PHOTOGRAPH THIS SHEET

AD A094294

DTIC ACCESSION NUMBER

III

LEVEL

INVENTORY

[redacted] TASK 3. EXPERIMENTAL INVESTIGATION OF SUPPRESSION PRINCIPLES VOLUME II - PARAMETRIC TESTING and SOURCE MEASUREMENTS. FINAL REPT., DEC. '78, REPT. NO. R78AEG627
CONTRACT DOT-OS-30034 FAA-RD-76-79-3-2

DISTRIBUTION STATEMENT A
Approved for public release
Distribution Unlimited

DISTRIBUTION STATEMENT

ACCESSION FOR
NTIS GRA&I
DTIC TAB
UNANNOUNCED
JUSTIFICATION

BY
DISTRIBUTION /
AVAILABILITY CODES

DIST	AVAIL AND/OR SPECIAL
A	

DISTRIBUTION STAMP

DTIC
ELECTE
JAN 29 1981
S D
D

DATE ACCESSIONED

81 1 27 008

DATE RECEIVED IN DTIC

PHOTOGRAPH THIS SHEET AND RETURN TO DTIC-DDA-2

DTIC FORM OCT 79 70A

DOCUMENT PROCESSING SHEET

REPORT NO. FAA-RD-76-79, III - II

R78AEG627

AD A094294

HIGH VELOCITY JET NOISE SOURCE LOCATION AND REDUCTION

TASK 3 - EXPERIMENTAL INVESTIGATION OF SUPPRESSION PRINCIPLES

Volume II - Parametric Testing and Source Measurements

TECHNICAL CONTRIBUTORS:

J.F. Brausch
W.S. Clapper
P.F. Scott
M.A. Smith
E.J. Stringas
R.W. Whittaker

GENERAL ELECTRIC COMPANY
AIRCRAFT ENGINE GROUP
CINCINNATI, OHIO 45215

DECEMBER 1978

FINAL REPORT

Document is available to the U.S. public through the National Technical Information Service, Springfield, Virginia 22161.

Prepared for

U.S. DEPARTMENT OF TRANSPORTATION
FEDERAL AVIATION ADMINISTRATION
Systems Research & Development Service
Washington, D.C. 20590

NOTICE

The contents of this report reflect the views of the General Electric Company which is responsible for the facts and the accuracy of the data presented herein. The contents do not necessarily reflect the official views or policy of the Department of Transportation. This report does not constitute a standard, specification or regulation.

1. Report No.	2. Government Accession No.	3. Recipient's Catalog No.
FAA-RD-76-79, III - II		

4. Title and Subtitle	5. Report Date
High Velocity Jet Noise Source Location and Reduction, Task 3 - Experimental Investigation of Suppression Principles Volume II - Parametric Testing and Source Measurements	December 1978
	6. Performing Organization Code

7. Author(s).	8. Performing Organization Report No.
J.F. Brausch, W.S. Clapper, R.J. Stringas, R. Whittaker. W.S. Clapper (Task 3 Technical Director and Editor) E.J. Stringas (Technical Project Manager)	R78AEG627
	10. Work Unit No.

9. Performing Organization Name and Address	11. Contract or Grant No.
General Electric Company Group Advanced Engineering Division Aircraft Engine Group Cincinnati, Ohio 45215	DOT-OS-30034
	13. Type of Report and Period Covered
	Technical Report October 1974-April 1978

12. Sponsoring Agency Name and Address	14. Sponsoring Agency Code
U.S. Department of Transportation Federal Aviation Administration Systems Research and Development Service Washington, D.C. 20590	ARD-550

15. Supplementary Notes

This report is in partial fulfillment of the subject program. Related documents to be issued in the course of the program include final reports of the following Tasks: Task 1 - Activation of Facilities and Validation of Source Location Techniques; Task 1 Supplement - Certification of the General Electric Jet Noise Anechoic Test Facility; Task 2 - Theoretical Developments and Basic Experiments; Task 4 - Development/Evaluation of Techniques for "Inflight" Investigation; Task 5 - Investigation of "Inflight" Aero-Acoustic Effects; Task 6 - Noise Abatement Nozzle Design Guide. FAA Program Monitor, R.S. Zuckerman.

16. Abstract

Experimental investigations were conducted of suppression principles, including developing an experimental data base, developing a better understanding of jet noise suppression principles, and formulating empirical methods for the acoustic design of jet noise suppressors. Acoustic scaling has been experimentally demonstrated, and five "optimum" nozzles have been selected for subsequent anechoic free-jet testing.

A series of experimental tests was conducted to provide farfield acoustic data on 47 baseline and suppressor nozzle configurations and to provide aerodynamic nozzle performance on 18 of the configurations. Suppressor design parameters evaluated experimentally included: suppressor area ratio, radius ratio, flow management, inner stream geometry, element number and type, treated ejectors on multielement and unsuppressed inverted-coannular-flow nozzles.

Parametric testing established suppression levels for single and dual flow nozzles during static operation. Selective free-jet tests conducted on eight configurations were utilized to establish flight suppression levels for plug, chute, tube and hole nozzles. The aerodynamic performance test program illustrated that suppressed exhaust nozzles which incorporate elemental base areas as an integral part of the design are sensitive to external Mach number. In general suppressor element base drag was the most significant loss mechanism.

This volume is part of the four volume set that constitutes the Task 3 final report. The other volumes are: Volume I - Verification of Suppression Principles and Development of Suppression Prediction Methods, Volume III - Suppressor Concepts Optimization, and Volume IV - Laser Velocimeter Time Dependent Cross Correlation Measurements.

17. Key Words (Suggested by Author(s))	18. Distribution Statement
Jet Noise, Suppression, Aerodynamic Performance, Freejet, Jet Plume Characteristics	Document is available to the U.S. public through the National Technical Information Service, Springfield, Virginia 22161.

19. Security Classif. (of this report)	20. Security Classif. (of this page)	21. No. of Pages	22. Price*
Unclassified	Unclassified	823	

*For sale by the National Technical Information Service, Springfield, Virginia 22151

NASA-C-168 (Rev. 6-71)

METRIC CONVERSION FACTORS

Approximate Conversions to Metric Measures

Symbol	When You Know	Multiply by	To Find	Symbol
		LENGTH		
		*2.5		
		30		
		0.9		
		1.5		
		AREA		
		6.5		
		0.09		
		0.8		
		2.6		
		0.4		
		MASS (weight)		
		28		
		0.45		
	(2000 lb)	0.9		
		VOLUME		
		5		
		15		
		30		
		0.24		
		0.47		
		0.95		
		3.8		
		0.03		
		0.76		
		TEMPERATURE (exact)		
°F	Fahrenheit temperature	5/9 (after subtracting 32)	Celsius temperature	°C

*1 in = 2.54 centimeters. For other exact conversions and more detailed tables, see NBS Misc. Publ. 286, Units of Weights and Measures, Price $2.25, SD Catalog No. C13.10:286.

Approximate Conversions from Metric Measures

Symbol	When You Know	Multiply by	To Find	Symbol
		LENGTH		
mm	millimeters	0.04	inches	in
cm	centimeters	0.4	inches	in
m	meters	3.3	feet	ft
m	meters	1.1	yards	yd
km	kilometers	0.6	miles	mi
		AREA		
cm^2	square centimeters	0.16	square inches	in^2
m^2	square meters	1.2	square yards	yd^2
km^2	square kilometers	0.4	square miles	mi^2
ha	hectares (10,000 m^2)	2.5	acres	
		MASS (weight)		
g	grams	0.035	ounces	oz
kg	kilograms	2.2	pounds	lb
t	tonnes (1000 kg)	1.1	short tons	
		VOLUME		
ml	milliliters	0.03	fluid ounces	fl oz
l	liters	2.1	pints	pt
l	liters	1.06	quarts	qt
l	liters	0.26	gallons	gal
m^3	cubic meters	35	cubic feet	ft^3
m^3	cubic meters	1.3	cubic yards	yd^3
		TEMPERATURE (exact)		
°C	Celsius temperature	9/5 (then add 32)	Fahrenheit temperature	°F

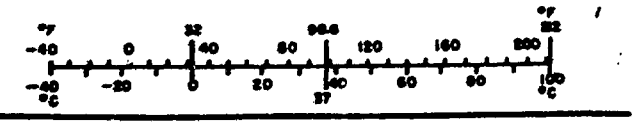

PREFACE

This report describes the work performed under Task 3 of the DOT/FAA High Velocity Jet Noise Source Location and Reduction Program (Contract DOT-OS-30034). The objectives of the contract were:

- Investigation, including scaling effects, of the aerodynamic and acoustic mechanisms of various jet noise suppressors.
- Analytical and experimental studies of the acoustic source distribution in such suppressors, including identification of source location, nature, and strength and noise reduction potential.
- Investigation of in-flight effects on the aerodynamic and acoustic performance of these suppressors.

These investigations are expected to lead to the preparation of a design guide report for predicting the overall characteristics of suppressor concepts, from models to full scale, static to in-flight conditions, as well as a quantitative and qualitative prediction of the phenomena involved.

The work effort in this program was organized under the following major Tasks, each of which is reported in a separate Final Report:

Task 1 - Activation of Facilities and Validation of Source Location Techniques.

Task 2 - Theoretical Developments and Basic Experiments.

Task 3 - Experimental Investigation of Suppression Principles.

Task 4 - Development and Evaluation of Techniques for "In flight" Investigation.

Task 5 - Investigation of "In flight" Aero-Acoustic Effects on Suppressed Exhausts.

Task 6 - Preparation of Noise Abatement Nozzle Design Guide Report.

Task 1 was an investigative and survey effort designed to identify acoustic facilities and test methods best suited to jet noise studies. Task 2 was a theoretical effort complemented by theory verification experiments which extended across the entire contract period of performance.

The subject of the present, Task 3, report series (FAA-RD-76-79 III - I, II, III, and IV) was formulated as a substantial part of the contract effort to gather various test data on a wide range of high velocity jet nozzle suppressors. These data, together with supporting theoretical advances from Task 2, have led to a better understanding of jet noise and jet noise

suppression mechanisms, as well as to a validation of scaling methods. Task 3 helped to identify several "optimum" nozzles for simulated in-flight testing under Task 5, and to provide a extensive, high-quality, data bank leading to formulation of methods and techniques useful for designing jet noise suppressors for application in the Task 6 design guide as well as in future studies.

Task 4 was similar to Task 1, except that it dealt with the specific test facility requirements, measurement techniques, and analytical methods necessary to evaluate the "in flight" noise characteristics of simple and complex suppressor nozzles. This effort provided the capability to conduct the "flight" effects test program of Task 5.

TABLE OF CONTENTS

Section		Page
1.0	SUMMARY	1
2.0	INTRODUCTION	10
3.0	PARAMETRIC ACOUSTIC TESTING AND SOURCE MEASUREMENTS	12
	3.1 Description of Test Models	14
	3.2 Definition of Test Matrices	34
	3.2.1 Acoustic Test Matrices	34
	3.2.2 Laser Velocimeter Test Matrix	45
	3.2.3 Ellipsoidal Mirror Test Matrices	48
	3.3 Data Acquisition and Data Reduction Procedures	49
	3.3.1 Acoustic Data	49
	3.3.1.1 Acoustic Data Acquisition	49
	3.3.1.2 Acoustic Data Reduction	52
	3.3.1.3 Air Attenuation Corrections	54
	3.3.1.4 Data Corrections to a Free-Field Environment JENOTS	54
	3.3.1.5 Data Scaling Procedure	55
	3.3.1.6 Power Level Calculations	55
	3.3.1.7 Acoustic Data Normalization	55
	3.3.2 Laser Velocimeter Data	57
	3.3.3 Ellipsoidal Mirror Data	63
	3.4 Data Analysis	67
	3.4.1 Tests Related to Baseline Nozzle Configurations	67
	3.4.1.1 Baseline Conical Nozzles (Models 1, 14)	67
	3.4.1.2 Convergent-Divergent Plug Nozzle Study	85
	3.4.1.3 Plug Nozzle Radius Ratio Study	96
	3.4.1.4 Baseline Dual-Flow Study	107
	3.4.1.5 Dual Flow Parametric Study	124
	3.4.1.6 Unsuppressed Annular Jet Study	135
	3.4.1.7 Summary	150
	3.4.2 Tests Related to Suppressors Influenced by Geometric and Cycle Variations, Single- and Dual-Flow Nozzles	150
	3.4.2.1 Chute Area Ratio and Radius Ratio Studies	151
	3.4.2.2 Flow Management and Inner Stream Geometry Studies	199
	3.4.2.3 Flow Segment	282
	3.4.2.4 Element Type Studies	301
	3.4.2.5 Treated Ejector Applications	321
	3.4.2.6 Summary of Suppression Levels	358

TABLE OF CONTENTS (Continued)

Section		Page
	3.4.3 Tests to Evaluate the Influence of Simulated Flight	358
	3.4.3.1 Simulated Flight Investigation for Several Configurations	358
	3.4.3.2 Shock Noise Studies	405
	3.4.4 Laser Velocimeter Results	411
	3.4.5 Ellipsoidal Mirror (EM) Testing	432
	3.4.5.1 Data Analysis	432
4.0	AERODYNAMIC PERFORMANCE TEST PROGRAM	445
	4.1 General Program Objectives and Scope	445
	4.2 Test Facility Description	446
	4.3 Model Description	450
	4.3.1 Annular Suppressed Models	450
	4.3.2 104-Tube Model	457
	4.3.3 Eight-Lobe Suppressor Model	457
	4.3.4 Reference Nozzle	457
	4.4 Data Reduction Procedures	463
	4.4.1 Flow Rates	463
	4.4.2 Flow Coefficients	463
	4.4.3 Thrust Measurements	464
	4.4.4 Thrust Coefficient	466
	4.4.5 Pressure Data	466
	4.5 Test Results and Discussion	467
	4.5.1 Data Quality	467
	4.5.2 Annular Nozzle Thrust Coefficients	472
	4.5.3 Effect of Suppressor Element Number	472
	4.5.4 Effect of Suppressor Area Ratio	477
	4.5.5 Effect of Inner Nozzle Area (Inner Radius Ratio)	477
	4.5.6 Effect of Inner Plug Axial Location	482
	4.5.7 Effect of Inner Nozzle Area (Radius Ratio) and Plug Location on Element Base Pressure	482
	4.5.8 Effect of Suppressor Ventilation on Performance	488
	4.5.9 Effect of External Mach Number	488
	4.5.10 104-Tube Nozzle Test Results	488
	4.5.11 Eight Lobe Nozzle Test Results	488
	4.5.12 Suppressor Flow Coefficients	495
	4.6 Conclusions	495
5.0	RESULTS AND CONCLUSIONS	497

TABLE OF CONTENTS (Concluded)

Section		Page
Appendix A	Test Model Definitions	501
Appendix B	Acoustic Test Matrices, Aerodynamic Test Conditions	543
Appendix C	General Electric Air-Attenuation Model	586
Appendix D	Summary of the Ellipsoidal Mirror Development	597
Appendix E	Error Analysis of the Ellipsoidal Mirror Technique	635
Appendix F	Aerodynamic Performance Details	654
References		821

LIST OF SYMBOLS

Symbols

A	Nozzle Exhaust Area, ft^2
a_o	Ambient Speed of Sound, ft/sec
AR	Suppressor Area-Ratio; Determined by the Total Nozzle Area, Excluding Any Plug, to the Flow Area of the Nozzle
C_D, CD	Flow Coefficient
C_f	Skin Friction Coefficient
C_{f_g}, C_T	Thrust Coefficient
C_V	Peak Thrust Coefficient
D	Diameter, ft or Chute-Base Drag, lbf
d	Chute Ventilation Depth, ft
D_{E_i}	Ejector Inlet Diameter, ft
D_{eq}	$\sqrt{(4\ \text{Area}/\pi)}$
D_f	Friction Drag, lbf
D_s	Shroud Diameter at Tip, ft
DBTF	Duct-Burning Turbofan
EPNL	Effective Perceived Noise Level, EPNdB
F	Force or Thrust, lbf
f	Frequency, Hz
F_p	Pressure Force, lbf
F_S	Ideal Gross Thrust, lbf
F_9	Stream Thrust Parameters, lbf
f_9	Dimensionless Stream Thrust Parameter
G	Ellipsoidal Mirror Gain, dB
H	Diffraction Window Function
h	Annulus Height, ft
L_E	Ejector Length, ft
M	Mach Number; Jet or Free Stream
m	Known Value of a Parameter
N	Number of Elements
n	Number of Samples Taken of a Given Parameter
N_θ	Velocity Index

LIST OF SYMBOLS

Symbols

N_{SH}	Normalized Shock Cell Noise, dB
OAPWL	Overall Sound Power Level, dB
OASPL	Overall Sound Pressure Level, dB
P	Pressure, lbf/in.^{2}
PNL	Perceived Noise Level, PNdB
P_T/P_a, P_T/P_o, PR	Nozzle total Pressure Ratio
R, r	Radius, ft
R_p	Plug Radius, ft
Rr	Radius Ratio, determined by the ratio of the inner radius to the outer radius for the particular flow passage.
R/R_o, r/r_o	Normalized Radial Location when referring to Jet Plume Laser Velocimeter Surveys
SPL	Sound Pressure Level, dB
T	Temperature, $^\circ$ R
t	Time, Seconds
TF	Turbofan
U, V	Mean Velocity, ft/sec, Jet or Free stream
U' u'	Local Turbulent Velocity, ft/sec
VCE	Variable Cycle Engine
W	Weight Flow Rate, lbm/sec
$W_{C/S}$, P	Chute or Spoke Width at Plug, ft
$W_{C/S}$, S	Chute or Spoke Width at Shroud, ft
W_p, S	Flow Width at Shroud, ft
W_p, P	Flow Width at Plug, ft
X	Axial Distance, ft
$\bar{X}$	mean of measured Values of a Parameter
X_{peak}	Peak Axial Noise Source Location For a Given Frequency, ft
X_s	Ejector Axial Spacing, ft
1/3 OBSPL	One-Third-Octave-Band SPL, dB
β	Shock Cell Noise Parameter, $\sqrt{M^2-1}$ or Bypass Ratio, W_o/W_i
Y	Plug half Angle, degrees

LIST OF SYMBOLS

Symbols

θ	Element Orientation Angle, Degrees
θ_I	Angle Relative to Inlet Axis, Degrees
λ	Wavelength, ft
ρ	Density, lbm/ft^3
ω, w	Jet Density Exponent

Subscript

a, o	Ambient
a, a/c, FS	Aircraft, Tunnel, Free stream or External
B, ch	Chute Base
c, i	Core or Inner Stream
ISA	International Standard Atmosphere
j	Jet
m, ma, mix	Mass-Averaged Conditions
o, f	Outer Stream or Fan Duct
s	Static Conditions
T	Total Conditions
1, 2, 3, 4	Control Planes Associated with Thrust Measurement Test Setup
8	Condition at Core (Inner) Flow Throat
9	Nozzle Exit Conditions of Inner (Core) Flow
18	Condition at Outer (Fan/Duct) Flow Throat

Superscript

i	Inner (Core) Stream
o	Outer (Fan/Duct) Stream
*	Denotes Sonic Conditions

LIST OF ILLUSTRATIONS

Figure		Page
1-1.	Evaluation of Noise Mechanisms for a Conical Nozzle.	2
1-2.	Correlation Between Measured and Predicted Effective Perceived Noise Level, EPNL, for All Types of Suppressor Nozzles.	4
1-3.	Typical Peak Static Noise Suppression Characteristics.	6
1-4.	Summary of Range and Noise Characteristics for Several Baseline and Suppression Levels.	9
3-1.	Description of Geometric Parameters.	28
3-2(a).	Far-Field Acoustic Test Matrix, Model 1, JENOTS.	36
3-2(b).	Far-Field Acoustic Test Matrix, Model 14, Cell 41 Anechoic Facility.	36
3-3.	Far-Field Acoustic Test Matrix, Model 2, JENOTS.	37
3-4.	Far-Field Acoustic Test Matrix, Models 3, 4, and 5, JENOTS.	37
3-5.	Far-Field Acoustic Test Matrix, Models 6 and 8, JENOTS.	39
3-6.	Far-Field Acoustic Test Matrix, Model 8, JENOTS.	40
3-7(a).	Far-Field Acoustic Test Matrix, Model 9, JENOTS.	41
3-7(b).	Far-Field Acoustic Test Matrix, Models 10, 11, 12, and 13, JENOTS.	41
3-8.	Far-Field Acoustic Test Matrix, Models 14 Through 19, Cell 41 Anechoic Facility.	42
3-9.	Far-Field Acoustic Test Matrix, Models 20 and 21, Cell 41 Anechoic Facility.	42
3-10.	Far-Field Acoustic Test Matrix, Models 22 Through 32 and 36, Cell 41 Anechoic Facility.	43
3-11.	Far-Field Acoustic Test Matrix, Models 39 Through 45 and 47, JENOTS Free Jet.	46
3-12.	Schematic of Acoustic Data Acquisition Systems.	50

LIST OF ILLUSTRATIONS (Continued)

Figure		Page
3-13.	Data Reduction System, JENOTS and Cell 41.	53
3-14.	Schematic of Laser Velocimeter Optics Package.	59
3-15(a).	Laser Velocimeter and Ellipsoidal Mirror at JENOTS.	60
3-15(b).	Laser Velocimeter in Cell 41 Anechoic Facility.	60
3-16.	Schematic of Laser Velocity Measurements.	62
3-17.	Schematics and Summary of Ellipsoidal Mirror Characteristics.	65
3-18.	Summary of Conical (Models 1 and 14) Nozzle Peak OASPL Characteristics.	69
3-19.	Summary of Conical Nozzle (Models 1 and 14) Peak PNL Characteristics.	69
3-20.	Summary of Conical Nozzle (Models 1 and 14) 90° OASPL Characteristics.	70
3-21.	Summary of Conical Nozzle (Models 1 and 14) 90° PNL Characteristics.	70
3-22.	Summary of Conical Nozzle (Models 1 and 14) 50° OASPL Characteristics.	71
3-23.	Summary of Conical Nozzle (Models 1 and 14) 50° PNL Characteristics.	71
3-24.	Summary of Conical Nozzle (Models 1 and 14) Power Level Characteristics.	72
3-25.	Supersonic Jet OASPL Correlation with Shock Strength Parameter β, Conical Nozzle (Model 14).	74
3-26.	Supersonic Jet PNL Correlation with Shock Strength Parameter β, Conical Nozzle (Model 14).	75
3-27.	Impact of Shock Noise on OASPL and PNL Directivity Conical Nozzle (Model 14), $V_{ma} = V_j = 1600$ ft/sec.	77
3-28.	Impact of Shock Noise on Spectra Conical Nozzle (Model 14), $V_{ma} = V_j = 1600$ ft/sec.	78

LIST OF ILLUSTRATIONS (Continued)

Figure		Page
3-29.	Impact of Shock Noise on OASPL and PNL Directivity, Conical Nozzle (Model 14), $V_{ma} = V_j = 2000$ ft/sec.	79
3-30.	Impact of Shock Noise on Spectra, Conical Nozzle (Model 14), $V_{ma} = V_j = 2000$ ft/sec.	80
3-31.	Impact of Cycle Variation at Ambient Temperature on OASPL and PNL Directivity, Conical Nozzle (Model 1).	81
3-32.	Impact of Cycle Variation at Ambient Temperature on Spectra, Conical Nozzle (Model 1).	82
3-33.	Impact of Cycle Variation at 1500° R on OASPL and PNL Directivity, Conical Nozzle (Model 14).	83
3-34.	Impact of Cycle Variation at 1500° R on Spectra, Conical Nozzle (Model 14).	84
3-35.	Summary of C-D Plug Nozzle (Model 2) Peak Noise Characteristics.	86
3-36.	Summary of C-D Plug Nozzle (Model 2) 90° Noise Characteristics.	87
3-37.	Summary of C-D Plug Nozzle (Model 2) 50° Noise Characteristics.	88
3-38.	Summary of C-D Plug Nozzle (Model 2) Power Level Noise Characteristics.	89
3-39.	Correlation of Peak OASPL with Pressure Ratio for a C-D Plug Nozzle (Model 2).	93
3-40.	Polar OASPL Distributions at V_{ma} = 1000, 1250, 1640, and 2090 ft/sec.	94
3-41.	150° Spectra at V_{ma} = 1000, 1250, 1640, and 2090 ft/sec.	95
3-42.	Jet Density Exponent Correlation.	97
3-43.	Model Hardware for Parametric Nozzle Radius Ratio Study.	99
3-44.	Summary of Plug Nozzle Peak OASPL and Suppression Levels.	100
3-45.	Summary of Plug Nozzle Peak PNL and Suppression Levels.	101

LIST OF ILLUSTRATIONS (Continued)

Figure		Page
3-46.	Summary of Plug Nozzle 90° OASPL and Suppression Levels.	102
3-47.	Summary of Plug Nozzle 90° PNL and Suppression Levels.	103
3-48.	Summary of Plug Nozzle 50° OASPL and PNL Characteristics.	104
3-49.	Summary of Plug Nozzle OAPWL and Suppression Levels.	105
3-50.	Impact of Plug Radius Ratio on OASPL and PNL Directivity, V_{ma} = 1490 ft/sec.	108
3-51.	Impact of Plug Radius Ratio on OASPL and PNL Directivity, V_{ma} = 1490 ft/sec.	109
3-52.	Impact of Plug Radius Ratio on OASPL and PNL Directivity, V_{ma} = 1950 ft/sec.	110
3-53.	Impact of Plug Radius Ratio on Spectra, V_{ma} = 1950 ft/sec.	111
3-54.	Impact of Plug Radius Ratio on OASPL and PNL Directivity, V_{ma} = 2350 ft/sec.	112
3-55.	Impact of Plug Radius Ratio on Spectra, V_{ma} = 2350 ft/sec.	113
3-56.	Jet Density Exponent Correlation.	114
3-57.	Impact of Velocity Ratio on Spectra, AR = 2.0 Coplanar-Coannular Nozzle (Model 6).	116
3-58.	Impact of Velocity Ratio on Spectra, AR = 2.0 Coplanar-Coannular Nozzle (Model 6).	117
3-59.	Impact of Velocity Ratio on OASPL and PNL Directivity.	118
3-60.	Impact of Velocity Ratio on Spectra.	119
3-61.	Comparison of OASPL and PNL Directivity at V_o/V_i = 1.25, AR = 2.0 Coplanar-Coannular Nozzle (Model 6).	120
3-62.	Comparison of OASPL and PNL Directivity, V_o/V_i = 2.0, AR = 2.0 Coplanar-Coannular Nozzle (Model 6).	121
3-63(a).	Normalized Spectra, V_o/V_i = 1.25, AR = 2.0 Coplanar-Coannular Nozzle (Model 6).	122
3-63(b).	Normalized Spectra, V_o/V_i = 2.0, AR = 2.0 Coplanar-Coannular Nozzle (Model 6).	123

LIST OF ILLUSTRATIONS (Continued)

Figure		Page
3-64.	Peak PNL Coplanar-Coannular Nozzle Area Ratio Variation.	125
3-65.	Peak OASPL Coplanar-Coannular Nozzle Area Ratio Variation.	126
3-66.	90° PNL and OASPL Coplanar-Coannular Nozzle Area Ratio Variation.	127
3-67.	50° PNL and OASPL Coplanar-Coannular Nozzle Area Ratio Variation.	128
3-68.	OASPL and PNL Directivity Variation with Area Ratio, $V_o/V_i = 2.0$.	129
3-69.	OASPL and PNL Directivity Variation with Area Ratio, $V_o/V_i = 1.5$.	130
3-70.	OASPL and PNL Directivity Variation with Area Ratio, $V_o/V_i = 2.0$.	131
3-71.	Spectra Variation with Area Ratio, $V_o/V_i = 1.0$.	132
3-72.	Spectra Variation with Area Ratio, $V_o/V_i = 1.5$.	133
3-73.	Spectra Variation with Area Ratio, $V_o/V_i = 2.0$	134
3-74.	Coannular-Coplanar Nozzle Suppression Characteristics with Varying Nozzle Area Ratio.	136
3-75.	Impact of Cycle Variation on Suppression Characteristics of $A_o/A_i = 0.4$ Coplanar-Coannular Nozzle (Models 12 and 13).	137
3-76.	Impact of Cycle Variation on Suppression Characteristics of $A_o/A_i = 0.65$ Coplanar-Coannular Nozzle (Models 10 and 11).	138
3-77.	OASPL Directivity Variation with Area Ratio, $W_i/W_o < 0.1$.	139
3-78.	PNL Directivity Variation with Area Ratio, $W_i/W_o < 0.1$.	140
3-79.	Spectra Variation with Area Ratio, $V_{ma} = 2350$ ft/sec.	141
3-80.	Spectra Variation with Area Ratio, $V_{ma} = 1800$ ft/sec.	142
3-81.	Impact of Inner Flow Variation, $A_o/A_i = 0.4$, PNL and OASPL Directivity.	143
3-82.	Impact of Inner Flow Variation, Ao/Ai = 0.65, PNL and OASPL Directivity.	144

LIST OF ILLUSTRATIONS (Continued)

Figure		Page
3-83.	Impact of Inner Flow Variation on Spectra, A_o/A_i = 0.4 V_{ma} = 2400 ft/sec.	145
3-84.	Impact of Inner Flow Variation on Spectra, A_o/A_i = 0.4, V_{ma} = 1800 ft/sec.	146
3-85.	Impact of Inner Flow Variation on Spectra, A_o/A_i = 0.65 V_{ma} = 2400 ft/sec.	147
3-86.	Impact of Inner Flow Variation on Spectra, A_o/A_i = 0.65 V_{ma} = 1800 ft/sec.	148
3-87.	Summary of Plug Nozzle and Coplanar-Coannular Nozzle Peak PNL Suppression Levels.	149
3-88.	Annular Suppressor Area Ratio and Radius Ratio Variation on Turbojet.	152
3-89.	Impact of Area Ratio and Radius Ratio on Peak OASPL.	153
3-90.	Impact of Area Ratio and Radius Ratio on Peak PNL.	154
3-91.	Impact of Area Ratio and Radius Ratio on 90° PNL and OASPL.	155
3-92.	Impact of Area Ratio and Radius Ratio on 50° PNL and OASPL.	156
3-93.	Impact of Area Ratio and Radius Ratio on OAPWL.	157
3-94.	Impact of Area Ratio and Radius Ratio on PNL and OASPL Directivity, V_{ma} = 2625 ft/sec.	159
3-95.	Impact of Area Ratio and Radius Ratio on Spectra, V_{ma} = 2625 ft/sec.	160
3-96.	Impact of Area Ratio and Radius Ratio on PNL and OASPL Directivity, V_{ma} = 2150 ft/sec.	162
3-97.	Impact of Area Ratio and Radius Ratio on Spectra, V_{ma} = 2150 ft/sec.	163
3-98.	Impact of Area Ratio and Radius Ratio on PNL and OASPL Directivity, V_{ma} = 1400 ft/sec.	165

LIST OF ILLUSTRATION (Continued)

Figure		Page
3-99.	Impact of Area Ratio and Radius Ratio on Spectra, V_{ma} = 1400 ft/sec.	166
3-100.	Half-Span Suppressor Area Ratio and Radius Ratio Variation on Dual Flow.	167
3-101.	Impact of Area Ratio and Radius Ratio on Peak PNL, Dual Flow.	169
3-102.	Impact of Area Ratio and Radius Ratio on Peak OASPL, Dual Flow.	170
3-103.	Impact of Area Ratio and Radius Ratio on 90° PNL, Dual Flow.	172
3-104.	Impact of Area Ratio and Radius Ratio on 90° OASPL, Dual Flow.	173
3-105.	Impact of Area Ratio and Radius Ratio on 50° PNL, Dual Flow.	174
3-106.	Impact of Area Ratio and Radius Ratio on 50° OASPL, Dual Flow.	175
3-107.	Impact of Area Ratio and Radius Ratio on OAPWL, Dual Flow.	177
3-108.	Impact of Area Ratio and Radius Ratio on OASPL and PNL Directivity, V_{ma} = 2425 ft/sec, Dual Flow.	178
3-109.	Impact of Area Ratio and Radius Ratio on Spectra, V_{ma} = 2425 ft/sec, Dual Flow.	179
3-110.	Impact of Area Ratio and Radius Ratio on OASPL and PNL Directivity, V_{ma} = 1200 ft/sec, Dual Flow.	180
3-111.	Impact of Area Ratio and Radius Ratio on Spectra, V_{ma} = 1200 ft/sec, Dual Flow.	181
3-112.	Impact of Area Ratio and Radius Ratio on PNL and OASPL Directivity, V_{ma} = 1945 ft/sec, Dual Flow.	182
3-113.	Impact of Area Ratio and Radius Ratio on Spectra, V_{ma} = 1945 ft/sec, Dual Flow.	183

LIST OF ILLUSTRATIONS (Continued)

Figure		Page
3-114.	Annular Suppressor Area Ratio Variation at Constant Radius Ratio, Dual Flow.	185
3-115.	Area Ratio Variation at Constant Radius Ratio, Peak OASPL.	187
3-116.	Area Ratio Variation at Constant Radius Ratio, Peak PNL.	188
3-117.	Area Ratio Variation at Constant Radius Ratio, 90° OASPL.	189
3-118.	Area Ratio Variation at Constant Radius Ratio, 90° PNL.	189
3-119.	Area Ratio Variation at Constant Radius Ratio, 50° OASPL.	190
3-120.	Area Ratio Variation at Constant Radius Ratio, 50° PNL.	190
3-121.	Area Ratio Variation at Constant Radius Ratio, OAPWL.	191
3-122.	Area Ratio Variation at Constant Velocity Ratio, Peak OASPL.	192
3-123.	Area Ratio Variation at Constant Velocity Ratio, Peak PNL.	193
3-124.	Area Ratio Variation at Constant Radius Ratio, OASPL and PNL Directivity, V_{ma} = 2075 ft/sec.	194
3-125.	Area Ratio Variation at Constant Radius Ratio, Spectra, V_{ma} = 2075 ft/sec.	195
3-126.	Area Ratio Variation at Constant Radius Ratio, OASPL and PNL Directivity, V_{ma} = 1340 ft/sec.	196
3-127.	Area Ratio Variation at Constant Radius Ratio, Spectra, V_{ma} = 1340 ft/sec.	197
3-128.	Dual Flow Models for Velocity Ratio Investigation at A_o/A_i = 0.65.	202
3-129.	Dual Flow Models for Velocity Ratio Investigation at A_o/A_i = 0.65.	203
3-130.	Dual Flow Models for Velocity Ratio Investigation at A_o/A_i = 1.92 and 3.61.	204
3-131.	Peak PNL and OASPL Variation with V_o/V_i, Model 33.	205

LIST OF ILLUSTRATIONS (Continued)

Figure		Page
3-132.	90° PNL and OASPL Variation with V_o/V_i, Model 33.	206
3-133.	50° PNL and OASPL Variation with V_o/V_i, Model 33.	207
3-134.	Peak PNL and OASPL Variation with V_o/V_i, Model 34.	208
3-135.	90° PNL and OASPL Variation V_o/V_i, Model 34.	209
3-136.	50° PNL and OASPL Variation with V_o/V_i, Model 34.	210
3-137.	Peak PNL and OASPL Variation with V_o/V_i, Model 35.	211
3-138.	90° PNL and OASPL Variation with V_o/V_i, Model 35.	212
3-139.	50° PNL and OASPL Variation with V_o/V_i, Model 35.	213
3-140.	Impact of V_o/V_i on PNL and OASPL Directivity, Model 33, V_{ma} = 2010 to 2050 ft/sec.	216
3-141.	Impact of V_o/V_i on Spectra, Model 33, V_{ma} = 2010 to 2050 ft/sec.	217
3-142.	Impact of V_o/V_i on PNL and OASPL Directivity, Model 33, V_{ma} = 1685 ≅ 1840 ft/sec.	218
3-143.	Impact of V_o/V_i on Spectra, Model 33, V_{ma} = 1685 - 1840 ft/sec.	219
3-144.	Impact of V_o/V_i on PNL and OASPL Directivity, Model 34, V_{ma} = 2250 - 2390 ft/sec.	220
3-145.	Impact of V_o/V_i on Spectra, Model 34, V_{ma} = 2250 - 2390 ft/sec.	221
3-146.	Impact of V_o/V_i on PNL and OASPL Directivity, Model 34, V_{ma} = 1720 ≅ 1830 ft/sec.	222
3-147.	Impact of V_o/V_i on Spectra, Model 34, V_{ma} = 1720 - 1830 ft/sec.	223
3-148.	Peak PNL and OASPL Variation with V_o/V_i, Model 31.	225
3-149.	90° PNL and OASPL Varition with V_o/V_i, Model 31.	226
3-150.	50° PNL and OASPL Variation with V_o/V_i, Model 31.	227

LIST OF ILLUSTRATIONS (Continued)

Figure		Page
3-151.	Peak PNL and OASPL Variation with V_o/V_i, Model 31.	228
3-152.	90° PNL and OASPL Variation with V_o/V_i, Model 27.	229
3-153.	50° PNL and OASPL Variation with V_o/V_i, Model 27.	230
3-154.	Peak PNL and OASPL Variation with V_o/V_i, Model 26.	231
3-155.	90° PNL and OASPL Variation with V_o/V_i, Model 26.	232
3-156.	50° PNL and OASPL Variation with V_o/V_i, Model 26.	233
3-157.	Dual Flow Model for β Investigation at $A_o/A_i = 1.92$.	235
3-158.	Peak PNL Variation with β, Model 33.	237
3-159.	Peak OASPL Variation with β, Model 33.	238
3-160.	90° PNL and OASPL Variation with β, Model 33.	239
3-161.	50° PNL and OASPL Variation with β, Model 33.	240
3-162.	Peak PNL Variation with β, Model 34.	241
3-163.	Peak OASPL Variation with β, Model 34.	242
3-164.	90° PNL and OASPL Variation with β, Model 34.	243
3-165.	50° PNL and OASPL Variation with β, Model 34.	244
3-166.	Peak PNL Variation with β, Model 31.	245
3-167.	Peak OASPL Variation with β, Model 31.	246
3-168.	90° PNL and OASPL Variation with β, Model 31.	247
3-169.	50° PNL and OASPL Variation with β, Model 31.	248
3-170.	Peak PNL Variation with β, Model 23.	249
3-171.	Peak OASPL Variation with β, Model 23.	250
3-172.	90° PNL and OASPL Variation with β, Model 23.	251

LIST OF ILLUSTRATIONS (Continued)

Figure		Page
3-173.	50° PNL and OASPL Variation with β, Model 23.	252
3-174.	Dual Flow Models 23, 24, 25, and 26 for A_o/A_i and Inner Plug Geometry Variation.	255
3-175.	Dual Flow Models 28 and 29 for A_o/A_i and Inner Plug Geometry Variation.	256
3-176.	Schematic of Inner Plug Geometry Variations.	257
3-177.	Peak PNL Variation with A_o/A_i and Inner Plug Geometry, Models 23 - 26, $W_{Inner} = 15\% W_{Outer}$ Cycle.	258
3-178.	Peak OASPL Variation with A_o/A_i and Inner Plug Geometry, Models 23 - 26, $W_{Inner} = 15\% W_{Outer}$ Cycle.	259
3-179.	90° PNL and OASPL Variation with A_o/A_i and Inner Plug Geometry, Models 23 - 26, $W_{Inner} = 15\% W_{Outer}$ Cycle.	260
3-180.	50° PNL and OASPL Variation with A_o/A_i and Inner Plug Geometry, Models 23 - 26, $W_{Inner} = 15\% W_{Outer}$.	261
3-181.	Peak PNL Variation with A_o/A_i and Inner Plug Geometry, Models 23 - 26, $W_{Inner} = 30\% W_{Outer}$ Cycle.	262
3-182.	Peak OASPL Variation with A_o/A_i and Inner Plug Geometry, Models 23 - 26, $W_{Inner} = 30\% W_{Outer}$ Cycle.	263
3-183.	90° PNL and OASPL Variation with A_o/A_i and Inner Plug Geometry, Models 23 - 26, $W_{Inner} = 30\% W_{Outer}$ Cycle.	264
3-184.	50° PNL and OASPL Variation with A_o/A_i and Inner Plug Geometry, Models 23 - 26, $W_{Inner} = 30\% W_{Outer}$ Cycle.	265
3-185.	Peak PNL Variation with A_o/A_i and Inner Plug Geometry, Models 23 - 26, DBTF/Inverted Dual Flow Cycle.	266
3-186.	Peak OASPL Variation with A_o/A_i and Inner Plug Geometry, Models 23 - 26, DBTF/Inverted Dual Flow Cycle.	267
3-187.	90° PNL and OASPL Variation with A_o/A_i and Inner Plug Geometry, Models 23 - 26, DBTF/Inverted Dual Flow Cycle.	268
3-188.	50° PNL and OASPL Variation with A_o/A_i and Inner Plug Geometry, Models 23 - 26, DBTF/Inverted Dual Flow Cycle.	269

LIST OF ILLUSTRATIONS (Continued)

Figure		Page
3-189.	Peak PNL and OASPL Variation with Inner Plug Geometry, Models 28 and 29, DBTF/Inverted Dual Flow Cycle.	270
3-190.	90° PNL and OASPL Variation with Inner Plug Geometry, Models 28 and 29, DBTF/Inverted Dual Flow Cycle.	271
3-191.	50° PNL and OASPL Variation with Inner Plug Geometry, Models 28 and 29, DBTF/Inverted Dual Flow Cycle.	272
3-192.	Impact of A_o/A_i and Inner Plug Geometry on PNL and OASPL Directivity, Models 23 - 26, W_{Inner} = 30% W_{Outer} Cycle, V_{ma} = 2300 ft/sec.	275
3-193.	Impact of A_o/A_i and Inner Plug Geometry on Spectra, Models 23 - 26, W_{Inner} = 30% W_{Outer} Cycle, V_{ma} = 2300 ft/sec.	276
3-194.	Impact of A_o/A_i and Inner Plug Geometry on PNL and OASPL Directivity, Models 23 - 26, W_{Inner} = 30% W_{Outer} Cycle, V_{ma} = 1875 ft/sec.	277
3-195.	Impact of A_o/A_i and Inner Plug Geometry on Spectra, Models 23 - 26, W_{Inner} = 30% W_{Outer} Cycle, V_{ma} = 1875 ft/sec.	278
3-196.	Impact of A_o/A_i and Inner Plug Geometry on PNL and OASPL Directivity, Models 23 - 26, W_{Inner} = 30% W_{Outer} Cycle, V_{ma} = 1380 ft/sec.	279
3-197.	Impact of A_o/A_i and Inner Plug Geometry on Spectra, Models 23 - 26, W_{Inner} = 30% W_{Outer} Cycle, V_{ma} = 1380 ft/sec.	280
3-198.	Summary of Comparison of Suppressed Dual Flow with No Inner Flow to Full-Plug Turbojets.	281
3-199.	Half-Span Suppressor Element Number Variation on Dual Flow.	283
3-200.	Suppressor Element Number Variation, Peak Noise and Suppression Levels.	285
3-201.	Suppressor Element Number Variation, Peak PNL and Suppression Levels.	286

LIST OF ILLUSTRATIONS (Continued)

Figure		Page
3-202.	Suppressor Element Number Variation, Peak OASPL and Suppression Levels.	287
3-203.	Suppressor Element Number Variation, 90° PNL.	288
3-204.	Suppressor Element Number Variation, 90° OASPL.	289
3-205.	Suppressor Element Number Variation, 50° PNL.	290
3-206.	Suppressor Element Number Variation, 50° OASPL.	291
3-207.	Suppressor Element Number Variation, OAPWL.	292
3-208.	Suppressor Element Number Variation, OASPL and PNL Directivity, V_{ma} = 2425 ft/sec.	294
3-209.	Suppressor Element Number Variation, Spectra, V_{ma} = 2425 ft/sec.	295
3-210.	Suppressor Element Number Variation, OASPL and PNL Directivity, V_{ma} = 2100 ft/sec.	296
3-211.	Suppressor Element Number Variation, Spectra, V_{ma} = 2100 ft/sec.	297
3-212.	Suppressor Element Number Variation, OASPL and PNL Directivity, V_{ma} = 1200 ft/sec.	298
3-213.	Suppressor Element Number Variation, Spectra, V_{ma} = 1200 ft/sec.	299
3-214.	Element Type Variation on Turbojet.	302
3-215.	Variation of Element Type, Turbojet, Peak OASPL and Suppression Levels.	303
3-216.	Variation of Element Type, Turbojet, Peak PNL and Suppression Levels.	304
3-217.	Variation of Element Type, Turbojet, 90° OASPL and PNL.	306
3-218.	Variation of Element Type, Turbojet, 50° OASPL and PNL.	307
3-219.	Variation of Element Type, Turbojet, OAPWL and Suppression Levels.	308

LIST OF ILLUSTRATIONS (Continued)

Figure		Page
3-220.	Variation of Element Type, Turbojet, OASPL and PNL Directivity, V_{ma} = 2380 ft/sec.	309
3-221.	Variation of Element Type, Turbojet, Spectra, V_{ma} = 2380 ft/sec.	310
3-222.	Variation of Element Type, Turbojet, OASPL and PNL Directivity, V_{ma} = 2620 ft/sec.	311
3-223.	Variation of Element Type, Turbojet, Spectra, V_{ma} = 2620 ft/sec.	312
3-224.	Conversion of Half-Span Suppressor from Chutes to Spokes.	314
3-225.	Element Type Variation, Dual Flow, Peak PNL and Suppression Levels.	315
3-226.	Element Type Variation, Dual Flow, Peak OASPL and Suppression Levels.	316
3-227.	Element Type Variation, Dual Flow, 90° OASPL and PNL.	317
3-228.	Element Type Variation, Dual Flow, 50° OASPL and PNL.	318
3-229.	Element Type Variation, Dual Flow, Low System Area Ratio.	320
3-230.	Element Type Study, Dual Flow, Low System Area Ratio, Peak PNL.	322
3-231.	Element Type Study, Dual Flow, Low System Area Ratio, Peak OASPL.	323
3-232.	Acoustically Treated Ejector Application to Annular Suppressor, Turbojet.	324
3-233.	Details of the Acoustically Treated Ejector.	326
3-234.	Impact of Acoustically Treated Ejector, Turbojet, Peak PNL.	328
3-235.	Impact of Acoustically Treated Ejector, Turbojet, Peak OASPL.	329
3-236.	Impact of Acoustically Treated Ejector, Turbojet, 90° OASPL, PNL, and Suppression Levels.	330

LIST OF ILLUSTRATIONS (Continued)

Figure		Page
3-237.	Impact of Acoustically Treated Ejector, Turbojet, 50° OASPL, PNL, and Suppression Levels.	331
3-238.	Impact of Acoustically Treated Ejector, Turbojet, OAPWL and Suppression Levels.	332
3-239.	Impact of Acoustically Treated Ejector, Turbojet, OASPL, and PNL Directivity, V_{ma} = 2005 ft/sec.	334
3-240.	Impact of Acoustically Treated Ejector, Turbojet, Spectra, V_{ma} = 2005 ft/sec.	335
3-241.	Impact of Acoustically Treated Ejector, Turbojet, OASPL, and PNL Directivity, V_{ma} = 2625 ft/sec.	336
3-242.	Impact of Acoustically Treated Ejector, Turbojet, Spectra, V_{ma} = 2625 ft/sec.	337
3-243.	Acoustically Treated Ejector Application to Annular Suppressor, Dual Flow.	338
3-244.	Treated Ejector Application to Dual Flow, Peak PNL and Suppression Levels.	340
3-245.	Treated Ejector Application to Dual Flow, Peak OASPL and Suppression Levels.	341
3-246.	Treated Ejector Application to Dual Flow, DBTF Cycle, Peak OASPL, PNL, and Suppression Levels.	342
3-247.	Treated Ejector Application to Dual Flow, 90° OASPL, PNL, and Suppression Levels.	343
3-248.	Treated Ejector Application to Dual Flow, 50° OASPL, PNL, and Suppression Levels.	344
3-249.	Treated Ejector Application to Dual Flow, OAPWL and Suppression Levels.	345
3-250.	Treated Ejector Application to Dual Flow, OASPL and PNL Directivity, V_{ma} = 2095 ft/sec.	346
3-251.	Treated Ejector Application to Dual Flow, Spectra, V_{ma} = 2095 ft/sec.	347

LIST OF ILLUSTRATIONS (Continued)

Figure		Page
3-252.	Unsuppressed Coannular Nozzles with Acoustically Treated Ejector.	349
3-253.	Unsuppressed Coannular Nozzles with Treated Ejectors, Peak OASPL, PNL, and Suppression Levels.	350
3-254.	Unsuppressed Coannular Nozzles with Treated Ejectors, 90° OASPL and PNL.	351
3-255.	Unsuppressed Coannular Nozzles with Treated Ejectors, 50° OASPL and PNL.	352
3-256.	Unsuppressed Coannular Nozzle with Treated Ejectors, OAPWL and Suppression Levels.	353
3-257.	Summary of Results for Treated Ejector Application to Unsuppressed Coannular Systems.	355
3-258.	Unsuppressed Coannular Nozzles with Treated Ejectors, OASPL and PNL Directivity.	356
3-259.	Unsuppressed Coannular Nozzles with Treated Ejectors, Spectra.	357
3-260.	Typical Peak Static Noise Suppression Characteristics.	359
3-261.	Tests to Evaluate the Influence of Simulated Flight, Summary of Suppressor Nozzle Families.	360
3-262.	Static and Flight Peak PNL Levels.	362
3-263.	Static and Flight PNL Suppression Levels.	363
3-264.	Static and Flight Peak PNL Levels.	365
3-265.	Static and Flight 90° PNL Levels.	366
3-266.	Conical Nozzle (Model 47) Velocity Indices.	368
3-267.	Plug Nozzle (Models 39 and 40) Velocity Indices	369
3-268.	Chute Nozzle (Models 41, 42, and 43) Velocity Indices.	370
3-269.	104-Tube (Model 44) and 104-Hole (Model 45) Nozzle Velocity Indices.	371
3-270.	Velocity Indices for Several Nozzles.	372

LIST OF ILLUSTRATIONS (Continued)

Figure		Page
3-271.	Comparison of Static and Flight Spectra, 104-Tube and 36-Chute Nozzles (Models 44 and 41).	373
3-272.	A Comparison of Flight Spectra for 104-Tube (Model 44) and 36-Chute (Model 42) Nozzles.	374
3-273.	Summary of Static and Flight PNL Suppression Characteristics (Models 39 and 40).	375
3-274.	Summary of Static and Flight Suppression Characteristics (Models 41 and 42).	376
3-275.	Summary of Static and Flight Suppression Characteristics (Models 44 and 45).	377
3-276.	0.85 Radius Ratio Plug Nozzle (Model 40) PNL and OASPL Directivity, V_{ma} = 2400 ft/sec.	378
3-277.	0.85 Radius Ratio Plug Nozzle (Model 40) PNL and OASPL Directivity, V_{ma} = 2000 ft/sec.	379
3-278.	0.85 Radius Ratio Plug Nozzle (Model 40) Spectra, V_{ma} = 2400 ft/sec.	380
3-279.	0.85 Radius Ratio Plug Nozzle (Model 40) Spectra, V_{ma} = 2000 ft/sec.	381
3-280.	0.789 Radius Ratio Plug Nozzle (Model 39) PNL and OASPL Directivity, V_{ma} = 2400 ft/sec.	382
3-281.	0.789 Radius Ratio Plug Nozzle (Model 39) PNL and OASPL Directivity, V_{ma} = 2000 ft/sec.	383
3-282.	0.789 Radius Ratio Plug Nozzle (Model 39) Spectra, V_{ma} = 2000 ft/sec.	384
3-283.	0.789 Radius Ratio Plug Nozzle (Model 39) Spectra, V_{ma} = 2000 ft/sec.	385
3-284.	AR = 2.5 36-Chute, Turbojet (Model 41), PNL and OASPL Directivity, V_{ma} = 2400 ft/sec.	386
3-285.	AR = 2.5 36-Chute, Turbojet (Model 41), PNL and OASPL Directivity, V_{ma} = 2400 ft/sec.	387
3-286.	AR = 2.5 36-Chute, Turbojet (Model 41), Spectra, V_{ma} = 2400 ft/sec.	388

LIST OF ILLUSTRATIONS (Continued)

Figure		Page
3-287.	AR = 2.5 36-Chute, Turbojet (Model 41) Spectra, V_{ma} = 2000 ft/sec.	389
3-288.	AR = 2.5 36-Chute with Auxiliary Flow (Model 42), PNL and OASPL Directivity, V_{ma} = 2000 ft/sec.	390
3-289.	AR = 2.5 36-Chute with Auxiliary Flow (Model 42), PNL and OASPL Directivity, V_{ma} = 2000 ft/sec.	391
3-290.	AR = 2.5 36-Chute with Auxiliary Flow (Model 42), Spectra, V_{ma} = 2400 ft/sec.	392
3-291.	AR = 2.5 36-Chute with Auxiliary Flow (Model 42), Spectra, V_{ma} = 2000 ft/sec.	393
3-292.	AR = 2.5 36-Chute with Abrupt Step (Model 43), PNL and OASPL Directivity, V_{ma} = 2400 ft/sec.	394
3-293.	AR = 2.5 36-Chute with Abrupt Step, (Model 43) PNL and OASPL Directivity, V_{ma} = 2000 ft/sec.	395
3-294.	AR = 2.5 36-Chute with Abrupt Step (Model 43), Spectra, V_{ma} = 2400 ft/sec.	396
3-295.	AR = 3.5 36-Chute with Abrupt Step (Model 43), Spectra, V_{ma} = 2000 ft/sec.	397
3-296.	104-Tube Nozzle (Model 44), PNL and OASPL Directivity, V_{ma} = 2400 ft/sec.	398
3-297.	104-Tube Nozzle (Model 44), Spectra, V_{ma} = 2400 ft/sec.	399
3-298.	104-Hole Nozzle (Model 45), PNL and OASPL Directivity, V_{ma} = 2400 ft/sec.	400
3-299.	104-Hole Nozzle (Model 45), PNL and OASPL Directivity, V_{ma} = 2080 ft/sec.	401
3-300.	104-Hole Nozzle (Model 45), Spectra, V_{ma} = 2400 ft/sec.	402
3-301.	104-Hole Nozzle (Model 45), Spectra, V_{ma} = 2080 ft/sec.	403
3-302.	Summary of Conical Nozzle (Model 47) Forward Quadrant Noise Trends.	406
3-303.	Summary of 50° Spectra Characteristics.	407

LIST OF ILLUSTRATIONS (Continued)

Figure		Page
3-304.	0.85 Radius Ratio Plug Nozzle (Model 40) 50° Spectra at Constant Pressure Ratio.	408
3-305.	0.85 Radius Ratio Plug Nozzle (Model 40) Directivity at Constant Pressure Ratio.	409
3-306.	The Effect of Pressure Ratio Variation on the Directivity and Spectra Characteristics of a 104-Hole Nozzle (Model 45).	410
3-307.	Summary of Peak Mean Velocity Decay Characteristics.	413
3-308.	Turbulence Intensity Levels at Location of Peak Mean Velocity.	414
3-309.	Peak Turbulence Intensity Levels.	415
3-310.	Centerline Velocity Decay Characteristics.	416
3-311.	Centerline Velocity Decay Characteristics.	417
3-312.	AR = 2.0 36-Chute (Model 16) and 36-Spoke (Model 18) Nozzles, Mean Velocity and Turbulence Profiles.	418
3-313.	AR = 2.0 36-Chute (Model 16) and 36-Spoke (Model 18) Nozzles, Mean Velocity and Turbulence Profiles.	419
3-314.	Effect of Area Ratio on Peak Axial Velocity Decay Characteristics.	421
3-315.	Impact of Suppression Area Ratio on Radial Mean Velocity and Turbulence Intensity Profiles.	422
3-316.	Impact of Suppressor Area Ratio on Mean Velocity and Turbulence Intensity Profiles.	423
3-317.	Impact of a Treated Ejector on the Mean Velocity and Turbulence Profiles of a 36-Chute Nozzle.	424
3-318.	Centerline Velocity Decay for 3.56-inch Conical Nozzle (Reference 12) V_{ref} = 2200 ft/sec.	425
3-319.	0.85 Radius Ratio Plug Nozzle (Model 40) Centerline Mean Velocity Decay Characteristics.	427
3-320.	8-Lobe Nozzle (Model 46), Static and Flight.	428

LIST OF ILLUSTRATIONS (Continued)

Figure		Page
3-321.	36-Chute Nozzle (Model 41) Mean Velocity Decay Characteristics, Static and Flight.	429
3-322.	104-tube Nozzle (Model 44) Mean Velocity Characteristics, Static and Flight.	430
3-323.	104-Tube Nozzle (Model 44) Turbulence Intensity Characteristics, Static and Flight.	431
3-324.	Integral Closure Check for AR = 2.0 36-Chute Nozzle, V_o = 2384 ft/sec, V_i = 1187 ft/sec.	433
3-325.	Integral Closure Check for AR = 1.75 20-Shallow-Chute Nozzle, V_o = 2375 ft/sec, V_i = 1167 ft/sec.	433
3-326.	Integral Closure Check for AR = 2.0 36-Chute Nozzle with Treated Ejector, V_o = 1803 ft/sec, V_i = 1173 ft/sec.	434
3-327.	Integral Closure Check for AR = 2.0 36-Chute Nozzle, V_i = 2378 ft/sec.	434
3-328.	Integral Closure Check for AR = 2.5 36-Spoke Nozzle, V_o = 2382 ft/sec, V_i = 1269 ft/sec.	435
3-329.	Effect of Element Number of Multispoke (Shallow Chute) Dual-Flow Suppressor Noise Source Distributions.	437
3-330.	Effect of Chute Area Ratio on Multichute Dual-Flow Suppressor Noise Source Distributions.	438
3-331.	Comparison of Noise Source Distributions for Multichute and Multispoke Dual-Flow Suppressors.	439
3-332.	Comparison of Noise Source Distributions for Multichute Dual-Flow and Turbojet Suppressors.	440
3-333.	Comparison of Noise Source Distributions for Multichute Dual-Flow and Turbojet Suppressors with Ejectors.	441
3-334.	Effect of an Ejector on Multichute Dual-Flow Suppressor Noise Source Distributions.	442
3-335.	Effect of an Ejector on Multichute Turbojet Suppressor Noise Source Distributions.	443
3-336.	Axial Distributions of Sound Source Intensity for a 40-Shallow-Chute Dual-Flow Suppressor (Model 32).	444

LIST OF ILLUSTRATIONS (Continued)

Figure		Page
4-1.	Typical Model Installation.	447
4-2.	Schematic of Model Air Supply.	448
4-3.	Schematic of Model Thrust-Measuring System.	449
4-4.	Schematic of Annular Suppressed Nozzle Showing Key Geometric Variables.	451
4-5.	Summary of Annular Suppressor Models Tested.	453
4-6.	Schematic of Dual-Flow Suppressor Installation.	458
4-7.	104-Tube Nozzle.	459
4-8.	104-Tube Nozzle Geometric Details.	460
4-9.	8-Lobe Nozzle.	461
4-10.	Supersonic Tunnel Association (STA) Nozzle.	462
4-11.	Control Volume Applied to Model Test Setup.	465
4-12.	STA Static Performance with the 1.248-in.-Diameter Outer Flowmeter.	469
4-13.	STA Static Performance with the 1.1398-in.-Diameter Inner Flowmeter.	470
4-14.	Wind-On STA Nozzle Thrust Coefficients.	471
4-15.	STA Nozzle Bias and Standard Deviation on Static Thrust Coefficient.	473
4-16.	STA Nozzle Bias and Standard Deviation on Flow Coefficient.	474
4-17.	Effect of Suppressor Element Number and Inner Flow on Nozzle Gross Thrust Coefficients of Shallow-Chute Nozzles.	476
4-18.	Effect of Suppressor Element Number and Free-Stream Mach Number on Nozzle Performance of Shallow-Chute Nozzles.	478
4-19.	Effect of Suppressor Element Number and Outer Flow on Nozzle Gross Thrust Coefficients of Shallow-Chute Nozzles.	479

LIST OF ILLUSTRATIONS (Continued)

Figure		Page
4-20.	Effect of Suppressor Area Ratio and Inner Flow on Nozzle Gross Thrust Coefficients of Deep-Chute Nozzles.	480
4-21.	Effect of Suppressor Area Ratio and Free-Stream Mach Number on Nozzle Performance of Deep-Chute Nozzles.	481
4-22.	Effect of Inner Radius Ratio and Free-Stream Mach Number or Nozzle Performance of Shallow-Chute Nozzles.	483
4-23.	Inner Radius Ratio Performance Trends, Deep-Chute Models.	484
4-24.	Inner Plug Axial Position Performance Trends, Shallow-Chute Models.	485
4-25.	Inner Plug Axial Location Performance Trends, Deep-Chute Models.	486
4-26.	Inner Plug Effects on Suppressor Base Pressures, $M_0 = 0.36$, $P_{T_i}/P_a = 2.5$.	487
4-27.	Comparis›n of Chute and Spoke Model Performance.	489
4-28.	Performance Trends with External Mach Number Shallow-Chute Models.	490
4-29.	Performance Trends with External Mach Number, Deep Chutes.	491
4-30.	104-Tube Nozzle Performance Trends.	492
4-31.	104-Tube Nozzle Base Drag Losses.	493
4-32.	Eight-Lobe Performance Chartacteristics.	494
A-1.	Model 1 - 4.64-in.-Diameter Conical Nozzle, Adapted to JENOTS. Model 14 - 4.64-in.-Diameter Conical Nozzle, Adapted to Cell 41, Anechoic.	502
A-2.	Model 2 - Convergent-Divergent Plug, Single Flow.	503
A-3.	Model 3 - Converging Plug, $R_r = 0.59$, Single Flow.	504
A-4.	Model 4 - Converging Plug, $R_r = 0.789$, Single Flow.	505
A-5.	Model 5 - Converging Plug, $R_r = 0.853$, Single Flow.	506

LIST OF ILLUSTRATIONS (Continued)

Figure		Page
A-6.	Model 6 - Dual-Flow Coannular Coplanar, A_o/A_i = 2.0. Model 9 - Coannular Coplanar, A_o/A_i = 2.0, Normal Fan Operation, Low Inner Flow.	507
A-7.	Model 7 - Dual-Flow Coannular Coplanar, A_o/A_i = 0.65. Models 10 and 11 Coannular Coplanar, A_o/A_i = 0.65, Normal Fan Operation, Low Inner Flow and No Inner Flow, Respectively.	508
A-8.	Model 8 - Dual-Flow Coannular Coplanar, A_o/A_i = 0.4. Models 12 and 13 - Coannular Coplanar, A_o/A_i = 0.4, Normal Fan Operation, Low Inner Flow and No Inner Flow, Respectively.	509
A-9.	Model 15 - 36 Chute, AR = 2.5, R_r = 0.653 Turbojet.	510
A-10.	Model 16 - 36 Chute, AR = 2.0, R_r = 0.716 Turbojet.	511
A-11.	Model 17 - 36 Chute, AR = 1.5, R_r = 0.782 Turbojet	512
A-12.	Model 18 - 36 Spoke, AR = 2.0, R_r = 0.716 Turbojet.	513
A-13.	Model 19 - 36 Chute, AR = 2.0, R_r = 0.716 Turbojet with Acoustically Treated Secondary Ejector.	514
A-14.	Model 20 - 62 Tube/Plug, AR = 2.95 Turbojet.	515
A-15.	Model 21 - 32 Chute, AR = 210, R_r = 0.498 Turbojet.	516
A-16.	Model 22 - 36 Chute, AR = 2.5, R_r^o = 0.653 Outer Suppressor; A_o/A_i = 1.92, R_o^i = 0.779 Inner Plug, Retracted.	517
A-17.	Model 23 - 36 Chute, AR = 2.0, R_r^o = 0.716 Outer Suppressor; A_o/A_i = 1.92, R_o^i = 0.779 Inner Plug, In-Line.	518
A-18.	Model 24 - 36 Chute, AR = 2.0, R_r^o = 0.716 Outer Suppressor; A_o/A_i = 1.92, R_r^i = 0.779 Inner Plug, Retracted.	519
A-19.	Model 25 - 36 Chute, AR = 2.0, R_r^o = 0.716 Outer Suppressor; A_o/A_i = 3.61, R_r^i = 0.89 Inner Plug, In-Line.	520

LIST OF ILLUSTRATIONS (Continued)

Figure		Page
A-20.	Model 26 - 36 Chute, AR = 2.0, R_r^o = 0.716 Outer Suppressor; A_o/A_i = 3.61, R_r^i = 0.589 Inner Plug, Retracted.	521
A-21.	Model 27 - 36 Chute, AR = 1.5, R_r^o = 0.782 Outer Suppressor; A_o/A_i = 1.92, R_r^i = 0.779 Inner Plug, Retracted.	522
A-22.	Model 28 - 36 Spoke, AR = 2.0, R_r^o = 0.716 Outer Suppressor; A_o/A_i = 1.92, R_r^i = 0.779 Inner Plug, Retracted.	523
A-23.	Model 29 - 36 Spoke, AR = 2.0, R_r^o = 0.716 Outer Suppressor; A_o/A_i = 1.92, R_r^i = 0.779 Inner Plug, In-Line.	524
A-24.	Model 30 - 20 Shallow Chute, AR = 1.75, R_r^o = 0.717 Outer Suppressor; A_o/A_i = 1.92, R_r^i = 0.779 Inner Plug, Retracted.	525
A-25.	Model 31 - 30 Shallow Chute, AR = 1.75, R_r^o = 0.717 Outer Suppressor; A_o/A_i = 1.92, R_r^i = 0.779 Inner Plug, Retracted.	526
A-26.	Model 32 - 40 Shallow Chute, AR = 1.75, R_r^o = 0.717 Outer Suppressor; A_o/A_i = 1.92, R_r^i = 0.779 Inner Plug, Retracted.	527
A-27.	Model 33 - 36 Chute, AR = 2.5, R_r^o = 0.783 Outer Suppressor; A_o/A_i = 0.65, R_r^i = 0.674 Inner Plug, Retracted.	528
A-28.	Model 34 - 36 Chute, AR = 3.0, R_r^o = 0.783 Outer Suppressor; A_o/A_i = 0.65, R_r^i = 0.674 Inner Plug, Retracted.	529
A-29.	Model 35 - 36 Spoke, AR = 2.5, R_r^o = 0.783 Outer Suppressor; A_o/A_i = 0.65, R_r^i = 0.674 Inner Plug, Retracted.	530
A-30.	Model 36 - 36 Chute, AR = 2.0, R_r^o = 0.716 Outer Suppressor; A_o/A_i = 1.92, R_r^i = 0.779 Inner Plug, Retracted with Acoustically Treated Ejector.	531

LIST OF ILLUSTRATIONS (Continued)

Figure		Page
A-31.	Model 37 - Coannular-Noncoplanar Dual Plug Nozzle, R_r^o = 0.853, A_o/A_i = 1.59, R_r^i = 0.800 with Acoustically Treated Secondary Ejector.	532
A-32.	Model 38 - Coannular-Noncoplanar Dual Plug Nozzle, R_r^o = 0.926, A_o/A_i = 0.71, R_r^i = 0.800 with Acoustically Treated Secondary Ejector.	533
A-33.	Model 39 - Converging Plug, Single Flow, R_r = 0.789.	534
A-34.	Model 40 - Converging Plug, Single Flow, R_r = 0.85.	535
A-35.	Model 41 - 36 Chute, AR = 2.5, R_r = 0.78 Turbojet.	536
A-36.	Model 42 - 36 Chute, AR = 2.5, R_r^o = 0.78 Outer Suppressor with Induced Flow Through A_o/A_i = 0.65, R_r^i = 0.674 Inner Plug, Retracted.	537
A-37.	Model 43 - 36 Chute, AR = 2.5, R_r^o = 0.78 Outer Suppressor with Abrupt Step Over A_o/A_i = 0.65, R_r^i = 0.674 Inner Plug, Retracted.	538
A-38.	Model 44 - 104 Elliptical Tubes, AR = 2.8.	539
A-39.	Model 45 - 104 Elliptical Holes, AR = 2.8.	540
A-40.	Model 46 - 8-Lobe Daisy, AR = 2.1.	541
A-41.	Model 47 - 4.0-in.-Diameter Conical.	542
C-1.	JENOTS Data: SPL Spectra, FSDR Program Calculation.	587
C-2.	JENOTS Data: SPL Spectra, FSDR Program Calculation.	588
C-3.	Revised Atmospheric Correction Factors.	589
C-4.	Revised Atmospheric Absorption.	590
C-5.	Atmospheric Attenuation Factors.	591
C-6.	Total Absorption of Sound in Air as a Function of Frequency.	592
D-1.	Test Set-Up for Ellipsoidal Mirror Surveys.	598

LIST OF ILLUSTRATIONS (Continued)

Figure		Page
D-2.	18-inch-Diameter Shallow-Disk EM with 9-foot Working Distance.	599
D-3.	34.654-inch-Diameter Deep-Dish EM with 15-foot Working Distance.	600
D-4.	"Reverse Mounting" Microphone Fixture for Deep-Dish Ellipsoidal Mirror.	601
D-5.	Ellipsoidal Mirror Set-Up of JENOTS.	602
D-6.	Ellipsoidal Mirror Set-Up in the Anechoic Facility.	602
D-7.	Set-Up of Mirror and Noise Source for Calibration of 18-inch EM.	605
D-8.	Set-Up of Reference Microphone and Noise Source for Calibration of 18-inch EM.	606
D-9.	Gain of the 18-inch-Diameter Ellipsoidal Mirror.	607
D-10.	Normalized Window Function Width for the 18-inch-Diameter Ellipsoidal Mirror.	608
D-11.	Gain of the Deep-Dish Ellipsoidal Mirror.	609
D-12.	Normalized Window Function Width for the Deep-Dish Ellipsoidal Mirror.	610
D-13.	Equipment Schematic for EM Data Processing, General Electric Acoustic Vane.	612
D-14.	95% Confidence Interval Curves as a Function of Frequency and Integration Time.	613
D-15.	Typical Brush Chart from EM Data Reduction.	614
D-16.	Integral Closure Check for 3.56-inch Conical Nozzle, $V = 2253$ ft/sec, $V_{a/c} = 0$.	621
D-17.	Axial Distribution of Sound Source Intensity (16,000 Hz, 1/3 Octave Band).	622

LIST OF ILLUSTRATIONS (Continued)

Figure		Page
D-18.	Axial Distribution of Sound Source Intensity (6300 Hz, 1/3 Octave Band).	623
D-19.	Axial Distribution of Sound Source Intensity (2500 Hz, 1/3 Octave Band).	624
D-20.	Axial Distribution of Sound Source Intensity (1000 Hz, 1/3 Octave Band).	625
D-21.	Axial Location of Peak Sound Source Intensity.	627
D-22.	Source Spectrum at Station 18 (x/D = 5.9).	628
D-23.	Source Spectrum at Station 46 (x/D = 30.6).	629
D-24.	Resolution of the Deep-Dish Ellipsoidal Mirror (Point Source Measurement), 4000 Hz.	633
D-25.	Resolution of the Deep-Dish Ellipsoidal Mirror (Point Source Measurement).	634
E-1.	Assumed Measurement Geometry.	636
E-2.	95% Confidence Internal Curves as a Function of Data Record Number.	645
E-3.	Details of Test Cases Used in Numerical Analysis.	651
F-1.	Geometric Details of Configuration SC-1, N = 20, Baseline Plug.	661
F-2.	Geometric Details of Configuration SC-2, N = 30, Baseline Plug.	662
F-3.	Geometric Details of Configuration SC-3, Modified Baseline Plug.	663
F-4.	Geometric Details of Configuration SC-4, N = 30, Full Plug.	664
F-5.	Geometric Details of Configuration SC-5, N = 30, Forward Baseline Plug.	665

LIST OF ILLUSTRATIONS (Continued)

Figure		Page
F-6.	Geometric Details of Configuration SC-6, N = 40, Baseline Plug.	666
F-7.	Geometric Details of Configuration DC-1, AR = 1.5, Baseline Plug.	667
F-8.	Geometric Details of Configuration DC-2, AR = 1.5, Full Plug.	668
F-9.	Geometric Details of Configuration DC-3, AR = 2.0, Baseline Plug.	669
F-10.	Geometric Details of Configuration DC-4, AR = 2.0, Modified Baseline Plug.	670
F-11.	Geometric Details of Configuration DC-5, AR = 2.0, Full Plug.	671
F-12.	Geometric Details of Configuration DC-6, AR = 2.0, Forward Plug.	672
F-13.	Geometric Details of Configuration DC-7, AR = 2.5, Baseline Plug.	673
F-14.	Geometric Details of Configuration DC-8, AR = 2.5, Full Plug.	674
F-15.	Geometric Details of Configuration DC-3 (Spoke), N = 36, AR = 2.0, Baseline Plug.	675
F-16.	Supersonic Tunnel Association (STA) Boattail Static-Pressure Instrumentation.	677
F-17.	Annular Nozzle Outer Shroud Static Pressures.	678
F-18.	Outer Plug Static Pressures.	679
F-19.	Inner Plug Static Pressures.	680
F-20.	Suppressor Element Base Static Pressures.	681
F-21.	104-Tube Nozzle Instrumentation.	682
F-22.	Configuration SC-1 Performance.	684

Figure		Page
F-23.	Configuration SC-2 Performance.	685
F-24.	Configuration SC-3 Performance.	686
F-25.	Configuration SC-4 Performance.	687
F-26.	Configuration SC-5 Performance.	688
F-27.	Configuration SC-6 Performance.	689
F-28.	Configuration DC-1 Performance.	690
F-29.	Configuration DC-2 Performance.	691
F-30.	Configuration DC-3 Performance.	692
F-31.	Configuration DC-4 Performance.	693
F-32.	Configuration DC-5 Performance.	694
F-33.	Configuration DC-6 Performance.	695
F-34.	Configuration DC-7 Performance.	696
F-35.	Configuration DC-8 Performance.	697
F-36.	Configuration DC-3 (Spoke) Performance.	698

LIST OF TABLES

Table		Page
1-1.	Summary of Nozzle Static and Projected Flight Peak PNL Suppression Characteristics.	7
3-1.	Description of Test Models and Test Types.	15
3-2.	Test Model Comparisons Summary.	30
3-3.	Far-Field Acoustic Test Matrix Description, Models 22-32 and 36, Cell 41 Anechoic Facility.	44
3-4.	Laser Velocimeter Test Matrix, Aero Cycle Conditions.	47
3-5.	JENOTS Ground Reflections Corrections (ΔdB's to be Added to SPL's).	56
3-6.	Summary of Nozzle Static and Projected Flight Peak PNL Suppression Characteristics.	364
4-1.	Nozzle Configuration Description.	452
4-2.	Annular Nozzle Performance Summary.	475
B-1.	Model No. 1: 4.64-inch-Diameter Conical, Adapted to JENOTS.	544
B-2.	Model No. 2: Convergent-Divergent Plug, Single Flow.	546
B-3.	Model No. 3: Convergent Plug, R_r = 0.59, Single Flow.	547
B-4.	Model No. 4: Convergent Plug, R_r = 0.789, Single Flow.	548
B-5.	Model No. 5: Convergent Plug, R_r = 0.853, Single Flow.	549
B-6.	Model No. 6: Dual-Flow Coannular-Coplanar, A_o/A_i = 2.0.	550
B-7.	Model No. 7: Dual-Flow Coannular-Coplanar, A_o/A_i = 0.5.	552
B-8.	Model No. 8: Dual-Flow Coannular-Coplanar, A_o/A_i = 0.4.	553
B-9.	Model No. 9: Coannular-Coplanar, A_o/A_i = 2.0, Low Inner Flow.	553
B-10.	Model No. 10: Dual-Flow Coannular-Coplanar, A_o/A_i = 0.65, Low Inner Flow.	554
B-11.	Model No. 11: Coannular-Coplanar, A_o/A_i = 0.65, No Inner Flow.	555

LIST OF TABLES (Continued)

Table		Page
B-12.	Model No. 12: Coannular-Coplanar, A_o/A_i = 0.4, Low Inner Flow.	555
B-13.	Model No. 13: Coannular-Coplanar, A_o/A_i = 0.4, No Flow.	556
B-14.	Model No. 14: 4.64-inch-Diameter Conical, Adapted to Cell 41, Anechoic.	557
B-15.	Model No. 15: 36 Chute, AR = 2.5, R_r = 0.653, Turbojet.	558
B-16.	Model No. 16: 36 Chute, AR = 2.0, R_r = 0.716, Turbojet.	559
B-17.	Model No. 17: 36 Chute, AR = 1.5, R_r = 0.782, Turbojet.	559
B-18.	Model No. 18: 36 Spoke, AR = 2.0, R_r = 0.716, Turbojet.	560
B-19.	Model No. 19: 36 Chute, AR = 2.0, R_r = 0.716, Turbojet with Acoustically Treated Secondary Ejector.	560
B-20.	Model No. 20: 72 Tube/Plug, AR = 2.95, Turbojet.	561
B-21.	Model No. 21: 32 Chute, AR = 2.0, R_r = 0.498, Turbojet.	561
B-22.	Model No. 22: 36 Chute, AR_i = 2.5, R_r^o = 0.653 Outer Suppressor; A_o/A_i = 1.92, R_r^i = 0.779 Inner Plug, Retracted.	562
B-23.	Model No. 23: 36 Chute, AR_i = 2.0, R_r^o = 0.716 Outer Suppressor; A_o/A_i = 1.92, R_r^i = 0.779 Inner Plug, In-Line.	563
B-24.	Model No. 24: 36 Chute, AR_i = 2.0, R_r^o = 0.716 Outer Suppressor; A_o/A_i = 1.92, R_r^i = 0.779 Inner Plug, Retracted.	564
B-25.	Model No. 25: 36 Chute, AR_i = 2.0, R_r^o = 0.716 Outer Suppressor; A_o/A_i = 3.61, R_r^i = 0.89 Inner Plug, In-Line.	565
B-26.	Model No. 26: 36 Chute, AR_i = 2.0, R_r^o = 0.716 Outer Suppressor; A_o/A_i = 3.61, R_r^i = 0.89 Inner Plug, Retracted.	566
B-27.	Model No. 27: 36 Chute, AR_i = 1.5, R_r^o = 0.782 Outer Suppressor; A_o/A_i = 1.92, R_r^i = 0.779 Inner Plug, Retracted.	567
B-28.	Model No. 28: 36 Spoke, AR_i = 2.0, R_r^o = 0.716 Outer Suppressor; A_o/A_i = 1.92, R_r^i = 0.779 Inner Plug, Retracted.	568
B-29.	Model No. 29: 36 Spoke, AR_i = 2.0, R_r^o = 0.716 Outer Suppressor; A_o/A_i = 1.92, R_r^i = 0.779 Inner Plug, In-Line.	569

LIST OF TABLES (Continued)

Table		Page
B-30.	Model No. 30: 20 Shallow Chute, AR = 1.75, R_r^o = 0.717 Outer Suppressor; A_o/A_i = 1.92, R_r^i = 0.779 Inner Plug, Retracted.	570
B-31.	Model No. 31: 30 Shallow Chute, AR = 1.75, R_r^o = 0.717 Outer Suppressor; A_o/A_i = 1.92, R_r^i = 0.779 Inner Plug, Retracted.	571
B-32.	Model No. 32: 40 Shallow Chute, AR = 1.75, R_r^o = 0.717 Outer Suppressor; A_o/A_i = 1.92, R_r^i = 0.779 Inner Plug, Retracted.	572
B-33.	Model No. 33: 36 Chute, AR = 2.5, R_r^o = 0.783 Outer Suppressor; A_o/A_i = 0.65, R_r^i = 0.674 Inner Plug, Retracted.	573
B-34.	Model No. 34: 36 Chute, AR_i = 3.0, R_r^o = 0.783 Outer Suppressor; A_o/A_i = 0.65, R_r^i = 0.674 Inner Plug, Retracted.	574
B-35.	Model No. 35: 36 Spoke, AR_i = 2.5, R_r^o = 0.783 Outer Suppressor; A_o/A_i = 0.65; R_r^i = 0.647 Inner Plug, Retracted.	575
B-36.	Model No. 36: 36 Chute, AR_i = 2.0, R_r^o = 0.716 Outer Suppressor; A_o/A_i = 1.92; R_r^i = 0.779 Inner Plug, Retracted with Acoustically Treated Secondary Ejector.	576
B-37.	Model No. 37: Coannular-Noncoplanar Dual Plug Nozzle, R_r^o = 0.853, A_o/A_i = 1.59, R_r^i = 0.800 with Acoustically Treated Secondary Ejector.	577
B-38.	Model No. 38: Coannular-Noncoplanar Dual Plug Nozzle, R_r^o = 0.926, A_o/A_i = 0.71, R_r^i = 0.800 with Acoustically Treated Secondary Ejector.	577
B-39.	Model No. 39: Converging Plug, Single-Flow, R_r = 0.789.	578
B-40.	Model No. 40: Converging Plug, Single-Flow, R_r = 0.85.	579
B-41.	Model No. 41: 36 Chute, AR = 2.5, R_r = 0.78 Turbojet.	580
B-42.	Model No. 42: 36 Chute, AR = 2.5, R_r^o = 0.78 Outer Suppressor with Induced Flow Through A_o/A_i = 0.65, R_r^i = 0.674 Inner Plug, Retracted.	581
B-43.	Model No. 43: 36 Chute, AR = 2.5, R_r^o = 0.78 Outer Suppressor with Abrupt Step Over A_o/A_i = 0.65, R_r^i = 0.674 Inner Plug, Retracted.	582
B-44.	Model No. 44: 104 Elliptical Tube, AR = 2.8.	583

LIST OF TABLES (Concluded)

Table		Page
B-45.	Model No. 45: 104 Elliptical Hole, AR = 2.8.	584
B-46.	Model No. 47: 4.0-inch-Diameter Conical.	585
C-1.	Listing of the GE Air-Attenuation Correction Computer Program.	593
E-1.	Sum and Sum of Squares of Row Elements of Typical A^{-1} EM Matrices.	646
E-2.	Theoretical Statistical Errors for a Single Point Source at Center of Measurement Set - 18-inch Elliptical Mirror.	653

1.0 SUMMARY

The High Velocity Jet Noise Source Location and Reduction Program (Contract DOT-OS-30034) was conceived to bring analytical and experimental knowledge to bear on understanding the fundamentals of jet noise for simple and complex suppressors.

Task 3, the subject of this report, involved the experimental investigation of suppression principles, including developing an experimental data base, developing a better understanding of jet noise suppression principles, and formulating empirical methods for the acoustic design of jet noise suppressors. Acoustic scaling has been experimentally demonstrated, and five "optimum" nozzles were selected for anechoic, free-jet testing in Task 5.

Volume I - Verification of Suppression Principles and Development of Suppression Prediction Methods - Some of the experimental studies (reported in Volume II) involved acquisition of detailed, far-field, acoustic data and of aerodynamic jet-flow-field data on several baseline and noise-abatement nozzles. These data were analyzed and used to validate the theoretical jet noise prediction method of Task 2 (referred to as M*G*B, designating the authors' initials) and to develop and validate the empirical noise-prediction method presented herein (referred to as M*S, designating the last name initials of the authors).*

The Task 2 theoretical studies conclude that four primary mechanisms influence jet noise suppression: fluid shielding, convective amplification, turbulent mixing, and shock noise. A series of seven suppressor configurations (ranging from geometrically simple to complex) were evaluated in Task 3 to establish the relative importance of each of the four mechanisms. Typical results of this evaluation of noise mechanisms are summarized in Figure 1-1 in terms of perceived noise level (PNL) directivity for a conical nozzle. In general, mechanical suppressors exhibit a significant reduction in shock noise relative to a baseline conical nozzle, reduce the effectiveness of fluid shielding (increase rather than suppress noise), reduce the effectiveness of convective amplification (reduce noise), and produce a modest reduction in turbulent mixing noise. The largest amount of shock noise reduction correlates with the suppressor which has the smallest characteristic dimension. Fluid shielding decreases because suppressors cause the mean velocity and temperature of the jet plume to decay faster than the conical baseline. A reduction in convection Mach number (and hence in convective amplification) occurs because a suppressor plume decays very rapidly. Turbulent mixing noise is reduced through alteration of the mixing process that results from segmenting the exhaust jet.

*The Task 3 empirical (M*S) method was initially intended for nozzle geometries which could not be modeled in the purely analytical Task 2 (M*G*B) method (a multielement nozzle with a treated ejector, for example).

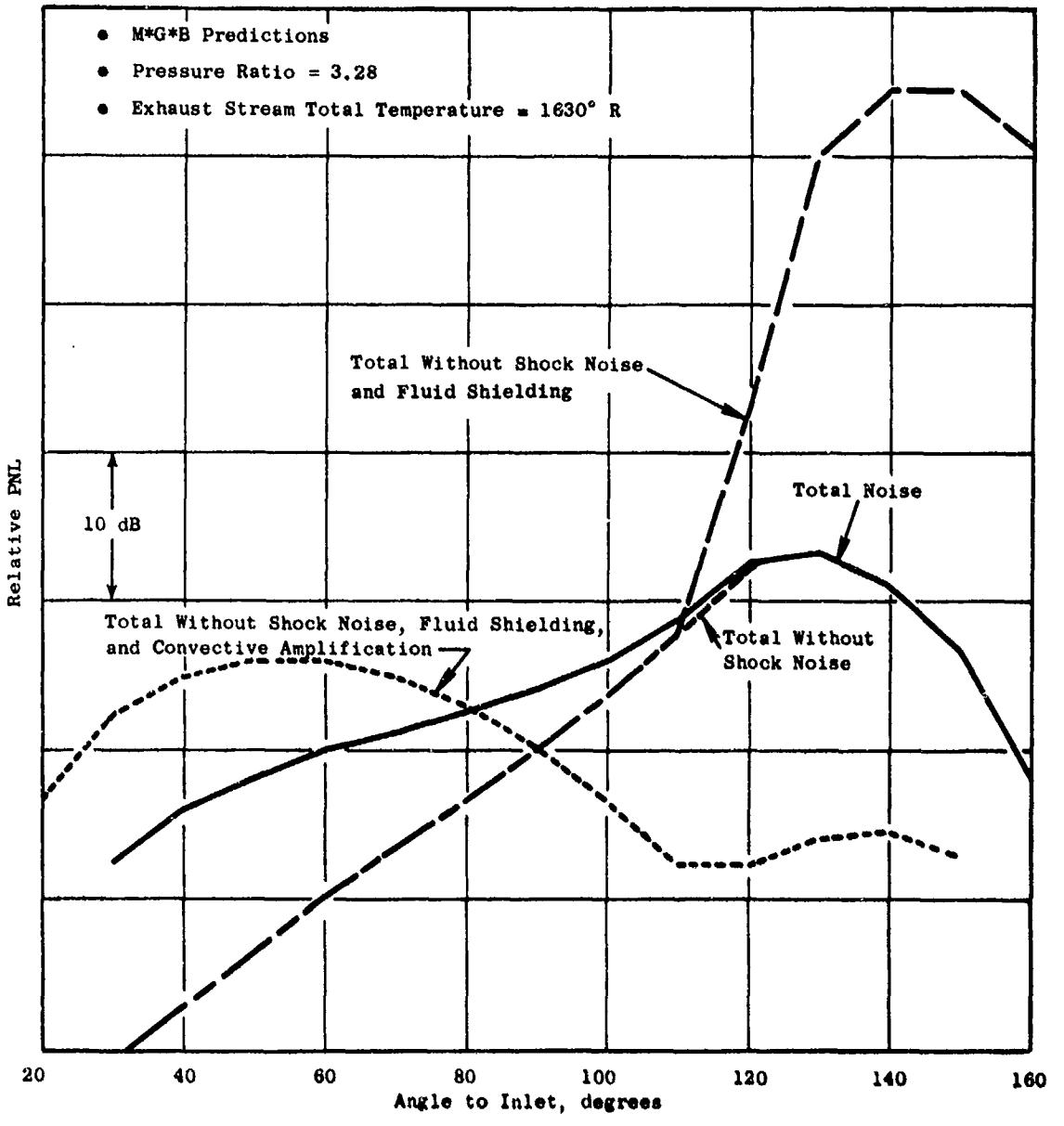

Figure 1-1. Evaluation of Noise Mechanisms for a Conical Nozzle.

Aerodynamic flow-field measurements (mean-velocity profiles) were demonstrated to be useful in verifying the flow-field predictions which were calculated by the M*G*B (theoretical) noise-prediction program. Noise source location devices such as the Ellipsoidal Mirror (EM) were demonstrated to be less useful than the Laser Velocimeter (LV) for the M*G*B theory verification studies because the LV provides data which may be directly compared with predictions made using the M*G*B program. Axial and radial mean-velocity profiles are typical examples of such comparisons.

The empirical M*S jet noise prediction method has been developed to predict the static acoustic characteristics of multielement suppressors applicable to both advanced turbojets and variable-cycle engines (which are representative of power plants for future supersonic cruise aircraft). The effect of external flow on the M*S jet noise prediction is discussed in the Task 6 Design Guide Report. Inputs required to use the M*S computational procedure include: element type, element number, suppressor area ratio and radius ratio, chute-spoke planform and cant angle plus pulg contour. The prediction accuracy is estimated to be ± 3.3 Effective Perceived Noise Decibels (EPNdB) at a 95% confidence level. Figure 1-2 illustrates the correlation between measured and predicted EPNLs for all types of suppressors.

The merits of both the M*S and M*G*B computational techniques can be stated as follows. The empirical (M*S) jet noise prediction method, based on correlations of scale-model jet data, serves as a useful preliminary design and prediction tool for selecting the basic nozzle type (chute, spoke, multitube, etc.) and primary geometric parameters (element number, area ratio, etc.) for a given application. It is also useful in evaluating the acoustic performance of a given suppressor nozzle, provided the nozzle is one of the types from which the correlation was derived. Further, the method is useful for doing parametric studies since the computation procedure is relatively simple and economical of both computer time and cost. The theoretical (M*G*B) prediction method, on the other hand, is more suited to detailed design and analysis of a suppressor nozzle. It can supply detailed information on the jet plume flow development as well as the far-field acoustic characteristics. It is also capable of evaluating changes in nozzle planform shape, element placement and spacing, etc. In addition, the theoretical prediction model is a useful diagnostic tool, capable of assessing the relative roles the various mechanisms play in the noise suppression process, and can also serve as a source location analysis tool.

Volume II - Parametric Testing and Source Measurements - A parametric experimental series was conducted to provide far-field acoustic data on 47 baseline and suppressor nozzle configurations and to provide aerodynamic nozzle performance on 18 of the configurations. The data presented in this volume were taken for use in the current program as well as to provide an extensive, high-quality, data base for future studies. The impact of varying the area ratio and velocity ratio of dual-flow, baseline nozzle configurations was investigated, and the importance of shock noise was assessed. The impact of varying area ratio and element number was parametrically studied for both single and dual-flow suppressors; core plug geometry, velocity ratio, and

- Flyover calculation using static data corrected to free-field conditions.
- The "Reference" level is the predicted value of noise for each nozzle, at a specified set of thermodynamic conditions, plus an arbitrary value of 100 dB.

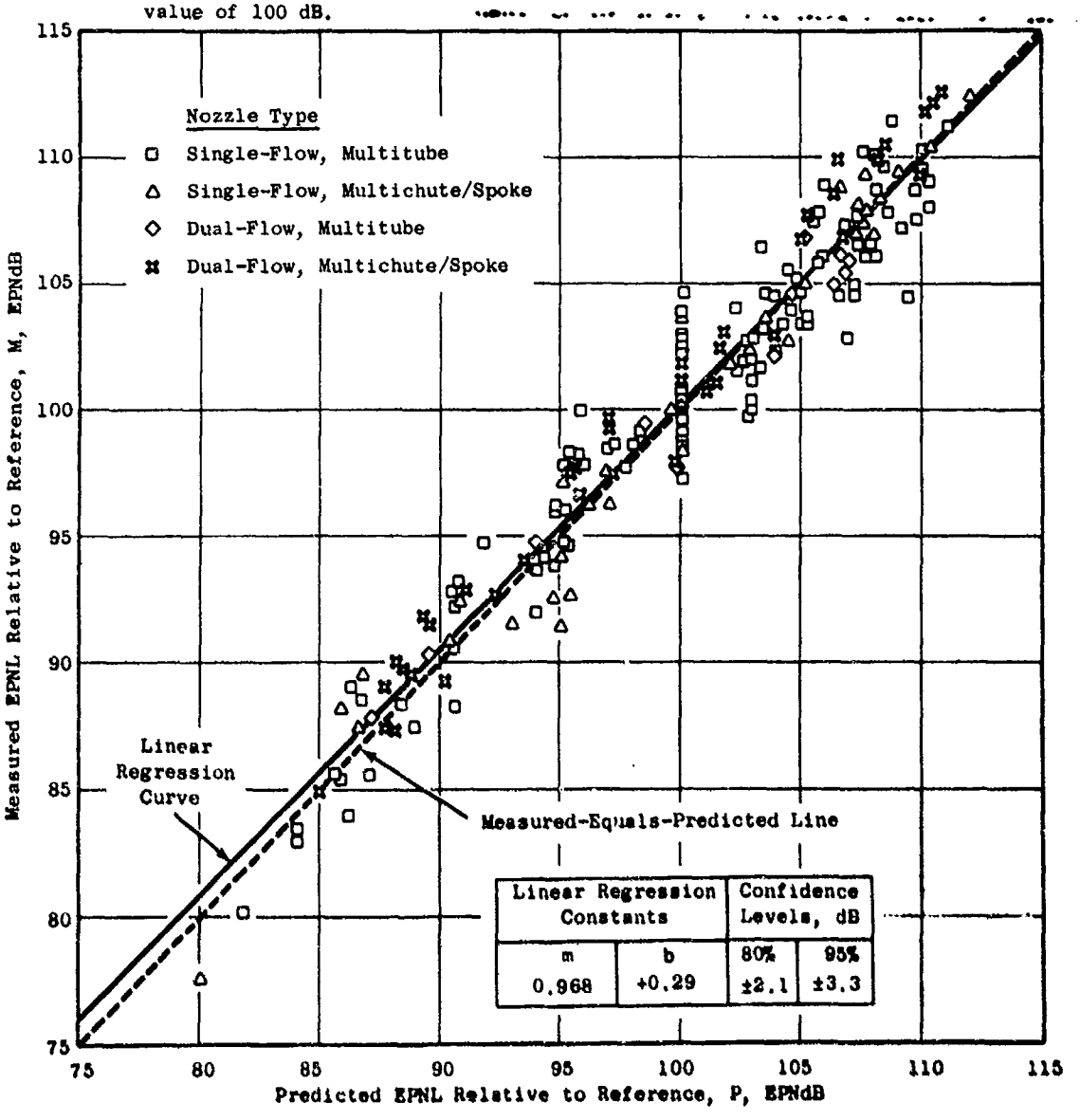

Figure 1-2. Correlation Between Measured and Predicted Effective Perceived Noise Level, EPNL, for all Types of Suppressor Nozzles.

weight flow ratio were evaluated for dual-flow suppressors. These studies establish absolute static suppression levels on the basis of normalized maximum PNL, for several families of suppressor nozzles, as illustrated in Figure 1-3.

Parametric testing identified the following primary trends for single-flow and for dual-flow suppressors during static operation:

Single Flow

- Suppression increases with increasing area ratio at high jet velocity.
- Suppression decreases with increasing area ratio at low jet velocity.
- Suppression level is affected by element type (spoke systems suppress slightly better than chutes).

Dual Flow

- Suppression increases with increasing area ratio.
- Suppression increases with increasing element number at high jet velocity.
- Suppression level is affected by core plug geometry [by 2 to 3 decibels (dB)].
- Suppression increases 3 to 4 dB when a treated ejector is added to a suppressor configuration.

Selective, free-jet tests conducted on eight configurations indicate that suppression generally decreases in flight. Typical static versus free-jet results are shown in Table 1-1.

The aerodynamic performance test data recorded on 18 of the configurations at both static and wind-on conditions is also included in this volume. Base pressure measurements were taken on several of the models in order to determine base drag (which is thought to be responsible for the poor aerodynamic performance of most mechanical suppressors in flight). These wind tunnel tests identified the following primary trends in aerodynamic performance:

- Performance decreases with increasing element number.
- Performance increases with increasing chute depth.
- Performance increases with increasing ratio of inner flow area to outer flow area.

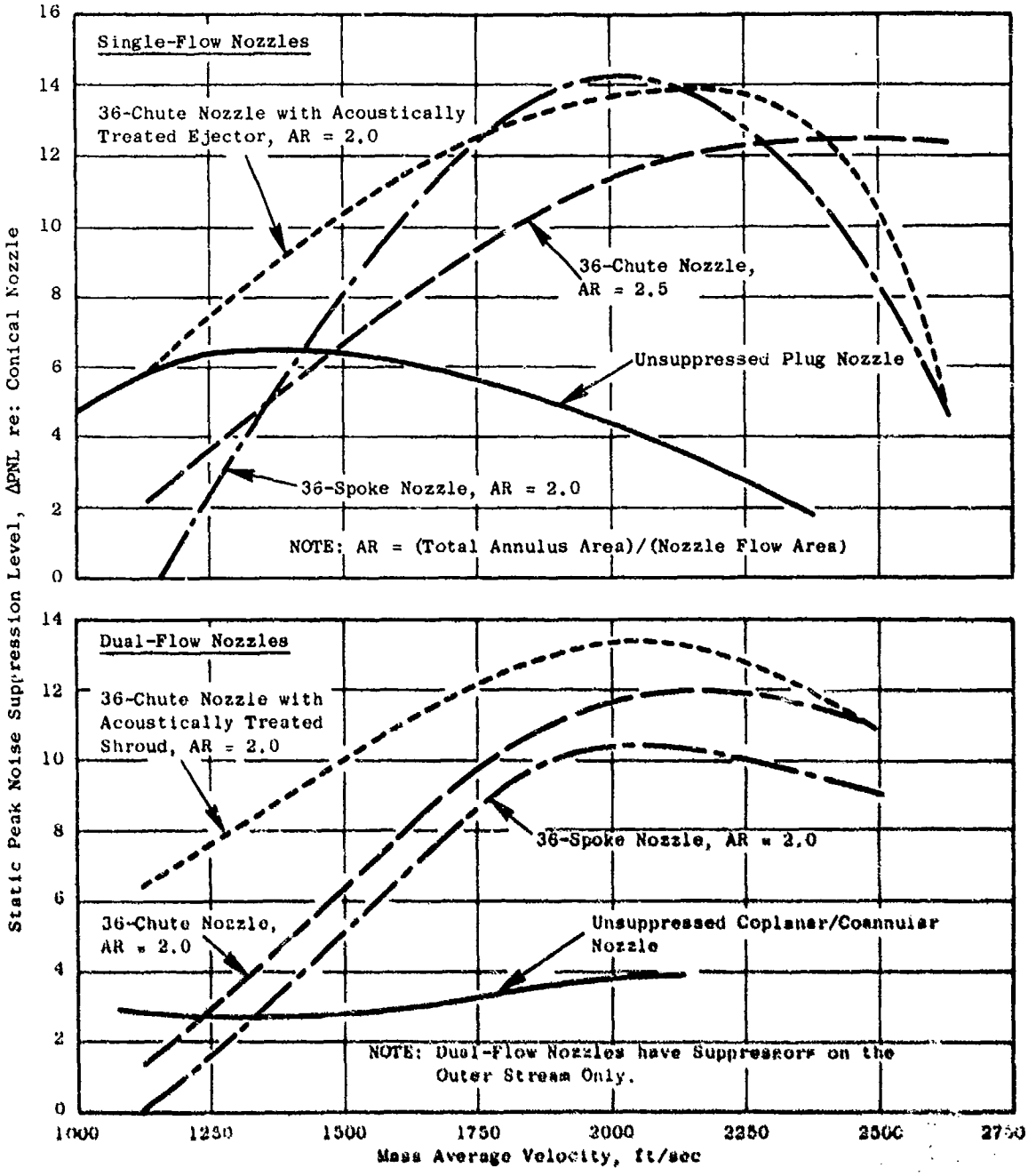

Figure 1-3. Typical Peak Static Noise Suppression Characteristics.

- Performance is affected by element type (chutes perform better than spokes because spokes have higher base drag).

The base pressure correlations provide a procedure for predicting suppressor nozzle aerodynamic performance.

Table 1-1. Typical Summary of Nozzle Static and Projected Flight Peak PNL Suppression Characteristics.

- Suppression Levels are Relative to a Conical Nozzle at Equivalent Flight Conditions
- V_j = 2500 ft/sec

Configuration	Suppression Level, db	
	Static	Flight
Plug Nozzle - 0.789 Radius Ratio	1.3	3.0
Plug Nozzle - 0.85 Radius Ratio	2.3	3.7
8-Lobe Nozzle	5.6	5.6
AR = 2.5 36-Chute Nozzle	13.5	10.9
AR = 2.5 36-Chute Nozzle with Auxiliary Flow	12.5	9.4
104-Tube Nozzle	12.0	12.0

Volume III - Suppressor Concepts Optimization - Several studies were conducted to attempt an optimization of suppressor concepts. The end product of this overall effort was to design five nozzles for static and free-jet testing in Task 5. Trade studies of performance versus suppression, aircraft integration studies, and development of a figure of merit method of analysis all make up the activities in this "optimization" process.

Trade studies of suppression versus aerodynamic performance indicate that a properly selected and designed mechanical suppressor can attain a delta suppression to delta thrust coefficient ratio ($\Delta PNL/\Delta C_{F_g}$) of almost 3.0 (based on static suppression and wind-on aerodynamic performance).

The aircraft integration study consisted of ranking nine baseline and suppressor nozzles with respect to performance level, suppression level, weight, impact on aircraft mission range, and noise footprint. In general, suppression level was found to be the most important design variable, with performance and weight ranking second and third, respectively.

The appropriate figure of merit, considering all the design variables, was found to be aircraft range. However, use of range as the figure of merit requires that the aircraft mission be specified, and several techniques for cursorily ranking the suppressors based solely on suppression level, performance, and weight may also be identified. A summary of the range versus noise

characteristics of typical nozzle configurations is presented in Figure 1-4. Once a noise goal is specified, adding a suppressor provides a significant range improvement over an unsuppressed system because adding a suppressor is less costly than reducing noise by enlarging the engine to reduce jet velocity.

The design of the five optimum nozzles was based on data from previous studies, performed by government and industry, on the M*G*B and M*S models discussed above and on the parametric data obtained in the acoustic and aerodynamic performance test series reported in Volume II. The configurations were designed and fabricated for open-throat, anechoic, free-jet testing in Task 5. The configurations chosen for evaluation were: (1) a 32-chute, single-flow nozzle; (2) a 40-shallow-chute, dual-flow nozzle; (3 and 4) a 36-chute, dual-flow nozzle, with and without a treated ejector; and (5) a 54-element, co-planar-mixer, plug nozzle.

Demonstration of acoustic scaling for several suppressor configurations was conducted to assure the adequacy of using scale-model results to project full-scale suppression levels. Full-scale data were obtained on several suppressor configurations using J79 and J85 engines. The suppressors evaluated were: (1) a baseline conical nozzle, (2) a 32-chute nozzle with and without a treated ejector, (3) an 8-lobe nozzle, and (4) a 104-tube nozzle. Scale-model data were obtained for these same configurations to allow comparison of scale-model and full-scale results. In general, peak full-scale suppression levels projected from scale-model data were verified by the full-scale engine results. Directivity patterns were duplicated within ±2 PNdB (the largest differences occurring with the conical nozzle configuration). Some spectral anomalies were observed for select cases; however, they were not of sufficient magnitude to invalidate the scale-model results. The conclusion resulting from this study is that full-scale noise levels can be predicted from scale-model test results using Strouhal scaling laws.

Volume IV - Laser Velocimeter Time Dependent Cross Correlation Measurements - In-jet/in-jet and in-jet/far-field exhaust noise diagnostic measurements conducted using a Laser Velocimeter (LV) are reported in this volume. Measurements were performed on a conical nozzle and a coannular plug nozzle. Two-point, space/time measurement using a two-LV system were completed for the conical nozzle. Measurements of mean velocity, turbulent velocity, eddy convection speed, and turbulent length scale were made for a subsonic ambient jet and for a sonic heated jet. For the coannular plug nozzle, a similar series of two-point, laser-correlation measurements were performed. In addition, cross correlations between the laser axial component of turbulence and a far-field acoustic microphone were performed.

Volumes I, II, III, and IV contain the results of a comprehensive effort to identify and integrate the theoretical studies, parametric test data, acoustic and performance diagnostic measurements, and system studies. A logical procedure has evolved for conducting suppressor design trade-offs.

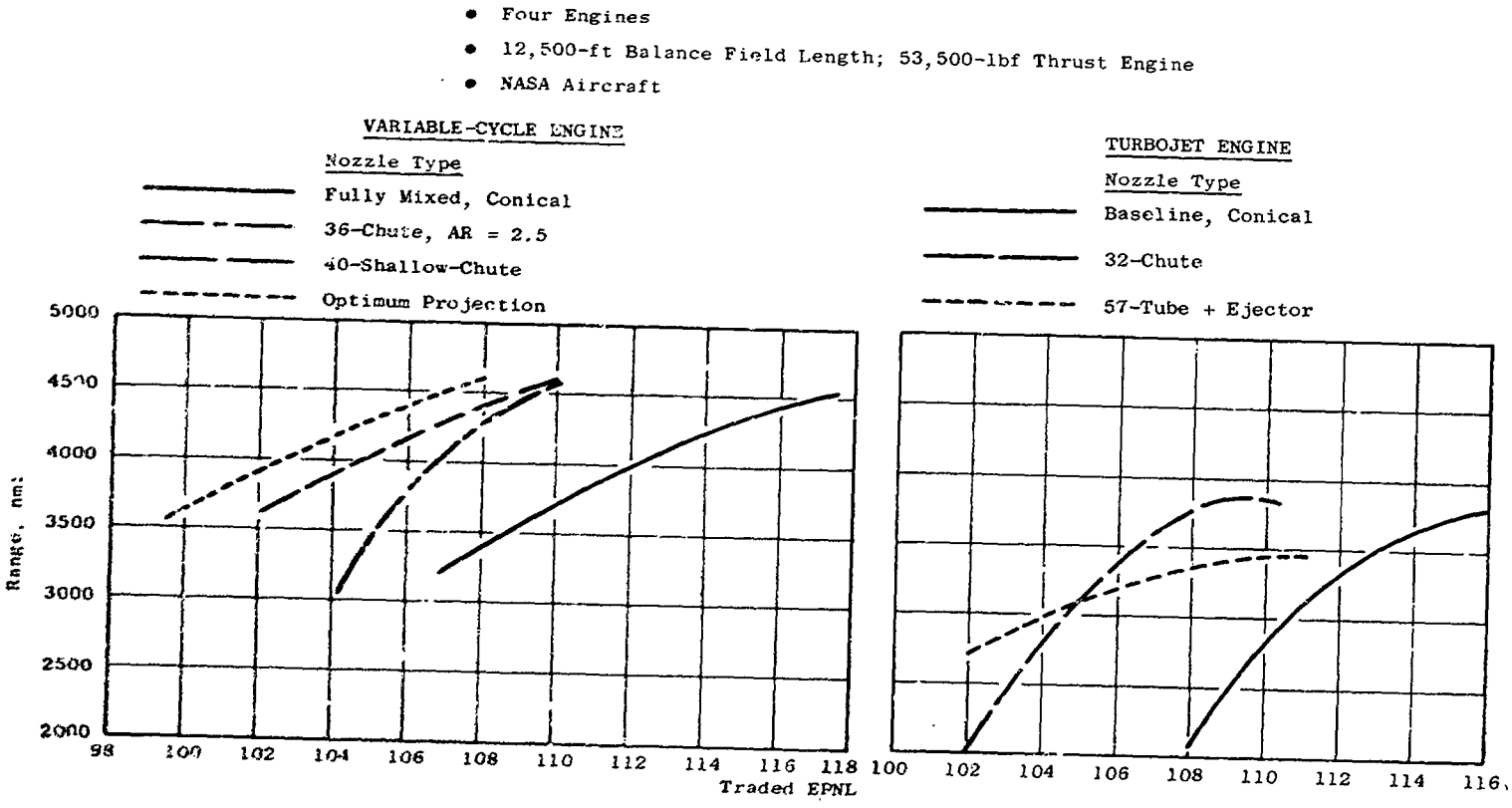

Figure 1-4. Summary of Range and Noise Characteristics for Several Baseline and Suppression Levels.

2.0 INTRODUCTION

The first 20 years of commercial aircraft operation with jet propulsion have clearly demonstrated the need for effective high velocity jet noise suppression technology in order to meet community acceptance. Aircraft system studies show that an efficient jet noise suppression device is required if a commercial supersonic aircraft is to be economically viable as well as environmentally acceptable. The current state of the art of high velocity jet noise suppression would make a supersonic transport (SST), with advanced technology engines, meet 1969 noise rules (at best). This state of the art is represented by the material in References 1 through 6.

Reference 1 describes analytical and experimental investigations which were conducted in the early 1960's. This study established a basis for development of mathematical and empirical methods for the predictions of jet-flow-field, aerodynamic characteristics and for determining the directional characteristics of jet noise suppressors. This work was limited in the sense that the suppressors evaluated had only modest suppression potential, and the measurement techniques available did not allow the acquisition of high-frequency, spectral data necessary to establish full-scale, PNL suppression levels.

The development of commercial SST vehicles by the U.S. and by the British-French multinational corporation in the 1960's placed extreme emphasis on the need for effective and efficient noise suppression devices. Phase I of work, conducted by the Boeing and General Electric companies, is summarized in References 2 and 3. Primary emphasis was on jet noise suppressor development through model and engine testing applicable to an afterburning turbojet engine. Suppressor designs were based primarily on empirical methods. Phase II of this effort, References 4 and 5, continued the suppressor development with a stronger emphasis placed on the integration of analytical studies and experimental test data. Specifically, the Boeing Company concentrated on optimization of tube-type suppressor systems and related semiempirical prediction methods. General Electric focused on the development both of chute and of tube-type suppressor systems with primary emphasis placed on optimization of chute-type suppressor nozzles.

Similar studies were conducted by the British and French in development of the Concorde, and typical results are summarized in Reference 6.

The design technology represented in References 1 through 6 is primarily semiempirical. The absence of general design rules based on engineering principles led to the government's formulation of the High Velocity Jet Noise Program, Contract DOT-OS-30034, in 1973. The purpose has been to achieve fundamental understanding, on a quantitative basis, of the mechanisms of jet noise generation and suppression and to develop design methods.

This report presents the results of Task 3 of the contract. It provides the experimental data base which was used in conjunction with the supporting

theories from Task 2 to develop a better understanding of jet noise and jet noise suppression.

The report is organized into four volumes (FAA-RD-76-79, III - I, II, III, IV) and is presented in a format consistent with the Task 3 work plan division of subtasks. Volume I is entitled "Verification of Suppression Principles and Development of Suppression Prediction Methods." Volume II, under this cover, is a data report entitled "Parametric Testing and Source Measurements," and Volume III is an analysis report entitled "Suppressor Concepts Optimization." Volume IV is an analysis report entitled "Laser Velocimeter Time Dependent Cross Correlation Measurement."

Volume I uses the data base (Volume II) and the Task 2 theoretical model (Reference 7) to postulate the suppression mechanisms. Volume I also presents an independent, empirical, static-jet-noise-prediction method which was developed from engineering correlations of the test data. Volume II presents the data and results of the parametric acoustic tests, the aerodynamic performance tests, and the Laser Velocimeter tests. Volume III presents the results of a trade study of performance versus suppression, an aircraft integration study, a "figure of merit" methodology, and a summary of the five "optimum" nozzles selected for testing in Task 5. An acoustic-scaling investigation was conducted to support the suppressor concepts optimization activities and is presented as an Appendix to Volume III. Volume IV presents the results of the in-jet/in-jet and in-jet/far-field cross correlation investigations.

The work reported in the present volume represents the experimental data base obtained to accomplish the general objectives of Volume I, "Verification of Suppression Principles and Development of Suppression Prediction Methods." Far-field acoustic data and select flow field, source characteristics, and aerodynamic performance data were obtained for a series of baseline nozzles and for several families of noise-abatement nozzles. Section 3.0 presents the Acoustic Test Program, and Section 4.0 presents the Aerodynamic Performance Test Program.

Schematics and pertinent dimensions for each of the nozzles evaluated for noise level are summarized in Appendix A. Appendix B contains a summary of the acoustic data and corresponding thermodynamic conditions. The air-attenuation model used for correcting acoustic data to standard-day conditions is summarized in Appendix C. Appendices D and E summarize the development of the ellipsoidal mirror and the results of an error-analysis study. Appendix F contains schematics of the models tested for aerodynamic performance and a detailed summary of the test data.

3.0 PARAMETERIC ACOUSTIC TESTING AND SOURCE MEASUREMENTS

This study consists of the selection, design, and procurement of test nozzles plus test and measurement efforts. Primarily, it provided the following data for analysis and evaluation during the Verification of Suppression Principles and Development of Suppression Prediction Methods studies presented in Volume I and the Suppressor Concepts Optimization studies presented in Volume III.

A. Detailed acoustic data were obtained on seven generic nozzles for data/theory comparison and verification of suppression principles and the initial development of the suppression prediction methods. These nozzles represented baselines and several families of noise-abatement suppressors. They started with simple, unsuppressed single-flow nozzles (conical and annular with plug), progressed in complexity to an unsuppressed coannular-coplanar dual-flow nozzle and culminated in four suppressor nozzle families of complex geometry, i.e., lobed, multitube, multichute, and high radius-ratio annular nozzle with multichute suppressor and plug. Measurements of both flow-field details and limited noise-source characteristics were obtained in addition to the far-field acoustic measurements.

B. Detailed static far-field acoustic data and select flow-field and source-characteristic data were obtained on an additional 32 models (models within A above, not included). Primary purpose was to amass the parametric design data required to experimentally establish the effect of varying geometric parameters for several groups of baseline and noise-abatement nozzles. The nozzles and parametric geometry variations were selected to adequately develop data applicable to (1) advanced suppression concepts appropriate for a future dual-flow variable cycle engine (VCE), and (2) the more conventional multielement suppressor concepts in conjunction with turbojet cycle applications. The data bank was used also in developing, checking, and improving the suppression prediction/correlation method described in Volume I.

C. Far-field acoustic data plus select flow-field and source characteristic data were obtained (where appropriate) on eight baseline and suppressor configurations within a static and simulated flight environment, free-jet, for the following purposes:

   1. To provide flight effect data to guide the designs of the five "optimum suppressors" described in Volume III.

   2. To evaluate the impact of "flight" on shock noise generation.

D. Wind tunnel static and simulated flight aerodynamic performance data (see Section 4.0) were obtained on a select group of baseline and noise-abatement nozzles. A total of 18 configurations was evaluated, through a joint NASA/GE effort, in the Lewis Research Center's 6 x 8-foot wind tunnel. These aerodynamic performance data were also used to perform the aircraft integration studies and to guide the designs of the five optimum suppressors described in Volume III.

The following criteria were used to influence selection of the models for parametric testing.

A. Configurations were made representative of several types of engine exhaust systems, i.e., turbojet, turbofan, and variable cycle (VCE) high-speed aircraft engines.

B. Designs were selected to achieve varying levels of suppression, anticipating the need to develop trend relationships among suppression, thrust decrement, and overall system impact. Increasing levels of achievable suppression were anticipated in the following nozzle configuration progression: plugs, lobed, turbojet multichute, turbojet multitube, VCE multichute, duct burning turbofan (DBTF) multichute, and VCE/DBTF multichute/ejector.

C. Design parameters were varied to influence noise generation, and configurations were selected to shed light on critical points in suppression theory. Among the major design parameters were radius ratio, area ratio, degree of segmentation, element characteristic dimensions, plug geometry, base design, treated ejector application, and flow management (bypass ratio, velocity ratio, isothermal and isovelocity cycle management).

D. Models were developed and tests were structured to establish the following effects on noise generation: equivalence of chute-to-spoke and tube-to-hole elements, dual-flow influences, flight effects on suppression, and the importance of shock noise under flight conditions.

Fulfilling the general scope of this study, and meeting the design criteria and key elements listed above, required a total of 47 model configurations structured around the following list of nozzle families and design considerations:

- Conical (convergent) baseline nozzles
- Simplistic single-flow plug nozzle (convergent, convergent-divergent, and varying plug radius ratio)
- Unsuppressed dual-flow (coannular-coplanar) nozzles

- Unsuppressed annular jet nozzles (with ventilated and nonventilated base)
- Chute area ratio, segmentation (element number), and spoke-versus-chute studies for turbojet suppression
- Influence of flow management on chute suppressor and base design studies for VCE suppression
- Dual-flow chute suppressors for turbofan systems
- Acoustically treated ejector applications
- Simulated flight invescigations

3.1 DESCRIPTION OF TEST MODELS

Within this study, 47 test model configurations were evaluated, 34 with new test hardware and 13 with previously manufactured hardware from DOT/FAA Contracts DOT-FA72 WA-2894 and FA-SS-71-13 as well as from NASA-Lewis Contract NAS3-18008. (This does not include the models reported in Volume III, Suppressor Concepts Optimization). All model hardware was of high manufacturing quality, normally designed to be subjected to gas stream conditions up to, or in excess of, T_T = 1800° R and P_T/P_O = 4.0. Most configurations used Hastelloy X as base material and higher strength alloys for the suppressor elements. Particular attention was addressed to producing high-quality flowpath lines and to sealing against leakage, whether from stream-to-stream or from stream-to-ambient environment. Many of the configurations were designed using a modular building-block approach, with interchangeable parts, so that consistency of physical flowpath geometry was maintained and only geometric parameters under study were physically varied. Model hardware was of fixed-point (nonvariable) design. Duplication of typical engine flow lines was normally maintained for one to two equivalent flow diameters upstream of the exit plane before transitioning adaptive hardware. Abrupt changes in internal flow lines were avoided and engine obstructions such as turbine struts were not simulated.

Turbojet simulation models ranged in size from 3.8 to 6.9-inch equivalent flow diameter. Dual-flow outer nozzles ranged from 3.2 to 6.5-inch equivalent diameter and inner nozzles from 2.9 to 4.7 inch. Each was selected to allow efficient operation of the individual acoustic facility burners over a wide range of planned cycle conditions and to allow incorporation of multielement suppressors whose characteristic frequency range of interest falls within the 80-KHz measuring capability of facility equipment. This allowed accomplishment of proper scaling of acoustic spectra data to engine size.

Table 3-1 organizes the test models. Each configuration is identified with its proper model number, model title, flowpath line schematic and photograph. These numbers and titles will serve as consistent identification

Table 3-1. Description of Test Models and Test Types.

Model No.	Title	Flowpath Schematic	Model Photograph	Design Flow Areas $\frac{A_o, \text{ in.}^2}{A_1, \text{ in.}^2}$	Type of Test Performed (JFJ = JENOTS Free Jet, J = JENOTS, C = Cell 41)			Model Details Appendix A Figure Number
					Far-Field Acoustics	LV	EM	
1	4.64-in.-Diameter Conical Adapted to JENOTS		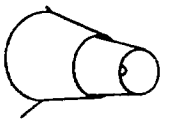	-- / 16.82	J	J	--	A-1
2	Convergent-Divergent Plug, Single Flow			-- / 37.40	J	J	J	A-2
3	Converging Plug, R_t = 0.59, Single Flow			-- / 33.63	J	--	--	A-3
4	Converging Plug, R_t = 0.789, Single Flow	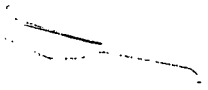		-- / 10.85	J	--	--	A-4

Table 3-1. Description of Test Models and Test Types (Continued).

Model No.	Title	Flowpath Schematic	Model Photograph	Design Flow Areas A_o, in.^{2} / A_i, in.^{2}	Type of Test Performed (JFJ = JENOTS Free Jet, J = JENOTS, C = Cell 41) Far-Field Acoustics	LV	EM	Model Details Appendix A Figure Number
5	Converging Plug, R_r = 0.853, Single Flow	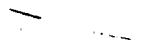		-- / 6.73	J	--	--	A-5
6	Dual-Flow Coannular Coplanar, A_o/A_i = 2.0	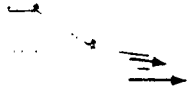		33.63 / 16.82	J	J	J	A-6
7	Dual-Flow Coannular Coplanar, A_o/A_i = 0.65			10.85 / 16.82	J*	J	--	A-7
8	Dual-Flow Coannular Coplanar, A_o/A_i = 0.4			6.73 / 16.82	J	--	J	A-8

* Data from NASA-Lewis DBTF Program Contract No. NAS3-18008 (Applies Only to Model No. 7)

Table 3-1. Description of Test Models and Test Types (Continued).

Model No.	Title	Flowpath Schematic	Model Photograph	Design Flow Areas $\frac{A_o, \text{ in.}^2}{A_i, \text{ in.}^2}$	Type of Test Performed (JFJ = JENOTS Free Jet, J = JENOTS, C = Cell 41)			Model Details Appendix A Figure Number
					Far-Field Acoustics	LV	EM	
9	Coannular Coplanar, A_o/A_i = 2.0, Low Inner Flow	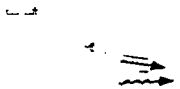		33.63 / 16.82	J	--	--	A-6
10	Coannular Coplanar, A_o/A_i = 0.65, Low Inner Flow		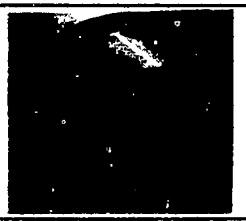	10.85 / 16.82	J	J	--	A-7
11	Coannular Coplanar, A_o/A_i = 0.65, No Inner Flow			10.85 / 16.82	J	J	--	A-7
12	Coannular Coplanar, A_o/A_i = 0.4, Low Inner Flow			6.73 / 16.82	J	--	J	A-8

Table 3-1. Description of Test Models and Test Types (Continued).

Model No.	Title	Flowpath Schematic	Model Photograph	Design Flow Areas $\frac{A_o, \text{ in.}^2}{A_i, \text{ in.}^2}$	Type of Test Performed (JFJ = JENOTS Free Jet, J = JENOTS, C = Cell 41)			Model Details Appendix A Figure Number
					Far-Field Acoustics	LV	EM	
13	Coannular Coplanar, A_o/A_i = 0.4, No Inner Flow			6.73 / 16.82	J	--	--	A-8
14	4.64-in.-Diameter Conical, Adapted to Cell 41, Anechoic		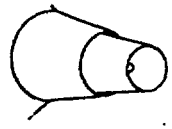	-- / 16.82	C	--	--	A-1
15	36 Chute, AR = 2.5, R_T = 0.653 Turbojet		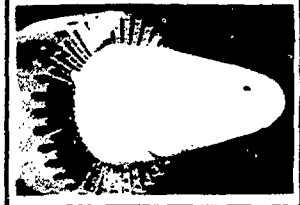	-- / 23.76	C	--	--	A-9
16	36 Chute, AR = 2.0, R_T = 0.716 Turbojet		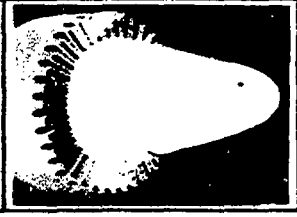	-- / 23.76	C	C	C	A-10

Table 3-1. Description of Test Models and Test Types (Continued).

Model No.	Title	Flowpath Schematic	Model Photograph	Design Flow Areas $\frac{A_o, \text{ in.}^2}{A_1, \text{ in.}^2}$	Type of Test Performed (JFJ = JENOTS Free Jet, J = JENOTS, C = Cell 41)			Model Details Appendix A Figure Number
					Far-Field Acoustics	LV	EM	
17	36 Chute, AR = 1.5, R_r = 0.782 Turbojet		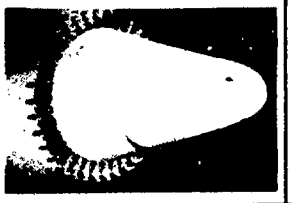	-- ----- 23.76	C	--	--	A-11
18	36 Spoke, AR = 2.0, R_r = 0.716 Turbojet		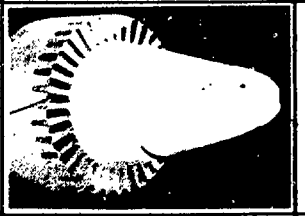	-- ----- 23.76	C	C	--	A-12
19	36 Chute, AR = 2.0, R_r = 0.716 Turbojet with Acoustically Treated Secondary Ejector		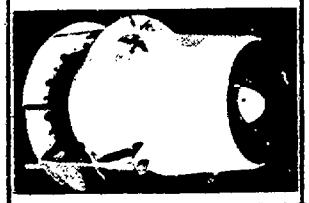	-- ----- 23.76	C	--	C	A-13
20	72 Tube/Plug, AR = 2.95 Turbojet	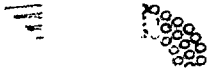	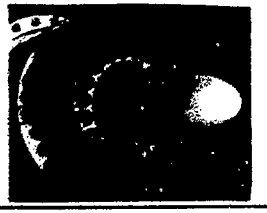	-- ----- 30.87	C	C	C	A-14

Table 3-1. Description of Test Models and Test Types (Continued).

Model No.	Title	Flowpath Schematic	Model Photograph	Design Flow Areas A_o, in.^{2} / A_i, in.^{2}	Type of Test Performed (JFJ = JENOTS Free Jet, J = JENOTS, C = Cell 41) Far-Field Acoustics	LV	EM	Model Details Appendix A Figure Number
21	32 Chute, AR = 2.0, A_r = 0.498 Turbojet	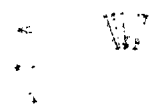	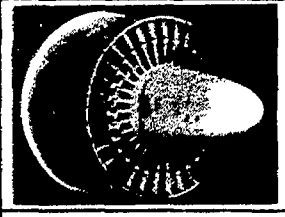	-- / 30.83	C	--	C	A-15
22	36 Chute, AR = 2.5, R_T^o = 0.653 Outer Suppressor; A_o/A_i = 1.92, R_T^i = 0.779 Inner Plug, Retracted	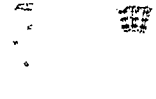	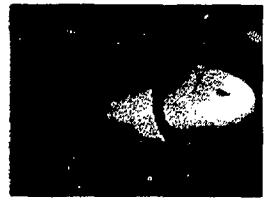	23.76 / 12.39	C	C	--	A-16
23	36 Chute, AR = 2.0, R_T^o = 0.716 Outer Suppressor; A_o/A_i = 1.92, R_T^i = 0.779 Inner Plug, In-Line	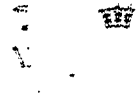		23.76 / 12.39	C	--	C	A-17
24	36 Chute, AR = 2.0, R_T^o = 0.716 Outer Suppressor; A_o/A_i = 1.92, R_T^i = 0.779 Inner Plug, Retracted		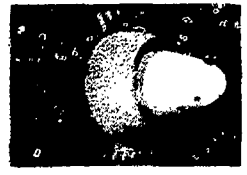	23.76 / 12.39	C	C	C	A-18

Table 3-1 Description of Test Models and Test Types (Continued).

Model No.	Title	Flowpath Schematic	Model Photograph	Design Flow Areas A_o, in.^{2} / A_i, in.^{2}	Type of Test Performed (JrJ = JENOTS Free Jet, J = JENOTS, C = Cell 41) Far-Field Acoustics	LV	EM	Model Details Appendix A Figure Number
25	36 Chute, AR = 2.0, R_f^o = 0.716 Outer Suppressor; A_o/A_i = 3.61, R_f^i = 0.89 Inner Plug, In-Line			23.76 / 6.58	C	--	C	A-19
26	36 Chute, AR = 2.0, R_f^o = 0.716 Outer Suppressor; A_o/A_i = 3.61, R_f^i = 0.89 Inner Plug, Retracted			23.76 / 6.58	C	--	--	A-20
27	36 Chute, AR = 1.5, R_f^o = 0.782 Outer Suppressor; A_o/A_i = 1.92, R_f^i = 0.779 Inner Plug, Retracted			23.76 / 12.39	C	C	--	A-21
28	36 Spoke, AR = 2.0, R_f^o = 0.716 Outer Suppressor; A_o/A_i = 1.92, R_f^i = 0.779 Inner Plug, Retracted			23.76 / 12.39	C	--	--	A-22

Table 3-1. Description of Test Models and Test Types (Continued).

Model No.	Title	Flowpath Schematic	Model Photograph	Design Flow Areas A_o, in.^{2} / A_i, in.^{2}	Type of Test Performed (JFJ = JENOTS Free Jet, J = JENOTS, C = Cell 41) Far-Field Acoustics	LV	EM	Model Details Appendix A Figure Number
29	36 Spoke, AR = 2.0, R_c^o = 0.716 Outer Suppressor; A_o/A_i = 1.92, R_c^i = 0.779 Inner Plug, In-Line			23.76 / 12.39	C	--	--	A-23
30	20 Shallow Chute, AR = 1.75, R_c^o = 0.717 Outer Suppressor; A_o/A_i = 1.92, R_c^i = 0.779 Inner Plug, Retracted			23.76 / 12.39	C	--	C	A-24
31	30 Shallow Chute, AR = 1.75, R_c^o = 0.717 Outer Suppressor; A_o/A_i = 1.92, R_c^i = 0.779 Inner Plug, Retracted			23.76 / 12.39	C	--	C	A-25
32	40 Shallow Chute, AR = 1.75, R_c^o = 0.717 Outer Suppressor; A_o/A_i = 1.92, R_c^i = 0.779 Inner Plug, Retracted			23.76 / 12.39	C	--	C	A-26

Table 3-1. Description of Test Models and Test Types (Continued).

Model No.	Title	Flowpath Schematic	Model Photograph	Design Flow Areas A_o, in.^{2} / A_i, in.^{2}	Type of Test Performed (JFJ = JENOTS Free Jet, J = JENOTS, C = Cell 41)			Model Details Appendix A Figure Number
					Far-Field Acoustics	LV	EM	
33	36 Chute, AR = 2.5, R_r^o = 0.783 Outer Suppressor; A_o/A_i = 0.65, R_r^i = 0.674 Inner Plug, Retracted	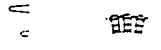	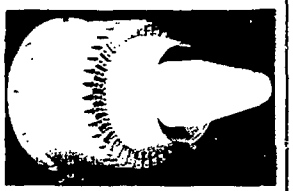	11.12 / 17.21	C	--	C	A-27
34	36 Chute, AR = 3.0, R_r^o = 0.783 Outer Suppressor; A_o/A_i = 0.65, R_r^i = 0.674 Inner Plug, Retracted		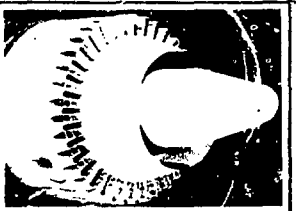	11.12 / 17.21	C	--	C	A-28
35	36 Spoke, AR = 2.5, R_r^o = 0.783 Outer Suppressor; A_o/A_i = 0.65, R_r^i = 0.674 Inner Plug, Retracted	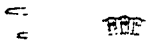	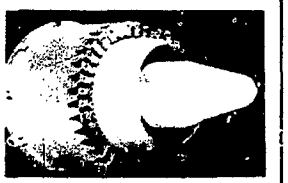	11.12 / 17.21	C	--	C	A-29
36	36 Chute, AR = 2.0, R_r^o = 0.715 Outer Suppressor; A_o/A_i = 1.92, R_r^i = 0.779 Inner Plug, Retracted with Acoustically Treated Secondary Ejector			23.76 / 12.39	C	C	C	A-30

Table 3-1. Description of Test Models and Test Types (Continued).

Model No.	Title	Flowpath Schematic	Model Photograph	Design Flow Areas A_o, in.^{2} / A_i, in.^{2}	Type of Test Performed (JFJ = JENOTS Free Jet, J = JENOTS, C = Cell 41) Far-Field Acoustics	LV	EM	Model Details Appendix A Figure Number
37	Coannular-Noncoplanar Dual Plug Nozzle, R_T^o = 0.853, A_o/A_i = 1.59, R_T^i = 0.800, with Acoustically Treated Secondary Ejector			18.05 / 11.35	C	--	--	A-31
38	Coannular-Noncoplanar Dual Plug Nozzle, R_T^o = 0.926, A_o/A_i = 0.71, R_T^i = 0.800, with Acoustically Treated Secondary Ejector	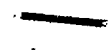		8.01 / 11.35	C	--	--	A-32
39	Converging Plug, Single Flow, R_r = 0.789			-- / 11.05	JFJ	JFJ	JFJ	A-33
40	Converging Plug, Single Flow, R_r = 0.85		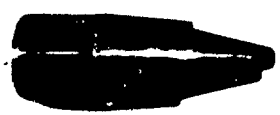	-- / 11.05	JFJ	JFJ	JFJ	A-34

Table 3-1. Description of Test Models and Test Types (Continued).

Model No.	Title	Flowpath Schematic	Model Photograph	Design Flow Areas $\frac{A_o, \text{ in.}^2}{A_1, \text{ in.}^2}$	Type of Test Performed (JFJ = JENOTS Free Jet, J = JENOTS, C = Cell 41)			Model Details Appendix A Figure Number
					Far-Field Acoustics	LV	EM	
41	36 Chute, AR = 2.5, R_T = 0.78 Turbojet		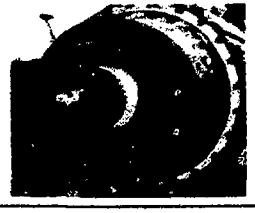	-- ----- 11.12	JFJ	JFJ	JFJ	A-35
42	36 Chute, AR = 2.5, R_T^o = 0.78 Outer Suppressor with Induced Flow Through A_o/A_1 = 0.65, R_T^i = 0.674 Inner Plug, Retracted	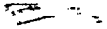		11.12 ----- 17.21	JFJ	JFJ	JFJ	A-36
43	36 Chute, AR = 2.5, R_T^o = 0.78 Outer Suppressor with Abrupt Step Over A_o/A_1 = 0.65, R_T^i = 0.674 Inner Plug, Retracted			11.12 ----- 17.21	JFJ	JFJ	JFJ	A-37
44	104 Tube, AR = 2.8			-- ----- 13.03	JFJ	JFJ	JFJ	A-38

Table 3-1. Description of Test Models and Test Types (Concluded).

Model No.	Title	Flowpath Schematic	Model Photograph	Design Flow Areas $\frac{A_o, \text{ in.}^2}{A_i, \text{ in.}^2}$	Type of Test Performed (JFJ = JENOTS Free Jet, J = JENOTS, C = Coil 41)			Model Details Appendix A Figure Number
					Far-Field Acoustics	LV	EM	
45	104 Hole, AR = 2.8	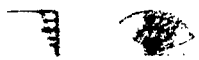	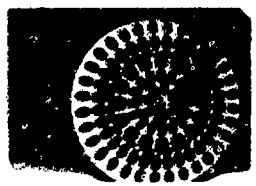	-- / 13.03	JFJ	JFJ	JFJ	A-39
46	8 Lobe, AR = 2.1	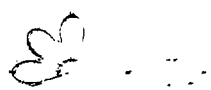		-- / 12.63	--	JFJ	--	A-40
47	4.0-in.-Diameter Conical			-- / 12.57	JFJ	--	JFJ	A-41

throughout the volume. Each configuration was subjected to far-field acoustic testing plus select laser velocimeter plume documentation and/or ellipsoidal mirror microphone source measurement on GE-Evendale facilities according to the following codes, as shown on the tables.

- J = JENOTS (Jet Engine Noise Outdoor Test Stand)
- JFJ = JENOTS Free Jet
- C = Cell 41 Anechoic Facility

Select configuration designs were also evaluated for aerodynamic performance in the joint GE/NASA-Lewis test program discussed in Section 4.0. Independent, but identical, aerodynamic hardware sets were manufactured in proper wind tunnel size.

Figure 3-1 defines geometric parameters associated with the overall model systems, the individual outer and inner streams, the multielement suppressors, and the ejectors.

The last column of Table 3-1 identifies Figures A-1 through A-41 of Appendix A which show in detail the physical dimensions of each model component. The individual models are categorized and discussed in the following paragraphs.

Models 1 through 13 in Table 3-1 were tested statically in the JENOTS facility, validated within this program's Task 1 (Reference 8). Model 1 is a 4.64-inch-diameter conical nozzle which established the baseline to which suppression levels were referenced.

Models 2 through 5 are single-flow plug nozzles. Model 2 has a convergent-divergent internal flowpath with an expansion area ratio of 1.22 Models 3, 4, and 5 establish a series of convergent plug nozzles for which radius ratio varies at values of 0.59, 0.789 and 0.853, respectively. The core plug is maintained consistent for the three models and the shroud is changed; therefore, a true plug radius ratio effect is established.

Models 6 through 13 are versions of coannular-coplanar geometries with variations in groups as follows:

A. Models 6, 7, and 8 maintain core geometry and vary fan shrouds to accomplish A_0/A_1 values of 2.0, 0.65, and 0.4, respectively. These were tested at typical dual-flow cycle conditions.

B. Models 9, 10, and 12 are similar in geometry to Models 6, 7, and 8; however, inner flow was regulated to rates of $\leq$10% of the outer flow.

C. Models 11 and 13 are similar in geometry to Model sets 7/10 and 8/12, respectively; however, core blank-off hardware was installed

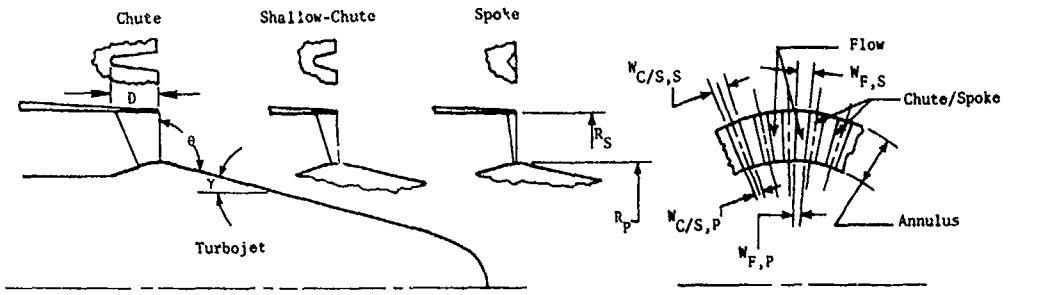

(a) Schematic of Turbojet and Suppressor

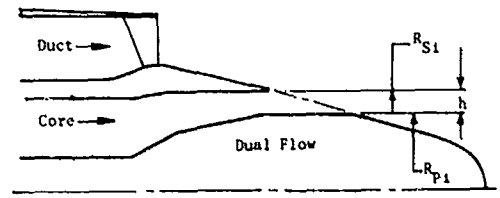

(b) Schematic, Dual-Flow, Core Plug In-Line

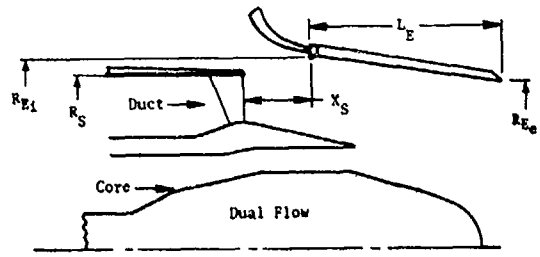

(c) Schematic, Dual-Flow, Core Plug Retracted with Ejector

System

- Turbojet; Single Flow
- Dual Flow; Turbofan (TF), Duct-Burning Turbofan (DBTF), Variable Cycle Engine (VCE)
  - Outer Stream/Duct/Fan Used Interchangeably
  - Inner Stream/Core Used Interchangeably
  - Area Ratio, A_o/A_i, Duct Area/Core Area
  - Bypass Ratio, W_o/W_i, Duct Weight Flow/Core Weight Flow
  - Velocity Ratio, V_o/V_i, Duct Ideal Velocity/Core Ideal Velocity

Duct Suppressor

- Chute - Good Ventilation Capability, Stowage within Plug Required
- Shallow Chute - Moderate Ventilation Capability - Stowage on Plug Surface
- Spoke - No Ventilation Capability - Stowage on Plug Surface
- Segmentation, N, Number of Elements
- Area Ratio, AR, Full Annular Area/Flow Area
- Radius Ratio, R_r^o, Plug Radius (R_P at Hub)/Shroud Radius (R_S at Tip)
- Chute or Spoke Width Ratio, $W_{C/S,S}/W_{C/S,P}$, Width at Shroud/Width at Plug
- Flow Width Radio, $W_{F,S}/W_{F,P}$, Width at Shroud/Width at Plug
- Depth to Width Ratio, $D/W_{C/S,S}$, Chute Depth/Chute Width at Shroud
- Plug Half Angle, γ
- Element Orientation Angle, θ

Core

- Radius Ratio, R_r^i, Plug Radius (R_{P_i})/Shroud Radius (R_{S_i})
- Annulus Height, h
- Plug Location: In-Line (Schematic b), Retracted (Schematic c)

Ejector (Single and Dual Flow)

- Ejector Inlet Radius, R_{E_i}
- Ejector Exit Radius, R_{E_e}
- Ejector Length, L_E
- Ejector Axial Spacing, X_S

Figure 3-1. Description of Geometric Parameters.

so that positive flow shut-off was accomplished. The system, therefore, reverts to a single annular flow exiting over an inner cavity of low base pressure.

Table 3-2 summarizes the comparisons which can be made through use of the test data acquired on Models 3 through 13.

Models 14 through 38 (Table 3-1) were tested statically in the General Electric Anechoic Chamber (Evendale, Ohio) which was also validated within Task 1 (Reference 9). Model 14 is a 4.64-inch-diameter conical nozzle (same geometry as Model 1) but adapted to the anechoic chamber. Models 15 through 21 are single-flow turbojet configurations with annular multielement suppressors around a plug geometry and are categorized as follows:

A. Models 15, 16, and 17 maintain 36-element segmentation and vary area ratio and radius ratio through values of 2.5/0.653, 2.0/0.716 and 1.5/0.782, respectively.

B. Model 18 maintains similar geometry to Model 16 except the chutes are converted to zero-ventilation spokes.

C. Model 19 maintains the suppressor/plug geometry of Model 16 but adds an acoustically treated secondary ejector.

D. Models 20 and 21 were previously designed and tested under DOT/FAA Supersonic Transport Noise Reduction Technology Contracts DOT-FA72WA-2894 and FA-SS-71-13, respectively, (References 3 and 4). In this program they were adapted to the anechoic facility and selected for test to fill identified data voids in turbojet suppression technology of generic multielement/plug systems of low radius ratio.

Models 22 through 38 are dual-flow nozzle configurations with geometries typical in application to DBTF/VCE systems. They are categorized as follows:

A. Models 22, 24, and 27 maintain 36-element segmentation and common inner flowpath geometry which maintain A_o/A_i at 1.92, but vary suppressor area ratio and radius ratio through values of 2.5/0.653, 2.0/0.716 & 1.5/0.782, respectively, similar to the same parametric variations on the turbojet systems of Models 15, 16, and 17 above.

B. Models 23, 24, 25 and 26 maintain 36-element segmentation and suppressor area ratio of 2.0 but vary system A_o/A_i with values of 1.92 and 3.61, plus alter inner plug positioning from an in-line geometry (Models 23 and 25) to a retracted geometry (Models 24 and 26). These inner plug geometry changes assess the impact of varying the inner stream flow injection method within the dual-flow system.

Table 3-2. Test Model Comparisons Summary.

Variable Parameter	Mode	Model No.	A_o/A_i	Annulus R_r	Description
Radius Ratio	Single Flow	3	---	0.59	Convergent Flowpath-Plug Centerbody
		4	---	0.789	Convergent Flowpath-Plug Centerbody
		5	---	0.853	Convergent Flowpath-Plug Centerbody
A_o/A_i	Conventional Dual Flow	6	2.0	0.59	Coannular Coplanar
		7	0.65	0.789	Coannular Coplanar
		8	0.4	0.853	Coannular Coplanar
	Low Inner Flow $W_i \leq 0.1\ W_o$	9	2.0	0.59	Coannular Coplanar
		10	0.65	0.789	Coannular Coplanar
		12	0.4	0.853	Coannular Coplanar
	No Inner Flow	11	0.65	0.789	Coannular Coplanar
		13	0.4	0.853	Coannular Coplanar
Variation Through Conventional Dual Flow/ Low Inner Flow/ No Inner Flow/ Plug	Constant A_o/A_i and R_r	6	2.0	0.59	Conventional Dual Flow
		9	2.0	0.59	Low Inner Flow
		3	2.0	0.59	Plug Centerbody
	Constant A_o/A_i and R_r	7	0.65	0.789	Conventional Dual Flow
		10	0.65	0.789	Low Inner Flow
		11	0.65	0.789	No Inner Flow
		4	0.65	0.789	Plug Centerbody
	Constant A_o/A_i and R_r	8	0.4	0.853	Conventional Dual Flow
		12	0.4	0.853	Low Inner Flow
		13	0.4	0.853	No Inner Flow
		5	0.4	0.853	Plug Centerbody

Table 3-2. Test Model Comparisons Summary (Concluded).

Variable Parameter	Mode	Model No.	Outer			Inner			System
			Element Description	Area Ratio, AR	Radius Ratio, R_r^o	Annulus Height, h	Radius Ratio, R_r^i	Plug Geometry	Area Ratio, A_o/A_i
Suppressor Area Ratio and Radius Ratio	• Turbojet	15	36 Chute	2.5	0.653	Not Applicable			
		16	36 Chute	2.0	0.716				
		17	36 Chute	1.5	0.782				
	• Dual Flow	22	36 Chute	2.5	0.653	0.70	0.779	Retracted	1.92
		24	36 Chute	2.0	0.716	0.70	0.779	Retracted	1.92
		27	36 Chute	1.5	0.782	0.70	0.779	Retracted	1.92
Suppressor Area Ratio	• Dual Flow • Constant Radius Ratio	34	36 Chute	3.0	0.783	1.034	0.674	Retracted	0.65
		33	36 Chute	2.5	0.783	1.034	0.674	Retracted	0.65
		27	36 Chute	1.5	0.782	0.70	0.779	Retracted	1.92
Flow Management, Auxiliary Injection Geometry	• Dual Flow • Chutes	23	36 Chute	2.0	0.716	0.70	0.779	In-Line	1.92
		24	36 Chute	2.0	0.716	0.70	0.779	Retracted	1.92
		25	36 Chute	2.0	0.716	0.35	0.89	In-Line	3.61
		26	36 Chute	2.0	0.716	0.35	0.89	Retracted	3.61
	• Dual Flow • Spokes	28	36 Spoke	2.0	0.716	0.70	0.779	Retracted	1.92
		29	36 Spoke	2.0	0.716	0.70	0.779	In-Line	1.92
Flow Management, Auxiliary Injection Rate	• Dual Flow	23	36 Chute	2.0	0.716	0.70	0.779	In-Line	1.92
		24	36 Chute	2.0	0.716	0.70	0.779	Retracted	1.92
		28	36 Spoke	2.0	0.716	0.70	0.779	Retracted	1.92
		31	36 Shallow Chute	1.75	0.717	0.70	0.779	Retracted	1.92
Segmentation, Element Number	• Dual Flow	30	20 Shallow Chute	1.75	0.719	0.70	0.779	Retracted	1.92
		31	30 Shallow Chute	1.75	0.719	0.70	0.779	Retracted	1.92
		32	40 Shallow Chute	1.75	0.719	0.70	0.779	Retracted	1.92
Suppressor Element Type	• Dual Flow	24	36 Chute	2.0	0.716	0.70	0.779	Retracted	1.92
		28	36 Spoke	2.0	0.716	0.70	0.779	Retracted	1.92
		23	36 Chute	2.0	0.716	0.70	0.779	In-Line	1.92
		29	36 Spoke	2.0	0.716	0.70	0.779	In-Line	1.92
	• Turbojet	16	36 Chute	2.0	0.716	Not Applicable			
		18	36 Spoke	2.0	0.716				
	• Dual Flow	33	36 Chute	2.5	0.783	1.034	0.674	Retracted	0.65
		35	36 Spoke	2.5	0.783	1.034	0.674	Retracted	0.65
Application of Acoustically Treated Ejector	• Dual Flow	24	36 Chute	2.0	0.716	0.70	0.779	Retracted	1.92
		36	36 Chute	2.0	0.716	0.70	0.779	Retracted	1.92
	• Turbojet	16	36 Chute	2.0	0.716	Not Applicable			
		19	36 Chute	2.0	0.716				
	• Unsuppressed Annular Dual Flow	37	Annular	---	0.853	0.634	0.800	Retracted	1.59
		38	Annular	---	0.926	0.634	0.800	Retracted	0.71

C. Models 28 ard 29 maintain the same annular suppressor geometry of Model 23 except the chutes are converted to zero-ventilation spokes. This model set was designed to further assess the impact of inner plug geometry changes within a dual-flow system but now with an outer stream suppressor utilizing spokes.

D. Models 30, 31, and 32 comprise a nozzle set designed to evaluate the impact of degree of segmentation, using 20, 30 and 40 shallow chutes. Suppressor area ratio and radius ratio are common at $_i$ 1.75 and 0.717, respectively. Inner plug geometry is held with R_r^i = 0.779 and the plug in the retracted position. System area ratio is constant at A_o/A_i = 1.92.

E. Models 33, 34, and 35 form a set of configurations evolved around the basic geometry of Model 33, which comes from the NASA-Lewis Duct Burning Turbofan Contract NAS3-18008 (Reference 10). The model was upgraded to adapt to the anechoic test rig. Model 35 is Model 33 converted to a zero-ventilation spoke configuration, and Model 34 adds a new area ratio = 3.0 annular chute suppressor. System area ratio is consistent with A_o/A_i = 0.65, and R_r^i = 0.674 inner plug is common in the retracted position.

F. Model 36 adds an acoustically treated secondary ejector to the basic geometry of Model 24, similar on this dual-flow model set to the turbojet set of Models 16 and 19.

G. Models 37 and 38 are acoustically treated ejector applications to coannular, noncoplanar dual-flow plug nozzles, the basic nozzle without ejector being previously evaluated under NASA-Lewis Contract NAS3-19777 (Reference 11). Inner plug geometry is maintained at R_r^i = 0.800 and outer shrouds are interchanged to affect R_r^o and A_o/A_i values of 0.853/1.159 and 0.926/0.71, respectively.

Table 3-2 summarizes the comparisons which can be made through use of test data acquired on Models 15 through 38. The general categories of variable parameters investigated are grouped as follows:

- Suppressor area ratio and radius ratio - each varying but not independently: applicable to turbojet Models 15, 16, and 17 and to dual-flow system Models 22, 24, and 27.

- Suppressor area ratio variation with constant radius ratio, Models 27, 33, and 34, applicable to dual-flow systems.

- Flow management with respect to inner stream injection geometry, assessing impact of inner plug location and inner plug radius ratio with accompanying variation in system area ratio: on dual-flow systems, relative chute suppressors (Models 23 through 26), and relative to spoke suppressor (Models 28 and 29).

- Flow management with respect to inner stream injection rate, meaning inner flow nominally equal to 0, 15, and 30% of outer flow on four select independent geometry nozzles: Models 23, 24, 28, and 31.

- Degree of segmentation of suppressed annulus of dual-flow system: Models 30, 31, and 32.

- Suppressor element type in terms of chute versus spoke on dual-flow systems, Model sets 24/28, 23/29, and 33/35 and on turbojet. Model set 16/18.

- Application of acoustically treated secondary ejector to suppressed dual flow (Model set 24/36) to suppressed turbojet (Model set 16/19) and to unsuppressed annular dual flow (Model set 37/38).

The Model Series 39 through 47 in Table 3-1 was tested statically and in the free-jet mode in the JENOTS facility to gain an early assessment of the influence of simulated flight for several baseline and suppressor configurations and to evaluate shock noise within a simulated flight environment. The models can be categorized as follows:

- Models 39 and 40 are single-flow plug nozzles of convergent flowpath geometry and with radius ratios of 0.789 and 0.85, respectively.

- Model set 41, 42, and 43 share a 36-chute annular suppressor of AR = 2.5 and R_r = 0.78. Model 41 is a single-flow turbojet configuration. Model 42 utilizes induced tertiary flow ducted through hollow struts to simulate a dual-flow system having an inner plug with retracted position geometry and with R_r = 0.674 and A_o/A_1 = 0.65. Model 43 closes off the induced flow passage of Model 42 and allows the annular suppressed jet to dump over the abrupt step of the inner plug geometry.

- Models 44 and 45 are 104 elliptical tube and hole configurations, respectively, to evaluate the influence of tube base ventilation within a wind-on environment.

- Model 46 is an 8-lobe daisy configuration of AR = 2.1.

- Model 47 is a 4-inch-diameter conical nozzle with both internal and external contoured flow lines.

Models 44, 46, and 47 are direct scale-model versions of J85-size nozzles tested within the joint GE/SNECMA* moving-frame validation test program on the Bertin Aerotrain. The full-size 8-lobe nozzle and the 104-tube nozzle were also tested on the Gates Learjet-25C and F-106 aircraft, respectively (Reference 12).

*SNECMA - Société Nationale D'Etude et De Construction de Moteurs D'Aviation.

3.2 DEFINITION OF TEST MATRICES

3.2.1 Acoustic Test Matrices

Of the 47 models enumerated in Table 3-1, 45 were tested for far-field acoustic data within this study. The nozzles represent various system applications, i.e., turbojet, turbofan, duct burning turbofan, and variable cycle engine. The systems range in complexity from simple conical and coplanar coannular baselines, to complex dual-flow plug nozzles with multielement suppressors and acoustically-treated secondary ejectors. Additionally, the purposes for test varied with individual nozzles and nozzle sets to:

1) Develop a detailed data base for use in Volume 1, "Verification of Suppression Principles and Development of Suppression Prediction Methods."

2) Develop parametric data for systematic variations in suppressor geometry.

3) Evaluate shock noise.

4) Establish noise dependency on flow-management parameters such as Wo/Wi, Ao/Ai, inner flow injection geometry and velocity/temperature control.

5) Obtain an early evaluation of simulated free-jet environment influence, etc.

The test matrices for the nozzles varied extensively in order to best develop the data base required to fulfill the specific objectives for the particular configuration. These test matrices are discussed in this section in terms of "nominal" values of aerodynamic parameters; i.e., ranges of P_T/P_o, T_T, V_j, V_o/V_i, W_o/W_i, etc., and in terms of their applicability to individual models or sets. However, to make the test results presented more meaningful, and the data acquired more useful, "specific" aerodynamic test values are necessary. These "as-measured" test values are tabulated in Appendix B, one table for each nozzle configuration. The tables also list pertinent acoustic data (scaled to an engine size of 338 $in.^2$ as discussed in Section 3.3.1.5) and conventionally-used data-normalization parameters.

The models are grouped, and test matrices discussed in the following ten sets:

Set	Model No.'s	Set Description
A	1 and 14	Conical Baseline - JENOTS and Cell 41 Anechoic Facility Adaptations
B	2	Convergent/Divergent Plug - JENOTS
C	3-5	Single-flow plug nozzle parametric radius ratio study - JENOTS

Set	Model No.'s	Set Description
D	6 and 8-13	Coannular coplanar nozzle geometries tested as dual flow, nominal outer stream operation with low inner flow, and nominal outer stream operation with no inner flow - JENOTS
E	15-19	Suppressed turbojet configurations studying suppressor area ratio, radius ratio, element type, and application of acoustically treated ejector - Cell 41 Anechoic Facility
F	20 and 21	Multielement annular suppressors on turbojet/plug system of low radius ratio - Cell 41 Anechoic Facility
G	22-32 and 36	Suppressed dual-flow configurations studying suppressor area ratio, radius ratio, element type, variation of inner stream geometry, flow management, and application of acoustically-treated ejector; all on systems of moderate to high radius ratio - Cell 41 Anechoic Facility
H	33, 34 and 35	Suppressed dual-flow configurations studying suppressor area ratio and element type on models of low system area ratio (A_o/A_i = 0.65) - Cell 41 Anechoic Facility
I	37 and 38	Acoustically-treated ejector application to coannular noncoplanar dual-flow plug nozzles - Cell 41 Anechoic Facility
J	39-45 and 47	Free-jet assessment of the influence of simulated flight on several baseline and suppressor configurations: conical, plug, chute, tube, and hole - JENOTS free jet

Set A - The 4.64-inch-diameter conical nozzle, as adapted to JENOTS (Model 1), was tested per the matrix of Figure 3-2(a) and as adapted to Cell 41 Anechoic Facility (Model 14) was tested per the matrix of Figure 3-2(b). Lines of constant total temperature at values of ambient, 700°, 850°, 1000°, 1250°, 1300°, 1450°, and 1500° R were primarily used. Constant stagnation temperature lines at 1000° and 1500° R also were used on Model 14.

Set B - Model 2, convergent-divergent flowpath plug, used the matrix of Figure 3-3 following (a) a typical turbojet operating line; (b) isovelocity lines at 1000, 1250, 1640, and 2090 ft/sec to establish noise dependency on jet density/temperature; (c) isotemperature lines of 1000°, 1250°, 1500°, 1750° and 2000° R to establish noise/velocity dependency.

Set C - Models 3, 4, and 5 (plug parametric radius ratio study) utilized the test matrix of Figure 3-4. Each of the three models was tested along the simulated turbojet engine cycle line. Additionally, Model 4 (R_r = 0.789) was subjected to a more detailed parametric matrix of (a) isovelocity lines

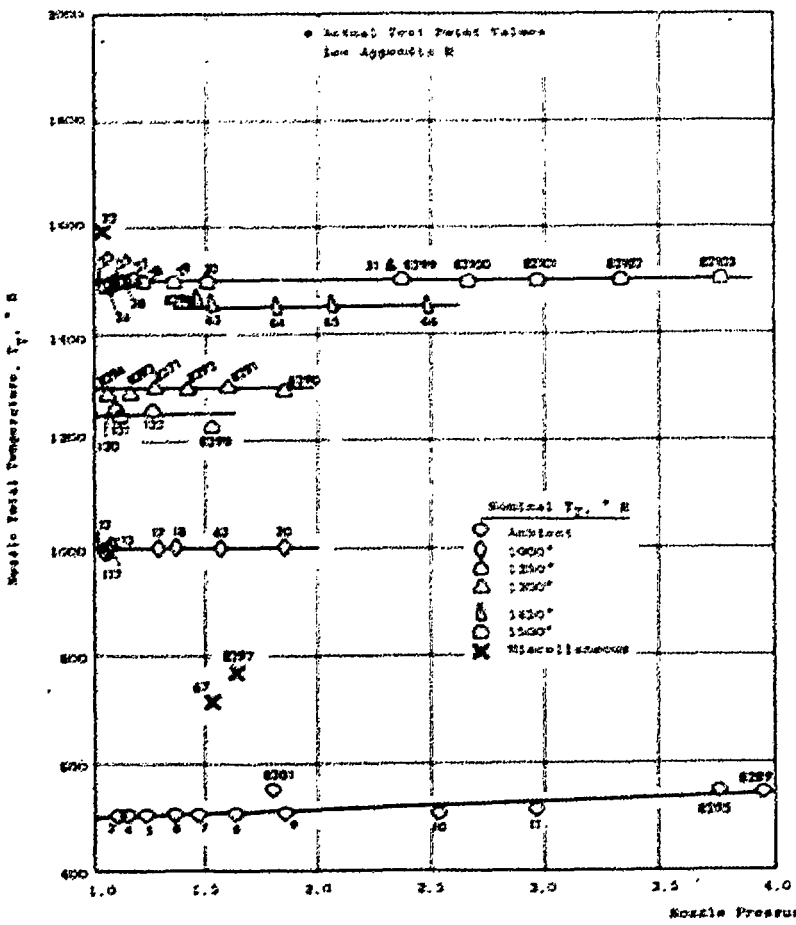

Figure 3-2(a). Far-Field Acoustic Test Matrix, Model 1, JENOTS.

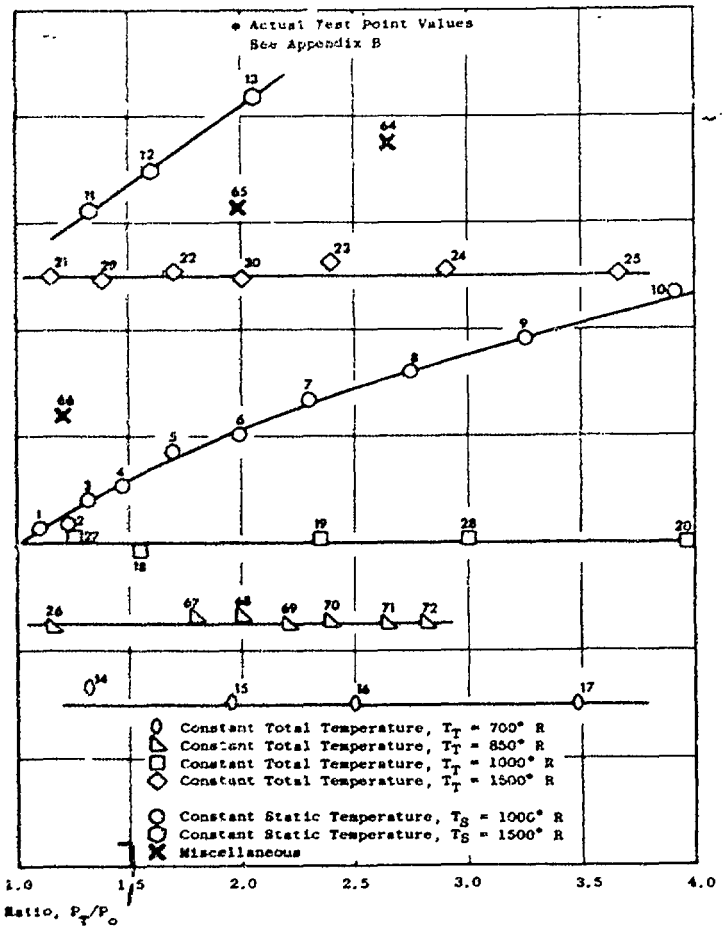

Figure 3-2(b). Far-Field Acoustic Test Matrix, Model 14, Cell 41 Anechoic Facility.

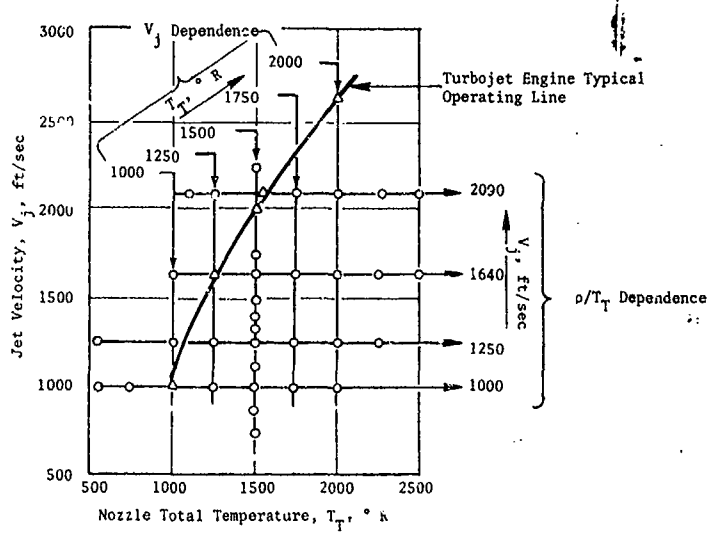

Figure 3-3. Far-Field Acoustic Test Matrix, Model 2, JENOTS.

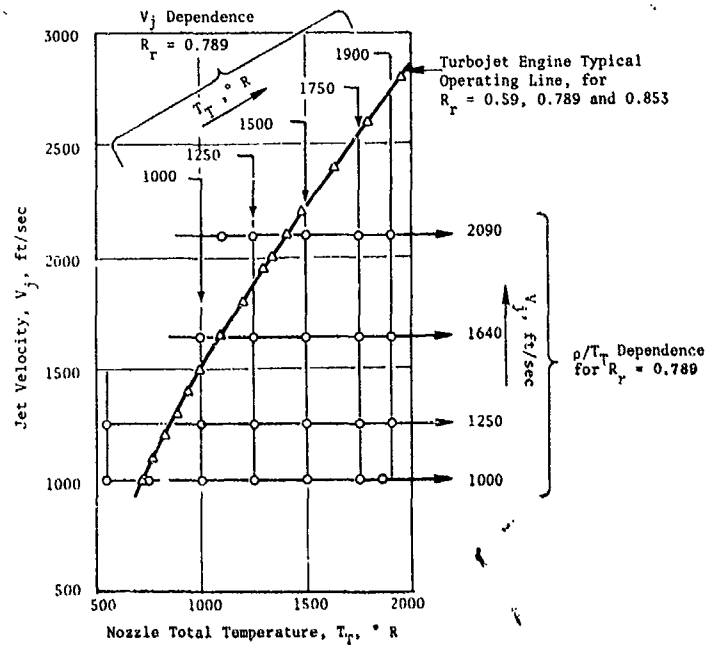

Figure 3-4. Far-Field Acoustic Test Matrix, Models 3, 4, and 5, JENOTS.

at 1000, 1250, 1640, and 2090 ft/sec to establish noise dependency on jet density/temperature, and (b) isotemperature lines of 1000°, 1250°, 1500°, 1750° and 1900° R to establish noise/velocity dependency.

Set D - Models 6 and 8 are dual-flow coannular-coplanar configurations of A_o/A_i = 2.0 and 0.4, respectively. They were tested using the nominal matrix of Figure 3-5. The inner stream was maintained at specific temperature/velocity conditions while the outer stream varied to effect a range of $1.0 \leq V_o/V_i \leq 2.0$. (Match symbols and data points of "inner velocity", left of figure, to those of "outer velocity", right of figure.) The test matrix was patterned along that of the duct burning turbofan matrix of Reference 10. Model 7 (of A_o/A_i = 0.65) was acoustically tested within the referenced program and the available far-field data will be used for comparisons within this report. Model 8 was further tested using the matrix of Figure 3-6 which maintained equal inner and outer stream temperatures at ambient and 1500° R and varied V_o/V_i from 0 to 5.0

Models 9, 10, and 12 of A_o/A_i = 2.0, 0.65, and 0.4 respectively, used the same physical hardware as Models 6, 7, and 8. The outer stream was operated in the conventional high-flow velocity mode but the inner weight flow and velocity were substantially reduced to determine the effect of low inner flow on generated noise. Matrices for the outer stream cycle are in Figure 3-7(a) for Model 9 and in Figure 3-7(b) for Models 10 and 12. While utilizing these outer stream cycles, the inner stream parameters ranged within ambient $\leq T_{Ti}$, ° R, $\leq$ 1000; $50 \leq V_i$, ft/sec $\leq$ 320 and $W_i \leq$ 10% of W_o.

Models 11 and 13 (of A_o/A_i = 0.65 and 0.4) again used the same physical hardware as Models 7 and 8 but provided positive shut-off of the inner flow. These models utilized the test matrix of Figure 3-7(b).

Set E - Models 15 through 19, single-flow turbojets, used conventional and advanced turbojet cycle lines as per Figure 3-8. The 16-point matrix had parameters of $1.7 \leq P_T/P_o \leq 3.9$, $730 \leq T_T$, °R ≤ 1760 and $1200 \leq V_j$, ft/sec ≤ 2650.

Set F - Models 20 and 21, conventional single-flow low radius ratio multitube and multichute annular plug suppressors, used the test matrix of Figure 3-9.

Set G - The suppressed dual-flow configurations, Models 22 through 32 and 36, normally used a 37 test point matrix depicted graphically in Figure 3-10 and based on the description within Table 3-3. Data points 1 through 20 were used to evaluate noise variation with flow management. Points 1-8 (for Models 23, 24, 28, and 31, only) used no inner flow; therefore, the outer flow exited over an abrupt step in the inner flowpath and the nozzle essentially reverted to a single-flow system. Positive shut-off of the inner flow was assured by using blank-off hardware within the inner stream. Points 9 through 14 metered the inner flow to be approximately 15% of the outer flow rate and points 15 through 20 raised that percentage to 30.

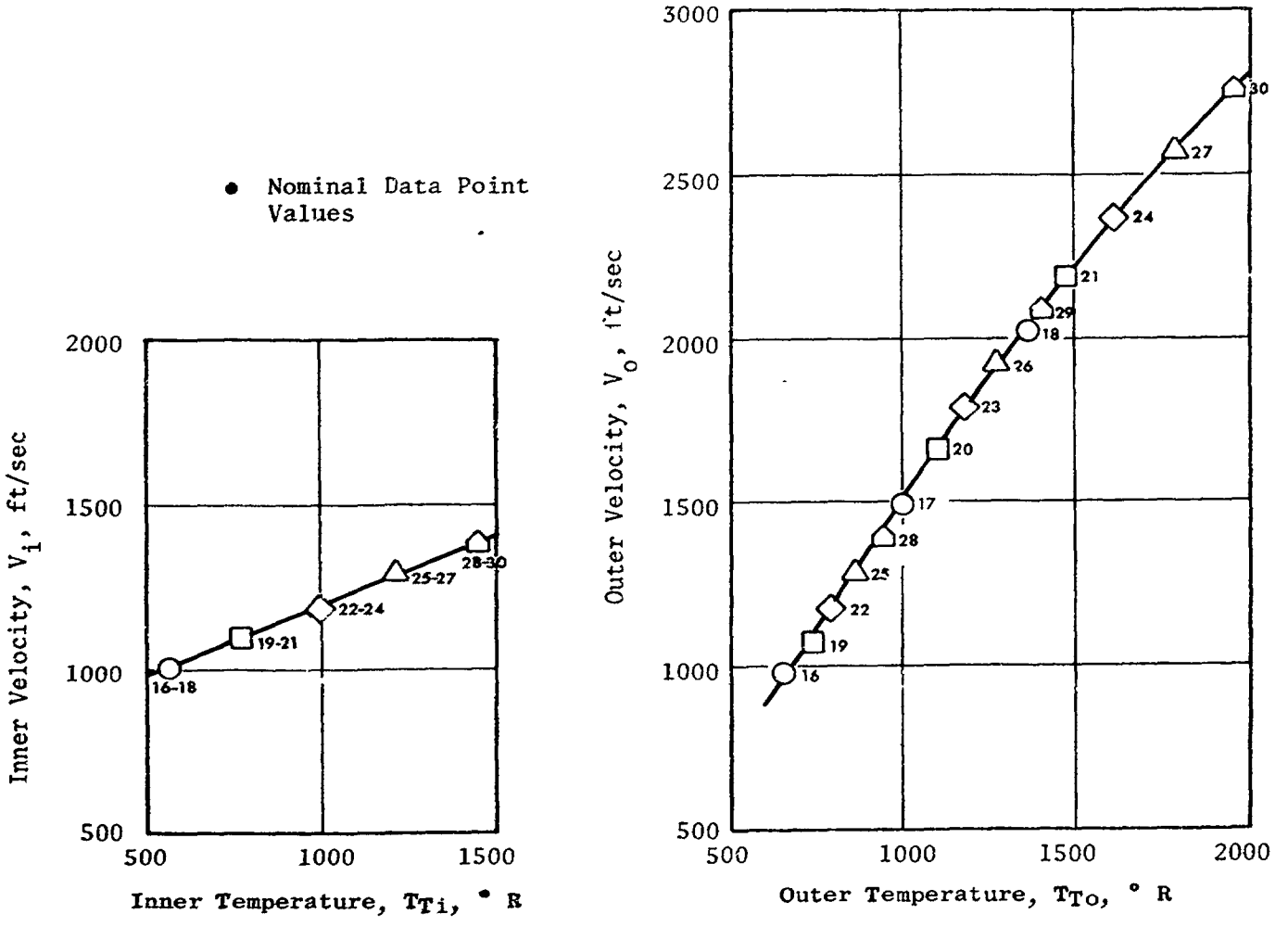

Figure 3-5. Far-Field Acoustic Test Matrix, Models 6 and 8, JENOTS.

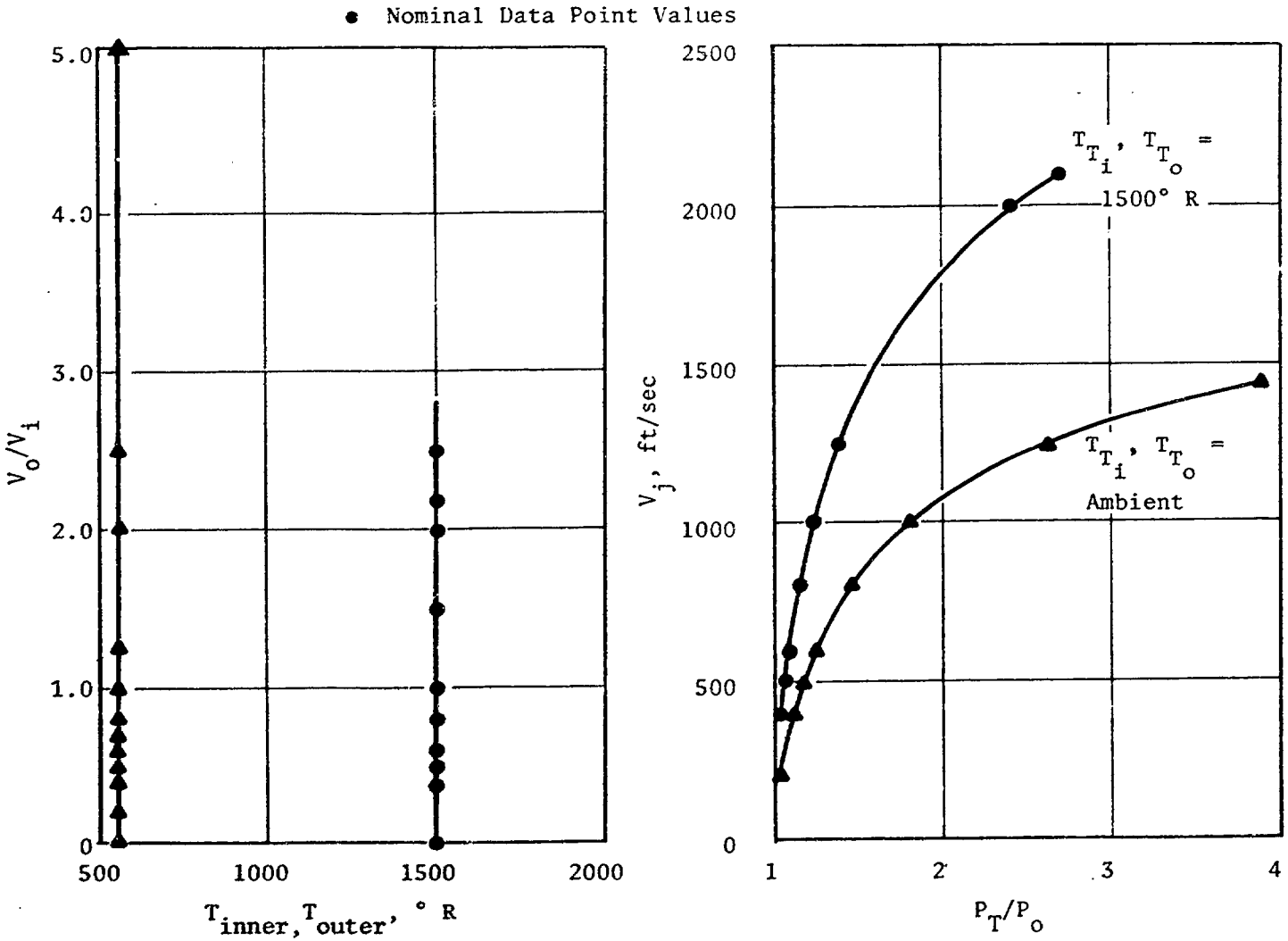

Figure 3-6. Far-Field Acoustic Test Matrix, Model 8, JENOTS.

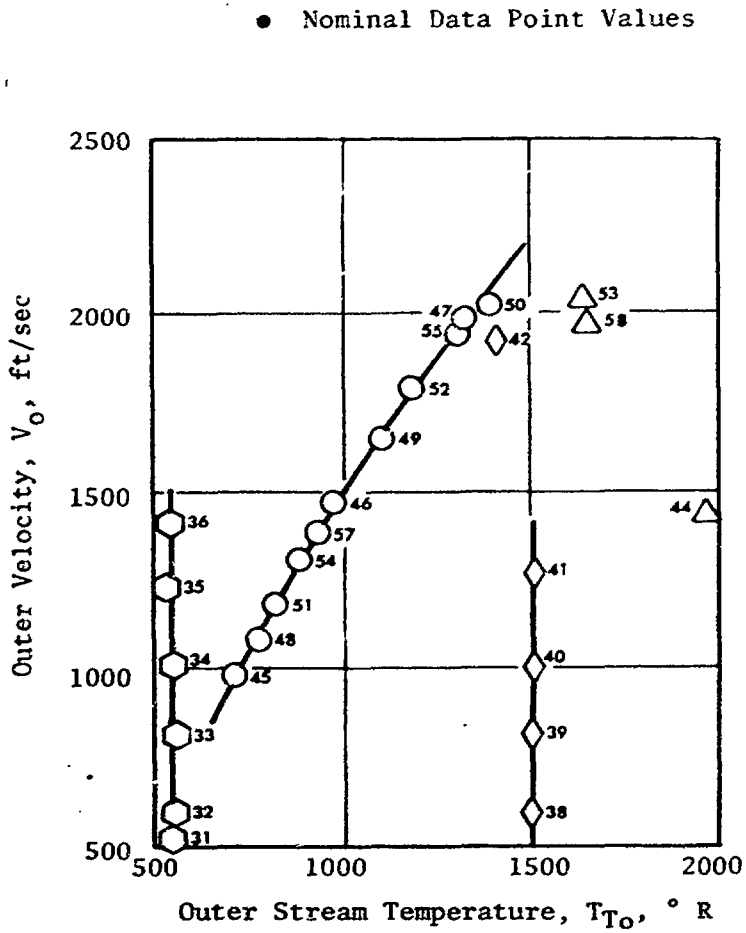

Figure 3-7(a). Far-Field Acoustic Test Matrix, Model 9, JENOTS.

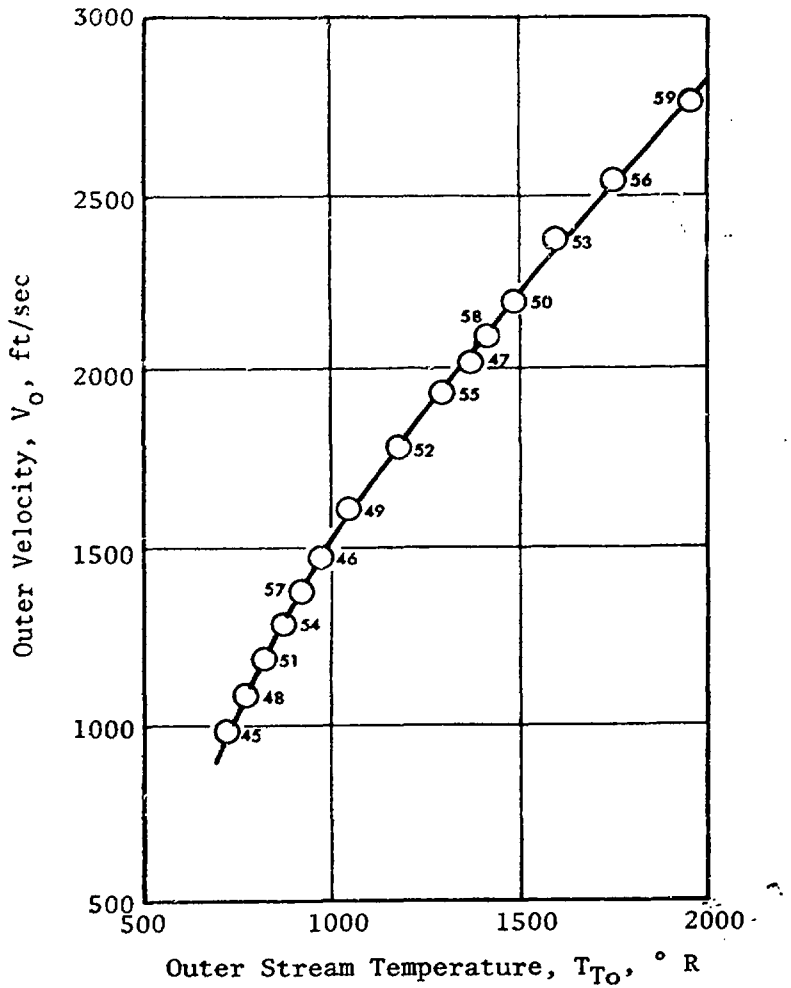

Figure 3-7(b). Far-Field Acoustic Test Matrix, Models 10, 11, 12, and 13, JENOTS.

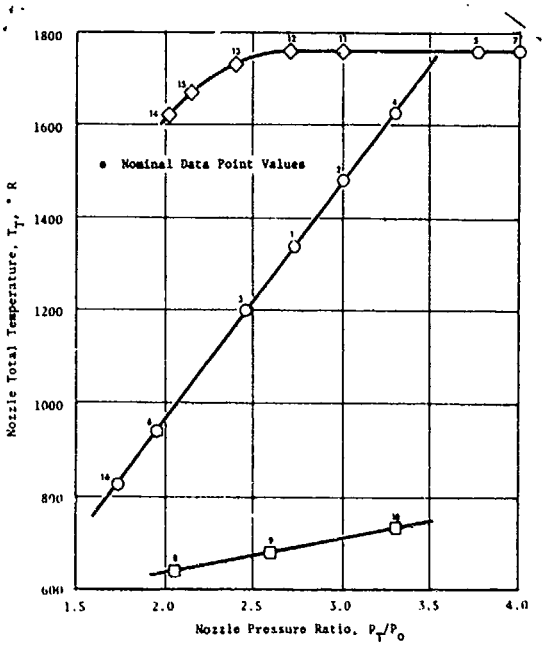

Figure 3-8. Far-Field Acoustic Test Matrix, Models 15 Through 19, Cell 41 Anechoic Facility.

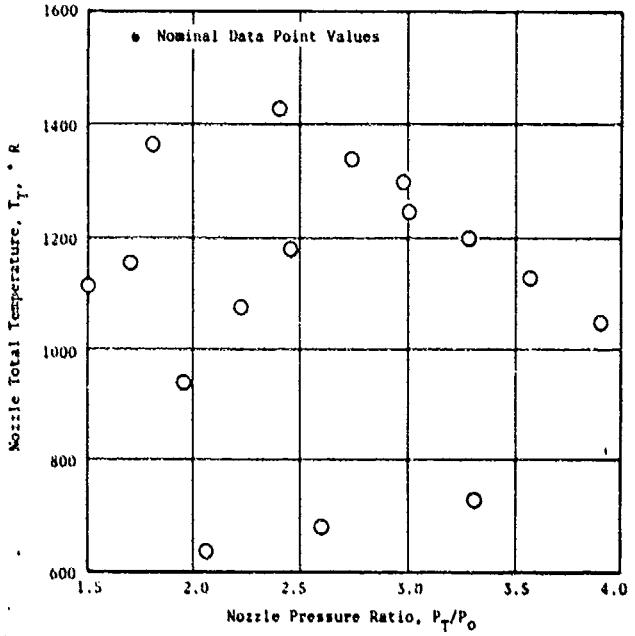

Figure 3-9. Far-Field Acoustic Test Matrix, Models 20 and 21, Cell 41 Anechoic Facility.

- Nominal Values of Outer and Inner Stream Aerodynamic Test Conditions Interrelating $(T_T)_{o,\,i}$; $(P_T/P_o)_{o,\,i}$; and $V_{o,i}$

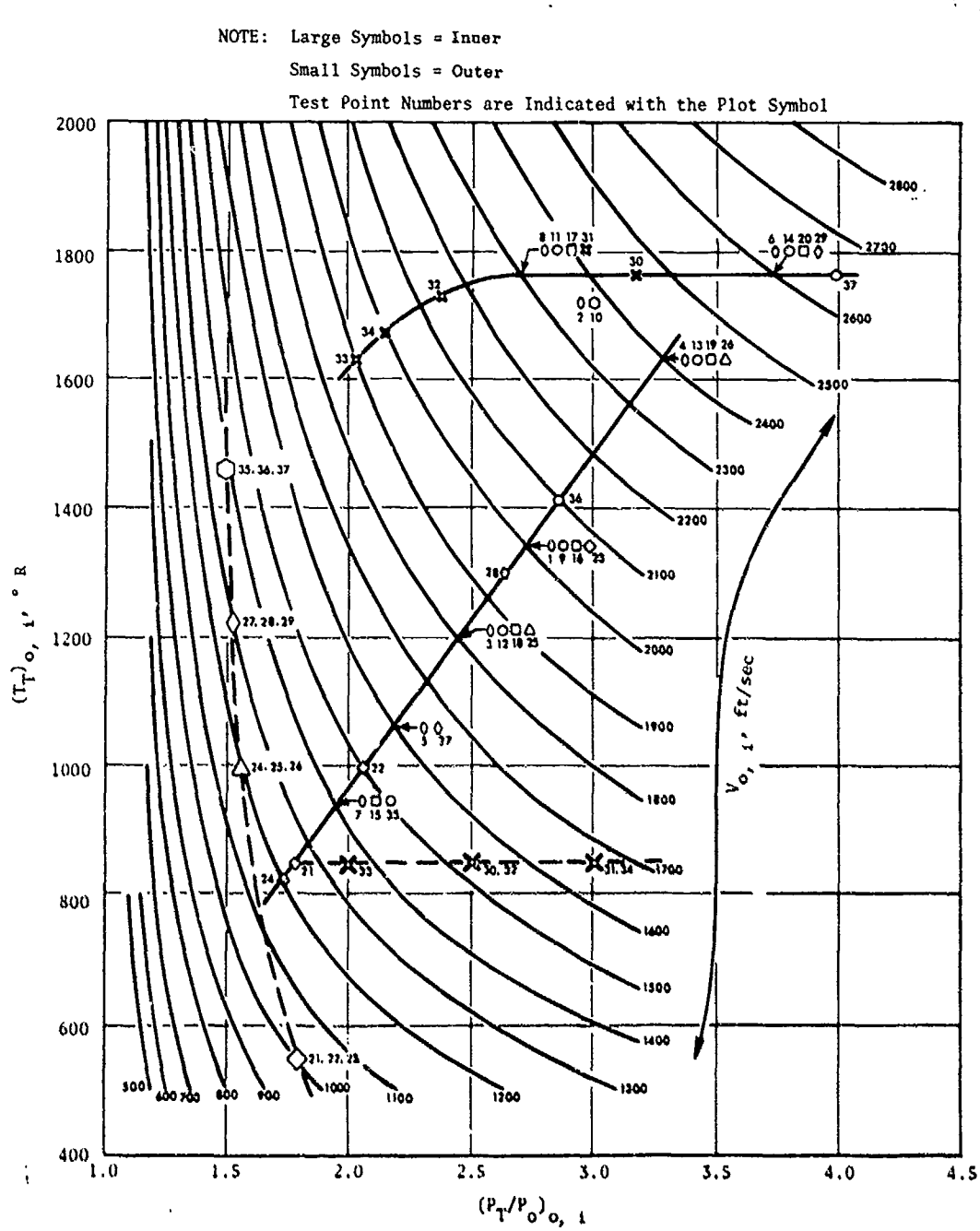

Figure 3-10. Far-Field Acoustic Test Matrix, Models 22 Through 32 and 36, Cell 41 Anechoic Facility.

Table 3-3. Far-field Acoustic Test Matrix Description - Models 22-32 and 36 - Cell 41 Anechoic Facility.

	Objective	Data Point Nos.	Outer Stream				Inner Stream
DUAL FLOW	Establish influence of inner core flow over 0 to 30% range	1-8	2.2-3.75	940-1760	1400-2300		No inner flow - abrupt step
		9-11	2.45-3.75	1340-1760	2000-2600	High	Inner flow metered to 15% of outer flow
		15-20	1.95-3.75	940-1760	1400-2600	High	Inner flow metered to 30% of outer flow
	Inverted dual flow and DBTF cycles	21-29 and 35-37	1.73-3.99	825-1760	1200-2680	1.0-2.0	Inner stream at 1000, 1200, 1300, and 1400 ft/sec
	AST/VCE cycle	30-34	2.0-3.2	1625-1760	1900-2450	1.2-1.6	Inner stream at 850° R and 1350-1660 ft/sec
			P_T/P_o	T_T, ° R	V_o, ft/sec	$\frac{V_o}{V_i}$	

Simulation of inverted dual flow and DBTF cycles was accomplished with Points 21 through 29 plus 35 through 37, within a V_o/V_i range of 1.0-2.0. Points 30 through 34 simulated Advanced Supersonic Transport/Variable Cycle Engine (AST/VCE) cycles.

Set H - Models 33, 34,and 35 followed a matrix similar to that of Set G; however, it was expanded to be more consistent with the test matrix of Reference 10 (DBTF program). Additionally, the data point series which simulates the 0, 15, and 30% inner flow cases was expanded from the matrix of Set G (see Appendix B for details).

Set I - Models 37 and 38 applied an acoustically treated secondary ejector to basic coannular/noncoplanar dual-flow plug nozzles; an abbreviated form of the Set G matrix was utilized. Basically, parts of the inverted dual-flow/DBTF cycle matrix (Points 22, 23, and 27-29) and the AST/VCE cycle matrix were used (see Figure 3-10 and Table 3-3). Several other data points were added; see the detailed tables in Appendix B.

Set J - Configurations within this set, Models 39-45 and 47, utilized the overall test matrix of Figure 3-11 but with data points selectively chosen for each individual configuration. The overall matrix primarily followed: (a) a typical turbojet engine operating line; (b) isovelocity lines at 1640 and 2090 ft/sec; (c) isotemperature lines at 1000°, 1400°, and 1690° R; (d) simulation of the J85 and advanced turbojet operating lines to tie in with tests performed in Task 4 (Reference 12).

In referring to the individual model data tabulations in Appendix B, many of the data points were tested at free-stream velocities of 150 and 275 ft/sec, in addition to the normal static test. Itemization of specific data points for each model is as follows:

- Models 39 and 40, plug nozzles of R_r = 0.789 and 0.85, used test points 3 through 12, primarily the turbojet operating line. Additionally, Model 40 used points 15-17, 19, and 21-24, forming isovelocity lines at 1640 and 2090 ft/sec.

- Models 41, 42, and 43 used data points 3, 4, 6, 7, and 9-12, again primarily the turbojet operating line.

- Models 44 and 45, the 104-tube and 104-hole nozzle nozzles, used points 9, 11-18, and 20. Model 45 also used points 25-30.

- Model 47, 4.0-inch conical nozzle, used data points 12 and 30 through 37, basically for shock noise evaluation within static and wind-on environments.

3.2.2 Laser Velocimeter Test Matrix

Laser velocimeter measurements of jet plumes were conducted on a total of 21 different model configurations as indicated in Table 3-1. Table 3-4

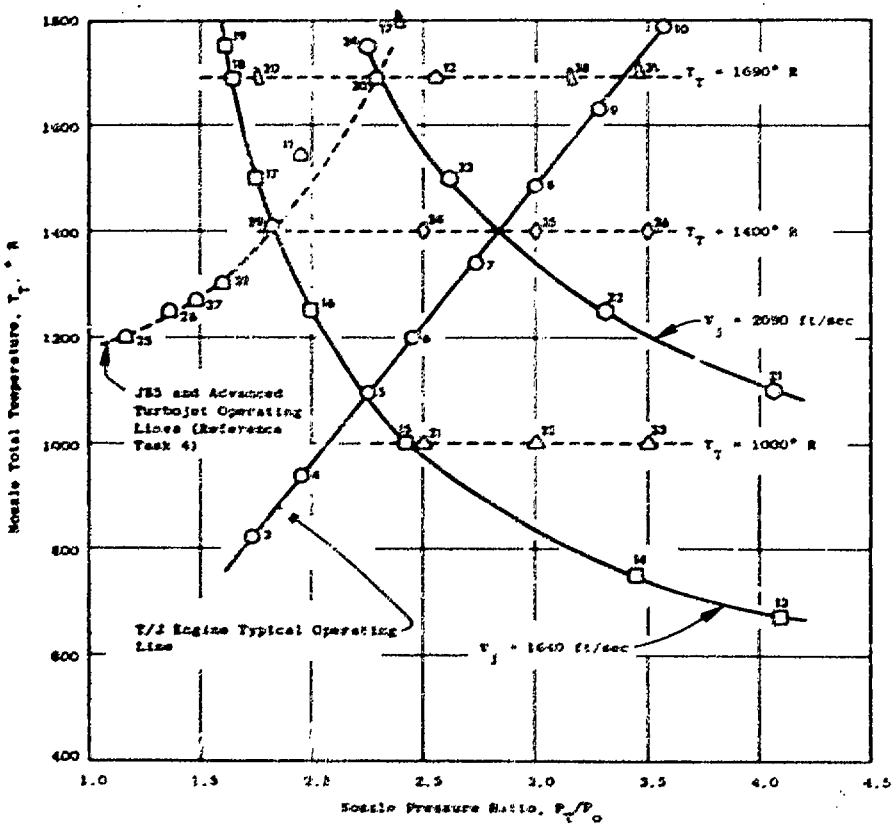

a) Cycle Matrix Shown as a Function of P_T/P_o and T_T

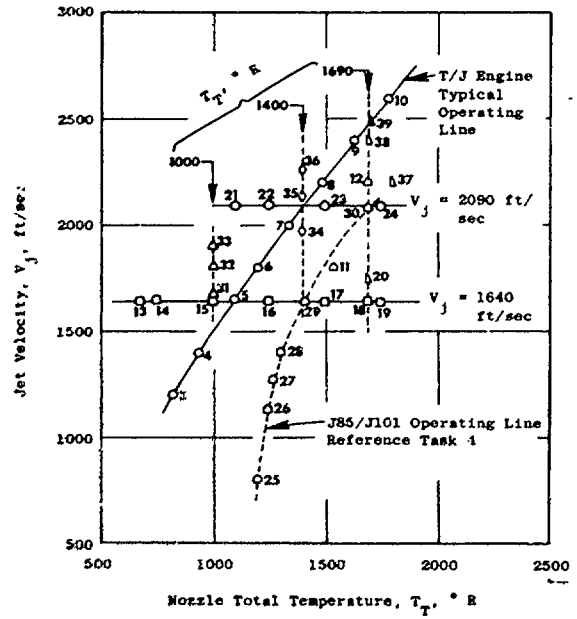

b) Cycle Matrix Shown as a Function of T_T and V_j

Figure 3-11. Far-Field Acoustic Test Matrix, Models 39 Through 45 and 47, JENOTS Free Jet.

Table 3-4. Laser Velocimeter Test Matrix; Aero Cycle Conditions.

Model No.	Inner			Outer			Free Stream
	$(P_T/P_0)_i$	T_{T_i} (°R)	V_i (ft/sec)	$(P_T/P_0)_o$	T_{To} (°R)	V_o (ft/sec)	V_{FS} (ft/sec)
1	1.79	565	1000				
1	1.56	1000	1200				
1	1.221	1500	1000	Not Applicable			
2	2.52	1550	2090				
2	1.99	1250	1640				
2	1.36	1000	1000				
6	1.77	553	1000	1.022	550	200	
6	1.77	555	1300	1.09	555	400	
6	1.81	535	1000	1.224	535	600	
6	1.78	550	1000	1.43	550	800	
6	1.79	545	1000	1.79	545	1000	
6	1.62	650	1000	2.19	650	1250	
6	1.51	530	500	1.82	530	1000	
6	1.22	1500	1000	1.032	1500	400	
6	1.22	1500	1000	1.073	1500	600	
6	1.22	1500	1000	1.22	1500	1000	
6	1.22	1500	1000	2.16	1500	2000	
7	1.56	1000	1200	1.73	825	1200	
7	1.56	1000	1200	2.45	1200	1800	
7	1.56	1000	1200	3.28	1630	2400	
10				1.73	825	1200	
10	$M_i = 10\%\ M_o$			2.45	1200	1800	
10				3.28	1630	2400	
11	Not Applicable			2.45	1200	1800	
16	1.73	825	1200				
16	3.28	1630	2400				
18	1.73	825	1200				
18	3.28	1630	2400	Not Applicable			
18	1.93	930	1400				
18	2.63	1200	1800				
20	1.45	1110	1200				
20	3.28	1630	2400				
22	1.56	1000	1200	3.28	1630	2400	
24	1.56	1000	1200	3.28	1630	2400	
27	1.56	1000	1200	3.28	1630	2400	
28	1.56	1000	1200	3.28	1630	2400	
39	1.73	825	1200				
39	3.28	1630	2400				
40	1.73	825	1200				
40	3.28	1630	2400				
43	1.73	825	1200				825
40	3.28	1630	2400				825
43	1.73	825	1200				
43	3.28	1630	2400				
43	1.73	825	1200				825
43	3.28	1630	2400				825
43	1.73	825	1200				
43	3.28	1630	2400				
43	1.73	825	1200	Not Applicable			825
43	3.28	1630	2400				825
43	1.73	825	1200				
43	3.28	1630	2400				
43	1.73	825	1200				825
43	3.28	1630	2400				825
44	1.73	1630	1200				
44	1.73	1630	1200				825
43	3.28	1630	2400				
43	1.73	1630	1200				
43	1.73	1630	1200				825
43	3.28	1630	2400				1630
48	2.52	1630	2520				
48	1.73	1630	1200				825
48	3.28	1630	2400				
48	1.73	1630	1200				825

summarizes these configurations as well as the aerodynamic test conditions for each model at which LV measurements were taken. Of the 21 total models, 14 were tested at the JENOTS Facility and the remaining 7 within the Cell 41 Anechoic Facility Thirteen of the models were single flow (simulating turbojet systems) and eight were dual flow. Models progressed in complexity from simple baseline conical to unsuppressed annular plug; to annular flow over a blunt base; to dual-flow coannular coplanar; to mechanical suppressors of the lobe, chute/spoke, and tube/hole families. Table 3-4 also shows that seven of the JENOTS configurations were tested under static (V_{FS} = 0) as well as free stream (V_{FS} = 150 or 275 ft/sec) environments.

3.2.3 Ellipsoidal Mirror Test Matrices

Ellipsoidal mirror measurements of source intensity distributions in Task 3 were conducted on a total of 26 different nozzle configurations as shown in Table 3-1. Of these, 14 configurations were tested at the Cell 41 Anechoic Facility using the 34.654-inch-diameter deep-dish mirror, and 12 were tested at the JENOTS Facility using the 18-inch-diameter shallow-dish mirror. The ellipsoidal mirror test matrix was planned to allow an assessment of various geometric and operating parameters on the jet noise source distributions of suppressor nozzles by comparison of measured source distributions for specific data points. Results can be expressed as Strouhal Number ($fDeq/V_o$) versus normalized axial distance (X_{peak}/D_{eq}) where Deq is the equivalent circular diameter based on nozzle area, V_o is the ideally expanded jet velocity and X_{peak} is the peak source location for a given frequency, f. For dual-flow configurations Deq is calculated from total area (inner plus outer streams) and V_o is based on the higher velocity of the outer stream. Comparisons of data can be made for the following parameters: (a) degree of segmentation using 20/30/40 shallow chutes, (b) area ratio impact on dual-flow 36-chute suppressors, (c) element-type comparison of spoke versus chute on 36-element dual-flow suppressor, (d) 36-element on dual-flow versus on single-flow turbojet, and (e) application of treated ejector on turbojet and dual-flow systems.

Results of EM tests are discussed in Section 3.4.5, Ellipsoidal Mirror Microphone Measurements.

3.3 DATA ACQUISTION AND DATA REDUCTION PROCEDURES

3.3.1 Acoustic Data

As shown in Table 3-1, 21 models were tested on the General Electric JENOTS Scale-model acoustic test facility and 26 were tested in the Cell 41 Anechoic Facility. The JENOTS facility is described in detail in the Task 1 final report (Reference 8) and includes the acoustic arena, burner systems, single and coannular flow systems, aerodynamic instrumentation and data acquisition, and acoustic data acquisition and reduction.

The sound field consists of 14 microphones arranged at 10° intervals around a 40' arc from 30° - 160°. The microphones are elevated 16' above the ground on specially designed "gooseneck" mounts to minimize the influence of reflections. Nozzle centerline height is 55" above the concrete pad. Test Model No. 2 used the single-flow with afterburner setup and all others used the coannular flow system with the acoustically-treated plenum section.

The Cell 41 Anechoic Facility is described in detail in the Task 1 Supplement Report (Reference 9). Reference 9 includes the facility operational domain, the burner systems, acoustic plenum/silencer system, microphone system, anechoic quality of the facility, contamination of measurements, analysis of variance - overall precision of the acoustic measurements, and general certification of the facility. Model numbers 14 through 38 of this study were tested in this facility.

3.3.1.1 Acoustic Data Acquisition

The acoustic data acquisition systems for JENOTS and Cell 41 are shown schematically in Figure 3-12. The JENOTS system is composed of B&K microphone/cathode follower powered and conditioned by a B&K 2801 power supply, followed by 3 feet of line to a specially designed 10-dB, fixed-gain preamplifier which drive 150 feet of cable terminating at the variable-gain differential input amplifiers to the Sangamo Sabre IV tape recorder. The signal is recorded on tape for future playback in the data reduction room. The microphone type used to obtain 80-KHz data is the B&K 4135 without grid caps. The cathode follower used most often is the B&K 2615 preamplifier although B&K 2619 is also used. The purpose of the cathode follower is to give a very high input impedance with small load to the microphone and a low-output impedance allowing the connection of long cables between the preamplifier and relatively low impedance amplifiers in the circuit. The B&K 2619 uses a field-effect transistor to give higher input impedance and lower inherent noise than Type B&K 2615. The cathode follower also supplies the microphone with a 200-volt polarization from the power supply.

The B&K 2801 power supply is operated in the direct-output mode to avoid sensitivity loss. The frequency response of the various preamplifiers is not influenced by the power supply when used in this position. This power supply does have optional 50-ohm and 200-ohm transformer outputs for use in eliminating amplifier oscillation and dampening RC resonance. The JENOTS systems,

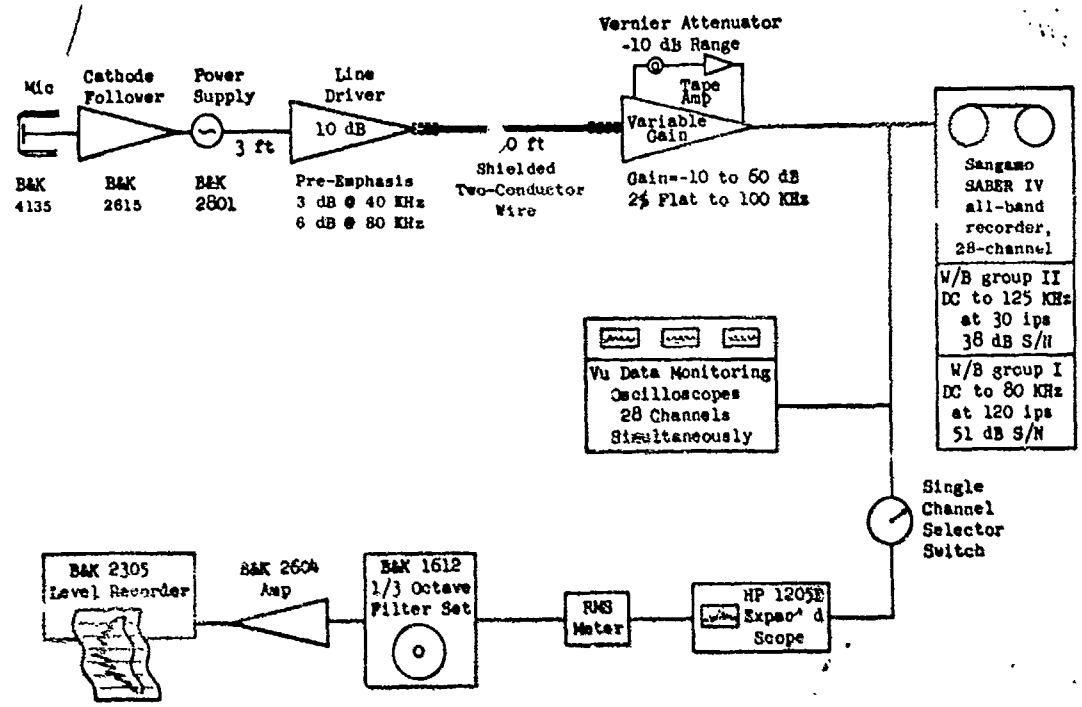

(a) JENOTS Data Acquisition System.

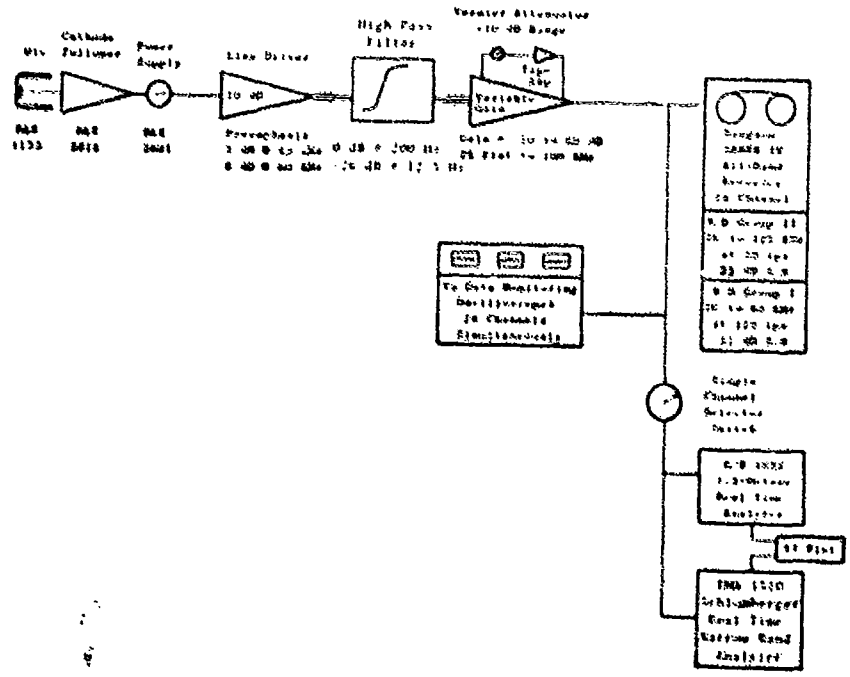

(b) Coil 41 Accurate Fertility Data Acquisition System.

Figure 3-12. Schematics of Acoustic Data Acquisition Systems.

however, are free of such problems due to the unloading of the power supply by the preamplifier. Three feet from the output of the power supply is a fixed 10-dB amplifier for driving the signal to the tape recorder amplifier. In anticipation of the low sound levels experienced at high frequency, the circuitry was designed with a frequency response that "preemphasized" the high-frequency signals such that it has a 3 dB increase at 40 KHz and an additional 3 dB between 40 KHz to 80 KHz. This increases the ability to measure low-amplitude high-frequency data. Two-conductor shielded wires were chosen for the 150 feet of lead from the line driver to the tape recorder amplifier to eliminate stray signal pickup. The cable introduces an effective 0.0458-μf capacitance to the circuit.

The amplifier at the tape recorder was designed by GE and has a variable gain from -10 dB to +60 dB. The amplifier delivers a 4-volt, peak-to-peak signal to the tape recorder electronics at the normal calibration signal level. This setting will allow a 6 dB over range without distortion. The amplifiers are flat within 5% from 5 Hz to 100 KHz. Each amplifier has an adjustable vernier attenuator which can give any desired measure of attenuation between 0 and 10 dB. During test calibration, this vernier is usually adjusted to make the 124-dB pistonphone calibration signal the full-scale (1.4 V/rms) input to the tape recorder. The 10-dB steps in the tape recorder amplifier then directly correspond to 10-dB steps in OASPL from 124 dB. The vernier can be moved to the fixed position, in which case, the signal goes directly into the 10-dB-step tape recorder amplifier. The output of each amplifier channel has a V-Data Monitoring oscilloscope for continual inspection of all signals for any clipping or deterioration of the signal due to excessive crest factor (peak value/rms).

The Sangamo Sabre IV 4930 magnetic tape recorder/reproducer has IRIG wideband and RM wideband Group I and Group II capability. In normal JENOTS operation all data are recorded on 1-inch in Wideband Group II at 30 ips, having a flat frequency response in excess of 100 KHz when used in conjunction with the B&K 4135 microphone. The voice channel is recorded direct.

The JENOTS recorder was modified to record 28 tracks and to improve its signal-to-noise dynamic range from the normal 32 dB to 39 dB over all frequencies. This lower noise floor was obtained by individual channel tuning by the Sangamo Electric Company at the factory. Playback capability of two data channels plus voice for on-site data investigation is also available.

The Cell 41 Anechoic Facility data acquisition is similar to that of JENOTS, utilizing B&K 4135 condenser microphones without grid caps, transistorized 2619 cathode followers and 2801 power supplies ; obtaining acoustic data through the 80 KHz 1/3-octave center frequency. The output of the power supply is similarly connected to a line driver adding 10 dB of amplification to the signal. Preemphasis to the high-frequency portion of the signal is also used. In order to remove low-frequency noise, high-pass filters with attenuations of approximately 26 dB at 12.5 KHz decreasing to 0 dB at 200 Hz were installed in the system.

The tape recorder's amplifying characteristics are similar to those of JENOTS. The prime system used for recording acoustic data is a Sangamo Sabre IV 28-track FM recorder. The system is set up for Wideband Group I (intermediate band double extended) at 120-ips tape speed. Operating at 120-ips tape speed provides the improved dynamic range necessary for obtaining the high-frequency/low-amplitude portion of the acoustic signal. The tape recorder is set up for ±40% carrier deviation with a recording level of 8 volts peak-to-peak. During recording, the signal is displayed on a calibrated master oscilloscope, and signal gain is adjusted to maximum without exceeding the 8-volt peak-to-peak level.

High-pass filters were incorporated in the acoustic data acquisition systems to enhance high-frequency data previously lost in the tape recorder electronic noise floor for microphones from 110° to 160°. The microphone signal below the 20 KHz 1/3-octave band was filtered out, and the gain was increased to boost the signal to noise ratio. For microphones from 110° to 160°, both the filtered and unfiltered signals were recorded on tape. For data below 20 KHz the unfiltered signal was used to calculate the sound pressure levels while for high frequencies the filtered signal was used. The entire jet noise spectra at a given angle was then obtained by computationally merging these two spectra.

3.3.1.2 Acoustic Data Reduction

Acoustic data reduction is conducted in the General Electric AEG Instrumentation and Data Room (IDR) and is similar for both JENOTS and Cell 41 Anechoic systems as shown schematically in Figure 3-13. The data tapes are played back on a CEC3700B tape deck with electronics capable of reproducing signal characteristics with the specifications indicated for Wideband Group I and Group II. During acoustic testing, a tone is inserted on the tape recorder to mark the point on the tape where recording of the microphone signal for a given acoustic test point is initiated. During the data-reduction phase a tape control unit automatically shuttles the tape, initiating an integration-start signal to the analyzer at this tone as the tape moves in its forward motion. This motion continues until an integration-complete signal is received. Then the tape control unit switches to the next channel, the tape rewinds, and the process is repeated. When all channels are complete, the tape moves forward to the next data point on the magnetic tape.

All 1/3-octave analyses are performed on a General Radio 1921 1/3-octave analyzer. Normal integration time is set for 32 seconds to ensure good integration for the low-frequency content. The analyzer has a 1/3-octave filter set for 12.5 Hz to 100 KHz and has a rated accuracy of ±1/4 dB in each band. Each data channel is passed through an interface to the GEPAC 30 computer where the data are corrected for the frequency response of the microphone and the data acquisition system and corrected to standard day (59° F, 70% relative humidity) atmospheric attenuation conditions per methods discussed in Section 3.3.1.3 for JENOTS and Cell 41 Anechoic Facilities. The output of the computer is passed to a Terminet 300 console where the corrected sound pressure level (SPL) can be printed out on sheets for "quick look"

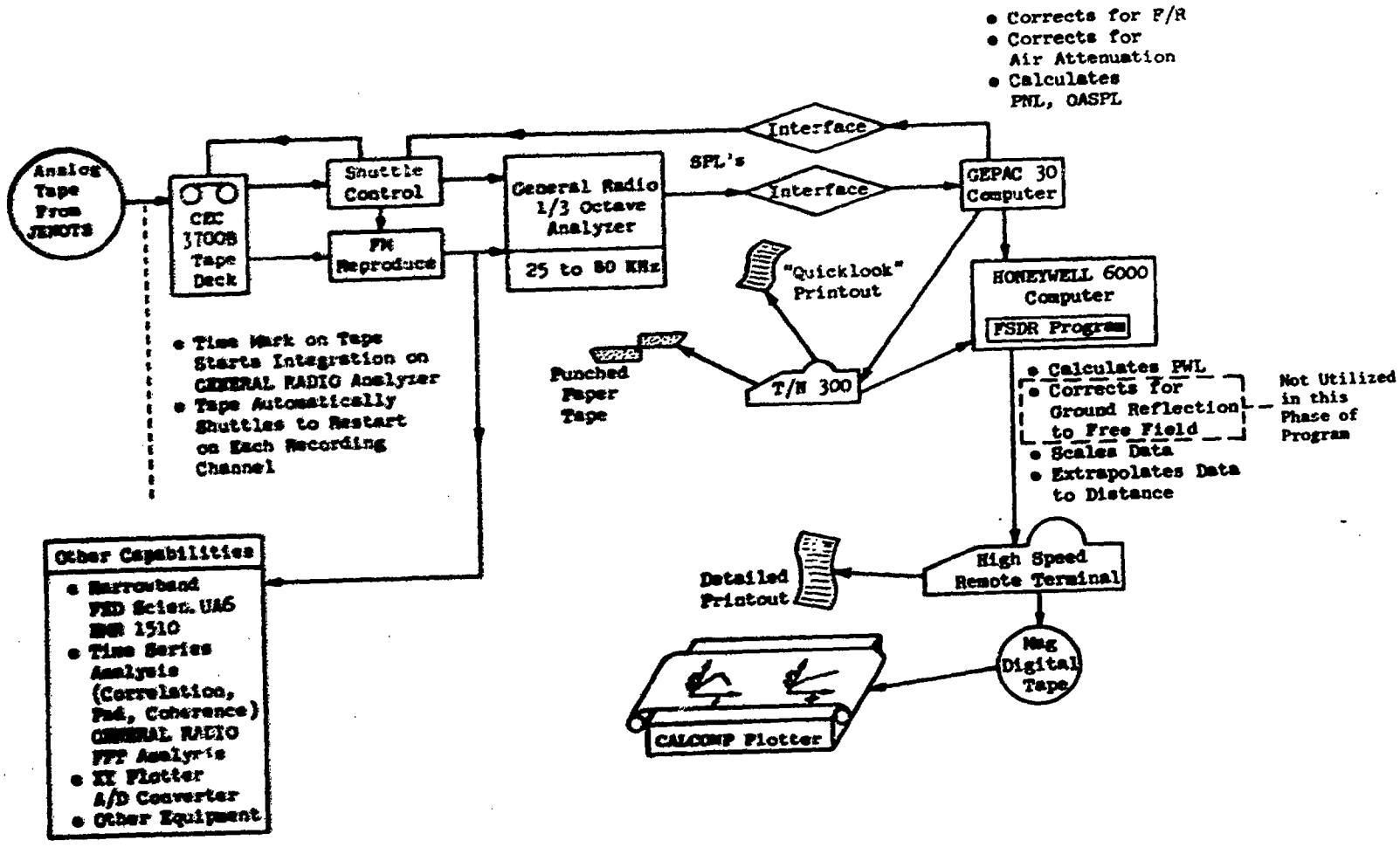

Figure 3-13. Data Reduction System, JENOTS and Cell 41.

analysis. For calculation of acoustic power, corrections for ground reflections to free field, scaling to other nozzle sizes, or extrapolations to different far-field distances, the data are sent to the Honeywell 6000 computer for processing through the full-scale data reduction (FSDR) program where the appropriate calculations are performed. This step is accomplished by accessing the SPL's stored on magnetic tape in the 6000 computer through a 1200-band Modem. The data printout is accomplished on a high-speed "remote" terminal. A magnetic tape is also written for CALCOMP plotting of the data.

3.3.1.3 Air Attenuation Corrections

Acoustic testing is subject to continual changes in meteorological conditions. Correspondingly, the attenuation of sound over the distance from the jet source to the microphone will vary with the environmental fluctuations of temperature and humidity due to differences in atmospheric absorption. It is common practice to attempt to account for these differences by either (1) correcting the data for air attenuation from the measured day values to a "standard day" of 59° F and 70% relative humidity (as has been done for data within this study) or by (2) removing all the air attenuation from the data. These corrections have been calculated using References 13 and 14. This work extended the experimental data of Reference 15 (Harris) taken at 68° F to other temperatures using the theoretical work of Reference 16 (Knesner). Reference 15 experiments, however, were only performed to the 12.5-KHz narrowband, and its corrections are limited to the 8-KHz 1/3-octave band. The need for corrections at higher frequencies led to an extension to 80 KHz (Reference 17). These corrections were developed by extrapolations of the Reference 13 and 14 (ARP866) curves, tempered by the continual experience of comparing scaled jet spectra of nozzles ranging from 1 inch to 4 feet in diameter. The Reference 17 air attenuation model was found to be best suited to the JENOTS outdoor test data and was applied to all data taken on that facility. The model, developed using References 13, 15, and 20, is discussed in Appendix C and also is presented in the form of a computer program listing which is used to generate the high frequency correction factors. Reference 10 discusses the air attenuation correction status in more detail, with particular application to the JENOTS facility data, and presents comparisons of data corrected by use of several techniques. To develop air attenuation corrections for application to acoustic data taken in the more controlled environment of the Cell 41 Anechoic Facility, an extension of Reference 14 to the 80-KHz 1/3 octave band was programmed and used.

3.3.1.4 Data Corrections to a Free-Field Environment-JENOTS

The ground presence at JENOTS affects the propagation of noise reflection/absorption. The approach taken to convert the measured noise data to the "free field" was based on theoretical analysis of the ideal case of an infinitely hard surface, a point source of broadband noise, and a stable homogenous medium (Reference 18). The analysis was modified by a series of tests and parametric studies conducted in Task 1 of this program (Reference 8). This involved the determination of the ground impedance phase factor and

reflection coefficient, an estimate of the scattering phenomenon, and a correction for the distributed source effects of the jet. The results of the calculations are shown in Table 3-5. These values were incorporated into the data reduction program as standard ground reflection corrections for all JENOTS data.

3.3.1.5 Data-Scaling Procedure

The primary function of a scaling procedure is to present test data in a useful form for engineering evaluation. Prior to scaling, the model SPL's are conditioned as described in Section 3.3.1.2 for frequency response of the microphone and the data acquisition system. The JENOTS data are corrected to "free field" per Section 3.3.1.4. These model SPL's are then corrected to the source by removal of extra ground attenuation (per Reference 19) and air attenuations based on the measured ambient meterological conditions, per Section 3.3.1.3. The spectrum frequencies are shifted on a 1/3-octave basis as a function of nozzle diameter ratio (e.g., $\sqrt{A_{full\ scale}/A_{model\ scale}}$). For all data within this study, a full-scale area of 338 $in.^2$ is used; that of the J79 engine's fixed area exhaust nozzle, used for the Acoustic Scaling Demonstration in Volume III. The absolute level is adjusted by the weight flow ratio (which is assumed equal to the square of the diameter ratio). The resultant spectrum is extrapolated to the desired arc or sideline using the inverse square law (20 log distance) and standard day atmospheric absorption as per Section 3.3.1.3. Extra ground attenuation (EGA) is not used in the extrapolation procedure. For most configurations within this study, "full-scale" data were developed at a 160-ft arc and a 2400-ft sideline.

3.3.1.6 Power Level Calculations

The method used to calculate sound power levels from the corrected SPL's is to integrate sound pressure levels assigned to strip areas based on the input microphone radius and acoustic angles of interest. The method used in the computer program is detailed in Appendix B of Reference 10. All levels are corrected to represent full-spherical radiation.

3.3.1.7 Acoustic Data Normalization

For presentation of acoustic results, the data normalization technique developed in Reference 11, modified for inclusion of static ideal gross thrust, was adopted. Reference 11 concluded that the mixed stream properties best govern the overall noise levels (OAPWL, OASPL, $PNL_{max.}$). Selection of mixed stream velocity as the basis for data comparisons has a strong physical attractiveness as it expresses the noise in terms of a velocity calculation based on the thermodynamic conditions of both streams. It also allows comparison of noise values at the same ideal thrust and total mass flow which are meaningful propulsion performance parameters.

Table 3-5. JENOTS Ground Reflections Corrections (ΔdB's to be Added to SPL's).

Frequency (Hz)	θ_I Angle Referenced Inlet													
	30	40	50	60	70	80	90	100	110	120	130	140	150	160
50	-4.99	-4.97	-4.93	-4.88	-4.82	-4.75	-4.66	-4.55	-4.41	-4.24	-4.03	-3.77	-3.46	-3.1
63	-4.45	-4.41	-4.35	-4.29	-4.21	-4.1	-3.98	-3.82	-3.64	-3.42	-3.16	-2.86	-2.52	-2.19
80	-4.0	-4.0	-3.34	-3.23	-3.1	-2.95	-2.76	-2.53	-2.27	-1.96	-1.61	-1.22	-0.83	-0.47
100	-4.0	-4.0	-3.0	-3.0	-3.0	-2.0	-0.7	-0.34	-0.07	0	0	1.6	2.11	2.54
125	-3.5	-4.0	-3.5	-2.0	-2.5	-0.5	1.7	1.0	1.0	2.0	2.0	2.9	3.8	2.8
160	0	01.5	-2.5	-0.5	-1.0	1.5	2.7	1.5	3.0	3.0	2.0	3.0	3.2	2.2
200	-2.0	-1.5	-1.5	-1.0	-1.0	0.5	0	0	0.5	1.0	-0.17	-0.65	-1.03	0
250	0	0	0	-0.5	-1.5	-1.5	-2.5	-2.5	1.5	-1.0	-2.0	-4.48	-4.58	-2.39
315	1.5	0	-1.5	-1.5	-1.5	-1.8	-4.0	-1.5	-3.0	-3.0	-3.0	-4.9	-5.09	-2.0
400	-2.0	-4.2	-4.1	-3.5	-2.5	-3.2	-3.1	-2.34	-1.85	-1.34	-4.9	-0.37	-0.7	-4.3
500	-1.0	-1.0	0	-1.3	-1.1	-1.2	-1.1	-1.35	-1.14	-1.87	-2.1	+1.8	-0.5	-0.5
630	-1.64	-1.5	-1.0	-2.5	-2.0	-3.2	-2.1	-2.09	-2.03	-3.5	-3.5	-1.64	-1.3	-0.9
800	-1.55	-1.35	-1.12	-1.0	-1.0	-2.0	-2.1	-0.88	-1.22	-0.5	-1.05	-0.5	-0.8	+2.2
1000	-1.0	-2.44	-1.3	-2.36	-2.3	-2.13	-1.9	-1.72	-1.47	-1.22	-2.1	-1.9	-0.71	-0.8
1250	-1.97	-2.03	-2.10	-2.17	-2.24	-2.28	-2.3	-2.28	-2.24	-2.18	-2.12	-2.08	-2.04	-2.2
1600	-2.17	-1.5	-2.06	-1.98	-1.90	-1.83	-1.8	-1.83	-1.93	-2.07	-2.23	-2.36	-2.45	-2.5
2000	-0.74	-2.0	-2.8	-0.92	-1.11	-1.37	-1.7	-1.90	-2.05	-2.10	-2.06	-1.97	-1.88	-1.8
2500	-1.5	-2.0	-1.8	-2.84	-2.70	-2.52	-2.35	-2.29	-2.31	-2.37	-2.45	-2.51	-2.54	-2.56
3150	-2.5	-2.57	-2.60	-2.66	-2.78	-2.93	-3.1	-3.14	-3.07	-2.91	-2.75	-2.65	-2.6	-2.59
4000	-2.80	-2.78	-2.74	-2.66	-2.58	-2.55	-2.60	-2.67	-2.72	-2.72	-2.72	-2.72	-2.72	-2.71
5000	-2.6	-2.72	-2.77	-2.84	-2.90	-2.85	-2.60	-2.41	-2.36	-2.44	-2.52	-2.56	-2.58	-2.59
6300	-2.70	-2.68	-2.64	-2.59	-2.56	-2.64	-2.90	-2.97	-2.85	-2.72	-2.68	-2.66	-2.66	-2.66
8000	-2.75	-2.76	-2.75	-2.73	-2.67	-2.60	-2.70	-2.80	-2.78	-2.74	-2.72	-2.71	-2.7	-2.7
10000	-2.69	-2.69	-2.68	-2.67	-2.67	-2.71	-2.80	-2.70	-2.60	-2.63	-2.65	-2.65	-2.65	-2.65
12500	-2.70	-2.70	-2.71	-2.69	-2.69	-2.70	-2.70	-2.70	-2.66	-2.66	-2.66	-2.66	-2.66	-2.66
16000	-2.61	-2.61	-2.61	-2.60	-2.58	-2.56	-2.70	-2.60	-2.57	-2.57	-2.57	-2.57	-2.57	-2.57
20000	-2.63	-2.63	-2.63	-2.62	-2.61	-2.61	-2.70	-2.56	-2.60	-2.60	-2.59	-2.59	-2.59	-2.59
25000	-2.71	-2.71	-2.71	-2.70	-2.70	-2.69	-2.70	-2.68	-2.68	-2.67	-2.67	-2.67	-2.67	-2.66
31500	-2.74	-2.73	-2.73	-2.73	-2.72	-2.72	-2.70	-2.71	-2.71	-2.70	-2.70	-2.69	-2.69	-2.69
40000	-2.71	-2.71	-2.71	-2.71	-2.70	-2.70	-2.70	-2.69	-2.68	-2.68	-2.68	-2.67	-2.67	-2.67
50000	-2.73	-2.73	-2.73	-2.73	-2.72	-2.72	-2.70	-2.71	-2.70	-2.70	-2.70	-2.69	-2.69	-2.69
63000	-2.70	-2.70	-2.70	-2.69	-2.69	-2.68	-2.70	-2.68	-2.67	-2.67	-2.66	-2.66	-2.66	-2.65
80000	-2.72	-2.72	-2.72	-2.71	-2.71	-2.71	-2.70	-2.70	-2.69	-2.69	-2.68	-2.68	-2.68	-2.68

In general, acoustic data will be presented as:

$$\text{Noise value} - 10 \log_{10} \left[F_s (T_o/T_{sm})^{\omega-1}\right] \text{ vs. } V_{ma},\ f, \text{ or } \theta$$

where:

Noise value = PNL, OASPL, OAPWL, OR 1/3 OBSPL

F_s = Static ideal gross thrust (sum of inner and outer streams)

T_o = Ambient temperature, ° R

T_{sm} = Static temperature corresponding to mass averaged velocity, V_{ma}, and total temperature, T_{Tma}, ° R.

ω = Jet density exponent (per SAE ARP 876) based on mass-averaged velocity, V_{ma}

$$V_{ma} = \frac{W_i V_i + W_o V_o}{W_i + W_o} \quad \text{(Mass-Averaged Jet Velocity, ft/sec)}$$

$$T_{Tma} = \frac{W_i T_{T_i} + W_o T_{T_o}}{W_i + W_o} \quad \text{(Mass-Averaged Total Temperature, ° R)}$$

where W and T_T are the exit plane values of mass flow and total temperature for the inner and outer (subscript i & o) streams, respectively, and f & θ are 1/3-octave-band center frequency and angle relative to inlet axis. In the case of turbojet test data, the flow parameters revert to the single-stream notation.

On occasion, for ease of data handling and presentation, the normalization seen on graphs will be:

Noise value -N, where:

$$N = 10 \log_{10} \left[F_s/10{,}000\ (T_o/T_{sm})^{\omega-1}\right]$$

The introduction of a 10,000-lb reference thrust shifts noise levels by 40 dB and allows plotting of all positive values of the low-level sideline noise data.

3.3.2 Laser Velocimeter Data

The laser velocimeter system was developed by General Electric during the AF/DOT Supersonic Jet Exhaust Noise Investigation (Reference 21) for measurement of mean and rms turbulent velocities in high-temperature, high-

velocity jets. The basic optics system is a differential Doppler, backscatter, single-package arrangement that has the proven feature of ruggedness for the severe acoustic environment. The LV is a noncontacting optical system in which the velocities of the seed particles are measured (in a single direction) as they pass through the fringes of an interference pattern created by two intersecting beams of coherent radiation. Figure 3-14 shows a schematic arrangement of the laser package used on this program. The laser beams are projected from below the lens, forming an angle, α, that keeps the major axis of the control volume ellipsoid to a minimum. The dimensions of the control volume are 0.25 inch for the major axis and 0.020 inch for the minor axis. The range of the LV control volume from the laser hardware was 85 inches. At this distance from the jet, a protective enclosure is not necessary. The three steering mirrors and the beam splitter are mounted on adjustable supports, all of the same aluminum alloy which eliminates temperature-alignment problems. References 21, 22, and 23 contain detailed descriptions of the system and its validation, as well as results for measurements on scale-model nozzles under static conditions.

The setup of the laser velocimeter (and ellipsoidal mirror) at JENOTS is shown in Figure 3-15(a) and the LV within the Cell 41 Anechoic Facility in Figure 3-15(b). At JENOTS the LV optics package is mounted on a remotely actuated platform on tracks parallel to the jet axis. Since the LV has a fixed working range of 85 inches, measurements at different points in the jet are accomplished by traversing the platform along three axes: horizontal, vertical, and axial (jet axis). Travel capabilities along the three axes are 32, 32, and 240 inches, respectively. Resolution is ±1/16 inch for each axis except for the last 208 inches of axial travel which has a resolution of ±1/8 inch.

Within the anechoic facility, the track is located on the northwest side of the chamber at a position approximately 13 feet from the nozzle axis. The traverse span ranges from approximately 2 feet below the nozzle discharge plane to approximately 17 feet above the nozzle discharge plane (see Reference 8).

The cart and lift have a rated load capacity of 3600 pounds. It rides on precision-aligned rails made of hardened steel for wear resistance and accurate positioning. The track extends through a sliding concrete hatch, via a hinged section of track, to the floor of the auxiliary room to permit interchanging the EN and LV systems as required. Traversing operation of the cart on the track can be accomplished from either the test chamber, auxiliary room, or control console. Remote position indication is provided by means of a 10-turn potentiometer driven off the winch shaft, with readout at the control console. The ability to record the position signal on magnetic tape in conjunction with the acoustic data for subsequent correlation is provided.

At both facilities the LV can be operated in a traversing mode to obtain continuous profiles of mean axial velocity, or it can be operated in a stationary mode to construct velocity histograms for determination of both mean and rms turbulent axial velocities at discrete points.

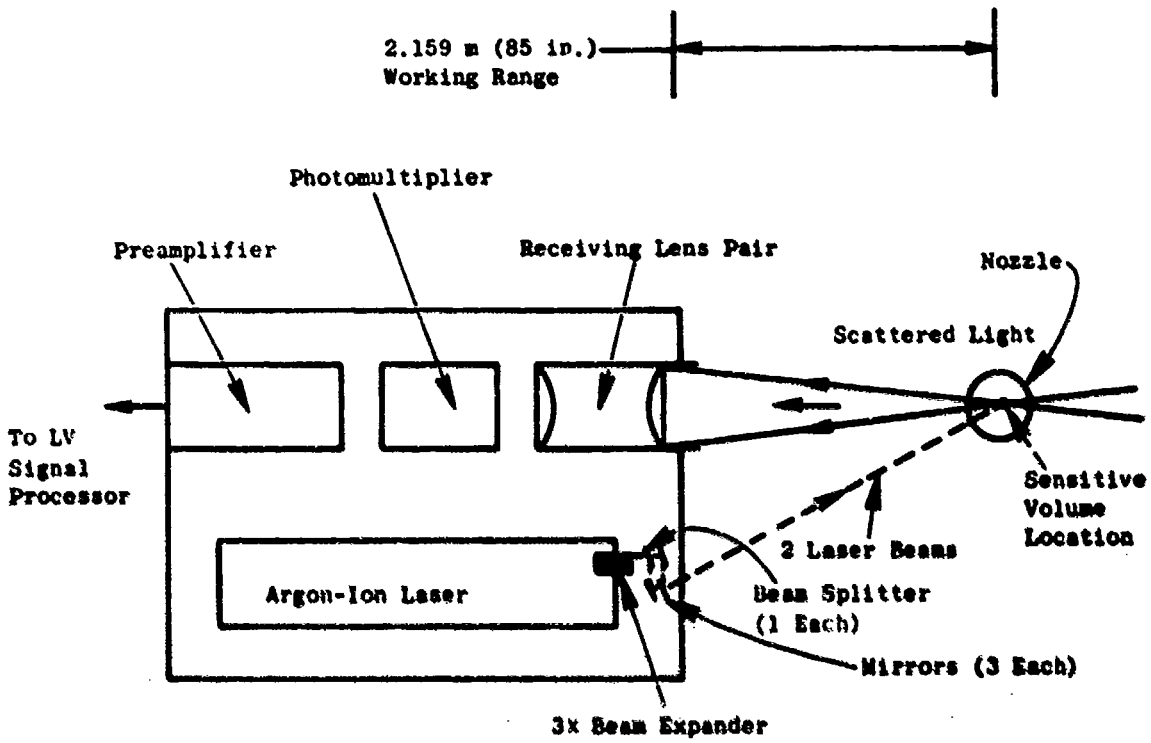

Figure 3-14. Schematic of Laser Velocimeter Optics Package.

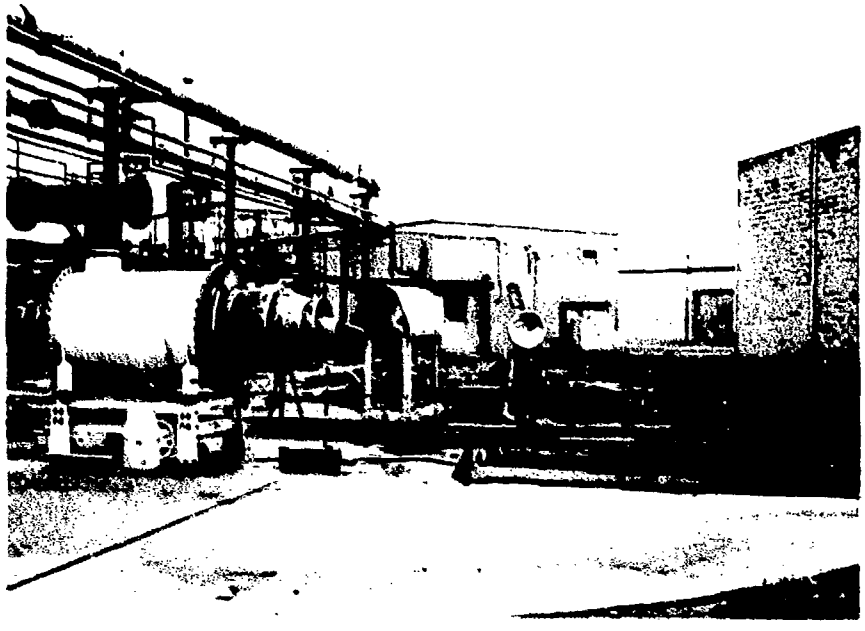

Figure 3-15(a). Laser Velocimeter and Ellipsoidal Mirror at JENOTS.

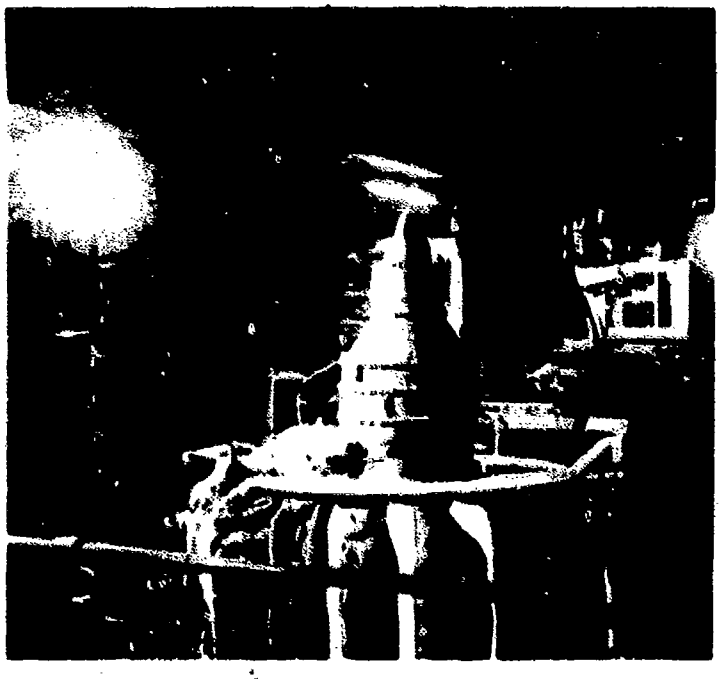

Figure 3-15(b). Laser Velocimeter in Cell 41 Anechoic Facility.

Traverses can be made along any of the three LV axes. In this mode of operation, the velocity levels and positions of incoming data are continuously recorded by an x-y plotter. Sampling rates on the order of at least 250 samples per inch of travel are typical for good definition. If data rates are low or details of a profile are not clear, the traversing speed can be reduced or portions of the traverse can be repeated one or more times. Better definition also can be obtained by executing the traverse as a series of "stutter" steps, with short pauses interspersed to accumulate additional data.

Histograms are located at strategic points to verify details from the mean velocity traverses and to obtain rms turbulence levels. The histogram is formed from a large number of samples, typically 500 to 1000.

Seeding is by injection of aluminum oxide (Al_2O_3) powder, a nominal 1-μm diameter, into the supply air to the burner and into the region of the nozzle so as to seed the entrained air. The powder-feeder equipment used is described in Reference 23 except that the fluidized bed column supply air was heated to about 250° F to prevent powder aggregation by moisture absorption.

This LV setup is used only for exhaust plume surveys and is removed during acoustic tests.

The concept of using laser velocimeter measurements for obtaining routine mean and turbulent-velocity profiles may be described in the following simple fashion. Two beams of monochromatic light intersect at a point in space and set up a fringe pattern of known spacing (see Figure 3-16). The flow is seeded with small particles which pass through the measuring volume; the light scattered from the particles is collected, and the laser signal processor measures the time it takes for the particles to pass through each fringe. Knowing the distance and the time for each validated particle enables the construction of the usual histogram (see insert on Figure 3-16). Then, by statistical techniques, the mean value (which corresponds to the mean velocity) and standard deviation (which corresponds to the turbulent velocity) are constructed. The method of calculation used to obtain the mean velocity and turbulent velocity from laser velocimeter measurements is described below.

A histogram is an estimate of the first-order probabilitiy density of the amplitude of a given sample. To obtain a velocity histogram, the time-dependent laser velocimeter velocity, V(t), is accumulated and divided into classes bounded by values of velocity increments, V_i. For each independent sample of velocity, a class interval is formed such that $V_i \leq V(t) \leq V_{i+1}$. During a measurement period, k_i number of velocity samples accumulated in each sample class, V_i. From the total sample of measured velocity points, the histogram is constructed as shown in Figure 3-16.

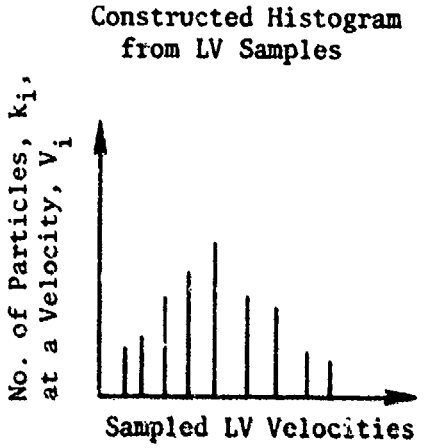

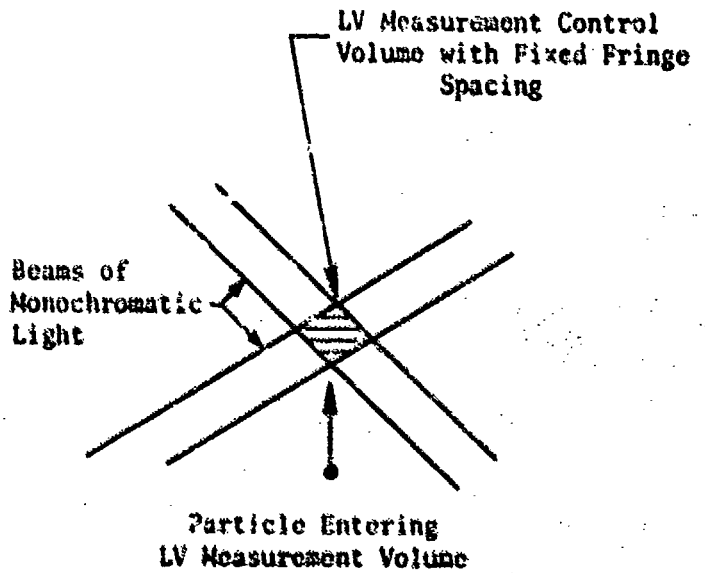

Figure 3-16. Schematic of Laser Velocity Measurements.

The mean velocity of the jet, $\bar{V}_j$, obtained from the discrete velocity samples is calculated by:

$$\bar{V}_j = \sum_{\substack{\text{All Class} \\ \text{Intervals}}} \left(\frac{V_{i+1} + V_i}{2} \right) \frac{k_i}{N}$$

where

$\frac{V_{i+1} + V_i}{2}$ is the value of the sampled axial velocity component at the center of the class interval.

K_i is the number of velocity samples in the class interval.

N is the total number of velocity samples ($\Sigma_i k_i$) in the histogram.

To obtain the axial turbulent velocity, u', from the sampled data contained in the histogram, the standard square root of the statistical variance is performed. This calculation is performed using the following equation:

$$u' = \left[\sum_{\substack{\text{All Class} \\ \text{Intervals}}} \frac{\left(\frac{V_{i+1}+V_i}{2} - \bar{V}_j \right)^2 k_i}{N} \right]^{1/2}$$

Reference 10 discusses the statistical errors for LV mean and turbulent velocity measurements. Discussions of LV turbulence spectra and in-jet far-field cross correlation measurements are treated in Reference 8.

3.3.3 Ellipsoidal Mirror Data

The ellipsoidal mirror (EM) was identified in Task 1 of this program (Reference 8) as a fast, flexible method of obtaining macroscopic noise source location information for a jet plume. Measurements were made on cold-flow, round, static jets to establish the basic capabilities of the technique. Measurements taken within Task 4 of this program (Reference 12) demonstrated the ability of the EM to detect variations of source distributions among different geometric nozzle configurations and between various levels of free-stream velocity for heated-flow jets. Task 3 continued the development of EM data acquisition and processing systems and further evaluated the accuracy of the technique. Appendix D is a comprehensive "Summary of Ellipsoidal Mirror Development" and treats in detail the development and evaluation of the EM technique. Task 3 additionally acquired heated-flow source location data on a total of 26 base-line and suppressor model configurations of the single (TJ) and dual-flow families. For the

test work, an 18-inch shallow-dish mirror and a 34.654-inch deep-dish mirror were used for the JENOTS and Cell 41 Anechoic Facility, respectively. Schematics and a summary of EM characteristics are presented in Figure 3-17. The mirror systems were calibrated for window function and gain; the window function representing the sensitivity of the system to discriminate between adjacent sources. Calibration results for the two systems in terms of gain and normalized window function width are also discussed in Appendix D. The deep-dish mirror, while not showing as good agreement with theoretical trends, showed higher gain and slightly narrower window function relative to the 18-inch shallow-dish mirror.

For each EM system, data are recorded on magnetic tape over a full length of "outbound" traverse. The microphone signal, DC cart position, and time code signals are all recorded using the standard acoustic data acquisition systems of the facilities discussion in Section 3.3.1.

Data reduction is a two-phase procedure consisting of (1) conversion of the raw analog data to digitized spectral distributions and (2) numerical processing (deconvolution procedure) of these results to correct for the effects of mirror gain and diffraction window function. After deconvolution, the distributions represent total source contributions at each axial position (i.e., a slice of jet measurements). Studies were performed for selection of the best deconvolution technique (the relaxation technique was selected) and for the effect of presmoothing data. These studies led to the adoption of improved data reduction procedures and also assessed the limitations and sources of errors from three areas: (1) theoretical limitations, (2) data acquisition errors, and (3) data processing errors and limitations. The major sources of errors encountered in processing EM data are:

1. Statistical errors due to insufficient averaging time.

2. Enhancement of ambient or electronic noise, or of statistical measurement errors, due to an ill-conditioned window function matrix.

3. Limits on achievable resolution due to numerical instabilities in the solution of an ill-conditioned set of equations.

4. Errors induced by uncertainty in window function measurements.

Data analysis can be interpreted as (1) axial source intensity distributions for individual 1/3-octave bands or (2) source spectra at discrete axial positons. The results are most readily summarized in terms of the axial locacation of the peak intensity for each frequency band: i.e., fD/V versus x/D.

For 1/3-octave band analyses, two processing cycles normally are performed using 1 and 4 second integration times for the JENOTS 18-inch mirror and 2 and 8 second times for the anechoic facility deep-dish mirror. The two cycles accommodate high and low frequency requirements over the 500 Hz to 40 KHz frequency range used.

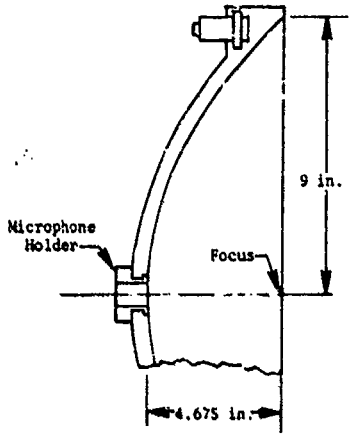

(a) 18-inch-Diameter Shallow-Dish EM with 9-foot Working Distance.

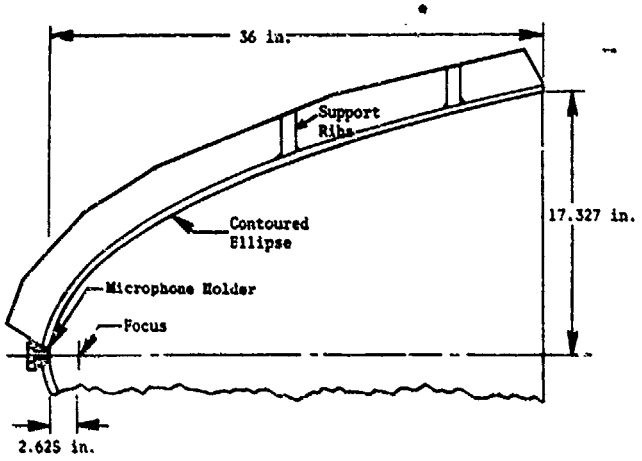

(b) 34.654-inch-Diameter Deep-Dish FM with 15-foot Working Distance.

(c) Summary of Ellipsoidal Mirror Characteristics.

Facility	Anechoic	JENOTS
Mirror Diameter	34.654 in.	18.0 in.
Mirror Length	36.0 in.	4.675 in.
Focal Length	2.625 in.	4.675 in.
Working Distance	180.0 in.	108.0 in.
Mirror Aperture	4° 44′	4° 48′
Eccentricity	0.971	0.930
Traverse Speed (Approximate)	1.9 ft/min	3.8 ft/min
Traverse Distance (Approximate)	20 ft	20 ft
Traverse Direction (Jet Axis)	Vertical	Horizontal
Microphone Type	¼ in. B&K 4136 Without Grid	¼ in. B&K 4136 Without Grid
Microphone Orientation	Toward Mirror	Toward Source

Figure 3-17. Schematics and Summary of Ellipsoidal Mirror Characteristics.

Mirror cart position is gaged from brush chart reduction of cart position signal, overall sound level, and time code.

Integral closure checks can be performed to see if the measured far-field noise signature can be calculated from the measured source distribution. This check does not guarantee that the source measurements are correct but establishes a confidence level in the results which can be used to identify ranges of variables for which a given technique is definitely not valid. Integral closure checks have shown (as a minimum) that the deconvolved source distributions generally appear to be valid over the 1-KHz to 20-KHz and 500-Hz to 10-KHz frequency ranges for the 18-inch shallow-dish and the 34.654-inch deep-dish mirrors, respectively.

An error analysis of the EM technique was also performed as a part of Task 3's continued evaluation of source measurements techniques and is treated in detail in Appendix E. This appendix evaluates the window function removal technique, or the way in which the acoustic sources are combined by the mirror to yield the measurement values. The appendix describes (1) the model for EM error analysis, (2) the technique for computing the estimate and invertability of the A-matrix, (3) estimator variance and bias, (4) errors induced by window function measurment uncertainty, and (5) a numerical evaluation study. The following conclusions were suggested.

1. A small elliptical mirror, such as the 18-inch mirror developed for this program, is capable of obtaining useful data when:

   - The source frequency is greater than 1000 Hz
   - The source dynamic range is less than 25 dB
   - The source spacing is greater than 0.5 inch
   - The measurement accuracy required is more than ±2.5 dB

2. The window function removal procedure is very sensitive to any error.

3. The presence of errors in analyzed data may be difficult to detect due to high correlation between adjacent errors. Check procedures should be included in the data reduction procedure to guarantee the data quality.

3.4 DATA ANALYSIS

The preceding sections have described the test models, test matrices, facilities, and data reduction procedures utilized in performing this study. This section will present the acoustic results in terms of noise characteristics as a function of velocity, directivity, and spectra. The data presented will, in most cases, be normalized per the parameters discussed in Section 3.3.1.7.

Section 3.4.1 presents the acoustic results of tests related to baseline nozzle configurations, e.g., conical, plug, and coplanar-coannular nozzles. Section 3.4.2 presents the acoustic results of tests designed to define the influence of geometric and cycle variations on the suppression characteristics of single- and dual-flow suppressor nozzles. Parameters investigated include chute area ratio, radius ratio, inner stream flow management and geometric variations, flow segmentation, element-type variation, and the application of treated ejectors. Section 3.4.3 pesents the suppression levels which occur in flight based on a series of scale-model free-jet measurements. Conical, plug, chute, and tube nozzle suppression characteristics are discussed. Sections 3.4.4 and 3.4.5 present the results of laser velocimeter and ellipsoidal mirror diagnostic measurements on several baseline and suppressor nozzles.

3.4.1 Tests Related to Baseline Nozzle Configurations

This section presents the acoustic results of tests related to baseline nozzle configurations. PNL, OASPL, and spectra acoustic characteristics are established for conical, plug, and coplanar-coannular nozzles. Sections 3.4.1.1 and 3.4.1.2 establish the noise characteristics of conical and convergent-divergent plug nozzles. The conical nozzle data are used as a reference to establish suppression levels throughout the rest of this report. Section 3.4.1.3 discusses the impact of plug radius ratio variation on the various noise parameters. Section 3.4.1.4 discusses the acoustic characteristics of a coplanar-coannular nozzle having an outer to inner flow area ratio, A_O/A_I, of 2.0. Section 3.4.1.5 presents the acoustic results of parametric test series using coplanar-coannular nozzles of A_O/A_I = 0.4, 0.65, and 2.0. The acoustic changes caused by reducing the inner flow to zero or less than 10% of the outer stream are discussed in Section 3.4.1.6.

3.4.1.1 Baseline Conical Nozzles (Models 1, 14)

This study was conducted to establish baseline noise levels using a conical nozzle, tested at both the JENOTS and Cell 41 Anechoic Facility. Subsequent test data for other baseline systems (i.e., C-D plug, high radius ratio plug, annular nozzles, and dual-flow coannular-coplanar nozzles) and for mechanically suppressed systems (i.e., single- and dual-flow multielement suppressors) are referenced to these conical nozzle data for gaging overall system acoustic effectiveness and to identify dominant regions of suppression. Since both JENOTS and the Cell 41 Anechoic Facility were used at

various stages of the Task 3 program (see Section 3.1, Table 3-1) to generate parametric noise data, a common baseline test for each facility was conducted. A 4.64-inch exit diameter conical nozzle was selected with a 2.3° internal converging flowpath angle, as per Appendix A, Figure 1. Adapted to the JENOTS facility, the nozzle is designated Model 1. The same nozzle adapated to the Cell 41 Anechoic Facility is designated Model 14.

To develop a referee data base across a wide span of cycle conditions, Models 1 and 14 were tested using the matrices of Section 3.2.1 Figure 3-2(a) and 3-2(b), respectively. The JENOTS test matrix included constant total temperature lines at T_T = amb, 1000°, 1250°, 1300°, 1450° and 1500° R. The Cell 41 Anechoic Facility matrix included (a) constant total temperature lines at 700°, 850°, 1000° and 1500° R, and (b) constant static temperature lines at 1000° and 1500° R. The matrices were developed to span the cycle conditions intended for subsequent suppressed nozzle tests. Additionally, the Model 14 matrix included sufficient test points to acquire parametric data influenced by shock cell noise. These data were used in Volume 1, Section 4.1 (Jet Noise Mechanisms) and within the subsequent studies of this volume in comparing nonconical nozzles to determine effectiveness of shock noise suppression. Details of the aerodynamic cycle data, along with basic noise information for both models, are included in the Appendix B tabulations.

Acoustic test results for the conical nozzles are presented in terms of normalized OASPL, PNL, and OAPWL versus mass-averaged velocity (V_{ma}). The mass-averaged velocity for a single-flow nozzle coincides with the fully expanded isentropic velocity. This is the format for most other baseline and suppressed nozzle configurations. See Section 3.3.1.7 (Acoustic Data Normalization) for definition of the normalization technique. The following data sets are included:

Figures 3-18 and 3-19	Peak OASPL and PNL
Figures 3-20 and 3-21	90° OASPL and PNL
Figures 3-22 and 3-23	50° OASPL and PNL
Figure 3-24	OAPWL

Part (a) of each graph is Model 1 (JENOTS) data corrected to free-field, and part (b) is Model 14 (Cell 41 Anechoic Facility) data. Each of the data sets have data-fitted curves applied. These data-fitted curves are used as the primary basis of comparing the PNL, OASPL, and OAPWL distributions with V_{ma}. For Figures 3-18, 3-19, and 3-24, i.e., peak OASPL, peak PNL and OAPWL, the data-averaged curves are transferred to part (c) of the graph where they are compared to predicted noise levels. For the 90° and 50° data sets, Figures 3-20 through 3-23, part (c) has only predicted noise levels and associated data-fitted curves generated using the Model 14 aero cycle data. To predict these noise levels, the method adopted in Volume 1, Section 3.3.2 (Conical Nozzles) was utilized. The method consists of the SAE ARP 876 proposed revision (see Volume 1, Appendix C) for predicting single-stream jet-mixing noise modified by increasing the predicted levels by 1.0 dB to bring it in line with the unapproved revision being considered in early 1978 by the SAE Jet Noise A-21 Subcommittee. The single-stream, shock-cell noise prediction procedure, Reference 24, proposed to the SAE Subcommittee, was also adopted.

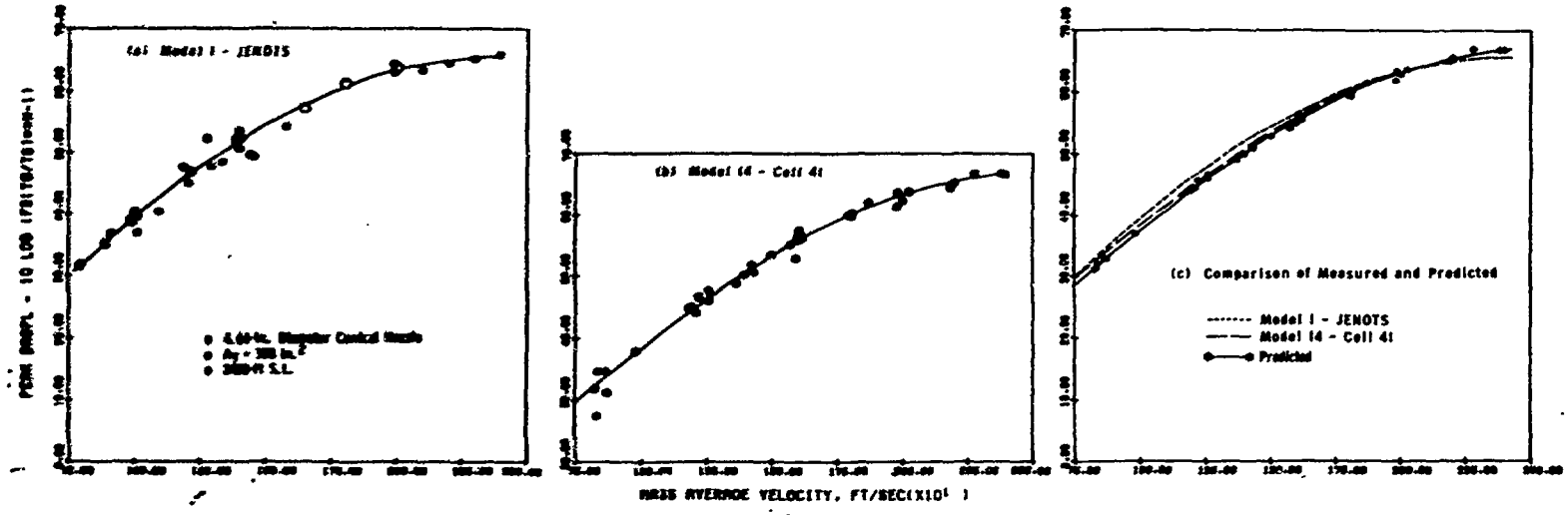

Figure 3-18. Summary of Conical Nozzle (Models 1 and 14) Peak OASPL Characteristics.

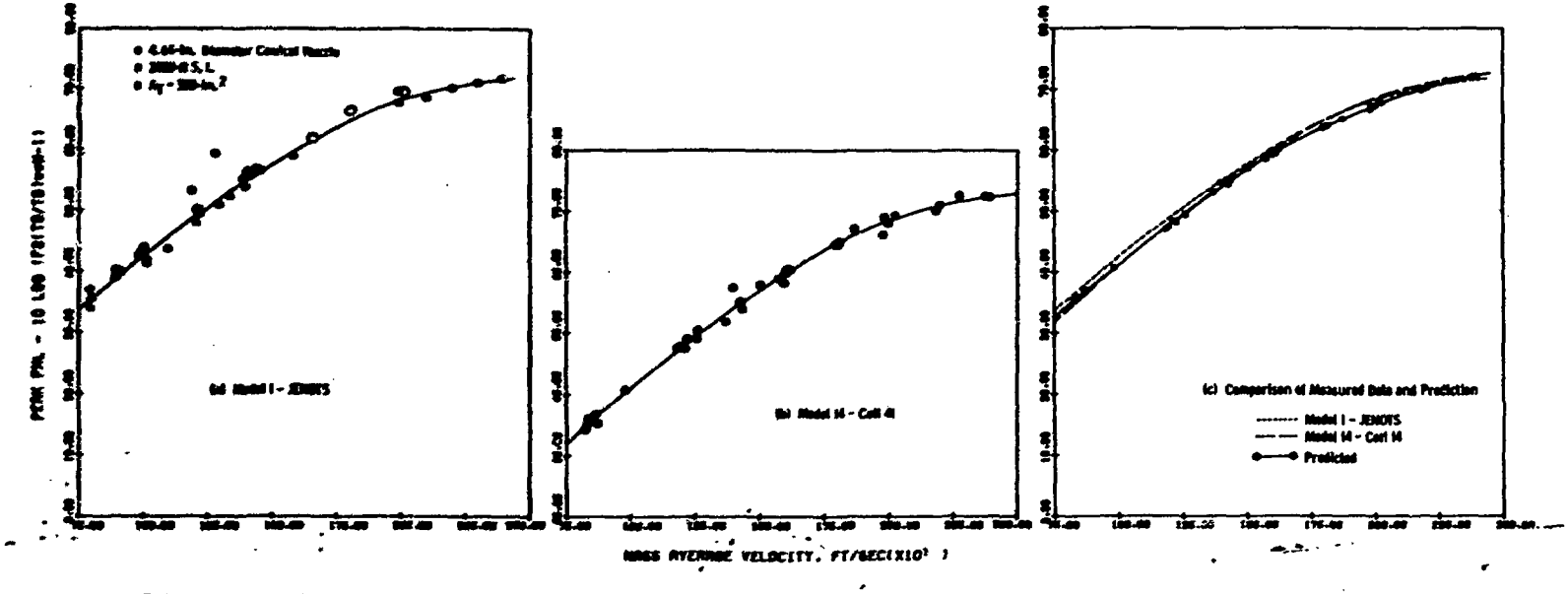

Figure 3-19. Summary of Conical Nozzle (Models 1 and 14) Peak PNL Characteristics.

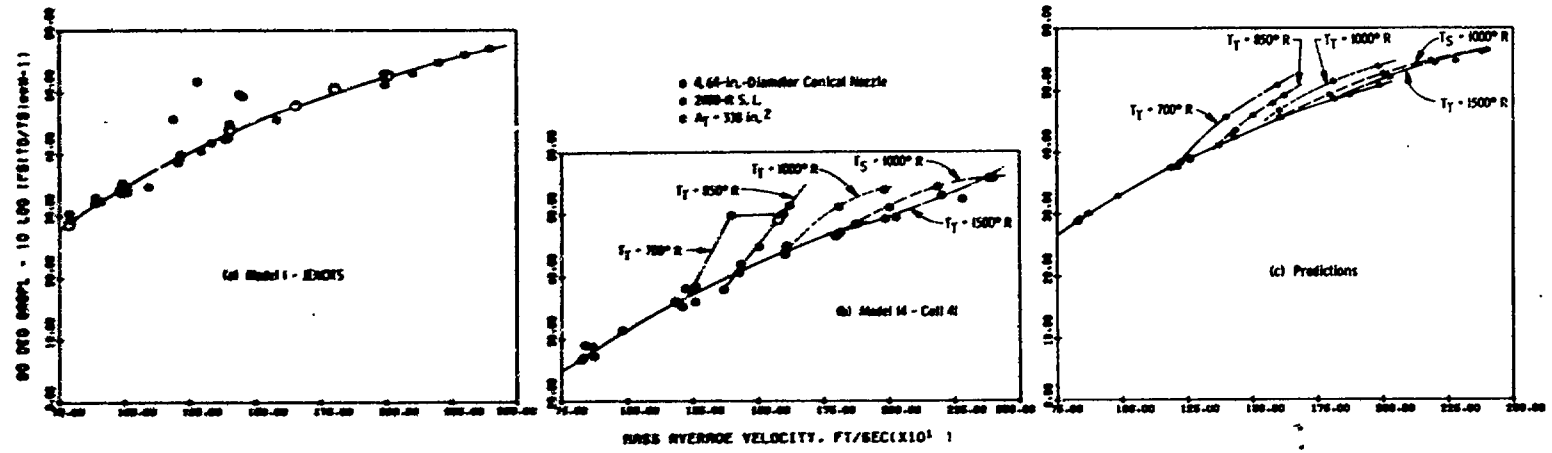

Figure 3-20. Summary of Conical Nozzle (Models 1 and 14) 90° OASPL Characteristics.

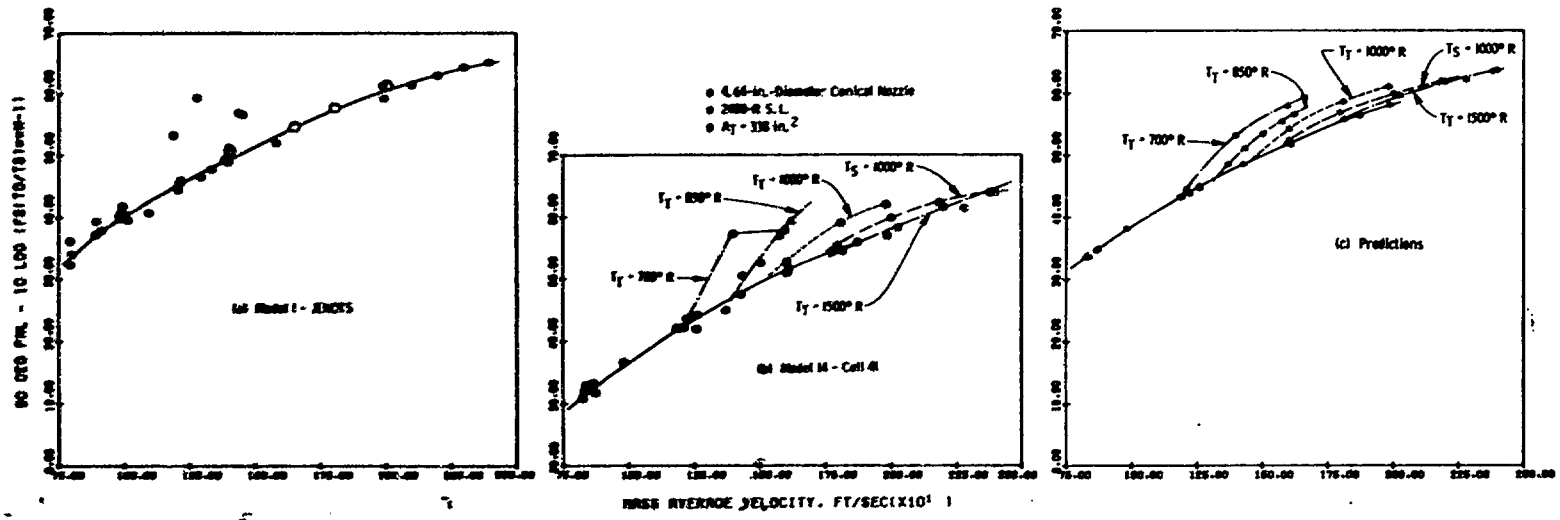

Figure 3-21. Summary of Conical Nozzle (Models 1 and 14) 90° PNL Characteristics.

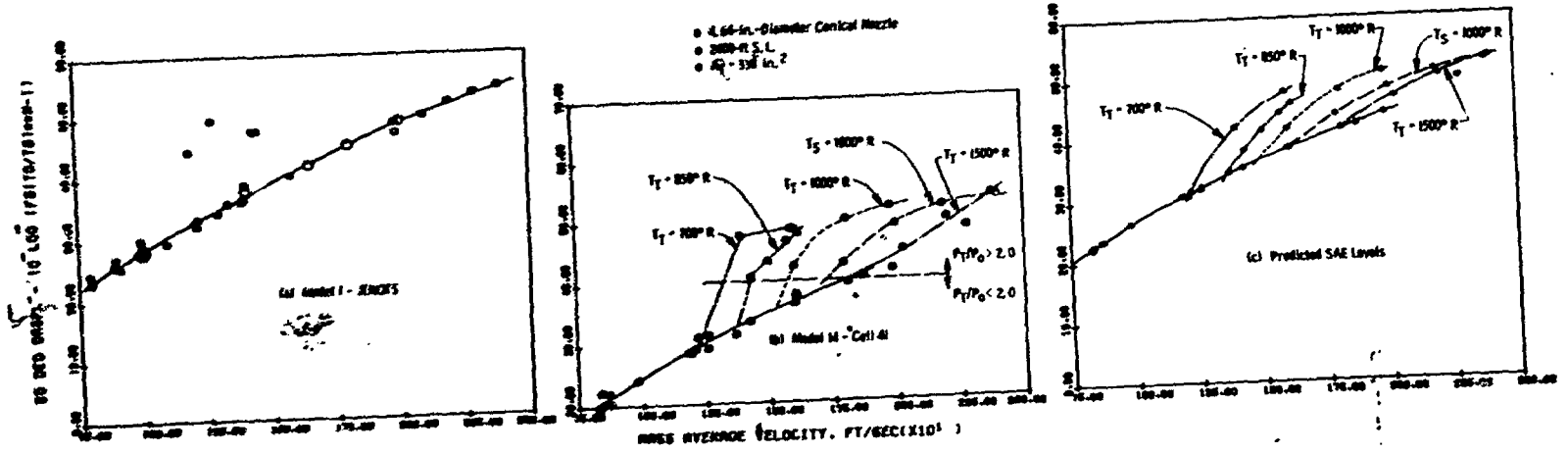

Figure 3-22. Summary of Conical Nozzle (Models 1 and 14) 50° OASPL Characteristics.

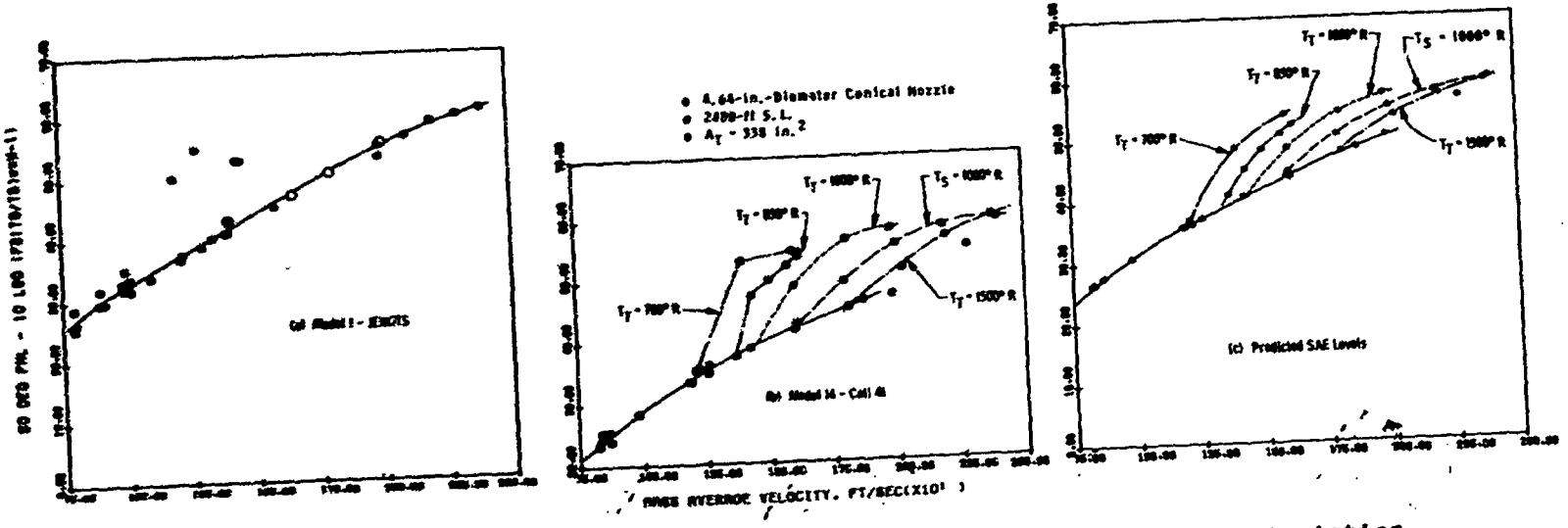

Figure 3-23. Summary of Conical Nozzle (Models 1 and 14) 50° PNL Characteristics.

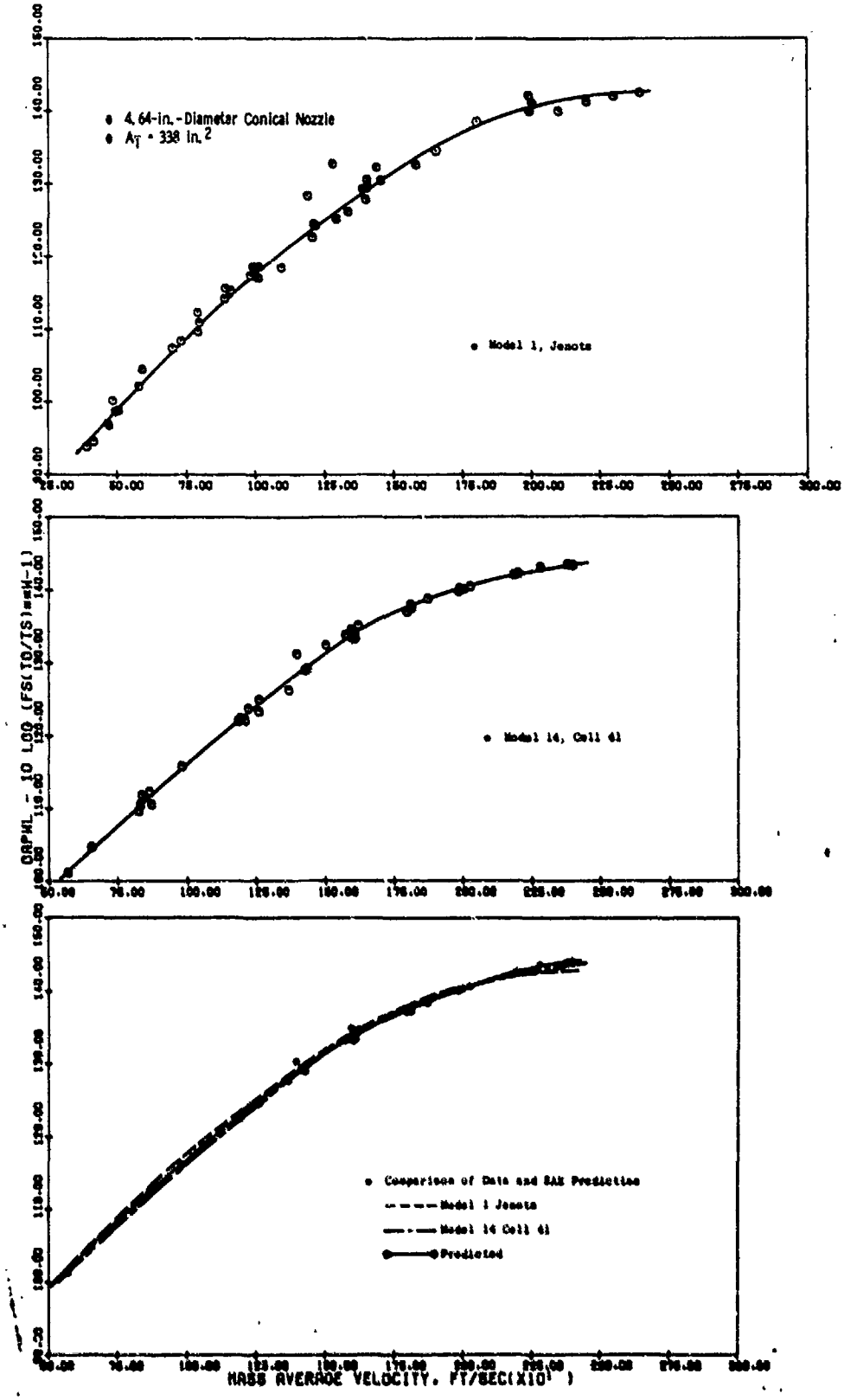

Figure 3-24. Summary of Conical Nozzle (Models 1 and 14) Power Level Characteristics.

The comparisons made in Figures 3-19 and 3-20, part (c), for peak OASPL and PNL show very good agreement among data from the two facilities, the data-averaged curves normally agreeing within ±0.5 dB. Relative to predicted data curves, the maximum deviation is about 1 to 2 dB in the midvelocity region, measured data falling above predicted.

Although the peak-noise variance for the two facilities is small, the individual facility conical nozzle data are used for comparing other test model results, rather than using a composite average. Similarly, when comparing individual data point PNL, OASPL, directivity, spectra, etc., single-point conical nozzle data from the same facility are used.

At 90° and 50° (Figures 3-20 through 3-23), deviations between the two baselines are more significant, particularly in the supercritical operational regime where Model 14 cycle conditions primarily followed a shock-cell noise evaluation matrix. For Model 14, variation of shock-cell influenced noise with V_{ma}, as a function of T_T = 700°, 850°, 1000°, and 1500° R and T_S = 1000° R, is distinctly identifiable in the broadside (90°) and forward quadrant (50°) data. Part (c) of Figures 3-20 through 3-23 shows predicted noise values based on the aero cycle data of Model 14. They, too, follow similar distinct trends associated with turbulent mixing noise at low velocity and with shock-cell generated noise in the supercritical regime of operation. Note that the data are all normalized with respect to temperature and the low-velocity (turbulent mixing noise dominated) points correlated well around the mean data line. The higher velocity supercritical pressure ratio points (dominated by shock-cell noise, which is independent of temperature) do not collapse around the mean line. An approximate distinction between points above and below P_T/P_0 = 2.0 is included on Figure 3-22. The predicted and measured power levels are summarized on Figure 3-24.

Shock-cell noise and its importance as a noise mechanism for supersonic choked jets is discussed in detail in Volume 1, Section 4.1 (Jet Noise Mechanisms), and in Task 2 (Reference 7) Section 4.6 (Shock-Cell Noise). According to experimental correlations for conical nozzles, it was shown that the OASPL should be only a function of the pressure ratio parameter as given by $\beta = \sqrt{M^2-1}$. Model 14 90° and 50° OASPL data from Figures 3-20 and 3-22 are replotted as a function of β in Figure 3-25, now unnormalized for temperature. The data for all temperature values now collapse close to a line which varies as β^4. Deviation from this line occurs at low values of β as the mixing noise begins to dominate the spectrum when shock strength diminishes. As an extension of this empirical correlation to the subjective PNL basis, Model 14 90° and 50° data from Figures 3-21 and 3-23 are replotted in Figure 3-26 versus the β parameter. They, too, show insensitivity to temperature and collapse well around the β^4 line.

To illustrate the acoustic characteristics of the conical baseline over isovelocity and isotemperature lines of cycle operation, the following OASPL and PNL directivity sets, plus spectra at 50°, 70°, 90°, 110°, 130° and 150°, are included:

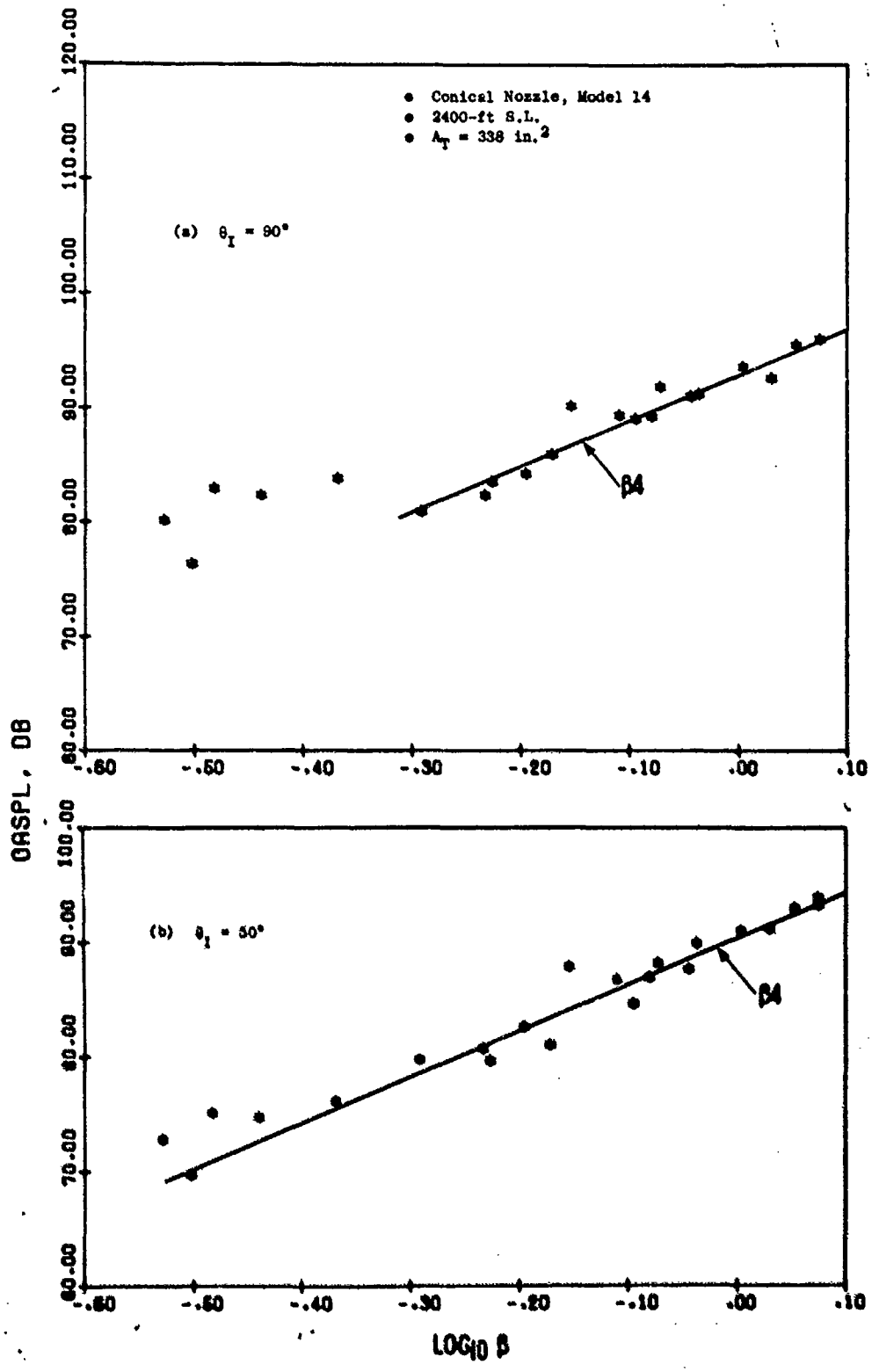

Figure 3-25. Supersonic Jet OASPL Correlation with Shock Strength Parameter β, Conical Nozzle (Model 14).

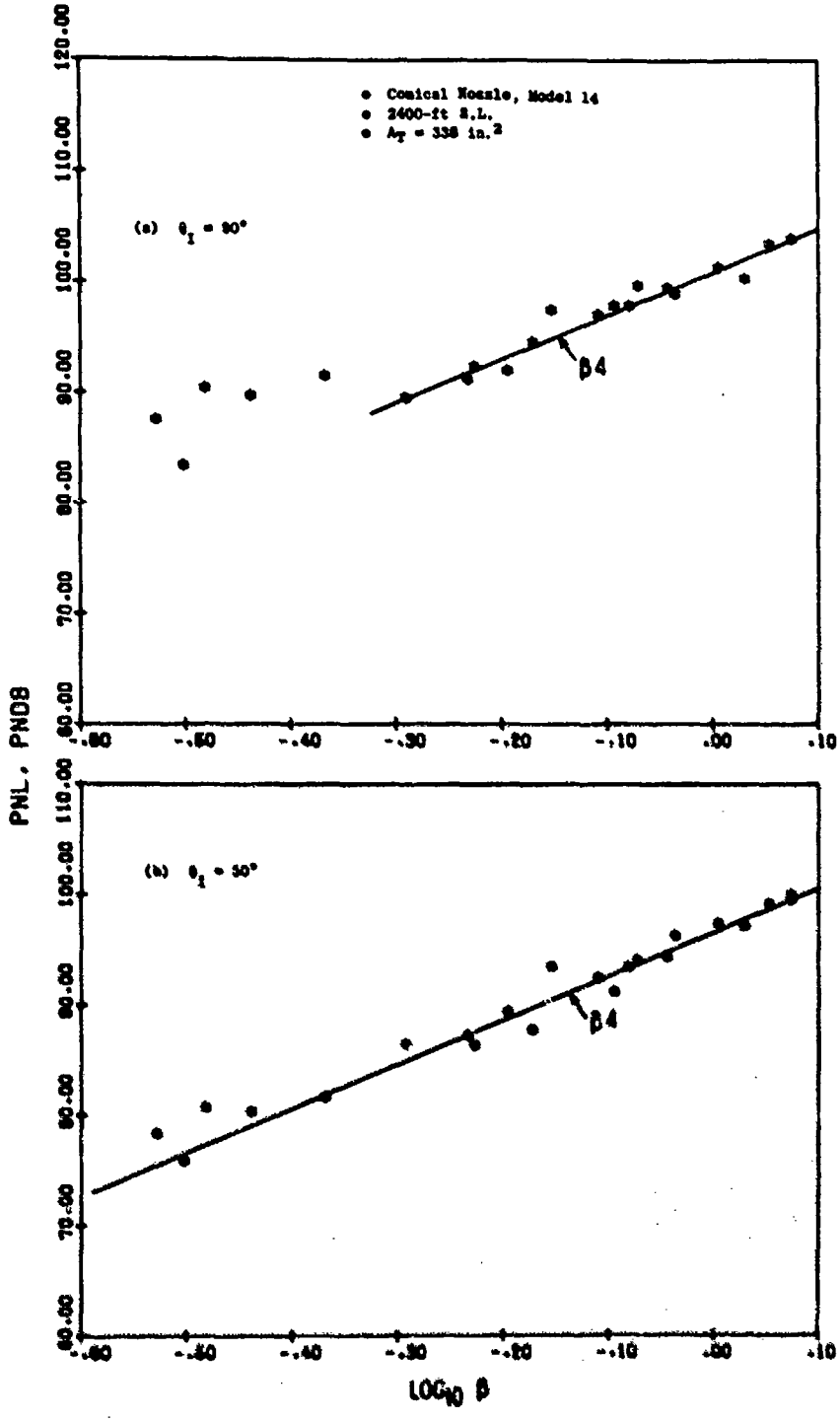

Figure 3-26. Supersonic Jet PNL Correlation with Shock Strength Parameter β, Conical Nozzle (Model 14).

Isovelocity

Figures 3-27 and 3-28, $V_j = V_{ma} = 1600$ fps; $1.6 \leq P_T/P_o \leq 3.49$; $1697 \geq T_T$, ° R ≥ 705

Figures 3-29 and 3-30, $V_j = V_{ma} = 2000$ fps; $2.06 \leq P_T/P_o \leq 3.96$; $1736 \geq T_T$, ° R ≥ 1004

Isotemperature

Figures 3-31 and 3-32, T_T = AMB; $1.10 \leq P_T/P_o \leq 3.94$; $402 \leq V_j = V_{ma}$, fps ≤ 1453

Figures 3-33 and 3-34, $T_T = 1500°$ R; $1.15 \leq P_T/P_o \leq 3.67$; $836 \leq V_j = V_{ma}$, fps ≤ 2380

The results given in Figures 3-27 through 3-30 for isovelocity data elicit the following observations:

- The data are not normalized for T_T, therefore, a wide variance in peak noise level is seen. If the data were normalized, closer agreement would result, similar to the Figure 3-18 and 3-19 peak noise plots. Normalization parameters for each data point are tabulated in Appendix B.

- For each data set, the transition is seen from the regions where noise is predominately influenced by turbulent mixing to where shock-cell noise dominates. For the 1600 fps data, the OASPL and PNL directivity patterns (Figure 3-27) follow standard turbulent-mixing noise distributions at low pressure ratio levels, particularly for the points with $P_T/P_o \leq 1.96$. Above that level, the directivity patterns show increasing influence of shock-cell noise: the $P_T/P_o = 2.30$ points showing influence at 120° and forward, and the higher P_T/P_o data being influenced even in the far aft sector. The spectra plots bear this out even through 130°.

  For the $V_j = 2000$ fps data set, slight shock-cell noise influence is seen even at the lowest $P_T/P_o = 2.06$ point, borne out in the 50° spectra. As P_T/P_o increases, the onset of influence moves further aft until, at highest $P_T/P_o = 3.96$, influence is seen at least to the 110° angular location.

- Shock-cell noise is quite broadband from mid to high frequency and clearly dominates the jet noise spectrum in the forward quadrant, as illustrated quantatively in the spectra plots.

From the Figure 3-31 through 3-34 plots for isotemperature data lines, further observations can be made:

- Within the T_T = amb data set, for highly supercritical data points at low to mid-velocity (1200 to 1450 fps), shock-cell noise totally

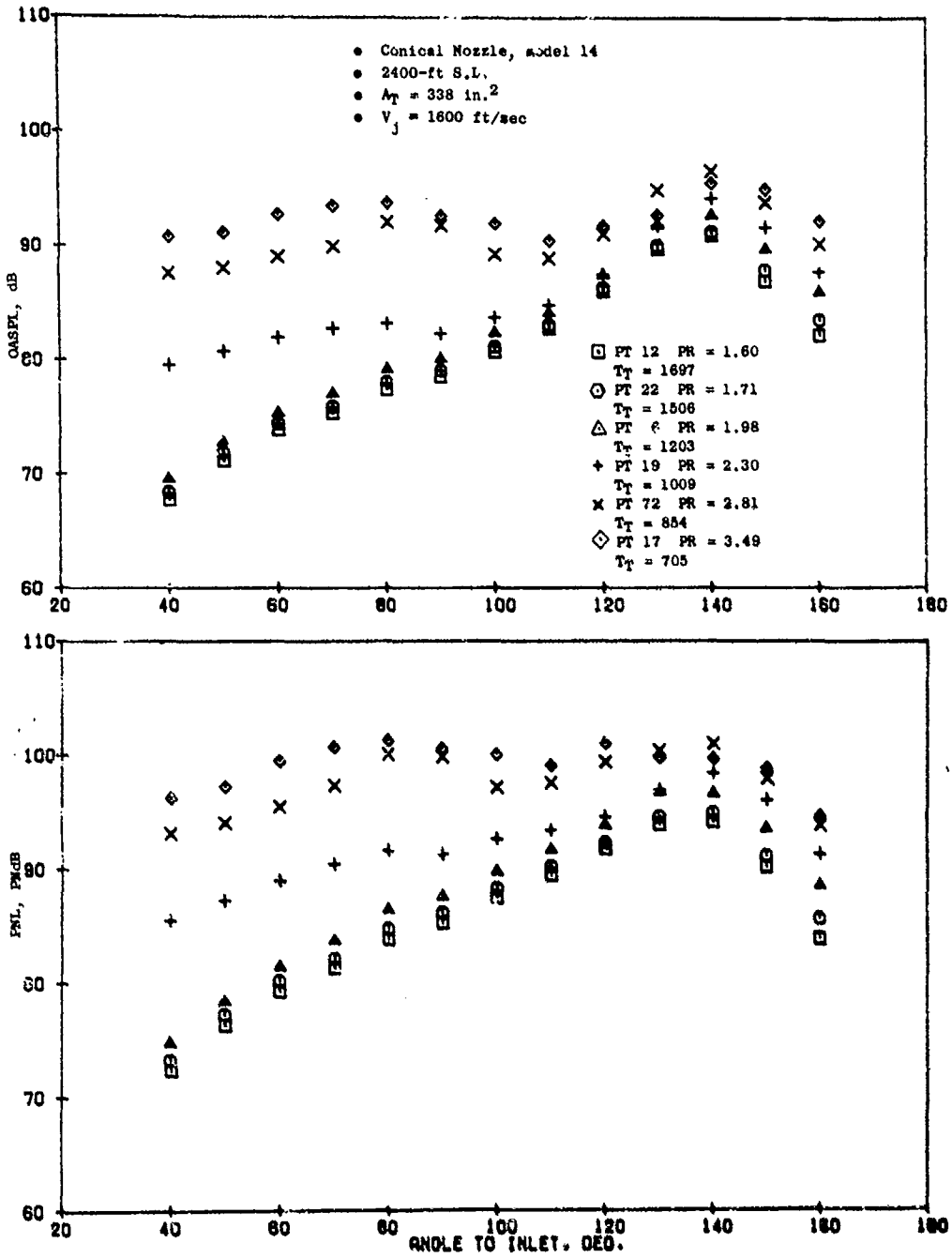

Figure 3-27. Impact of Shock Noise on OASPL and PNL Directivity Conical Nozzle (Model 14), $V_{ma} = V_j = 1300$ ft/sec.

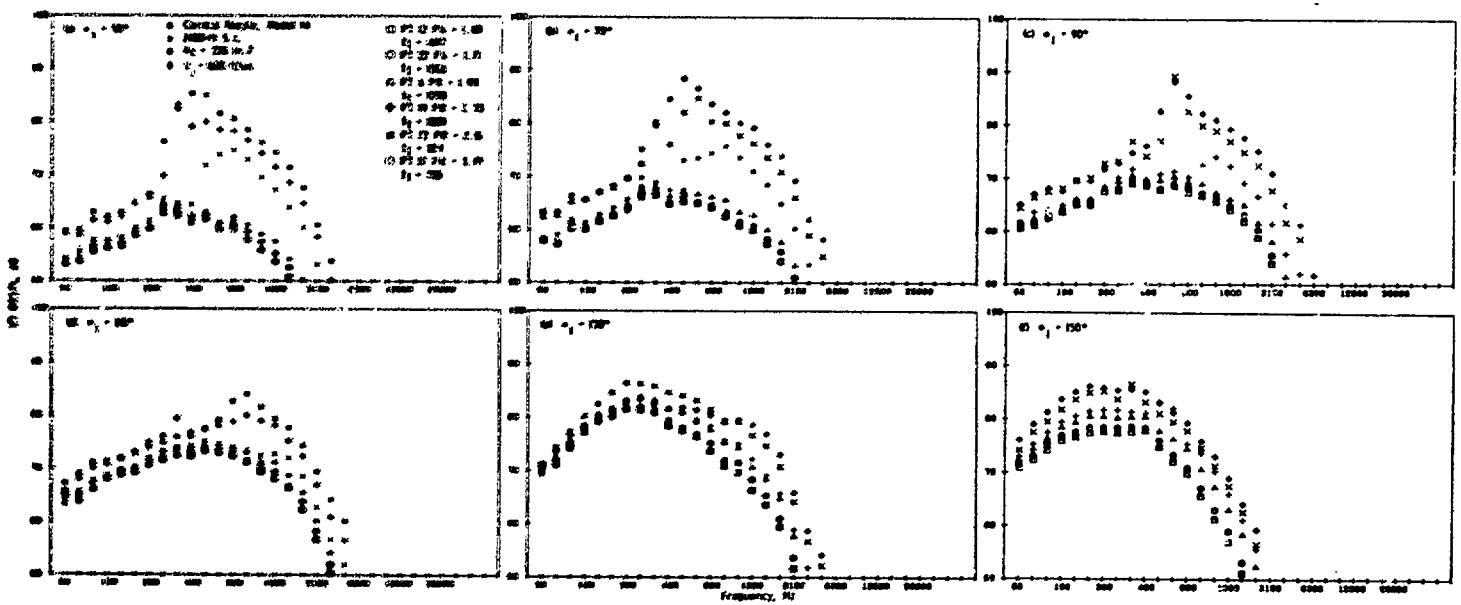

Figure 3-28. Impact of Shock Noise on Spectra Conical Nozzle (Model 14), $V_{ma} = V_j = 1600$ ft/sec.

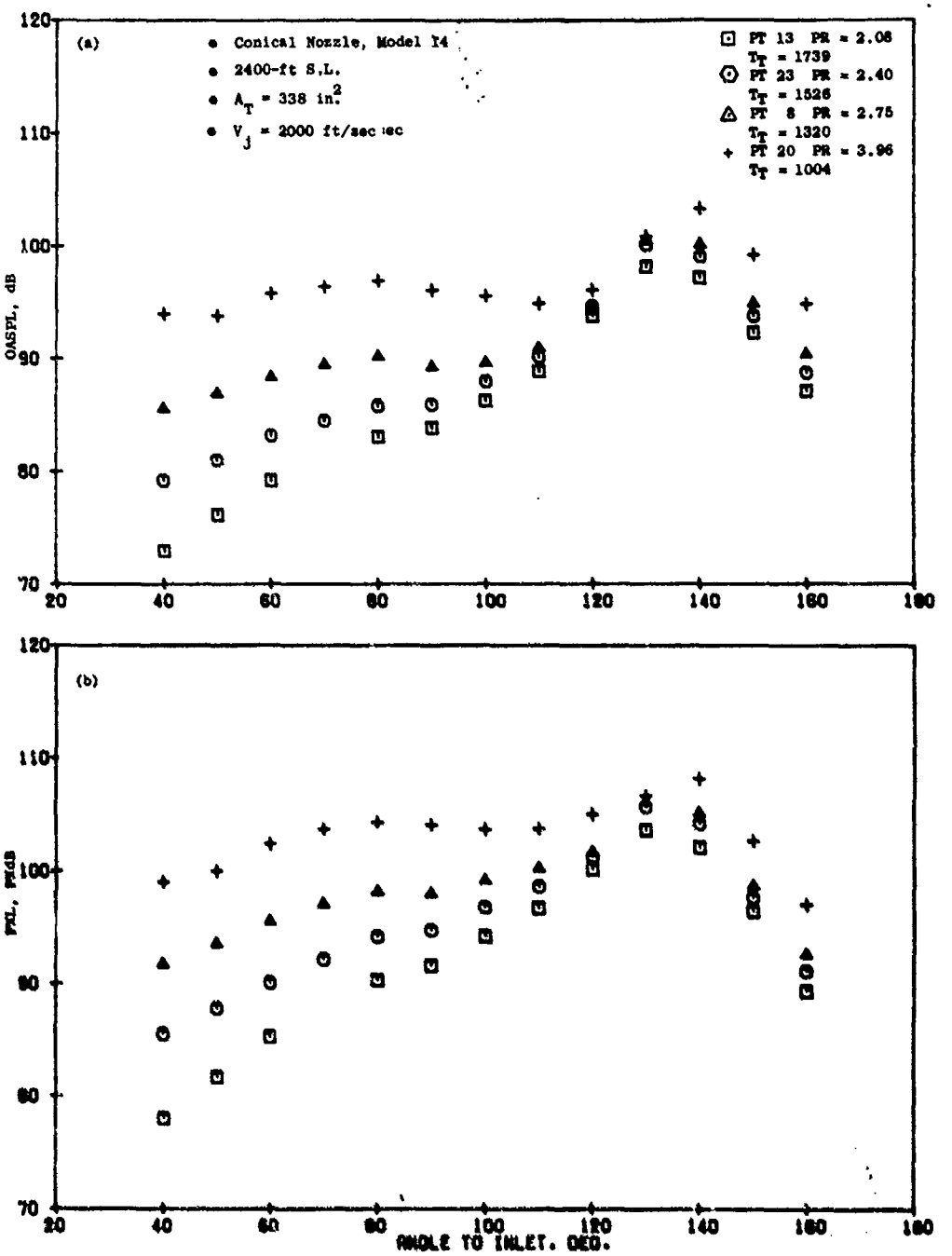

Figure 3-29. Impact of Shock Noise on OASPL and PNL Directivity, Conical Nozzle (Model 14), $V_{ma} = V_j$ = 2000 ft/sec.

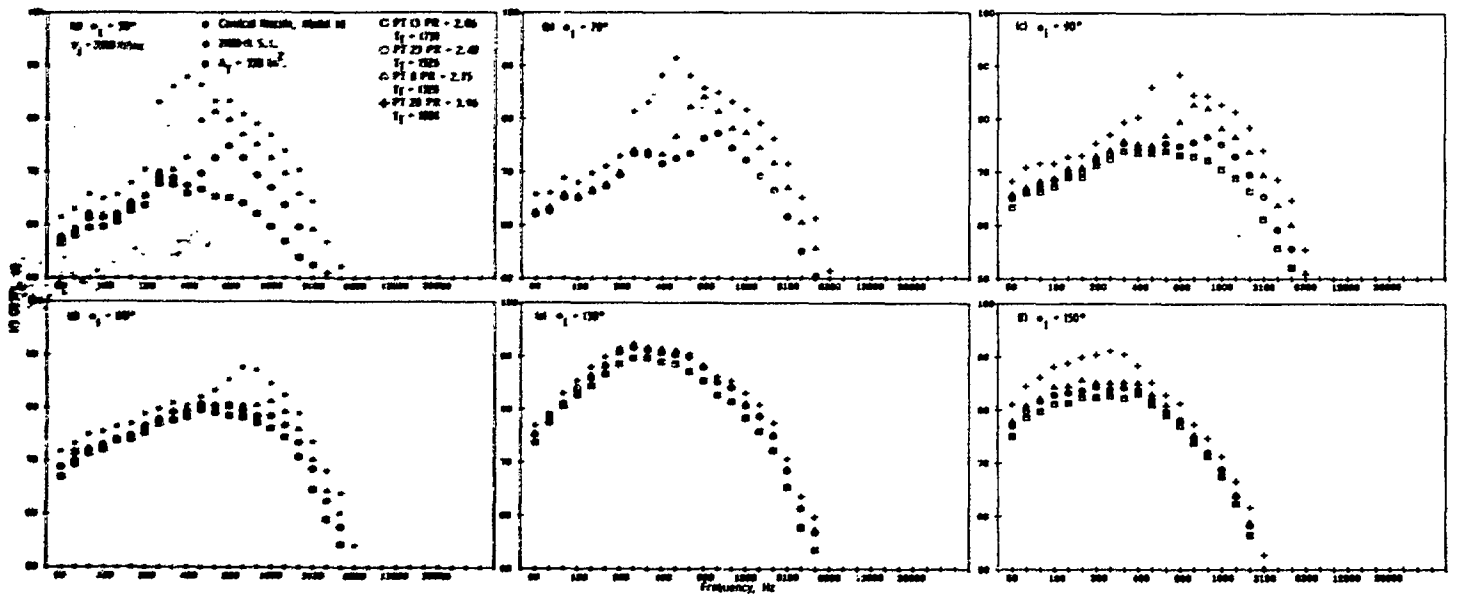

Figure 3-30. Impact of Shock Noise on Spectra, Conical Nozzle (Model 14), $V_{ma} = V_j = 2000$ ft/sec.

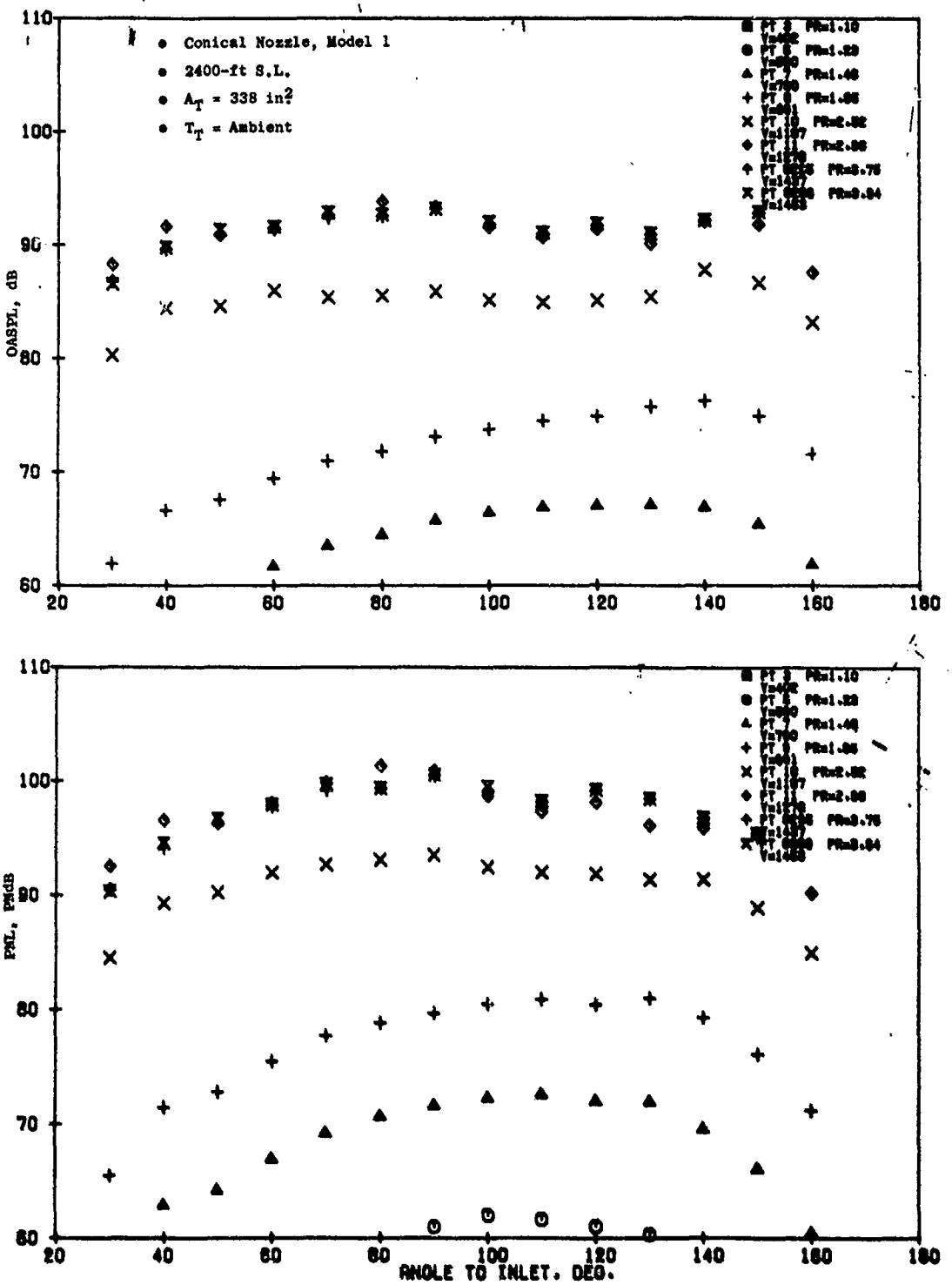

Figure 3-31. Impact of Cycle Variation at Ambient Temperature on OASPL and PNL Directivity, Conical Nozzle (Model 1).

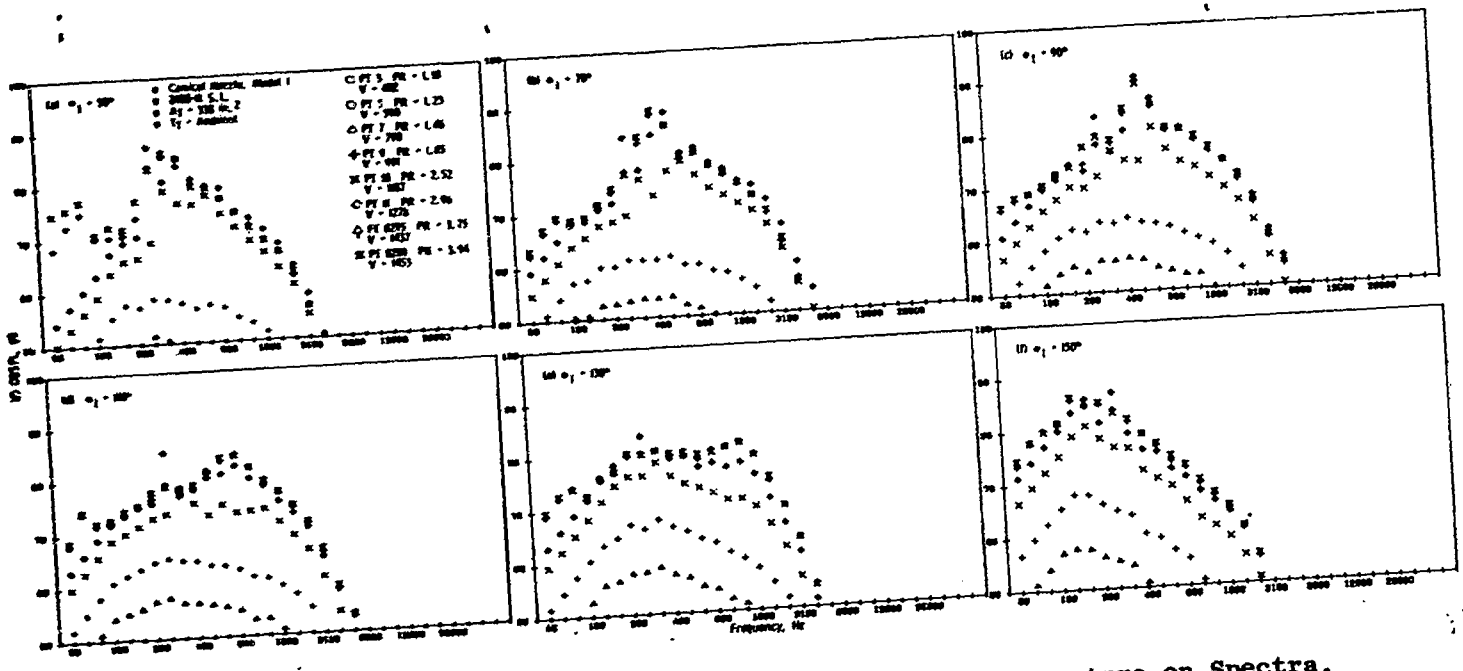

Figure 3-32. Impact of Cycle Variation at Ambient Temperature on Spectra, Conical Nozzle (Model 1).

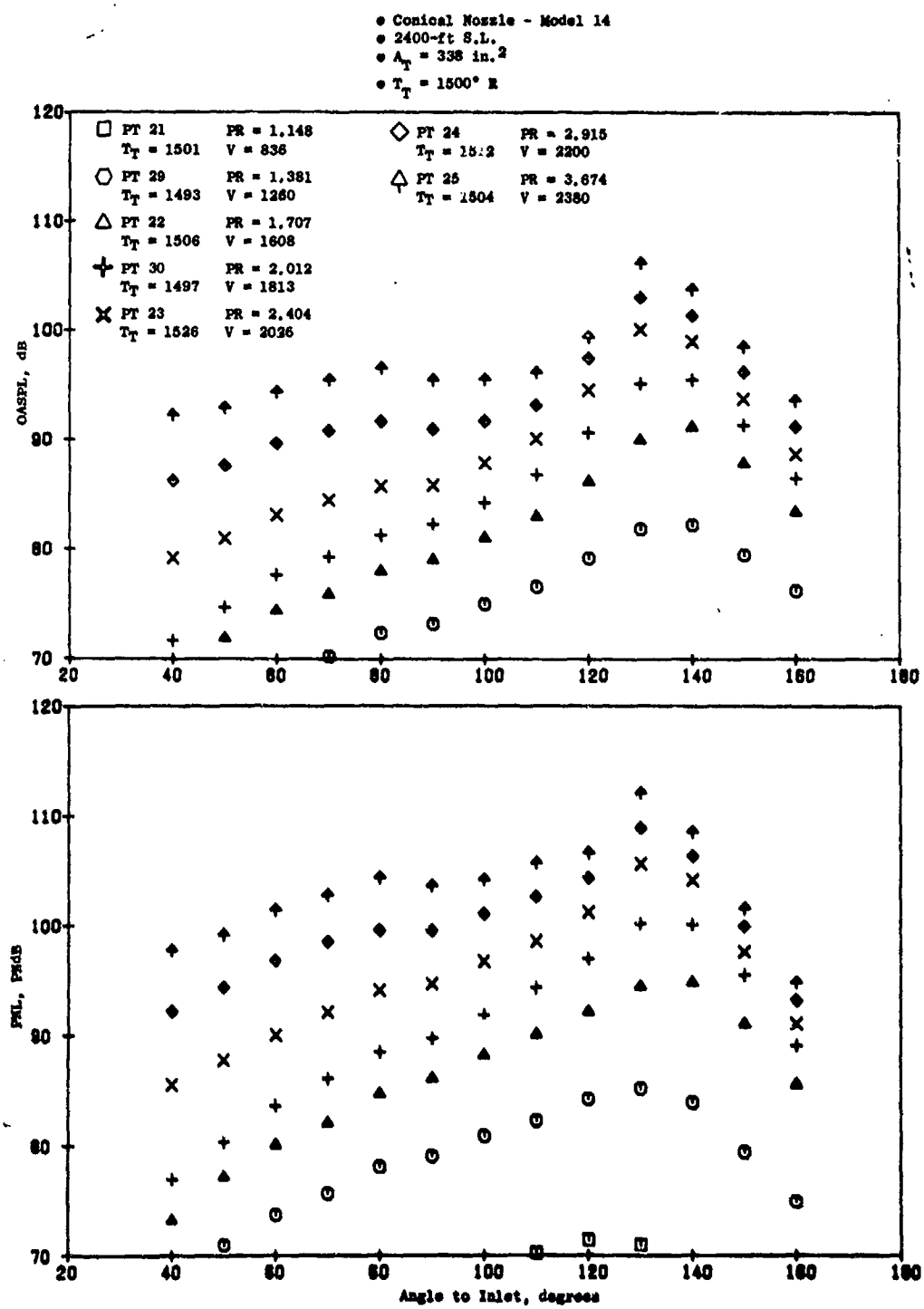

Figure 3-33. Impact of Cycle Variation at 1500° R on OASPL and PNL Directivity, Conical Nozzle (Model 14).

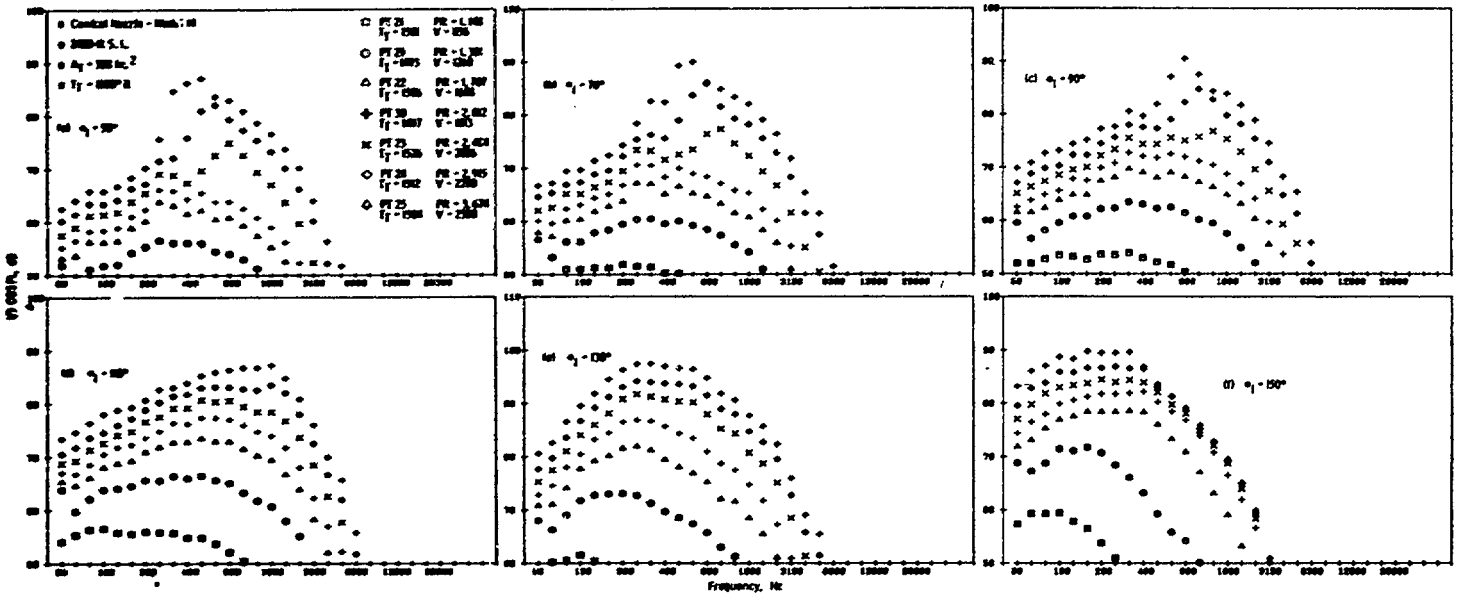

Figure 3-34. Impact of Cycle Variation at 1500° R on Spectra, Conical Nozzle (Model 14).

- dominates all but the most aft noise angles. The OASPL is nearly omnidirectional, i.e., independent of observer angle, θ_j. The very low velocity points ($P_T/P_O \leq 1.85$) also show fairly flat directivity patterns; however, this is characteristic of low-velocity turbulent-mixing noise.

- At higher T_T = 1500° R, again shock-cell noise dominates the forward quadrant angles at supercritical P_T/P_O; however, the regime of dominance is not as distinct as with the isovelocity data set.

For comparisons of baseline spectra and directivity to other models within later studies of this volume, individual conical nozzle data points are selected to best match the P_T/P_O, T_T and V_j cycle of the particular nozzle in study. By doing so, a true measure of suppressor effectiveness can be made.

3.4.1.2 Convergent-Divergent Plug Nozzle Study (Model 2)

An investigation of the acoustic characteristics of a convergent-divergent (C-D) internal flowpath plug nozzle was conducted in this study. This nozzle system represents a realistic turbojet engine configuration with a geometry significantly different than a conical nozzle or simple converging plug nozzle. The nozzle, Model 2, is shown in Figure 3-1 and details are in Appendix A, Figure 2. The C-D flowpath has an exit-to-throat area ratio of 1.22 and equivalent flow diameter ratio of 1.10. At the throat, the plug-to-shroud radius ratio is 0.66, and at the exit plane it is 0.55. The plug has a 3° half-angle within the area of the straight cylindrical shroud, followed by a 10° half angle flowpath extending to the contoured plug end.

Acoustic testing was performed at JENOTS and followed the matrix of Section 3.2.1, Figure 3-3, including the following:

- Turbojet engine typical operating line

- Isotemperature lines at T_T = 1000°, 1250°, 1500°, 1750°, 2000°, and 2250° R

- Isovelocity lines at $V_j = V_{ma}$ = 1000, 1250, 1640, and 2090 ft/sec.

The isovelocity lines were established primarily to derive the temperature dependency of noise for this type of nozzle, similar to that established for a conical nozzle by Hoch, et.al. (Reference 25).

Acoustic test results on a normalized overall basis versus jet velocity are presented for the following:

Figure 3-35 Peak OASPL & PNL
Figure 3-36 90° OASPL & PNL
Figure 3-37 50° OASPL & PNL
Figure 3-38 OAPWL

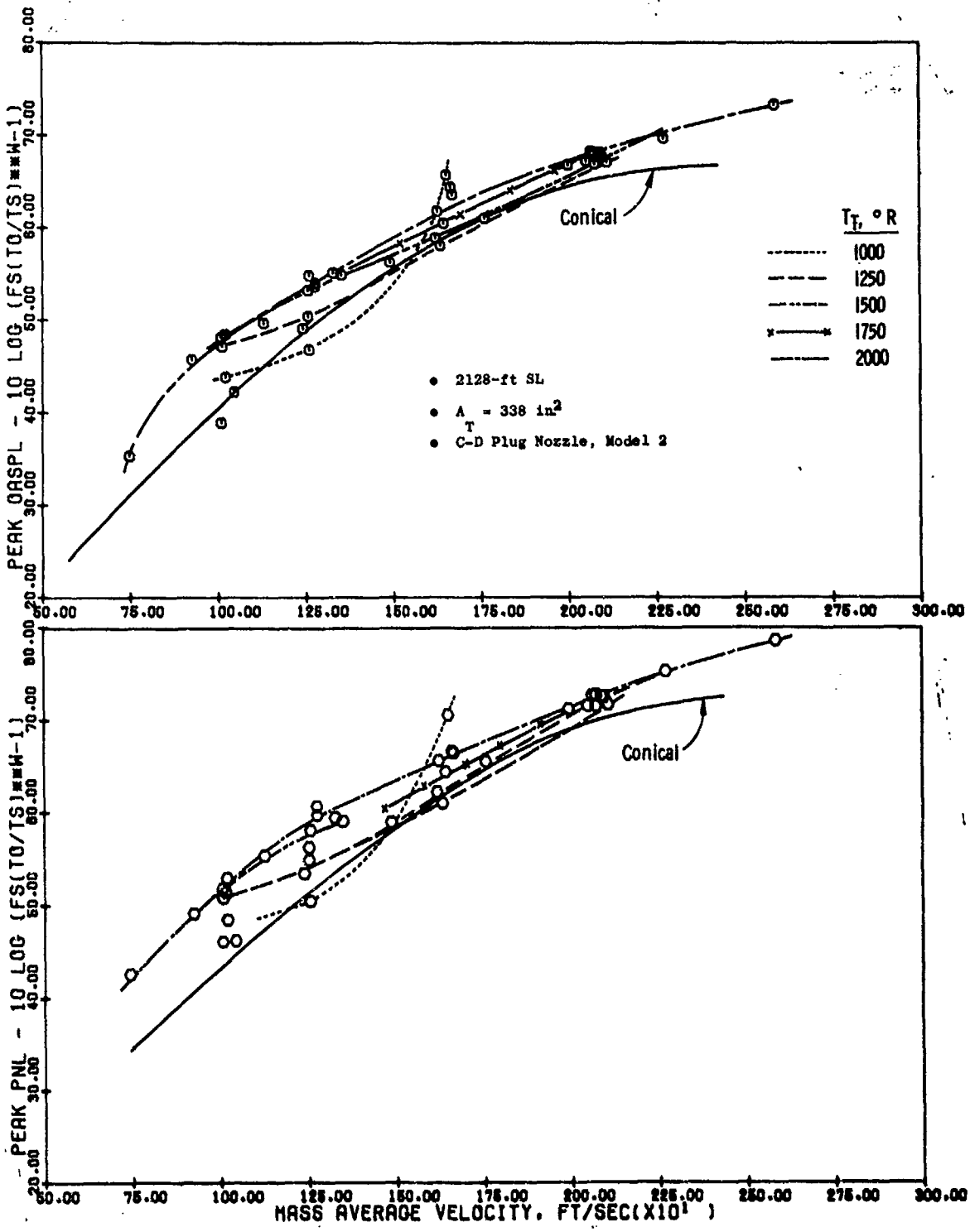

Figure 3-35. Summary of C-D Plug Nozzle (Model 2) Peak Noise Characteristics.

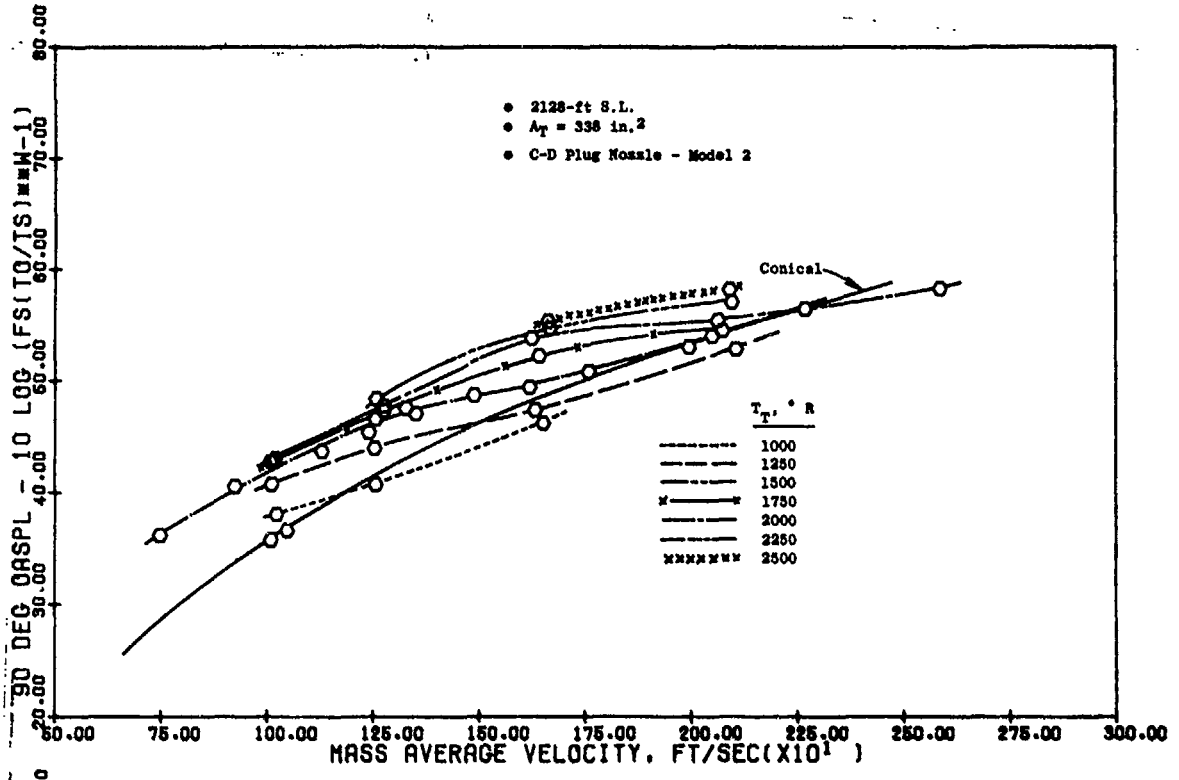

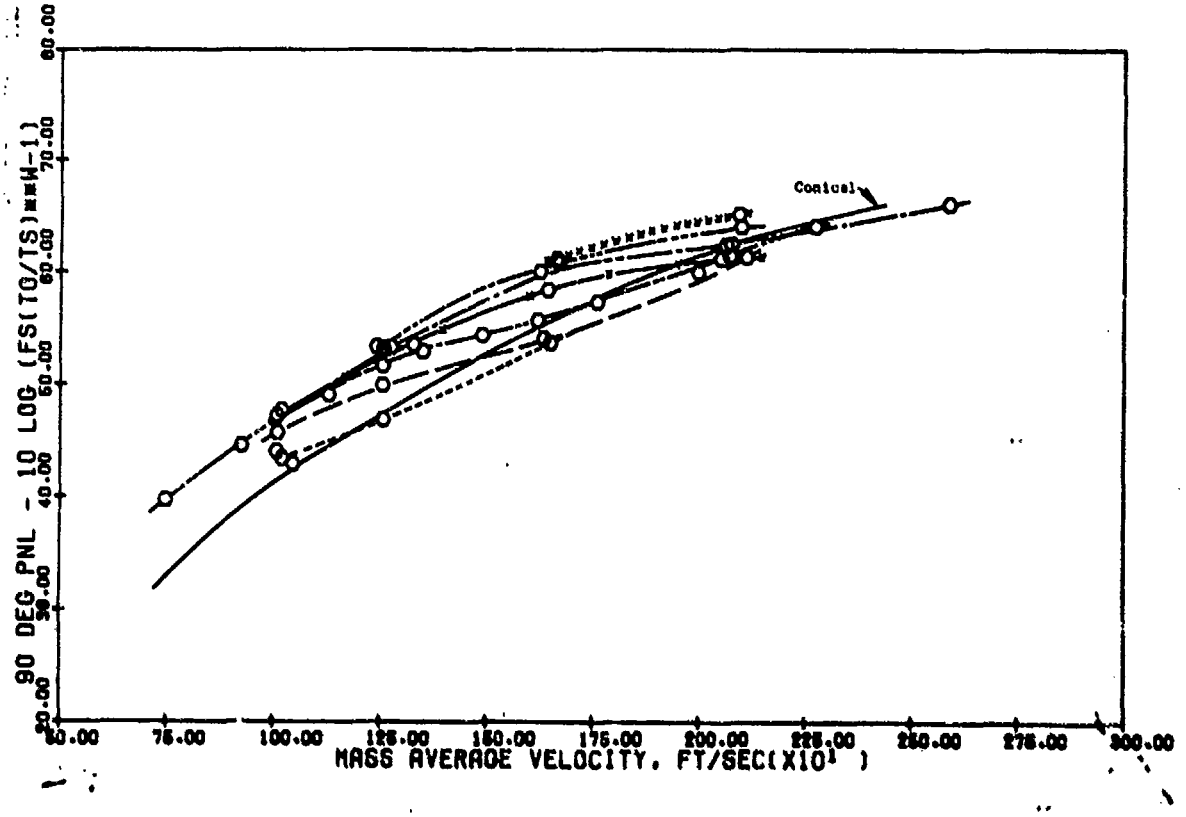

Figure 3-36. Summary of C-D Plug Nozzle (Model 2) 90° Noise Characteristics.

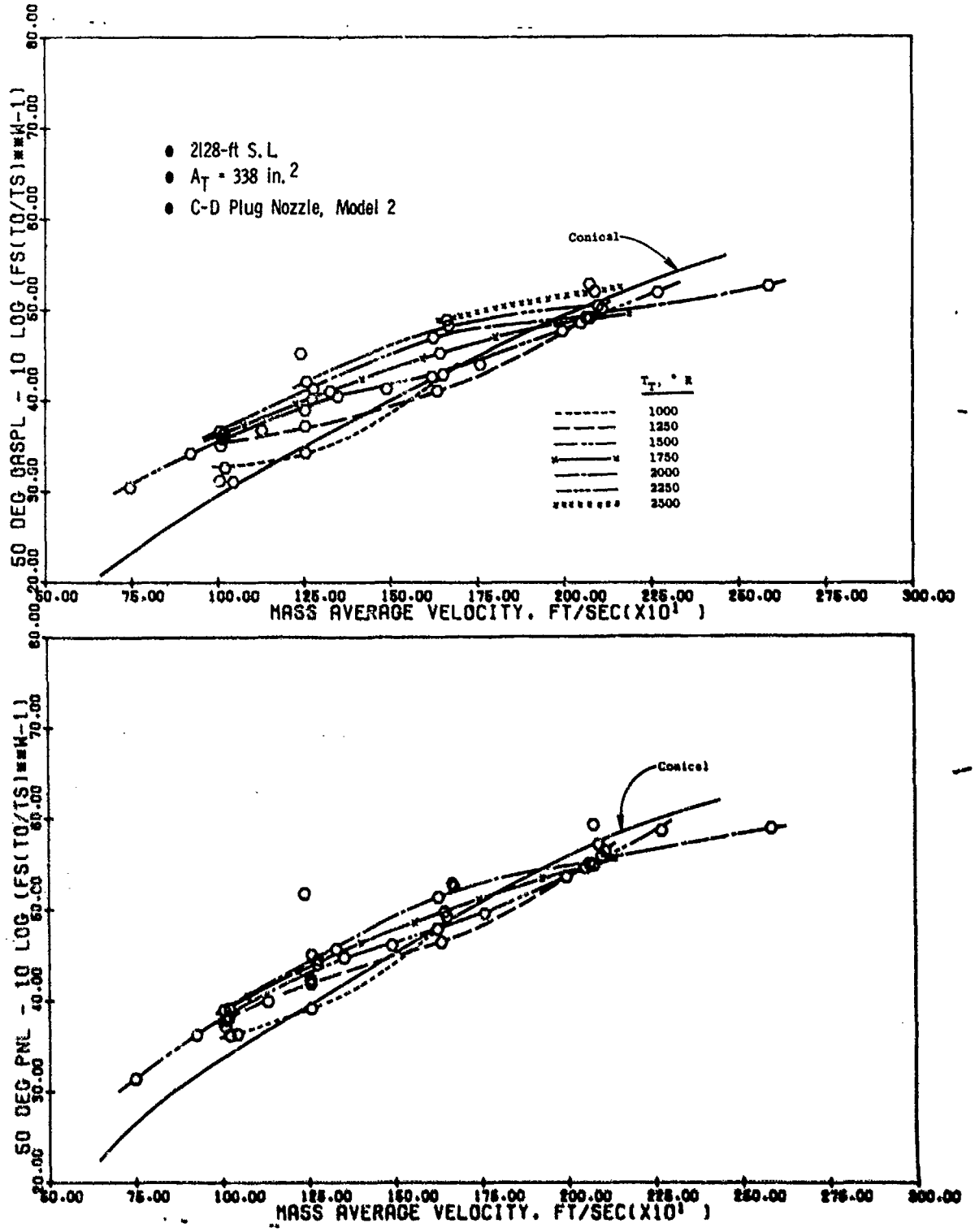

Figure 3-37. Summary of C-D Plug Nozzle (Model 2) 50° Noise Characteristics.

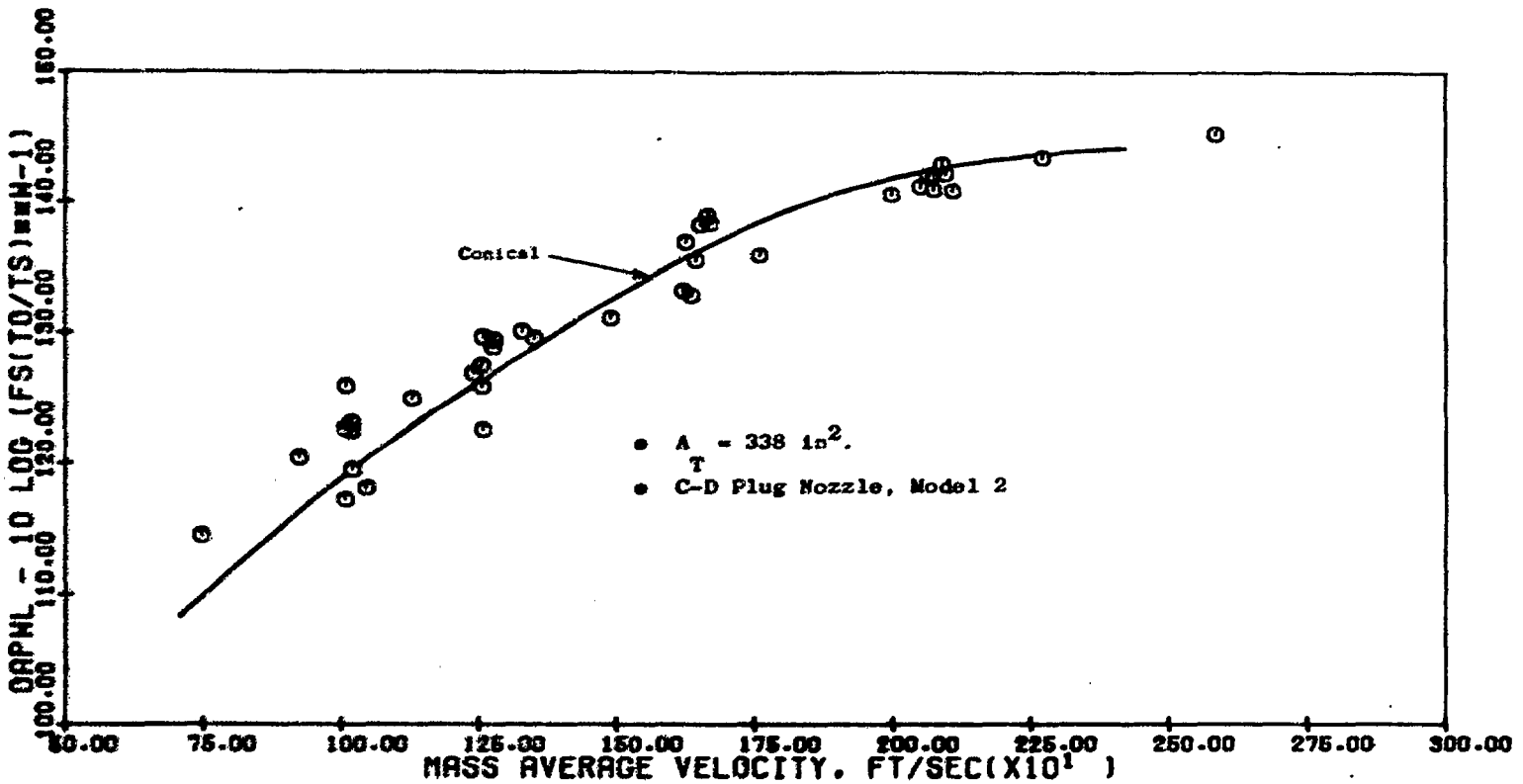

Figure 3-38. Summary of C-D Plug Nozzle (Model 2) Power Level Noise Characteristics.

The above data are presented on a 2128-foot sideline rather than at the standard of 2400-foot sideline, adopted for this report because initial data reduction for this nozzle was at 2128-feet. The conical nozzle data-fitted curves are, therefore, also corrected to the 2128-foot sideline.

Acoustic data trends are observed to be quite dissimilar to those of other model series in that:

a. Collapse of the data with use of the temperature (density) normalization is not observed even at peak noise angles suggesting a strong influence of other than turbulent mixing noise.

b. Noise levels at low velocity (1000 ft/sec) vary as much or more than at high velocity (2090 ft/sec), exactly opposite to the trend of the Section 3.4.1.1 Baseline Conical Nozzles.

c. Normalized noise levels at a particular jet velocity show trends with temperature. Constant temperature lines can be derived, as seen in each data plot.

d. Most noise levels are above the referee conical baseline, at all velocity values, also indicative of other than turbulent mixing noise influence.

Operation above supercritical pressure ratio begins to introduce shock-cell associated noise in puretone and broadband form in conical nozzle data. The resulting noise levels do not correlate with conventional temperature scaling methods because shock cell noise is nontemperature dependent. Operation of a conical nozzle near and below choking pressure ratio generates turbulent mixing noise, which, when normalized with temperature (density), collapses well around a single mean curve.

The flowpath design and operational characteristics must be examined more closely to understand the noise levels of the C-D nozzle. Assuming a one-dimensional flow approximation, flow conditions within and aft of the C-D system are established as a function of nozzle area ratio (A_{exit}/A_{throat} or A_9/A_8) and nozzle pressure ratio, P_T/P_0. For Model 2's C-D flowpath, the nozzle should be shock-free at M = 1.55 or P_T/P_0 = 3.90. Subsonic Mach number and P_T/P_0 corresponding to this A_9/A_8 are 0.58 and 1.24, respectively. Therefore, the following flow patterns are anticipated for the range of nozzle pressure ratios evaluated:

(a) For $P_T/P_0 < 1.24$, the flow throughout the nozzle is subsonic, the velocity and Mach number are maximum at the throat plane.

(b) For $P_T/P_0 = 1.24$, the flow is accelerated to M = 1 at the throat plane and subsequently decays to a subsonic velocity at the exit plane.

(c) For $1.24 < P_T/P_o < 2.61$, the flow is accelerated to M = 1 at the throat and to supersonic conditions within the divergent section. A normal shock wave is formed within the divergent part of the nozzle, across which total pressure and velocity of the flow decreases. The flow at the exit from the nozzle is subsonic.

(d) At $P_T/P_o = 2.61$, the location of the normal shock wave is at the exit plane of the divergent section. This pressure ratio is calculated from the expression:

$$P_T/P_o = \frac{2\gamma}{\gamma+1}(M^2_{exit}) - \frac{\gamma-1}{\gamma+1};$$

where M_{exit} corresponds to supersonic isentropic expansion from M = 1 at A_8 to $M = M_{exit}$ at A_9.

(e) For $2.54 < P_T/P_o < 3.90$, the flow attains M = 1 at the throat and accelerates to supersonic in the divergent section. As the flow leaves the nozzle supersonically, shock patterns (oblique and normal) form outside the nozzle, across which the flow is decelerated.

(f) At $P_T/P_o = 3.90$, the flow attains M = 1 at the throat and is accelerated isentropically to supersonic velocity, attaining M = 1.54 at the exit plane. The flow ideally is without shock structure throughout.

(g) Above $P_T/P_o = 3.90$, the flow can again become shock infested.

The following observations aid in understanding the generated noise patterns:

(a) Only (b) and (f) of the above flow patterns (at $P_T/P_o = 1.24$ and 3.90) expand the flow isentropically, corresponding to the normal flow pattern associated with a convergent nozzle for which the isentropic fully expanded velocity is calculated as V_{ms}. This is the main parameter against which noise is plotted for comparison to the conical nozzle data. Flow stream characteristics of a C-D system may not lend to correlation using the isentropic velocity calculation based on nozzle P_T/P_o and T_T. Operation between P_T/P_o of 1.24 to 2.61 results in an internal normal shock which reduces velocity, the loss dependent on shock strength. The exit plane velocity will not correspond to the isentropic expansion velocity calculation.

(b) Since a shock structure can be generated within the nozzle diverging section for $1.24 < P_T/P_o < 2.61$, low velocity noise can be influenced by shock-cell formations. In contrast, conical nozzle shock-cell noise influence is not observed until $P_T/P_o > 1.86$.

(c) For the P_T/P_O = 1.24 to 2.61 range of operation, dominance of either turbulent mixing noise or shock-associated noise depends on the competitive influence of: (a) increased shock-strength associated with higher operating pressure ratio and, (b) relative change in exit velocity associated with the increase in P_T/P_O, tempered by greater loss across the stronger internal normal shock.

(d) Shock-associated noise generated internally may not exhibit the same characteristics as externally generated shock-cell noise for convergent nozzles.

(e) Other sources of noise may exist, i.e., internally generated noise associated with an interaction of the shock structure and flow disturbances such as those associated with turbulence of combustion, upstream support strut wakes, or from nozzle wall boundary layers. This interaction may also significantly boost jet mixing noise levels.

(f) For operation in the 2.61 < P_T/P_O < 3.90 regime, where external shock structure is expected to be present, the more omnidirectional characteristic of shock-cell noise associated with convergent flow nozzles should be present and shock-cell noise will compete with turbulent mixing noise for predominance.

Changes in noise characteristics are expected to be pressure ratio dependent, of significant magnitude, and broadband in content, based on the above considerations.

As a preliminary attempt at correlation of peak noise, 120-foot arc peak OASPL and 2120-foot sideline peak OASPL are plotted versus nozzle P_T/P_O at the isovelocity lines of 1000, 1250, 1640 and 2090 ft/sec in Figure 3-39. Pressure ratio ranges corresponding to anticipated flow regimes are indicated. Additionally, Figure 3-40 presents 120-foot polar OASPL distributions for the four isovelocity lines and Figure 3-41 contains 1/3 OBSPL spectra at 150° relative to the inlet (normally the peak noise angle for each of the four velocity points).

The following observations are noted based on a review of the above data figures, consistent with the previous observations (a) through (f):

- For $P_T/P_O \leq 1.24$, peak OASPL levels vary within 1 dB (at 1000 ft/sec) on a nonnormalized basis. When normalized for T_T, the variance drops to 0.3 dB; the closer correlation anticipated for turbulent mixing noise.

- For pressure ratio range of operation where an internal shock is expected, i.e., 1.24 < P_T/P_O < 2.61, Figure 3-39, correlation of Peak OASPL with P_T/P_O, indicates a changing trend with velocity change. At 1000 and 1250 ft/sec noise decreases as P_T/P_O increases at 1640 ft/sec the level remains near constant, and at 2090 ft/sec the peak OASPL increases. This may be in line with the

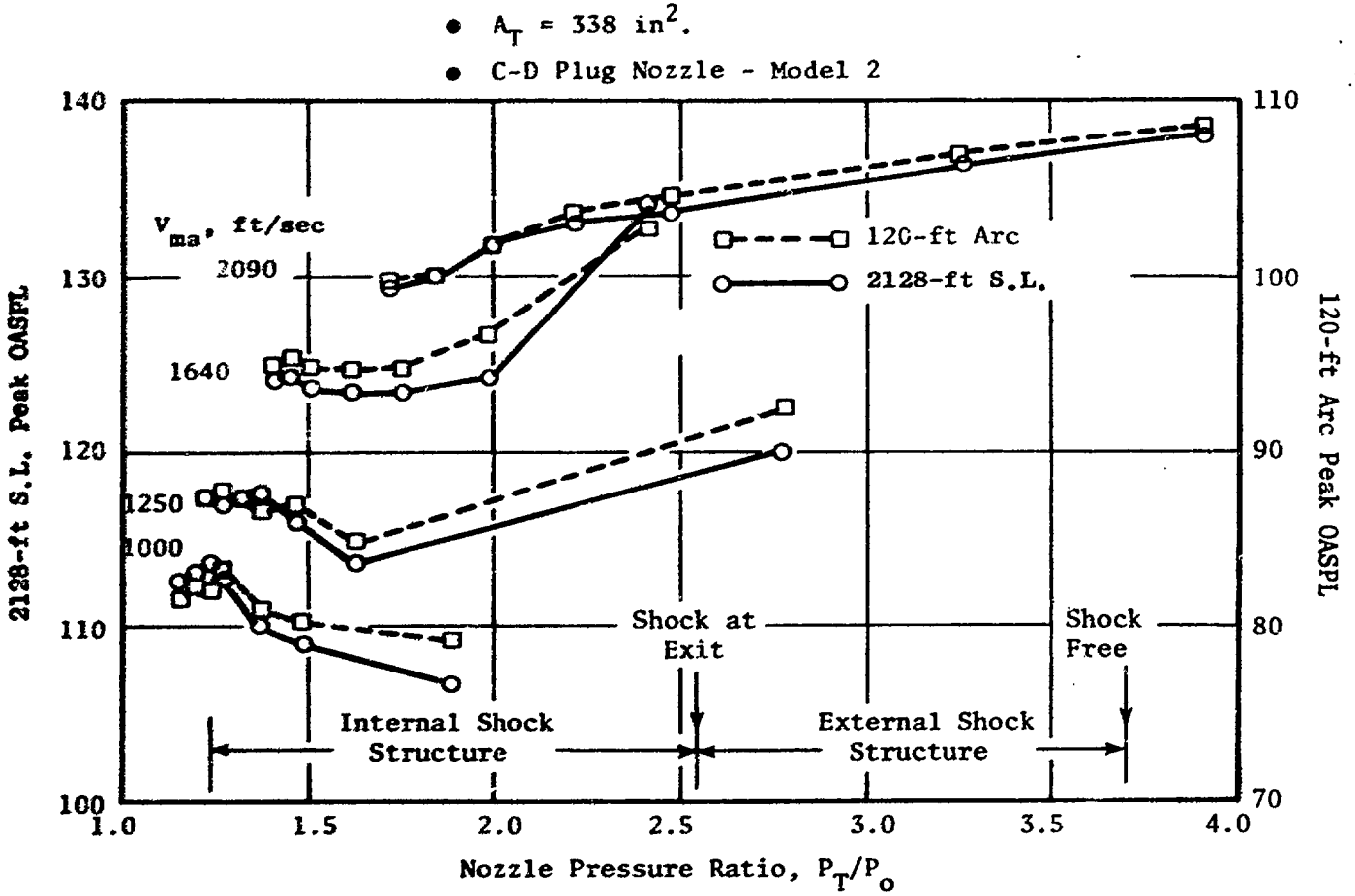

Figure 3-39. Correlation of Peak OASPL with Pressure Ratio for a C-D Plug Nozzle (Model 2).

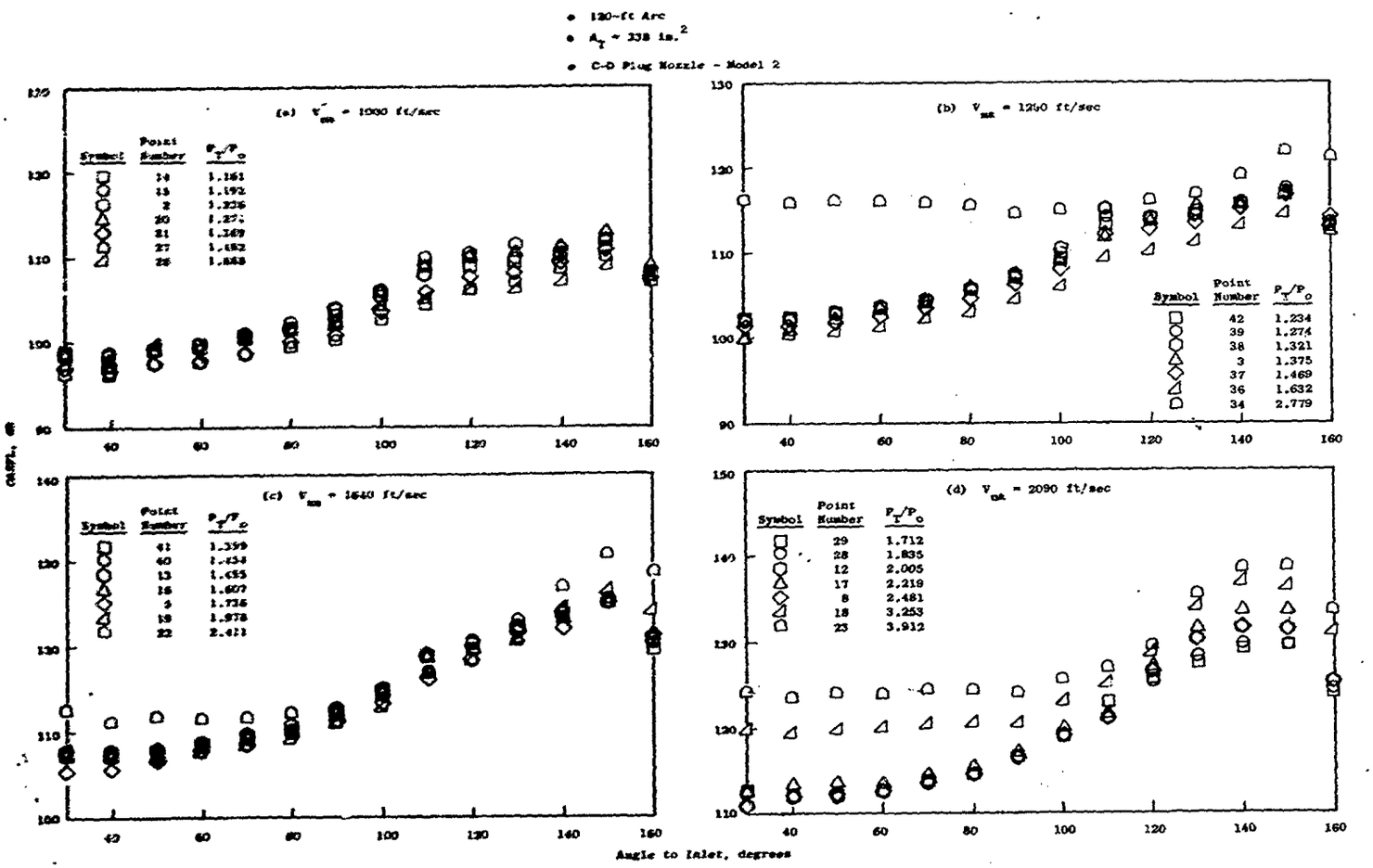

Figure 3-40. Polar OASPL Distributions at V_{ma} = 1000, 1250, 1640, and 2090 ft/sec.

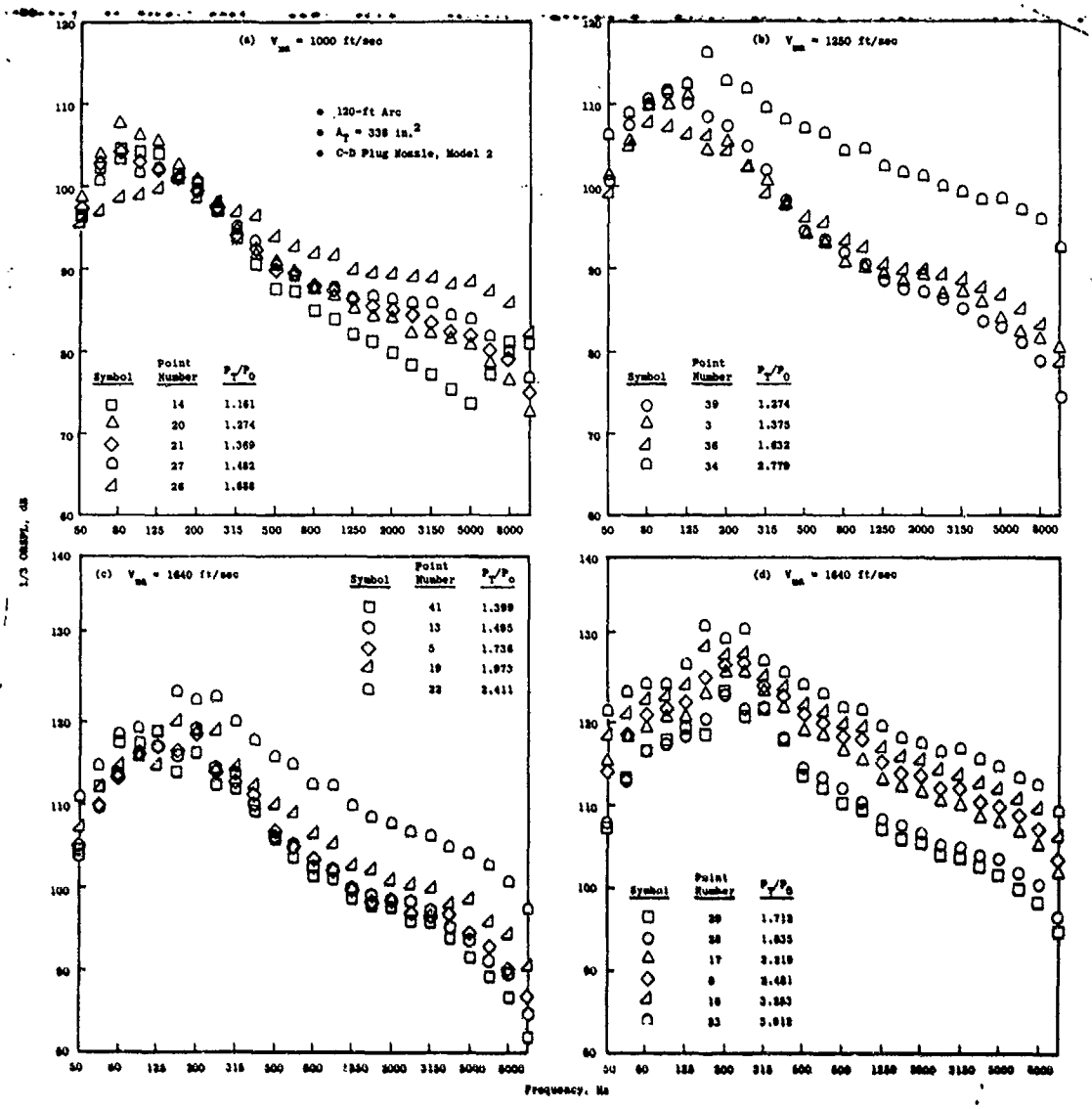

Figure 3-41. 150° Spectra at V_{ma} = 1000, 1250, 1640, and 2090 ft/sec.

previous observation (c). The OASPL and 1/3 OBSPL data of Figures 3-40 and 3-41, within this range of operation, indicate smooth transition in levels at all angles. Spectrum changes are mostly broadband in content.

- For the pressure ratio range of operation where an external shock structure is anticipated, $2.61 < P_T/P_O < 3.90$, the more omnidirectional characteristic associated with conical nozzle shock-cell noise persists [previous observation (f)], and competition for dominance of either turbulent mixing or shock noise is more pronounced. At 1000 ft/sec all points are below $P_T/P_O = 2.54$ and no external shock structure is expected; therefore, directivity and spectra changes are all uniform. At 1250 ft/sec, for the $P_T/P_O = 2.79$ point, inlet and broadside noise levels are raised substantially while aft-to-peak levels increase moderately. Spectra at 150° show noise increases to be very broadband from ≈ 160 Hz through 10KHz. At 1640 ft/sec, where maximum $P_T/P_O = 2.41$ (< 2.54 where shock sits at the exit plane) OASPL directivity shows no abrupt rise in the forward quadrant; however, aft angle 150° spectra still shows a fairly broadband increase in noise levels, indicating possibility of strong aft directed shock noise. At 2090 ft/sec, the $P_T/P_O = 2.48$ point maintains low forward quadrant noise whereas the $P_T/P_O = 3.25$ and 3.91 points increase forward quadrant and broadside OASPL proportionately with P_T/P_O change. Spectra changes at 150° are again broadband and consistent with P_T/P_O changes.

A jet density correlation was derived using the isovelocity data lines at V_{ma} = 1000, 1250, 1640 and 2090 ft/sec obtained through systematic variation of P_T/P_O and T_T. Nonnormalized OAPWL and peak OASPL values are plotted versus 10 $\log_{10}$ (ρ_j/ρ_{isa}) in Figure 3-42. Straight lines are fitted through each velocity set by least squares curve fit. The resulting line slopes yield the density exponent (ω) for the correlation of jet noise dependence on density. Each line of data, therefore, establishes the value of ω for that particular velocity and these ω values versus $\log_{10} V_{ma}/a_o$ are also plotted in Figure 3-42 for both OAPWL and peak OASPL. The figures also show comparison to the conical nozzle ω dependency established by Hoch, et.al. (Reference 25). Differences are quite substantial and again illustrate the distinctly different noise characteristics of a C-D nozzle (Model 2) system.

3.4.1.3 Plug Nozzle Radius Ratio Study (Models 3, 4, and 5)

The plug nozzle may be thought of as a basic building block. In its simplest form, it is the basic propulsion nozzle geometry normally used for increasing aerodynamic efficiency. In its more complex form, it is the base structure around which multielement annular suppressors are incorporated. Through use of a translating cylindrical shroud, it reverts to geometry similar to that of the convergent-divergent system of the previous section. The C-D flowpath is essential for proper flow expansion guidance in cruise flight mode, necessary to optimize aerodynamic performance.

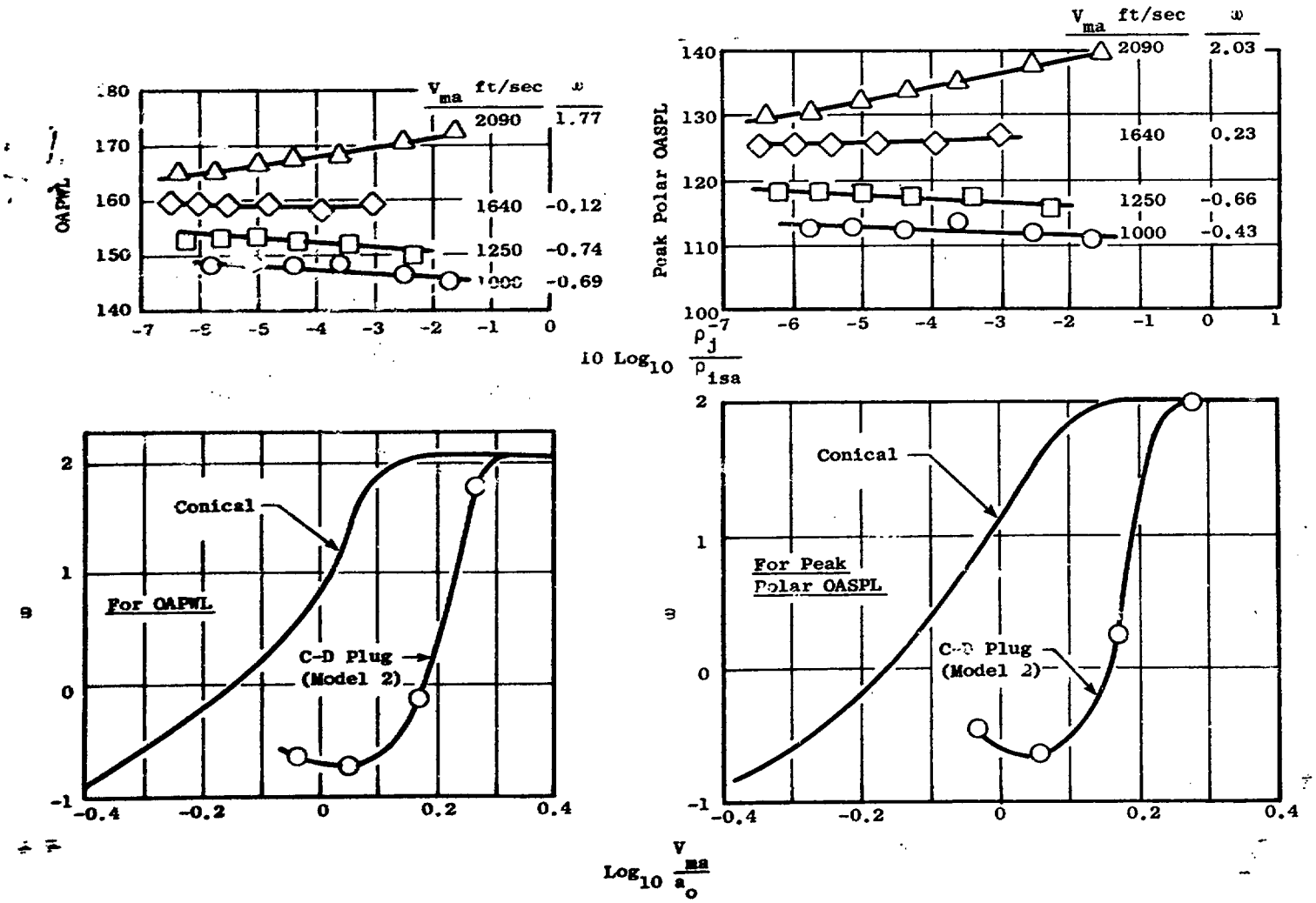

Figure 3-42. Jet Density Exponent Correlation.

The far-field acoustic characteristics of three different annular plug nozzles were measured within this study to establish noise level variation as a function of plug geometry, primarily plug radius ratio. Additionally, information was obtained for use in Task 2, Section 4.6.7, "Experimental Evaluation of Annular Plug Nozzle Shock Cell Noise Characteristics," and Section 4.7.8, "Data Theory Comparisons." Temperature (density) dependence information was also obtained to establish noise ω dependency similar to that done by Hoch, et al. (Reference 25) for conical nozzles and to that of the previous section for the C-D plug (Model 2). This noise data allows documentation of the dependency of the plug system in a general manner similar to the conical nozzle.

The three configurations tested are shown in Figure 3-43 with details in Appendix A, Figures 3, 4, and 5. The models maintain the 10° half-angle core plug of 2.40" radius over the plug peak. The plug flowpath is contoured to simulate conventional engine flowlines. Interchangeable converging shrouds of R_S = 4.071, 3.041 and 2.815" are used to effect plug-to-shroud radius ratios (R_r) of 0.59, 0.789 and 0.853 for Models 3, 4, and 5, respectively.

The models were tested at JENOTS with the far-field acoustic matrix of Section 3.2.1, Figure 3-4. Each used the simulated turbojet engine cycle line, and Model 4, of representative R_r = 0.789, was selected for a more detailed parametric test matrix consisting of:

- Isovelocity lines at 1000, 1250, 1640, and 2090 ft/sec, similar to that of Model 2 of the previous section to establish noise dependency on jet density/temperature.
- Isotemperature lines of 1000°, 1250°, 1500°, 1750°, and 1900° R, to establish noise/velocity dependency.

Previous suppression levels associated with plug nozzles were low to moderate (1 to 3 ΔPNL) in level, primarily associated with plugs of low radius ratio. The current plug-baseline systems were developed to evaluate several design principles. An increase in plug radius ratio for a fixed area nozzle pushes the flow to a smaller annulus, further removed from the nozzle centerline and should, therefore, increase peripheral mixing area. Smaller annulus slit height (higher radius ratio) is associated with reduction in shock-cell noise. The smaller annulus height, relative to a fixed plug length, enhances the possibility for greater physical shielding of high-frequency noise.

Data results for the parametric radius ratio study, along the simulated turbojet engine cycle line, are presented as follows; each scaled and normalized per Section 3.3.1.7 then plotted versus V_{ma} with Δ suppression plots included as appropriate:

Figure 3-44 and 3-45	Peak OASPL and PNL
Figure 3-46 and 3-47	90° OASPL and PNL
Figure 3-48	50° OASPL and PNL
Figure 3-49	OAPWL

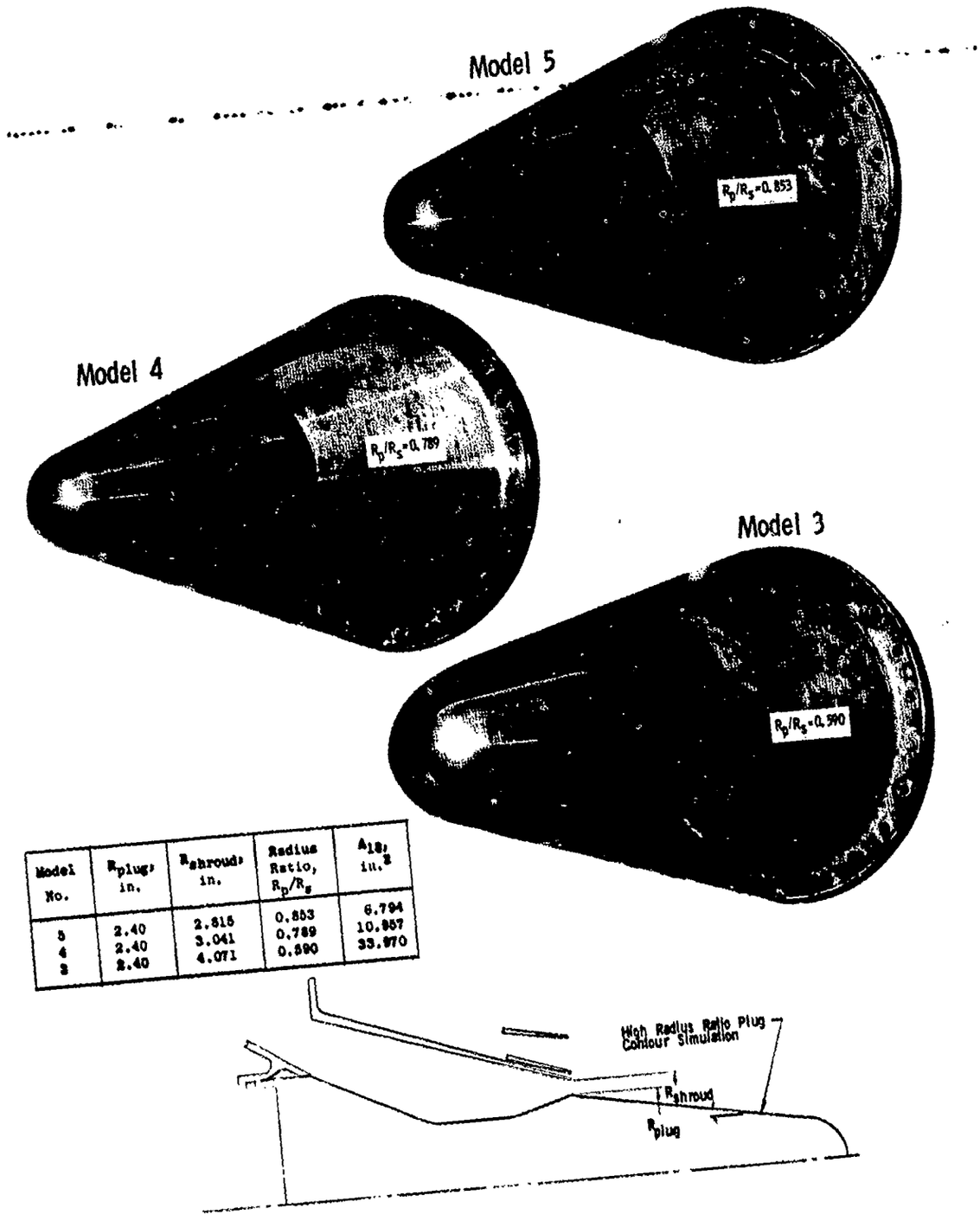

Model No.	R_{plug}, in.	R_{shroud}, in.	Radius Ratio, R_p/R_s	A_{18}, $in.^2$
5	2.40	2.815	0.853	6.794
4	2.40	3.041	0.789	10.857
3	2.40	4.071	0.590	33.970

Figure 3-43. Model Hardware for Parametric Nozzle Radius Ratio Study.

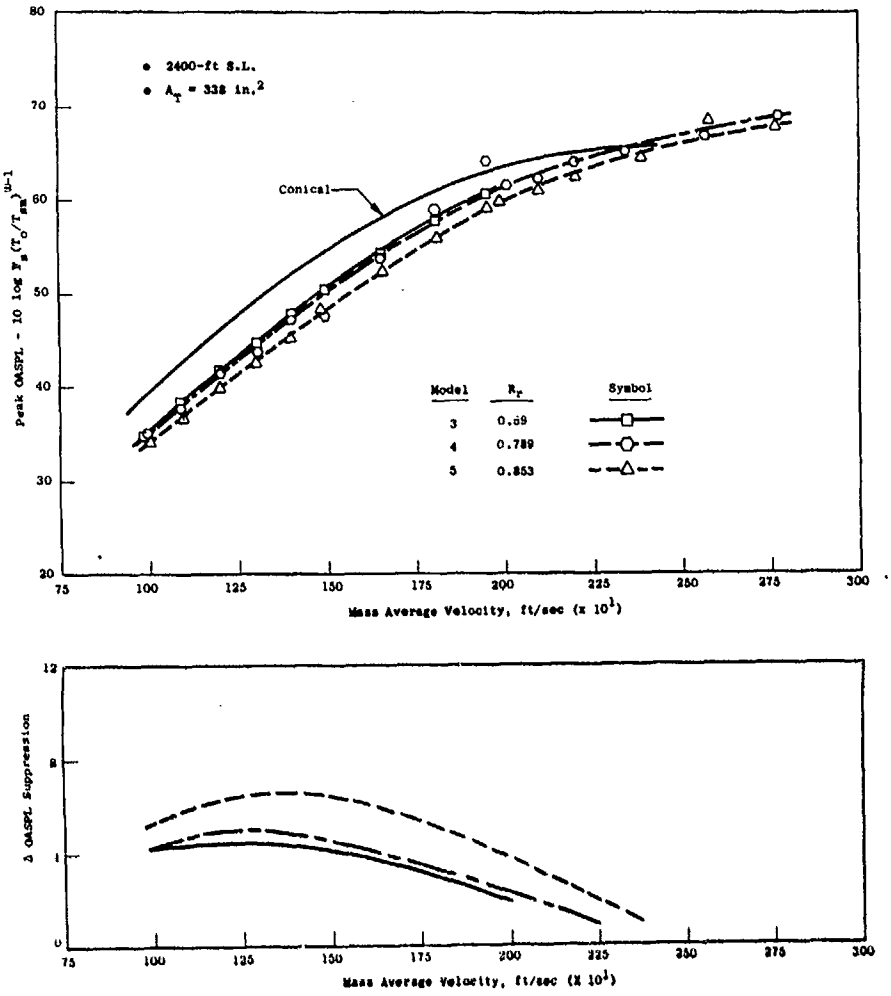

Figure 3-44. Summary of Plug Nozzle Peak OASPL and Suppression Levels.

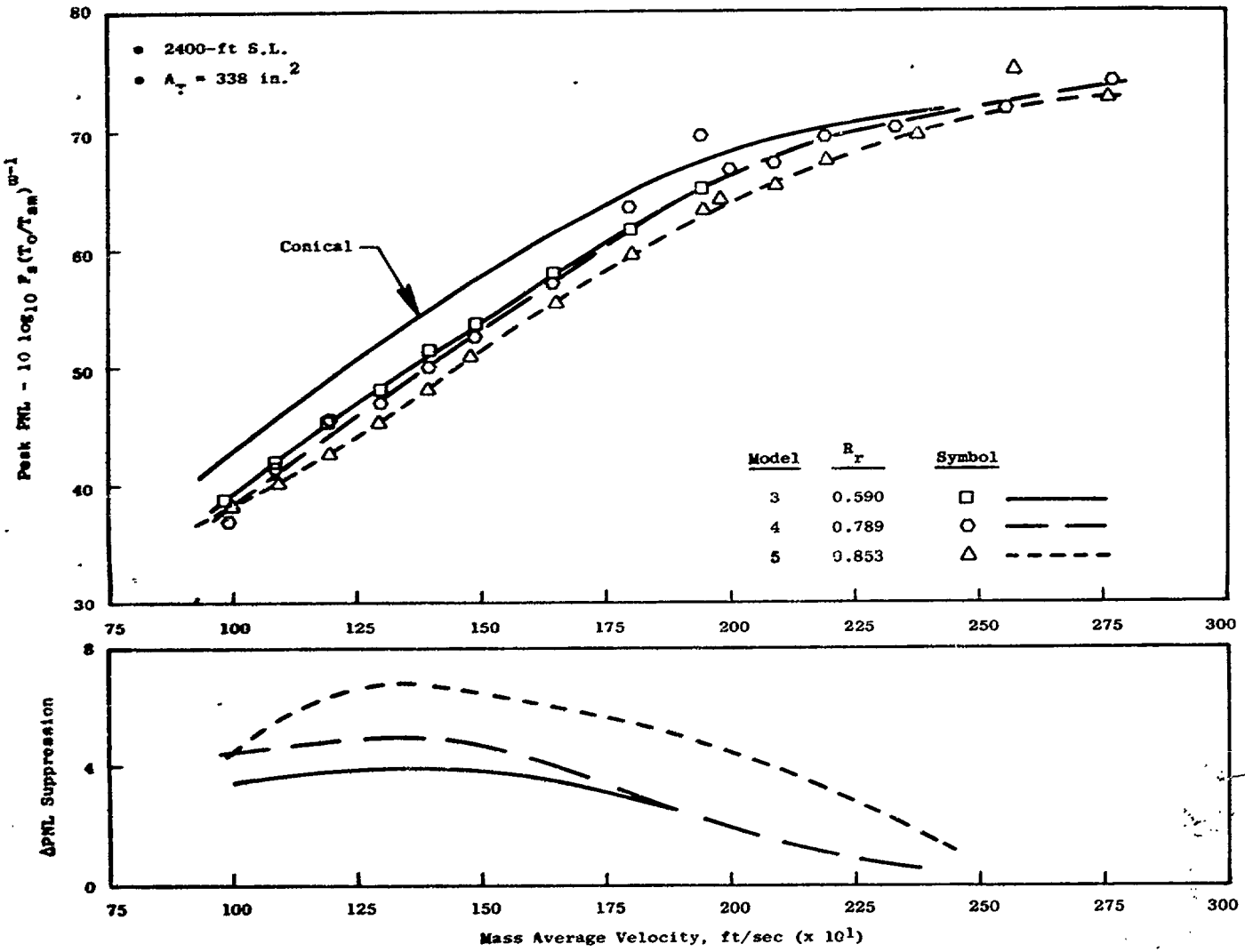

Figure 3-45. Summary of Plug Nozzle Peak PNL and Suppression Levels.

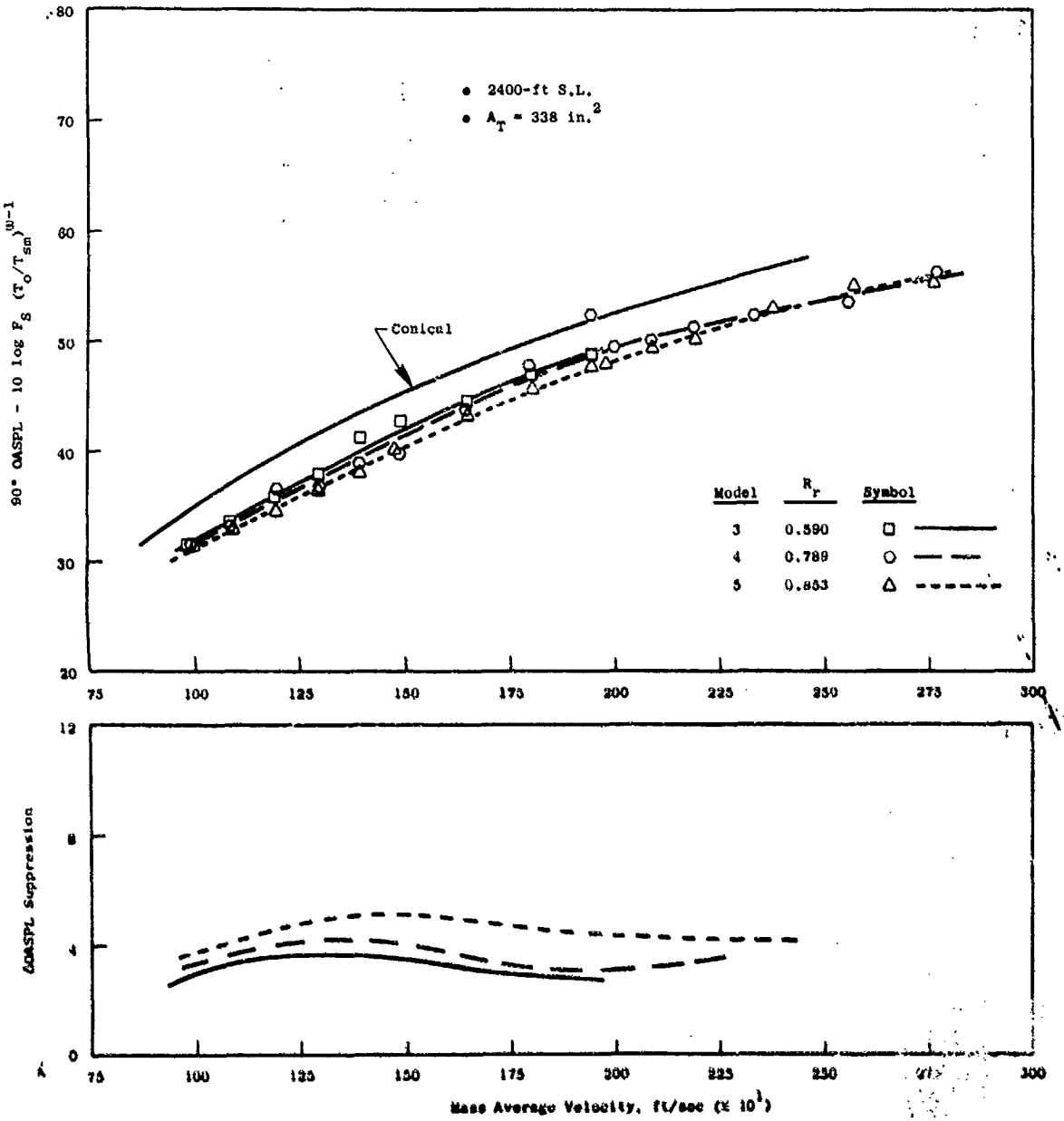

Figure 3-46. Summary of Plug Nozzle 90° OASPL and Suppression Levels.

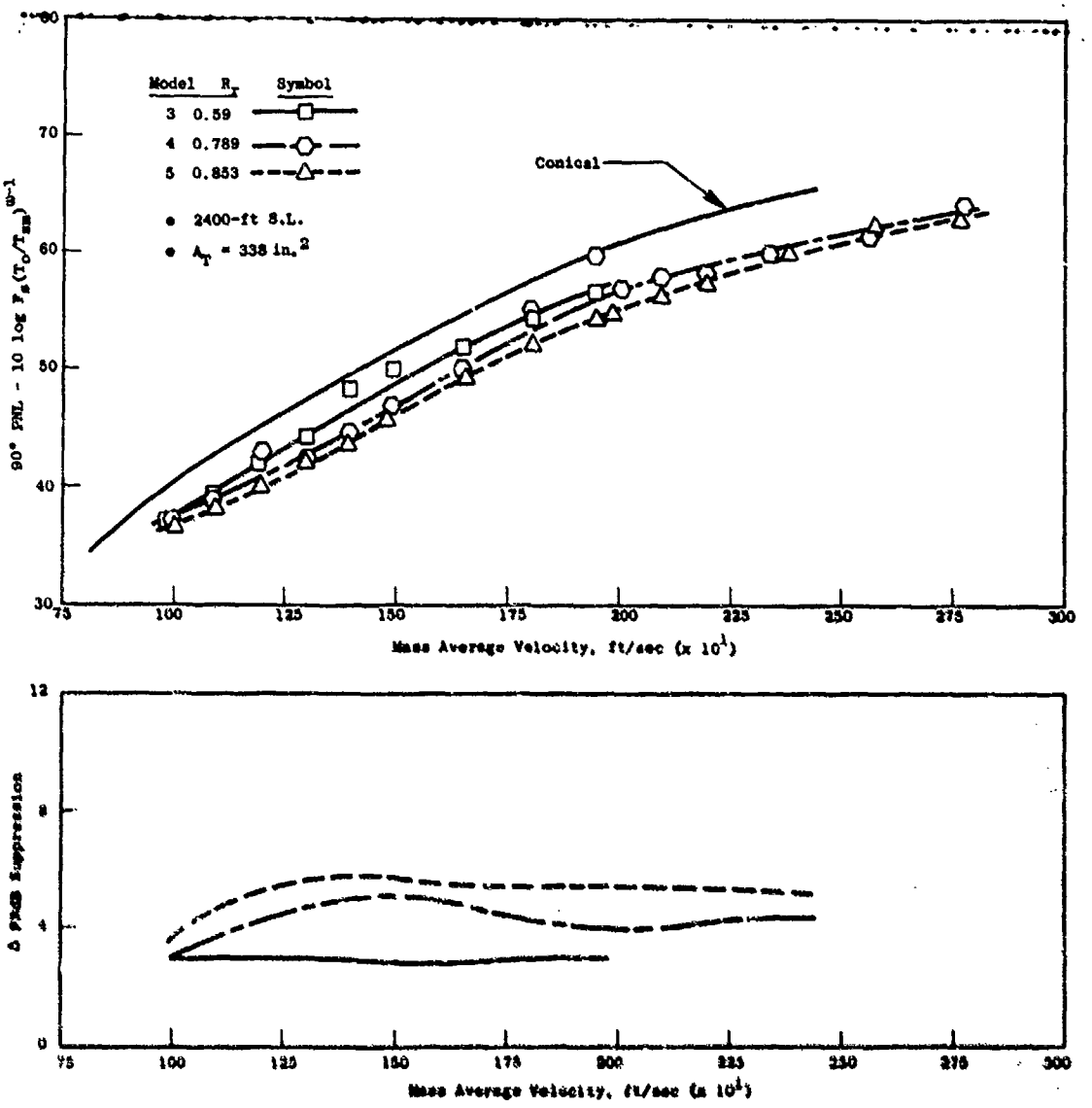

Figure 3-47. Summary of Plug Nozzle 90° PNL and Suppression Levels.

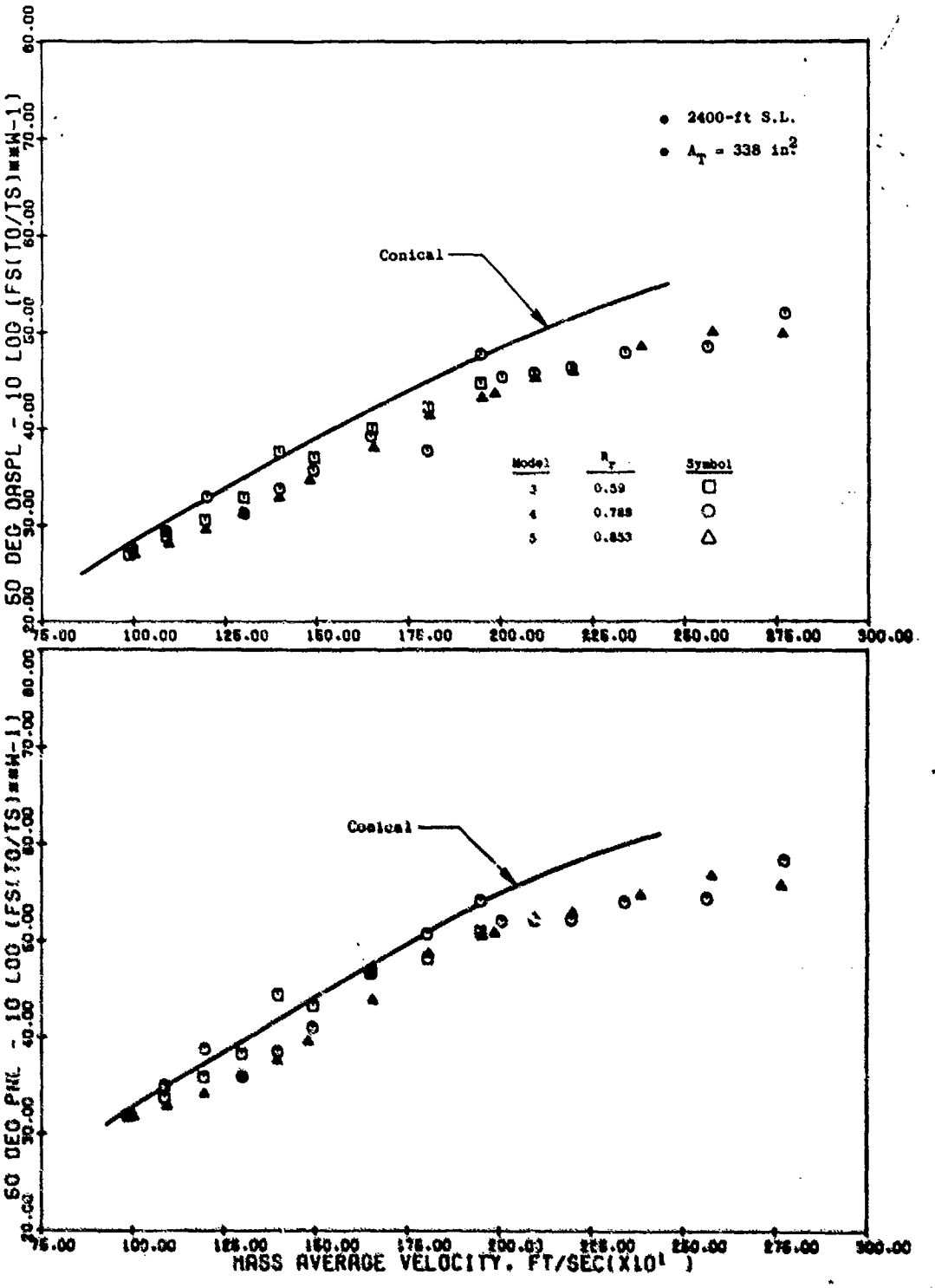

Figure 3-48. Summary of Plug Nozzle 50° OASPL and PNL Characteristics.

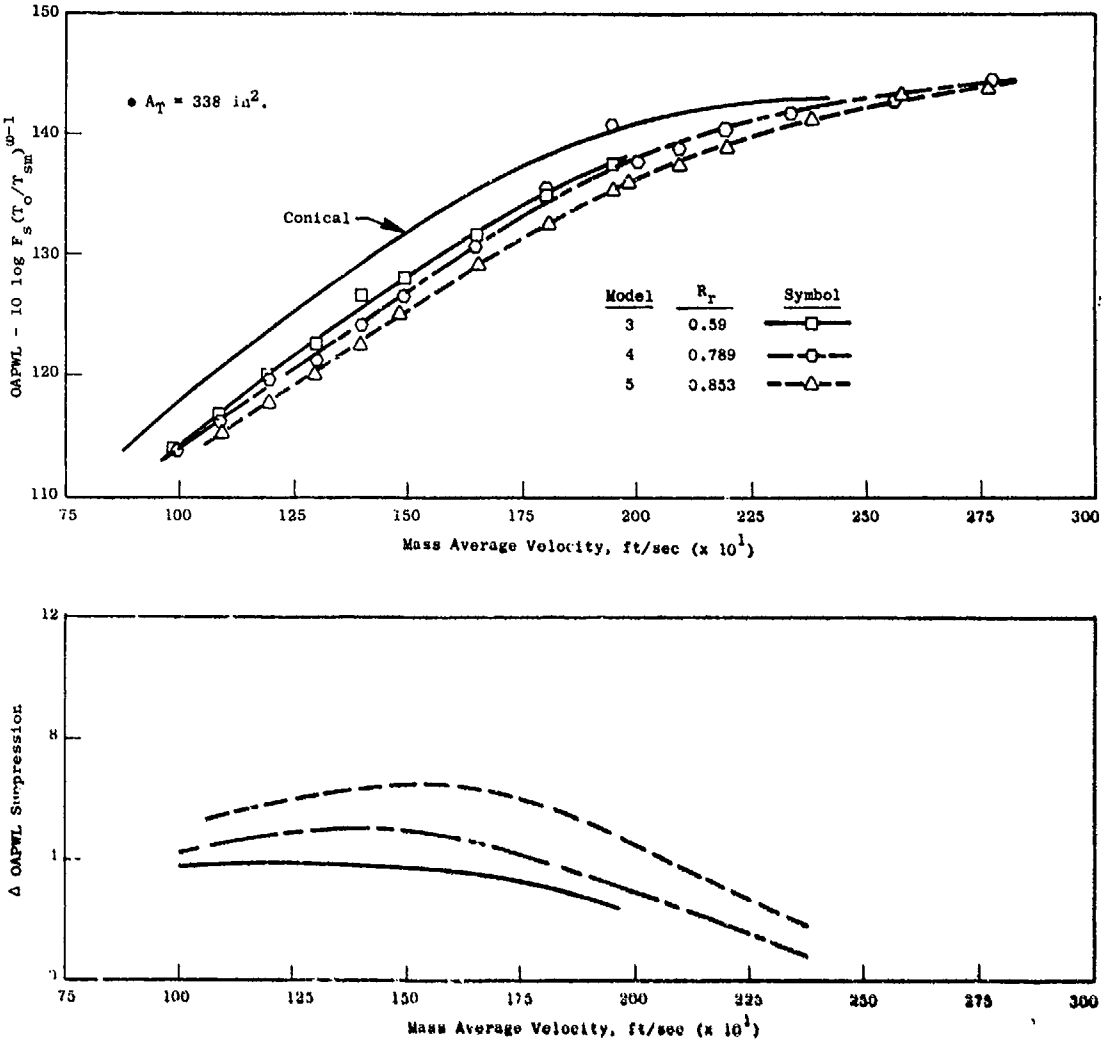

Figure 3-49. Summary of Plug Nozzle OAPWL and Suppression Levels.

Figures 3-44 through 3-47 show definite trends of suppression increase with higher radius ratio at peak and 90° for both OASPL and PNL. Maximum suppressions of 6.6 ΔPNL/6.8 ΔOASPL are seen at peak and 5.7 ΔPNL/5.1 ΔOASPL at 90° attained by the R_r = 0.853 plug (Model 5). Velocity region of max. suppression occurs at 1200 to 1500 ft/sec, considerably different than the higher velocity range for suppressors. Peak noise level suppression drops off considerably at high velocity; however, 90° suppression is fairly constant across the test velocity range. Since the 90° suppression levels are fairly well carried over to peak angles in the aft quadrant for low velocity, it is an indicator that a reduction in turbulent mixing noise is the primary suppression mechanism. A total variance of approximately 2.0 Δpeak OASPL and 3 Δpeak PNL is seen from the R_r = 0.59 to 0.853 excursion, maximum change occurring between the 0.789 (Model 4) and 0.853 (Model 5) plugs.

Data collapse quite consistently around the mean data-fitted curves, except for several points above the mean lines which possibly contain some shock-cell noise influence. At 50°, the PNL and OASPL levels are not as conducive to curve fitting, again indicating the presence of other than turbulent-mixing noise. Section 4.6.7 of Task 2 addresses shock-cell noise characteristics and correlations for these three annular plug nozzles. It has indicated that the annular jet formed between the nozzle shroud and plug centerbody may produce significantly different shock-cell patterns than an equivalent-flow-area conical nozzle when operating at underexpanded pressure ratios. The presence of the plug or centerbody provides a guided-expansion surface for the supersonic expansion/compression process. Additionally, the turbulent boundary layer on the plug surface may interact with the impinging shocks, modifying their characteristics.

Measured OASPL values for all supercritical nozzle pressure ratios correlate well at $\theta_I \approx 30°$ and 50° (where shock-cell noise is expected to dominate) when plotted versus β following typical conical nozzle β^4 dependency. A method of normalizing shock cell noise (N_{sh}) was formulated as:

$$N_{sh} = \text{OASPL} - 40 \log_{10}(\beta) - 20 \log_{10}(D_{eq}/r_o)$$ Task 2 Report, Equation 263 (Reference 7)

Data correlated very well at 30°, 50° and 70° when normalized in this manner and plotted versus β. A consistent trend of lower shock-cell noise (from 3 to 5 dB below conical) is observed as radius ratio is increased. As mentioned previously, this can be associated with decreasing annulus slit height as R_r increases and, subsequently, reduces the potential for strong shock structure development.

Comparisons of 50° nonnormalized spectra at P_T/P_o = 2.65, 3.28, and 3.55 were also done in the Task 2, Section 4.6.7, and showed that conical nozzle spectra shape is not maintained for a plug nozzle. A tendency to form two peaks was seen, their separation increasing with increasing radius ratio. The spectra were also more broadband in character than equivalent conical nozzle spectra.

For a more detailed comparison of PNL, OASPL and 1/3 OBSPL characteristics for the three radius ratio models tested along the simulated turbojet operating cycle line, the following are included:

- Figures 3-50 and 3-51 P_T/P_O = 2.07, T_T = 985° R, V_{ma} = 1490 ft/sec
- Figures 3-52 and 3-53 P_T/P_O = 2.65, T_T = 1295° R, V_{ma} = 1950 ft/sec
- Figures 3-54 and 3-55 P_T/P_O = 3.27, T_T = 1535° R, V_{ma} = 2350 ft/sec

Observations from the data plots include:

- Directivity patterns are quite consistent among the three radius ratio models with a general lowering of levels across all angles as R_T increases.
- Broadside and forward quadrant noise levels, even at high P_T/P_O, are quite low compared to shock-cell infested conical nozzle patterns.
- A tendency is observed toward double-humped spectra, particularly for low velocity data.
- Some shock-cell tones are present in the forward quadrant angle's spectra and occasionally at 90° to 110°.
- Changes in spectra levels from model to model occur fairly well broadband, particularly at low V_{ma}. At high velocity, spectra are quite similar in level and shape, bearing out the little change seen in PNL and OASPL at high V_{ma}.

Jet-density correlation, using data acquired at V_{ma} = 1000, 1250, 1640 and 2090 ft/sec on Model 4, was done similar to the procedure described in the previous section for the C-D plug (Model 2). Nonnormalized OAPWL and peak OASPL are plotted versus 10 $\log_{10}$ (ρ_o/ρ_{isa}) in Figure 3-56. Values of ω are tabulated and plotted versus $\log_{10}$ V_{ma}/a_o. Curves are shown through the data points to compare to the conical nozzle density dependence established by Hoch, et al. (Reference 25). Minor variations relative to the conical nozzle are seen, indicating that the choice of the conical nozzle curve for data correlation is sound.

3.4.1.4 Baseline Dual Flow Study

An AR = 2.0 coplanar-coannular nozzle, Model 6, was tested on JENOTS to establish the acoustic characteristics of a typical dual flow coplanar-coannular nozzle. Appendix A, Figure A-6 should be referred to for detailed geometric characteristics. The acoustic test matrix included cold inner and outer flow streams having a velocity ratio range of V_o/V_i = 0 to 5.0, plus hot inner and outer streams (≈1500° R) over a V_o/V_i = 0 to 2.5. The test matrix is described in Section 3.2.1 and the test conditions are documented

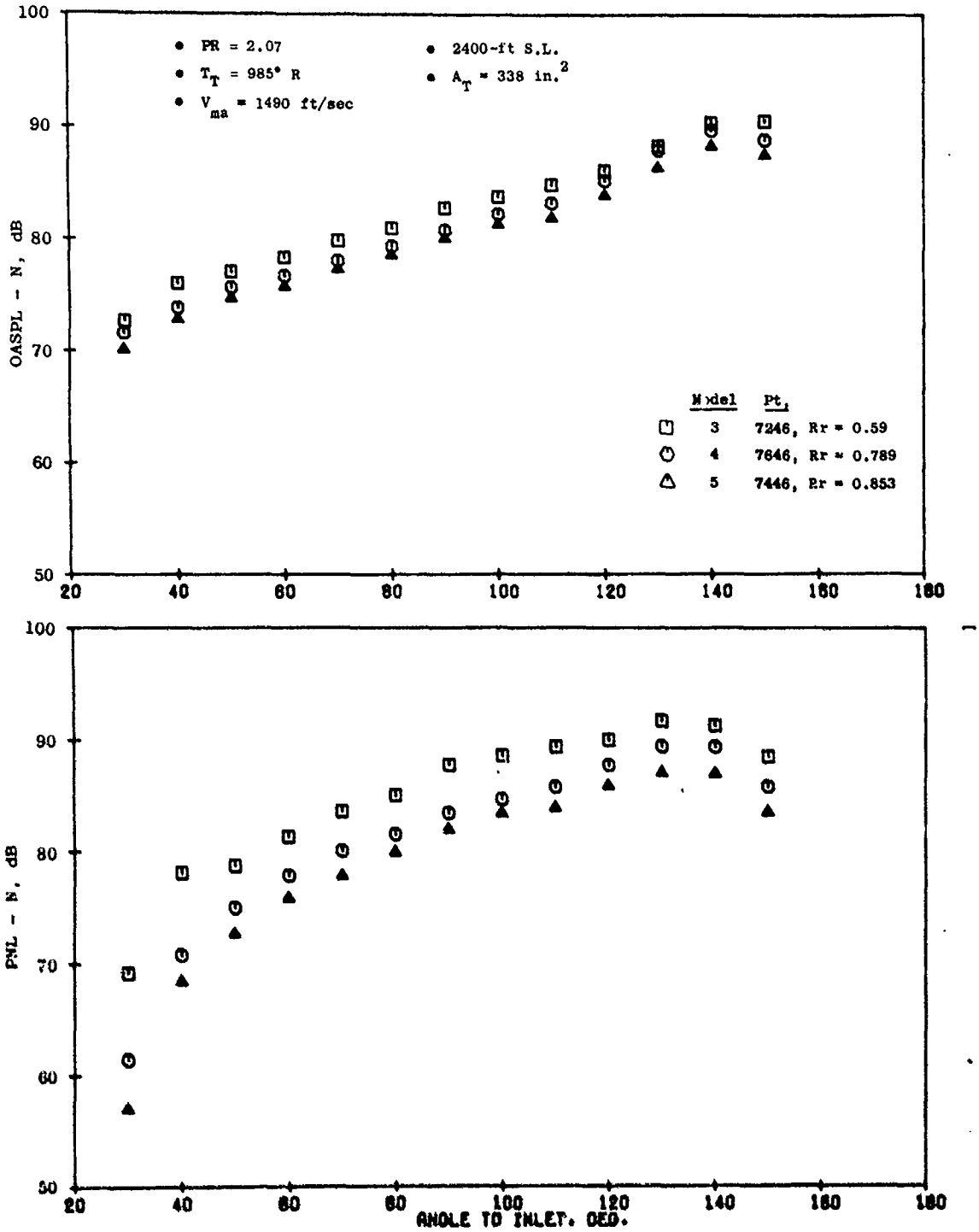

Figure 3-50. Impact of Plug Radius Ratio on OASPL and PNL Directivity, V_{ma} = 1490 ft/sec.

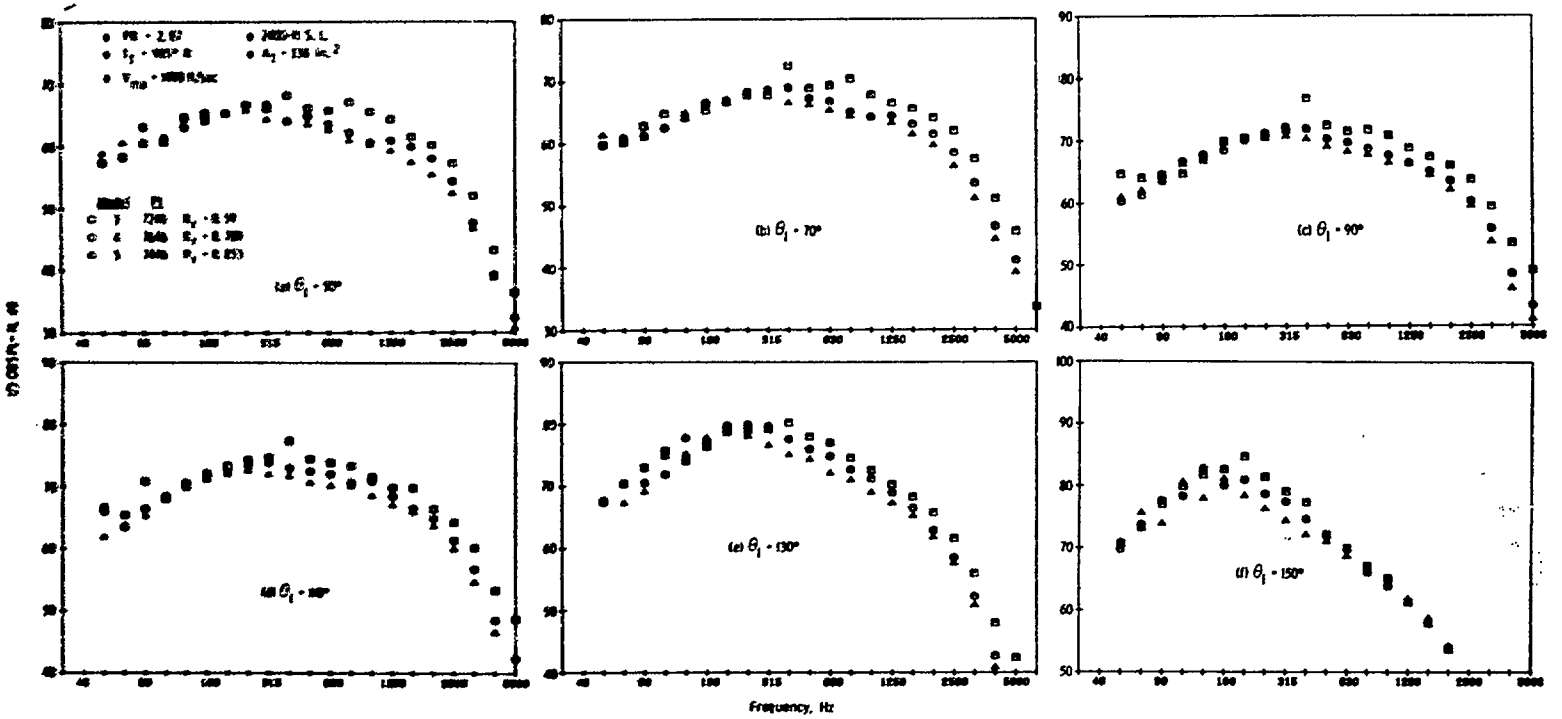

Figure 3-51. Impact of Plug Radius Ratio on OASPL and PNL Directivity, V_{ma} = 1490 ft/sec.

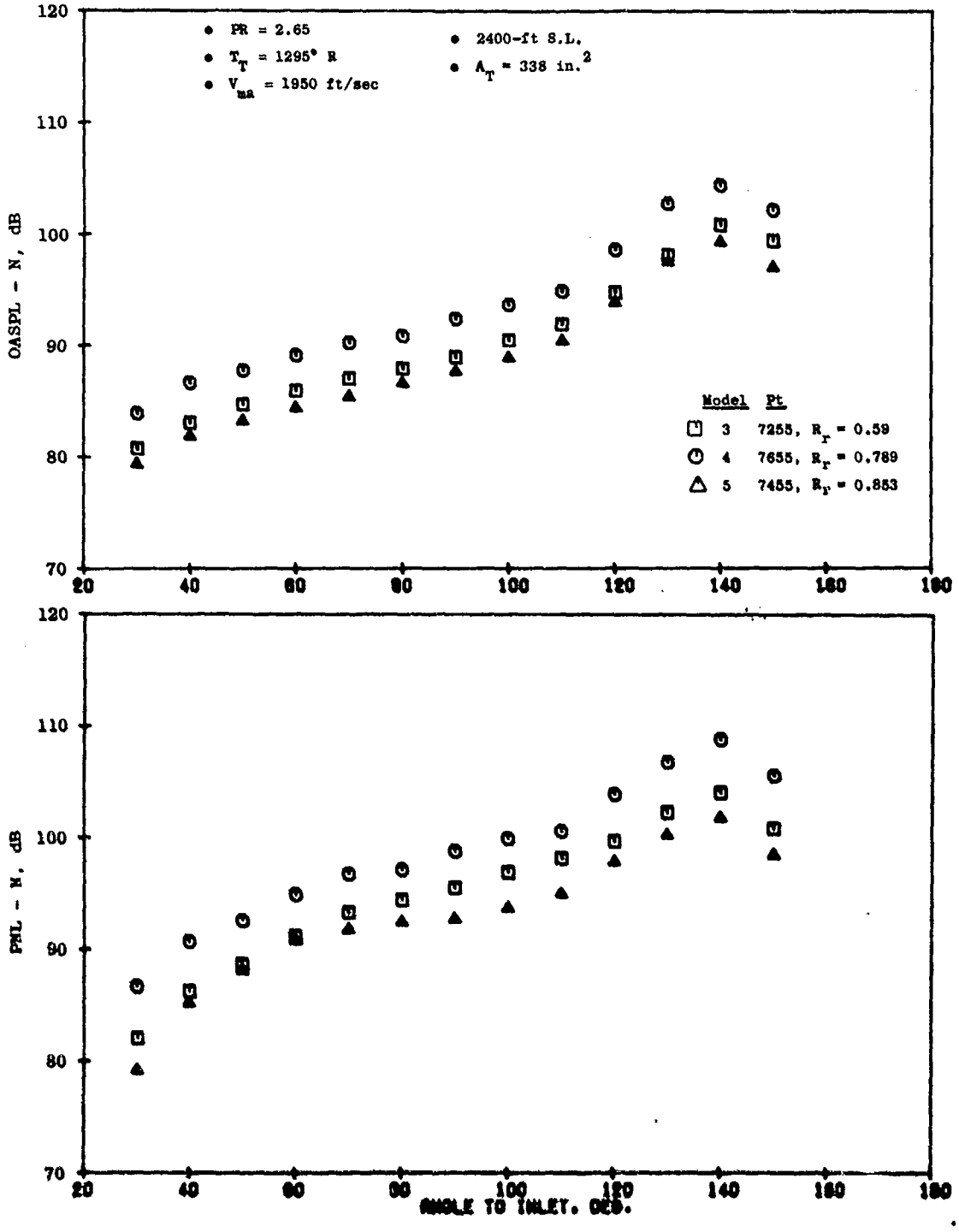

Figure 3-52. - Impact of Plug Radius Ratio on OASPL and PNL Directivity, V_{ma} = 1950 ft/sec.

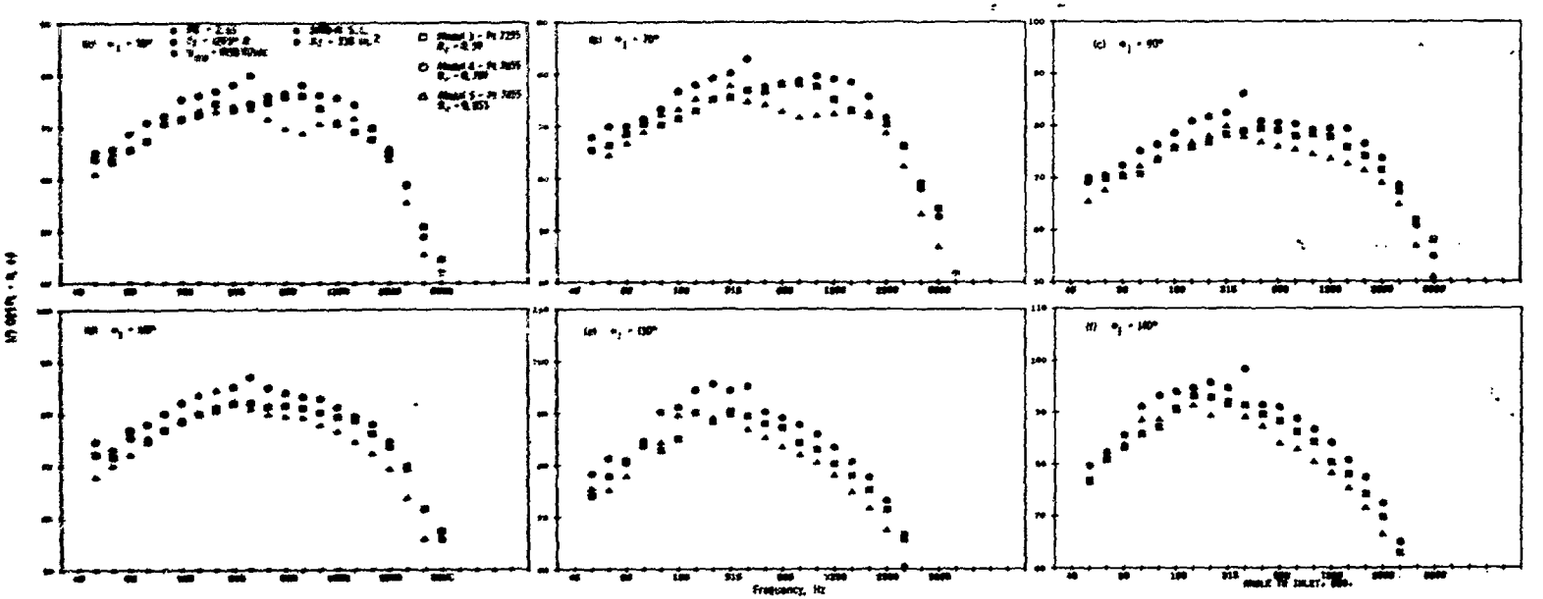

Figure 3-53. Impact of Plug Radius Ratio on Spectra , V_{ma} = 1950 ft/sec.

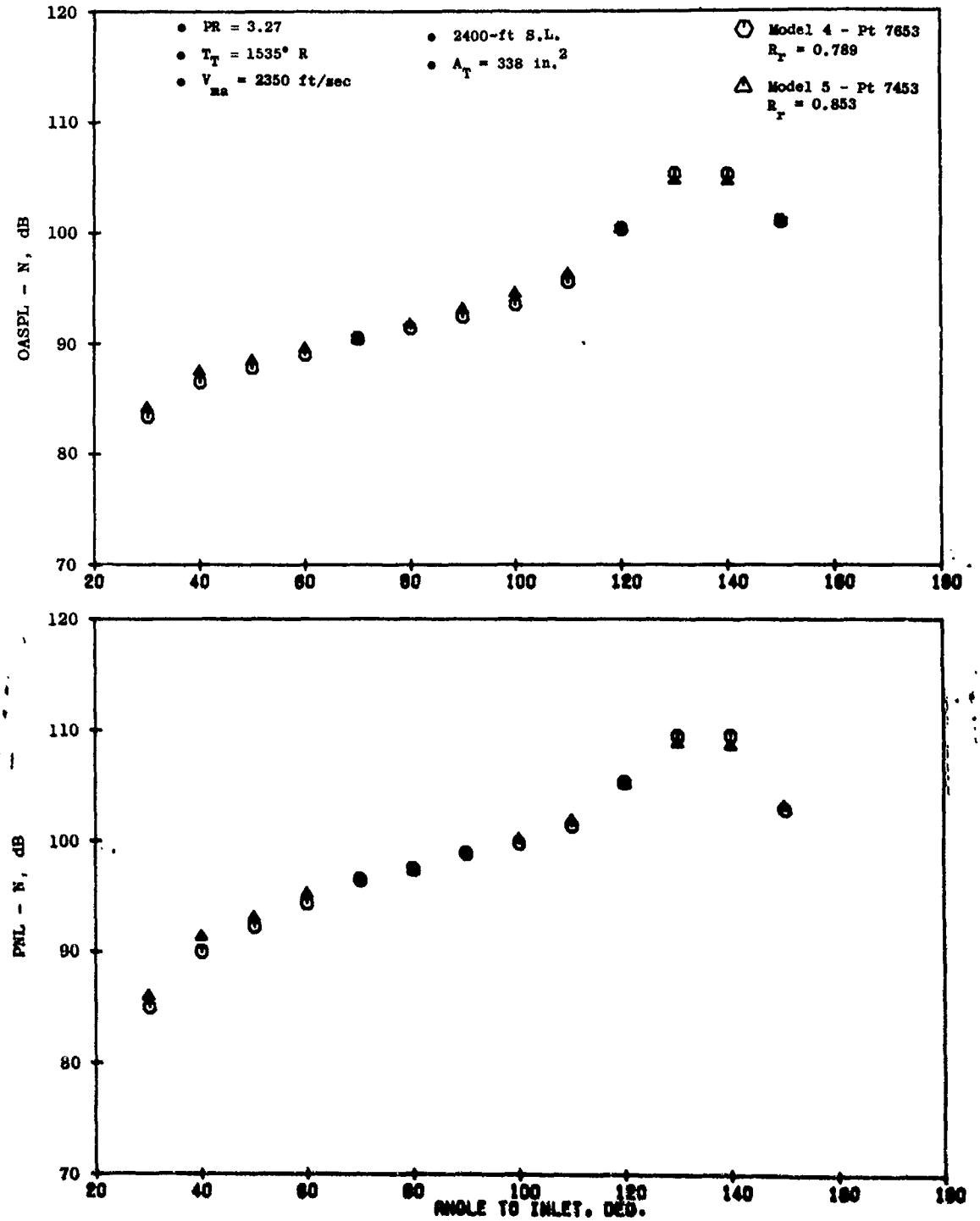

Figure 3-54. Impact of Plug Radius Ratio on OASPL and PNL Directivity, V_{ma} = 2350 ft/sec.

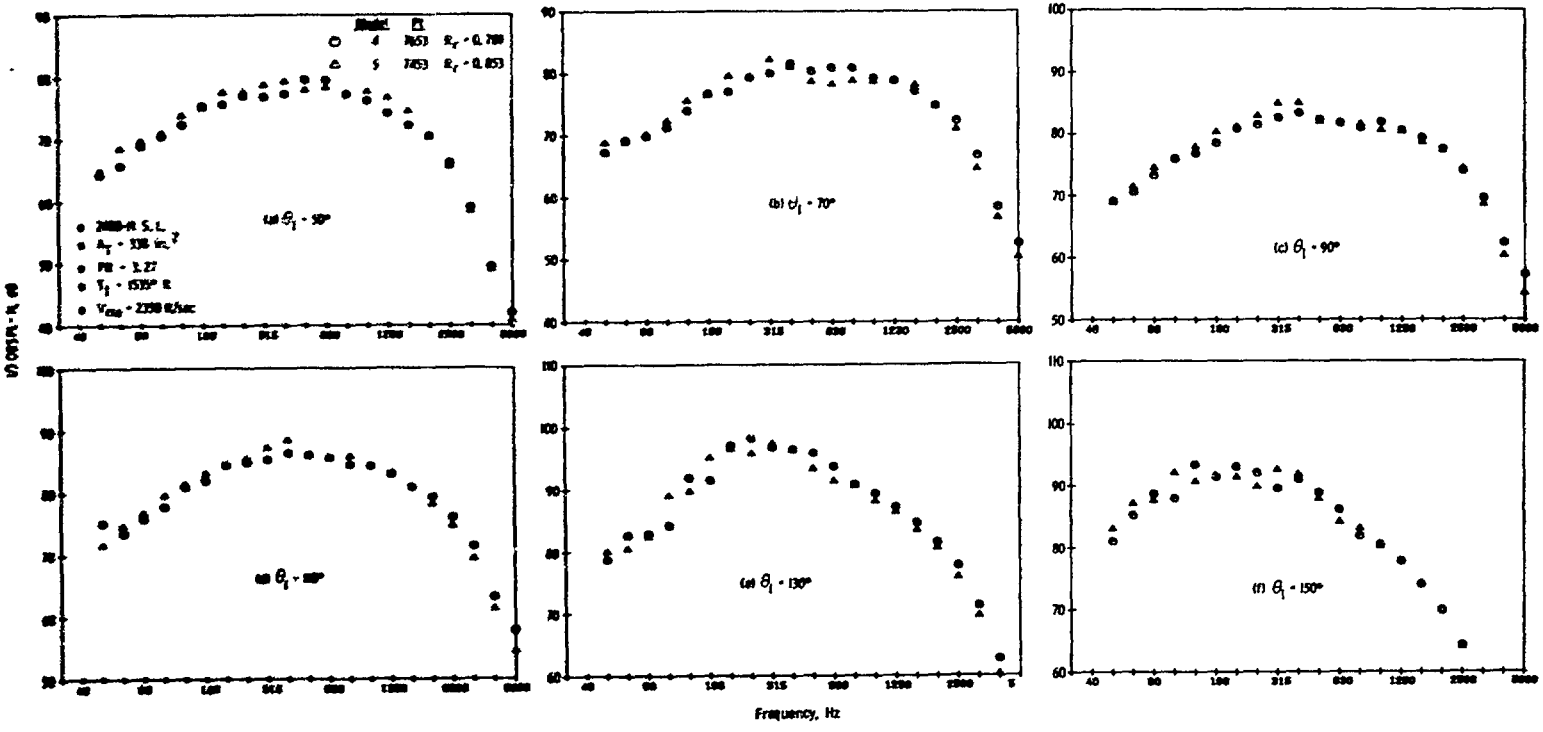

Figure 3-55. Impact of Plug Radius Ratio on Spectra, V_{ma} = 2350 ft/sec.

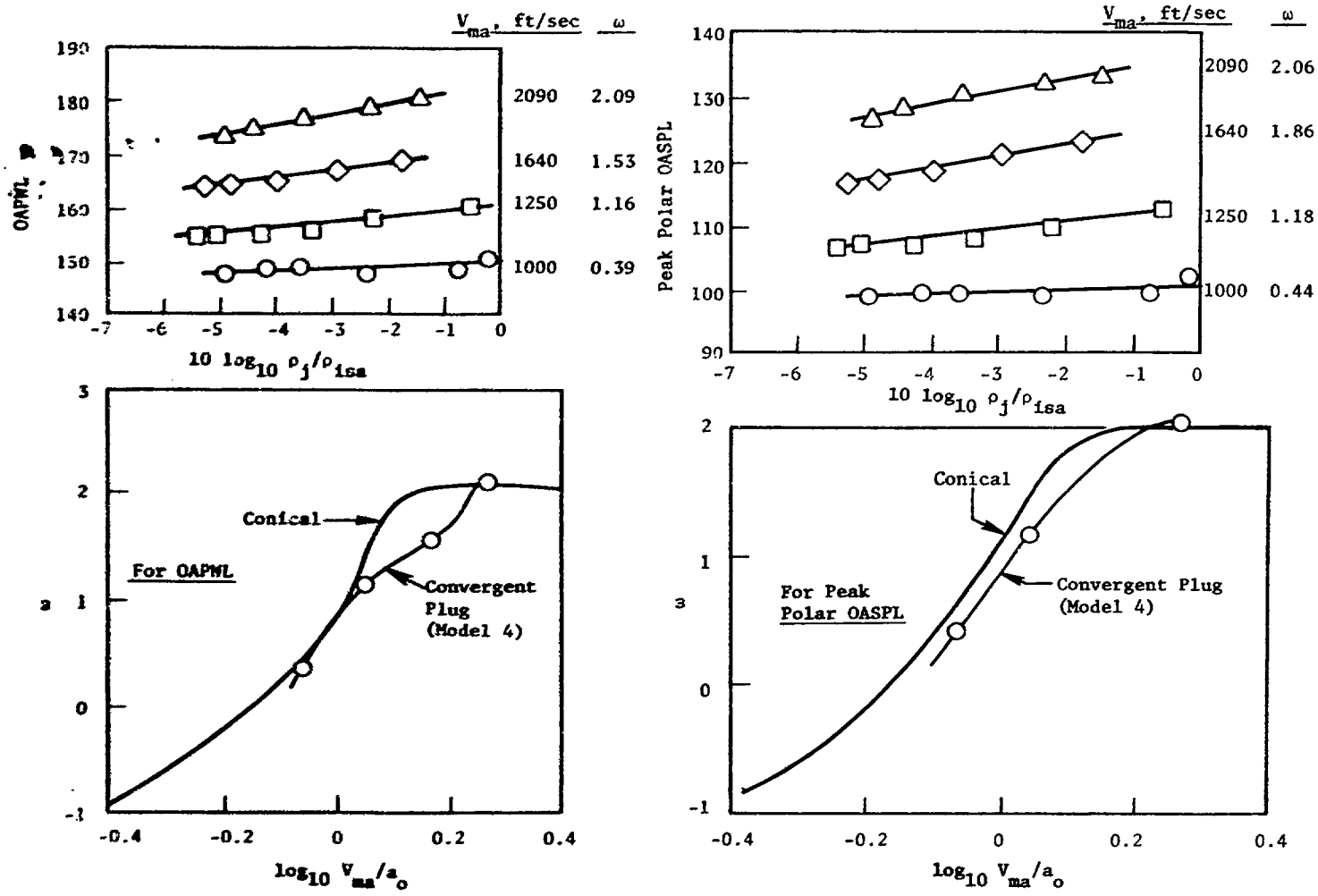

Figure 3-56. Jet Density Exponent Correlation.

on Table 6 of Appendix B. Conventional bypass as well as inverted flow cycle conditions were evaluated. A conventional bypass cycle is defined as when $V_o/V_i < 1.0$. An inverted flow cycle is when $V_o/V_i > 1.0$.

These data were used to support the theory/data comparisons presented in Section 4.7.8 of the Task 2 final report, Reference 7 and in Section 4.3.4 of Volume I of this report.

The PNL and OASPL directivity characteristics for velocity ratios (V_o/V_i) ranging from 0.17 to 1.27 are presented on Figure 3-57. The inner stream velocity was held constant at 1000 ft/sec. The data have been normalized as discussed in Section 3.3.1.7. The minimum noise level is observed to occur at a velocity ratio of 0.5 to 0.6. This is similar to the results presented in References 26, 27, and 28. Typical spectra comparisons at angles of 50°, 90° and 140° are presented on Figure 3-58. The spectra comparisons indicate that the level of noise reduction at a velocity ratio of 0.5 is relatively frequency independent in the aft quadrant and frequency dependent in the forward quadrant. The apparent deviation of the V_o/V_i = 1.27 data in the forward quadrant is due to the presence of shock noise, as demonstrated by the shape of the 60° spectra.

A similar data set was obtained holding the outer velocity, V_o, constant at 1000 ft/sec and varying the inner velocity, V_i, resulting in $0.63 < V_o/V_i < 2.66$. Also, the stagnation temperature of the inner stream was maintained at 1290° R. In contrast to the previous case, the minimum noise did not occur in the velocity ratio region of 0.5 to 0.6, but was observed to decrease as velocity ratio increased. Normalized PNL and OASPL directivity characteristics are presented on Figure 3-59 to support this observation. A 17 dB reduction in OASPL in the aft quadrant is observed as V_o/V_i increases from 0.63 to 2.86. Spectra are presented on Figure 3-60 to illustrate that the noise reduction with increasing velocity ratio primarily occurs in the low to midfrequency range.

The data are examined further by normalizing and comparing the data points for both sets on the basis of mixed flow velocity as defined in Section 3.3.1.7. This parameter was not effective in collapsing these two data sets into a unified line in the low velocity regime.

The nozzle was also evaluated at several conditions where both mass average velocity and velocity ratio were held constant. Typical directivity examples are presented for inverted flow cycles of V_o/V_i = 1.25 and 2.0 on Figures 3-61 and 3-62, respectively. The normalization parameter generally causes the collapse of the directivity pattern at a given mass average velocity while velocity ratio is held constant. This observation is also correct for the velocity ratio of 2.0 as illustrated by Figure 3-62. Typical spectra comparisons are presented on Figures 3-63(a) and (b) to verify the observations based on the directivity characteristics. In general, the spectra at the various angles indicate that this normalization parameter is effective in correlating the test data.

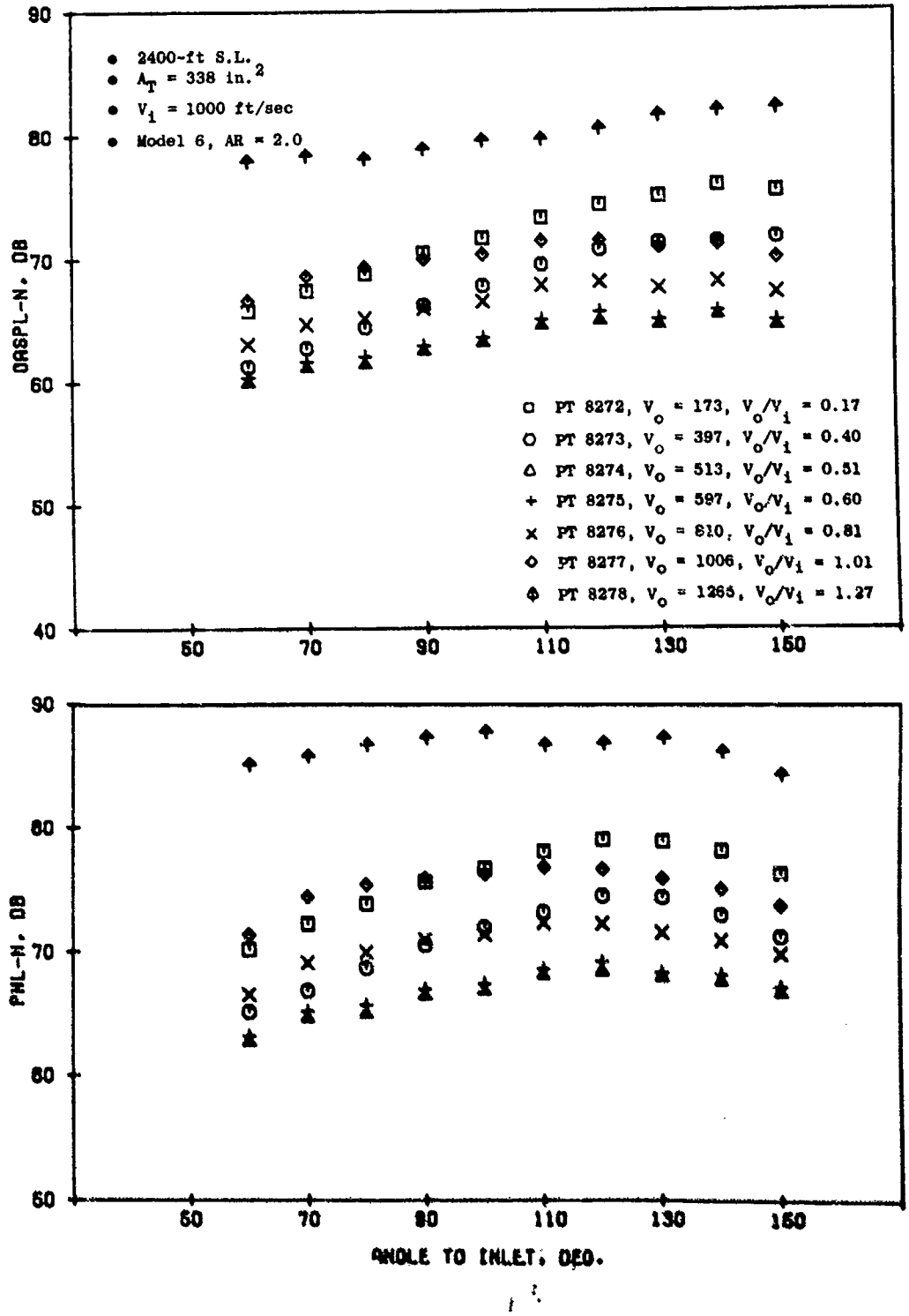

Figure 3-57. Impact of Velocity Ratio on OASPL and PNL Directivity, AR = 2.0 Coplanar-Coannular Nozzle (Model 6).

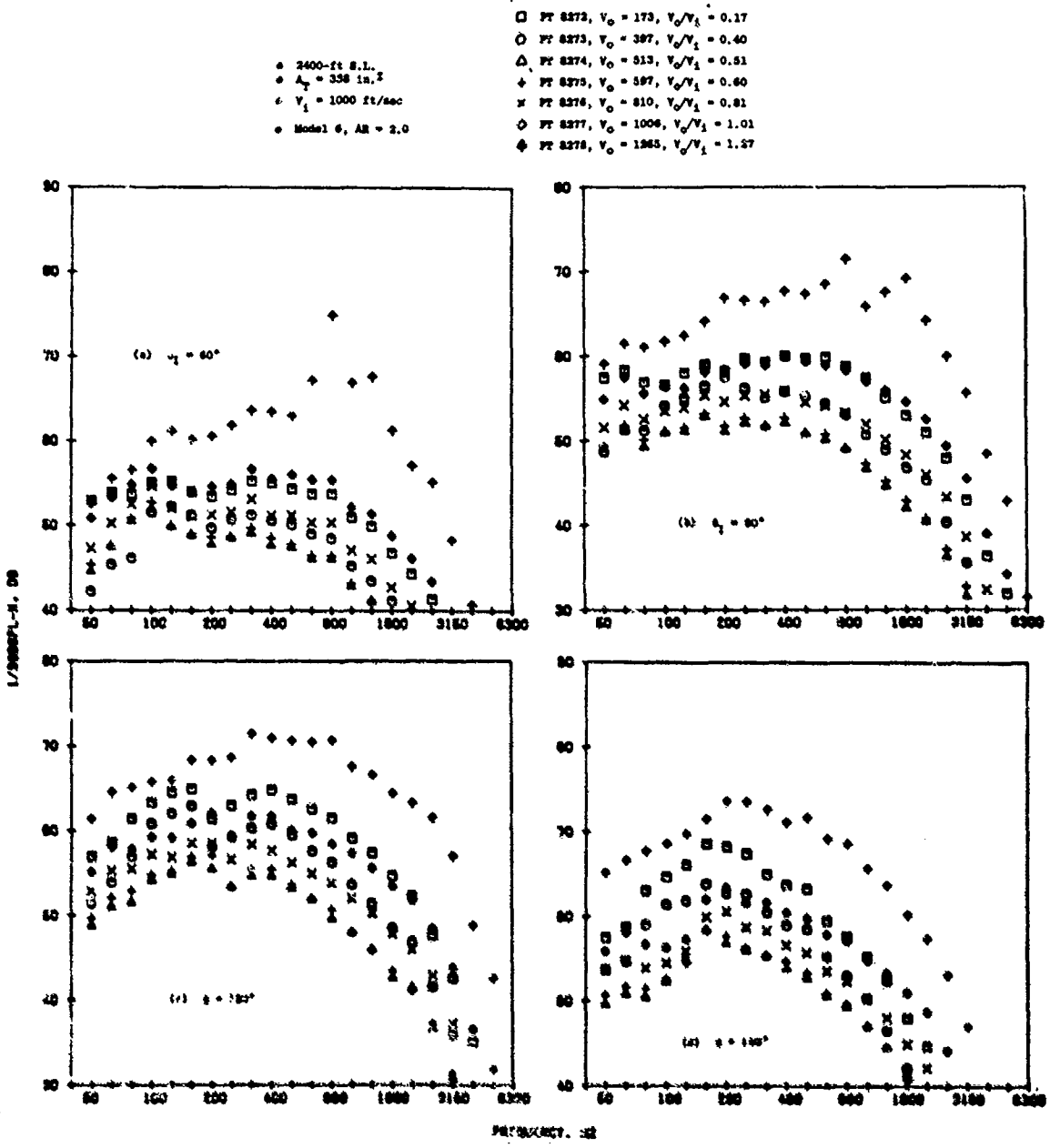

Figure 3-58. Impact of Velocity Ratio on Spectra, AR = 2.0 Coplanar-Coannular Nozzle (Model 6).

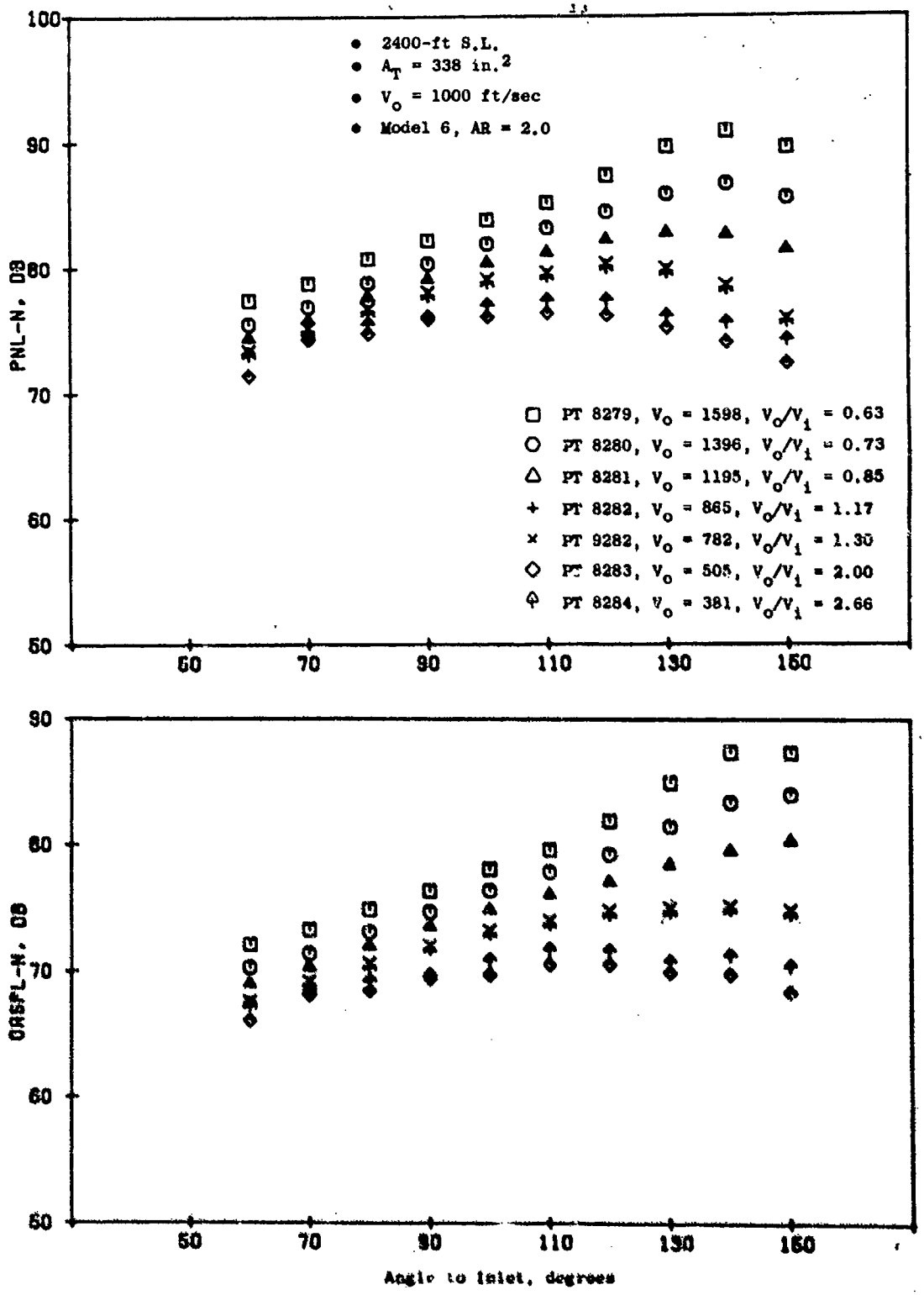

Figure 3-59. Impact of Velocity Ratio on OASPL and PNL Directivity.

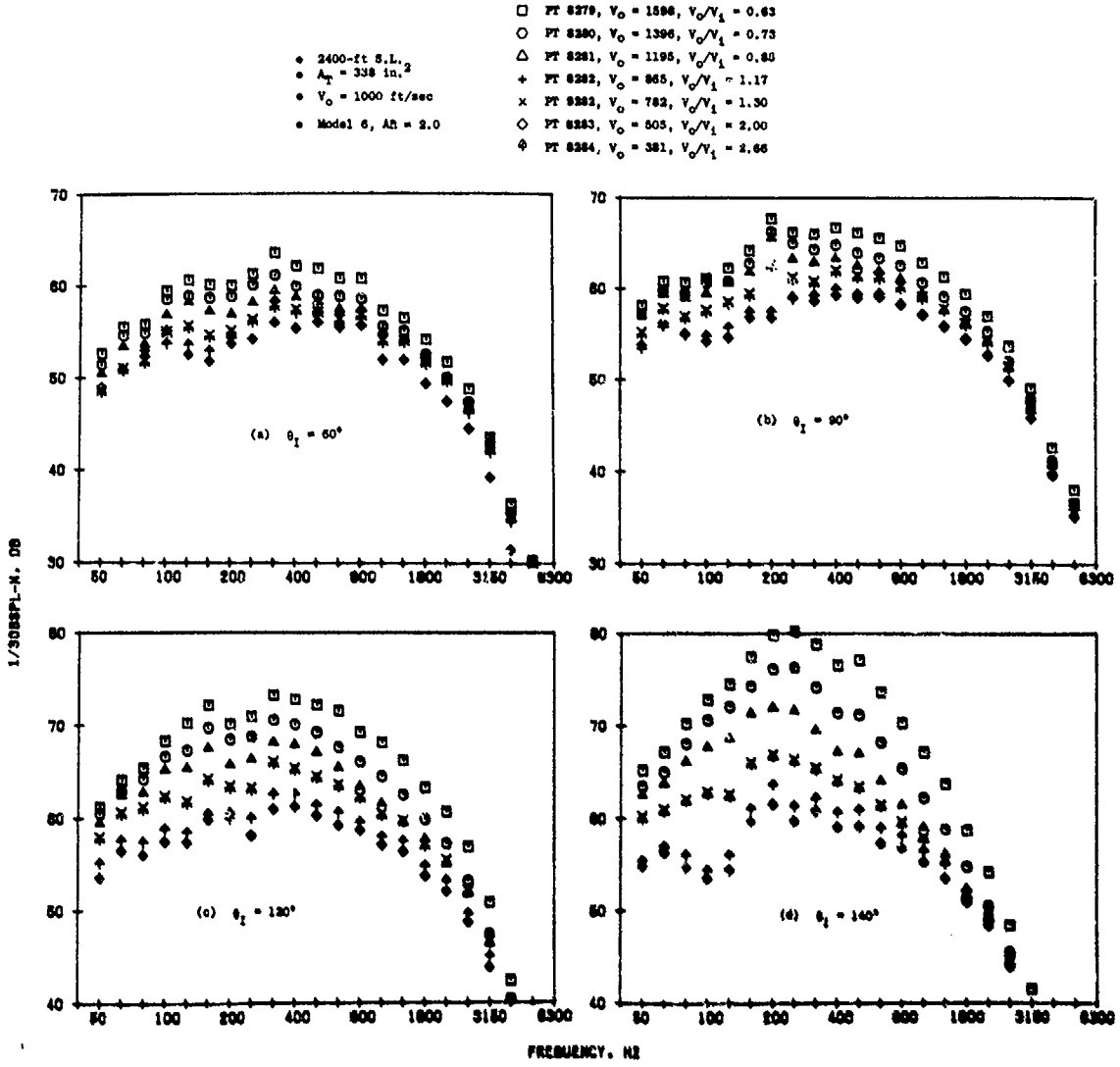

Figure 3-60. Impact of Velocity Ratio on Spectra.

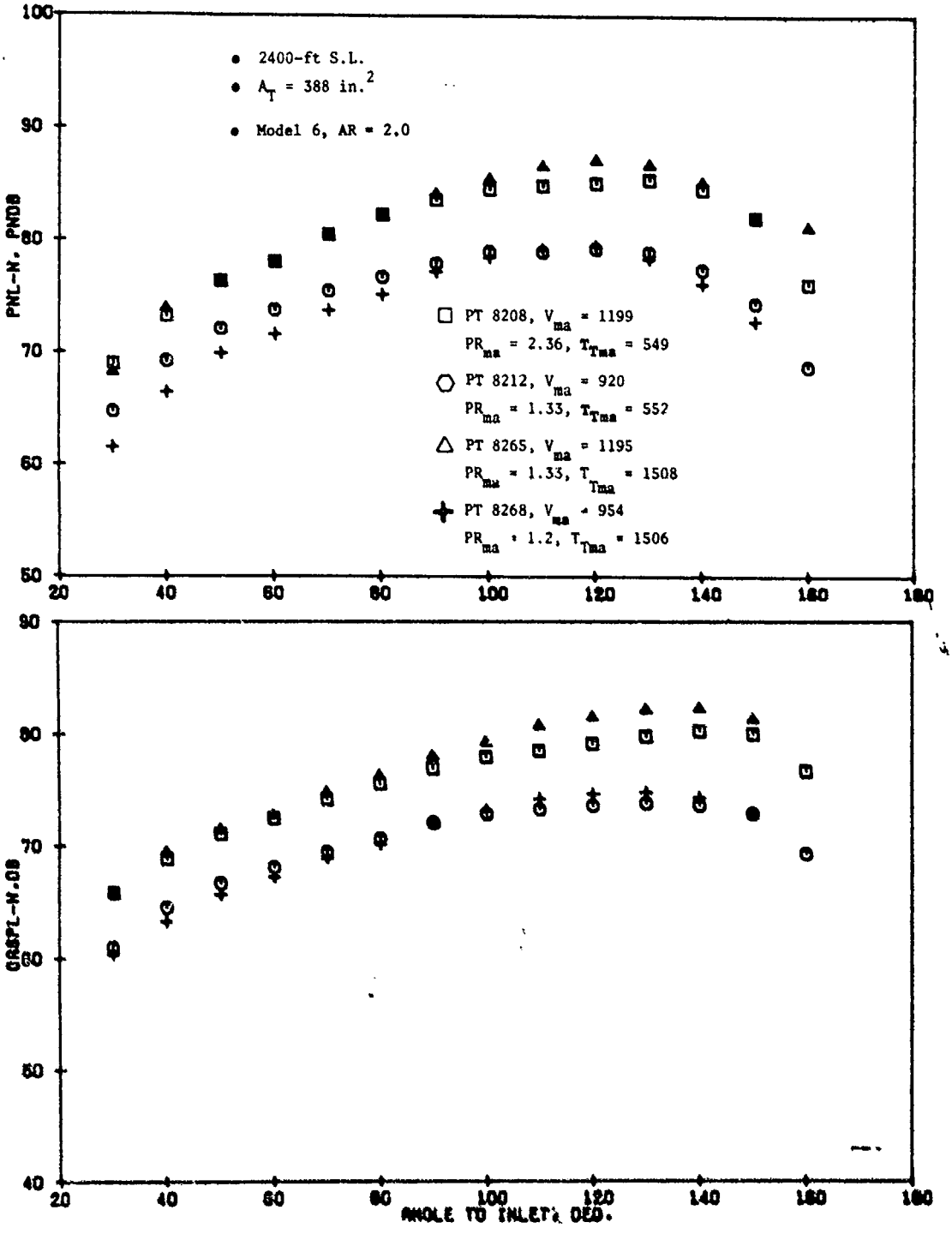

Figure 3-61. Comparison of OASPL and PNL Directivity at V_o/V_i = 1.25, AR = 2.0 Coplanar-Coannular Nozzle (Model 6).

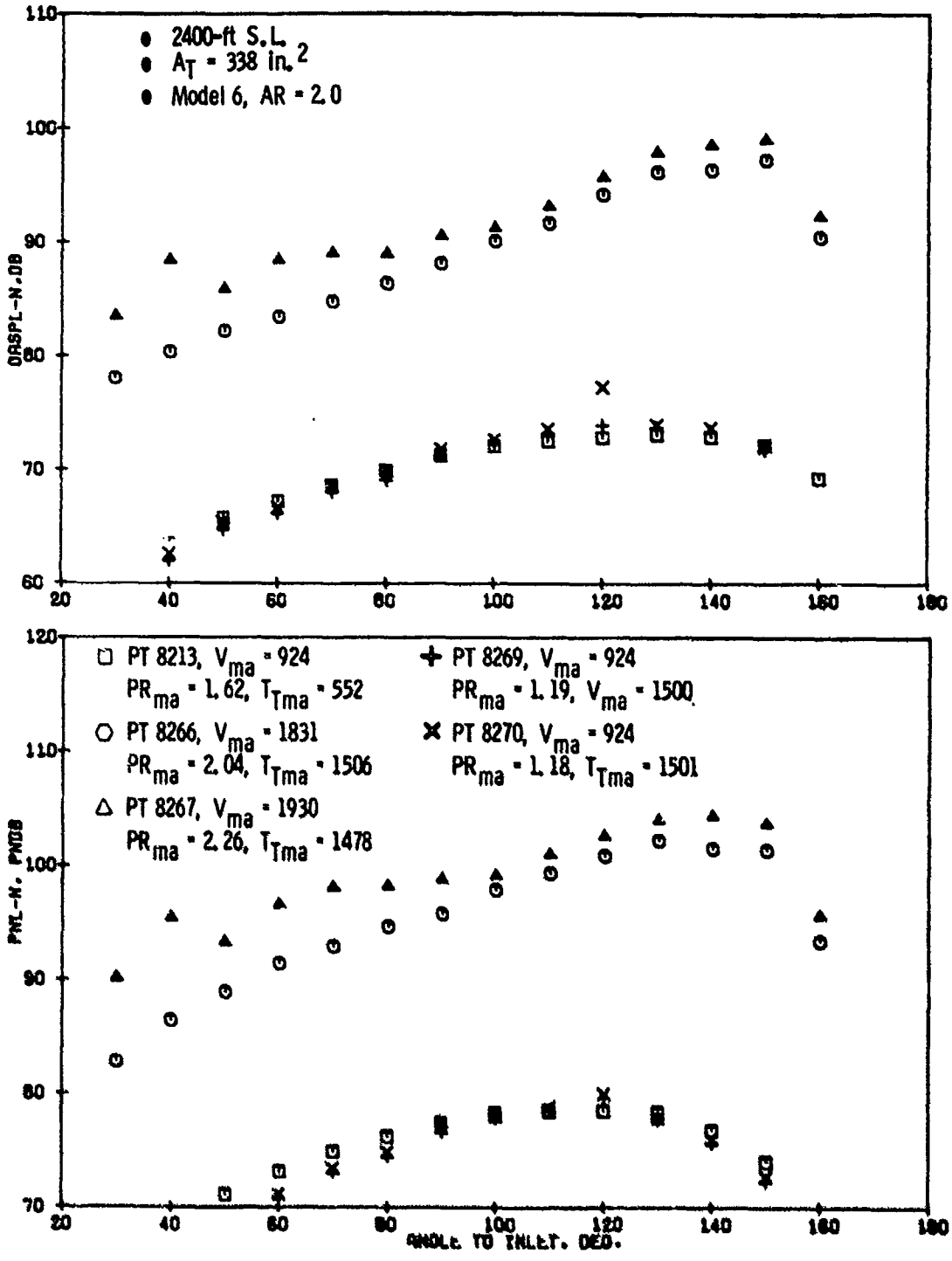

Figure 3-62. Comparison of OASPL and PNL Directivity, V_o/V_i = 2.0, AR = 2.0 Coplanar-Coannular Nozzle (Model 6).

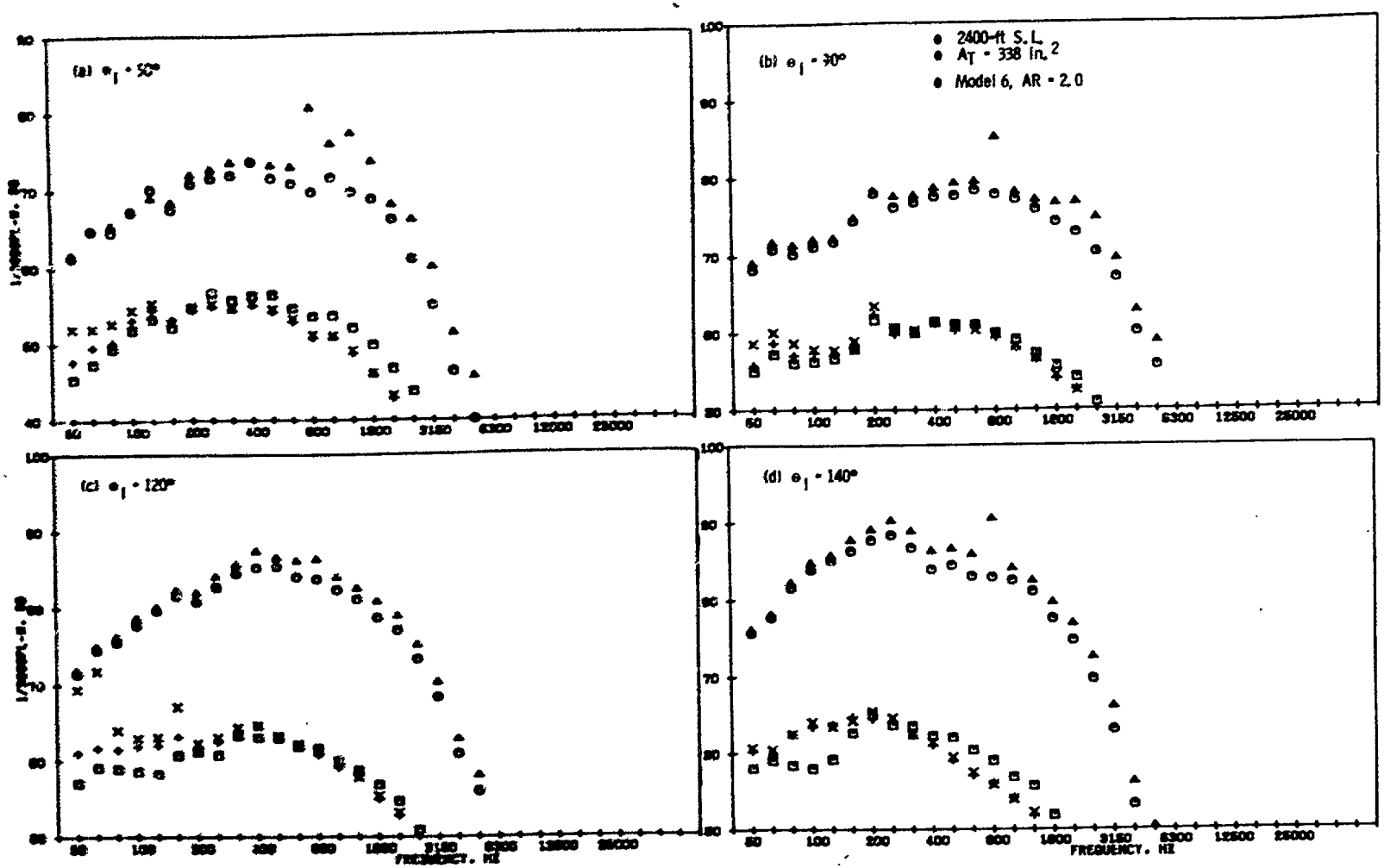

Figure 3-63(a). Normalized Spectra, V_o/V_i = 1.25, AR = 2.0 Coplanar-Coannular Nozzle (Model 6).

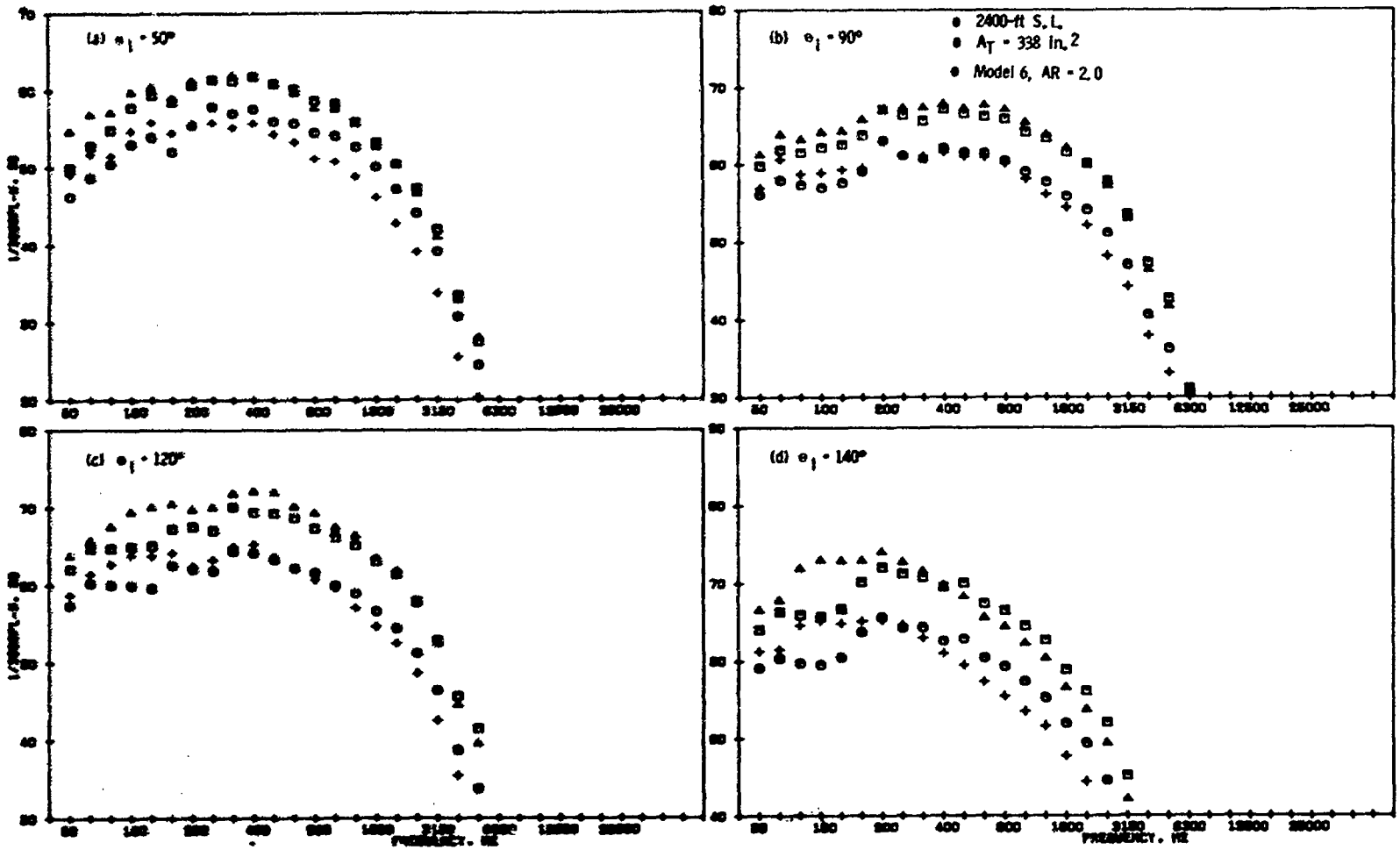

Figure 3-63(b). Normalized Spectra, V_o/V_1 = 2.0, Coplanar-Coannular Nozzle (Model 6).

3.4.1.5 Dual-Flow Parametric Study (Models 6, 7, and 8)

Test data similar to that described in the previous section were obtained on AR = 0.65 (Model 7) and 0.4 (Model 8) coplanar-coannular nozzles. In conjunction with the previous results, they will be used to evaluate the impact of nozzle area ratio on suppression characteristics for inverted-flow cycles.

The geometric characteristics of these nozzles are defined on Figures A-7 and A-8 in Appendix A. The thermodynamic conditions are summarized on Tables 7 and 8 in Appendix B.

Normalized PNL levels for the three nozzles are on Figure 3-64, along with conical nozzle data; presented as a reference for establishing suppression level. No consistent trend of suppression with area ratio is observed. The maximum suppression level obtained is 4 dB and occurs at both velocity ratios of 1.5 and 2.0. Peak OASPL comparisons on Figure 3-65 exhibit similar trends, however, suppression levels up to 5 dB are observed. Normalized OASPL and PNL characteristics at 90° are summarized on Figure 3-66. Trends are similar to those observed at the peak noise angle with the exception that the absolute level of suppression has decreased. Comparisons at 50° are presented on Figure 3-67 and show suppression level to increase as velocity ratio decreases. The variation of noise level with nozzle area ratio is a function of velocity ratio.

Directivity and spectra comparisons are presented on Figures 3-68 through 3-73. PNL and OASPL directivity characteristics are evaluated for velocity ratios of 1.0, 1.5 and 2.0. The inner velocity, is held constant at 1000 ft/sec and the data are normalized for thrust and temperature. Comparisons at a velocity ratio of 1.0, on Figure 3-68, show no significant change in PNL or OASPL characteristics as area ratio varies. Similarly at velocity ratios of 1.5 and 2.0, on Figures 3-69 and 3-70, a reduction of 3 to 9 dB occurs as area ratio decreases from 2.0to 0.4. The variation in noise level is a function of area ratio, velocity ratio, and acoustic angle; the maximum variation occurring at a velocity ratio of 2.0. Noise level variation with area ratio is significant when holding inner stream cycle conditions constant and normalizing for thrust and temperature. On the basis of constant mass average velocity, V_{mg}, this variation is reduced and demonstrates that noise may be correlated using this parameter. Spectra variations at 50°, 90°, 120° and 140° are summarized on Figure 3-71 for a velocity ratio of 1.0. With the exception of frequencies below 160 Hz, where the data are strongly influenced by ground reflection, the spectrum shapes and levels are equivalent. Similar comparisons for velocity ratios of 1.5 and 2.0 are summarized on Figures 3-72 and 3-73. The difference between the three configurations is frequency dependent. Comparison of the 50° spectra for velocity ratios of 1.5 and 2.0 illustrates a change in spectrum shape as the outer stream pressure ratio increases. Also the variation in level due to nozzle area ratio is found to increase significantly compared to the 1.5 velocity ratio comparisons. This is attributed to shock noise occurring in the forward quadrant. The comparisons also suggest that reduction of the outer stream annulus height is an effective way to reduce shock noise as discussed in Section 4.6.7, Reference 7.

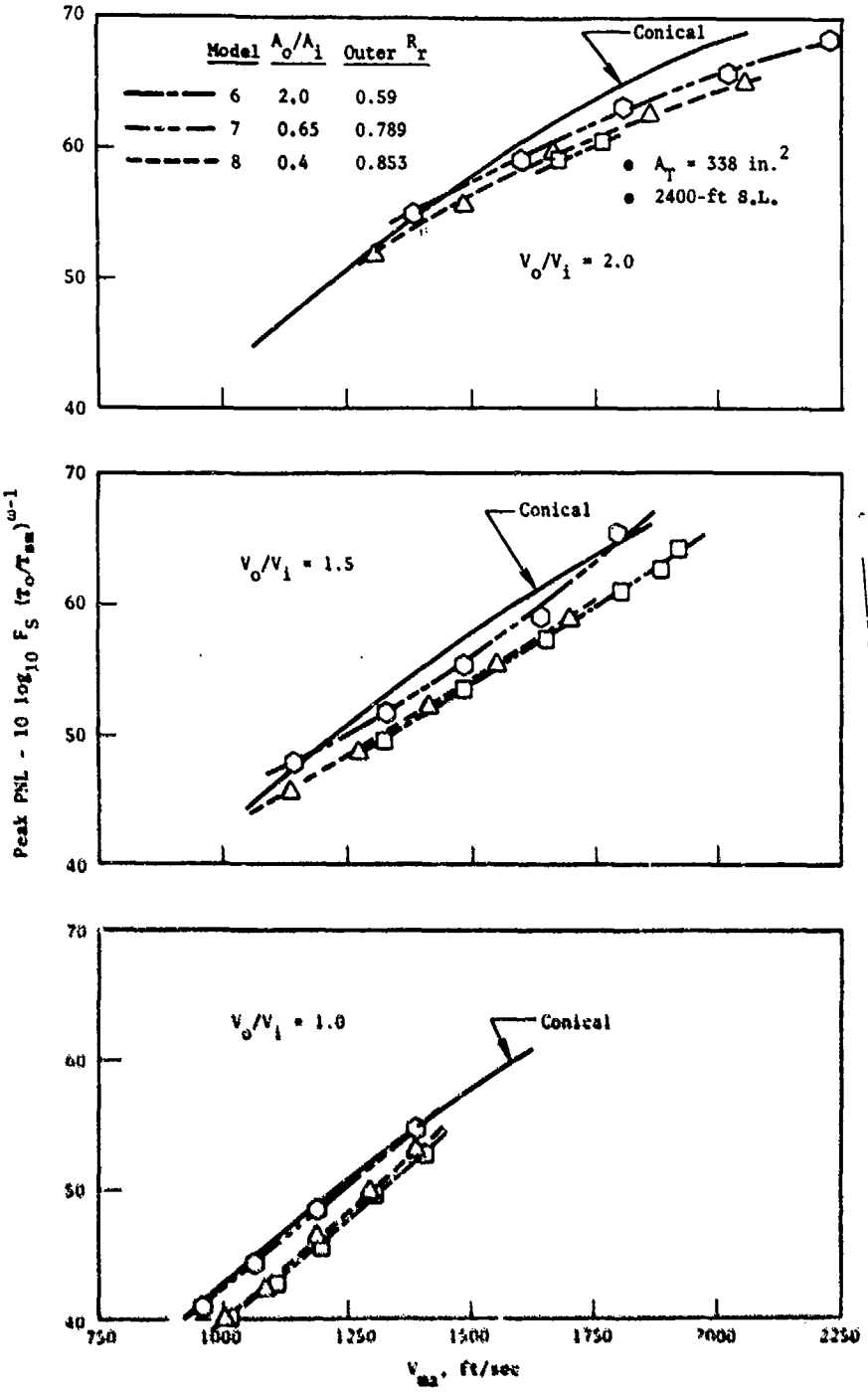

Figure 3-64. Peak PNL Coplanar-Coannular Nozzle Area Ratio Variation.

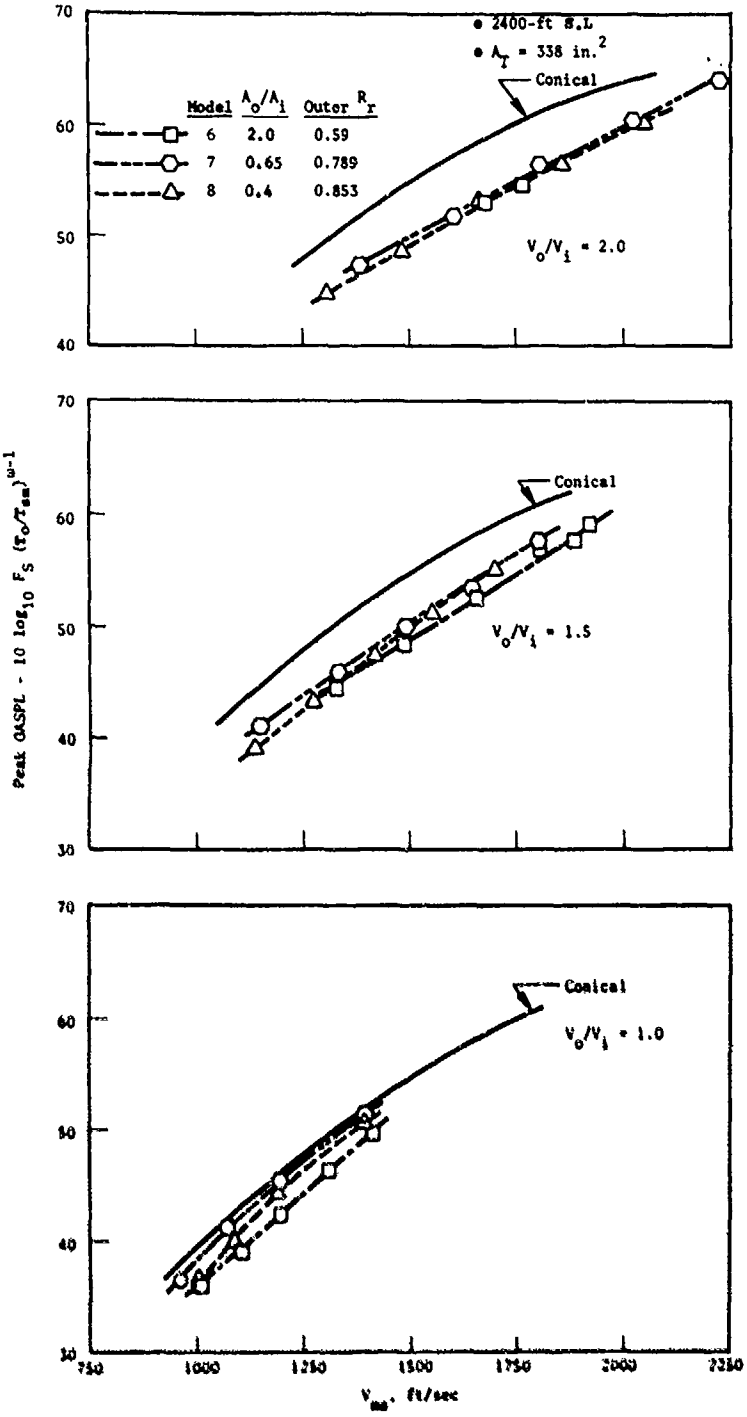

Figure 3-65. Peak OASPL Coplanar-Coannular Nozzle Area Ratio Variation.

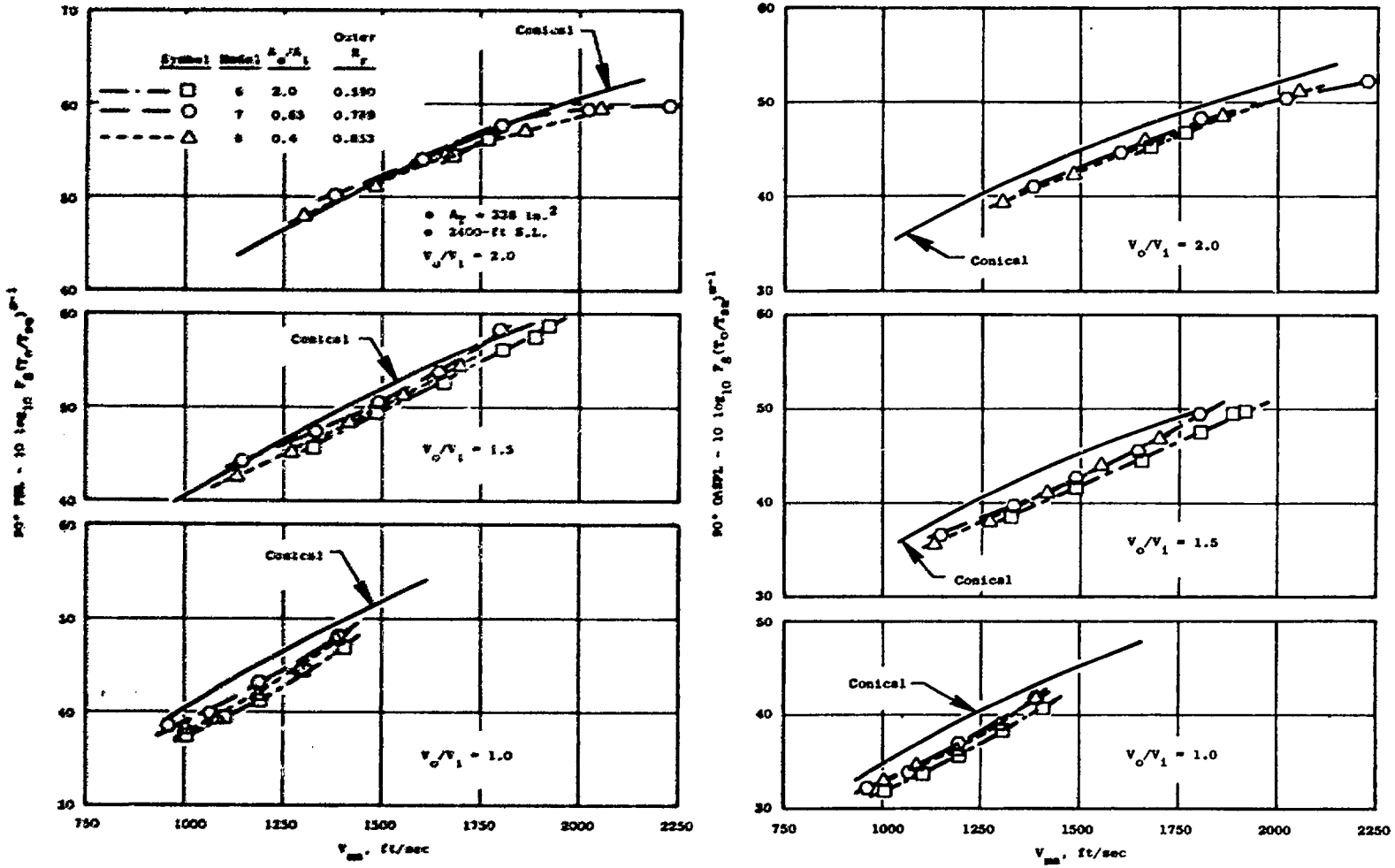

Figure 3-66. 90° PWL and OASPL Coplanar-Coannular Nozzle Area Ratio Variation.

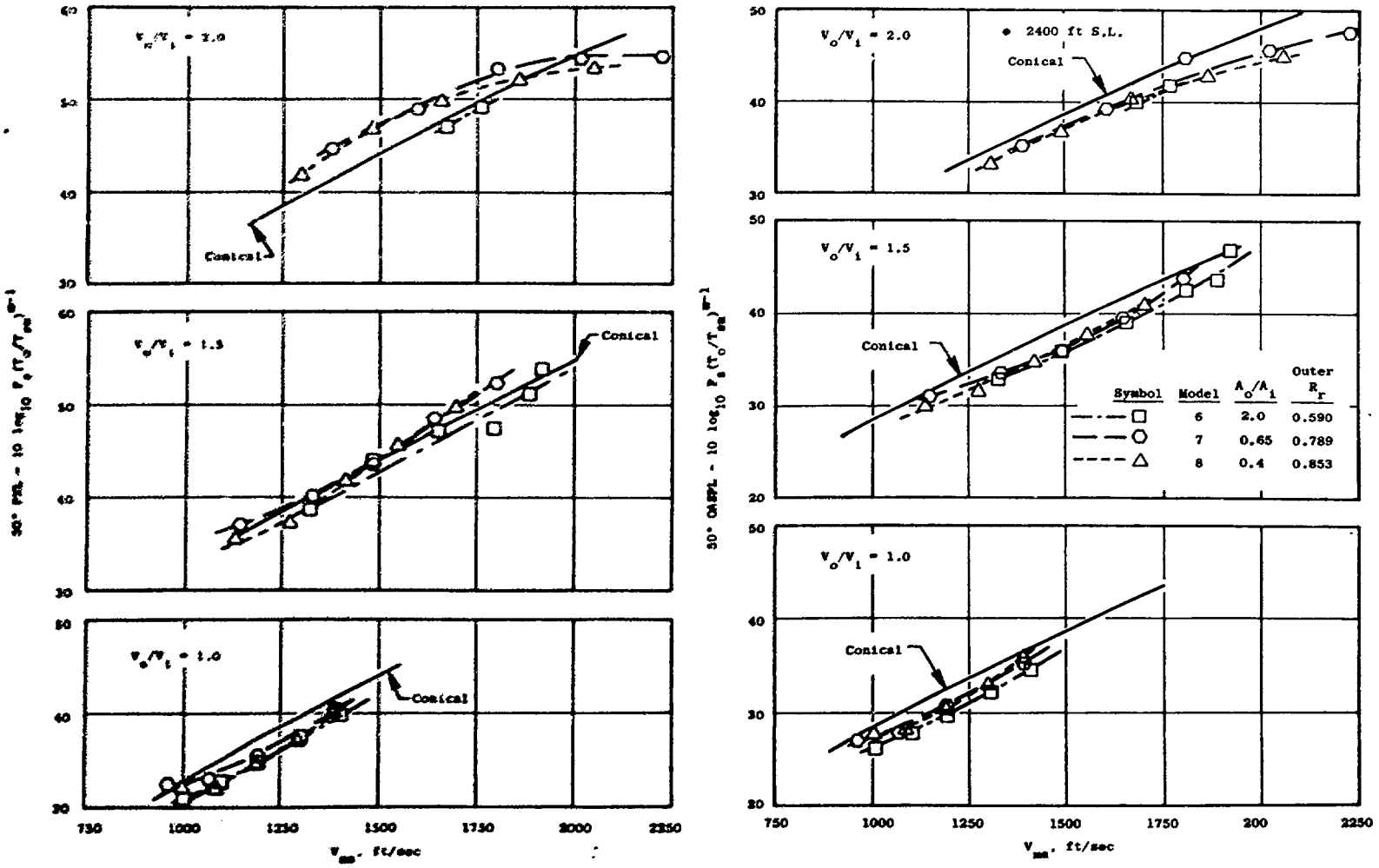

Figure 3-67. 50° PNL and OASPL Coplanar-Coannular Nozzle Area Ratio Variation.

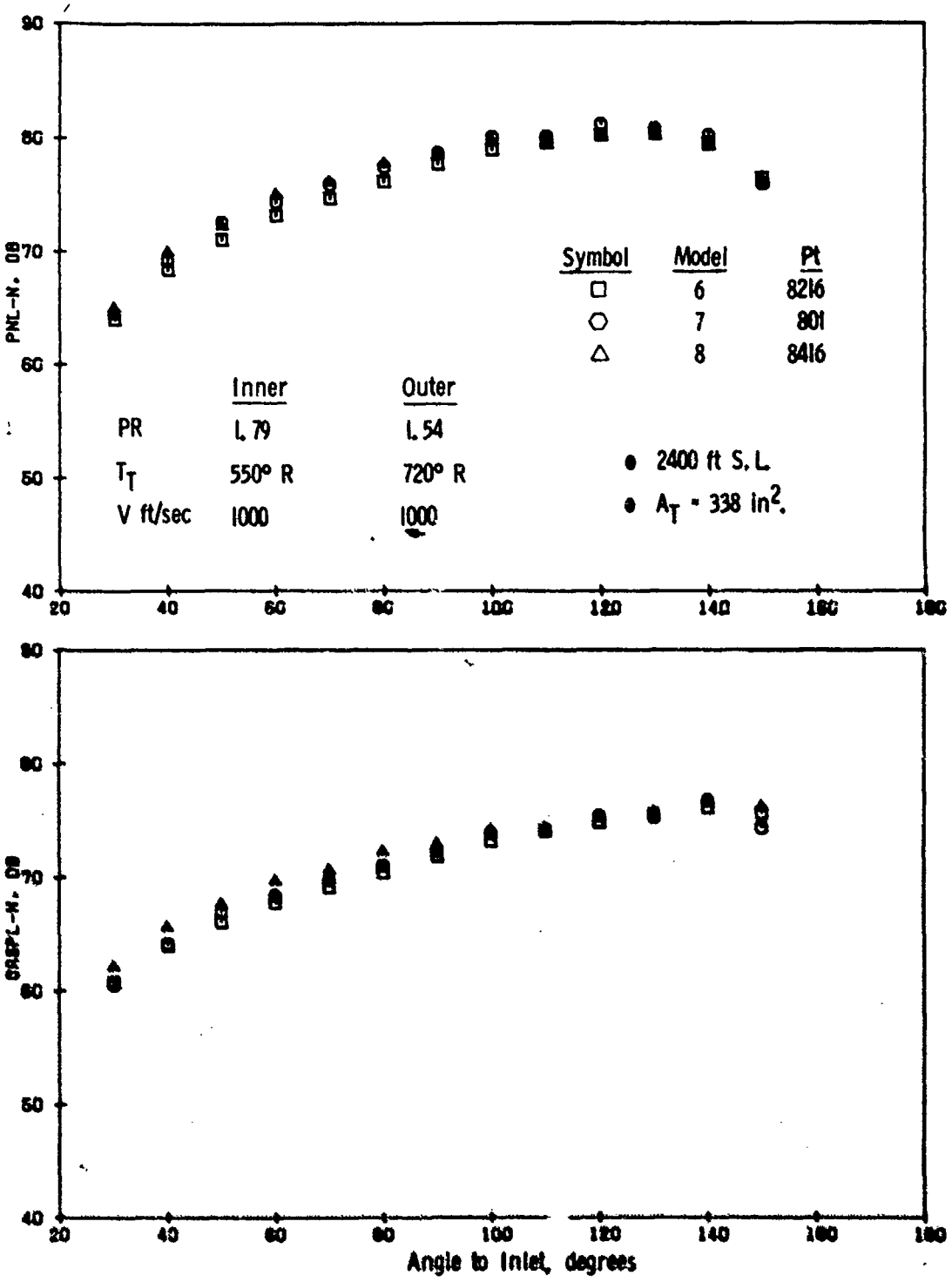

Figure 3-68. OASPL and PNL Directivity Variation with Area Ratio, V_o/V_i = 1.0.

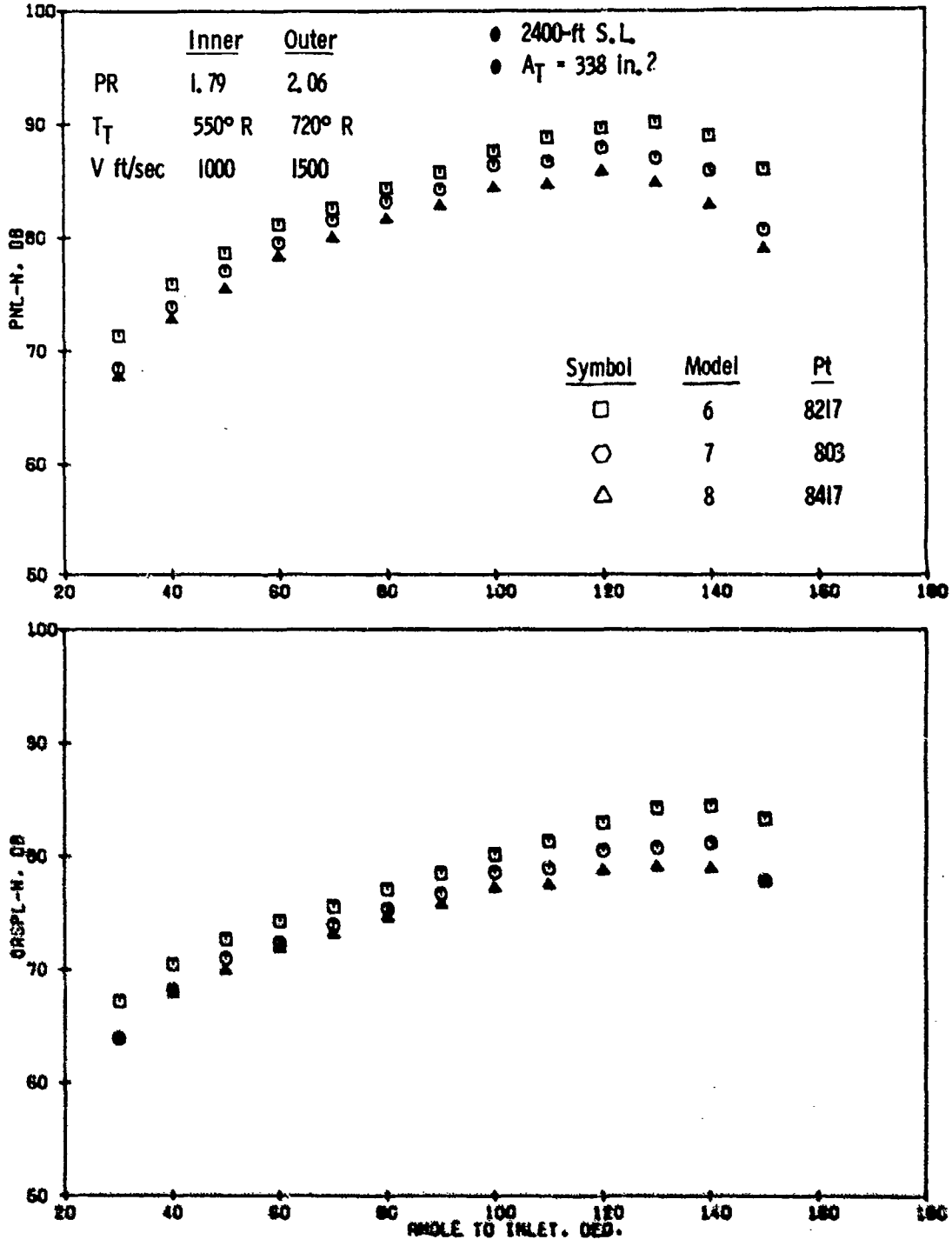

Figure 3-69. OASPL and PNL Directivity Variation with Area Ratio, V_o/V_i = 1.5.

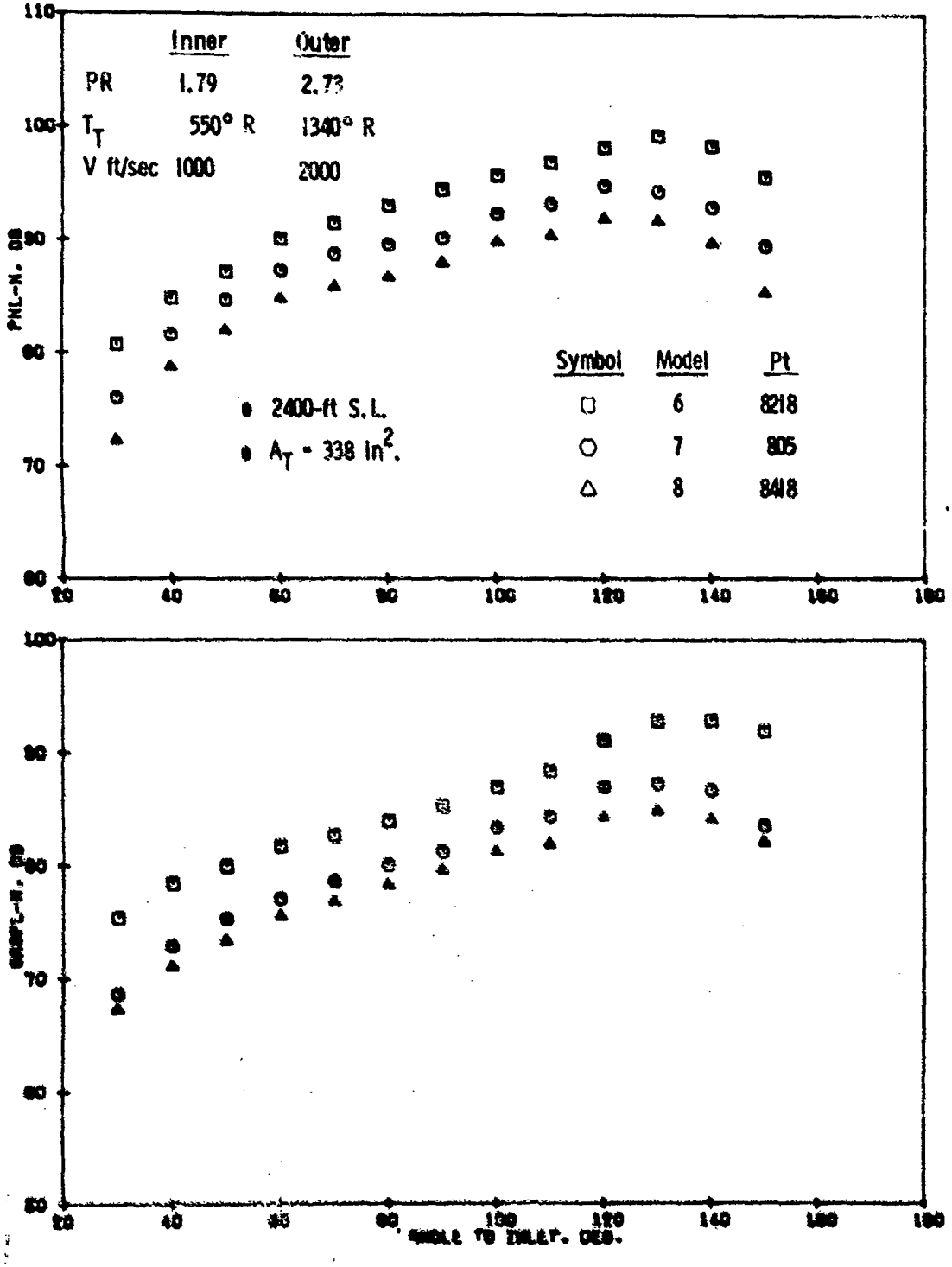

Figure 3-70. OASPL and PNL Directivity Variation with Area Ratio, V_O/V_1 = 2.0.

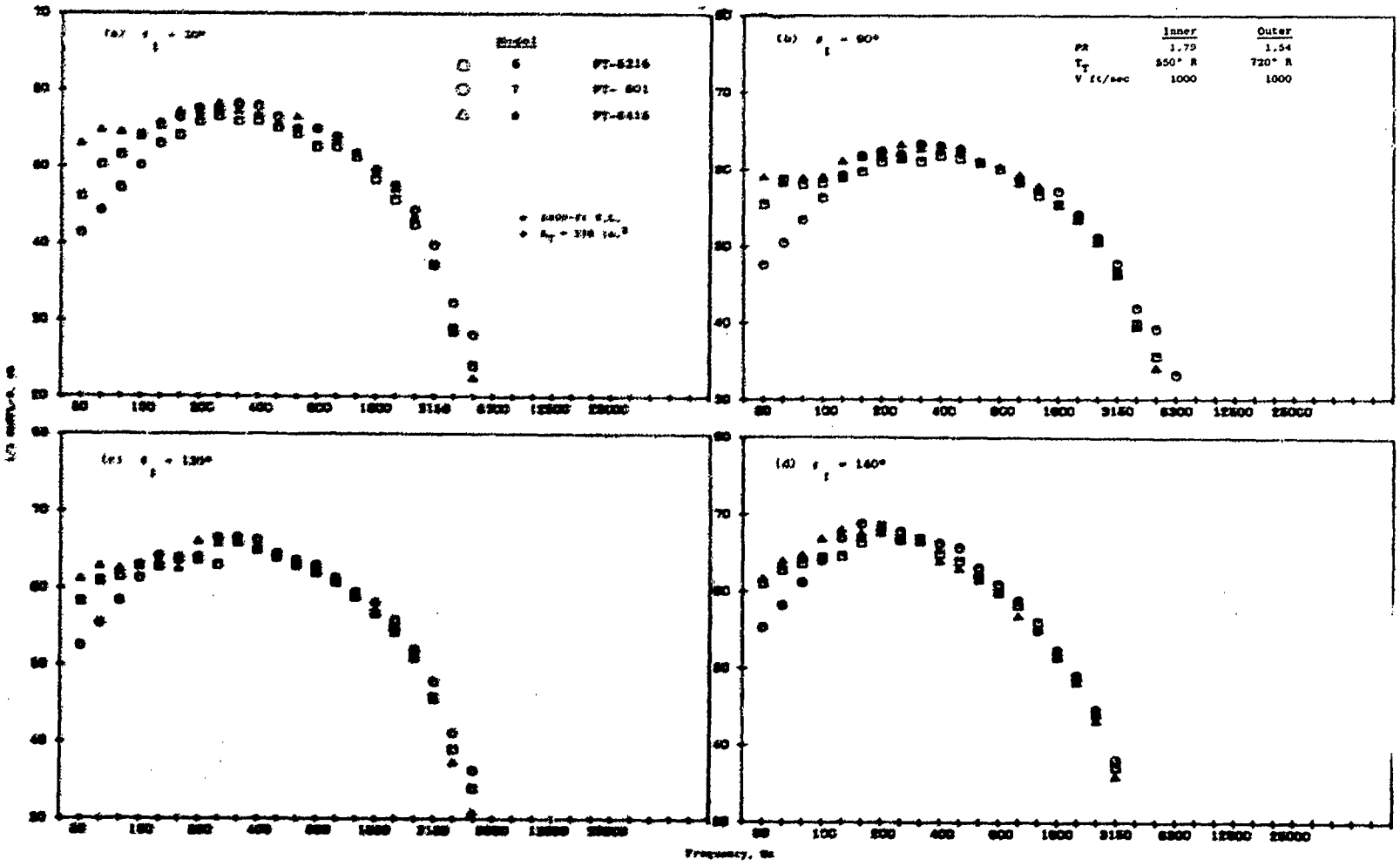

Figure 3-71. Spectra Variation with Area Ratio, $V_O/V_1 = 1.0$.

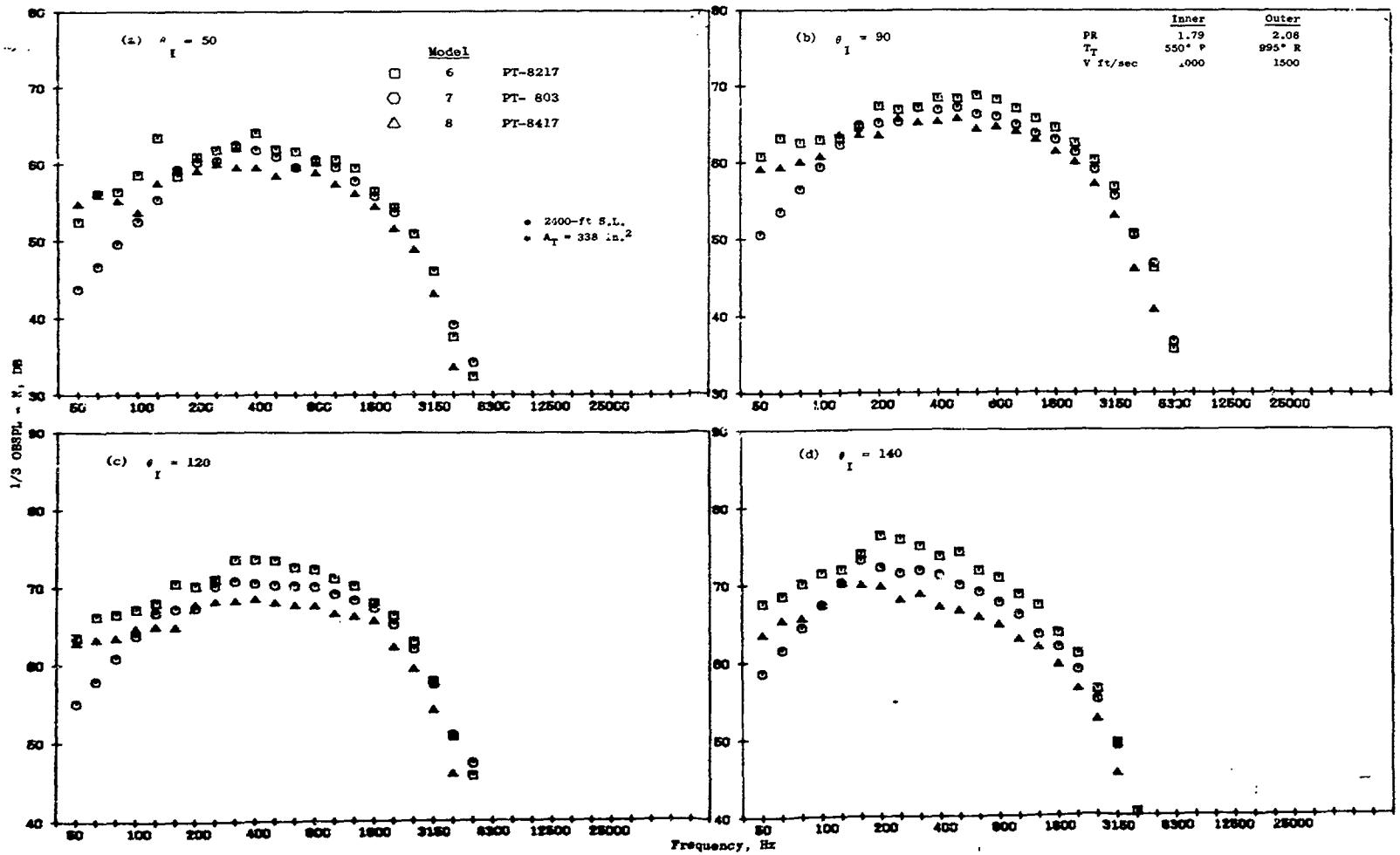

Figure 3-72. Spectra Variation with Area Ratio, V_o/V_i = 1.5.

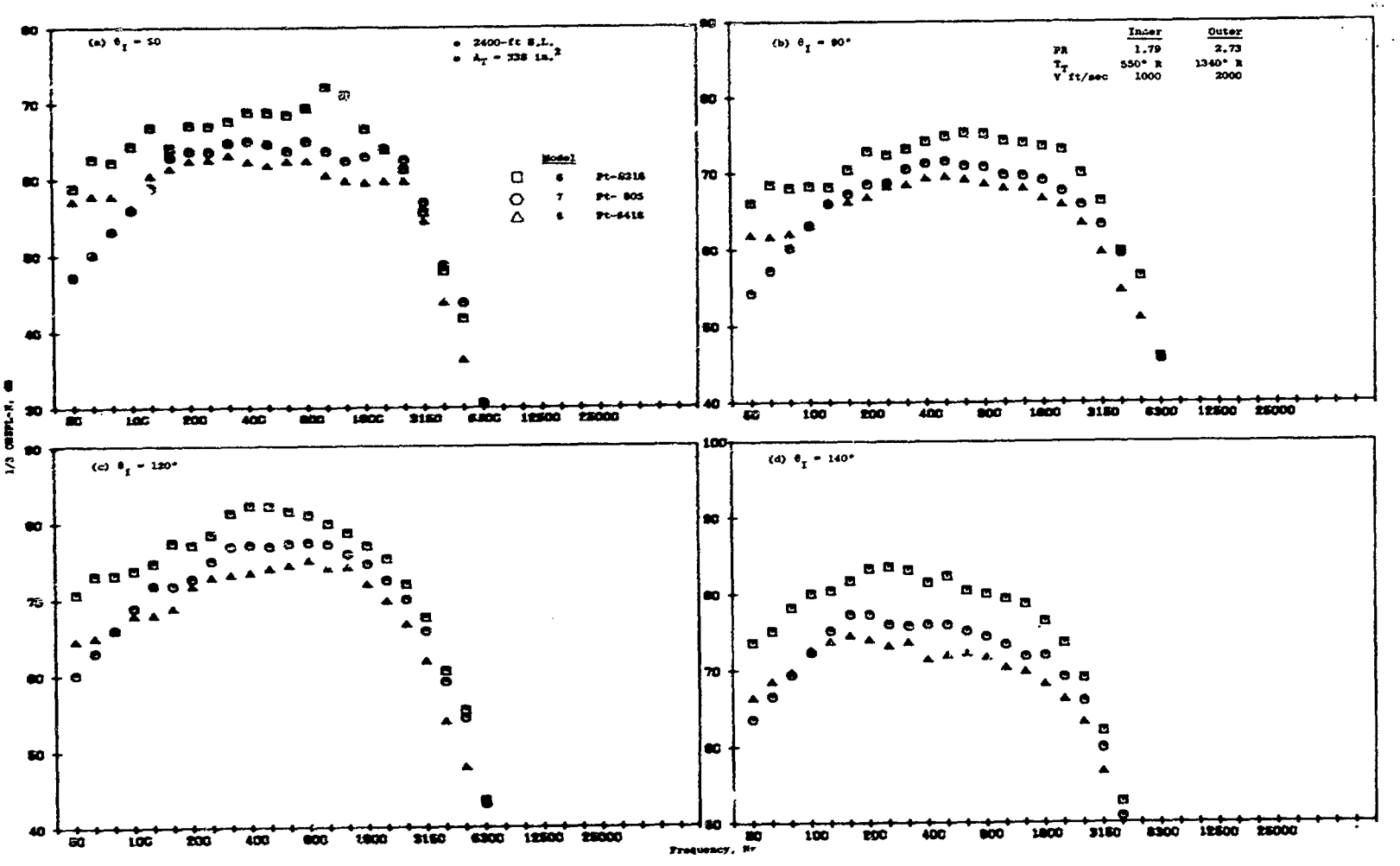

Figure 3-73. Spectra Variation with Area Ratio, V_O/V_i = 2.0.

3.4.1.6 Unsuppressed Annular Jet Study

In addition to conventional and inverted flow cycles, coplanar coannular nozzles were also tested at cycle conditions where (a) the inner stream flow was reduced to zero and (b) it was held to be less than 10% of the outer stream: termed testing with "low inner flow."

The low inner flow configurations were nozzles 9, 10, and 12 having A_o/A_i = 2.0, 0.65 and 0.4, respectively. The zero inner flow nozzles were configurations 11 and 13 have A_o/A_i = 0.65 and 0.4, respectively.

The detailed geometric parameters of these exhaust nozzles are summarized on Figures A-9 through A-13 in Appendix A. The theromodynamic conditions are summarized on Tables 9 thru 13 in Appendix B.

Normalized peak and 90° suppression levels as a function of velocity are summarized for the low inner flow test series on Figure 3-74(a). Suppression levels increase as area ratio decreases; >8 peak PNdB being measured for the A_i/A_o = 0.4 nozzle (Model 12) in contrast to only 4 peak PNdB for A_i/A_o = 2.0 (Model 9). This trend is significantly different than discussed in the previous section for inverted-flow cycles, where suppression level was only a weak function of area ratio.

The influence of zero inner flow for the A_o/A_i = 0.4 coplanar-coannular nozzle (Model 13) is summarized on Figure 3-75. The reduction of inner flow to zero is found to decrease the average suppression at the peak noise angle by 3 to 7 PNdB. Significant changes in the noise levels at 90° are also observed.

A similar comparison for the A_o/A_i = 0.65 configuration (Model 11) is presented on Figure 3-76. Suppression is also observed to decrease with reduction of the inner flow to zero, however, the decrease in suppression is from 1 to 3 dB. The absolute level of suppression also decreases when compared with the A_o/A_i = 0.4 configuration (Model 13).

Normalized PNL and OASPL directivity patterns are presented on Figures 3-77 and 3-78 for outer stream velocities of 2350 ft/sec and 1800 ft/sec. Peak noise level is decreased as area ratio decreases. The noise levels of the three nozzles are within 1 dB at 90°. Selected spectra comparisons at these conditions are on Figures 3-79 and 3-80, along with conical data at comparable conditions. The 50° spectra at 2350 ft/sec illustrates the classical shock noise spectrum shape. The peak frequency of shock noise increases as area ratio decreases and suppression relative to the conical nozzle in the aft quadrant occurs in the mid to high frequency regime.

Similar directivity and spectra comparisons for A_o/A_i = 0.4 and 0.65 coplanar-coannular nozzles, having no inner flow or low inner flow conditions, are summarized on Figures 3-82 thru 3-87. The reduction of the inner flow to zero causes an increase in noise level, particularly in the aft quadrant. The PNL change in the forward quadrant is not as significant as OAPSL, indicating a low frequency variance. This observation is supported by the spectra comparisons presented. The trends are similar for the A_o/A_i = 0.4

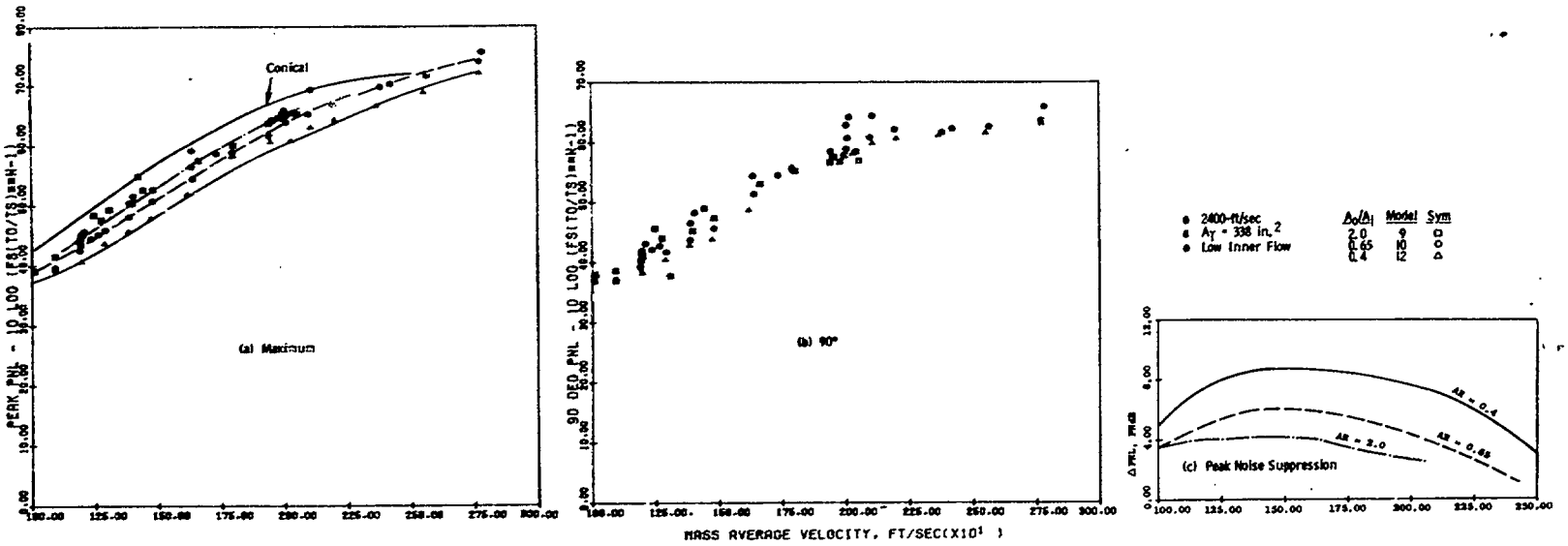

Figure 3-74. Coannular-Coplanar Nozzle Suppression Characteristics with Varying Nozzle Area Ratio.

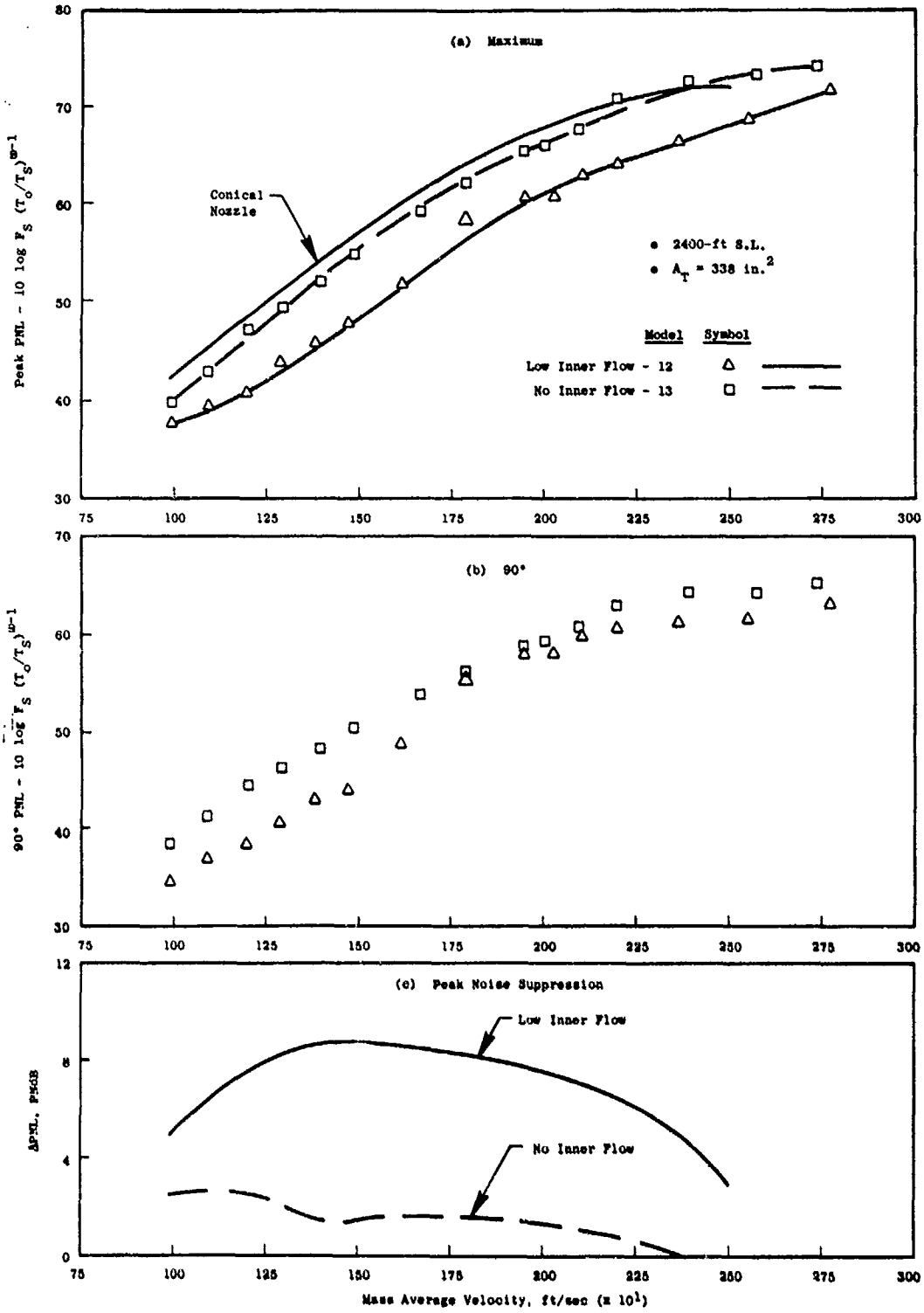

Figure 3-75. Impact of Cycle Variation on Suppression Characteristics of A_o/A_i = 0.4 Coplanar-Coannular Nozzle (Models 12 and 13).

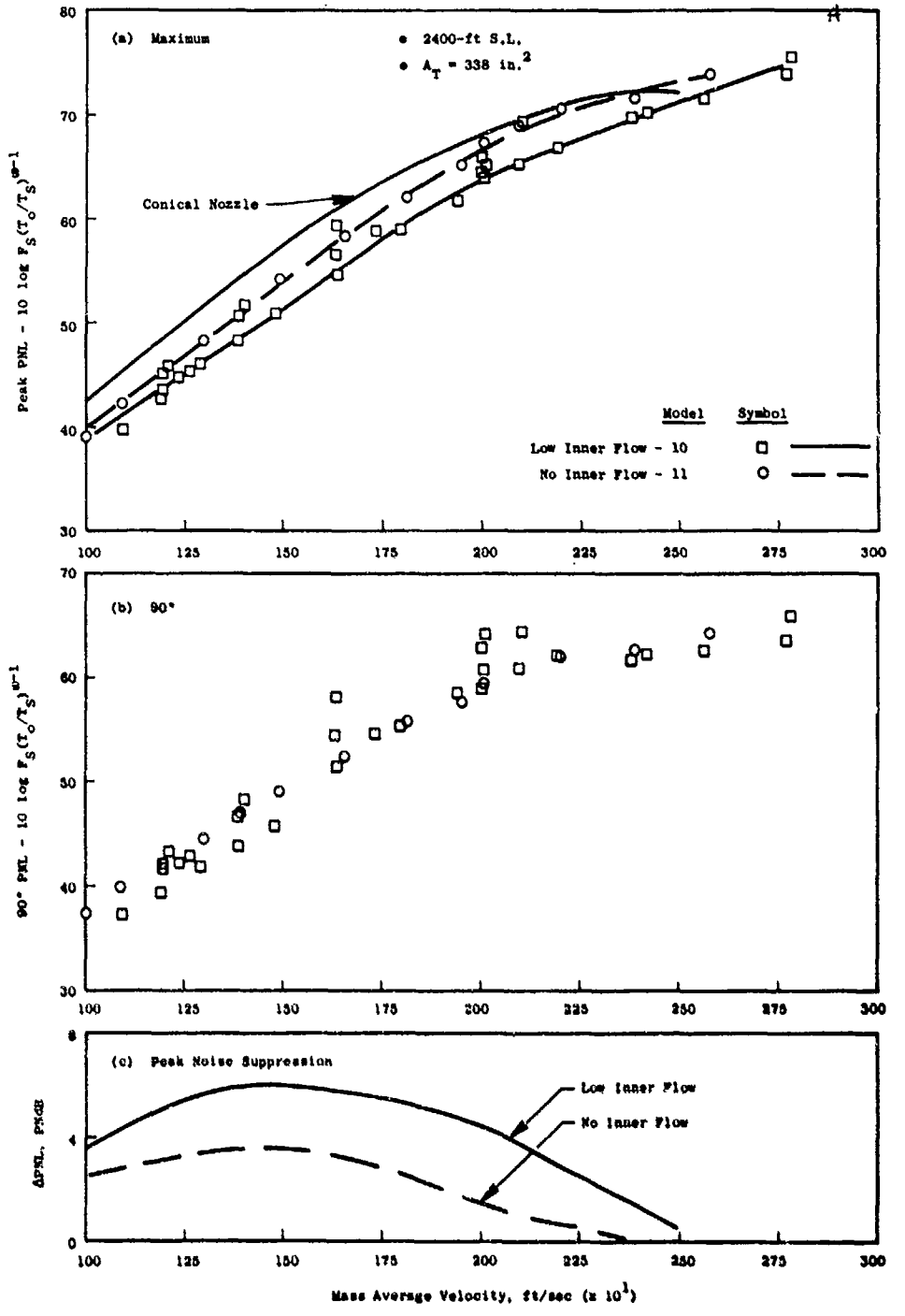

Figure 3-76. Impact of Cycle Variation on Suppression Characteristics of A_o/A_i = 0.65 Coplanar-Coannular Nozzle (Models 10 and 11).

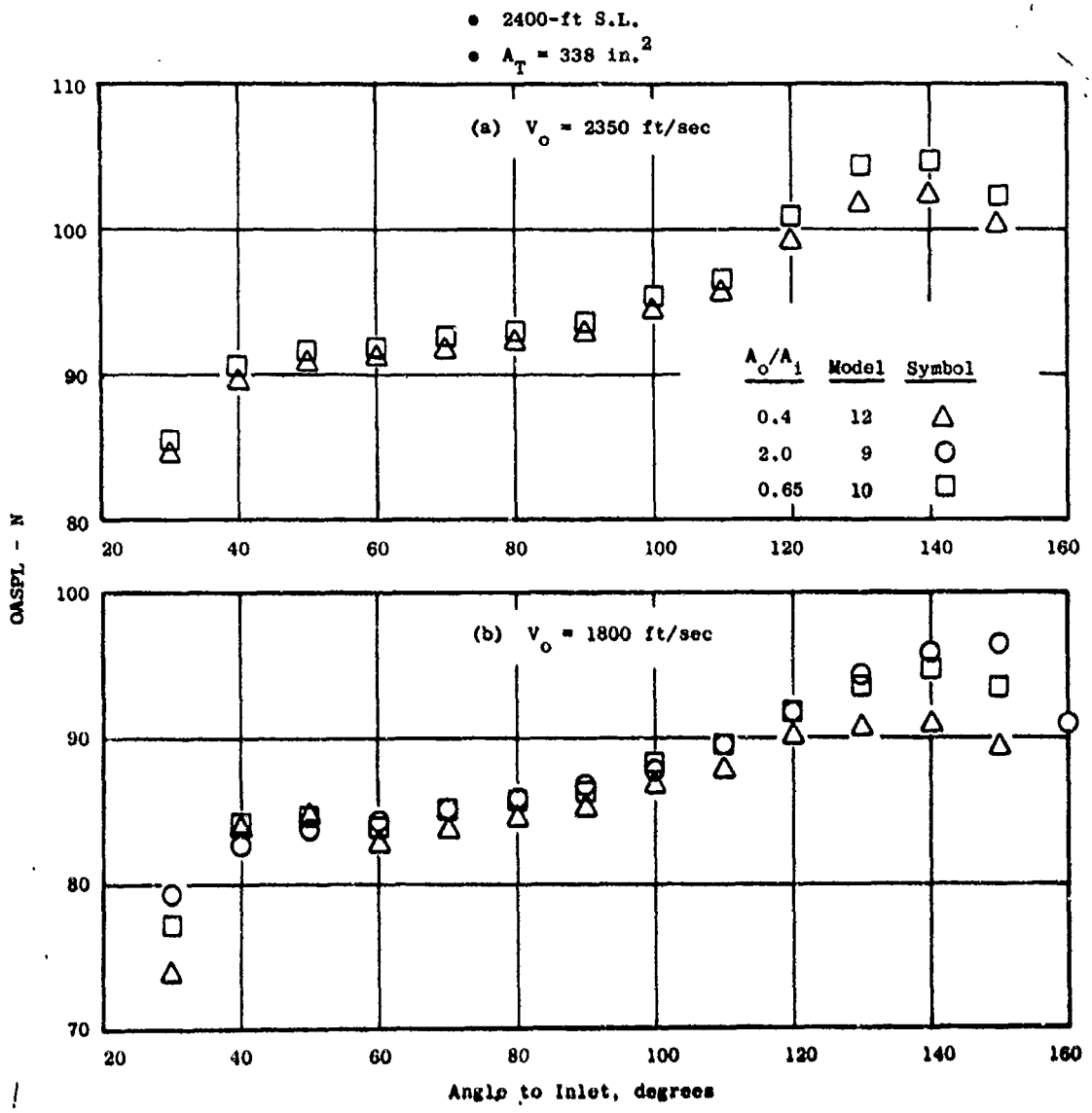

Figure 3-77. OASPL Directivity Variation with Area Ratio, $W_i/W_o < 0.1$.

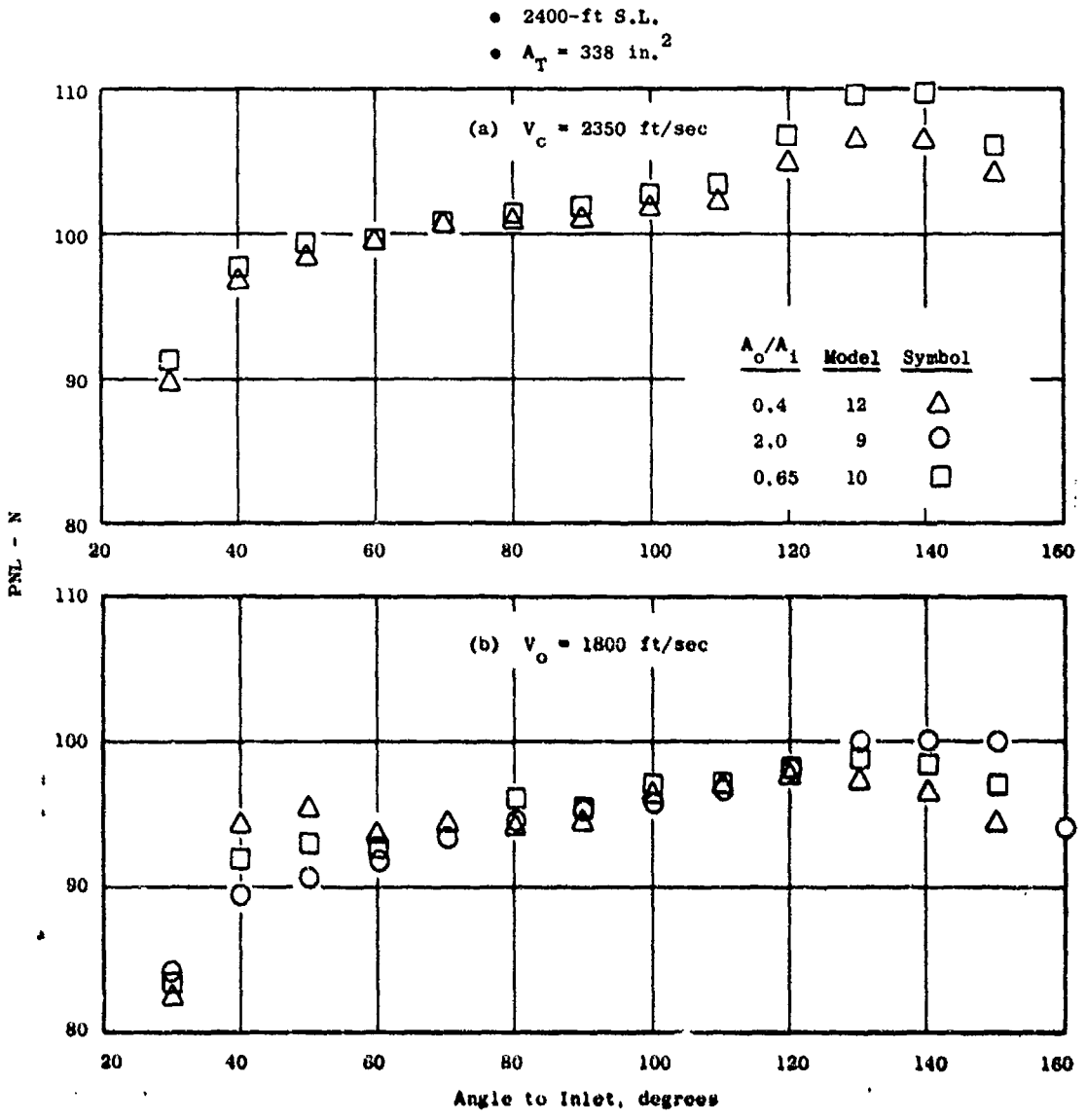

Figure 3-78. PNL Directivity Variation with Area Ratio, $W_i/W_o < 0.1$.

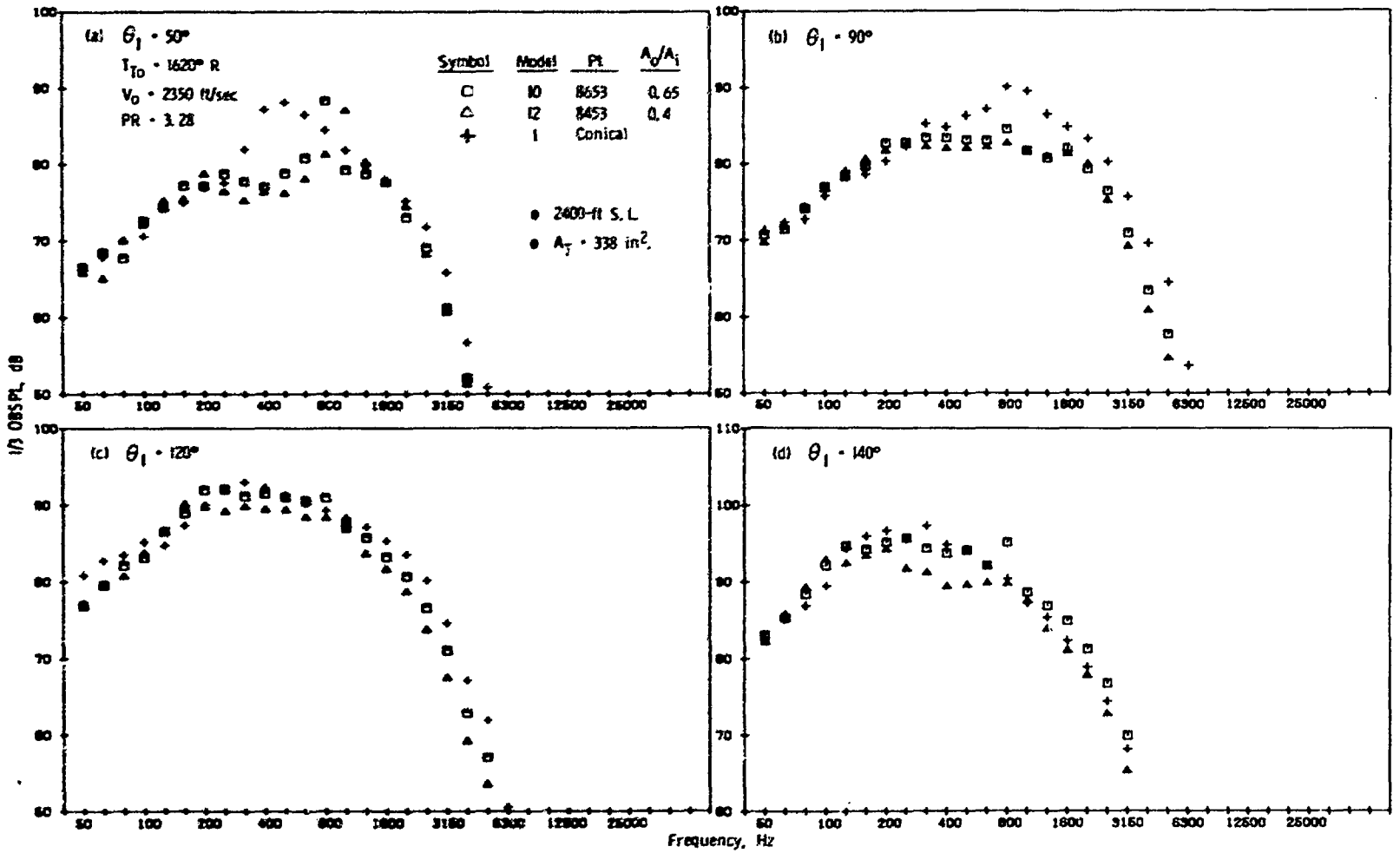

Figure 3-79. Spectra Variation with Area Ratio, V_{ma} = 2350 ft/sec.

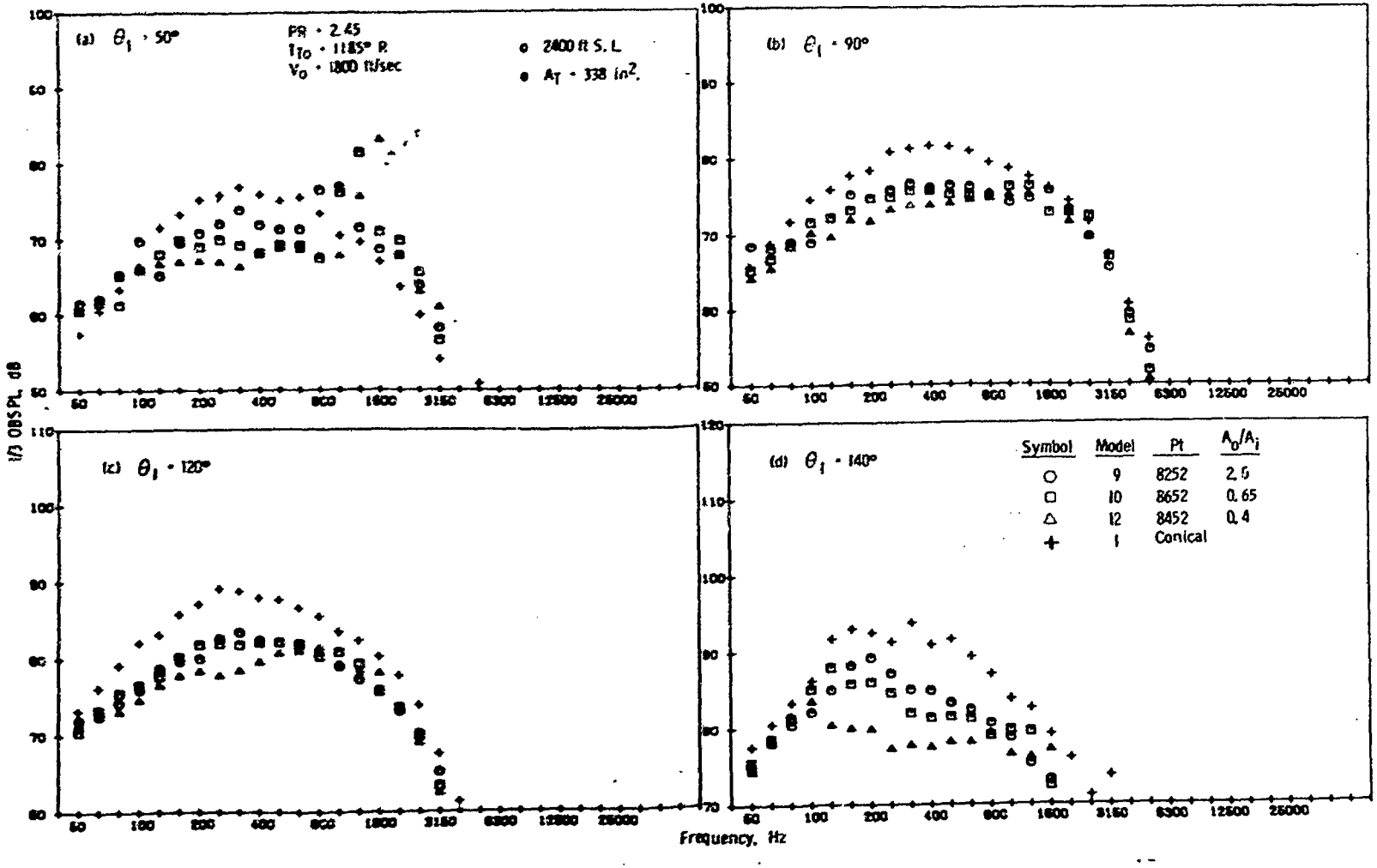

Figure 3-80. Spectra Variation with Area Ratio, V_{ma} = 1800 ft/sec.

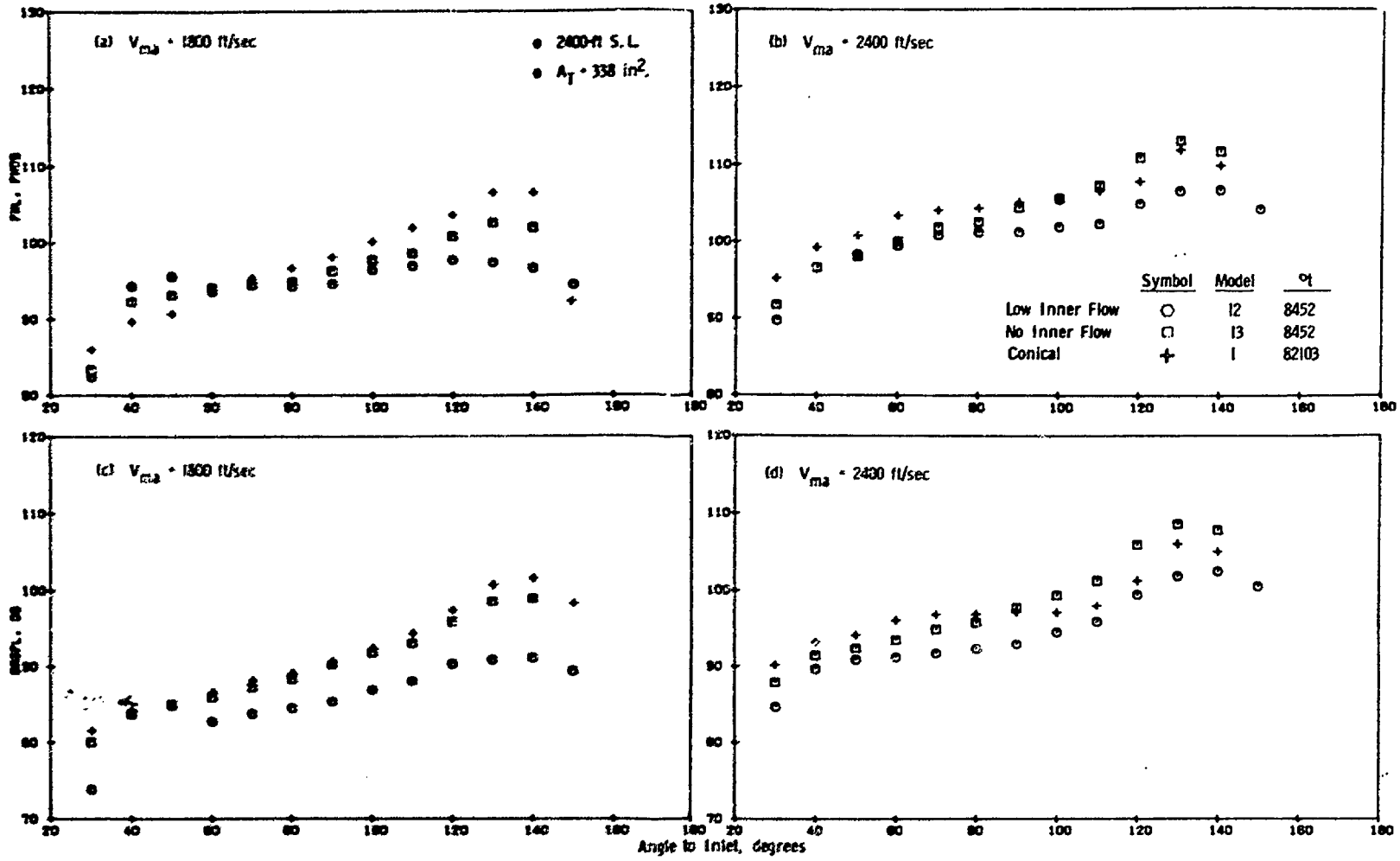

Figure 3-81. Impact of Inner Flow Variation, A_O/A_1 = 0.4, PNL and OASPL Directivity.

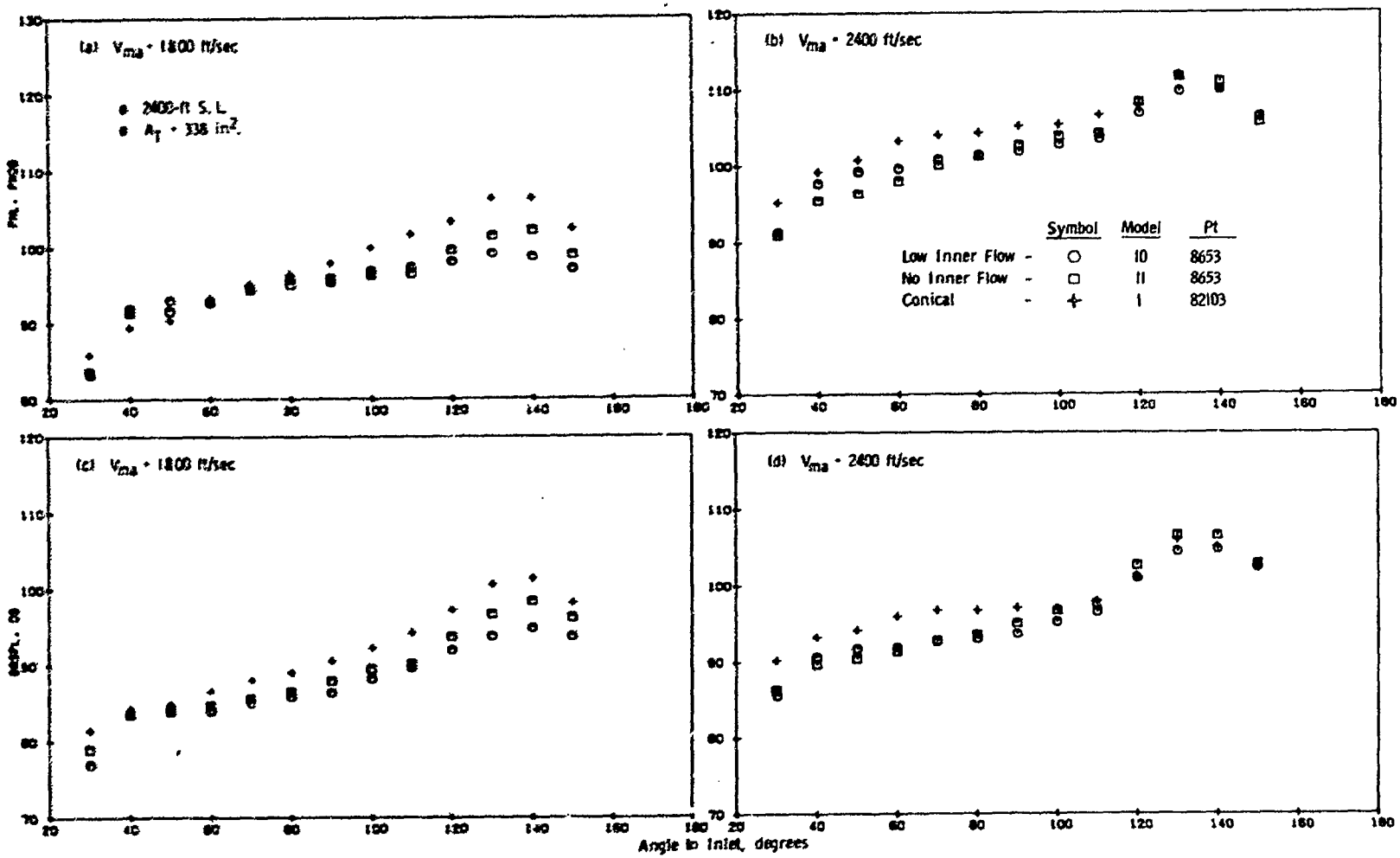

Figure 3-82. Impact of Inner Flow Variation, A_o/A_1 = 0.65, PNL and OASPL Directivity.

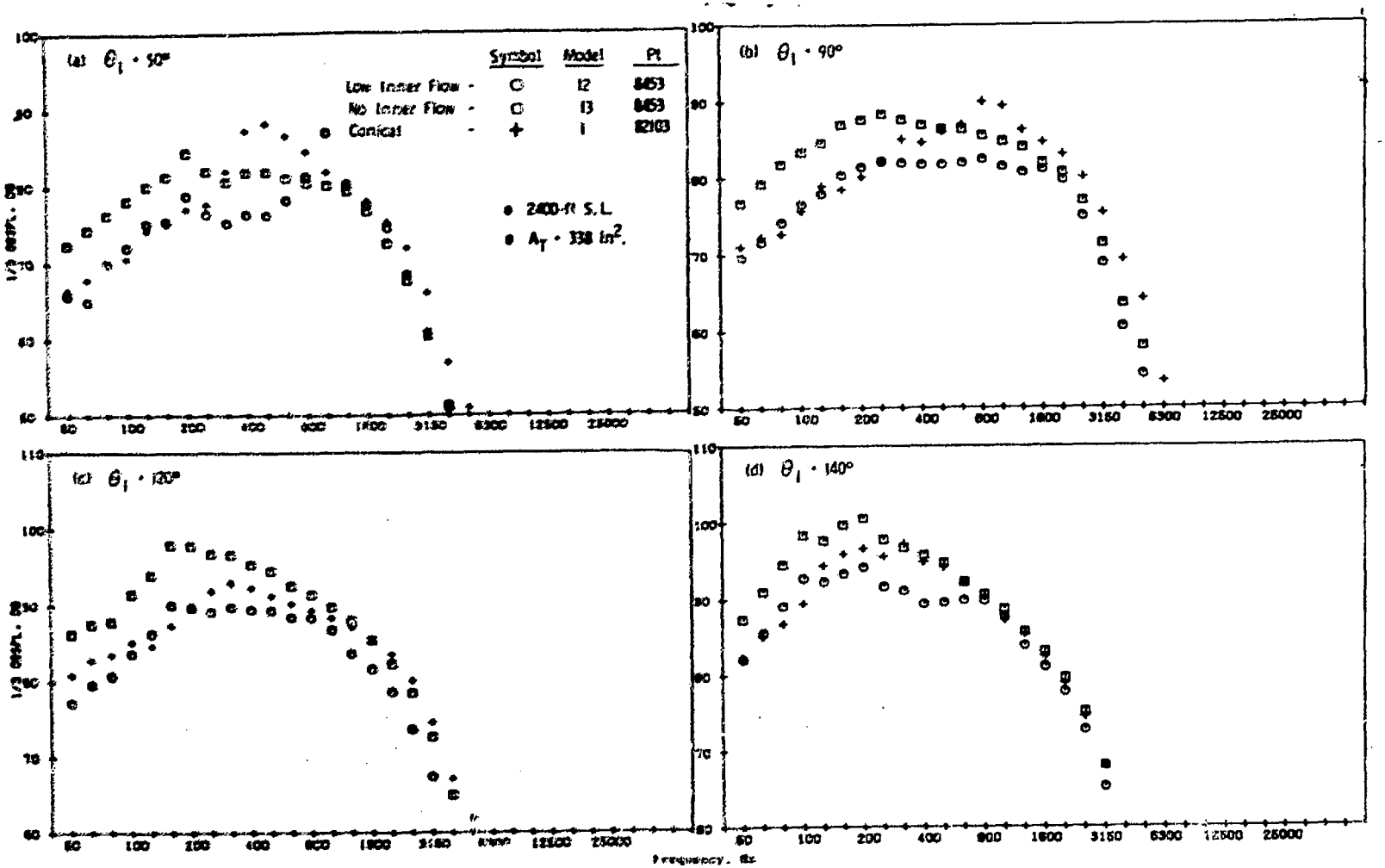

Figure 3-83. Impact of Inner Flow Variation on Spectra, A_O/A_i = 0.4, V_{ma} = 2400 ft/sec.

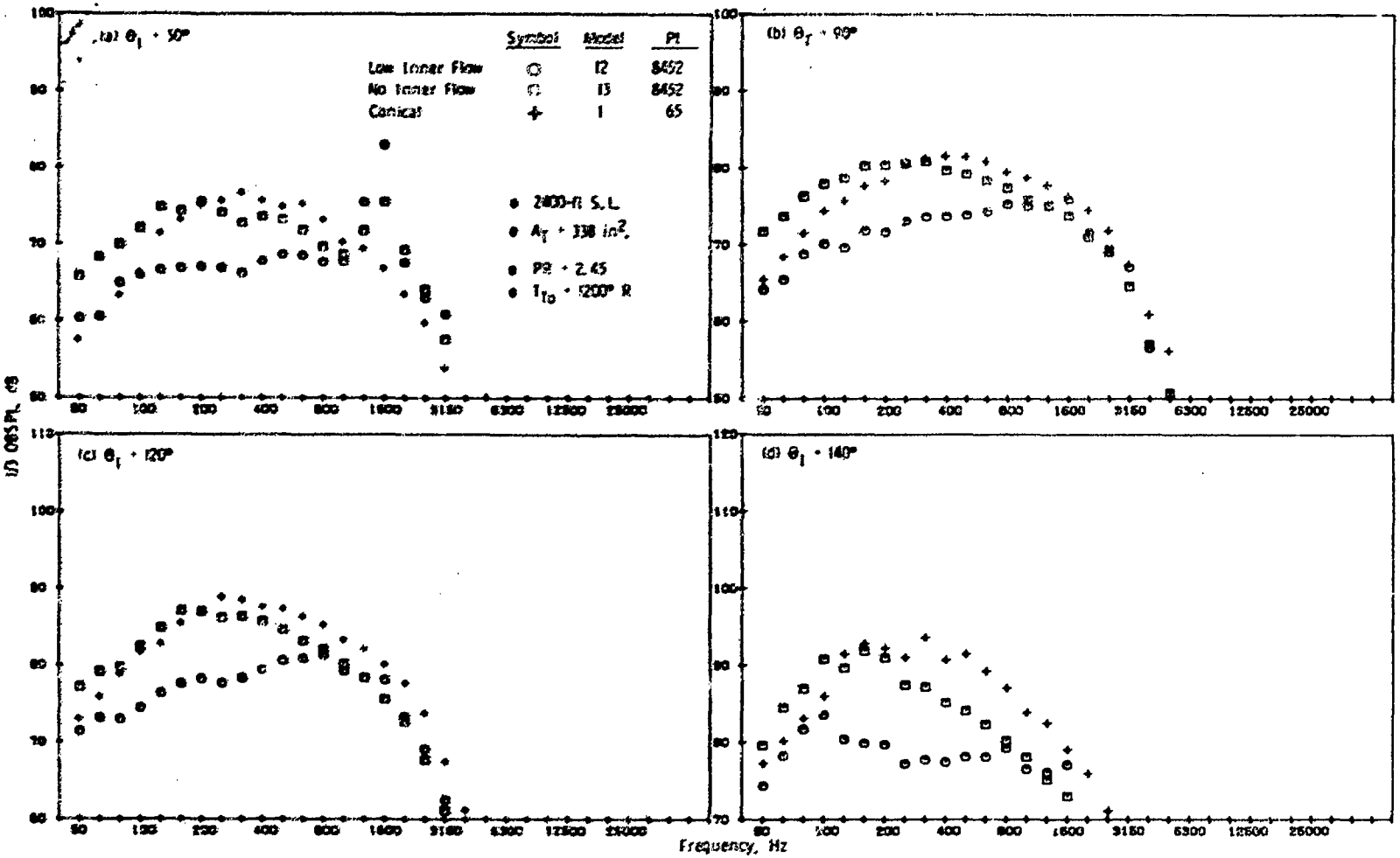

Figure 3-84. Impact of Inner Flow Variation on Spectra, A_O/A_i = 0.4, V_{ma} = 1800 ft/sec.

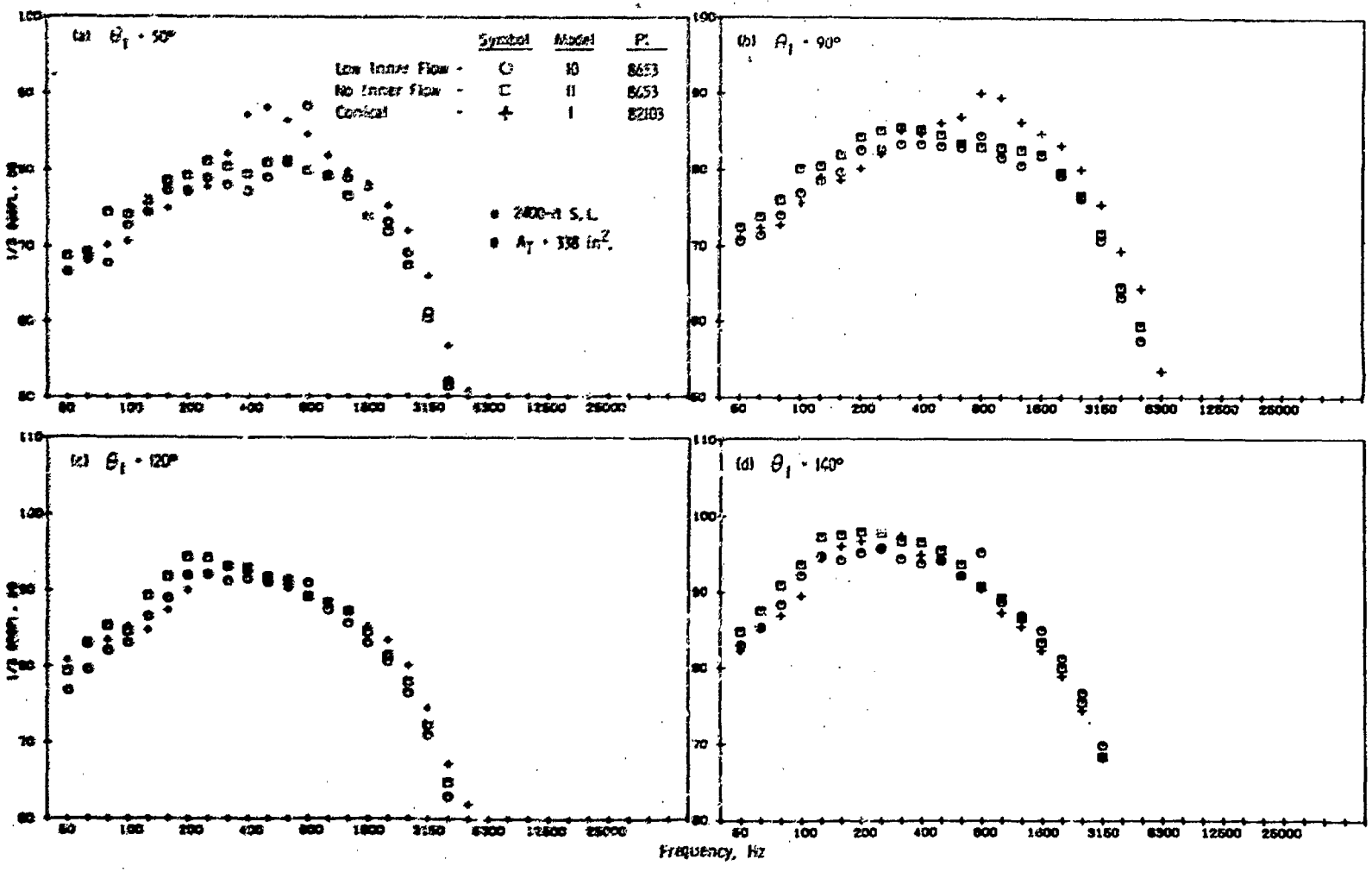

Figure 3-85. Impact of Inner Flow Variation on Spectra, A_o/A_1 = 0.65, V_{ma} = 2400 ft/sec.

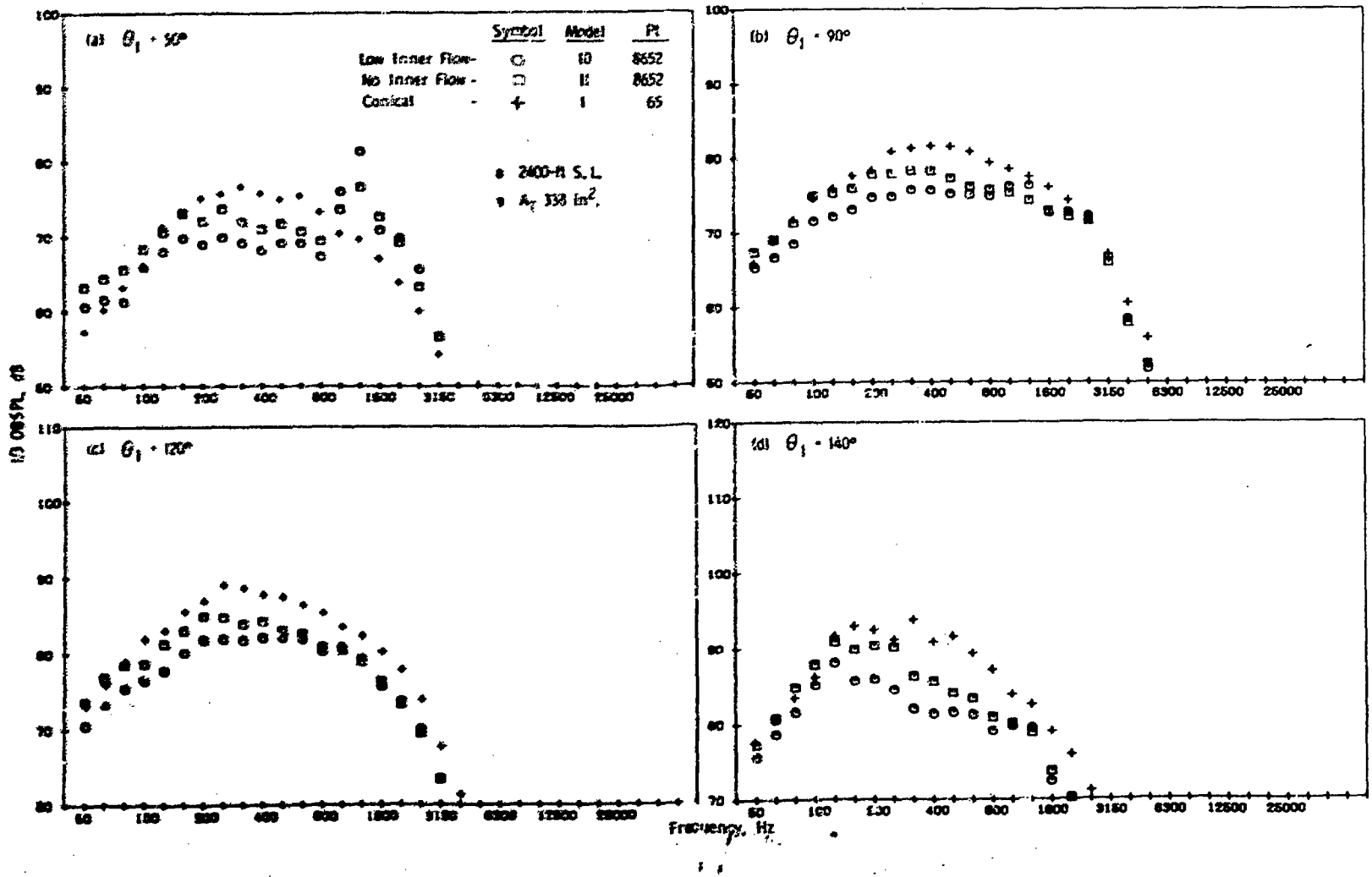

Figure 3-86. Impact of Inner Flow Variation on Spectra, A_o/A_i = 0.65, V_{ma} = 1800 ft/sec.

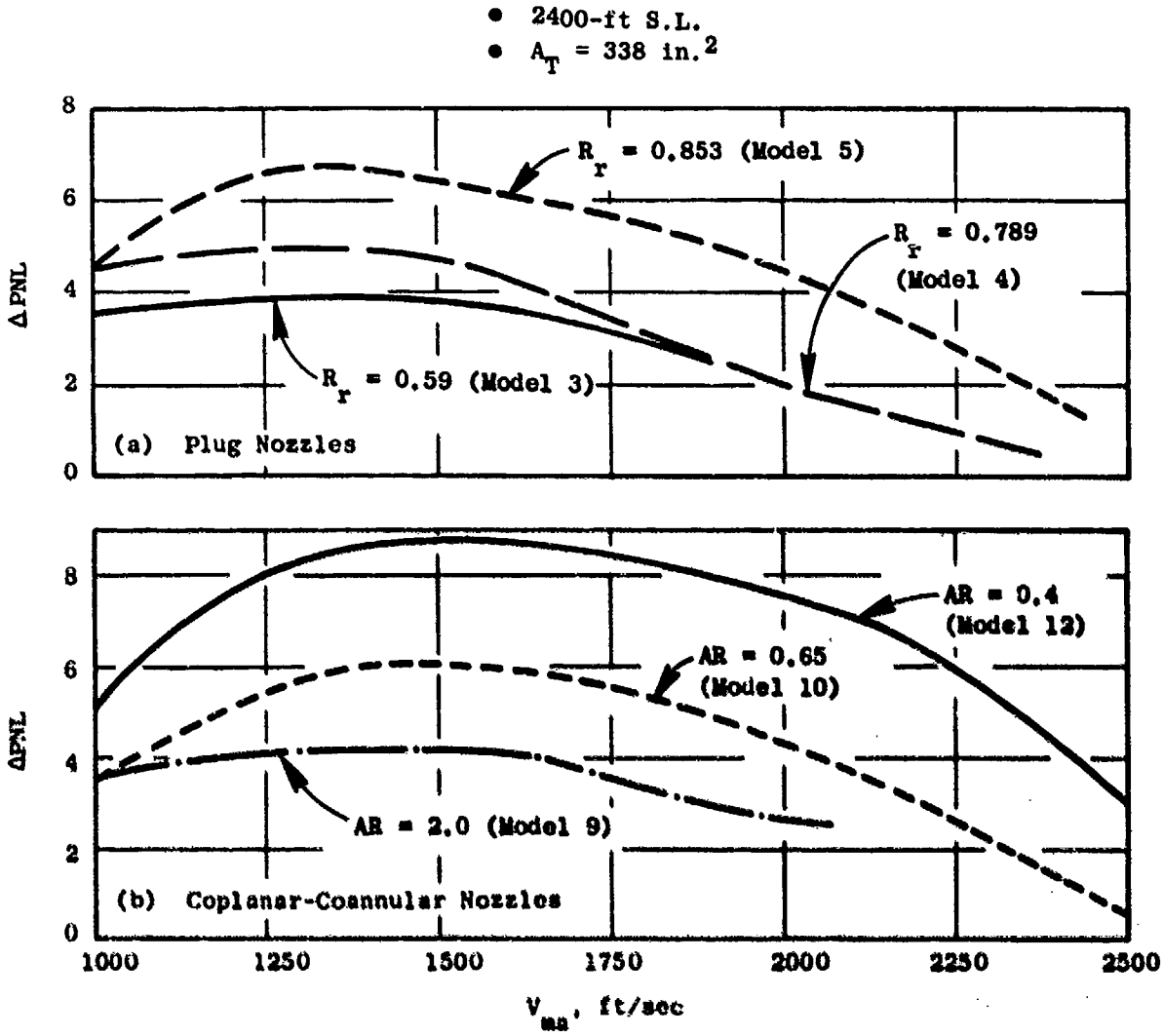

Figure 3-87. Summary of Plug Nozzle and Coplanar-Coannular Nozzle Peak PNL Suppression Levels.

(Models 12 and 13) and 0.65 (Models 10 and 11) nozzles, however, sensitivity of directivity and spectra characteristics to inner stream conditions increases as flow area ratio decreases.

3.4.1.7 Summary

Conical nozzle reference noise levels have been established on the basis of PNL and OASPL variation with velocity, PNL and OASPL directivity, and spectra. These levels will be used as a reference for establishing suppression levels. Measured conical noise levels correlated well with those predicted using existing methods.

Parametric variation of plug nozzle radius ratio showed that the suppression increased with radius ratio as illustrated on Figure 3-87. Parametric studies utilizing coplanar-coannular nozzles having A_o/A_i = 0.4, 0.6 and 2.0 indicated that for inverted flow cycles, only slight variation of suppression level occurred with change in area ratio. However, a similar study utilizing these configurations showed that if inner-to-outer flow ratio was held to less than 10%, a significant variation of suppression level with area ratio occurred as illustrated on Figure 3-87. Reduction of the inner flow to zero caused a significant loss of suppression.

3.4.2 Tests Related to Suppressors Influenced by Geometric and Cycle Variations, Single- and Dual-Flow Nozzles

This section presents the results of a series of acoustic studies to establish suppression depending on geometric and cycle variations. Both single and dual flow exhaust nozzles were considered. A suppressor design implemented on a single flow nozzle was termed a full span suppressor. The implementation of a suppressor on a dual flow nozzle is termed a half span suppressor, as it extends only across the outer flow stream.

Section 3.4.2.1 presents the results of studies performed to determine the influence of suppressor area ratio and radius ratio on a series of 36-chute nozzles implemented as both half span and full span suppressors. Flow management and inner stream geometry variations are discussed in Section 3.4.2.2. Flow management principles include variation of outer to inner stream parameters of velocity ratio, V_o/V_i, weight flow ratio, $\beta = W_o/W_i$, and area ratio, A_o/A_i. Flow segmentation studies discussed in Section 3.4.2.3 utilized half span suppressors having 20, 30 and 40 shallow-chutes implemented on a common flowpath geometry. The element type studies in Section 3.4.2.4 utilized 36-spoke and 36-chute nozzles, as both half span and full span suppressors, to establish suppression trends. Studies to evaluate treated ejectors are discussed in Section 3.4.2.5.

In each section the peak noise suppression level was established as a function of jet velocity; referenced to the conical nozzle data of Section 3.4.1.1 The suppression level was found to vary significantly with jet velocity and with several of the geometric parameters evaluated.

3.4.2.1 Chute Area and Radius Ratio Studies

Area Ratio and Radius Ratio Variable, Turbojet (Models 15, 16 and 17)

This study investigated the influence of changing suppressor nozzle area ratio and radius ratio on a turbojet exhaust nozzle system (see Figure 4.3-1 for description of parameters). Models 15, 16 and 17 of Figure 3-88 were used. Detailed schematics of the test configurations are in Appendix A, Figures 9, 10 and 11. The aft plug geometry (15° half-angle and plug length) was maintained, as well as the flow area of 23.76 in.^{2} and segmentation with 36 elements. For consistency of design, the chute depth to width ratio, D_c/W_c, was maintained at 2.54 at the shroud and at 1.53 at the hub.

The following values applied to the model set:

Model No.	Area Ratio	$A_{Blocked}$, in.^{2}	R_p, in.	R_s, in.	R_r	θ_{plug}, deg.
15	2.5	35.64	3.739	5.738	0.653	7.42
16	2.0	23.76	4.00	5.571	0.716	11.61
17	1.5	11.88	4.22	5.399	0.782	15.86

The acoustic test matrix was defined in Section 3.2.1, Figure 3-8 and utilized both the conventional turbojet cycle line and the high T_T cycle line.

Acoustic results are presented as peak OASPL and PNL levels along with curve-fitted-data suppression trends relative to the conical baseline in Figures 3-89 and 3-90. Each figure has data separated into the conventional turbojet and high T_T cycle lines. OASPL and PNL at 90° are presented in Figure 3-91, 50° OASPL and PNL in Figure 3-92 and overall power levels in Figure 3-93. In reviewing the figures it is seen that:

- On a peak OASPL basis, Figure 3-89:
  - Maximum suppression levels of 16 and 15 dB are seen for the the AR = $2.5/R_r$ = 0.653 suppressor (Model 15) on the high T_T and conventional turbojet cycle lines, respectively.
  - As area ratio increases from 1.5, Model 17, to 2.5, Model 15, (and radius ratio subsequently decreases from 0.782 to 0.653) the peak OASPL suppression is substantially improved at all mid-to-high V_{aa} values; an increase in suppression of 6 to 8 ΔdB is seen at 2250 ft/sec, as an example.
  - At very low V_{aa} each suppressor performs equivalently, yet all maintain a suppression level near 8 to 9 ΔPOASPL.

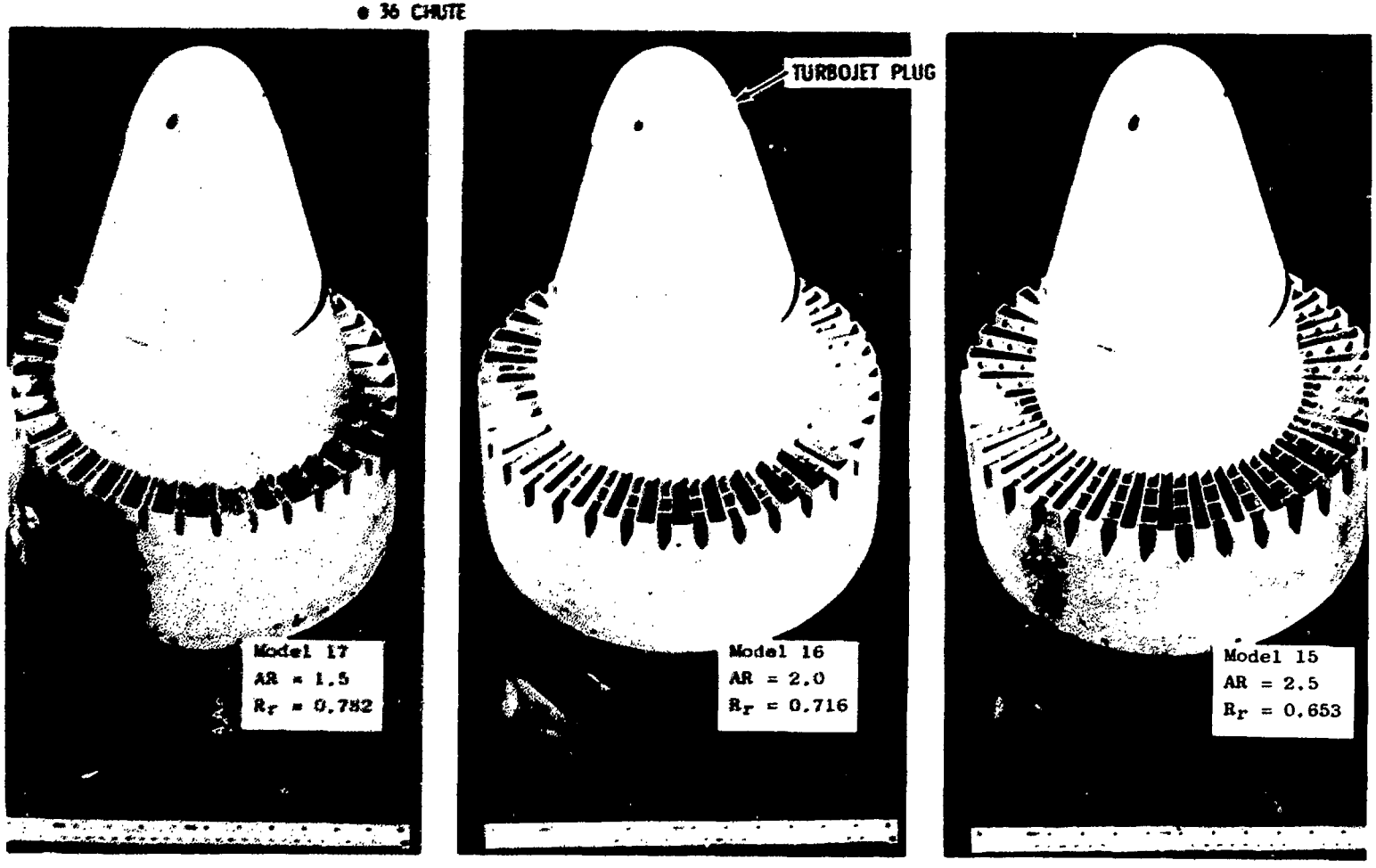

Figure 3-88. Annular Suppressor Area Ratio and Radius Ratio Variation on Turbojet.

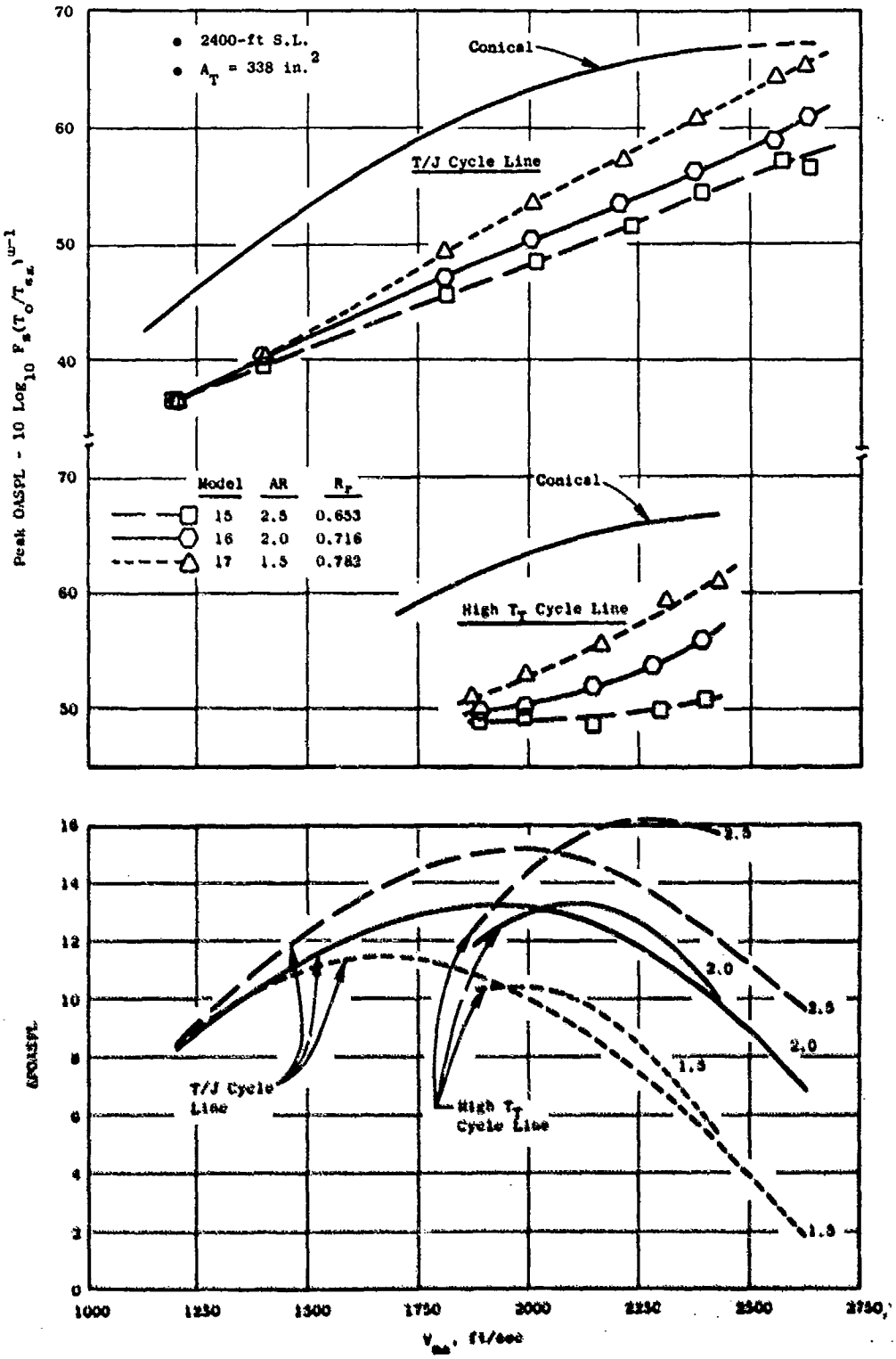

Figure 3-89. Impact of Area Ratio and Radius Ratio on Peak OASPL.

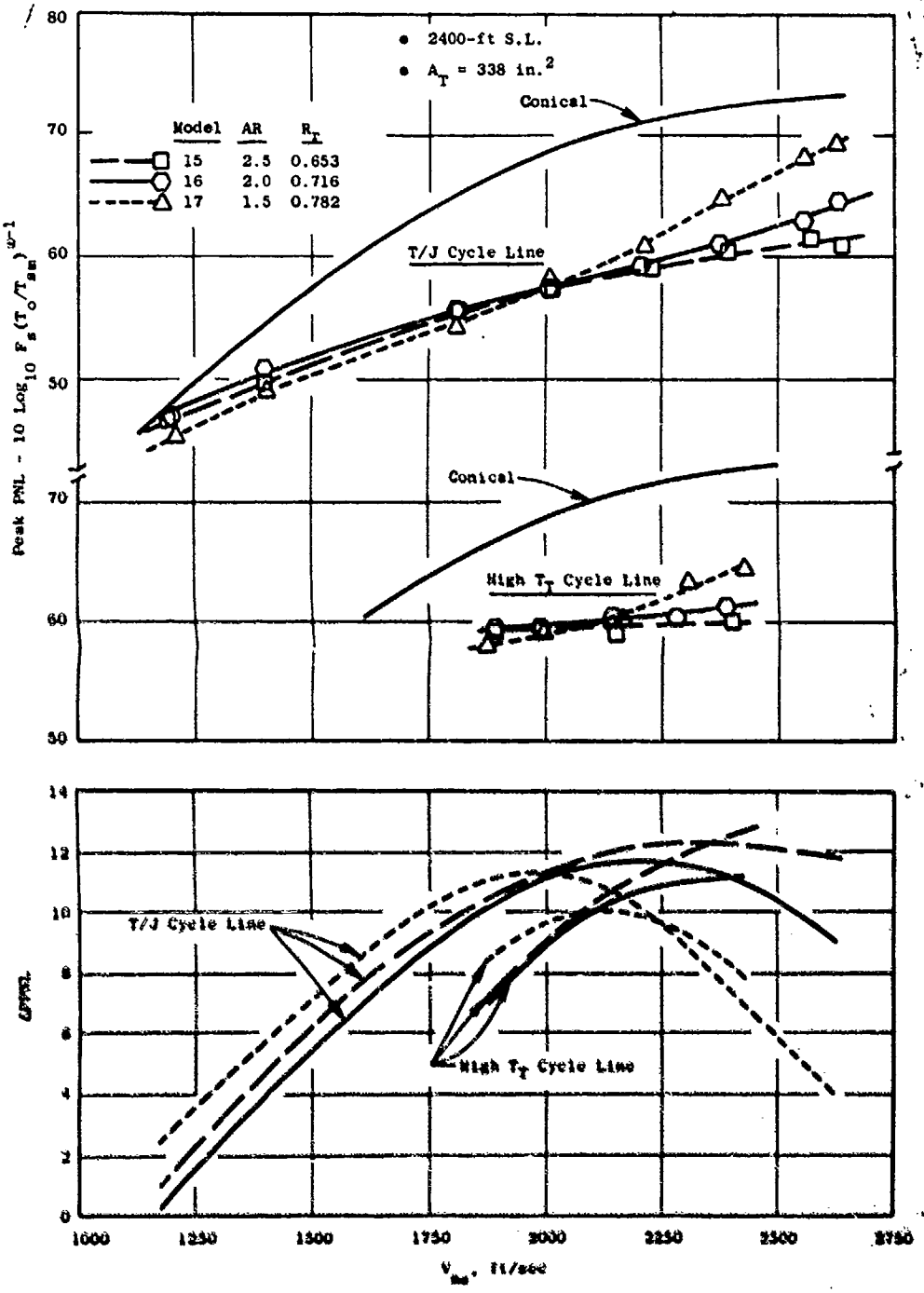

Figure 3-90. Impact of Area Ratio and Radius Ratio on Peak PNL.

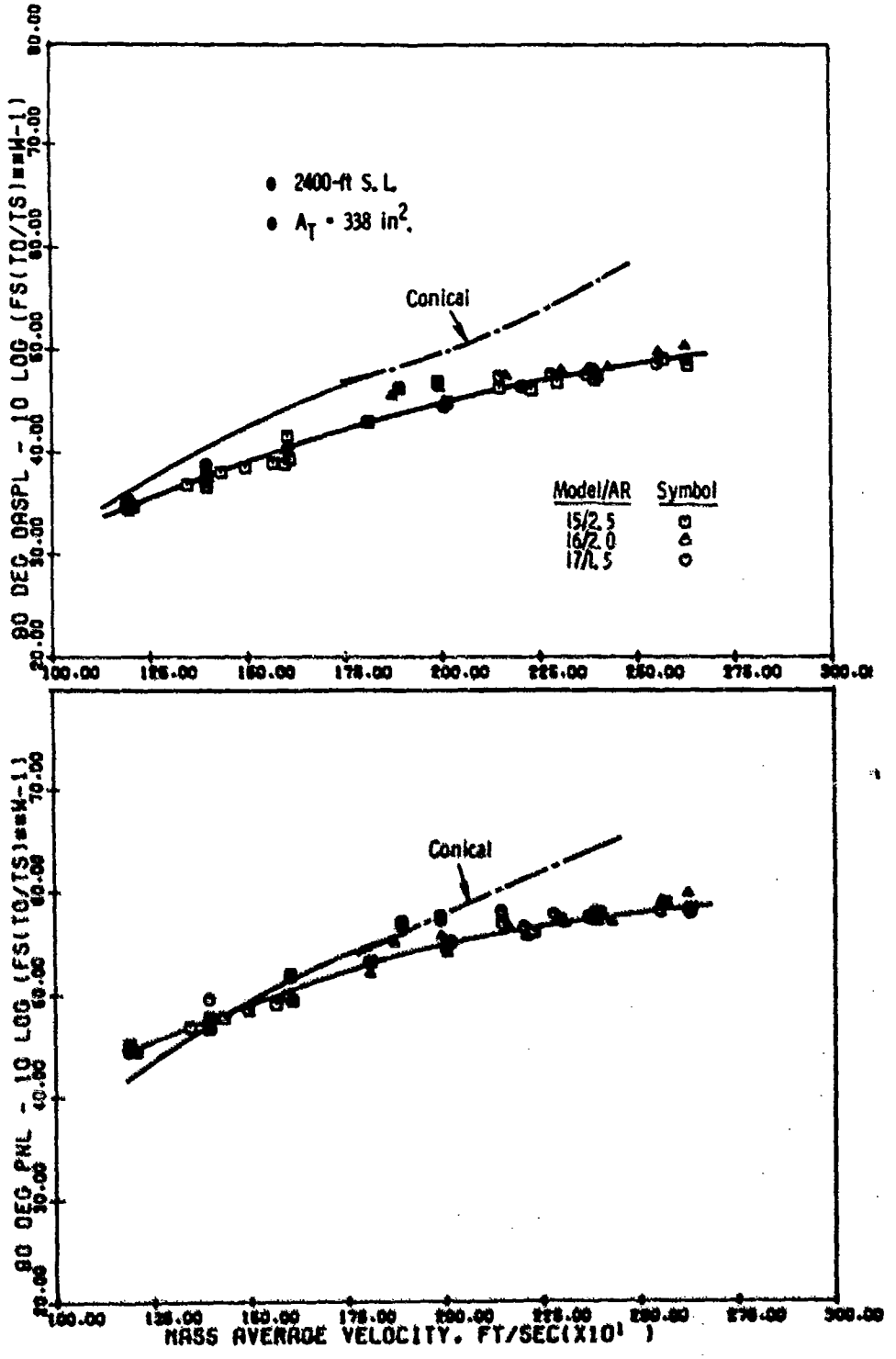

Figure 3-91. Impact of Area Ratio and Radius Ratio on 90° PNL and OASPL.

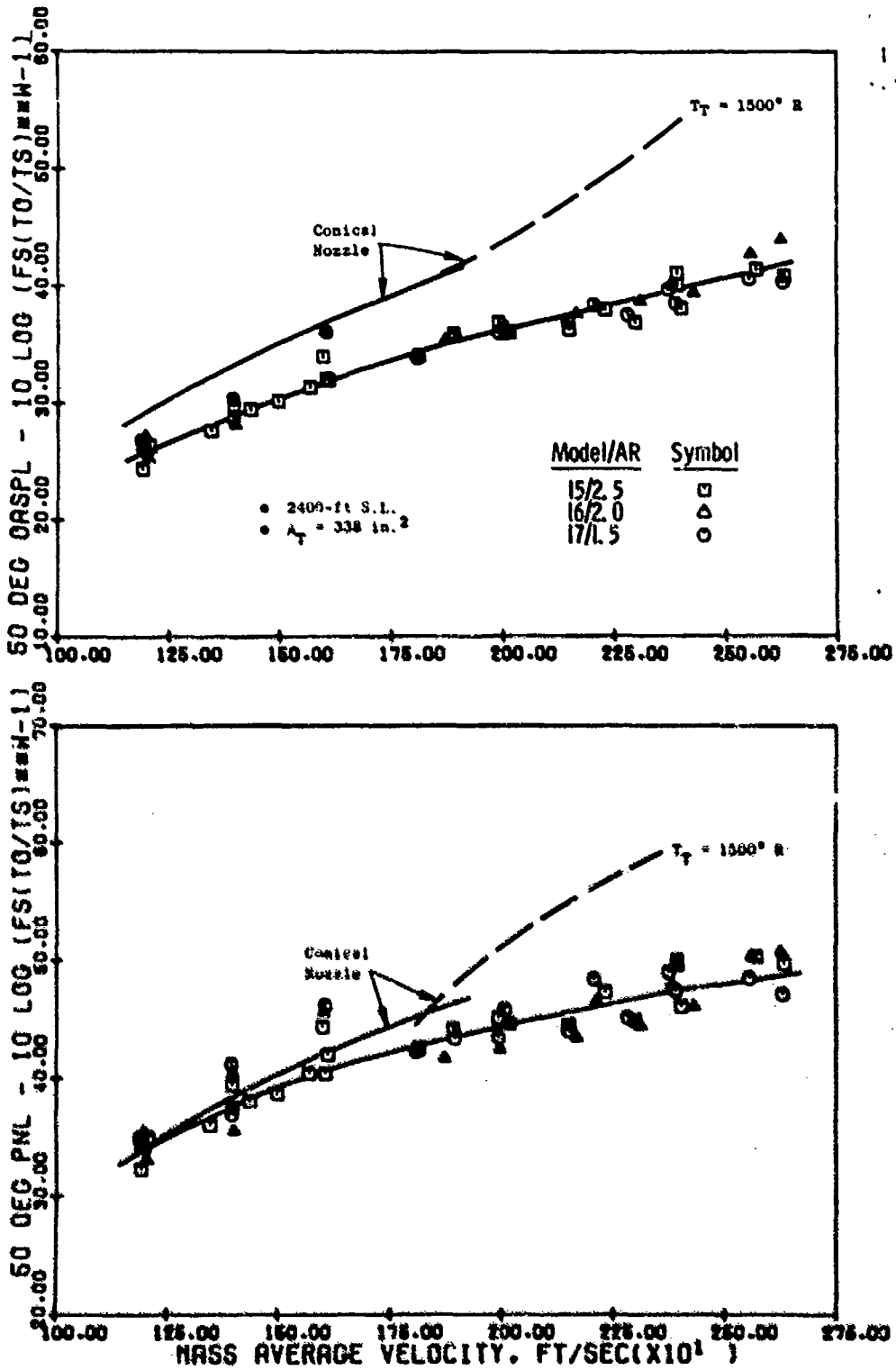

Figure 3-92. Impact of Area Ratio and Radius Ratio on 50° PNL and OASPL.

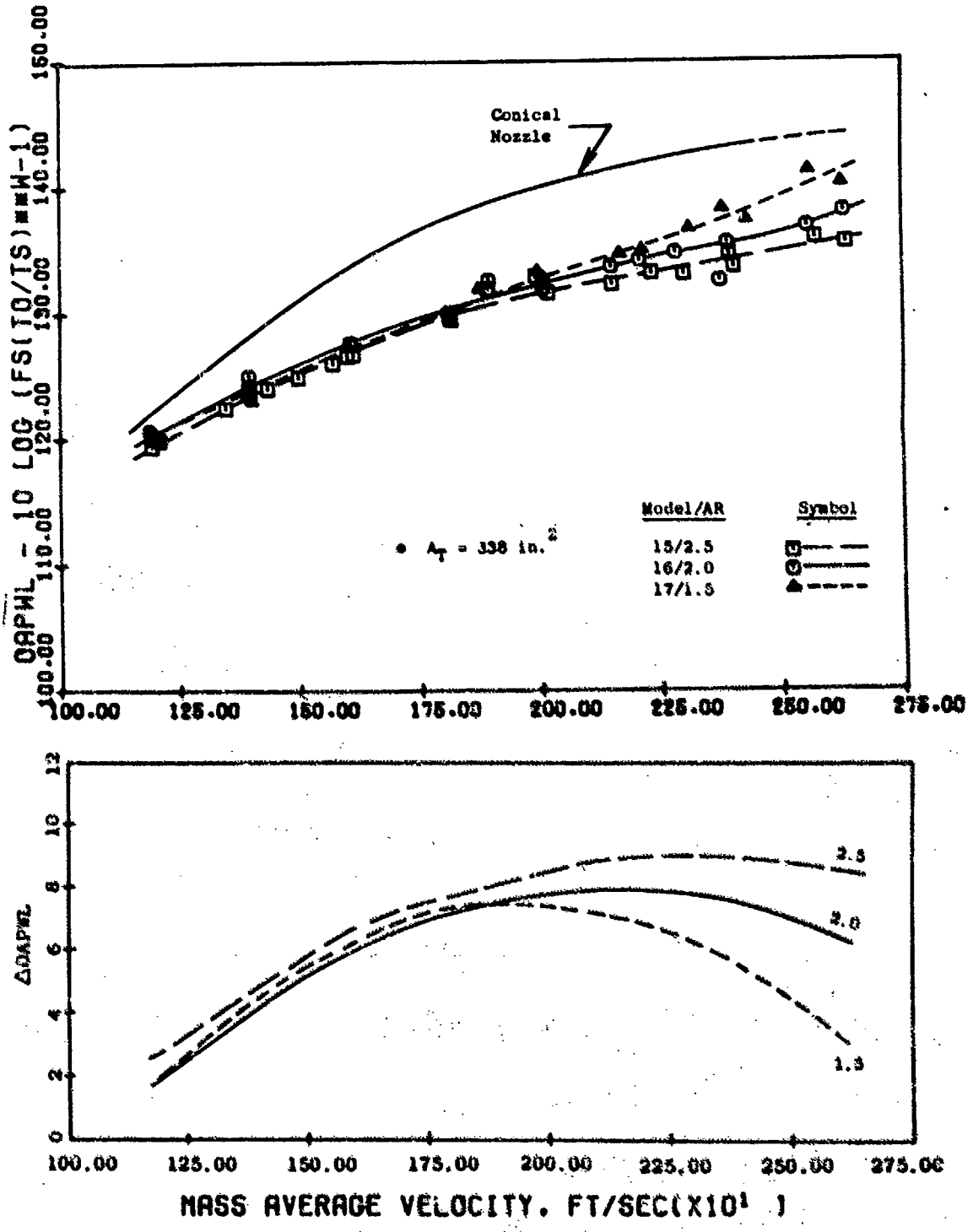

Figure 3-93. Impact of Area Ratio and Radius Ratio on OAPWL.

- On a peak PNL basis, Figure 3-90:

  - A maximum suppression level of near 12 to 12.5 dB is seen for the AR = 2.5/R_T = 0.653 suppressor (Model 15) for both the conventional turbojet and high T_T cycle lines of test.

  - Suppression variance with area ratio/radius ratio is very predominant, particularly at high V_{ma}. The trend with area ratio reverses at low V_{ma}; the magnitude in span of suppression was lower than in the high velocity region. At high V_{ma}, the change in AR from 1.5, Model 17, to 2.5, Model 15, (and in radius ratio from 0.782 to 0.653 is seen to enhance suppression by 4.5 to 5 dB at V_{ma} = 2400 ft/sec, as an example. At low V_{ma}, the lower area ratio (1.5)/higher radius ratio (0.782), Model 17, performs most effectively, showing approximately a 2 dB suppression gain relative to the AR = 2.5 suppressor (Model 15).

- At 90°, Figure 3-91, on both an OASPL and PNL basis, minimal distinction is seen among the three area ratio models, and between the conventional turbojet and high T_T cycle lines. A significant level of suppression relative to the conical nozzle is retained, both on a PNL and OASPL basis but not of the magnitude measured at peak noise angles in the aft quadrant.

- At 50°, Figure 3-92, distinction between the three area ratio/radius ratio models and between the two cycle lines is a little more predominant than at 90°. Suppression relative to the conical nozzle is also somewhat higher due to reduction in the shock-cell noise contribution which normally adds to the conical nozzle noise signature in the forward quadrant at supercritical operating conditions.

- On an OAPWL basis, Figure 3-93, the data trends are similar to those of the peak OASPL and Peak PNL plots, showing suppression improvement with area ratio increase at high V_{ma} and a near equivalency at low V_{ma}. Maximum suppression of 9 dB is seen for the area ratio = 2.5 at 2250 ft/sec.

To illustrate the more detailed changes in noise characteristics associated with changing area ratio and radius ratio, sets of PNL and OASPL directivity plus spectra plots are included as follows:

Figures 3-94 and 3-95 Data Point 7, V_{ma} = 3625 ft/sec, TJ Cycle Line
Figures 3-96 and 3-97 Data Point 13, V_{ma} = 2150 ft/sec, High T_T Cycle Line
Figures 3-98 and 3-99 Data Point 6, V_{ma} = 1400 ft/sec, TJ Cycle Line.

Examination of the first data set shows that at the highest measured test point: a) The aft quadrant directivity patterns are distinctly sharper for the lower area ratio/higher radius ratio, b) at broadside the levels are nearly identical, and c) in the inlet quadrant, distinct differences in

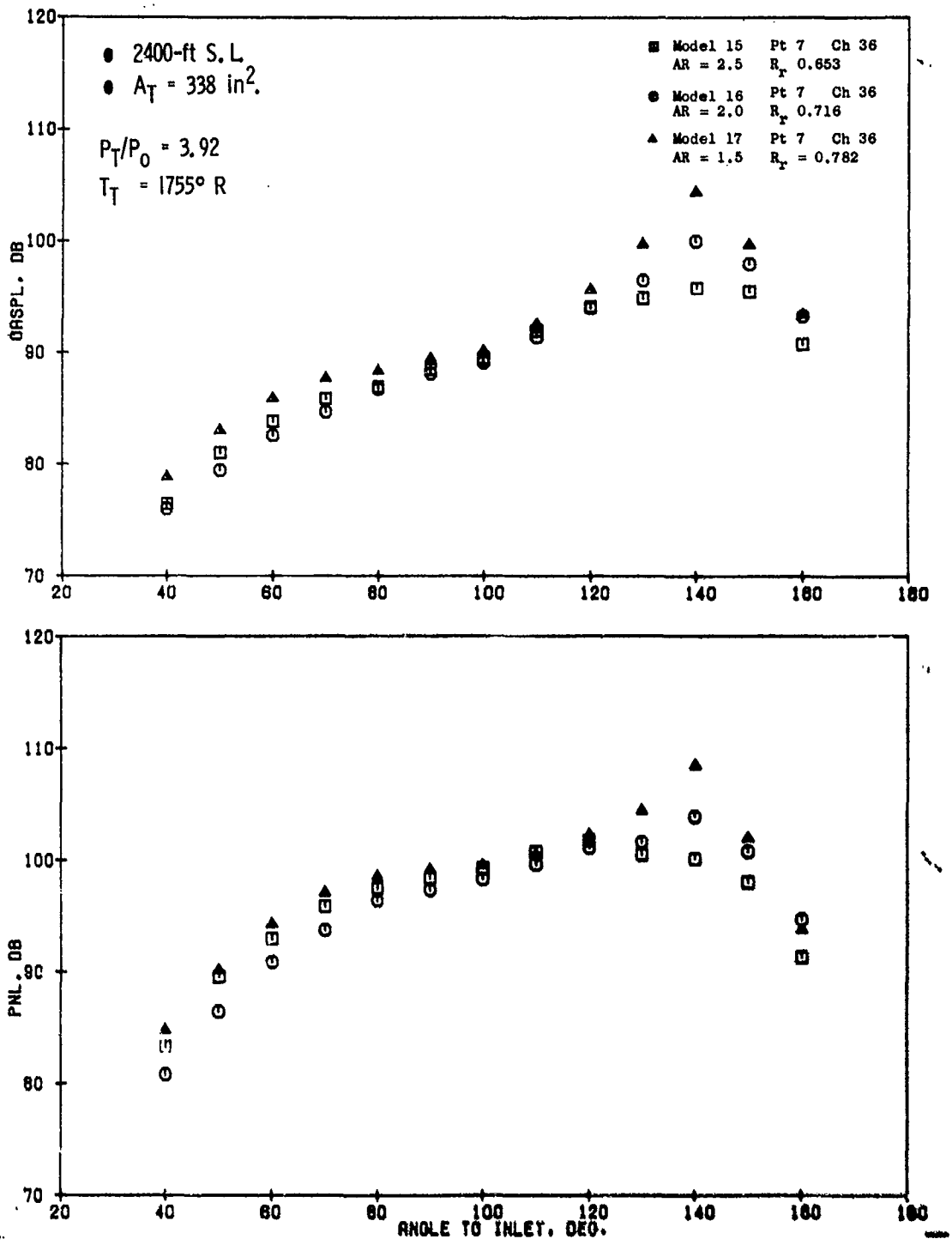

Figure 3-94. Impact of Area Ratio and Radius Ratio on PNL and OASPL Directivity, V_{ms} = 2625 ft/sec.

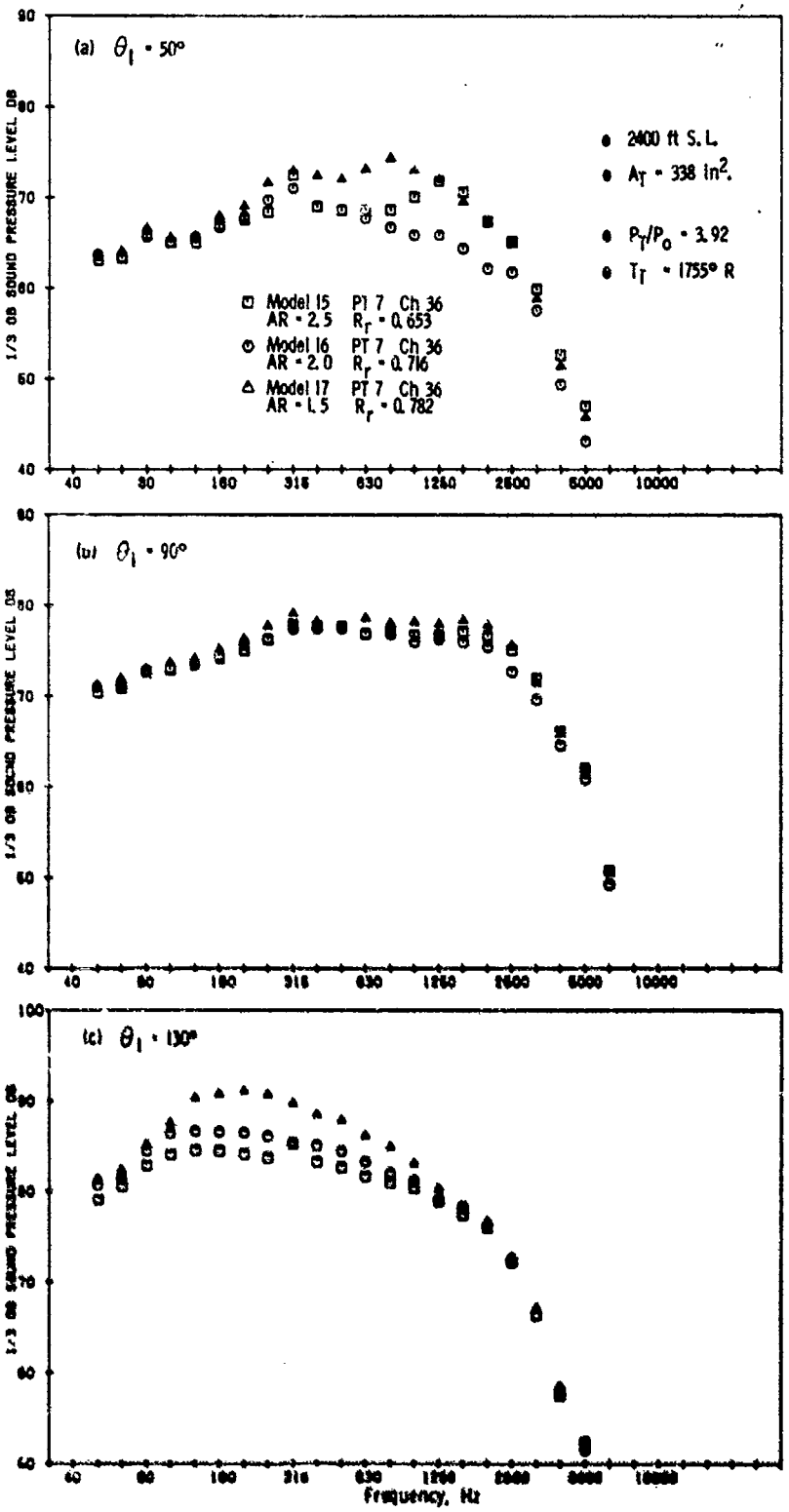

Figure 3-95. Impact of Area Ratio and Radius Ratio on Spectra, V_{aa} = 2625 ft/sec.

levels are seen but not of the magnitude observed at peak noise angles. The highest area ratio/lowest radius ratio is always the best suppressor in the aft quadrant but then show equivalency to, or slightly poorer performance than, the area ratio = 2.0 nozzle (Model 16) within the forward quadrant. The lowest area ratio/highest ratius ratio is the poorest suppressor at all angles.

An increase in area ratio will generally decrease noise at a supercritical operating point as the effect is to produce more rapid plume decay. This is observed in the aft angle 130° spectra, Figure 3-95, where post merged low-to-intermediate frequency noise is significantly lower for the higher area ratio. For this reason the normal double-humped spectra characteristics of multi-element suppressors are not seen.

At 90° the spectra shapes are all nearly similar as were the PNL and OASPL levels.

Within the inlet quadrant, changes in spectra are primarily in the mid to high frequency range and bear out changes seen in the OASPL/PNL directivity patterns.

Looking at the second data set, Figures 3-96 and 3-97 at V_{ma} = 2150 ft/sec, where peak PNL's are nearly the same for the three area ratio models but peak OASPL's show a spread of about 7 dB, the following are observed:

- Peak PNL's occur at 120°, 110° and 140° for AR = 2.5, 2.0 and 1.5, respectively. OASPL directivity shifts to be peaked at the further aft angles.

- PNL directivity is fairly flat broadside and in the near aft quadrant (90° to 140°) with peaks occurring at 120°, 110° and 140° for AR = 2.5 (Model 15), 2.0 (Model 16) and 1.5 (Model 17), respectively, whereas OASPL directivity peaks further aft.

- The very sharp aft quadrant and near level forward quadrant directivity patterns of the conical nozzle are not present for the suppressors. Shock-cell noise is the primary suppressor mechanism responsible for the forward quadrant suppression, the forward quadrant angles showing about 6APNL below the conical at 80° and approximately 19 APNL at 40°, with even greater Δ's for OASPL.

- Looking more closely at 50°, OASPL's are identical but PNL varies about 3 dB; the spectra showing a crossover of high and low frequency influence with area ratio variation. This indicates a delicate balance between the high frequency premerged and low frequency postmerged jet noise characteristics.

- Broadside, at 90°, the same spectral crossover with area ratio is maintained.

- In the aft quadrant (120° to 150°) spectra suppression relative to the conical is primarily in the mid-to-high frequency range with

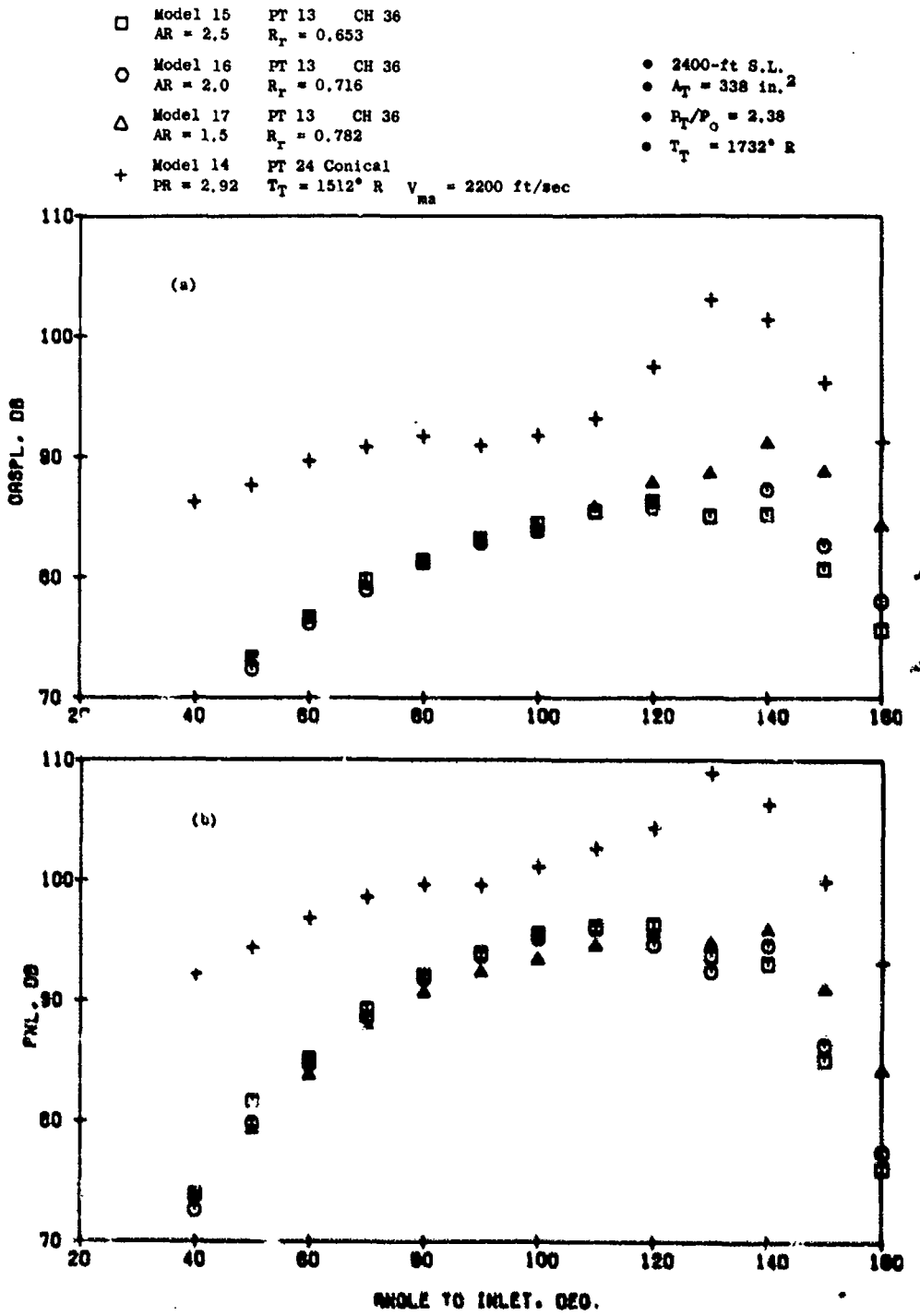

Figure 3-86. Impact of Area Ratio and Radius Ratio on PNL and OASPL Directivity, V_{ma} = 2150 ft/sec.

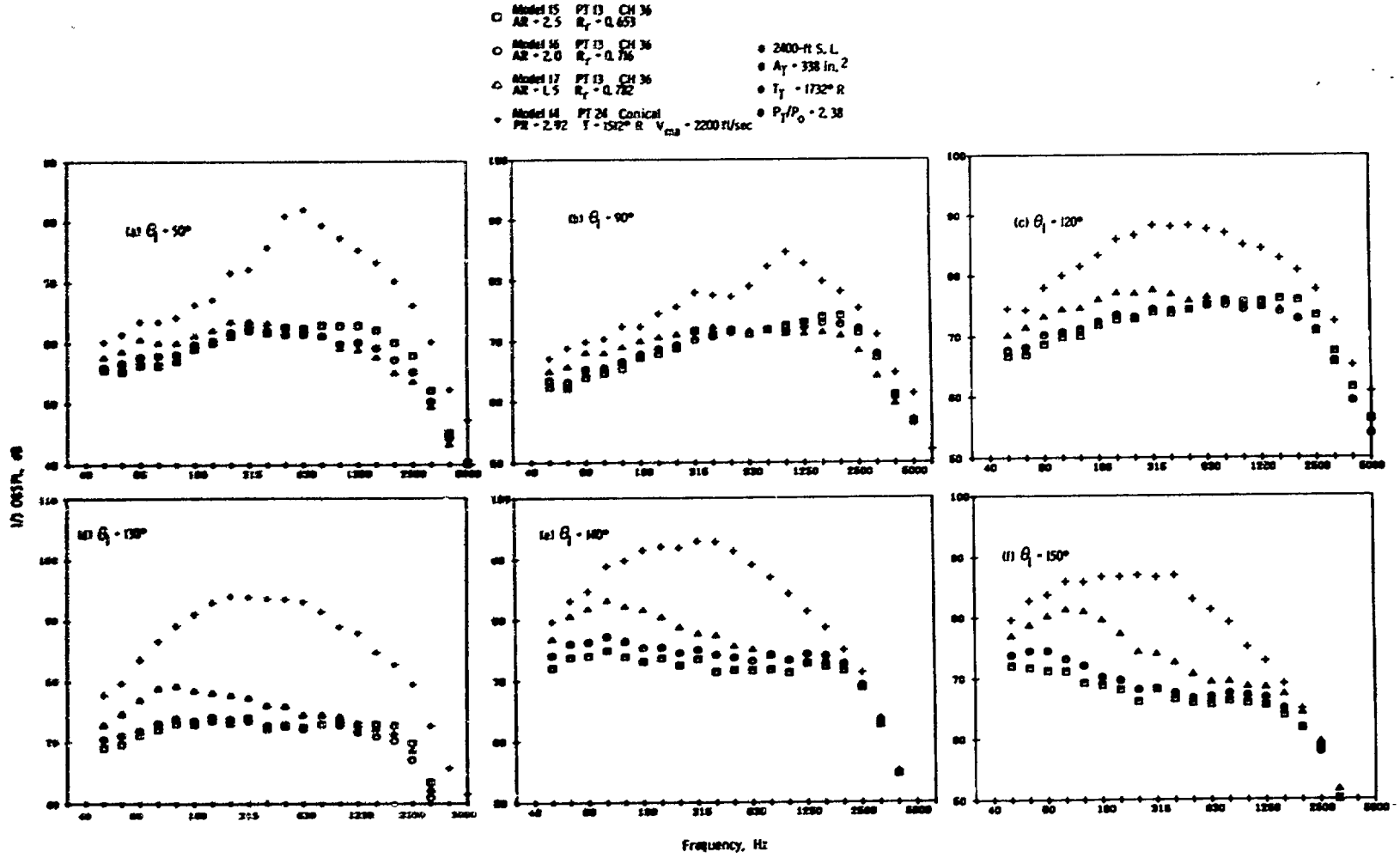

Figure 3-97. Impact of Area Ratio and Radius Ratio no Spectra, V_{ma} = 2150 ft/sec.

lower area ratio indicating quicker merging of individual jets and, therefore, generating a higher content of low frequency noise. Very high frequency premerged noise at far aft angles (e.g., 150°) still shows significantly different levels for the three models, reversed from the pattern at inlet angles (e.g., 50°) but they no longer control OASPL or PNL.

For the third data set, Figures 3-98 and 3-99 at V_{ma} = 1400 ft/sec, where the three models still maintain approximately 10 ΔPOASPL and 4 to 5.5 ΔPPNL suppression, the following observations are noted:

- Noise variance with area ratio/radius ratio is minor as PNL and OASPL directivity patterns show, except in the very aft quadrant where higher area ratio still maintains best PNL and OASPL suppression and shows variance relative to the lowest area ratio of 3 ΔPNL to 5 ΔOASPL at 160°.

- The crossover of noise directivity patterns with changing area ratio still exists as it did at mid and high-velocity. The higher area ratio is noisier at inlet angles and quieter in the aft quadrant, crossover normally occurring in the 100° to 140° region.

Area Ratio and Radius Ratio Variable, Dual Flow (Models 22, 24 and 27)

This study extended the previous investigation to a dual flow exhaust nozzle system. Models 22, 24, and 27 of Figure 3-100 were used, each maintaining the 36-chute suppressors of Models 15, 16 and 17, respectively, with area ratios and radius ratios of 2.5/0.653, 2.0/0.716 and 1.5/0.782. In place of the full plug turbojet geometry, an inner plug of 0.7" annulus step height was used in the retracted position. This set the outer to inner area ratio, A_o/A_i, at 1.92. Inner plug radius ratio was 0.779. Figures 16, 18 and 21 of Appendix A detail the model geometries. The inner stream geometry does not utilize a mechanical suppressor. The suppressor is applied only to the outer stream and is termed a half span suppressor.

Farfield acoustic testing in the Cell 41 Anechoic Facility followed the matrix described in Section 3.2.1, Figure 3-10 and Table 3-3. Each model used the following cycle series:

- W_i = 15% W_o
- W_i = 30% W_o
- DBTF/Inverted Dual Flow cycle with $1.0 \leq V_o/V_i \leq 2.0$
- AST/VCE

Additionally, Model 24 was tested with no inner flow while maintaining normal outer stream cycle conditions.

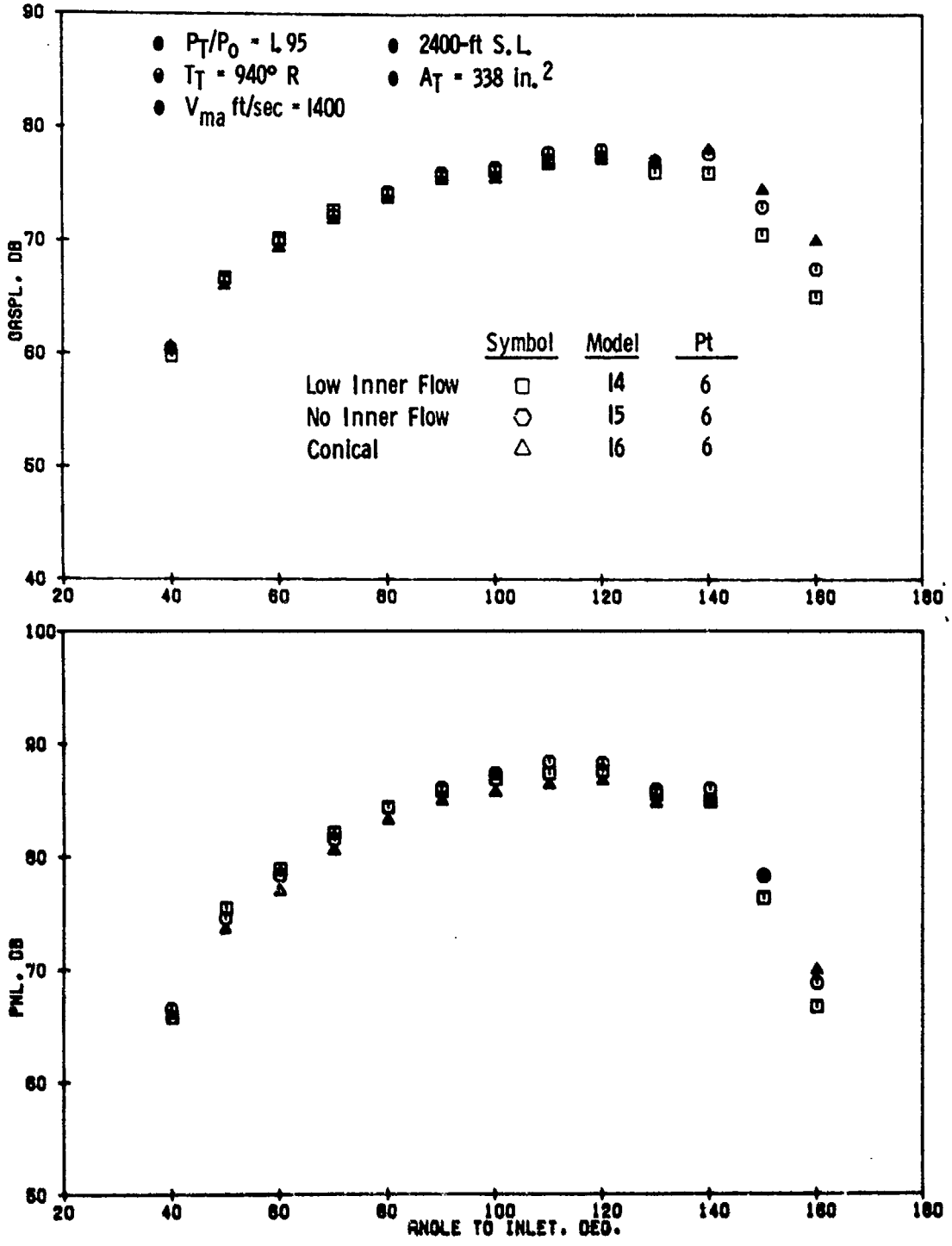

Figure 3-98. Impact of Area Ratio and Radius Ratio on PNL and OASPL Directivity, V_{ma} = 1400 ft/sec.

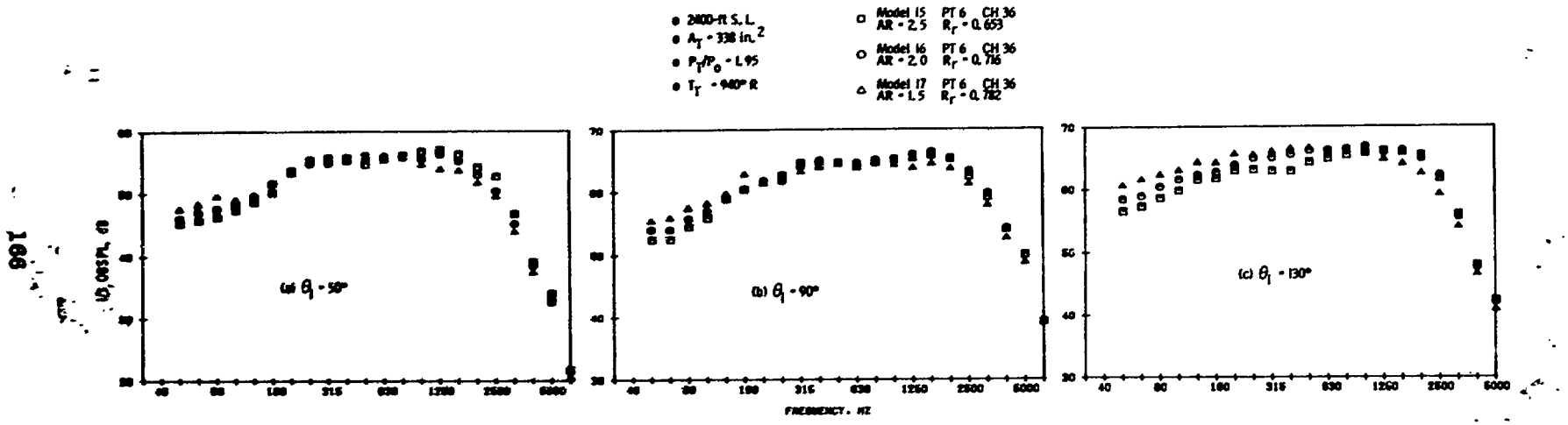

Figure 3-99. Impact of Area Ratio and Radius Ratio on Spectra, V_{ma} = 1400 ft/sec.

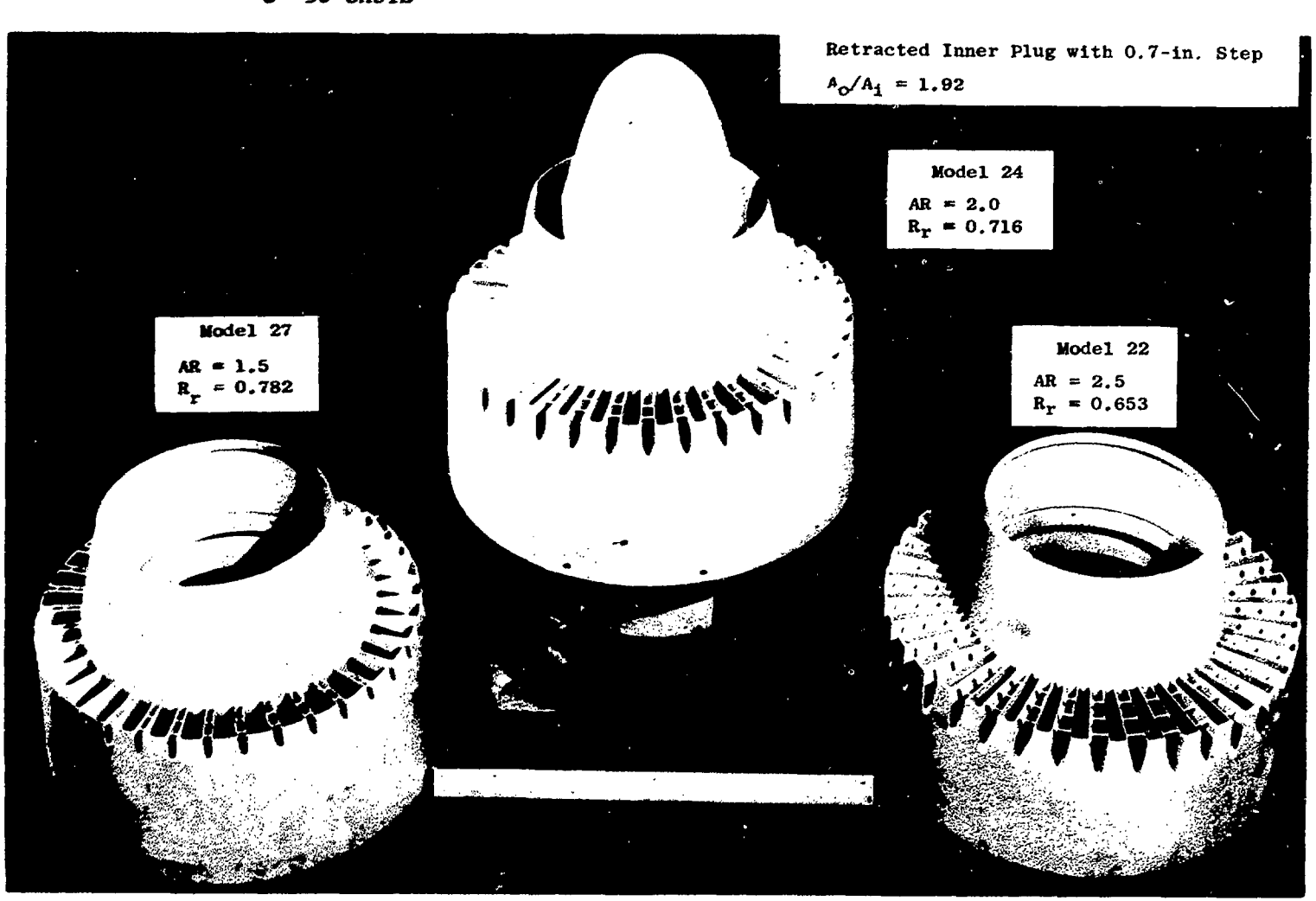

Figure 3-100. Half-Span Suppressor Area Ratio and Radius Ratio Variation on Dual Flow.

Acoustic results on a peak PNL basis, Figure 3-101, are shown for three data sets, i.e., (a) for all data points, (b) for the W_i = 30% W_o cycle, and (c) for the DBTF/Inverted Dual Flow cycle. The results shown are selected as representative of all the data cycle sets. For area ratio = 1.5 (Model 27) the three data-fitted curves are nearly duplicates, except that the DBTF cycle peaks at 11 ΔPPNL suppression instead of at 10 as did the other two. For the AR = 2.0, the three curves behave similarly within approximately ±0.3 ΔPPNL, peak suppressions being at 9 to 9.5 ΔPPNL. The three data curves for the area ratio 2.5 nozzle, Model 22 are generally the same with ±0.3 dB at high V_{ma} but show a spread of nearly 2 ΔPPNL at low V_{ma}. The above observations indicate that outer to inner stream cycle variations, within the range tested, do not significantly alter suppressor performance; if the measurements are normalized with respect to thrust, mixed flow density, and correlated as a function of V_{ma}. In general:

- The area ratio and radius ratio excursions within the test range show a noise variance of 1.5 ΔPPNL min. to 3.5 max.; magnitude of variance dependent on cycle V_{ma}.

- The low area ratio/high radius ratio is consistently better at low-to-intermediate V_{ma}, just as it was for the full span turbojet nozzle application.

- Peak suppression levels of 11, 9.5 and 10.4 for area ratios for 1.5 (Model 27), 2.0 (Model 24) and 2.5 (Model 22), respectively, are somewhat below those of the same applications to the turbojet which were 11.5, 12.0 and 12.5; indicating that a full span turbojet suppressor is slightly more efficient than a half span suppressor application to a dual flow system.

- The AR = $2.5/R_r$ = 0.653 suppressor (Model 22) is consistently poorer at low V_{ma} and potentially better at high V_{ma}. On the turbojet system the same was true at high V_{ma}, but, at low V_{ma} little distinction was seen between the AR = 2.0 and 2.5 (Models 24 and 22 respectively).

- The maximum PPNL suppression level for the AR = 2.5 nozzle, Model 22, occurs at a higher velocity than for the 1.5 (Model 27) and 2.0 (Model 24) and in some instances the maximum value may not have been achieved within the test range.

- Peak PNL suppression curves for each area ratio model show a trend crossover occurring in the 2000 to 2350 ft/sec V_{ma} range, generally consistent with the 2000 to 2100 ft/sec range of the single flow system.

Peak OASPL data are presented in the same manner in Figure 3-102 as were peak PNL data, namely, (a) for all data points, (b) for W_i = 30% W_o and (c) for DBTF/Inverted Dual Flow. The following are noted:

- Consistency of data for the three cycle sets is very good, particularly when comparing equivalent curve-fitted trends of ΔPOASPL where variance for each model is within ±0.5 dB.

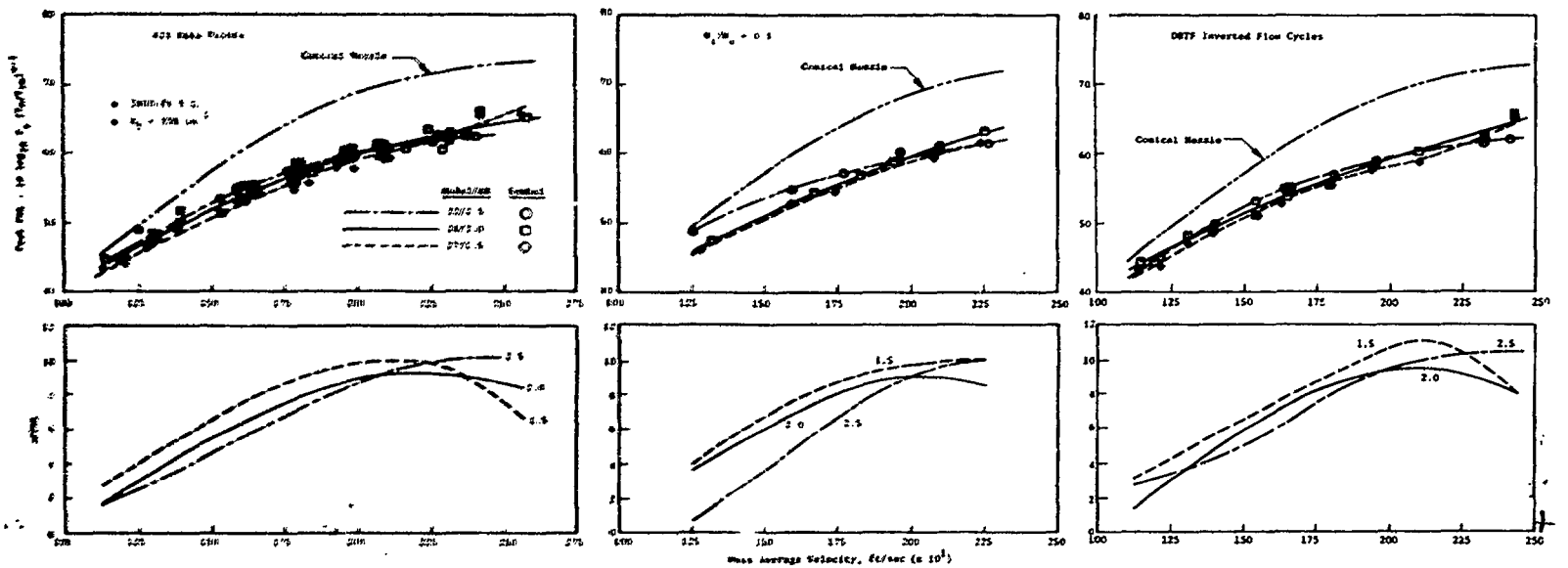

Figure 3-101. Impact of Area Ratio and Radius Ratio on Peak PNL, Dual Flow.

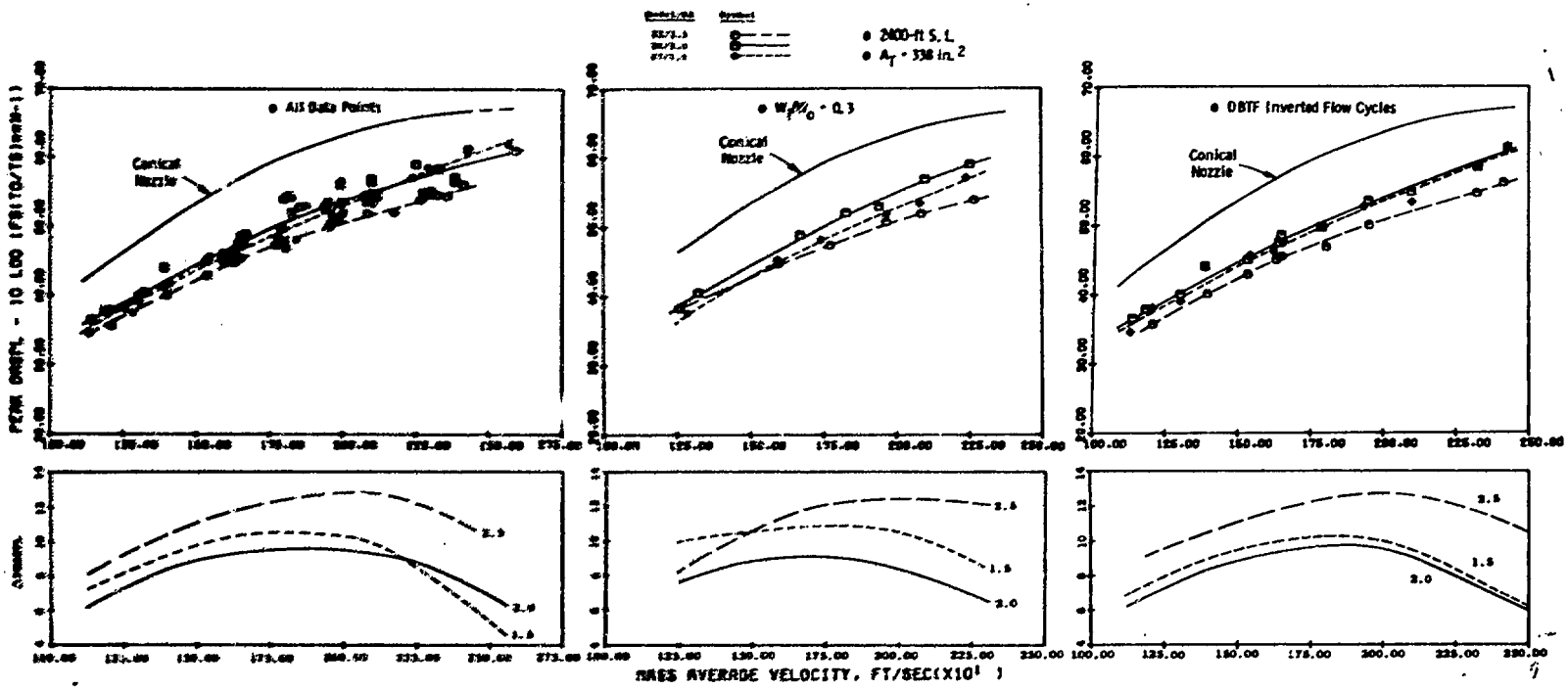

Figure 3-102. Impact of Area Ratio and Radius Ratio on Peak OASPL, Dual Flow.

- Variance in area ratio/radius ratio over the design range yielded a min. to max. ΔPOASPL of 2 to 5 dB, greater than the 1.5 to 3.5 ΔdB span experienced on PPNL.

- Maximum levels of peak OASPL suppression are also lower than those of the previous turbojet full span suppressors, i.e., 11, 9.5 and 12.5 ΔPOASPL for dual flow area ratios = 1.5, 2.0 and 2.5, respectively, compared to 11, 13 and 15.5 for equivalent turbojet models. This again implies that suppression of the full stream is somewhat more effective than suppressor application to the outer annulus alone.

- The relationship for sequence of models in improving suppression from 1.5 to 2.0 to 2.5 seems to hold up on the peak OASPL basis.

- Crossover of ΔPOASPL trend curves in the mid-to-high V_{ma} range is not seen for the area ratio = 2.5 nozzle, Model 22, as it was on the ΔPPNL basis. Area ratio of 2.5 is consistently the best suppressor, even at low V_{ma}. Maximum POASPL suppression levels are higher than they were for PPNL at about 12.5 to 13 ΔPOASPL versus 10 to 10.5 ΔPPNL.

- The AR = 2.0 nozzle, Model 24, is almost always the poorest POASPL suppressor; however, AR = 1.5 exhibits near the same noise levels, within 0.5 to 2 dB across the V_{ma} range.

Data at 90°, Figure 3-103 for PNL and Figure 3-104 for OASPL, indicate that some suppression is retained broadside (primarily on the OASPL basis), particularly at mid-to-high V_{ma} where shock-cell noise is prevalent in the conical nozzle but negligible, if at all present, in the segmented suppressors. Suppression levels relative to the conical nozzle are of similar magnitude to those of the previous section's full span turbojet suppressors.

On both a PNL and OASPL basis, a maximum variation of 3 dB is seen among the three models on the W_i = 30% W_o cycle data. No consistent trend of PNL with area ratio is evident, but OASPL progressively increases as AR changes from 2.0 to 1.5 to 2.5.

Similar 50° data, Figure 3-105 for PNL and Figure 3-106 for OASPL show substantial forward quadrant suppression, even at low V_{ma}, much higher levels than at broadside. At high V_{ma}, with supercritical pressure ratio, levels are very significantly below those of the conical nozzle due to absence of shock-cell noise.

OASPL levels for the three models are fairly near the same level and no distinction between area ratio is made, except for the W_i = 30% W_o cycle where a spread of 2 dB is seen.

On the PNL basis, variation of AR/R_r shows the AR = 2.5 (Model 22) to now be highest in level and the AR = 1.5 (Model 27) to consistently maintain the highest suppression in the forward quadrant.

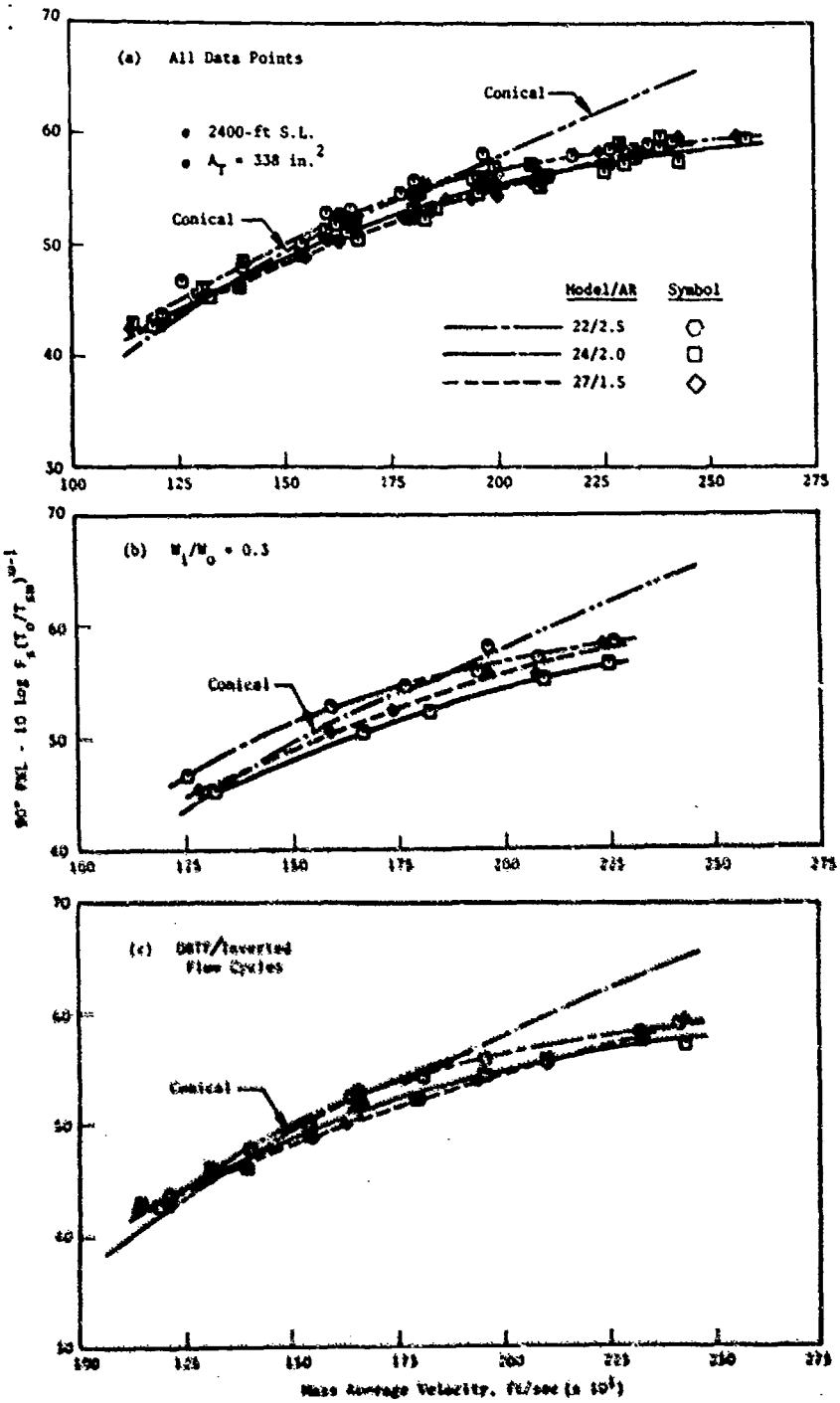

Figure 3-103. Impact of Area Ratio and Radius Ratio on 90° PNL, Dual Flow.

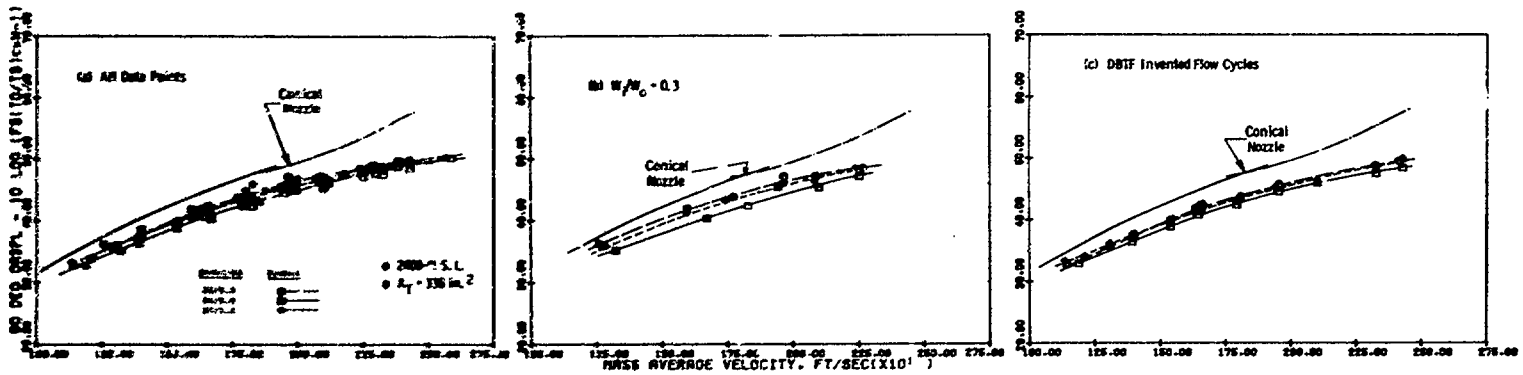

Figure 3-104. Impact of Area Ratio and Radius Ratio on 90° OASPL, Dual Flow.

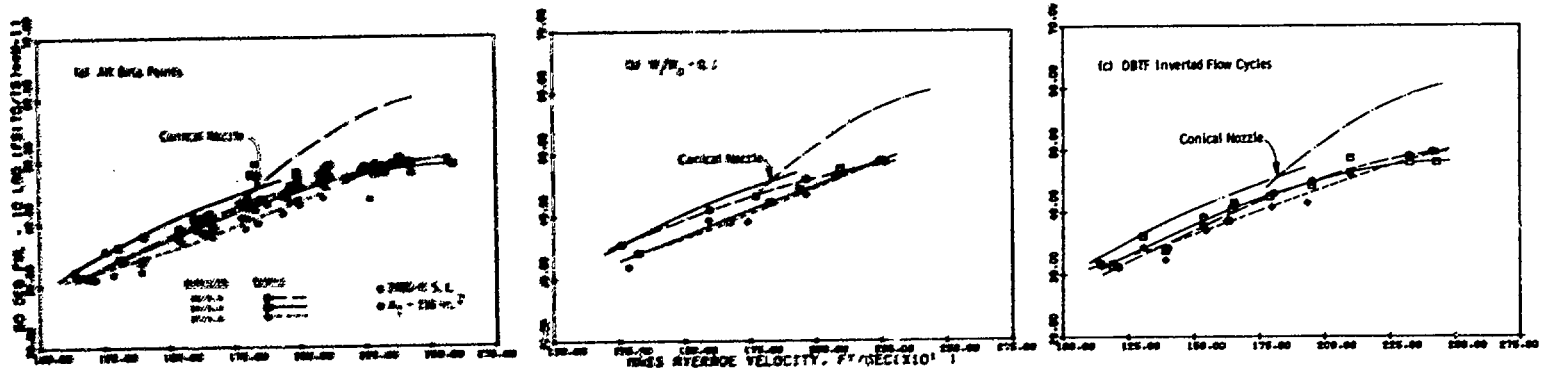

Figure 3-105. Impact of Area Ratio and Radius Ratio on 50° PNL, Dual Flow.

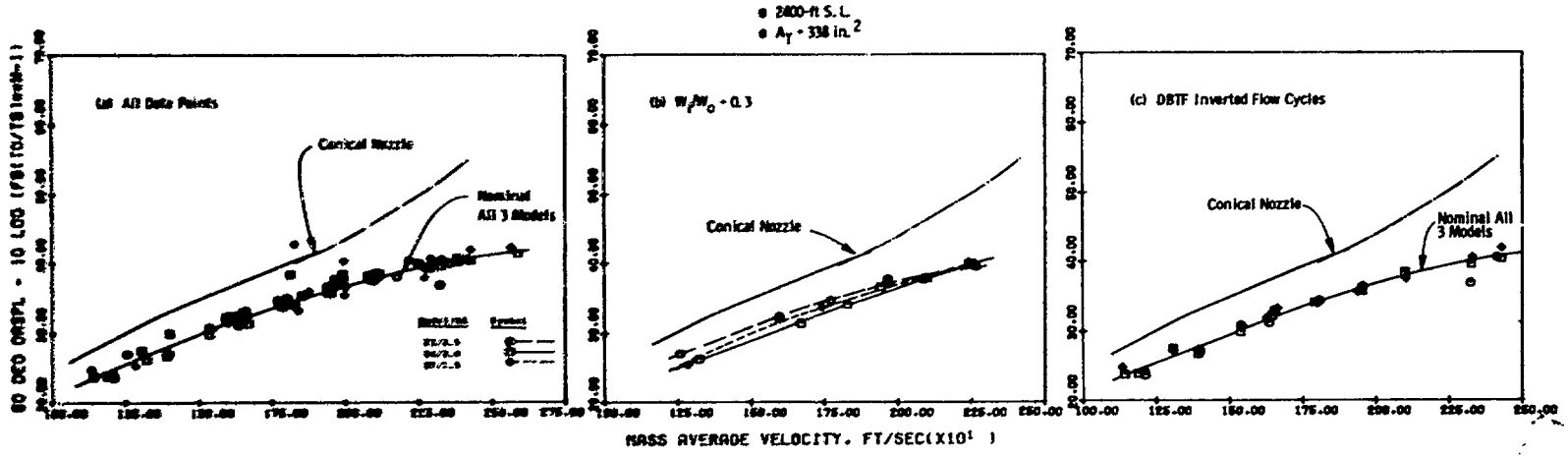

Figure 3-106. Impact of Area Ratio and Radius Ratio on 50° OASPL, Dual Flow.

OAWPL data are included as Figure 3-107 to show that no significant variation with cycle or area ratio/radius ratio is present.

For more detailed variations in noise characteristics of PNL & OASPL directivity plus spectra, the following data sets from the DBTF cycle matrix were selected for inclusion:

Figures 3-108 and 3-109 Data Point 37, V_{ma} = 2425 ft/sec,
Figures 3-110 and 3-111 Data Point 24, V_{ma} = 1200 ft/sec,
Figures 3-112 and 3-113 Data Point 36, V_{ma} = 1945 ft/sec,

The following observations are made from the first data set at high V_{ma}:

- OASPL and PNL directivity bear out the trends of noise at peak, 90° and 50° versus V_{ma} in that significant suppression is seen at peak, minimum at broadside and then somewhat higher levels in the forward quadrant.

- Noise directivity of the suppressor nozzles has shifted from the conventional conical nozzle pattern to now peak somewhat further aft. At mid-to-low V_{ma} the suppressor's directivity patterns more closely match those of the conical or tend to shift peak noise more toward the broadside locations. Directivity patterns are not uniform among the three area ratios in that the 1.5 (Model 27) and 2.0 (Model 24) are more peaked than the smooth distribution of the 2.5 (Model 22). Maximum variation in suppressor noise levels is seen in the peak aft quadrant; however, levels are more uniform and within a maximum spread of about 3 dB in the forward quadrant.

- Spectra at this high V_{ma} point, for inlet to broadside angles, have the characteristic flat to somewhat double-humped distribution with suppression primarily in the midfrequency range where conical nozzle shock-cell tone and broadband noise are normally dominant. At further aft and peak angles, the spectra lose the high frequency second hump associated with the premerged jets and they more closely resemble the conical nozzle. Suppression is still primarily maintained in a broad band of frequencies, primarily centered in midrange. At all angles, the very low-frequency noise levels associated with the postmerged jets are similar in level to the conical.

Best suppression on a flight transformed basis would be from the AR = 2.5 nozzle, Model 22, (see θ = 130° and 140°) where high frequency noise is somewhat below that of the 2.0 (Model 24) and 1.5 (Model 27), in addition to the greatly reduced midfrequency levels.

At the low V_{ma} point (1200 ft/sec and both streams operating subcritically):

- OASPL and PNL directivities are consistent with plots of peak noise versus V_{ma}, showing 3-4 ΔPPNL and 7-9 ΔPOASPL. At 90°, PNL levels

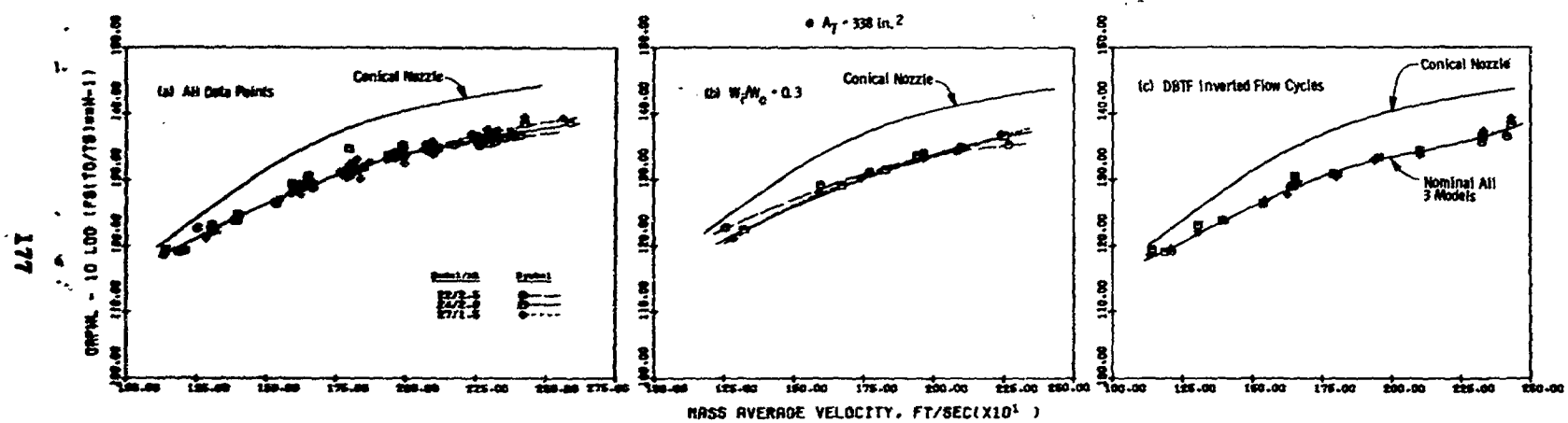

Figure 3-107. Impact of Area Ratio and Radius Ratio on OAPWL, Dual Flow.

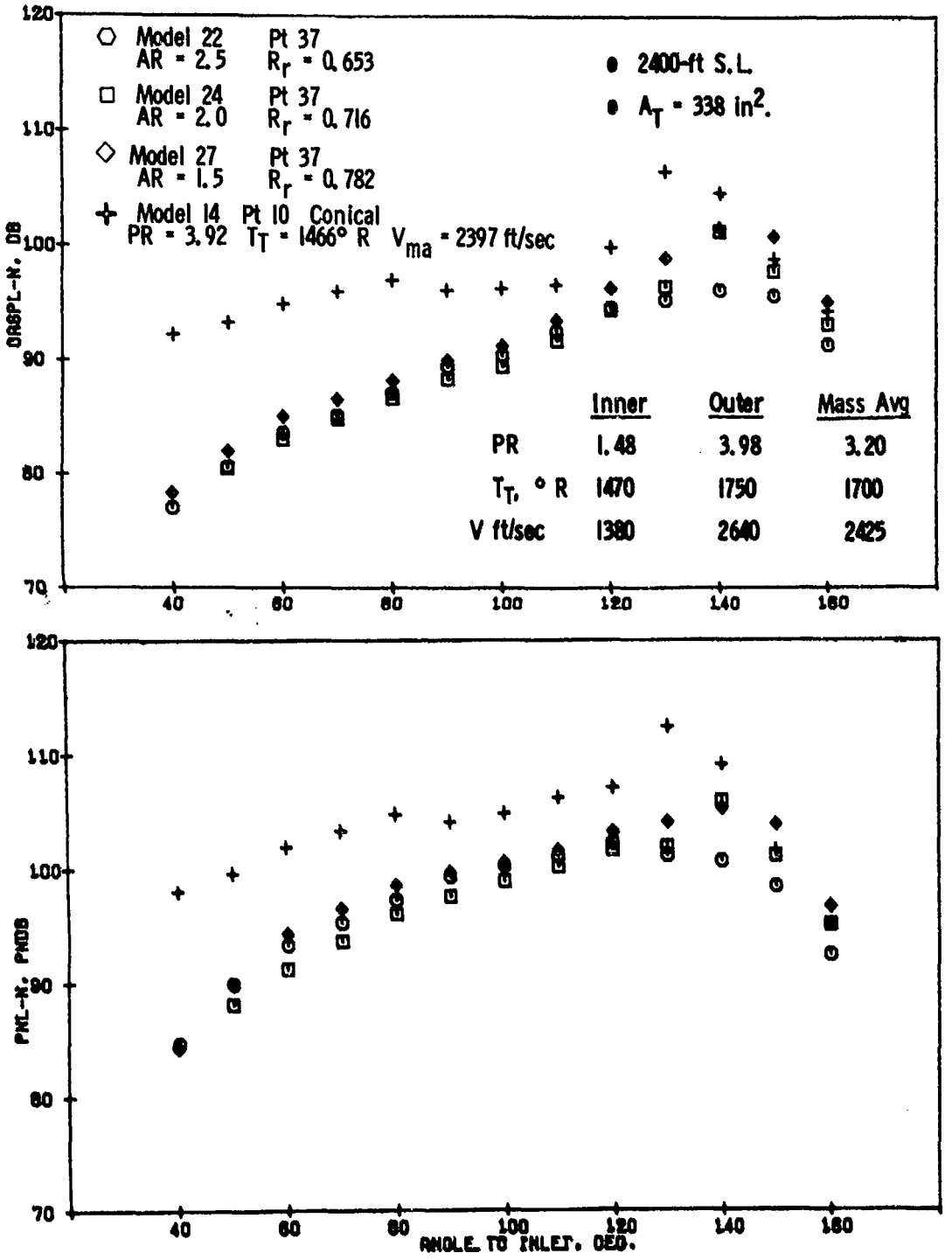

Figure 3-108. Impact of Area Ratio and Radius Ratio on OASPL and PNL Directivity, V_{ma} = 2425 ft/sec, Dual Flow.

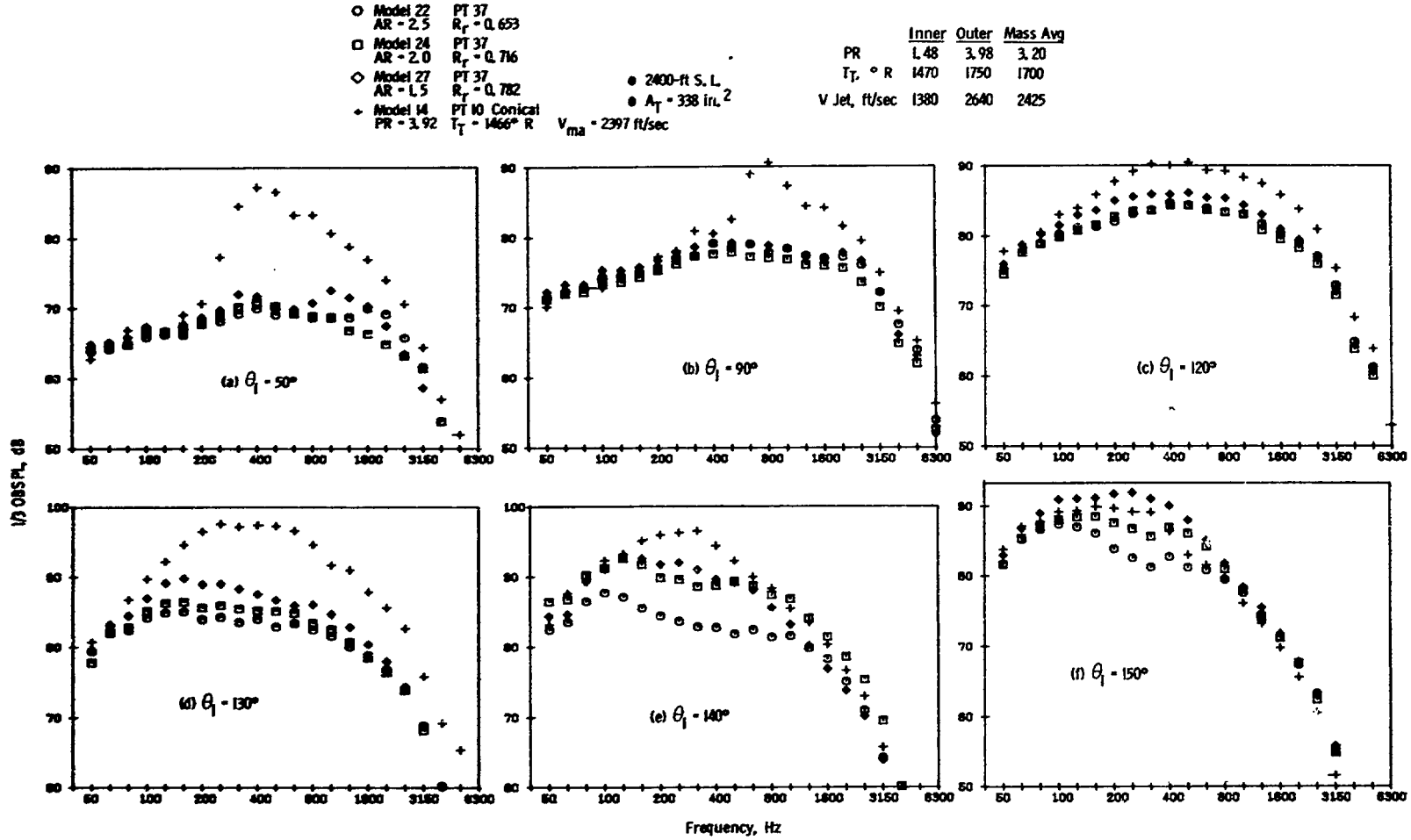

Figure 3-109. Impact of Area Ratio and Radius Ratio on Spectra, V_{ma} = 2425 ft/sec, Dual Flow.

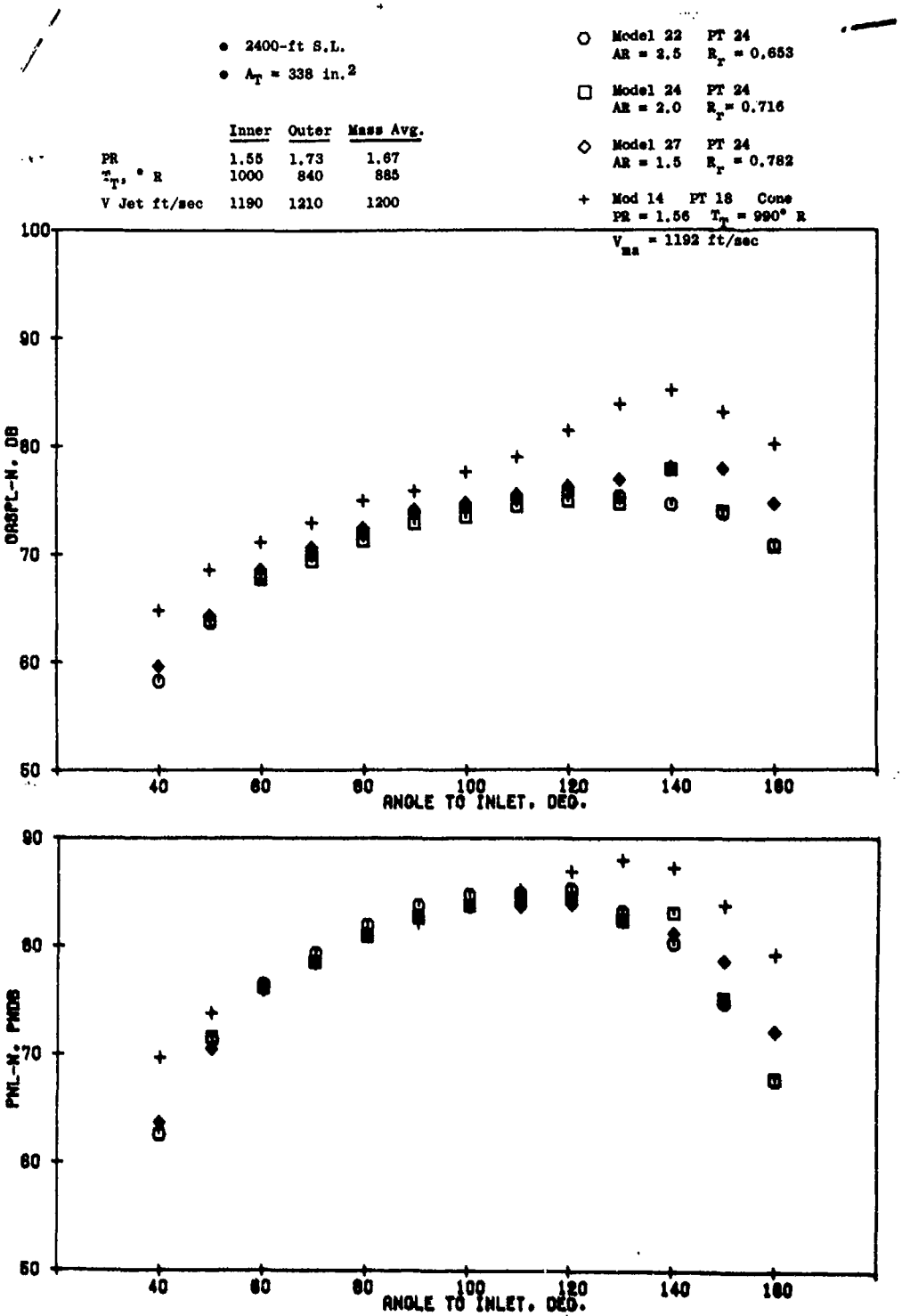

Figure 3-110. Impact of Area Ratio and Radius Ratio on OASPL and PNL Directivity, V_{mp} = 1200 ft/sec, Dual Flow.

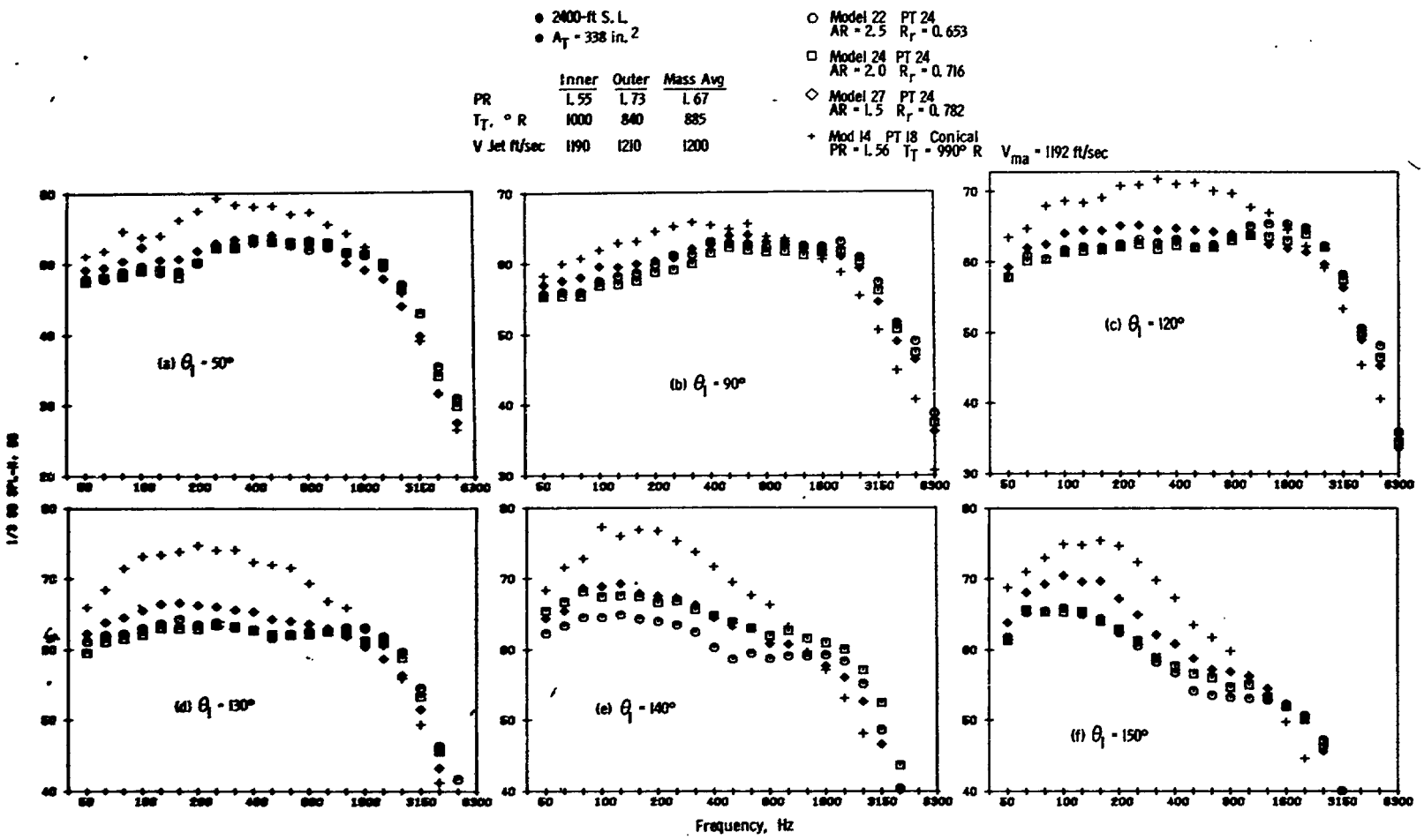

Figure 3-111. Impact of Area Ratio and Radius Ratio on Spectra, V_{ma} = 1200 ft/sec, Dual Flow

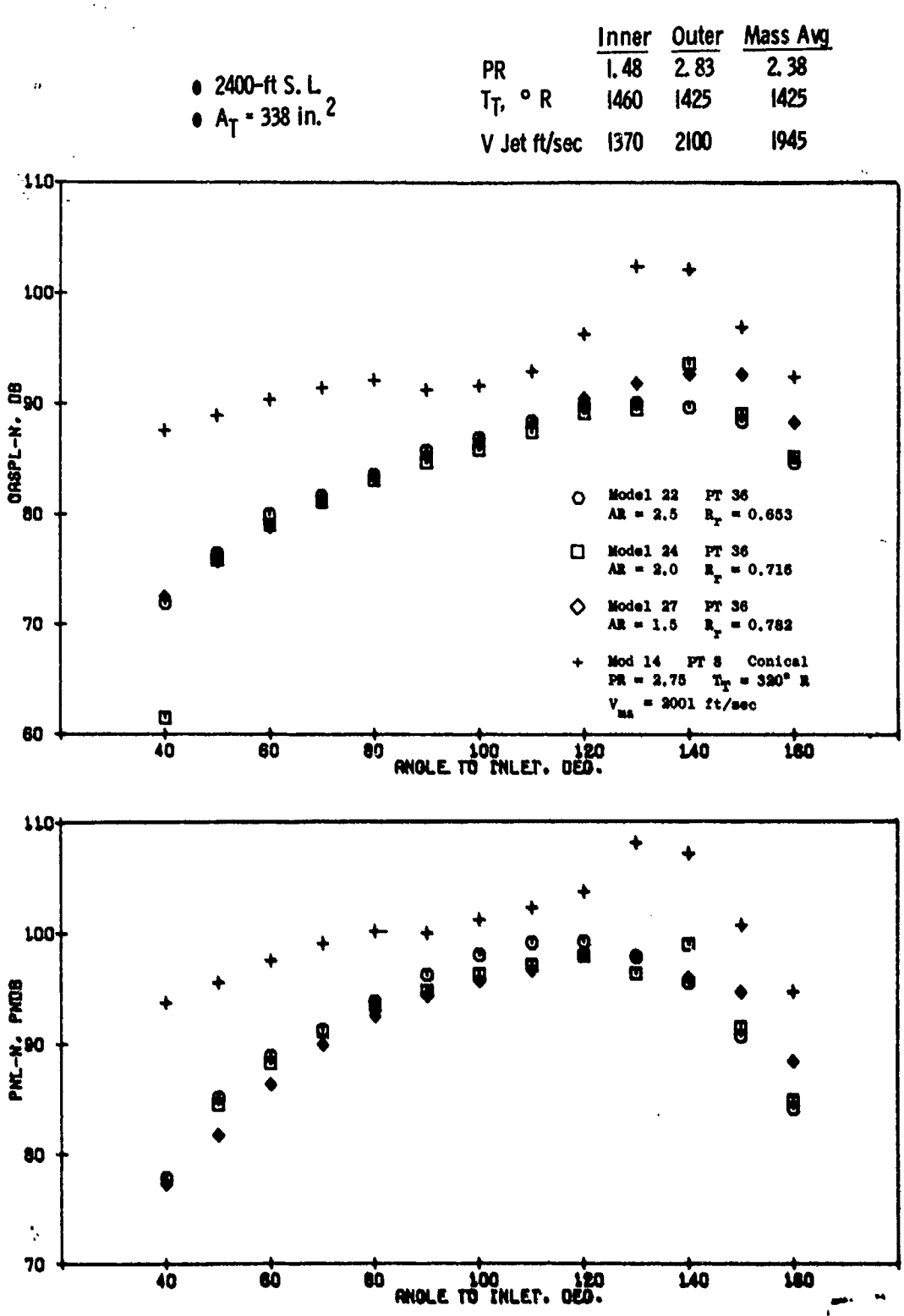

Figure 3-112. Impact of Area Ratio and Radius Ratio on PNL and OASPL Directivity, V_{ma} = 1945 ft/sec, Dual Flow.

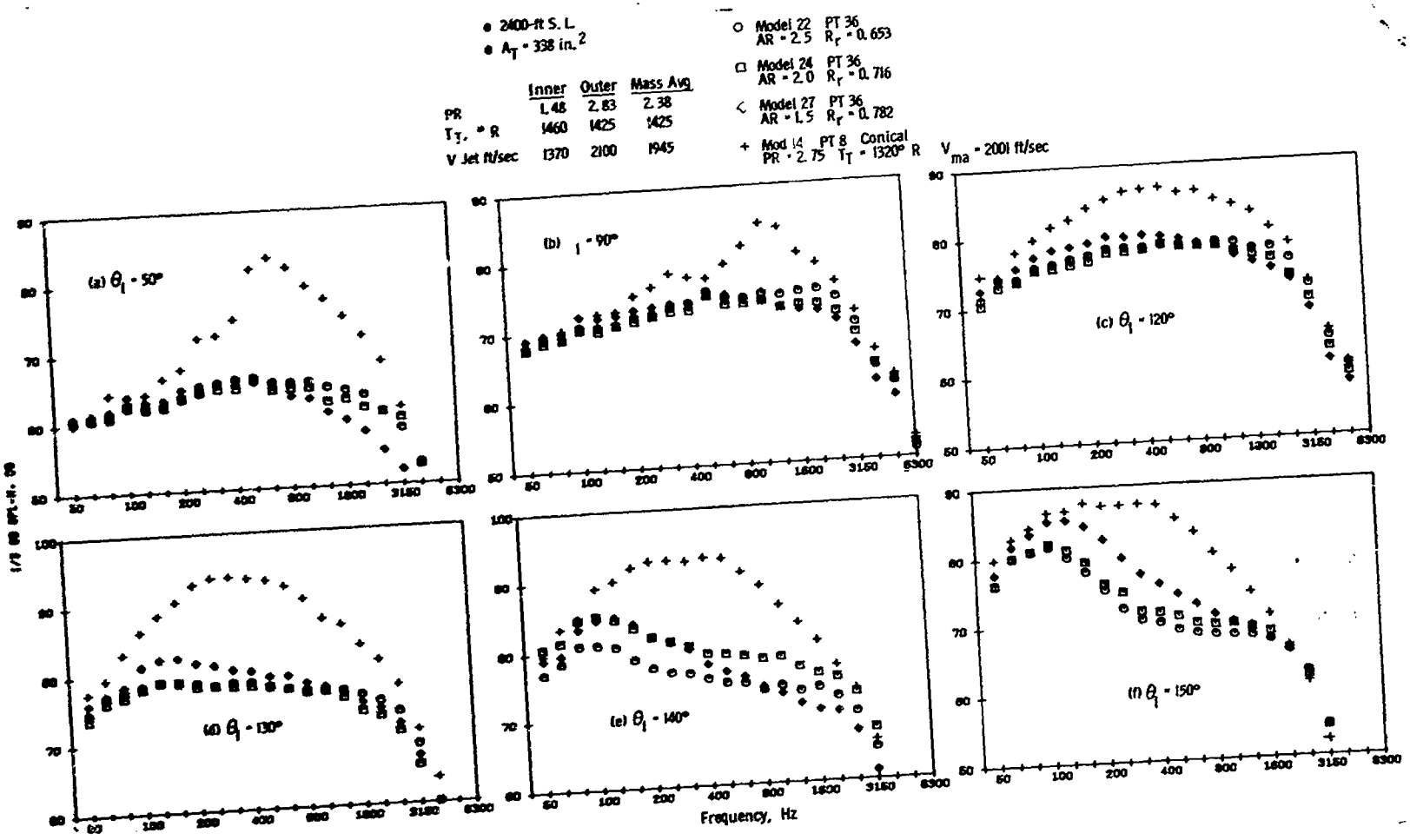

Figure 3-113. Impact of Area Ratio and Radius Ratio on Spectra, V_{ma} = 1945 ft/sec, Dual Flow.

are slightly above the conical nozzle (as the conical nozzle was also operated subcritically and had no shock-cell noise) and OASPL levels show 2-3 dB suppression. At 50°, ΔPNL and ΔOASPL are somewhat greater than at broadside.

- In general the variance in noise level with changing area ratio is primarily seen only in the aft quadrant and with maximum variance of about 4 PNL and OASPL at 150°. The AR = 2.5 (Model 22) is seen to generally be the best suppressor on a directivity basis.

- Plots at 50°, 90° and 120° to 150° show slightly greater predominance of the premerged high frequency spectra at aft quadrant and peak angles. Suppression relative to the conical nozzle is still primarily maintained in the midfrequency range but with high-frequency noise levels approaching those of the baseline much sooner than at high V_{ma} and with some low frequency noise suppression observed, dissimilar to that observed at high V_{ma} for comparable angles.

For consistency of data presentation in comparison to similar data on the full span turbojet suppressor models of the previous section, Figures 3-112 and 3-113 are included for a midvelocity point at V_{ma} = 1945 ft/sec.

Area Ratio Variable, Radius Ratio Constant, Dual Flow (Models 33 and 34)

The purpose of this study was to isolate acoustic performance as a function of area ratio alone, maintaining constant suppressor radius ratio. Models 33 and 34 were utilized per Figure 3-114, each with a nominal value of 0.78 suppressor radius ratio and with a suppressor area ratio of 2.5 and 3.0, respectively. Schematics of the detailed system geometries are per Appendix A, Figures A-27 and A-28. Model 33 of AR = 2.5, from the NASA-Lewis/GE Duct Burning Turbofan program NAS3-18008 (Reference 10), was adapted to the Cell 41 Anechoic Facility. Model 34 adds a new AR = 3.0 annular chute suppressor to the same inner stream geometry. Pertinent parameters for the models are:

	Outer				Inner				System
Model No.	Flow Area, $in.^2$	No. of Chutes	Area Ratio	Radius Ratio	Flow Area, $in.^2$	Step Height, in.	Plug Location	Radius Ratio	Area Ratio
33	17.21	36	2.5	0.783	11.12	1.034	Retracted	0.674	0.65
34	17.21	36	3.0	0.783	11.13	1.034	Retracted	0.674	0.65

- 36 Chute
- Radius Ratio = 0.78

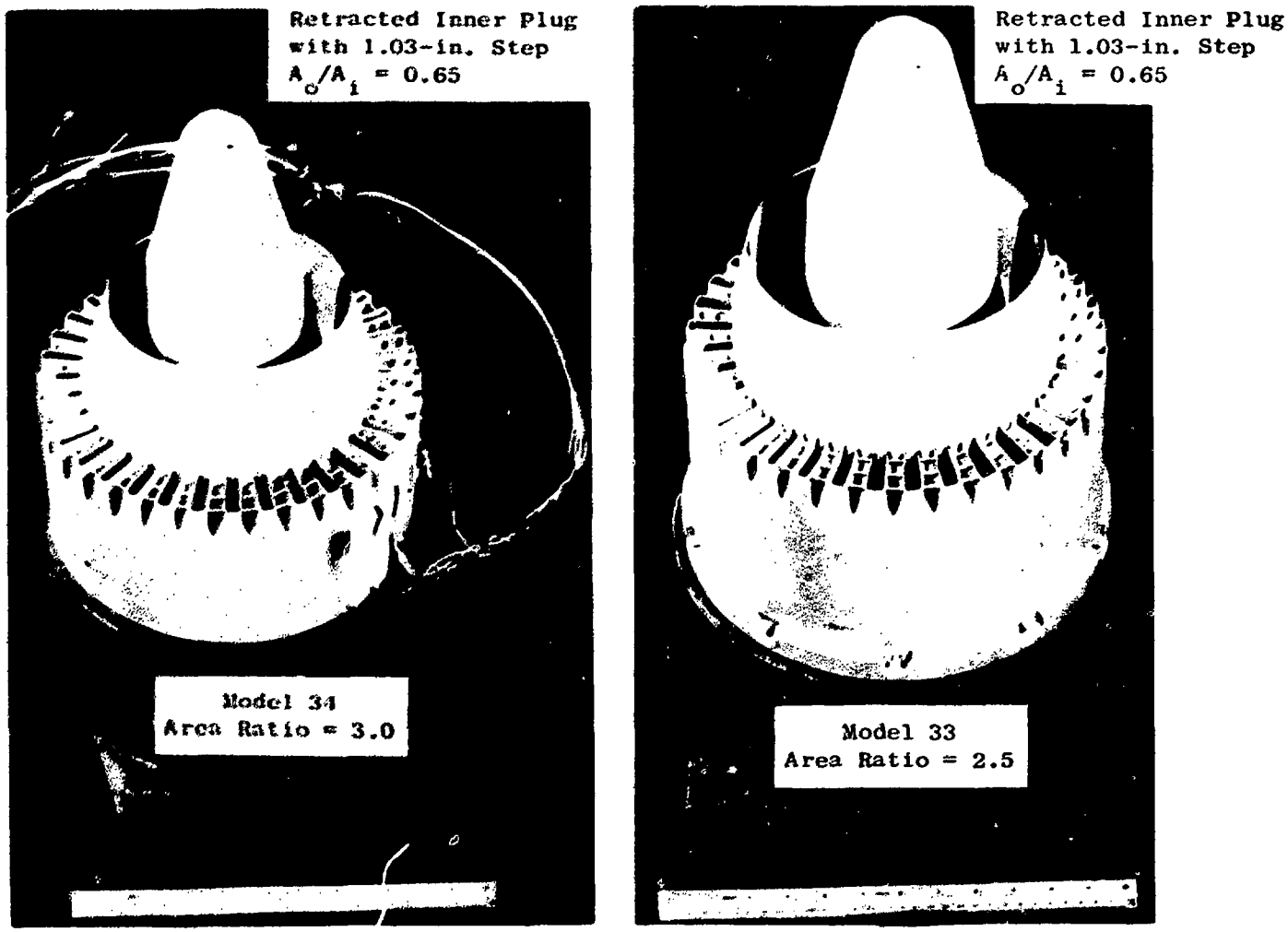

Figure 3-114. Annular Suppressor Area Ratio Variation at Constant Radius Ratio, Dual Flow.

As shown in the tabulation, Models 33 and 34 maintained the same inner flowpath geometry and flow area ratio of 0.65 and thus formed a true variation of suppressor area ratio at constant suppressor radius ratio.

Far-field acoustic testing was performed in the Cell 41 Anechoic Facility following a matrix similar to Section 3.2.1, Figure 3-10 and Table 3-3, but expanded to be more consistent with the test matrix of the DBTF Program (Reference 10). The following cycle series was used.

- W_i = 0, 15, and 30% W_o
- DBTF/Inverted Dual Flow Cycle
- AST/VCE

Comparative acoustic data plots for the two models are included in the following format for the W_i = 0, 15, and 30% W_o cycles, each normalized and versus V_{ma}.

- Figures 3-115 and 3-116 peak OASPL and PNL
- Figures 3-117 and 3-118 90° OASPL and PNL
- Figures 3-119 and 3-120 50° OASPL and PNL
- Figure 3-121 OAPWL

Acoustic data for Models 33 and 34 were presented and discussed in Section 3.4.2.2 (System Velocity Ratio Variation at Fixed A_o/A_i and Duct Suppressor Geometry). It was shown that noise levels for low system area ratio, A_o/A_i = 0.65, vary widely with cycle V_o/V_i, particularly studied within the dBTF/Inverted Dual Flow cycle matrix for $0.6 \leq V_o/V_i \leq \infty$. Within this section, for isolation of suppressor area ratio impact on acoustic performance, comparisons between the two models at fixed values of V_o/V_i = 0.6, 0.8, 1.0, 1.25, 1.5, 2.0, and ∞ (no inner flow) are included in Figures 3-122 and 3-123 for peak OASPL and peak PNL.

Supporting OASPL and PNL directivity data plus 1/3 OBSPL spectra, selected as representative of the wide data matrix, are included in the following graphs:

- Figures 3-124 and 3-125 W_i = 30% W_o, V_{ma} = 2075 ft/sec
- Figures 3-126 and 3-127 W_i = 30% W_o, V_{ma} = 1340 ft/sec

Review of the data elicits the following general observations:

- Levels of peak OASPL/PNL suppression vary considerably with the particular cycle under consideration. Maximum Δ peak PNL values are seen to be approximately 19/13.5, 16.3/11.5, and 13.5/9.7 for W_i = 0, 15, and 30% W_o cycles for the AR = 2.5 suppressor (Model 33) and 18.5/13, 16.7/12, and 15.5/10.7 for the AR = 3.0 nozzle (Model 34). This results in a spread of 5.5/3.7 and 3.1/2.3 peak OASPL/PNL. A greater spread is seen in the DBTF cycle where $0.6 \leq V_o/V_i \leq \infty$, as per data of Section 3.4.2.2.

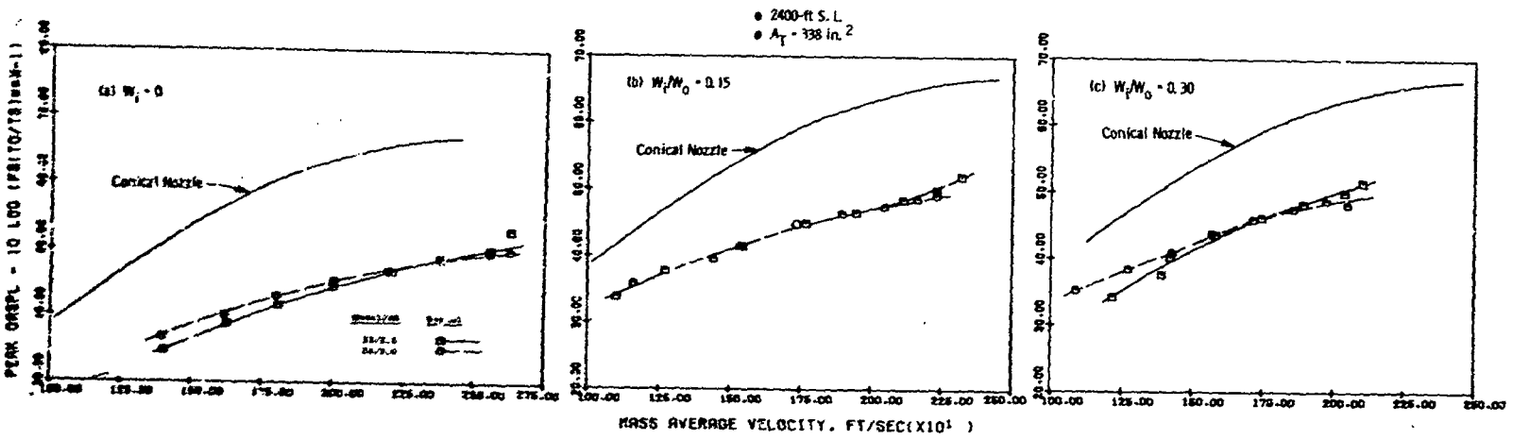

Figure 3-115. Area Ratio Variation at Constant Radius Ratio, Peak OASPL.

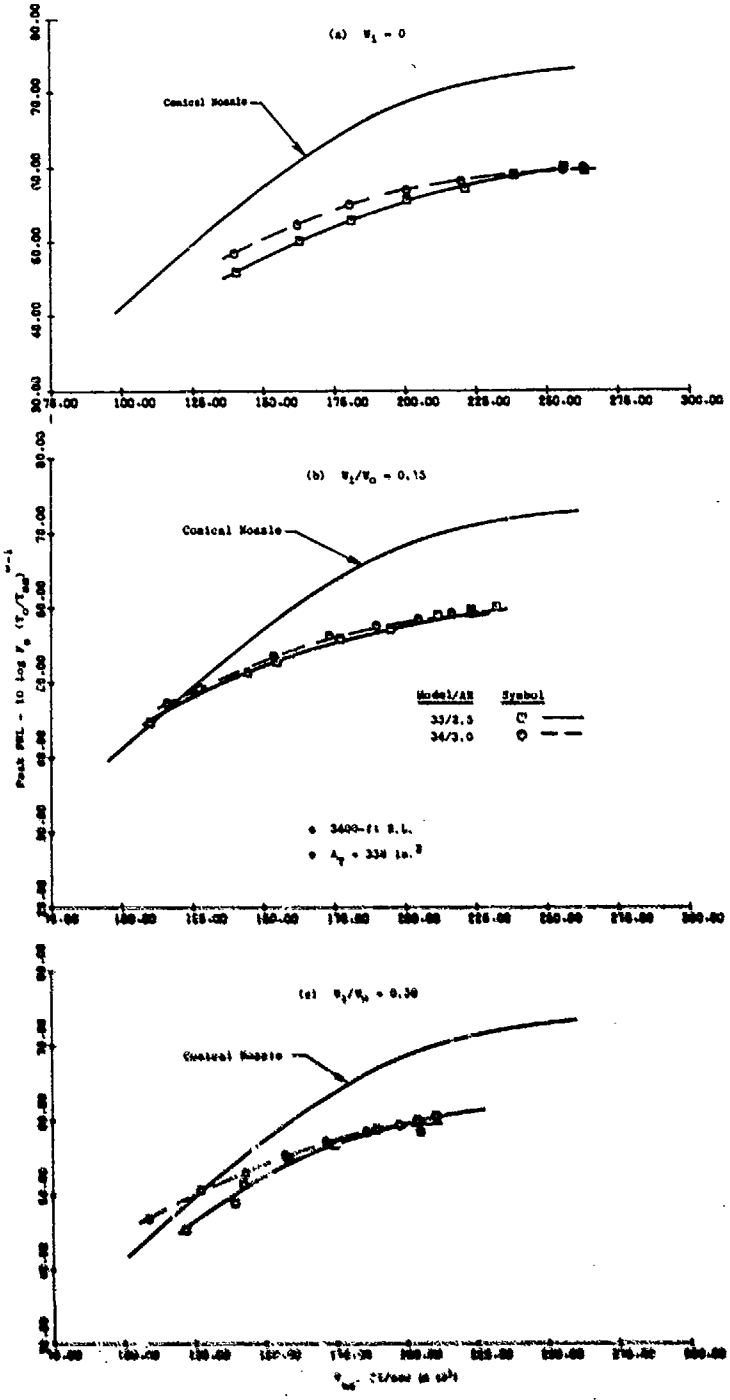

Figure 3-116. Area Ratio Variation at Constant Radius Ratio, Peak PNL.

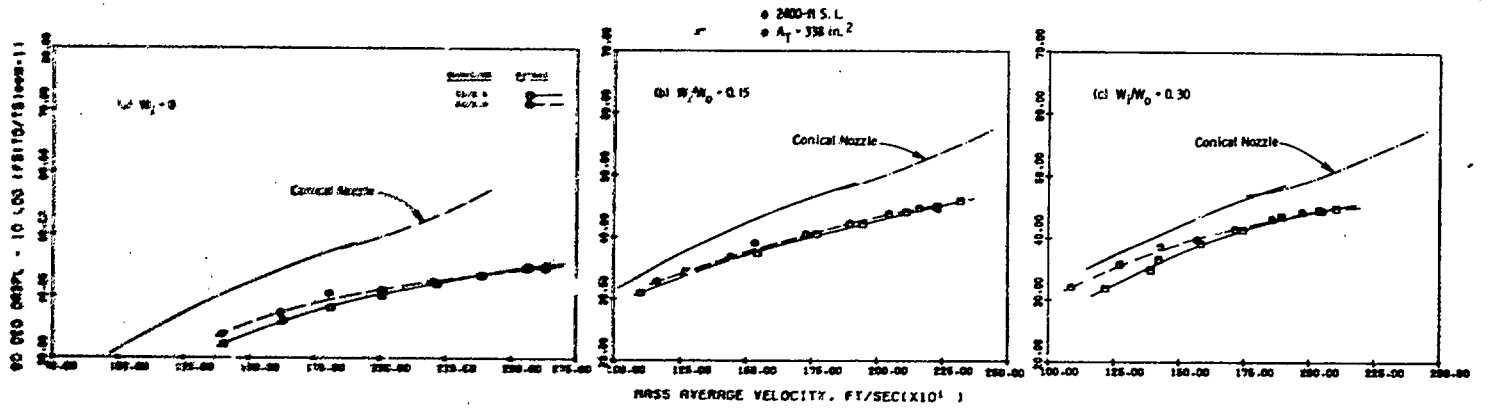

Figure 3-117. Area Ratio Variation at Constant Radius Ratio, 90° OASPL.

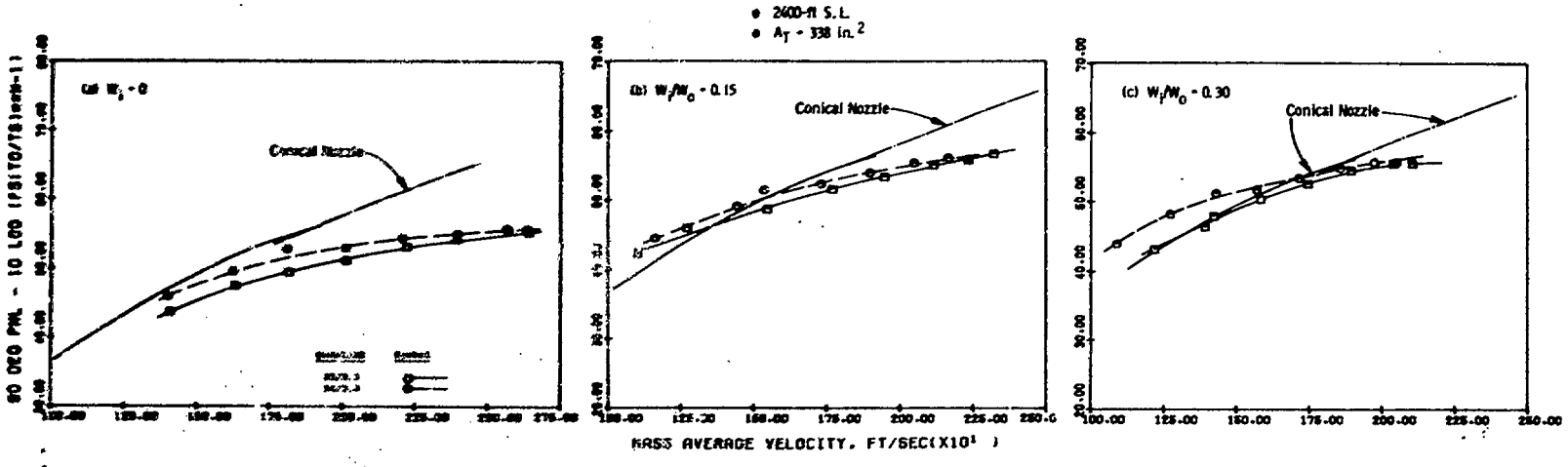

Figure 3-118. Area Ratio Variation at Constant Radius Ratio, 90° PNL.

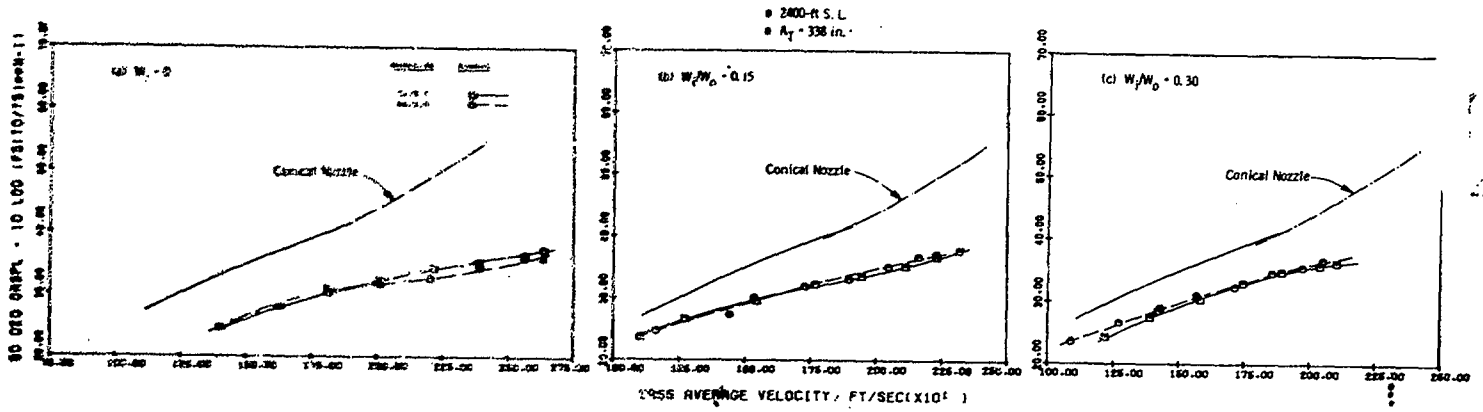

Figure 3-119. Area Ratio Variation at Constant Radius Ratio, 50° OASPL.

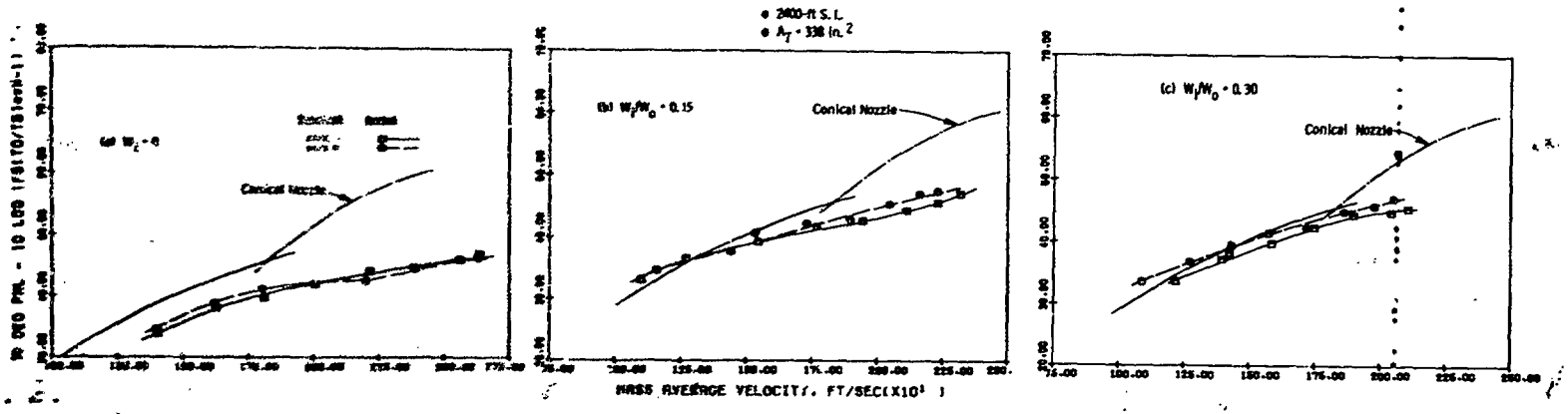

Figure 3-120. Area Ratio Variation at Constant Radius Ratio, 50° PNL.

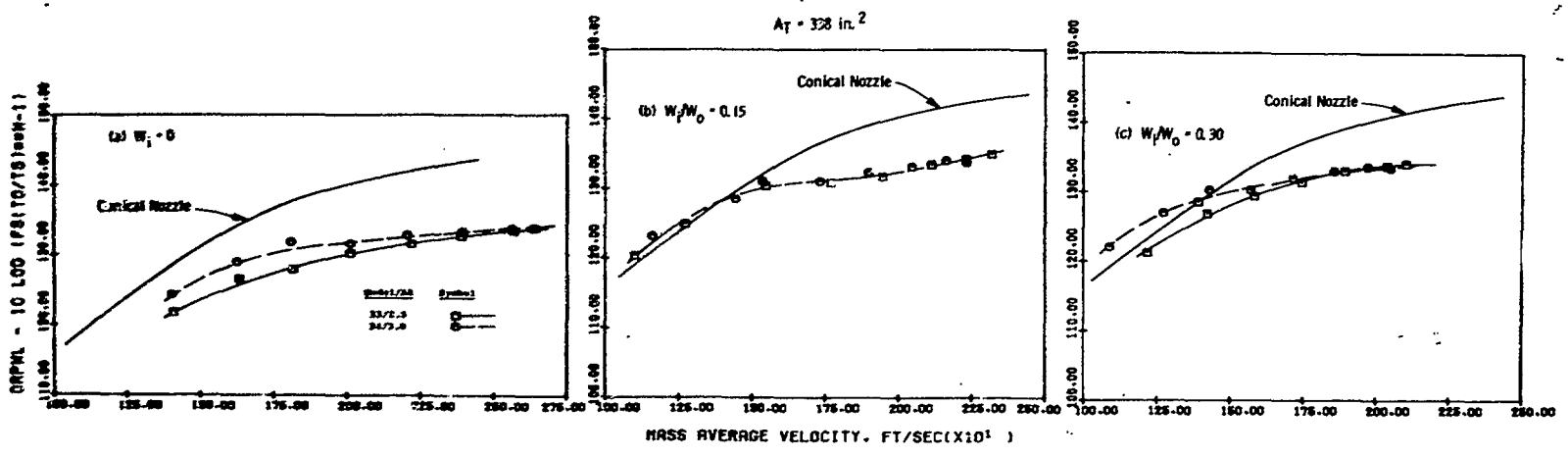

Figure 3-121. Area Ratio Variation at Constant Radius Ratio, OAPWL.

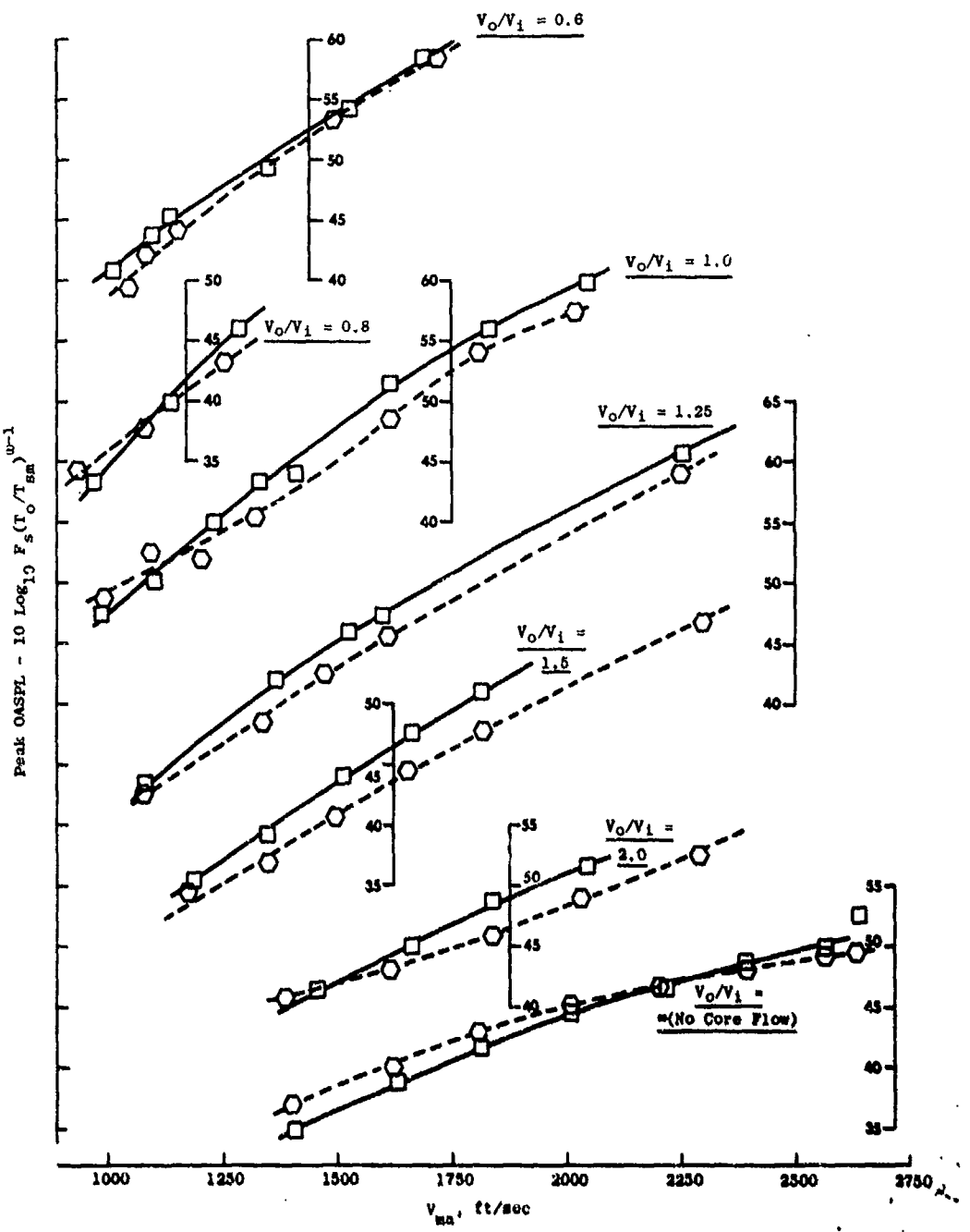

Figure 3-122. Area Ratio Variation at Constant Velocity Ratio, Peak OASPL.

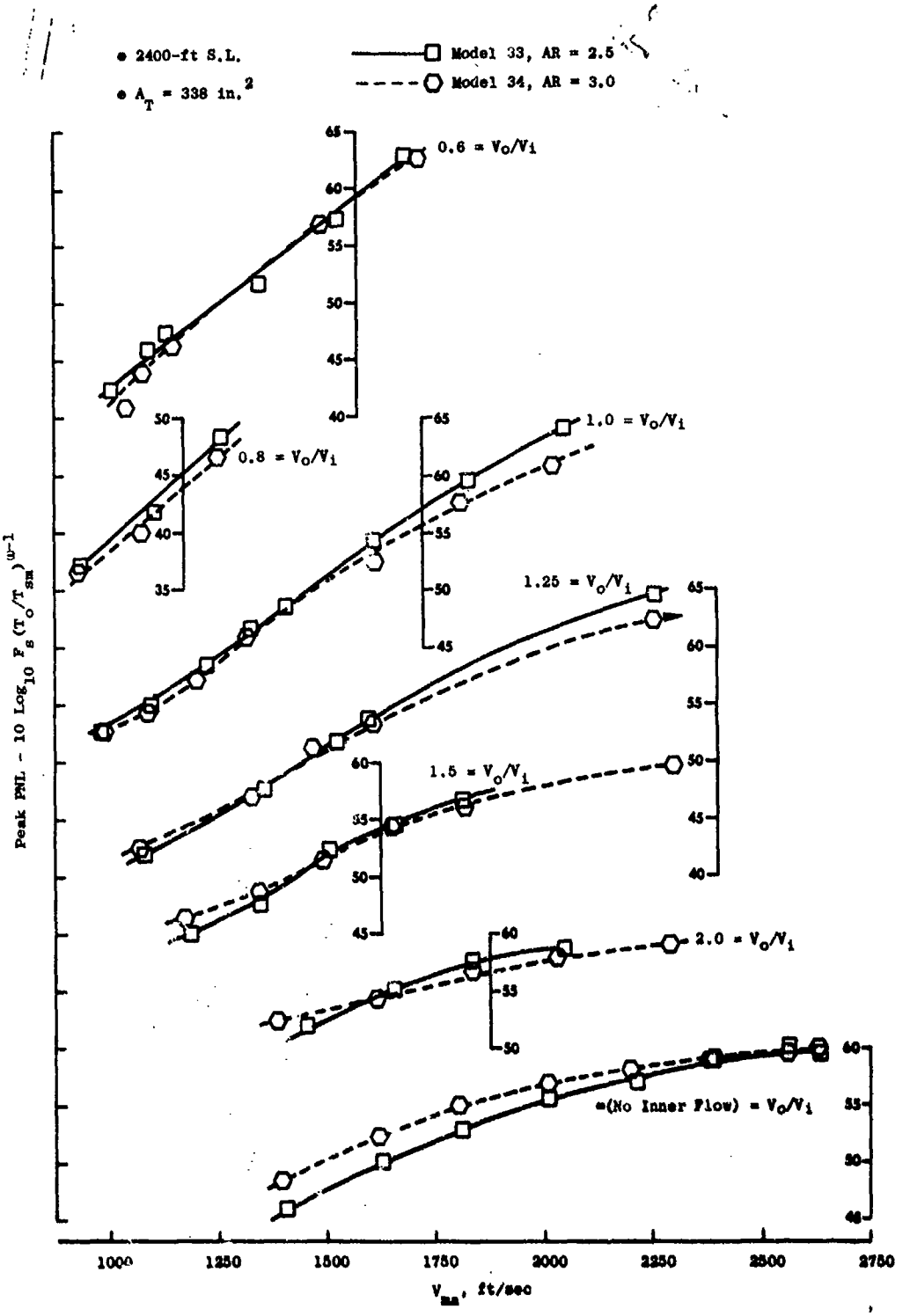

Figure 3-123. Area Ratio Variation at Constant Velocity Ratio, Peak PNL.

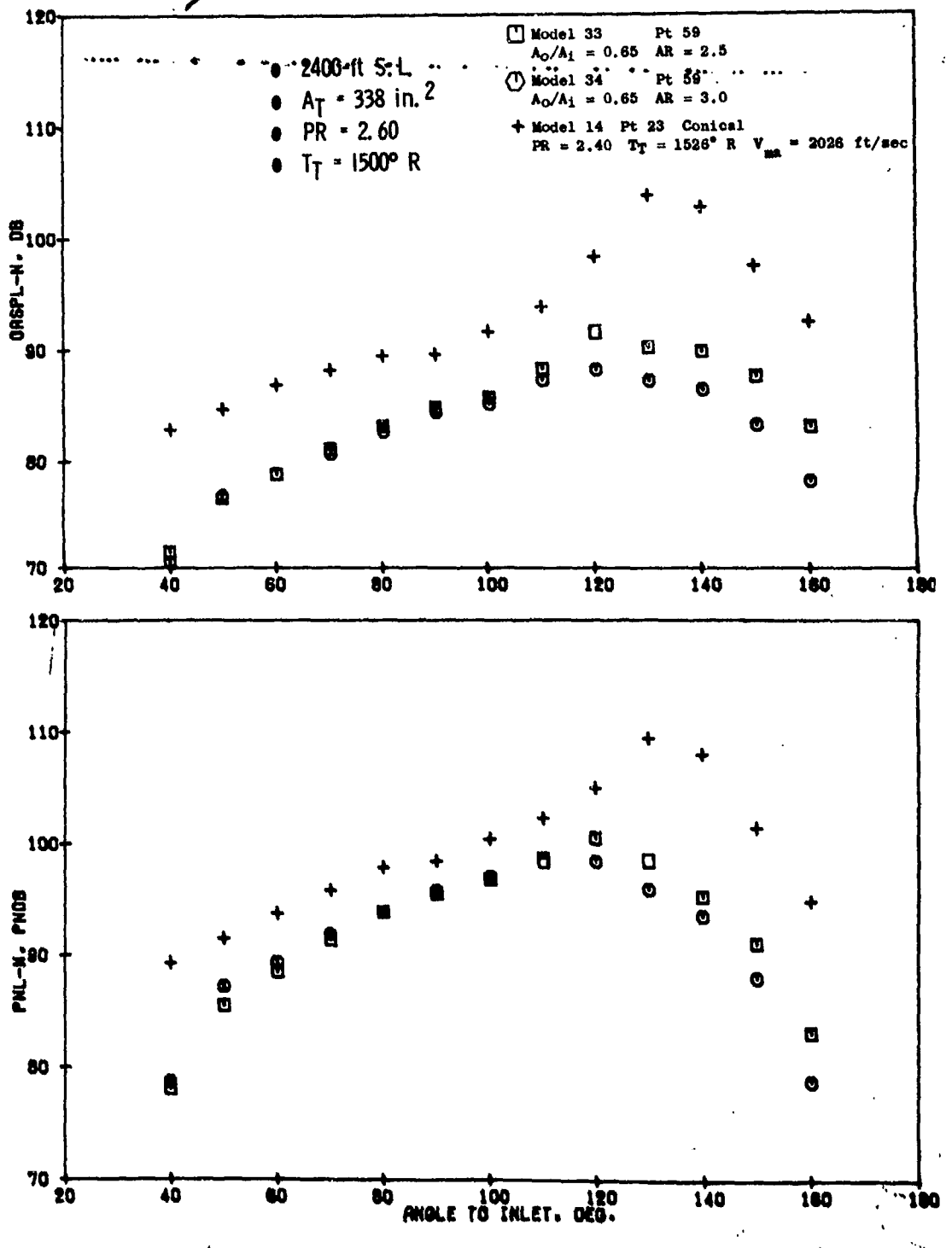

Figure 3-124. Area Ratio Variation at Constant Radius Ratio, OASPL and PNL Directivity, V_{ma} = 2075 ft/sec.

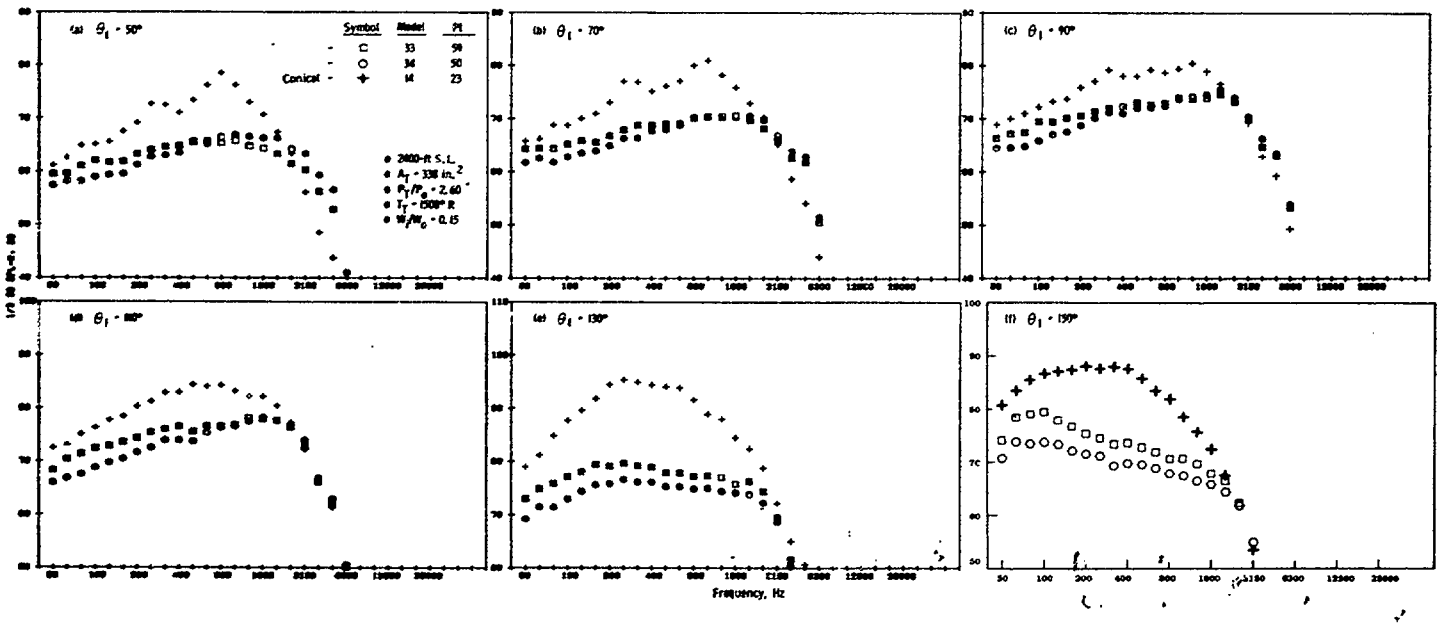

Figure 3-125. Area Ratio Variation at Constant Radius Ratio, Spectra, V_{ma} = 2075 ft/sec.

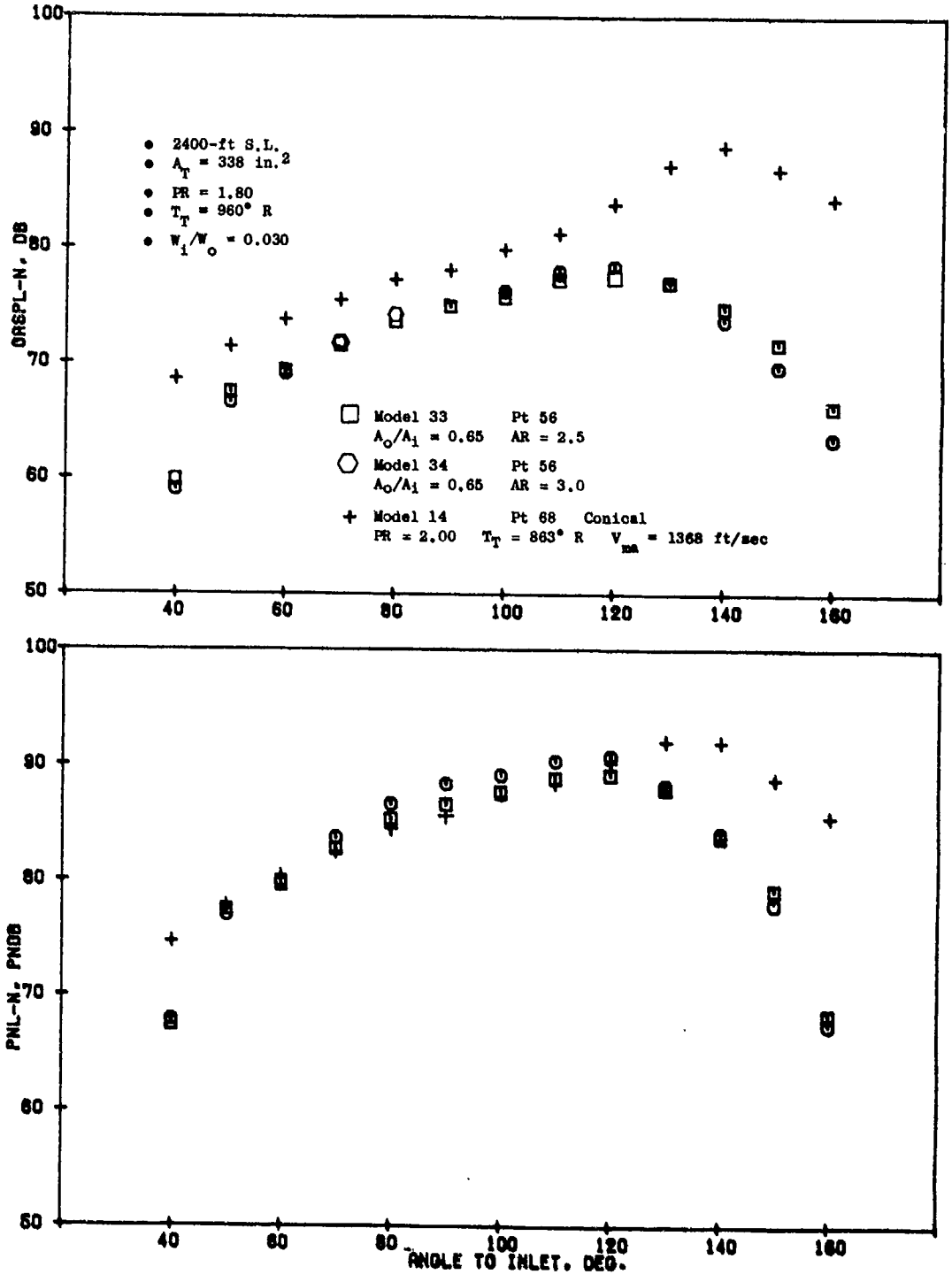

Figure 3-126. Area Ratio Variation at Constant Radius Ratio, OASPL and PNL Directivity, V_{ma} = 1340 ft/sec.

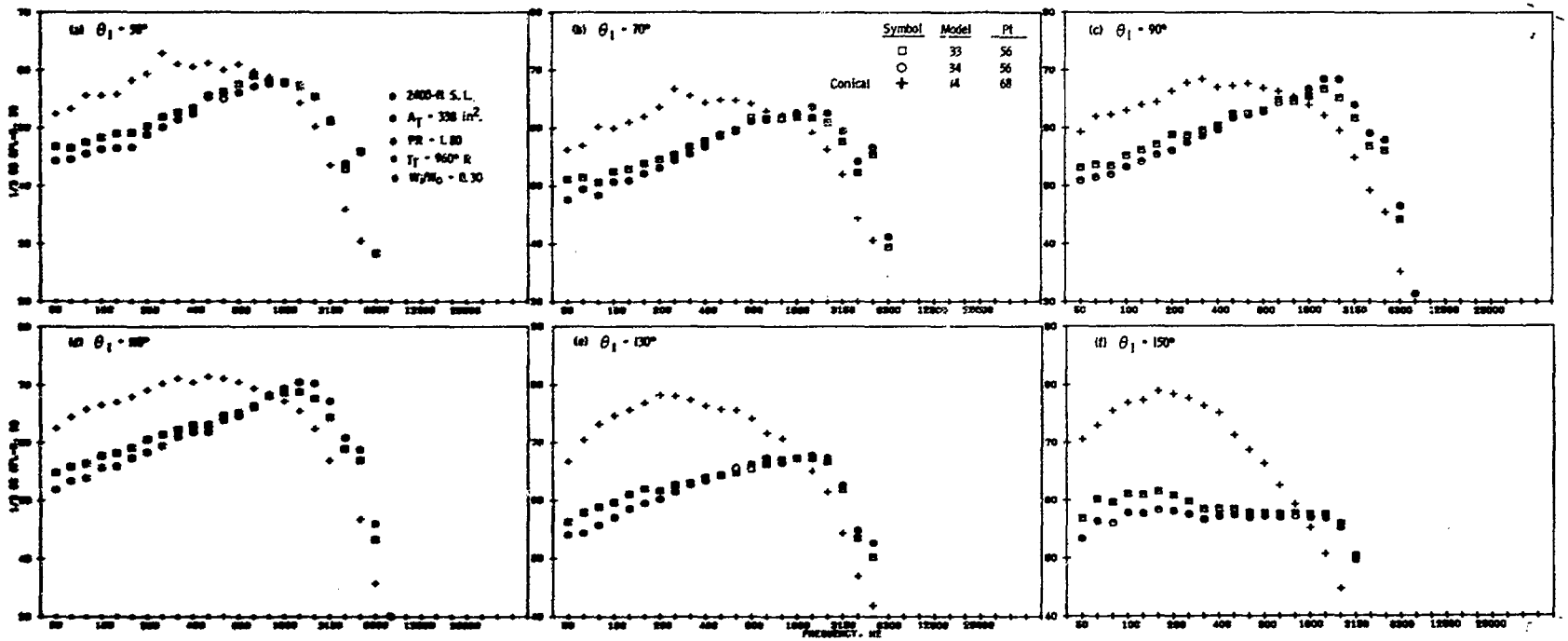

Figure 3-127. Area Ratio Variation at Constant Radius Ratio, Spectra, V_{ma} = 1340 ft/sec.

- On a peak OASPL/PNL basis for the W_i = 0, 15, and 30% W_o cycle, Figures 3-115 and 3-116 show suppression trends with area ratio are similar to those of the previous section's trends of area ratio/radius ratio variation on a dual flow system in that; (a) at low V_{ma}, the lower AR = 2.5 (Model 33) shows consistently better suppression from 0 to 3 on peak OASPL and from 1 to 4 on peak PNL, (b) at high V_{ma} the higher AR = 3.0 (Model 34) consistently shows a potential for better suppression with improvements of 1 to 2 seen on peak OASPL and 0 to 1 on peak PNL, and (c) the crossover in trend occurs in the V_{ma} range of 2000-2250 ft/sec. This occurs for both peak PNL and peak OASPL whereas in the previous section for area ratio and radius ratio variation on a dual flow system, it was not a consistent trend on peak OASPL.

- At 90°, Figures 3-117 and 3-118, some suppression is retained broadside for most cycles, particularly for OASPL and most noticeably at mid-to-high V_{ma} where shock-cell noise is not predominant in the segmented jets flow field. For all cycles and for both PNL and OASPL, the lower AR = 2.5 (Model 33) is consistently the better suppressor, indicating levels of 1 to 4 lower PNL noise and from 0 to 2 lower OASPL noise than the AR = 3.0 (Model 34).

- Similarly at 50°, Figures 3-119 and 3-120, substantial forward quadrant suppression is seen relative to the conical nozzle; greater than at broadside. Basic differences between the two area ratios are not obvious as differences in levels are mostly nominal, and where they do occur, they form no consistent trend for the various data sets. This is consistent with the previous section's variation of area ratio and radius ratio on the OASPL basis where 50° data showed no distinguishable preference with area ratio variation. On the PNL basis, the previous data showed lower area ratio to maintain better suppression by several ΔPNL.

- OAPWL data for the three chosen cycles, Figure 3-121, indicate similarity of levels to better suppression by the lower AR = 2.5 nozzle, Model 33, from 0 to 4 ΔOAPWL looking from high to low V_{ma}. Previous data showed no significant variation with area ratio and radius ratio.

- Reviewing Figures 3-122 and 3-123, peak OASPL and peak PNL comparisons for the DBTF cycle at constant V_o/V_i = 0.6, 0.8, 1.0, 1.25, 1.5, 2.0, and ∞ (no inner flow) shows: (a) consistent trends of improved OASPL suppression with higher AR = 3.0 (Model 34) for all velocity ratios and V_{ma} values, except when inner flow was completely shut off (V_o/V_i = ∞); and (b) peak PNL trends are similar to those of Figure 3-116 for W_i = 0, 15, and 30% W_o, in that at low V_{ma} the low AR (Model 33) is the better suppressor and at high V_{ma} the higher AR = 3.0 (Model 34) shows potential for greater suppression.

- The OASPL and PNL directivity data of Figures 3-124 and 3-126 indicate (a) differences in OASPL level are primarily observed in the

aft quadrant for both high V_{ma} = 2075 ft/sec and the low V_{ma} = 1340 ft/sec, maximum variance of 5 ΔOASPL being seen at 160° for the high V_{ma} point, and (b) for PNL, low V_{ma} variance is broadside where high V_{ma} variance is in the aft quadrant with a maximum ΔPNL of 4 seen at 160° for the high V_{ma} point. Thus, no exceptionally large differences are seen in the AR = 2.5 to 3.0 range. The data are consistent with previous observations on the peak basis in that at low V_{ma} the AR = 2.5 (Model 33) has lower noise level and at high V_{ma} the AR = 3.0 (Model 34) is the better suppressor.

- Supporting spectra (Figures 3-125 and 3-127) indicate that major differences in noise content are in the low frequency range associated with the postmerged jets and in all cases indicate lower levels associated with the AR = 3.0 (Model 34). This would suggest more rapid decay of the premerged individual jet plumes prior to coalescence into a common jet, thereby resulting in a lower merged velocity. Spectra comparisons at high frequency show dominance of the AR = 3.0 (Model 34) at low V_{ma}, thus, showing better suppression for the AR = 2.5 (Model 33) as the high frequency levels are controlling both OASPL and PNL. At V_{ma} = 2075 ft/sec the high frequency spectra for the AR = 3.0 (Model 34) are normally lower level than the AR = 2.5 (Model 33), thus effecting the previously observed improved performance.

3.4.2.2 Flow Management and Inner Stream Geometry Studies

System overall parameters of area ratio (A_o/A_i), velocity ratio (V_o/V_i), and by-pass ratio ($\beta = W_o/W_i$) are developed in detail to establish the basic propulsion nozzle for each dual flow system considered for application of an annular half span suppressor. Detailed individual stream aerodynamic cycle composition in terms of $P_{T_{i,o}}/P_o$, $T_{i,o}$ and $V_{i,o}$ are selected consistent with state-of-the-art component and cycle designs to provide system efficiency. These variables were also found to sharply influence the acoustic effectiveness of a system which incorporates an annular mechanical suppressor. Three studies were performed to develop qualitative and quantitative suppressor design directions. These are:

(a) System Velocity Ratio Variation With Fixed A_o/A_i and Fixed Outer Stream Suppressor Geometry.

Outer to inner stream velocity ratio variance over a range of $0.6 \leq V_o/V_i \leq \infty$ has been considered for various annular suppressors. Detailed results are presented for six representative chute, spoke and shallow-chute models; three at $A_o/A_i = 0.65$, two at 1.92 and one at 3.61. The results indicate that V_o/V_i influence is most predominant on low area ratio systems, due to the more controlling influence of the inner stream.

(b) System β Variation With Fixed A_o/A_i and Fixed Outer Stream Geometry.

Outer to inner stream weight flow ratio, β, at fixed values of ∞, 6.7, and 3.3 (corresponding to W_i = 0, 15 and 30% of W_o) have been considered in application to seven models. Detailed results from four of these models are discussed and consistently indicate increased acoustic efficiency of the annular suppressor with increase in β.

(c) System Area Ratio and Inner Stream Plug Geometry Variation - Fixed Outer Stream Suppressor Geometry

A controlled study was considered utilizing six models to isolate the impact on suppression potential due to system area ratio changes, within the practical range for a variable cycle engine (VCE) system (A_o/A_i = 1.92 and 3.61). Changes in inner stream plug geometry were evaluated, duplicating practical engine designs to induce low amounts of flow into the inner stream. Results indicate that higher system area ratio (effectively forcing a greater portion of the flow through the suppressed annulus) yields higher suppression. Inner flow geometry variance has minor impact on suppression for the high A_o/A_i system and mixed results for the low A_o/A_i system.

System Velocity Ratio Variation at Fixed A_o/A_i and Outer Stream Suppressor Geometry

This study attempted to isolate the influence of velocity ratio (V_o/V_i) for a dual flow system. Systematic variation of velocity ratio was accomplished with fixed system area ratios (A_o/A_i) and utilizing select multi-element annular suppressors, independent of any attempt to maintain consistent values of by-pass ratio ($\beta = W_o/W_i$). This was accomplished on Models 22 to 32 and 36, of A_o/A_i = 1.92 and 3.61, utilizing the DBTF/Inverted Dual Flow test matrix of Section 3.2.1, which set values of V_o/V_i at 1.0, 1.25, 1.5 and 2.0 and on Models 33, 34 and 35 utilizing an expanded DBTF/Inverted Dual Flow test matrix with V_o/V_i's = 0.6, 0.8, 1.0, 1.25, 1.5, 2.0 and ∞ (no inner flow). Of these various models, six were selected for presentation of results herein, as follows:

		Outer Stream				Inner Stream				
Model No.	System A_o/A_i	Element Description	AR	$\frac{H}{D}$	Flow Area, In.^{2}	Step Height In.	Plug Location	$\frac{H}{D}$	Flow Area, In.^{2}	Appendix A Figure Reference
33	0.65	36 Chute	2.5	0.783	17.21	1.034	Retracted	0.674	11.12	27
34	0.65	36 Chute	3.0	0.783	17.21	1.034	Retracted	0.674	11.12	28
35	0.65	36 Spoke	2.5	0.783	17.21	1.034	Retracted	0.674	11.12	29
31	1.92	30 Shallow Chute	1.75	0.717	23.76	0.70	Retracted	0.779	12.39	25
27	1.92	36 Chute	1.5	0.783	23.76	0.70	Retracted	0.779	12.39	21
26	3.61	36 Chute	2.0	0.716	23.76	0.33	Retracted	0.89	8.58	20

The last column of the above chart refers to the detailed geometric definitions for each model in Appendix A. The first three suppressors, Models 33, 34 and 35 of Figure 3-128, are of A_o/A_i = 0.65, the next two, Models 31 and 27 of Figure 3-129, are of A_o/A_i = 1.92, and the last, Model 26 of Figure 3-130, is of A_o/A_i = 3.61. Results are discussed as an aggregate for each A_o/A_i value. The three basic varieties of the spoke/chute family of segmented suppressors are represented, i.e., deep-chutes, spokes and shallow-chutes. All models are of relatively high suppressor radius ratio, R_r^o = 0.716 to 0.783, consistent with advanced technology suppressor systems. Suppressor area ratio range of 1.5 to 2.5 is also represented.

Results of peak, 90° and 50° PNL and OASPL are presented in the following Figures for the three models of A_o/A_i = 0.65, each data set normalized as per Section 3.3.1.7 and plotted versus V_{ma}.

Model No.	Peak	90°	50°
33	3-131	3-132	3-133
34	3-134	3-135	3-136
35	3-137	3-138	3-139

Partial acoustic results from the three models are discussed in other sections of this report (Section 3.4.2.1 "Area Ratio Variable, Radius Ratio Constant - Dual Flow" compares Model 33 and 34's Area Ratio = 2.5 and 3.0 results, and Section 3.4.2.4 "Element Type Study-Dual Flow of Low System Area Ratio" compares Model 33 and 35 chute versus spoke results).

Observations of results from the above curves in relation to the goal of isolating the impact of system velocity ratio are as follows:

- When isolated on data-fitted curves at constant V_o/V_i values, peak OASPL and PNL acoustic results form progressive and consistent trends of noise level. Trends on a peak OASPL basis are consistently progressive from V_o/V_i = 0.6 to ∞ for all three models, at any V_{ma}. The noise levels are consistent with or slightly in excess of, the conical baseline at V_o/V_i = 0.6, and they vary progressively until ΔOASPL suppression levels approach 19 dB in the $2000 \leq V_{ma}$, ft/sec, ≤ 2500 range for V_o/V_i = ∞, for each model. V_o/V_i = ∞ is attained when the inner flow is curtailed completely (by use of a positive shutoff mechanism placed about one diameter upstream of the inner exit plane). A blunt base region remains at the inner exit annulus, over which the outer stream flow expands.

- At mid-to-high V_{ma}, maximum PNL suppression levels of 13.5 to 16 PNdB are observed for the three models. The peak PNL levels decrease uniformly as V_o/V_i increases, but do not display the same magnitude of change as on peak OASPL. At lower V_{ma}, a reversing of noise level trends is seen at the higher V_o/V_i ratios and levels of suppression are substantially reduced.

- A_o/A_1 = 0.65
- 1.03-in. Core Annulus Height
- Plug Retracted

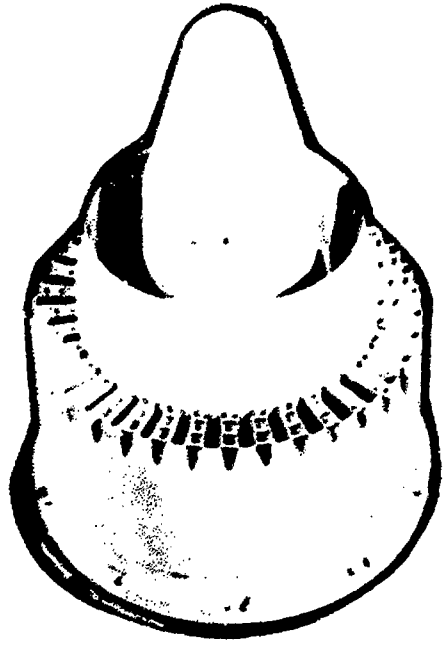

Model 33
36-Chute, AR = 2.5

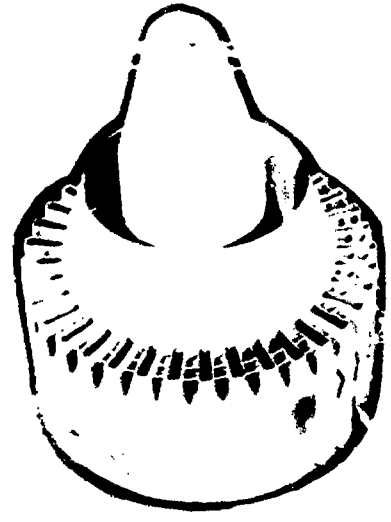

Model 34
36-Chute, AR = 3.0

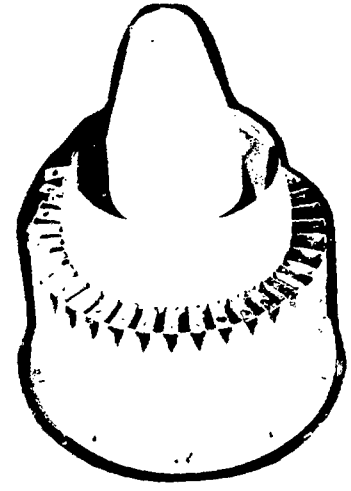

Model 35
36-Spoke, AR = 2.5

Figure 3-128. Dual-Flow Models for Velocity Ratio Investigation at A_o/A_i = 0.65.

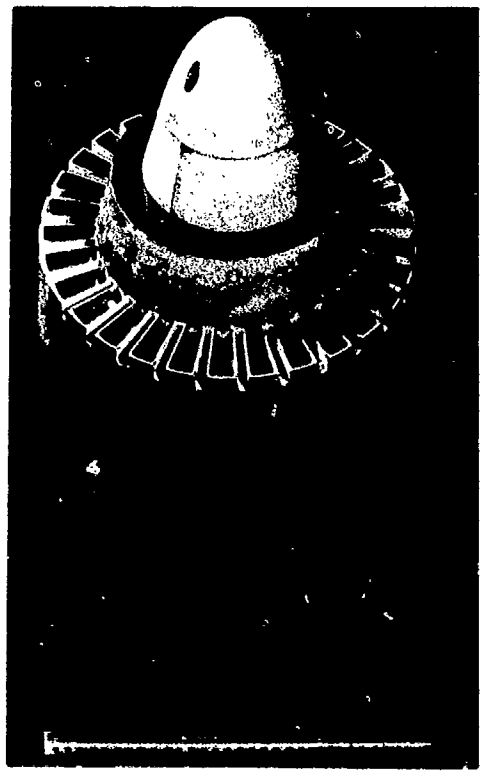

Model 31 30-Shallow Chute, AR = 1.75
R_f^o = 0.717, R_f^i = 0.779 Core Plug, Retracted
A_o/A_i = 1.92

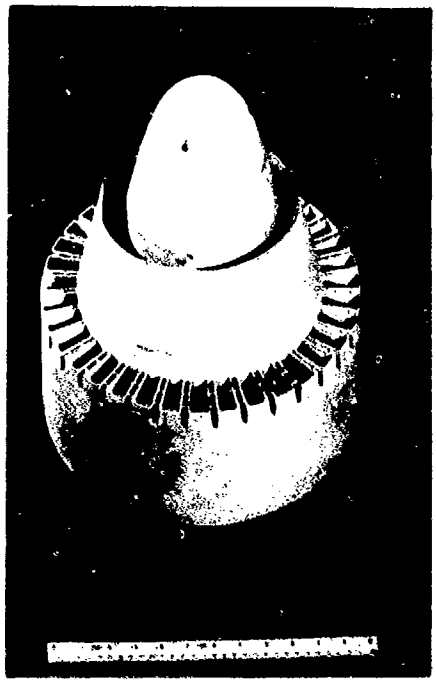

Model 27 36-Chute, AR = 1.5
R_f^o = 0.782, R_f^i = 0.779 Core Plug, Retracted
A_o/A_i = 1.92

Figure 3-129. Dual-Flow Models for Velocity Ratio Investigation at A_o/A_i = 1.92.

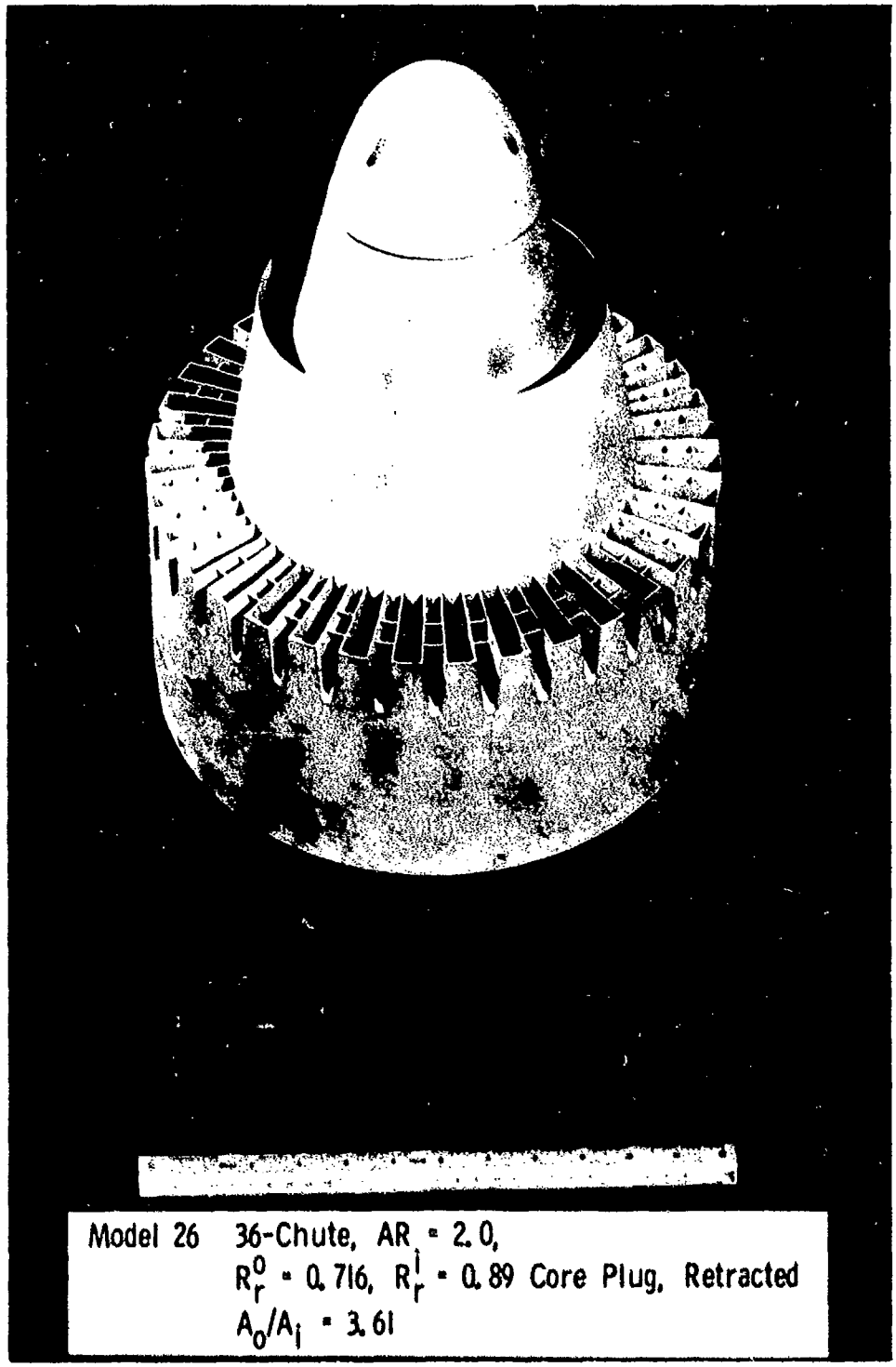

Figure 3-130. Dual-Flow Models for Velocity Ratio Investigation at A_o/A_i = 3.61.

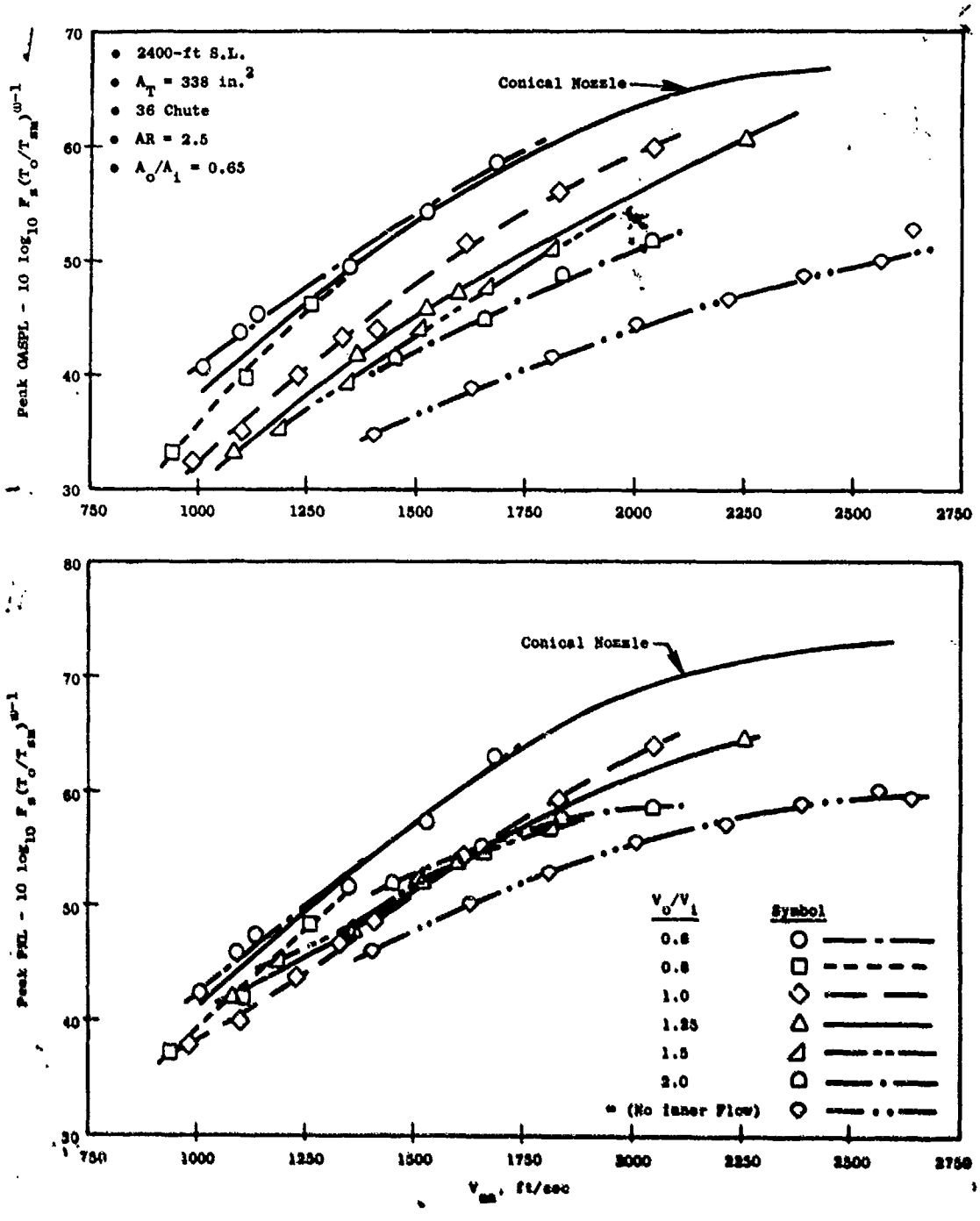

Figure 3-131. Peak PNL and OASPL Variation with V_o/V_i, Model 33.

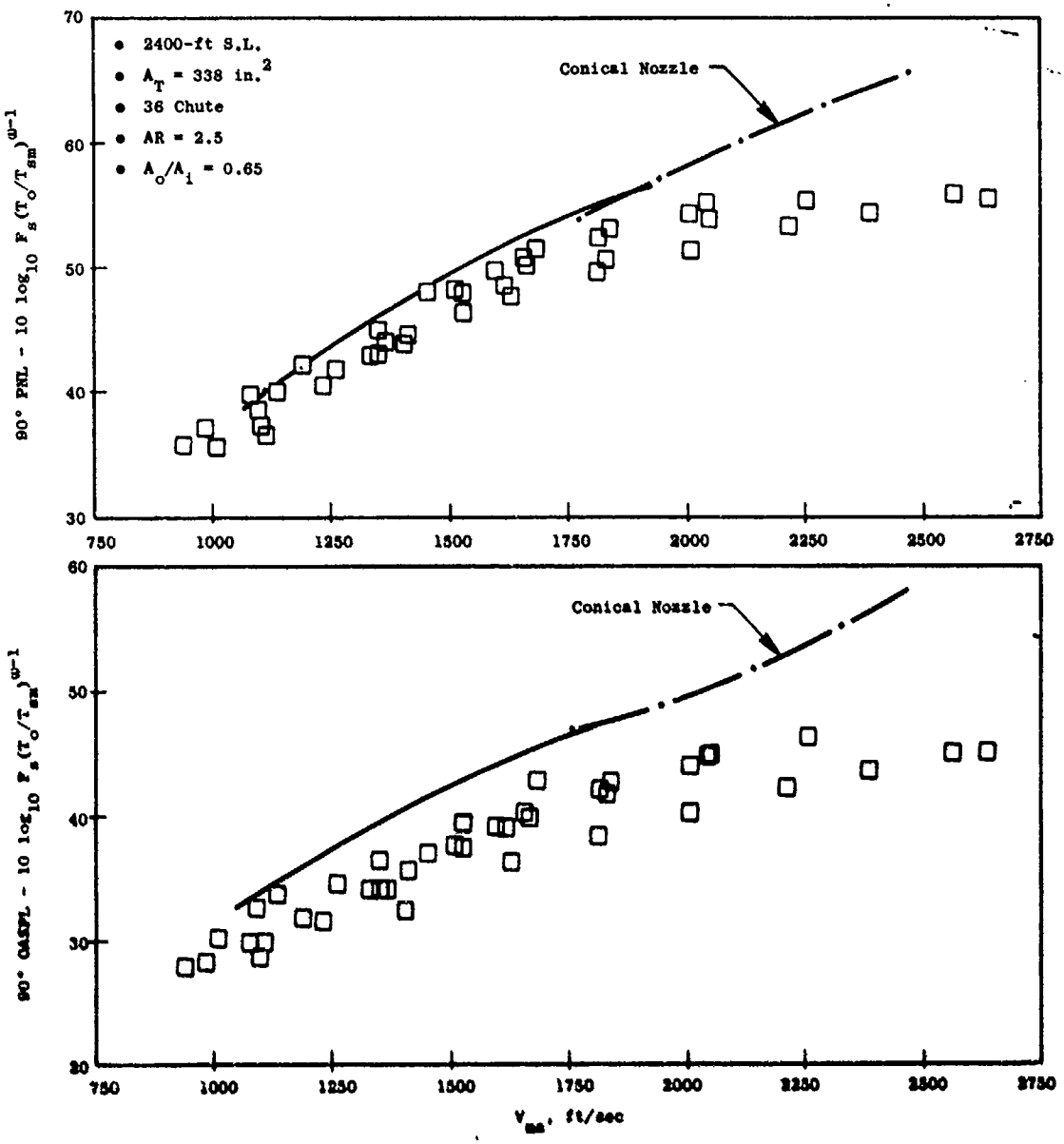

Figure 3-132. 90° PNL and OASPL Variation with V_o/V_i, Model 33.

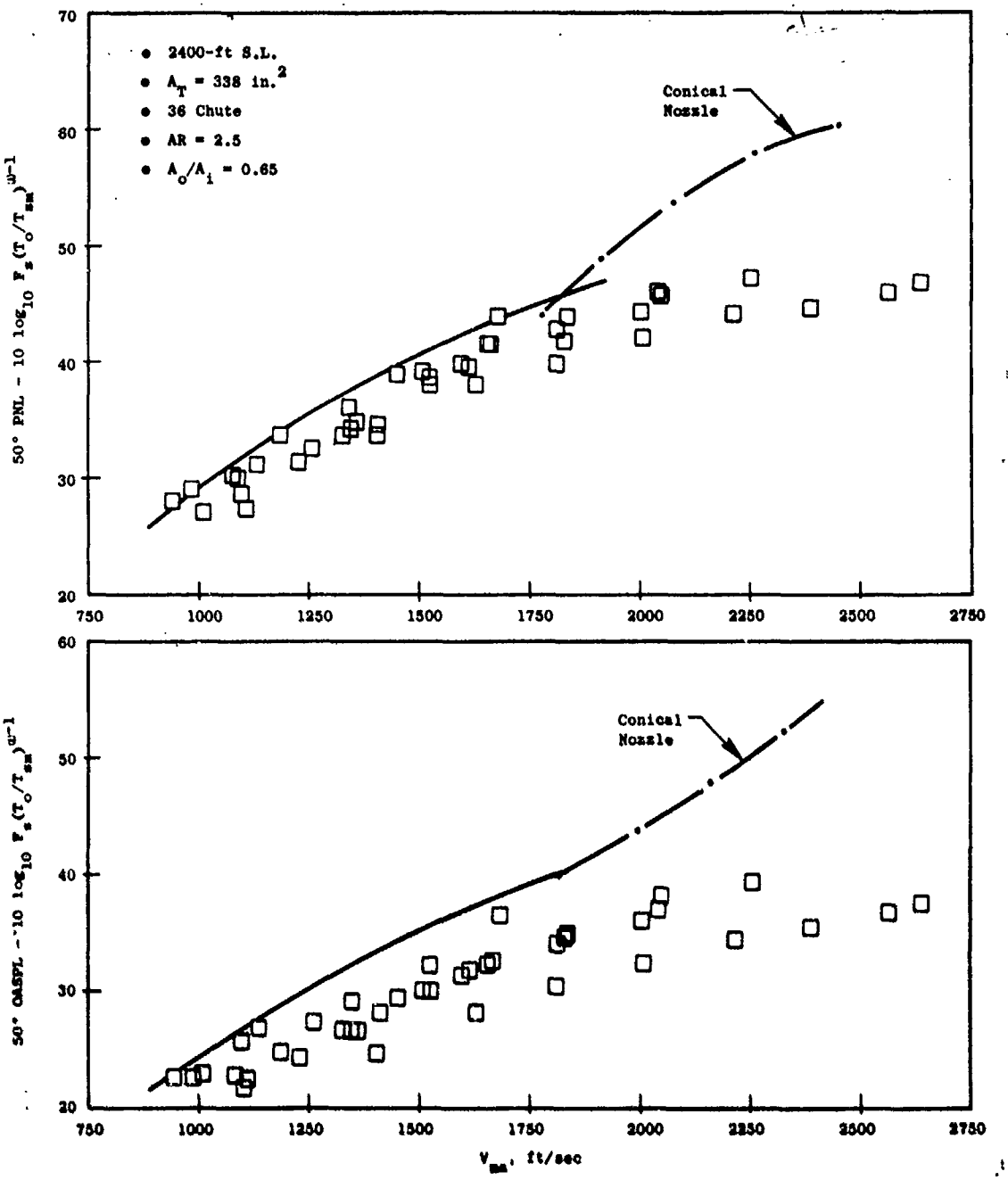

Figure 3-133. 50° PNL and OASPL Variation with V_o/V_i, Model 33.

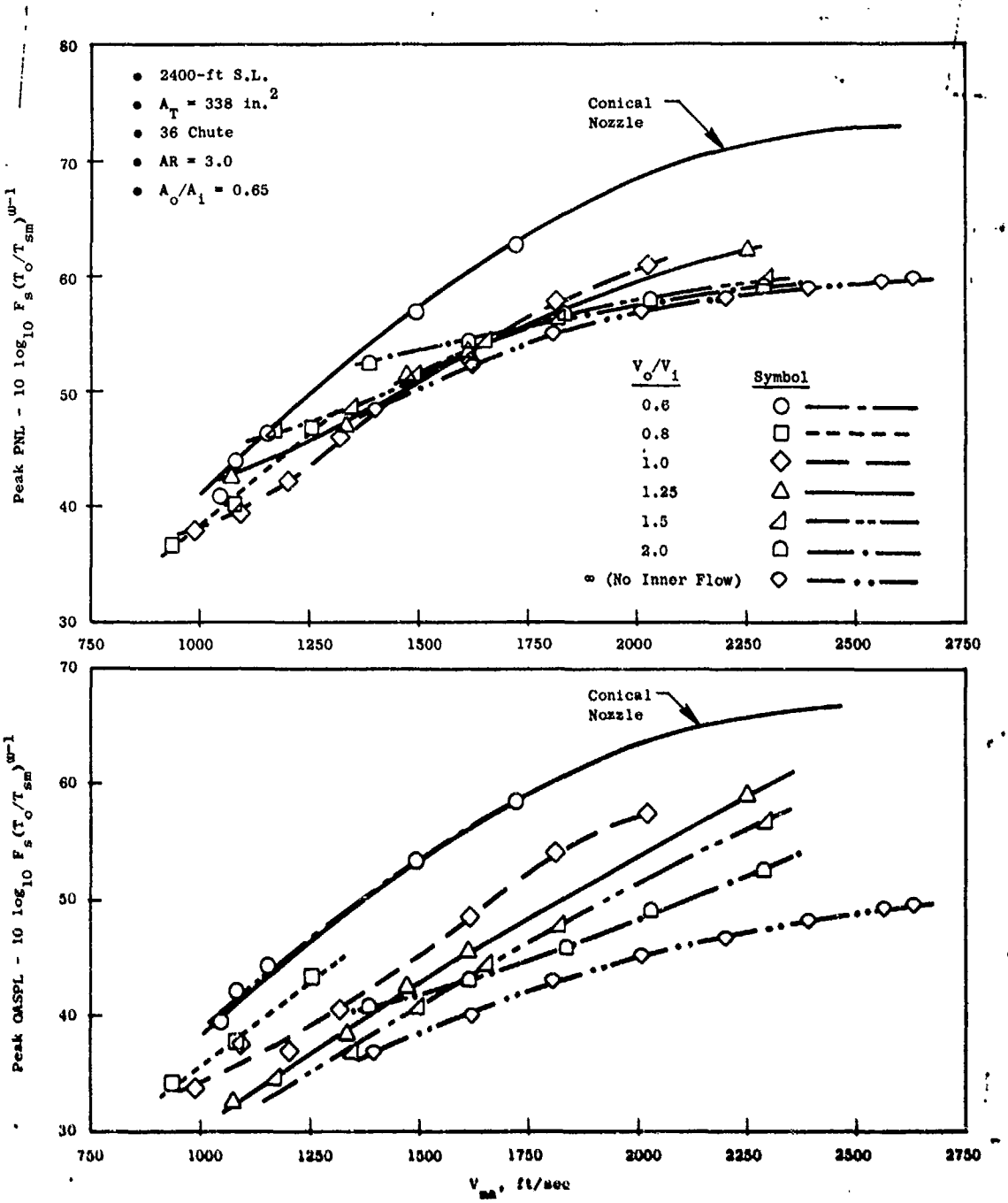

Figure 3-134. Peak PNL and OASPL Variation with V_o/V_i, Model 34.

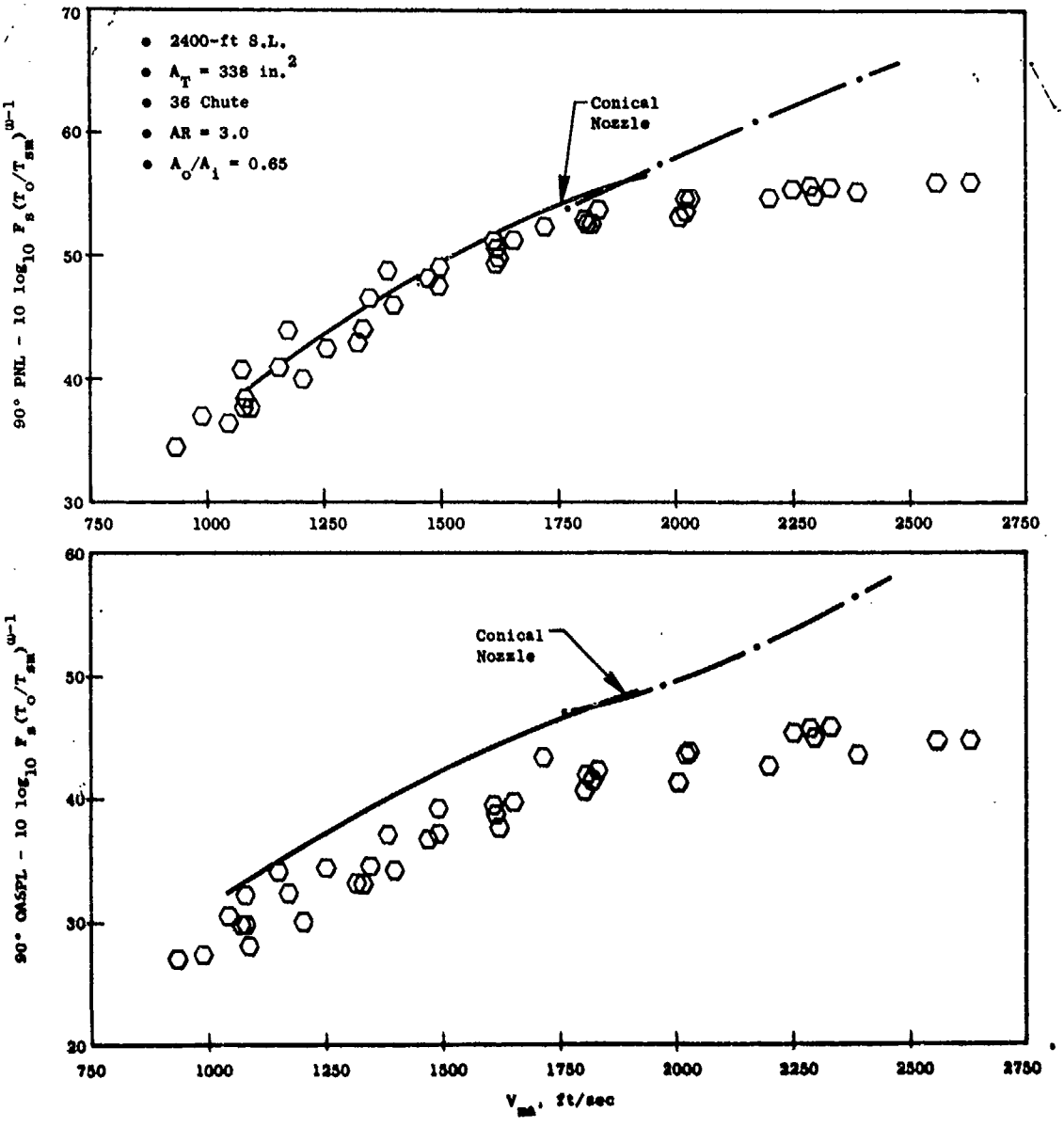

Figure 3-135. 90° PNL and OASPL Variation with V_o/V_i, Model 34.

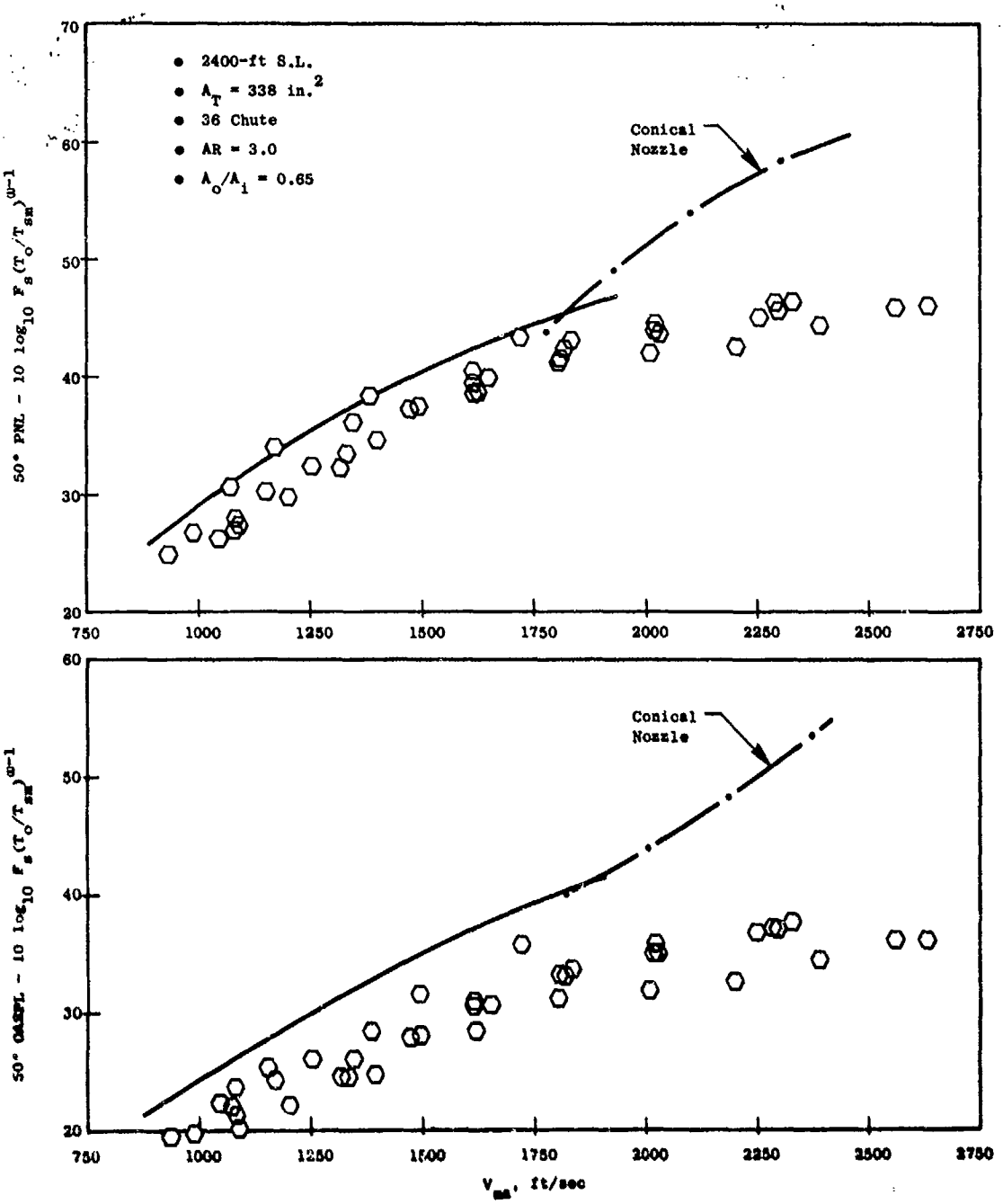

Figure 3-136. 50° PNL and OASPL Variation with V_o/V_i, Model 34.

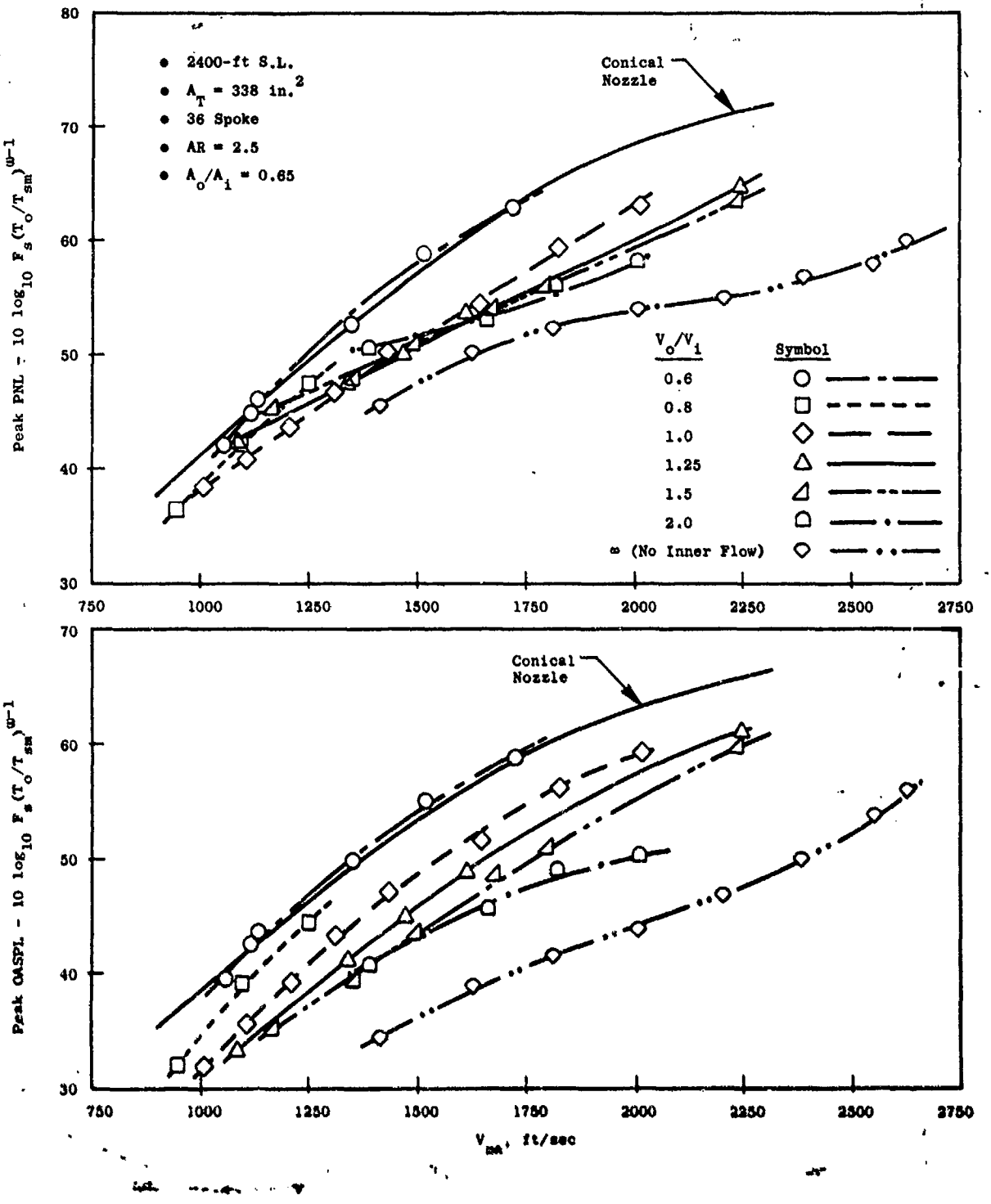

Figure 3-137. Peak PNL and OASPL Variation with V_o/V_i, Model 35.

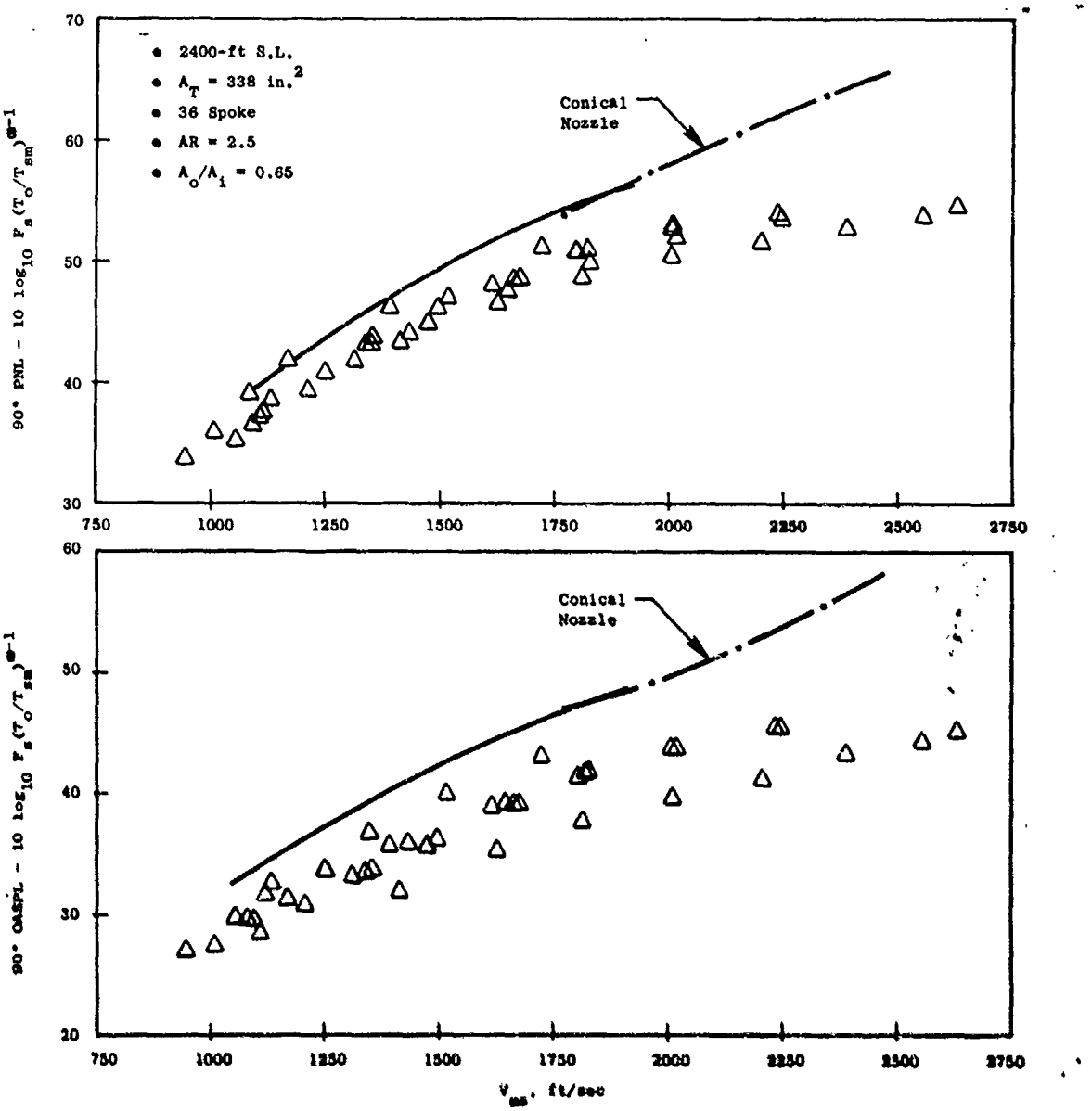

Figure 3-138. 90° PNL and OASPL Variation with V_o/V_i, Model 35.

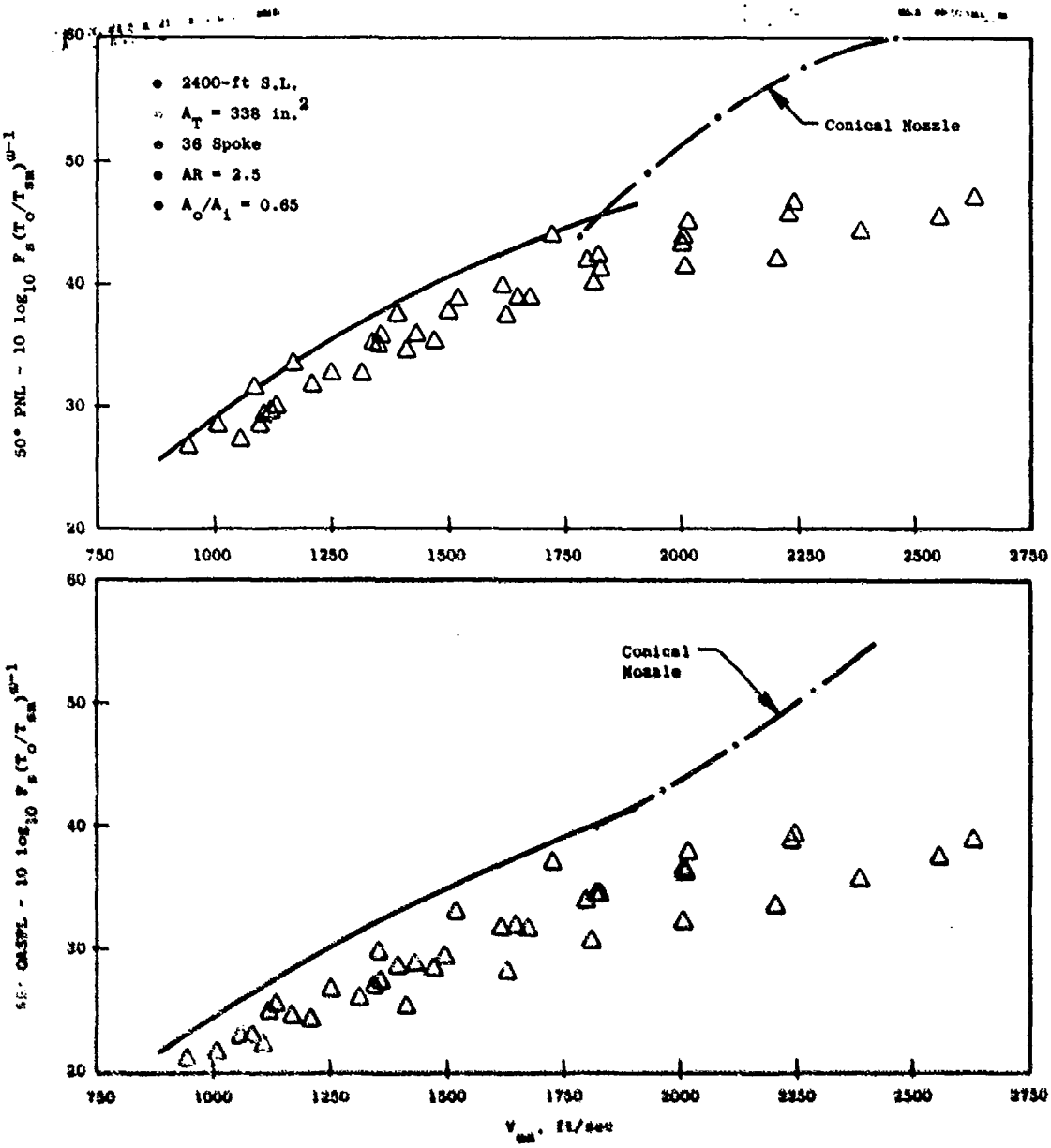

Figure 3-139. 50° PNL and OASPL Variation with V_o/V_i, Model 35.

- β excursions for the individual V_o/V_i cycle lines are:

V_o/V_i	β
0.6	0.6 - 0.9
0.8	0.4 - 1.0
1.0	0.5 - 1.0
1.25	0.5 - 1.2
1.5	0.6 - 1.3
2.0	0.6 - 1.3
∞	∞

Normally at a fixed V_{ma}, the inner and outer stream cycle conditions selected for the test will result in increased β as V_o/V_i is increased. Therefore, in addition to gradual dominance of the noise caused by the outer stream velocity increase, the outer stream weight flow increase also increases the noise. For the V_o/V_i = 0.6 line, where V_o is 40% less than V_i, and W_o is 10 to 40% less than W_i, total predominance of the inner stream would be expected. Suppression normally attributed to the annular plug effect (R_r^i = 0.674) is not apparent. For the V_{ma} range tested, as V_o/V_i increases and the outer stream dominates both velocity and mass flow, the effectiveness of the segmented suppressor becomes more paramount and levels of suppression gradually increase.

- The greater the loss of peak PNL suppression as oposed to peak OASPL suppression at low V_{ma}, and the much higher level of peak OASPL suppression than peak PNL suppression at high V_{ma} indicates that a complex and changing interaction exists in the spectral composition for dominance of high or low frequency. This is related to relative noise levels of the inner and outer streams and depends on the individual stream cycle composition in addition to any possible inner/outer flow interactions affecting noise generation.

- Figures 3-132, 3-135 and 3-138 show substantially less suppression for the 90° PNL and OASPL data compared to the aft quadrant, however, significant levels of suppression are still attained. A primary observation, in relation to this study's goal, is that discrete trends with system velocity ratio variation are not nearly as discernible as they were at the peak noise angle. Data are therefore presented without individual curve fits for fixed V_o/V_i values. In assembling the data, however, a fairly distinct data trend was observed for the V_o/V_i = ∞ case. Appendix B contains the specific acoustic and aerodynamic cycle information.

- At 50°, Figures 3-133, 3-136 and 3-139, the PNL and OASPL data are similar to the 90° data. Again, trends are not as discernible with set velocity ratio and information is plotted without data-fitted curves.

To illustrate the more detailed changes in noise characteristics associated with system velocity ratio influence at fixed system A_o/A_i and fixed annular suppressor geometry, the following representative sets of PNL and OASPL directivities plus spectra plots are included; selected from Model 33 and 34's data banks:

Figures 3-140 and 3-141	Model 33, V_{ma} = 2010 - 2050 ft/sec
Figures 3-142 and 3-143	Model 33, V_{ma} = 1685 - 1840 ft/sec
Figures 3-144 and 3-145	Model 34, V_{ma} = 2250 - 2390 ft/sec
Figures 3-146 and 3-147	Model 34, V_{ma} = 1720 - 1830 ft/sec

The following general observations are made:

- PNL and OASPL directivity for the first data set on Model 33, where V_o/V_i = 1.0, 2.0 and ∞ are compared, show major and systematic changes for 120° and aft. Significant, yet not as systematic, reductions occur broadside and in the forward quadrant, the largest change occuring between V_o/V_i of 2.0 and ∞.

- Spectra for the same data set show very broad changes in composition, particularly in the aft quadrant at 140°, for V_o/V_i = 1.0 ($V_o \simeq V_i \simeq$ 2050 ft/sec, β = 0.7). The inner stream low frequency noise dominates, and high frequency associated with the segmented suppressor is very low. As velocity ratio increases to 2.0 ($V_o \simeq$ 2600 ft/sec, $V_i \simeq$ 1300 ft/sec, β = 1.3), the low frequency contribution to the spectra is extremely reduced. When inner flow is cut completely, only a fairly flat spectra remains at 140°, where normally an annular suppressor spectra would be more low frequency dominated.

  Changes with V_o/V_i at 120° are similar to 140°, but not of the same magnitude. In general both OASPL and PNL are low-to-mid frequency dominated for the aft quadrant, therefore, changes at low frequencies control both, and substantiate the large variances seen at higher V_{ma} in Figure 3-131.

- At 90° and 50°, the low V_o/V_i spectra are more equally balanced for low and high frequency composition. Changes again are primarily observed in the low-to-mid frequencies. Low frequency no longer fully controls OASPL and PNL, therefore, the changes in these values are minor compared to those in the aft quadrant.

- The second data comparison for Model 33 at V_{ma} from 1685 to 1840 ft/sec for values of V_o/V_i of 0.6, 1.0, 1.5, 2.0 and ∞, indicates both PNL and OASPL trends similar to the previous comparison. Aft

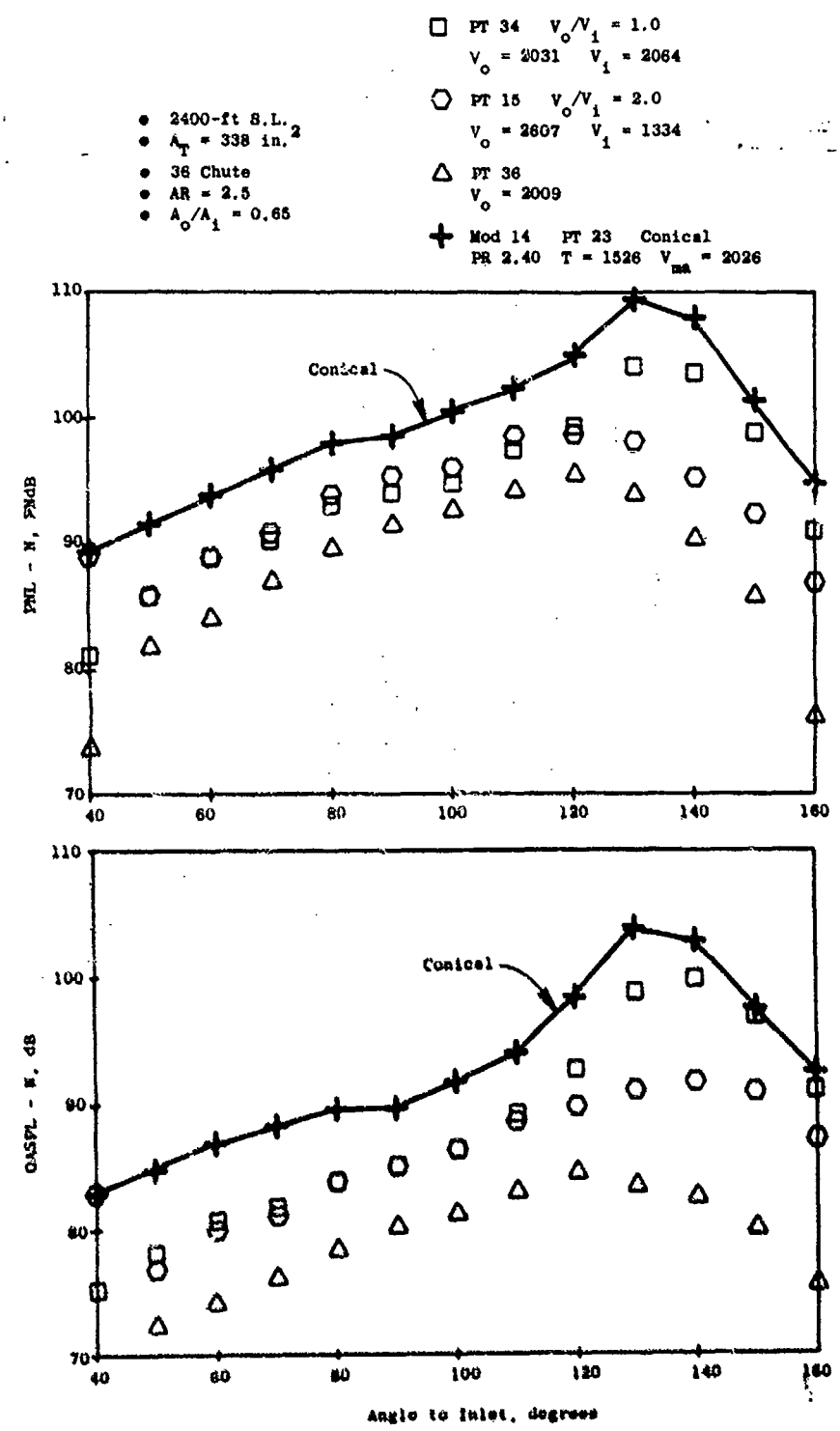

Figure 3-140. Impact of V_o/V_i on PNL and OASPL Directivity, Model 33, V_{ma} = 2010 to 2050 ft/sec.

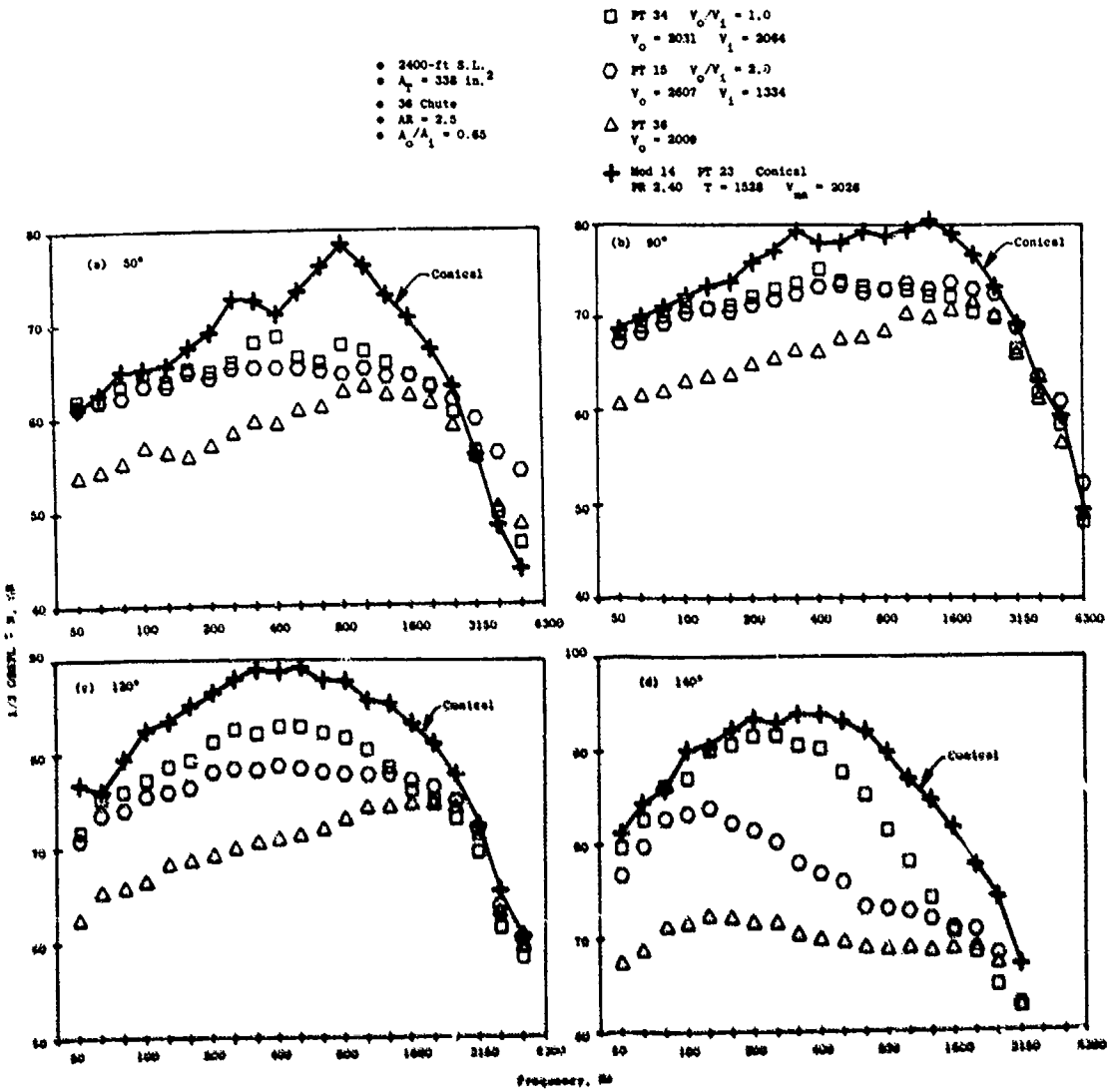

Figure 3-141. Impact of V_o/V_i on Spectra, Model 33, V_{mb} = 2010 to 2050 ft/sec.

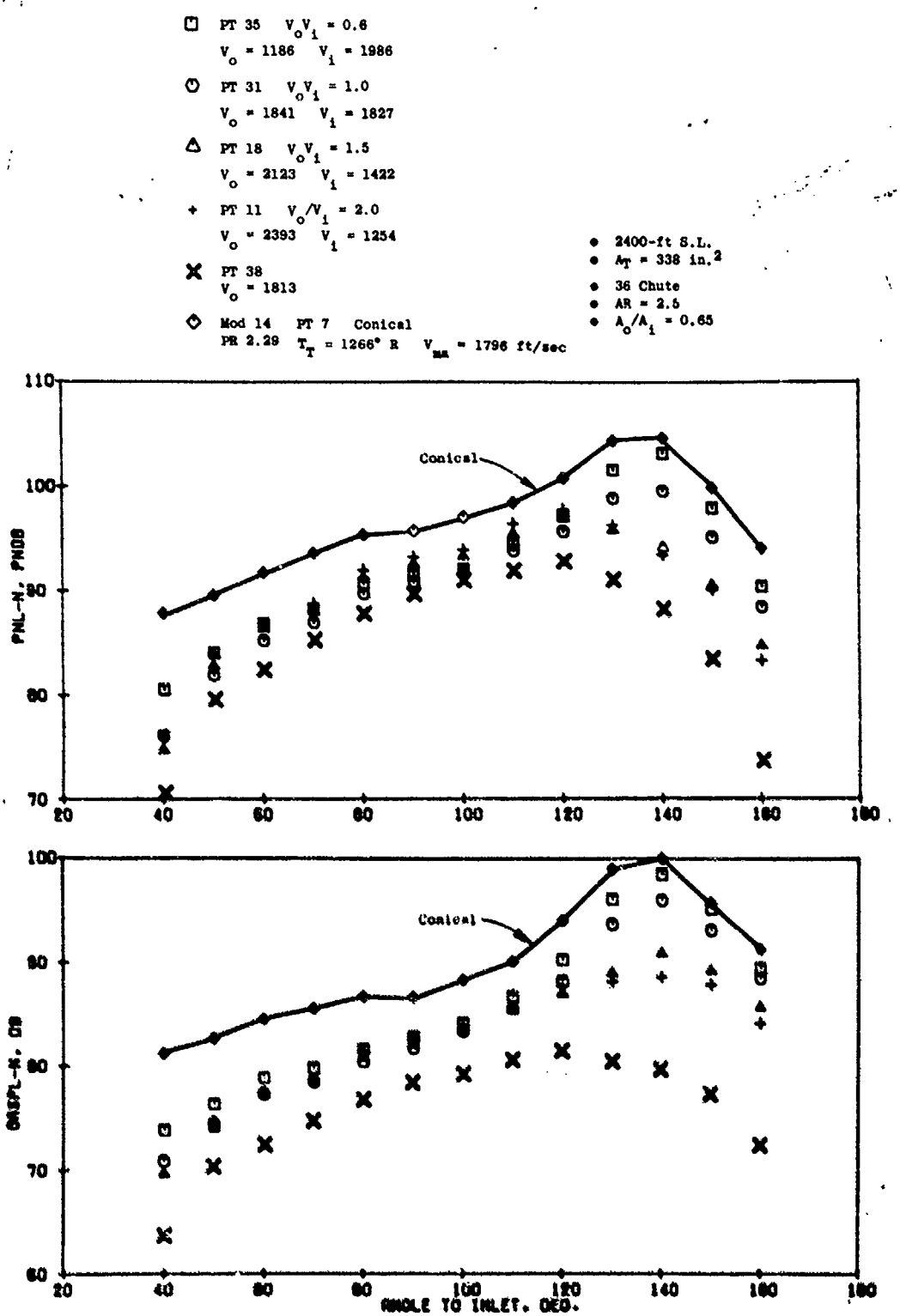

Figure 3-142. Impact of V_o/V_i on PNL and OASPL Directivity, Model 33, V_{max} = 1685-1840 ft/sec.

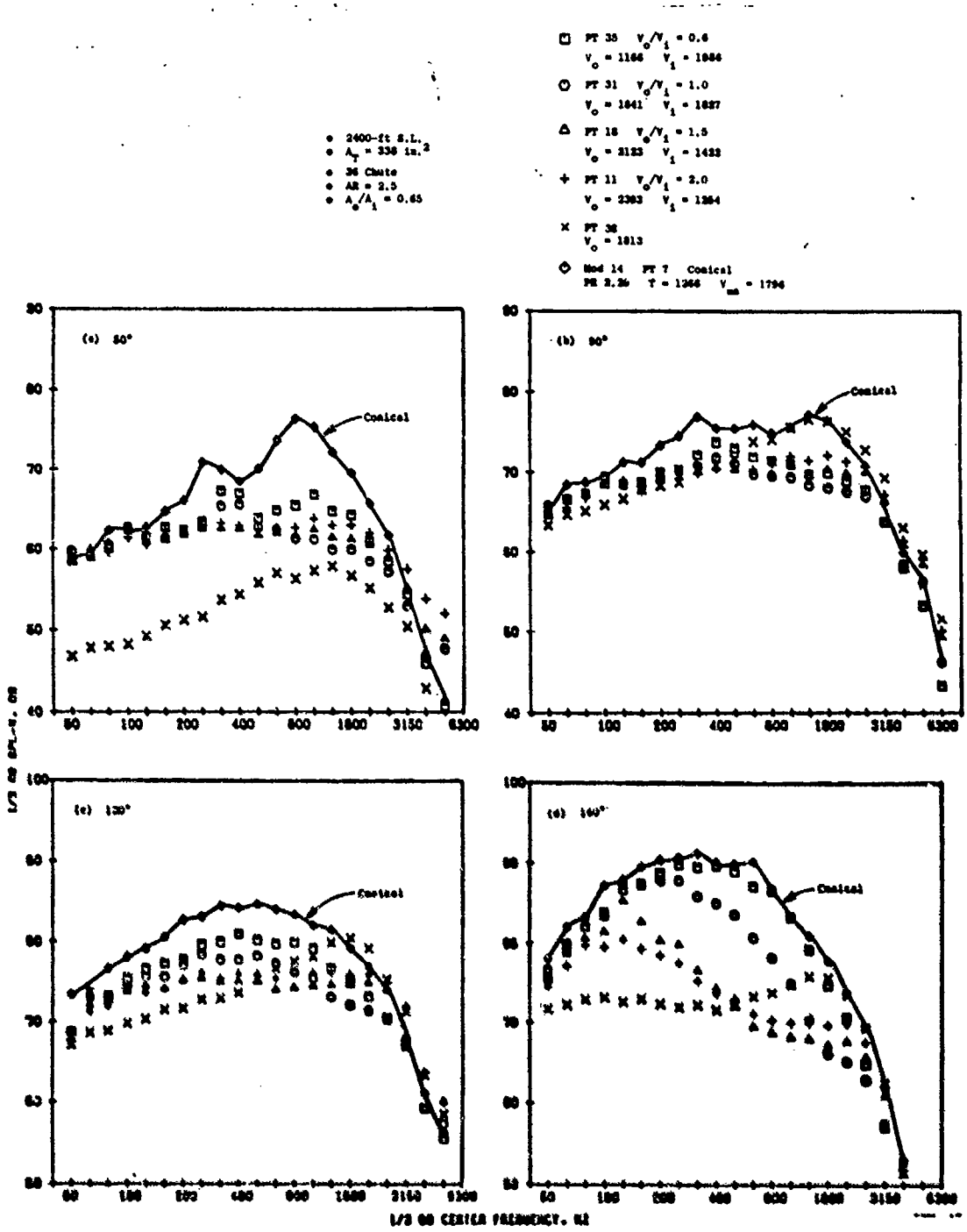

Figure 3-143. Impact of V_o/V_i on Spectra - Model 33 - V_{mr} = 1685-1840 ft/sec.

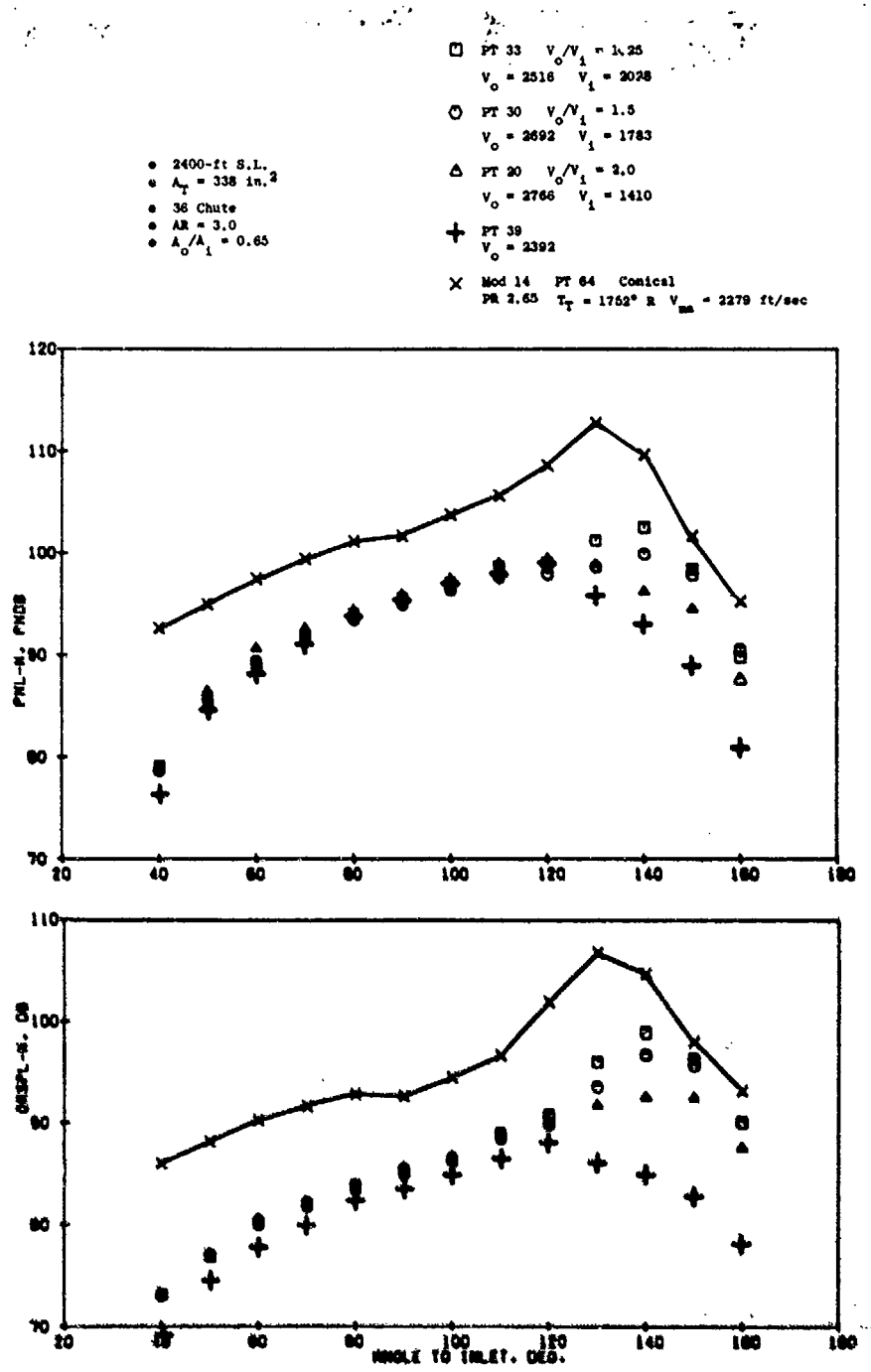

Figure 3-144. Impact of V_o/V_i on PNL and OASPL Directivity, Model 34, V_{ma} = 2250-2390 ft/sec.

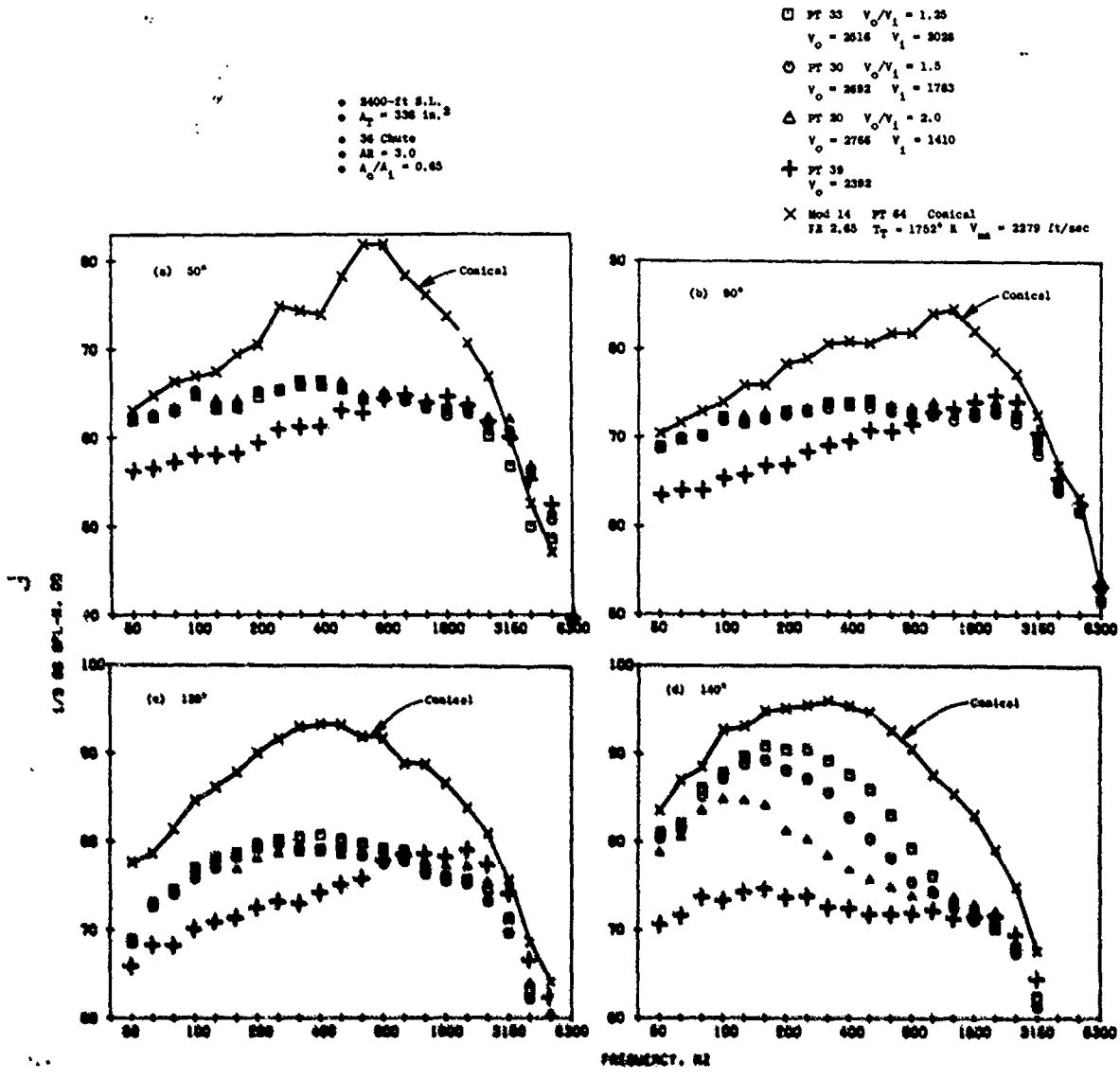

Figure 3-145. Impact of V_o/V_i on Spectra, Model 34, V_{max} = 2250-2390 ft/sec.

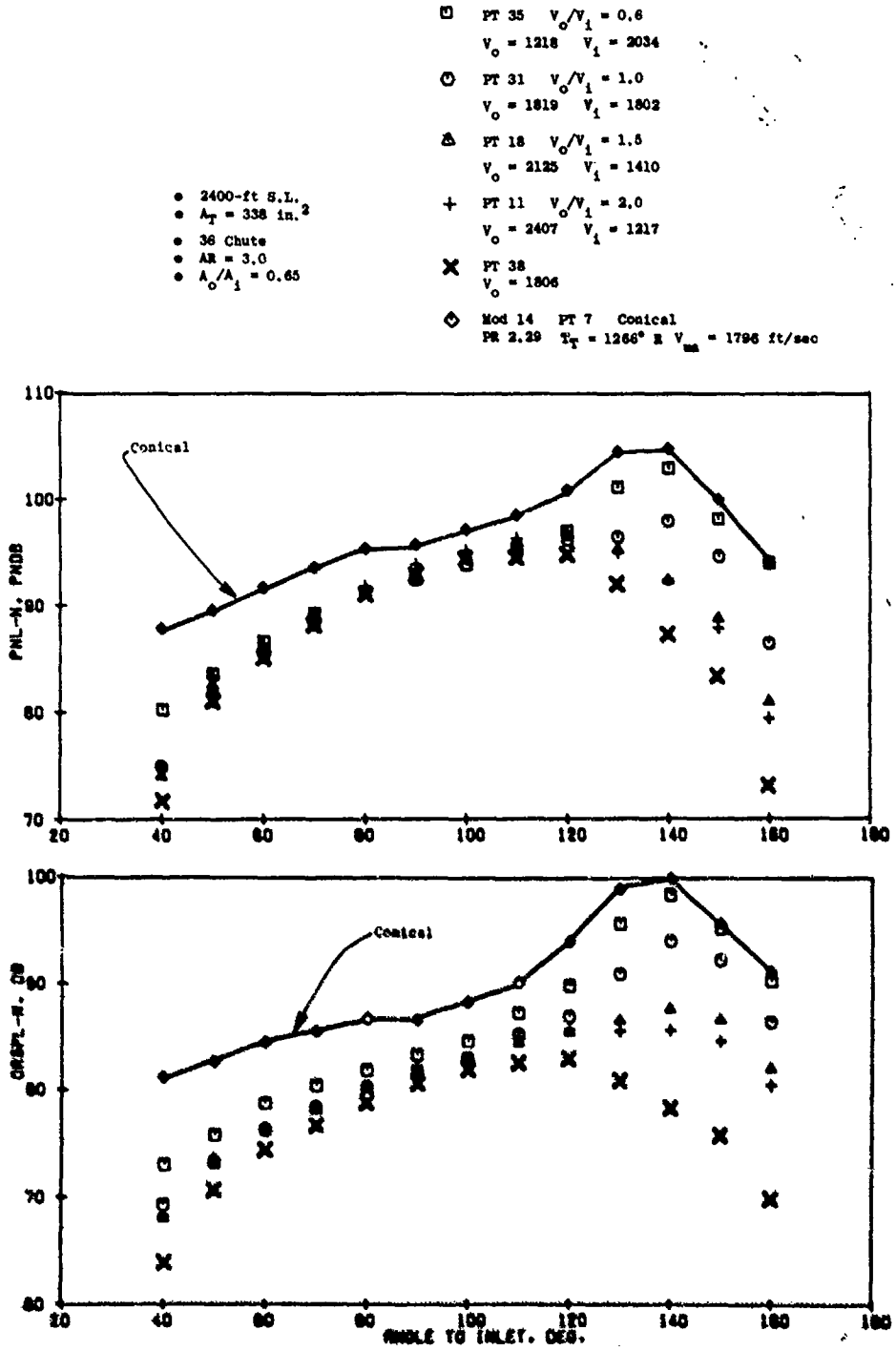

Figure 3-146. Impact of V_o/V_i on PNL and OASPL Directivity, Model 34, V_{ma} = 1720-1830 ft/sec.

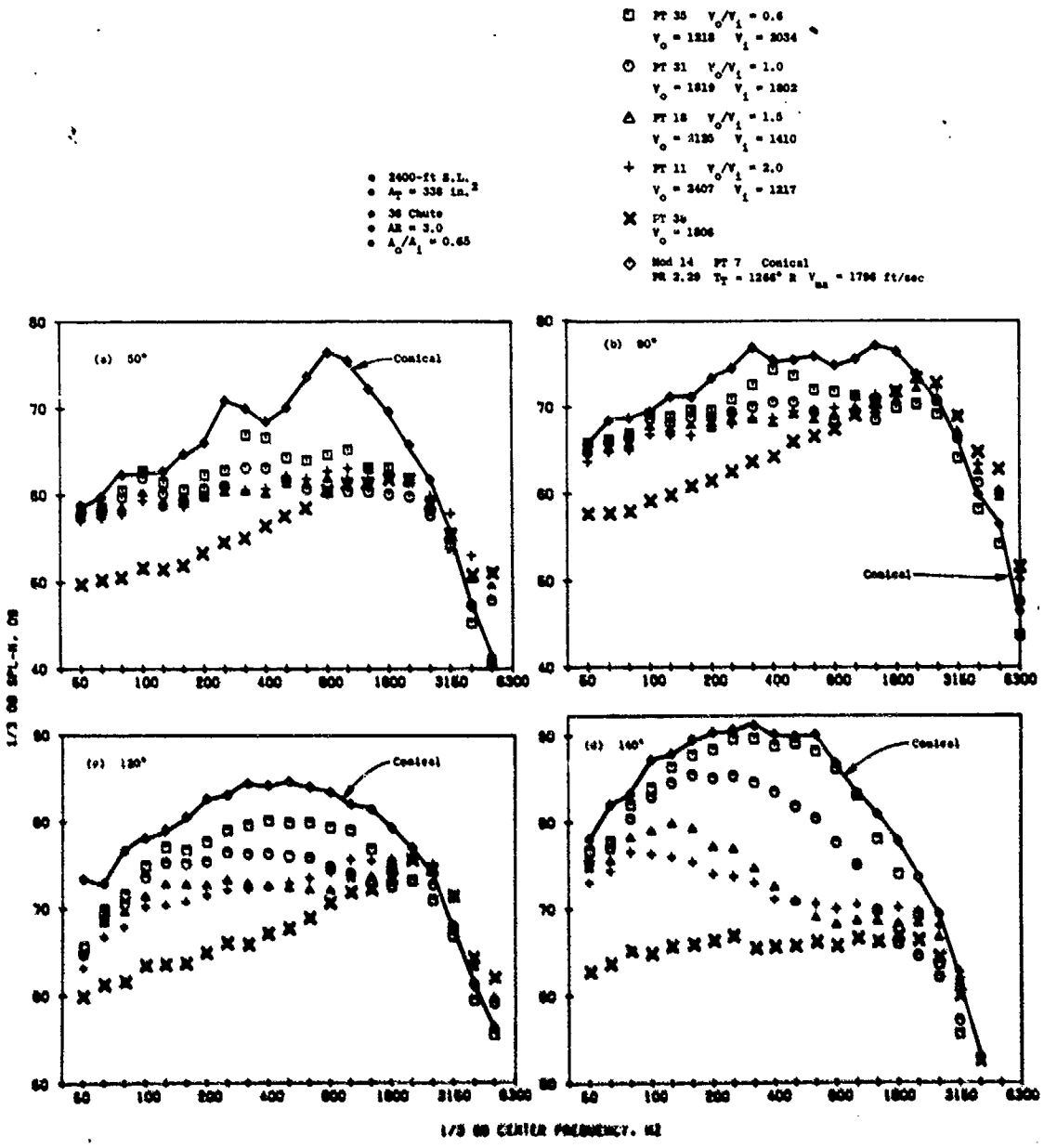

Figure 3-147. Impact of V_o/V_i on Spectra, Model 34, V_{ma} = 1720-1830 ft/sec.

quadrant changes are very systematic and progress with system velocity ratio change as shown in Figure 3-131. Broadside and forward quadrant changes, as mentioned previously, are not as distinguishable, except for $V_o/V_i = \infty$.

- Spectra comparisons at aft angles for this data set show low V_o/V_i = 0.8 spectra shapes approaching the conical nozzle. Suppression starts primarily in mid-frequency at V_o/V_i = 1.0 and is then more broadband from low-to-mid frequency for V_o/V_i = 1.5 to 2.0. Terminating inner flow again results in near flat spectra. In general the broadside and forward quadrant spectra changes are mainly at mid-to-high frequency for V_o/V_i = 0.8 to 2.0. When inner flow is terminated, the low frequency levels are also substantially reduced. Again, the mid-to-high frequencies control PNL and OASPL and therefore the low-to-mid frequency reductions do not significantly reduce either.

- Model 34 data comparisons, Figures 3-144 thru 3-147, exhibit trends similar to those of Model 33.

Results of peak, 90°, and 50° PNL and OASPL are included in the following figures for Models 31 and 27 at A_o/A_i = 1.92.

Model No.	Peak	90°	50°
31	3-148	3-149	3-150
27	3-151	3-152	3-153

For this model set the DBTF/Inverted Dual Flow cycle matrix consisted of 12 data points at select values of V_o/V_i = 1.0, 1.25, 1.5 and 2.0. Therefore, it did not cover the expanded range of the previous A_o/A_i = 0.65 models and broad results are not as conclusive. Data for these two models are partially presented elsewhere in this report (Section 3.4.2.3 "Flow Segmentation Study" for Model 31, comparing 20, 30 and 40 elements and Section 3.4.2.1 "Area Ratio and Radius Ratio Variable - Dual Flow" for Model 27, comparing area ratios/radius ratios of 1.5/0.782, 2.0/0.716, and 2.5/0.653). The results are presented in those sections as data fitted curves through the aggregate of test points. They normally show that the variance from the mean line is small enough to consider no distinguishable noise trend with V_o/V_i.

The last model of the six selected for data presentation is Model 26 (36-chute of A_o/A_i = 3.61). Peak, 90° and 50° PNL/OASPL data are presented in Figures 3-154, 3-155 and 3-156, respectively for this model. The parameter β ranges from 2.8 to 8.8, therefore the outer stream dominates in noise generation. Little variance is distinguishable for the four V_o/V_i settings, and what little exists is less than the variance seen in the A_o/A_i = 1.92 system. No inner/outer flow interaction mechanism seems to be present to enhance the suppression above that of a basic suppressed annulus.

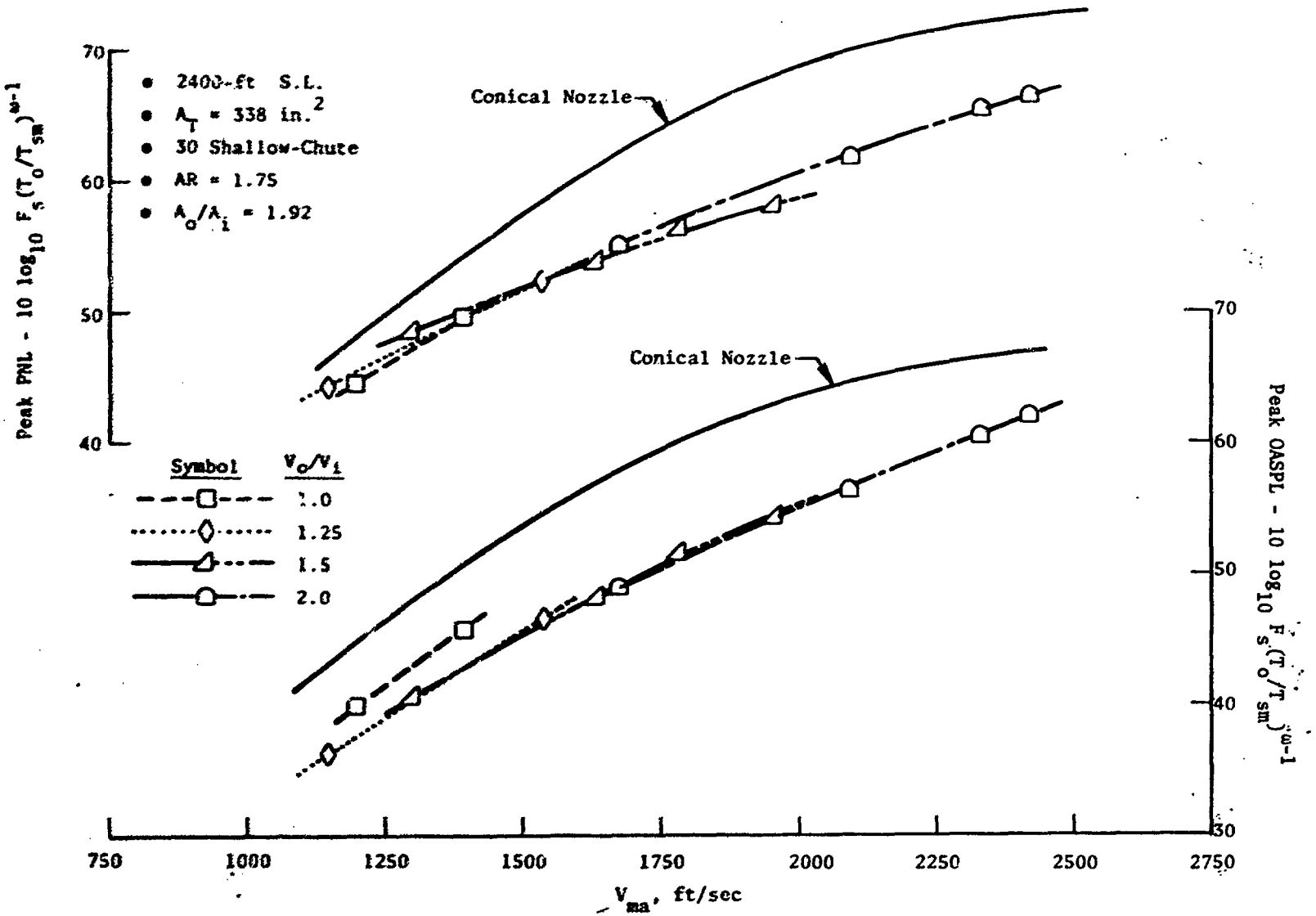

Figure 3-148. Peak PNL and OASPL Variation with V_o/V_i, Model 31.

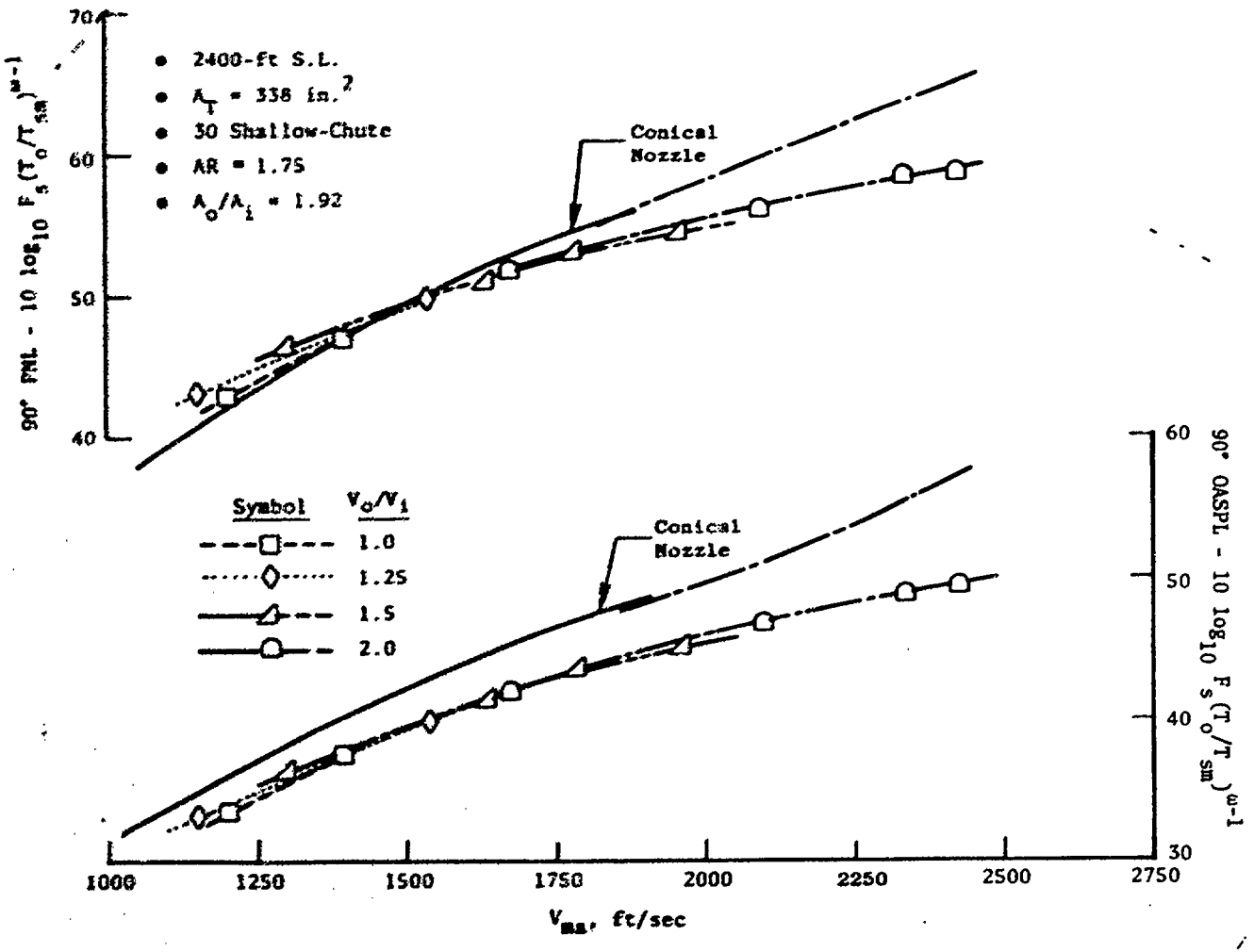

Figure 3-149. 90° PNL and OASPL Variation with V_o/V_i, Model 31.

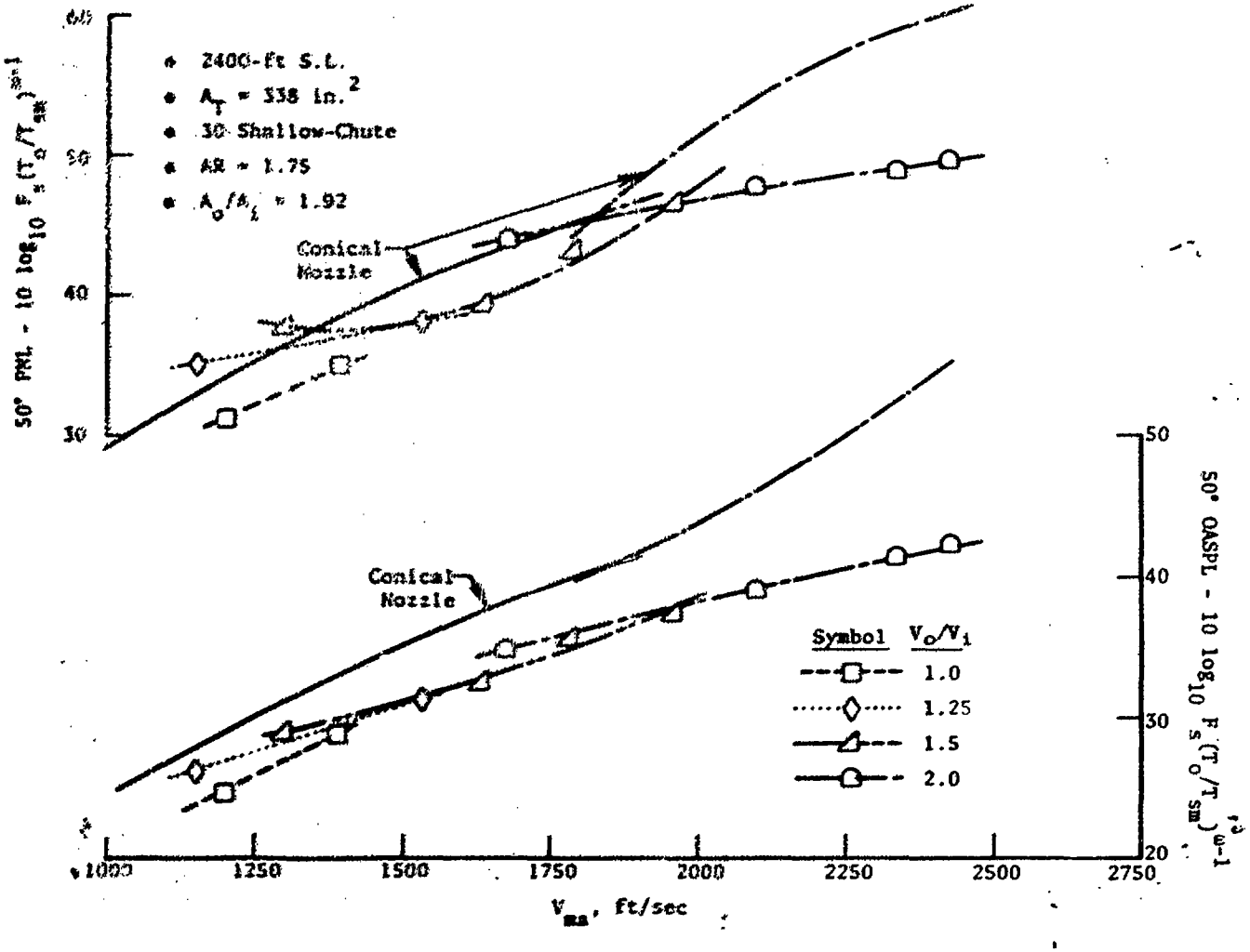

Figure 3-150. 50° PNL and OASPL Variation with V_o/V_i, Model 31.

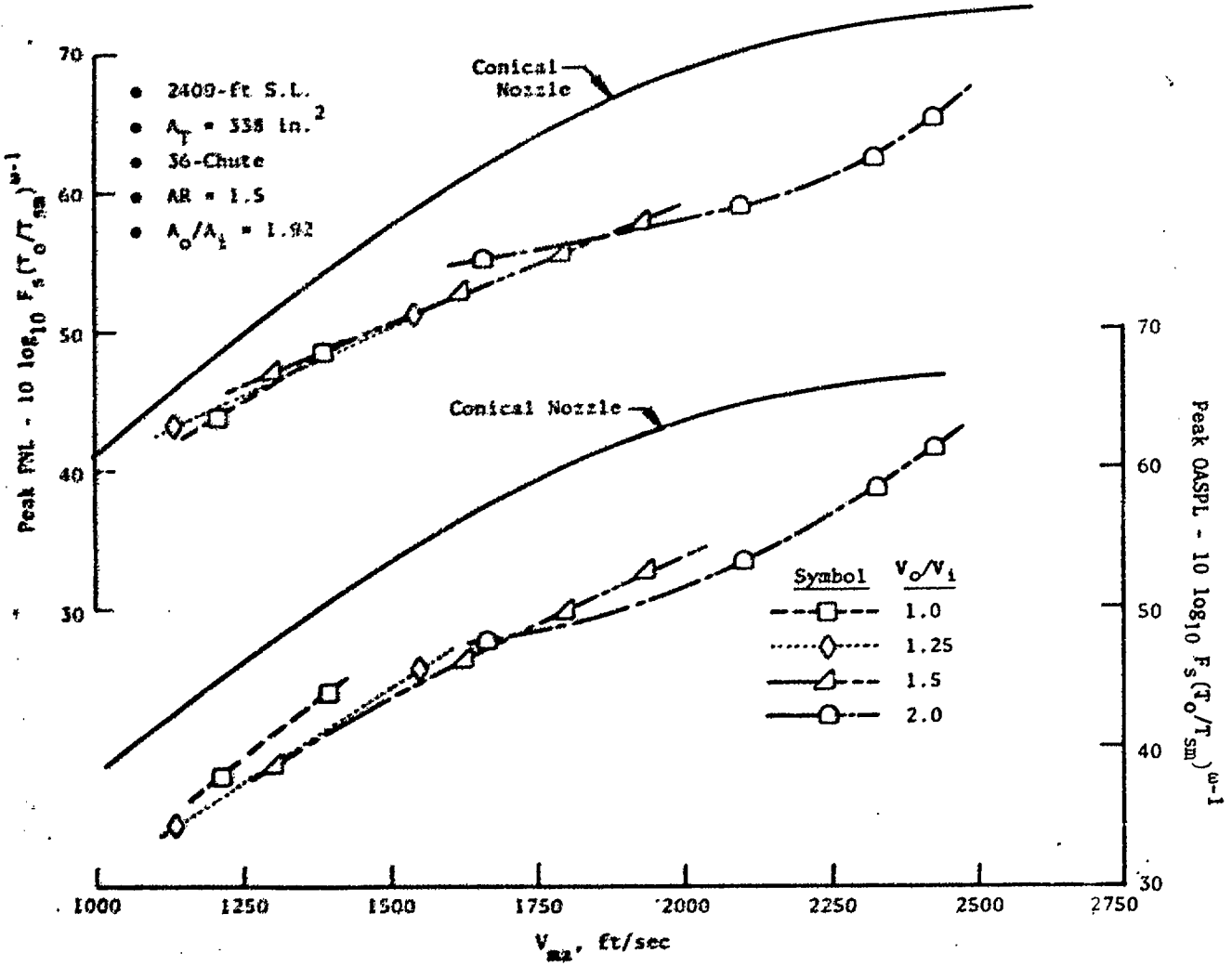

Figure 3-151. Peak PNL and OASPL Variation with V_o/V_i, Model 27.

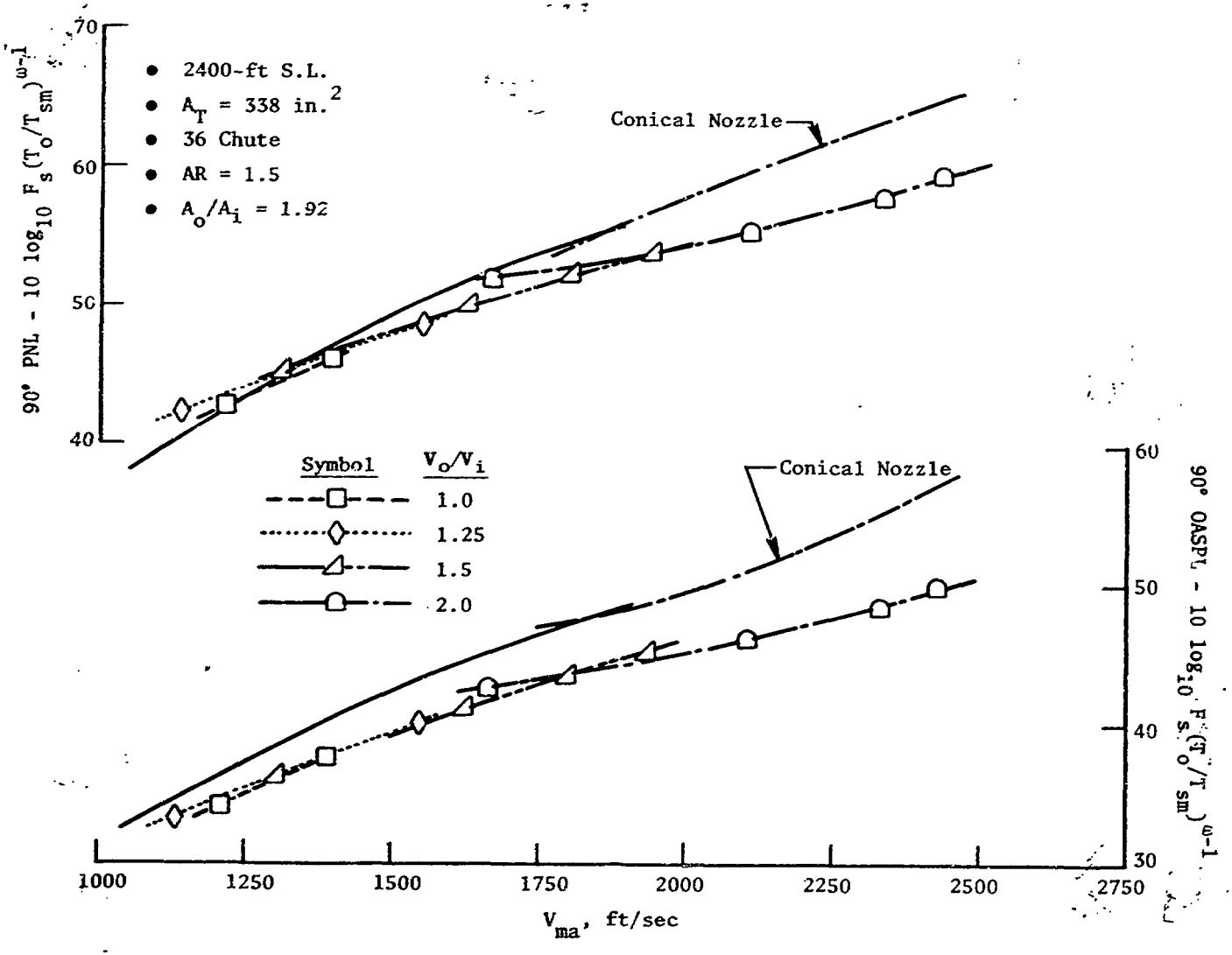

Figure 3-152. 90° PNL and OASPL Variation with V_o/V_i, Model 27.

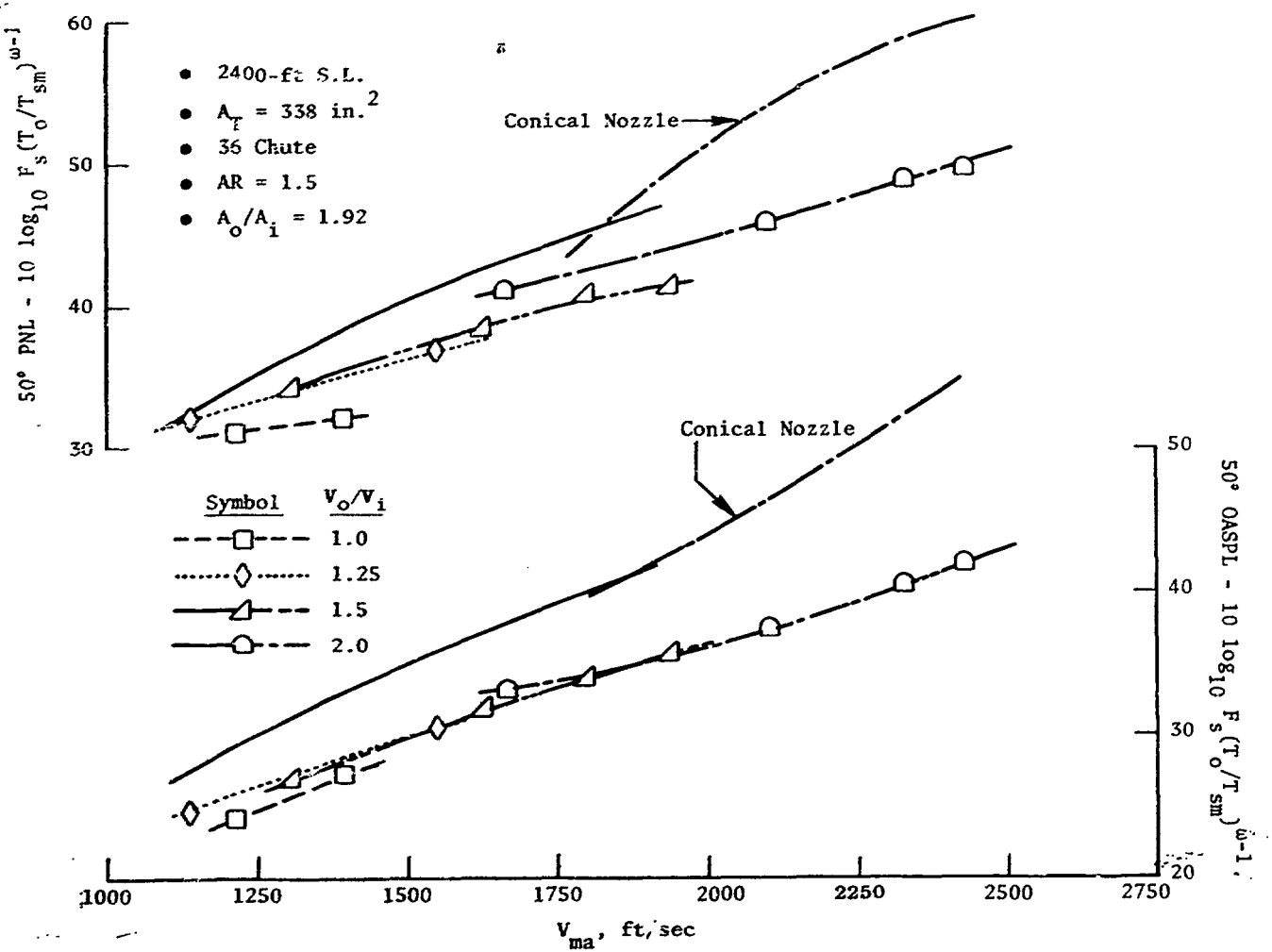

Figure 3-153. 50° PNL and OASPL Variation with V_o/V_i, Model 27.

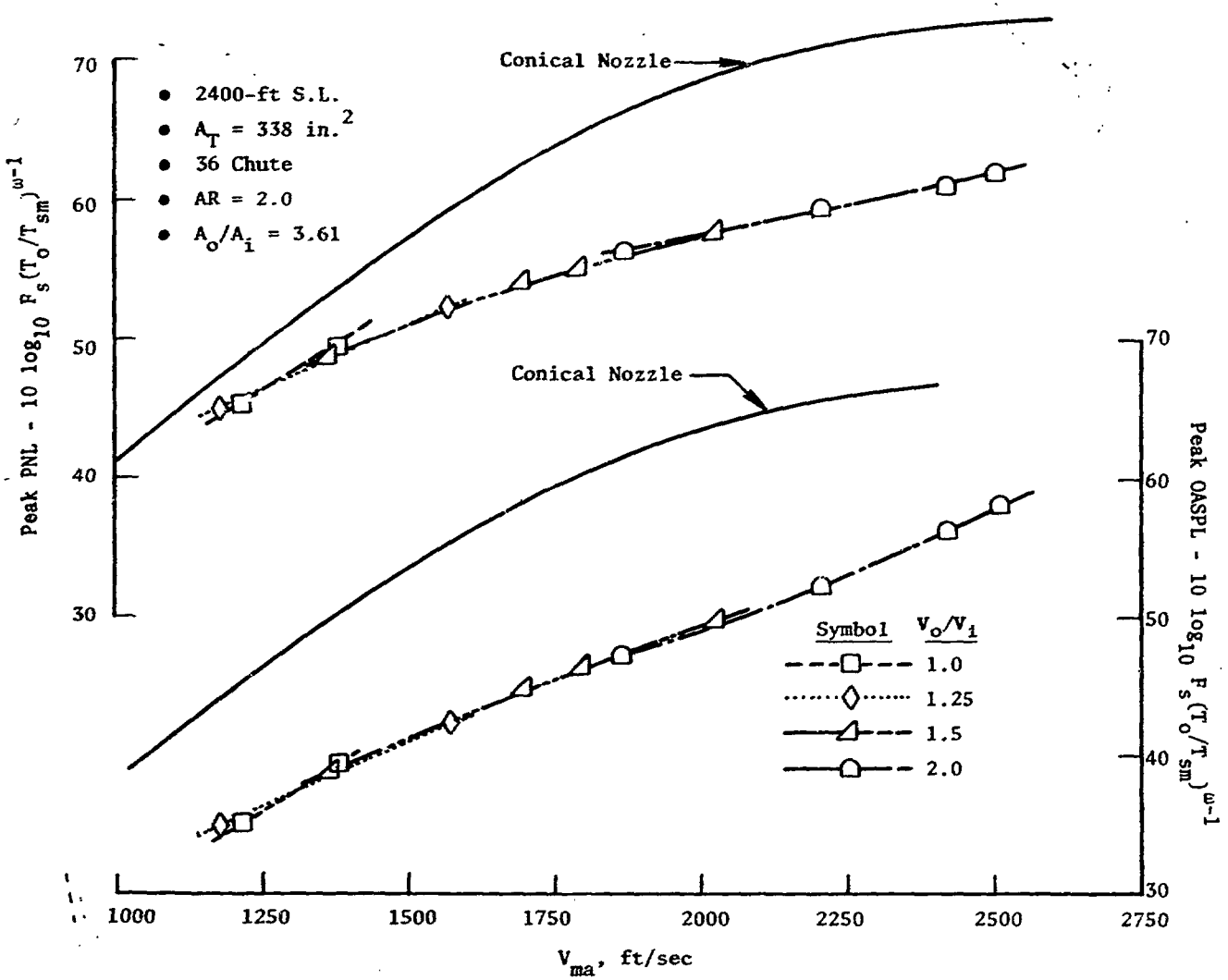

Figure 3-154. Peak PNL and OASPL Variation with V_o/V_i, Model 26.

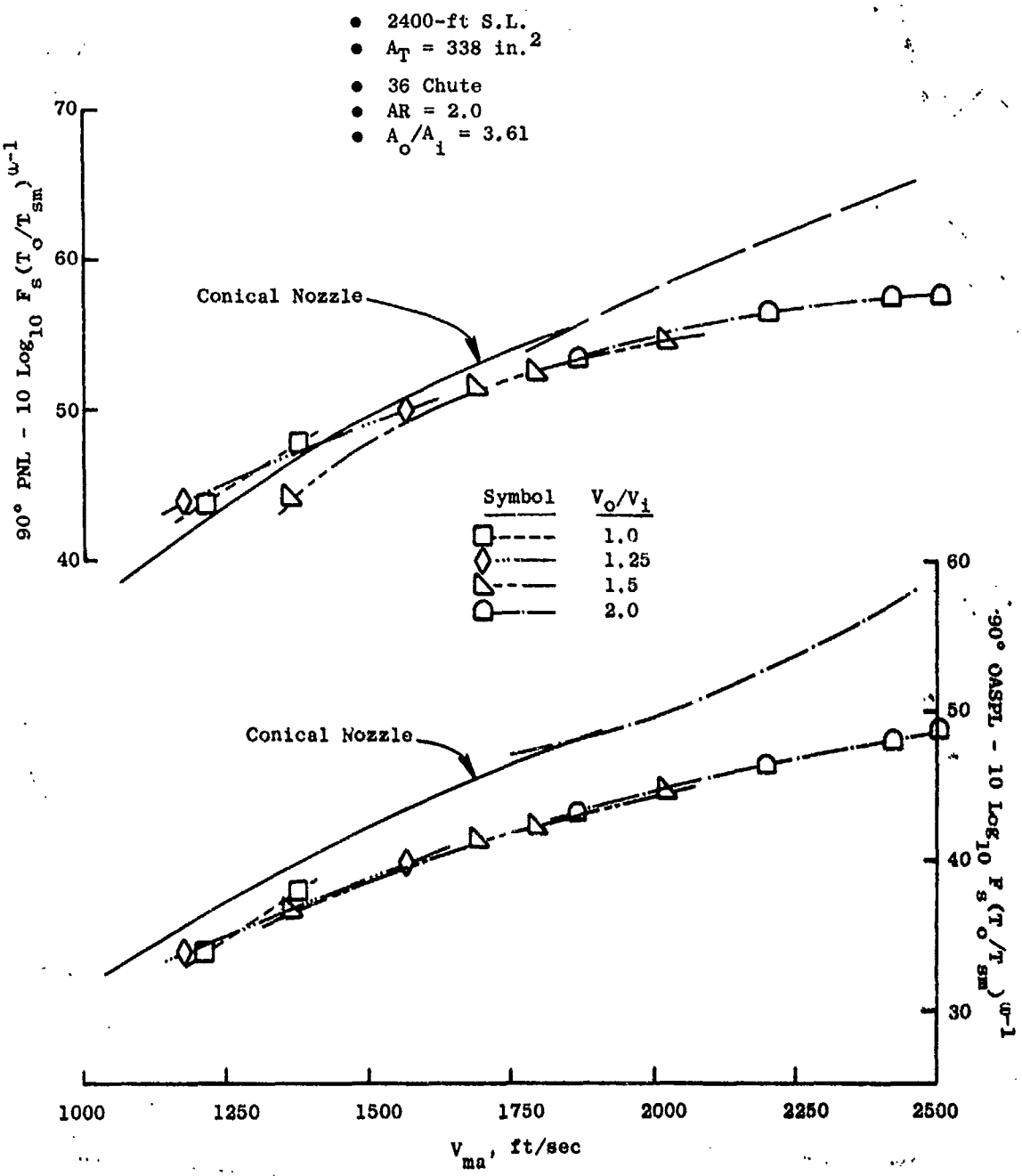

Figure 3-155. 90° PNL and OASPL Variation with V_o/V_i, Model 26.

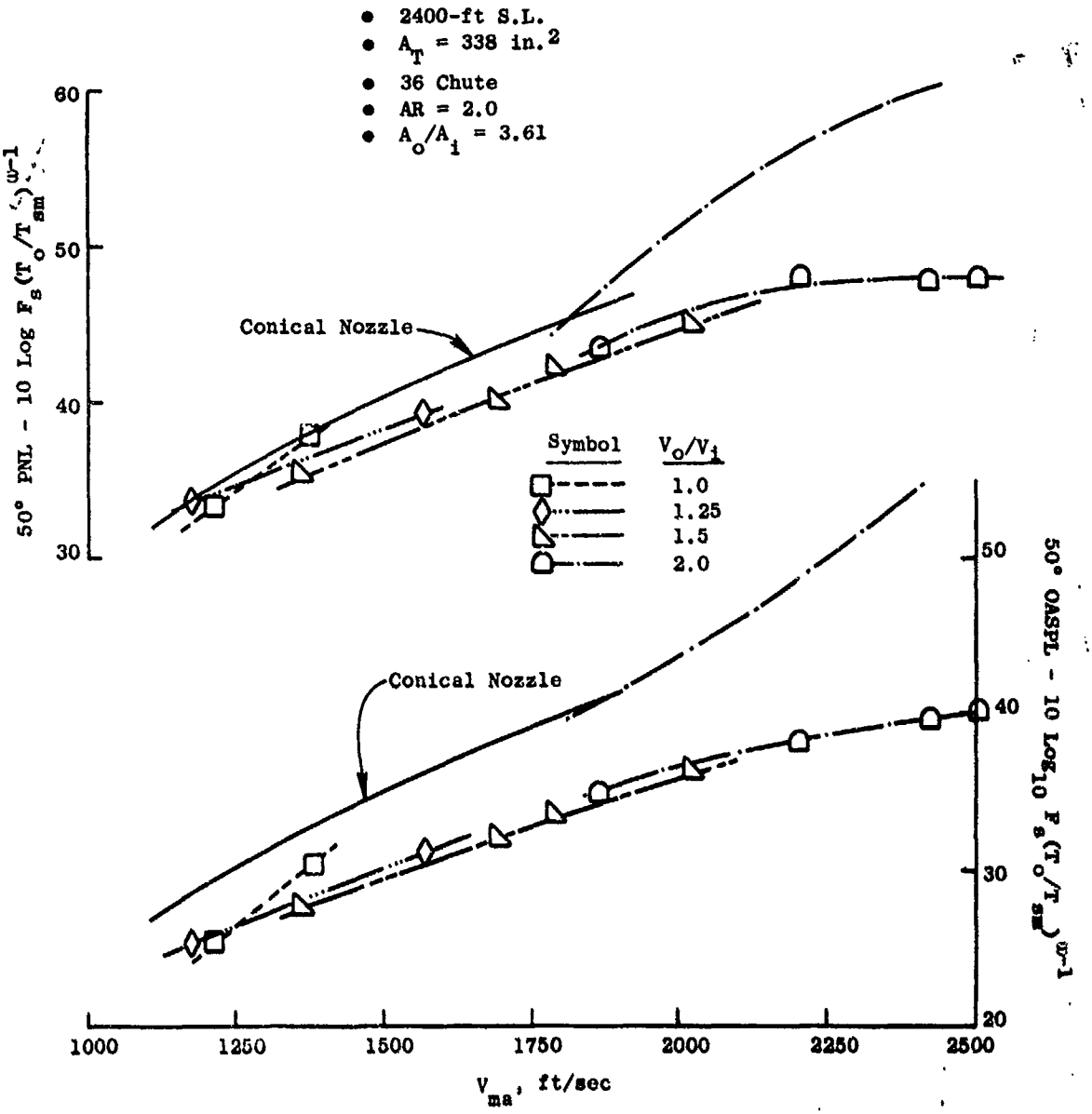

Figure 3-156. 50° PNL and OASPL Variation with V_o/V_i, Model 26.

System β Variation at Fixed A_o/A_i and Duct Suppressor Geometry

This study continues the theme of system variation investigations. The previous section isolated the influence of system velocity ratio and this section isolates the impact of system weight flow ratio, β. Primary emphasis is placed on systems which utilize low amounts of inner flow, in an effort to extend preliminary results of the NASA-Lewis/GE Duct-Burning Turbofan Program (Reference 10). These results indicate that unsuppressed coannular and suppressed annular systems show enhanced suppression with low amounts of inner stream flow.

Seven test configurations were utilized, varying system area ratio and annular suppressor geometry, and the following four were selected for presentation of results herein:

		Outer Stream				Inner Stream				Appendix A Figure Reference
Model No.	System A_o/A_i	Element Description	AR	R_2^o	Flow Area, $in.^2$	Step Height in.	Plug Location	R_2^i	Flow Area, $in.^2$	
33	0.65	36-Chute	2.5	0.783	17.21	1.03	Retracted	0.674	11.12	27
34	0.65	36-Chute	3.0	0.783	17.21	1.03	Retracted	0.674	11.12	28
31	1.92	30-Shallow Chute	1.75	0.717	23.76	0.70	Retracted	0.779	12.39	25
23	1.92	36-Chute	2.0	0.716	23.76	0.70	In-Line	0.779	12.39	17

The first three models are the same as in the previous section (shown in Figures 3-129 and 3-130). A photo of Model 23 is included as Figure 3-157. The last column of the above chart references the detailed geometry sketches for each model as shown in Appendix A. Three of the configurations have annular deep-chute suppressors and Model 31 has an annular shallow-chute suppressor. The first two models have A_o/A_i of 0.65 and the remaining two have A_o/A_i of 1.92. The suppressor area ratio range is 1.75 to 3.0 and the radius ratio range is 0.716 to 0.783. Each model is representative of an advanced technology dual flow system with half-span suppressor application.

Systematic variation of weight flow ratio was accomplished using preselected β values of 3.3, 6.7 and ∞. This corresponded to metering inner stream flow rates at 30, 15 and 0% of the outer stream. The $\beta = \infty$ case is attained when the inner flow is curtailed completely by use of a positive shut-off mechanism placed about one diameter upstream of the inner flow exit plane. Through this β variation, for the two A_o/A_i systems selected, the system velocity ratio varied as follows:

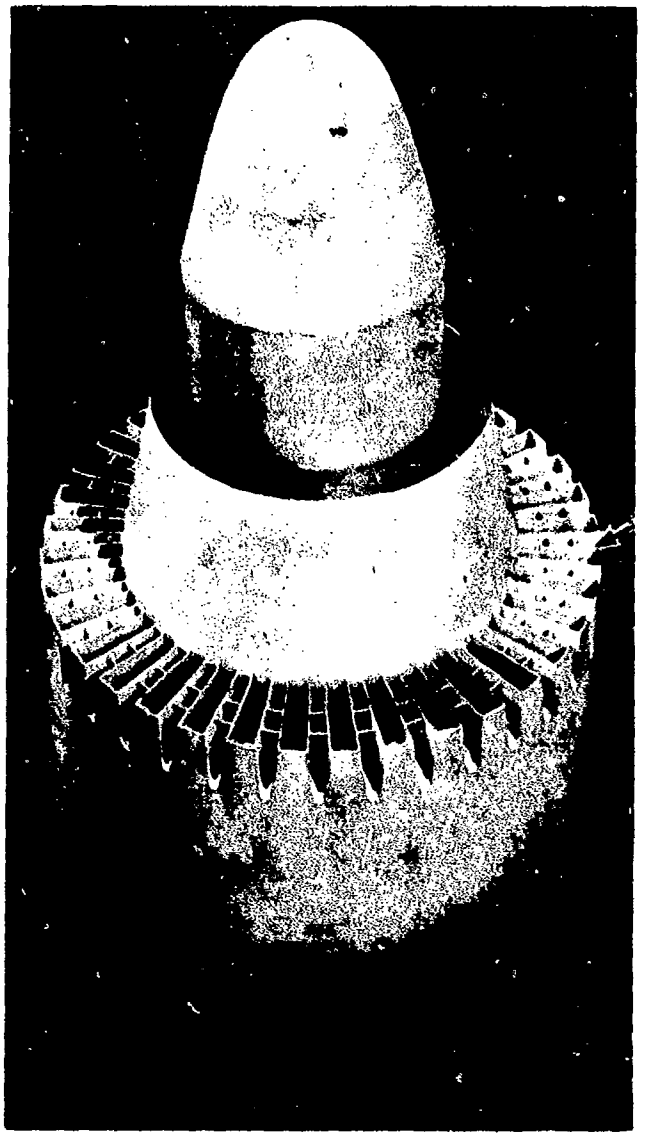

Model 23

- 36 Chute, AR = 2.0
- $R_r^o = 0.716$, $R_r^i = 0.779$ In-Line Inner Plug
- $A_o/A_i = 1.92$

Figure 3-157. Dual Flow Model for β Investigation at $A_o/A_i = 1.92$.

A_o/A_i	β	$\approx V_o/V_i$
0.65	6.7	6 - 14
	3.3	6 - 11
1.92	6.7	2.5 - 8
	3.3	1 - 3

Acoustic results in terms of peak, 90° and 50° PNL and OASPL are presented individually for each model in the following figures. Each data set if normalized per Section 3.3.1.7 and plotted versus V_{ma}. The peak PNL and OASPL data sets have Δ plots showing suppression relative to the baseline convergent nozzle.

Model No.	Peak PNL	Peak OASPL	90° PNL & OASPL	50° PNL & OASPL
33	3-158	3-159	3-160	3-161
34	3-162	3-163	3-164	3-165
31	3-166	3-167	3-168	3-169
23	3-170	3-171	3-172	3-173

The following are observed:

- System weight flow ratio, β, is a strong parameter which influences peak PNL and peak OASPL significantly. The magnitude of influence is somewhat greater for low system A_o/A_i of 0.65 than for 1.92. The influence is fairly systematic, progressively decreasing suppression capability as β is lowered from ∞, to 6.7, to 3.3. Influence of β on the A_o/A_i = 0.65 system is fairly consistent over the V_{ma} test range, whereas, on the A_o/A_i = 1.92 systems, it's influence is primarily at mid-to-high V_{ma}; suppression variance decreasing on both PNL and OASPL basis.

- At A_o/A_i = 0.65 (Models 33 and 34), peak PNL changes up to 5 dB at low V_{ma} (between β = 3.3 and ∞) and up to 3 dB at high V_{ma}. The corresponding peak OASPL variances are about 5 and 6 dB, respectively.

- In the previous study, system velocity ratio varied over the $0.6 \leq V_o/V_i \leq \infty$ range, with small incremental and systematic variations exercised within the 0.6 to 2.0 range. Accompanying β ranged from 0.4 to 1.3. Variations in noise level appear to be primarily controlled by whichever stream's noise dominated the spectral composition. At preselected values of β of 3.3 and 6.7, V_o/V_i vari-

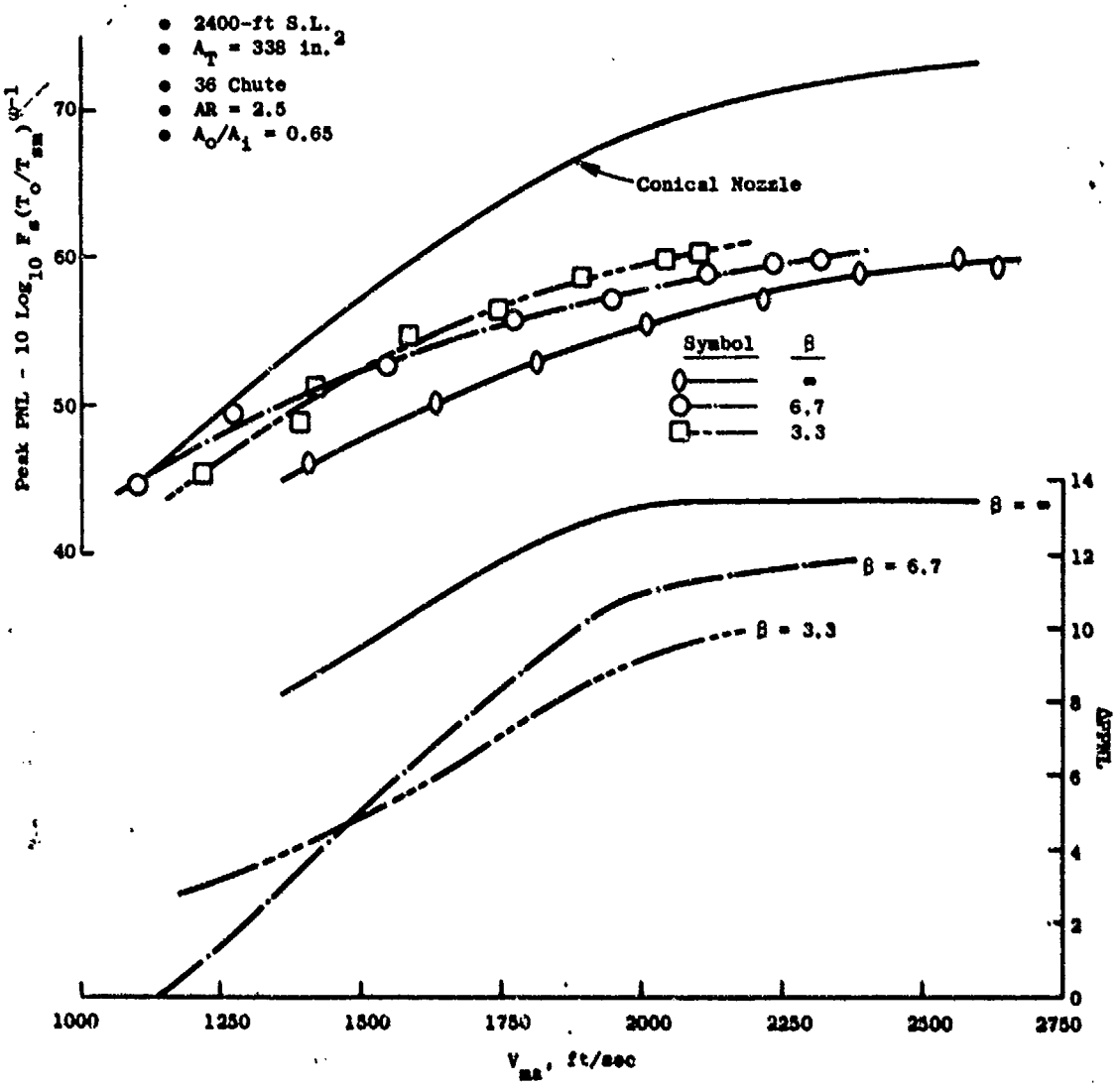

Figure 3-158. Peak PNL Variation with β, Model 33.

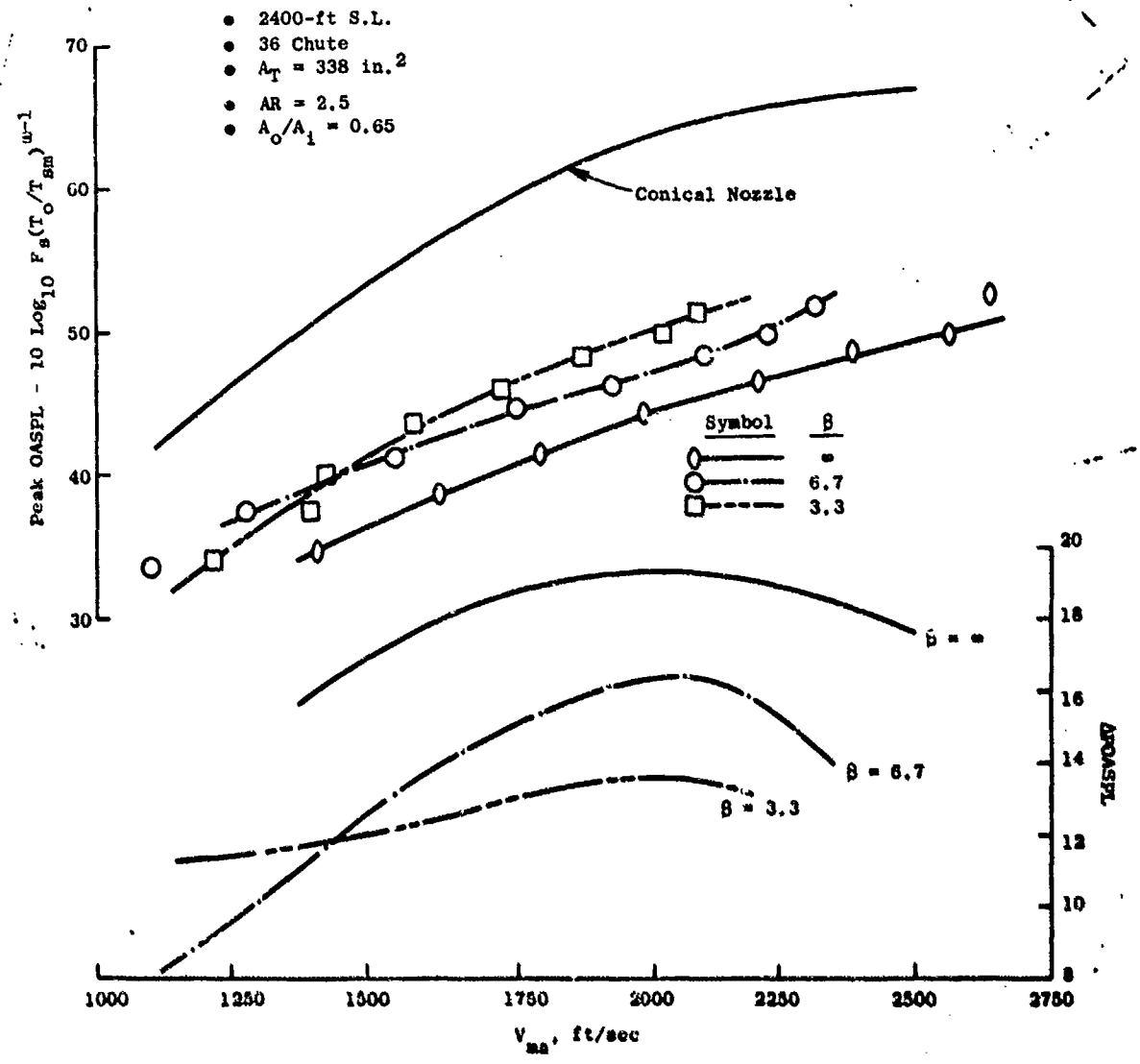

Figure 3-159. Peak OASPL Variation with β, Model 33.

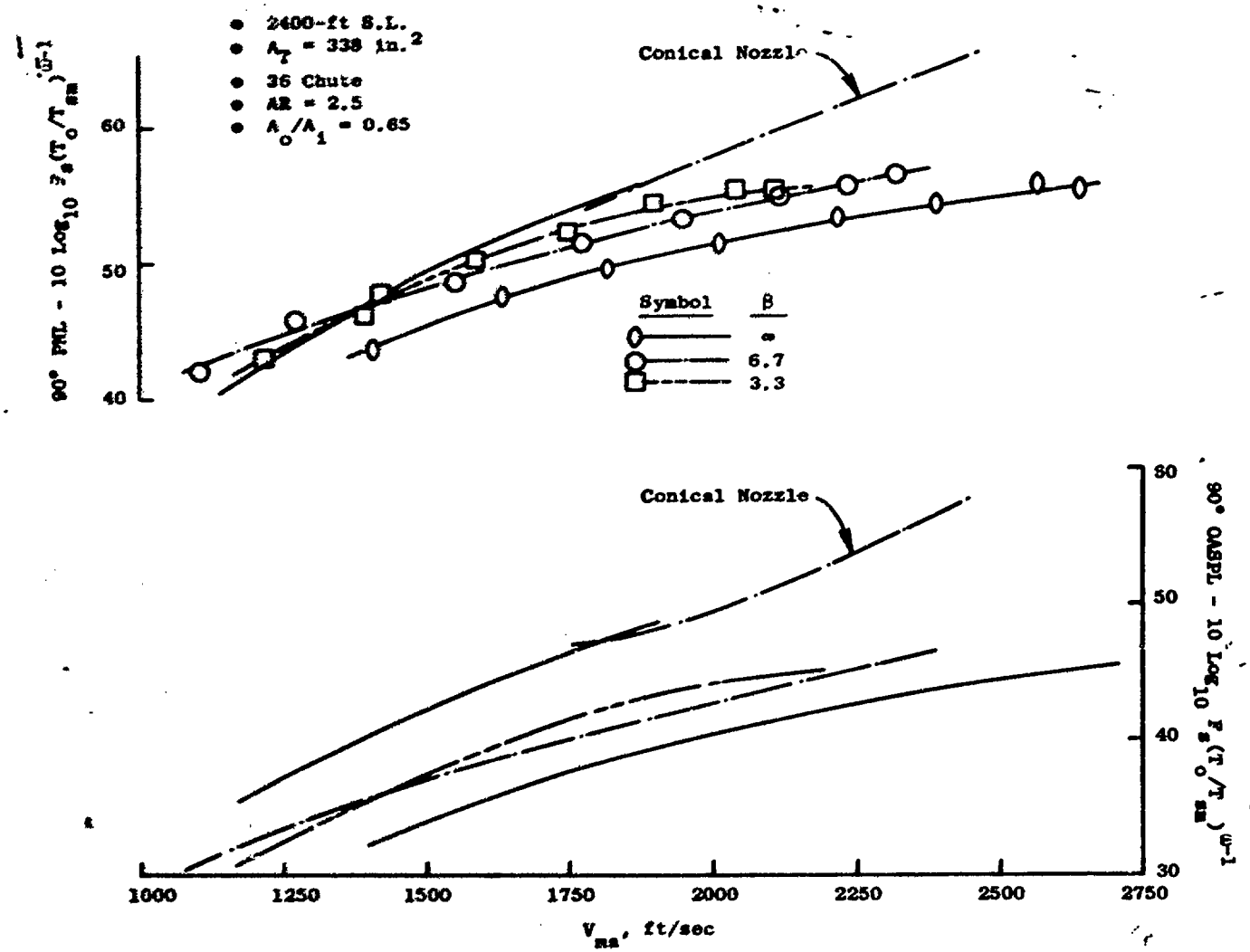

Figure 3-160. 90° PWL and OASPL Variation with β, Model 33.

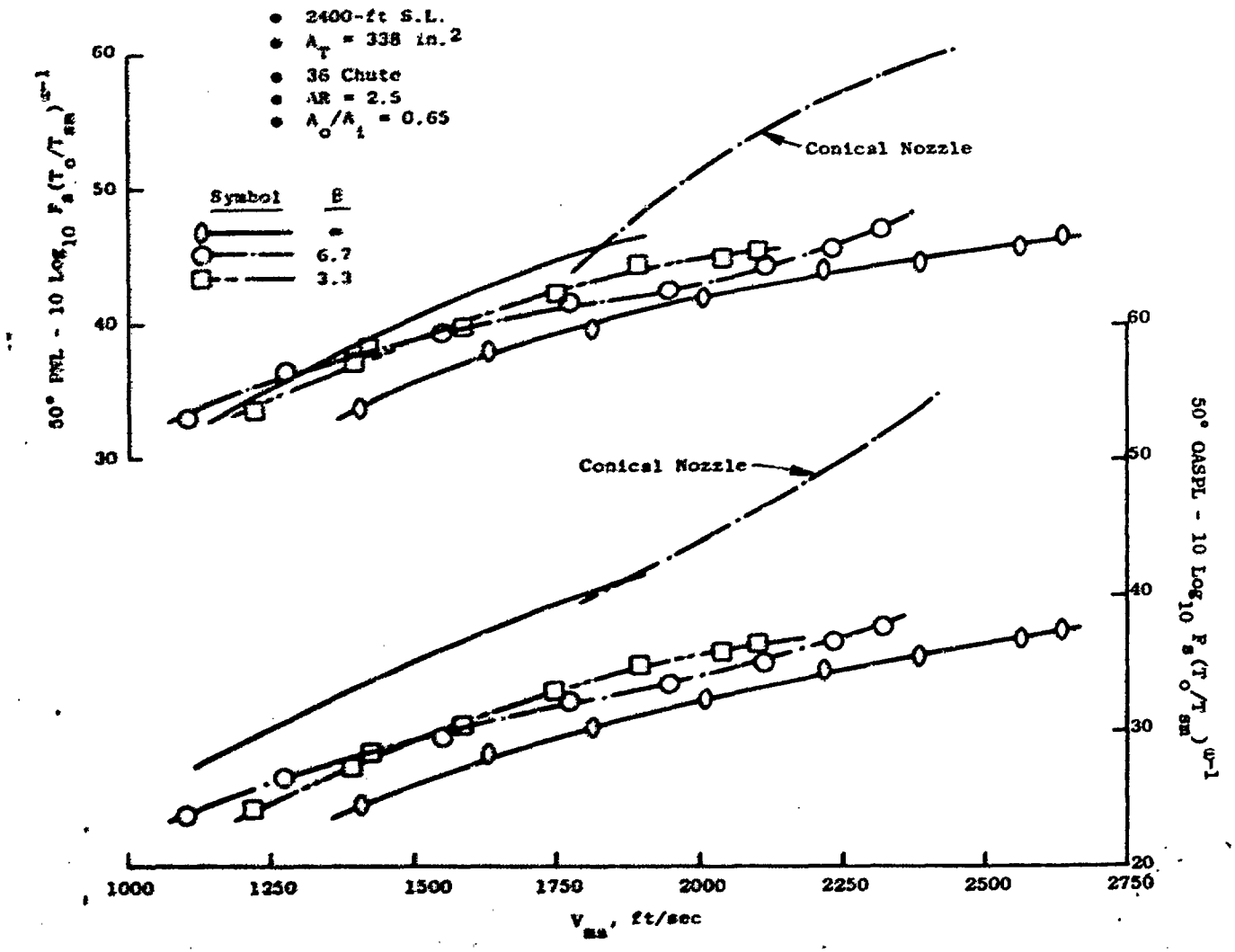

Figure 3-161. 50° PNL and OASPL Variation with β, Model 33.

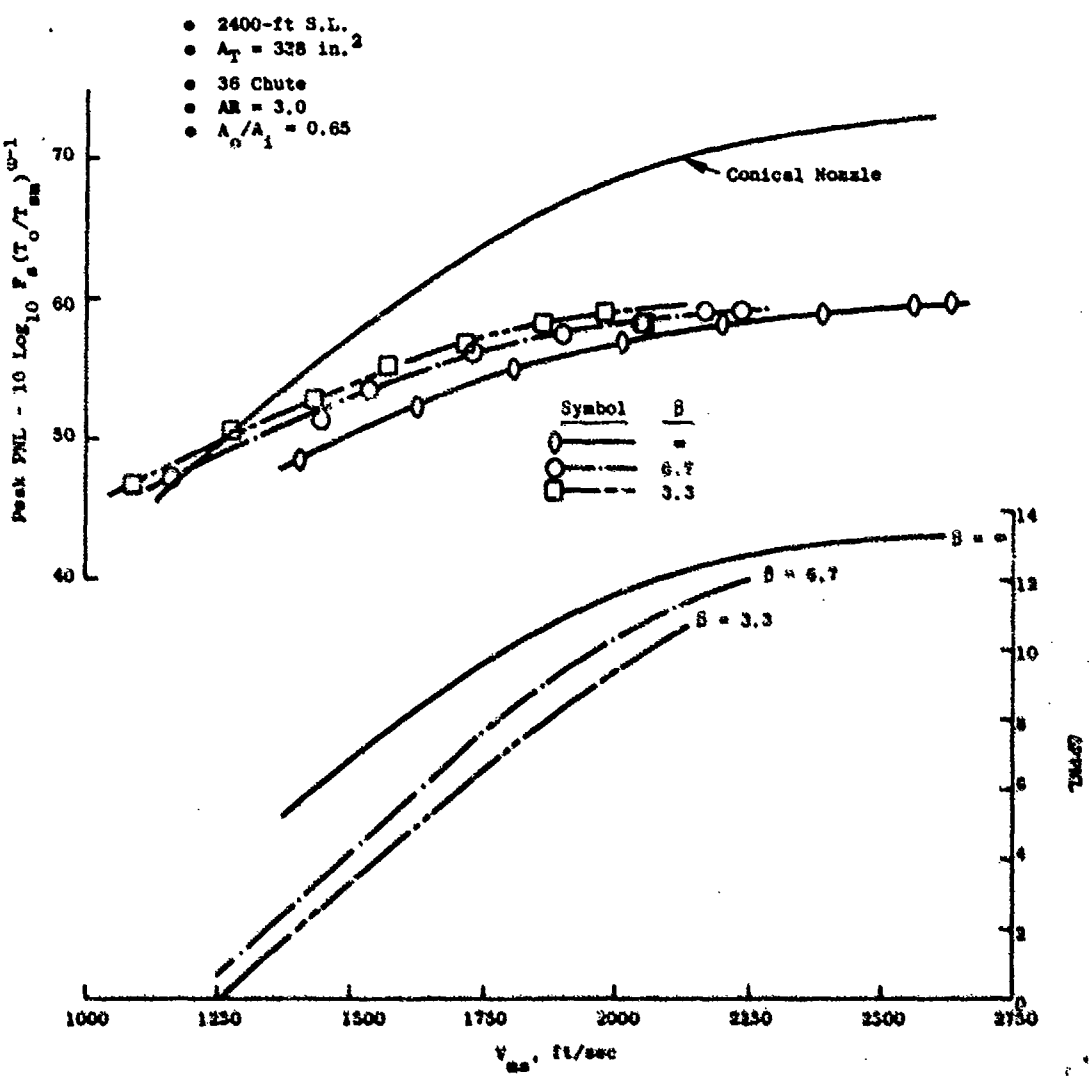

Figure 3-162. Peak PNL Variation with β, Model 34.

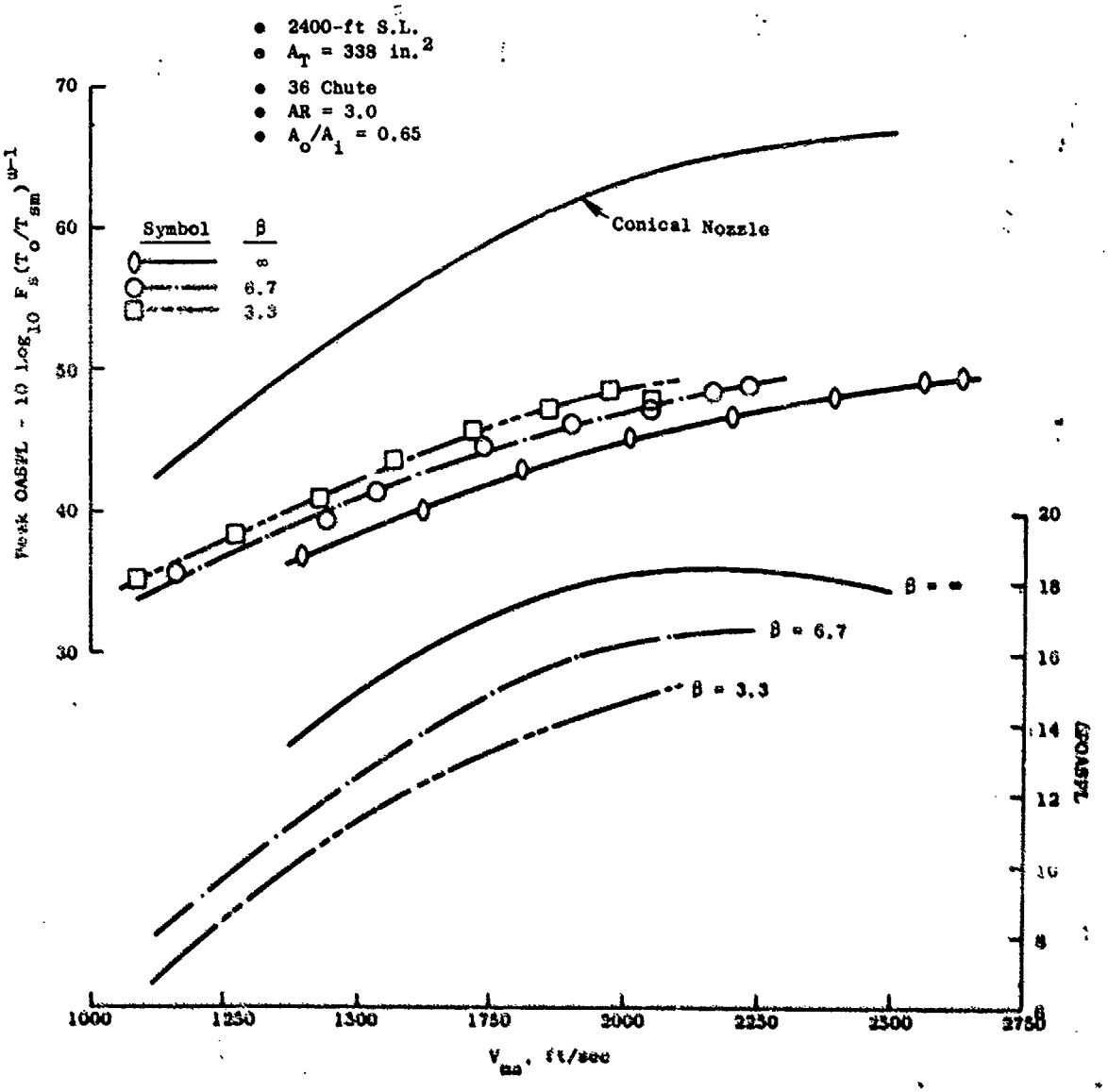

Figure 3-163. Peak OASPL Variation with β, Model 34.

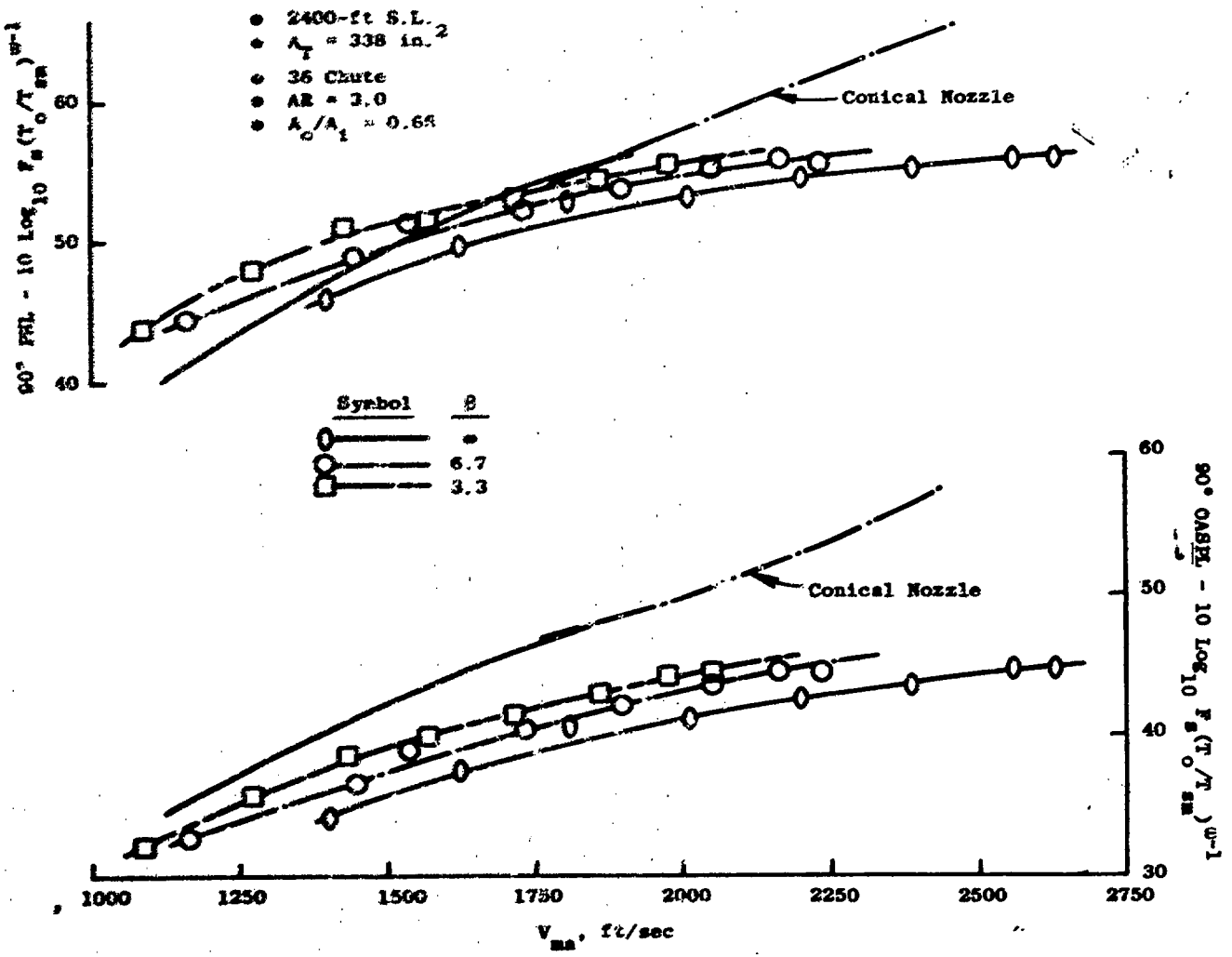

Figure 3-164. 90° PWL and OASPL Variation with β, Model 34.

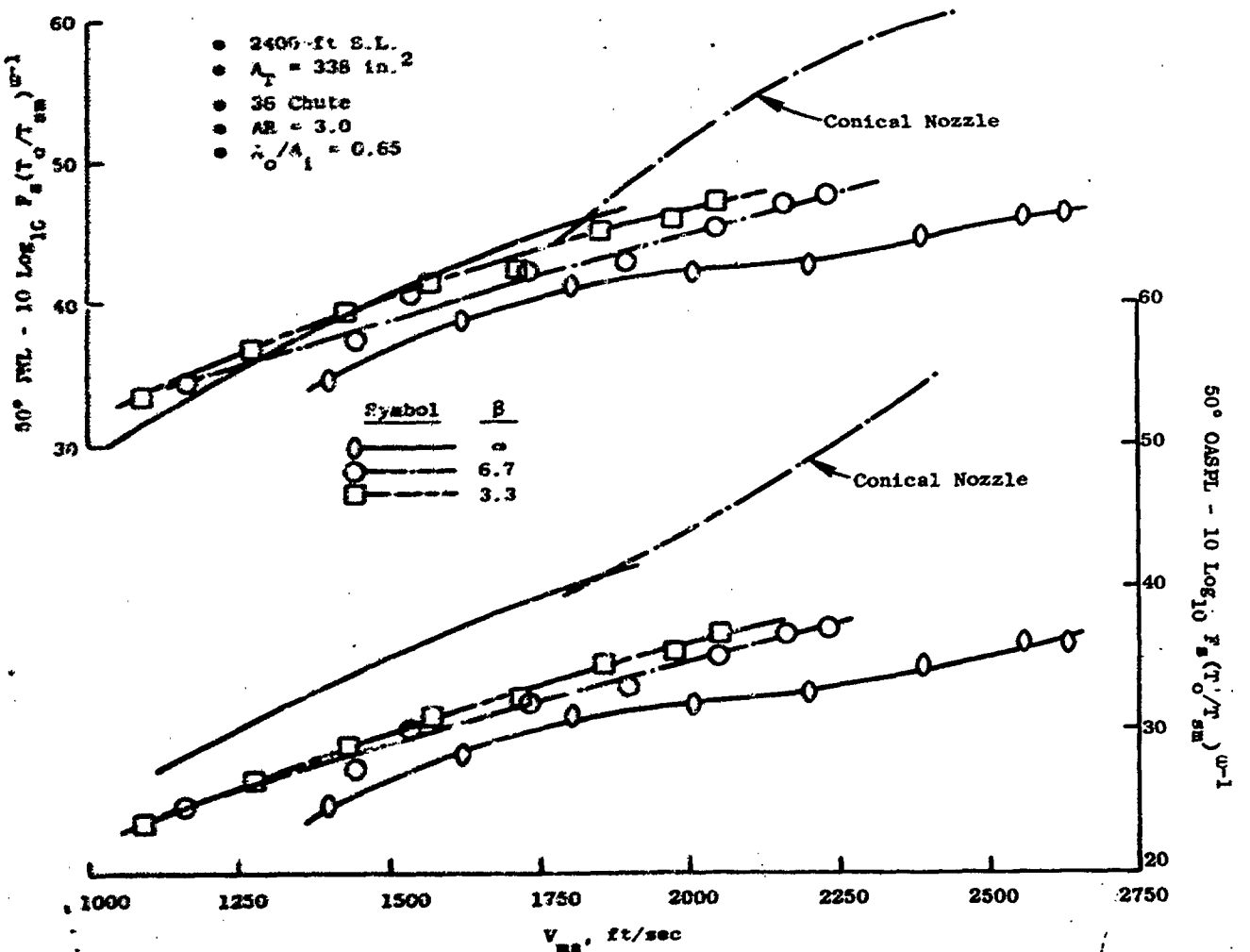

Figure 3-165. 50° PNL and OASPL Variation with β, Model 34.

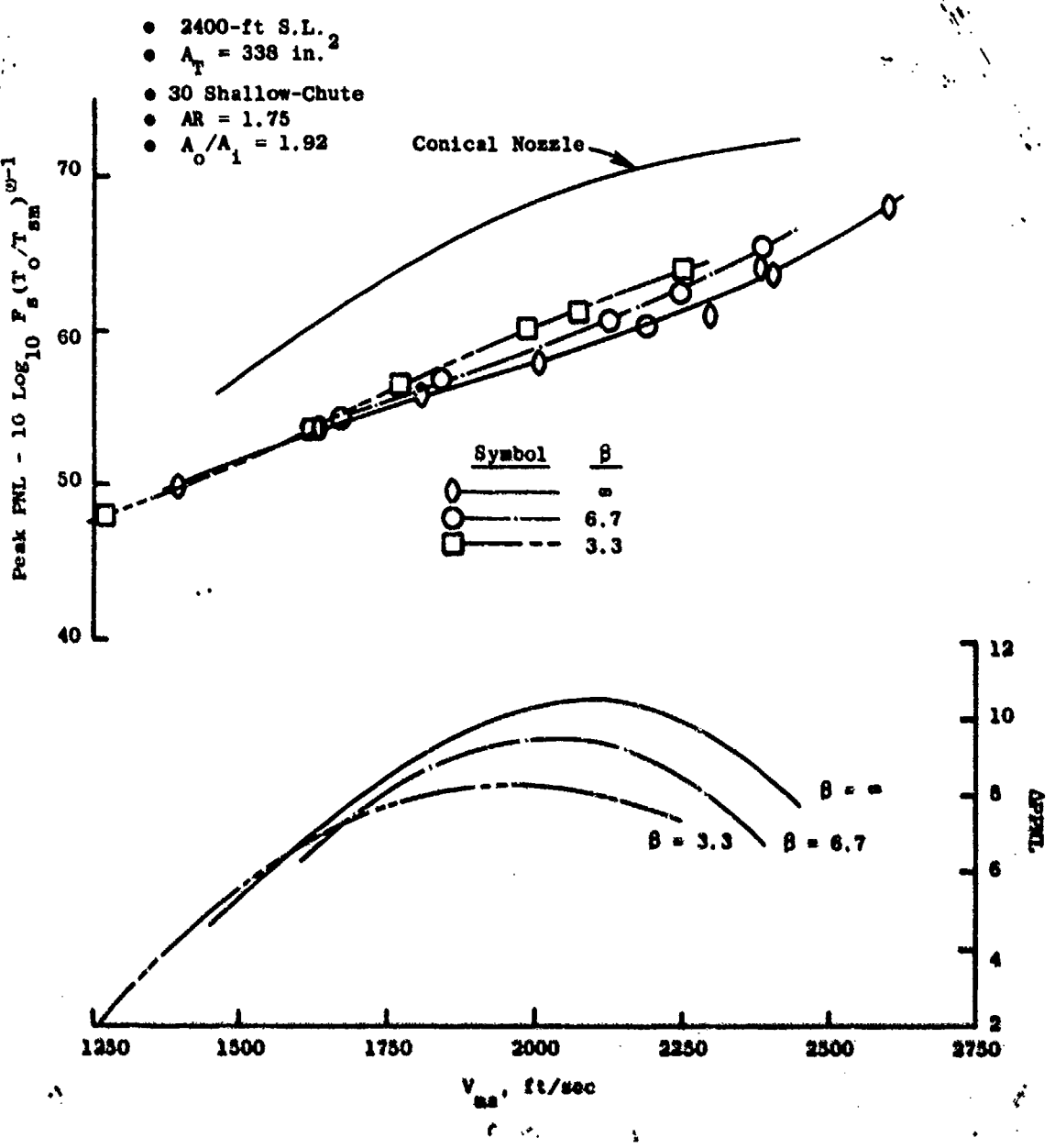

Figure 3-168. Peak PNL Variation with β, Model 31.

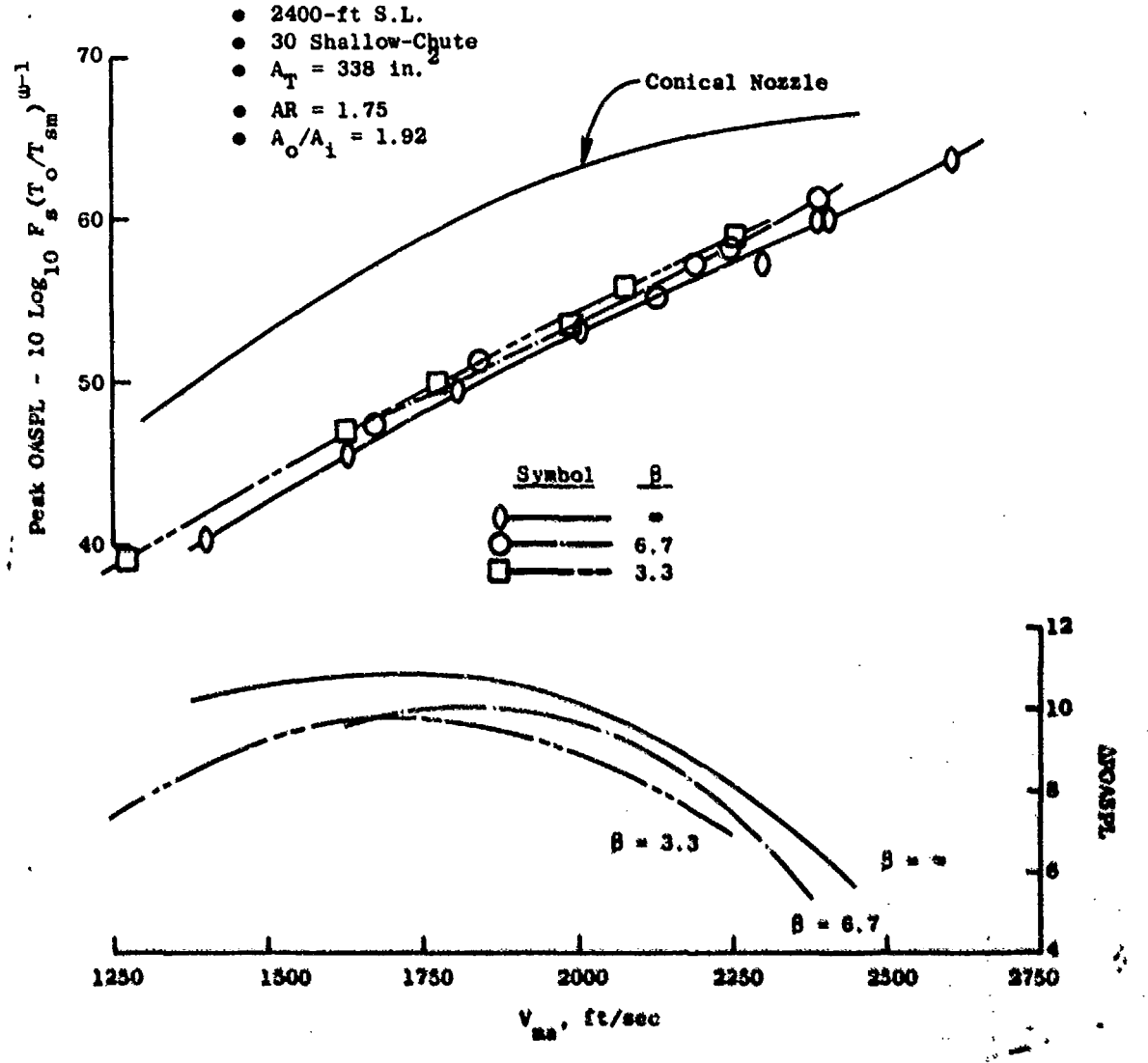

Figure 3-167. Peak OASPL Variation with β, Model 31.

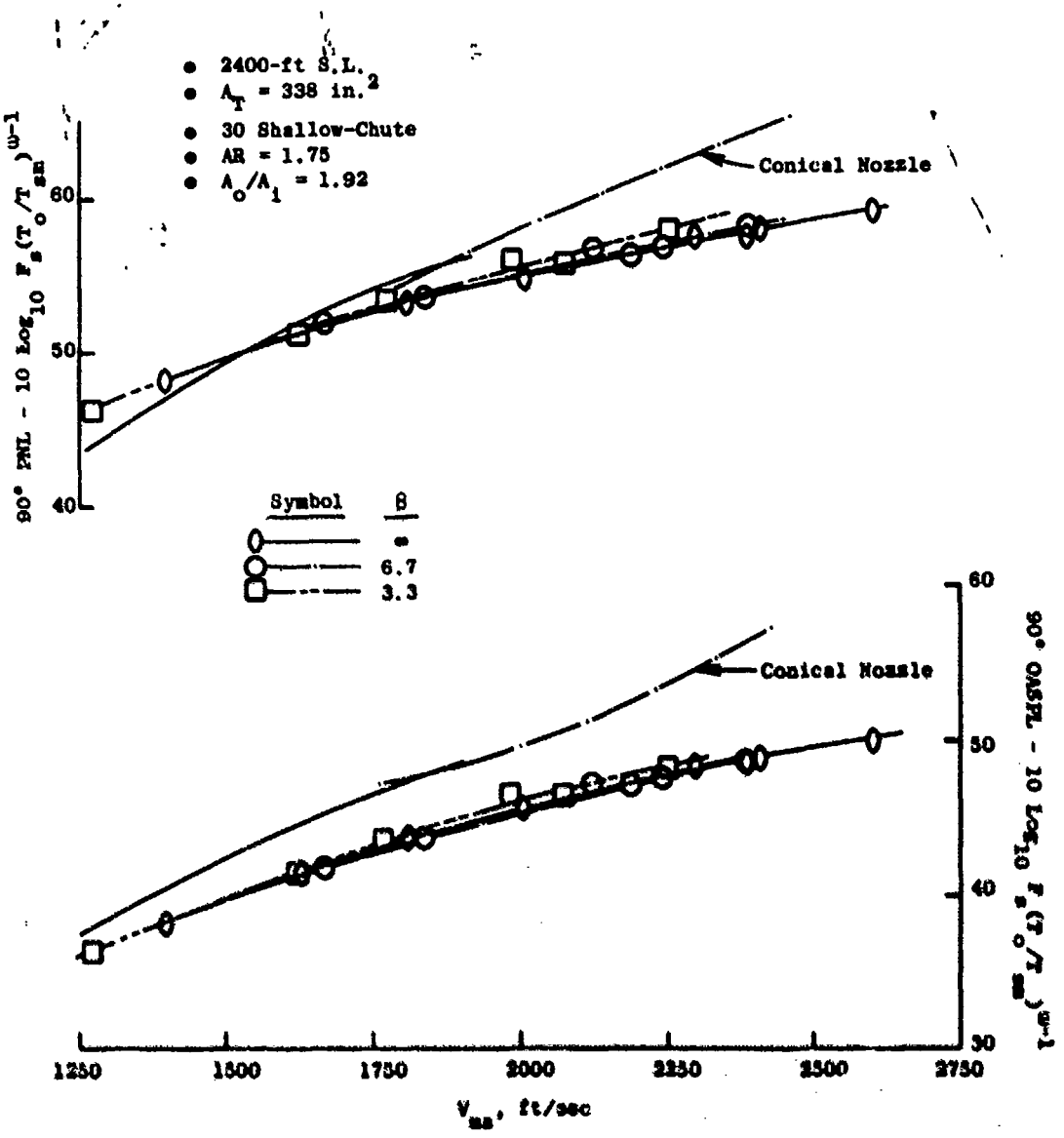

Figure 3-168. 90° PNL and OASPL Variation with β, Model 31.

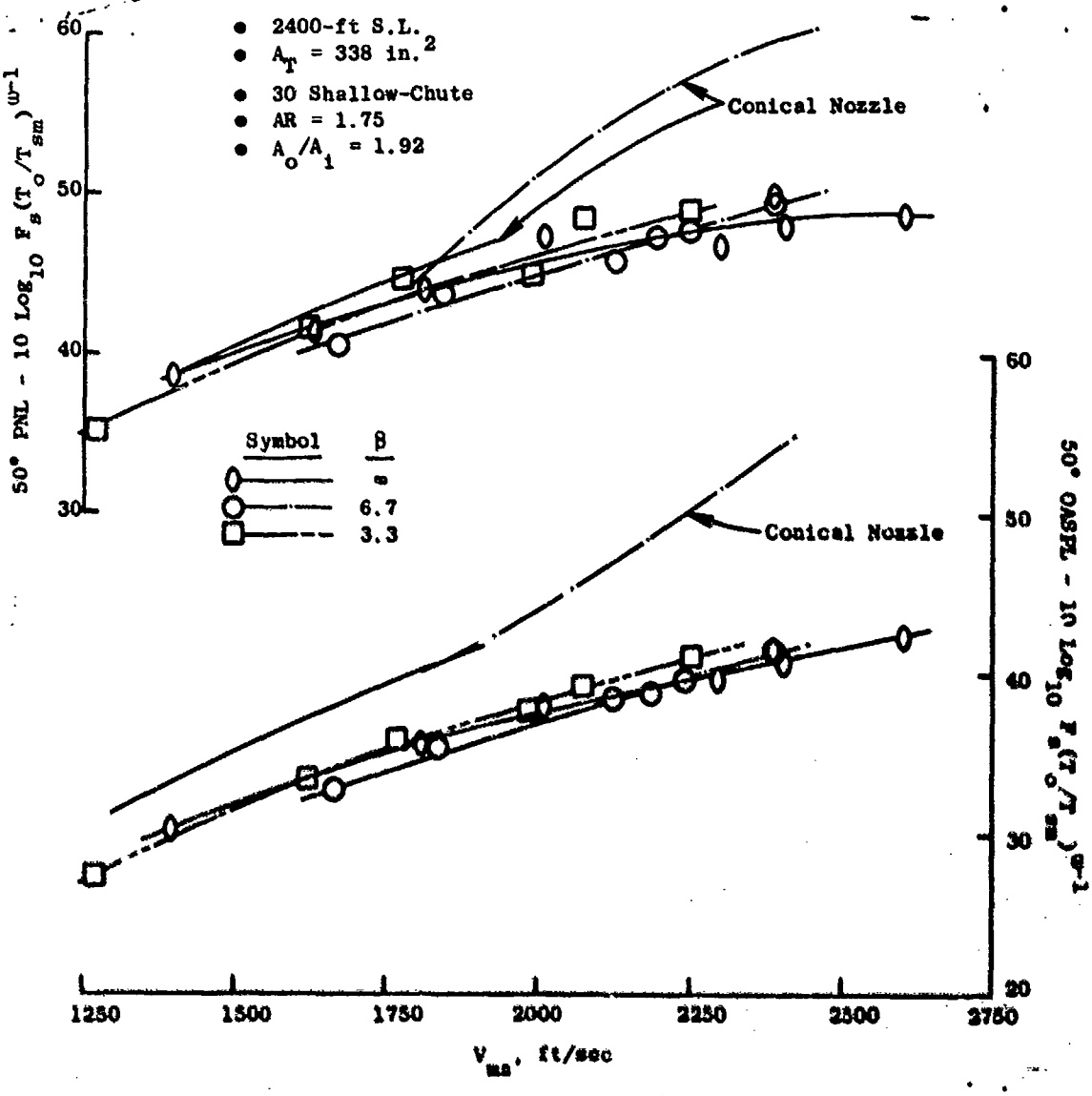

Figure 3-169. 50° PNL and OASPL Variation with β, Model 31.

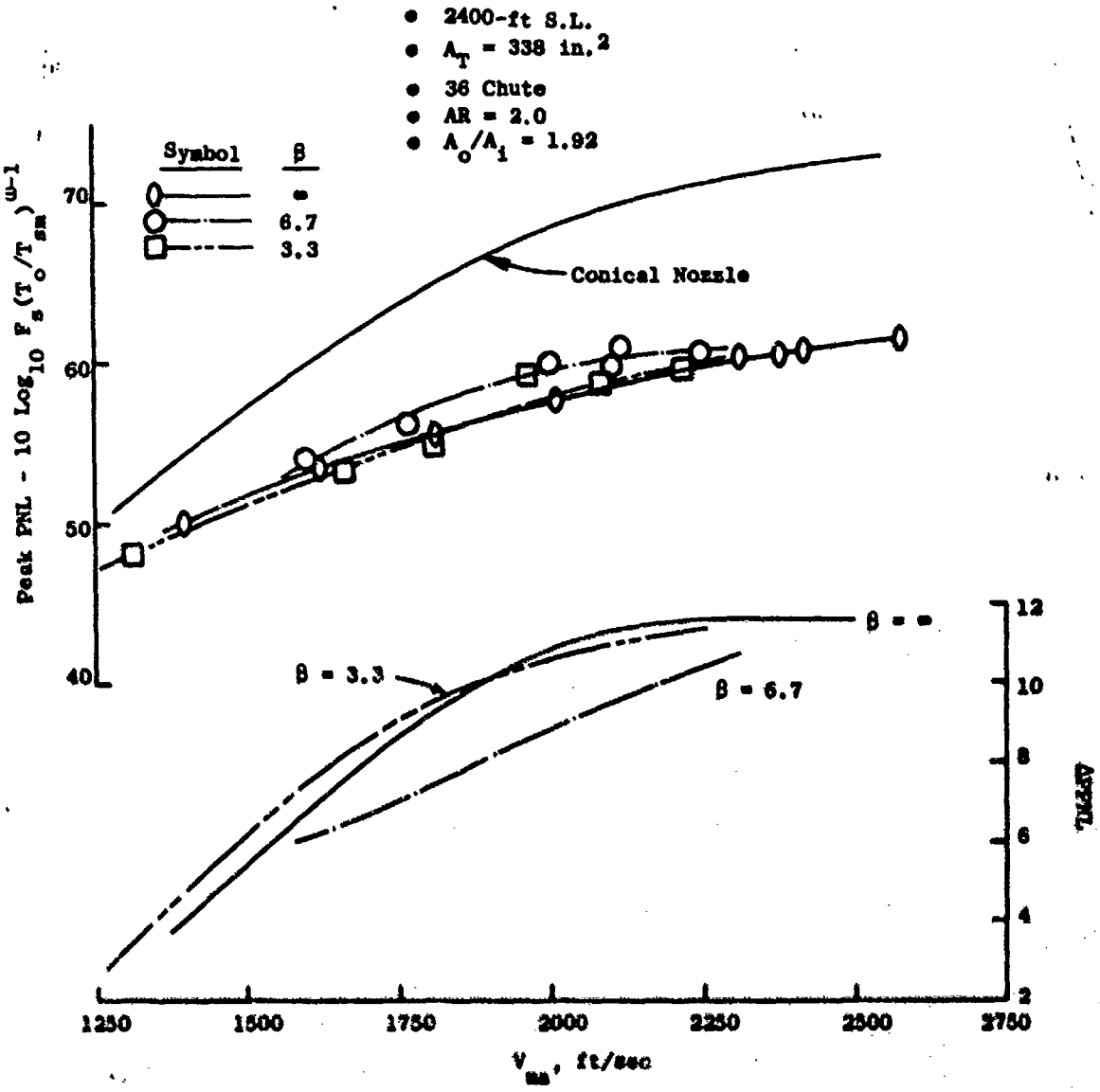

Figure 3-170. Peak PNL Variation with β, Model 23.

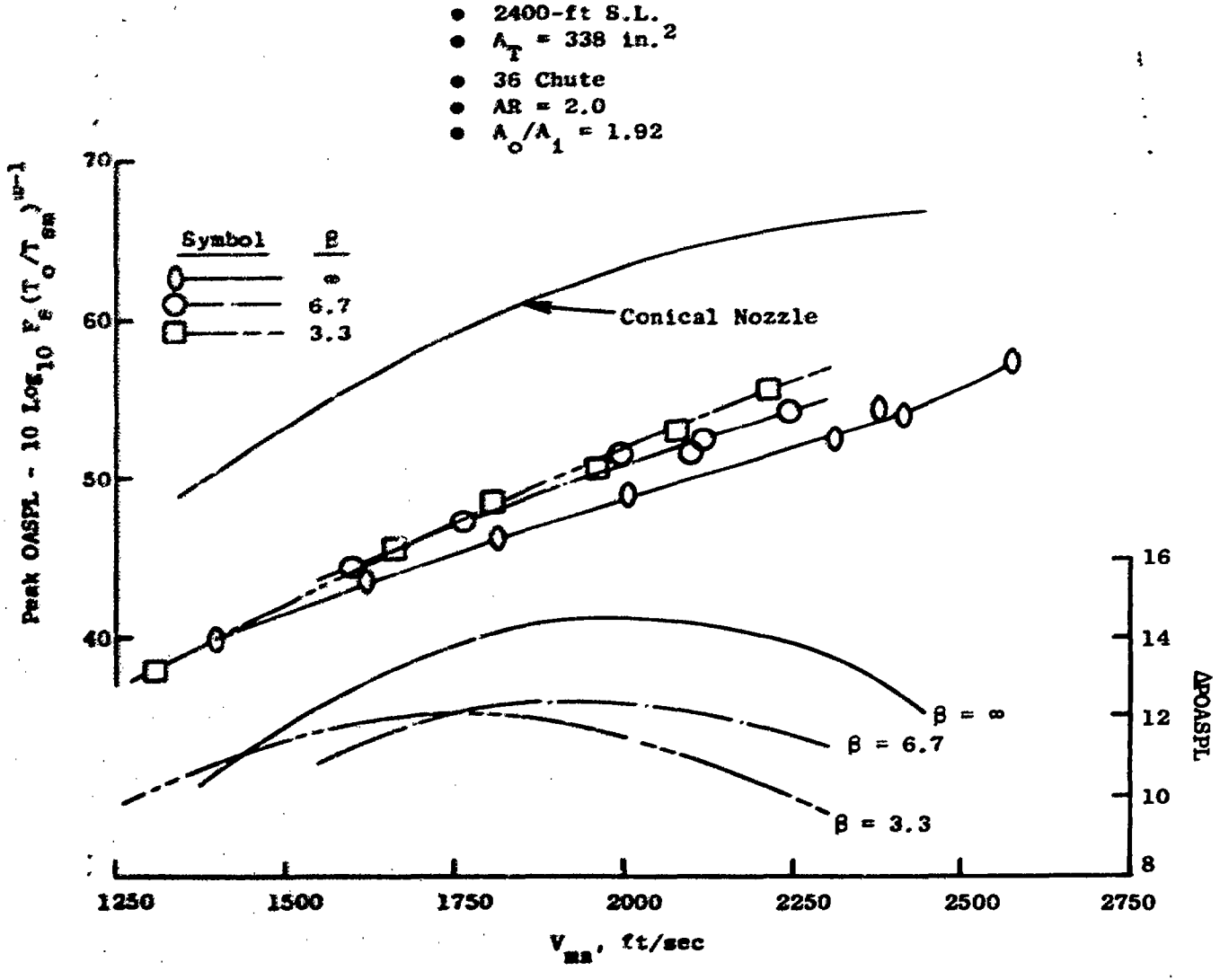

Figure 3-171. Peak OASPL Variation with β - Model 23.

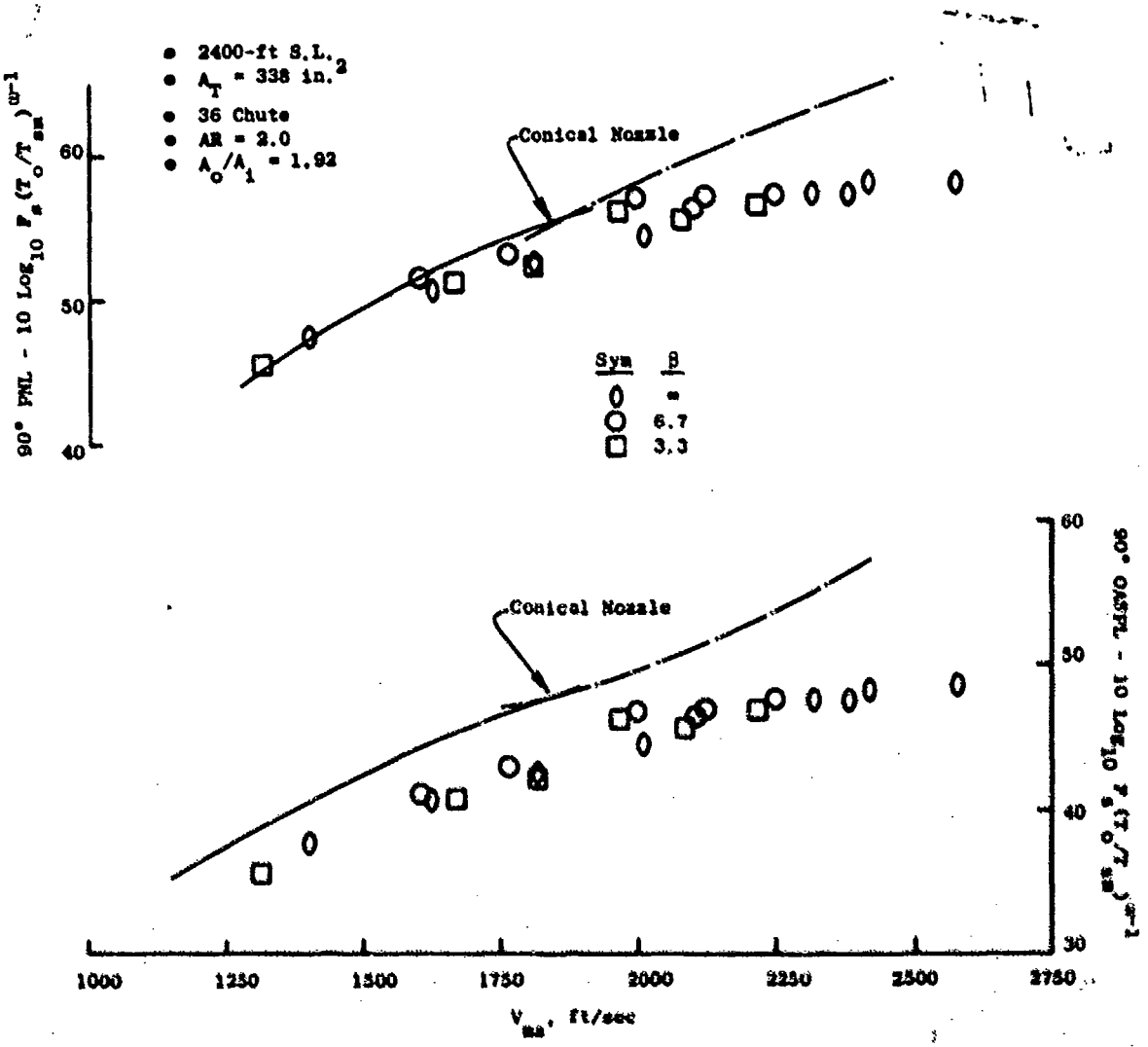

Figure 3-172. 90° PNL and OASPL Variation with β, Model 23.

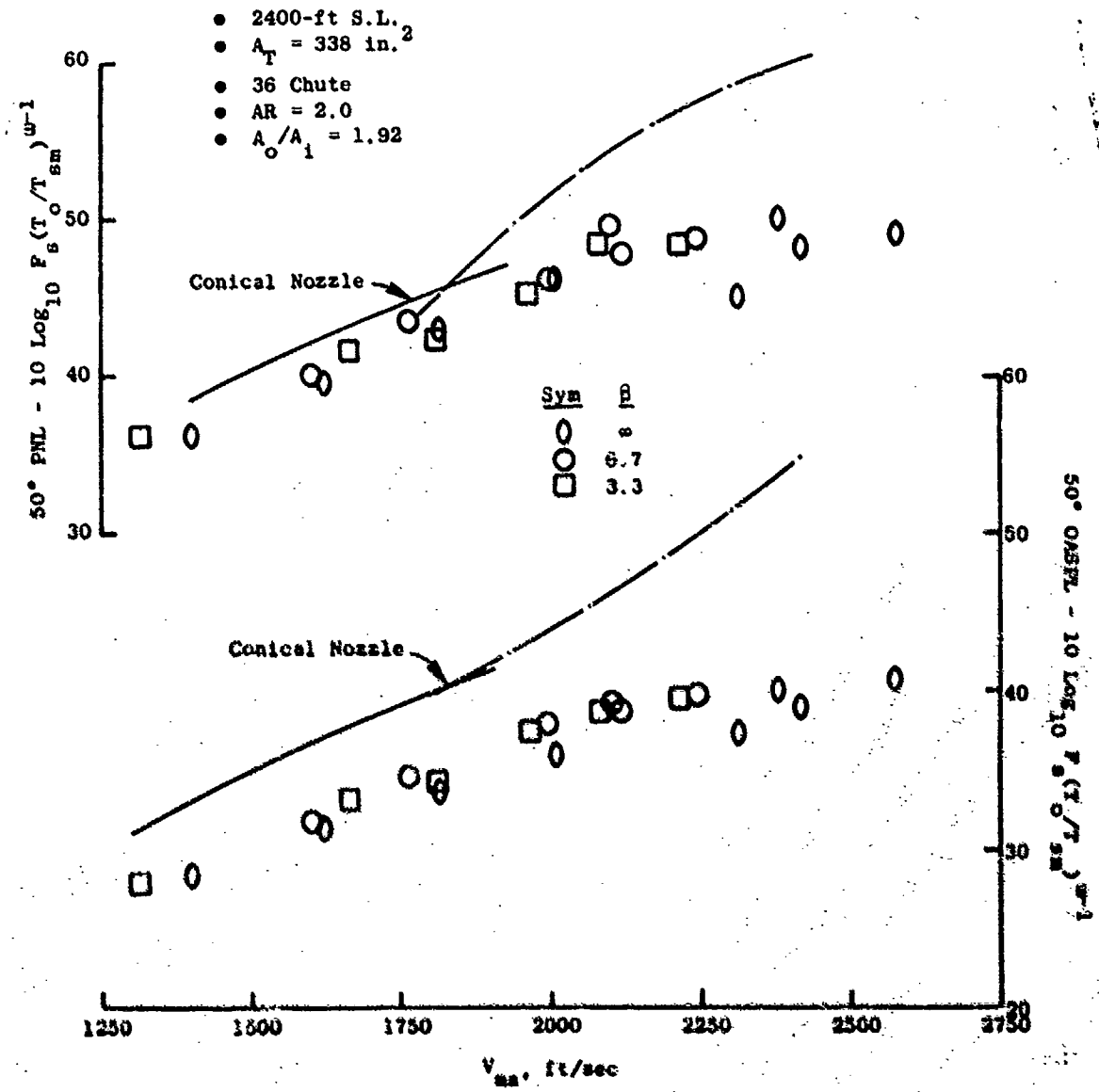

Figure 3-173. 50° PNL and OASPL Variation with β, Model 23.

ations range from 1 to 14. Therefore, flow and velocity dominance is always in the outer suppressed stream and inner stream flow and velocity are always minor on a thrust contribution basis. The resultant systematic changes in noise as β progress from 3.3 to 6.7 to ∞ are judged to be attributable to flow interaction mechanisms rather than pure inner/outer flow dominance.

- At 90° the β influence on PNL and OASPL is almost as strong and consistent as at peak angle for the A_o/A_i = 0.65 systems, but is configuration dependent for the A_o/A_i = 1.92 systems. Little variance is seen for Model 31, whereas the 90° data for Model 23 still shows considerable variance, but it is not progressively systematic.

- 50° data trends are quite similar to those at 90° and are configuration dependent. The A_o/A_i = 0.65 systems still exhibit distinct and progressive variance with β changes and the A_o/A_i = 1.92 Model 23 data again shows non-systematic variance. The Model 31 data however, show some magnitude of systematic variance, similar to that of the peak noise levels.

- Examination of the model definition table above and the detailed schematics of Appendix A shows that for Models 31 and 23, the area ratios were equivalent. However, Model 31 had a retracted inner geometry, similar to that of the A_o/A_i = 0.65 systems, and Model 23 had an in-line inner flow plug geometry. This difference may explain the variations in data seen between Models 31 and 23 and the closer match of Model 31's trends to those of the A_o/A_i = 0.65 systems.

<u>System Area Ratio and Inner Stream Plug Geometry Variation - Fixed Outer Stream Suppressor Geometry</u>

The last of the three studies supporting the impact of Flow Management/ Core Geometry considerations on noise was a controlled effort to isolate the effects of system area ratio and inner stream plug geometry. Each of these parameters was varied within the practical range for a variable cycle engine system. Six models were used, per the following chart:

		Outer Stream				Inner Stream				
Model No.	System A_o/A_i	Element Description	AR	R_p^o	Flow Area, $In.^2$	Step Height In.	Plug Location	R_p^i	Flow Area, $In.^2$	Appendix A Figure Reference
23	1.92	36-Chute	2.0	0.716	23.76	0.70	In-Line	0.779	12.39	17
24	1.92	36-Chute	2.0	0.716	23.76	0.70	Retracted	0.779	12.39	18
25	3.61	36-Chute	2.0	0.716	23.76	0.35	In-Line	0.89	6.58	19
26	3.61	36-Chute	2.0	0.716	23.76	0.35	Retracted	0.89	6.58	20
28	1.92	36-Spoke	2.0	0.716	23.76	0.70	Retracted	0.779	12.39	22
29	1.92	36-Spoke	2.0	0.716	23.76	0.70	In-Line	0.779	12.39	23

Photos of Models 23 through 26 are included in Figure 3-174. Figure 3-175 shows Models 28 and 29. The last column of the above chart refers to the detailed sketches of each model shown in Appendix A.

Variations of system area ratio and inner stream plug geometry were accomplished by using interchangeable modular inner stream hardware, schematically shown in Figure 3-176. An inner stream plug allowing 0.70" annulus height (schematics a and b), resulted in an inner flow area of 12.39 in.^{2} This, combined with the outer flow area of 23.76 in.^{2}, effected an A_o/A_i of 1.92. Using the 0.35" annulus height inner stream plug changed the inner flow area to 6.58 in.^{2} and the A_o/A_i to 3.61 (schematics c and d). In-Line inner stream plug geometry (schematics a and c) was altered to retracted, (schematics b and d) through removal of a support spacer.

As shown in the above table, two basic annular suppressors were used (36-chute and 36-spoke), each of AR = 2.0 and R_F = 0.716. Within model sets 23/25 and 24/26, system area ratio, A_o/A_i, varied from 1.92 to 3.61. The first set utilized an in-line plug, and the second set utilized a retracted plug geometry. Comparisons for inner stream geometry variations were made using model sets 23/24, 25/26 and 28/29 (the first and second sets with the 36-chute suppressor at A_o/A_i = 1.92 and 3.61, respectively, and the third set with the 36-spoke suppressor of A_o/A_i = 1.92).

The six models were tested in the Cell 41 Anechoic Facility per the matrix of Section 3.2.1, Figure 3-10 and Table 3-3, utilizing the cycle lines of:

- W_i = 15 and 30% W_o
- DBTF/Inverted Dual Flow
- AST/VCE

Data in terms of peak, 90° and 50° (PNL and OASPL) are presented in the following figures, normalized per Section 3.3.1.7 and plotted versus V_{ms}:

Model	W_i = 15% W_o	W_i = 30% W_o	DBTF/Inv. Dual Flow
23, 24, 25 & 26	3-177 to 3-180	3-181 to 3-184	3-185 to 3-188
28 and 29			3-189 to 3-191

Comparing the model sets for system area ratio variation (Models 23/25 and 24/26), the following observations are noted:

- Peak PNL for all three data cycle sets indicate that A_o/A_i = 3.61 is universally the better suppressor system, because a greater proportion of flow is passed through the segmented annular suppressor. Differences between Models 24 and 26, with retracted

- 36 Chute
- Area Ratio = 2.0
- Radius Ratio = 0.716

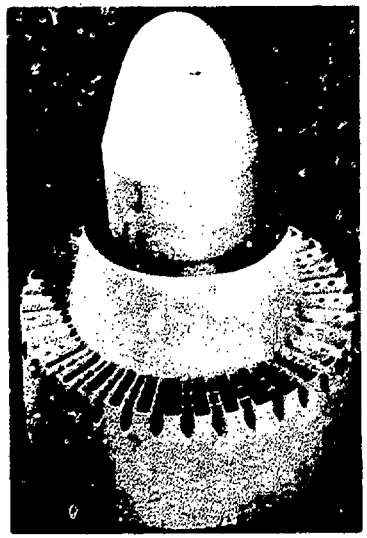

Model 23
In-Line Inner Plug
with 0.7-in. Step
A_o/A_i = 1.92

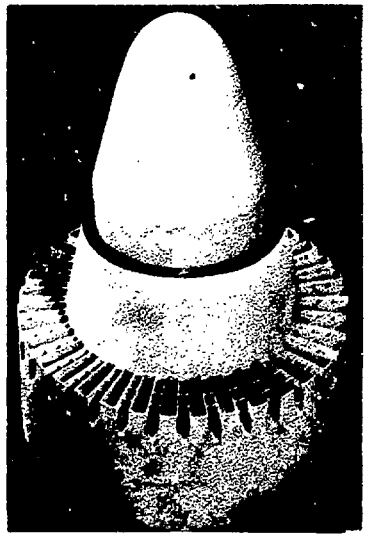

Model 25
In-Line Inner Plug
with 0.35-in. Step
A_o/A_i = 3.61

Model 24
Retracted Inner Plug
with 0.7-in. Step
A_o/A_i = 1.92

Model 26
Retracted Inner Plug
with 0.35-in. Step
A_o/A_i = 3.61

Figure 3-174. Dual Flow Models 23, 24, 25, and 26 for A_o/A_i and Inner Plug Geometry Variation.

- 36 Spoke
- Area Ratio = 2.0
- Radius Ratio = 0.716
- A_o/A_i = 1.92

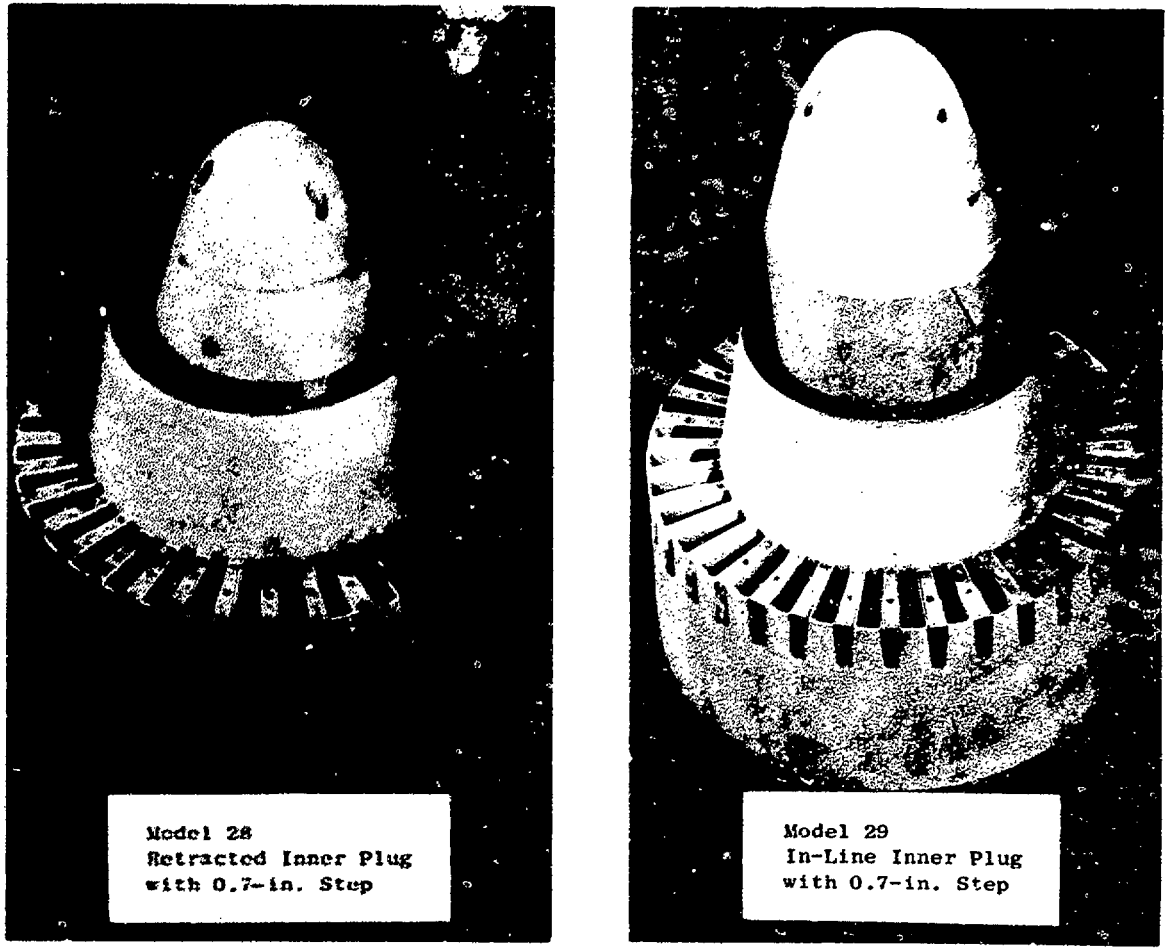

Figure 3-175. Dual Flow Models 28 and 29 for A_o/A_i and Inner Plug Geometry Variation.

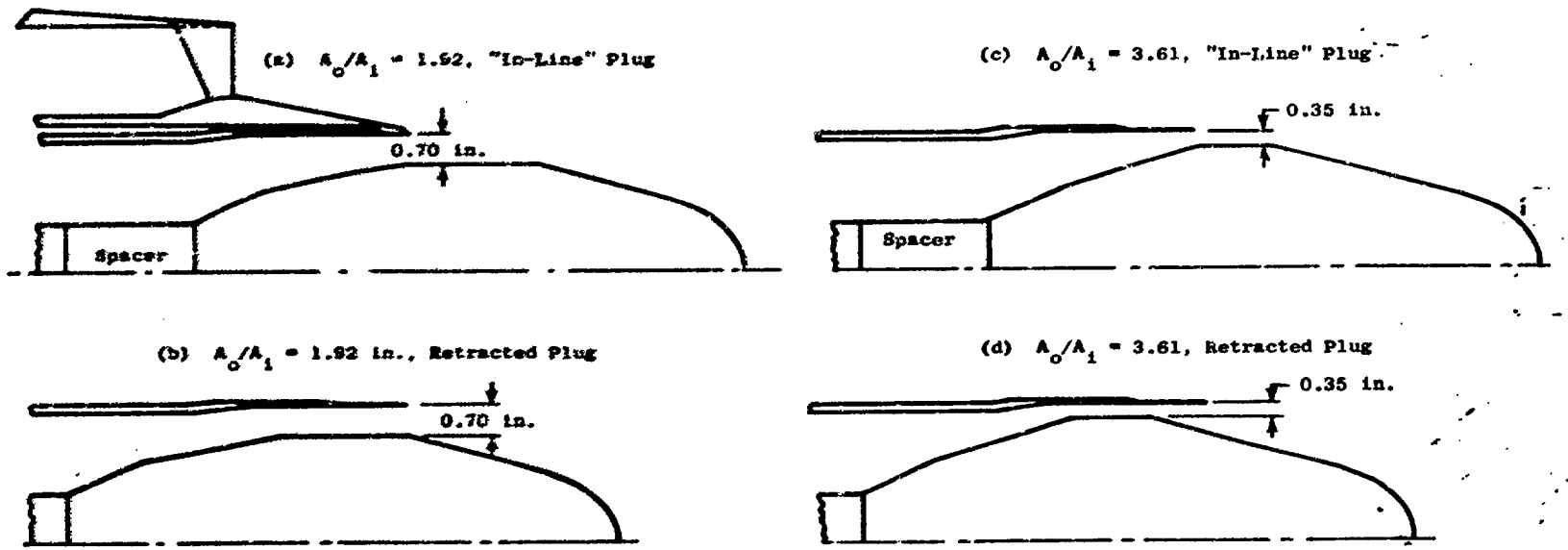

Figure 3-176. Schematic of Inner Plug Geometry Variations.

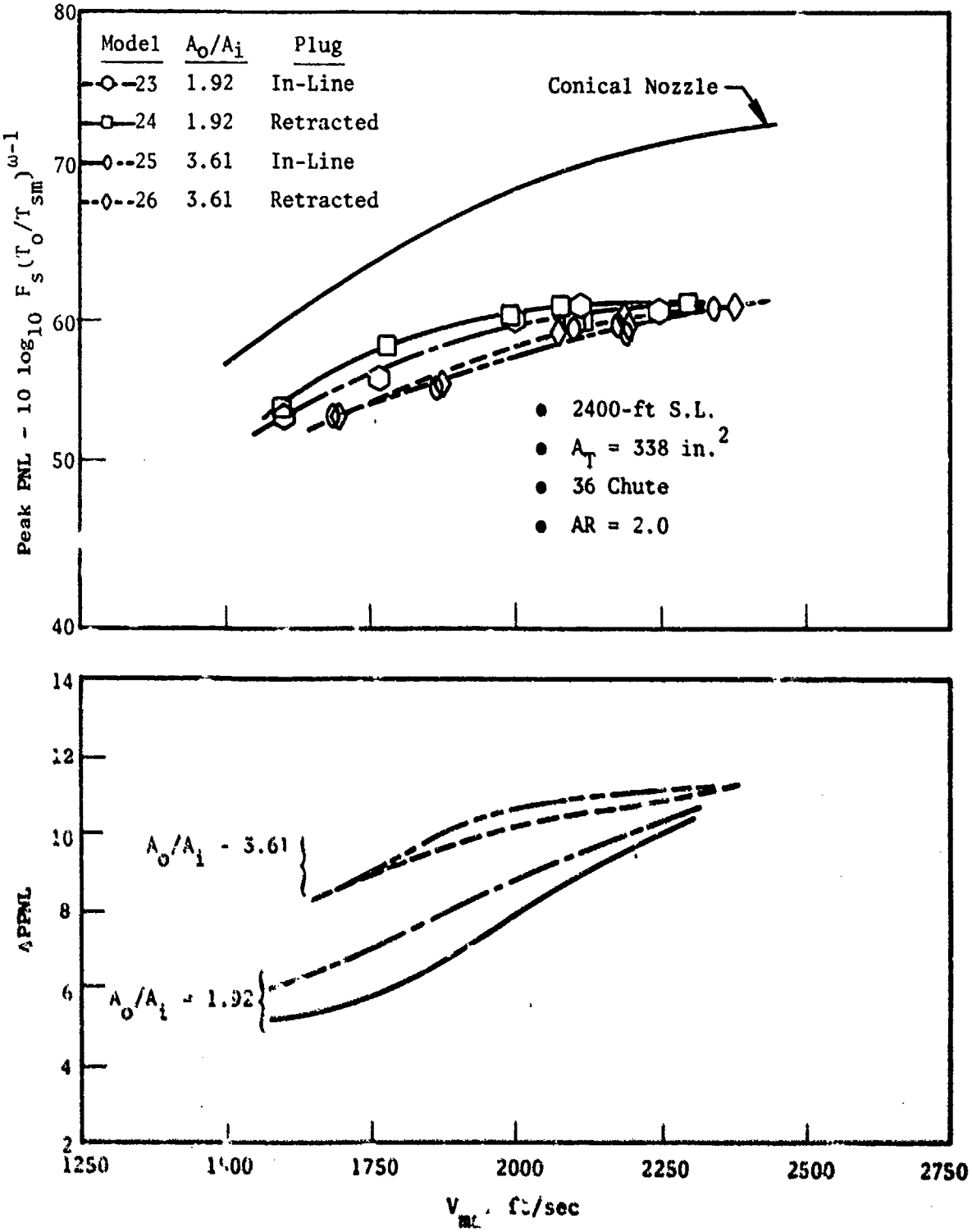

Figure 3-177. Peak PNL Variation with A_o/A_i and Inner Plug Geometry, Models 23 - 26, W_{Inner} = 15% W_{Outer} Cycle.

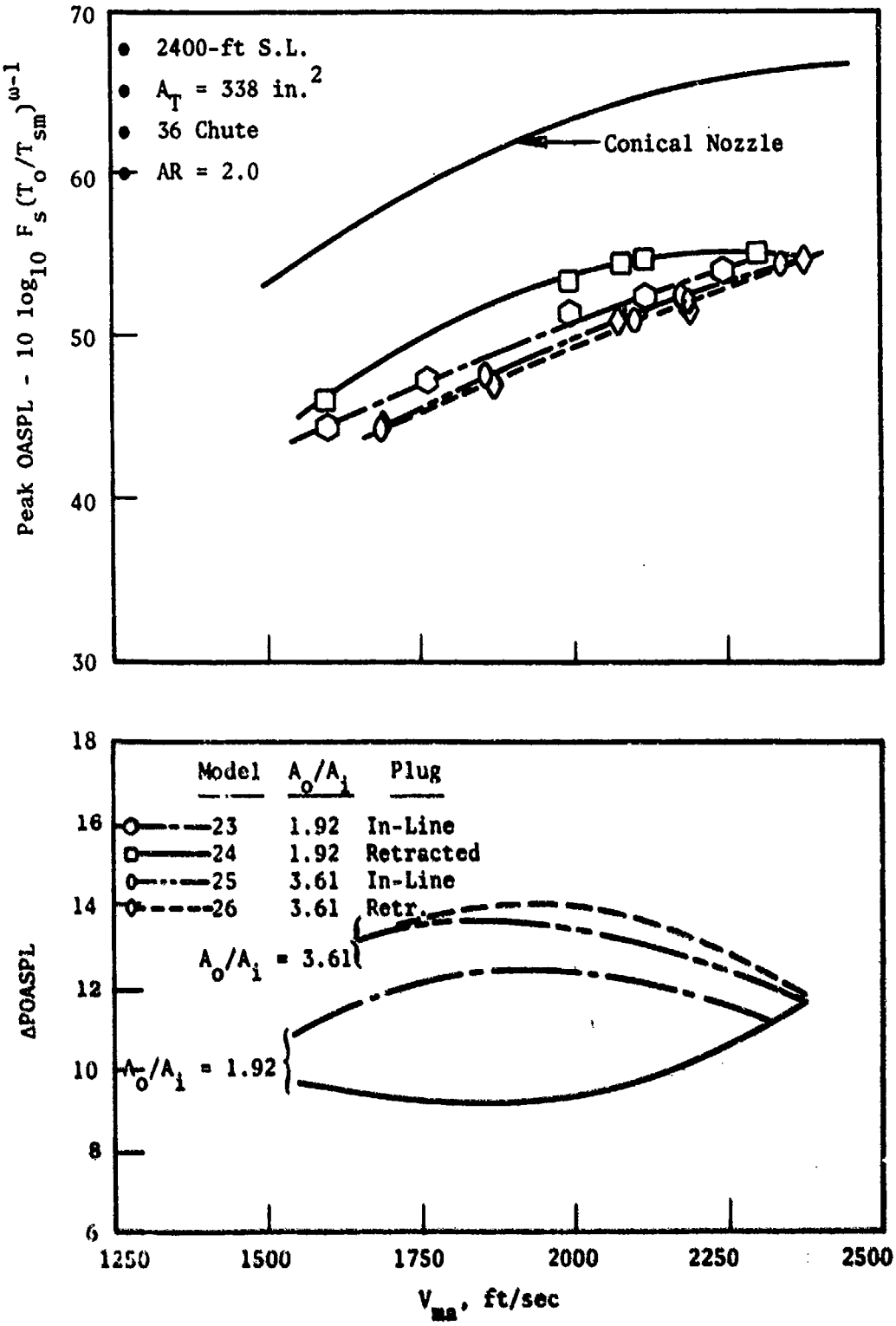

Figure 3-178. Peak OASPL Variation with A_o/A_i and Inner Plug Geometry, Models 23 - 26, W_{Inner} = 15% W_{Outer} Cycle.

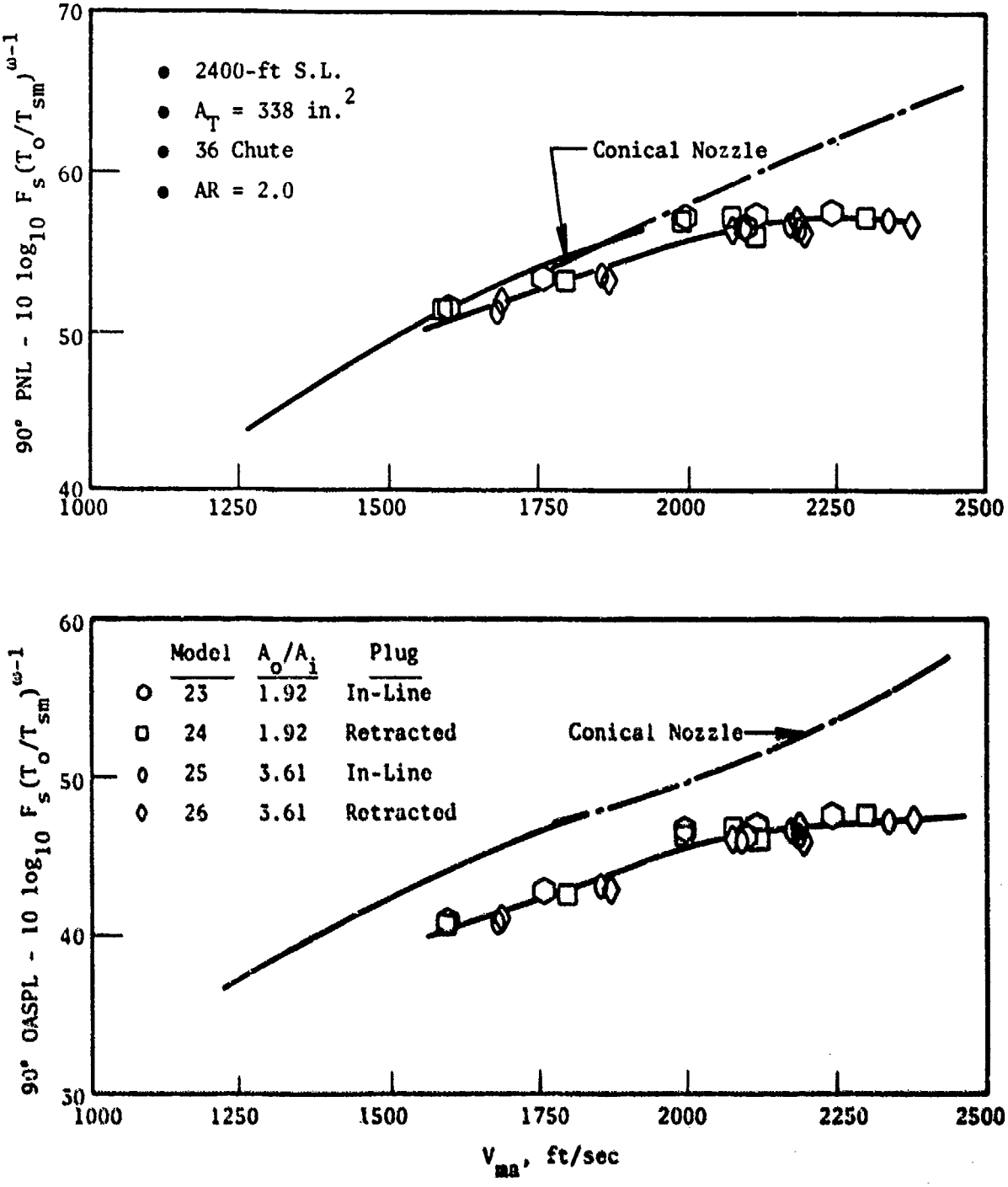

Figure 3-179. 90° PNL and OASPL Variation with A_o/A_i and Inner Plug Geometry, Models 23 - 26, $W_{Inner} = 15\% W_{Outer}$ Cycle.

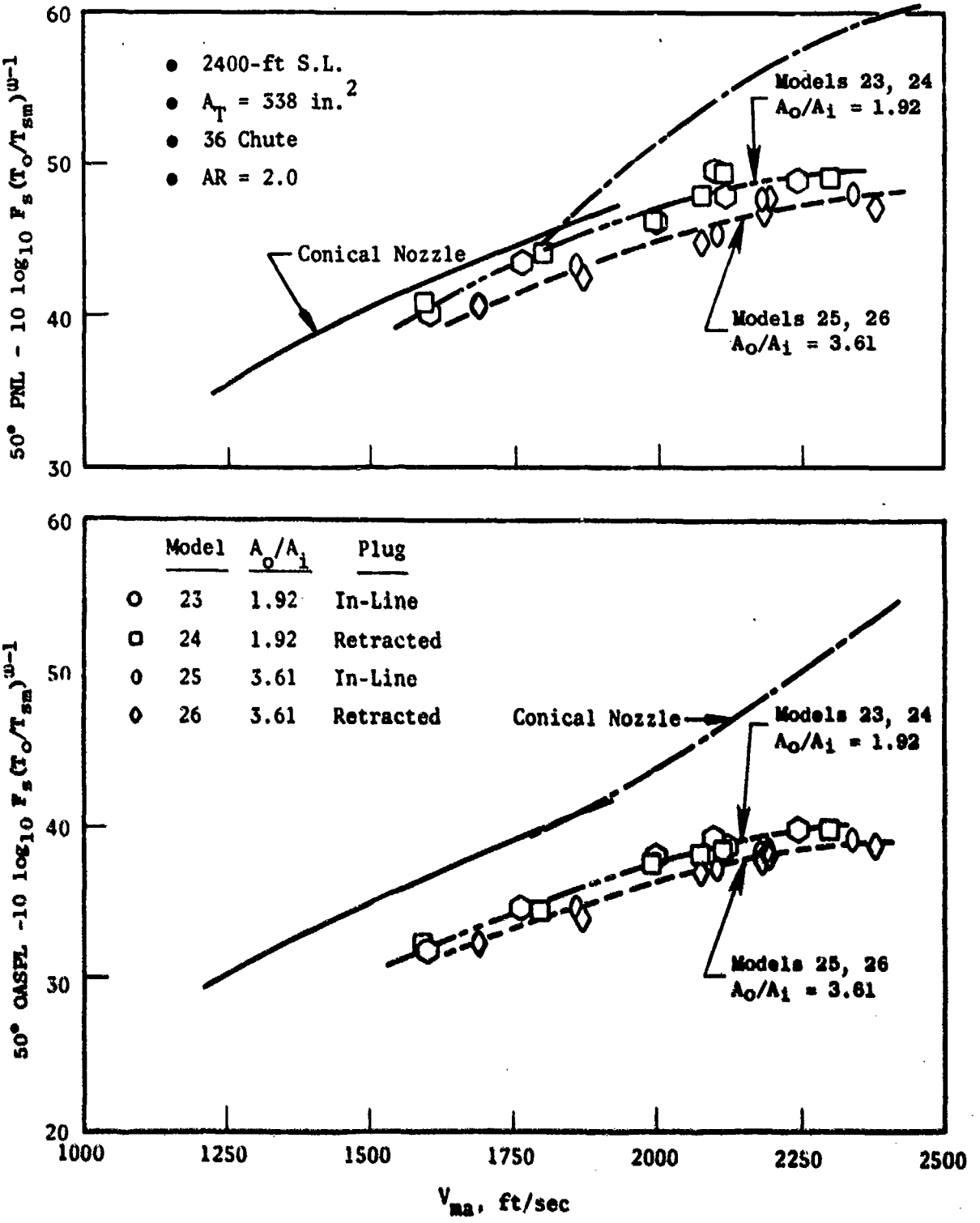

Figure 3-180. 50° PNL and OASPL Variation with A_o/A_i and Inner Plug Geometry, Models 23 - 26, W_{Inner} = 15% W_{Outer} Cycle.

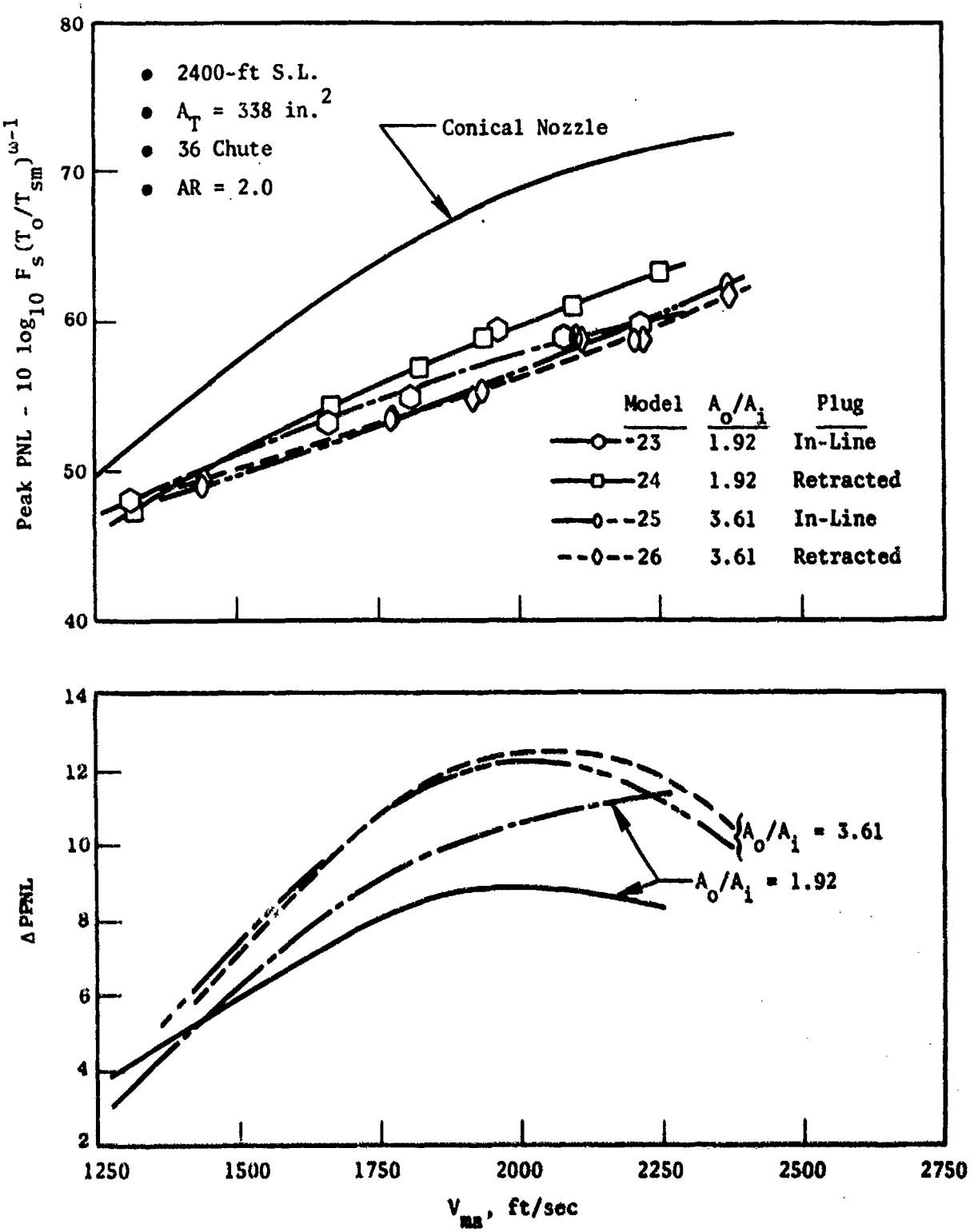

Figure 3-181. Peak PNL Variation with A_o/A_i and Inner Plug Geometry, Models 23 - 26, W_{Inner} = 30% W_{Outer} Cycle.

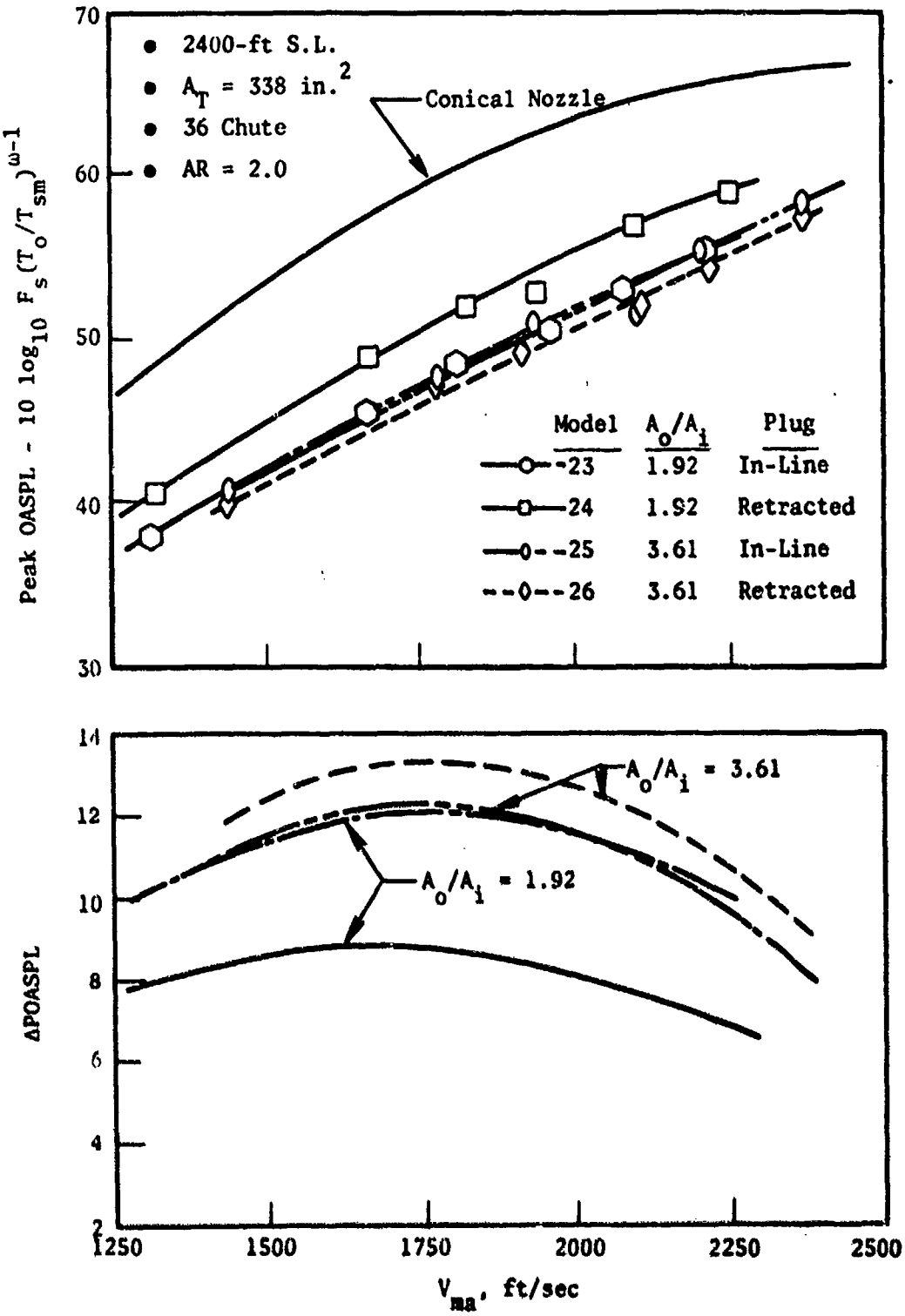

Figure 3-182. Peak OASPL Variation with A_O/A_i and Inner Plug Geometry, Models 23 - 26, W_{Inner} = 30% $W_{Outer\ Cycle}$.

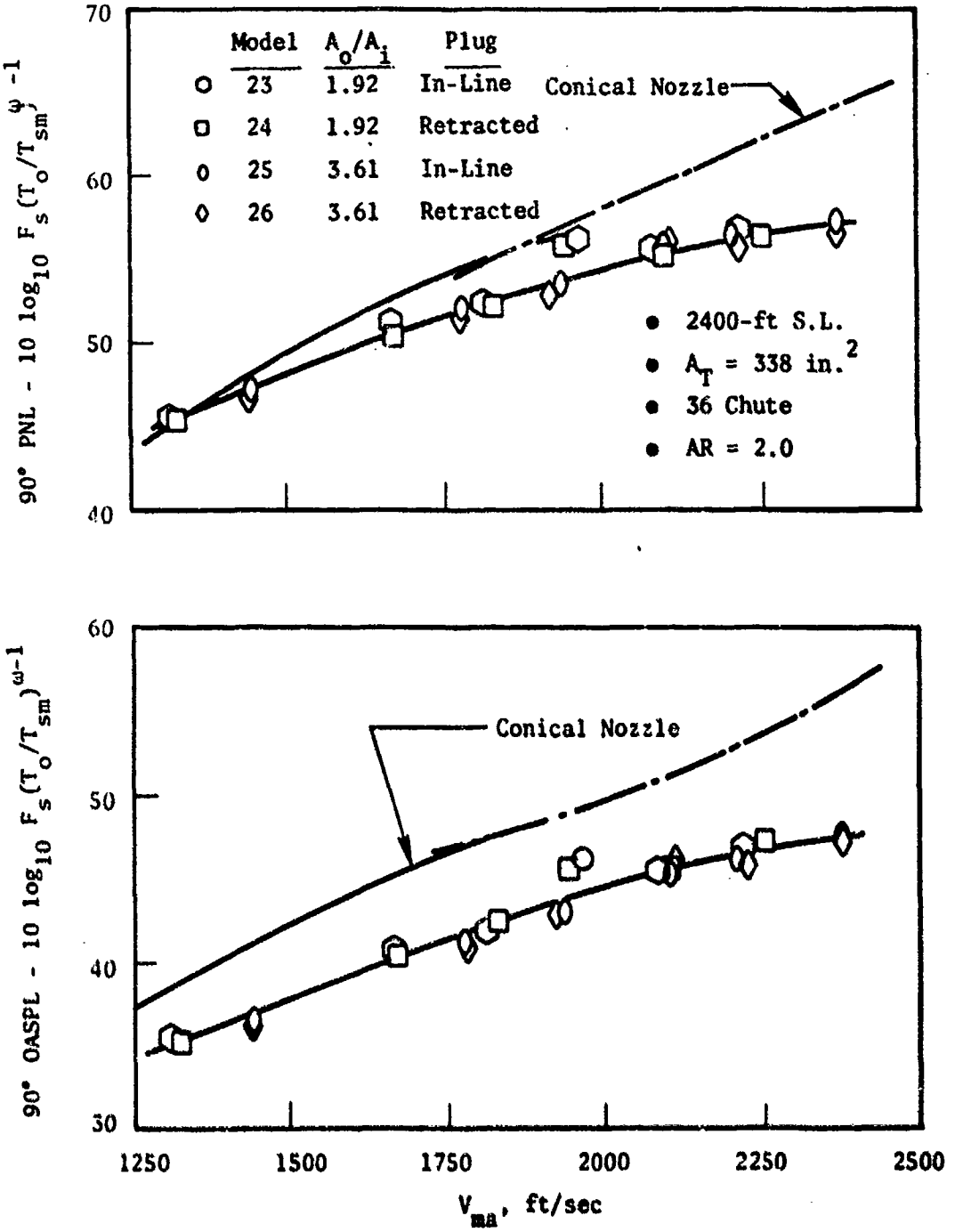

Figure 3-183. 90° PNL and OASPL Variation with A_o/A_i and Inner Plug Geometry, Models 23 - 26, W_{Inner} = 30% W_{Outer} Cycle.

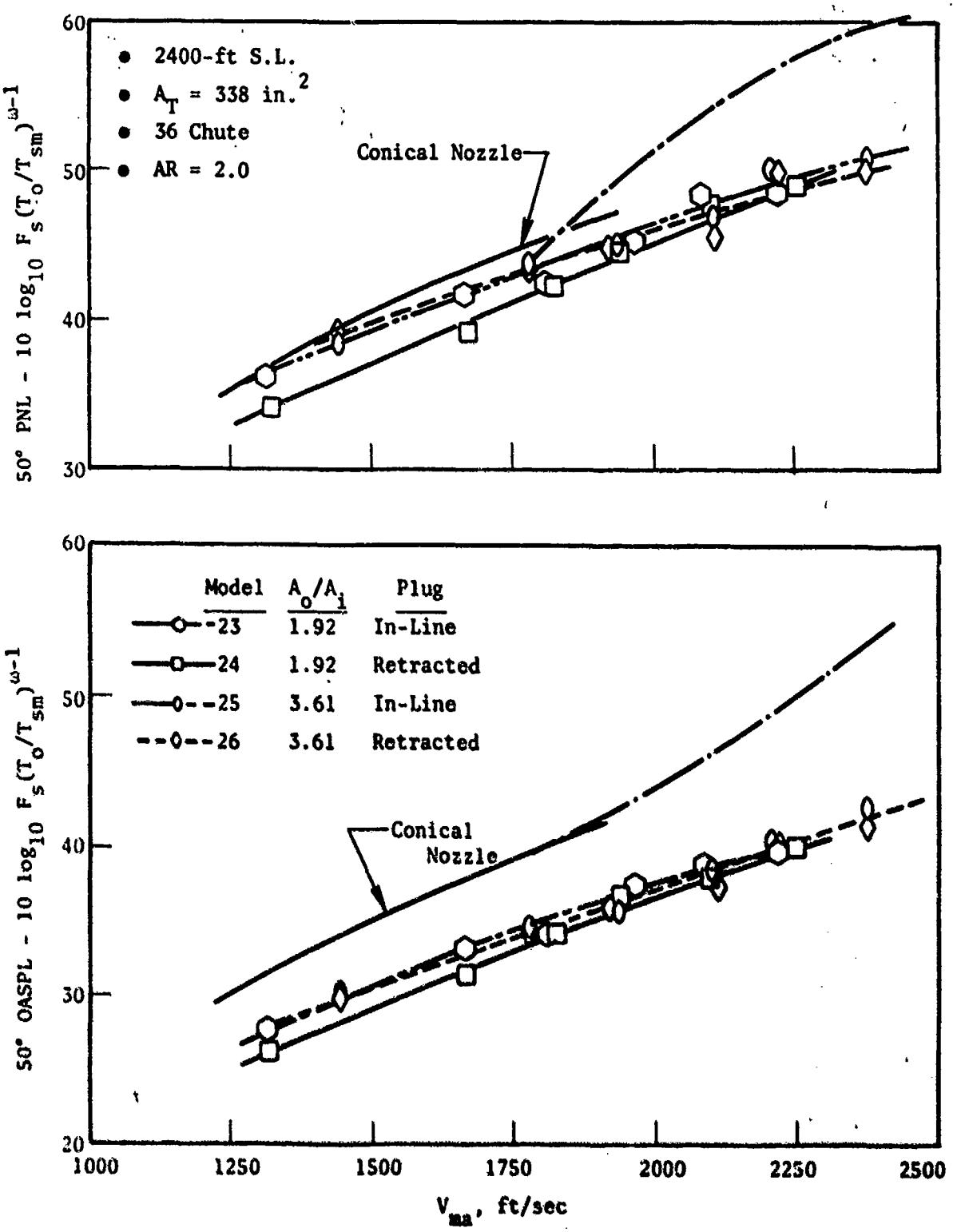

Figure 3-184. 50° PNL and OASPL Variation with A_o/A_i and Inner Plug Geometry, Models 23 - 26, $W_{Inner} = 30\% W_{Outer}$ Cycle.

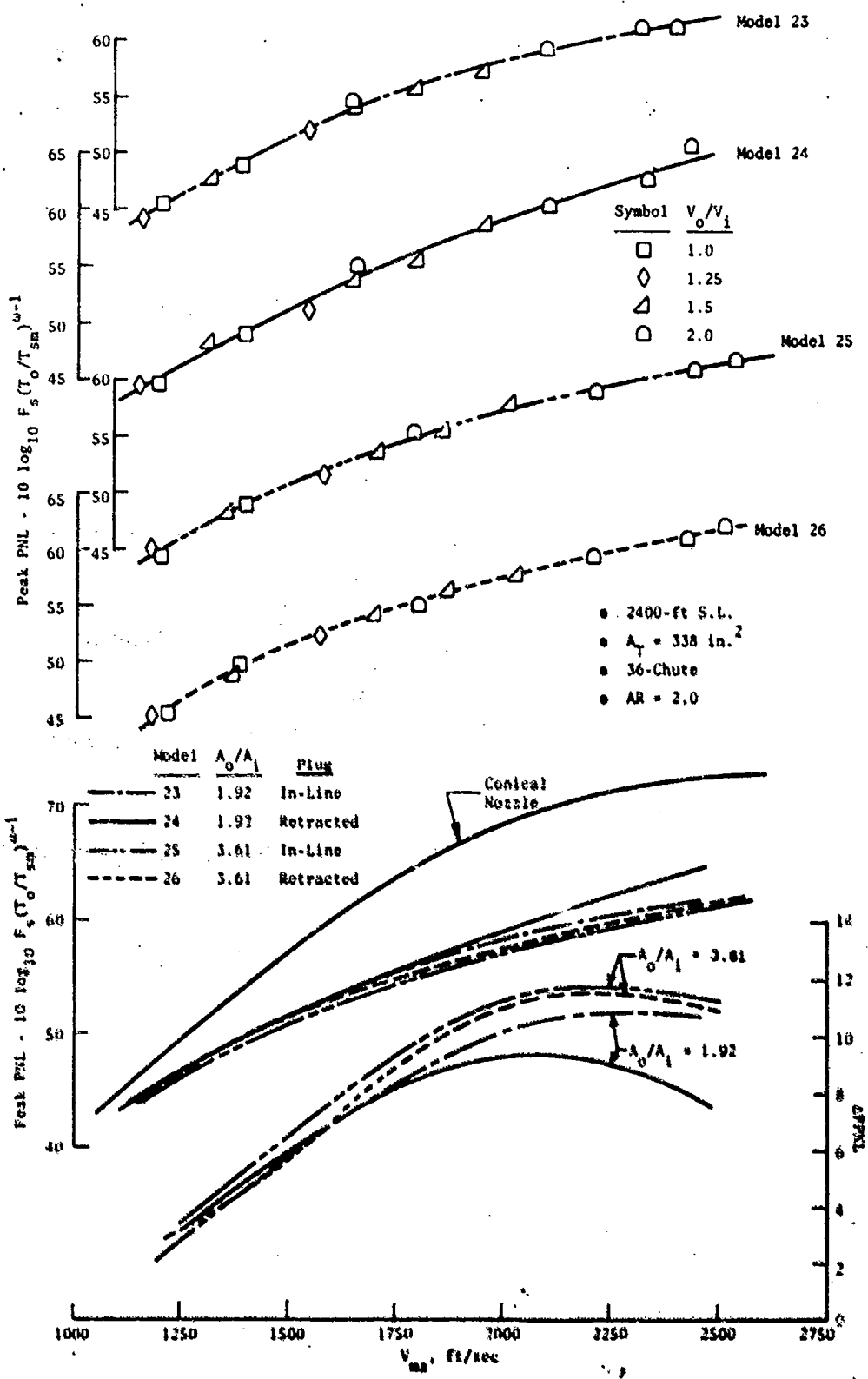

Figure 3-185. Peak PNL Variation with A_O/A_i and Inner Plug Geometry, Models 23-26, DBTF/Inverted Dual Flow Cycle.

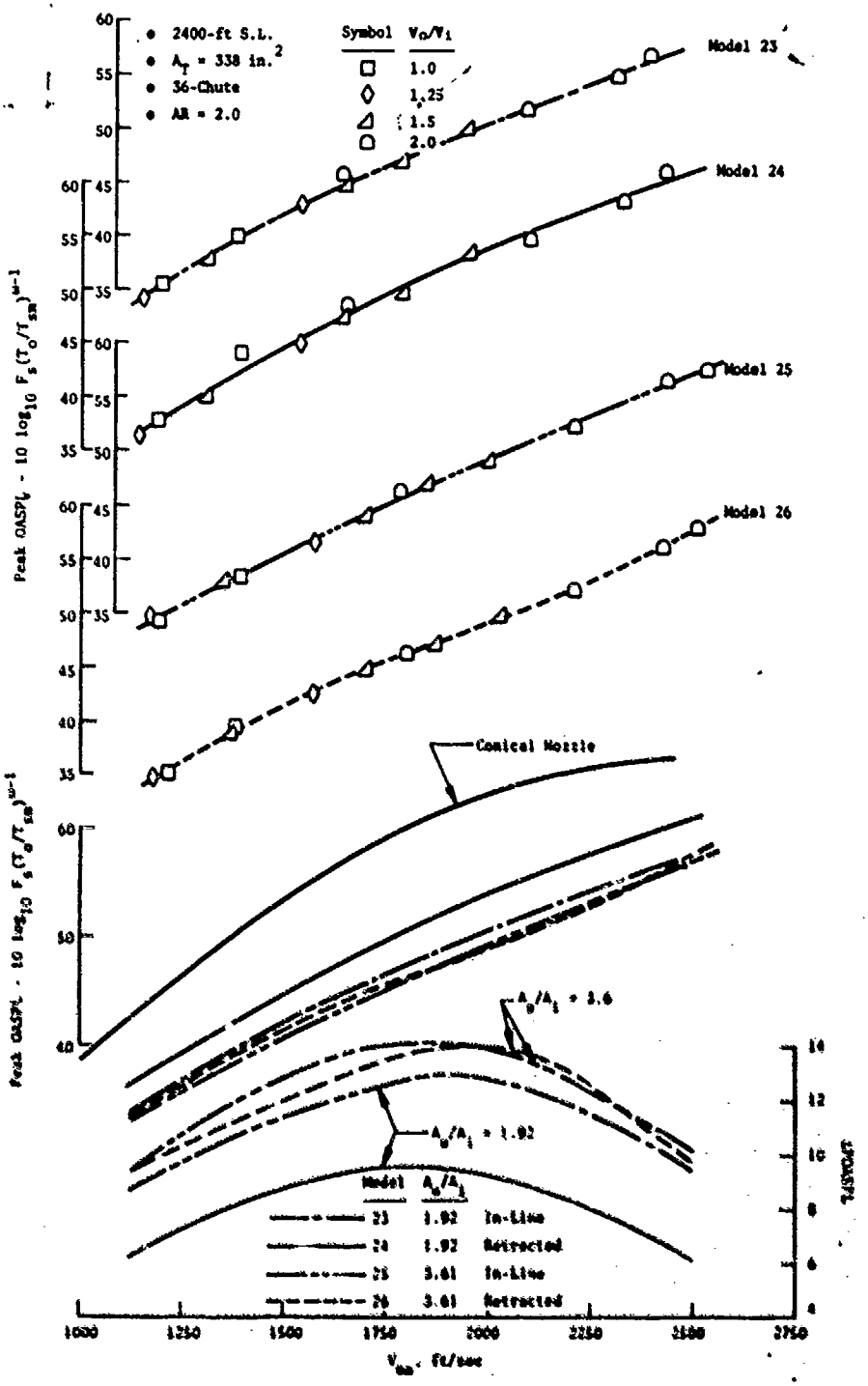

Figure 3-186. Peak OASPL Variation with A_o/A_i and Inner Plug Geometry, Models 23-26, DSTF/Inverted Dual Flow Cycle.

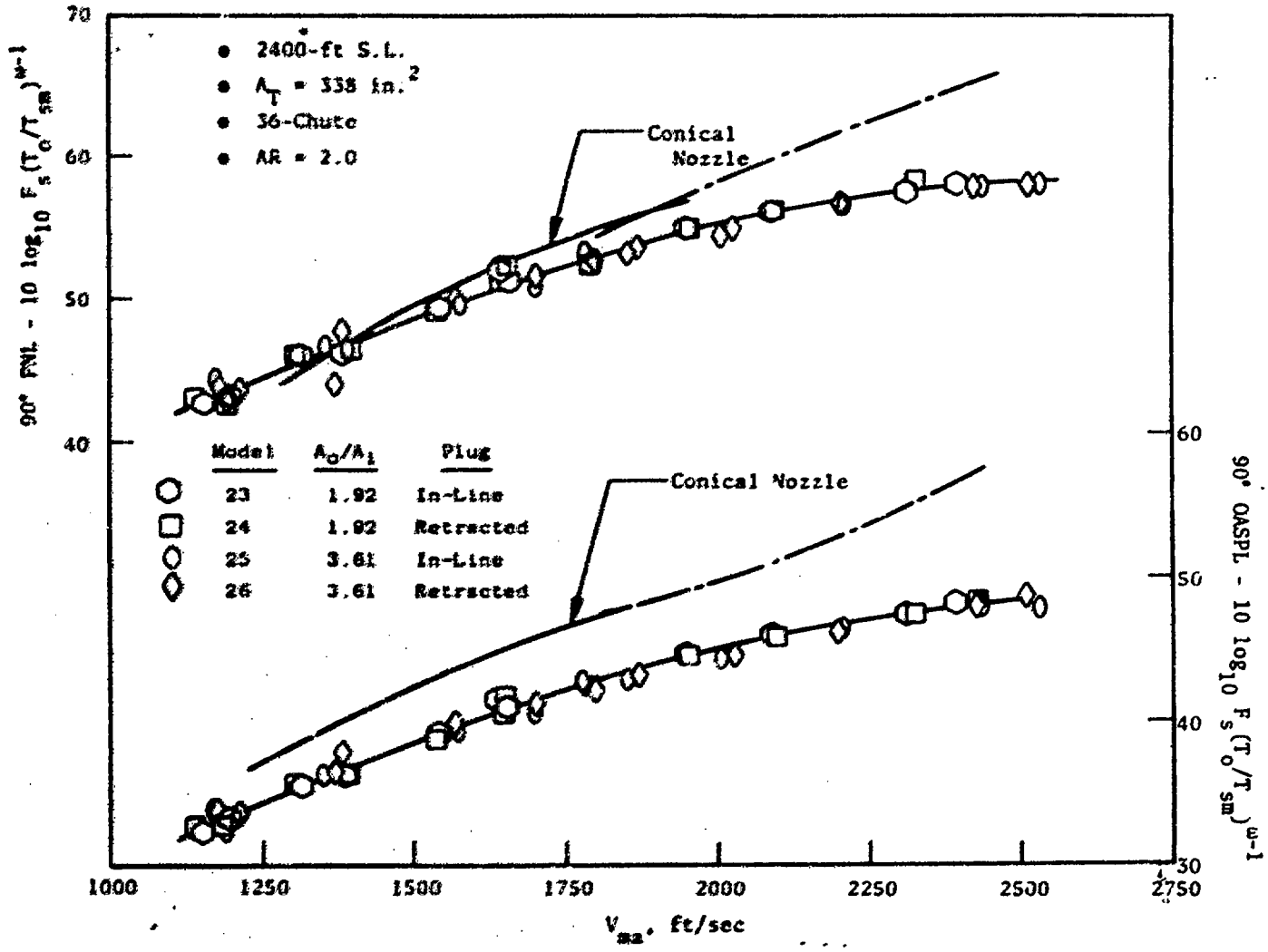

Figure 3-187. 90° PNL and OASPL Variation with A_o/A_i and Inner Plug Geometry, Models 23-26, DSTF/Inverted Dual Flow Cycle.

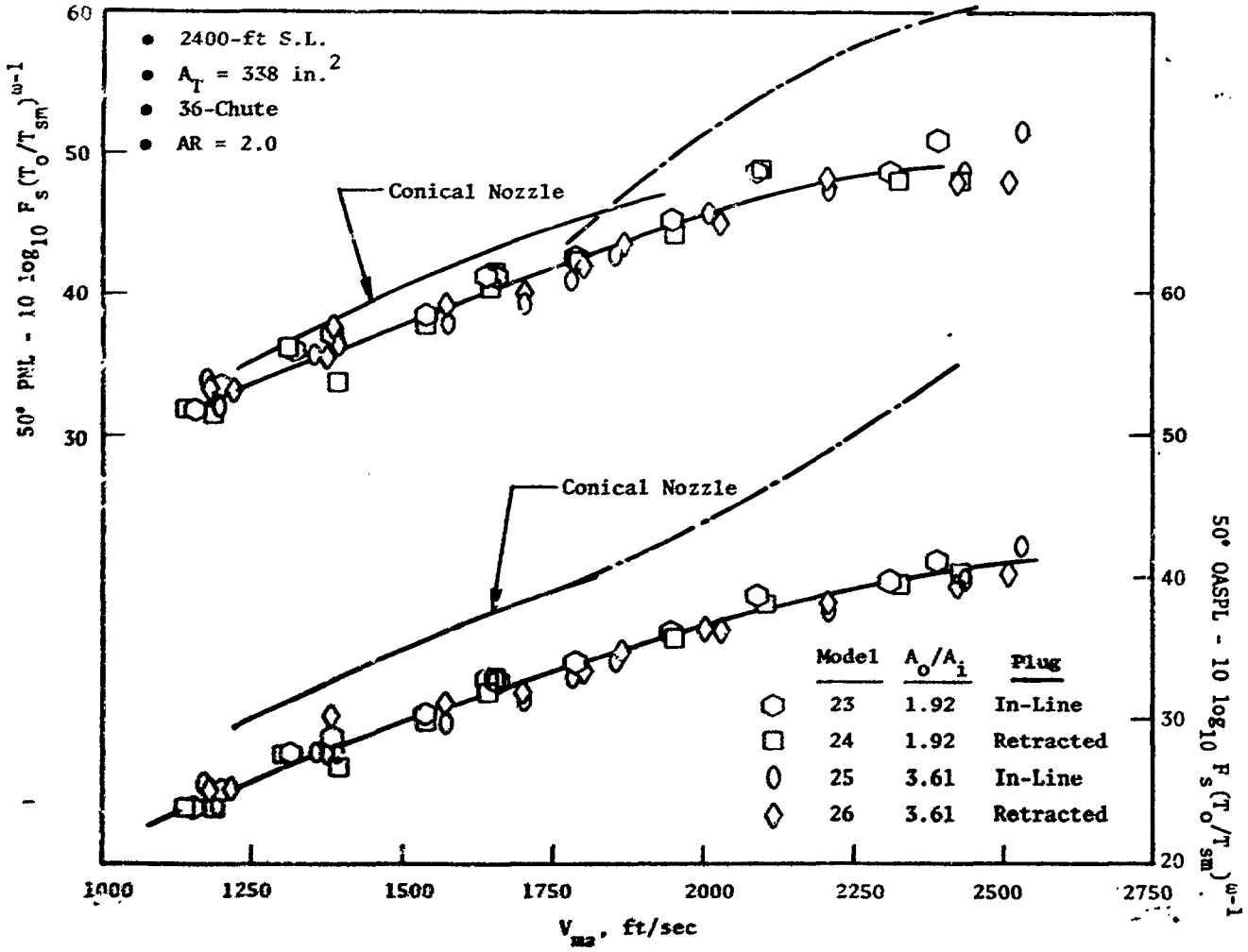

Figure 3-188. 50° PNL and OASPL Variation with A_o/A_i and Inner Plug Geometry, Models 23-26, DBTF/Inverted Dual Flow Cycle.

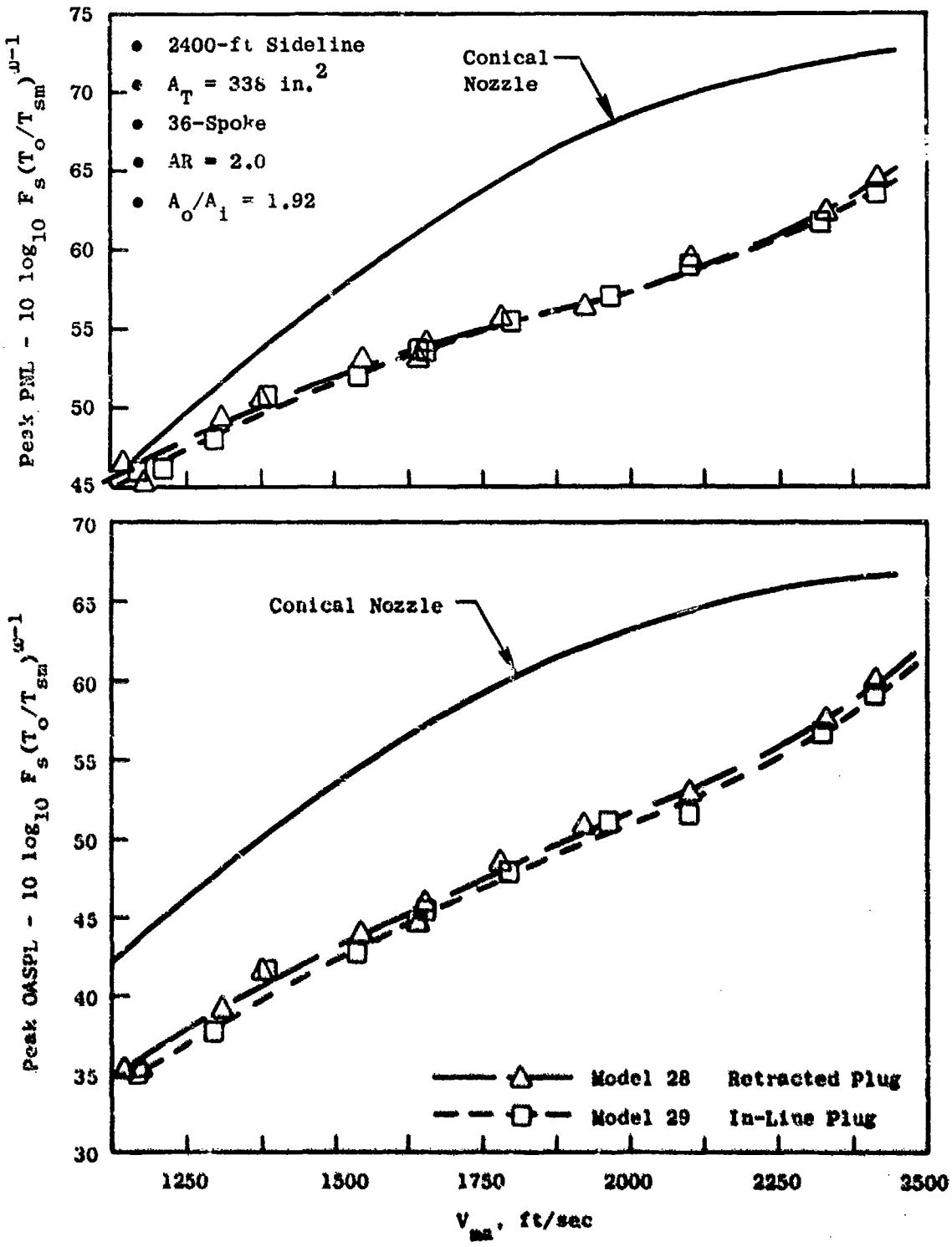

Figure 3-189. Peak PNL and OASPL Variation with Inner Plug Geometry, Models 28 and 29, DBTF/Inverted Dual Flow Nozzle.

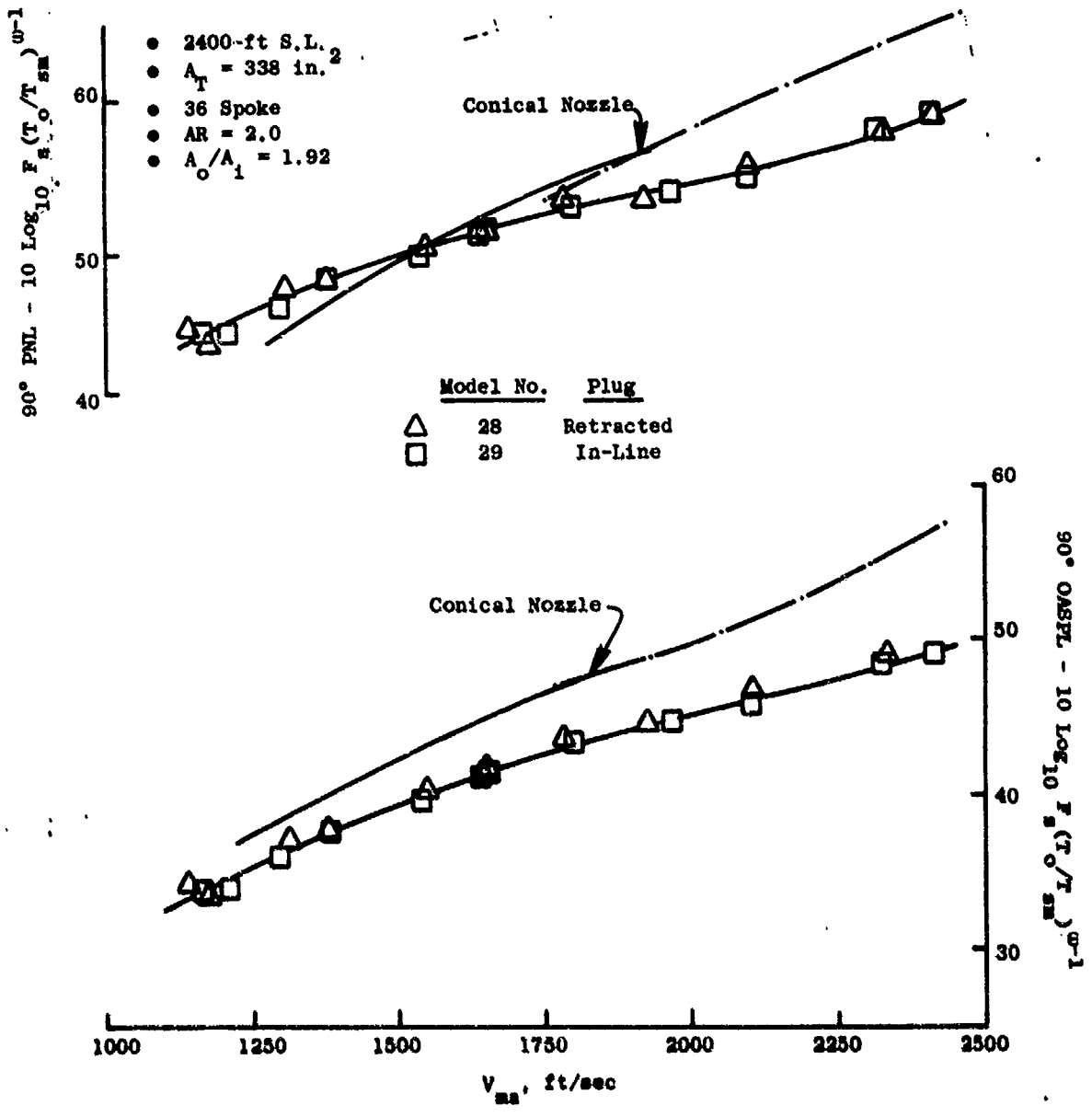

Figure 3-190. 90° PNL and OASPL Variation with Inner Plug Geometry, Models 28 and 29, DSTF/Inverted Dual Flow Cycle.

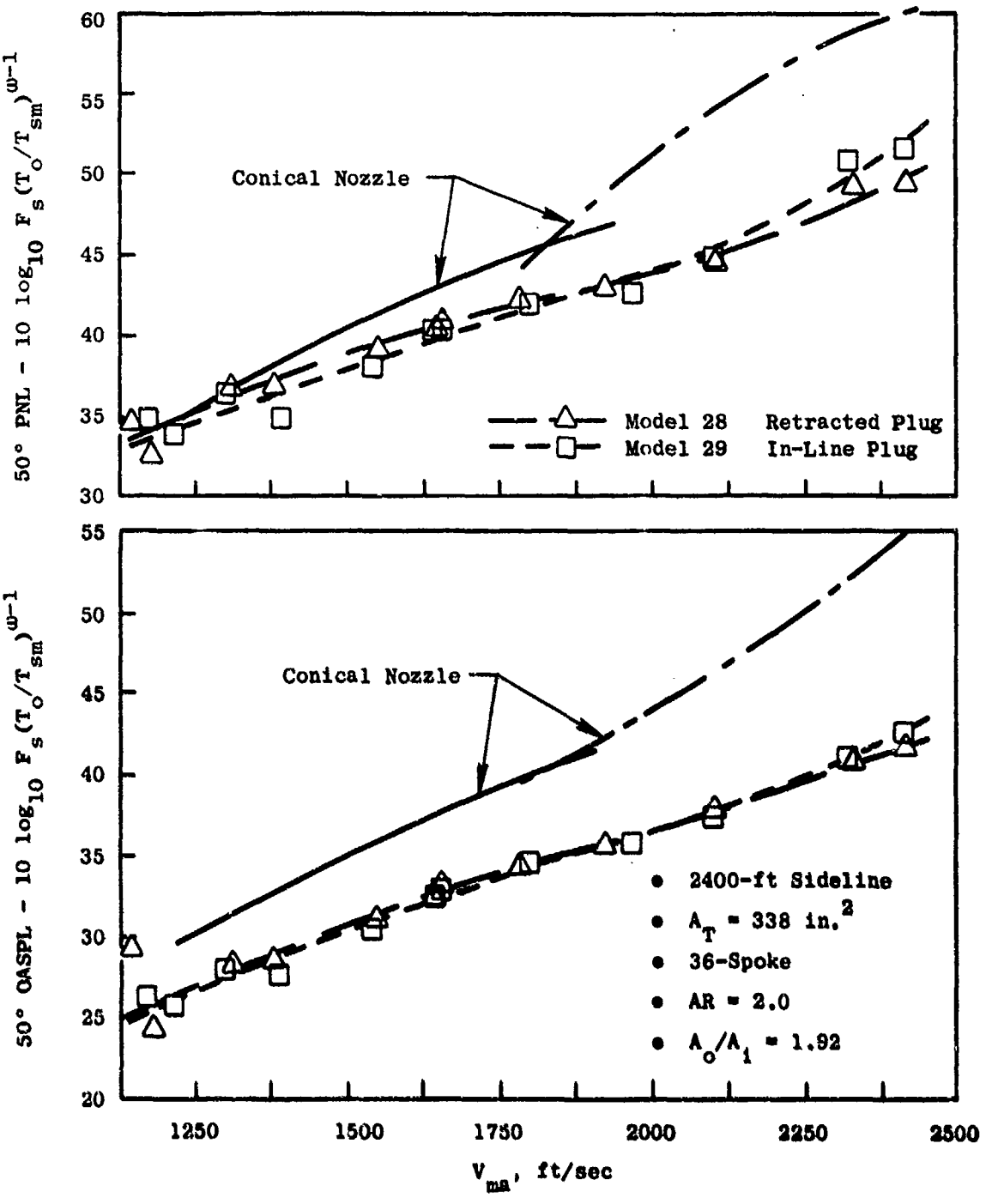

Figure 3-191. 50° PNL and OASPL Variation with Inner Plug Geometry, Models 28 and 29, DBTF/Inverted Dual Flow Cycle.

inner stream geometry, represent up to 3.5 dB greater suppression for higher area ratio at ≈ 2000 ft/sec V_{ma}. Differences between Models 23 to 25, with in-line plug geometry, however, are not as uniform in trend or magnitude.

- On the peak OASPL basis, trends similar to the peak PNL data are observed, with the higher A_o/A_i = 3.61 (Models 25 and 26) consistently exhibiting greater suppression than the A_o/A_i = 1.92 (Models 23 and 24). Model 26 shows up to ≈ 5 ΔdB greater suppression than Model 24 at mid-V_{ma} range, but again, Models 23 and 25 show much less variance.

- At 90°, on all three cycle lines, all four models have similar noise levels (no distinction observable for system area ratio change on either a PNL or OASPL basis).

- Results at 50° are generally similar to the 90° data, with no predominant distinction between models. The W_i = 15% W_o cycle data is an exception, where separate data-fitted-curves can be drawn through the aggregate of A_o/A_i = 1.92 and 3.61 data sets. This indicates ≈ 1 ΔOASPL and ≈ 2 ΔPNL greater suppression for the higher area ratio.

In comparing model sets for change in core geometry from in-line to retracted at fixed A_o/A_i (Model sets 23/24, 25/26 and 28/29) the following observations are noted:

- Model set 25/26 on all three cycle lines (Figures 3-177, 3-181 and 3-185), and Model set 28/29 on the DBTF/Inverted Dual Flow cycle line (Figure 3-189), show no significant difference in peak PNL noise levels with change in inner stream geometry, at any V_{ma} tested. These model sets are of A_o/A_i = 3.61 and 1.92, respectively. Model set 23/24, of in-line and retracted geometries, respectively, do show some variance, particularly at higher V_{ma}; the in-line geometry indicates somewhat greater suppression potential.

- Models 28 and 29 (Figure 3-189) show no pronounced difference in levels on a peak OASPL basis. Models 25 and 26 (Figures 3-178, 3-182 and 3-186) are basically equivalent except for ≈ 0.5 to 0.8 ΔdB greater suppression for the retracted position on the W_i = 30% W_o cycle line. Models 23 and 24 (Figures 3-178, 3-182 and 3-186) again show variance favoring the in-line geometry on each of the cycle lines tested.

- For 90° data, (Figures 3-179, 3-183, 3-187 and 3-190) for all model comparisons on all cycle lines, no distinction is seen between in-line and retracted core geometries.

- 50° PNL and OASPL (Figures 3-180, 3-184, 3-188 and 3-191) show no inner flow geometry preference except for the W_i = 30% W_o cycle

line where the Model 24 retracted inner stream plug shows ≈ 1 ΔOASPL and up to ≈ 2 ΔPNL greater suppression at low V_{ma} than the Model 23 in-line plug.

For the impact of system area ratio and inner stream geometry changes on PNL/OASPL directivity and spectra, the following representative data are included for Models 23, 24, 25 and 26, from the W_i = 30% W_o cycle line:

- Figures 3-192 and 3-193, V_{ma} = 2300 ft/sec
- Figures 3-194 and 3-195, V_{ma} = 1875 ft/sec
- Figures 3-196 and 3-197, V_{ma} = 1380 ft/sec

Summary-Flow Management and Inner Stream Geometry Studies

Flow Management and Inner Stream Geometry Studies for a dual-flow nozzle system incorporating an outer stream half-span mechanical suppressor have investigated the aerodynamic cycle and geometric nozzle variations which would most significantly impact noise suppression capability. Consideration has been given to: a) system velocity ratio (V_o/V_i); b) system weight flow ratio ($\beta = W_o/W_i$); c) system area ratio (A_o/A_i) and d) inner stream plug geometry. Primary design considerations evolved from a series of three distinct studies are as follows:

- Velocity ratio influence is most predominant in systems of low area ratio where the inner stream exerts more of a controlling influence. Progressive and systematic increases in peak OASPL suppression occur as V_o/V_i changes from 0.6 to ∞. Fairly systematic changes in peak PNL are also observed, but not of the magnitude or as progressively uniform as on peak OASPL. At broadside, and in the forward quadrant, systematic variation of noise levels with V_o/V_i variation is not evident.

- Highest suppression levels are attained when inner flow is completely terminated and the outer stream effectively discharges over an abrupt-step formed by the inner stream annulus. Peak PNL suppression levels of up to 13.5 dB were seen on the 2400 ft. sideline for Model 33, the 36 chute AR = 2.5, R_T^o = 0.783 system of A_o/A_i = 0.65. Figure 3-198 compares this closed inner stream system's suppression to levels attained by three full plug turbojet configurations; namely, Models 15 & 17, of AR, R_T = 2.5/0.653 and 1.5/0.782 discussed in Section 3.4.2.1 and Model 41 of AR, R_T = 2.5/0.78 presented in Section 3.4.3.1. In all cases the abrupt-step system showed greater suppression potential. It is recognized that this system may be unacceptable from an aero performance consideration. However, it does provide an upper limit in noise reduction which could conceivably be achieved by judiciously bleeding the inner flow.

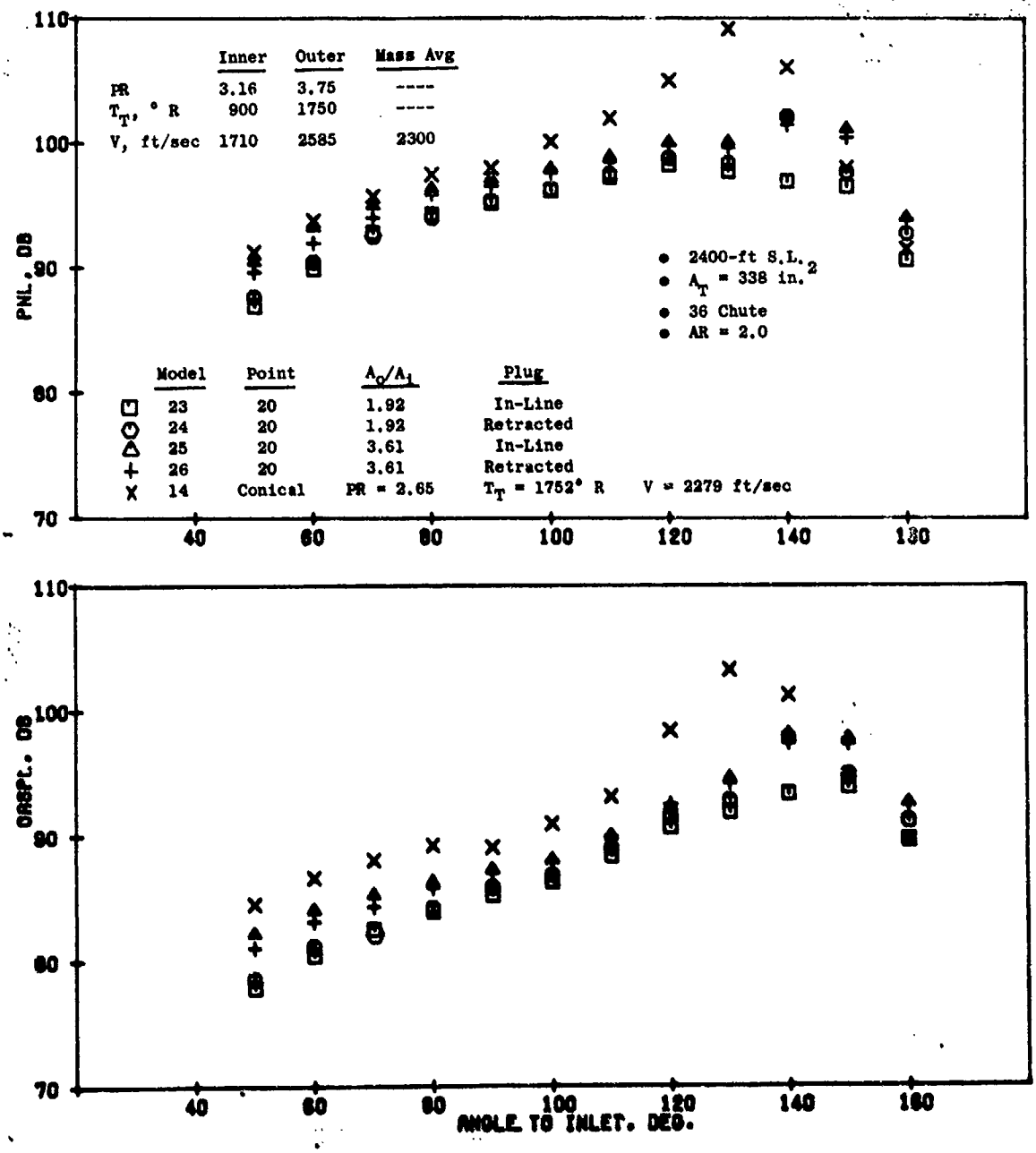

Figure 3-192. Impact of A_o/A_i and Inner Plug Geometry on PNL and OASPL Directivity, Models 23-26, W_{Inner} = 30% W_{Outer} Cycle, V_{ma} = 2300 ft/sec.

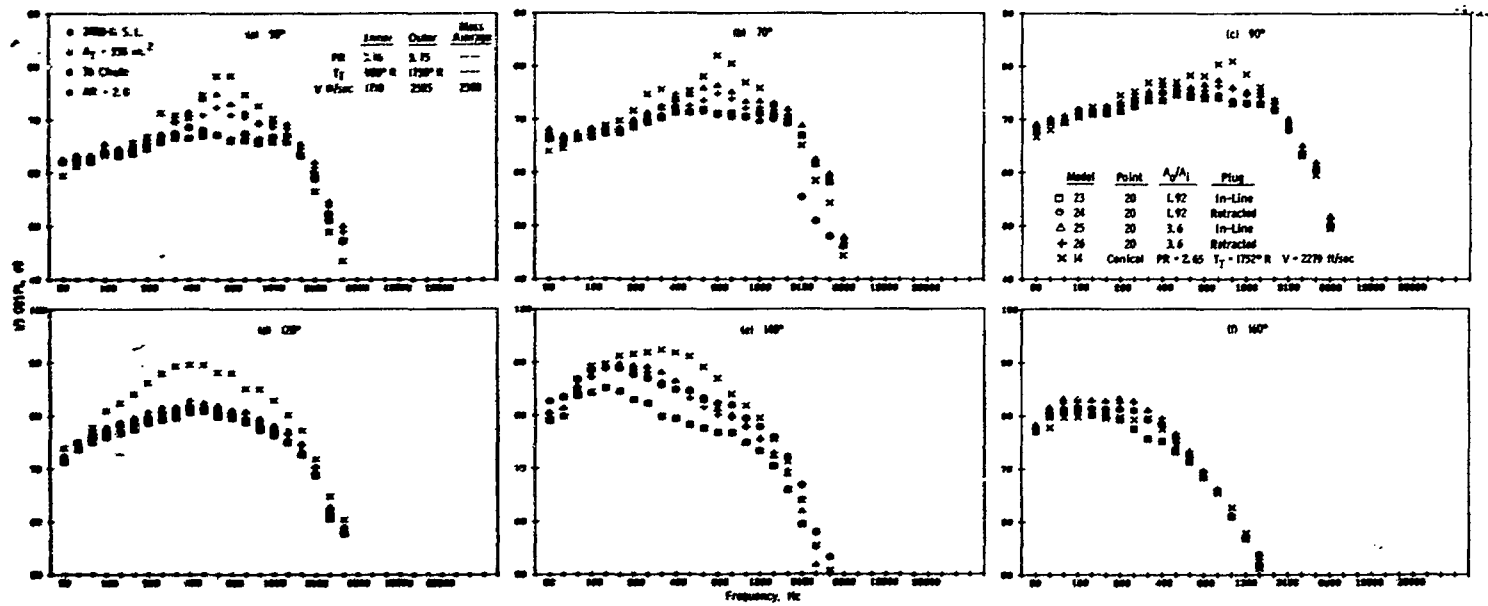

Figure 3-193. Impact of A_e/A_i and Inner Plug Geometry on Spectra, Models 23 - 26, W_{Inner} = 30% W_{Outer} Cycle, V_{ma} = 2300 ft/sec.

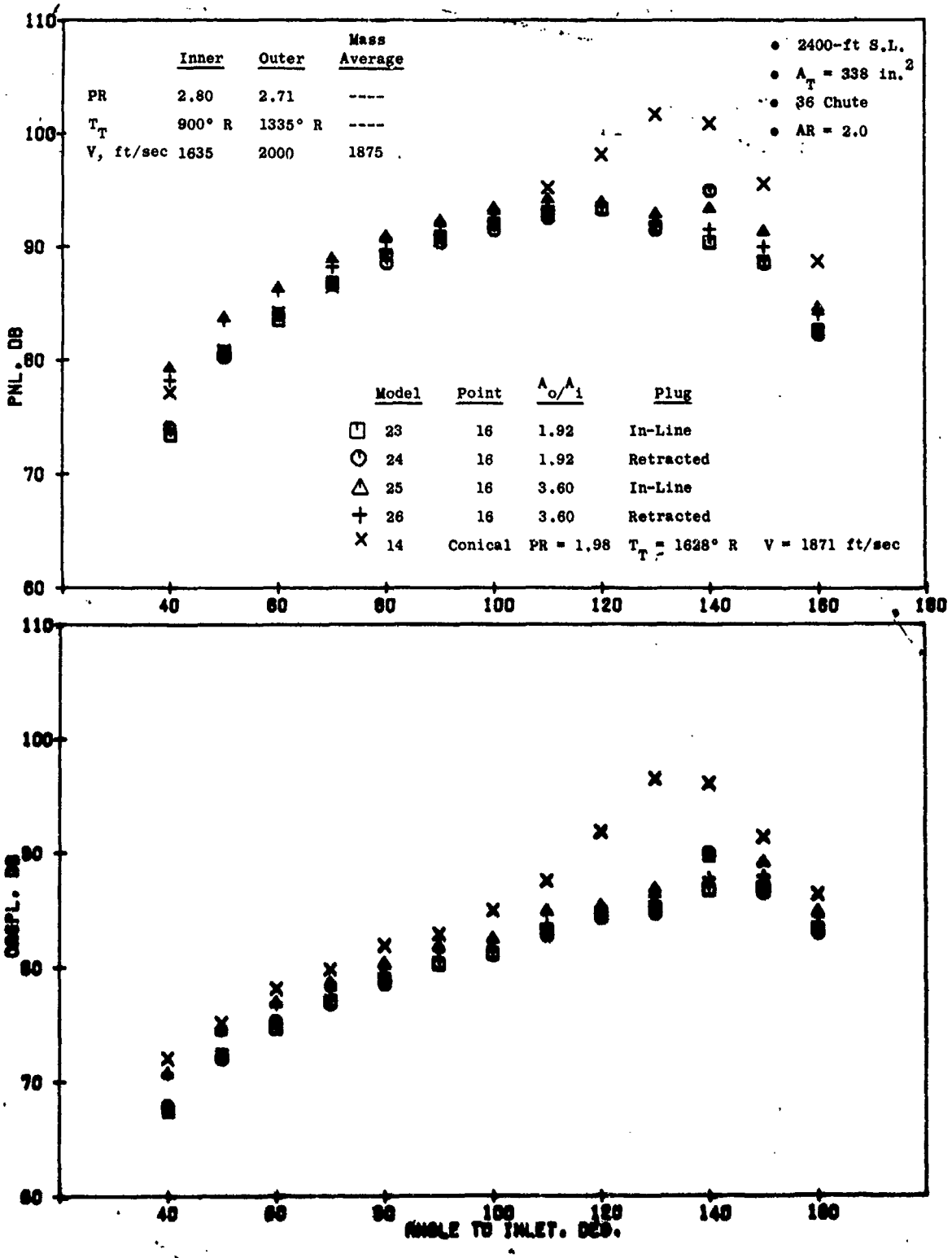

Figure 3-194. Impact of A_O/A_I and Inner Plug Geometry on PNL and OASPL Directivity, Models 23-26, W_{Inner} = 30% W_{Outer} Cycle, V_{ma} = 1875 ft/sec.

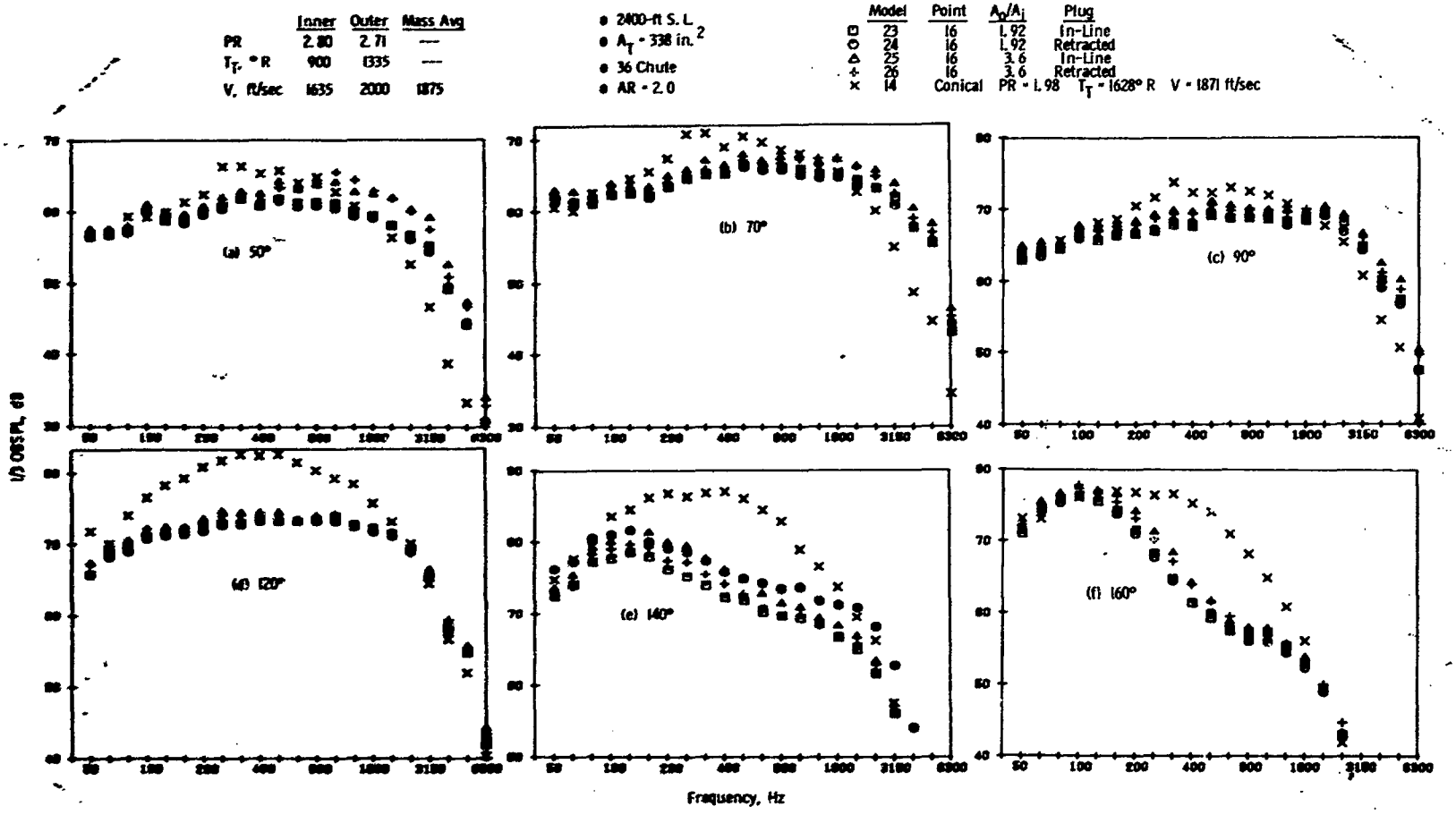

Figure 3-195. Impact of A_O/A_i and Inner Plug Geometry on Spectra, Models 23-26, W_{Inner} = 30% $W_{Outer\ Cycle}$, V_{ma} = 1875 ft/sec.

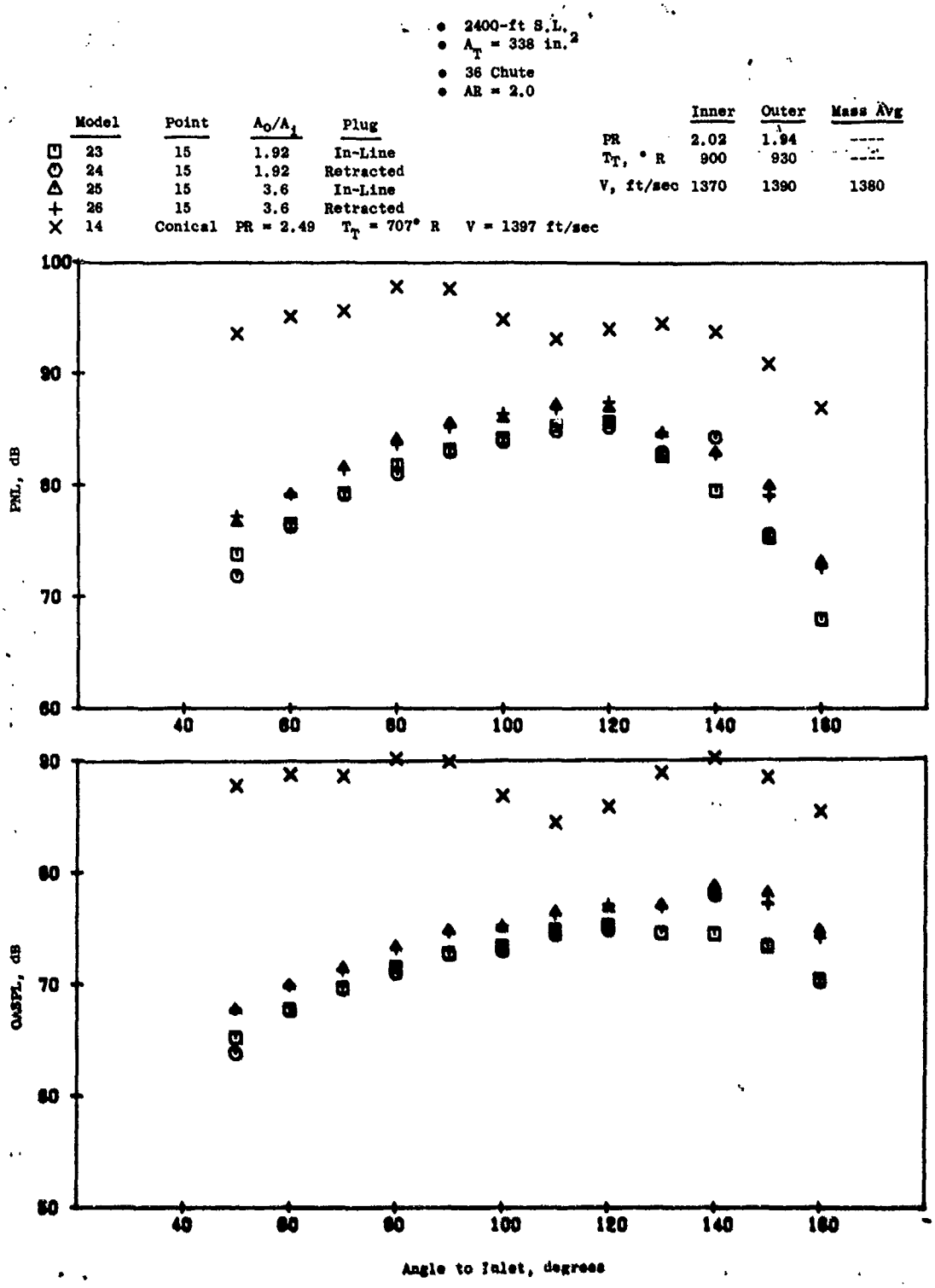

Figure 3-196. Impact of A_O/A_i and Inner Plug Geometry on PNL and OASPL Directivity, Models 23-26, W_{Inner} = 30% W_{Outer} Cycle, V_{ms} = 1380 ft/sec.

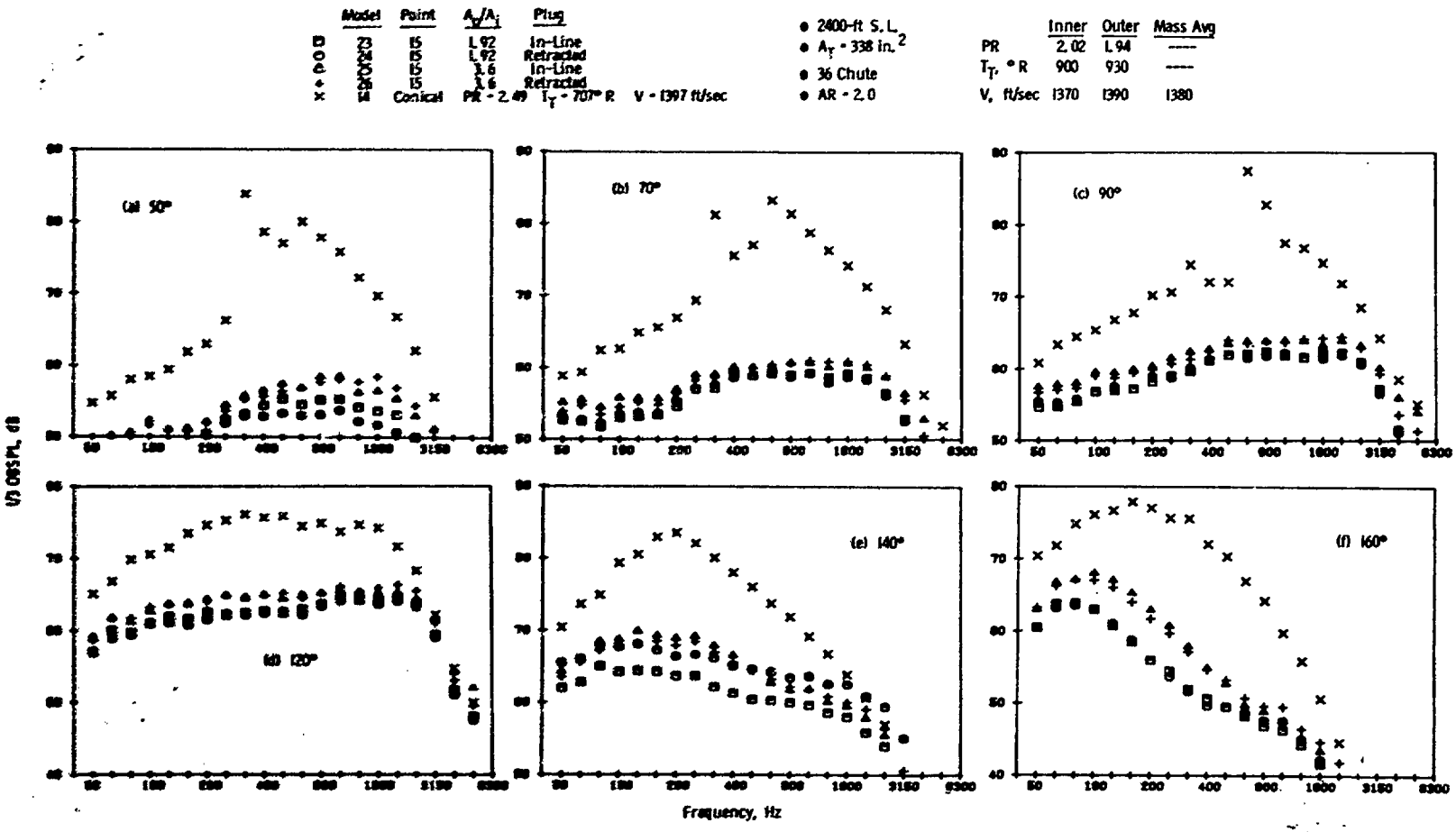

Figure 3-197. Impact of A_o/A_i and Inner Plug Geometry on Spectra, Models 23-26, W_{Inner} = 30% W_{Outer} Cycle, V_{ma} = 1380 ft/sec.

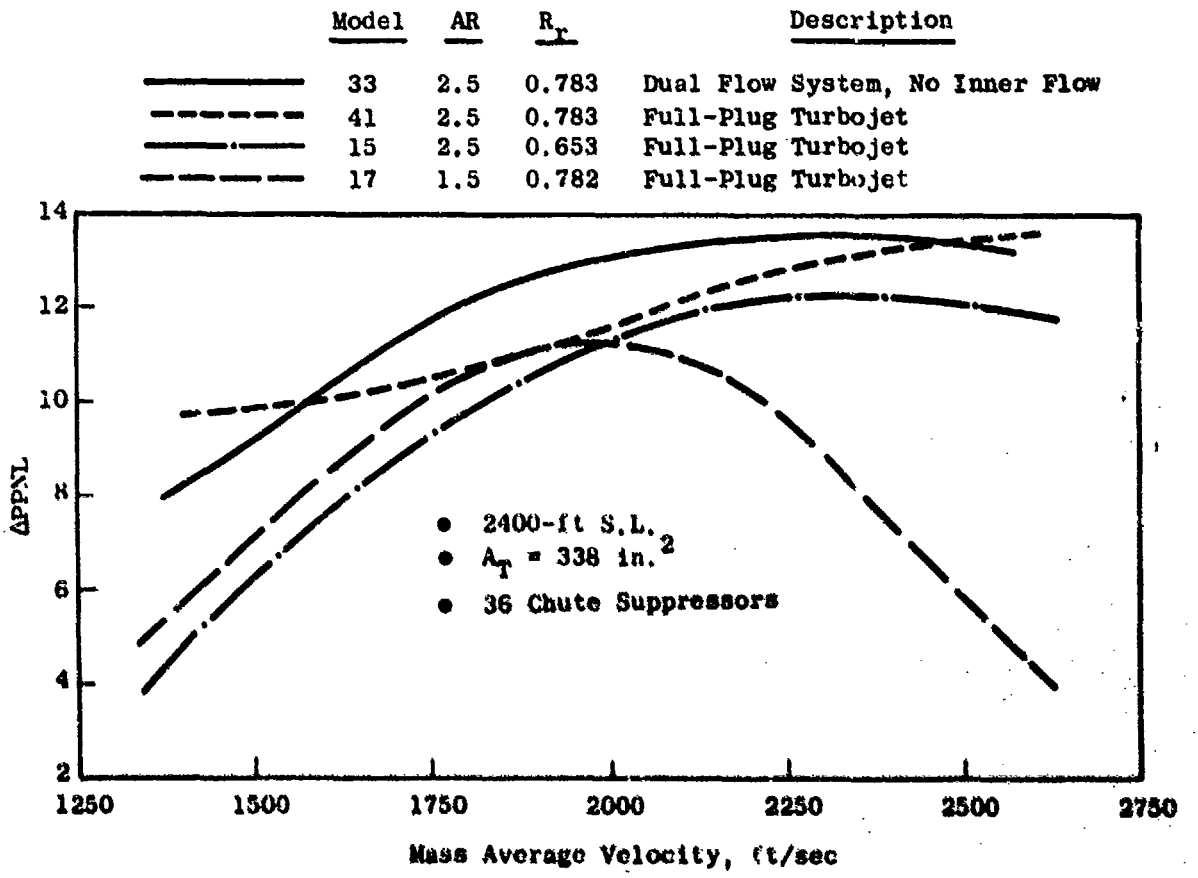

Figure 3-198. Summary Comparison of Suppressed Dual Flow with No Inner Flow to Full-Plug Turbojets.

- For systems of A_o/A_i = 1.92 the magnitude of noise variance with V_o/V_i is not present as it is for the low area ratio system, as the outer stream now controls the major portion of the system flow. Individual data sets, however, do show some distinct variance with velocity ratio within the range of 1.5 to 2.0.

- For A_o/A_i = 3.61, with β from 2.8 to 8.8, the outer stream dominates noise generation and little variance is discernible for $1.0 \leq V_o/V_i \leq 2.0$

- Injecting low amounts of inner flow to effect β values of 3.3, 6.7, and ∞ shows β to be a strong system parameter influencing suppression. The influence is greater for low system area ratio and changes are fairly systematic, decreasing suppression as β is lowered from ∞ to 3.3. Changes in peak PNL range from 5 to 3 ΔdB at low to high V_{ma} over the β range tested.

- System area ratio variation impacts suppression performance significantly. The high A_o/A_i value of 3.61 indicates peak PNL and peak OASPL suppression gains up to 3.5 and 5 ΔdB, respectively over the lower A_o/A_i counterparts. Impact is primarily in the aft quadrant with 90° showing no systematic trends and 50° only indicating higher A_o/A_i is still favorable.

- Inner stream geometry variation from the in-line to the retracted configurations has negligible impact on suppression. Variance within the model sets is not strong or consistent enough to substantiate any preference of geometry.

3.4.2.3 Flow Segmentation Study

The intention of this study was to investigate the impact of degree of segmentation of an annular duct supressor within a dual flow exhaust nozzle system. Models 30, 31, and 32 (Figure 3-199) of 20, 30 and 40 shallow chute element, respectively, were utilized. Detailed schematics of the models are in Appendix A, Figures 24, 25 and 26. Inner stream flowpath geometry was held constant using the 0.7-in. annulus height plug in the retracted position. Parameters of the outer flowpath held constant were:

- Flow area = 21.76 $in.^2$
- Blocked area = 17.82 $in.^2$
- Suppressor area ratio = 1.75
- Suppressor radius ratio = 0.717
- Shroud I.D. = 10.44 in.
- Plug O.D. = 7.48 in.
- Upstream flow geometry
- System area ratio, A_o/A_i, = 1.92

- Retracted Inner Plug with 0.7-in. Step
- Area Ratio = 1.75
- Radius Ratio = 0.717
- A_o/A_i = 1.92

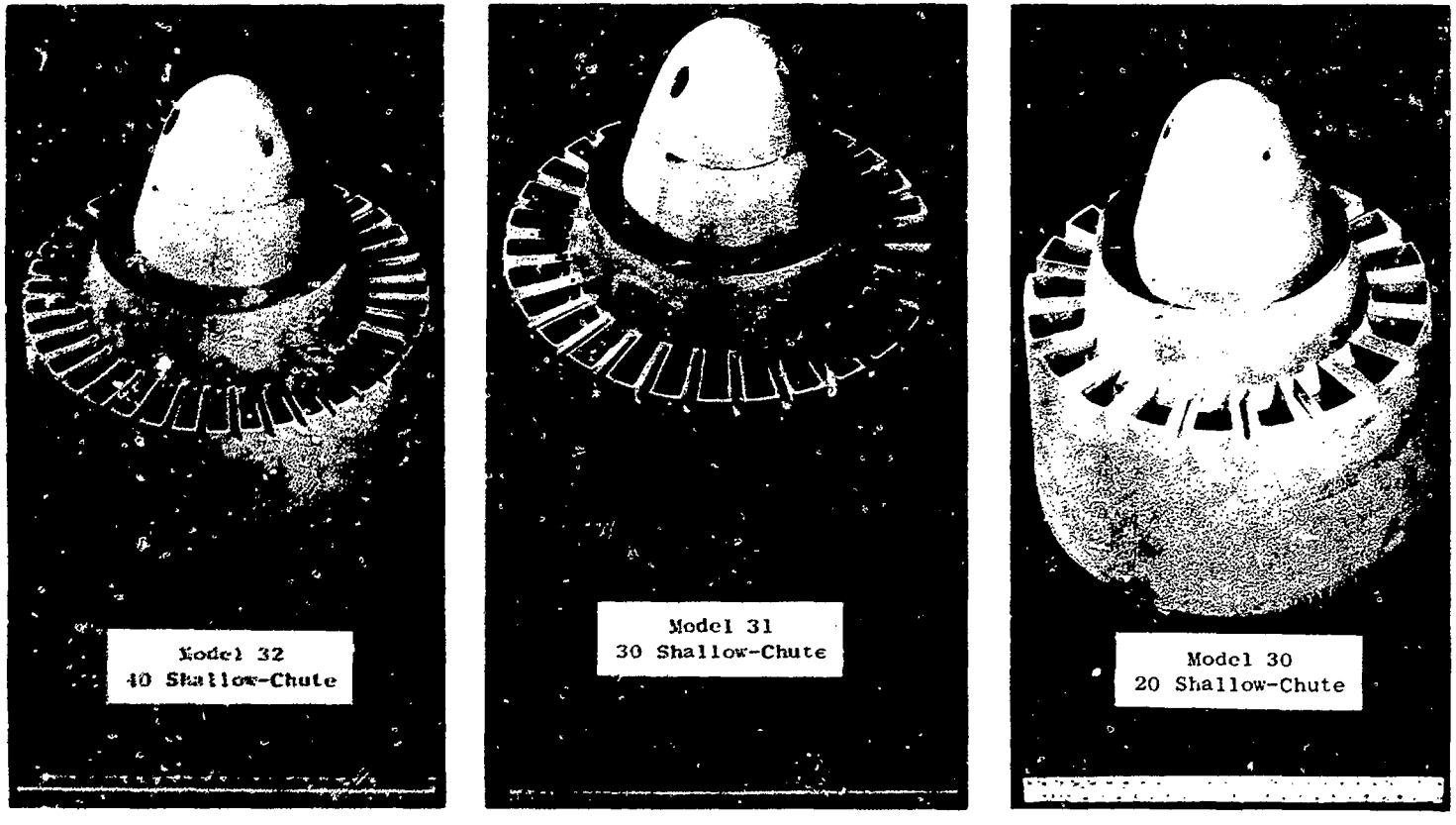

Figure 3-199. Half-Span Suppressor Element Number Variation on Dual Flow.

The only geometric variable was element number, more finely segmenting both flow and blocked areas as element number increased.

Acoustic test matrices were as described in Section 3.2.1, Figure 3-10 and Table 3-3, testing each model for the following cycle series:

- W_i = 15% W_o
- W_i = 30% W_o
- DBTF/Inverted Dual Flow with $1.0 \leq V_o/V_i \leq 2.0$
- AST/VCE

Model 31 was additionally tested with no inner flow while maintaining a normal outer flow cycle.

Acoustic results, if presented as an aggregate of all test data on the basis of peak noise levels, show (as in Figure 3-200) that:

- Maximum suppression levels of 10 ΔPPNL and 11.5 ΔPOASPL were attained.
- At low and intermediate V_{ma}, finer segmentation is more effective on a peak PNL basis; however, a switch to lower element number is more effective at V_{ma}>2250 ft/sec.
- On the peak OASPL basis the coarser segmentation of 20 elements (Model 30) is significantly more effective and no significant distinction is seen between the finer segmentation of 30 or 40 shallow-chutes (Models 31 and 32).

Closer evaluations of the data, as applicable to the individual cycles of a) W_i = 15% W_o b) W_i = 30% W_o, and c) DBTF/Inverted Dual Flow, are presented in the following:

Figures 3-201 and 3-202 Peak PNL & OASPL
Figures 3-203 and 3-204 90° PNL & OASPL
Figures 3-205 and 3-206 50° PNL & OASPL
Figure 3-207 OAPWL

Peak PNL data in Figure 3-201 for all three cycle lines show that finer segmentation yields more effective suppression at low and intermediate V_{ma}, and a maximum level of near 10 ΔPPNL is experienced. Degree of segmentation is relatively unimportant at $2000 \leq V_{ma} \leq 2250$ ft/sec, then coarser segmentation becomes more effective at V_{ma}>2250 ft/sec. Variance of up to 5 ΔPPNL is seen for the study excursion range of 20 to 40 elements, magnitude depending on cycle line and V_{ma} selected.

Figure 3-202, peak OASPL data for the three cycle curves, shows lower element number segmentation to be consistently more effective. A variance of 1 to 4 ΔPOASPL is seen from 20 to 40 elements, magnitude of variance always

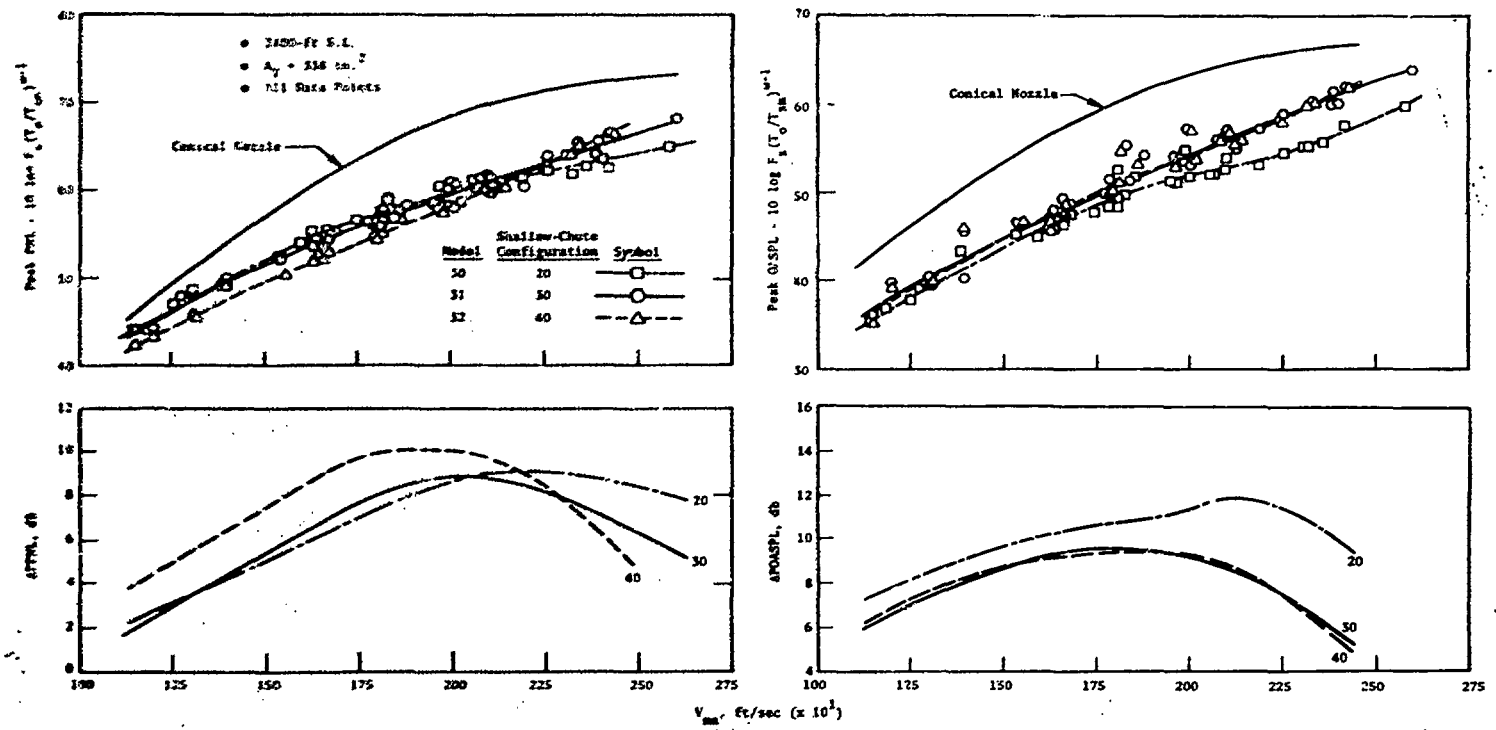

Figure 3-200. Suppressor Element Number Variation, Peak Noise and Suppression Levels.

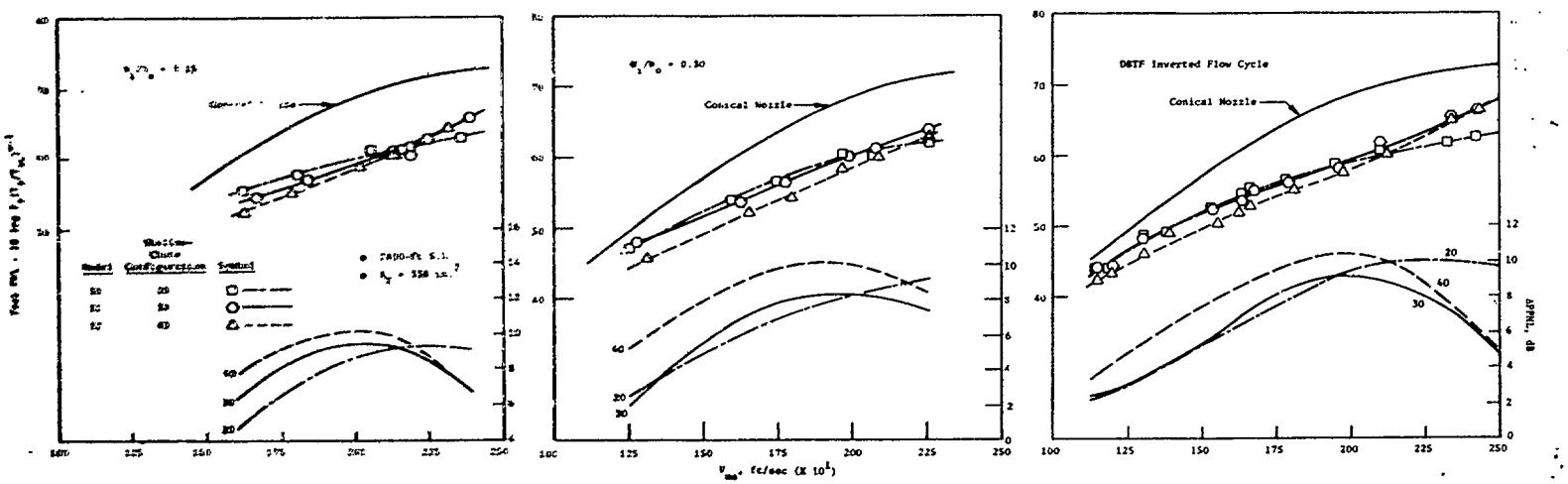

Figure 3-201. Suppressor Element Number Variation, Peak PNL and Suppression Levels.

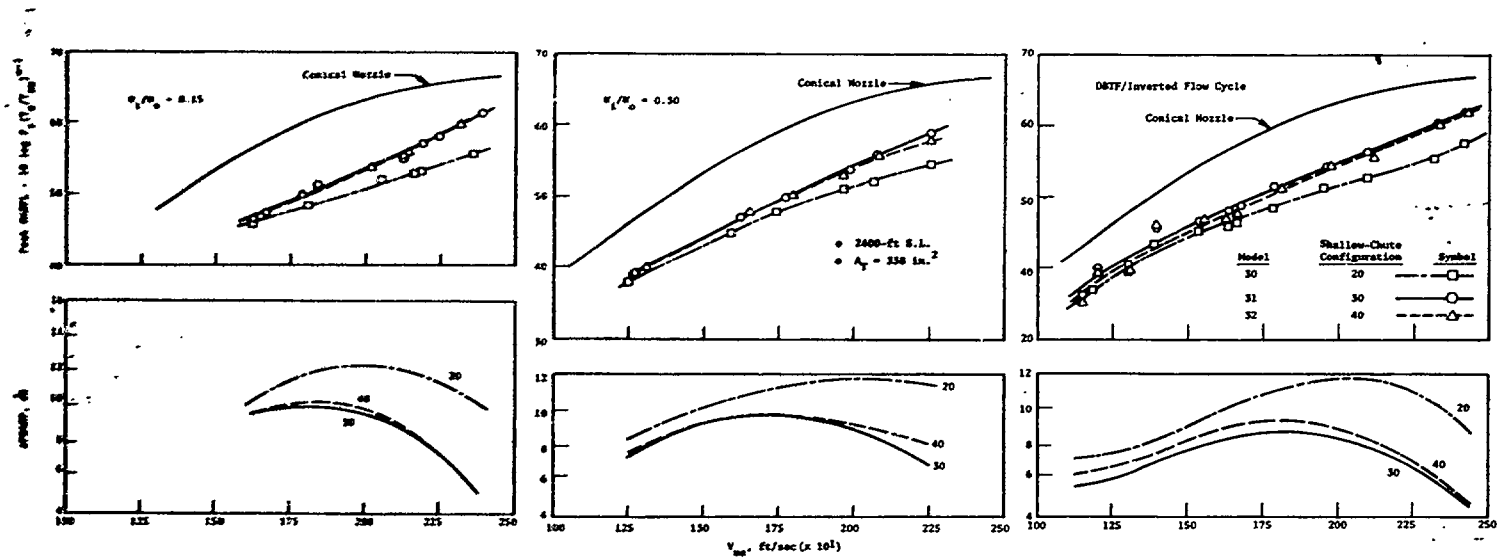

Figure 3-202. Suppressor Element Number Variation, Peak OASPL and Suppression Levels.

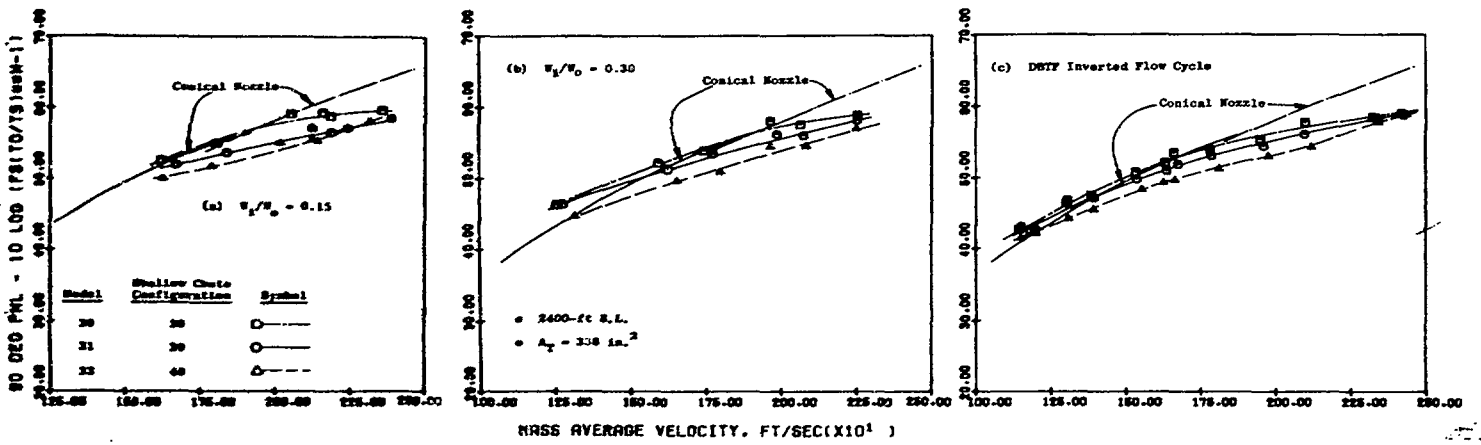

Figure 3-203. Suppressor Element Number Variation, 90° PNL.

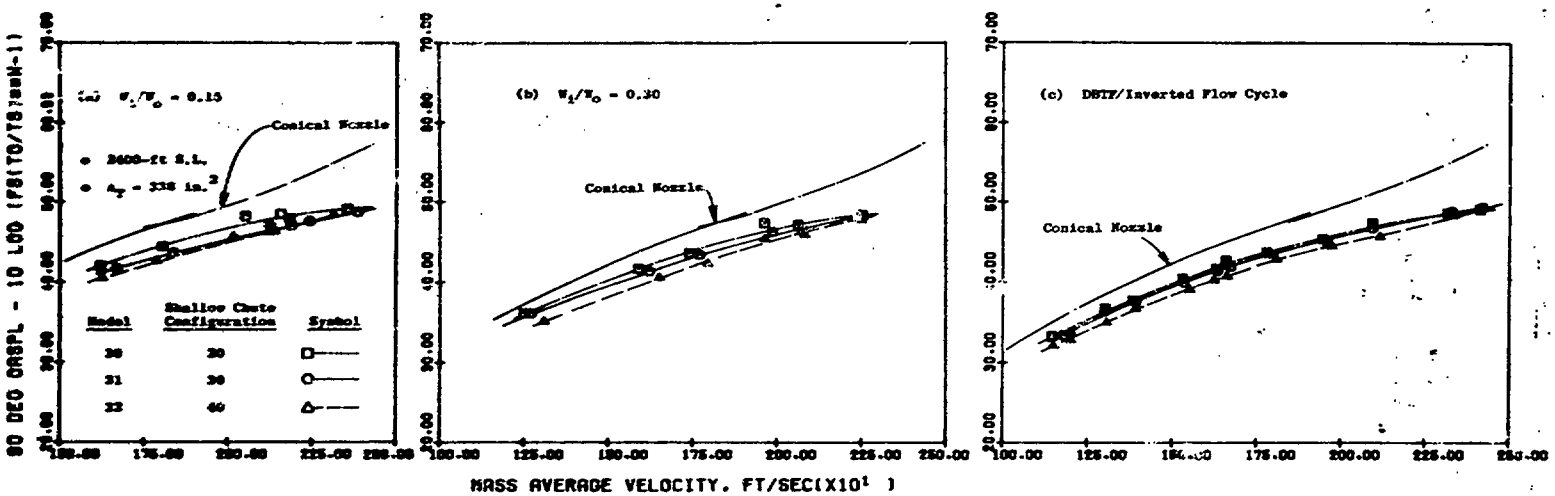

Figure 3-204. Suppressor Element Number Variation, 90° OASPL.

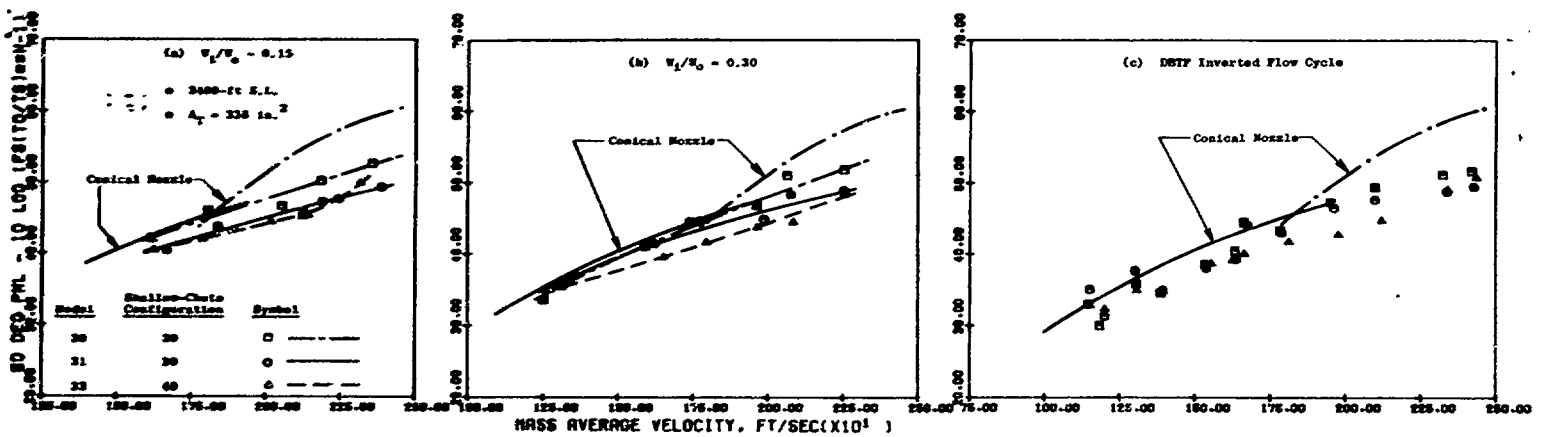

Figure 3-205. Suppressor Element Number Variation, 50° PNL.

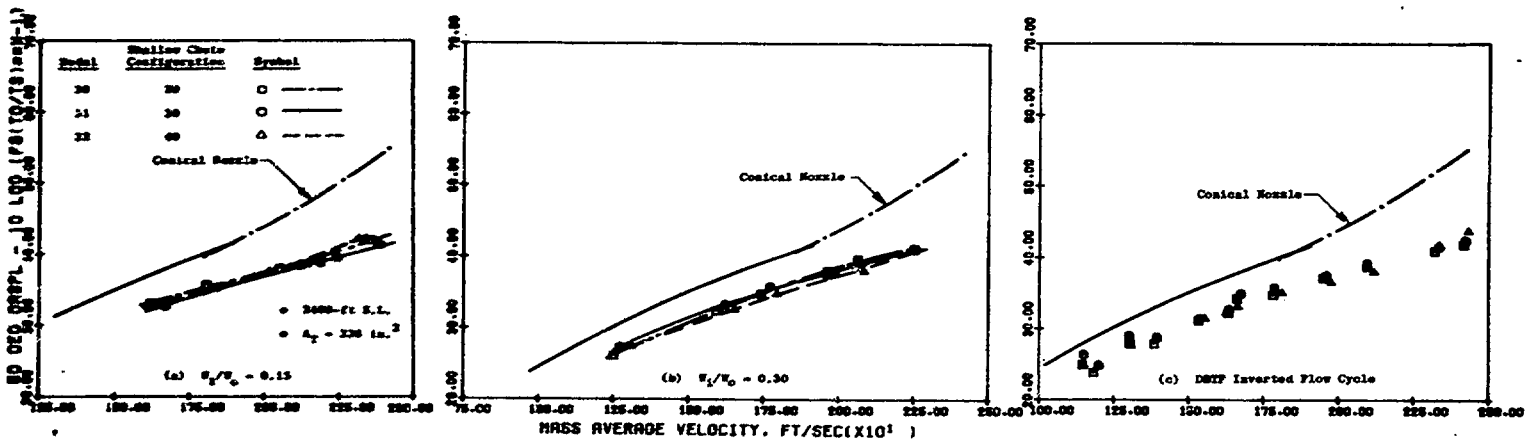

Figure 3-206. Suppressor Element Number Variation, 50°-OASPL.

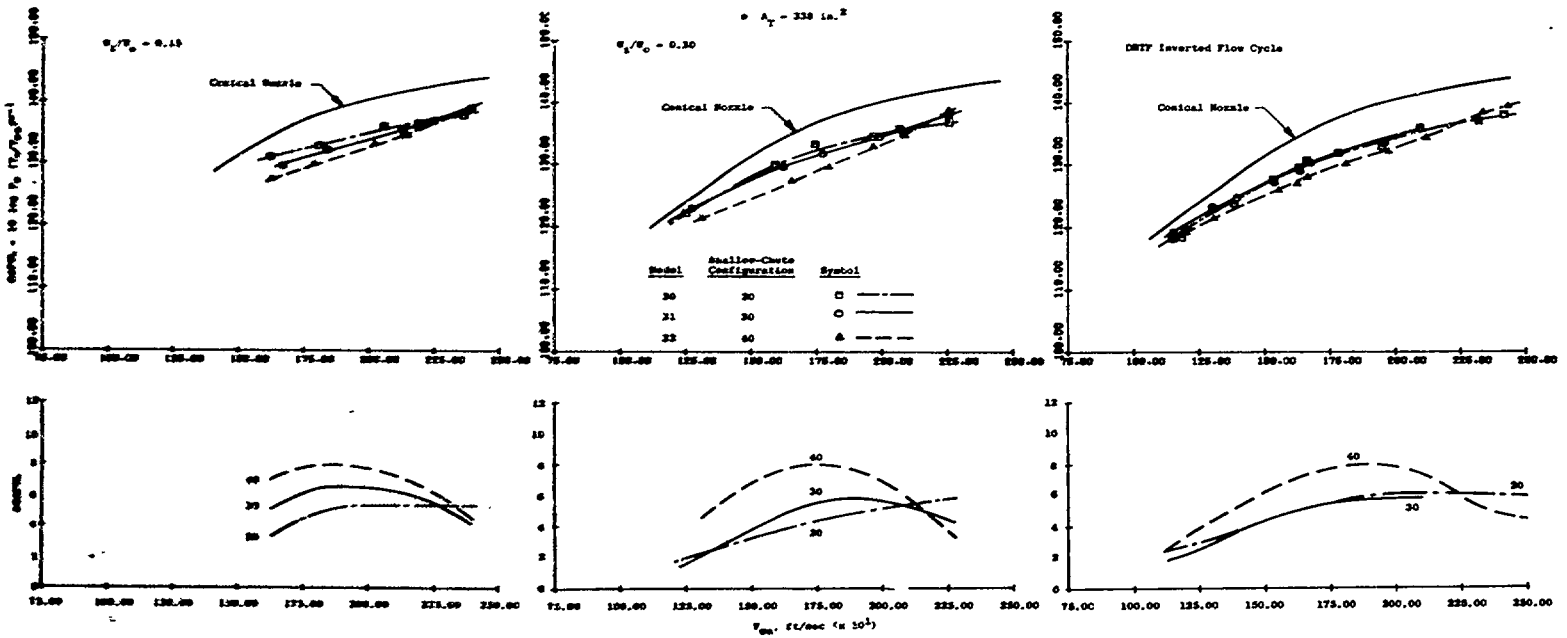

Figure 3-207. Suppressor Element Number Variation, OAPWL.

greater at higher V_{ma}. Distinction between 30 and 40 shallow-chute performance is nil. For the DBTF/Inverted Dual Flow cycle data, both for peak PNL and OASPL, minimal distinction is seen for V_o/V_i variance from 1.0 to 2.0; the data adhering well to smooth singular trend curves.

Figures 3-203 and 3-204, for 90° PNL and OASPL, show that PNL suppression is still attained at intermediate and high V_{ma} settings, but at low V_{ma} the self noise of the shallow-chutes raises the PNL levels slightly above the baseline. Moderate levels of OASPL suppression are maintained at all V_{ma} values. Finer segmentation is more effective at all cycles, at all velocity values and for both PNL and OASPL, a nominal 3 to 4 ΔPNL greater suppression afforded by 40 (Model 32) relative to 20 elements (Model 30).

Figures 3-205 and 3-206, for 50° PNL and OASPL, show that substantial PNL and OASPL suppression is maintained in the forward quadrant, both at low V_{ma} where turbulent mixing noise is prevalent and at higher V_{ma} (supercritical pressure ratio) where the suppressor very significantly lowers noise levels relative to the conical noise levels. On an OASPL basis, little distinction is seen in fineness of segmentation, whereas higher element number still offers significant improvement on a PNL basis.

OAPWL trends with V_{ma}, Figure 3-207, are consistent with those of PPNL in that (a) finer segmentation is more effective at low and intermediate V_{ma}, (b) degree of segmentation is relatively unimportant for $2000 \leq V_{ma} \leq 2250$, and (c) trend is for more effective suppression with fewer element at $V_{ma} > 2250$ ft/sec.

For a more detailed evaluation of suppressor segmentation influence on PNL and OASPL directivity plus spectra characteristics, the following data sets from the DBTF cycle are included as representative of the overall test results.

Figures 3-208 and 3-209 Data Point 37, V_{ma} = 2425 ft/sec, V_o/V_i = 1.9

Figures 3-210 and 3-211 Data Point 26, V_{ma} = 2100 ft/sec, V_o/V_i = 2.0

Figures 3-212 and 3-213 Data Point 24, V_{ma} = 1200 ft/sec, V_o/V_i = 1.0

A general review of the above data suggests:

- The PNL angular variation of these multielement suppressors hint at the classical migration of maximum noise angles at lower inlet angles relative to the conical nozzle.
- At high V_{ma} (supercritical pressure ratio in the outer stream), large amounts of inlet angle suppression are seen. The primary suppression mechanism is reduction of the strong puretone and broadband shock-cell noise, prevalent in the conical nozzle noise signature.

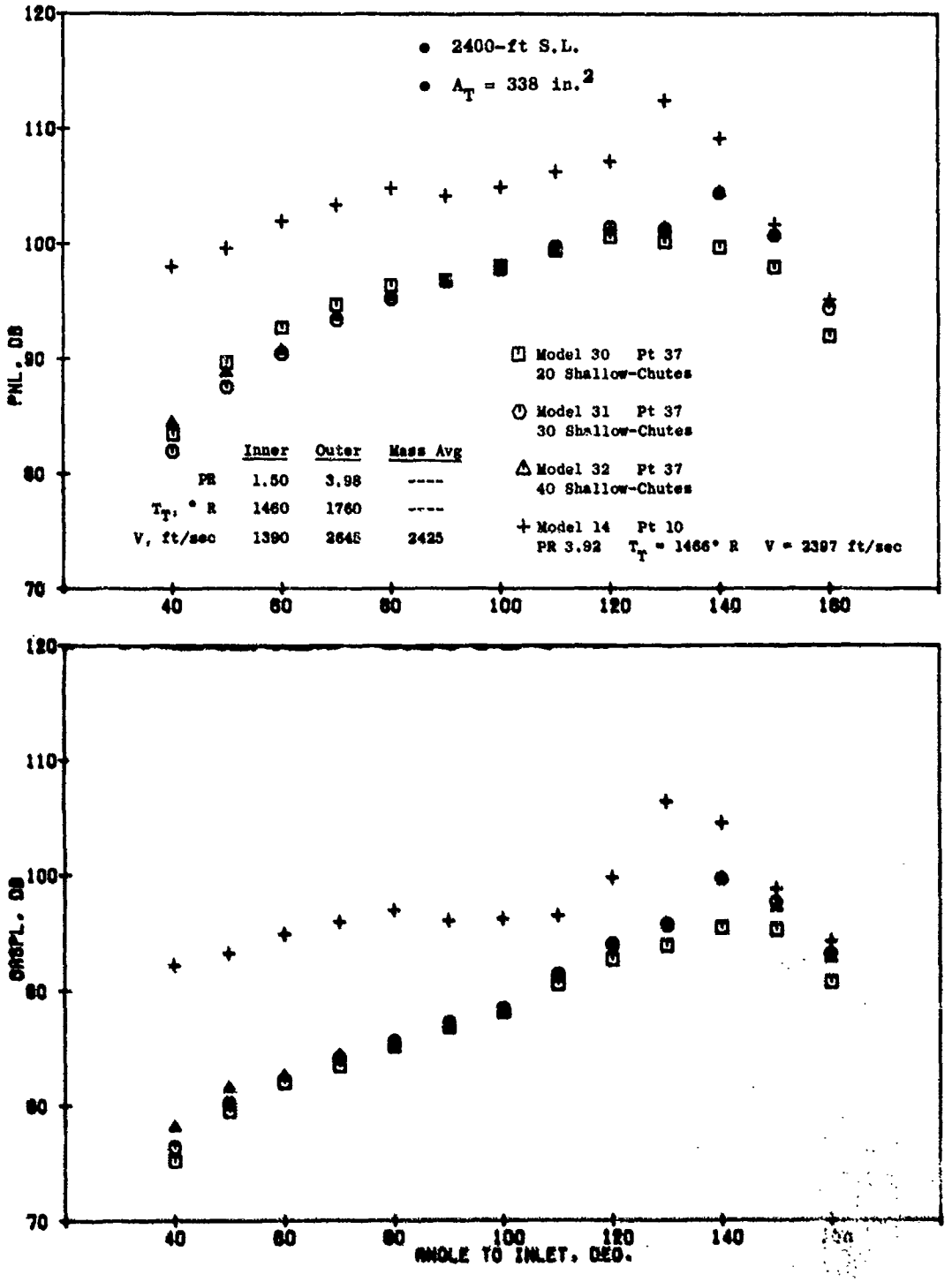

Figure 3-208. Suppressor Element Number Variation, OASPL and PNL Directivity, V_{ma} = 2425 ft/sec.

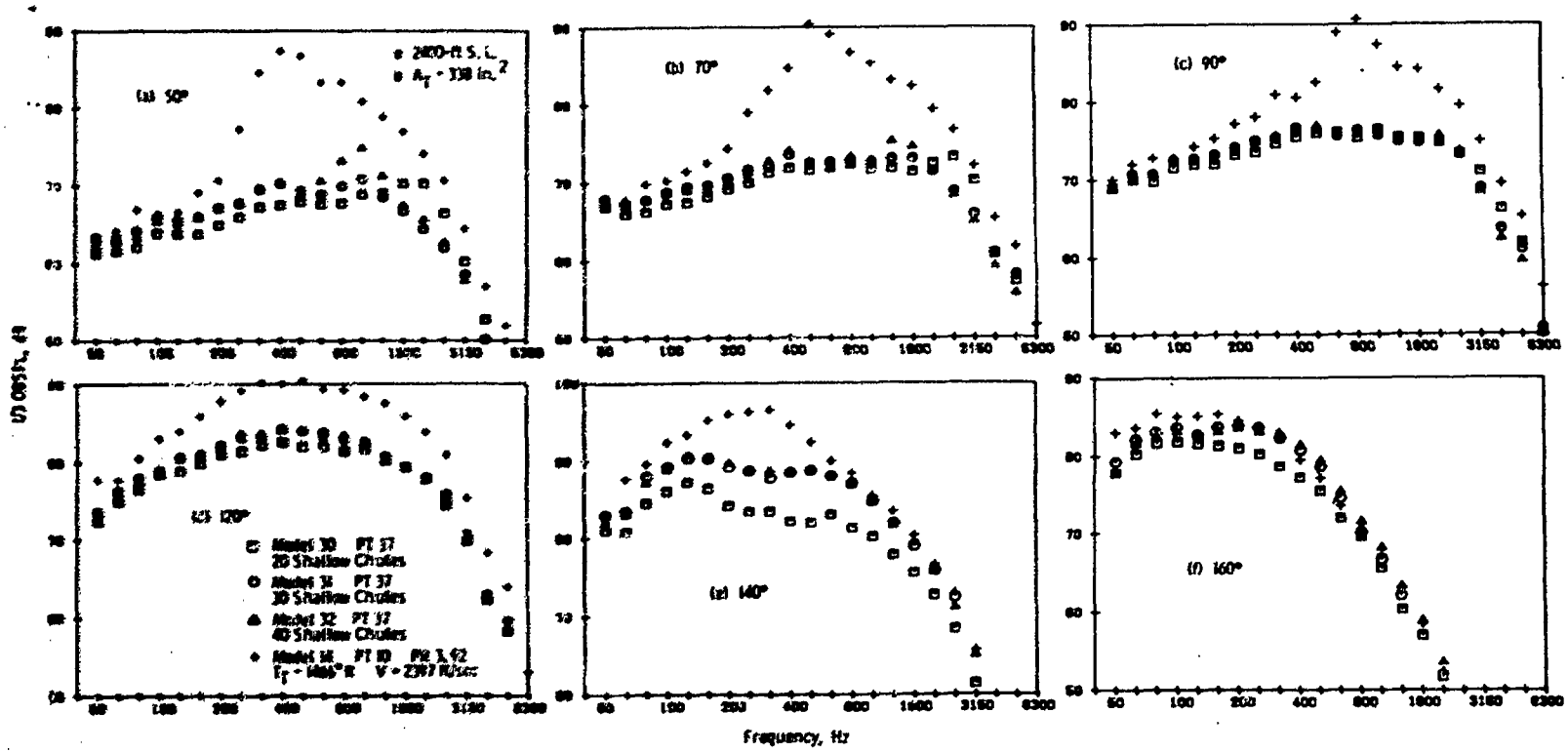

Figure 3-209. Suppressor Element Number Variation, Spectra, V_{ma} = 2425 ft/sec.

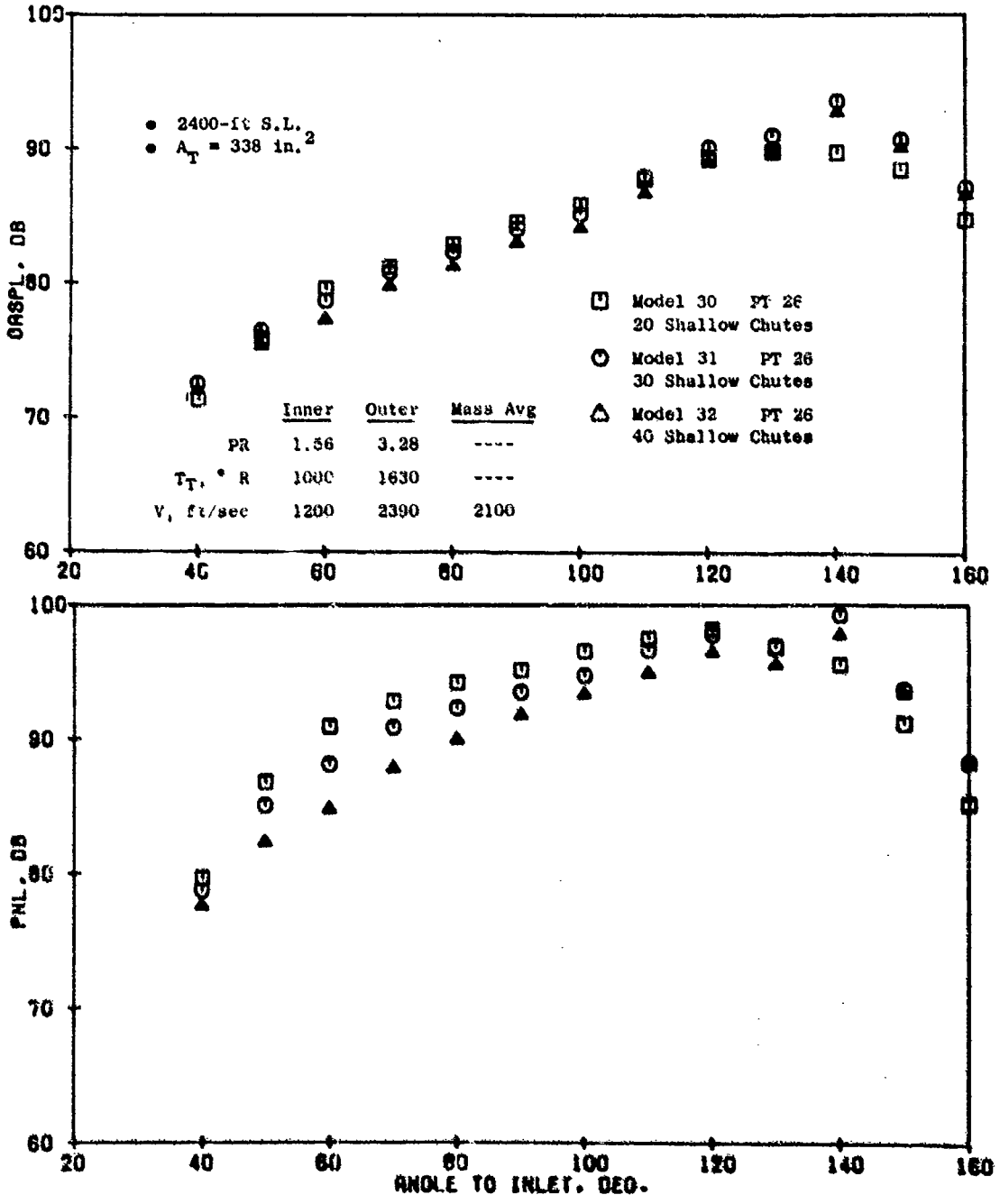

Figure 3-210. Suppressor Element Number Variation, OASPL and PNL Directivity, V_{ma} = 2100 ft/sec.

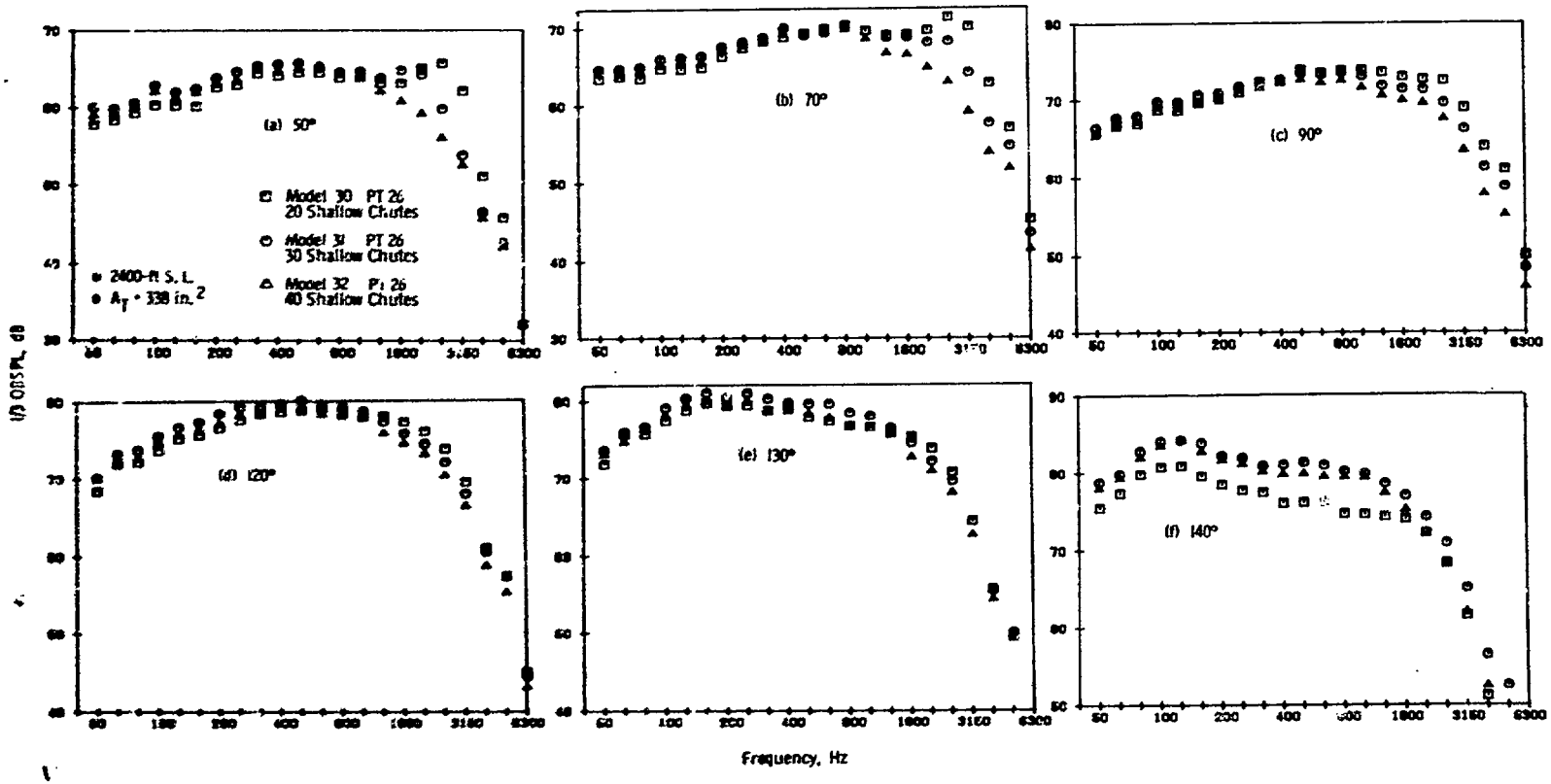

Figure 3-211. Suppressor Element Number Variation, Spectra, V_{ma} = 2100 ft/sec.

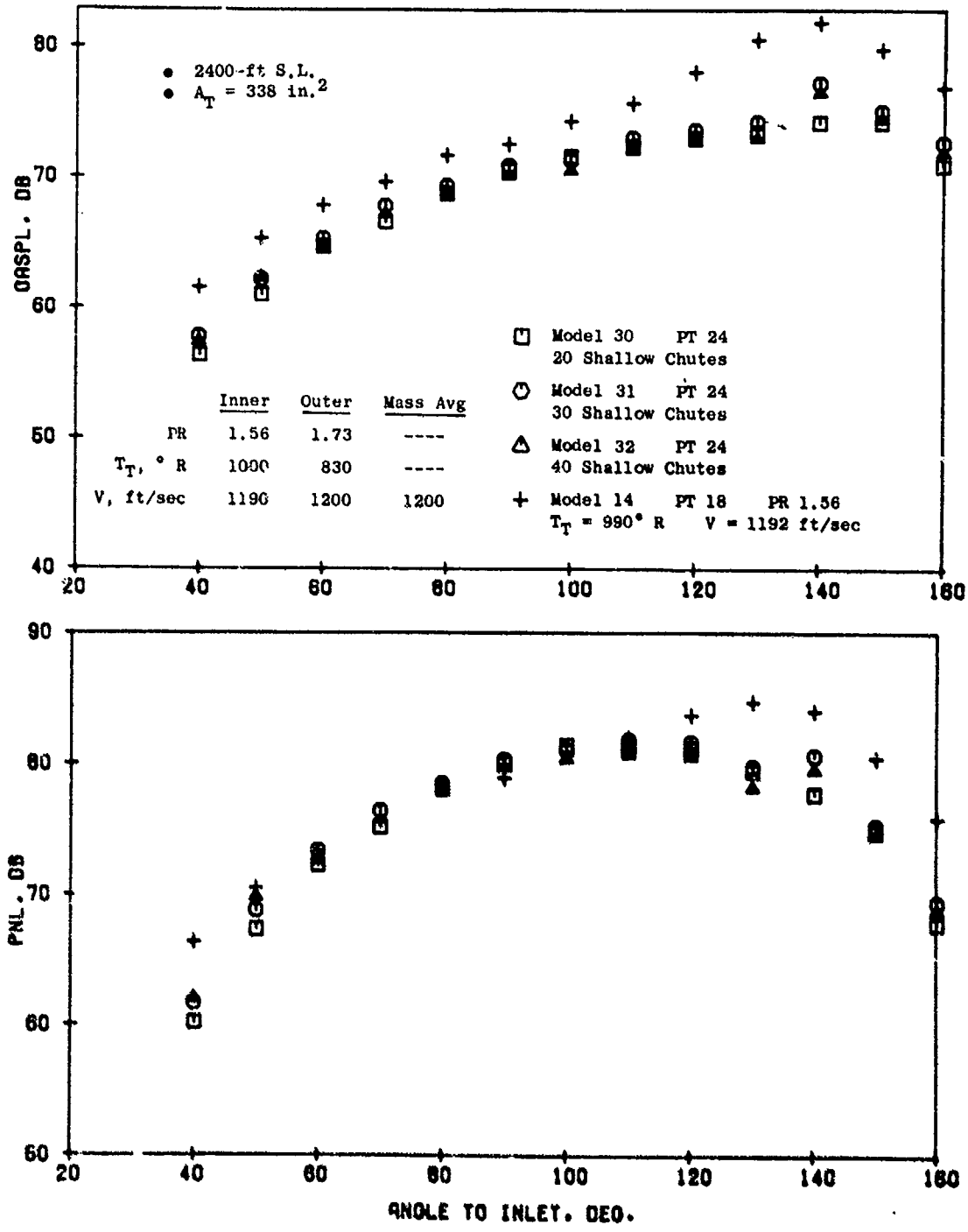

Figure 3-212. Suppressor Element Number Variation, OASPL and PNL Directivity, V_{ma} = 1200 ft/sec.

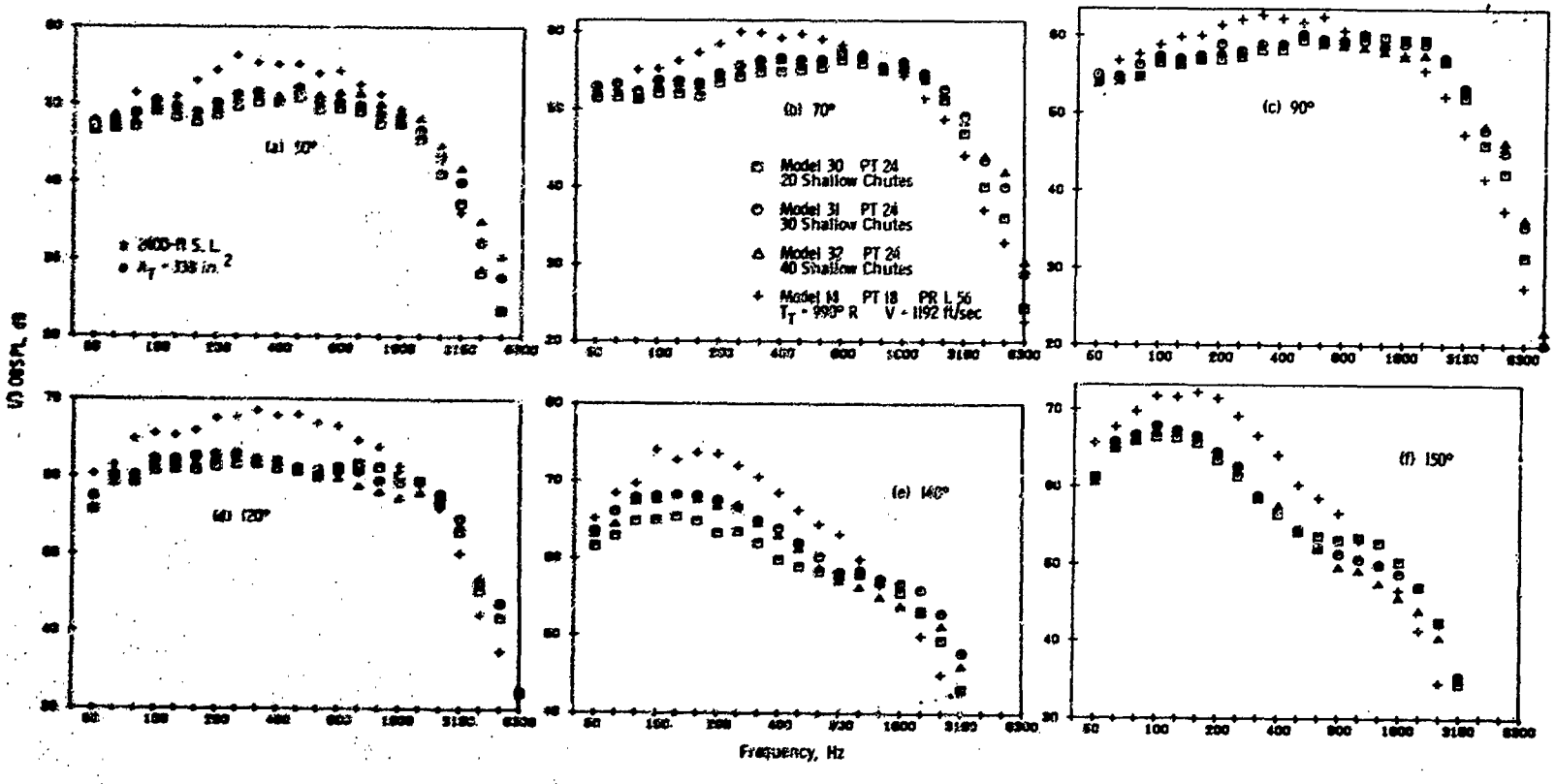

Figure 3-213. Suppressor Element Number Variation, Spectra, V_{ma} = 1200 ft/sec.

- The multielement suppressor's noise signature is observed to be a fair balance of pre and postmerged jet noise sources. At forward quadrant angles, the double humped spectra distribution, and in cases dominance of the premerged or high frequency noise, is normally seen. As expected at aft quadrant peak noise angles, the low frequency noise portion of the spectra tends to contribute more to the total noise with increasing velocity. This result implies greater importance of the merged-flow region in ultimately defining the velocity range of noise suppression.

In depth examination of the first data set, Figures 3-208 and 3-209 at V_{ma} = 2425 ft/sec, suggests the following:

- At peak noise angles, significant suppression relative to the conical nozzle is realized by the shallow chute models, particularly for 20 element segmentation (Model 30). Aft quadrant suppression is low to nil. Forward quadrant suppression is extremely high, up to 12 ΔPNL and 13 ΔOASPL at 50° due to reduced shock noise. The conical nozzle and outer stream cycle pressure ratios were at 3.92 and 3.98, respectively, for this data set. Slight amounts of shock noise influence can still be detected in the suppressed nozzle spectra at 50 and 70°.

- In the aft quadrant, suppressor spectra shape closely approximates that of the conical nozzle; at 120° fairly broadband suppression is observed, at 140° midfrequency levels are best reduced and at 150°, little-to-no suppression is present.

For the intermediate V_{ma} = 2100 ft/sec data set, Figures 3-210 and 3-211, the following are observed:

- Little variance is seen in peak PNL level but peaks shift from 120° for the 20 element to 140° for the 30 and 40 element suppressors. At the 140° location, spectra are similar for the 30 and 40 shallow-chute, Models 31 and 32, and suppression for the 20 element, Model 30 is quite broadband.

- The 20 shallow-chute, Model 30 noise is highest at inlet and broadside angles then lowest at aft angles on both PNL and OASPL bases, a full reversal of trends.

- Variation in PNL at forward angles is more pronounced than for OASPL. This is because low and intermediate frequency spectra are near to the same levels for the three models, and essentially control OASPL. In contrast, larger variance in PNL is controlled by high frequency spectra, still somewhat influenced by tone and broadband shock noise for the 20 and 30 element models. The larger characteristic flow dimensions and wider spacing between individual jets of the more coarsely segmented streams allow for development of shock structure and for radiation of associated tone and broadband noise before shock structure has decayed or has been destroyed

by merging of the individual jets. The duct stream was operating at a supercritical pressure ratio of 3.28 for this test point.

The third data set, Figures 3-212 and 3-213, is at $V_o = V_i = V_{ma} = 1200$ ft/sec. Significant PNL suppression occurs only in the peak and aft quadrant angles and is fairly broadband in frequency range. Low element number is slightly more effective at most angles. This is attributable to suppression of the controlling low and midfrequency spectra, even though high frequency noise levels are normally above those of the 30 and 40 element models.

3.4.2.4 Element Type Studies

Previous technology on multielement suppressors had indicated that ventilation capability of the segmenting element is an important parameter in the overall suppressor selection and system design. From an installed performance viewpoint, well ventilated chutes had substantially less thrust loss then low or nonventilated spokes, due primarily to the differences in base drag associated with the chute/spoke blockage area. Spokes, however, are mechanically far easier to implement within a nozzle system than chutes. They can be stowed on the plug surface and deployed simply for suppressor activation. Deeply ventilated chutes, due to their large size, must be stowed within the plug itself and are significantly more complex to deploy.

Data previously available for comparing chute to spoke performance was on a turbojet annular suppressor of low duct radius ratio. The current studies extend this data base to systems of high duct radius ratio for applications of full span suppressors to turbojets and of half-span suppressors on dual flow systems of moderate and low system area ratio, i.e., $A_o/A_i = 1.92$ and 0.65.

Element Type Study, Turbojet

The impact of varying element design from a fully ventilated chute to a nonventilated spoke was investigated on a full plug turbojet system within this study. Models 16 and 18 were used per Figure 3-214 photo and Figures 10 and 12 of Appendix A. The base model was a 36-chute suppressor of area ratio = 2.0 and radius ratio = 0.716. Removable filler inserts were used to convert from a well-ventilated chute to a nonventilated spoke designed to be flush with the shroud outer flowpath and with the chute exit plane. The acoustic test matrix for these turbojet configurations followed the matrix Section 3.2.1, Figure 3-8, using conventional turbojet and high TT cycle lines.

Review of the acoustic results in terms of peak OASPL in Figure 3-215 and peak PNL in Figure 3-216, (each showing the two cycle line results separately) indicates:

- A maximum suppression level of 13.5 dB is achieved relative to the conical nozzle by the spoke, on both a peak OASPL and a peak PNL basis.

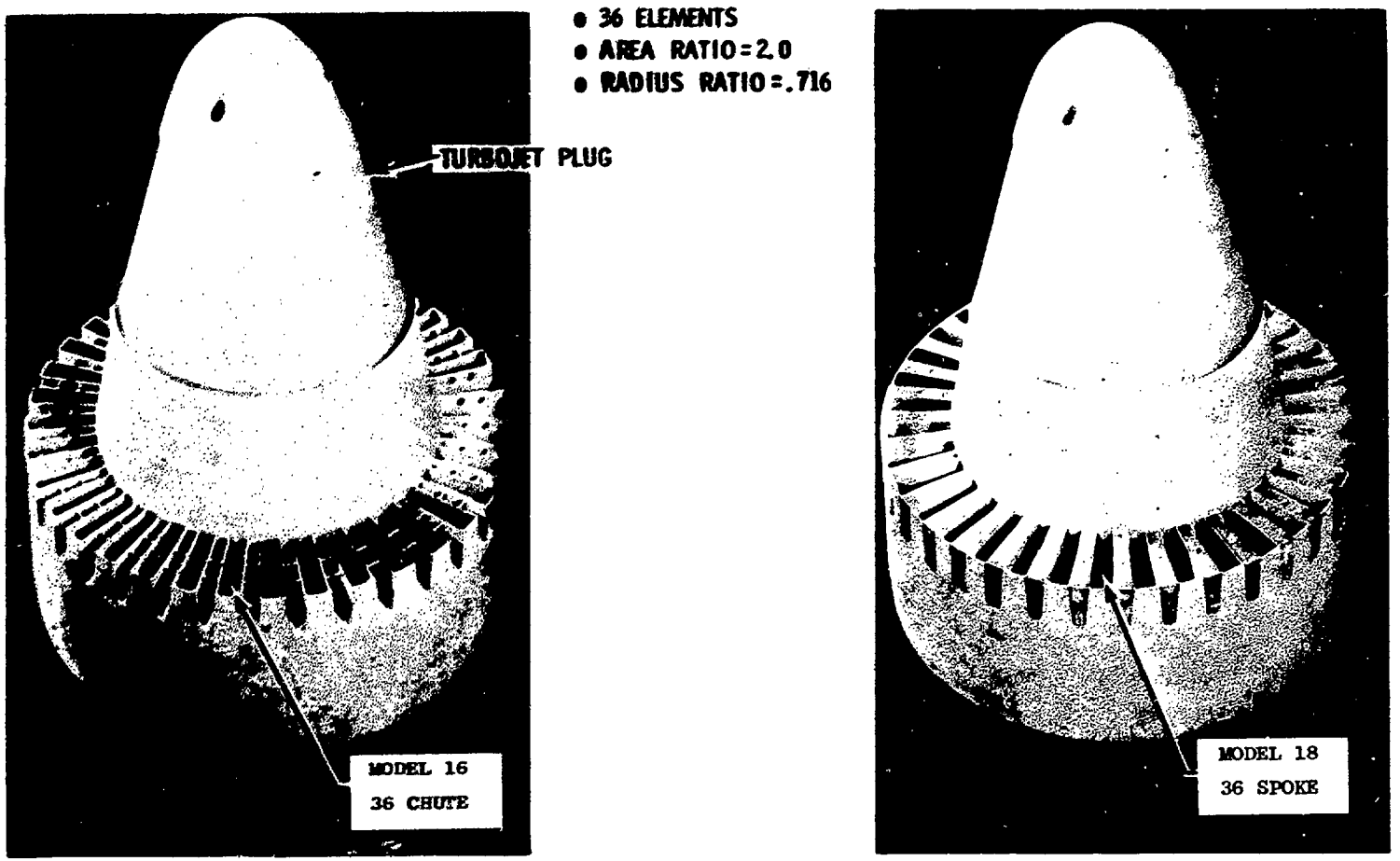

Figure 3-214. Element Type Variation on Turbojet.

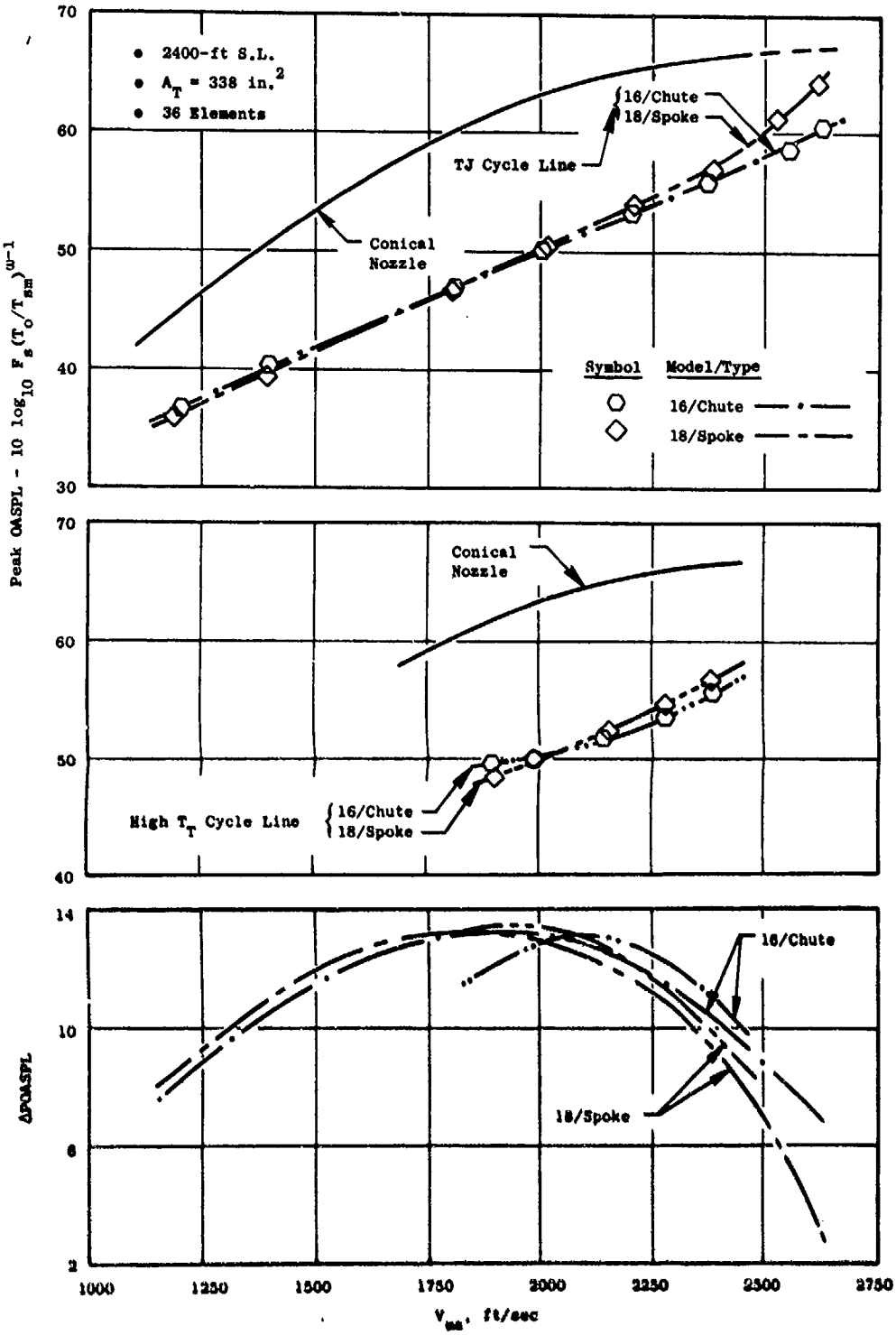

Figure 3-215. Variation of Element Type, Turbojet, Peak OASPL and Suppression Levels.

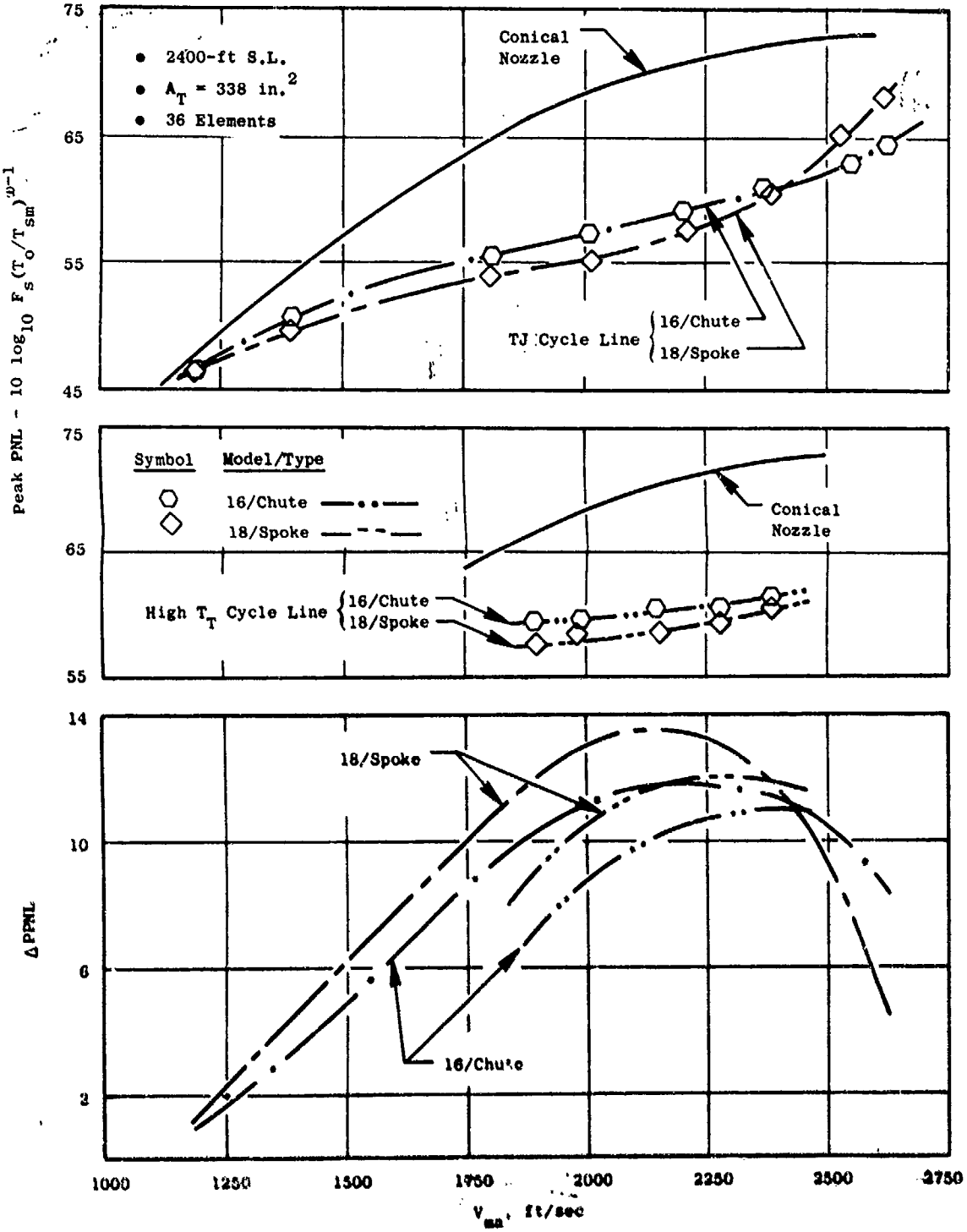

Figure 3-216. Variation of Element Type, Turbojet, Peak PNL and Suppression Levels.

- On the peak OASPL basis, the spokes and chutes are equivalent except at high velocity where the spokes becomes less effective than the chutes.

- In the high V_{ma} range, the spokes become substantially noisier than the chutes.

At 90°, Figure 3-217, spokes are more effective than chutes, from 1 to 2.5 ΔPNL in the mid-V_{ma} range, and become equivalent to chutes at the highest V_{ma} tested.

At 50°, Figure 3-218, results show that effectiveness of element type is more dependent on cycle line, the high T_T cycle line showing equivalence of spoke/chute and the conventional turbojet cycle line showing the spokes significantly more effective on a PNL basis.

On an overall power level basis, Figure 3-219, trends are the same as for peak PNL, showing spokes superior at mid-V_{ma}, then equivalent to or poorer than chutes at high V_{ma}.

Primary areas of interest on a PNL and OASPL directivity and spectral distribution basis are presented in:

Figure 3-220 OASPL and PNL vs θ at V_{ma} = 2380 ft/sec

Figure 3-221 Spectra at 50, 90 and 130° at V_{ma} = 2380 ft/sec

Figure 3-222 OASPL and PNL vs θ at V_{ma} = 2620 ft/sec

Figure 3-223 Spectra at 50, 90 and 130° at V_{ma} = 2620 ft/sec

The above two data sets exemplify the distinct difference in suppression characteristics at mid and high velocity points.

For the first set at 2380 ft/sec, the OASPL distributions are similar at all angles, particularly broadside and in the aft quadrant, while PNL is similar at peak and aft, but much lower for the spoke in the forward quadrant. The 130° spectra bear out similar frequency distribution; but at 90° and 50°, the high frequency levels of the chute are much more predominant. Distribution and level suggest a broadband shock cell noise influence at this highly supercritical pressure ratio of 3.28.

At the higher V_{ma} = 2620 ft/sec data point, PNL and OASPL distributions are similar for the spoke and chute except near peak angle and in the far forward quadrant, where the spoke is now noisier than the chute. At 130° the spectra suggest this is a low frequency jet mixing noise phenomena; and at 50°, the difference is primarily in higher frequency bands, again associated with shock-cell noise at this high pressure ratio of 3.92.

As in the previous spectra at lower V_{ma}, shock-noise was present for only one of the designs (not the same one), suggesting a phenomena associated

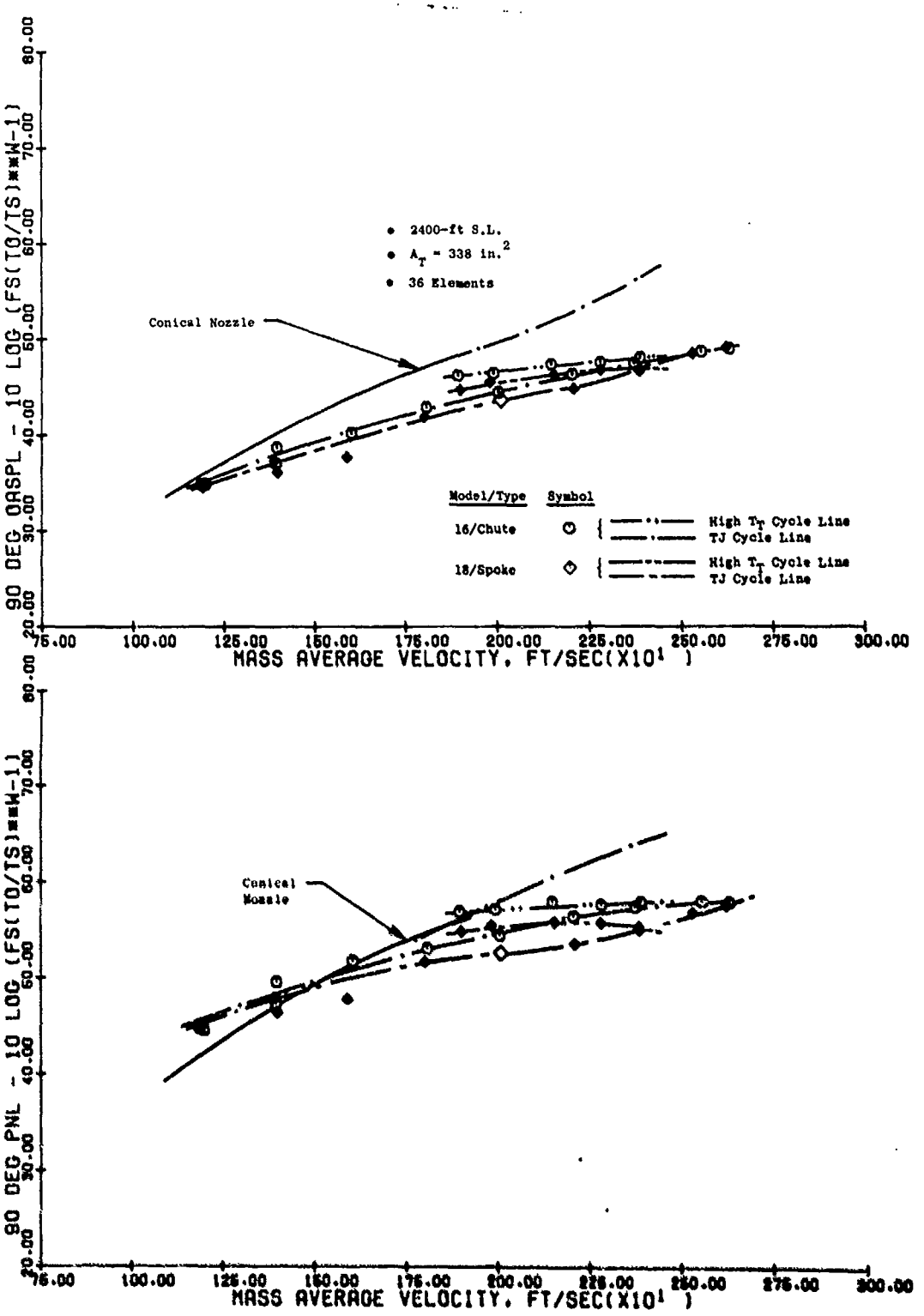

Figure 3-217. Variation of Element Type, Turbojet, 90° OASPL and PNL.

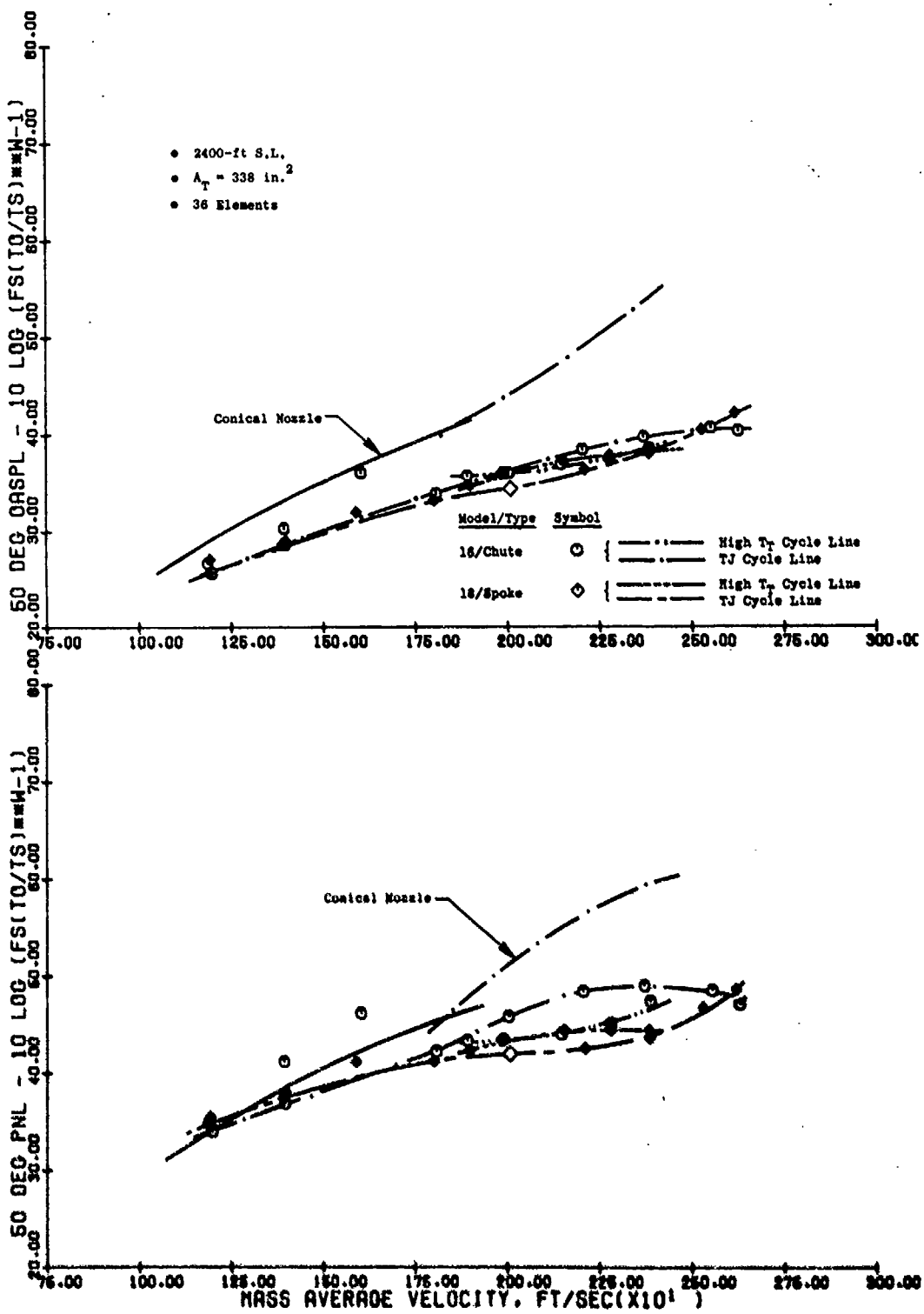

Figure 3-218. Variation of Element Type, Turbojet, 50° OASPL and PNL.

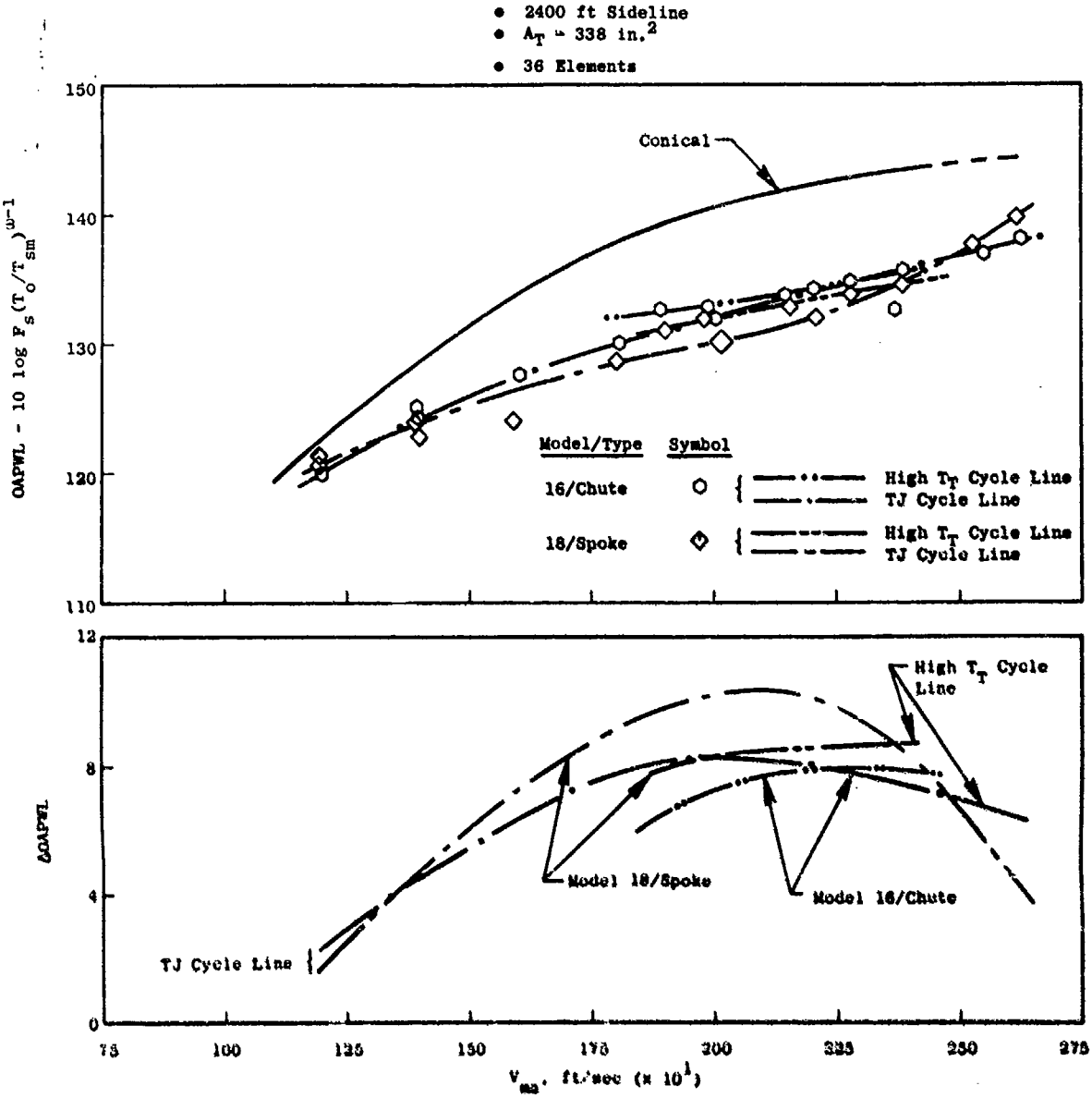

Figure 3-219. Variation of Element Type, Turbojet, OAPWL and Suppression Levels.

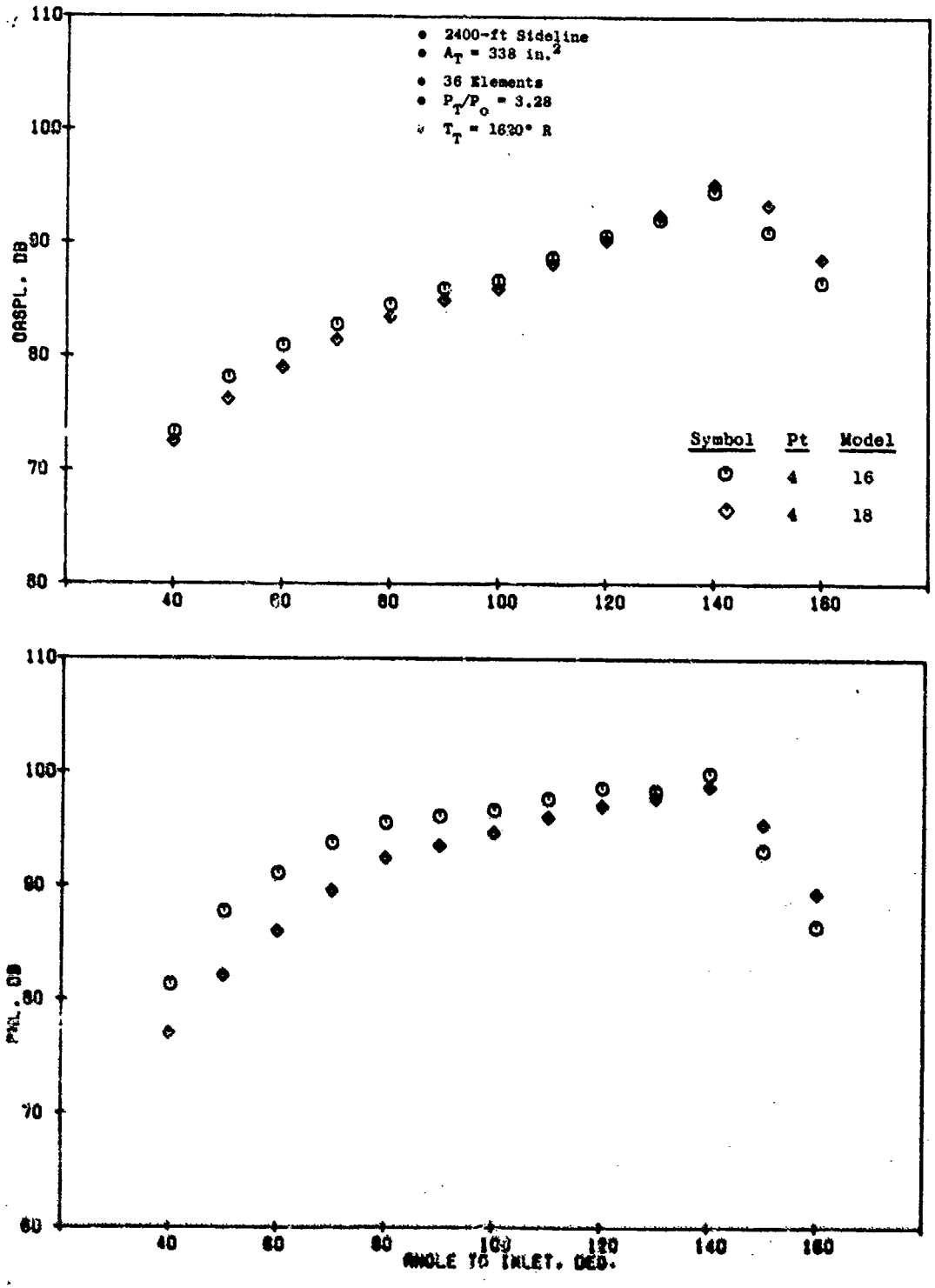

Figure 3-220. Variation of Element Type, Turbojet, OASPL and PNL Directivity, V_{aa} = 2380 ft/sec.

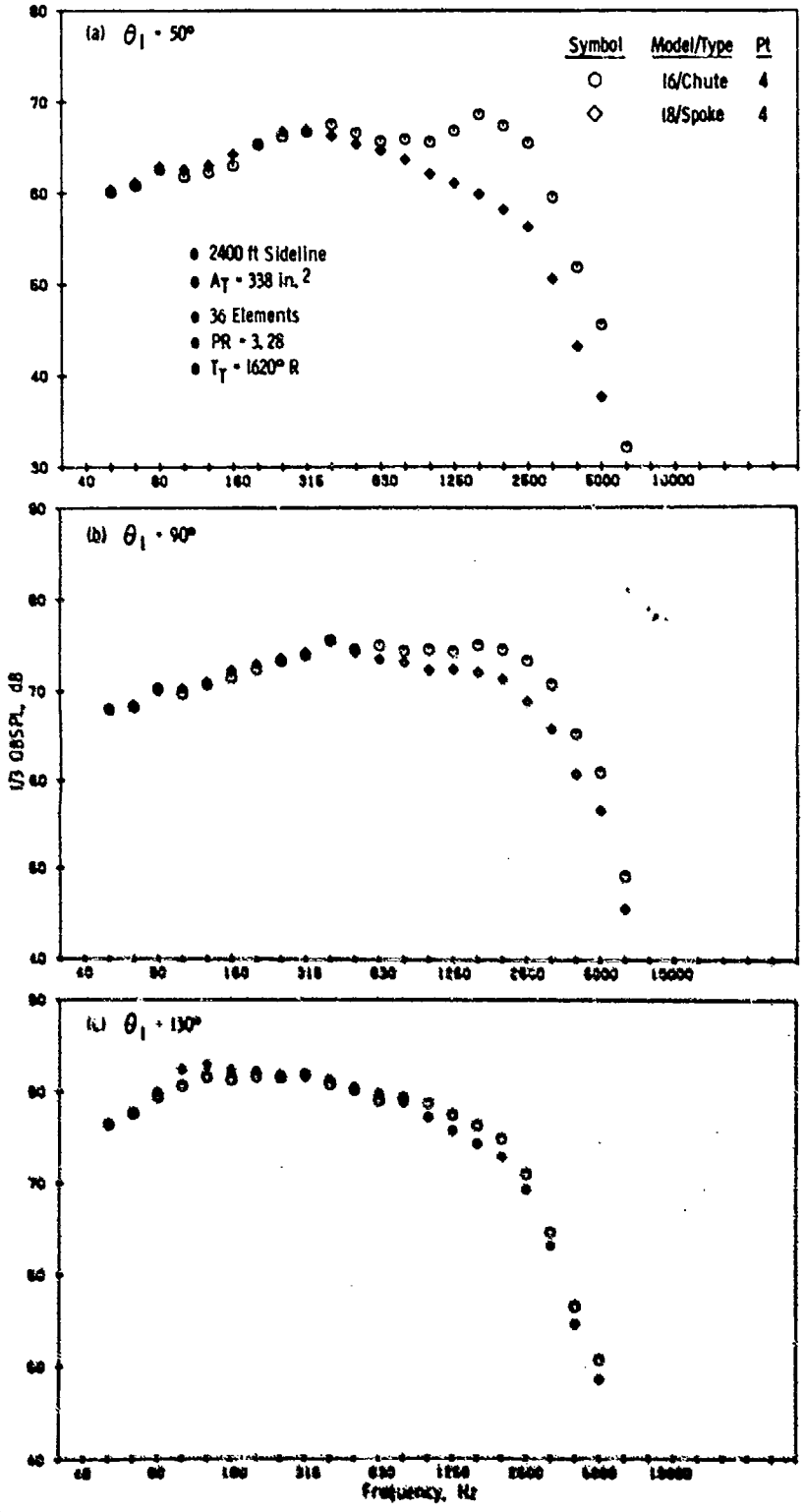

Figure 3-221. Variation of Element Type, Turbojet, Spectra, V_{ms} = 2380 ft/sec.

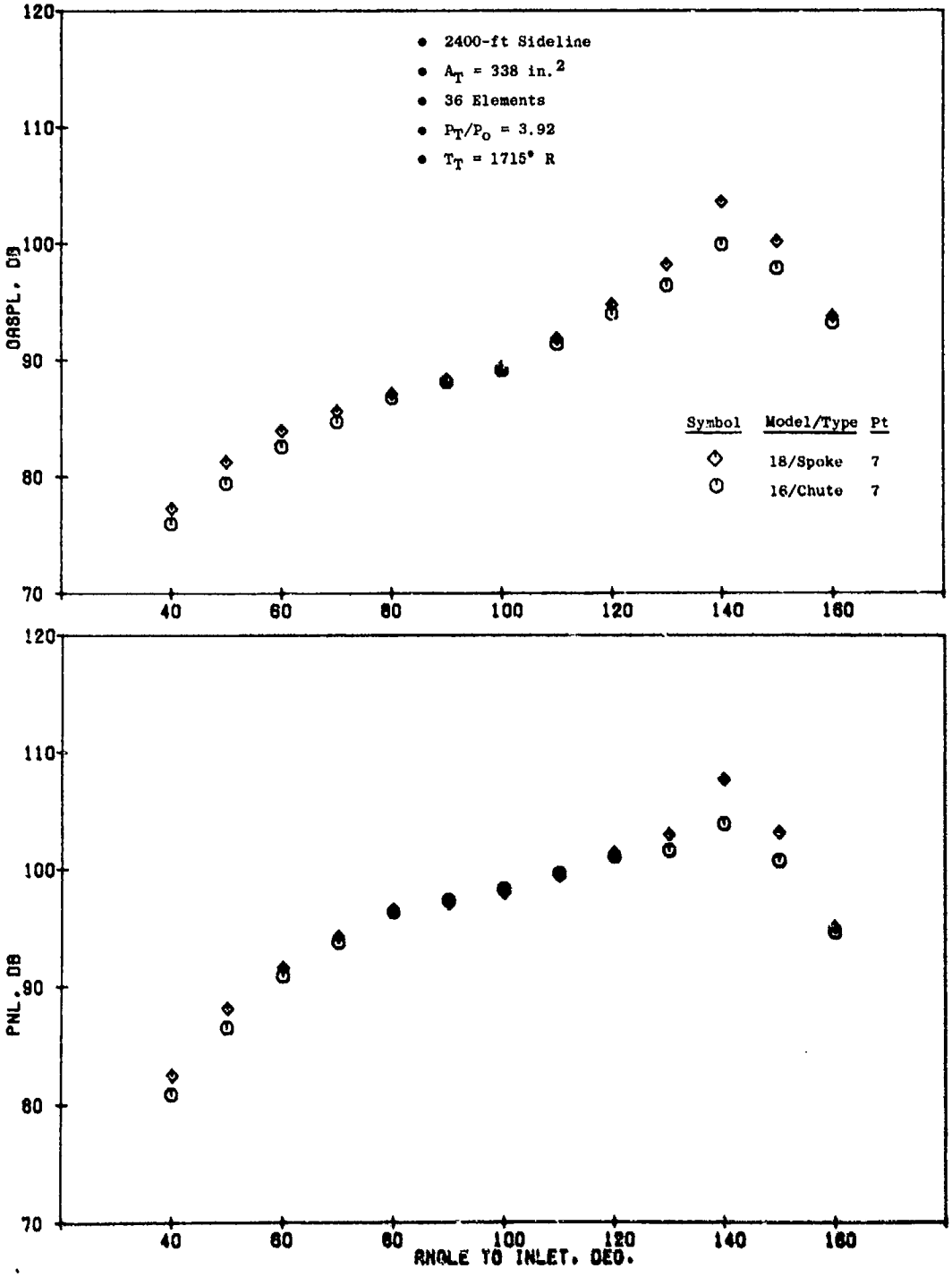

Figure 3-222. Variation of Element Type, Turbojet, OASPL and PNL Directivity, V_{ms} = 2620 ft/sec.

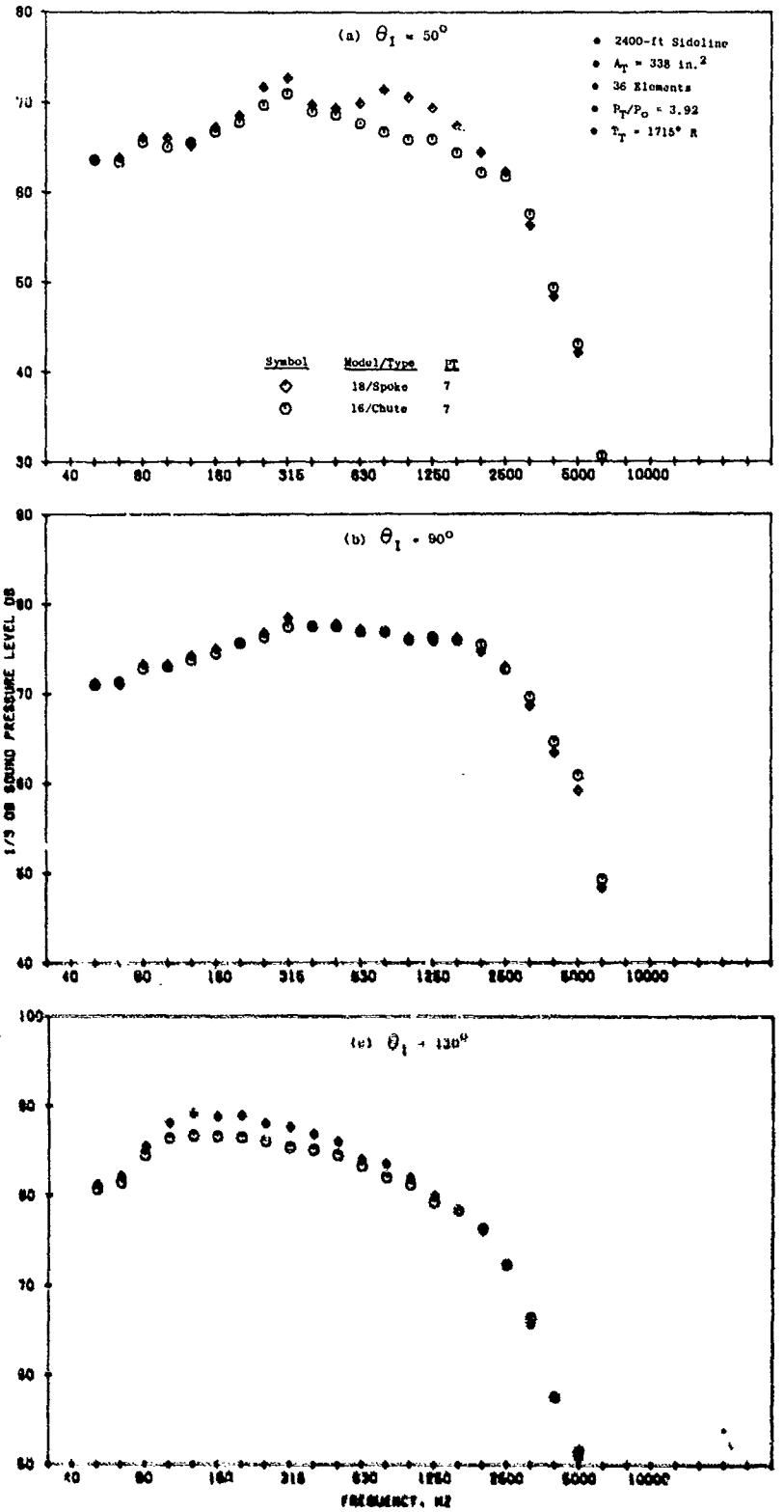

Figure 3-223. Variation of Element Type, Turbojet, Spectra, V_{ma} = 2620 ft/sec.

with the large variance in ventilation capability and its resultant impact on mixing potential and base pressurization, effecting the potential to generate strong shock-cell noise.

Element Type Study - Dual Flow of High System Area Ratio

This study extended investigation of varying element type from the deeply ventilated chutes to nonventilated spokes, but now on a dual flow nozzle with system area ratio of 1.92. Models 24 and 28 were used, Figure 3-224 photo and details in Appendix A, Figures 18 and 22. Model 24 was similar to Model 16 of the previous study in that the annular suppressor has 36 elements, AR = 2.0 and R_r^o = 0.716. Model 24 has a core plug of 0.7" annulus height located in the retracted position. Model 28 used the same filler inserts as Model 18 to convert the base chute model to the spoke configuration.

The acoustic test matrix for these dual flow models was per Section 3.2.1, Figure 3-10 and Table 3-3, using the following cycle lines:

- W_i = 0, 15 and 30% W_o
- DBTF/Inverted Dual Flow
- AST/VCE

The following study results are included, selected from the DBTF/Inverted Dual Flow and W_i = 30% W_o cycle lines and are representative of overall cycle trends:

- Figure 3-225 Peak PNL
- Figure 3-226 Peak OASPL
- Figure 3-227 90° OASPL and PNL
- Figure 3-228 50° OASPL and PNL

Review of the data indicates:

- On the basis of peak OASPL, Figure 3-226, spokes attain a maximum suppression level slightly greater than 12 dB; approximately 3 dB higher suppression than the chutes. This maximum suppression level is slightly under the 3.5 ΔPOSPL attained on Model 18 spoke/turbojet system; however, peak suppression levels on both turbojet and dual flow systems are attained by spokes.
- A significant margin of better performance by the spokes is observed for the dual-flow system over the test velocity range. This is contrary to the results of the turbojet application, where spokes and chutes were essentially equivalent except at high V_{ma} where spokes became somewhat less effective than chutes.

- **Area Ratio = 2.0**
- **Radius Ratio = 0.716**

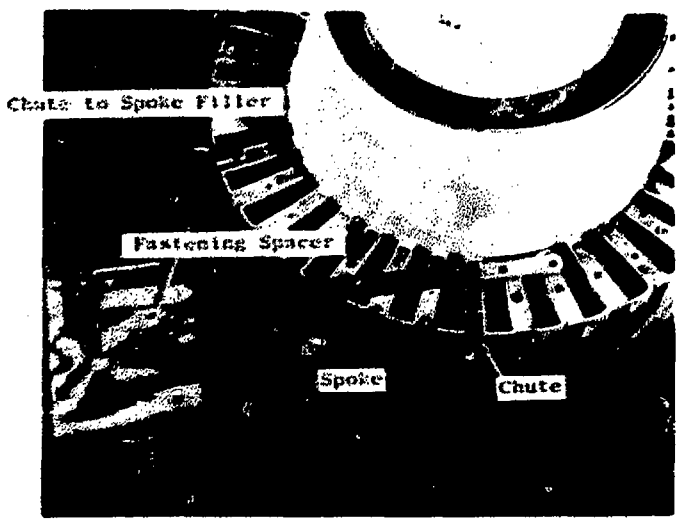

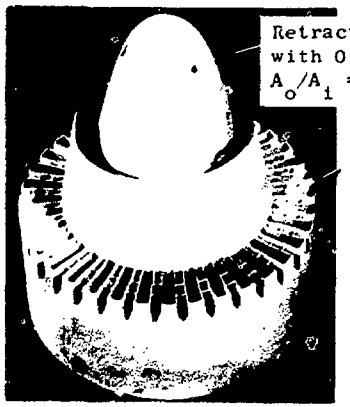

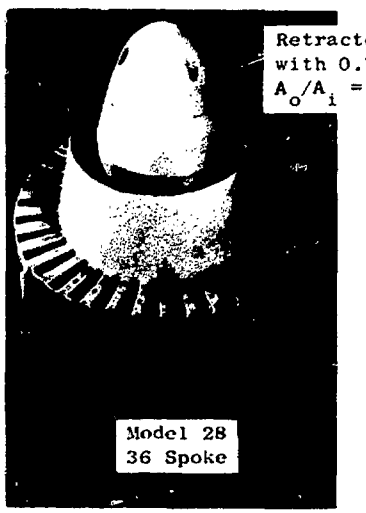

Figure 3-224. Conversion of Half-Span Suppressor from Chutes to Spokes.

- 2400-ft Sideline
- A_T = 338 in.^{2}
- 36 Elements

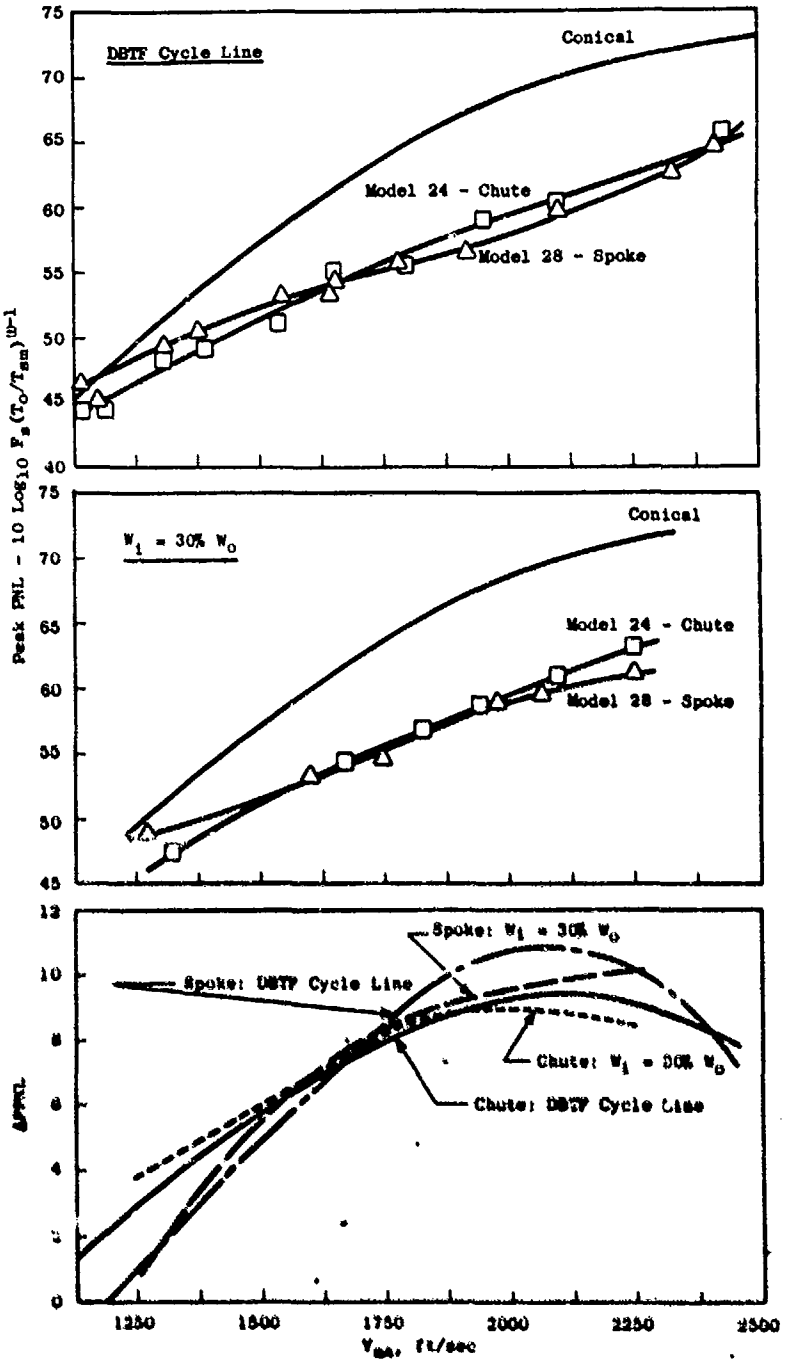

Figure 3-225. Element Type Variation, Dual Flow, Peak PNL and Suppression Levels.

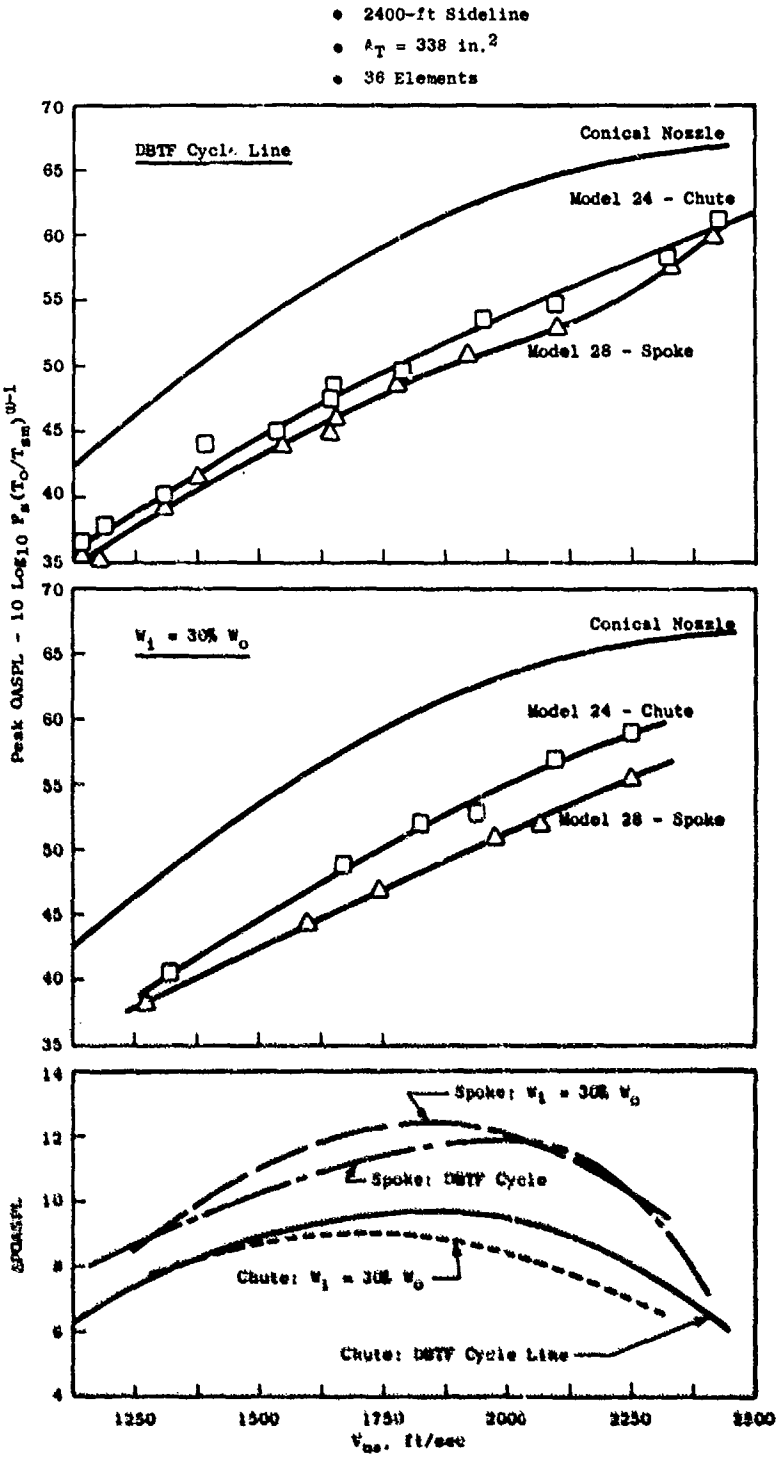

Figure 3-226. Element Type Variations, Dual Flow, Peak PNL and Suppression Levels.

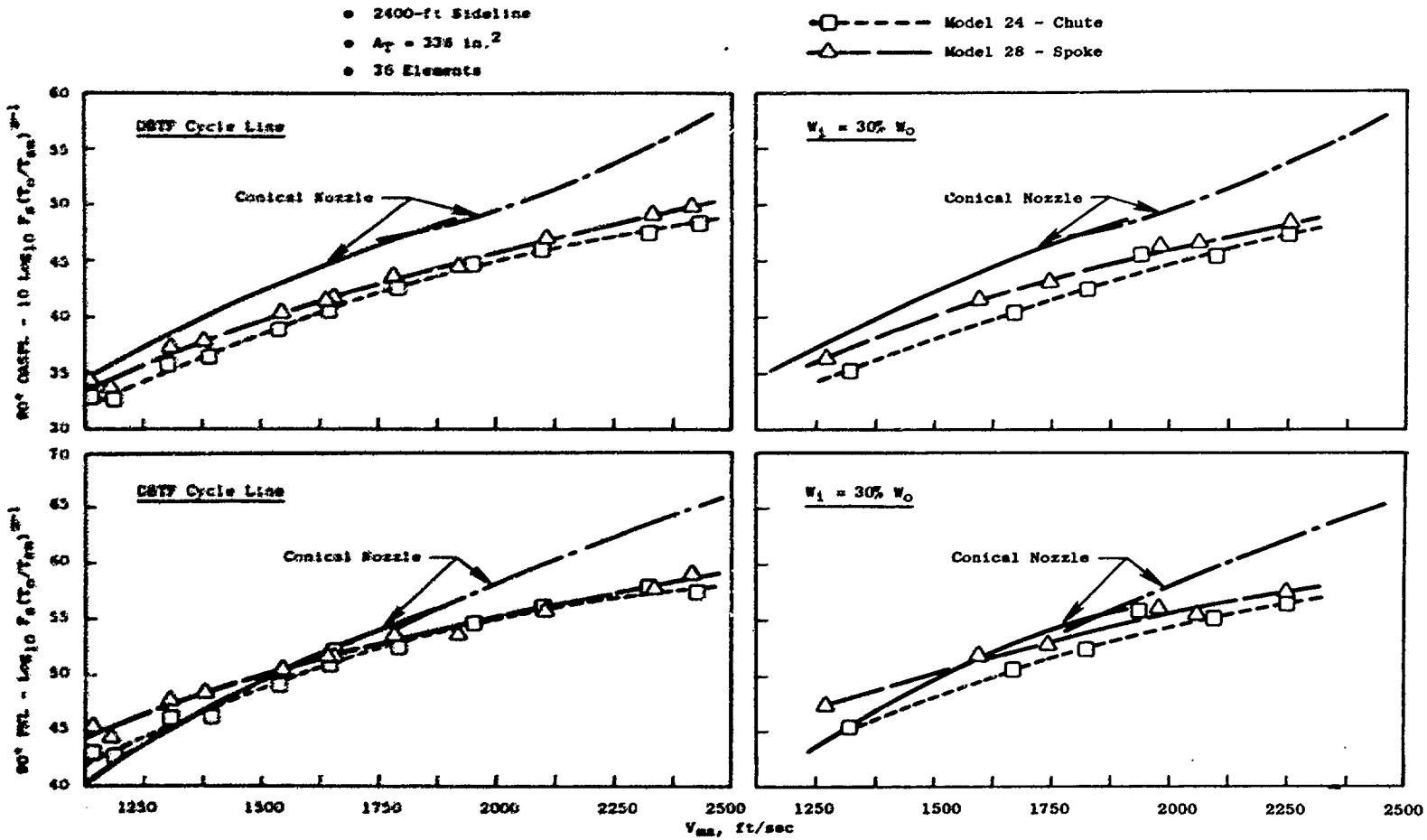

Figure 3-227. Element Type Variation, Dual Flow, 90° OASPL and PNL.

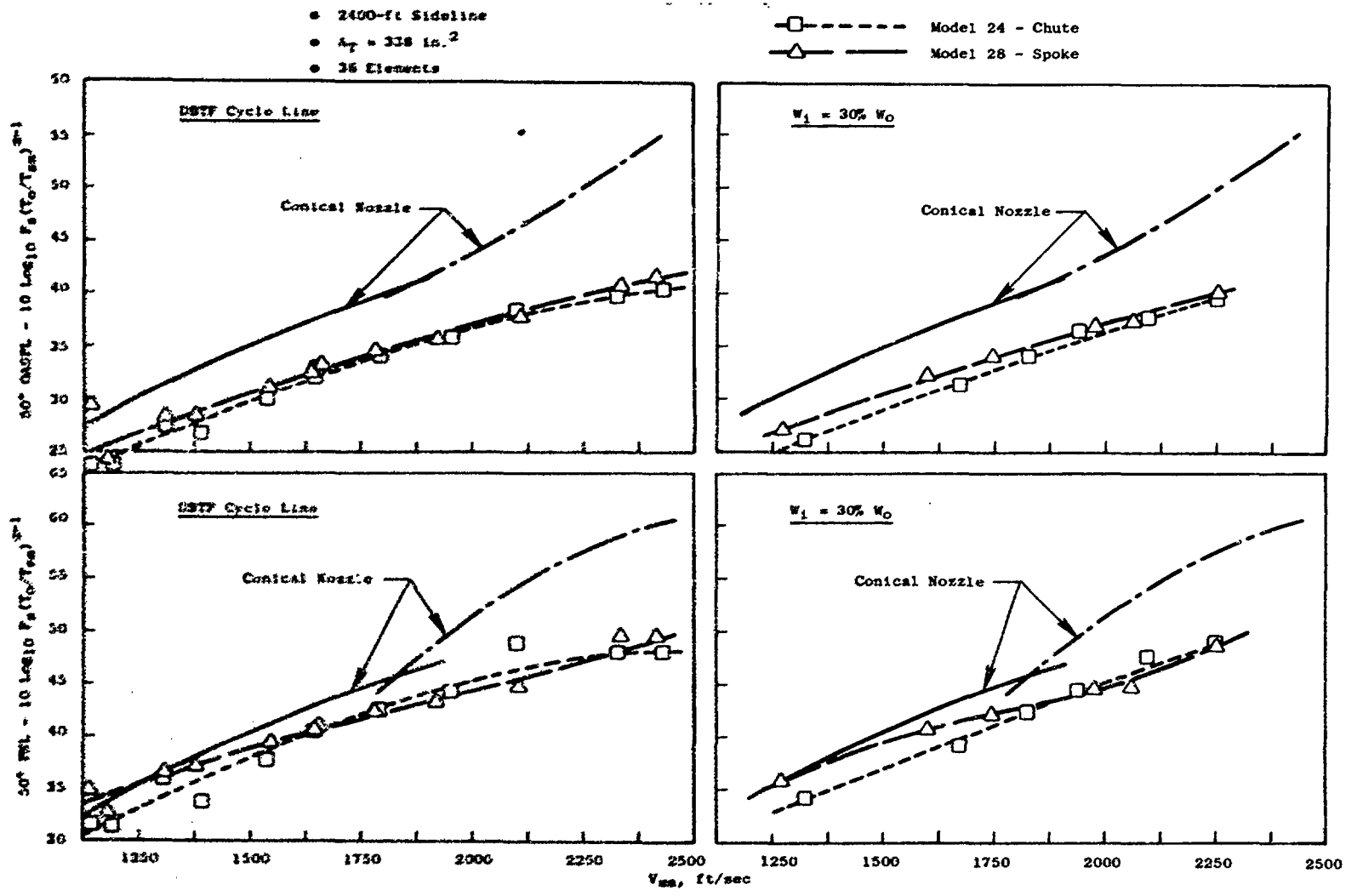

Figure 3-228. Element Type Variation, Dual Flow, 50° OASPL and PNL.

- On the basis of peak PNL, Figure 3-225, a maximum suppression level of about 10.5 dB is observed, which is significantly less than the 13.5 ΔPPNL attained by turbojet spokes. In the mid-to-high velocity range, the spokes are from 0.5 to 1.5 dB more effective than chutes for either cycle line presented. The span of increased effectiveness of the spokes is not observed, as it was for the spoke/chute-turbojet systems. At lower velocity and chutes (Model 24) are slightly more effective than the spokes (Model 28).

- Review of the 90 and 50° data, Figures 3-227 and 3-228, shows in most instances that the spoke loses its performance edge and is either equivalent to or somewhat noiser than the chutes. This again is somewhat dissimilar to the turbojet application where spokes retained significant suppression advantage at broadside and forward quadrant angles.

Element Type Study - Dual Flow of Low System Area Ratio

This third study of element type variation compares deeply-ventilated chutes to nonventilated spokes, on a dual flow system of $A_o/A_i = 0.65$. Models 33 and 35 were used (Figure 3-229) and detailed schematics of Appendix A Figures 27 and 29 show chute and spoke nozzles, respectively. Model 33 of suppressor area ratio = 2.5, from the NASA-Lewis/GE Duct Burning Turbofan Program, NAS3-18008, (Reference 10) was adapted to the Cell 41 Anechoic Facility. Model 35 converted Model 33 to nonventilated spokes through application of filler inserts, maintaining the same inner flowpath geometry. Pertinent parameters for the models are:

		Outer			Inner				
Model No.	El. No & Type	Flow Area, $in.^2$	Area Ratio	Radius Ratio	Flow Area, $in.^2$	Step Height, in.	Plug Location	Radius Ratio	System Area Ratio
33	36 Chute	17.21	2.5	0.783	11.12	1.034	Retracted	0.674	0.65
35	36 Spoke	17.21	2.5	0.783	11.12	1.034	Retracted	0.674	0.65

Far-field acoustic testing was performed in the Cell 41 Anechoic Facility following a matrix similar to Section 3.2.1, Figure 3-10 and Table 3-3, but expanded to be more consistent with the matrix of the Reference 10 DBTF program. The following cycle series was used:

- W_i = 0, 15 and 30% W_o
- DBTF/Inverted Dual Flow Cycle
- AST/VCE

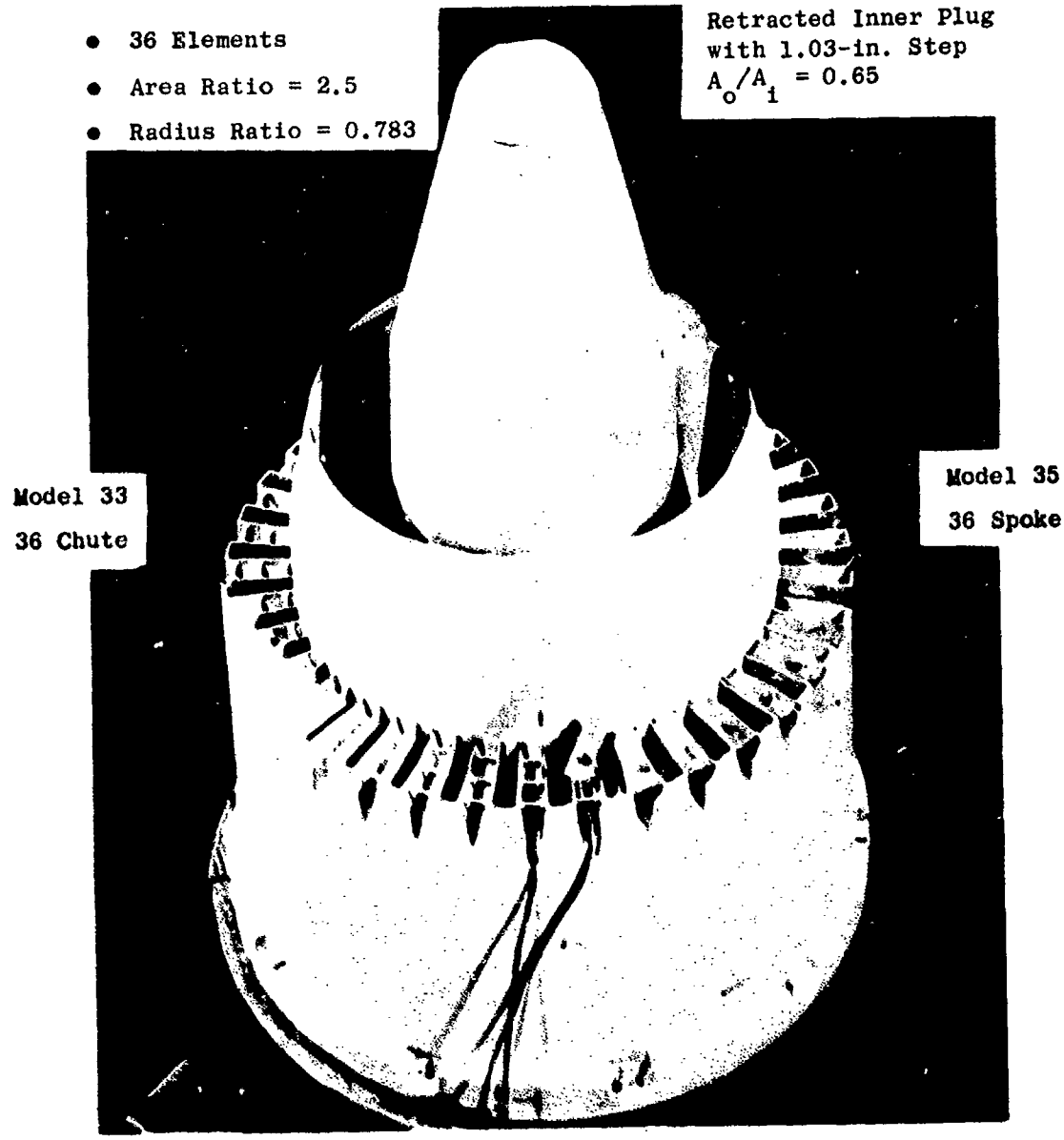

Figure 3-229. Element Type Variation, Dual Flow, Low System Area Ratio.

Primary acoustic data for the two models, tested within the DBTF/Inverted Dual Flow cycle matrix are presented and discussed in Section 3.4.2.2 (System Velocity Ratio Variation at Fixed A_o/A_i and Duct Suppressor Geometry). It is shown that noise levels for systems of low area ratio, e.g. $A_o/A_i = 0.65$, vary widely with cycle velocity ratio, V_o/V_i the inner flow more strongly governs the overall system. Within this section, for isolation of suppressor element type impact on acoustic performance, comparisons between the two models at fixed values of $V_o/V_i = 0.6, 0.8, 1.0, 1.25, 1.5, 2.0$ and ∞ (no inner flow) are included in Figure 3-230 for peak PNL and in Figure 3-231 for peak OASPL, selected to be representative of all test data.

For the peak PNL data, again, only minor variances are seen, particularly at low V_o/V_i. For $V_o/V_i \geq 1.5$, a slight margin of better performance by 1 to 2.5 ΔPNL is seen for the spokes. On the previous study's spoke/chute application to a dual flow system of $A_o/A_i = 1.92$, from mid-to-high V_{ma}, the spokes were also slightly better by 0.5 to 1.5 ΔPNL than the chutes. For the turbojet system at low-to-mid V_{ma}, the spokes were better than the chutes by approximately 2 ΔPNL at 2000 to 2200 ft/sec, but at high V_{ma}, the spokes become substantially noisier than their counterparts.

On the basis of peak OASPL, very little difference is seen between spokes and chutes for any V_o/V_i ratio; the small variance that exists shows no significant trend. If any distinctions had to be extracted from the data they would be: a) At low V_o/V_i the chute (Model 33) is slightly noisier than the spoke (Model 35), b) at intermediate values of V_o/V_i the two are near comparable with only a slight margin of better chute performance at high V_{ma}, and c) at the very high V_o/V_i the chute is normally about 1 ΔOASPL quieter. These results are compatible with those of the two previous studies where turbojet application showed spokes and chutes almost the same except for the small advantage by chutes at high V_{ma}, and dual flow application showed the spokes somewhat better at any V_{ma}.

With the small variance observed in suppression potential between deeply-ventilated chutes and nonventilated spokes, acoustic performance may not be the principle design consideration. Aerodynamic performance differences and mechanical implementation considerations will have a strong influence in the ultimate selection process. These aspects are discussed in Volume III.

3.4.2.5 Treated Ejector Applications

Treated Ejector Application, Turbojet

The potential for additional noise reduction of annular suppressed jets was evaluated through application of an acoustically treated ejector to a basic turbojet propulsion nozzle. Models 16 and 19, as shown in Figure 3-232 and in the detailed schematics of Appendix A, Figures A-10 and A-19, were used. The basic Model 16 as described in Section 3.4.2.1 "Area Ratio and Radius Ratio Variable, Turbojet" consists of a 36-chute, AR = 2.0, $R_T^D = 0.716$

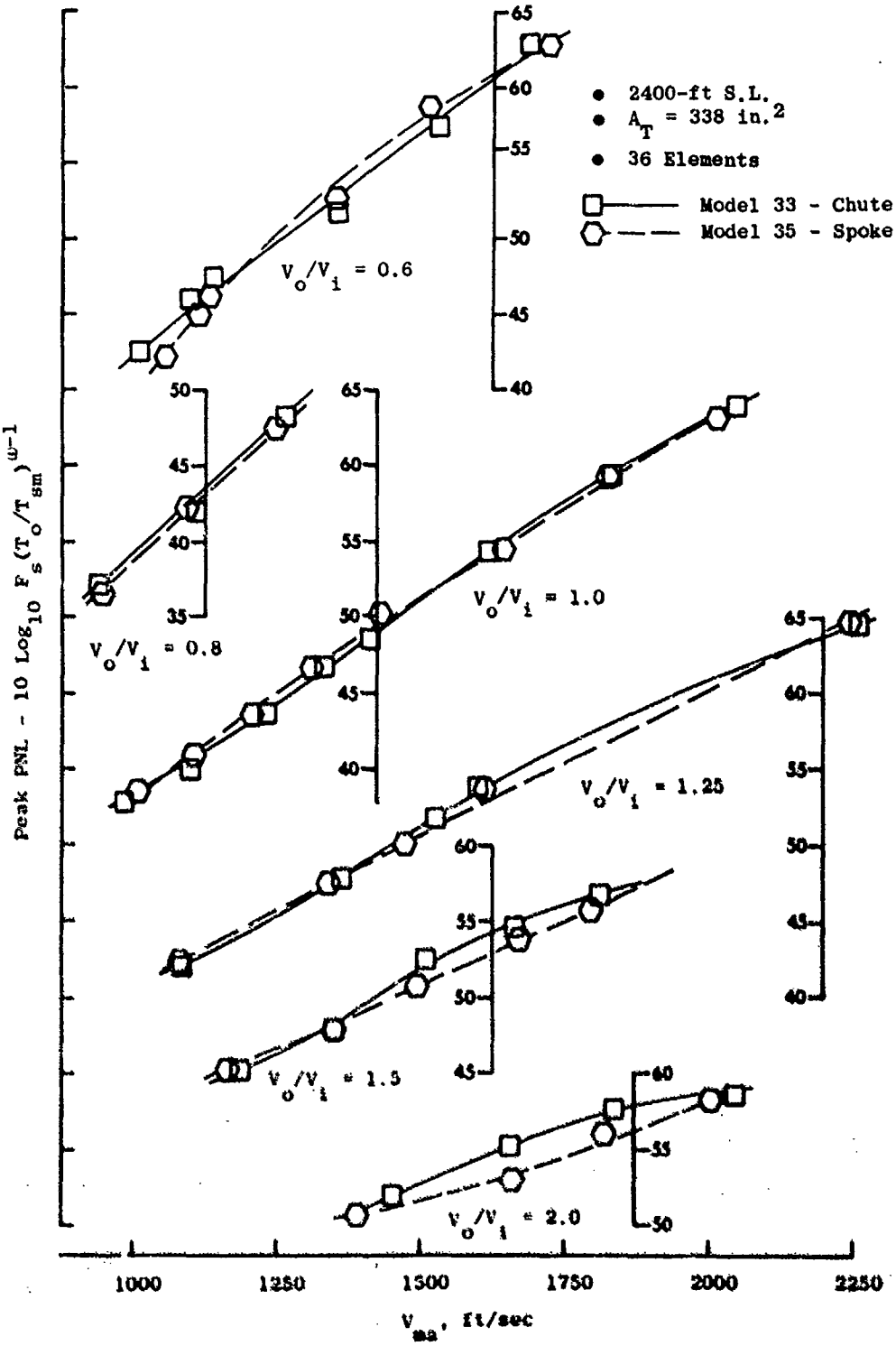

Figure 3-230. Element Type Study, Dual Flow, Low System Area Ratio, Peak PNL.

366

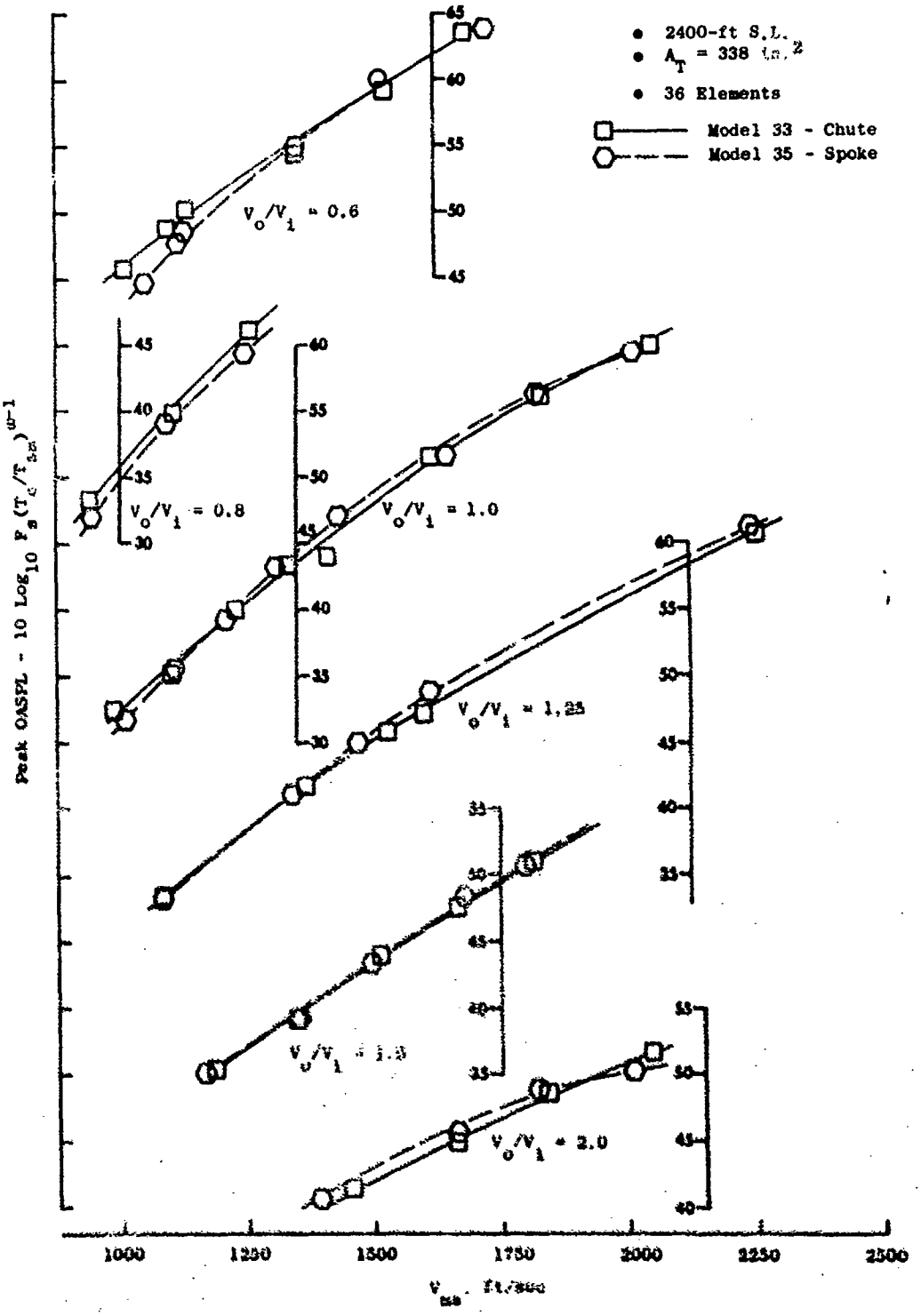

Figure 3-231. Element Type Study, Dual Flow, Low System Area Ratio, Peak OASPL.

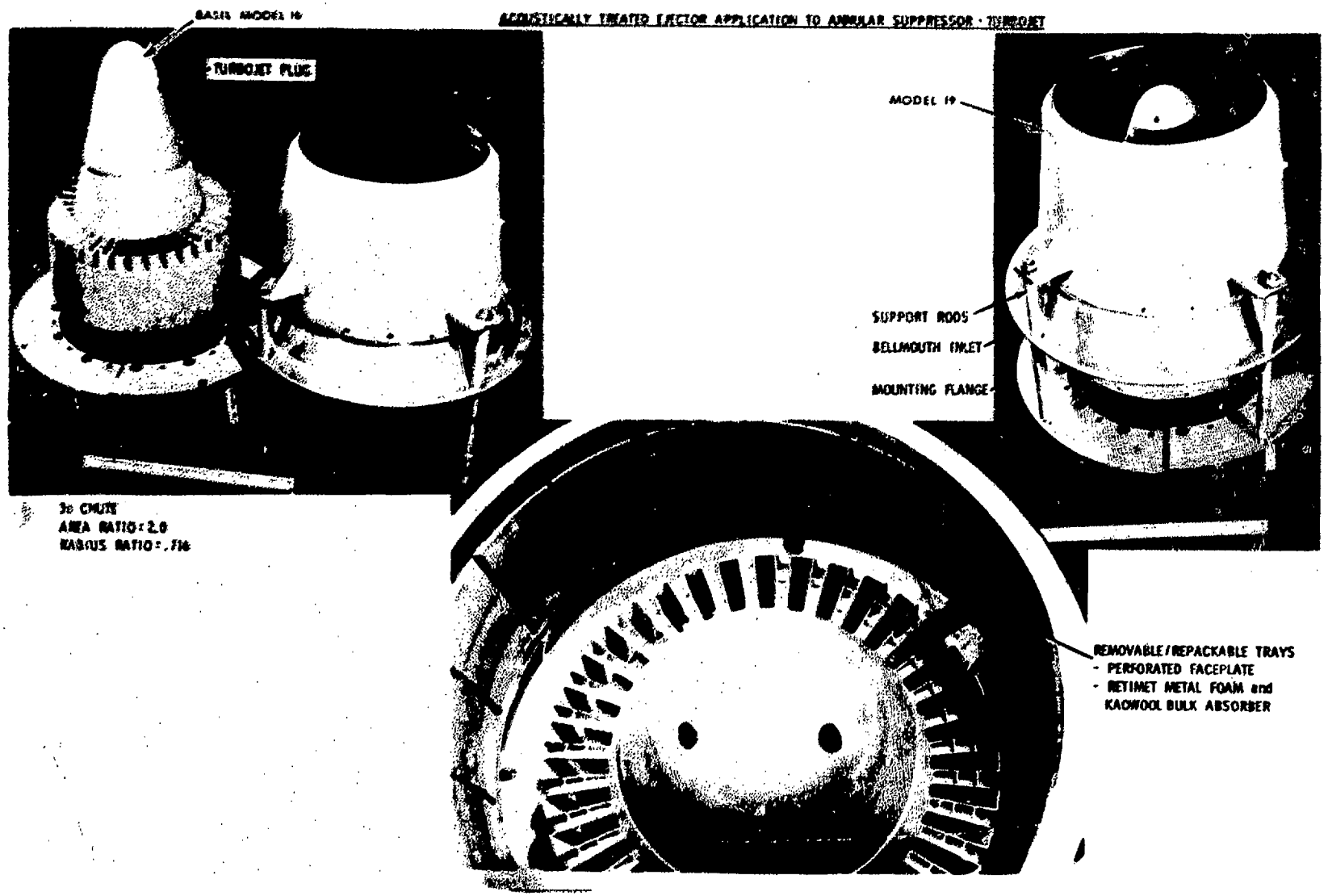

Figure 3-232. Acoustically Treated Ejector Application to Annular Suppressor, Turbojet.

annular suppressor on a full-plug turbojet. The acoustic performance of the basic segmented suppressor was expected to be enhanced, partially due to physical shielding of the ejector shroud, but primarily due to energy absorption by the acoustic treatment within the wall. Highly segmented annular suppressors redistribute acoustic energy to the higher frequency range where it is more effectively absorbed by a broadband bulk absorbing material. The basic design of the high-radius-ratio annular plug nozzle positions the suppressor elements, and their accompanying segmented jet noise sources, within close proximity of the ejector treatment. Previous suppressed annular plug/treated ejector systems, Reference 4, were of low radius ratio design and possibly did not benefit from this feature.

The ejector's internal flow lines were designed for good aerodynamic performance, using Figure 3-1 and the guidelines of Reference 10 as follows:

- Ejector inlet diameter to suppressor shroud diameter ratio (D_{E_i}/D_s) of 1.11 was set, a fairly tight fitting ejector design.

- Ejector axial positioning was set by the ratio of offset spacing to suppressor shroud radius (X_s/R_s) = 0.27; therefore, X_s = 1.5 in.

- Ejector length was established from practical system considerations and limitations, with ratio of ejector length to ejector inlet diameter (L_E/DE_i) set at 0.75 therefore, L_E = 9.28 in.) This terminates the ejector near the center plug's tip.

- Ejector exit diameter (D_{E_e}) was set by equating exit flow area to inlet flow area for proper flow filling within the ejector to prevent flow separation and base pressure loss. The inlet area considers ejector offset spacing and chute ventilation.

The acoustic treatment system design and material selections were based on a combination of approximate theoretical considerations and available experimental results. The bulk absorber material was selected to withstand high temperature in the nozzle exhaust environment and to have good acoustic absorption properties over a reasonably wide frequency range. Details of construction and packing of the ejector system are shown in Figure 3-233. Removable/repackable trays were used so that the bulk absorber material could be refurbished if degradation occurred due to exposure to the highly turbulent environment. Construction details are as follows:

- Cavity depth was approximately 0.43 in, faced with 37% porous perforated sheet metal using 0.045-in.-diameter holes on a straight line pattern with 0.067 in. spacing between centers, 225 holes/ $in.^2$, 24 gage material.

- The cavity was lined with approximately 0.1-in. thick 95% porous RETIMET NiCr Metal Foam, 60-70 cgs Rayls, to protect the ceramic fiber absorer from degradation. The remaining cavity depth was packed with KAOWOOL, a ceramic refractory fiber bulk absorber,

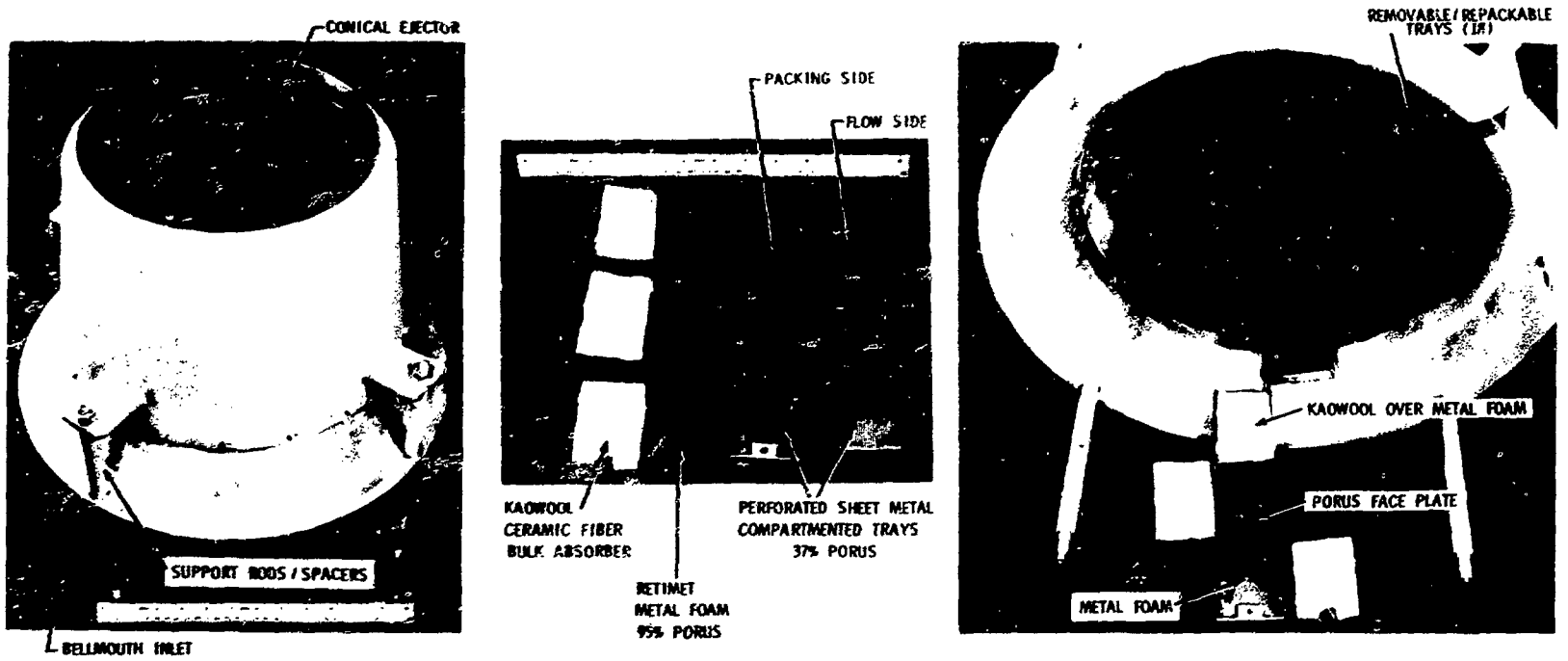

Figure 3-233. Details of the Acoustically Treated Ejector.

compressed to 3 lb/ft^3 density. The material has good absorption and insulation characteristics and is capable of sustained use at 2300° R without devitrifying.

A contoured bellmouth inlet was used for the static acoustic tests to provide idealized flow to the ejector, thus eliminating the possiblity of an extraneous noise source from flow separation around a sharp lip.

Acoustic tests were performed in the Cell 41 Anechoic Facility and followed the matrix of Section 3.2.1, Figure 3-8, using conventional and high T_T cycle lines.

Peak PNL acoustic results, Figure 3-234, are shown separately as applicable to the conventional turbojet and high T_T cycle lines, each relative to the conical baseline. The lower part of the graph shows the suppression level (ΔPPNL) of Model 19 referenced first to the conical nozzle for overall system suppression level, then referenced to Model 16 for gaging the effectiveness of the treated ejector application. Similar data plots for peak OASPL are shown in Figure 3-235. It is observed that maximum suppression levels of 15.5 ΔPPNL and 11.5 ΔPOASPL are achieved at V_{ma} ≈2100 to 2200 ft/sec. Peak PNL suppression drops drastically above and below the maximum value, to 5 ΔPPNL at high V_{ma}, and 7 at low V_{ma}. On a peak noise basis, the ejector is very effective, accounting for 5.5 ΔPPNL and approximately 4 ΔPOASPL at low V_{ma} and about 4 ΔPPNL and 2 ΔPOASPL at mid-V_{ma}. At highest V_{ma}, however, the suppression trend is actually reversed and the ejector application appears to generate greater noise than the nonejector system.

Comparing the turbojet cycle line to the high T_T cycle line, basic overall suppression levels relative to conical vary somewhat, particularly for ΔPPNL at 1800 to 2100 ft/sec. However, suppression levels attributable to the ejector alone are reasonably consistent.

At 90°, Figure 3-236, the Model 19 system yields suppression at all velocity values. This system has a distinct advantage over the basic nonejector Model 16, particularly in the low and midvelocity region where the system exhibits noise levels comparable to, or higher than, the baseline. Suppression attributable to the ejector alone (plotted as Model 19 relative to Model 16) shows levels and trends of ΔOASPL and ΔPNL closely matching those at peak angle.

Figure 3-237, 50° OASPL and PNL data, shows significant levels of suppression with the ejector relative to the conical baseline at all jet velocities. Suppression attributable to the ejector is fairly well maintained even within the forward quadrant, particularly on a ΔPNL basis in the low and midvelocity range. At high V_{ma} the loss of suppression and/or some noise enhancement is seen, similar to what occurred at the peak noise angles.

The overall power level data of Figure 3-238 show trends and ejector levels of effectiveness paralleling those of the PPNL data. Low and midvelocities show significant noise reduction relative to the basic system; high-velocity suppression is negated and/or shows noise enhancement.

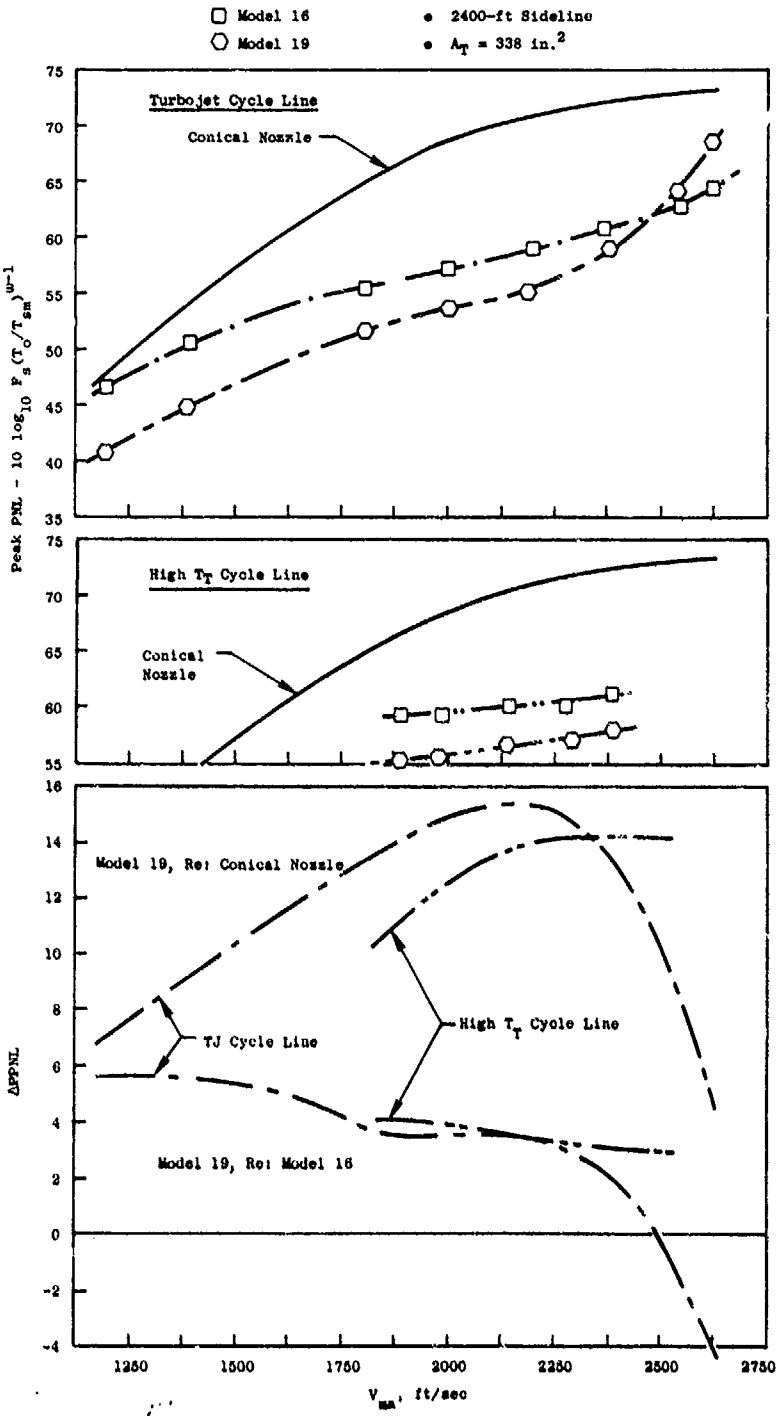

Figure 3-234. Impact of Acoustically Treated Ejector, Turbojet, Peak PNL.

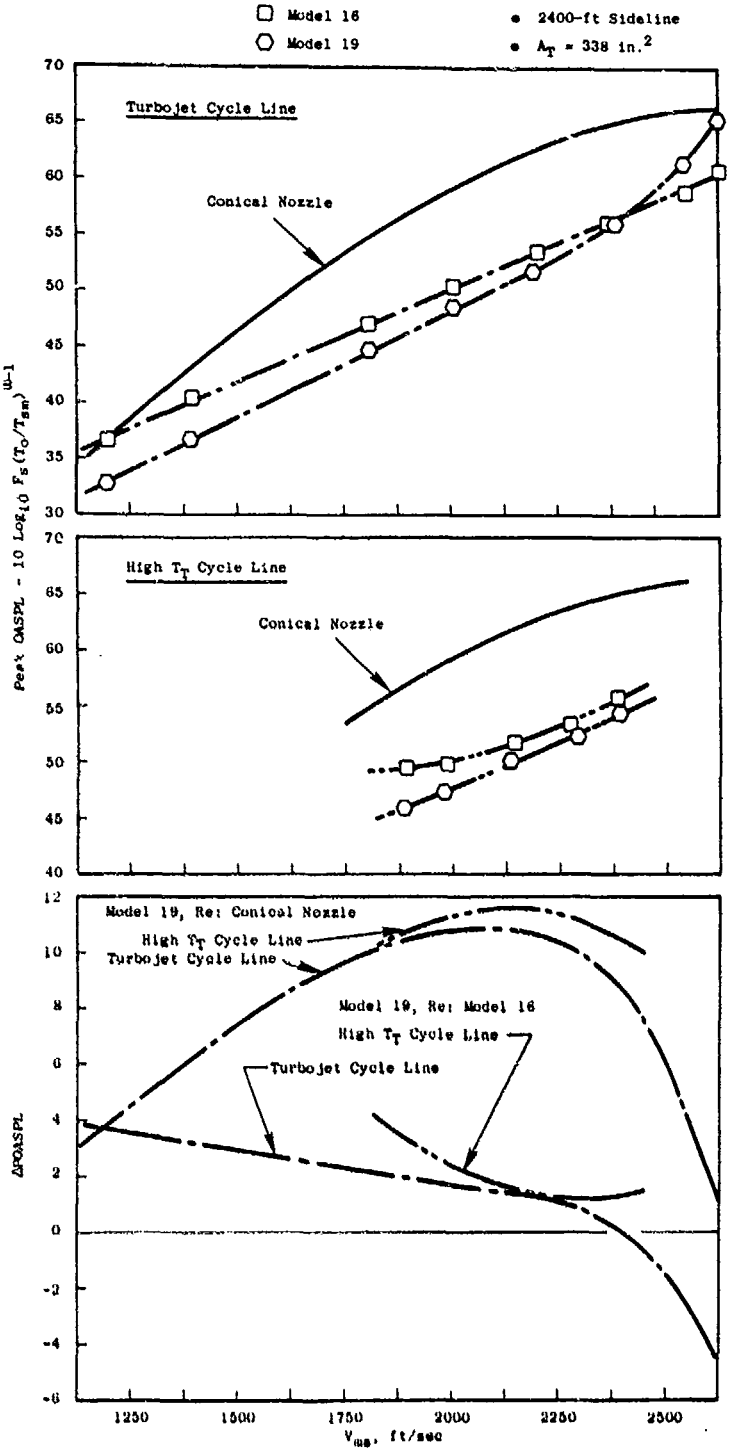

Figure 3-235. Impact of Acoustically Treated Ejector, Turbojet, Peak OASPL.

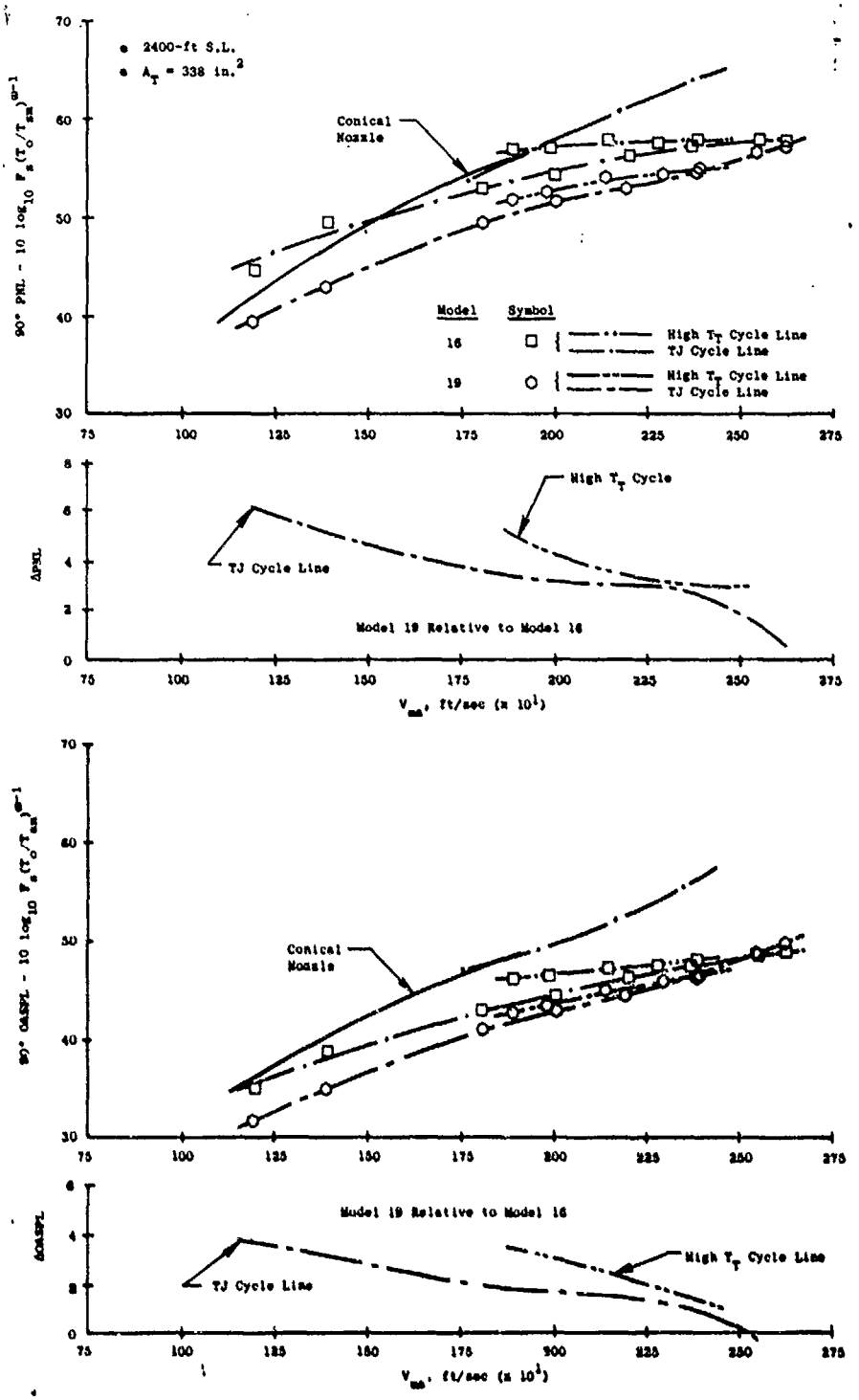

Figure 3-236. Impact of Acoustically Treated Ejector, Turbojet, 90° OASPL, PNL, and Suppression Levels.

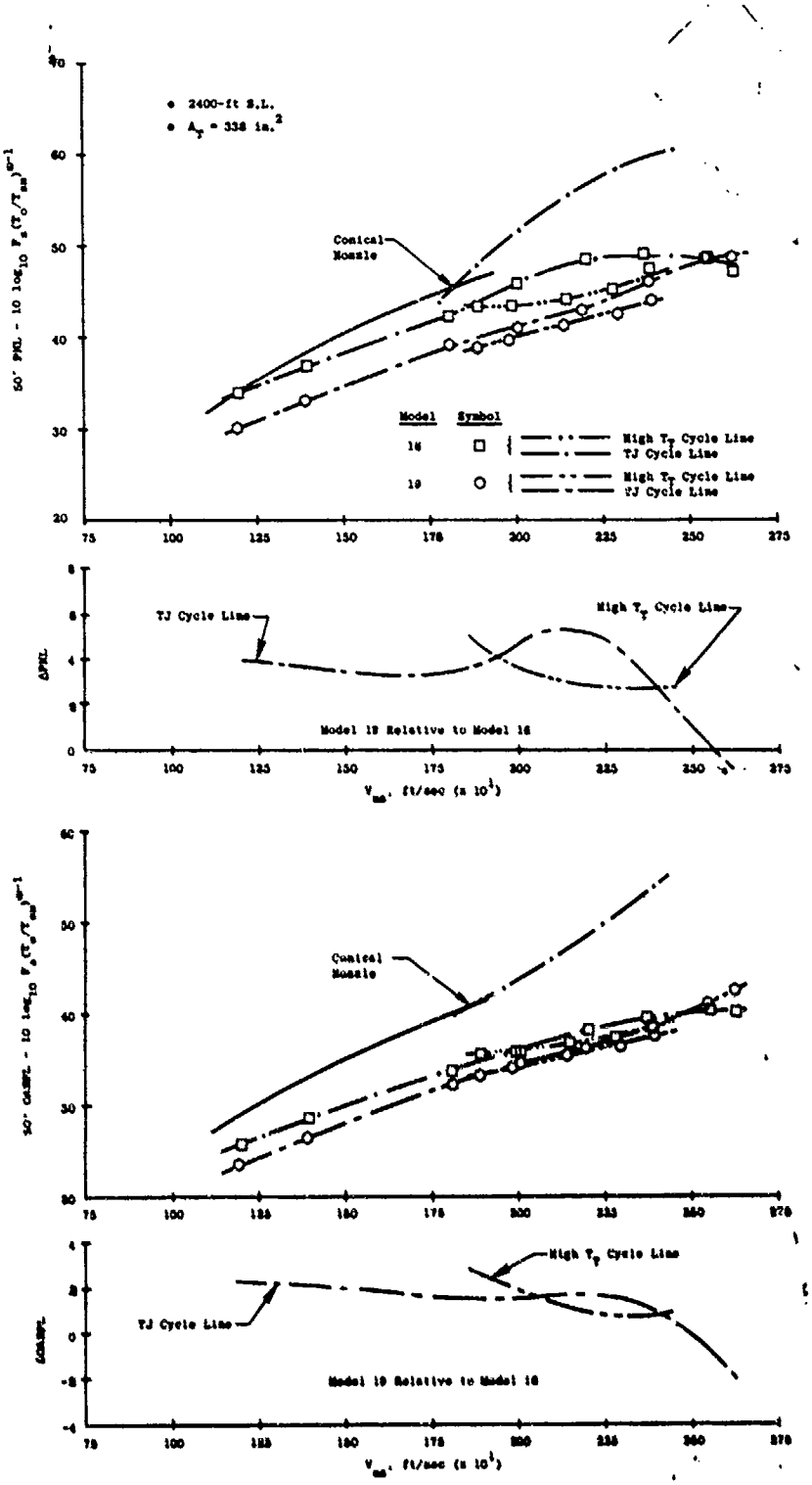

Figure 3-237. Impact of Acoustically Treated Ejector, Turbojet, 50° OASPL, PNL, and Suppression Levels.

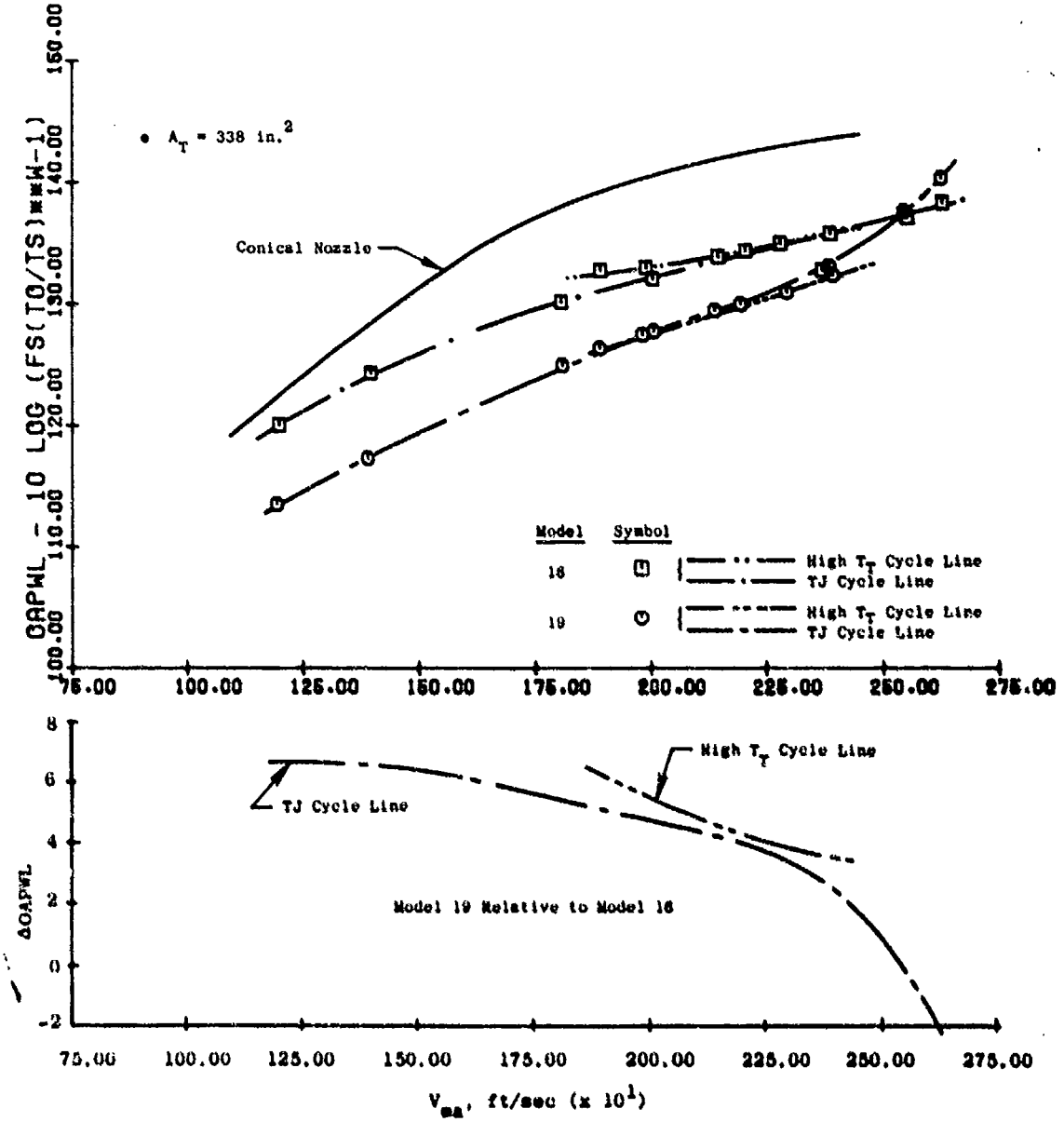

Figure 3-238. Impact of Acoustically Treated Ejector, Turbojet, OAPWL and Suppression Levels.

The following are included for a closer look at noise distribution with angle and at spectral composition.

- Figure 3-239 OASPL and PNL distributions at $V_{ma} \approx 2000$ ft/sec
- Figure 3-240 Spectra at select angles at $V_{ma} \approx 2000$ ft/sec
- Figure 3-241 OASPL and PNL distribution at $V_{ma} \approx 2625$ ft/sec
- Figure 3-242 Spectra at selected angles at $V_{ma} \approx 2625$ ft/sec

The first set of data at 2000 ft/sec reinforce the previous plots at peak, 90°, and 50°. Suppression of the total system is significant at all angles and suppression enhancement by application of the ejector is considerable in magnitude and fairly uniform for all angles. The spectra, Figure 3-240 illustrates that the significant change is in the high-frequency range, as anticipated.

Figure 3-241 and 3-242, at the high $V_{ma} = 2625$ ft/sec point, also reinforce the trends seen in peak, 90°, and 50° plots; the noise levels are generally greater with the ejector applied. This is correct to some extent for all angles, but principally in the forward and aft quadrants. On a spectral basis, the higher levels exist primarily over the low and midfrequency ranges with a slight amount of high-frequency suppression still achieved by the acoustic treatment.

Treated Ejector Application, Dual flow

This study extends the previous section's investigation to a dual flow application. Model 24 is the base configuration (Figure 3-243 and Figure A-18 in Appendix A) and the same 36-chute, AR = 2.0, $R_T^2 = 0.716$ annular suppressor as the base turbojet Model 16, modified with a retracted inner plug in lieu of the full turbojet plug. The inner stream is an annulus with a step height of 0.7 in. and the system area ratio (A_0/A_1) is 1.92. The same treated ejector as described in the previous section was applied (Figure 3-243 and Figure A-30 in Appendix A), maintaining axial spacing and ejector diameter to suppressor shroud diameter ratio (Model 36).

Acoustic testing in the Cell 41 Anechoic Facility followed the matrix of Section 3.2.1, Figure 3-10 and Table 3-3, using the cycle lines of:

- $W_i = 15\% W_0$
- $W_i = 30\% W_0$
- DBTF/Inverted Dual Flow
- AST/VCE

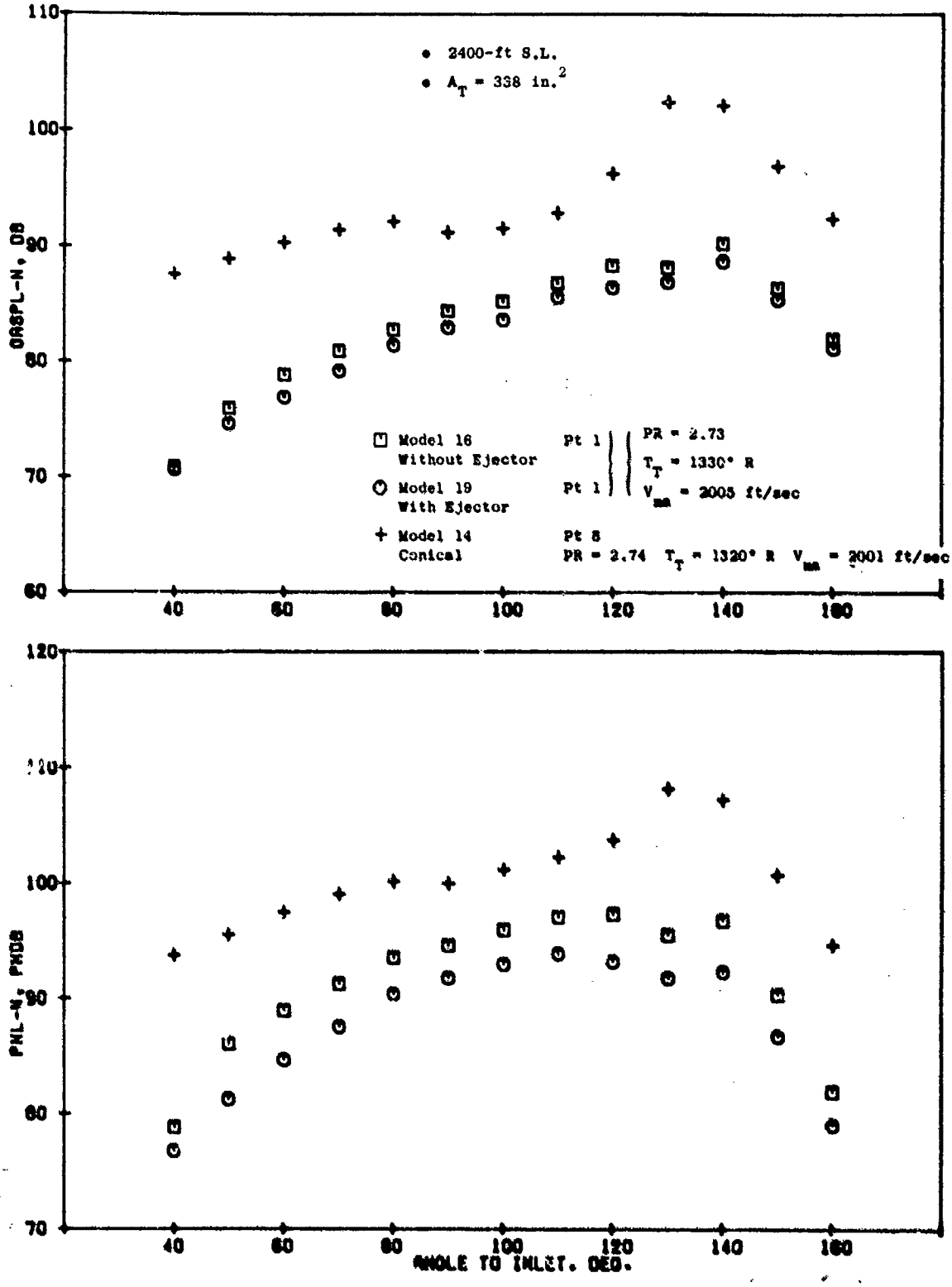

Figure 3-239. Impact of Acoustically Treated Ejector, Turbojet, OASPL and PNL Directivity, V_{ma} = 2005 ft/sec.

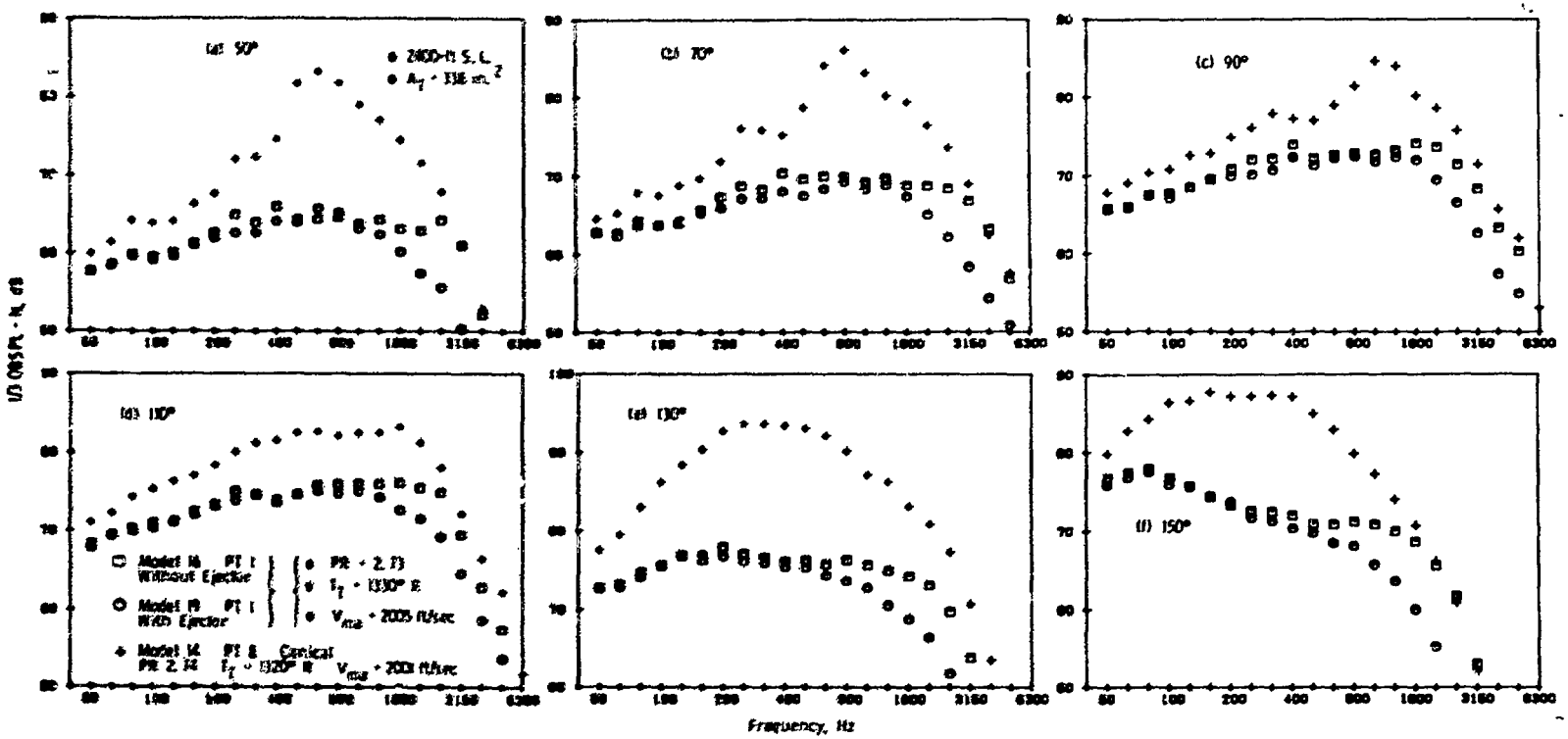

Figure 3-240. Impact of Acoustically Treated Ejector, Turbojet, Spectra, V_{max} = 2005 ft/sec.

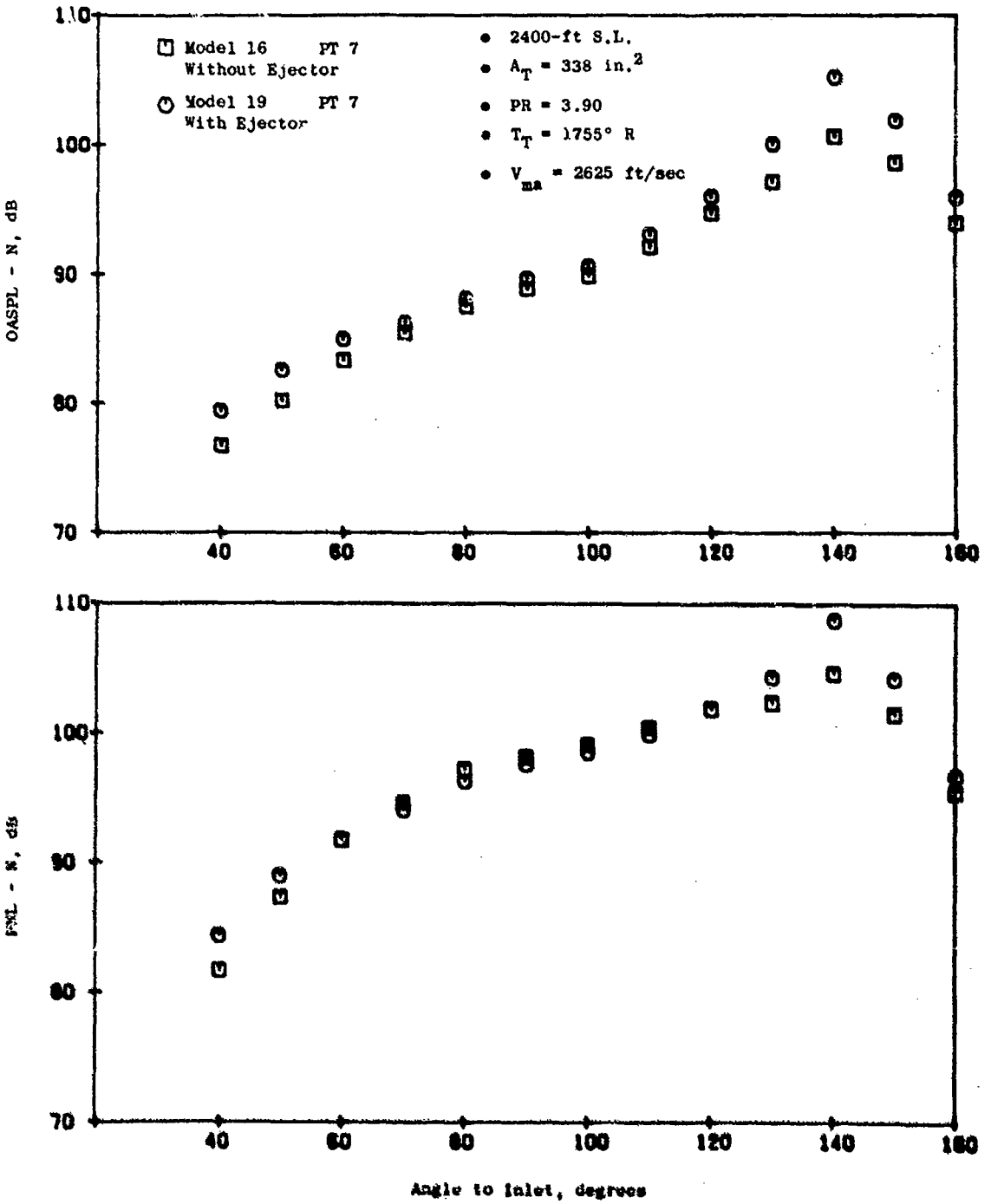

Figure 3-241. Impact of Acoustically Treated Ejector, Turbojet, OASPL, and PNL Directivity, V_{ma} = 2625 ft/sec.

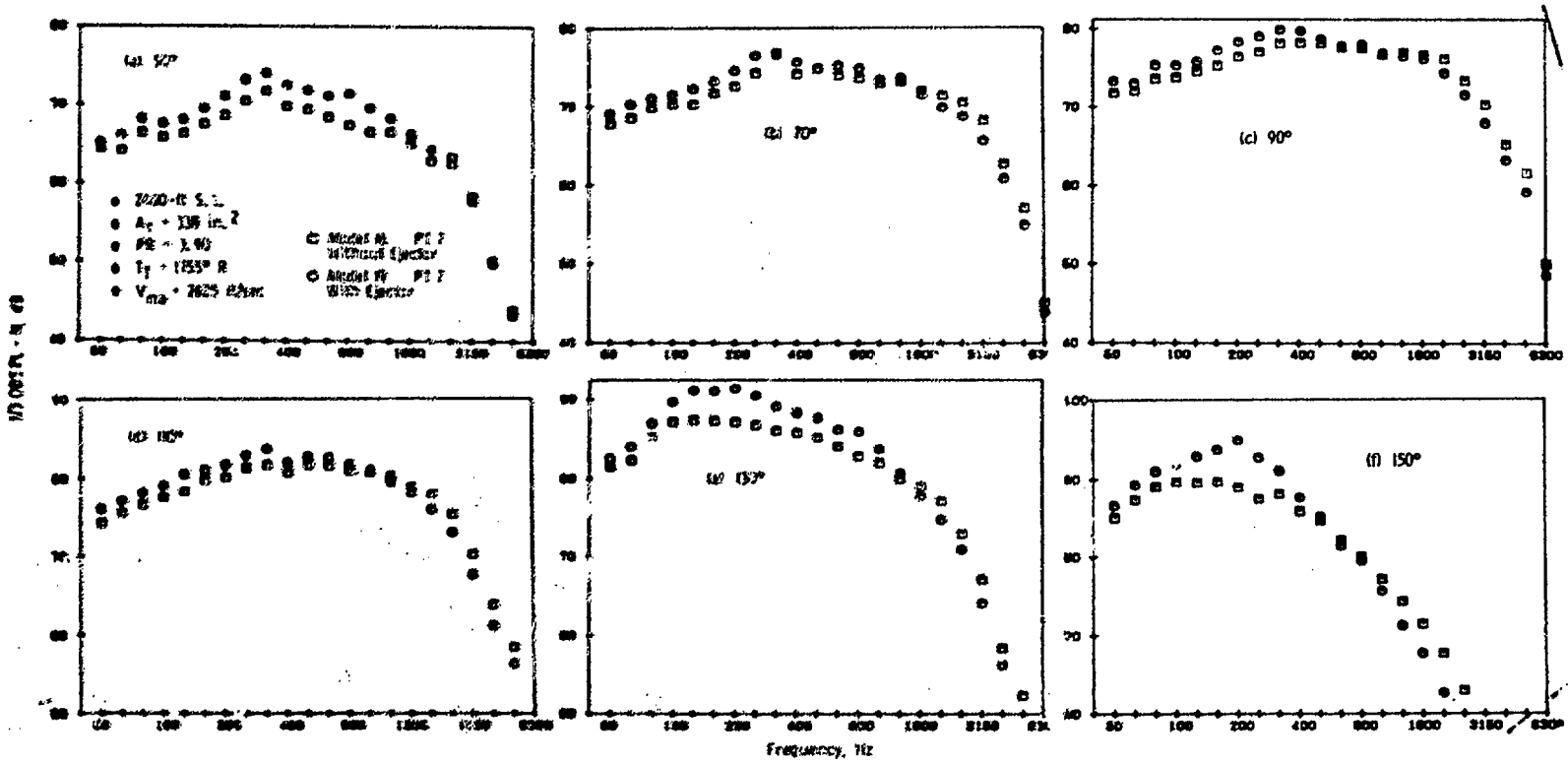

Figure 3-242. Impact of Acoustically Treated Ejector Application, Turbojet, Spectra, V_{ma} = 2625 ft/sec.

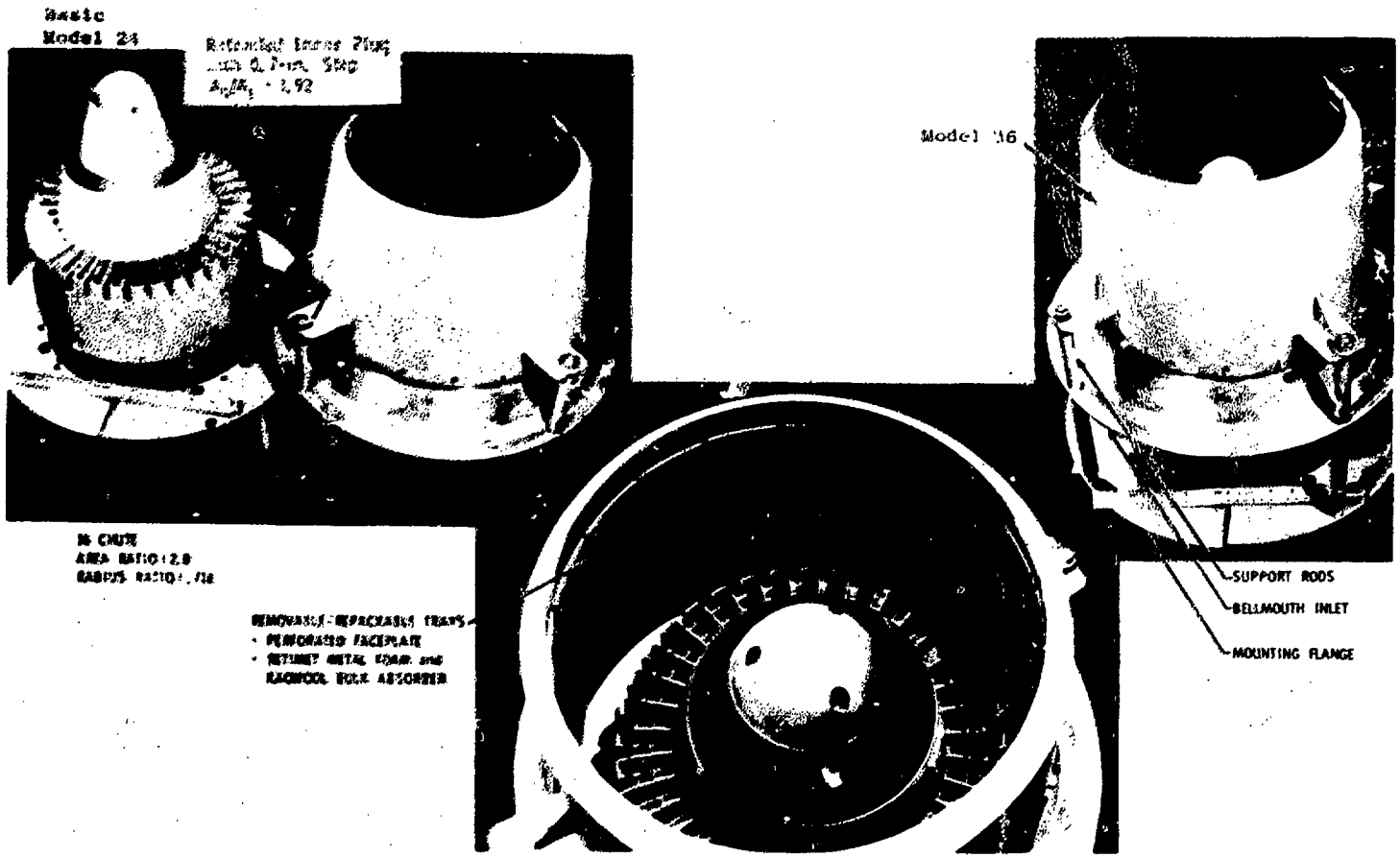

Figure 3-243. Acoustically Treated Ejector Application to Annular Suppressor, Dual Flow.

A summary of PPNL and POASPL levels for the 15%, 30%, and AST/VCE cycle lines is shown in Figures 3-244 and 3-245 along with suppression plots of the ejector Model 36 relative to the conical and relative to the non-ejector Model 24. The data indicate maximum system suppression levels of near 13 ΔPNL and 14 ΔOASPL in comparison to the previous 15.5 and 11.5 of the turbojet system. System overall suppression levels do not seem to drop off as rapidly at higher V_{ma} as is the case with the turbojet/ejector application.

Suppression attributable to the ejector alone averages 4 ΔPNL and 4.5 ΔOASPL over a wide V_{ma} range. This is dramatically different than the ejector application to the suppressed turbojet where maximum suppression values of 4 ΔPNL/5.5 ΔOASPL at low V_{ma} dissipated to noise enhancement at high V_{ma}.

PNL and OASPL data obtained from testing along the DBTF/Inverted Dual Flow cycle line are shown in Figures 3-246, 3-247, and 3-248 for peak, 90°, and 50°, respectively. Each of these figures also displays the suppression curves attributable only to application of the ejector, i.e., Model 36 relative to Model 24.

At 90°, noise reduction due to ejector application is still present, but at a reduced level from that at peak noise angle, maintaining 2-4 ΔPNL and 1-2 ΔOASPL across the test velocity range. This is also reduced from that achieved in the previous turbojet/ejector study. Additionally, the overall system suppression at 90° is somewhat less than the turbojet/ejector system.

At 50°, significant overall system suppression is regained relative to the conical nozzle, both on OASPL and PNL. This is observed primarily at high V_{ma} relative to the shock-cell infested conical nozzle, and to a lesser degree at low V_{ma}. Suppression levels attributable to the ejector alone are from 2-4 ΔPNL and up to 2 ΔOASPL. These levels are in concert with those achieved on the turbojet/ejector system. Again, as at 90° and peak angle, the additional suppression attributable to the ejector does not as readily dissipate with increasing V_{ma}, as was seen with the turbojet/ejector system.

An overall power level data plot is also included as Figure 3-249, and its trends fairly well parallel those of the PPNL/POASPL curves.

Figures 3-250 and 3-251 are included as typical examples of PNL and OASPL directivity and of spectral distributions. The data shown are from the AST/VCE cycle line at V_{ma} = 2095 ft/sec and were selected as representative of trends for most of the test points. Observations show, as in the case of turbojet/ejector data at low to moderate velocities, suppression attributable to the ejector persists at all angles, except the most aft, particularly on a PNL basis. The suppression is again attributable to acoustic absorption in the high-frequency regime.

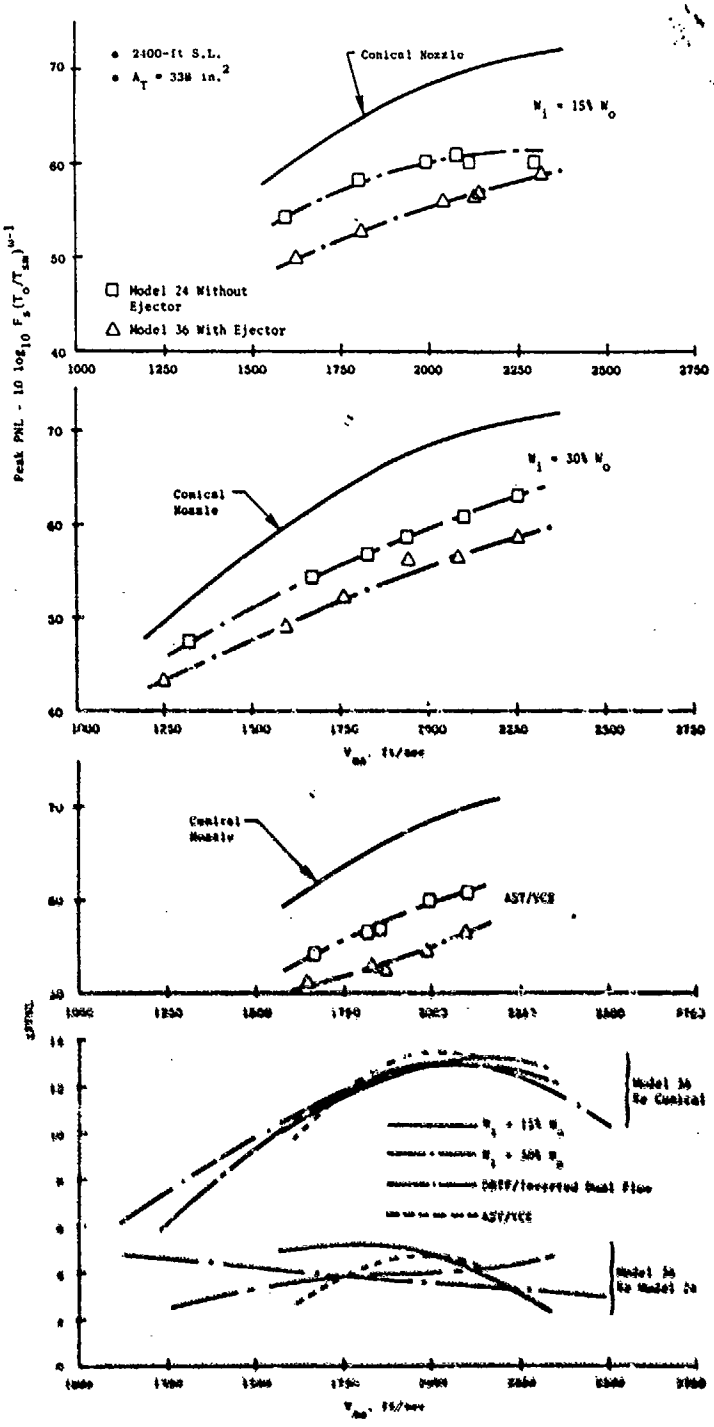

Figure 3-244. Treated Ejector Application to Dual Flow, Peak PNL and Suppression Levels.

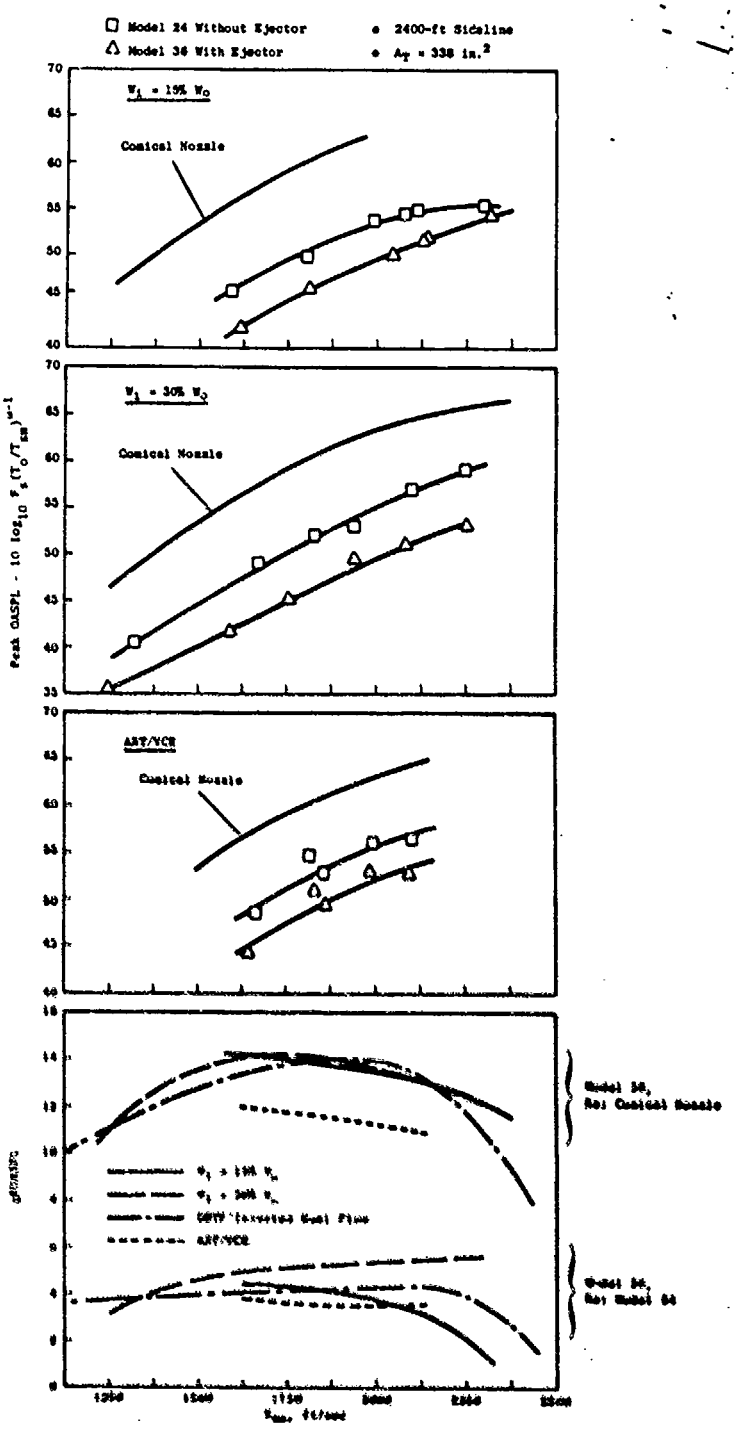

Figure 3-245. Treated Ejector Application to Dual Flow, Peak OASPL and Suppression Levels.

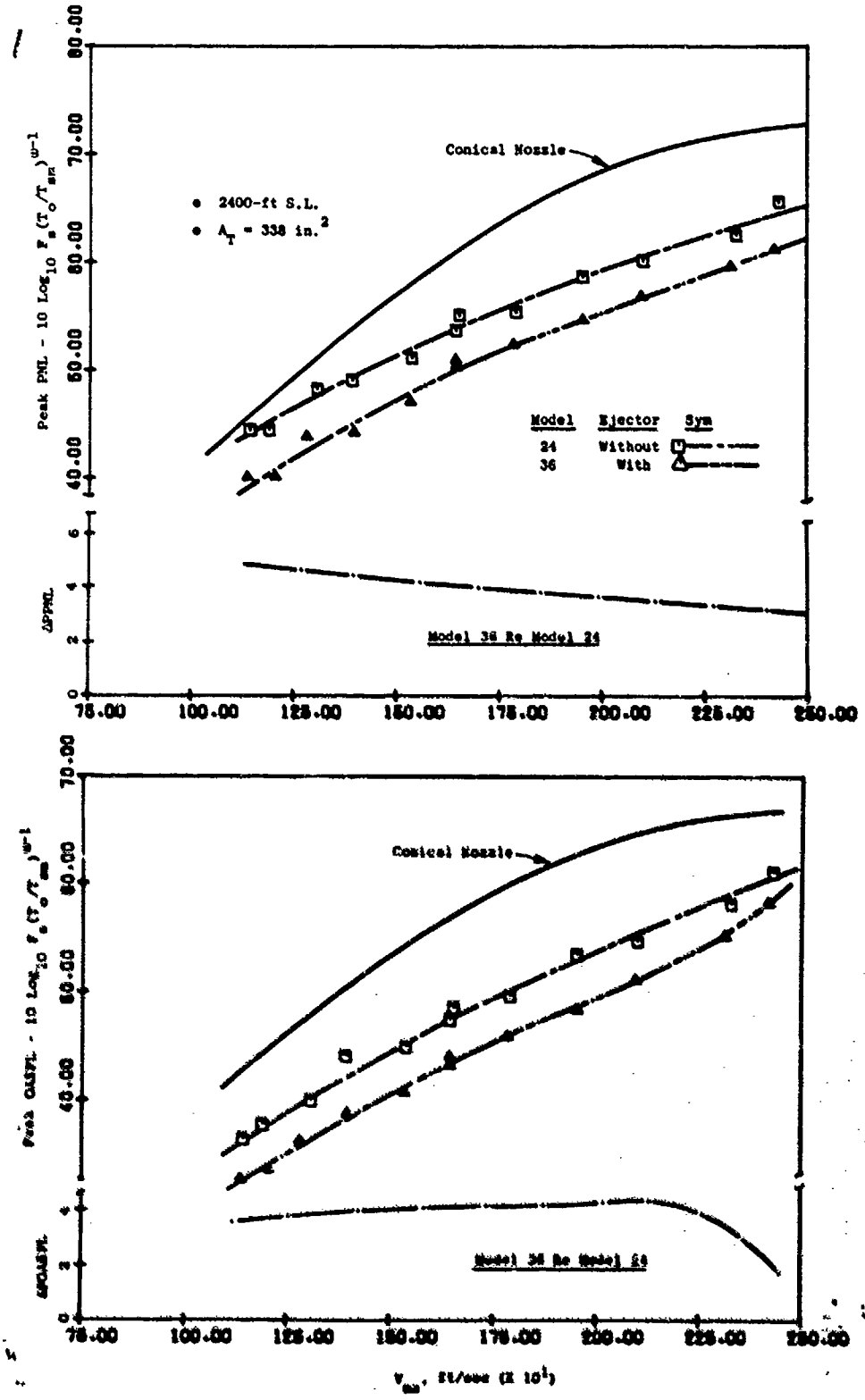

Figure 3-246. Treated Ejector Application to Dual Flow, Low-Bypass DSTP Cycle, Peak OASPL, PNL, and Suppression Levels.

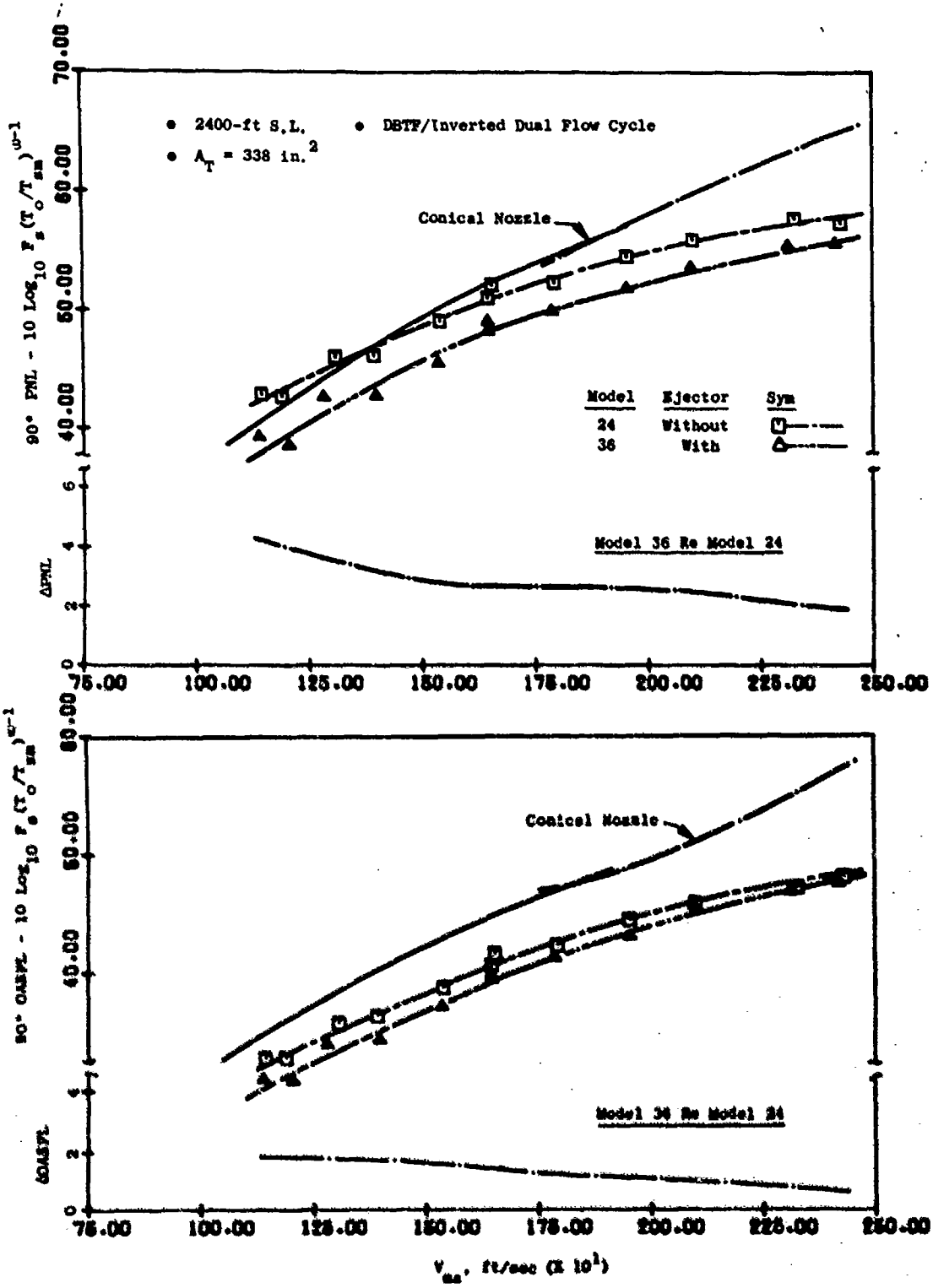

Figure 3-247. Treated Ejector Application to Dual Flow, 90° OASPL, PNL, and Suppression Levels.

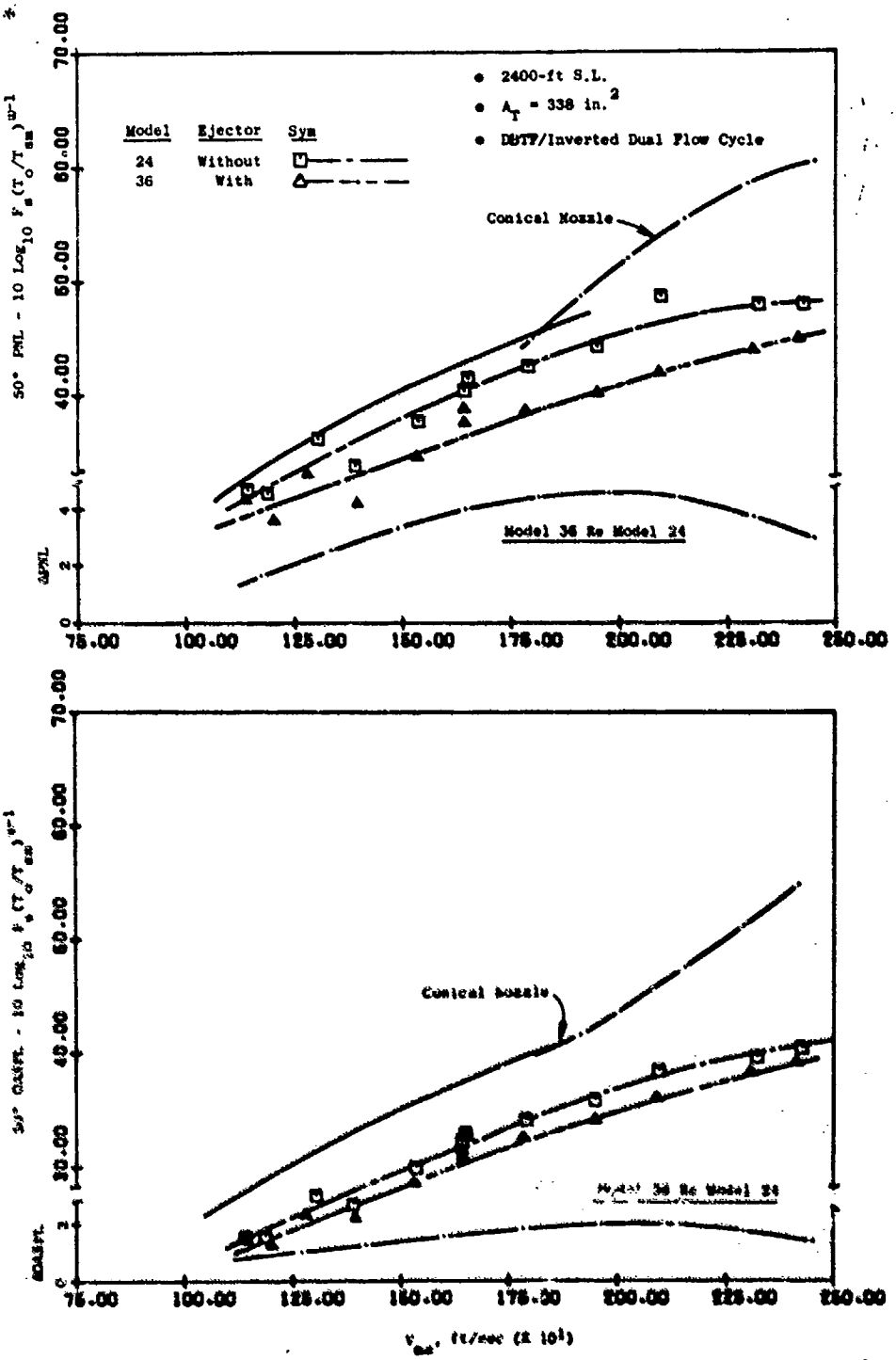

Figure 3-248. Treated Ejector Application to Dual Flow, 50° OASPL, PNL, and Suppression Levels..

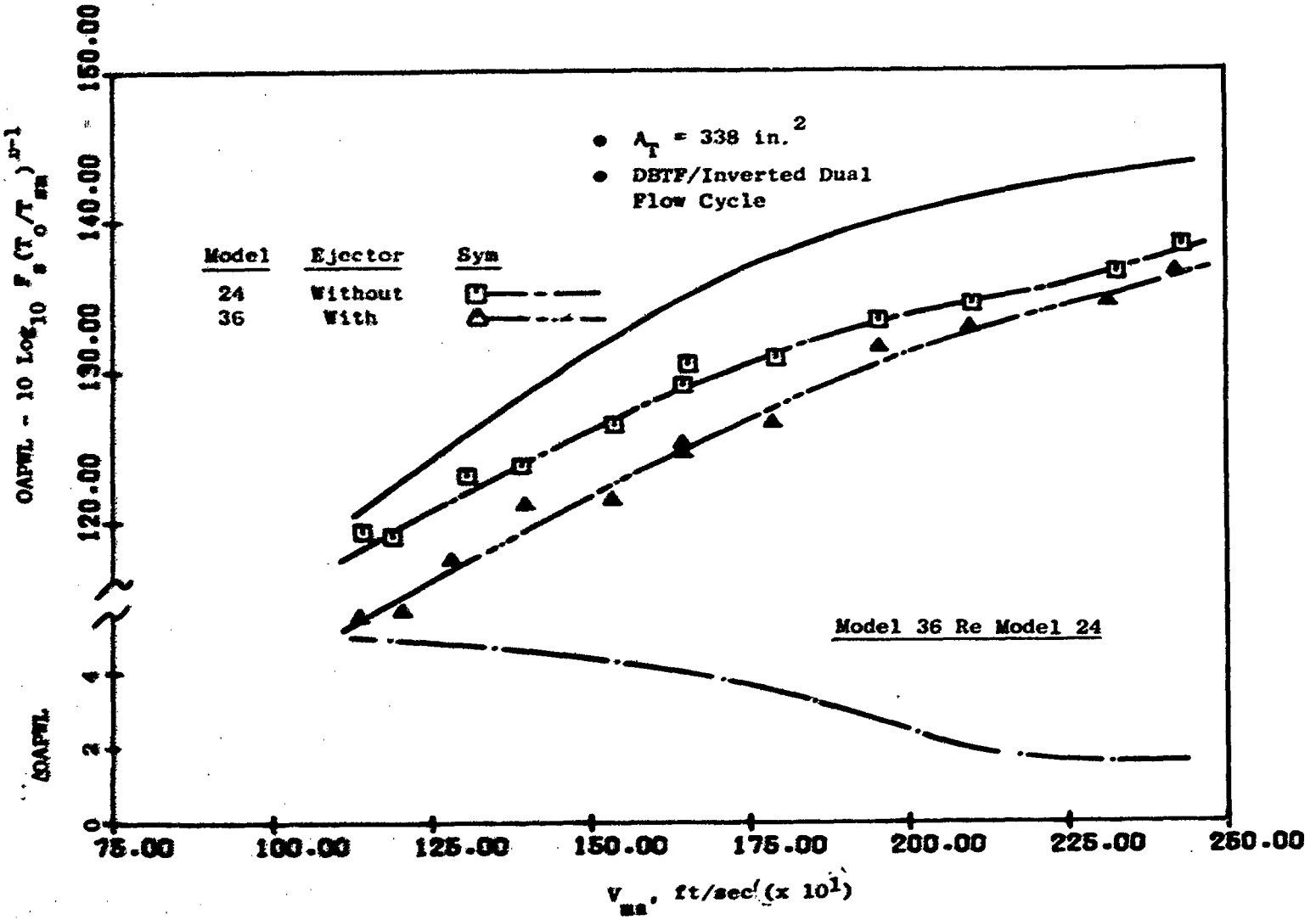

Figure 3-249. Treated Ejector Application to Dual Flow - OAPWL and Suppression Levels.

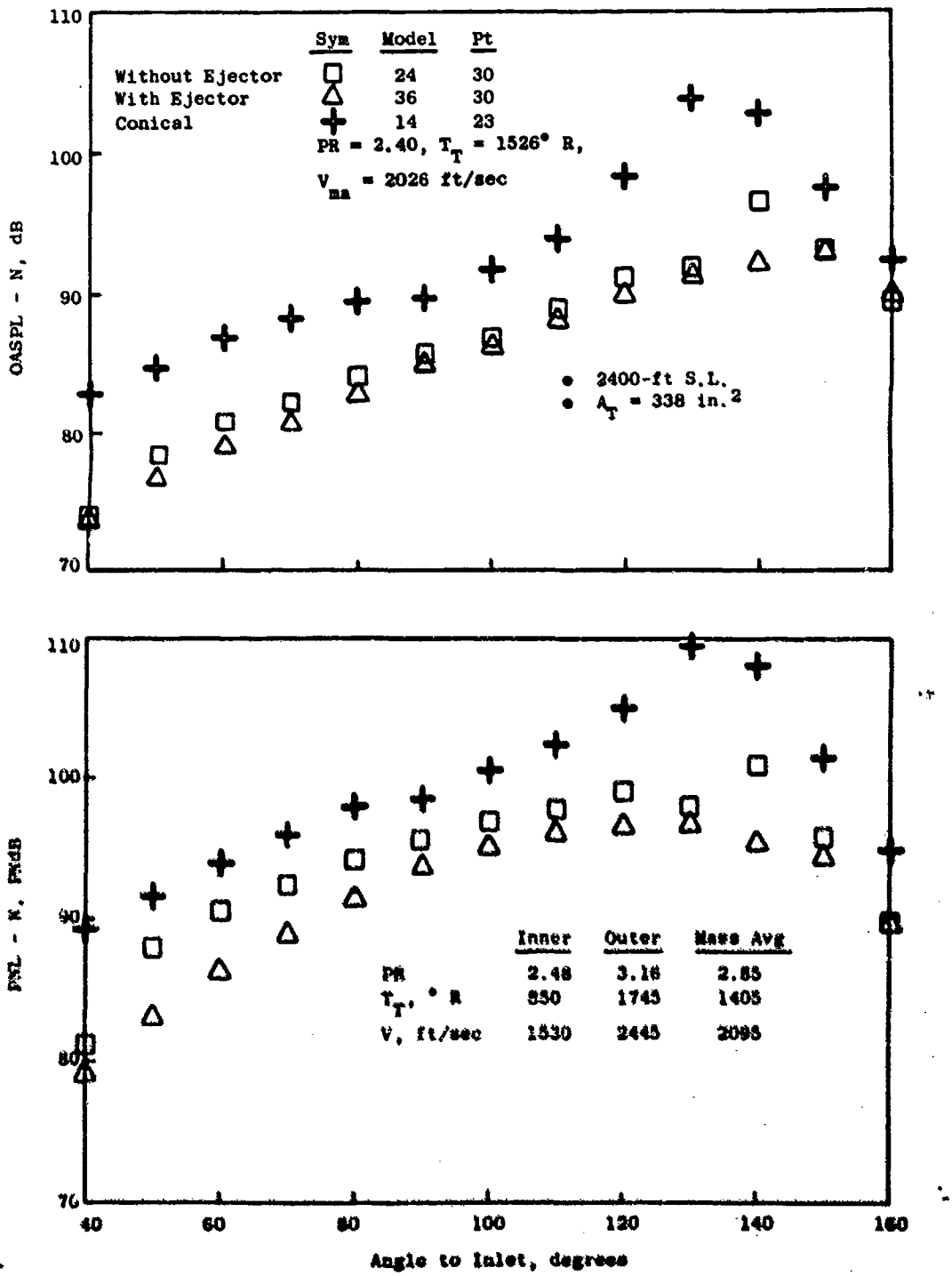

Figure 3-250. Treated Ejector Application to Dual Flow, OASPL and PNL Directivity, V_{ma} = 2085 ft/sec.

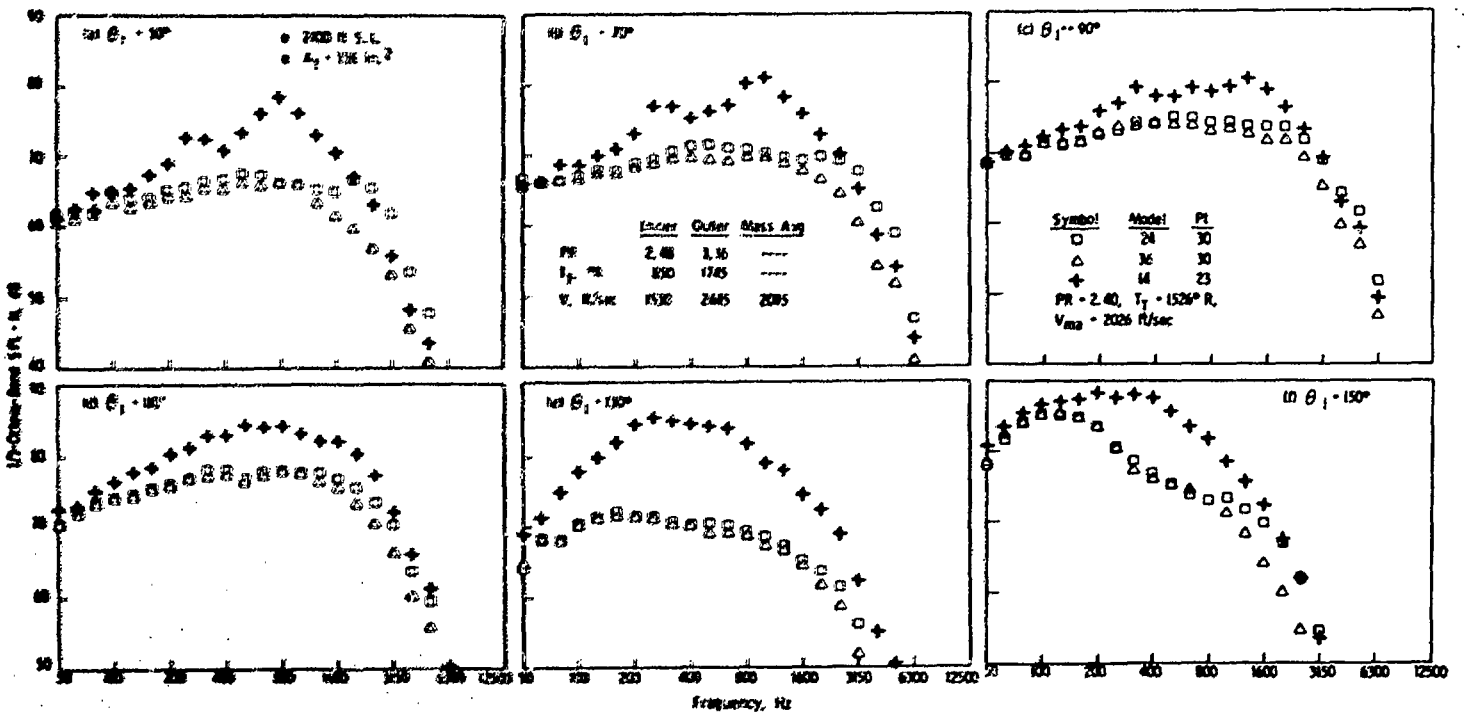

Figure 3-251. Treated Ejector Application to Dual Flow, Spectra, V_{ma} = 2095 ft/sec.

Treated Ejector Application, Unsuppressed Coannular Nozzles

The two previous sections evaluated application of an acoustically treated ejector to systems whose mid-to-high-frequency noise generation region was in close proximity to the nozzle exit plane which is inherent in the mechanics of highly segmented annular suppressors. The suppressor systems in themselves are mechanically more complex, heavier, and aerodynamically poorer than unsuppressed coannular-noncoplanar dual plug propulsion nozzles of equivalent thrust rating. The unsuppressed coannular nozzle on its own, due to the nature of its high duct radius ratio, normally affords suppression relative to the conical nozzle. It, too, may have mid-to-high frequency noise sources in near proximity of the nozzle exit plane. Location, frequency distribution, and noise levels are dependent on the physical geometry of the system and aerodynamic cycle. The small annulus heights associated with duct nozzles approach the characteristic dimensions (chute/flow widths and heights) associated with segmented suppressors. Therefore, application of a treated ejector to an unsuppressed coannular system was expected to possibly enhance acoustic performance sufficient to make the system favorably competitive to the more mechanically complex and heavier suppressor systems without ejectors.

For the study, Models 37 and 38 were used. Details are presented in Appendix A, Figures A-31 and A-32 and in Figure 3-252. Pertinent system parameters were as follows:

	Outer		Inner			System	Ejector			
Model No.	R_r^o	A_{Flow}, in.^{2}	D_s, in.	R_r^i	A_{Flow}, in.^{2}	A_o/A_i	D_{Ei}, in.	D_{Ei}/D_3	X_s/R_s	L_E/D_{Ei}
37	0.852	18.05	9.19	.800	11.35	1.59	11.0	1.20	0.29	0.76
38	0.926	8.01	8.46	.800	11.35	0.71	11.0	1.30	0.32	0.76

The basic coannular nozzles were from the NASA-Lewis contract NAS3-19777, (Reference 11) and the acoustic ejector was from the NASA-Lewis contract NAS3-18008 (Reference 10). The ejector design and packing were similar to that discussed in Section 3.4.2.5.

The acoustic test matrix within the Cell 41 Anechoic Facility followed an abbreviated form of Section 3.2.1 Figure 3-10 and Table 3-3 and basically uses parts of the D8TF/Inverted Dual Flow and the AST/VCE cycle matrices.

Acoustic results are presented as peak PNL/OASPL levels plus curves of suppression relative to the conical baseline in Figure 3-253, 90° OASPL/PNL in Figure 3-254, 50° OASPL/PNL in Figure 3-255, and overall power levels in Figure 3-256. Figure 3-253 shows that maximum suppression levels on a peak OASPL basis approach 5 and 4, and on a peak PNL basis approach 6.5 and 5 for Models 38 and 37, respectively. At 90° and 50°, noise levels approach those of the conical baseline.

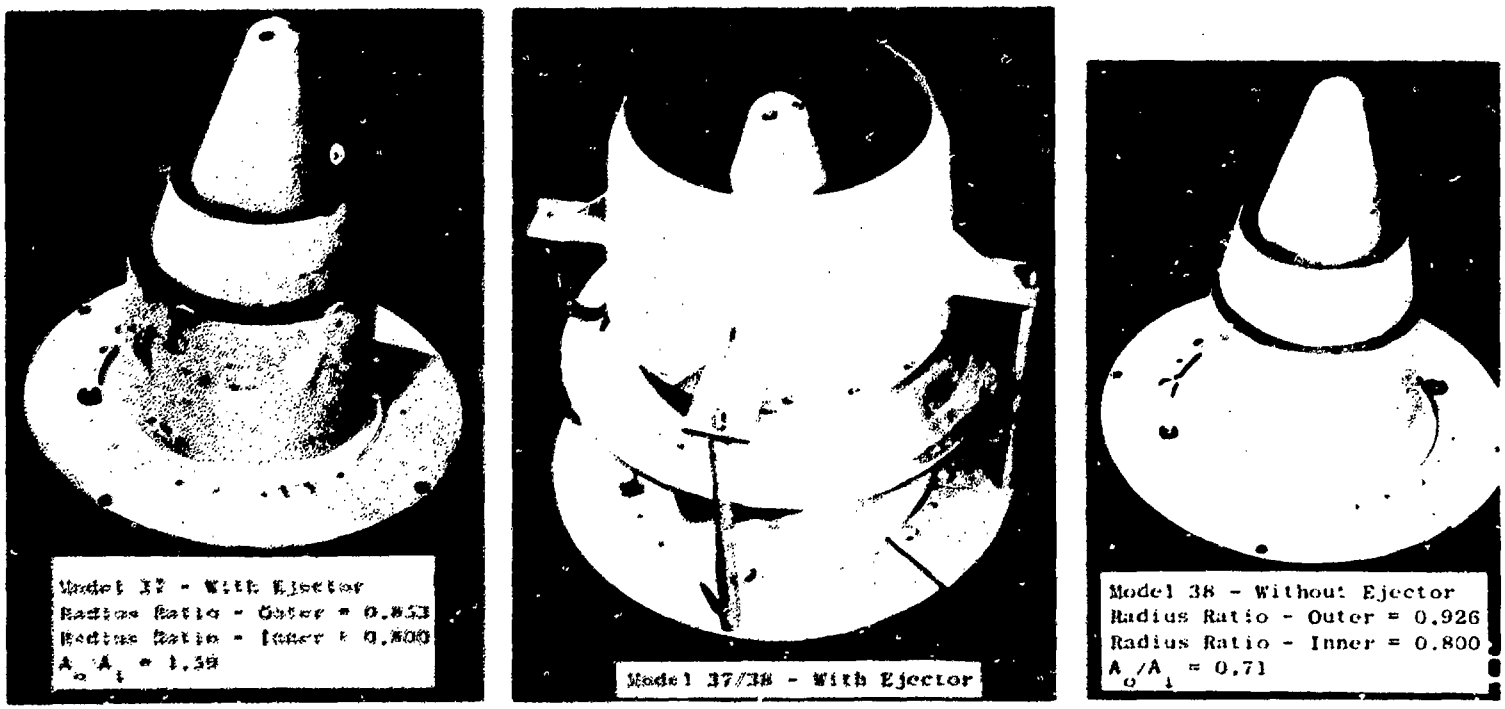

Figure 3-252. Unsuppressed Cosnnular Nozzles with Acoustically Treated Ejector.

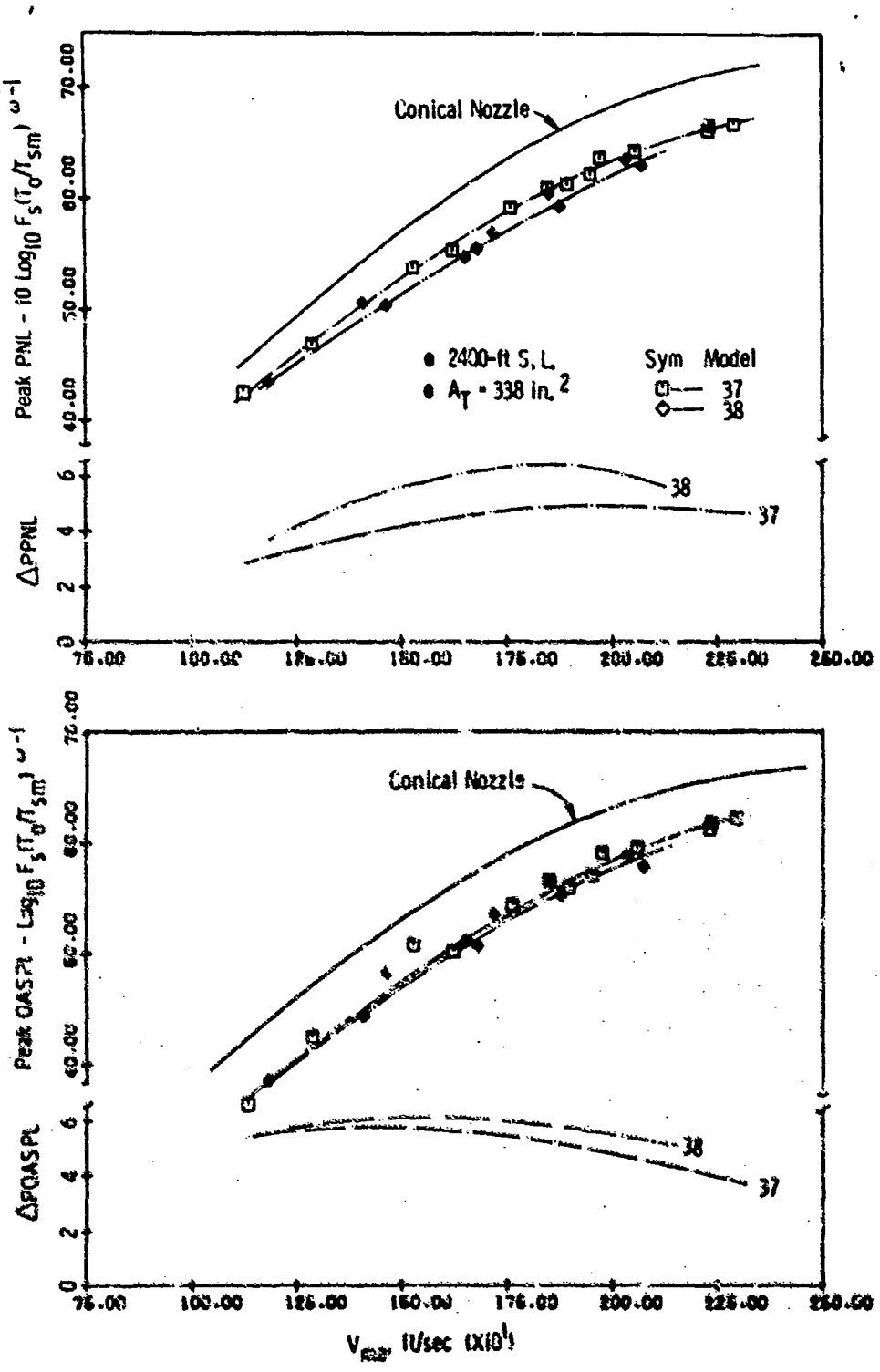

Figure 3-253. Unsuppressed Coannular Nozzles with Treated Ejectors, Peak OASPL, PNL, and Suppression Levels.

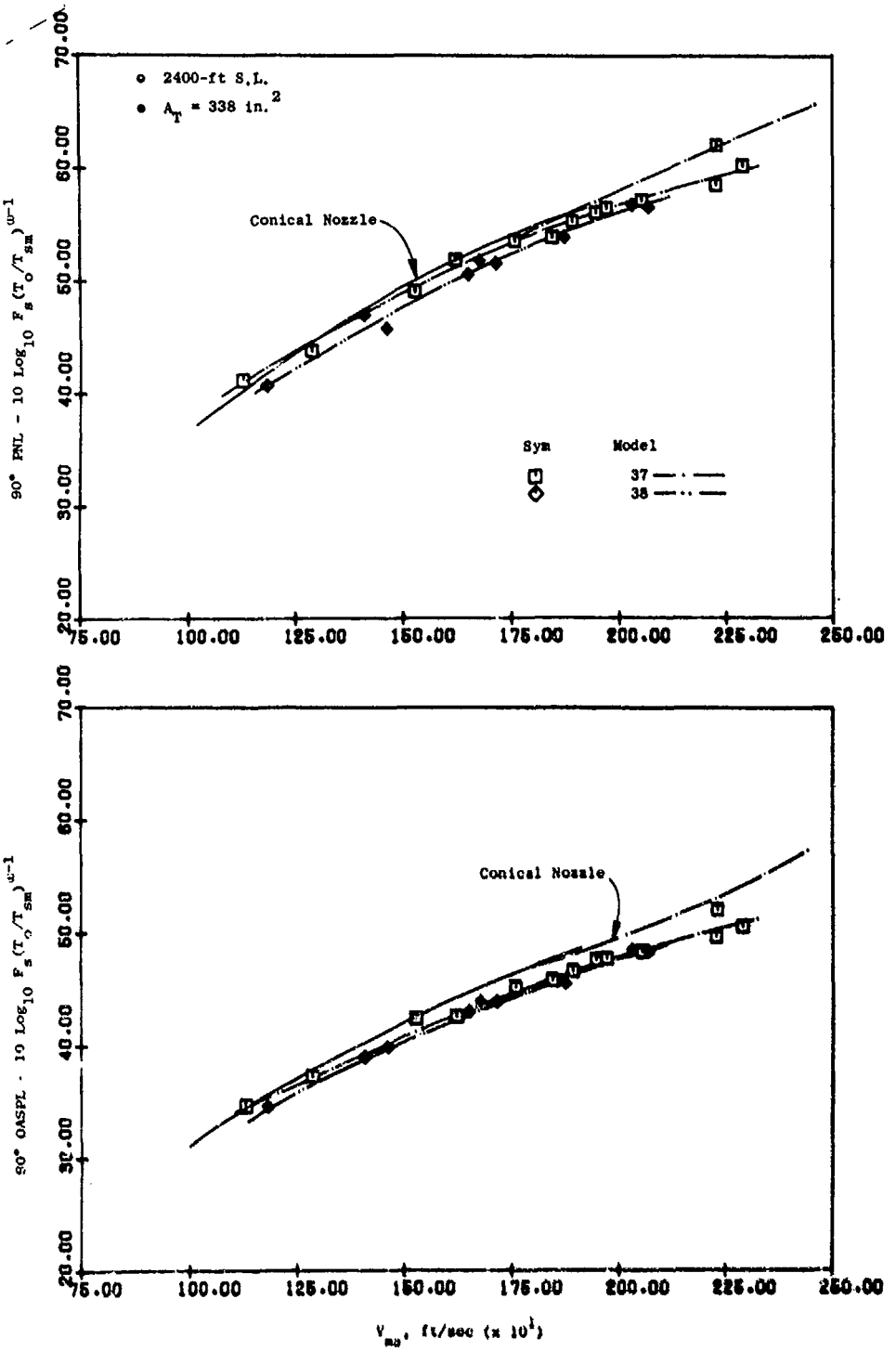

Figure 3-254. Unsuppressed Coannular Nozzles with Treated Ejectors, 90° OASPL and PNL.

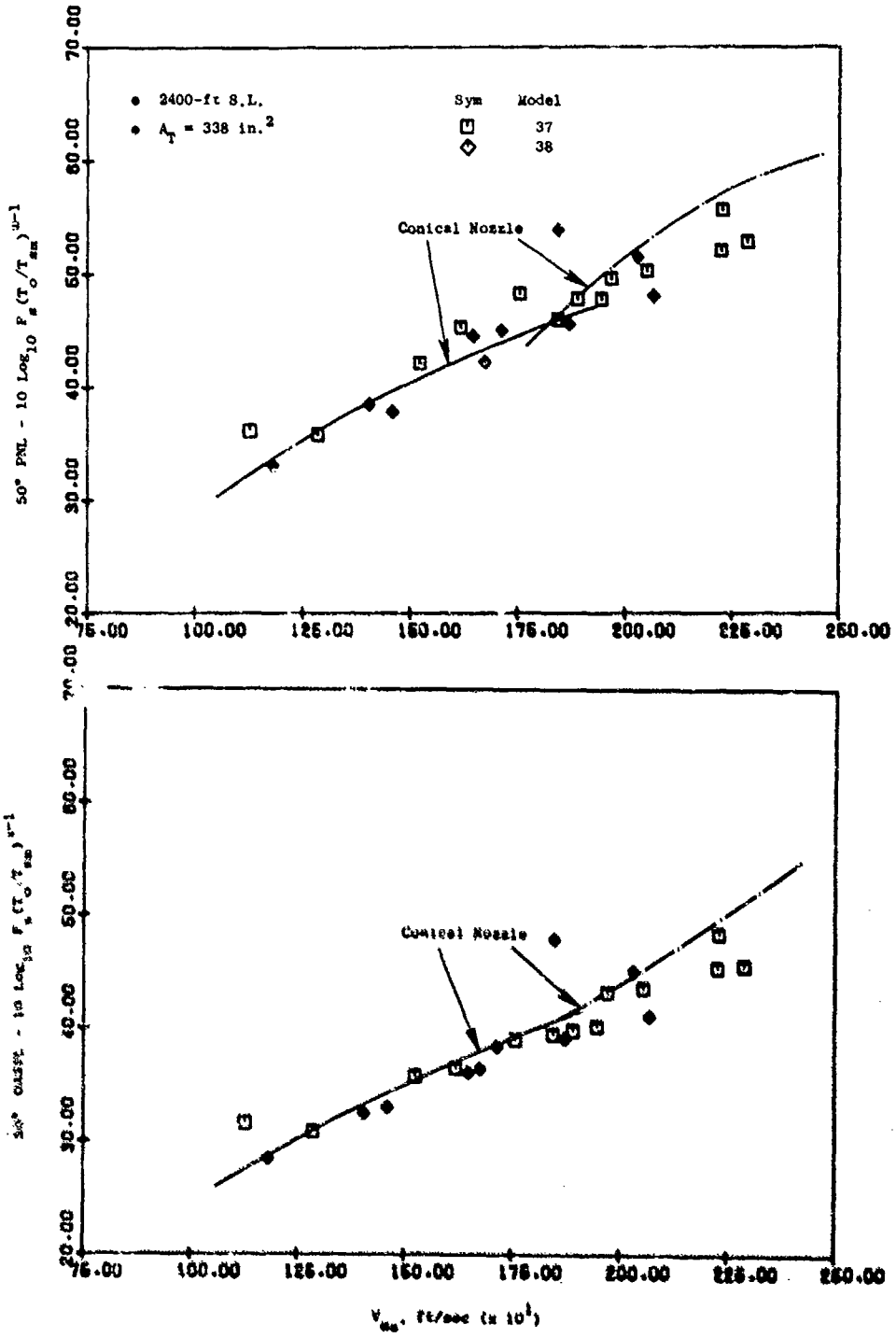

Figure 3-255. Unsuppressed Coannular Nozzles with Treated Ejectors, 50° OASPL and PNL.

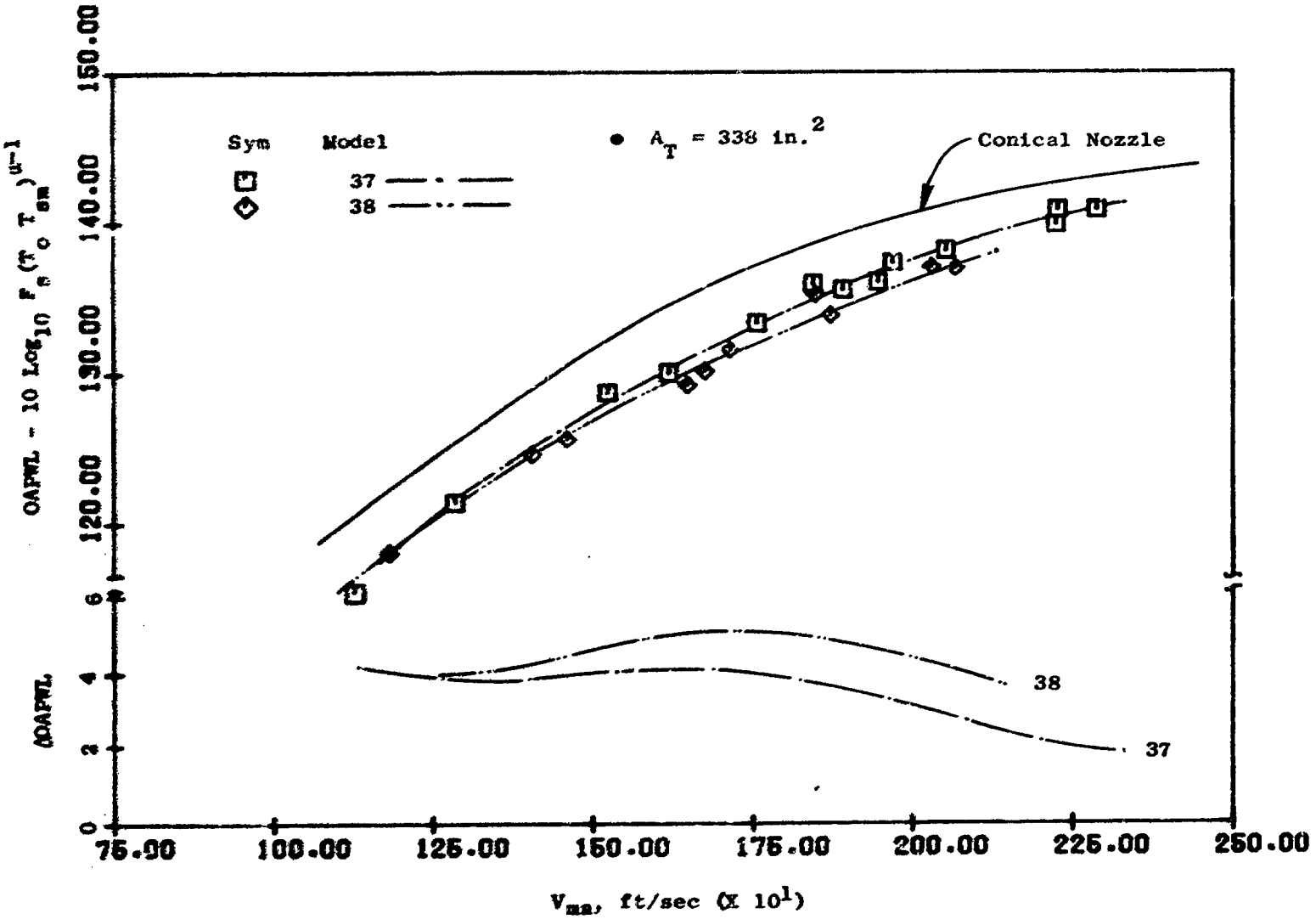

Figure 3-256. Unsuppressed Coannular Nozzle with Treated Ejectors, OAPWL and Suppression Levels.

To establish treated ejector effectiveness on its own, Figure 3-257 compares the peak PNL suppression trends of Models 37 and 38 (from Figure 3-253) to the levels established in Reference 11 for the basic nonejector coannular noncoplanar systems (Configurations 5 and 6, respectively, from Reference 11 for Models 37 and 38). This comparison points out that application of the treated ejector to the system of higher duct radius ratio (Configuration 6 and Model 38) increased peak PNL suppression levels to 6.5 dB, the ejector effecting near 2 PNL suppression on its own in the midvelocity range. This level is considerably less than the basic 4 ΔPPNL obtained with the treated ejector applied to a suppressed turbojet or suppressed dual flow system (Model 19 relative to Model 16 in Section 3.4.2.5 and Model 37 relative to Model 24 in Section 3.4.2.5). This is perhaps partially attributable to the ejector's looser fit to the base nozzle system (D_{E_j}/D_8 = 1.3 for Model 38 compared to 1.11 for Models 19 and 36). On the Model 37 system of lower duct radius ratio, the ejector performs well at high velocity and then loses all suppression potential at low V_{ma}, to the point of increasing system noise levels.

As an evaluation of the overall study goal (i.e., to determine whether an unsuppressed coannular plug system, through application of a treated ejector, can achieve suppression levels similar to a suppressed annular turbojet or dual flow system without ejector), Figure 3-257 also includes peak PNL suppression curves of Models 16 and 24 of the previous two sections. These were 36-chute, AR = 2.0 turbojet and dual flow suppressors, respectively. It is readily seen that, in the mid-to-high-velocity region associated with engine cycles at takeoff and community power settings, the performance of the ejected unsuppressed coannular systems is well below that of the more mechanically complex multielement systems. In fact, little or no suppression enhancement through ejector application is available at high velocity for either system studied.

To exemplify the more detailed noise characteristics of this type of system, a set of PNL and OASPL directivity and spectra plots is included. Figures 3-258 and 3-259 are at V_{ma} = 2060 ft/sec and show (a) PNL and OASPL distributions in concert with the previous peak, 90°, and 50° plots, (b) suppression is slightly greater for the higher duct radius ratio model at peak angle and toward the inlet but at 90° suppression for both models is nil, and (c) spectra distributions show suppression relative to the conical nozzle is primarily in the midfrequency range.

3.4.2.6 Summary of Suppression Levels

The preceding sections have described parametric test data which were used to establish the suppression levels for several types of nozzle configurations. Suppressor and system aerodynamic and geometric parameters evaluated experimentally included the following: suppressor area ratio, radius ratio, flow management (system velocity ratio, weight flow ratio, and area ratio), inner stream geometry, element number, element type, and treated ejectors on multielement and unsuppressed inverted-coannular-flow nozzles.

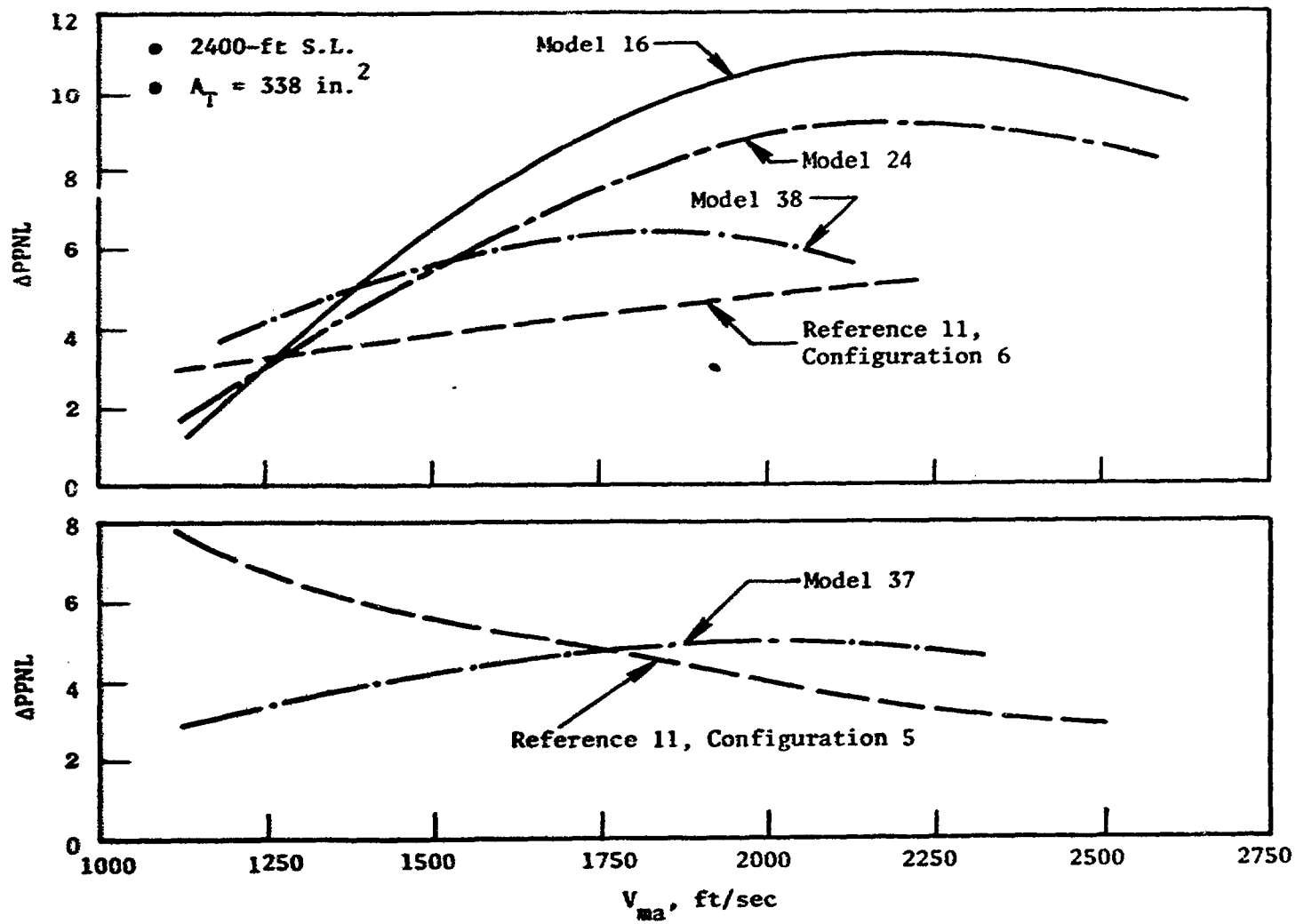

Figure 3-257. Summary of Results for Treated Ejector Application to Unsuppressed Coannular Systems.

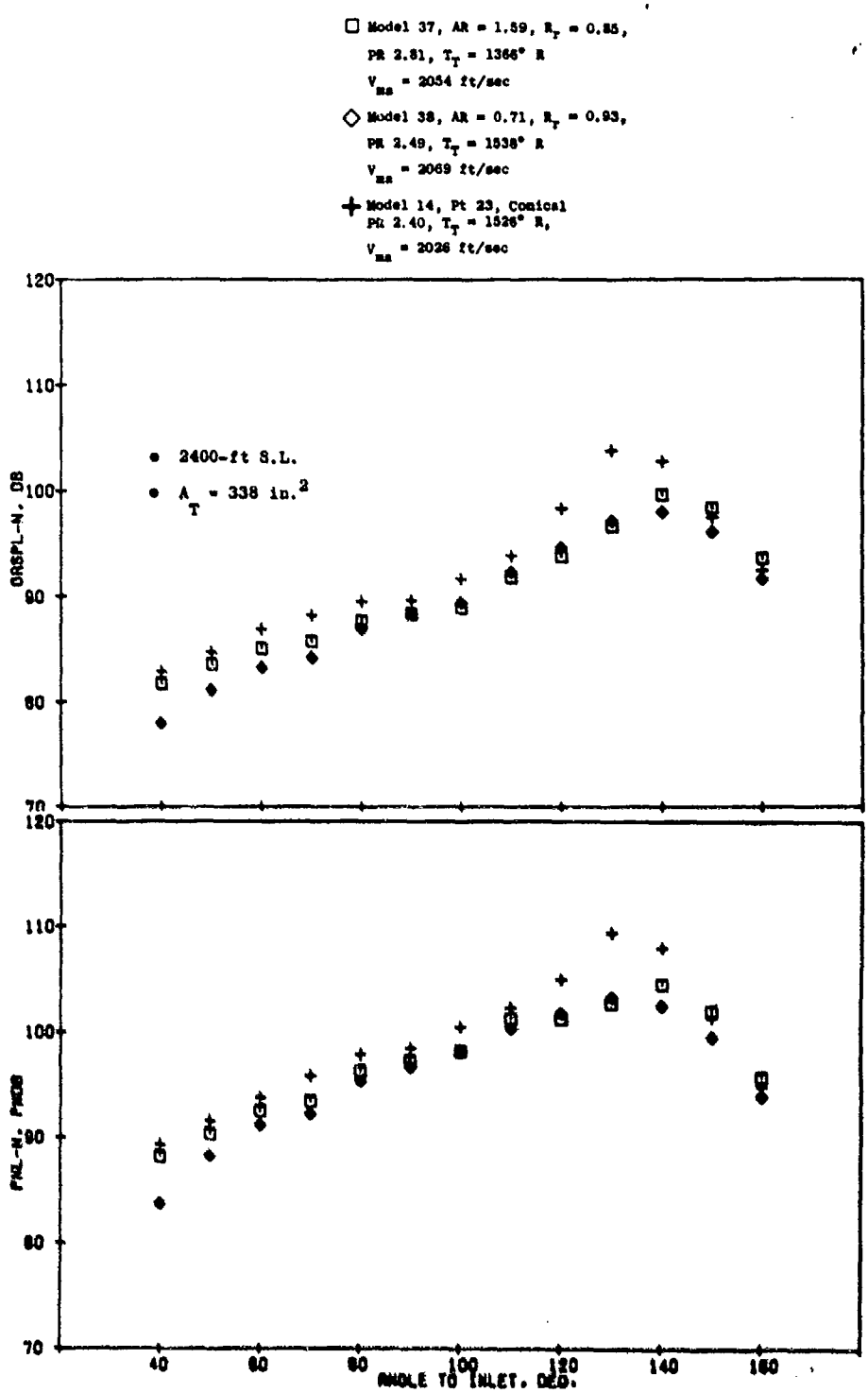

Figure 3-258. Unsuppressed Coannular Nozzles with Treated Ejectors, OASPL and PNL Directivity.

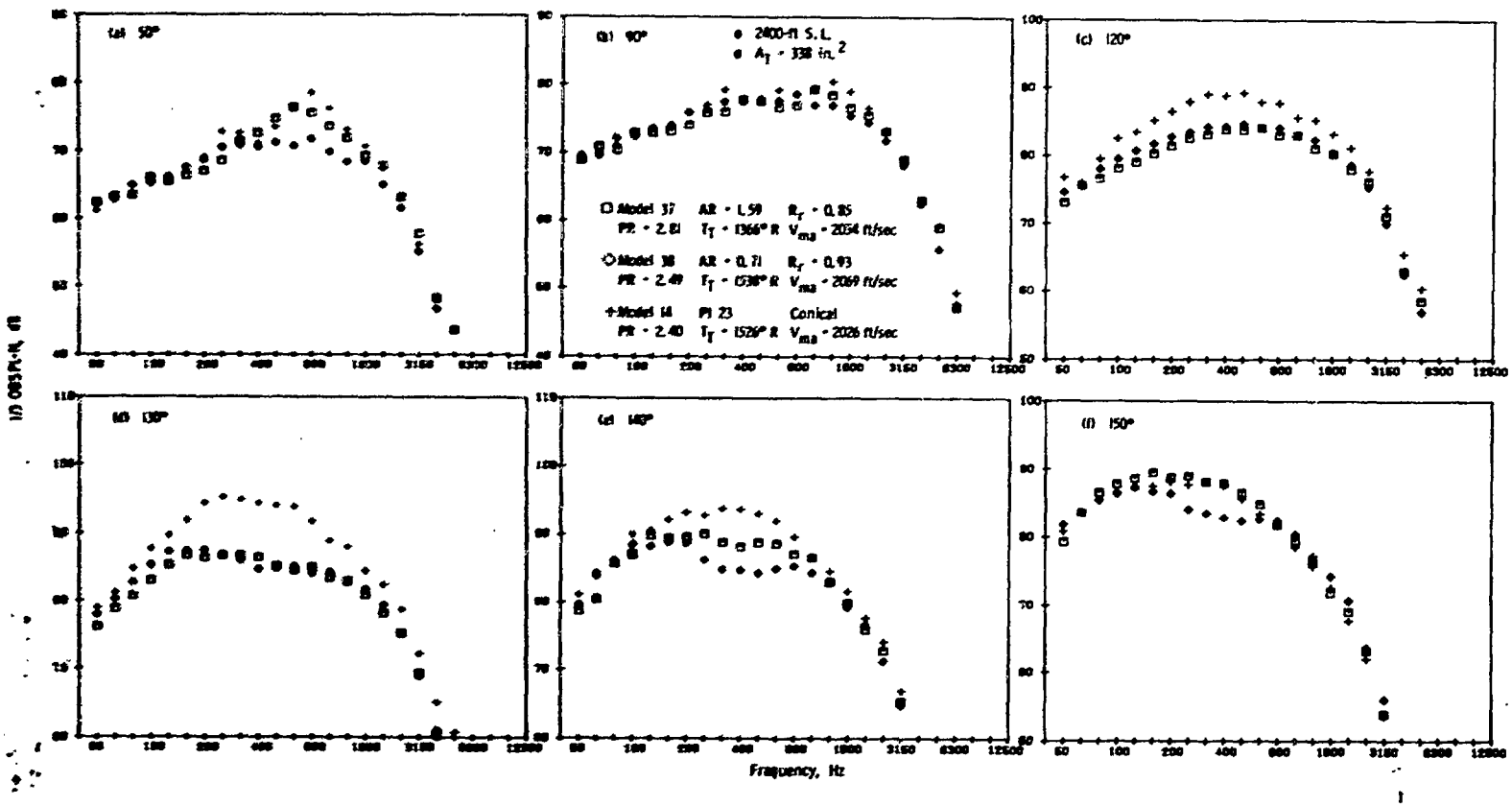

Figure 3-259. Unsuppressed Coannular Nozzles with Treated Ejectors, Spectra.

Figure 3-260 summarizes the typical suppression levels measured while testing half-span and full-span suppressors. Suppression levels are quoted relative to the conical reference nozzle. The configurations chosen in general are those which attained the highest suppression levels in their respective nozzle families.

Full-span suppressor designs which have static suppression levels in excess of 14 PNdB have been demonstrated. The 36-chute nozzle with acoustically treated ejector and 36-spoke configurations attained the highest suppression levels. Half-span suppressors implemented on the outer stream of dual flow nozzles resulted in measured peak suppression levels of 10 to 13 PNdB. The AR = 2.0 36-chute nozzle incorporating an acoustically treated ejector attained the highest suppresion. In general, suppression levels attained with half-span suppressors were slightly less than similar full-span suppressor designs. These slight acoustic differences dictate that aerodynamic performance and suppressor weight must also be considered in any ranking procedure for determining the best suppressor design. This procedure is discussed in Volume III of this report.

3.4.3 Tests to Evaluate the Influence of Simulated Flight

This section will present the results of a series of free-jet scale model tests on baseline and suppressor nozzles. All free-jet data have been transformed using the method presented in Reference 12. The transformation is accomplished by extracting the static directivity of the noise after correcting for refraction, turbulent scattering, and absorption effects and then employing a suitable multipole source decomposition to evaluate the proper dynamic effect.

3.4.3.1 Simulated Flight Investigation for Several Configurations

Eight nozzles, ranging from simple to complex geometry, were tested to determine their static and simulated flight acoustic characteristics. These nozzles were tested on the JENOTS free-jet facility (Reference 12). The model descriptions and test matrices are discussed in Sections 3.1 and 3.2.1, respectively. Photographs of the suppressor nozzle families evaluated are summarized on Figure 3-261. The ensuing discussions focus on answering four key questions, i.e.:

- Do suppressor nozzles provide a reduction in peak PNL level in flight relative to a conical nozzle? If so, is the magnitude of suppression equivalent to, greater than, or less than what is observed statically?
- Are the velocity indices of suppressor nozzles similar to those of a conical nozzle?

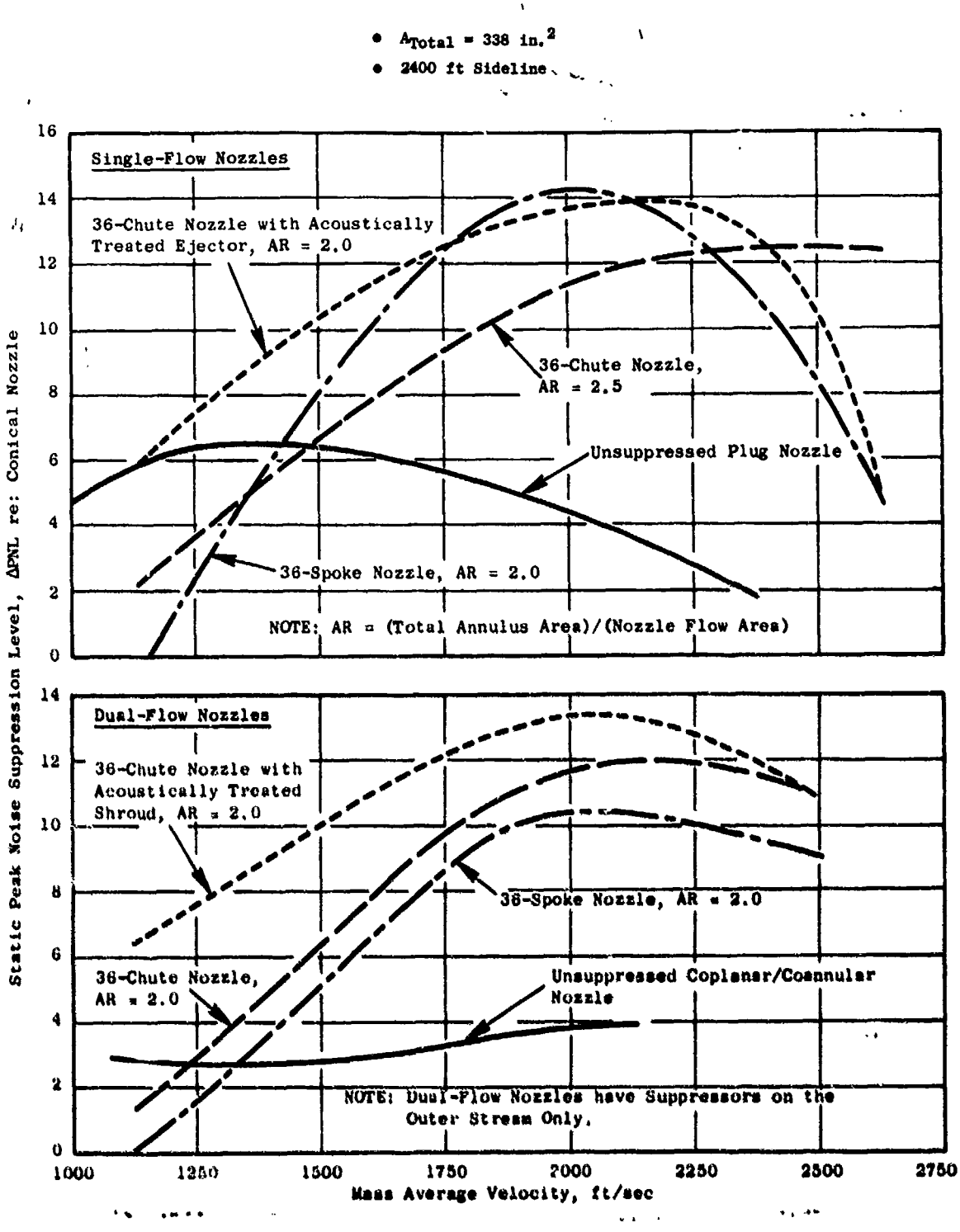

Figure 3-260. Typical Peak Static Noise Suppression Characteristics.

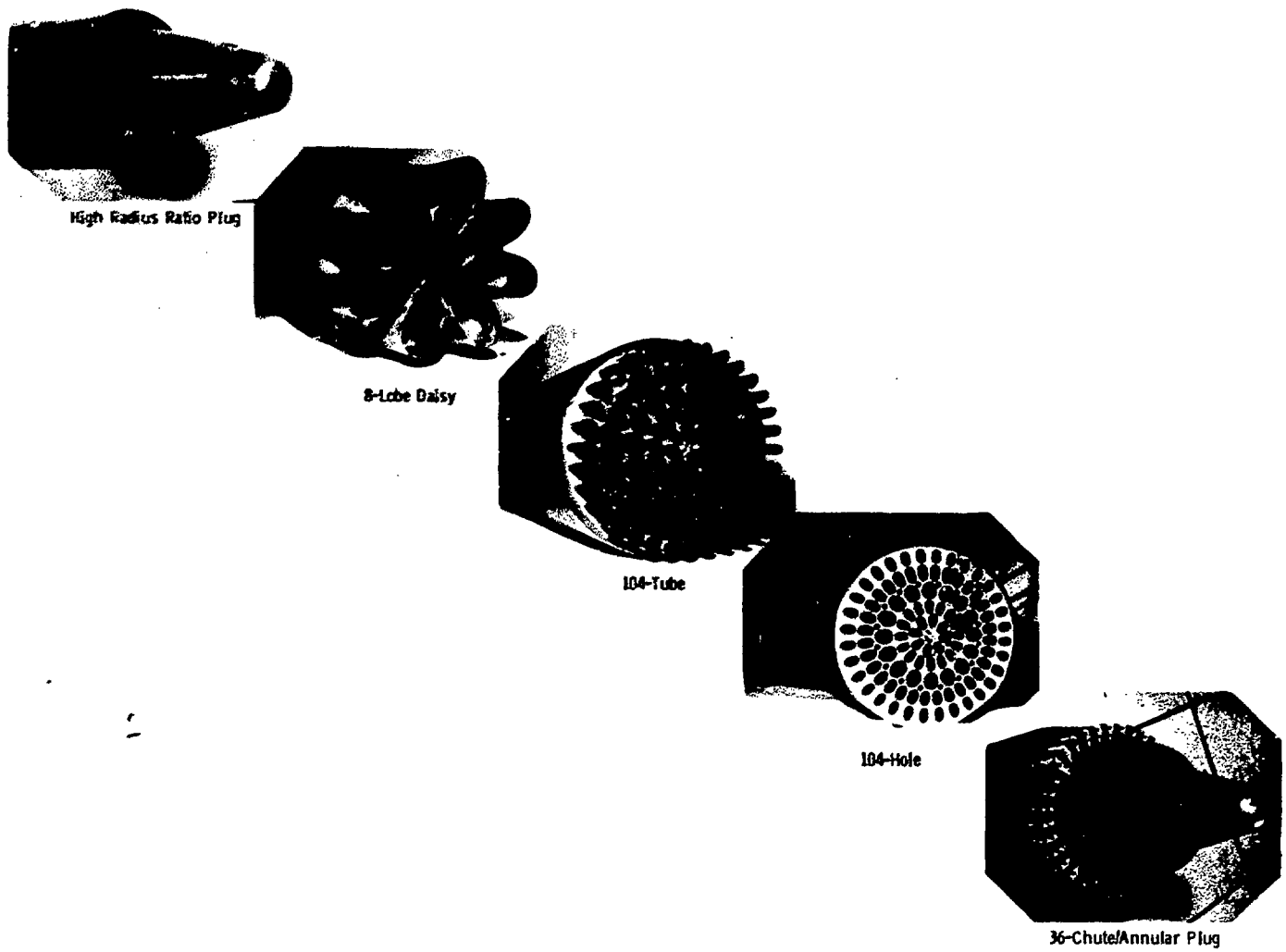

Figure 3-261. Tests to Evaluate the Influence of Simulated Flow, Summary of Suppressor Nozzle Families.

- What are the effects of flight on the spectral shapes of a suppressor nozzle?

- Is there a noise reduction at the 90° acoustic angle?

The level of peak PNL suppression as a function of velocity was established for both static and flight conditions by subtracting the normalized PNL levels presented on Figure 3-262 for select suppressor nozzles from those of the conical nozzle. The resulting suppression levels are summarized on Figure 3-263. The flight peak noise suppression of the 0.85-radius ratio plug nozzle is equivalent to the static suppression. An improvement of 1.5 to 2.0 ΔPNdB during flight occurs for the 0.789 radius ratio plug nozzle. The static suppression of each of the three chute nozzles was equivalent, whereas in flight a decrease occurs. Similar comparisons for 104-tube and 104-hole nozzles over a limited test matrix show flight and static suppression levels to be equivalent.

Table 3-6 summarizes typical static and flight peak noise suppression levels at a jet velocity of 2500 ft/sec. For baseline systems such as plug nozzles, the flight levels of suppression are near equivalent to the static levels and for the tube nozzle they are equivalent. The chute nozzles exhibit an approximate 3 PNdB loss of suppression in flight.

Peak OASPL and 90° PNL levels as a function of velocity are summarized on Figures 3-264 and 3-265, respectively. The peak OASPL reduction from static to flight is greater than on a PNL basis. The differences are configuration dependent. For example, chute nozzles exhibited a zero to 1-PNdB increase and a zero to 1-dB decrease on the basis of OASPL. Differences between peak PNL and OASPL noise trends are attributed to frequency-dependent spectra changes from static to flight. A greater reduction in OASPL indicates that low frequencies realize more reduction in flight than high frequencies; 90° PNL static and flight levels are within ±1 PNdB for the conical, 0.789 plug and 104-hole nozzles. The 0.85 radius ratio plug nozzle PNL levels increase from zero to 2 dB depending on the condition being compared. This increase is attributed to shock-cell noise dominance and is discussed in Section 3.4.3.2. The 36-chute nozzles show an increase in noise level of 3 to 4 dB, a trend which differs significantly from the other nozzle families.

PNL directivity characteristics for each of the nozzles are summarized in terms of velocity indices (N_θ) calculated by using the following equation:

$$N_\theta = \left[\frac{OASPL_{static} - OASPL_{flight} - 10 \log (1 - M_{a/c} \cos \theta)}{\log \frac{V_J}{V_J - V_{a/c}}} \right]$$

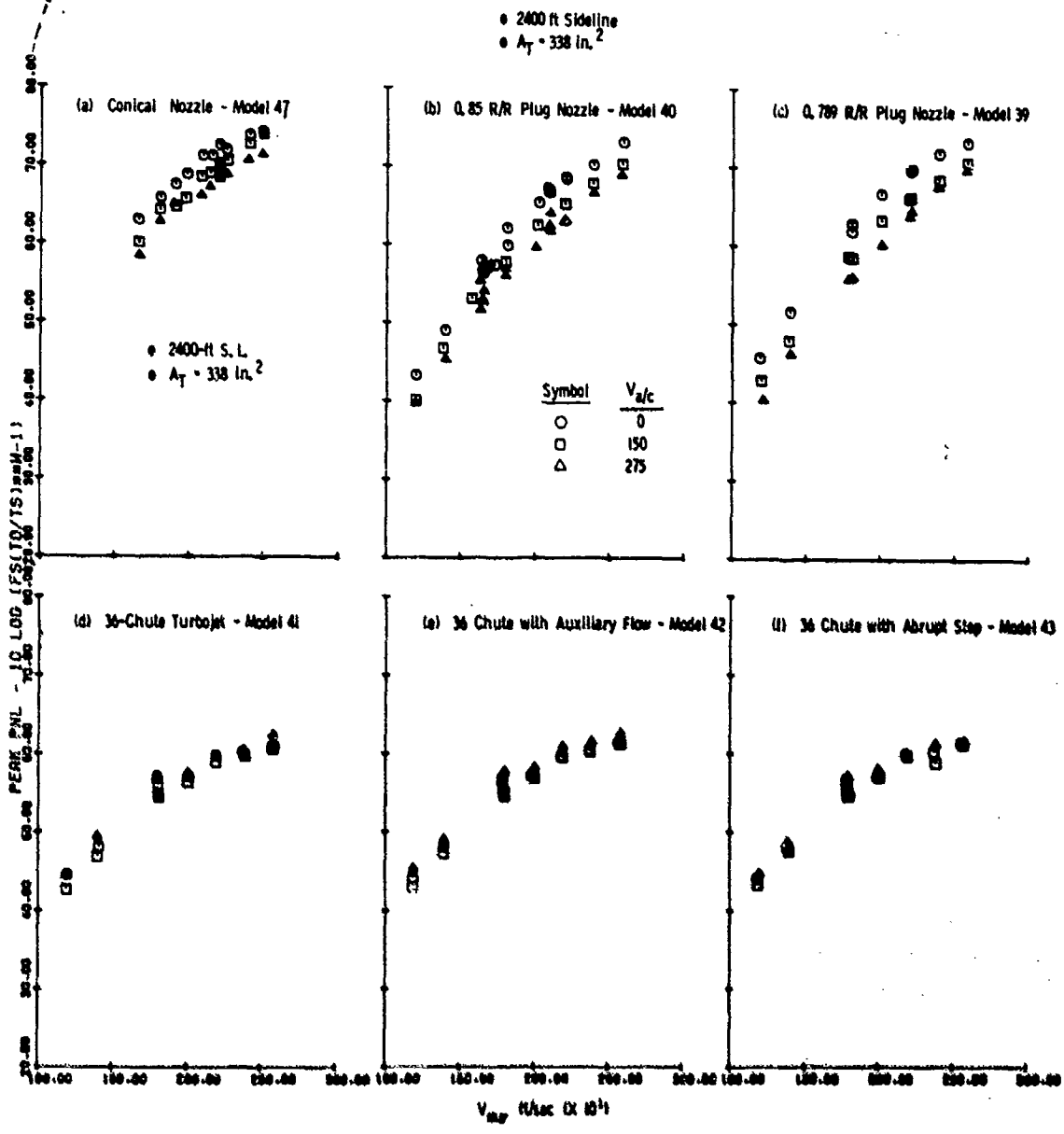

Figure 3-262. Static and Flight Peak PNL Levels.

40

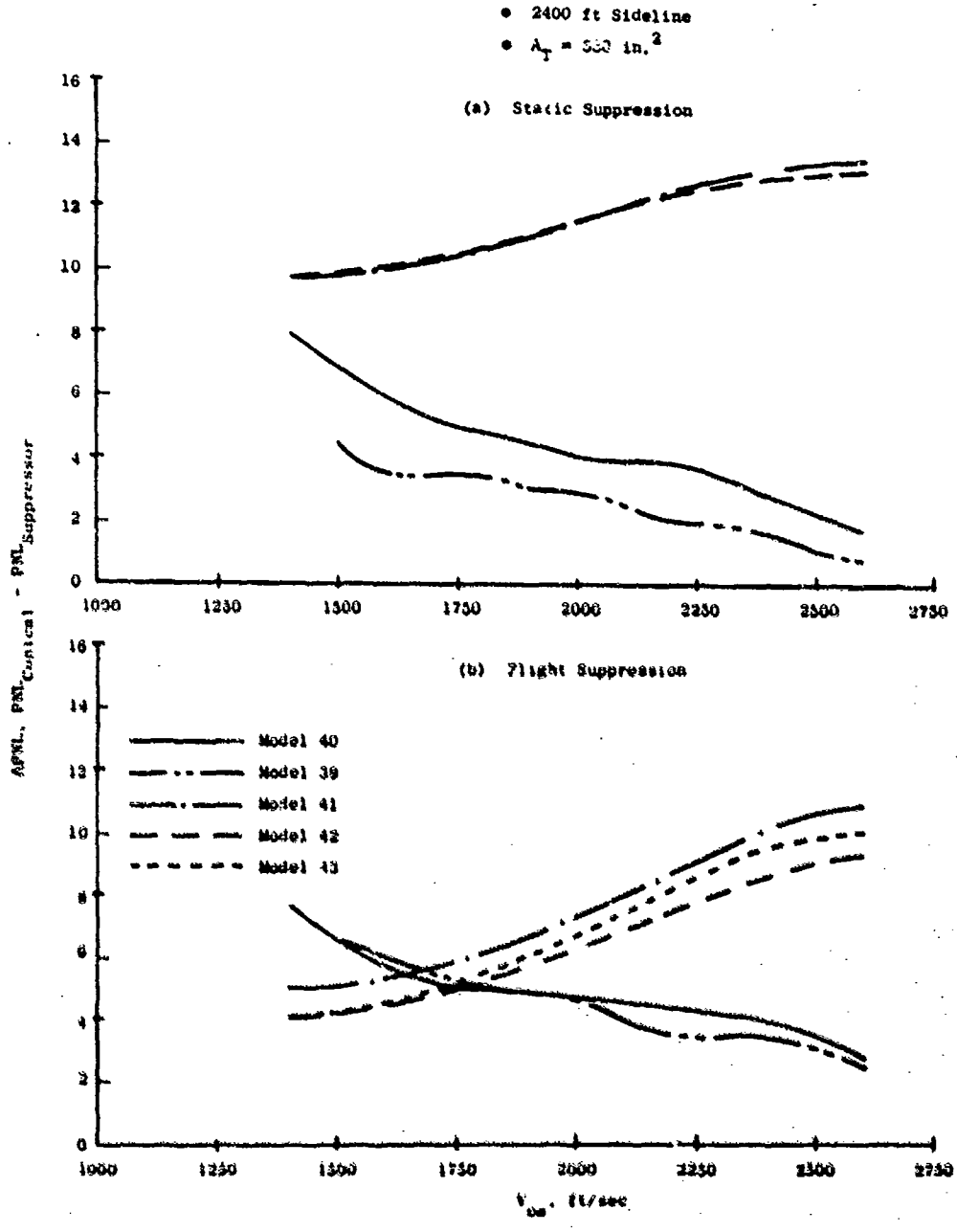

Figure 3-263. Static and Flight PWL Suppression Levels.

Table 3-6. Summary of Nozzle Static and Projected Flight Peak PNL Suppression Characteristics.

- Suppression Levels are Relative to a Conical Nozzle
- 2400-ft Sideline
- V_j = 2500 ft/sec
- A_T = 338 in.^{2}

Model No.	Configuration	Suppression Level, dB	
		Static	Flight
39	Plug Nozzle - 0.789 Radius Ratio	1.3	3.0
40	Plug Nozzle - 0.85 Radius Ratio	2.3	3.7
46	8-Lobe Nozzle	5.6	5.6
41	AR = 2.5 36-Chute Nozzle	13.5	10.9
42	AR = 2.5 36-Chute Nozzle with Auxiliary Flow	12.5	9.4
44	104-Tube Nozzle	12.0	12.0

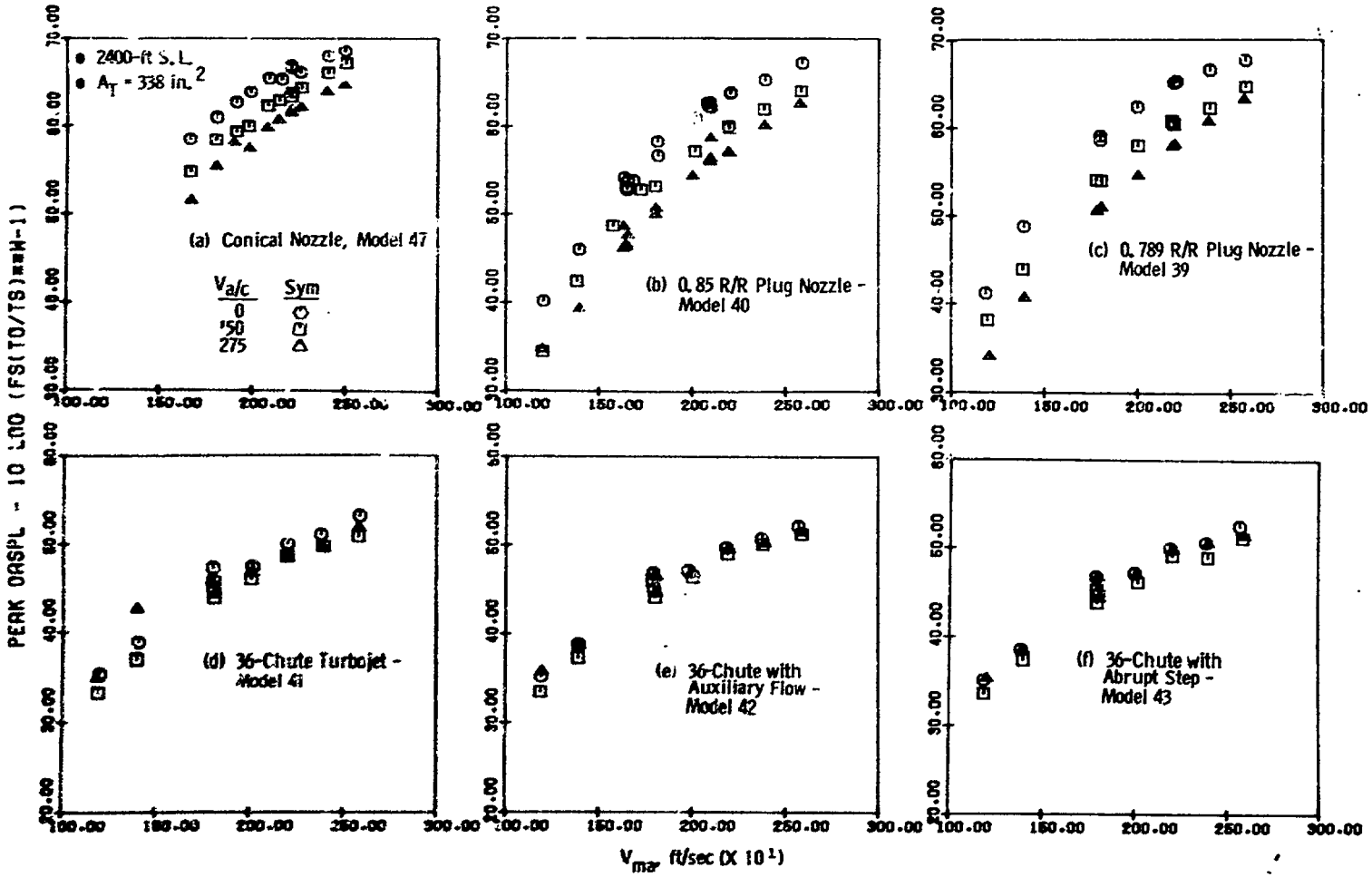

Figure 3-264. Static and Flight Peak OASPL Levels.

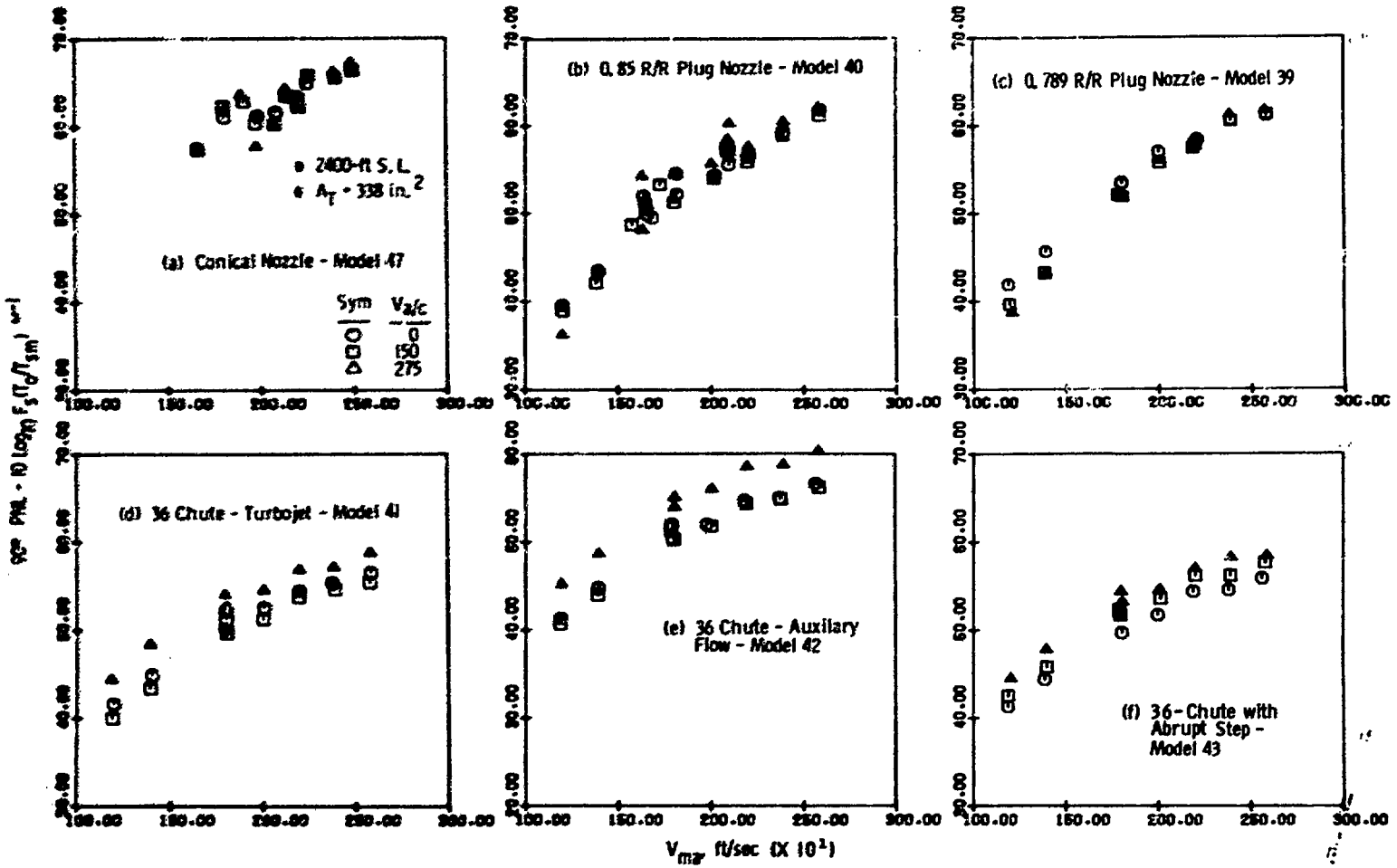

Figure 3-265. Static and Flight 90° PNL Levels.

Velocity indices were calculated for jet velocities ranging from 1800 ft/sec through 2600 ft/sec, as summarized on Figures 3-266 through 3-269. Data at free-jet velocities of 150 and 275 ft/sec were utilized. The velocity index parameter was not sufficient to collapse the data into one set of indices which is correct for all configurations. Plug nozzles and conical nozzles have similar indices in the aft quadrant. In the forward quadrant the effect of shock-cell noise is apparent. In general, for the conical nozzle (Figure 3-266) as pressure ratio increases, forward quadrant indices become negative which indicates a noise increase in flight. The suppressor nozzles exhibit a velocity pattern which is distinctly different from the conical nozzle and varies with nozzle type. Chute nozzles in particular show a sharp decrease in velocity index beginning at an acoustic angle of 130°.

The velocity indices are compared on Figure 3-270 for several configurations. The tube nozzle and plug nozzles have velocity index patterns of similiar shape and level. The conical nozzle deviates from these configurations, particularly in the forward quadrant, due to the presence of shock noise. Velocity indices of the chute nozzle configurations are significantly less than that of the other configurations at 130°. Examination of the spectra should provide some insight into the cause of this variation.

The spectra presented on Figures 3-271(a) and 3-271(b) are at 130° for both the chute (Model 41) and tube (Model 44) nozzles. Three spectra are presented for each configuration: static spectra and wind-on spectra before and after transformation. The reduction in the low frequency portion of the spectra is within 1 dB for both the chute and tube nozzle configurations. In the high frequency portion of the spectra, dominated by the premerged noise, both nozzles have a slight increase in level. However, the absolute level relative to the low frequency portion of the spectra is extremely different. The transformed spectra of the chute and tube nozzles are compared on Figure 3-272. There is a 10 dB difference in the high frequency portion of the spectra. The dominance of the high frequency noise is the reason for the lack of flight effect on these chute nozzles.

In addition to being analyzed on a velocity index basis, the directivity patterns were also analyzed on the basis of PNL suppression level as a function of angle for several jet velocities. Jet velocities of 2200 ft/sec and 2600 ft/sec are discussed in detail.

The acoustic suppression levels in terms of ΔPNL versus angle are summarized on Figures 3-273 through 3-275. Static and flight suppression levels, Figure 3-273, are equivalent for the plug nozzle. The chute nozzles, Figure 3-274, exhibit a loss of suppression in the aft quadrant and generally maintain suppression in the forward quadrant. The 104-tube (Model 44) and 104-hold (Model 45) nozzles, Figure 3-275, show essentially no change in suppression level relative to a conical nozzle (Model 47) in flight.

A summary of PNL, OASPL, and spectra comparisons for each of the configurations is presented in Figures 3-276 through 3-301 for jet velocities of [illegible]00 and 2000 ft/sec. Four acoustic angles of 50°, 90°, 110°, and 130° were

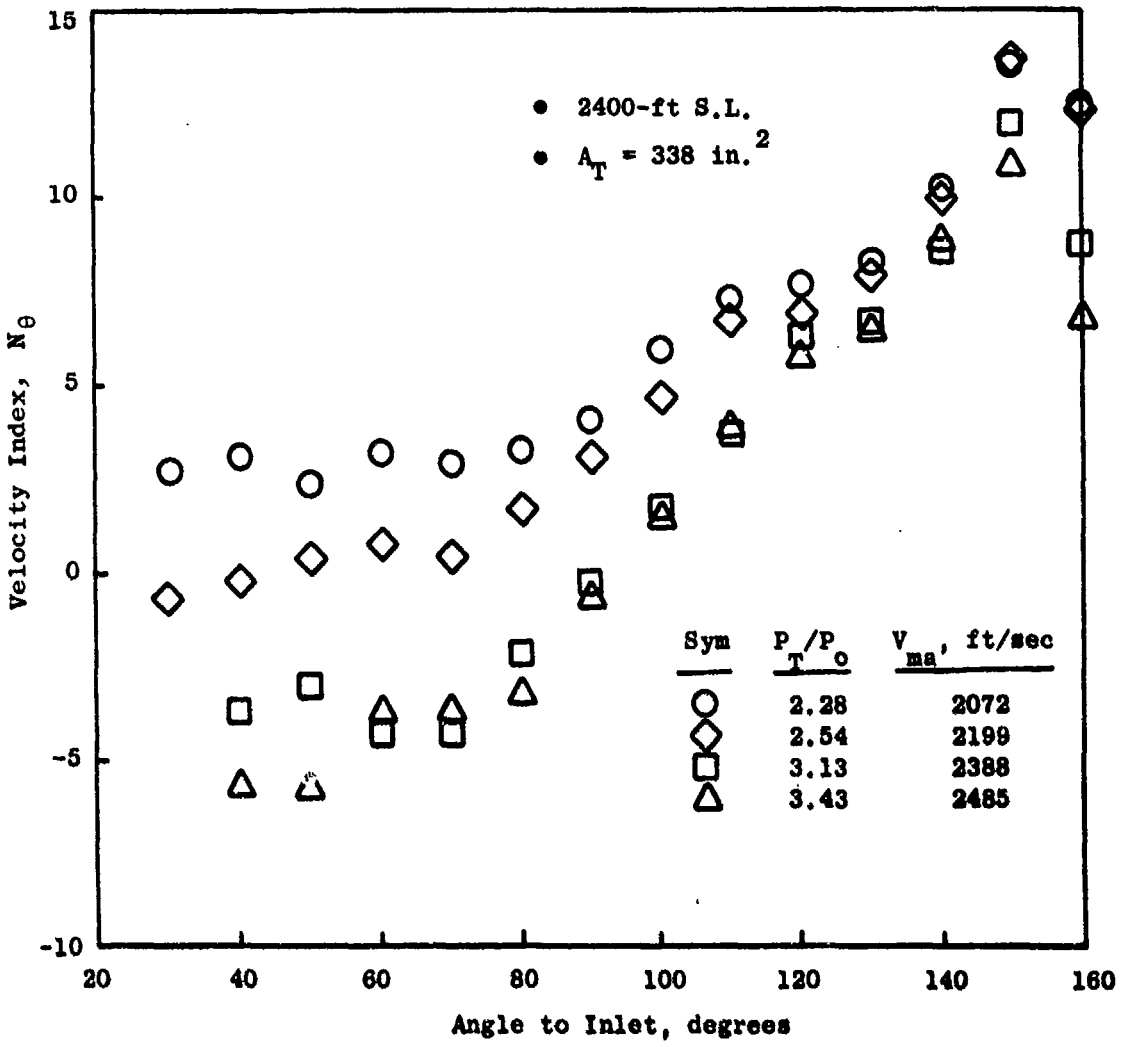

Figure 3-266. Conical Nozzle (Model 47) Velocity Indices.

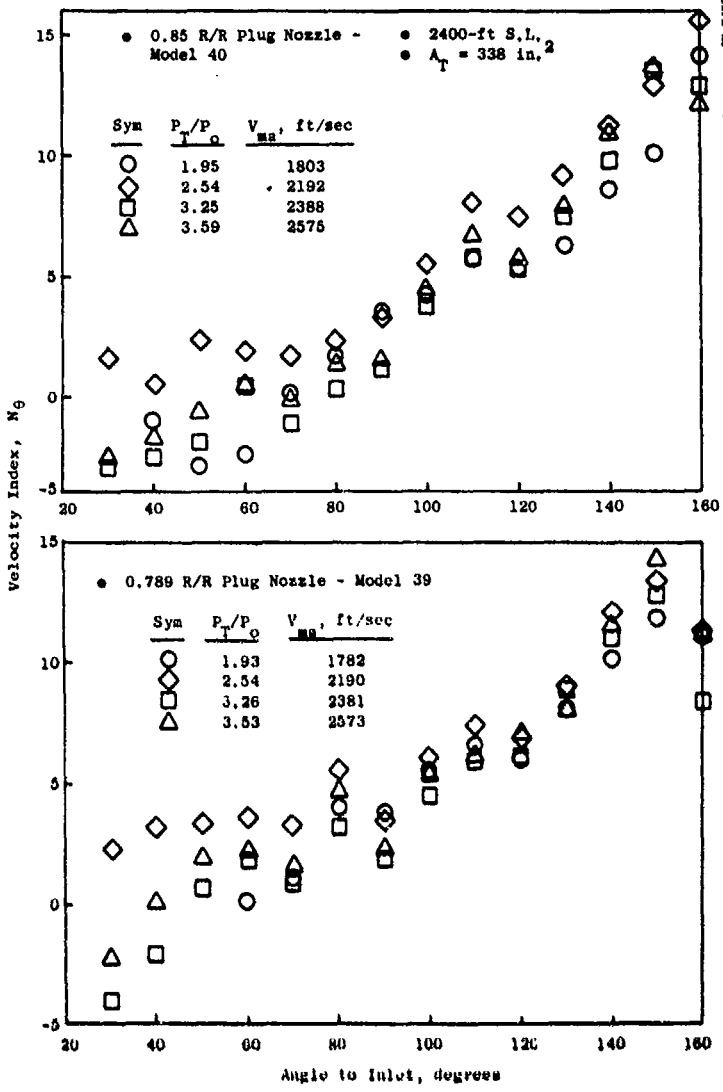

Figure 3-267. Plug Nozzle (Models 39 and 40) Velocity Indices.

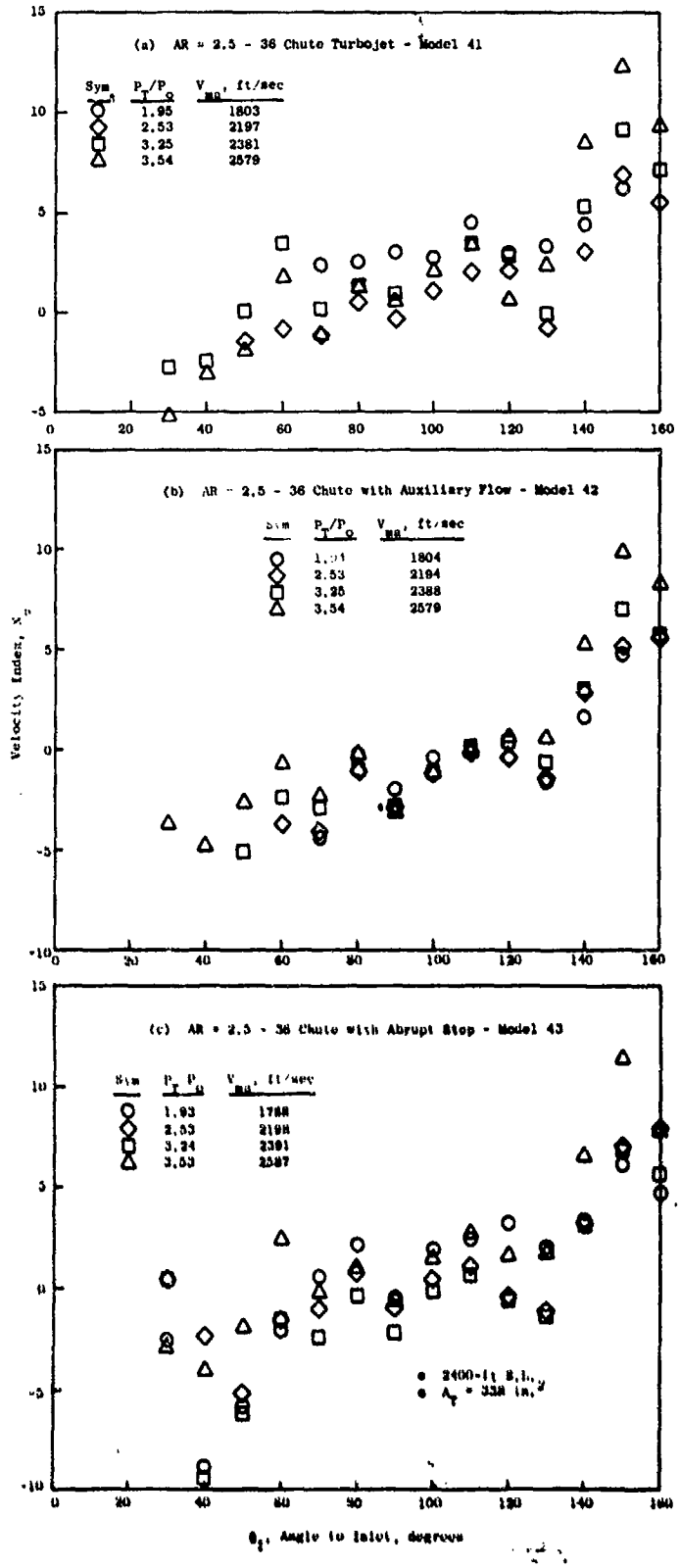

Figure 3-268. Chute Nozzle (Models 41, 42, and 43) Velocity Indices.

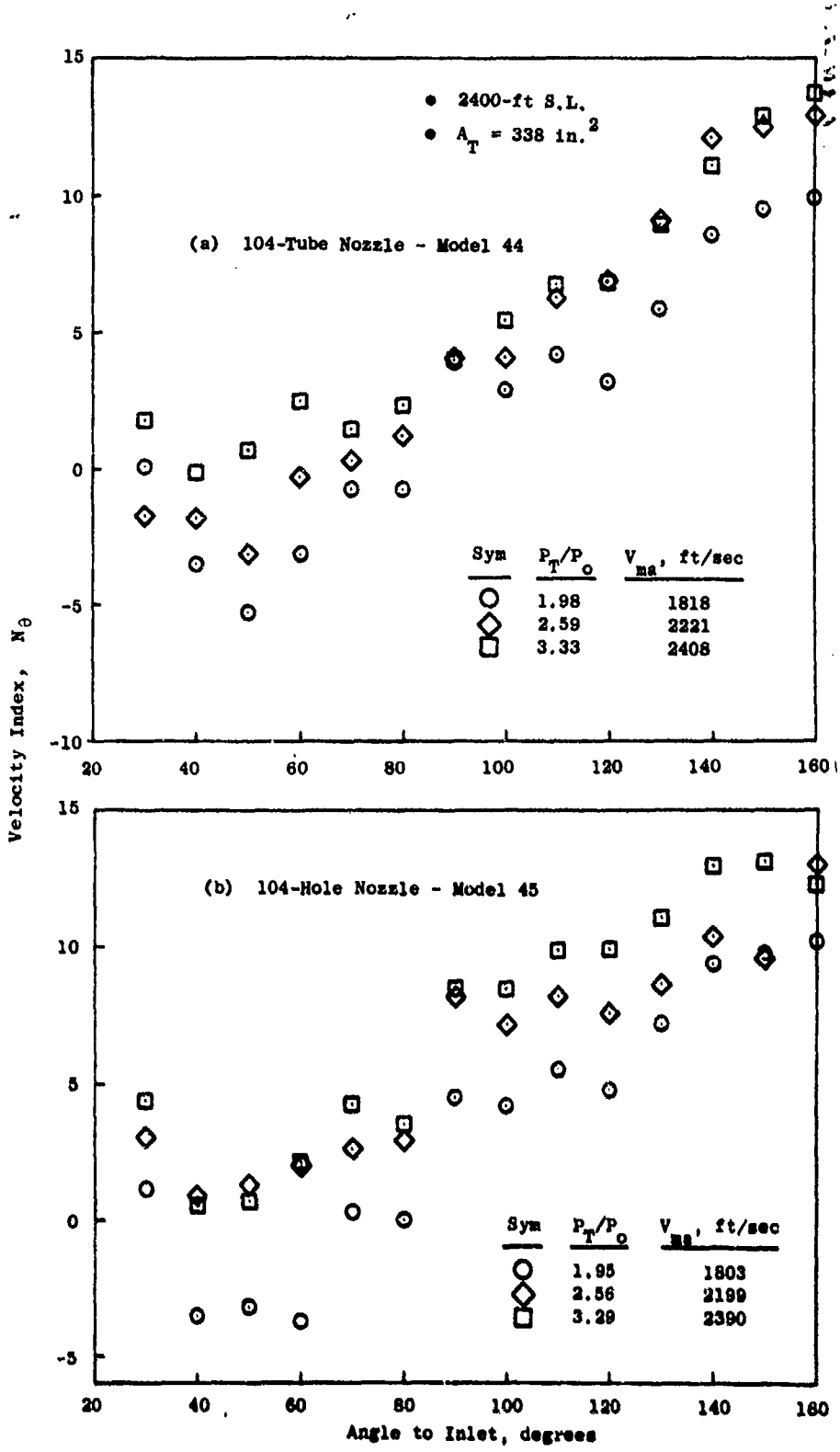

Figure 3-269. 104-Tube (Model 44) 104-Hole (Model 45) Nozzle Velocity Indices.

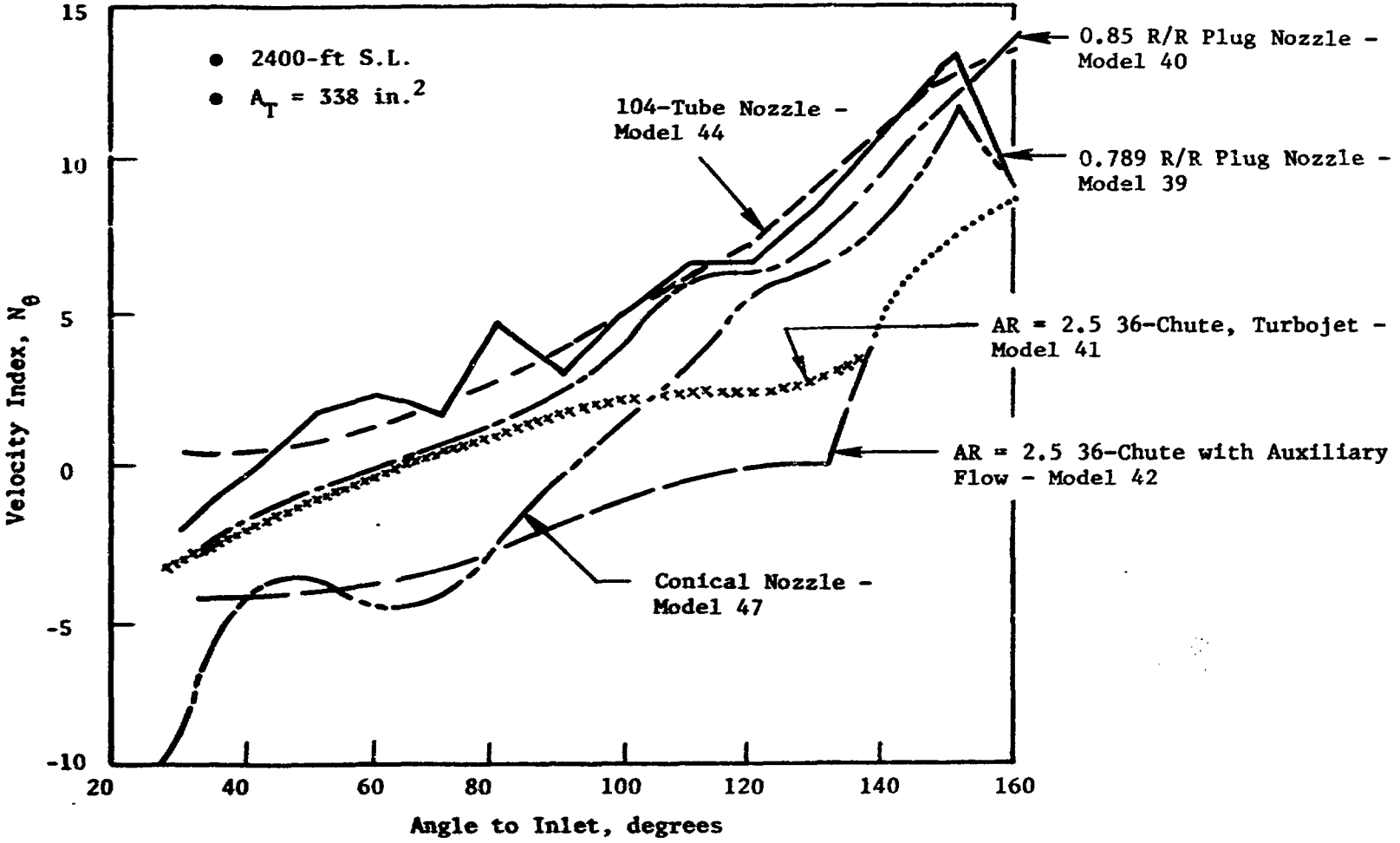

Figure 3-270. Velocity Indices for Several Nozzles.

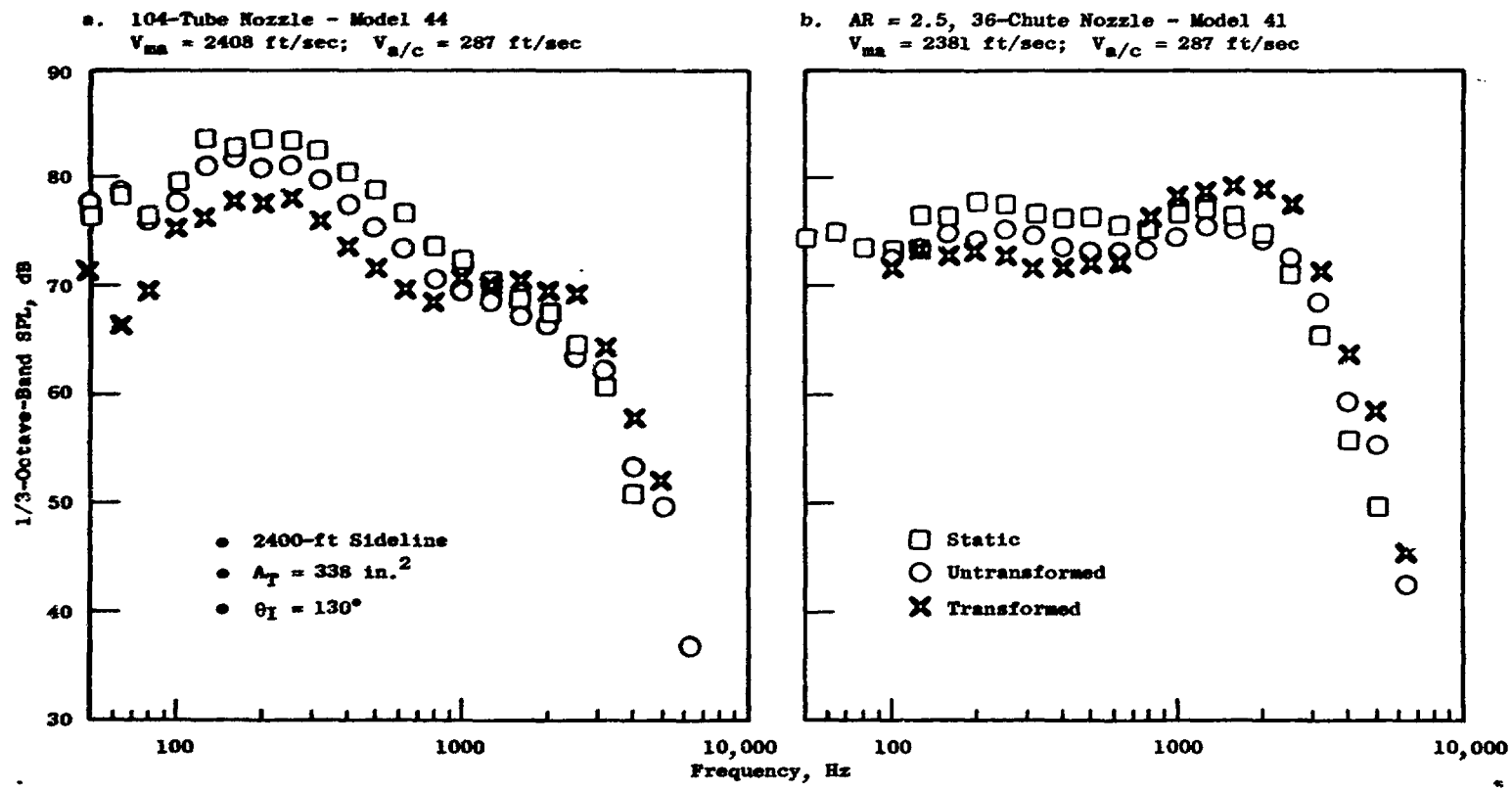

Figure 3-271. Comparison of Static and Flight Spectra, 104-Tube and 36-Chute Nozzles (Models 44 and 41).

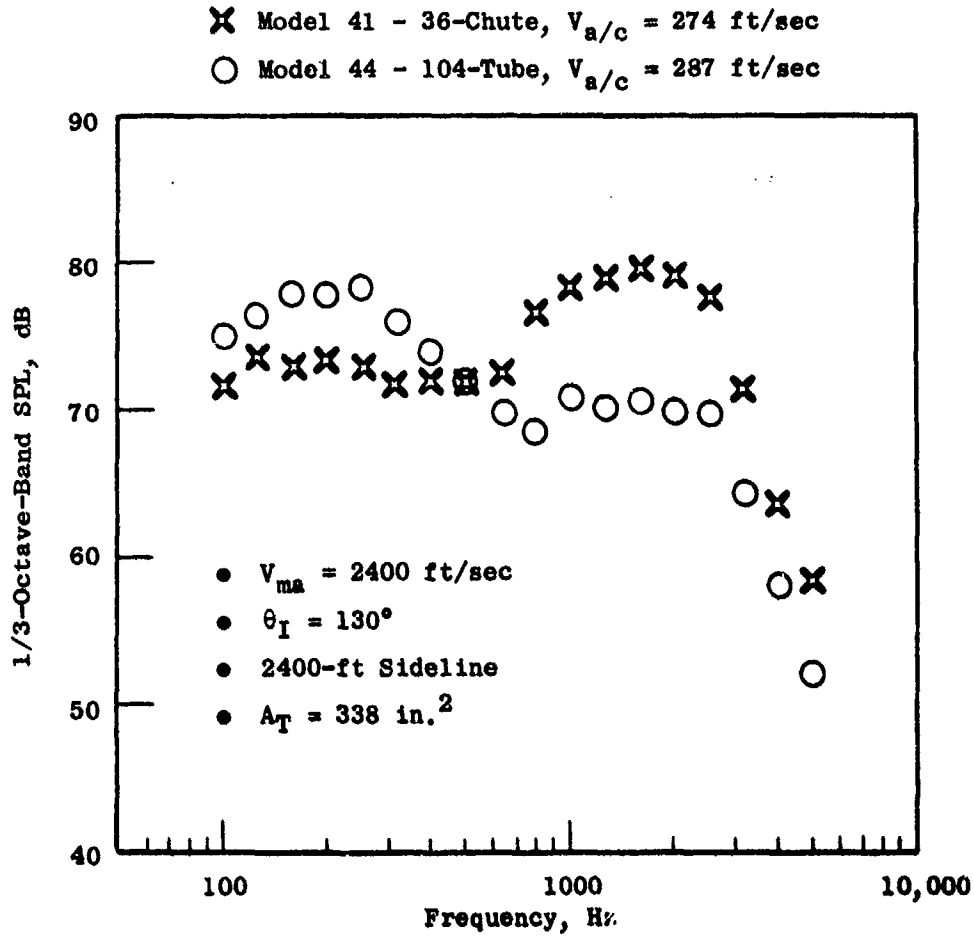

Figure 3-272. A Comparison of the Flight Spectra for 104-Tube (Model 44) and 36-Chute (Model 42) Nozzles.

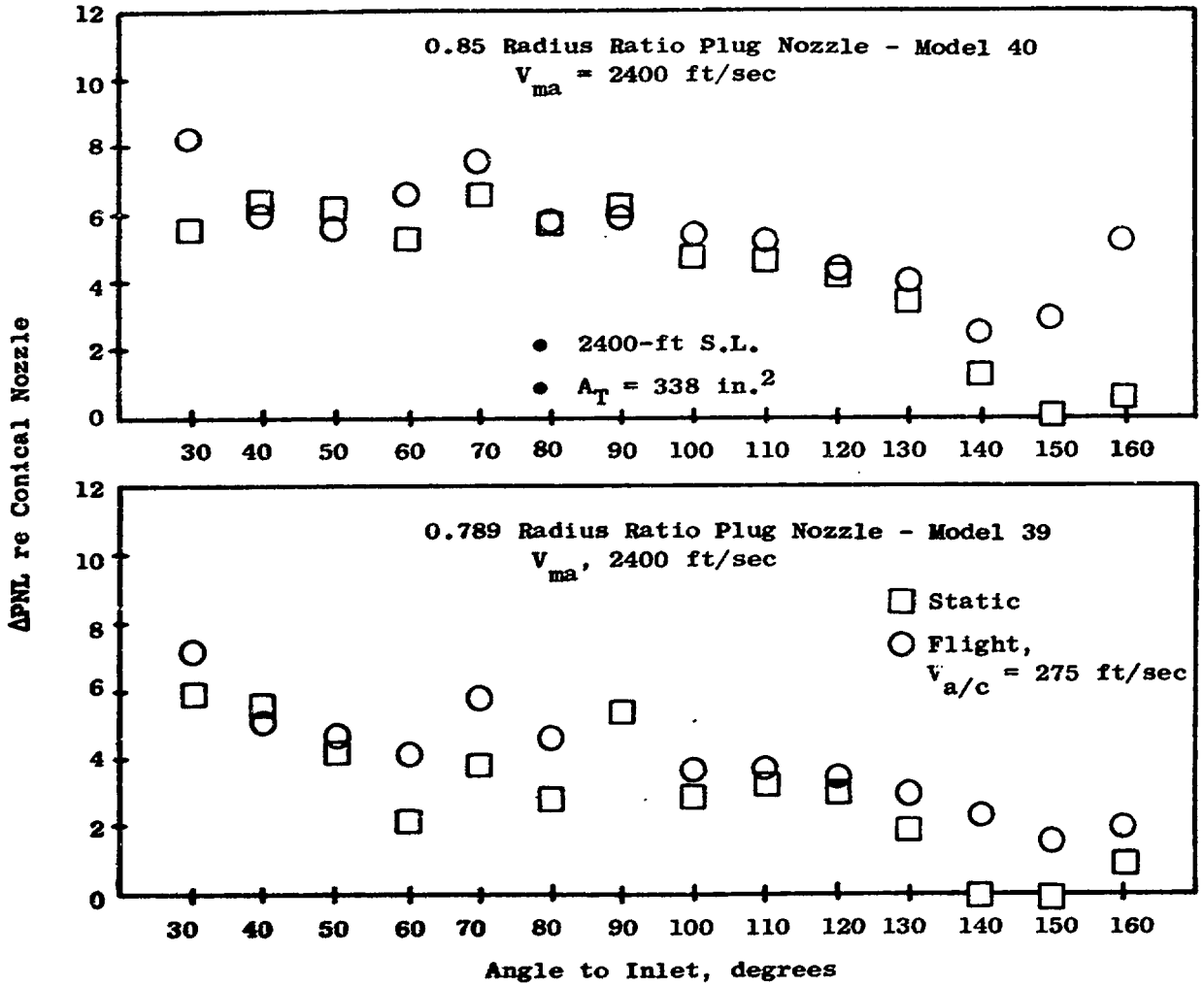

Figure 3-273. Summary of Static and Flight PNL Suppression Characteristics (Models 39 and 40).

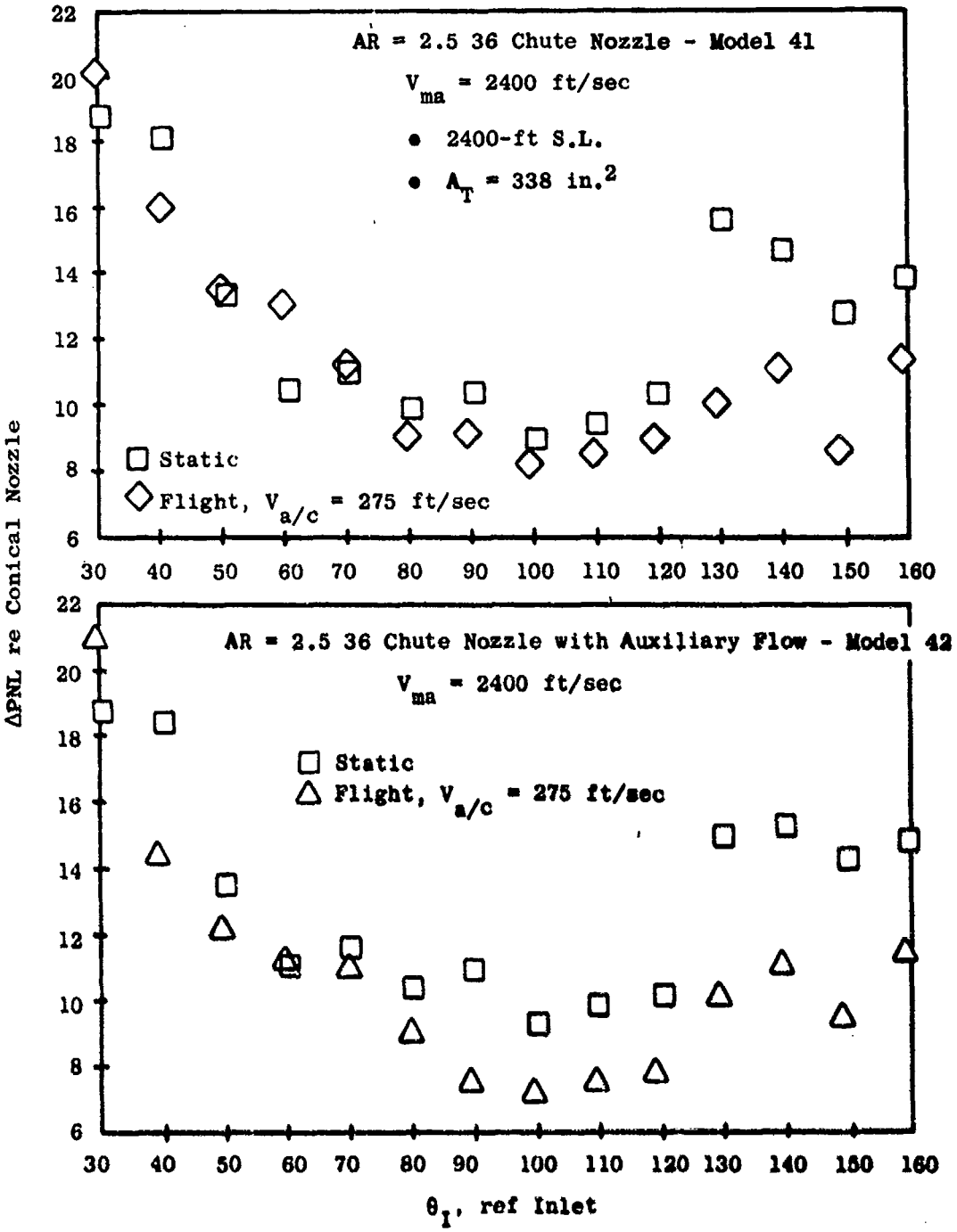

Figure 3-274. Summary of Static and Flight Suppression Characteristics (Models 41 and 42).

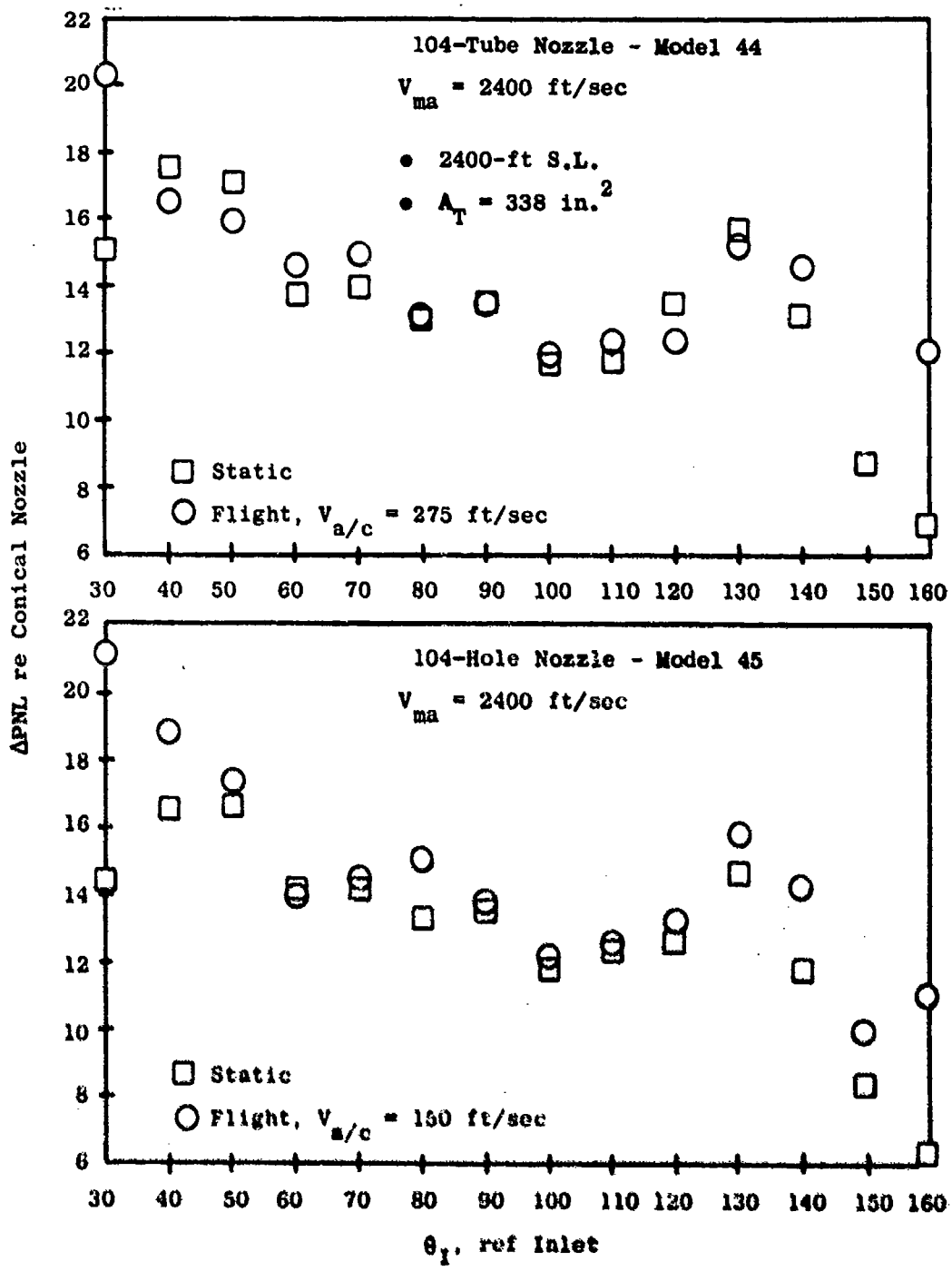

Figure 3-275. Summary of Static and Flight Suppression Characteristics (Models 44 and 45).

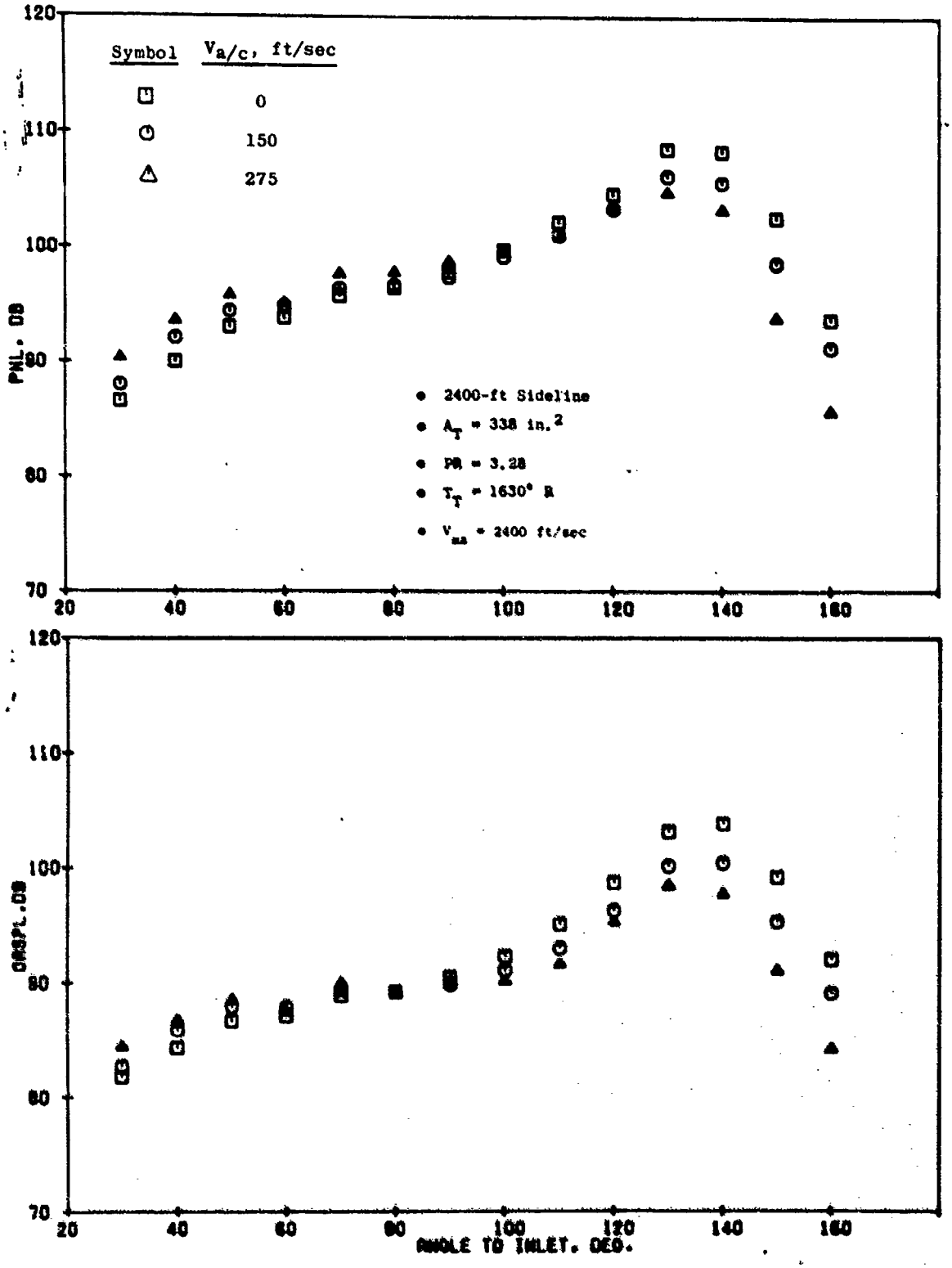

Figure 3-276. 0.85 R/R Plug Nozzle (Model 40) PNL and OASPL Directivity, V_{aa} = 2400 ft/sec.

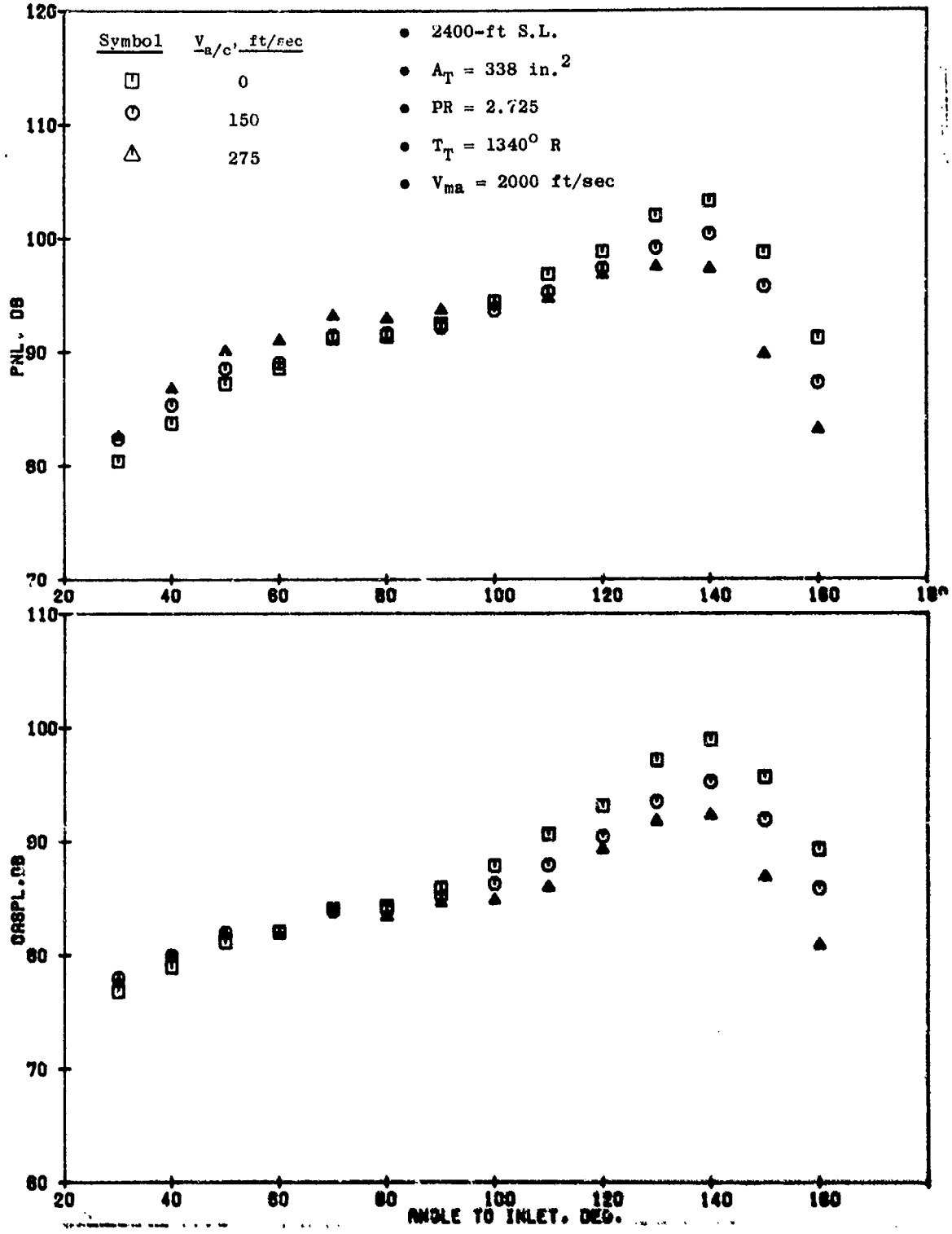

Figure 3-277. 0.85 R/R Plug Nozzle (Model 40) PNL and OASPL Directivity, V_{ma} = 2000 ft/sec.

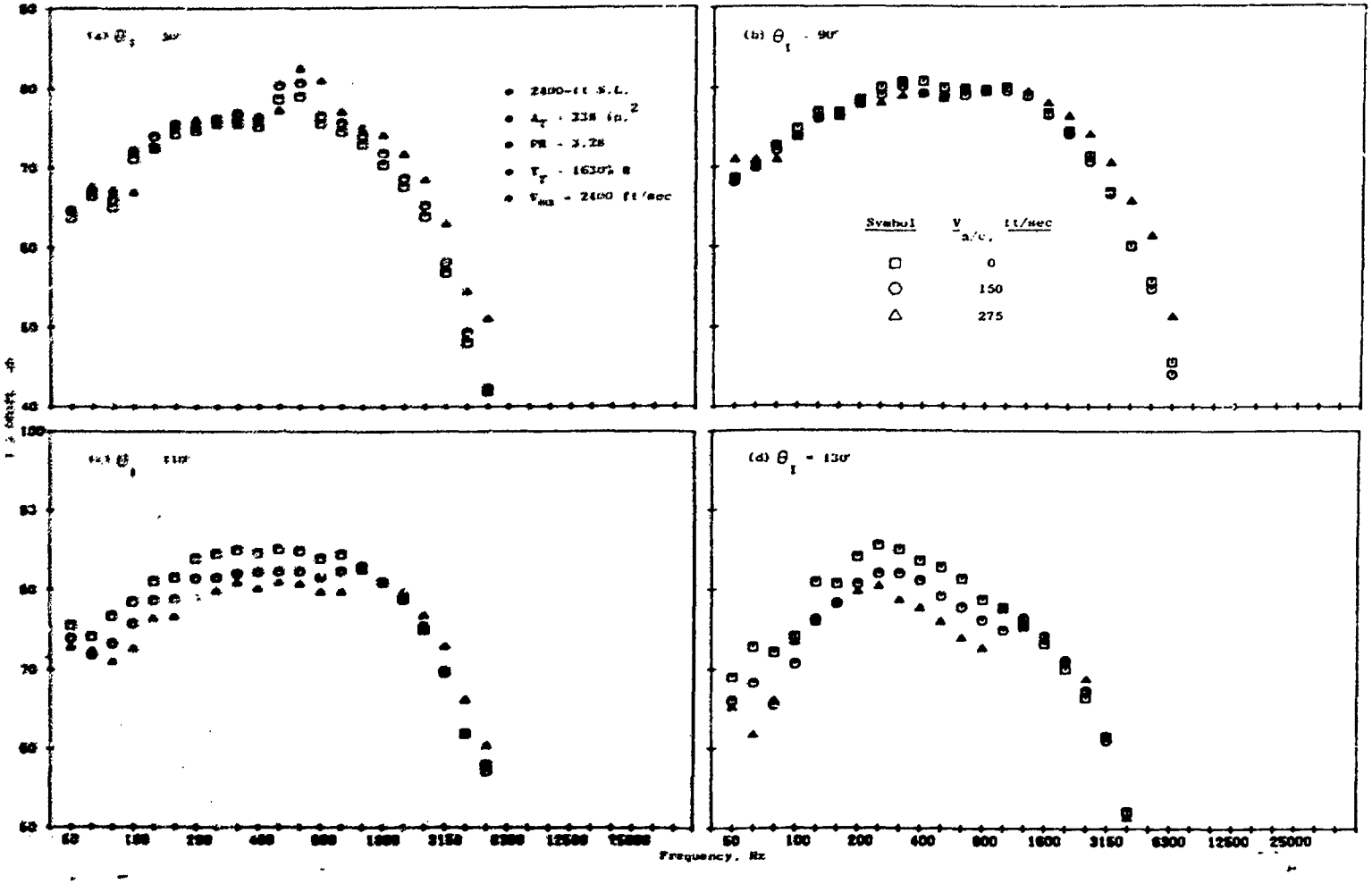

Figure 3-278. 0.85 Radius Ratio Plug Nozzle (Model 40) Spectra, V_{ma} = 2400 ft/sec.

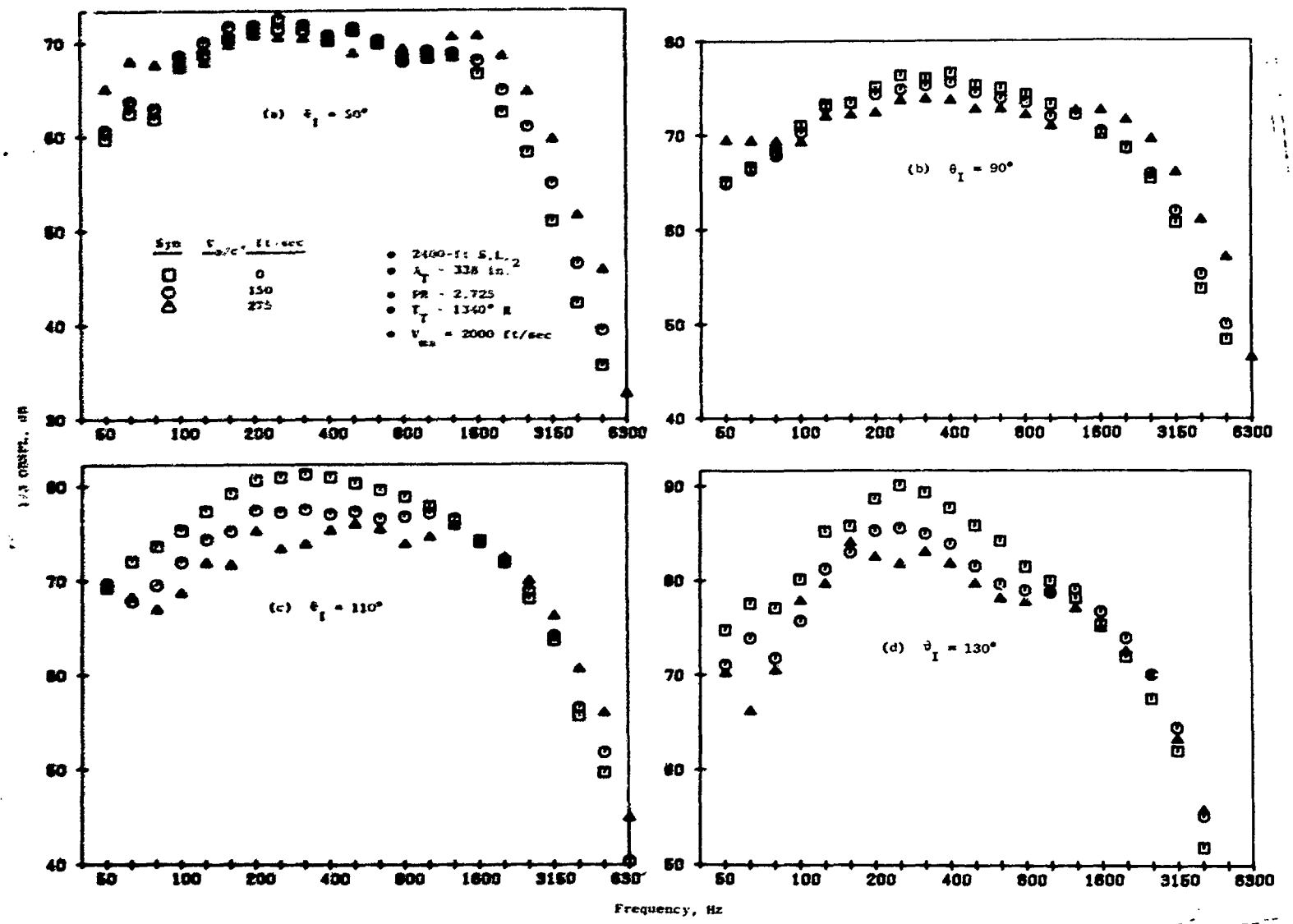

Figure 3-279. 0.85 Radius Ratio Plug Nozzle (Model 40) Spectra, V_{ma} = 2000 ft/sec.

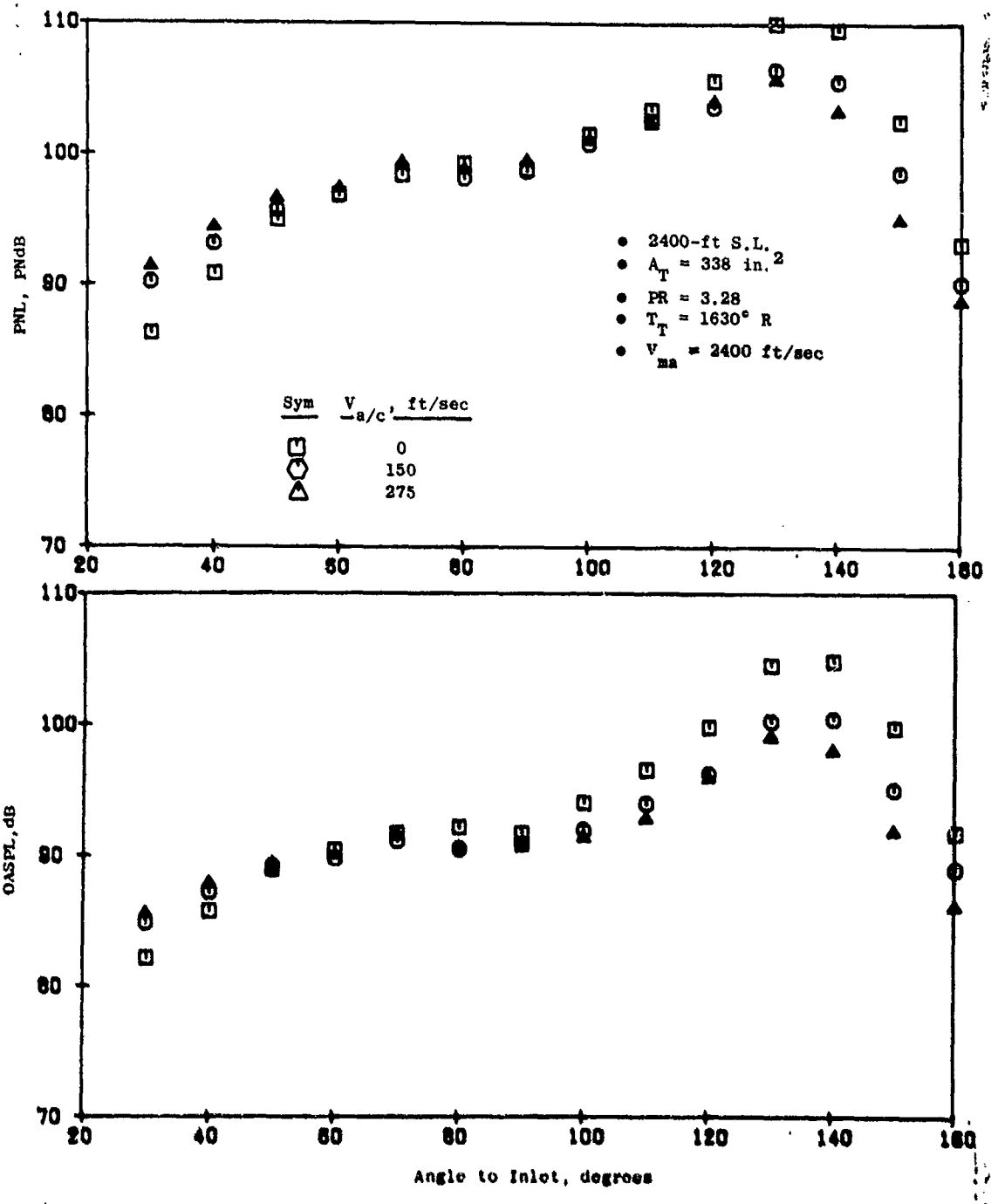

Figure 3-280. 0.789 Radius Ratio Plug Nozzle (Model 39) PNL and OASPL Directivity, V_{ma} = 2400 ft/sec.

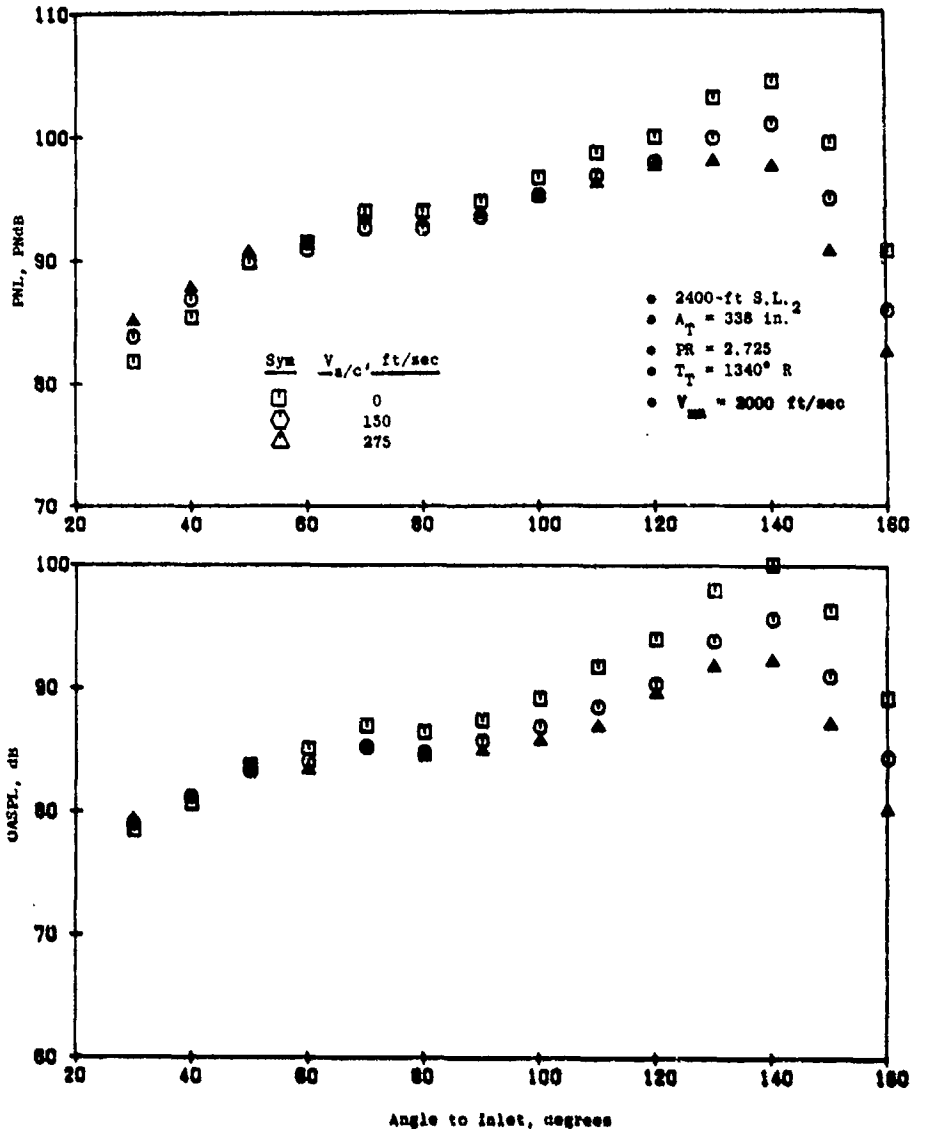

Figure 3-281. 0.789 Radius Ratio Plug Nozzle (Model 39) PNL and OASPL Directivity, V_{ma} = 2000 ft/sec.

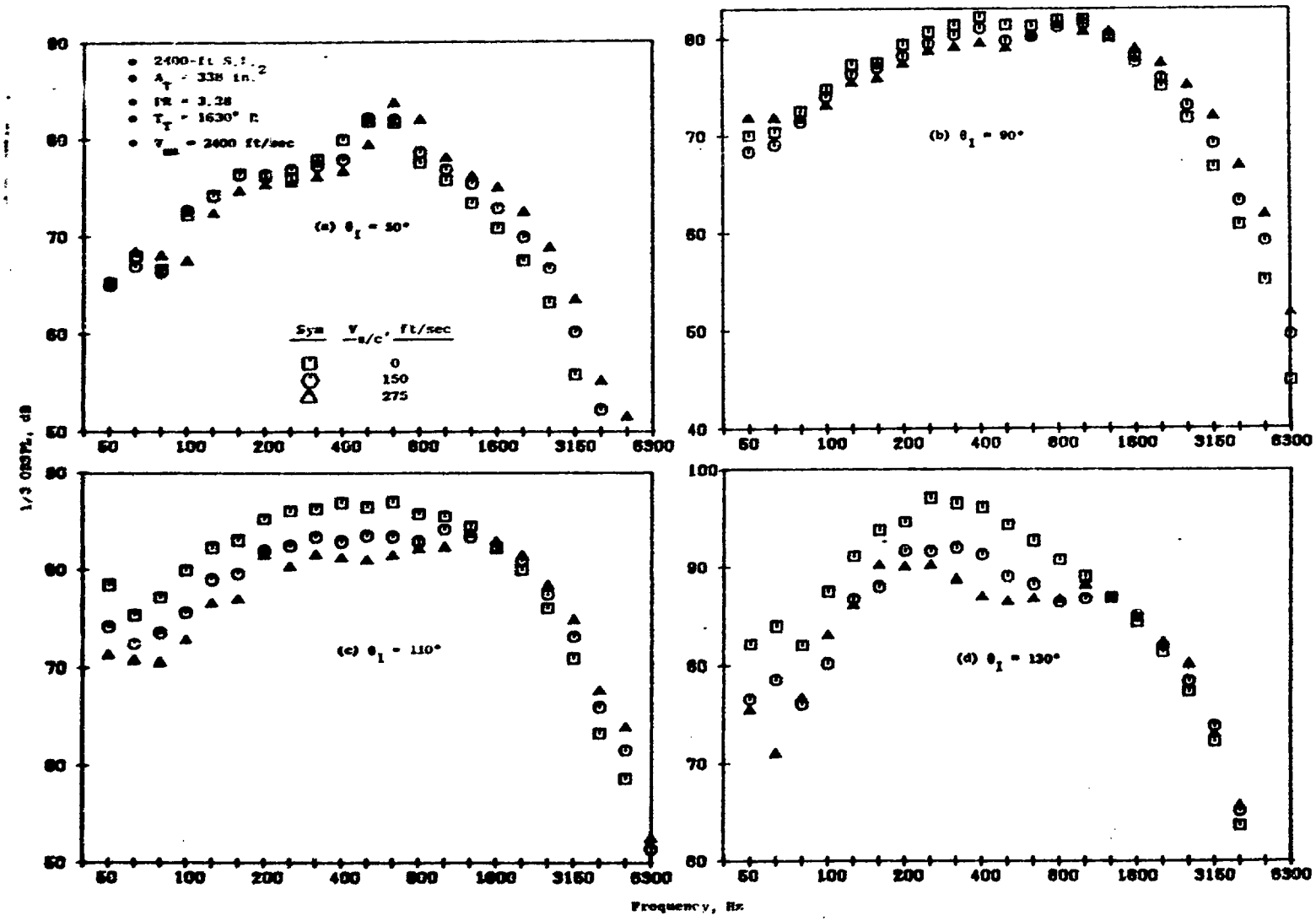

Figure 3-282. 0.789 Radius Ratio Plug Nozzle (Model 39) Spectra, V_{ma} = 2400 ft/sec.

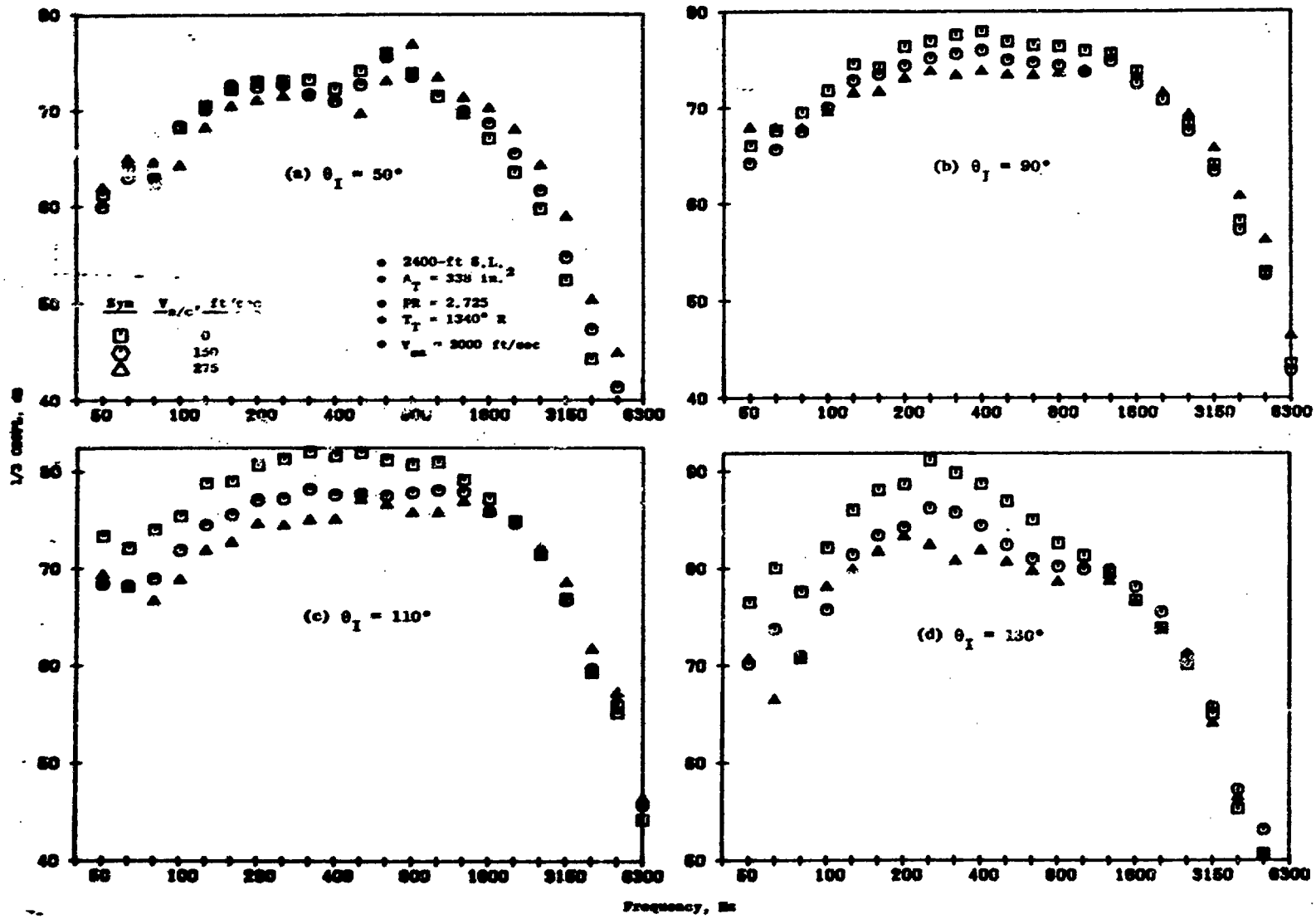

Figure 3-283. 0.789 Radius Ratio Plug Nozzle (Model 39) Spectra, V_{ma} = 2400 ft/sec.

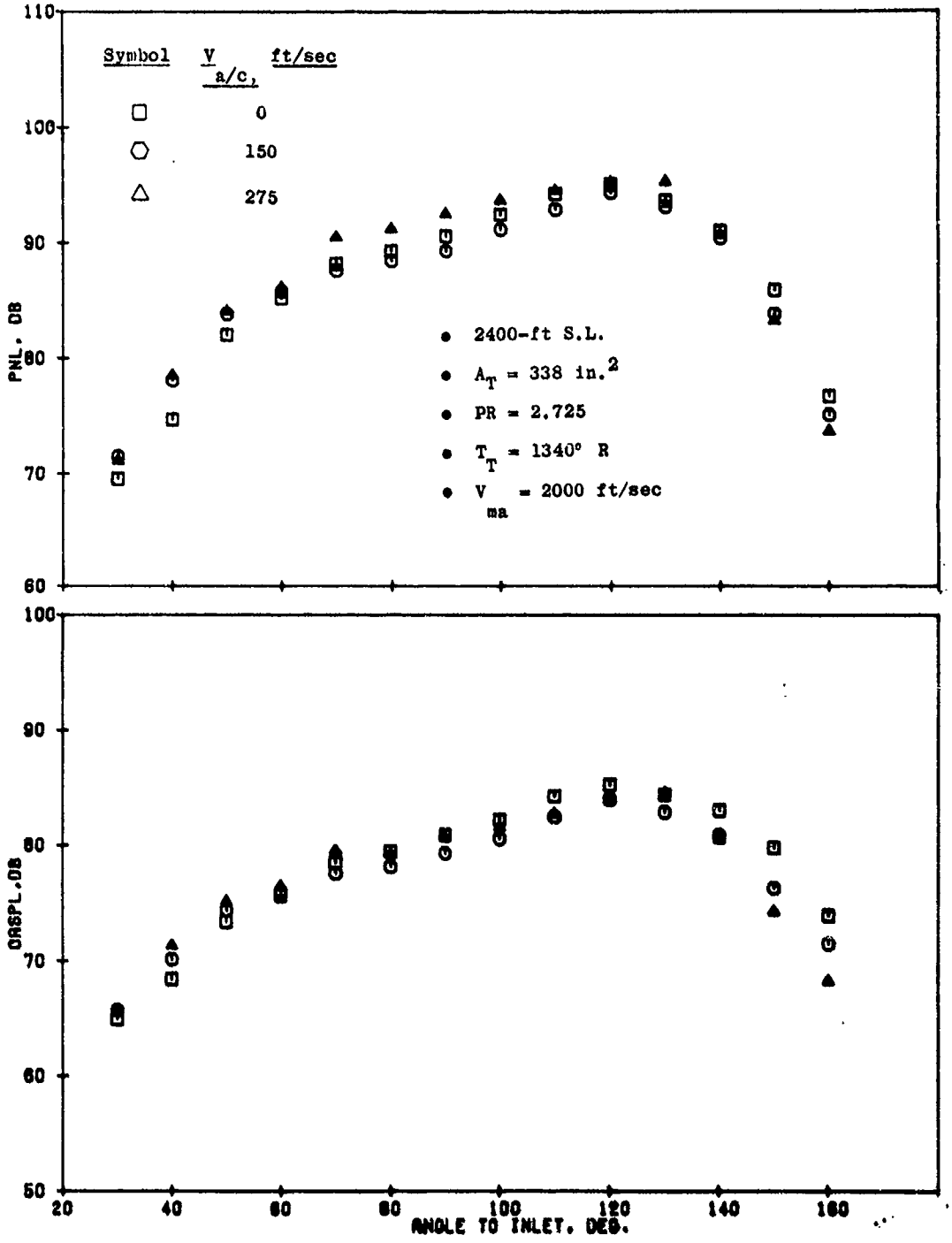

Figure 3-284. AR = 2.5 35-Chute, Turbojet (Model 41), PNL and OASPL Directivity, V_{ma} = 2000 ft/sec.

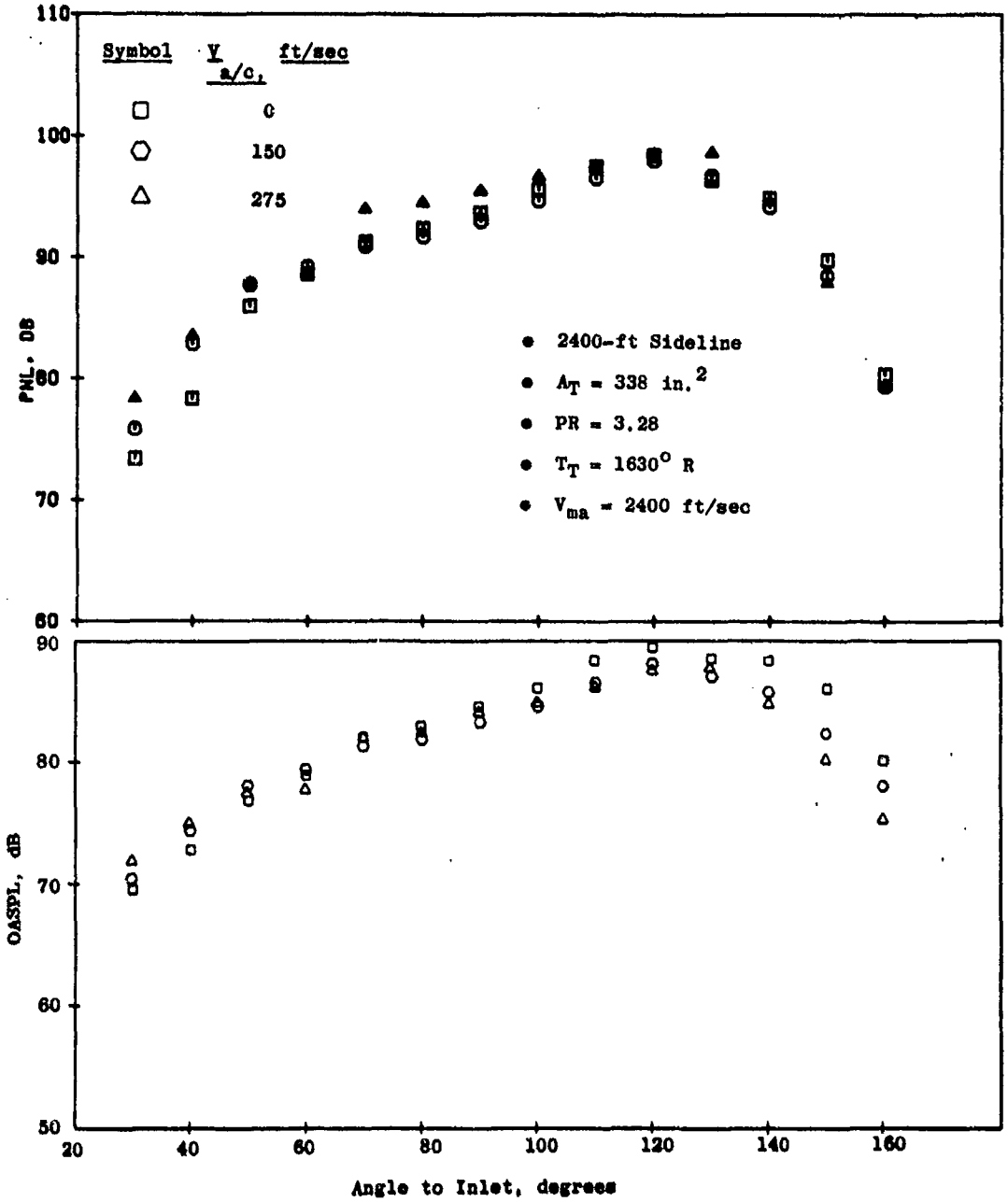

Figure 3-285. AR = 2.5 36-Chute (Model 41), Turbojet, PNL and OASPL Directivity, V_{ma} = 2400 ft/sec.

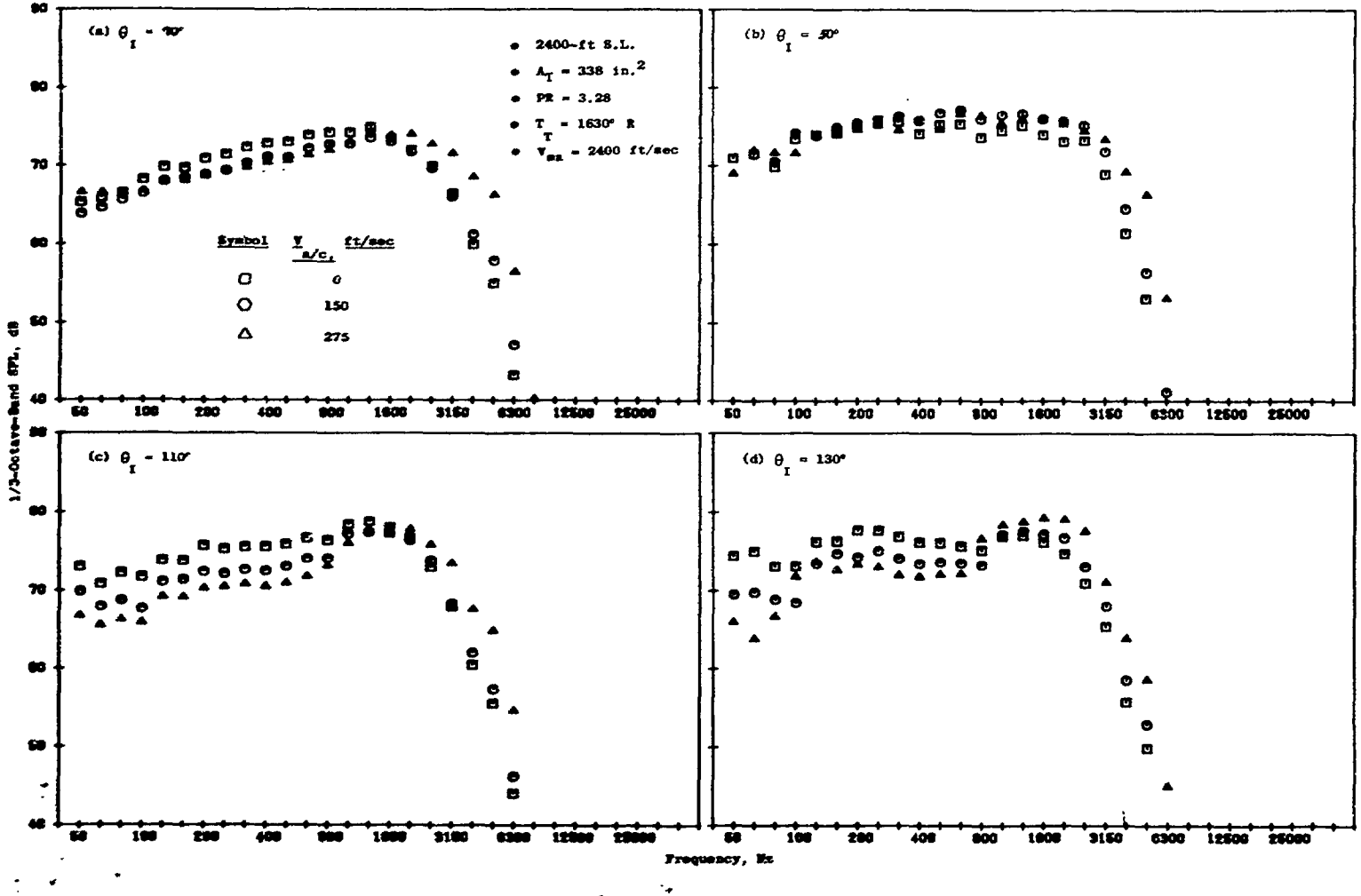

Figure 3-286. AR = 2.5 36-Chute (Model 41), Turbojet, Spectra, V_{ma} = 2400 ft/sec.

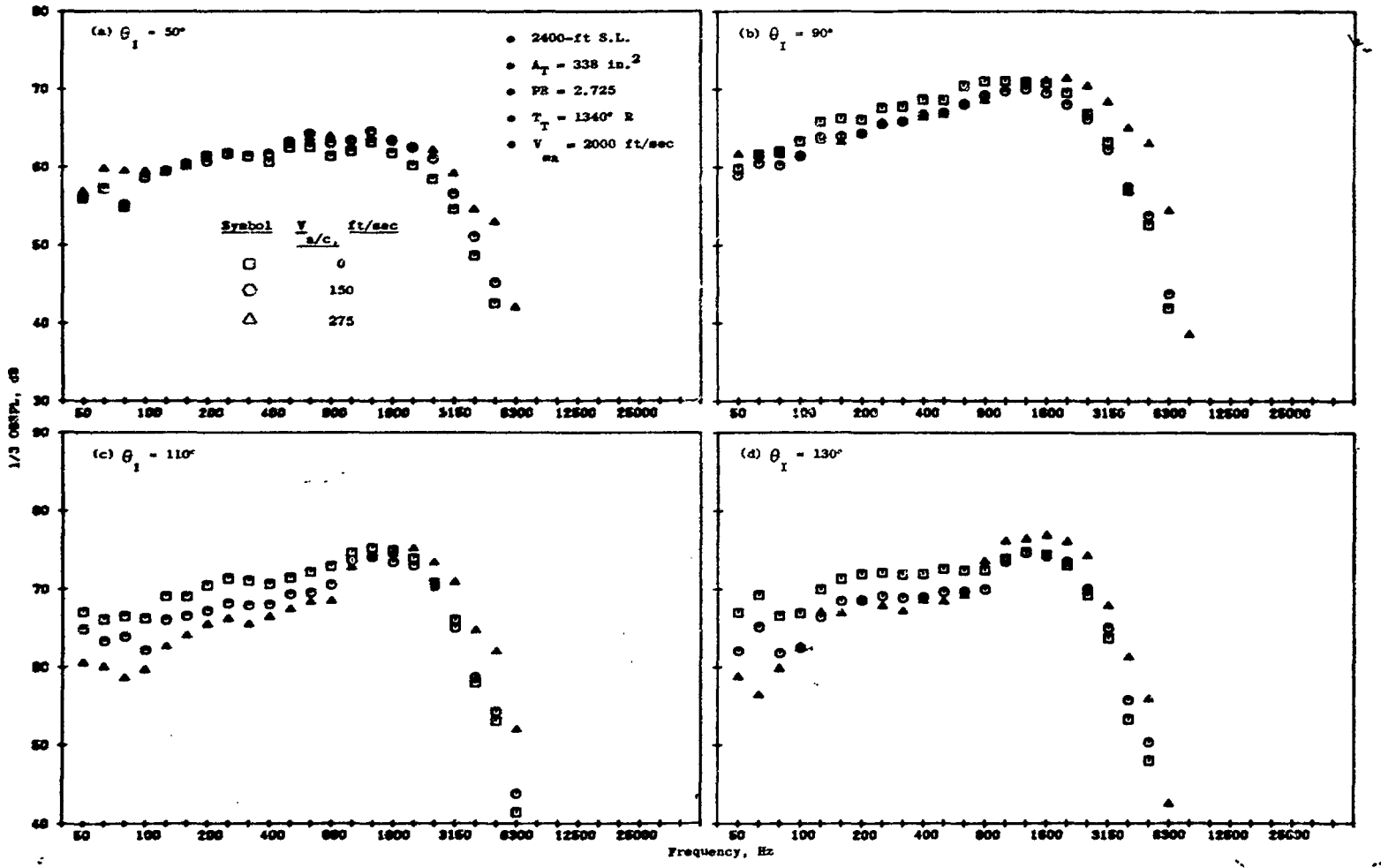

Figure 3-287. AR = 2.5 36-Chute, Turbojet (Model 41) Spectra, V_{ma} = 2000 ft/sec.

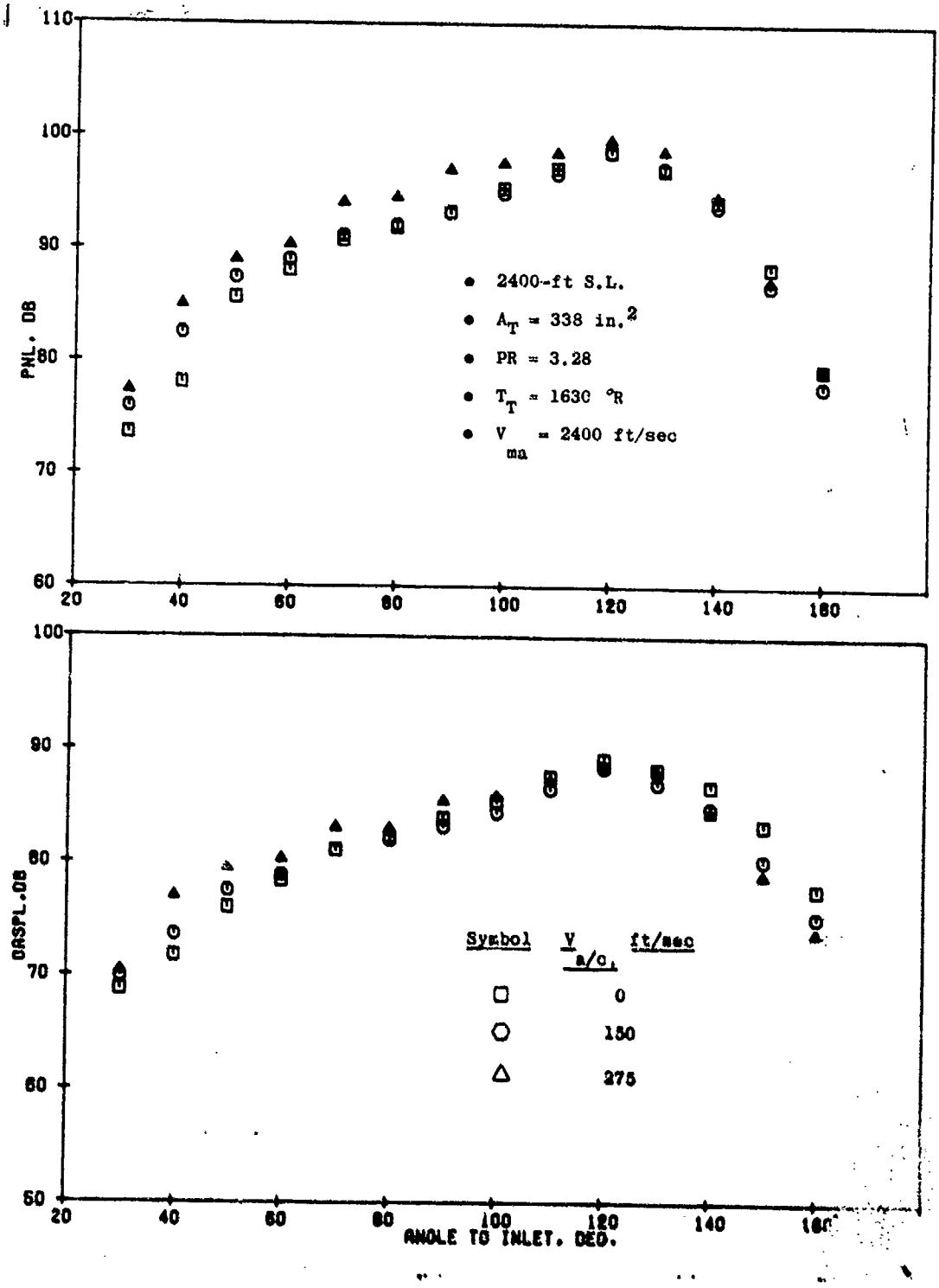

Figure 3-288. AR = 2.5 36-Chute with Auxiliary Flow (Model 42), PNL and OASPL Directivity, V_{ma} = 2400 ft/sec.

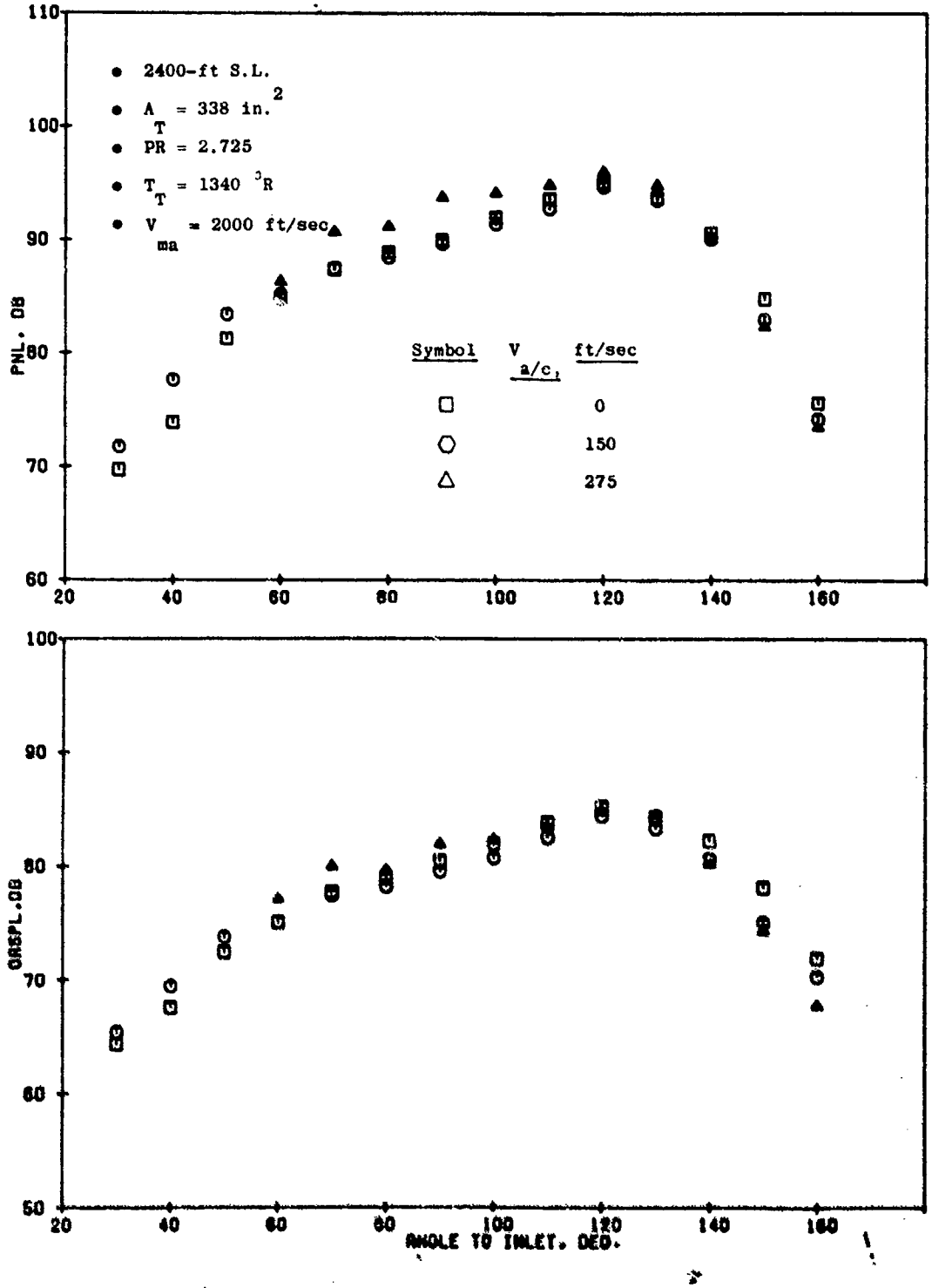

Figure 3-289. AR = 2.5 36-Chute with Auxiliary Flow (Model 42), PNL and OASPL Directivity, V_{ma} = 2000 ft/sec.

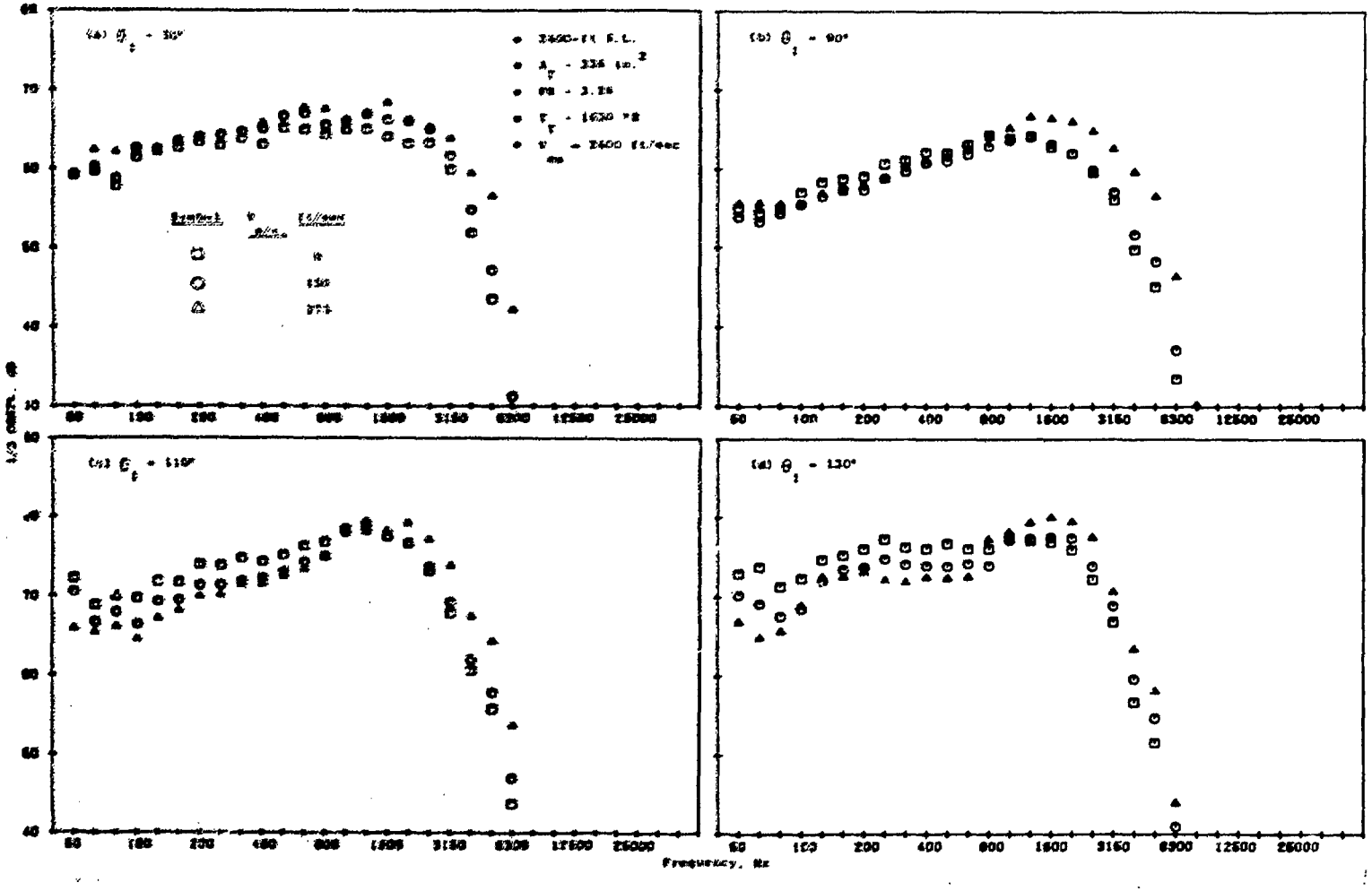

Figure 3-290. AR = 2.5 38-Chute with Auxiliary Flow (Model 42), Spectra, V_{ma} = 2400 ft/sec.

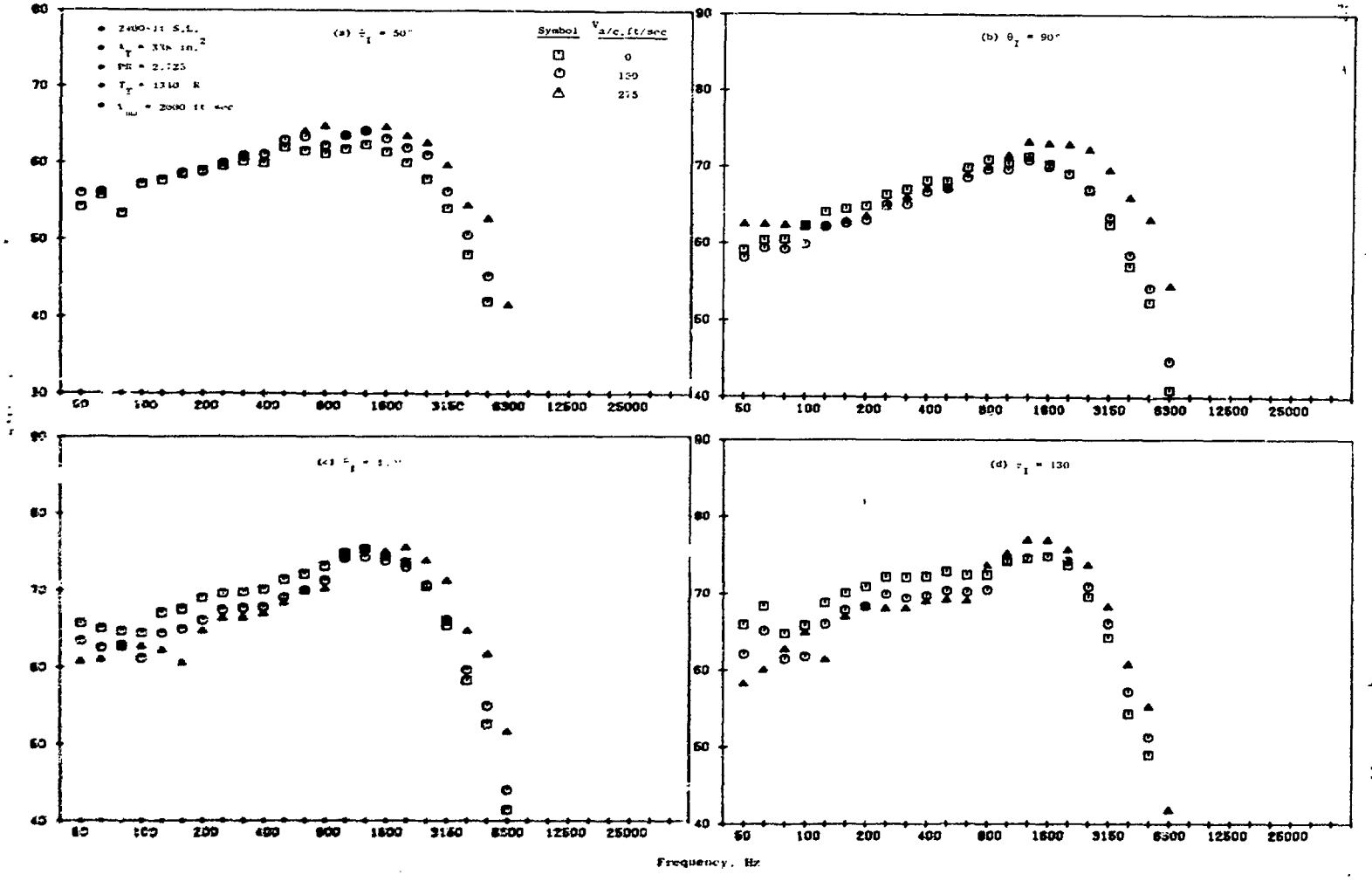

Figure 3-291. AR = 2.5 36-Chute with Auxiliary Flow (Model 42), Spectra, V_{ma} = 2000 ft/sec.

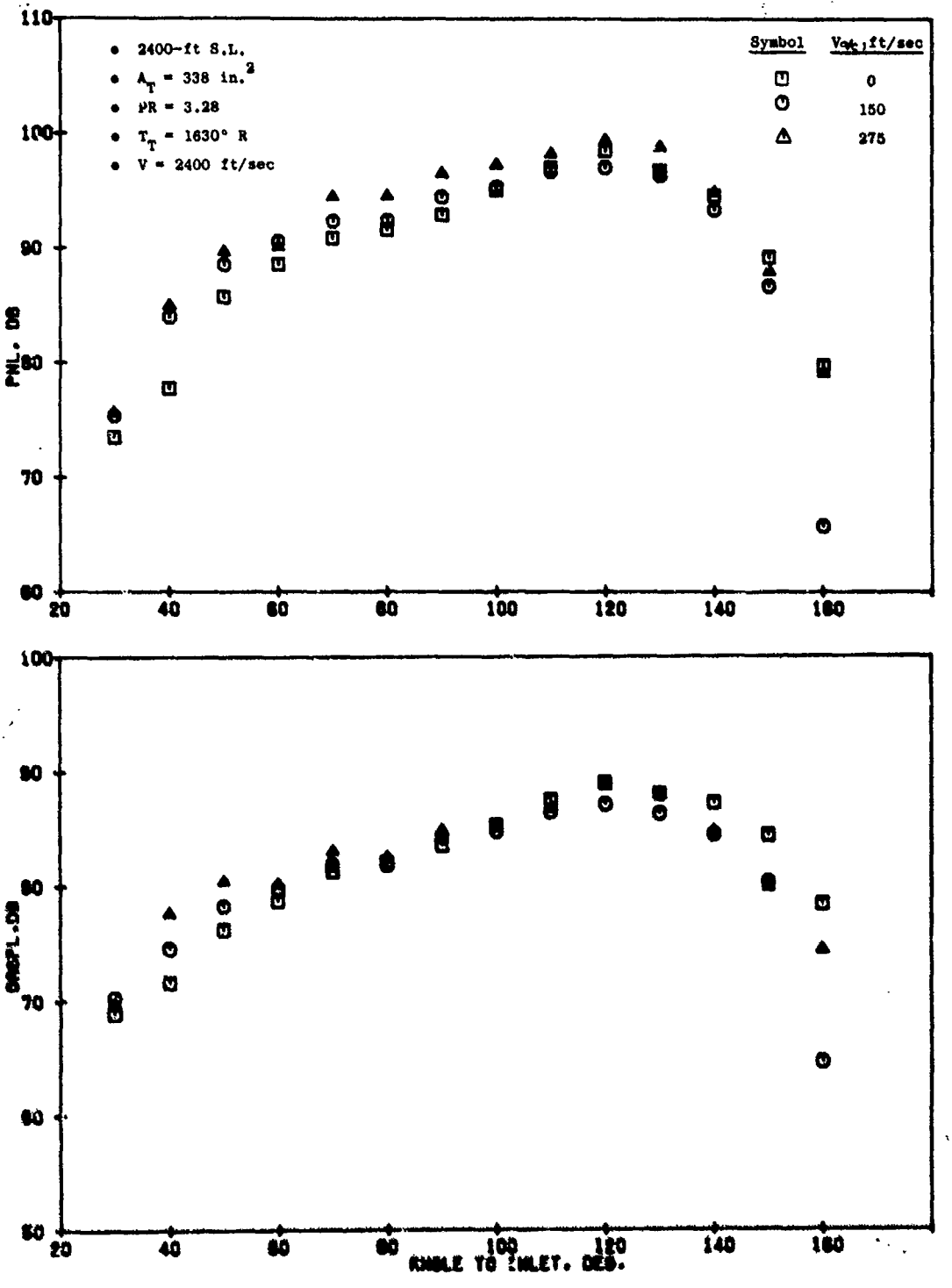

Figure 3-292. AR = 2.5 36-Chute with Abrupt Step (Model 43), PNL and OASPL Diectivity, V_{aa} = 2400 ft/sec.

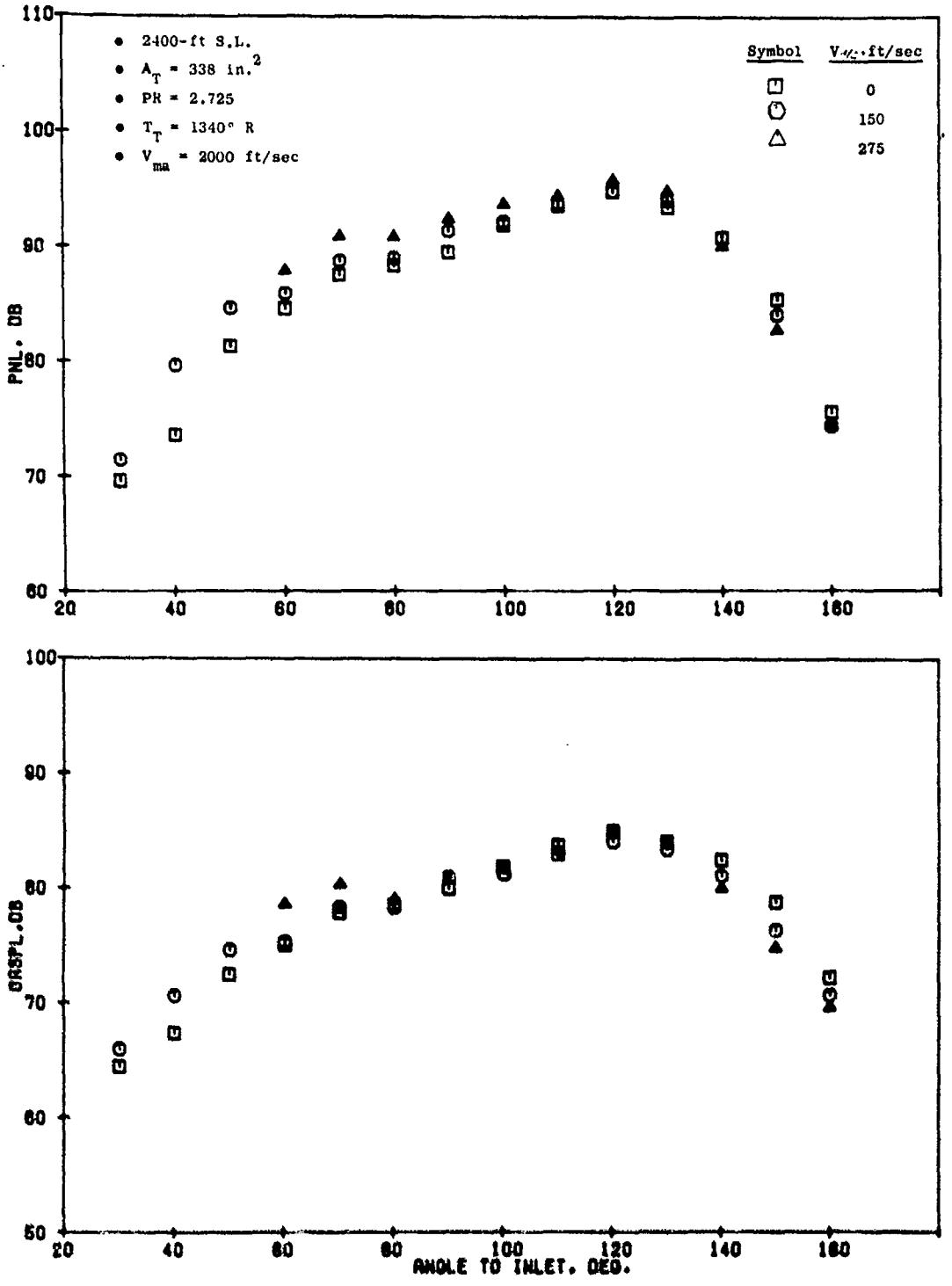

Figure 3-293. AR = 2.5 36-Chute with Abrupt Step (Model 43), PNL and OASPL Directivity, V_{ma} = 2000 ft/sec.

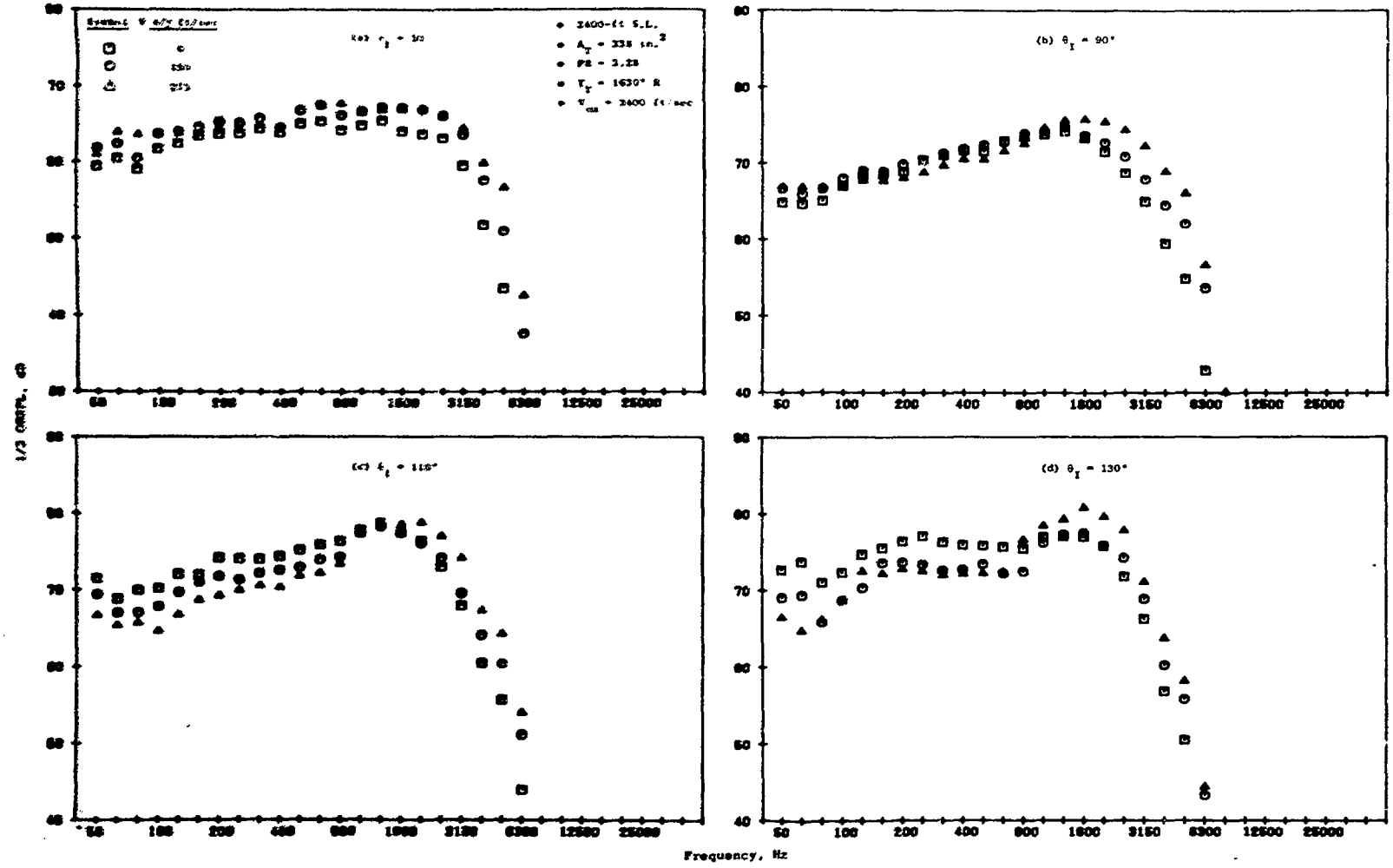

Figure 3-294. AR = 2.5 36-Chute with Abrupt Step (Model 43), Spectra, V_{ma} = 2400 ft/sec.

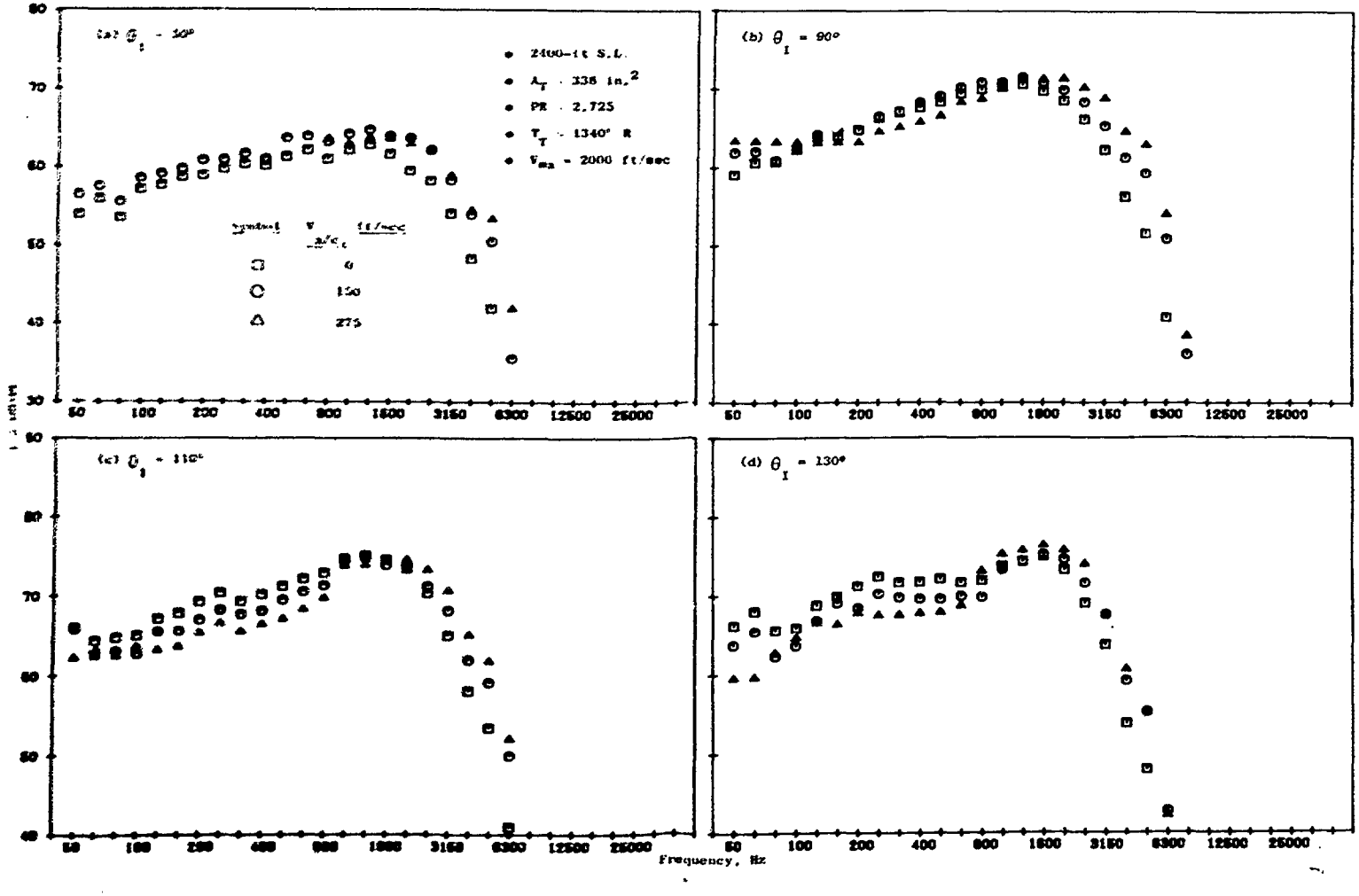

Figure 3-295. AR = 2.5 36-Chute with Abrupt Step (Model 43), Spectra, V_{ma} = 2000 ft/sec.

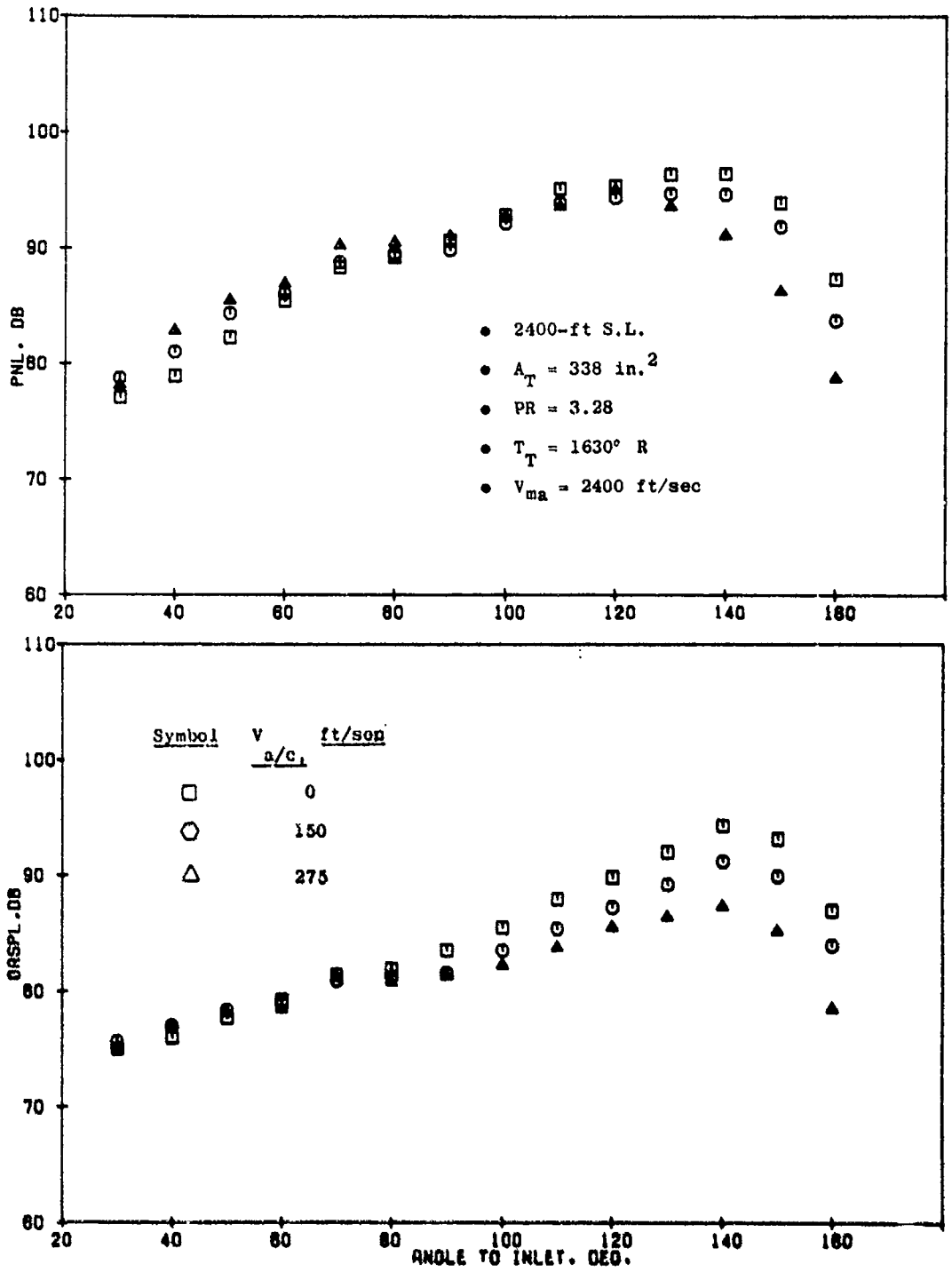

Figure 3-296. 104-Tube Nozzle (Model 44), PNL and OASPL Directivity, V_{ma} = 2400 ft/sec.

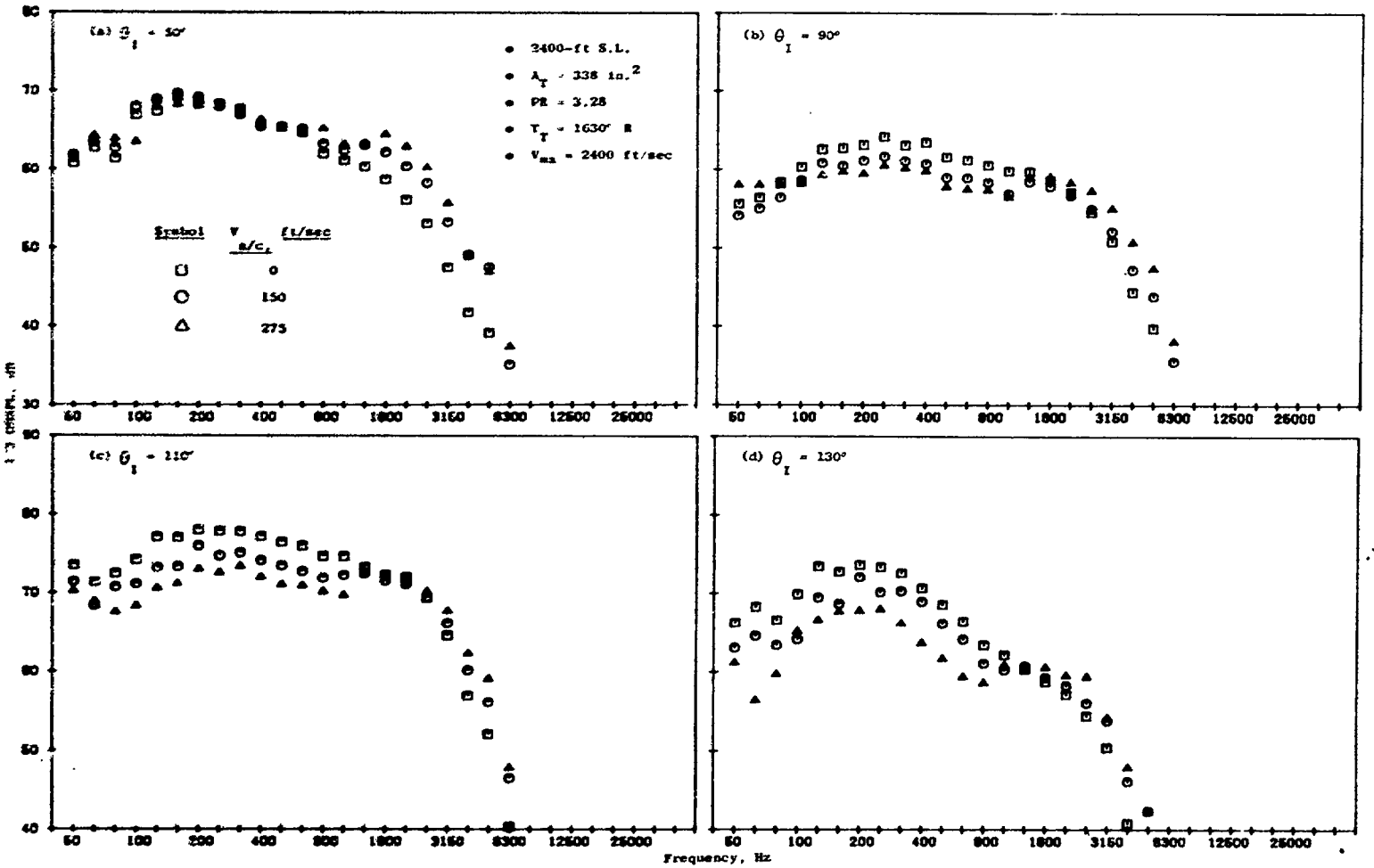

Figure 3-297. 104-Tube Nozzle (Model 44), Spectra, V_{ma} = 2400 ft/sec.

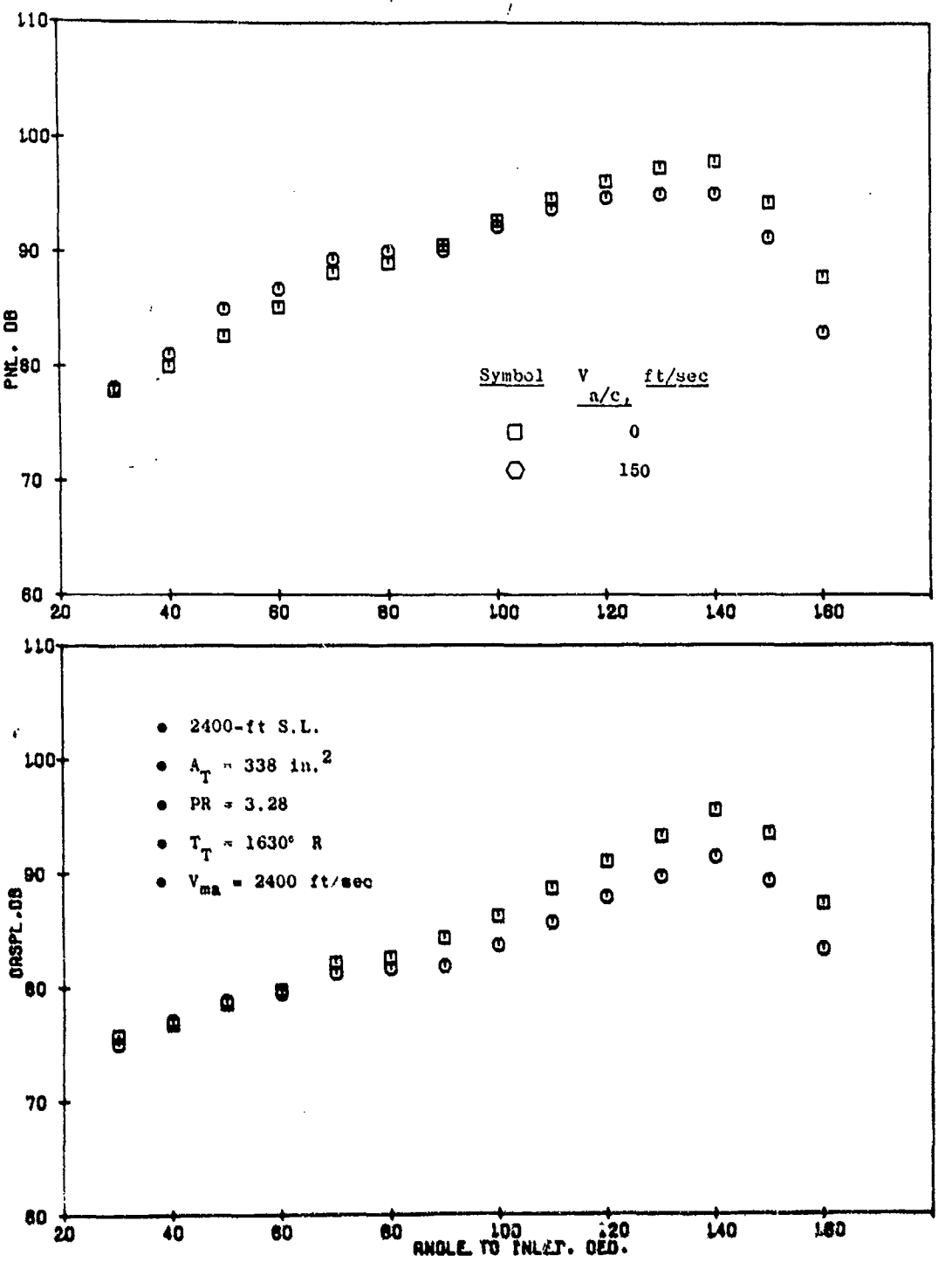

Figure 3-298. 104-Hole Nozzle (Model 45), PNL and OASPL Directivity, V_{ma} = 2400 ft/sec.

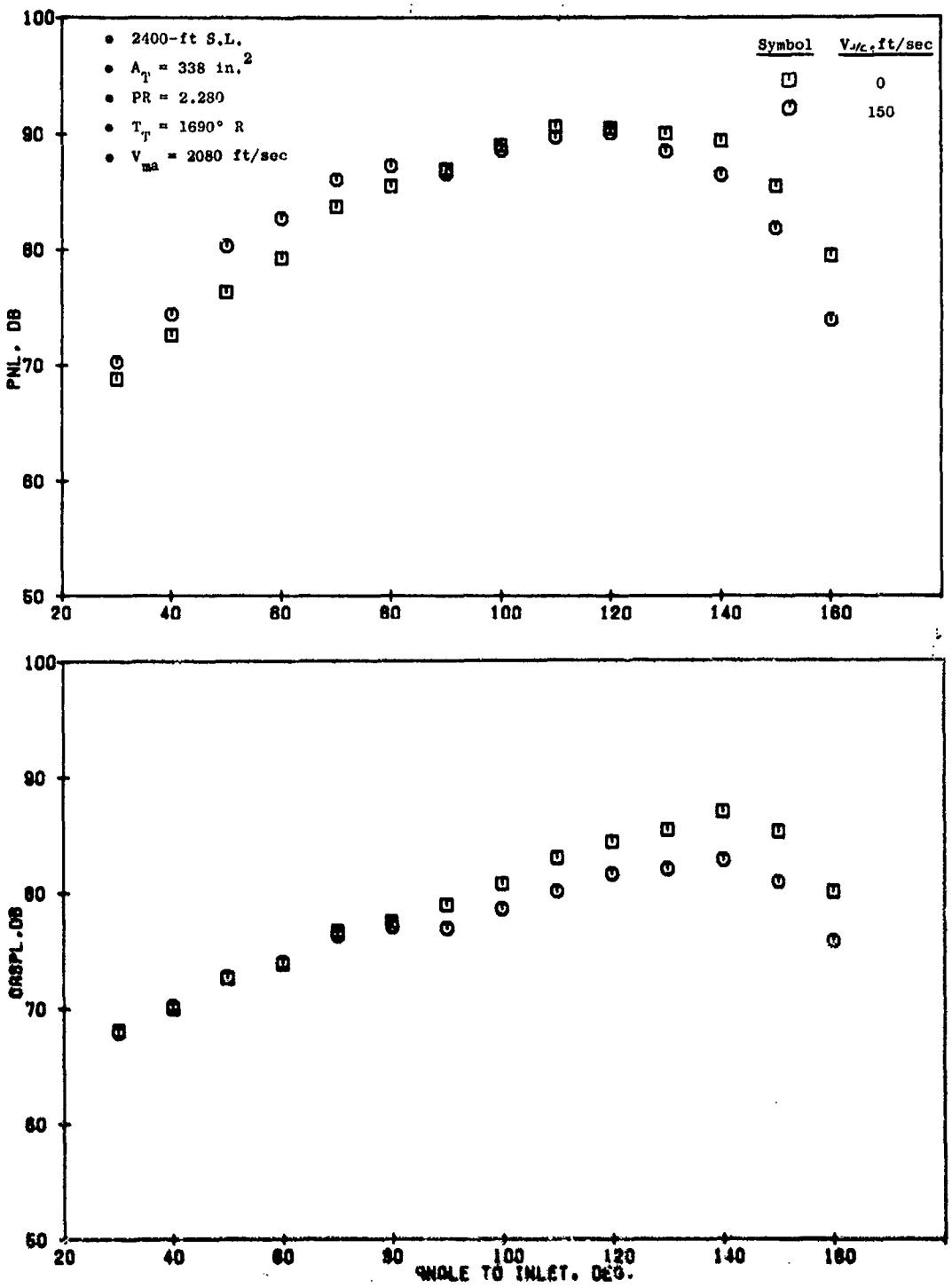

Figure 3-299. 104-Hole Nozzle (Model 45), PNL and OASPL Directivity, V_{ma} = 2080 ft/sec.

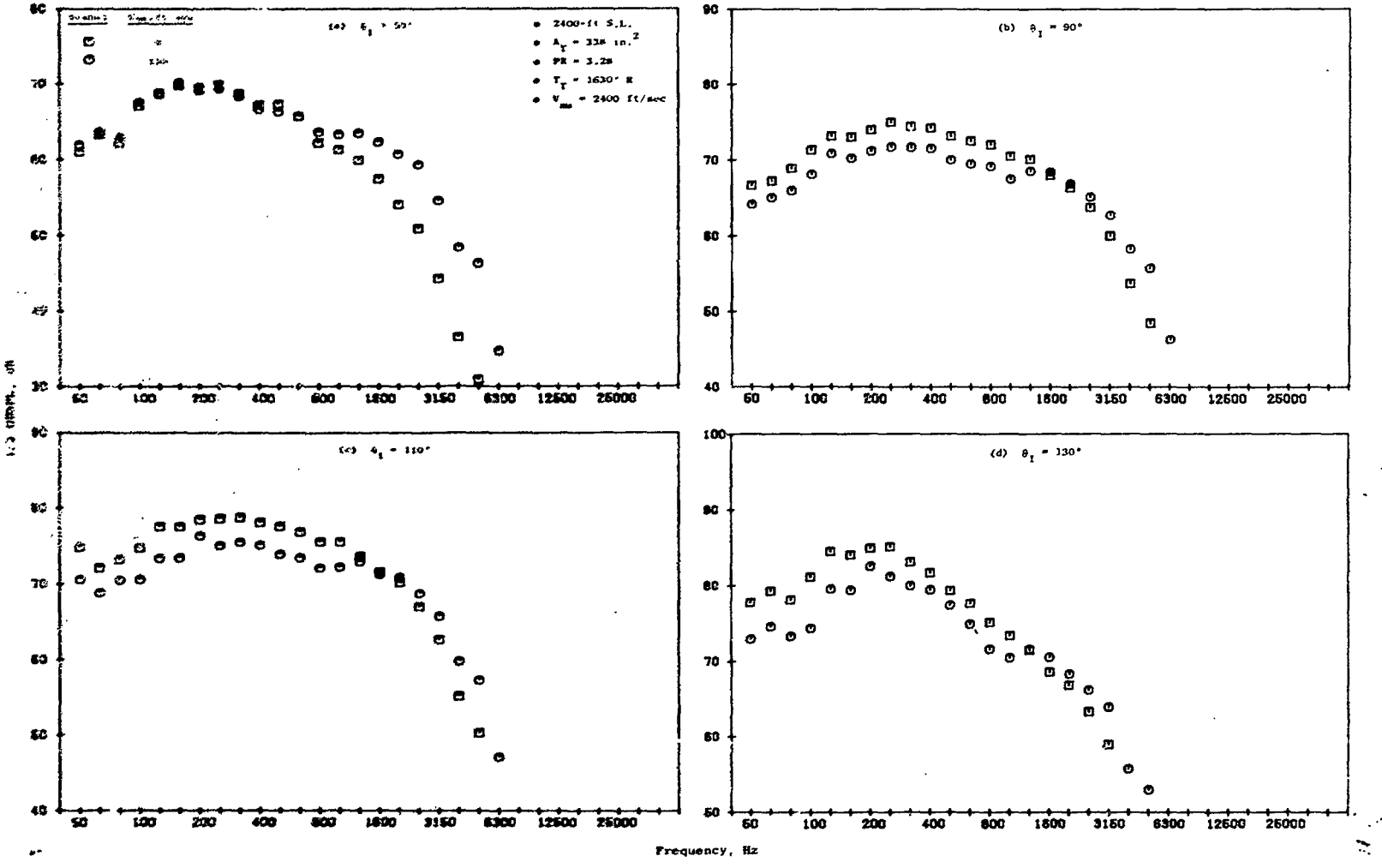

Figure 3-300. 104-Hole Nozzle (Model 45), Spectra, V_{ma} = 2400 ft/sec.

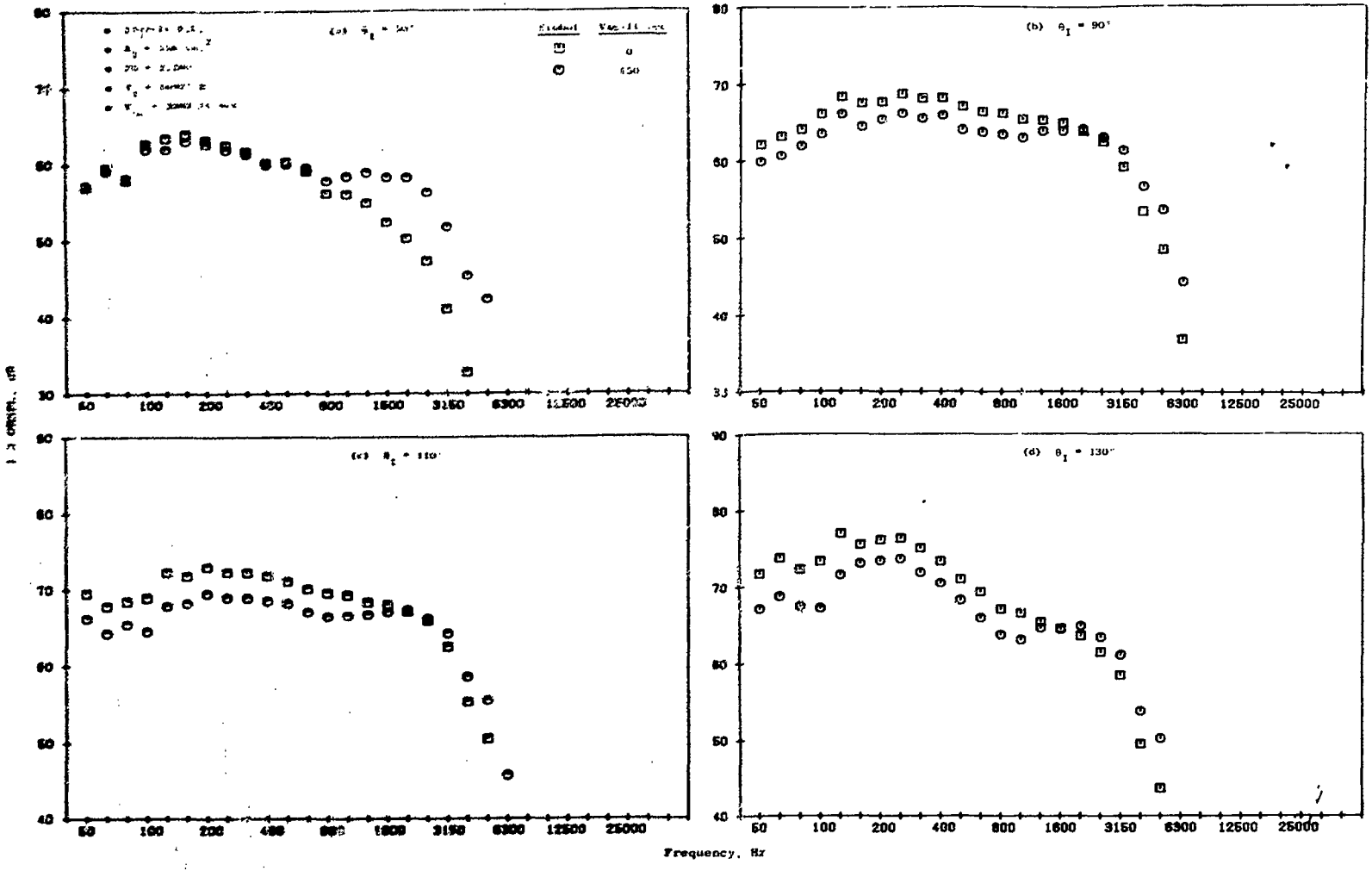

Figure 3-301. 104-Hole Nozzle (Model 45), Spectra, V_{ma} = 2080 ft/sec.

chosen for presentation. The following comments are pertinent for each of the suppressor families. The plug nozzles (Models 39 and 40), Figures 3-276 through 3-281, have very similar directivity patterns. The general simulated-flight trend is a significant noise reduction in the aft quadrant, no change at 90°, and a slight increase (on the order of 1 PNdB) at select angles in the forward quadrant. At 50°, the spectrum shape (Figures 3-278, 3-279, 3-282, and 3-283) is dominated by shock-cell noise; an increase of the peak spectrum level of 3 dB is observed. This corresponds exactly to the level which would be predicted by using 40 log $[1/1 - M \cos \theta_I]$.

The 90° spectra, Figures 3-278 and 3-279, show no change for the 0.85 radius ratio configuration, Model 40. The 0.789 radius ratio plug nozzle (Model 39) 90° spectra, Figures 3-282 and 3-283, has a modest low-frequency reduction with an increase occurring in the high frequency portion of the spectra. The spectra have a significant low and midfrequency reduction with no change in the high frequency portion of the spectrum.

The PNL, OASPL and spectra characteristics of the three chute configurations (Models 41, 42, and 43) are summarized on Figures 3-284 through 3-295. The patterns are distinctly different than those of the plug nozzle configurations. In general, aft angle suppression is observed for $\theta_I > 130°$ with level varying anywhere from 1 to 4 PNdB depending on the chute configuration. However, for $\theta_I \leq 130°$, the static and flight levels are generally within 2 dB. These trends are supported by the spectra comparisons presented in Figure 3-286. At 90° there is a low-frequency reduction but it is negated by an increase in the high-frequency noise. The trend at 130° is significantly different, as previously discussed. Low-frequency reduction on the order of 5 dB occurs; however, this again is negated by the increase in high-frequency noise. The relative levels of the high-frequency and low-frequency noise is the reason for a lack of flight effect.

The directivity and spectra characteristics of the 104-tube (Model 44) and 104-hole (Model 45) nozzles are presented on Figures 3-296 through 3-301. The changes in directivity pattern from static to flight are similar to those for the plug nozzle configuration. There is a significant reduction at the angle of maximum noise. At 90°, a modest reduction of 1 dB occurs with equivalent static and flight levels in the forward quadrant. Spectra comparison at 50° shows static and flight levels to be equivalent in the low frequency portion of the spectra with an increase in the high frequency portion of the spectra. At 90°, significant low-frequency suppression and a slight increase in the high-frequency portion of the spectra is observed.

Studies to evaluate the influence of simulated flight (using the free-jet technique) have established that a common set of velocity indices may not be established for both baseline and suppressor nozzles. The chute nozzles evaluated have shown a 3-PNdB loss in in-flight peak noise suppression due to dominance of the high frequency portion of the spectra (which realizes only a minimal flight effect). The minimization of high-frequency noise is considered to be a critical design parameter for a suppressor nozzle to realize a reduction of noise in flight.

3.4.3.2 Shock Noise Studies

The effect of shock noise, both statically and in simulated flight, was explored for five nozzles: a conical nozzle (Model 47), a 0.85 radius ratio plug nozzle (Model 40), an AR = 2.5 36-chute nozzle (Model 41), a 104-tube nozzle (Model 44), and a 104-hole nozzle (Model 45). The shock noise characteristics of the 8-lobe nozzle (Model 46) are discussed in detail in Reference 7.

According to the Harper-Bourne Fisher (HBF) theory (Reference 24) the OASPL, if dominated by shock-cell noise, should be only a function of the pressure ratio parameter β, given by the following equation:

$$\beta = \sqrt{M^2 - 1}$$

OASPL's at angles of 40° through 90° are presented as a function of β on Figure 3-302 for the conical nozzle (Model 47). At angles such as 40°, the shock noise appears to be dominant; this is reflected in the collapse of the data, for all temperatures, close to a line which varies as β^4. Transformed free-jet data are also presented on Figure 3-302. In general, the transformed results show an increase in noise due to the dynamic effect. The increase in level is a function of angle and β. However at negative values of β this noise increase in flight is not as apparent. The approximate level of increase is predicted by 40 log $[1/1 - M_{a/c} \cos \theta_I]$ in the β range where shock noise is clearly dominant.

Similar static OASPL comparisons were made at 50° for the 0.85 radius ratio plug nozzle (Model 40), AR = 2.5 36-chute nozzle (Model 41), 104-tube nozzle (Model 44), and 104-hole nozzle (Model 45). The plug nozzle did follow the classical β^4 line, but the other suppressors did not show a significant trend. Spectra comparisons for the four nozzles are shown on Figure 3-303. The conical and 0.85 R_r plug nozzles exhibit the spectrum shapes indicative of shock noise whereas the multielement suppressors do not.

Spectra comparisons for the 0.85 R_r plug nozzle (Model 40) at pressure ratios of 2.5, 3.0, and 3.5 are presented in Figure 3-304. The spectra for the three velocity conditions at a pressure ratio of 2.5 collapse in the frequency range of $400 \leq f \leq 5000$ Hz. Spectrum levels below 400 Hz increase as jet velocity increases. However, the frequency dependent trend is not repeated at pressure ratios of 3.0 and 3.5. The spectrum shapes are observed to be equivalent and suggest the spectrum is dominated by shock noise rather than jet noise. OASPL directivity comparisons were also made in a similar manner and are presented on Figure 3-305.

Shock noise dominates at a pressure ratio of 2.5 up to 70°, at a pressure ratio of 3.0 up to 90°, and at a pressure ratio of 3.5 up to 100°. In general, as nozzle pressure ratio is increased and total temperature is held constant, the region of shock noise dominance will extend into the aft quadrant.

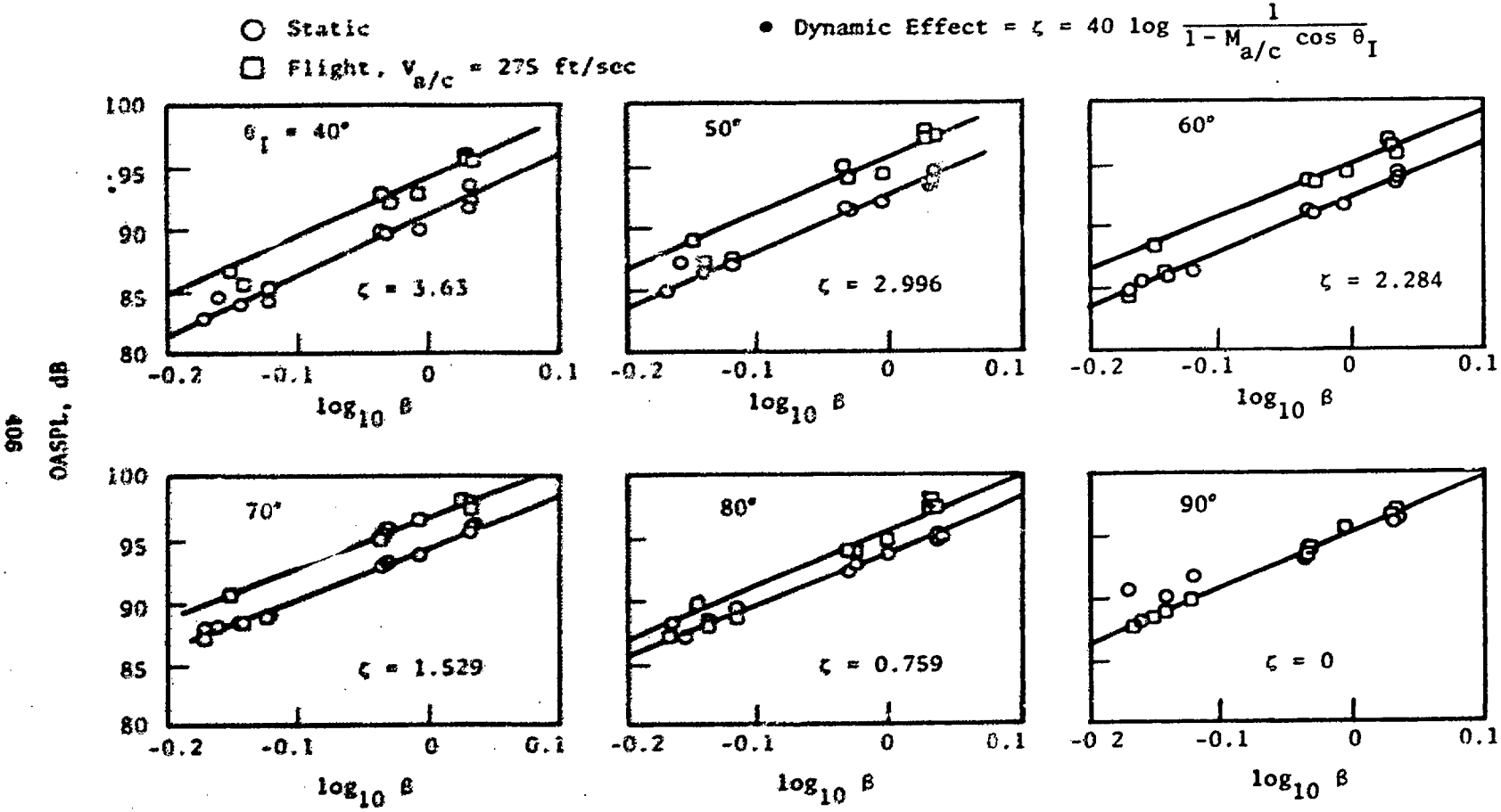

Figure 3-302. Summary of Conical Nozzle (Model 47) Forward Quadrant Noise Trends.

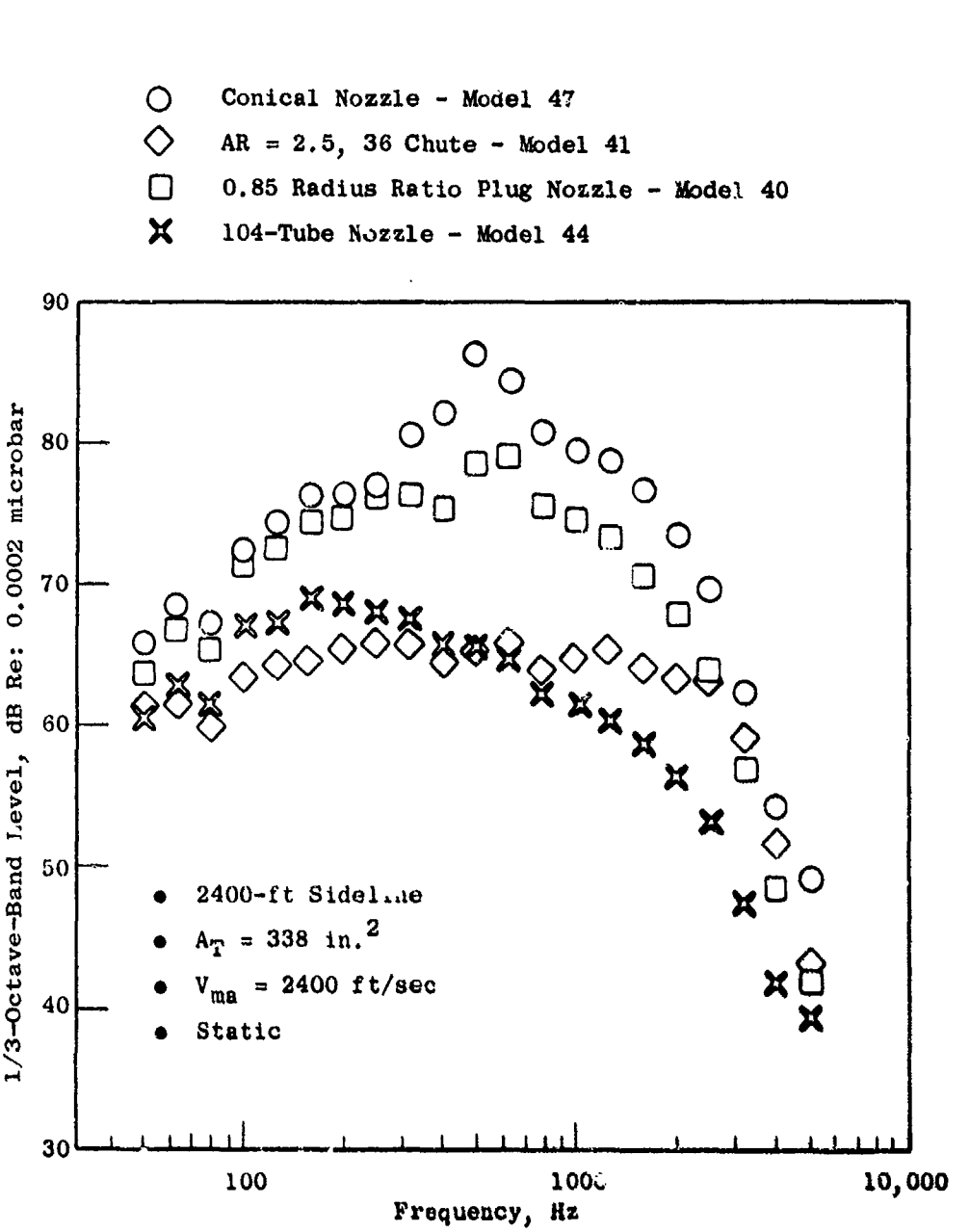

Figure 3-303. Summary of 50° Spectra Characteristics.

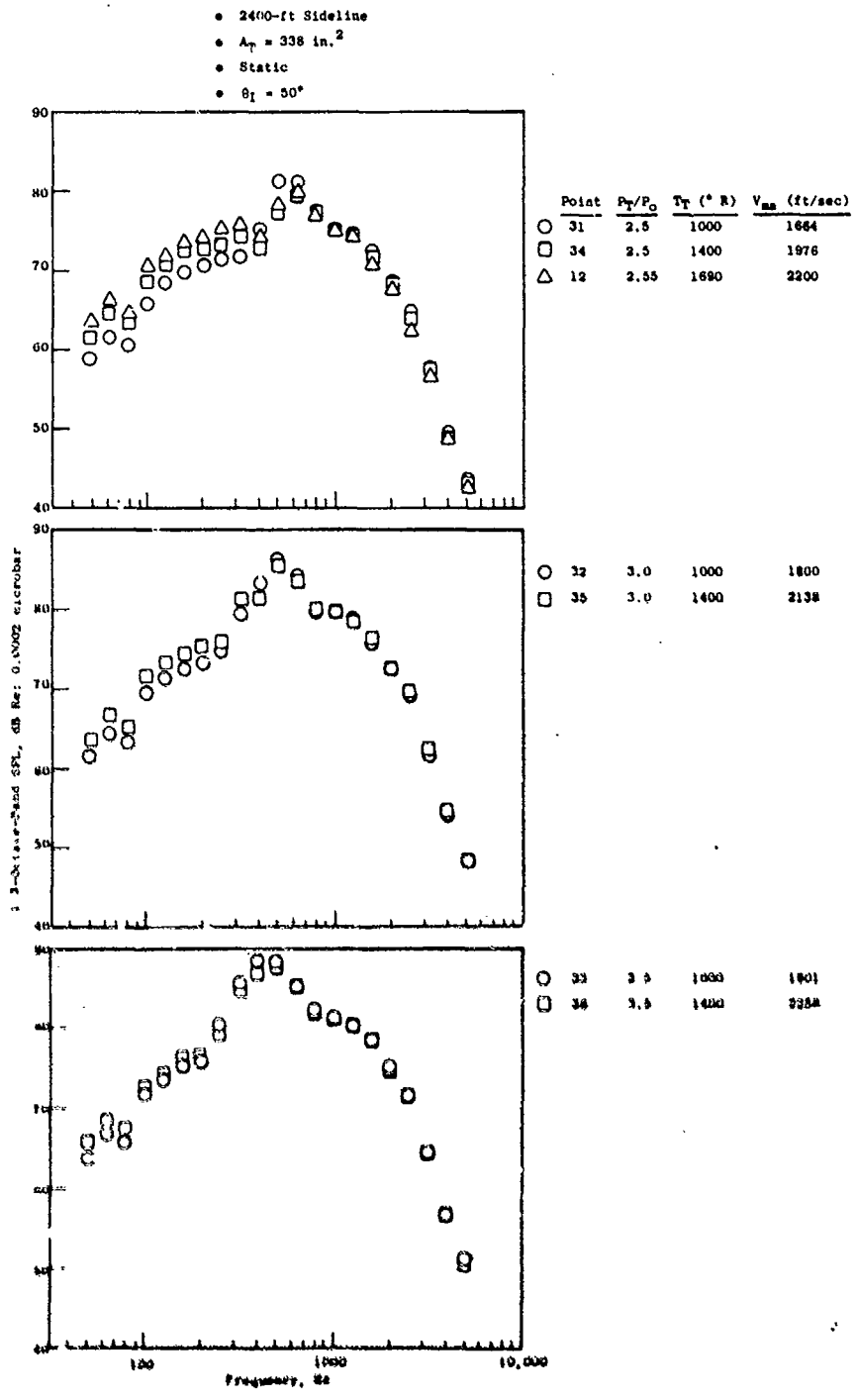

Figure 3-304. 0.85 Radius Ratio Plug Nozzle (Model 40) 50° Spectra at Constant Pressure Ratio.

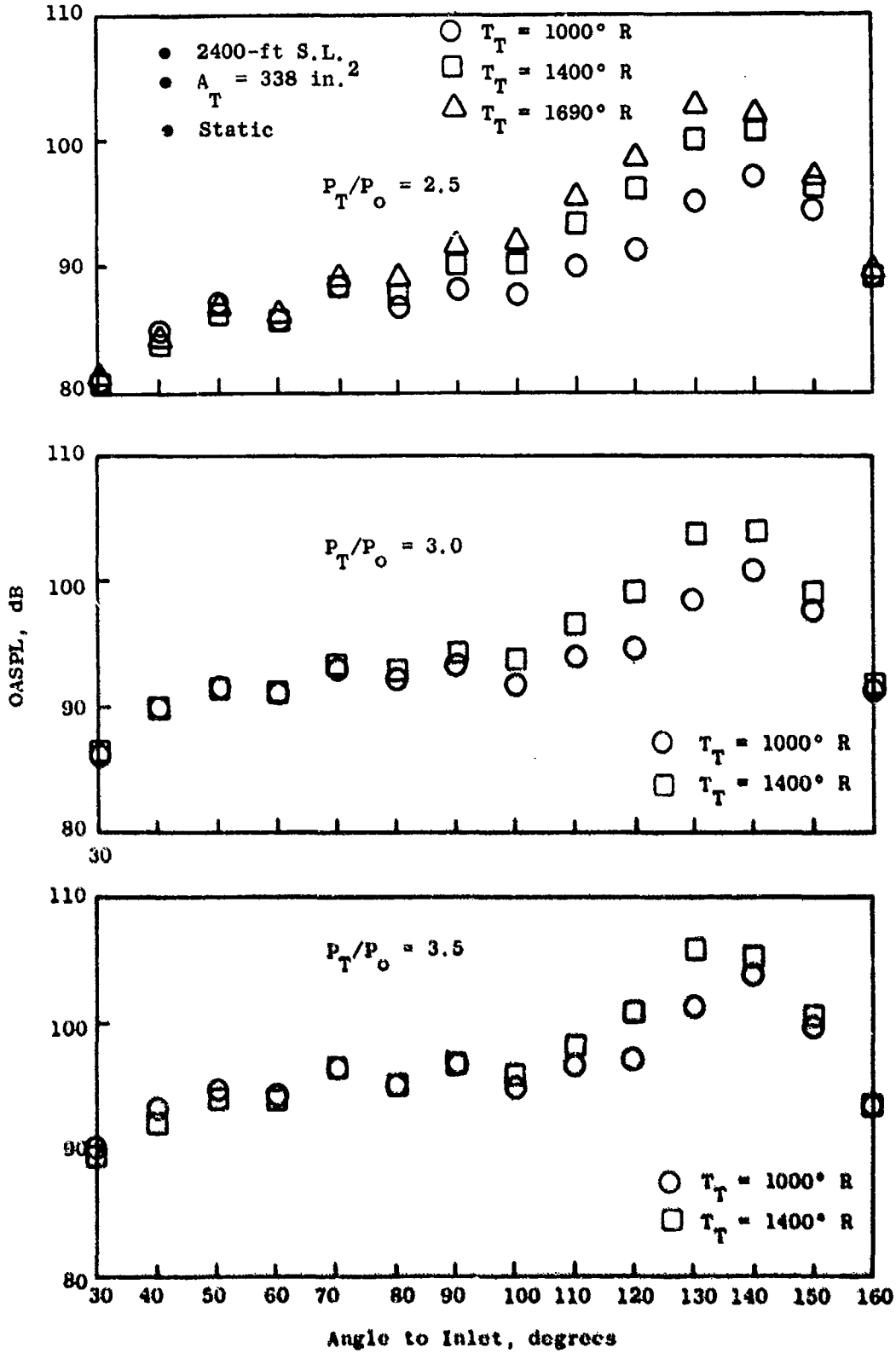

Figure 3-305. 0.85 Radius Ratio Plug Nozzle (Model 40) Directivity at Constant Pressure Ratio.

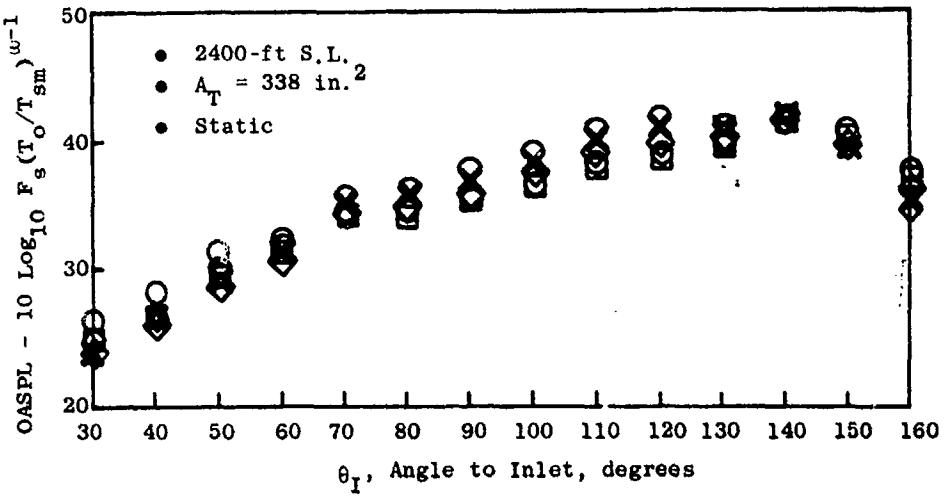

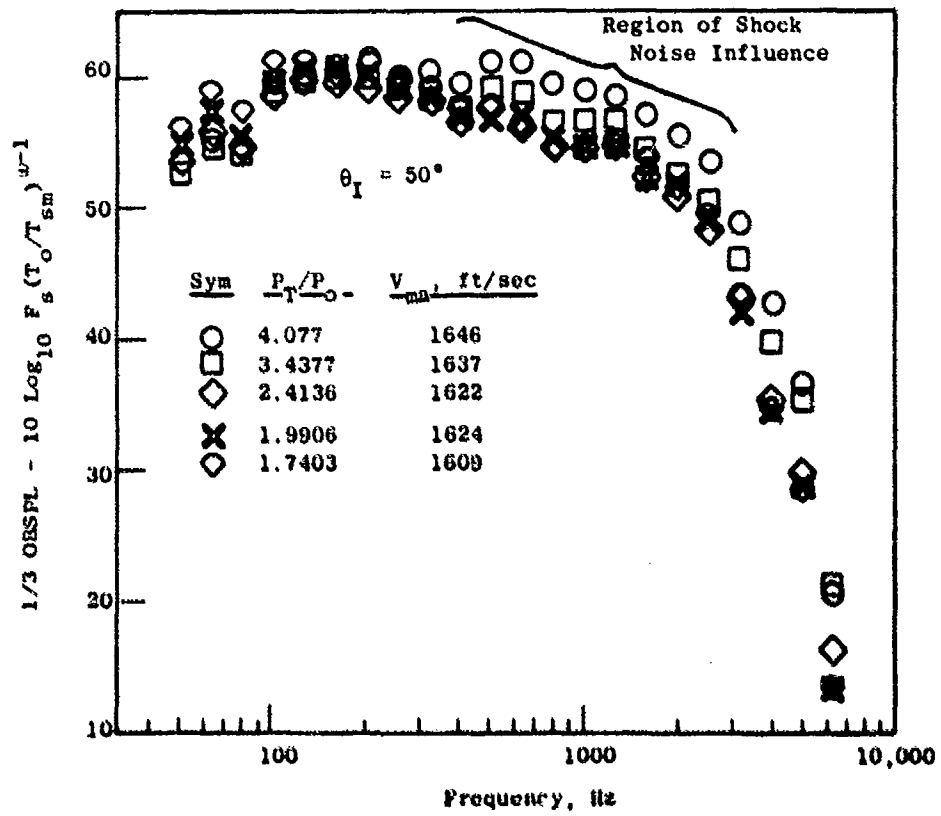

Figure 3-306. The Effect of Pressure Ratio Variation on the Directivity and Spectra Characteristics of a 104-Hole Nozzle (Model 45).

The 104-hole nozzle (Model 45) was chosen to illustrate the influence of shock noise on multielement suppressor nozzles. The results of this study were distinctly different than those observed for the conical (Model 47) and plug (Model 40) nozzles. Directivity and spectra comparisons are presented on Figure 3-306.

The directivity comparisons were made for five conditions where jet velocity varied from 1609 ft/sec to 1646 ft/sec. However, nozzle pressure ratio varied from 1.74 through 4.07. If the 104-hole nozzle was dominated by shock noise, the data would not collapse when normalized by the 10 log F_s $(T_o/T_{sm})^{\omega-1}$ factor. However, the levels for all five points do collapse within a ±1 dB band. This implies that the directivity pattern of this nozzle is not dominated by shock noise. Spectrum wise (θ_I = 50°), a variation with pressure ratio is observed in the frequency range of $400 \leq f \leq 6300$ Hz for the 3.43 and 4.0 pressure ratio conditions, suggesting a slight influence due to shock noise in spite of the apparent collapse of the OASPL data. However, at low pressure ratios the data collapse when normalized by this parameter.

The major results of this exploratory study show that shock noise dominates the forward quadrant noise levels at supercritical pressure ratios, that the region of shock noise influence increases at pressure ratio is increased and temperature is decreased, and that the shock noise levels follow a β^4 slope and are amplified in flight according the 40 log $[1/1 - M_{a/c} \cos \theta_I]$ based on transformed free-jet data.

Plug nozzles also have significant shock noise; however, on an absolute level it is less than for a conical nozzle. Complex suppressor nozzles, such as the 104-hole nozzle, do not have a significant shock-noise component.

3.4.4 Laser Velocimeter Results

Laser velocimeter (LV) measurements were conducted on baseline and several suppressor nozzles to determine if the mean velocity decay characteristics were similar for baseline and suppressor nozzles, and to determine if suppressor turbulence intensity levels were equivalent to a conical nozzle. The effects of geometric changes on the mixing characteristics of exhaust nozzles were also examined. These geometric studies included variation of element type, single versus dual flow, suppessor area ratio variation and the influence of a treated ejector. The baseline nozzles were tested on the JENOTS facility and the suppressor nozzles were tested in the anechoic chamber.

Laser velocimeter measurements were also taken on several baseline and suppressor configurations in a freejet on the JENOTS facility to establish the change in mixing characteristics with the addition of external flow.

The baseline nozzles evaluated include a conical nozzle (from Task 4, Reference 12), a 0.67 radius ratio convergent-divergent plug nozzle (Model 2), and an A_o/A_i = 1.0 coplanar-coannular nozzle (Model 6). Mean velocity and turbulence intensity profiles for the first two configurations were compared extensively with theoretical predictions in Section 4.5.8 of Reference 7 and

will not be repeated here except for selected comparisons. The results of this study are presented as mean-velocity decay characteristics and turbulence intensity levels for several baseline and multielement-suppressor nozzles. The test matrix and data reduction/acquisition were discussed in Sections 3.2.2 and 3.3.2, respectively.

Figure 3-307 summarizes mean-velocity decay characteristics for the conical (Reference 12) and two inverted-flow, coplanar-coannular nozzles (Models 6 and 7). The coannular data are normalized with respect to the area and the calculated isentropic velocity of the outer flow. The peak velocity decay is enhanced by the inverted-flow cycle in the $3.0 < X/D^{o}_{eq} < 11.0$ region reduced at $X/D^{o}_{eq} < 11$ for the range investigated. Turbulence intensity levels at the location of maximum mean velocity are summarized on Figure 3-308. Turbulence levels are approximately 3 to 4% in the region where the measured velocity is equivalent to the isentropic velocity. The maximum turbulence levels produced by the coplanar-coannular nozzles are observed to occur closer to the nozzle exit plane than was the case with the conical nozzle. Peak turbulence levels, which in general do not occur at the same location as the peak mean velocity, are summarized on Figure 3-309 for the conical nozzle and also for the 0.65 A_o/A_i coplanar-coannular nozzle (Model 7). The peak turbulence level of the coplanar-coannular nozzle is approximately 2% lower than for the conical nozzle and occurs nearer to the nozzle exit plane.

The AR = 2.0 coplanar-coannular nozzle (Model 6) was also tested to determine the influence of velocity ratio on the centerline mean-velocity decay characteristics. The studies were conducted with the inner and outer streams both operating at stagnation temperatures of ambient and 1500° R. The results are summarized on Figures 3-310 and 3-311. As velocity ratio (V_o/V_i) increases, the decay rate of the mean velocity is substantially reduced. The increase in stagnation temperature also enhances the velocity decay rate, when compared to ambient conditions.

Mean velocity and turbulence intensity levels were established for several single and dual flow suppressor nozzles. In general, the segmentations of the exhaust plume caused a more rapid decay of the mean velocity when compared to the unsuppressed case. The downstream, postmerged, mean velocity characteristics of the suppressor nozzles are very similar to the baseline configurations.

The mixing characteristics of two typical turbojet suppressor nozzles [AR = 2.0 36-chute (Model 16) and AR = 2.0 36-spoke (Model 18)] are summarized on Figures 3-312 and 3-313. The data were obtained by radial traverses on a chute or spoke centerline. Measured data for the 3.56 conical nozzle (Reference 12) is presented at locations where it is available. The spoke and chute nozzles both have very similar mean velocity profiles at axial locations in the X/D range from 0.4 to 24. The turbulence intensity levels are very similar, with the maximum variance occurring at $X/D \leq 1.0$. When compared to the conical nozzle, both configurations display a significant reduction in mean velocity up to an X/D of 8.0. At X/D = 16, the peak velocity level of the conical

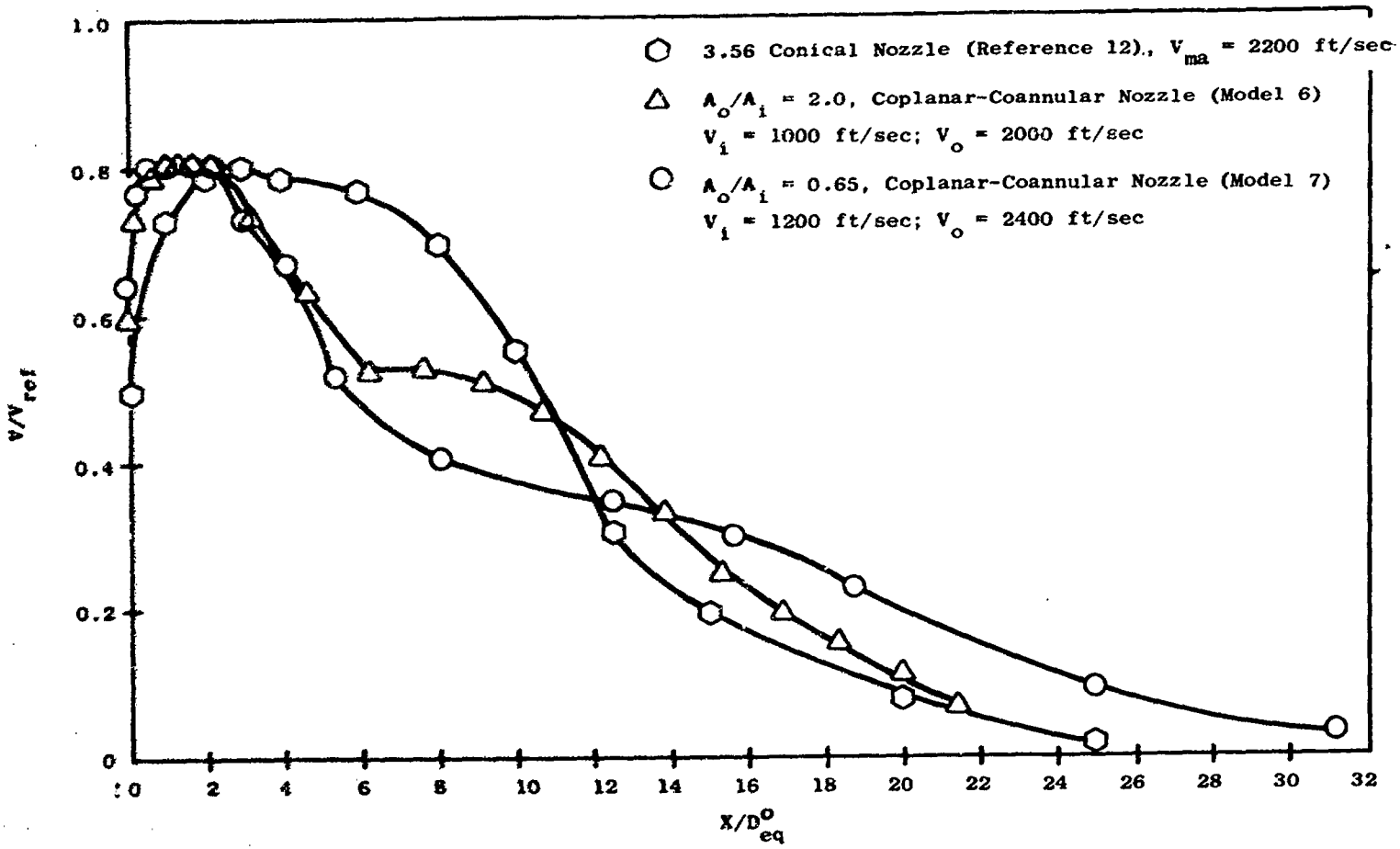

Figure 3-307. Summary of Peak Mean Velocity Decay Characteristics.

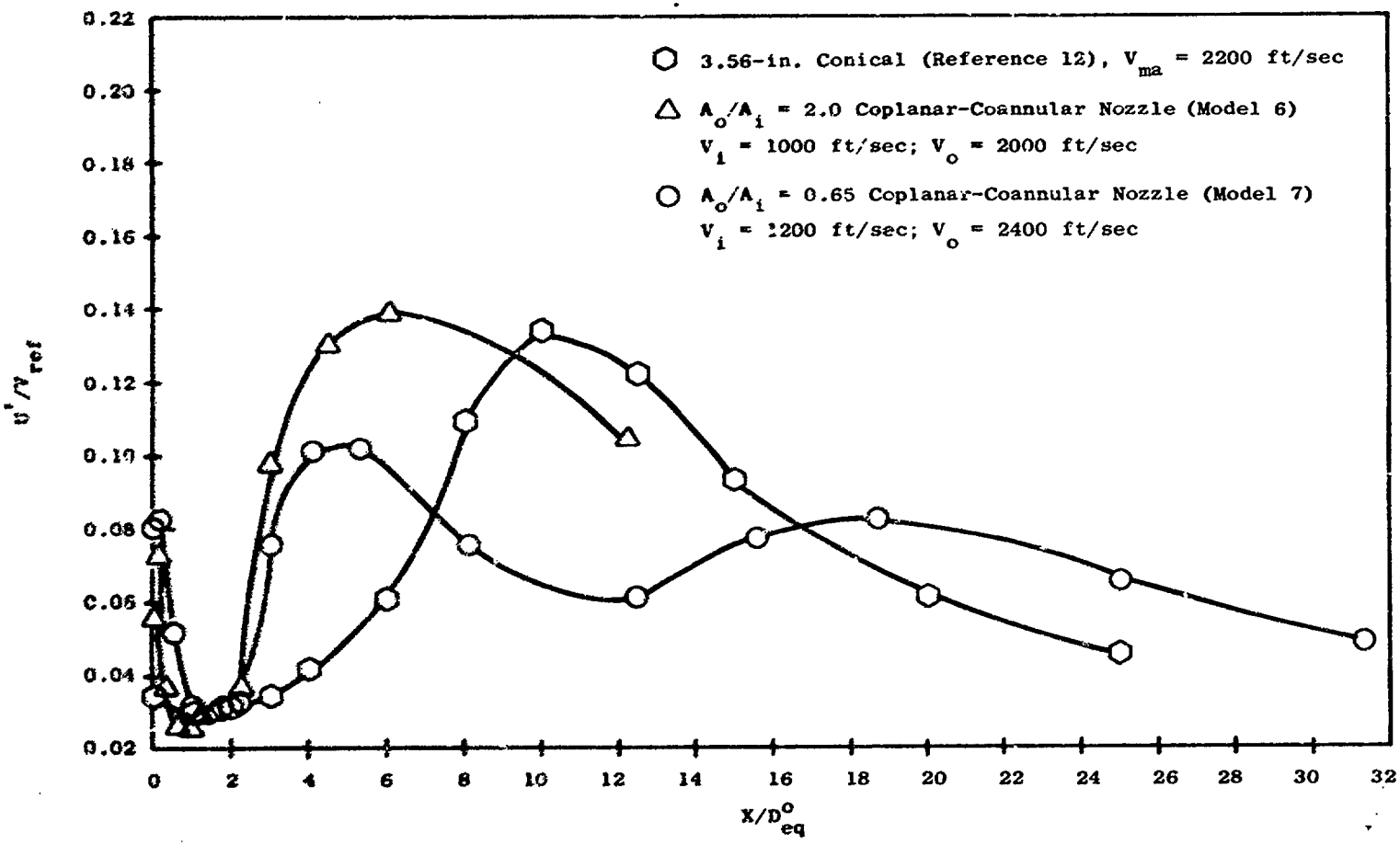

Figure 3-308. Turbulence Intensity Levels at Location of Peak Mean Velocity.

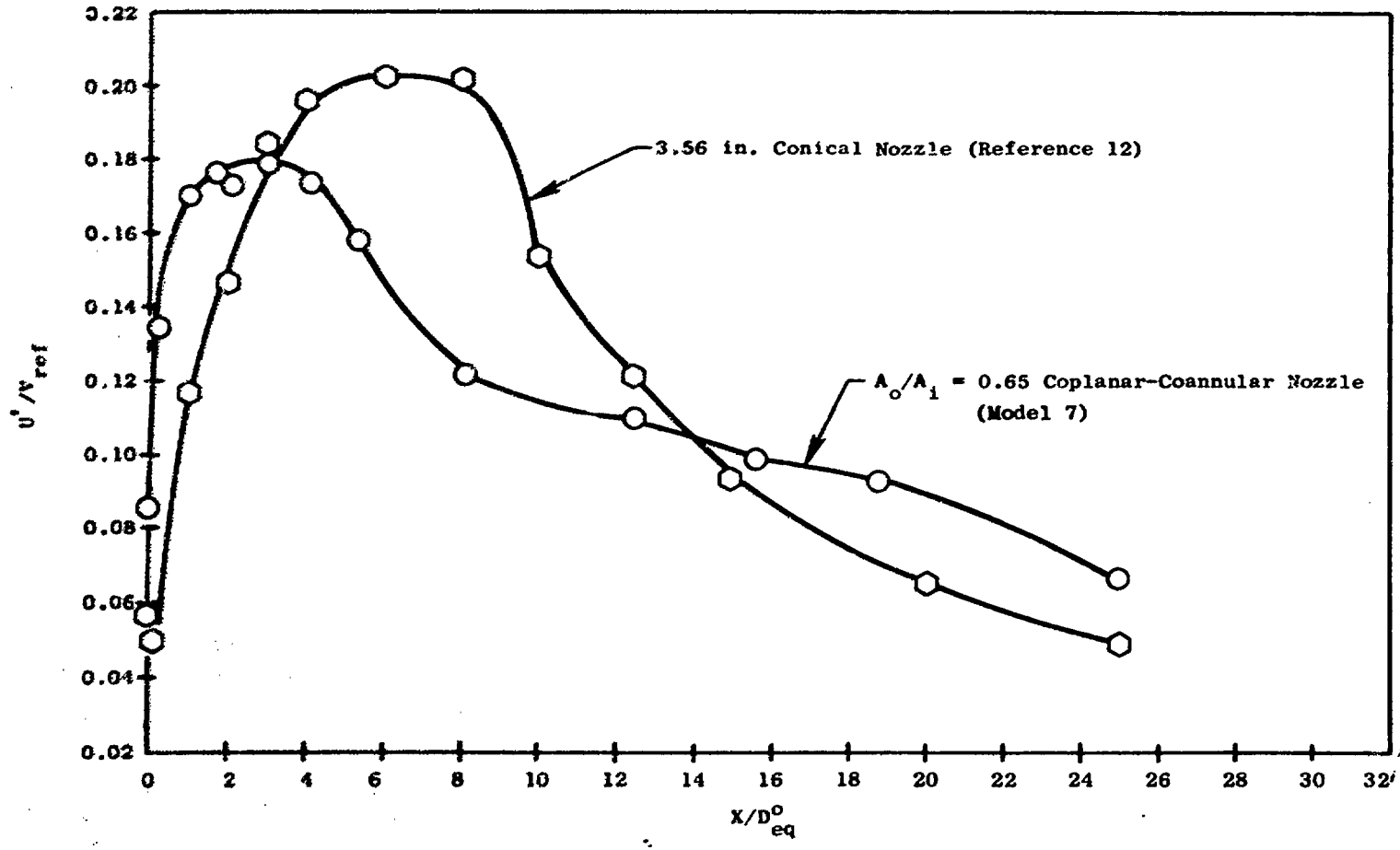

Figure 3-309. Peak Turbulence Intensity Levels.

- Model 6

A-1 V_i = 1000 ft/sec; V_o = 0
A-2 V_i = 1000 ft/sec; V_o = 200 ft/sec
A-3 V_i = 1000 ft/sec; V_o = 400 ft/sec
A-4 V_i = 1000 ft/sec; V_o = 600 ft/sec
A-5 V_i = 1000 ft/sec; V_o = 800 ft/sec
A-6 V_i = 1000 ft/sec; V_o = 1010 ft/sec
A-7 V_i = 1000 ft/sec; V_o = 1250 ft/sec
A-8 V_i = 500 ft/sec; V_o = 1000 ft/sec

- AR = 2.0
- A_o/A_i = 2.0, Coplanar-Coannular Nozzle
- $T_{T_o} = T_{T_i}$ = Ambient

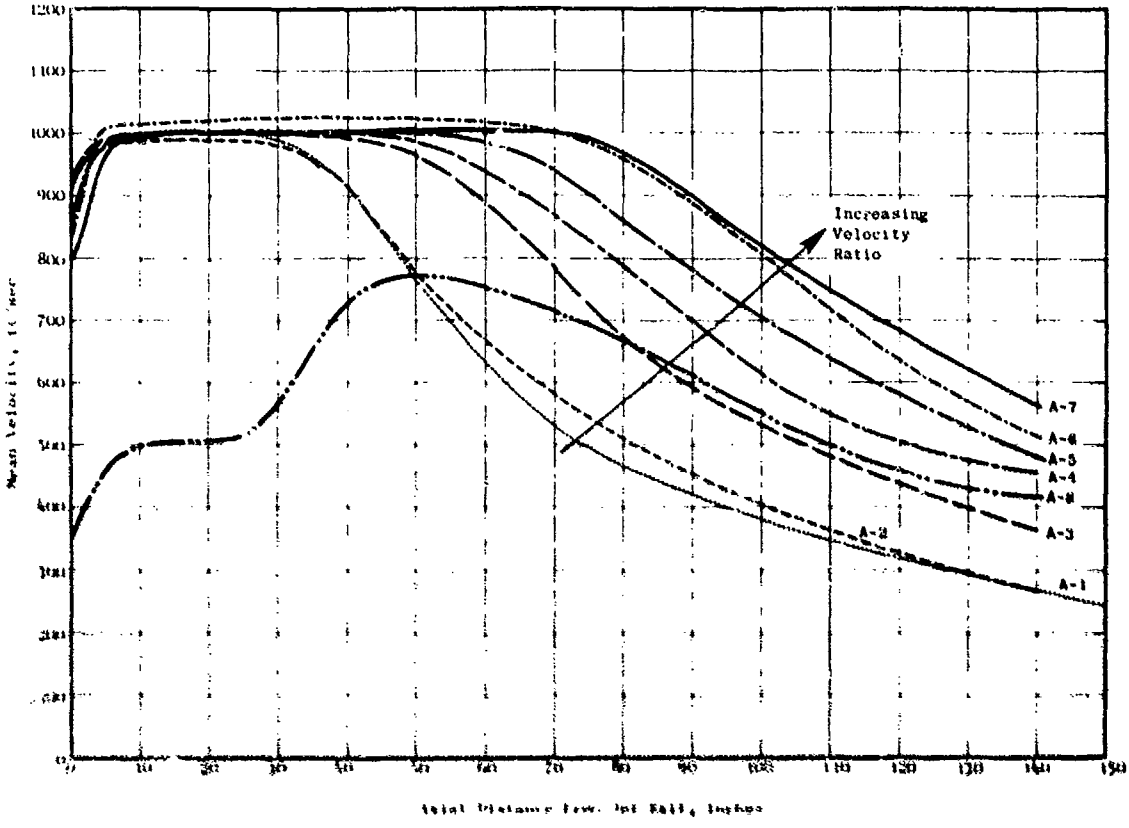

Figure 3-310. Centerline Velocity Decay Characteristics.

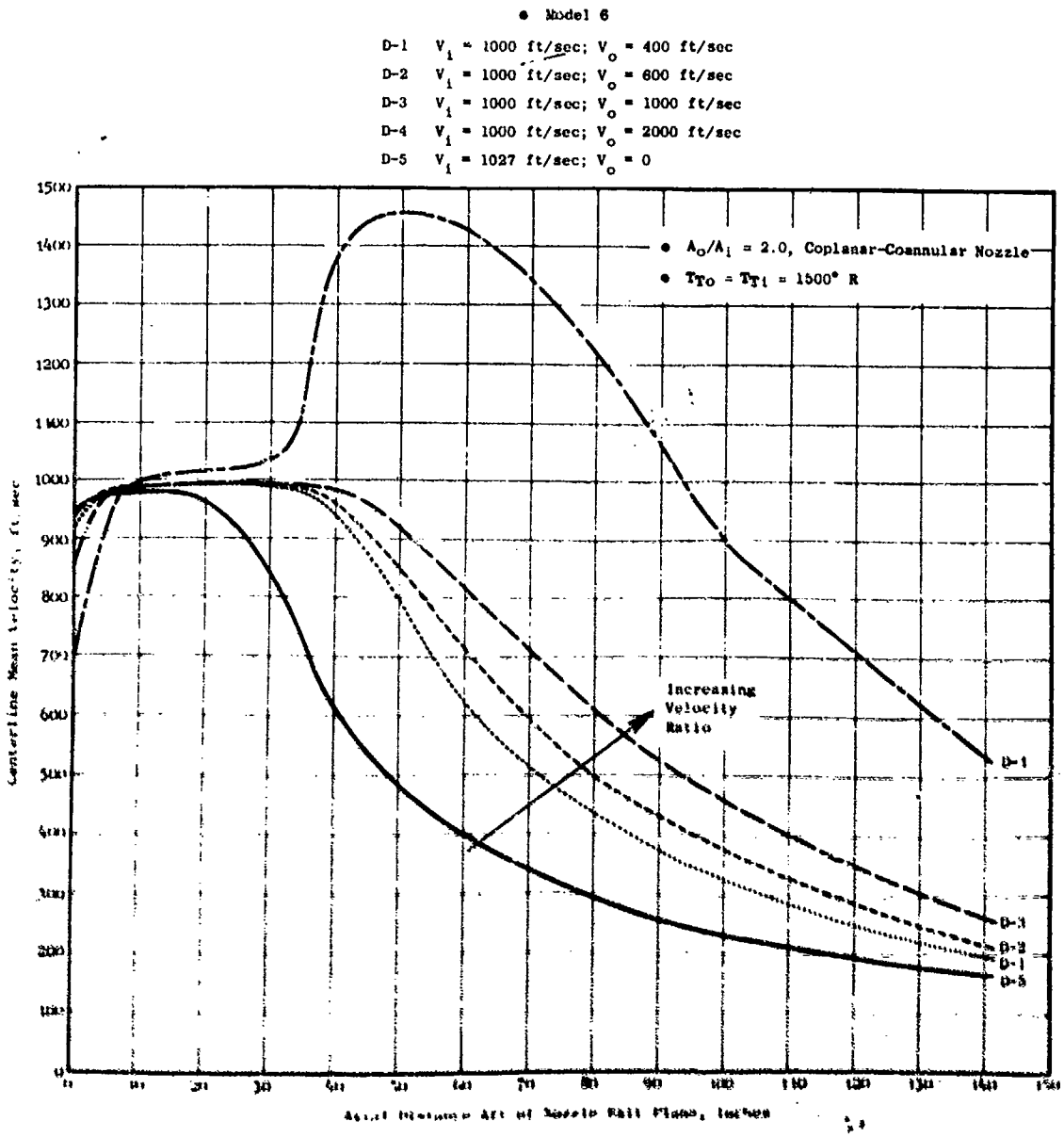

Figure 3-311. Centerline Velocity Decay Characteristics.

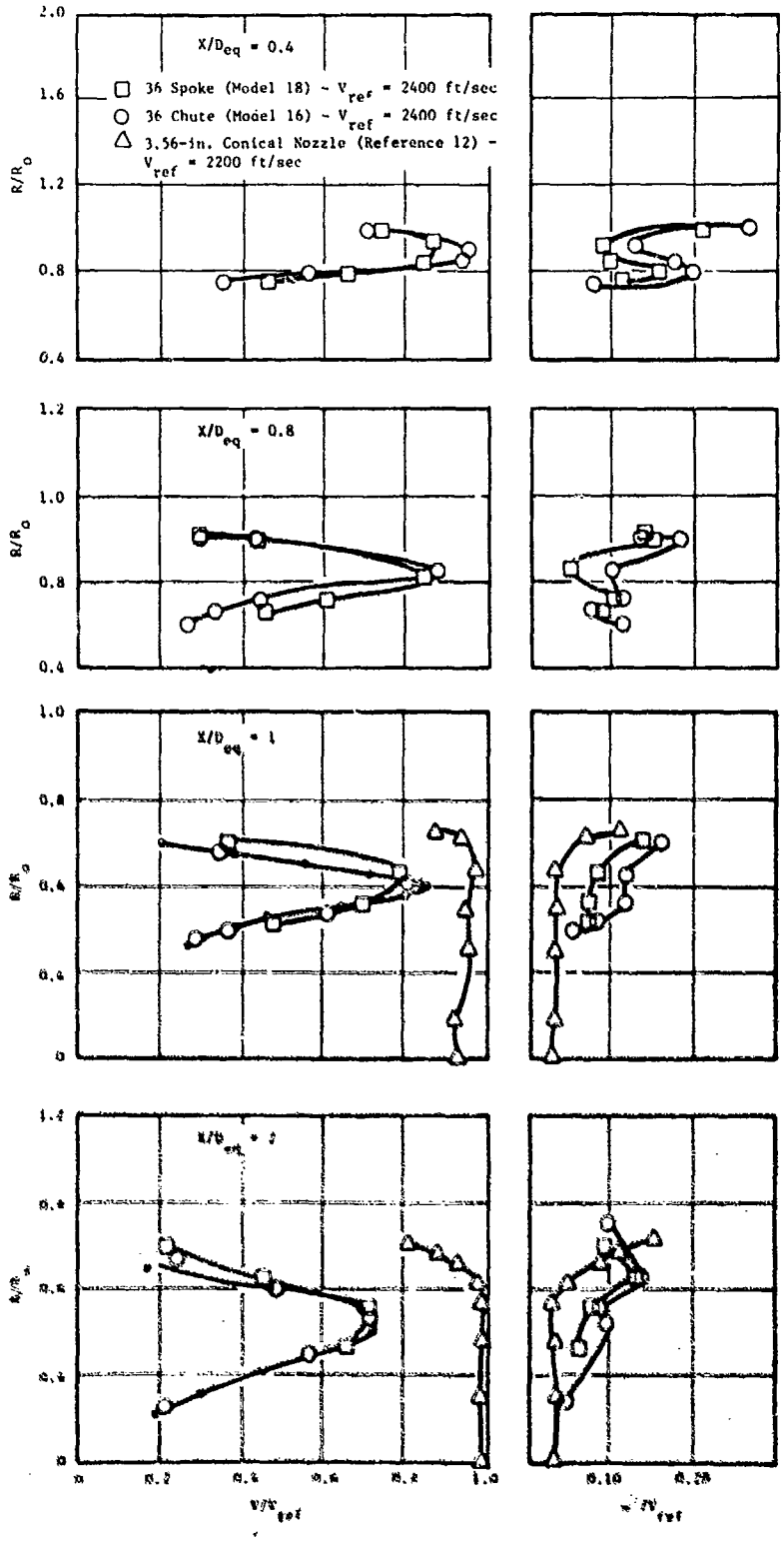

Figure 3-312. AR = 2.0 36-Chute (Model 16) and 36-Spoke (Model 18) Nozzles - Mean Velocity and Turbulence Profiles.

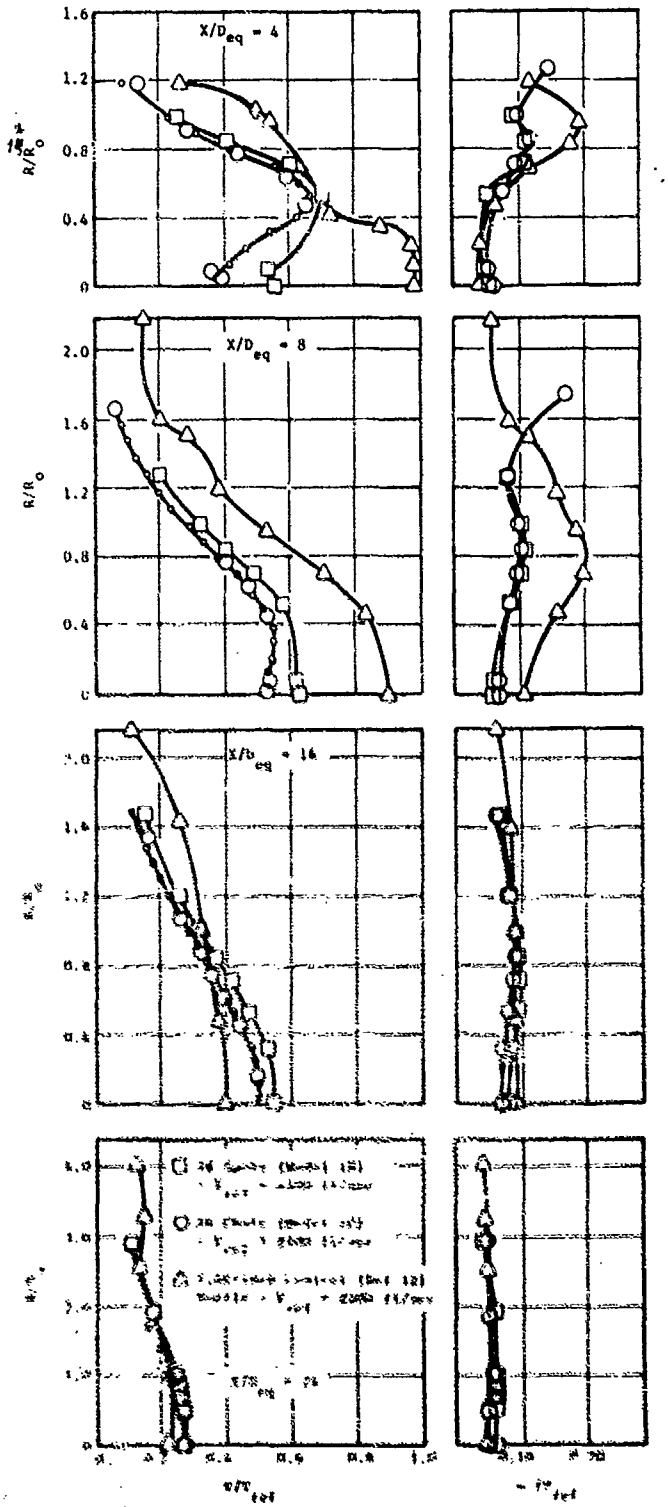

Figure 3-313. AR = 2.0 36 Chute and 36 Spoke Nozzles - Mean Velocity and Turbulence Profiles.

nozzle is actually less than the suppressor nozzles. The baseline and suppressor nozzles are equivalent at an X/D = 24.

Comparison of the spoke (Model 18) and chute (Model 16) mean velocity and turbulence profiles indicate only small differences between the configurations. The comparison of acoustic data for these configurations was presented in Section 3.4.2.4. The peak noise levels at the comparable cycle conditions for the plume are found to be essentially equivalent (which is supported by the similarity of the mean velocity and turbulence intensity comparisons).

Mean velocity and turbulence intensity measurements were made to determine the influence of suppressor area ratio variation. Models 22, 24 and 27 were utilized to perform this study. They were dual flow nozzles incorporating half-span suppressors having 36 elements. The acoustic data comparisons for these configurations are presented in Section 3.4.2.1. The outer stream velocity was 2400 ft/sec and the inner stream velocity was 1200 ft/sec. Figure 3-314 summarizes the decay characteristics of the peak velocity at whatever radial location it occurs. The AR = 2.5 nozzle configuration (Model 22) causes the most rapid decay in mean velocity. It is interesting to note that noise reduction potential was generally enhanced with excessive suppressor area ratio which in turn exhibited the more rapid velocity decay rates.

Detailed mean velocity and turbulence profiles are summarized on Figures 3-315 and 3-316, for several axial locations. The trend of noise with suppressor area ratio variation is best illustrated by the comparisons at X/D = 2.0 and X/D = 4.0. Minor differences in the turbulence intensity profiles are also apparent, however, they cannot be related to the noise generation process on a quantative basis.

A study was conducted with Model 24 as the base configuration and with Model 36 to determine the effect that adding a treated ejector has on the mean velocity and turbulence intensity profiles. These comparisons are summarized on Figure 3-317. The comparisons at X/D = 2.0 are at the exit plane of the ejector. The addition of the treated ejector resulted in only a minor change in the shape and level of the mean velocity and turbulence intensity profiles at the nozzle exit plane. A similar conclusion is drawn from the measurements made at the other axial locations. The acoustic comparisons presented in Section 3.4.2.7 showed a suppression improvement of 3-4 PNdB at the maximum noise angle. Since mean velocity and turbulence intensity profiles were shown to be similar, the beneficial effect of the ejector can probably be attributed to physical shielding and acoustic treatment effectiveness.

Measurements were also made on the JENOTS free-jet facility to determine the change in the mean velocity and turbulence intensity profiles in simulated flight. The characteristics are discussed below for a conical nozzle (Reference 12), plug nozzle (Model 40), chute nozzle (Model 41), and a 104-tube nozzle (Model 44).

The peak mean velocity decay characteristics for the conical nozzle (Reference 12) are summarized on Figure 3-318. The measurements show a slowing down of the mean velocity decay rate with increasing simulated aircraft velocity ($V_{a/c}$) as discussed in Reference 29. A similar type of comparison

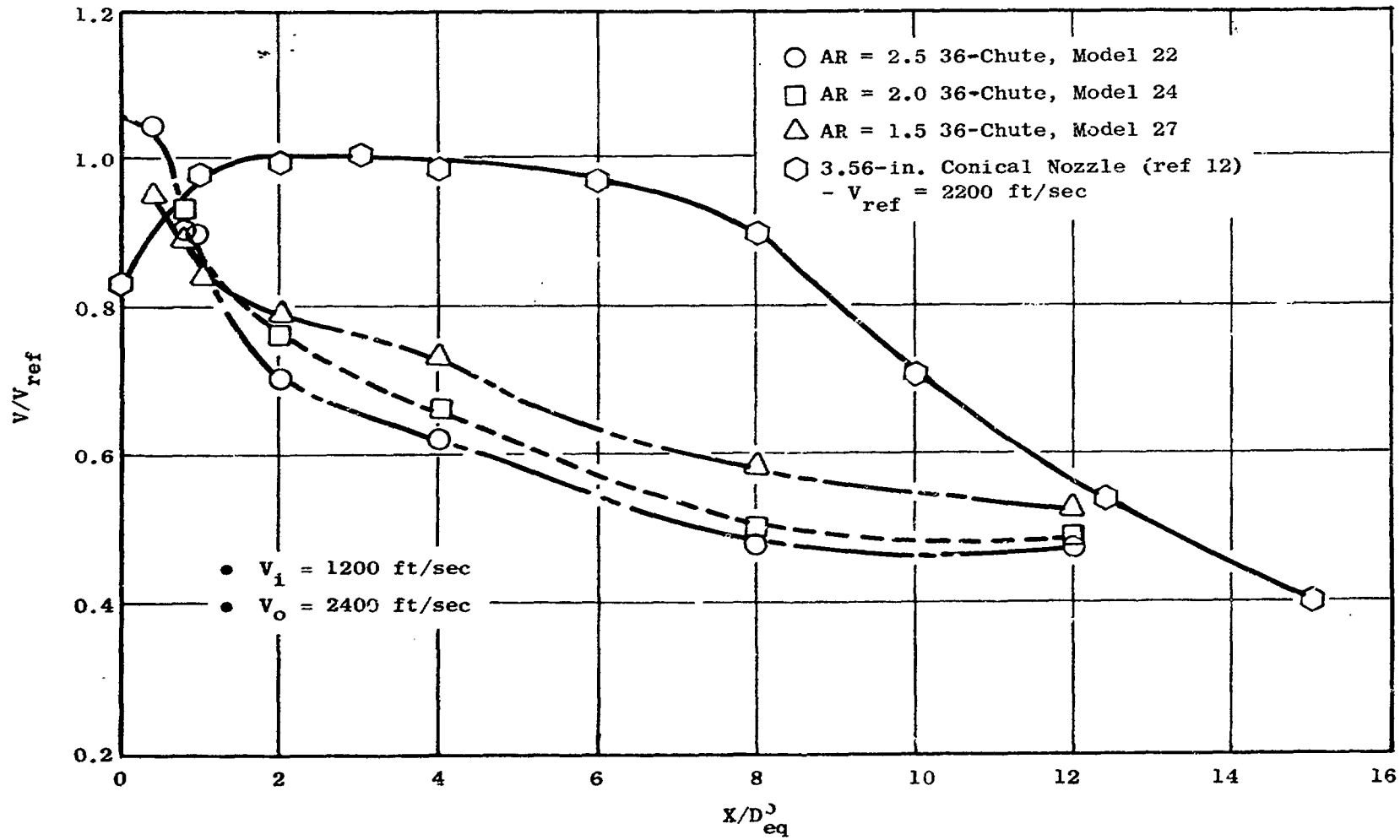

Figure 3-314. Effect of Area Ratio on Peak Axial Velocity Decay Characteristics.

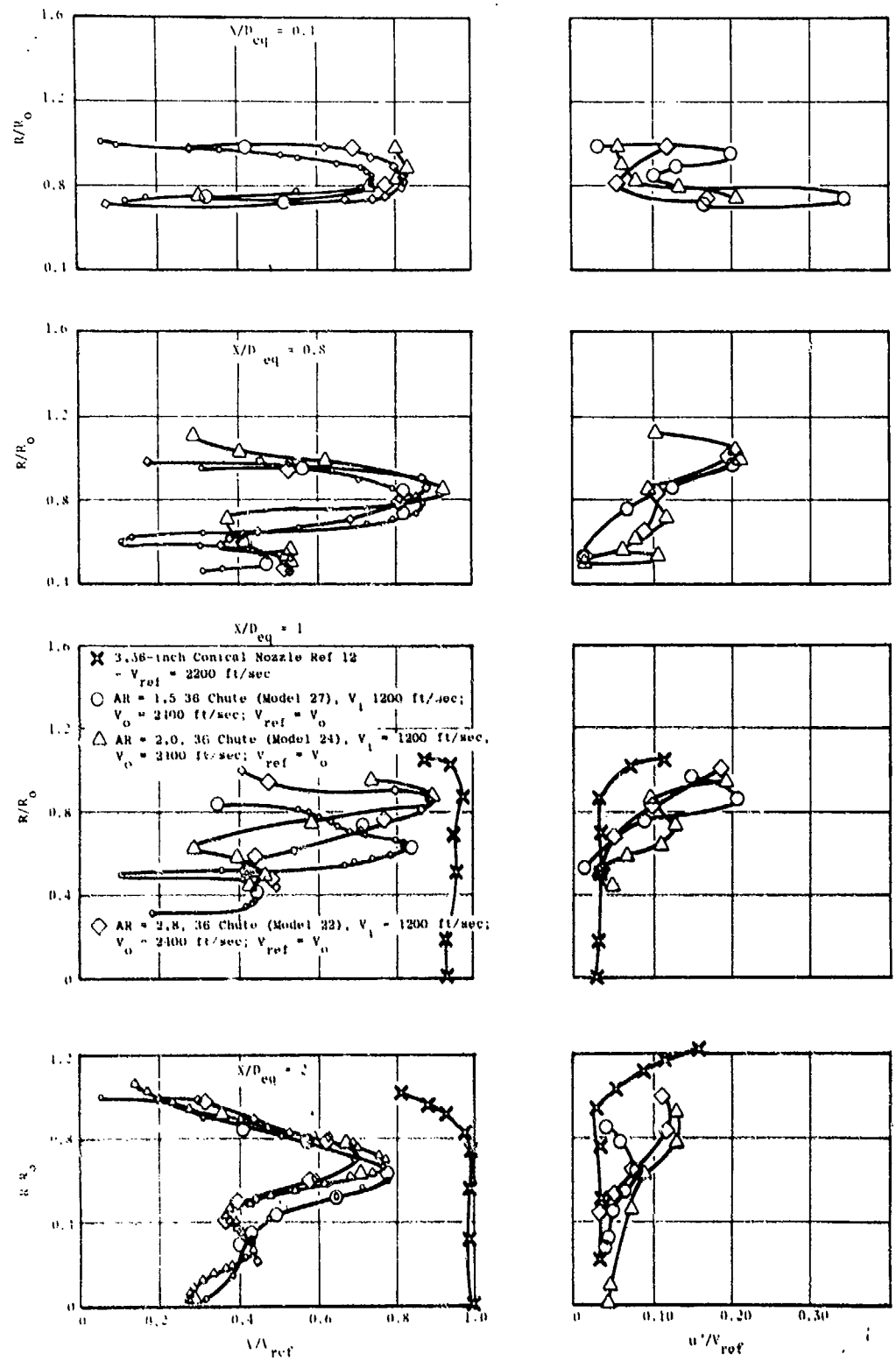

Figure 3-315. Impact of Suppressor Area Ratio on Radial Mean Velocity and Turbulence Intensity Profiles.

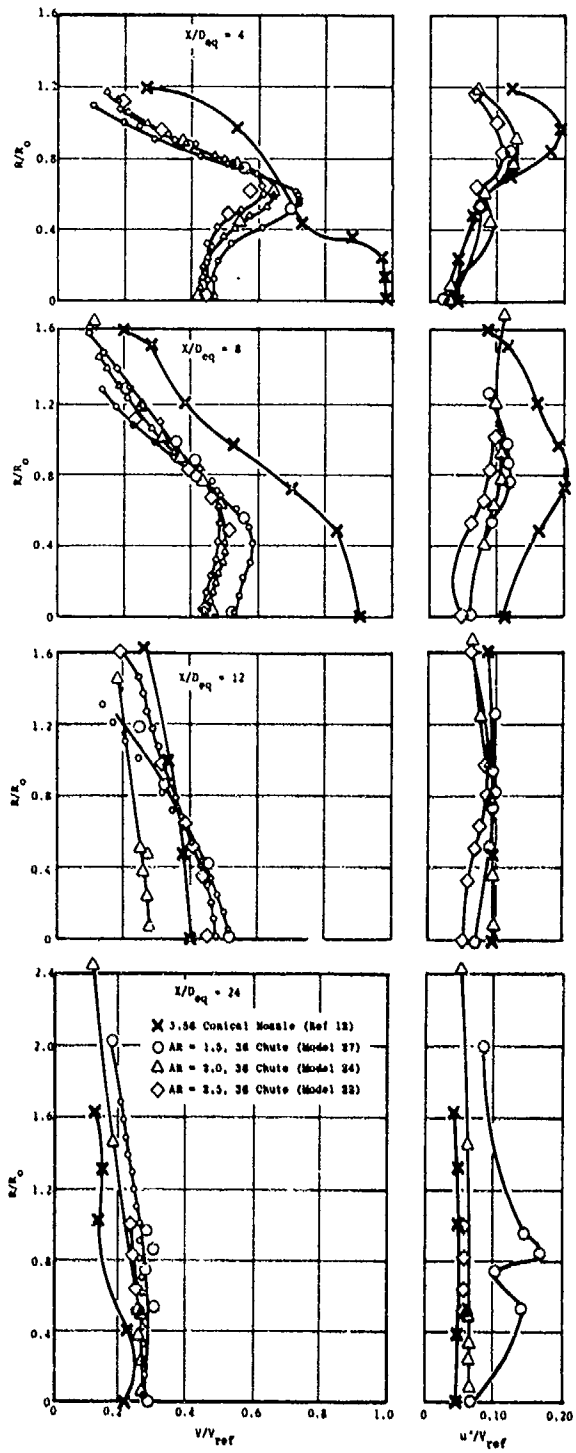

Figure 3-316. Impact of Suppressor Area Ratio on Mean Velocity and Turbulence Intensity Profiles.

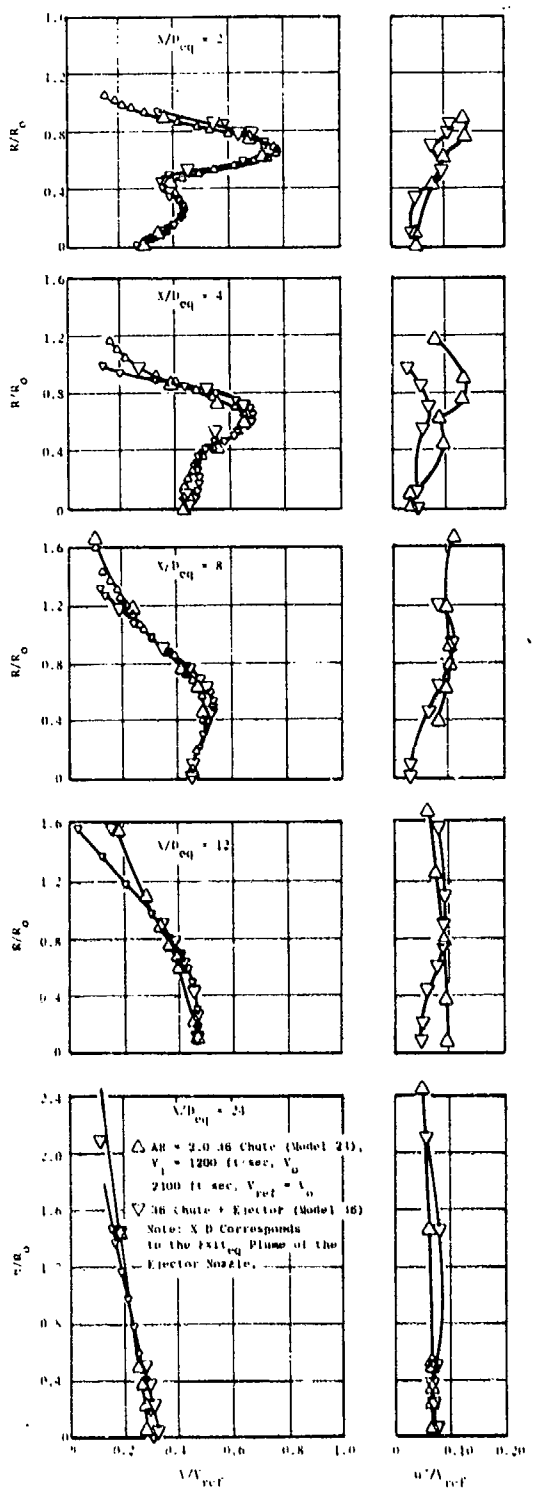

Figure 3-317. Impact of a Treated Ejector on the Mean Velocity and Turbulence Profiles of a 36 Chute Nozzle.

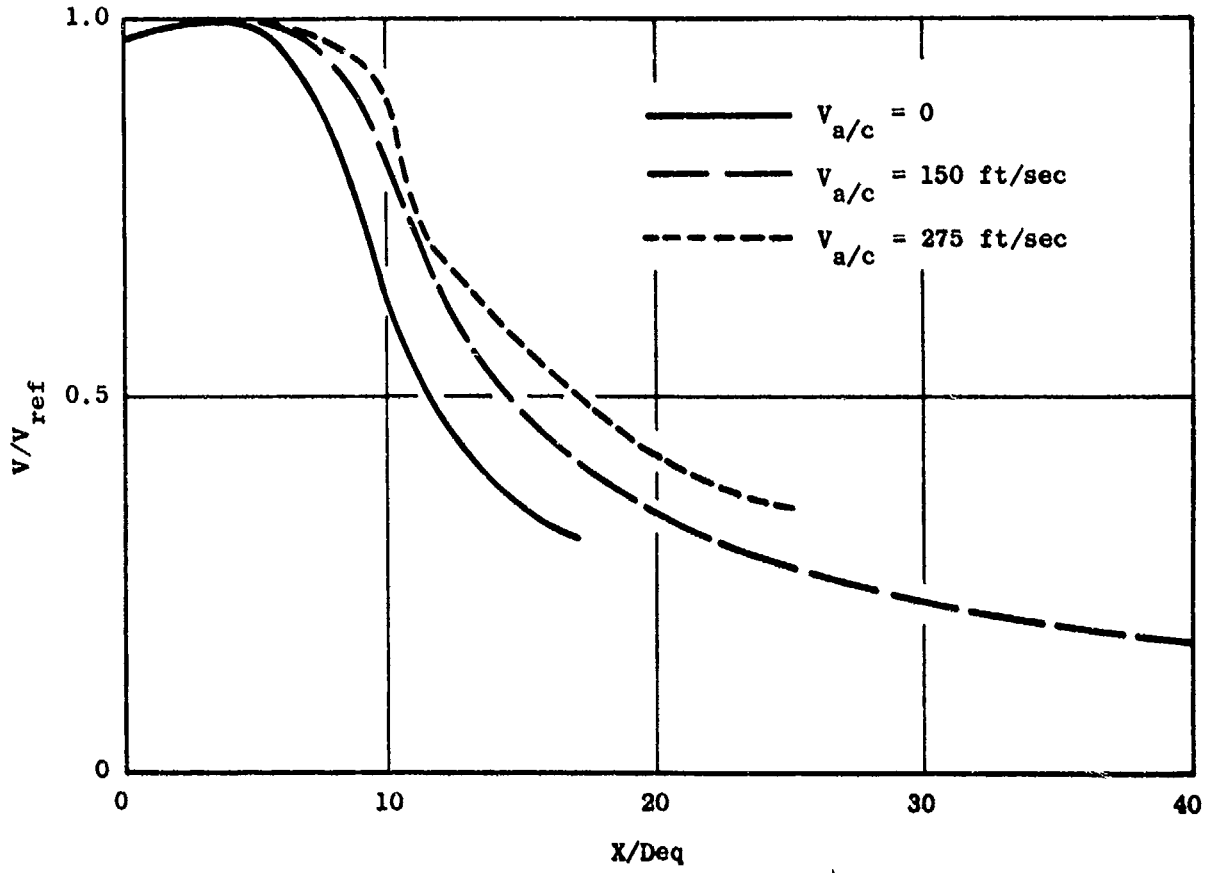

Figure 3-318. Centerline Velocity Decay for 3.56-inch Conical Nozzle (Reference 12), V_{ref} = 2200 ft/sec.

for the 0.85 R/R plug nozzle, Model 40, is presented on Figure 3-319. These data were obtained by performing a series of axial traverses at the nozzle centerline and at normalized radial locations. The trends are similar to the conical nozzle.

The 8-lobe nozzle (Model 46) static and flight mean velocity decay characteristics are summarized on Figure 3-320. The rate of velocity decay has increased significantly relative to the conical nozzle at X/D < 14. The region of maximum mean velocity gradient (0 < X/D < 4.0) appears to be only slightly sensitivity to forward flight. In the axial region of 4.0 < X/D < 15 the velocity decay rate of this configuration is enhanced rather than decreased as was the case for the conical nozzle. The static and flight peak turbulence intensity levels for this configuration are also summarized on Figure 3-320. The turbulence level near the nozzle exit plane is slightly increased in flight very near the nozzle exit plane (X/D < 2.0) and slightly reduced at other axial locations. The peak turbulence intensity levels also occur very near the nozzle exit plane.

Select measurements were made on the AR = 2.5 36-chute nozzle (Model 41). The mean velocity decay characteristics for this configuration, based on a series of axial traverses directly behind a flowing chute centerline at two radial locations, are summarized on Figure 3-321. The decay of the peak velocity near the nozzle exit plane is insensitive to flight. However at X/D > 12 where the segmentized jets have lost their individual identity (or coalesced), the characteristics exhibited are the same characteristics observed for the conical nozzle. Mean velocity and turbulence intensity levels for a 104-tube nozzle Model 44 are summarized on Figures 3-322 and 3-323. The measurements were made along the centerline of the nozzle and at the centerlines of inner, middle, and outer tubes. The centerline static and flight mean velocity comparisons show a trend identical to that exhibited by the AR = 2.5 36-chute nozzle (e.g., influence of free-stream velocity is observed up to X/D = 7, while beyond this point the velocity decay rate is slowed down). The mean velocity levels of inner and middle tubes are essentially identical up to X/D of 3 with a slight divergence of 2% to 5% between X/D of 2 and 6. The decay characteristics of the outer tube are more sensitive to free-stream velocity. Turbulence intensity levels are compared on Figure 3-223. The maximum turbulence intensity levels occur in the jet plume of the outer tube in the region of maximum mean velocity gradient. The levels are similar to those of the conical nozzle. In flight, minimal change in turbulence inensity levels occurs near the nozzle exit plane; in the region of the coalesced jet, the levels are reduced.

The prior data comparisons support the following conclusions. Suppressors generally cause the increase in mean velocity decay until the velocity reaches 60% or less of the fully expanded isentropic velocity. This point generally occurs within 10 to 15 equivalent nozzle diameters and is a function of the suppressor design. The axial location of peak turbulence intensity is a function of nozzle type, and generally occurs in the region where the mean velocity gradient is a maximum. For example, the peak turbulence intensity levels for the conical nozzle occurred at 6 < X/D < 8 whereas the peak turbulence intensity level for the chute nozzles occurred at X/D < 0.4.

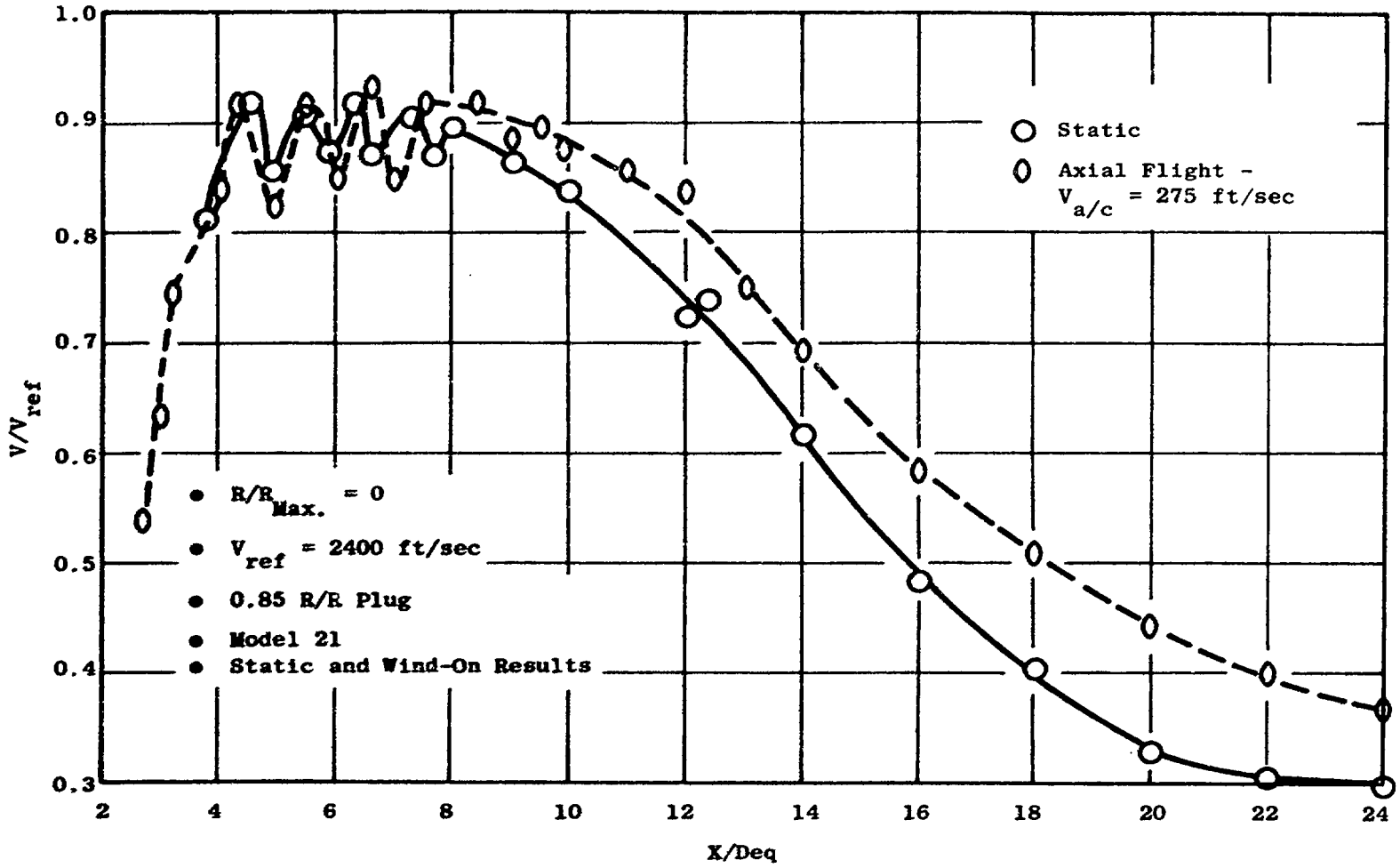

Figure 3-319. 0.85 Radius Ratio Plug Nozzle (Model 40) Centerline Mean Velocity Decay Characteristics.

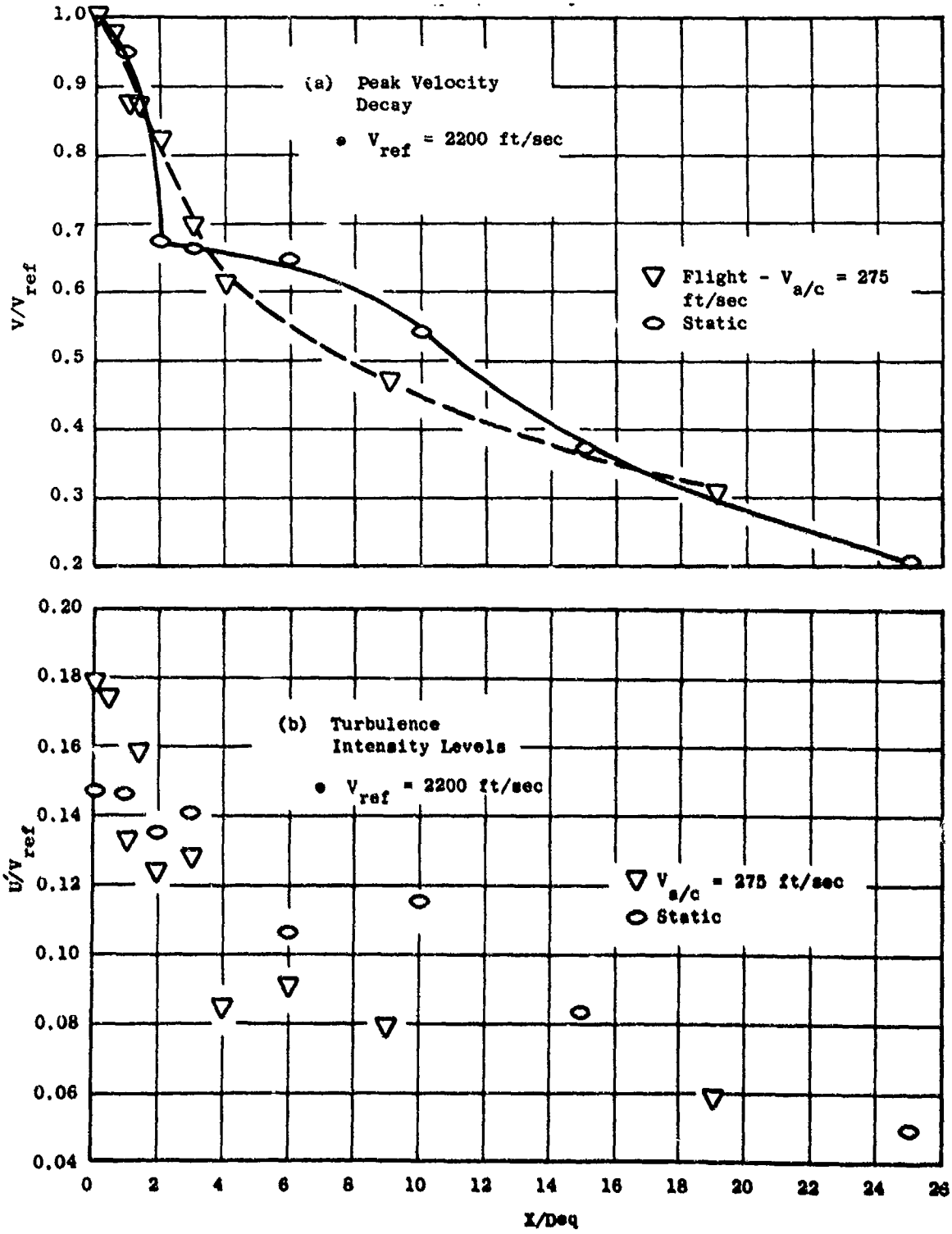

Figure 3-320. 8-Lobe Nozzle (Model 46), Static and Flight.

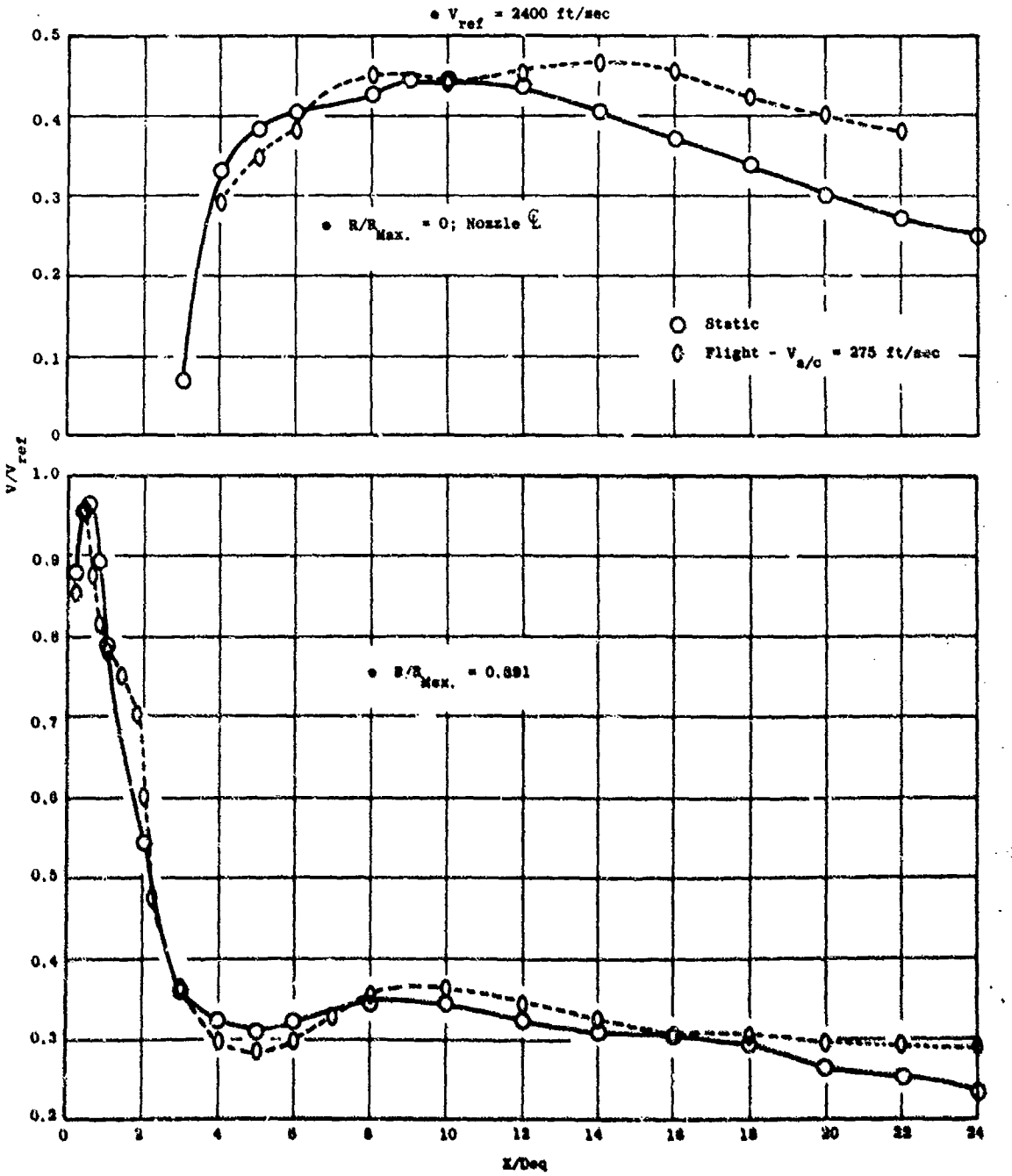

Figure 3-321. 36-Chute Nozzle (Model 41) Mean Velocity Decay Characteristics Static and Flight.

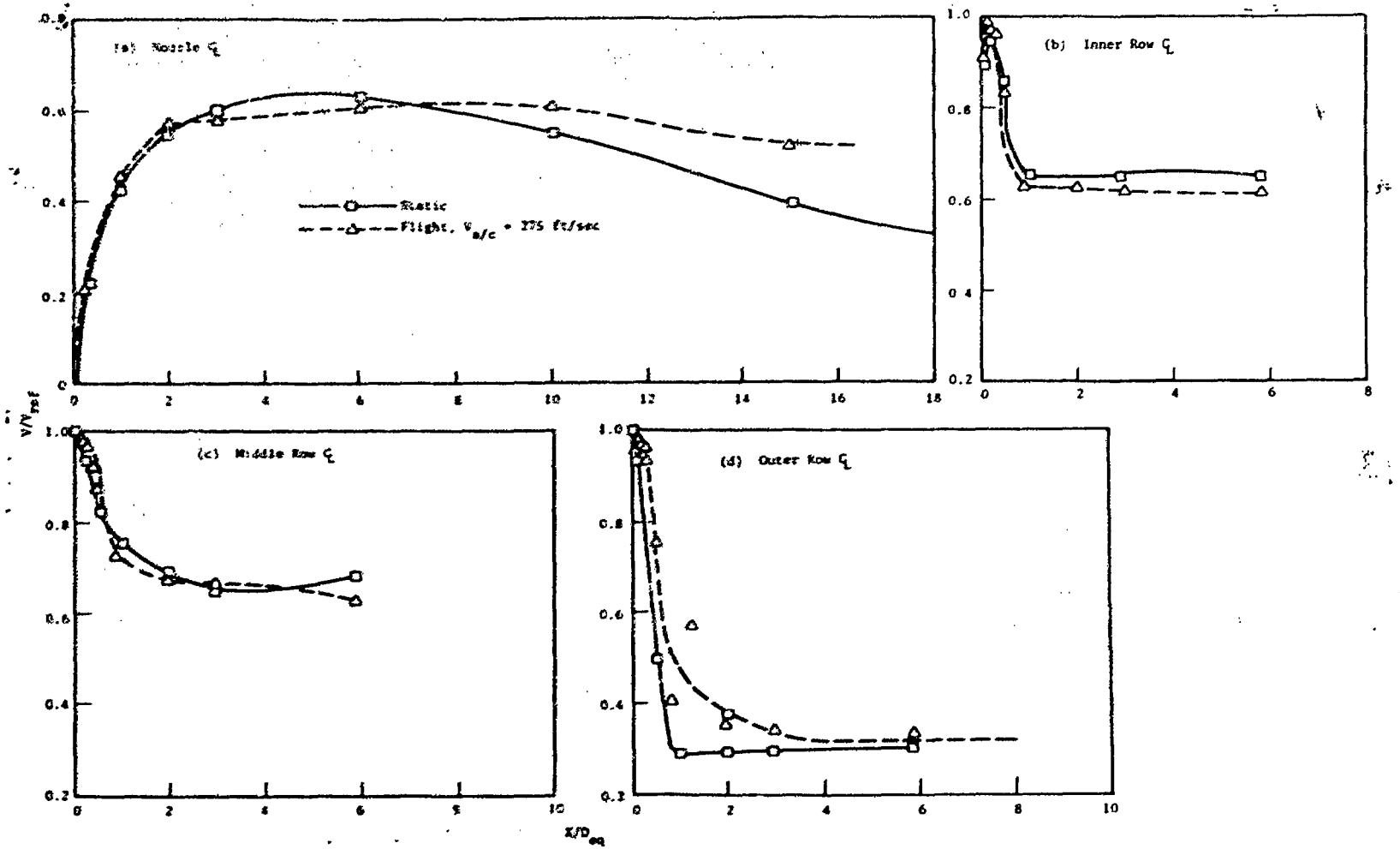

Figure 3-322. 104-Tube Nozzle (Model 44) Mean Velocity Characteristics, Static and Flight.

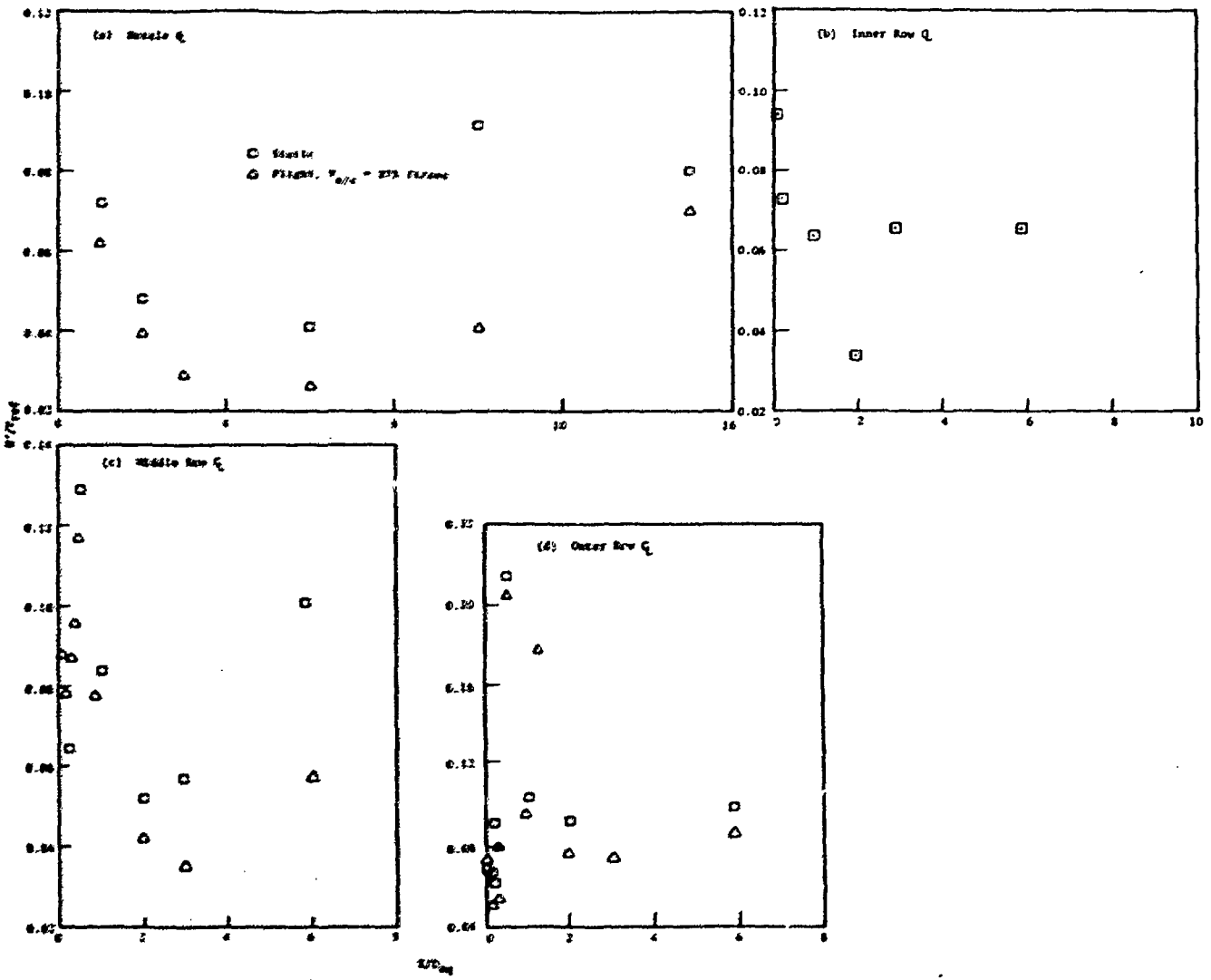

Figure 3-323. 104-Tube Nozzle (Model 44) Turbulence Intensity Characteristics, Static and Flight.

In general, for a complex multielement suppressor nozzle the region of peak turbulence intensity was found to occur within one equivalent nozzle diameter for the configurations evaluated. Although axial locations of peak turbulence intensity levels are a function of nozzle type, the absolute level ranges from 18 to 22% and does not correlate with exhaust nozzle type.

In simulated flight, the velocity decay rate for the conical nozzle was retarded (e.g., decayed at a much lower rate). The suppressor showed very little sensitivity to forward velocity with the exception of the downstream coalesced jet. Turbulence intensity levels were found to decrease in the coalesced jet in-flight compared to static. The levels near the exit plane were found to be generally comparable.

Overall, the laser velocimeter was demonstrated to be extremely useful in determining the differences in aerodynamic mixing characteristics of baseline and complex multielement suppressor nozzles. The aerodynamic data, in conjunction with the acoustic data bank, may be utilized to aid in the validation of current and future jet noise analytical prediction models.

3.4.5 Ellipsoidal Mirror (EM) Testing

This section presents the results of ellipsoidal mirror (EM) source location measurements made on several scale model suppressor nozzles during the Task 3 test program. EM testing was conducted on a total of twenty-two different nozzle configurations. Of these, fourteen configurations were tested at the jet noise anechoic facility using the 34.654-inch diameter deep-dish mirror, and eight were tested at the JENOTS free-jet facility, using the 18-inch-diameter shallow-dish mirror. Test setup and data acquisition were described in Section 3.3.3, and Appendices D and E describe the EM developments.

3.4.5.1 Data Analysis

The EM test matrix was planned to allow evaluation of several geometric and operating parameters by comparison of measured source distributions for specific data points. The results of these comparisons are presented in this section. The source distributions are expressed as Strouhal Number ($f\ D_{eq}/V_o$) versus normalized axial distance (X_{peak}/D_{eq}), where D_{eq} is the equivalent circular diameter based on nozzle area, V_o is the ideally expanded jet velocity and X_{peak} is the peak source location for a given frequency, f. For dual flow configurations, D_{eq} is calculated from total area (inner plus outer) and V_o is based on the higher velocity (outer) stream.

Integral closure checks were made for all EM data points in the test program. Typical results are shown in Figures 3-324 through 3-328 for measurements made in the anechoic facility with the deep-dish mirror. Note that the data obtained with 2-sec integration time yielded the best results, even at lower frequencies, and was subsequently used to completely define the majority of the source distributions.

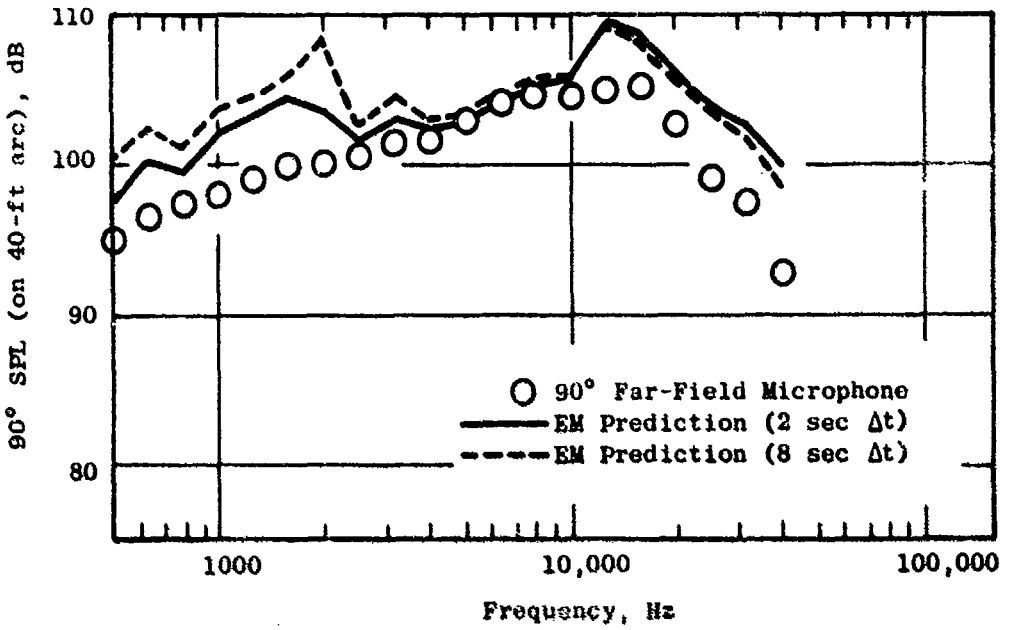

Figure 3-324. Integral Closure Check for AR = 2.0 36-Chute Nozzle, V_o = 2384 ft/sec, V_i = 1187 ft/sec.

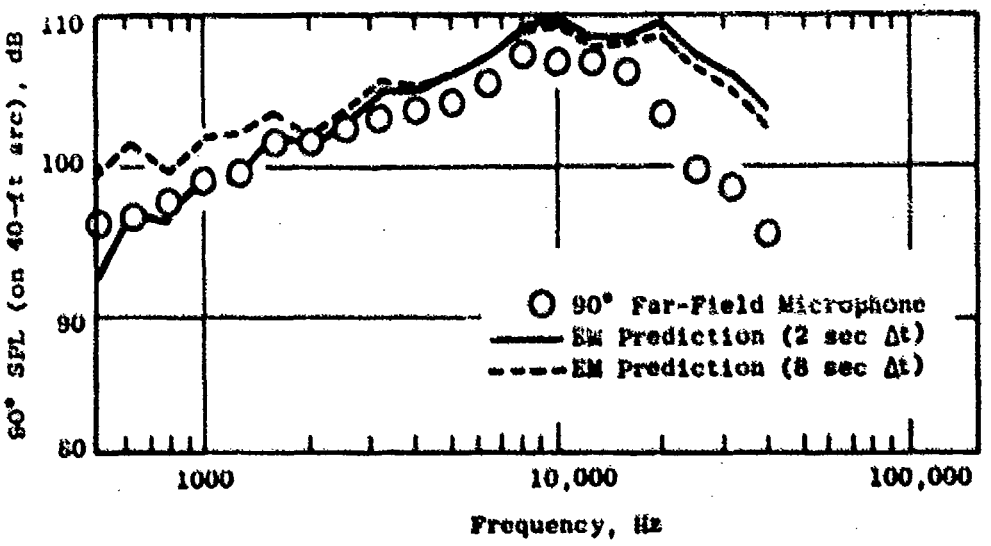

Figure 3-325. Integral Closure Check for AR = 1.75 20-Shallow-Chute Nozzle, V_o = 2375 ft/sec, V_i = 1167 ft/sec.

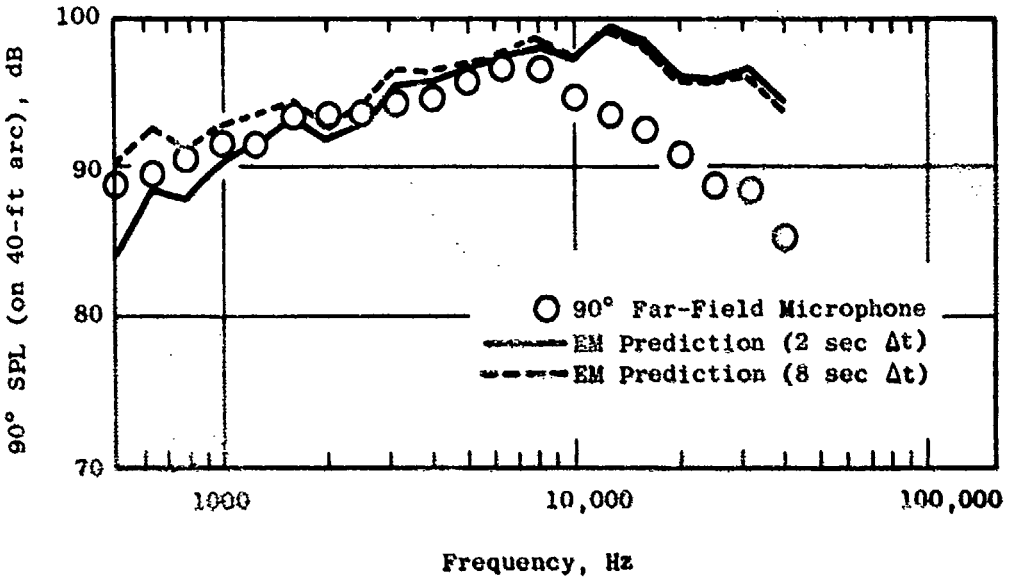

Figure 3-326. Integral Closure Check for AR = 2.0 36-Chute Nozzle with Treated Ejector, V_o = 1803 ft/sec, V_j = 1173 ft/sec.

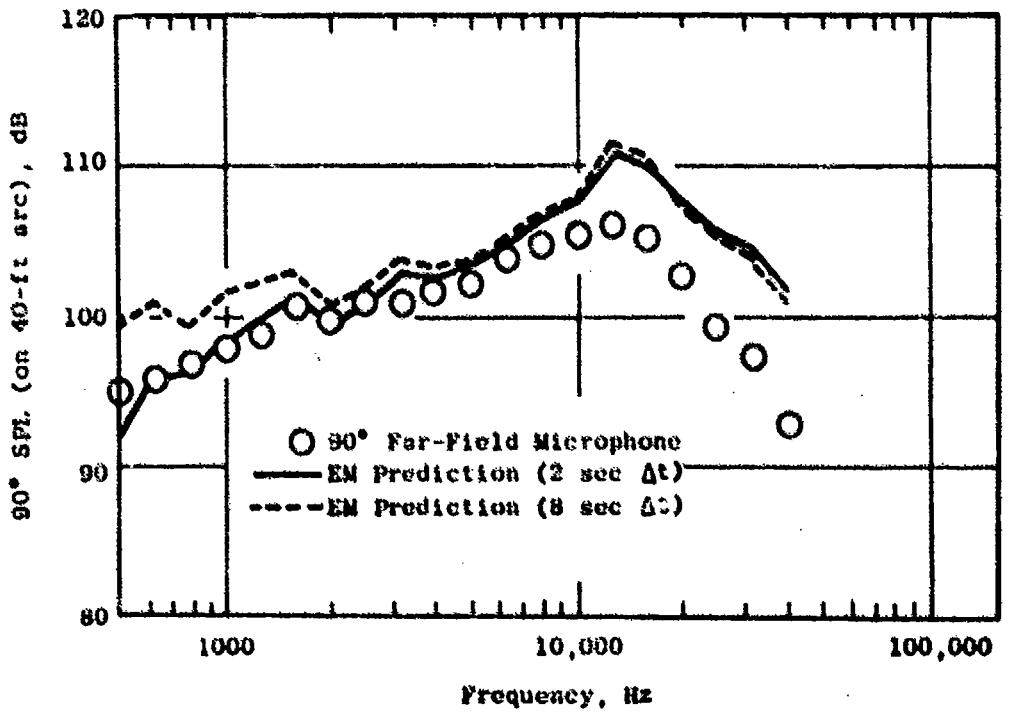

Figure 3-327. Integral Closure Check for AR = 2.0 36-Chute-Nozzle, V_j = 2375 ft/sec.

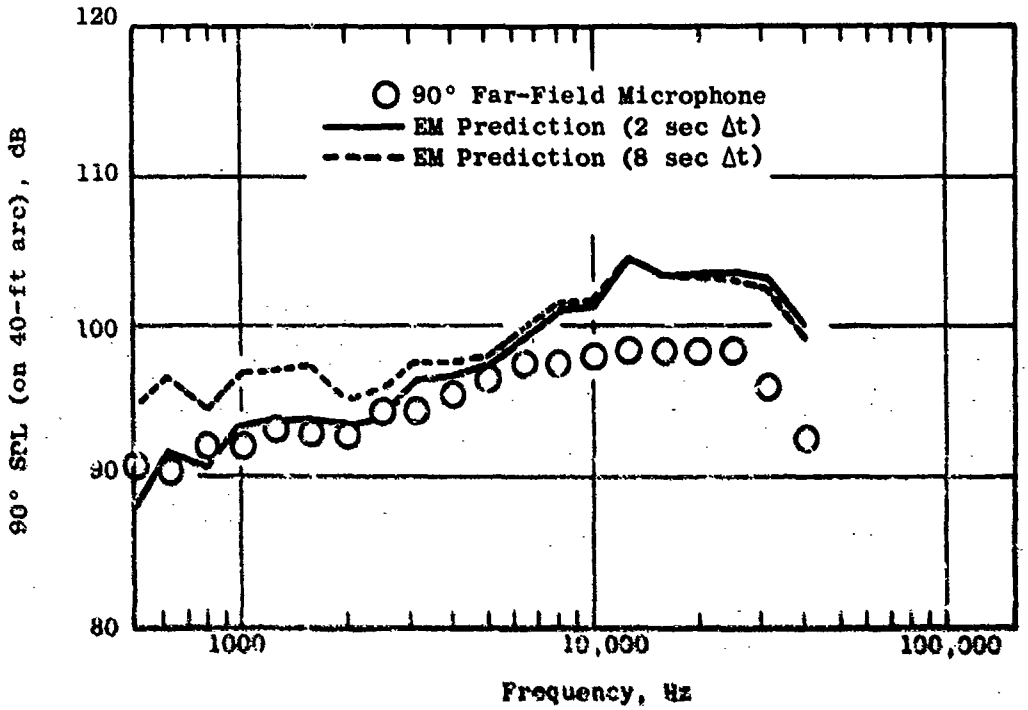

Figure 3-328. Integral Closure Check for AR = 2.5 36-Spoke Nozzle, V_o = 2382 ft/sec, V_j = 1269 ft/sec.

Figure 3-329 shows a comparison of peak source distributions for 20-, 30-, and 40-shallow-chute, dual-flow suppressors (Models 30, 31, and 32). While there is no significant difference between the 30- and 40-element data, high-frequency sources for the 20-element configuration peak farther downstream of the nozzle exit.

A comparison of peak source distributions for 36-chute, dual-flow suppressors with area ratios 2.5 and 3.0 (Models 33 and 34) is shown in Figure 3-330. The source distribution for area ratio 3.0 is seen to peak farther downstream at all frequencies.

Figure 3-331 shows a comparison of 36-chute and 36-spoke suppressors (Models 33 and 35). The source distribution for the chute nozzle peaks slightly closer to the nozzle exit for higher frequencies.

Figure 3-332 compares 36-chute dual-flow and turbojet suppressors (Models 24 and 16), while Figure 3-333 shows the same comparison with ejectors (Models 36 and 19). In both cases, the turbojet distributions peak farther downstream in the high and midfrequency ranges.

Figures 3-334 and 3-335 show the effect of ejectors on 36-chute nozzles for dual-flow (Models 24 and 36) and turbojet (Models 16 and 19) configurations, respectively. In each case, the peak high-frequency source distributions occur farther downstream with the ejector. There is no significant effect on low-frequency source distributions which normally peak downstream of the ejector exit.

Typical axial distributions of sound source intensity for a suppressor (Model 32) are shown in Figure 3-336. These 40-shallow-chute, dual-flow suppressor results confirm the expectation that source distributions become broader and flatter with decreasing frequency.

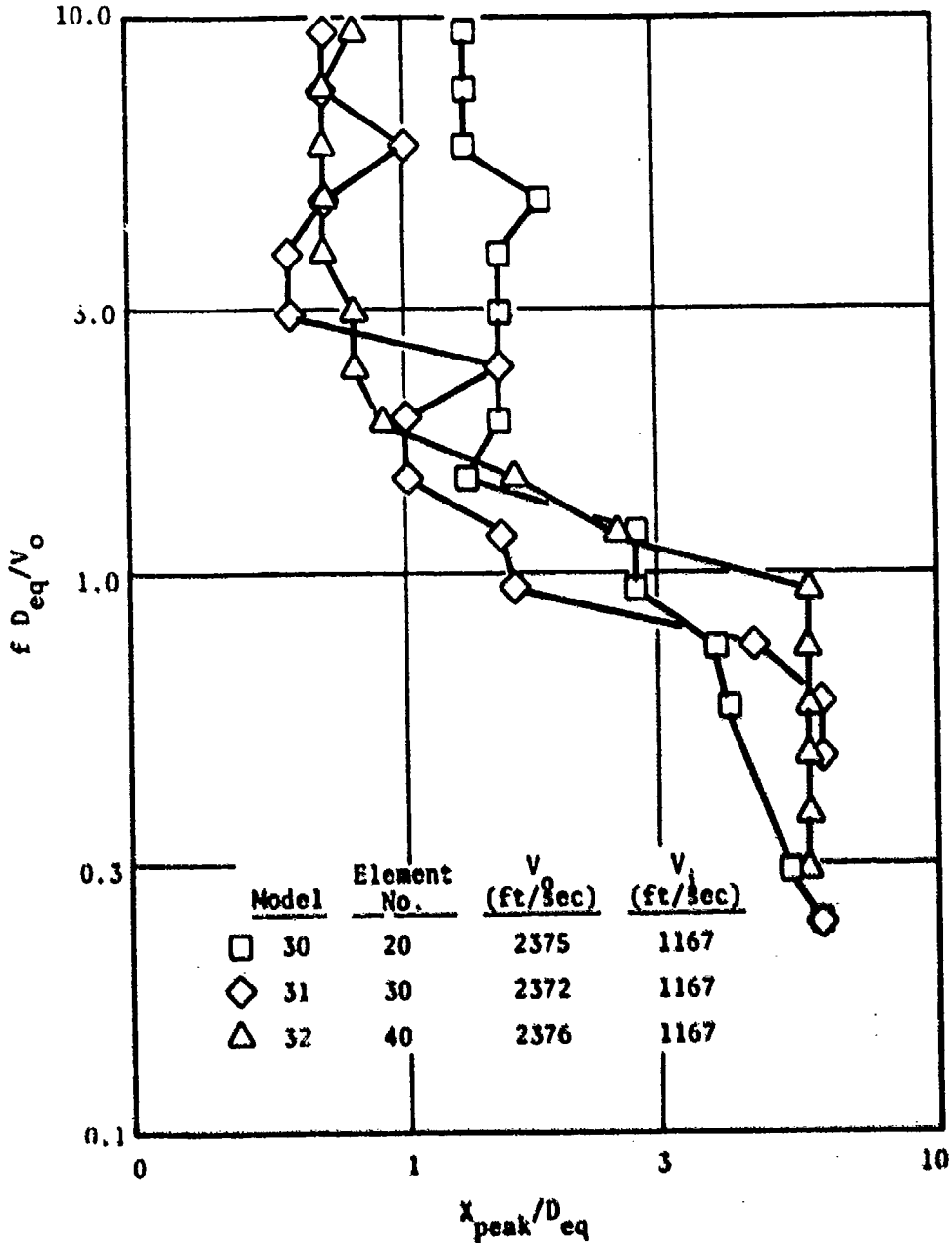

Figure 3-329. Effect of Element Number on Multispoke (Shallow Chute) Dual-Flow Suppressor Noise Source Distributions.

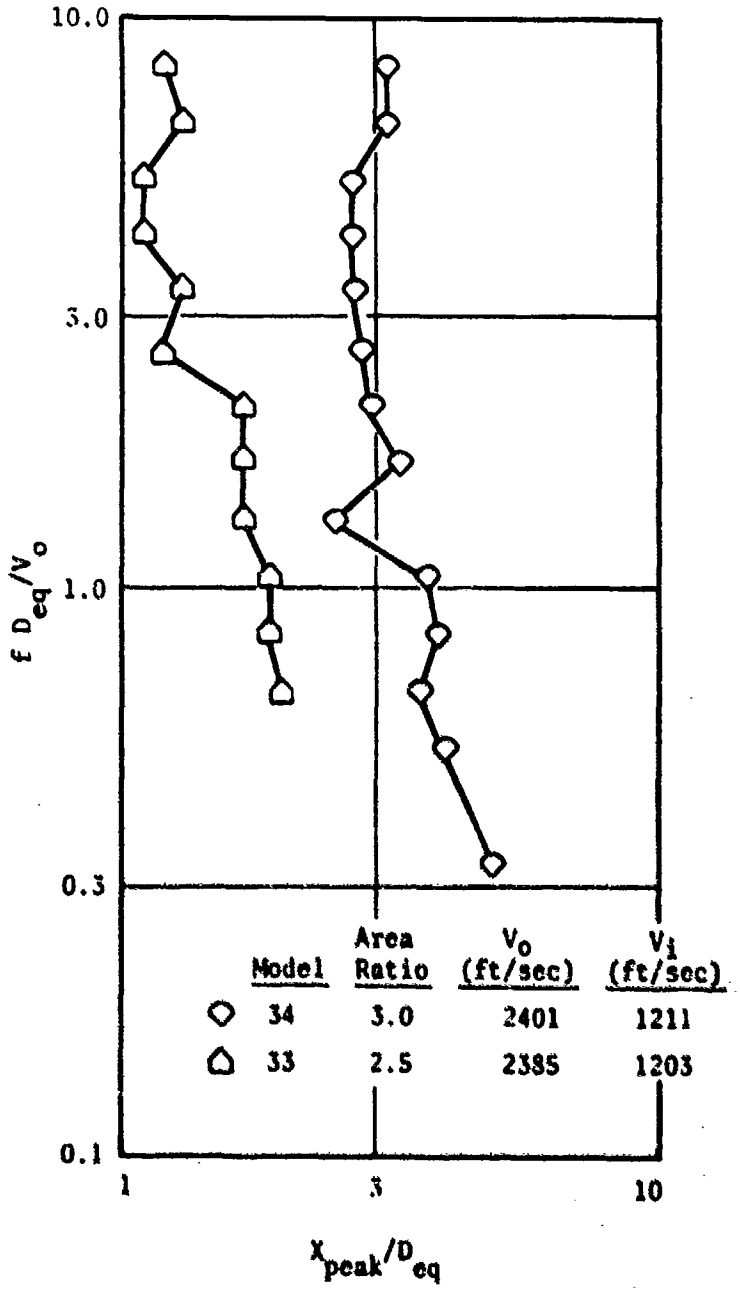

Figure 3-330. Effect of Chute Area Ratio on Multi-chute Dual-Flow Suppressor Noise Source Distributions.

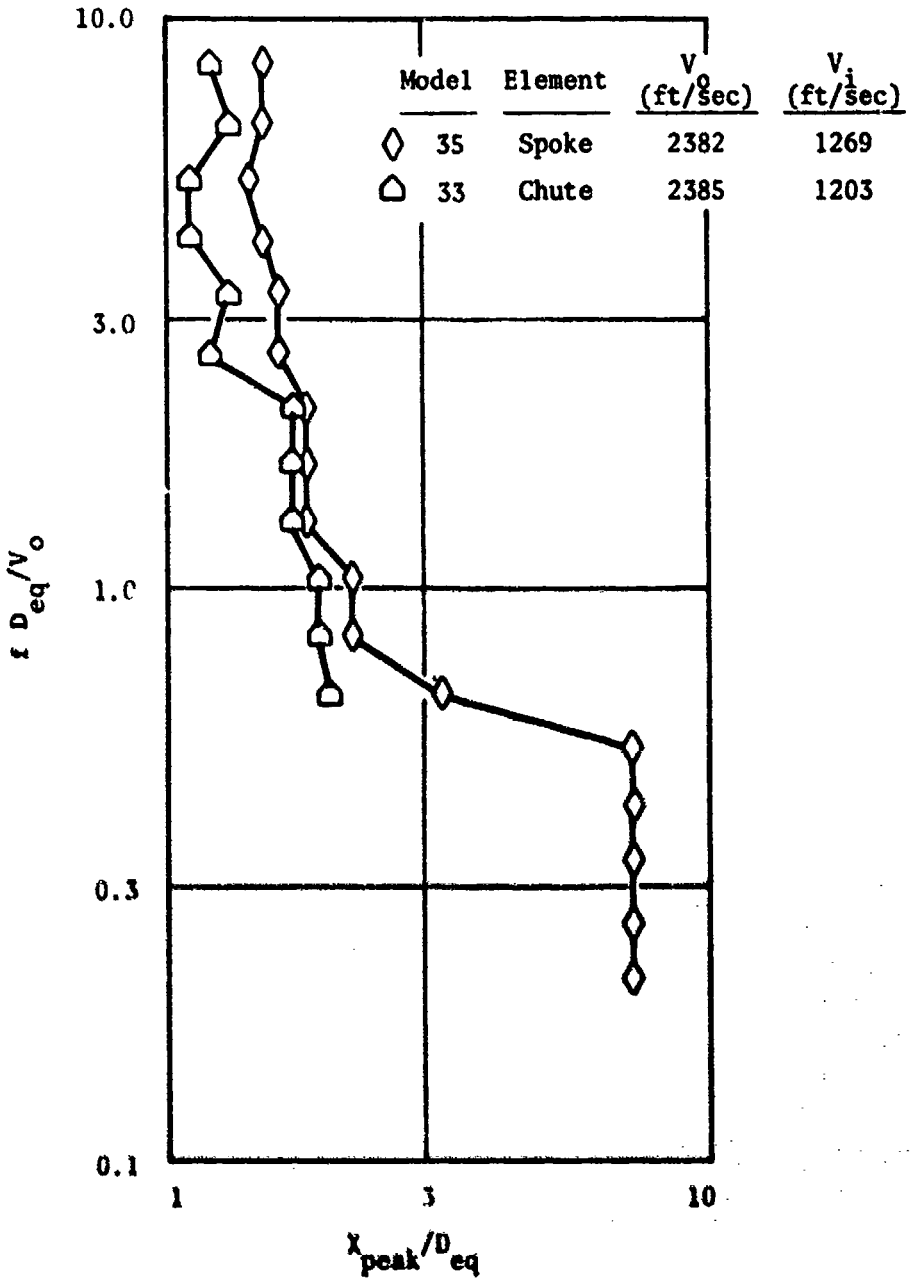

Figure 3-331. Comparison of Noise Source Distributions for Multichute and Multispoke Dual-Flow Suppressors.

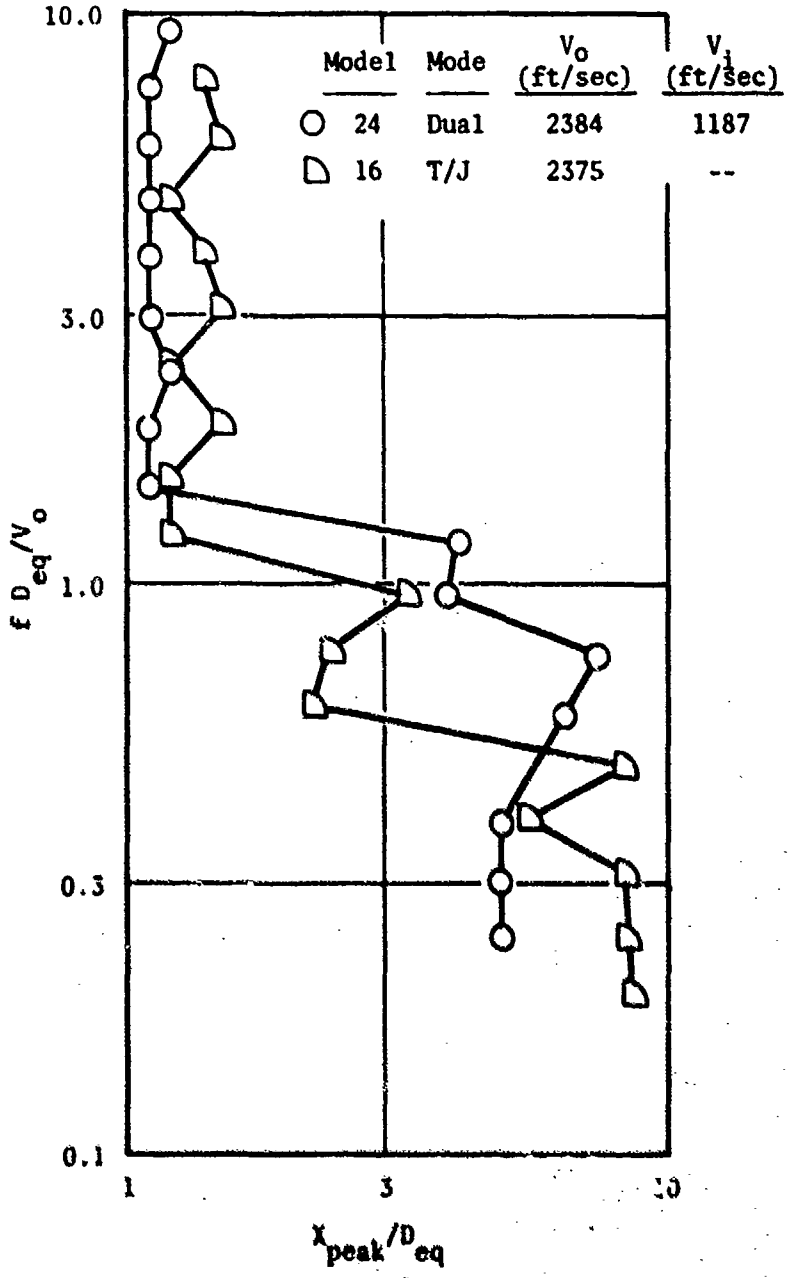

Figure 3-332. Comparison of Noise Source Distributions for Multichute Dual-Flow and Turbojet Suppressors.

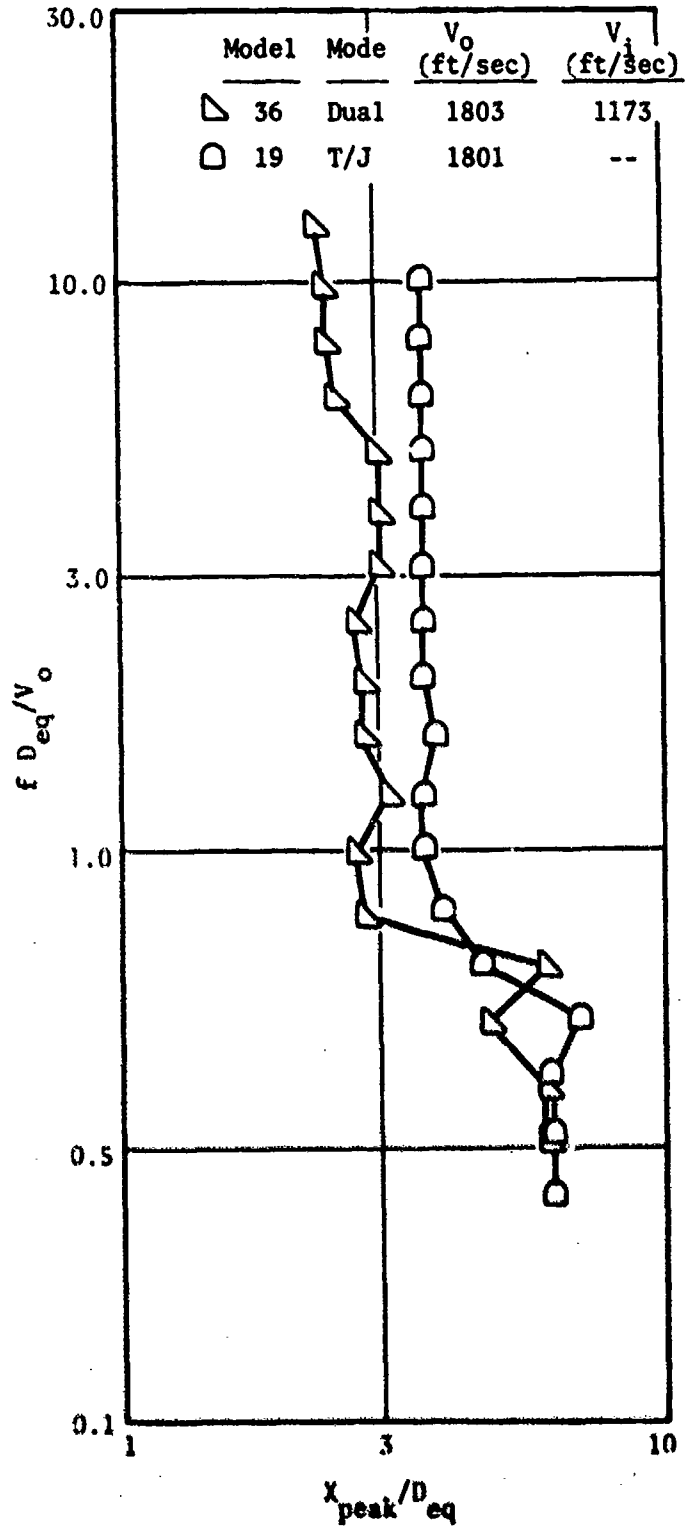

Figure 3-333. Comparison of Noise Source Distributions for Multichute Dual-Flow and Turbojet Suppressors with Ejectors.

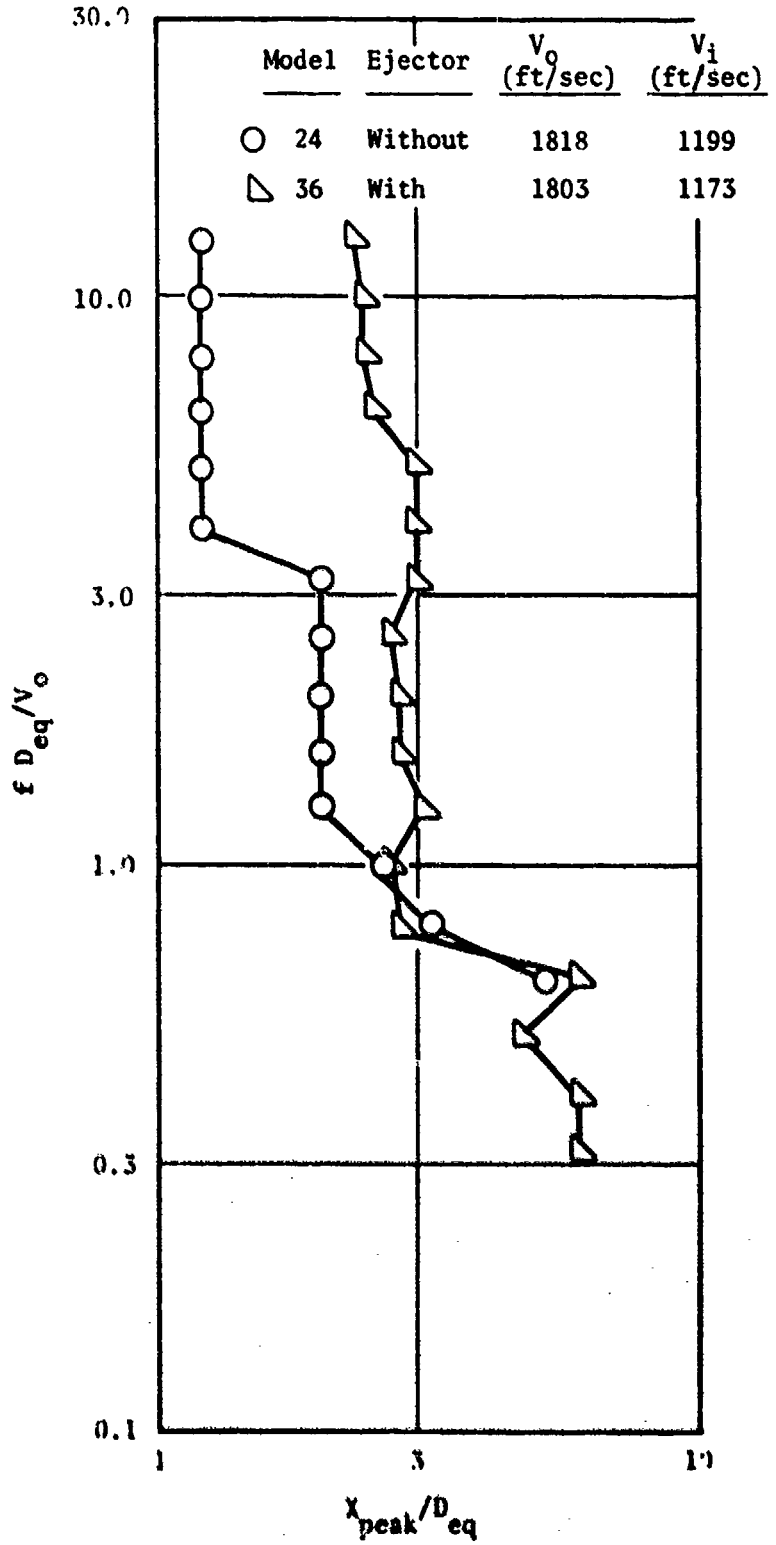

Figure 3-334. Effect of an Ejector on Multichute Dual-Flow Suppressor Noise Source Distributions.

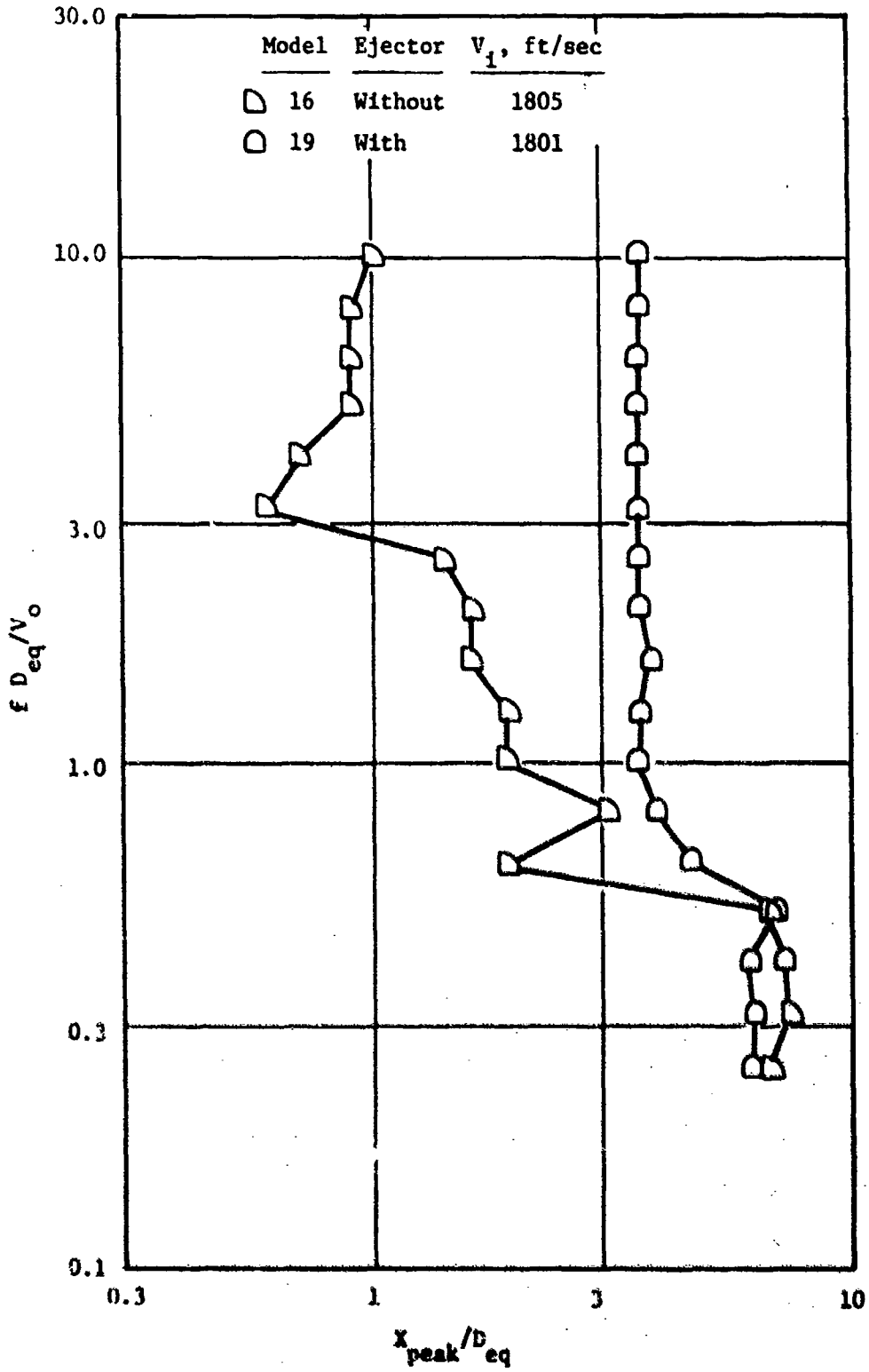

Figure 3-335 Effect of an Ejector on Multichute Turbojet Suppressor Noise Source Distributions.

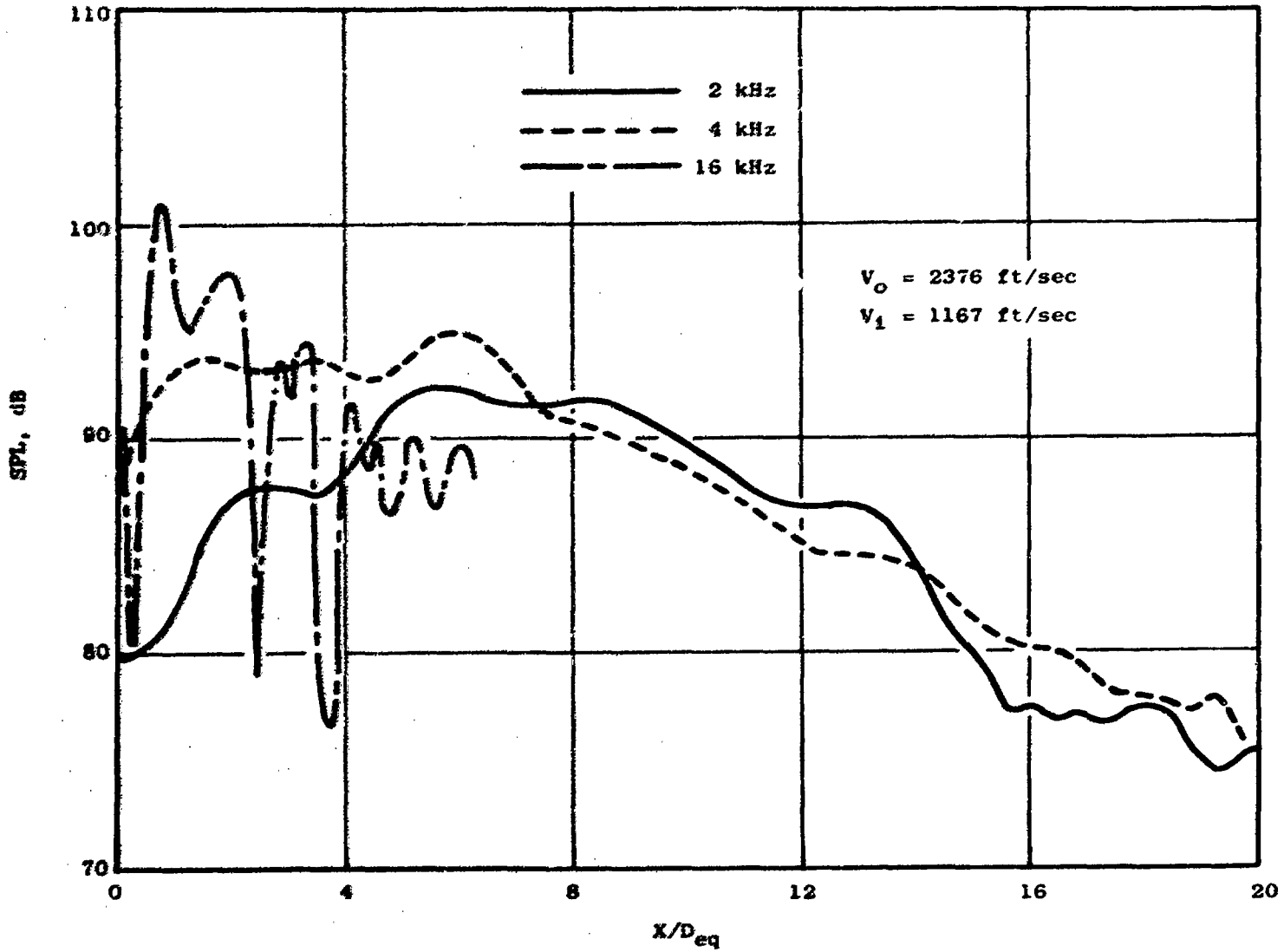

Figure 3-336. Axial Distributions of Sound Source Intensity for a 40-Shallow-Chute Dual-Flow Suppressor (Model 32).

4.0 AERODYNAMIC PERFORMANCE TEST PROGRAM

Historically, the introduction of mechanical jet noise suppression devices into the exhaust gases of turbine engines has resulted in significant losses in thrust, usually in proportion to the amount of suppression achieved. In addition, the base areas associated with suppressor elements introduce a performance (thrust loss) sensitivity to external flow conditions not normally encountered with nonsuppressing exhaust nozzles. The task of designing a viable jet noise suppressing exhaust system therefore depends heavily on an understanding of the effect of nozzle geometric parameters on in-flight suppression and performance. With this understanding, the designer can conduct trade studies leading to a low-noise exhaust system with good aerodynamic performance.

Past programs, such as the DOT Supersonic Transport Noise Reduction Technology Program, identified the annular (plug) nozzle with exit plane suppressor elements as a promising high velocity jet noise suppression system. A significant parametric data base on the effect of nozzle geometric variations, such as element number and area ratio, was, however, not available. More importantly, recent advances in engine technology (variable cycle engines) and acoustic work on the benefits of inverted flow nozzles with high radius ratios resulted in even greater voids in the available performance prediction technology base. Unknowns included the effect of inner nozzle geometry, location, and area on overall nozzle performance. In addition, high radius ratio, parametric jet noise suppressor performance data were unavailable. The current program provided the vehicle for filling these technology voids.

4.1 GENERAL PROGRAM OBJECTIVES AND SCOPE

The overall objective of the wind tunnel test program was to generate a comprehensive parametric data base on the aerodynamic performance of both dual- and single-flow annular nozzle/chute-type suppressor systems. These data would augment existing data from previous programs (such as the SST Phase II Program) and provide information necessary to conduct the trade studies and aircraft integration studies reported in Volume III, and provide design data for the noise abatement nozzle design guide (Task 6 of this program).

Specifically, the objectives of the aerodynamic performance test program were to obtain performance data under simulated flight conditions on the effects of suppressor area ratio, suppressor element number, and suppressor ventilation area. In the case of the dual flow nozzles, data were required on the effects of inner nozzle geometry. Suppressor element base pressure data were required as an integral part of the basic performance data. Previous programs had identified element base drag as the major contributor to exhaust system thrust loss. Parametric base pressure information would provide a basis for correlation of these data resulting in a performance

prediction tool for future design studies. The program involved the design and fabrication of model hardware, geometrically duplicating acoustic models described in Section 3.1, and testing in the Lewis Research Center 8- by 6-foot Wind Tunnel. Data obtained in the test program included nozzle thrust coefficients and model surface static pressures. Data were taken over a range of inner to outer stream pressure ratios representative of takeoff conditions with tunnel Mach numbers of 0.0, 0.36, and 0.45.

4.2 TEST FACILITY DESCRIPTION

The test program was conducted in the NASA-Lewis 8- by 6-foot supersonic wind tunnel. The test nozzles were mounted to a 8.5-inch diameter cylindrical sting which was supported in the test section by a perpendicular strut connected to the tunnel ceiling. A schematic and photograph illustrating this mounting system is shown in Figure 4-1. Air was supplied to the model through tubes running down the strut and emptying into coannular air passages leading aft to the model. The air source was a continuous supply of 450 psig compressor air which passed through a system of control valves, flowmeters, and into the strut. A schematic of the air supply system is shown in Figure 4-2. The outer nozzle air was metered through a 1.248 inch diameter choked venturi. The inner nozzle air supply was metered through either a 1.1398-inch or 0.3985-inch diameter choked venturi, depending on the flow rate required.

The nozzle thrust was measured with a load cell mounted in the forward portion of the sting as shown schematically in Figure 4-3. The coannular air passages in the sting were mounted to the load cell and were metric; i.e., forces on the coannular air passages were measured by the load cell. The air supply tubes internal to the strut were fixed to the tunnel ceiling and thus formed flexture columns bridging the nonmetric and metric portions of the test rig. Interactions resulting from the bridging are accounted for in the balance calibration. Airflow from the tubes entered the sting perpendicular to the sting axis and thus created no entering momentum force on the load cell. The air passages themselves where suspended inside the sting with bearings which supported the concentric passages and allowed the axial forces to be transmitted to the load cell. Static pressure instrumentation was located on the forward-facing portions of the internal metric hardware so that the tare force could be accounted for in cases where internal static pressures were different from ambient.

The load cell was calibrated by mounting the Supersonic Tunnel Association (STA) model on the sting and applying a known axial force along the centerline of the model and the load cell. This known force was generated by a hydraulic cylinder connected to a circular pad which applied force to the nozzle in an axial direction. The correlation of the known applied force and the millivolt output of the load cell comprised the desired calibration. The calibration was made from 0 to 1000 pounds, the maximum allowable balance load.

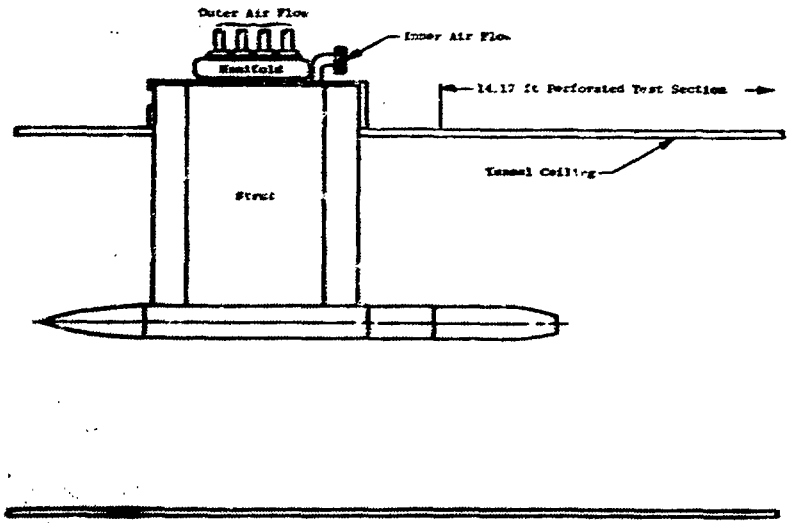

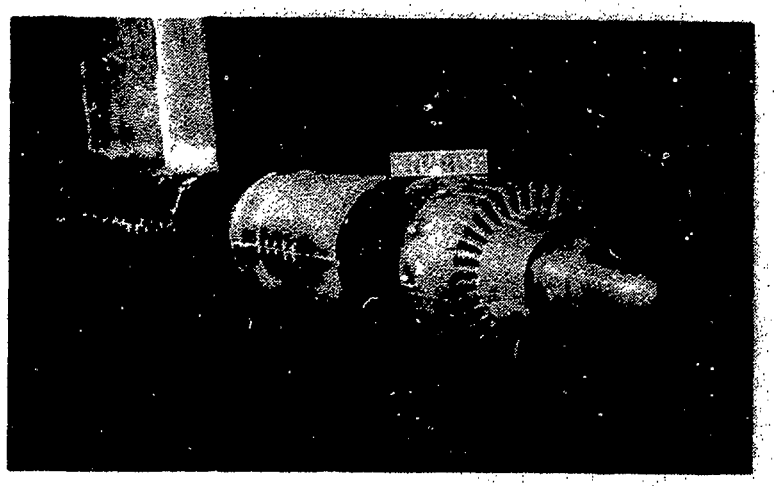

- Model Installed in 8 x 6 foot Supersonic Wind Tunnel
- Schematic of Model Mount System

Figure 4-1. Typical Model Installation.

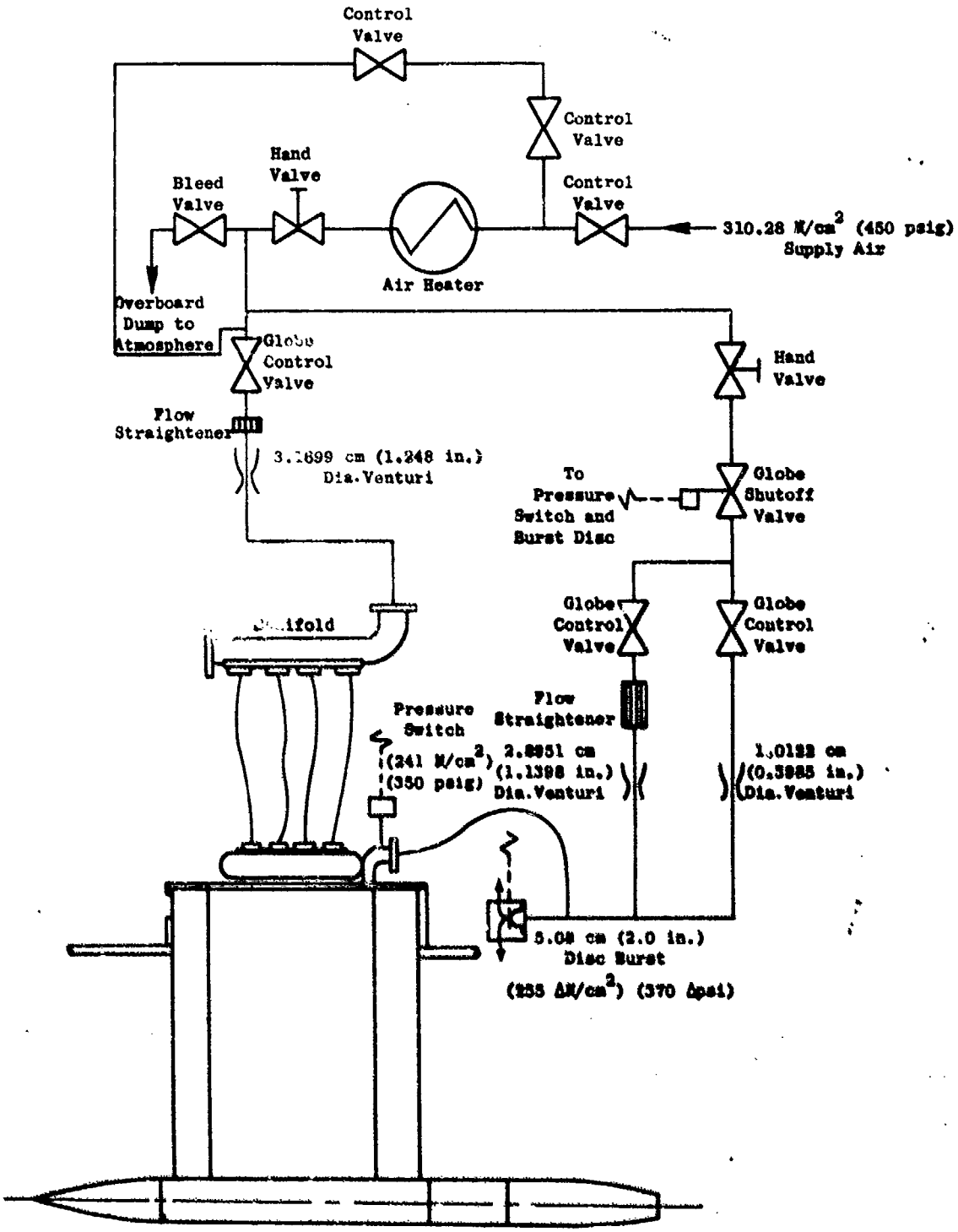

Figure 4-2. Schematic of Model Air Supply.

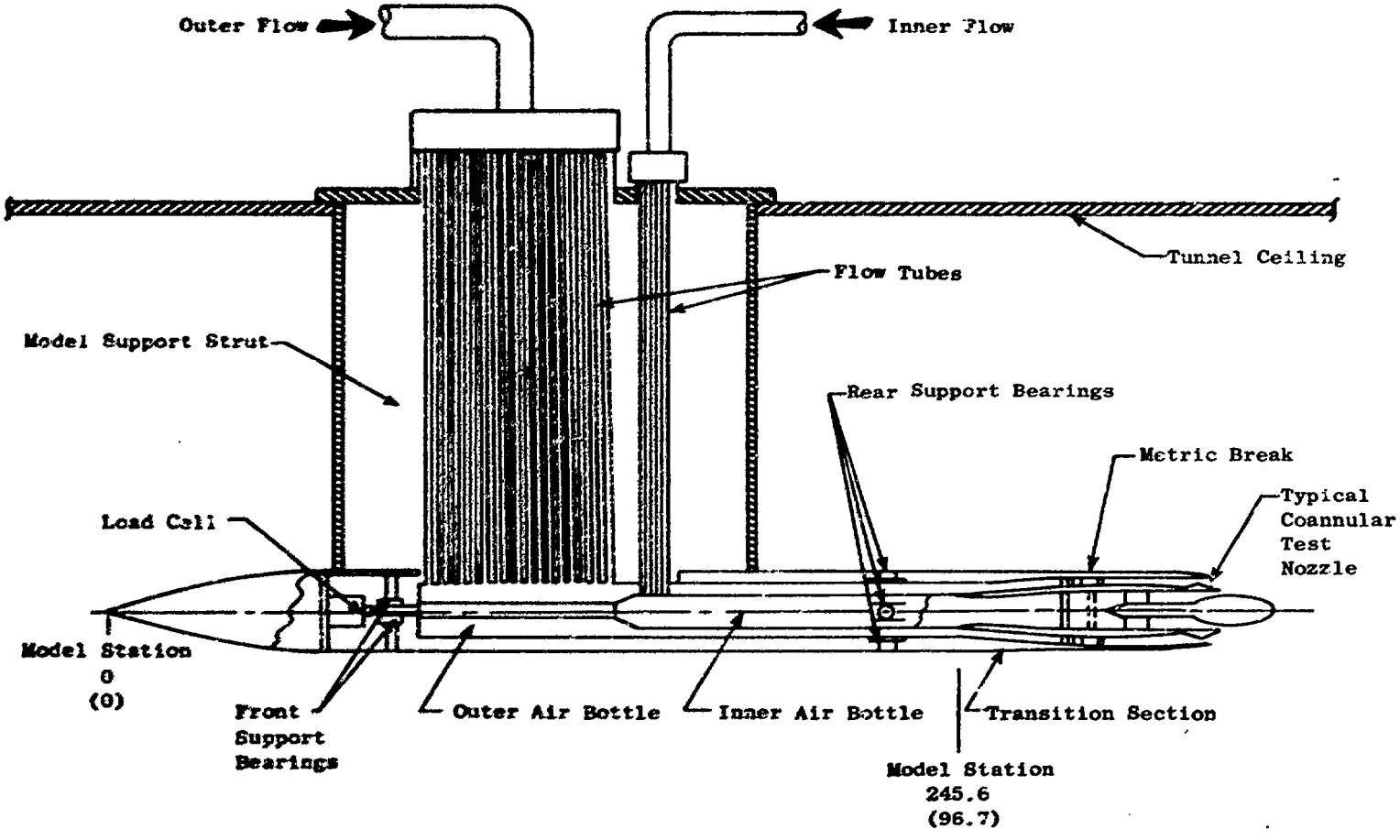

Figure 4-3. Schematic of Model Thrust-Measuring System.

4.3 MOLEL DESCRIPTION

The suppressor models tested in the NASA Lewis 8- by 6-foot supersonic wind tunnel included 15 annular suppressed nozzle configurations, a 104-tube nozzle, and an eight-lobe nozzle. The annular nozzles simulated both turbojet installations (single flow) and advanced, inverted-flow variable cycle engine installations (dual flow). In addition to the suppressor models, a reference nozzle, the Supersonic Tunnel Association (STA) model, was also tested. A description of these models is presented below. Details of the model geometries and instrumentation are presented in Appendix F.

4.3.1 Annular Suppressed Models

A schematic of a typical annular suppressed nozzle configuration is shown in Figure 4-4 to illustrate the variables investigated. Principle variables evaluated included: element number, N, for a given suppressor area ratio; suppressor area ratio, AR, for a given element number; inner nozzle area (or radius ratio); axial location of the inner plug, X; and chute ventilation area, or depth, d. Table 4-1 lists the configurations tested and key geometric variables. Figure 4-5 presents a pictorial summary of the models tested.

Basically the annular nozzles are representative of current concepts for supersonic transport exhaust systems. The two inner plug (15° half angle) axial locations represent either an expandable flap and seal design for inner area control ($X/D_{max.} = 0.412$) or a similar system with a translating plug ($X/D_{max.} = 0.161$).

The inner plug radius ratios tested represent a variation in engine cycle, i.e., the variation on the amount of fan flow relative to core flow for given pressure/temperature conditions in each stream. The $(R_r)_i = 0$ configurations are representative of a turbojet or mixed-flow turbofan design.

The shallow-chute suppressor designs, with a suppressor area ratio (AR) of 1.75, represent a potentially light, easily stowable system. Element number, N, was varied between 20 and 40, representing a practical range for this variable. Based on previous test experience, 20 represents a lower limit for reasonable suppression while 40 represents an upper limit for reasonable performance.

The deep-chute suppressor designs, with 36 elements, represent a system with good performance; i.e., the chute depth implies good ventilation for maintaining low base drag. The area ratio was varied between 1.5 and 2.5, again representing practical limits. In this case, 1.5 represents the lower limit for acoustic reasons and 2.5 an upper limit for mechanical design reasons.

In addition to the shallow-chute and deep-chute designs, a "spoke" suppressor was tested. The spoke suppressor has historically been an

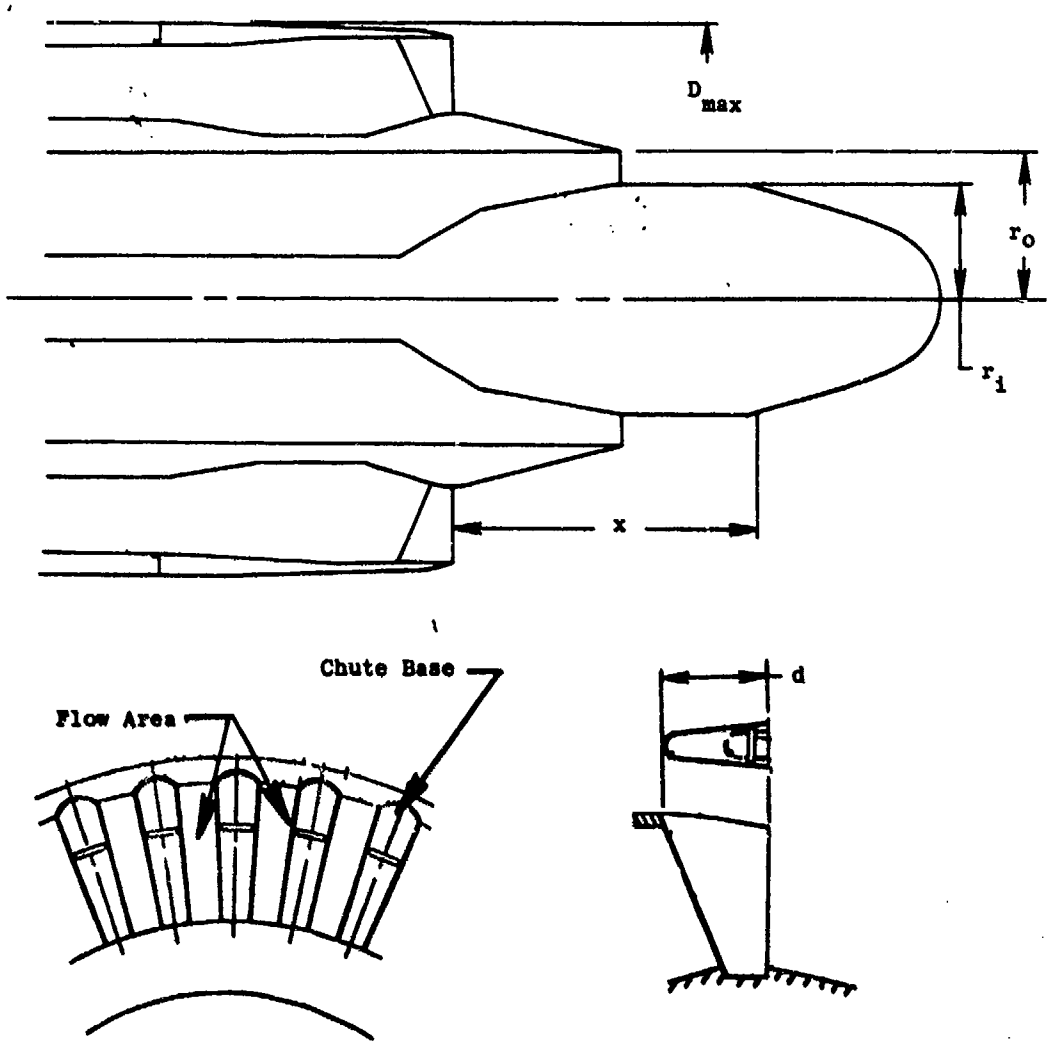

- Suppressor Area Ratio = $(A_o + A_{ch})/A_o$
  where: A_o = Total Outer Flow Area
  A_{ch} = Total Chute Base Area
- Element Number = N, Total Number of Suppressor Elements
- Chute Ventilation Depth = d
- Inner Nozzle Radius Ratio = $(R_r)_i = r_i/r_o$
  (r_o was Constant for all Dual Flow Configurations)
- Inner Plug Axial Spacing Ratio = x/D_{max}

Figure 4-4. Schematic of Annular Suppressed Nozzle Showing Key Geometric Variables.

Table 4-1. Nozzle Configuration Description.

Nozzle Configuration	Suppressor Type	N	AR	Inner Plug Description	$X/D_{max.}$	$(R_r)_i$
SC1	Shallow Chute	20	1.75	Baseline	0.412	0.78
SC2	Shallow Chute	30	1.75	Baseline	0.412	0.78
SC3	Shallow Chute	30	1.75	Reduced Area	0.412	0.89
SC4	Shallow Chute	30	1.75	Full	---	---
SC5	Shallow Chute	30	1.75	Forward	0.181	0.78
SC6	Shallow Chute	40	1.75	Baseline	0.412	0.78
DC1	Deep Chute	36	1.5	Baseline	0.412	0.78
DC2	Deep Chute	36	1.5	Full	---	---
DC3	Deep Chute	36	2.0	Baseline	0.412	0.78
DC4	Deep Chute	36	2.0	Reduced Area	0.412	0.89
DC5	Deep Chute	36	2.0	Full	---	---
DC6	Deep Chute	36	2.0	Forward	0.181	0.78
DC7	Deep Chute	36	2.5	Baseline	0.412	0.78
DC8	Deep Chute	36	2.5	Full	---	---
DC3 (Spoke)	Spoke	36	2.0	Baseline	0.412	0.78

Model	Suppressor Type	Number of Elements	Area Ratio	Flowpath	Photograph	Model Details in Figure No. (Appendix F)
SC-1	Shallow Chute	20	1.75	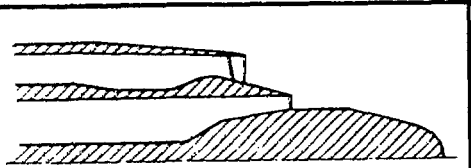	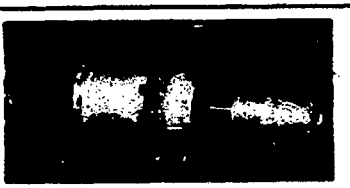	F-1
SC-2	Shallow Chute	30	1.75	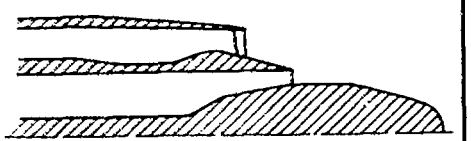		F-2
SC-3	Shallow Chute	30	1.75	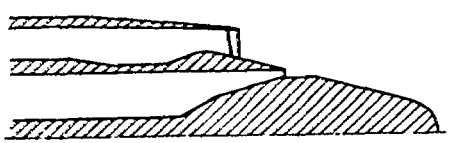		F-3
SC-4	Shallow Chute	20	1.75	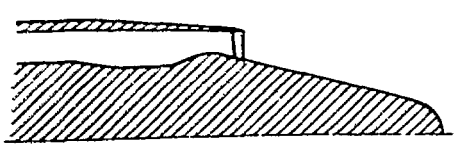		F-4

Figure 4-5. Summary of Annular Suppressor Models Tested.

Model	Suppressor Type	Number of Elements	Area Ratio	Flowpath	Photograph	Model Details in Figure No. (Appendix F)
SC-5	Shallow Chute	30	1.75	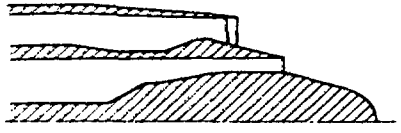		F-5
SC-6	Shallow Chute	40	1.75	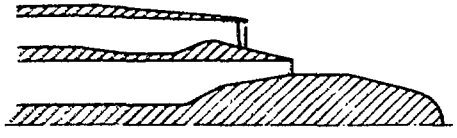	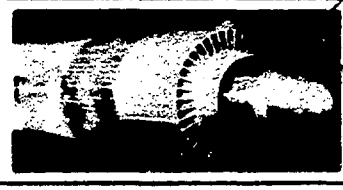	F-6
DC-1	Deep Chute	36	1.5	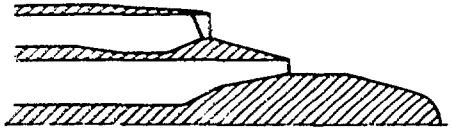		F-7
DC-2	Deep Chute	36	1.5	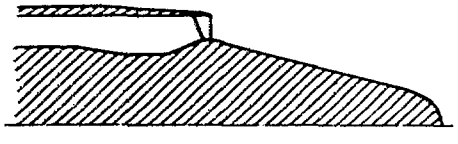	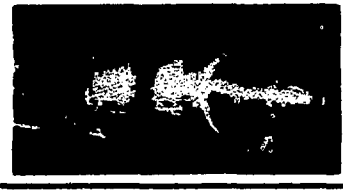	F-8

Figure 4-5. Summary of Annular Suppressor Models Tested (Continued).

Model	Suppressor Type	Number of Elements	Area Ratio	Flowpath	Photograph	Model Details in Figure No. (Appendix F)
DC-3	Deep Chute	36	2.0	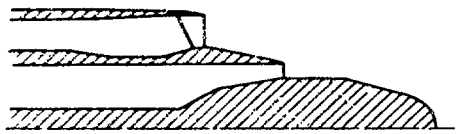		F-9
DC-4	Deep Chute	36	2.0	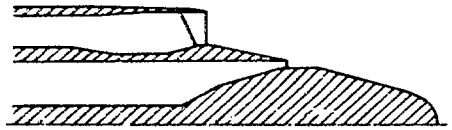		F-10
DC-5	Deep Chute	36	2.0	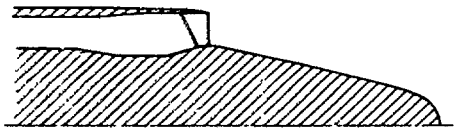	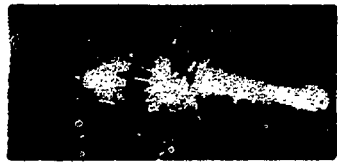	F-11
DC-6	Deep Chute	36	2.0	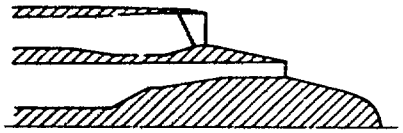		F-12

Figure 4-5. Summary of Annular Suppressor Models Tested (Continued).

Model	Suppressor Type	Number of Elements	Area Ratio	Flowpath	Photograph	Model Details in Figure No. (Appendix F)
DC-7	Deep Chute	36	2.5	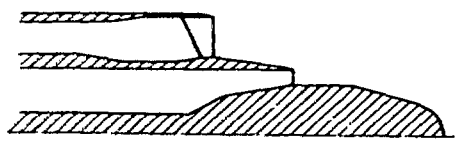	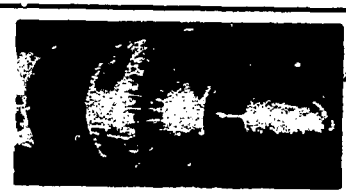	F-13
DC-8	Deep Chute	36	2.5	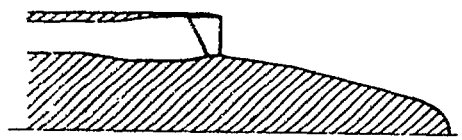	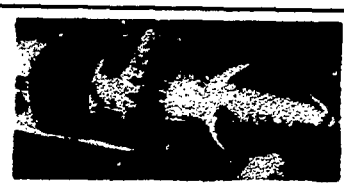	F-14
DC-3 (Spoke)	Spoke	36	2.0	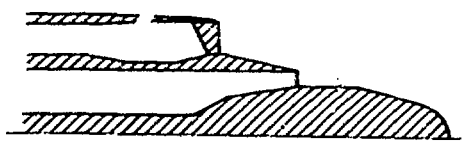	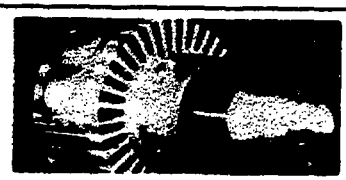	F-15

Figure 4-5. Summary of Annular Suppressor Models Tested (Concluded).

attractive concept due to its potential for low weight and ease of storage in the unsuppressed mode. The spoke configuration [model DC-3 (spoke)] was derived by filling the ventilation area of configuration DC-3 with inserts, as shown in Figure 4-5 and Figure F-15, Appendix F.

A schematic of a typical annular suppressed nozzle installed on the model support string is shown in Figure 4-6. Adapters connected the model flowpaths to the inner and outer air supply passages. The nozzle total pressure and temperature measurements were made with instrumentation rakes downstream of flow conditioners (choked plates and screens) to assure flat flow profiles. The outer diameter of the models was 8.0 inches, which required a reduction from the 8.5-inch diameter sting. This reduction was made via a nonmetric transition fairing. The metric break (the separation between the metric and nonmetric portion of the system) was provided by a 0.05-inch gap between the fairing and model shroud, as shown in Figure 4-6.

4.3.2 104-Tube Model

The 104-tube suppressor model was the same as that tested in the JENOTS free jet facility as described in Reference 12. A photograph of the model is shown in Figure 4-7. The model outer diameter is 7.245 inches and the physical throat area is 12.56 $in.^2$. The suppressor area ratio is 2.8. Key geometric parameters are shown in Figure 4-8.

4.3.3 Eight-Lobe Suppressor Model

The eight-lobe suppressor was also the same hardware tested in the JENOTS free jet under Task 4. A photograph of the model installed in the 8- by 6-foot wind tunnel is shown in Figure 4-9. The model outer diameter is 6.625 inches and the throat area is 13.121 $in.^2$. The model simulated a full-scale turbojet exhaust system which would utilize secondary air from the inlet to purge and cool the cavity between the nacelle and engine. The cooling air would exit at the trailing edge of the lobes. This secondary air gap can be seen in the closeup of the nozzle exit, Figure 4-9. For the wind tunnel test, the secondary airflow was not simulated.

4.3.4 Reference Nozzle

The Supersonic Tunnel Association (STA) nozzle was used as a reference and calibration device for the wind tunnel test series. This nozzle, shown in Figure 4-10, is basically a modified ASME nozzle with a circular-arc boattail. The use of the STA nozzle as a reference is described in detail in Section 4.5.1.

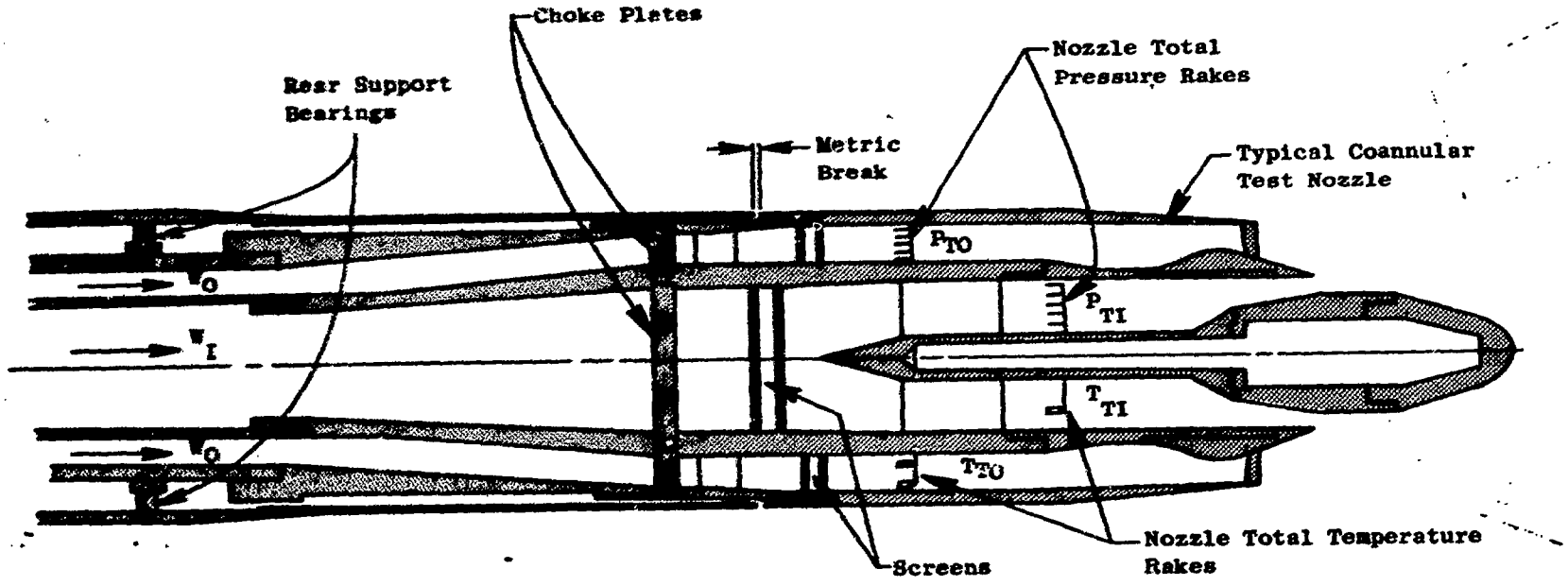

Figure 4-6. Schematic of Dual Flow Suppressor Installation.

Figure 4-7. 104 Tube Nozzle.

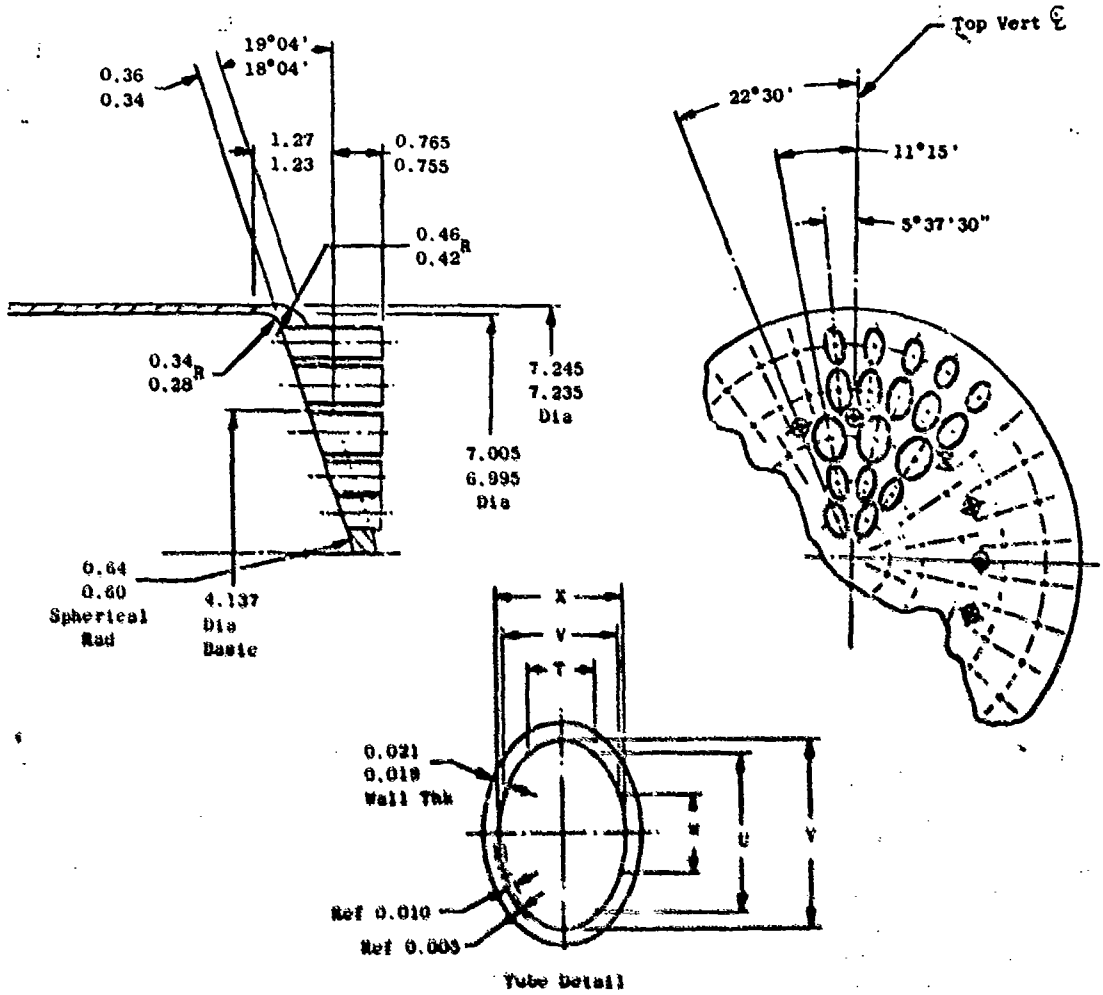

Tube	T Dim	U Dim	V Dim	W Dim	X Dim	Y Dim
A	0.113	0.420	0.227	0.227	0.260	0.465
B	0.130	0.488	0.273	0.273	0.317	0.529
C	0.149	0.558	0.365	0.368	0.466	0.589
D	0.113	0.420	0.227	0.227	0.260	0.465
E	0.113	0.420	0.227	0.227	0.260	0.465

Figure 4-8. 104 Tube Nozzle Geometric Details.

● 8-Lobe Nozzle Installation

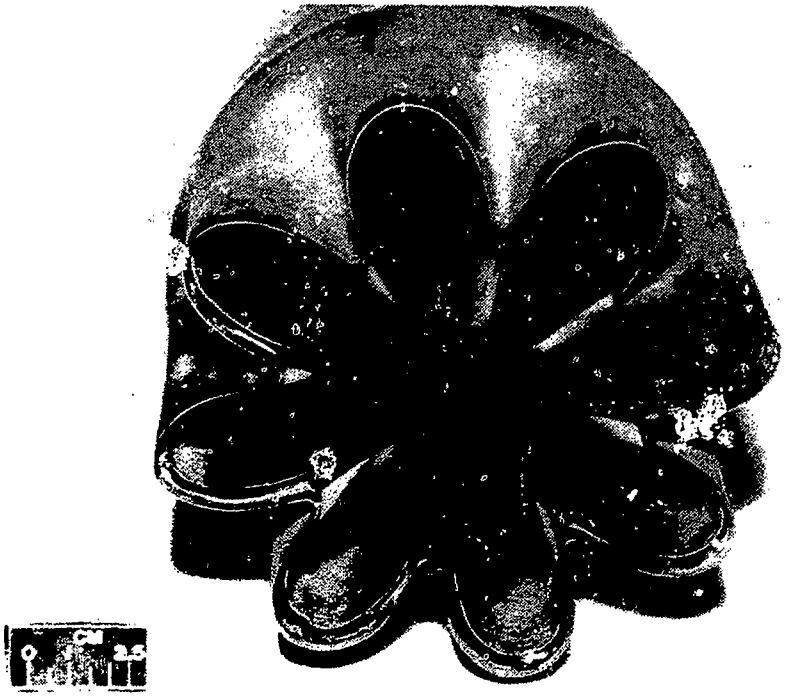

● Close-Up of 8-Lobe Nozzle Exit

Figure 4-9. 8-Lobe Nozzle.

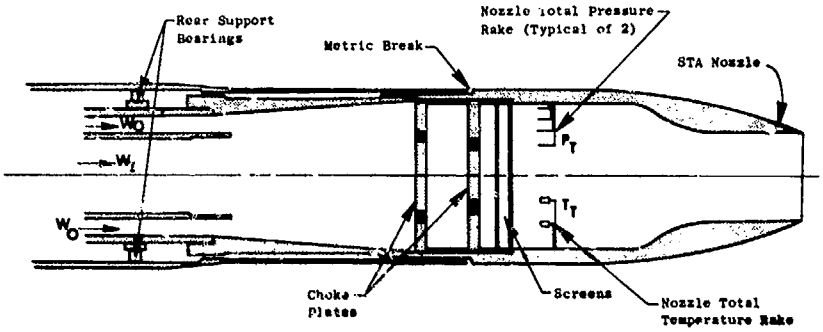

(a) Test Nozzle Internal Geometry and Instrumentation

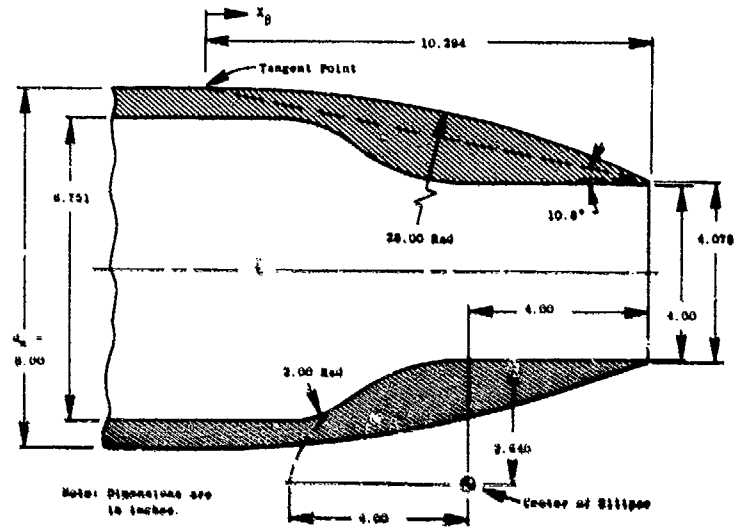

(b) Definition of Internal and External Flowpath

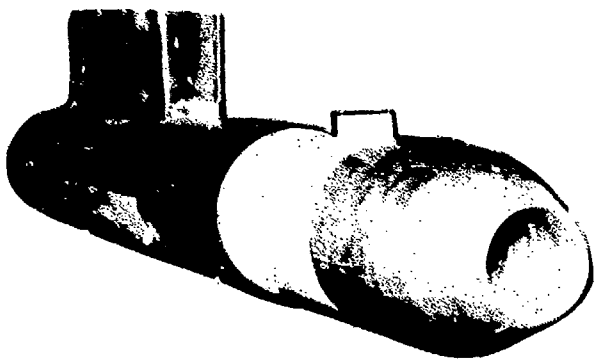

(c) Photograph of Nozzle

Figure 4-10. Supersonic Tunnel Association (STA) Nozzle.

4.4 DATA REDUCTION PROCEDURES

General descriptions of the methods used to determine model flow rates and nozzle thrust are contained in the following subsections. A more extensive detailing of the data reduction procedures is included in Appendix F.

4.4.1 Flow Rates

The mass flow through the outer nozzle was measured with a 1.248-inch throat diameter choked venturi meter, located as shown in Figure 4-2. The flow rate was calculated using the measured gas total temperature and pressure, T_{TV_o} and P_{TV_o}, respectively, and the equation:

$$W_o = C_{DV_o} \frac{K_{V_o} P_{TV_o} A_{V_o}}{\sqrt{T_{TV_o}}} \qquad (1)$$

where C_{DV_o} is the venturi flow coefficient. The critical flow factor, K_{V_o}, was calculated as a function of total pressure and temperature to account for real gas effects as given in Reference 36.

The mass flow through the inner nozzle was measured with either of two choked venturi meters located as shown in Figure 4-2. The flow for high inner flow rates was measured using the 1.1398-inch-throat-diameter venturi. The flow for the low inner flow rate testing was measured with the 0.3985-inch-throat-diameter venturi. For both meters, the flow rate was computed from a calibration of the meters made by the manufacturer utilizing the measured venturi pressure and total temperature.

4.4.2 Flow Coefficients

The flow coefficient of a nozzle is defined as the ratio of actual mass flow rate through the nozzle to the ideal isentropic flow rate at the temperature and pressure of the flow:

$$C_D = \frac{\text{measured flow}}{\text{ideal flow}} \qquad (2)$$

The ideal weight flow for the outer nozzle was calculated from the relation:

$$W_{I_o} = \frac{K_o A_o P_{T_o}}{\sqrt{T_{T_o}}} \frac{A^*}{A_o} \qquad (3)$$

where A_O, PT_O, and TT_O are the outer nozzle physical throat area, total pressure, and total temperature, respectively. The critical flow factor, K_O, was corrected for real gas effects; A^*/A_O is the ratio of the flow area at sonic conditions to the outer nozzle throat area ($A^*/A_O = 1.0$ for values of nozzle pressure ratios greater than 1.8929).

The inner nozzle ideal weight flow was calculated in a similar fashion using the inner nozzle throat area and the inner flow pressure and temperature. For the low inner flow testing, the inner nozzle total pressures required to supply the low flow rates were generally lower than ambient pressure due to the pumping effect of the outer flow. In these cases, the ideal flow rate and flow coefficients are meaningless and were not calculated.

4.4.3 Thrust Measurements

The thrust of the exhaust nozzles is defined as the axial exit momentum of the exhaust flow, plus the excess of exit pressure over ambient pressure times the exit area normal to the axis, minus the axial drag on the nozzle external surface, i.e.,

$$F = \int_{A_{exit}} d(wv)_{axial} + \int_{A_{exit}} (P-P_a)dA - D_{external} \qquad (4)$$

The external drag consists of both the pressure drag on the boattail surface and the and suppressor element bases, and the axial component of skin friction. Figure 4-11 shows a control volume applied to the test nozzles. The momentum equation in the axial direction for this control volume is:

$$F = F_{LC}+F_{AS}+A_1(P_1-P_a)+A_2(P_2-P_a)+A_3(P_3-P_a)+A_4(P_4-P_a) \qquad (5)$$

where F_{LC} is the axial force applied to the load cell and F_{AS} is the axial force applied at the boundary of the control volume by the air supply tubes. The static pressures P_1, P_2, P_3, and P_4 were measured with static taps at each of the four areas (Figure 4-11). The force measuring system was calibrated by applying known forces and correlating this force against the load cell output, as previously described in Section 4.2.

An adjustment was made to the measured thrust to account for external friction drag on the cylindrical section upstream of the nozzle shroud. The axial force on this 8.0-inch diameter section, which extended from the metric-break to the attach-point of the nozzle shrouds, was not included in the nozzle net thrust. The friction drag was calculated by the equation:

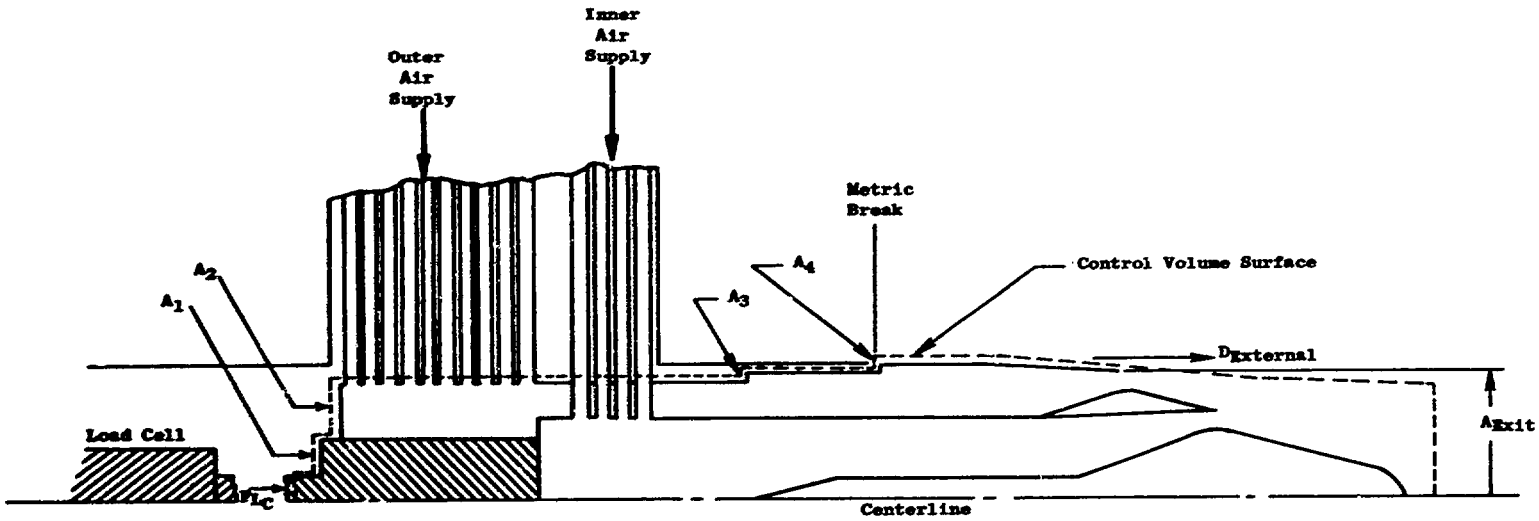

Figure 4-11. Control Volume Applied to Model Test Setup.

$$D_f = \frac{\gamma}{2} P_a \ M_a^2 \ A_c \ C_f \tag{6}$$

where A_c is the wetted surface area of the cylindrical section and C_f is the skin friction drag coefficient.

The thrust of the nozzles for this test was therefore given by:

$$F = F_{LC}+F_{AS}+A_1(P_1-P_a)+A_2(P_2-P_a)+A_3(P_3-P_a)+A_4(P_4-P_a)+D_f. \tag{7}$$

4.4.4 Thrust Coefficient

The thrust coefficient is the ratio of the measured nozzle thrust to the ideal thrust of the inner duct flow plus the ideal thrust of the outer duct flow. The ideal thrust for each stream equals the actual mass flow rate times the ideal velocity, i.e., the velocity of the stream expanded isentropically from the total pressure to the ambient pressure. The equation for the thrust coefficient is thus:

$$C_T = \frac{F}{W_o V_{I_o}+W_i V_{I_i}} \tag{8}$$

The ideal thrust for the nozzles was calculated using the dimensionless ideal-thrust function which is a function of only the nozzle pressure ratio.

During much of the low inner flow rate testing, the total pressure of the inner nozzle flow was lower than ambient. In these cases, the ideal thrust of the inner nozzle was set equal to zero.

For the static tests of the STA model, a dimensionless stream-thrust parameter was also calculated as:

$$f_g = \frac{F + P_a A_9}{P_T A_9} \tag{9}$$

where A_9 is the STA nozzle exit area.

4.4.5 Pressure Data

Total pressures in the models and static pressures on the model surfaces were measured with scanning valve/transducer arrangements. The individual static pressure readings were also nondimensionalized by the ambient pressure. Axial pressure forces on the aft-facing portions of the shroud, outer

plug, inner plug, and suppressor element bases were calculated by multiplying the difference between the static pressure at each tap and ambient by an incremental projected area represented by the particular tap and summing the products, i.e.,

$$F_p = \Sigma(P-P_a)\Delta A \tag{10}$$

These pressure forces were also nondimensionalized by the total ideal thrust of the nozzle:

$$\frac{F_p}{W_i V I_i + W_o V I_o} \tag{11}$$

Specific tap locations are presented in Appendix F.

4.5 TEST RESULTS AND DISCUSSION

4.5.1 Data Quality

Prior to testing the plug nozzle models in the 8- by 6-foot tunnel, a Supersonic Tunnel Association (STA) model was tested as a means of investigating the force and weight-flow measurement accuracy of the test equipment. The STA model assembly is shown in Figure 4-10. The model has a 4.0-inch diameter throat and an 8.0-inch maximum outside diameter, corresponding to the 8.0-inch maximum outside diameter of the annular nozzle models. Air could be supplied to the STA model using either the outer or inner flowpath as shown in the schematic of Figure 4-10. The tests were conducted with air supplied through either the 1.248-inch-diameter meter for the outer nozzle air supply or with air supplied by the larger of the two inner flowmeters, which was 1.1398 inch in diameter. The smaller of the two inner flowmeters was not tested with the STA model because flow sufficient to choke the STA model could not be supplied due to pressure limitations. This did not compromise the the facility checkout because the small meter was used only to meter flow for the low inner flow test points, where the flow rates ranged from one to six percent of the outer flow. Small errors in this measurement could not affect overall results.

The criteria against which the STA measurements were compared to determine the facility thrust and flow measurement accuracies were calculated values of STA thrust coefficient, flow coefficient, and dimensionless stream-thrust parameter for the static tests and previous measured values for wind-on testing. The calculated static values are derived from semi-empirical methods of calculating standard ASME long radius nozzle performance, as described in Reference 37. These ASME equations are modified to include the effect of a small difference in length of the internal flowpaths between the ASME and STA nozzles. The resulting equations, for nozzle pressure ratios equal to or greater than 1.89, are as follows:

$$C_D = 1 - 0.241\ RN^{-0.2}$$

$$C_V = 1 - 0.143\ RN^{-0.2}$$

$$F_9 = G(1 + 1.4\ C_D\ C_V)\ (0.52828)$$

where

$$G = 1.00012 + 9,9112 \times 10^{-6} \times P_T$$

and C_V is the peak thrust coefficient.

These equations are based on a large data base and provide an accurate method for calculating the static STA nozzle performance parameters. For the wind-on tests, the data are compared to previous results on the same STA model in the NASA Lewis 8- by 6-foot tunnel using different flowmetering and force measuring hardware. These previous tests are reported in Reference 38.

Comparisons of the measured static thrust and flow coefficients and stream-thrust parameter with the calculated values are shown in Figures 4-12 and 4-13 for the 1.248-inch and 1.1398-inch-diameter meters, respectively. Figure 4-14 compares the measured thrust coefficient to previous test results at Mach numbers of 0.36, 0.40, and 0.45. Agreement between the measured values and the calculated or previously determined data is good, as is the repeatability of the data (five to eight static points and two wind-on points were taken at most nozzle pressure ratios). Repeatability of the wind-on data was better than the static data, possibly due to the increased tunnel vibration which would reduce hysteresis in the support bearings.

The number of repeat points taken at static conditions allowed a statistical evaluation of the data. Standard deviations and the bias of the mean value of the data from the "known" (or calculated) value were calculated by the following equations:

$$\text{Standard Deviation} = \sqrt{\frac{\Sigma(X_i - \bar{X})^2}{n - 1}} \qquad (12)$$

$$\text{Bias} = \bar{X} - m$$

where

X_i = individual measured value of the parameter (e.g., thrust coefficient or flow coefficient)

$\bar{X}$ = mean of measured values of the parameter

m = known value of parameter

n = number of samples taken of the given parameter

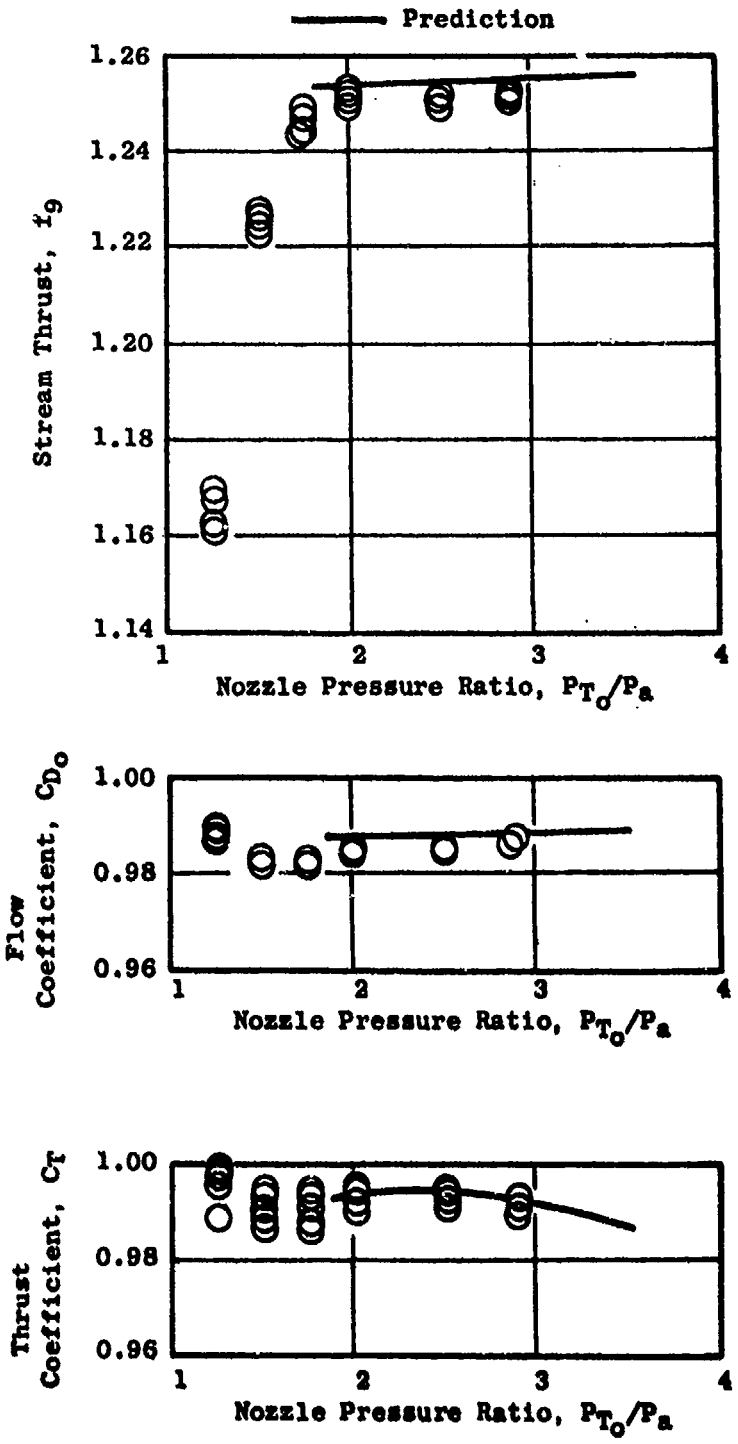

Figure 4-12. STA Static Performance with the 1.248-in.-Diameter Outer Flowmeter.

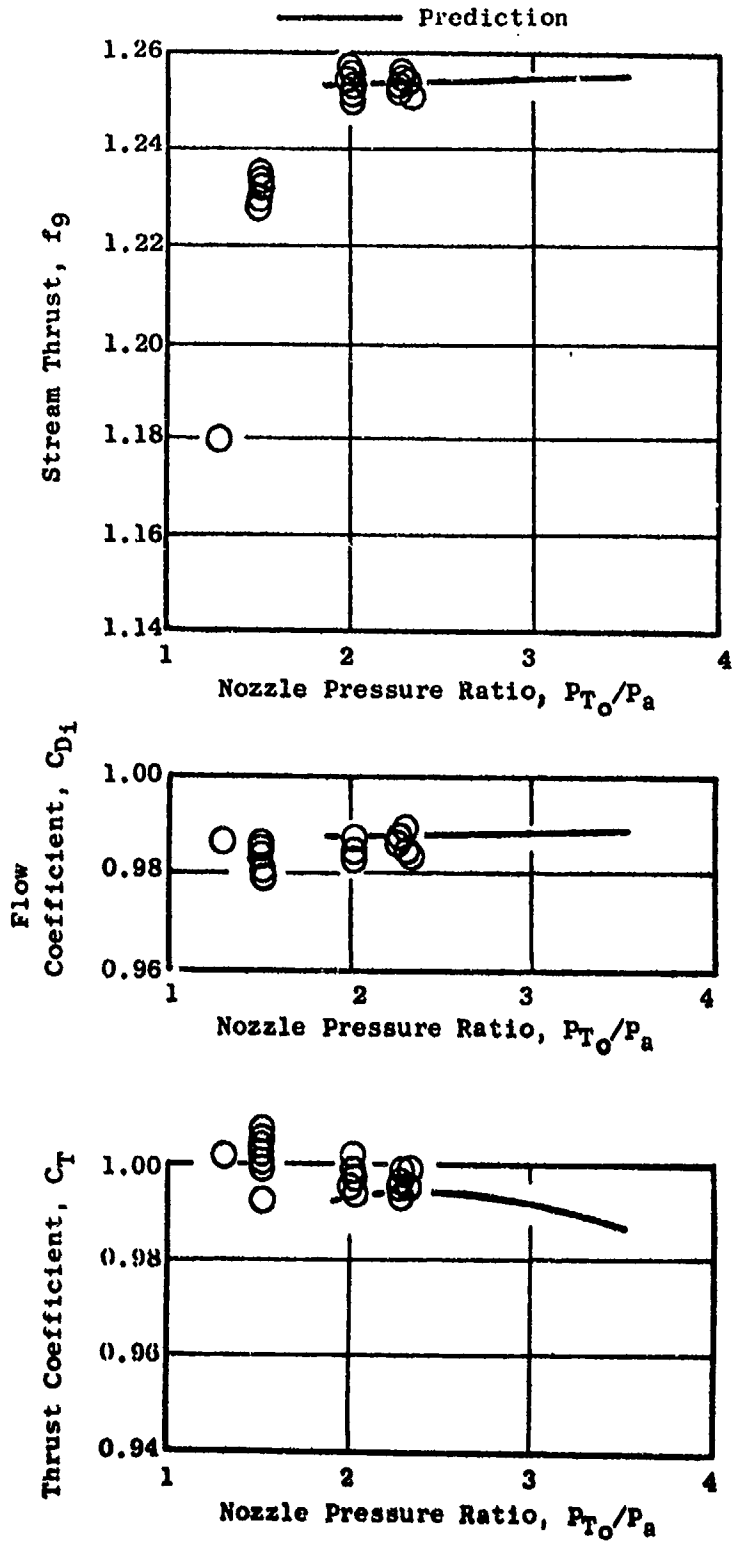

Figure 4-13. STA Static Performance with the 1.1398-in.-Diameter Inner Flowmeter.

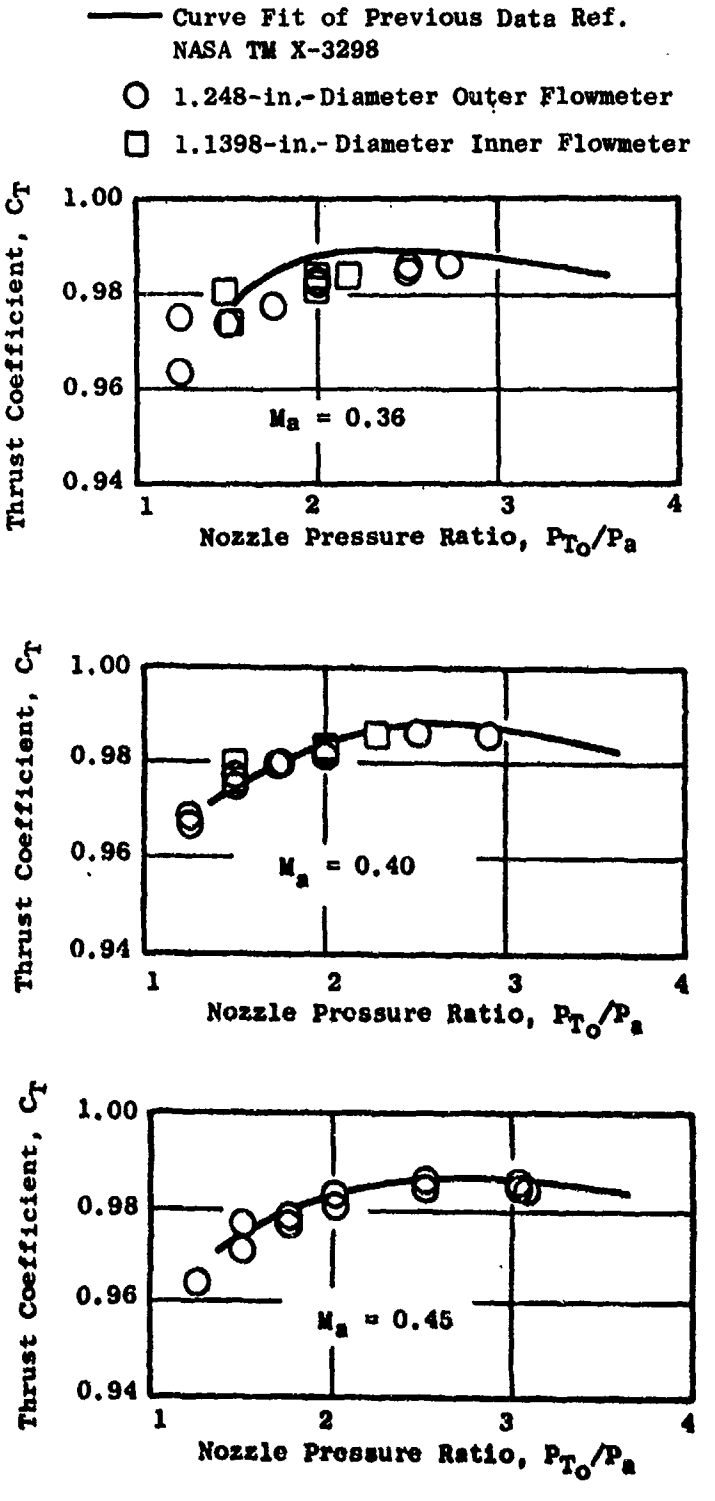

Figure 4-14. Wind-On STA Nozzle Thrust Coefficients.

Standard deviation calculations were made at each pressure ratio for which repeat points were taken. Bias calculations were made at each pressure ratio above 1.89 for which repeat points were taken, as the calculation procedure for the known values does not apply below this pressure ratio. The procedure used for taking repeat points was to set each data point once in the order of increasing nozzle pressure ratio and then repeat each point going down in pressure ratio, until a zero flow condition was reached; then the process was repeated. In some instances either wind-on test points or tests utilizing the other flowmeter were conducted between repeating cycles.

The results of the statistical analysis are shown in Figures 4-15 and 4-16 for the thrust coefficient and flow coefficient, respectively. The thrust coefficient deviation and bias were dependent on the magnitude of the nozzle thrust and are, therefore, plotted as a function of balance load in Figure 4-15. The flow coefficient parameters are shown as a function of the flowmeter total pressure over the range for which STA data were taken. The upper limit to the STA model airflow and force balance loading was the maximum supply pressure at the venturis, approximately 400 to 420 psia. These results indicate an accuracy and repeatability of greater than ±0.5% which are well within acceptable limits for the test program. Additional information can be found in Reference 38.

4.5.2 Annular Nozzle Thrust Coefficients

A total of 15 suppressed annular nozzle configurations was tested. All configurations were tested at tunnel Mach numbers of 0, 0.36, and 0.45. The outer nozzle pressure ratio was varied from 1.5 to 3.3. Two separate regimes of inner nozzle flow conditions were investigated; a "low" or bleed flow regime where the inner nozzle flow rate was varied from zero to six percent of the outer nozzle flow, and a "high" flow regime in which the inner stream pressure ratio was varied from 1.5 to 3.5.

Performance in terms of nozzle thrust coefficient, C_{fg}, is summarized for the 15 annular suppressed configurations in Table 4-II. The thrust coefficients presented in the table were selected at a nominal inner and outer nozzle pressure ratio, P_{T_I}/P_a and P_{T_O}/P_a, of 2.5. Both static (M_a = 0) and Mach 0.36 performance are listed. Table 4-2 illustrates the "spread" in performance obtained between the various configurations and also illustrates differences between static and wind-on performance. The detailed performance of each nozzle as affected by inner and outer nozzle pressure ratios and external flow conditions is included in Appendix F. Also contained in Appendix F are the summary off-line data printouts containing all key measured parameters.

4.5.3 Effect of Suppressor Element Number

The effect of the number of suppressor elements on performance, for a given suppressor area ratio, can be investigated by comparing model SC-1, SC-2, and SC-6 test results. Thrust coefficients are presented in Figure 4-17 as a function of suppressor element number and inner nozzle pressure

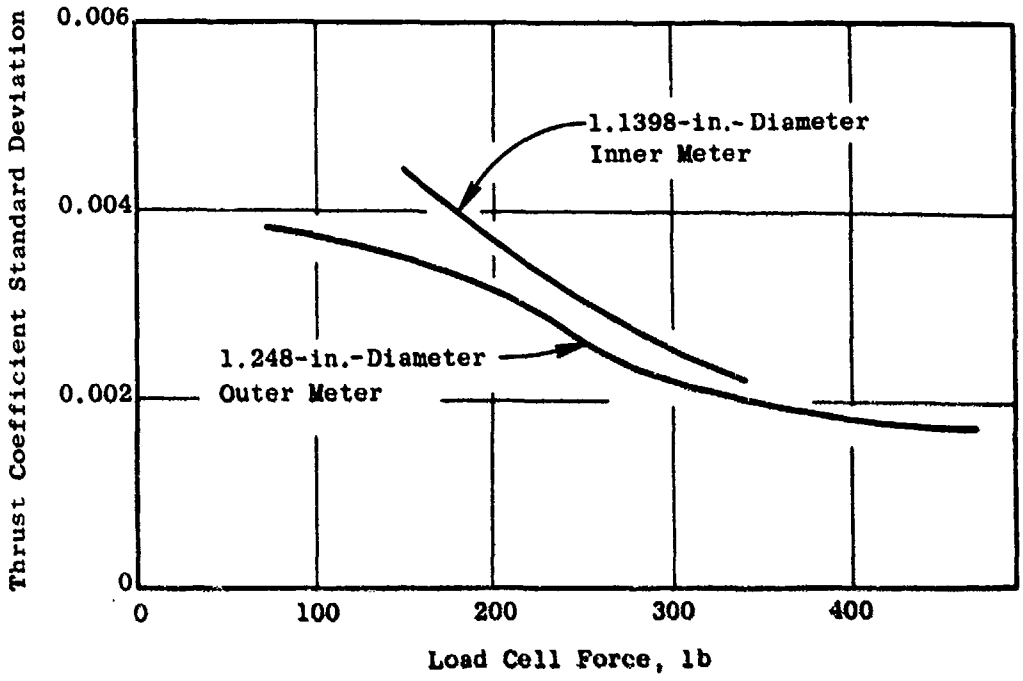

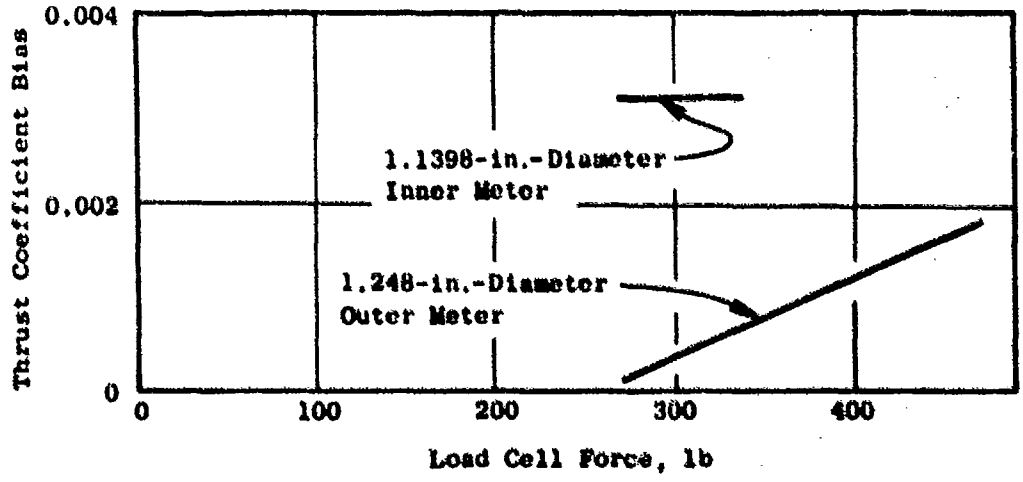

Figure 4-15. STA Nozzle Bias and Standard Deviation on Static Thrust Coefficient.

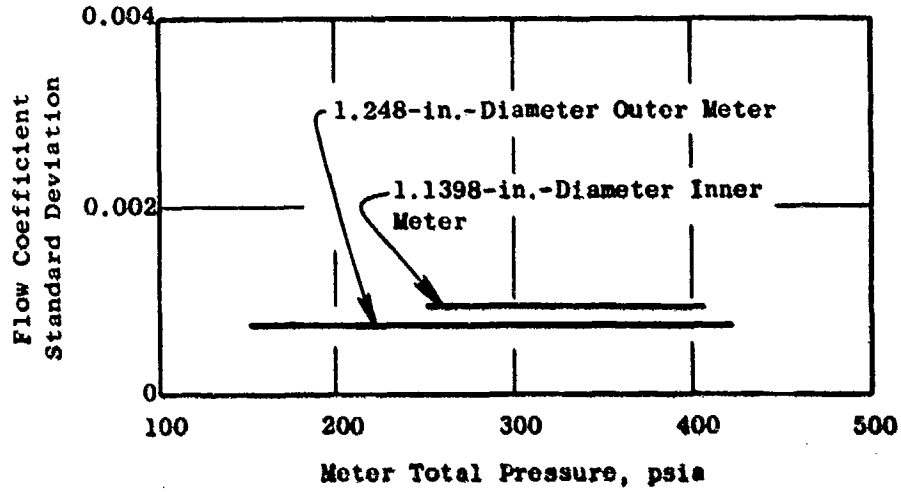

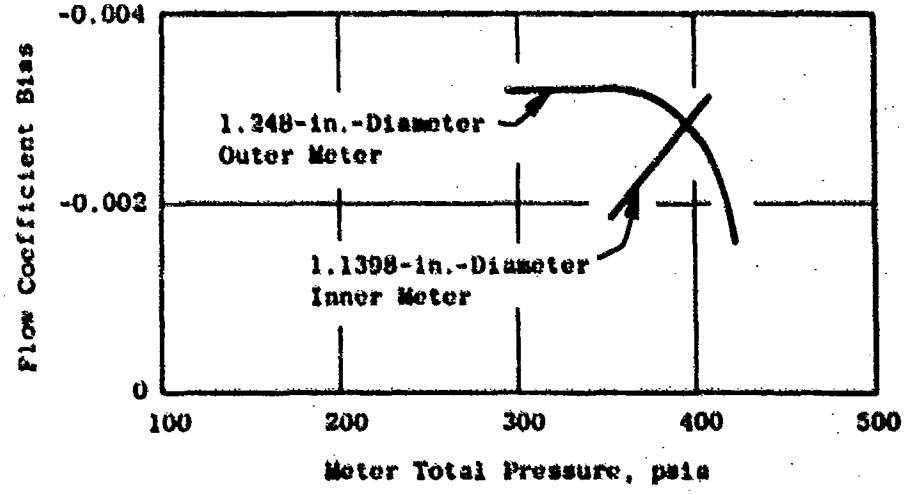

Figure 4-16. STA Nozzle Bias and Standard Deviation on Flow Coefficient.

Table 4-2. Annular Nozzle Performance Summary.

Area [illegible]	No. Elements	Description	Inner Plug Geometry: Full $(R_r)_i = 0$	Baseline $(R_r)_c = 0.78$	Reduced Area $(R_r) = 0.89$	Forward Plug
1.75	20	Shallow Chutes		0.929*(0.955)		
"	30	"	0.895(0.927)	0.914(0.934)	0.907(0.934)	0.918(0.941)
"	40	"		0.906(0.923)		
1.5	36	Deep Chutes	0.895(0.920)	0.920(0.933)		
2.0	"	"	0.877(0.910)	0.910(0.941)	0.894(0.936)	0.907(0.944)
2.0	"	Spokes		0.863(0.884)		
2.5	"	Deep Chutes	0.890*0.957)	0.913(0.958)		

* C_{fg} Overall at $P_{T_0}/P_a - P_{T_I}/P_a = 2.5$, $M_a = 0.36(0)$

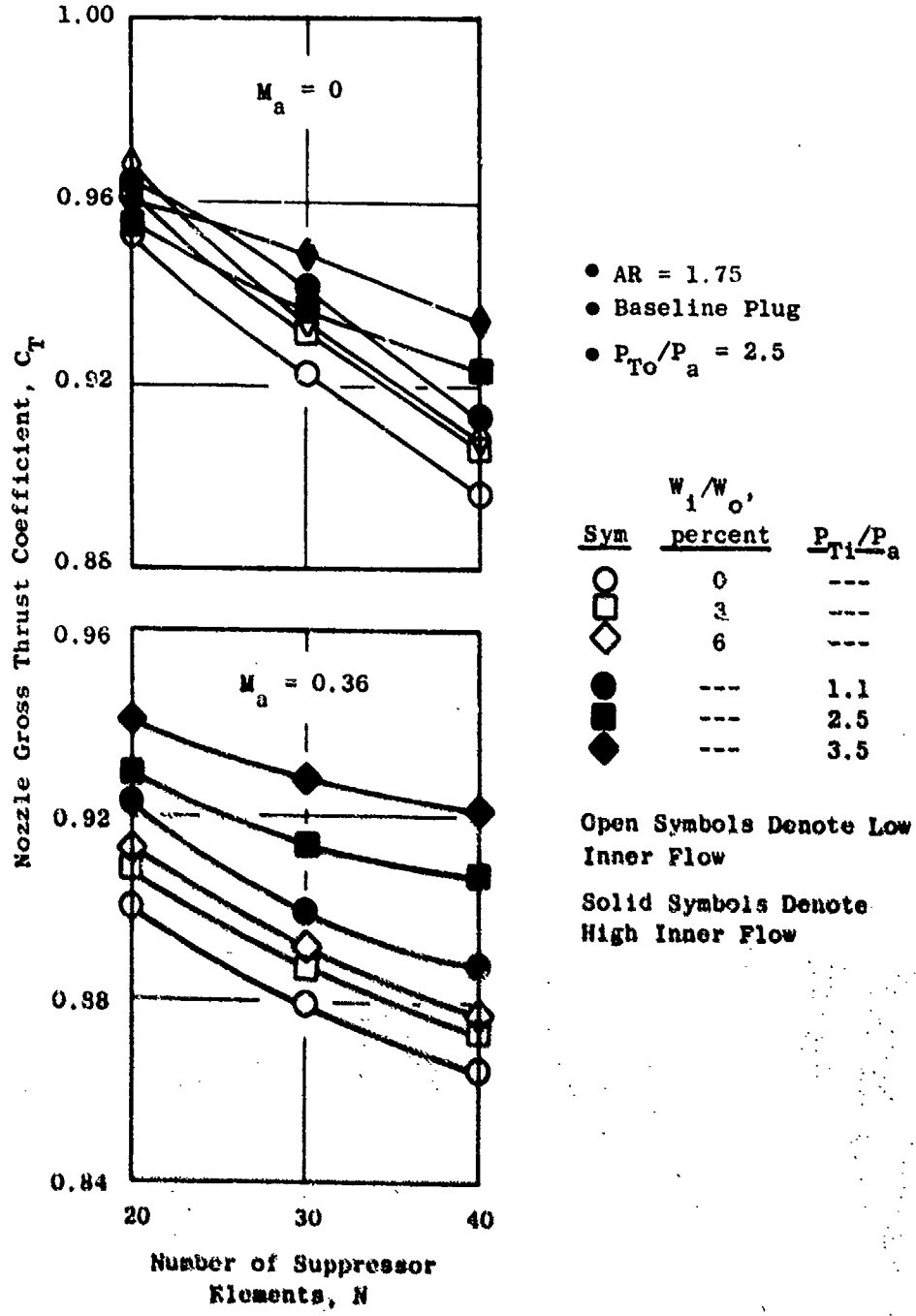

Figure 4-17. Effect of Suppressor Element Number and Inner Flow on Nozzle Gross Thrust Coefficients of Shallow-Chute Nozzles.

ratio for an outer pressure ratio of 2.5 at static and Mach 0.36 conditions. In all cases, performance decreases as element number increases. For an inner nozzle pressure ratio of 2.5, the thrust coefficient decreased from 0.929 for 20 elements to 0.907 for 40 elements. This decrease in nozzle performance with element number reflects the increase in element base drag as illustrated in Figure 4-18 where both performance and element base drag, in terms of ideal thrust, are shown as a function of element number and external Mach number for an inner and outer nozzle pressure ratio of 2.5.

Figure 4-19 presents trends in performance as a function of element number and outer pressure ratio for an inner pressure ratio of 2.5. Note that performance sensitivity to element number increases as outer pressure ratio increases. In summary, performance is adversely affected by an increase in the number of elements for a given suppressor area ratio at outer nozzle pressure ratios greater than 1.5.

4.5.4 Effect of Suppressor Area Ratio

The effect of suppressor area ratio on performance can be investigated by comparing test results for models DC-1, DC-3, and DC-7. Thrust coefficients as a function of suppressor area ratio and inner nozzle flow condition for a constant outer nozzle pressure ratio of 2.5 are presented in Figure 4-20. At static conditions, performance increases as area ratio increases for all inner flow conditions. At Mach 0.36, performance first decreases, then increases with area ratio for "low" flow conditions and remains relatively constant for "high" inner flow conditions. These trends appear to contradict element base pressure drag trends shown in Figure 4-21. Figure 4-21 illustrates the loss in gross thrust due to element base pressures as a function of suppressor area ratio for inner and outer nozzle pressure ratio of 2.5. Statically, the base drag loss does not vary with area ratio, while at Mach 0.36 and 0.45, drag increases with area ratio. The reason for this apparent anomaly is that, in conjunction with increasing area ratio, the plug half angle immediately downstream of the suppression was decreased. The angle was 15.8° for the area ratio 1.5 suppressor, 11.7° for the area ratio 2.0, suppressor, and only 7.4° for the area ratio 2.5 suppressor (see Appendix F). In addition, as area ratio was increased, the external shroud boattail angle and projected area were decreased. As a result, shroud and plug drag decreases tended to compensate for the increased element drag at Mach 0.36 and 0.45 as area ratio was increased. Based on previous experience with increasing area ratio, Reference 3, it could be expected that if the plug angle downstream of the suppressor were held constant as area ratio was increased, the performance trend at Mach 0.36 and 0.45 would follow the same trend as the element base pressure losses, i.e., lower performance with higher area ratios.

4.5.5 Effect of Inner Nozzle Area (Inner Radius Ratio)

Trends in performance as the inner nozzle area is varied can be investigated by comparing model SC-2, SC-3, and SC-4 (AR 1.75, 30 shallow

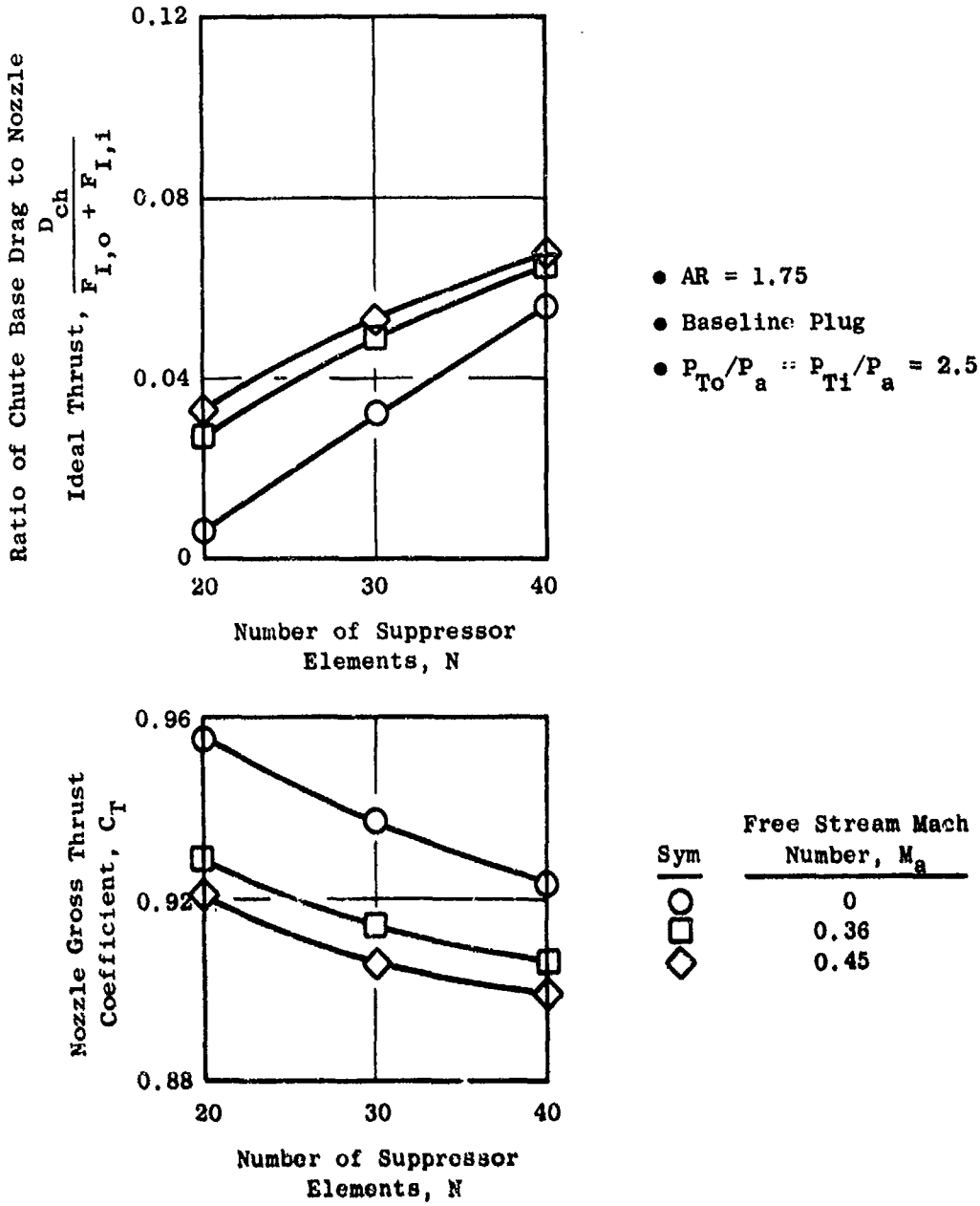

Figure 4-18. Effect of Suppressor Element Number and Free-Stream Mach Number on Nozzle Performance of Shallow-Chute Nozzles.

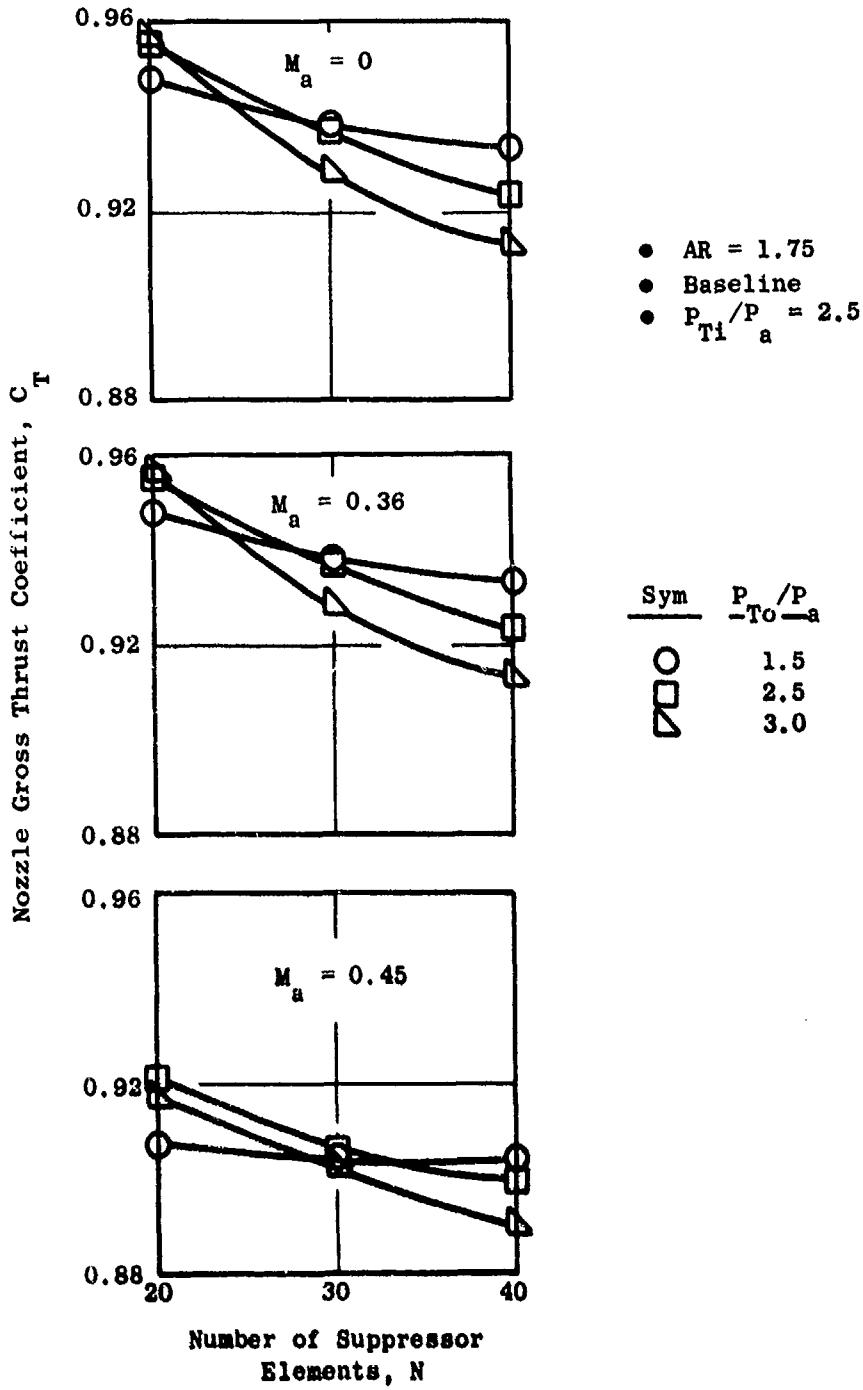

Figure 4-19. Effect of Suppressor Element Number and Outer Flow on Nozzle Gross Thrust Coefficients of Shallow-Chute Nozzles.

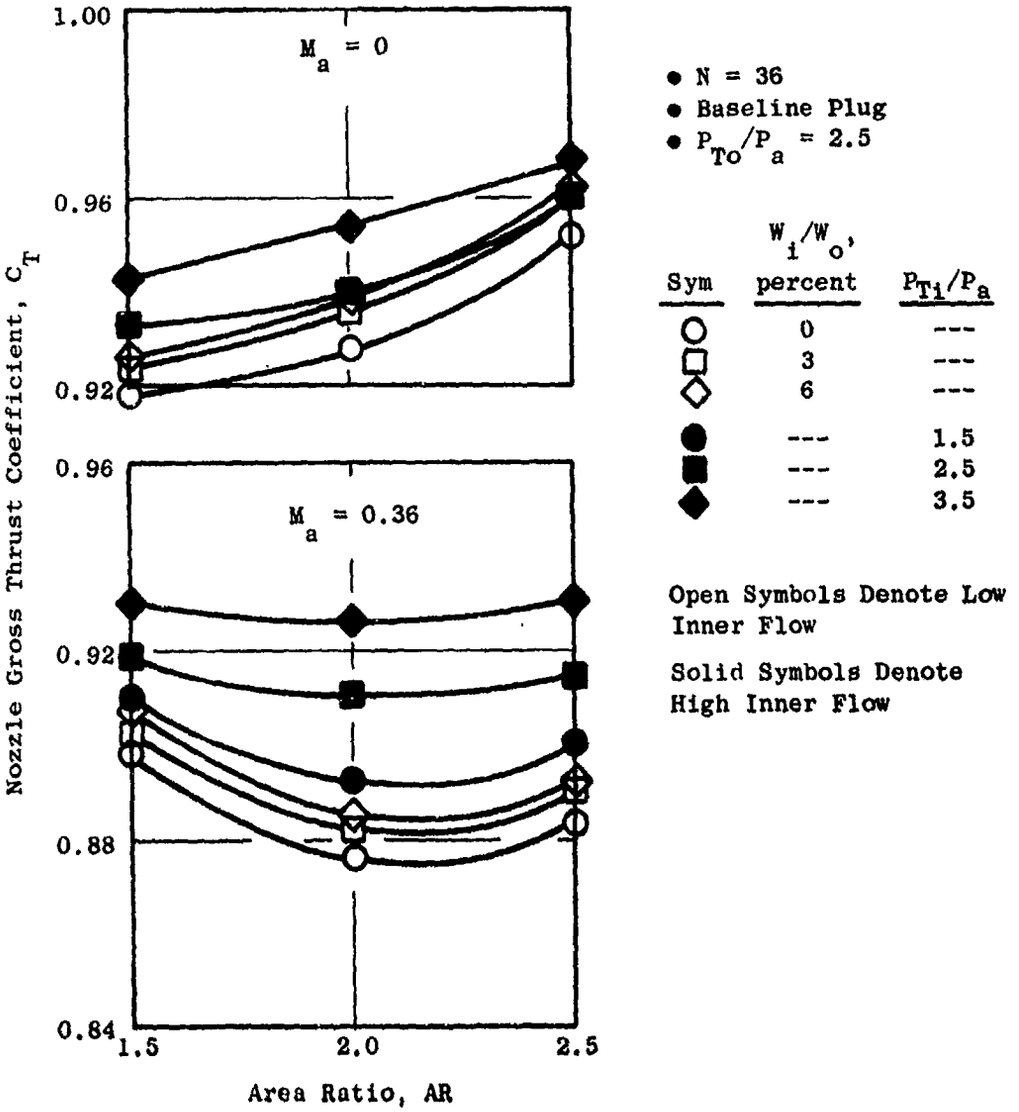

Figure 4-20. Effect of Suppressor Area Ratio and Inner Flow on Nozzle Gross Thrust Coefficients of Deep-Chute Nozzles.

Sym	Free Stream Mach Number, M_a
◇	0
□	0.36
○	0.45

- N = 36
- Baseline
- $P_{To}/P_a = P_{Ti}/P_a = 2.5$

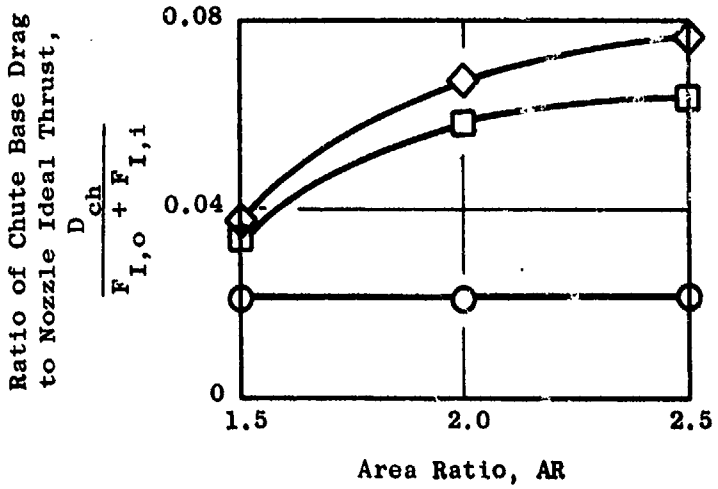

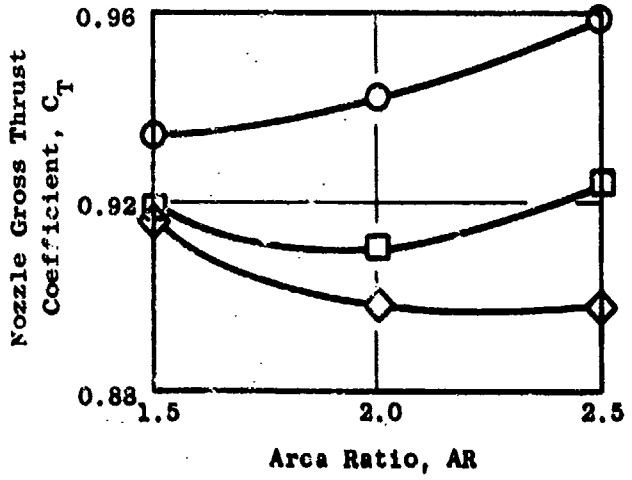

Figure 4-21. Effect of Suppressor Area Ratio and Free-Stream Mach Number on Nozzle Performance of Deep-Chute Nozzles.

chutes) and models DC-3, DC-4, and DC-5 (AR 2.0, 36 deep chutes). The effect of reducing the inner nozzle flow area (increasing radius ratio) on the performance of the area-ratio-1.75, 30-shallow-chute suppressor is presented in Figure 4-22 for a typical outer nozzle and inner nozzle pressure ratio of 2.5 and Mach numbers of 0, 0.36 and 0.45. As the inner nozzle area is decreased, performance is reduced. Figure 4-22 also shows the effect of inner nozzle area on the suppressor base drag. Note that the drag is referenced to the sum of the ideal thrusts of both inner and outer streams. If it were possible to measure the performance of the inner and outer nozzles independently, it could be expected that the outer flow losses would be high relative to the inner flow losses due to the influence of the suppressor. Therefore, as the ratio of unsuppressed to suppressed flow decreased, the total nozzle performance could be expected to decrease, as illustrated by the test results.

Trends for the 36-deep-chute, area-ratio-2.0 nozzle are presented in Figure 4-23. These trends are the same as those described above for the shallow-chute models.

4.5.6 Effect of Inner Plug Axial Location

The effect of inner plug axial location can be investigated by comparing the performance of models SC-2 and SC-5, 30-shallow-chute, area-ratio-1.75 suppressor, and models DC-3 and DC-6, 36-deep-chute, area-ratio-2.0 suppressor. The shallow-chute comparison is shown in Figure 4-24. Performance is compared as a function of outer nozzle pressure ratio for an inner nozzle pressure ratio of 2.5 at Mach 0, 0.36, and 0.45. At outer nozzle pressure ratios of 2.5 and less, axial position of the inner plug had very little effect on nozzle performance. At pressure ratios greater than 2.5, the forward plug location gave the higher level of performance.

Comparisons for the 36-deep-chute suppressor are shown in Figure 4-25. For this model, the effect of axial inner plug location is minimal except at Mach 0.45 where the forward position gives slightly better performance above pressure ratios of 2.5.

4.5.7 Effect of Inner Nozzle Area (Radius Ratio) and Plug Location on Element Base Pressure

The effect of inner nozzle geometry on suppressor element base pressure is shown in Figure 4-26 for Mach 0.36 and an inner nozzle pressure ratio of 2.5 for both the shallow-chute and deep-chute suppressors. The key here is that changes in inner plug area and axial location did not significantly influence the element base pressure. This could be expected based on the fact that the inner nozzle is downstream of the suppressor exit plane. The influence of inner nozzle changes should not feed upstream, especially in cases where the outer, or suppressed, stream pressure ratio is above choked.

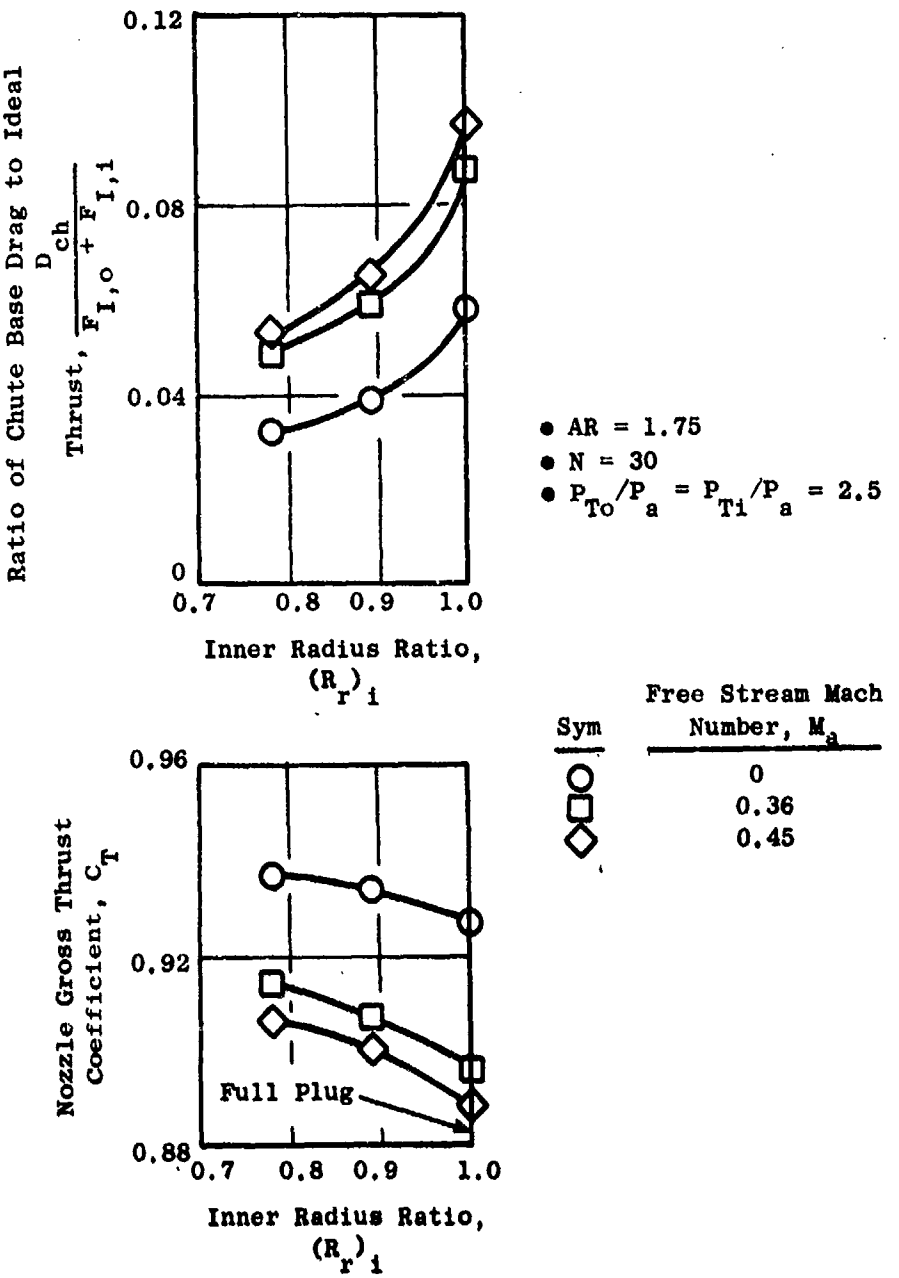

Figure 4-22. Effect of Inner Radius Ratio and Free-Stream Mach Number on Nozzle Performance of Shallow-Chute Nozzles.

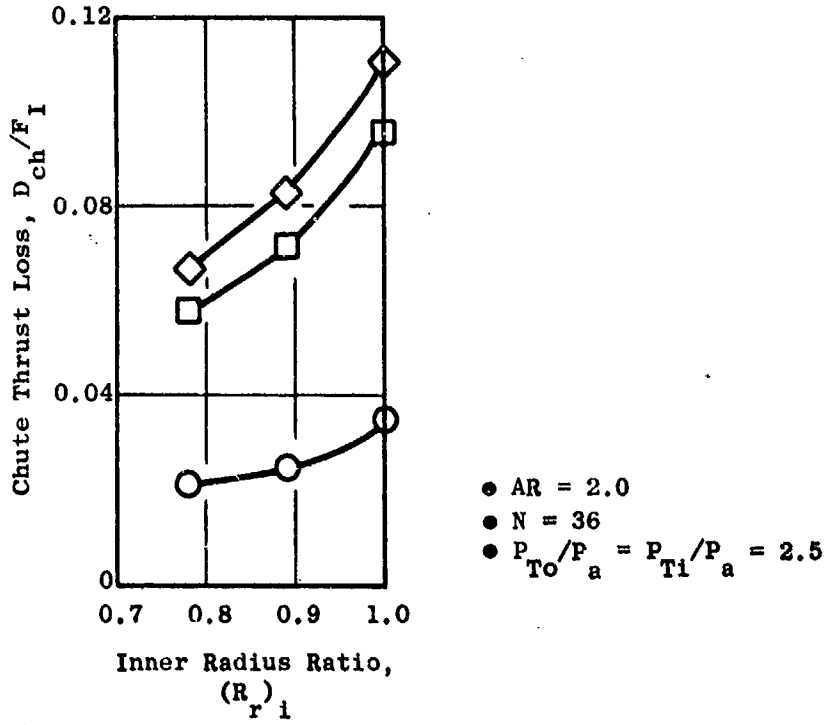

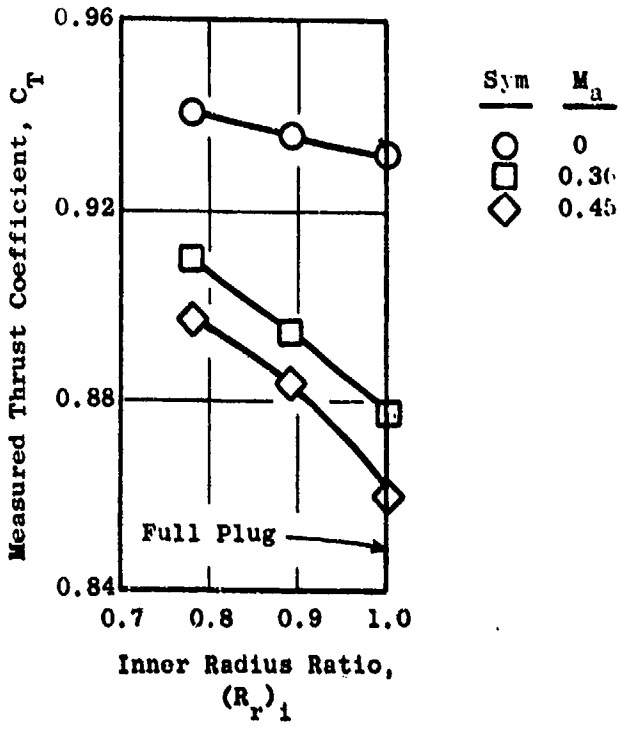

Figure 4-23. Inner Radius Ratio Performance Trends, Deep-Chute Models.

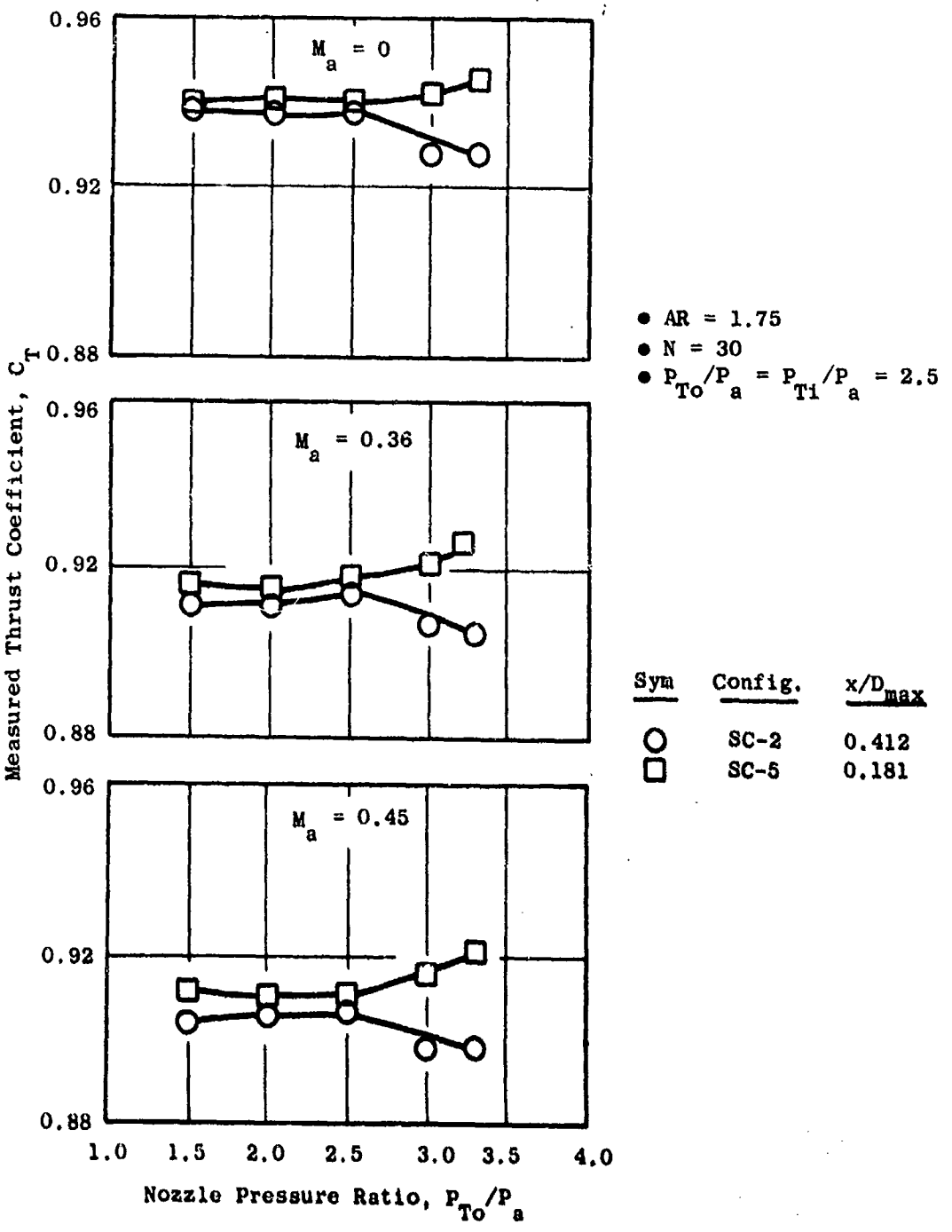

Figure 4-24. Inner Plug Axial Position Performance Trends, Shallow-Chute Models.

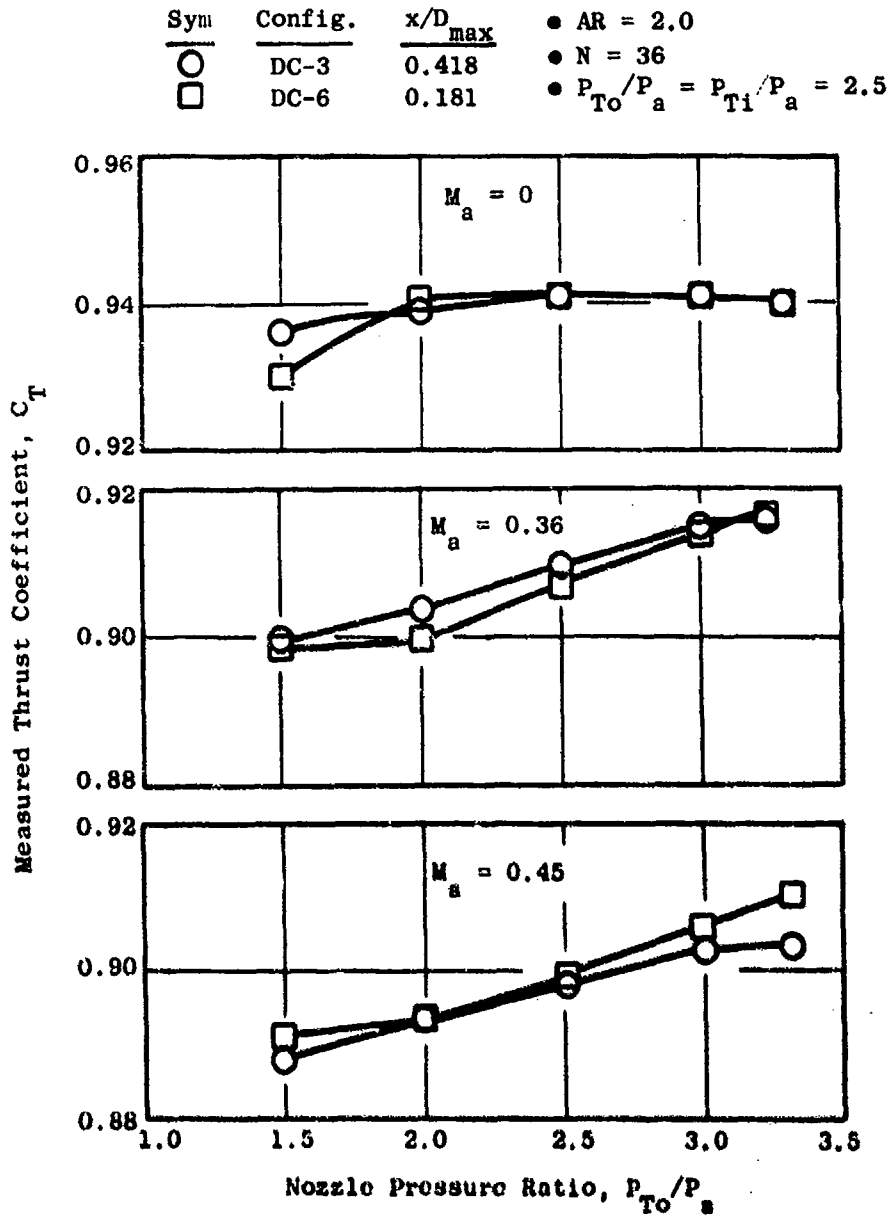

Figure 4-25. Inner Plug Axial Location Performance Trends, Deep-Chute Models.

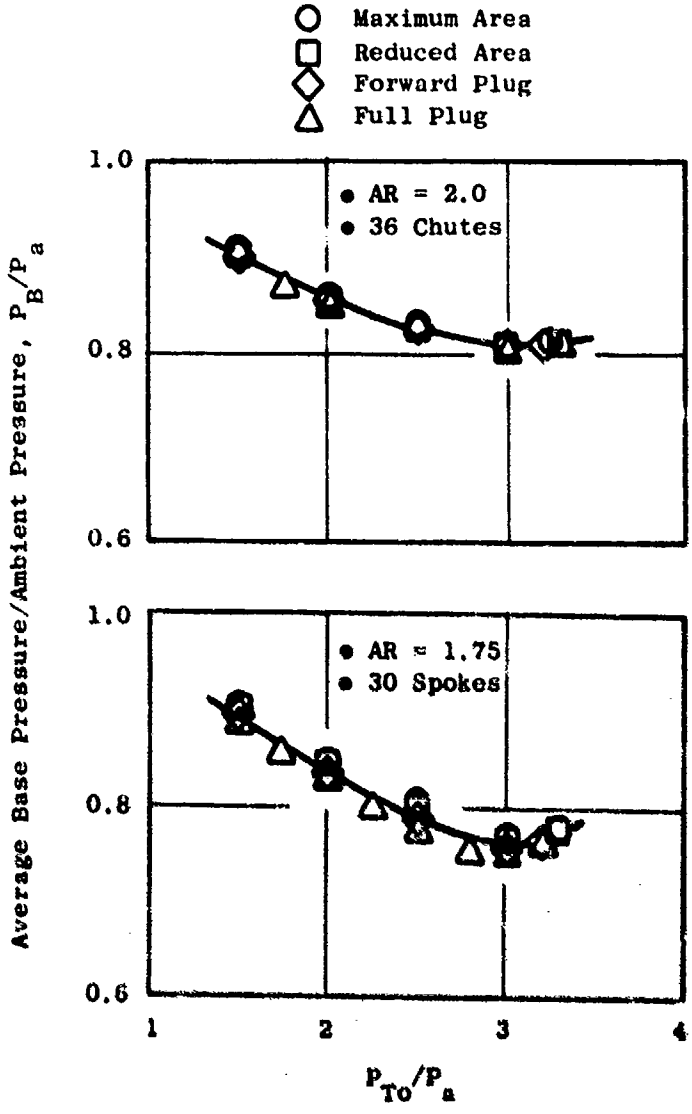

Figure 4-26. Inner Plug Effects on Suppressor Base Pressures, $M_o = 0.36$, $P_{Ti}/P_a = 2.5$.

4.5.8 Effect of Suppressor Ventilation on Performance

The importance of suppressor ventilation on performance is shown in Figure 4-27 where model DC-3, the 36-chute, area-ratio-2.0 suppressor is compared to model DC-3 (spoke). As was described in Section 4.3.1, inserts were placed in the suppressor to effectively eliminate base ventilation from the perimeter of the elements. As can be seen in Figure 4-27, elimination of the ventilation area significantly impacted nozzle performance, resulting in a loss of from three percent at low outer nozzle pressure ratios to seven percent at a pressure ratio of 3.0. It can be concluded from this test that good aerodynamic performance is highly dependent on the amount of available ventilation area.

4.5.9 Effect of External Mach Number

In all cases, increasing external Mach number had a detrimental effect on nozzle performance. Figure 4-28 shows trends in thrust coefficient as a function of tunnel Mach number for the shallow-chute models. The loss in thrust coefficient between Mach 0.45 and static conditions varied between 1.5% and 4%, depending on the configuration. The largest loss occurred for the full plug design, model SC-4.

Similar trends are shown in Figure 4-29 for the deep-chute models. The loss in thrust coefficient between static conditions and Mach 0.45 varied from 1.6% for the area-ratio-1.5 suppressor to 8.8% for the area-ratio-2.5 suppressor with full plug.

4.5.10 104-Tube Nozzle Test Results

Thrust coefficients for the 104-tube nozzle are shown in Figure 4-30. The peak static performance obtained was 0.887 at a nozzle pressure ratio of 3.1. At Mach 0.36, a thrust coefficient of 0.864 was obtained at a pressure ratio of 3.0. The suppressor base plate pressure drag is a major loss component for the 104-tube nozzle, as illustrated in Figure 4-31. In this Figure, both the overall thrust loss as measured by the force balance, and the base drag loss calculated by integrating static pressures, are compared. At a nozzle pressure ratio of 3.0 at Mach 0.36, the overall loss is 13.6%, of which 7.4% is base drag. Remaining losses include tube internal friction and tube entrance losses. As in the case of spoke and chute suppressors, external flow has a significant detrimental effect on performance, about 2.3% in thrust coefficient between static conditions and Mach 0.36.

4.5.11 Eight-Lobe Nozzle Test Results

Thrust coefficients for the 8-lobe nozzle are presented in Figure 4-32. Again, external Mach number has a significant adverse effect on performance.

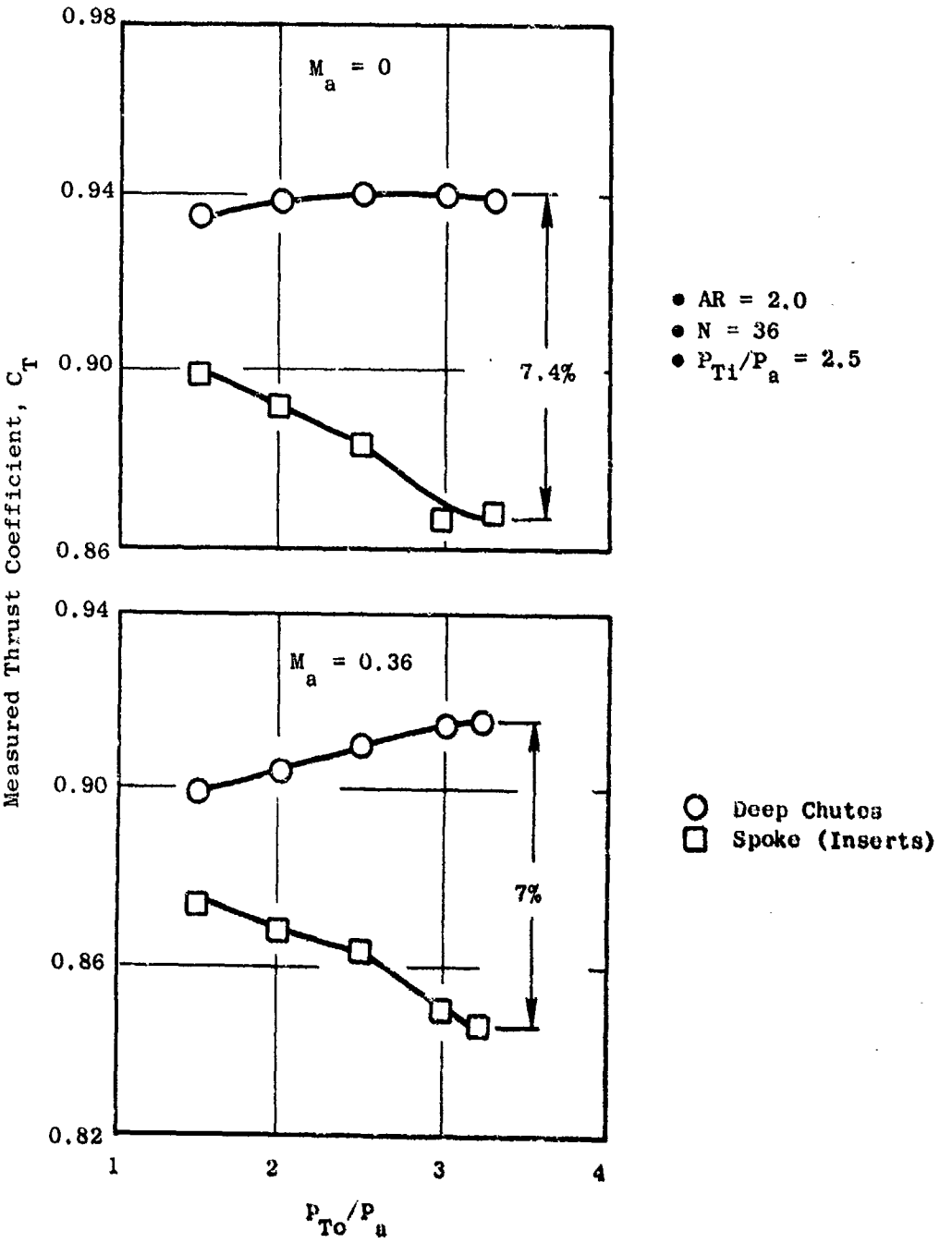

Figure 4-27. Comparison of Chute and Spoke Model Performance.

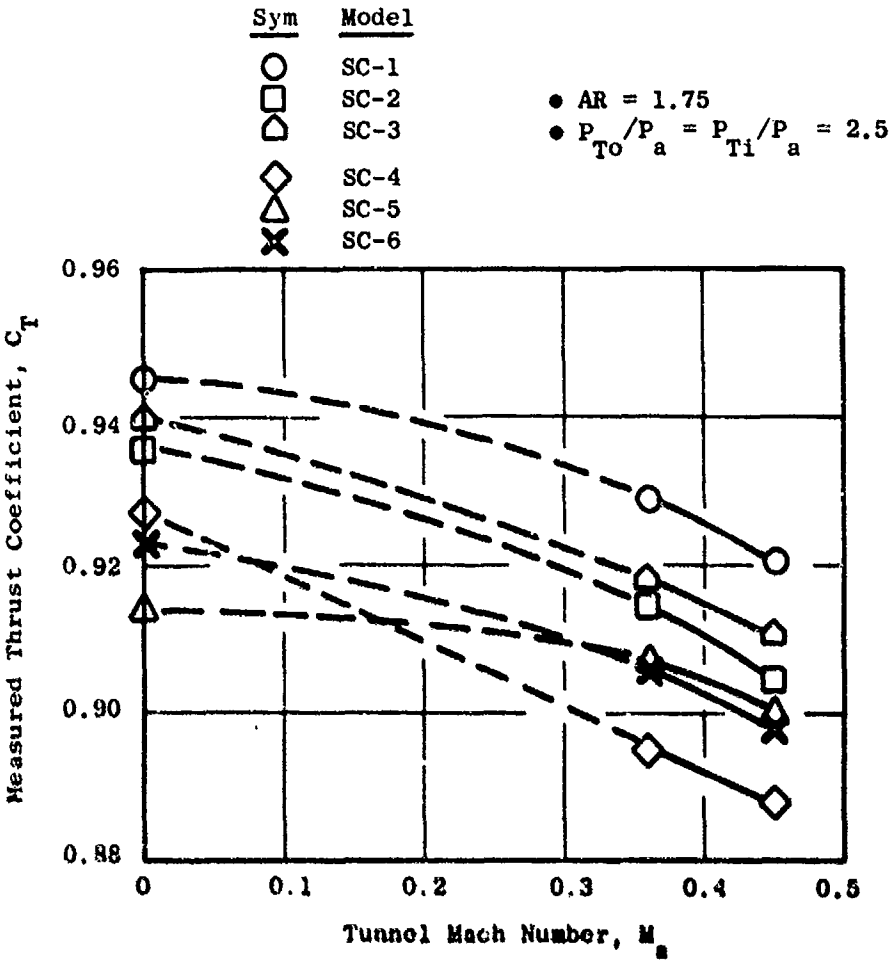

Figure 4-28. Performance Trends with External Mach Number Shallow-Chute Models.

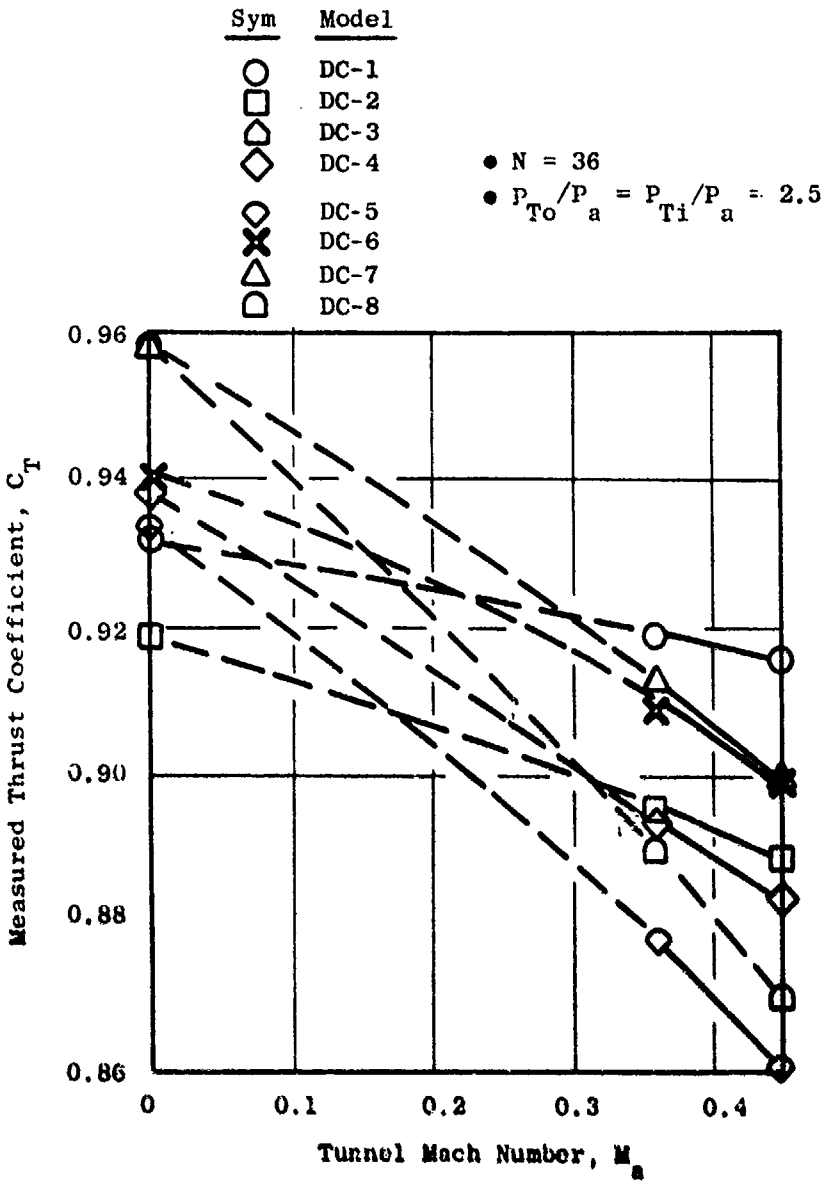

Figure 4-29. Performance Trends with External Mach Number, Deep Chutes

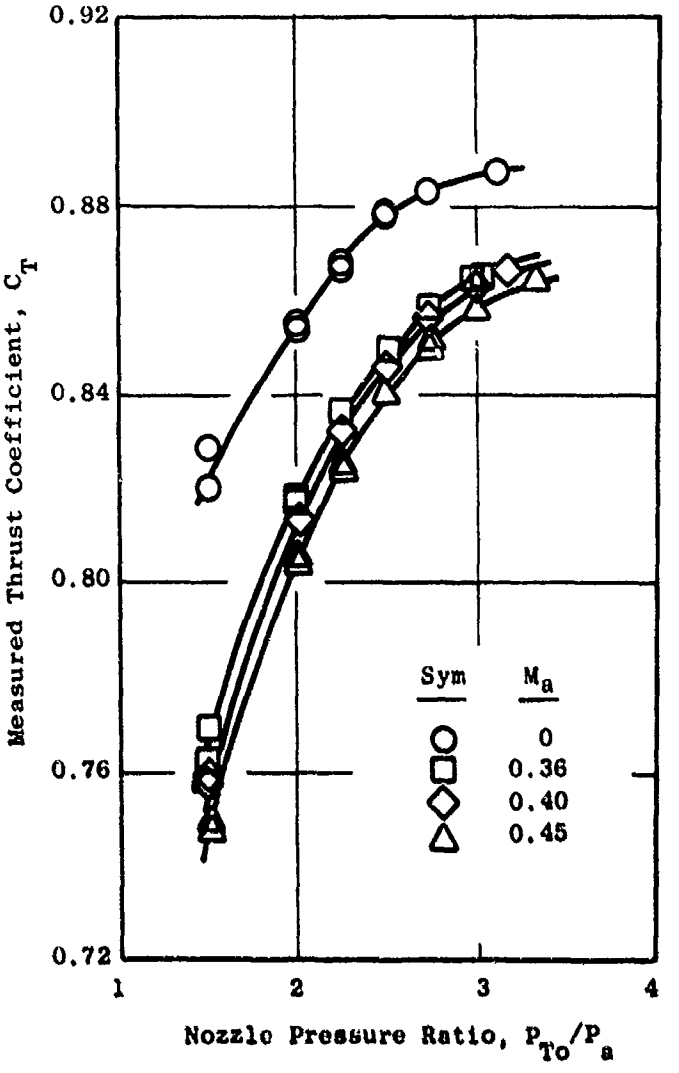

Figure 4-30. 104-Tube Nozzle Performance Trends.

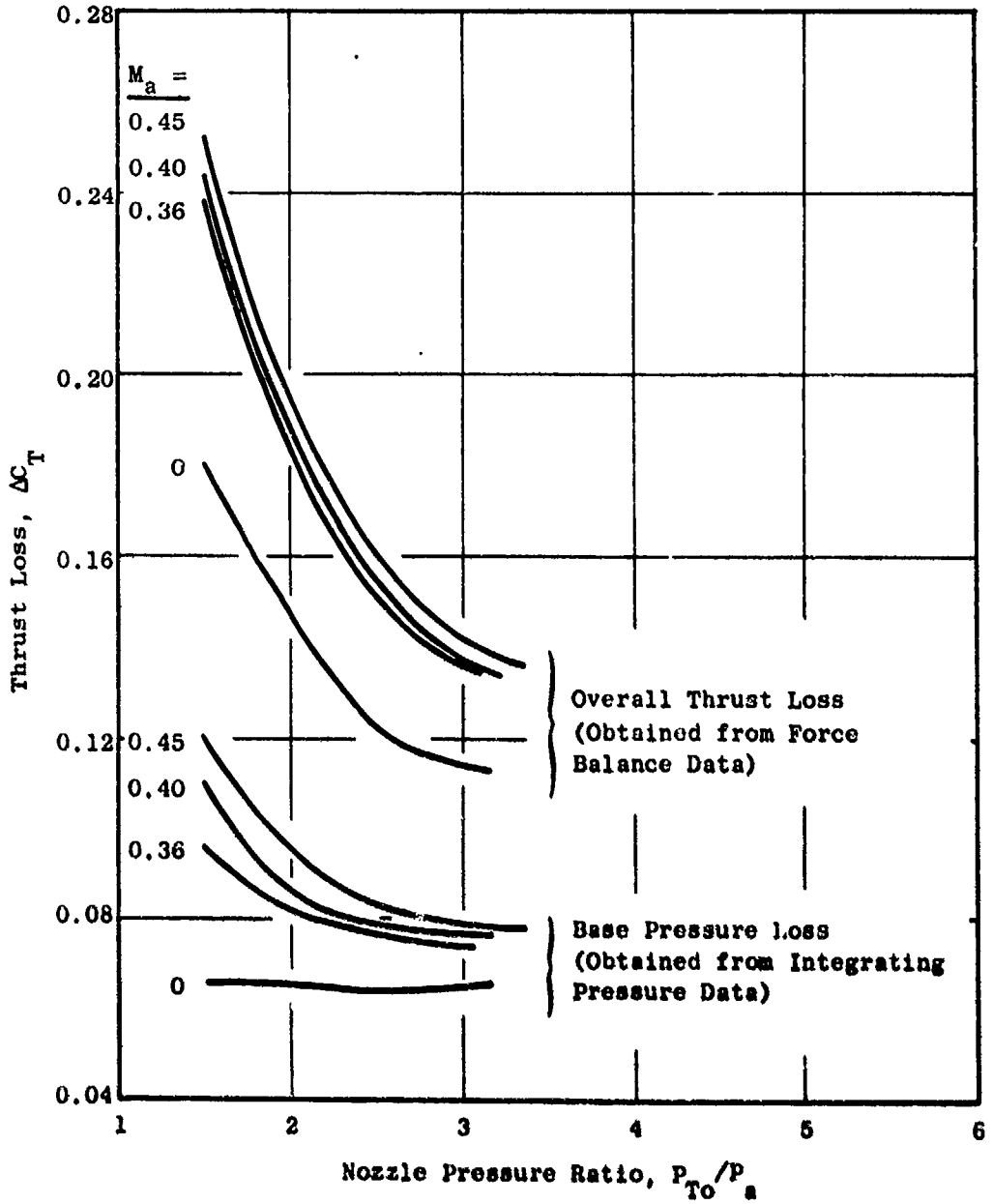

Figure 4-31. 104-Tube Nozzle Base Drag Losses.

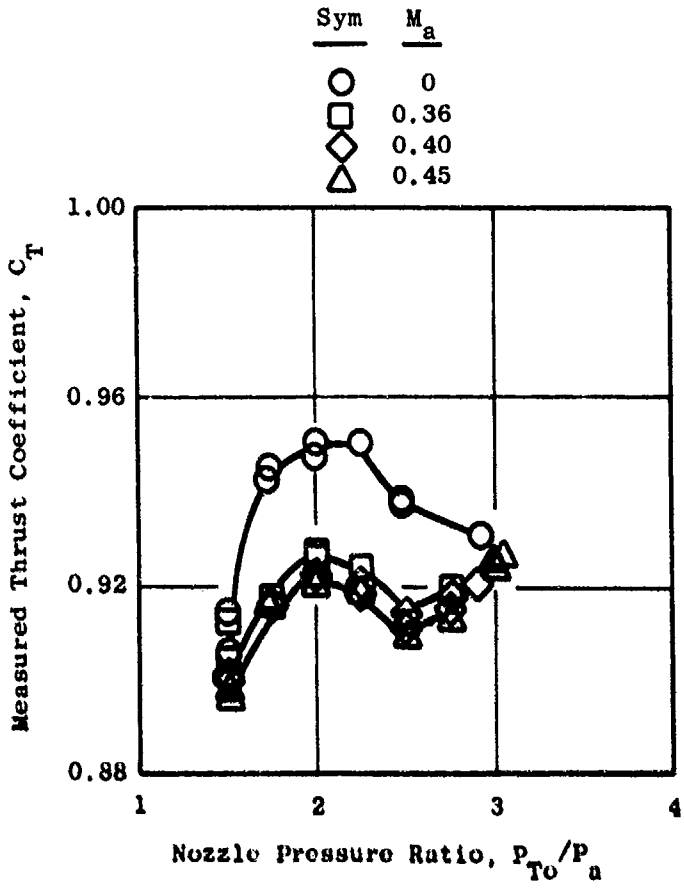

Figure 4-32. Eight-Lobe Performance Characteristics.

Statically, a thrust coefficient of 0.950 at a pressure ratio of 2.0 was measured, while at Mach 0.36, the thrust coefficient was 0.926. The performance of this nozzle would be significantly improved if secondary air were available to fill the gap between the primary nozzle and the outer shroud, as explained in Section 4.4.3. Because the model did not provide a passage for secondary air, the gap area would be "pumped" to less than ambient pressure by the primary jet, resulting in abnormally high base drag losses. In addition, secondary air would reduce the nozzle performance sensitivity to external flow.

4.5.12 Suppressor Flow Coefficients

Suppressor flow coefficients are functions only of suppressor geometry above choked pressure ratios. Flow coefficients are useful in the design of full scale exhaust systems for setting the nozzle physical throat area required to match engine cycle conditions. For scale model tests, they are also useful as a diagnostic tool. For example, a changing flow coefficient above choked conditions could be indicative of either a leak in the model system or a deflection in the suppressor elements with increased pressure (throat area changes). Nothing of this nature was encountered in this test. Flow coefficients are tabulated below for each suppressor configuration.

Suppressor Type	AR	N	CD_o
Shallow Chute	1.75	30	0.971
Shallow Chute	1.75	40	0.966
Deep Chute	1.5	36	0.968
Deep Chute	2.0	36	0.948
Deep Chute	2.5	36	0.978

Flow coefficients for each data point taken can be found in Appendix F in the off-line data summary tabulations.

4.6 CONCLUSIONS

The results of the aerodynamic performance test program again illustrate that exhaust nozzles which incorporate element base areas as an integral part of the jet noise suppression mechanism are sensitive to external Mach number. Static testing is an inadequate means of estimating the in-flight performance of a full scale system since not only performance levels, but trends with geometric variables may be different in flight than statically. This was demonstrated in the area ratio variation experiment where results indicated that, statically, performance increased with increasing area ratio. At Mach 0.45, however, performance decreased with increasing area ratio.

In general, the highest exhaust nozzle loss mechanism is suppressor element base drag. The so-called "base ventilation area" has a dramatic impact on element base drag as was demonstrated by the deep-chute versus

"spoke" experiment, which resulted in a greater than seven percent loss in thrust coefficient when the chute ventilation area was blocked.

The test results also illustrate that the number of elements, for a given suppressor area ratio, is an important variable as far as performance is concerned. Increasing the number of elements had a detrimental effect on performance. For a typical outer and inner nozzle pressure ratio of 2.5, at Mach 0.36, a 2.2% loss was recorded when the element number was increased from 20 to 30.

Increasing the area of the inner nozzle, for a given suppressor geometry, improved the overall performance of the exhaust system, as might be expected since the inner nozzle is "unsuppressed" and only small losses are incurred relative to the outer suppressed stream. Increasing the inner nozzle area while keeping the outer nozzle area constant resulted in increased total nozzle flow rate. Nozzles with no inner flow, i.e., simulated turbojet nozzles, exhibited the lowest performance since all engine flow passes through the mechanical suppressor.

Inner nozzle flow or geometric conditions had little or no effect on suppressor element base pressures. This allows some freedom in the design of the inner nozzle without fear of increasing suppressor base drag. However, care should be exercised in the design of the inner nozzle to prevent excessive inner flow performance losses. Although all inner plugs in this test program had essentially the same contours, test results reported in Reference 39 have shown that the shape of the inner plug can have a significant effect on performance.

In summary, the data taken in the NASA-Lewis Research Center 8- by 6-foot wind tunnel was of high quality, with accuracy and repeatability generally better than ±0.5% over the range of interest. The results of the test program significantly add to the data base already available for the design of advanced, high velocity jet noise suppressor systems. Specifically, these data were utilized in performing trade studies of performance versus suppression, and aircraft integration studies reported in Volume III. Also, correlation of these data was a key element in formulating performance prediction procedures for the Task 6 Design Guide.

5.0 RESULTS AND CONCLUSIONS

Task 3 of the High Velocity Jet Noise Program involved a series of parametric acoustic, aerodynamic and source measurement tests on baseline and suppressed nozzles. This report (Volume II of IV) has documented the model configurations, test efforts, and results.

Baseline conical nozzle acoustic data have been shown to agree well with present SAE prediction methods for jet mixing noise, especially with respect to peak noise level and to shock cell noise when correlated with $\sqrt{M^2-1}$. Plug nozzle studies have shown that suppression increases with radius ratio. Suppression levels up to 6 ΔPNdB have been achieved at high radius ratio. Coplanar-coannular nozzles with outer to inner flow area ratios of 0.4 to 2.0 have demonstrated inner to outer flow ratio to be an important design variable. Maximum suppression was achieved when W_o/W_i was less than 0.1. The variation with area ratio was minimal above this ratio. Complete blockage of the inner flow caused a significant loss in suppression.

Suppressor and system aerodynamic and geometric parameters evaluated experimentally included the following: suppressor area ratio, radius ratio, flow management (system velocity ratio, weight flow ratio and area ratio), inner stream geometry, element number, element type, and treated ejectors on multi-element and unsuppressed inverted coannular flow nozzles. Suppressor area ratio variation for single-flow nozzles has established that peak noise suppression increases with increasing area ratio at high jet velocity and decreases with increasing area ratio at low jet velocities. For example, a 5 PNdB difference existed between a 1.5 and a 2.5 area ratio nozzle at 2400 ft/sec. Minimal distinction was seen at 90°. The area ratio study conducted on dual-flow nozzles (with only the outer stream suppressed) shows a maximum of 3.5 peak PNdB variance between the configurations, with the suppression level dependent on jet velocity. Low-area-ratio, high-radius-ratio designs were consistently better at low to intermediate jet velocities, as they were for the full span turbojet nozzles. Peak noise suppression levels of 11, 9.5 and 10.4 for area ratios of 1.5, 2.0 and 2.5, respectively, were below those of the same suppressor applied to a single-flow turbojet (i.e., ΔPNL = 11.5, 12.0 and 12.5), suggesting that a full-span turbojet suppressor is slightly more efficient than a half-span suppressor applied to a dual-flow system.

Flow management and inner stream geometry studies were conducted utilizing a dual-flow nozzle system incorporating an outer stream half-span mechanical suppressor. These studies established that velocity ratio is an important design consideration with systems of low area ratio, e.g., A_o/A_i = 0.65. Highest suppression levels were attained when inner flow was completely eliminated. For systems of A_o/A_i = 1.92 and 3.6, variance due to velocity ratio was not as distinct and decreased as area ratio increased. Injecting low amounts of inner flow to effect bypass ratios of 3.3 and 6.7 showed bypass ratio to be a strong parameter influencing suppression. The influence was

greater for low system area ratio, with suppression decreasing as W_o/W_i was lowered from ∞ to 3.3. Increasing flow area ratio caused an increase in suppression of between 3.5 and 5 PNdB over its lower A_o/A_i counterparts. Inner stream plug geometry variation showed only minor change in suppression.

Flow segmentation studies showed that maximum suppression levels of 10 PNdB were attainable. Increasing element number was more effective at mass average velocity less than 2250 ft/sec. Reduction of element number was more effective above this velocity.

Spoke/chute element type studies on a full-span suppressor achieved a maximum suppression of 13.5 ΔPNdB. Spoke and chutes were found in general to exhibit equivalent peak noise suppression levels. At high mass average velocities, spoke suppressor effectiveness was diminished. A similar spoke/chute study on a half span suppressor showed a peak PNL suppression level of 10.5 PNdB, significantly less than the 13.5 peak PNL attained by the full-span application. The spoke nozzles were from 0.5 to 1.5 PNdB more effective than chutes.

Application of acoustically treated ejectors to half and full span 36-element suppressors was found to effect a significant increase in suppression. Similar application to an unsuppressed inverted-flow coannular plug nozzle was not as effective.

Studies to assess the influence of simulated flight using the freejet technique established that a common set of velocity indices may not be established for both baseline and suppressor nozzles. Chute nozzles in general have shown a 3 PNdB loss of suppression in flight due to dominance of the high frequency portion of the spectra, which realizes only a minimal flight effect. The minimization of high frequency noise has been demonstrated to be a critical design criterion for a suppressor if it is to realize a beneficial flight effect.

Laser velocimeter measurements established that suppressors enhance mean velocity decay until the velocity approached 60% or less of the fully expanded isentropic velocity. The axial location of peak turbulence intensity is a function of nozzle type and may be related to the region of maximum mean velocity gradient. Axial location of peak turbulence intensity was found to be a function of nozzle type; however, the absolute turbulence level range of 18 to 22% could not be correlated with exhaust nozzle type. Conical nozzle velocity decay rate was reduced in simulated flight. Complex suppressor nozzles showed very little sensitivity to forward velocity, until the downstream region of the coalesced jet. The turbulence intensity levels near the exit plane were found to be generally comparable. Overall, the laser velocimeter has been demonstrated to be extremely useful in determining the aerodynamic mixing characteristics for complex multi-element suppressor nozzles.

A wind tunnel test program illustrated that the aerodynamic performance of suppressed nozzles which incorporate elemental base areas as an integral

part of the design are sensitive to external Mach number. Static testing was shown to be an inadequate means of estimating in-flight performance of a potential full-scale suppressor. In-flight performance levels, as well as trends with geometric variables, may be different than static. The area ratio variation study demonstrated this result when static performance improved with increasing suppressor area ratio, and Mach 0.45 performance decreased with the same area ratio increase.

In general, suppressor element base drag is the most important loss mechanism. The so-called base ventilation area has a dramatic impact on element based drag as demonstrated by the seven percent loss in thrust coefficient incurred when a deep-chute ventilation area was blocked as a spoke.

Tests results also illustrate that suppressor segmentation is an important performance variable. Increasing element number decreased performance. For a typical outer and inner nozzle pressure ratio of 2.5, at flight Mach 0.36, a 2.2.% loss was associated with element number increase from 20 to 30.

Decreasing system area ratio (A_o/A_i) for a fixed half-span suppressor improved the overall system performance. This was anticipated, since the inner nozzle is unsuppressed and only small losses are incurred relative to the outer suppressed stream. Systems with no inner flow, i.e., turbojet nozzles, exhibited the highest performance loss, since all flow passes through the suppressor.

Inner nozzle flow rate and plug geometry variation had little or no effect on suppressor element base pressure. This allows some flexibility for inner nozzle design by eliminating concern of increasing base drag. Although inner plug geometries in this study maintained similar contours, results from previous studies have shown that inner plug shape can impact performance significantly.

The NASA-Lewis Research Center's 8-by-6-foot wind tunnel data was of high quality, with accuracy and repeatability generally better than $\pm 0.5\%$ over the range of interest. Study results significantly add to the aerodynamic performance data base available for the design of advanced, high velocity jet noise suppressor systems.

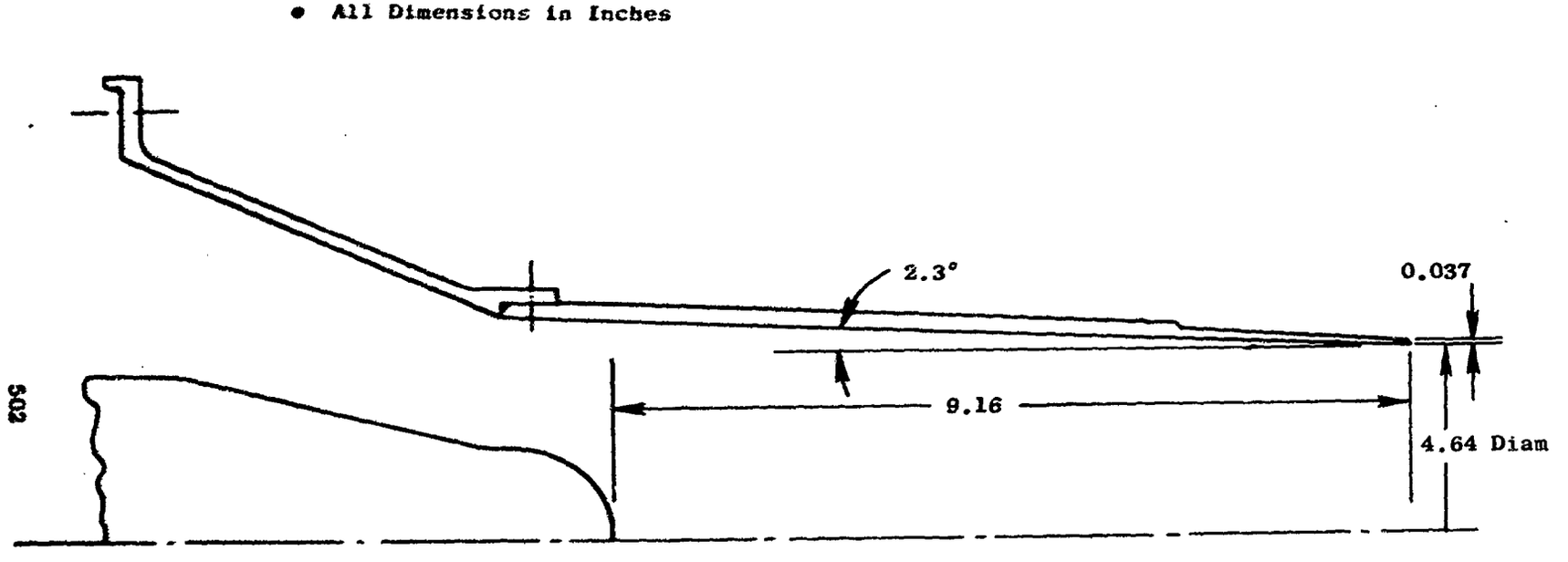

Figure A-1. Model 1 - 4.64-in.-Diameter Conical Nozzle Adapted to JENOTS. Model 14 - 4.64-in.-Diameter Conical Nozzle Adapted to Cell 41, Anechoic.

APPENDIX A

Figures A-1 through A-41 are dimensioned, schematic illustrations of the test models discussed in Section 4.3 of this document.

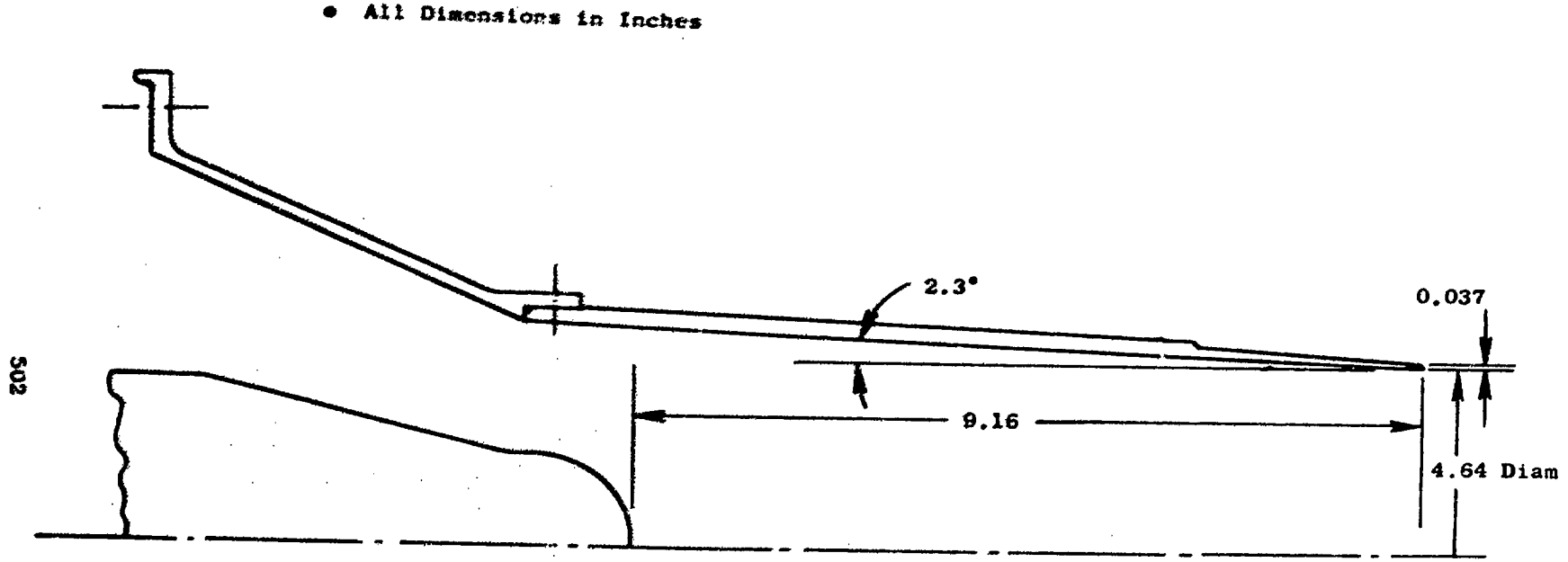

Figure A-1. Model 1 - 4.64-in.-Diameter Conical Nozzle Adapted to JENOTS. Model 14 - 4.64-in.-Diameter Conical Nozzle Adapted to Cell 41, Anechoic.

- $A_9/A_8 = 1.22$
- $D_{9\ eq}/D_{8\ eq} = 1.10$
- All Dimensions i. Inches

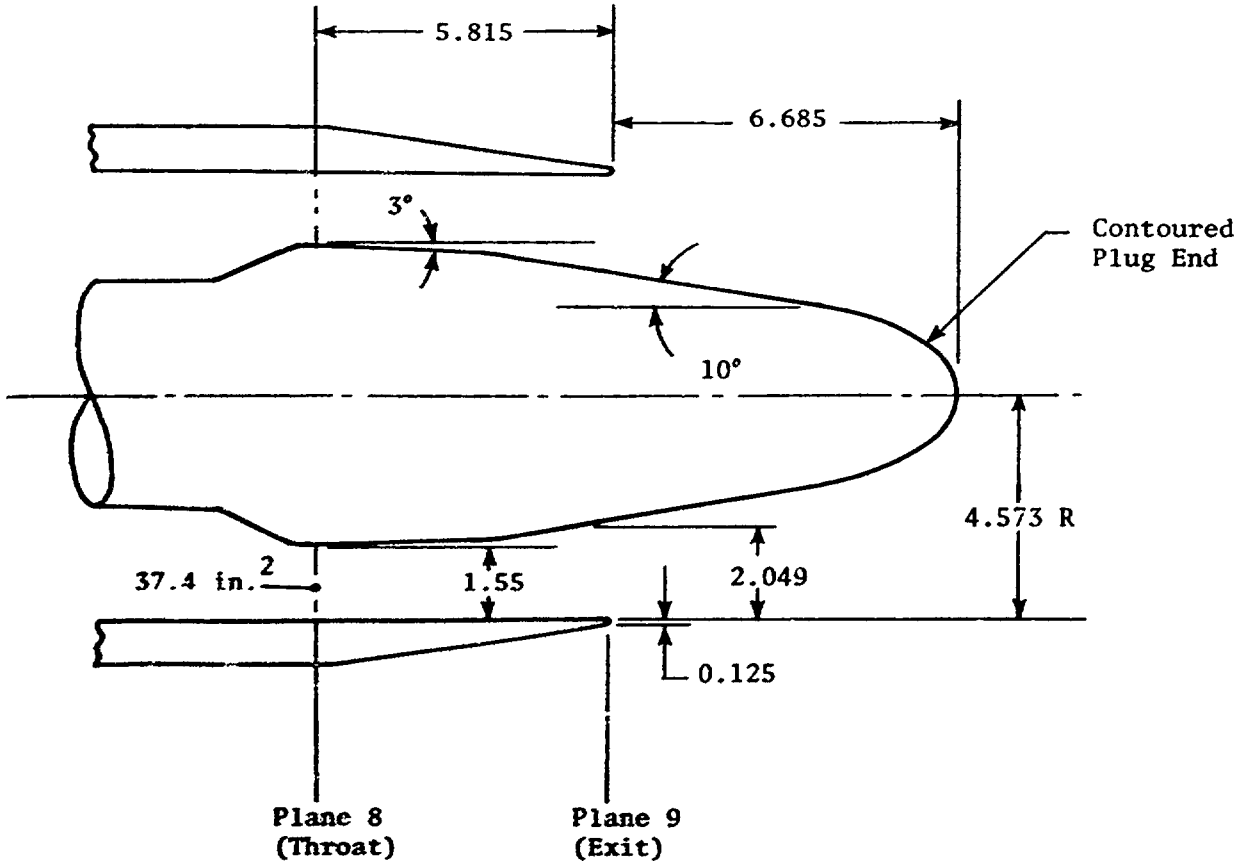

Figure A-2. Model 2 - Convergent-Divergent Plug, Single Flow.

- All Dimensions in Inches

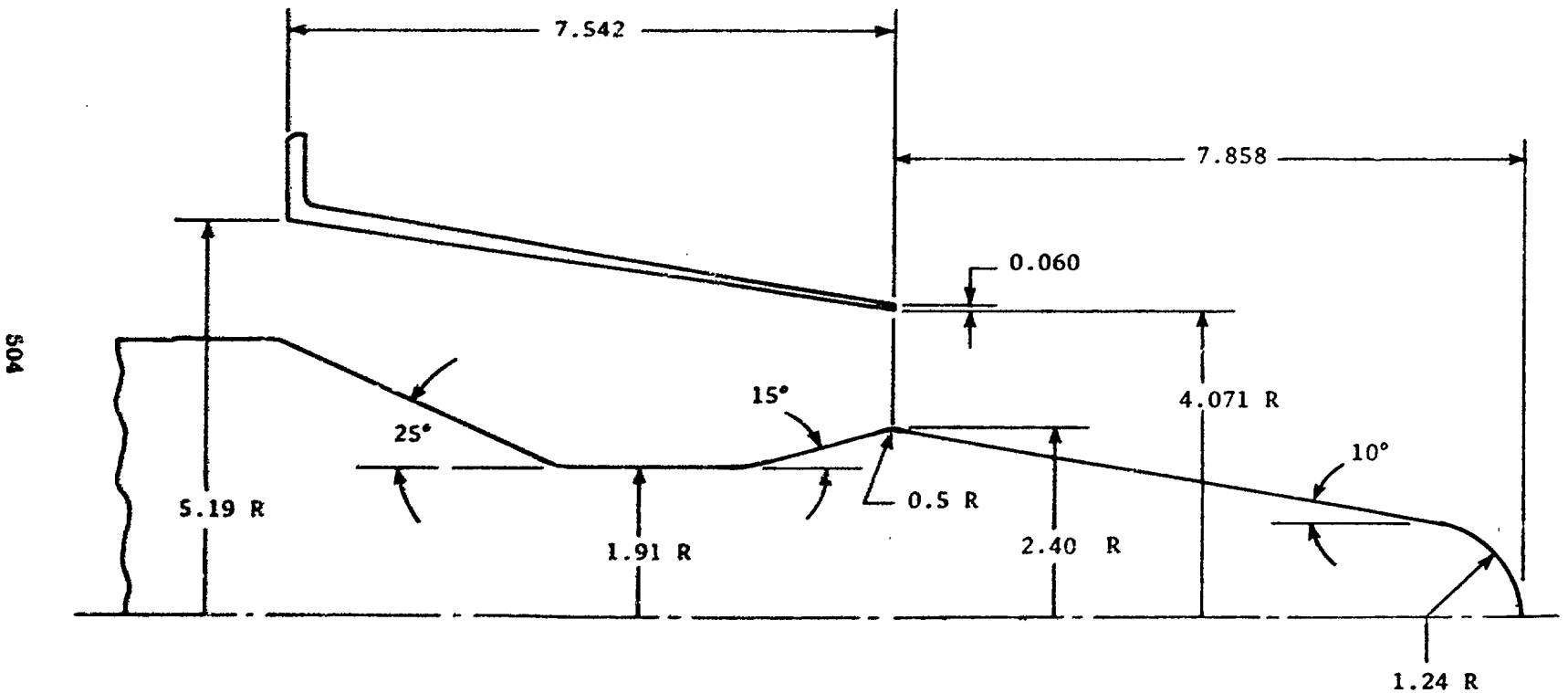

Figure A-3. Model 3 - Converging Plug, R_r = 0.59, Single Flow.

● All Dimensions in Inches

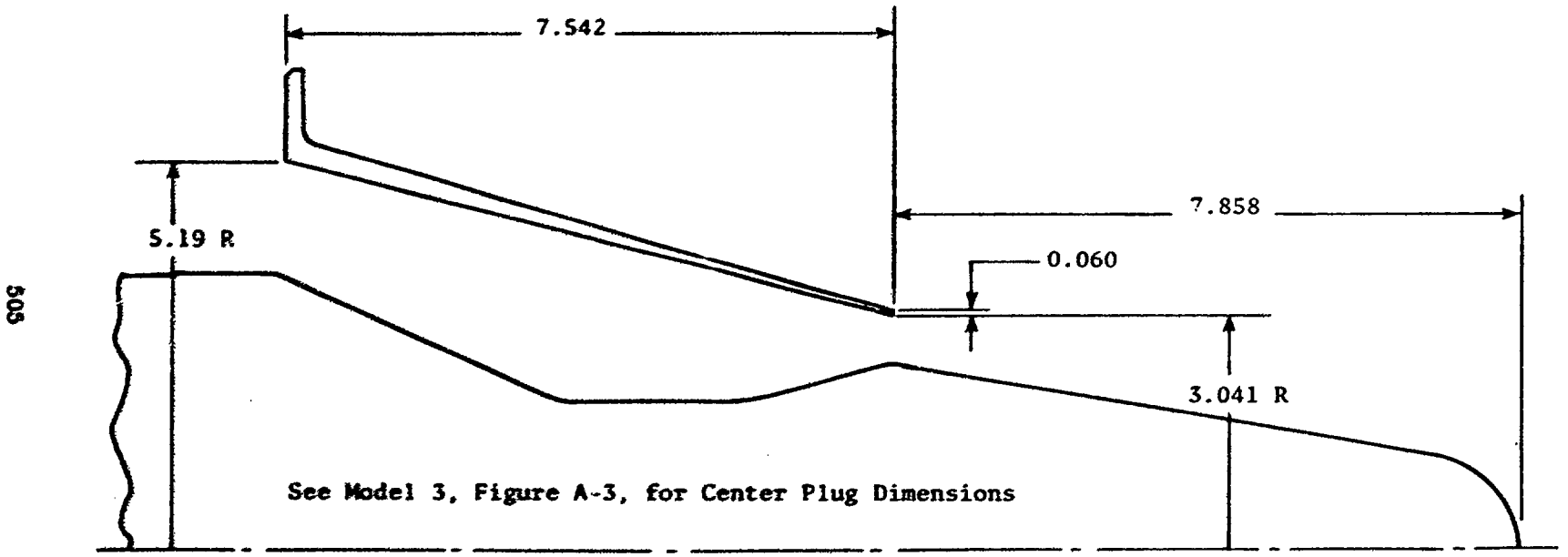

Figure A-4. Model 4 - Converging Plug, R_r = 0.789, Single Flow.

● All Dimensions in Inches

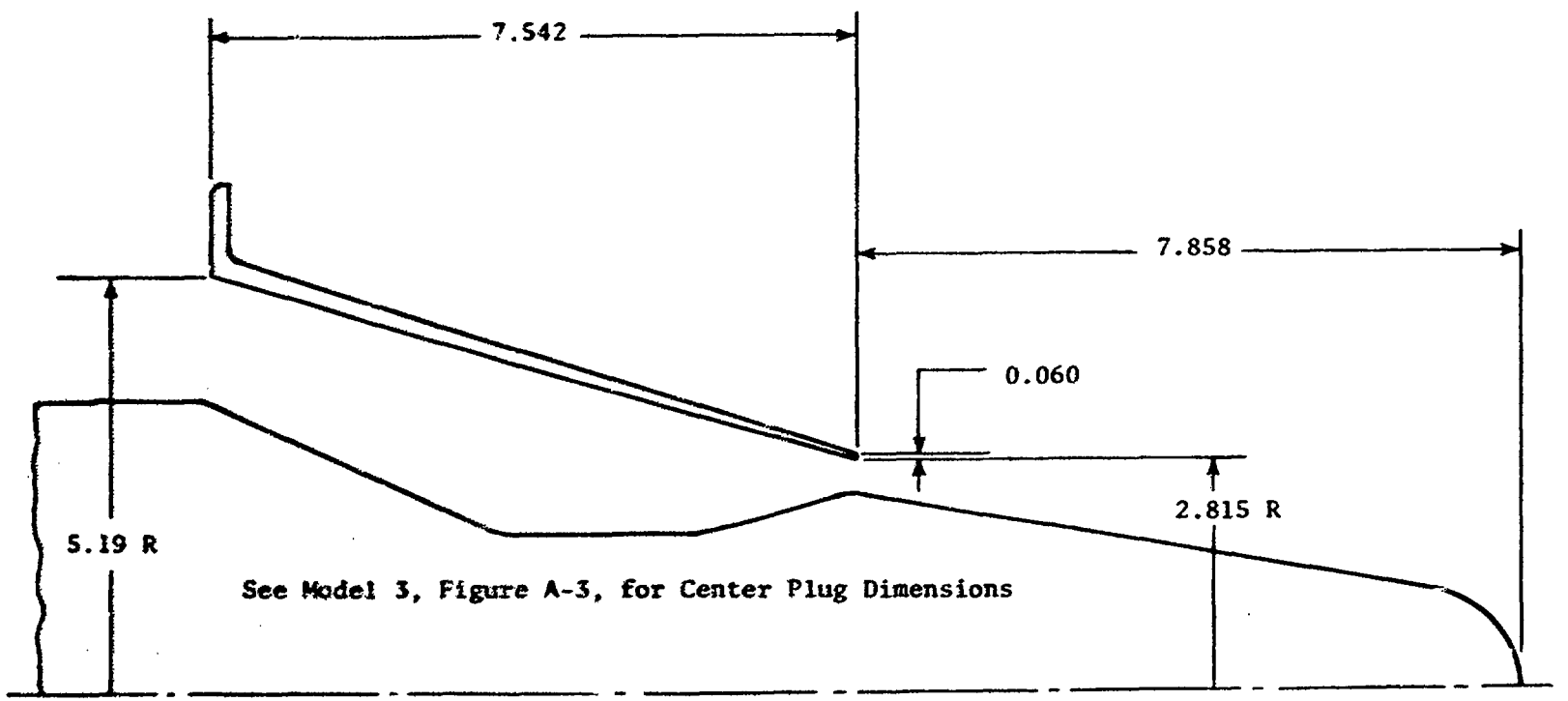

Figure A-5. Model 5 - Converging Plug, R_r = 0.853, Single Flow.

• All Dimensions in Inches

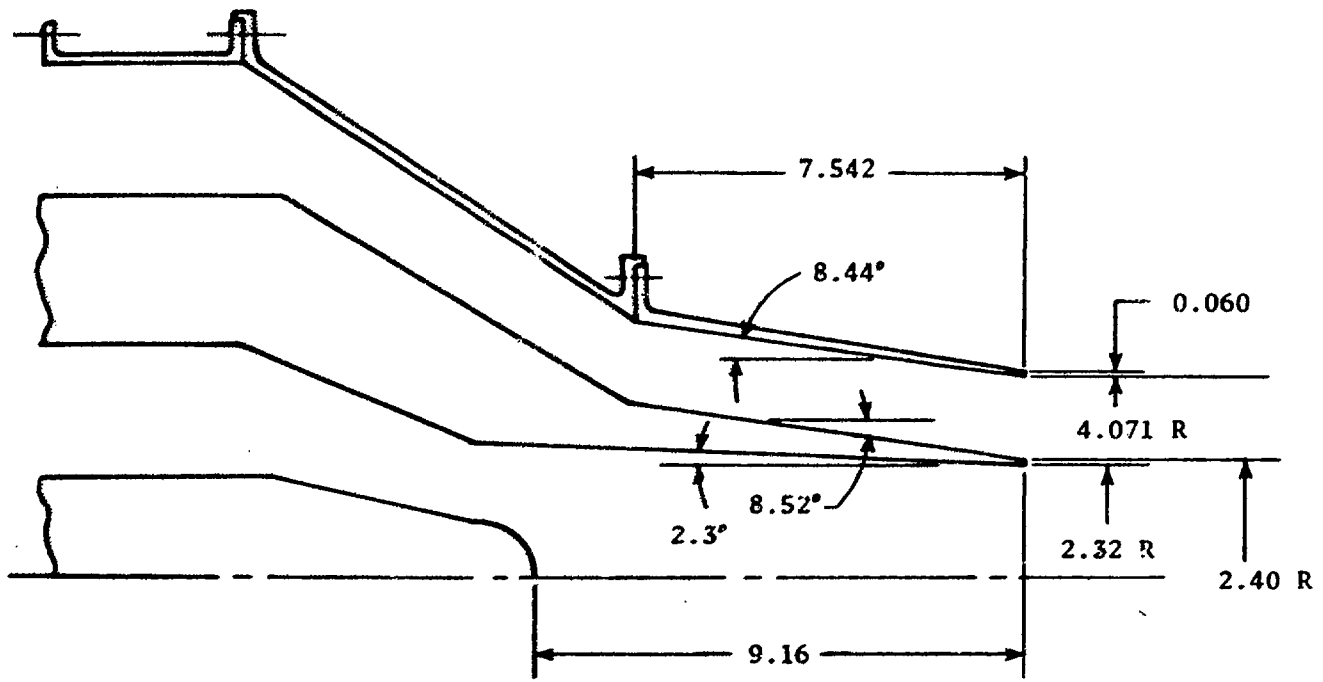

Figure A-6. Model 6 - Dual-Flow Coannular Coplanar, A_o/A_i = 2.0. Model 9 - Coannular Coplanar, A_o/A_i = 2.0, Low Inner Flow.

• All Dimensions in Inches

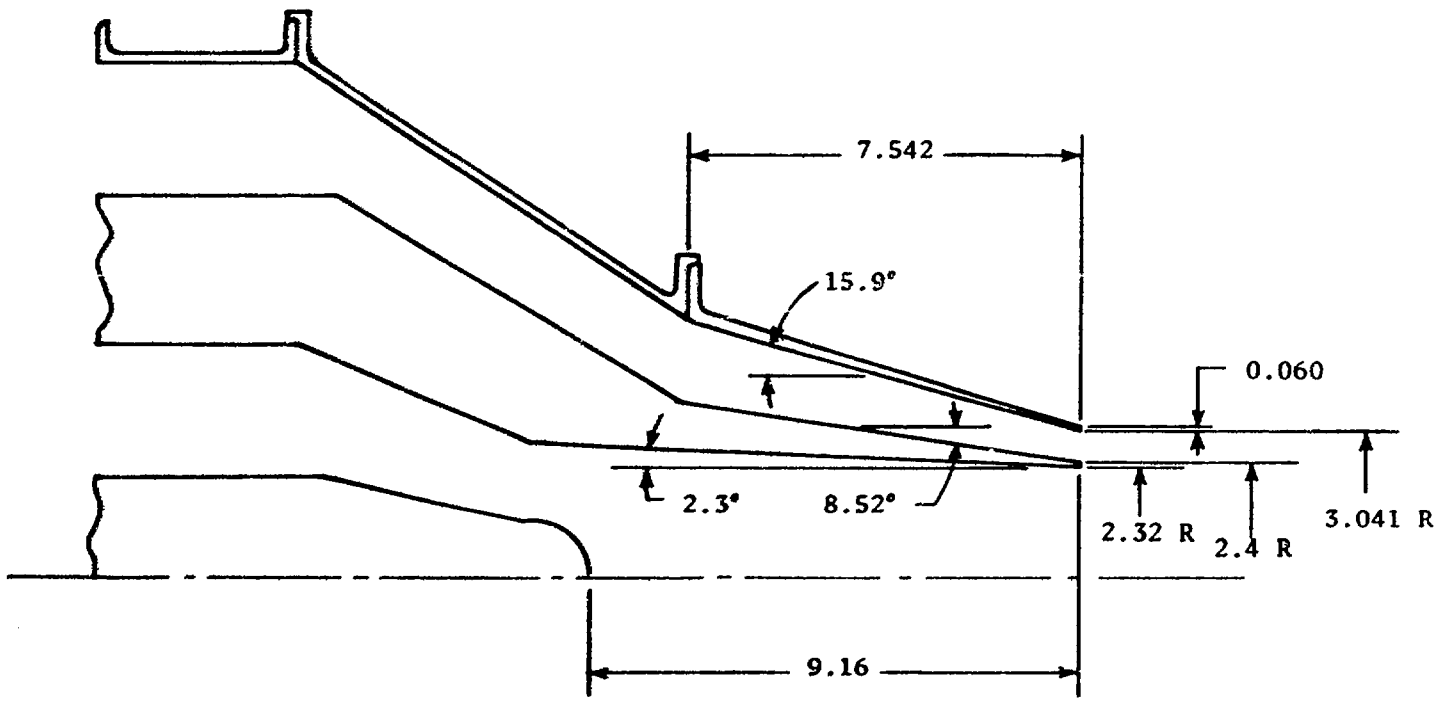

Figure A-7. Model 7 - Dual-Flow Coannular-Coplanar, A_o/A_i = 0.65. Models 10 and 11 - Coannular-Coplanar, A_o/A_i = 0.65, Low Inner Flow and No Inner Flow, Respectively.

• All Dimensions in Inches

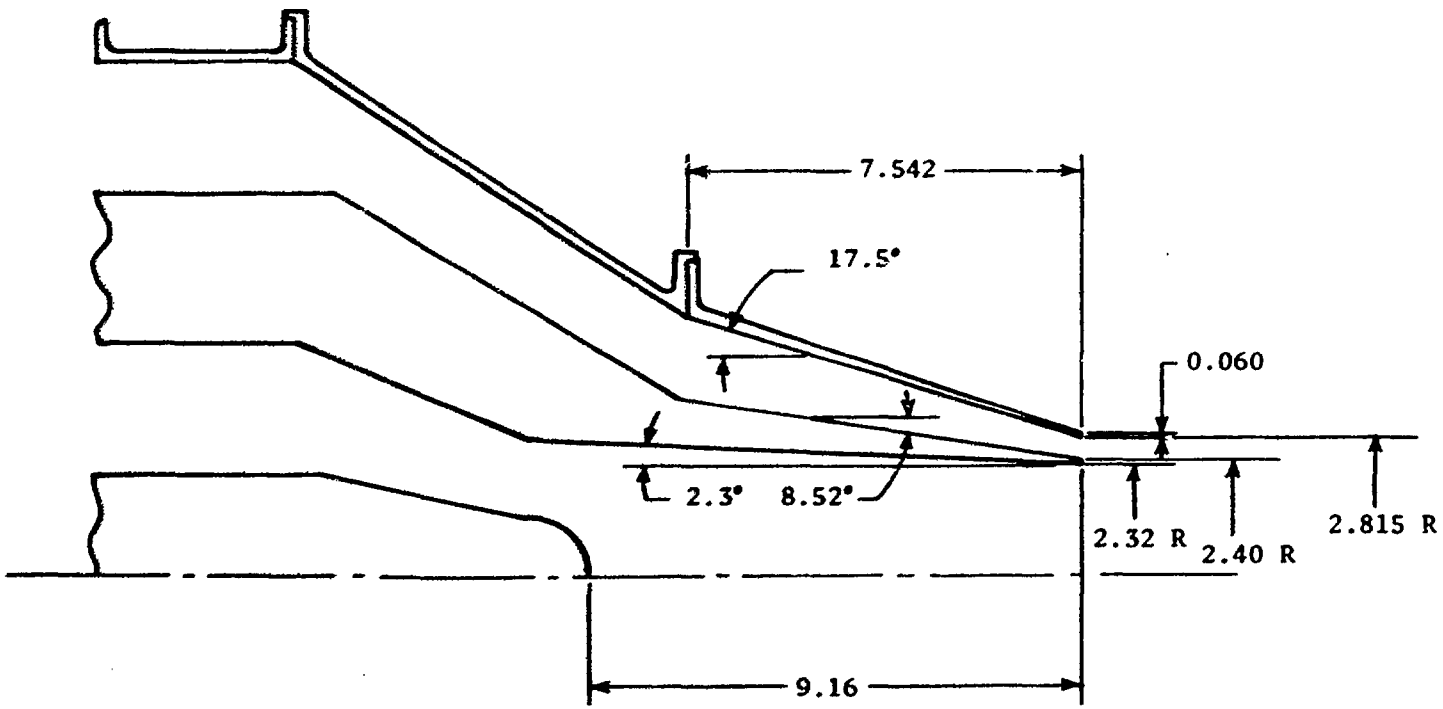

Figure A-8. Model 8 - Dual-Flow Coannular Coplanar, A_o/A_i = 0.4. Models 12 and 13 - Coannular Coplanar, A_o/A_i = 0.4, Low Inner Flow and No Inner Flow, Respectively.

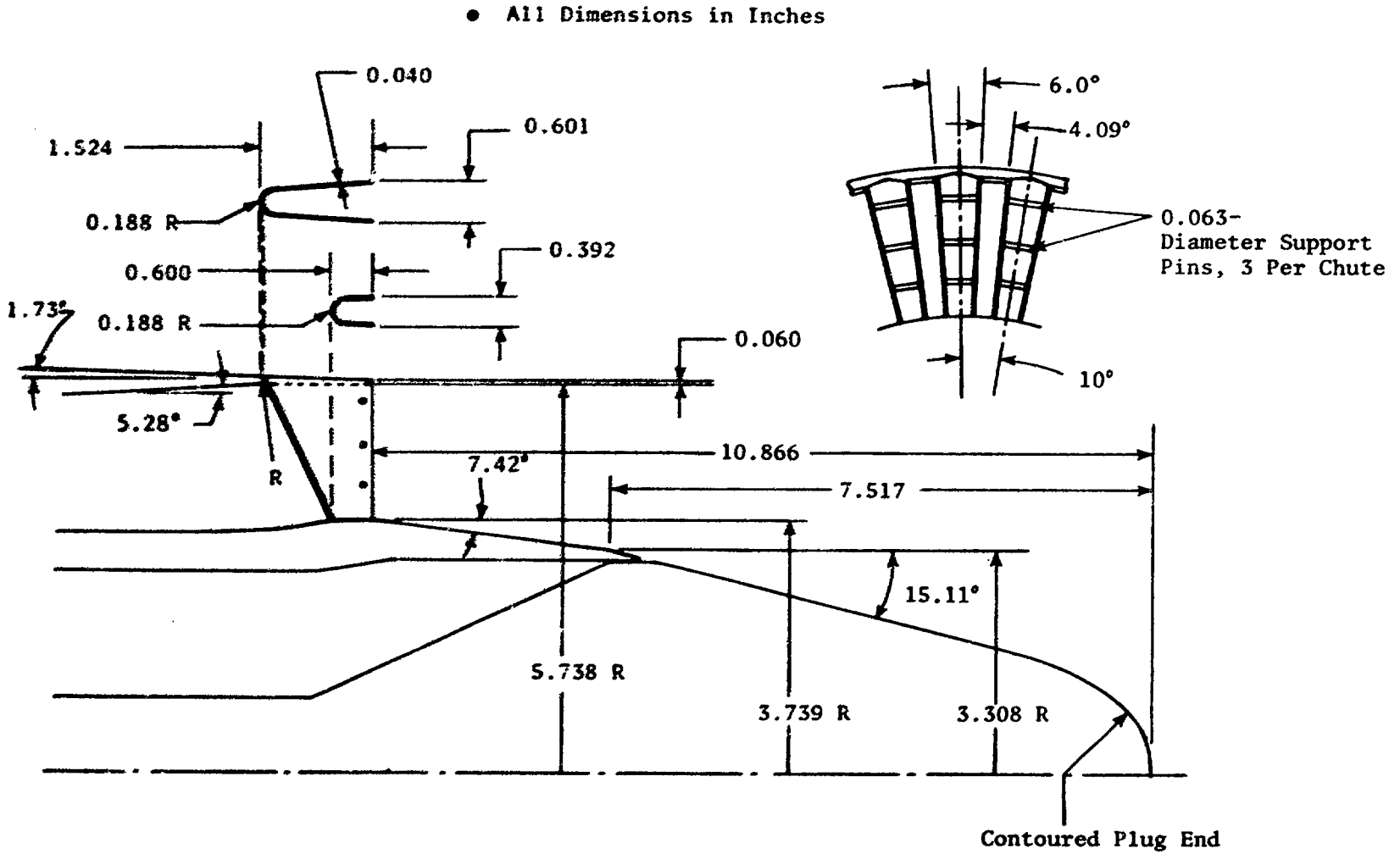

Figure A-9. Model 15 - 36-Chute, AR = 2.5, R_r = 0.653 Turbojet.

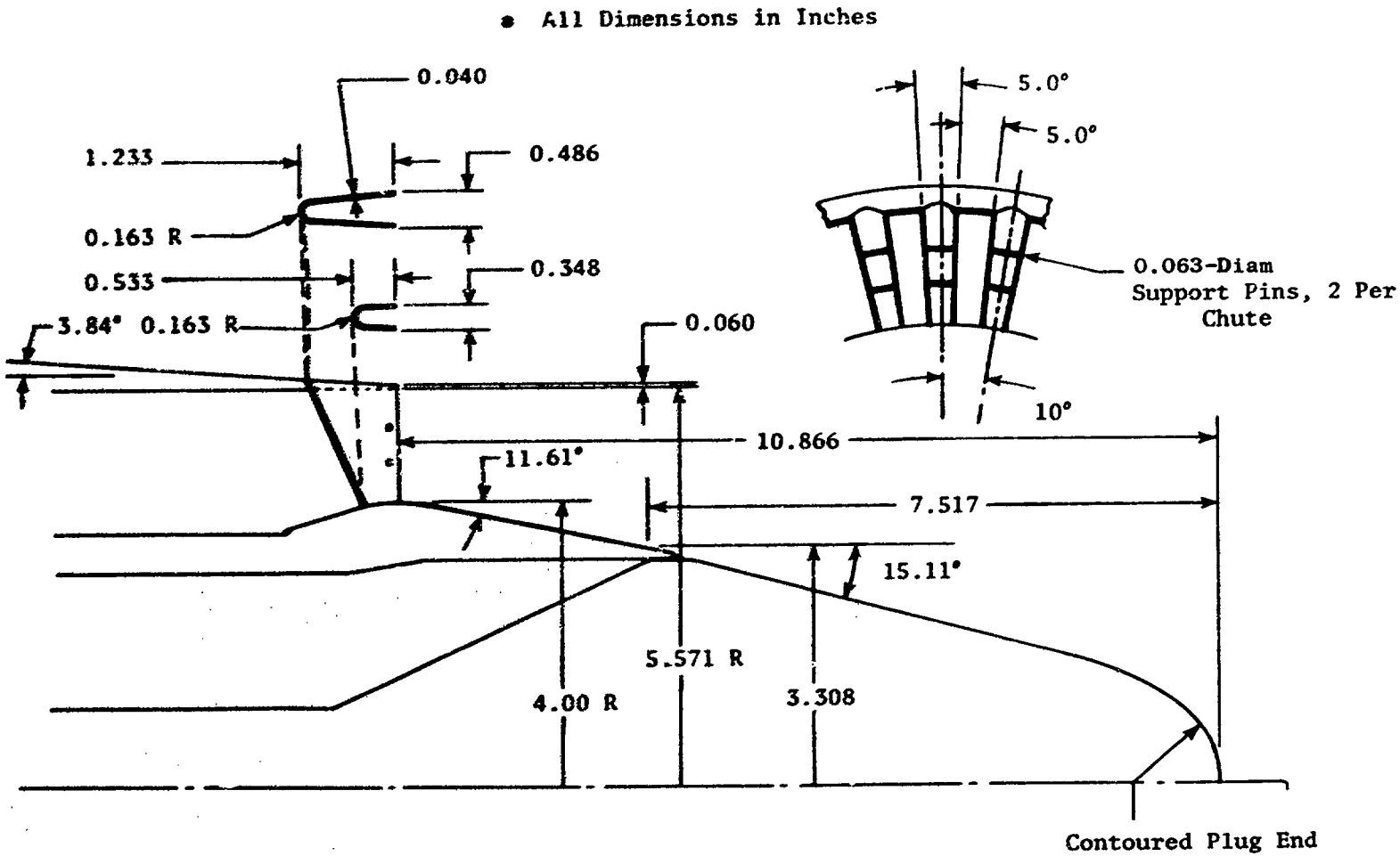

Figure A-10. Model 16 - 36-Chute, AR = 2.0, R_r = 0.716 Turbojet.

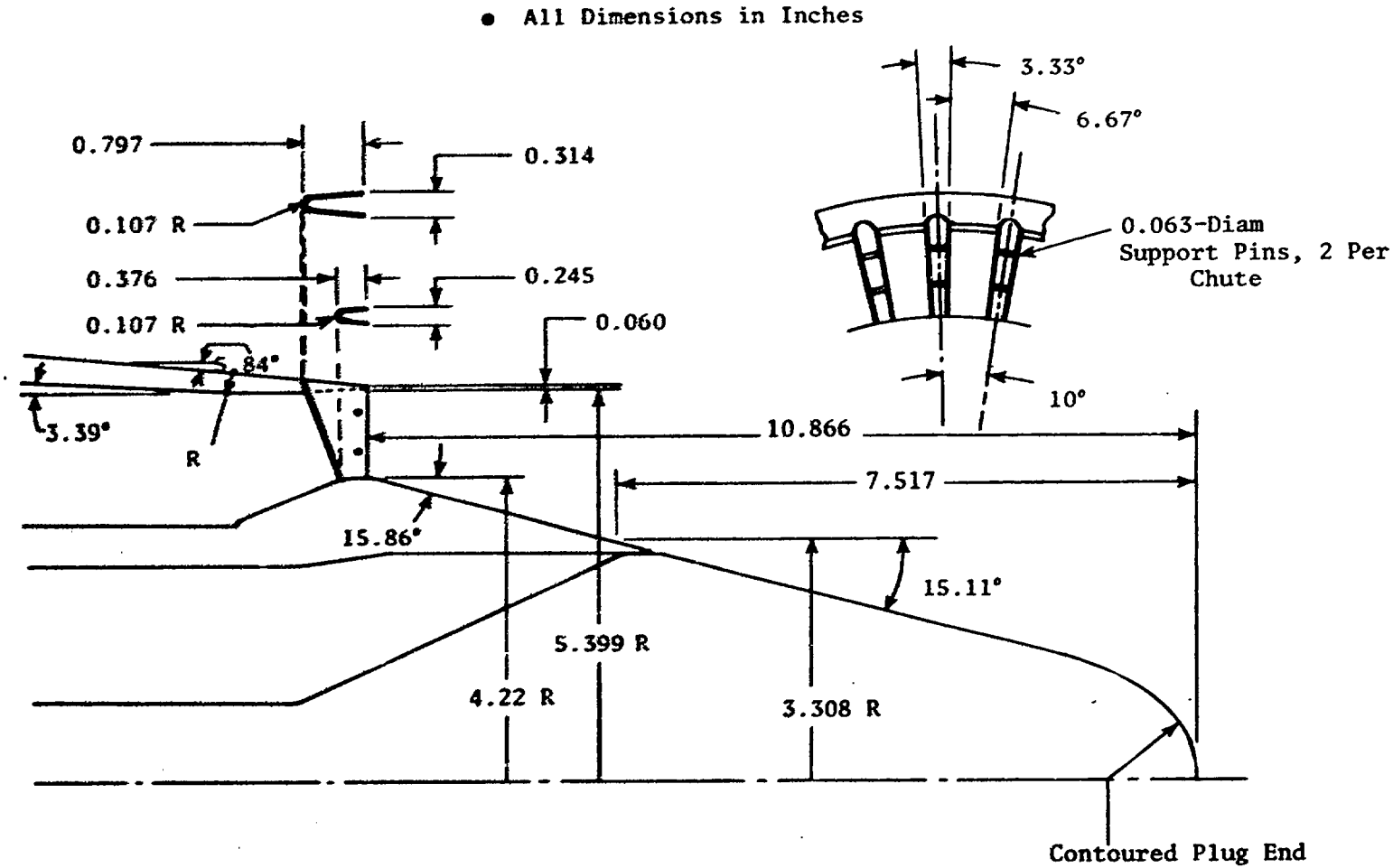

Figure A-11. Model 17 - 36-Chute, AR = 1.5, R_r = 0.782 Turbojet.

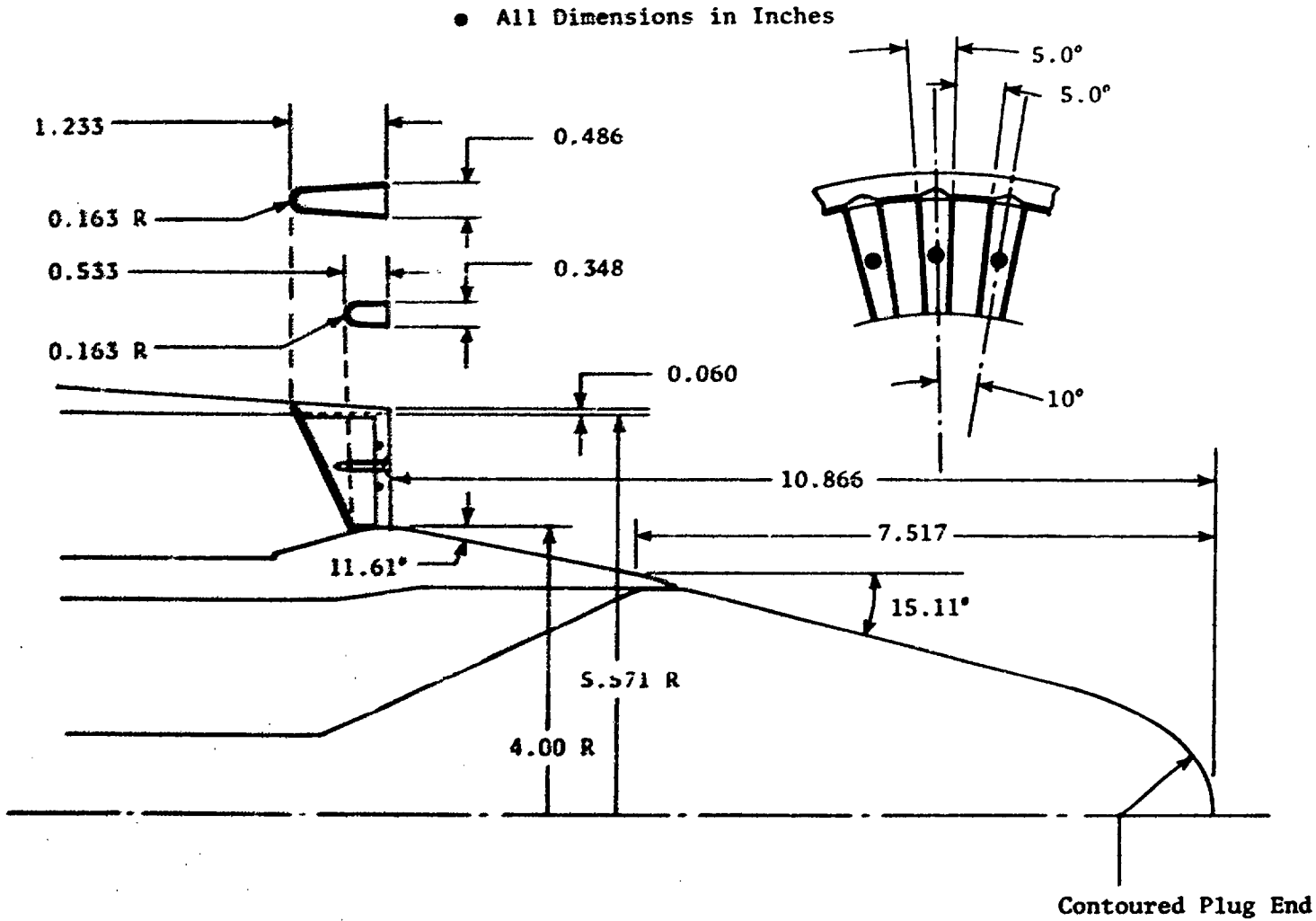

Figure A-12. Model 18 - 36-Spoke, AR = 2.0, R_r = 0.716 Turbojet.

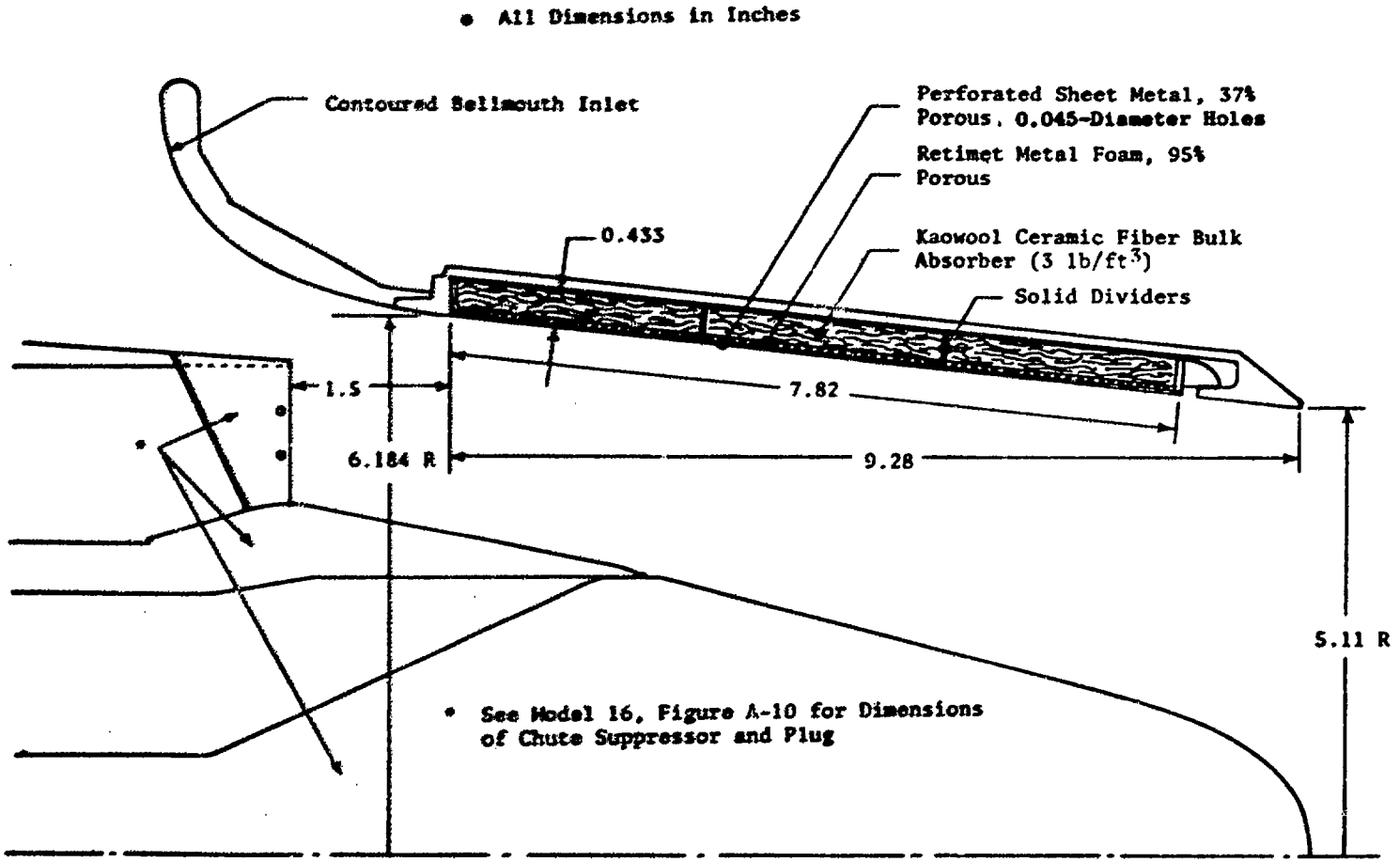

Figure A-13. Model 19 - 36-Chute, AR = 2.0, R_r = 0.716 Turbojet with Acoustically Treated Secondary Ejector.

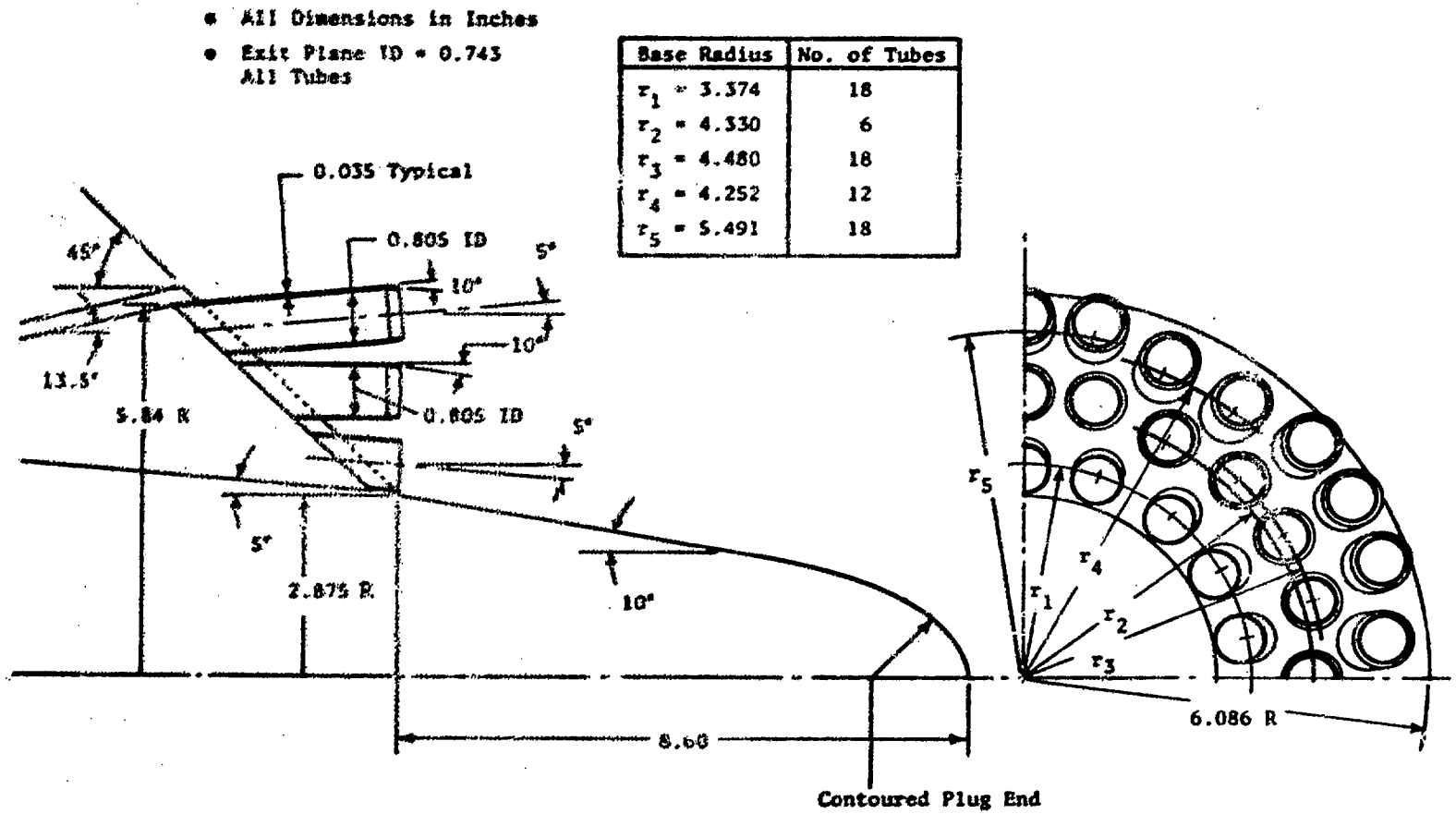

Base Radius	No. of Tubes
r_1 = 3.374	18
r_2 = 4.330	6
r_3 = 4.480	18
r_4 = 4.252	12
r_5 = 5.491	18

Figure A-14. Model 20 - 72-Tube/Plug, AR = 2.95 Turbojet.

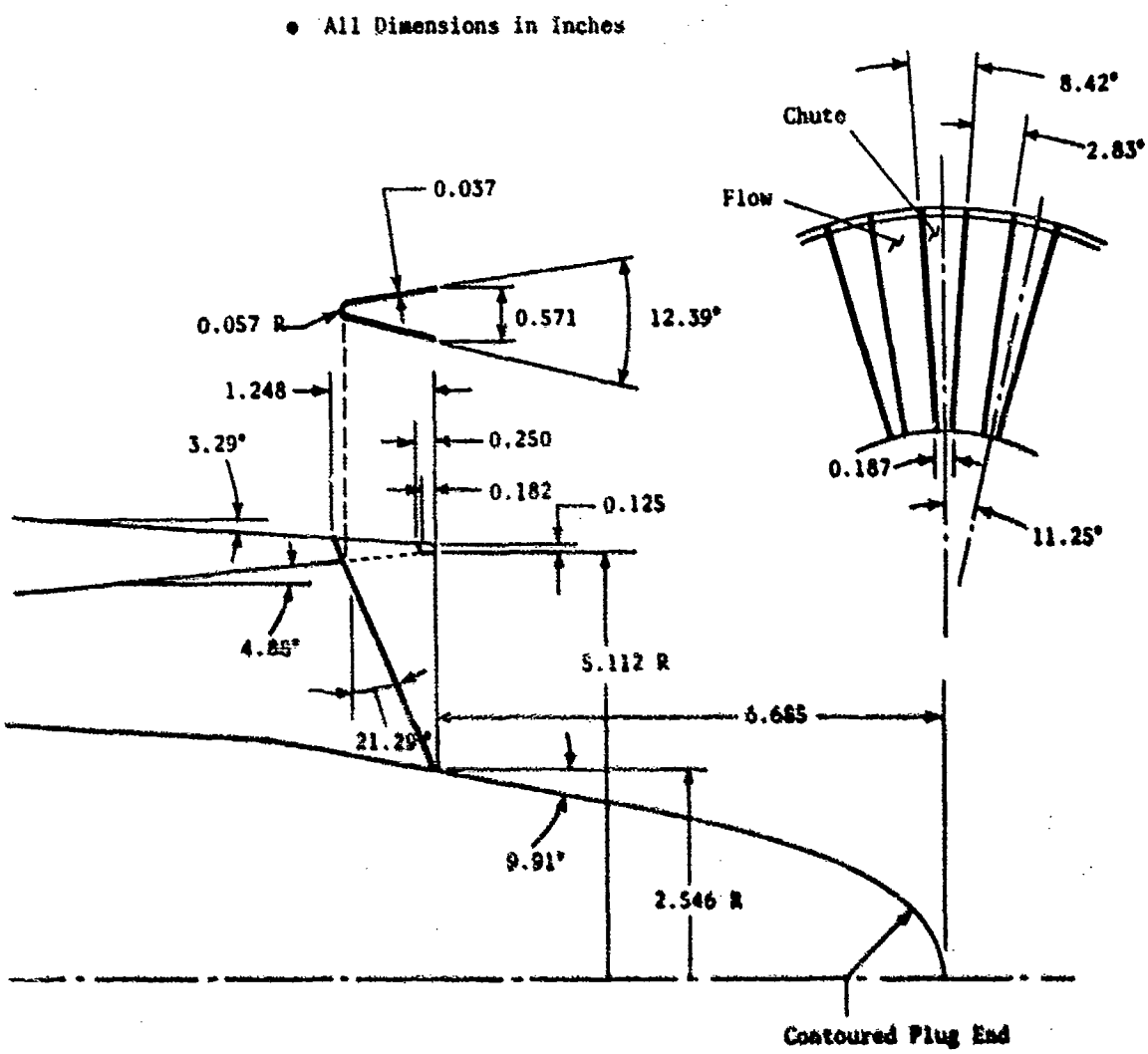

Figure A-15. Model 21 - 32-Chute, AR = 2.0, R_r = 0.498 Turbojet.

• All Dimensions in Inches

* See Model 15, Figure A-9 for Dimensions of Chute Suppressor

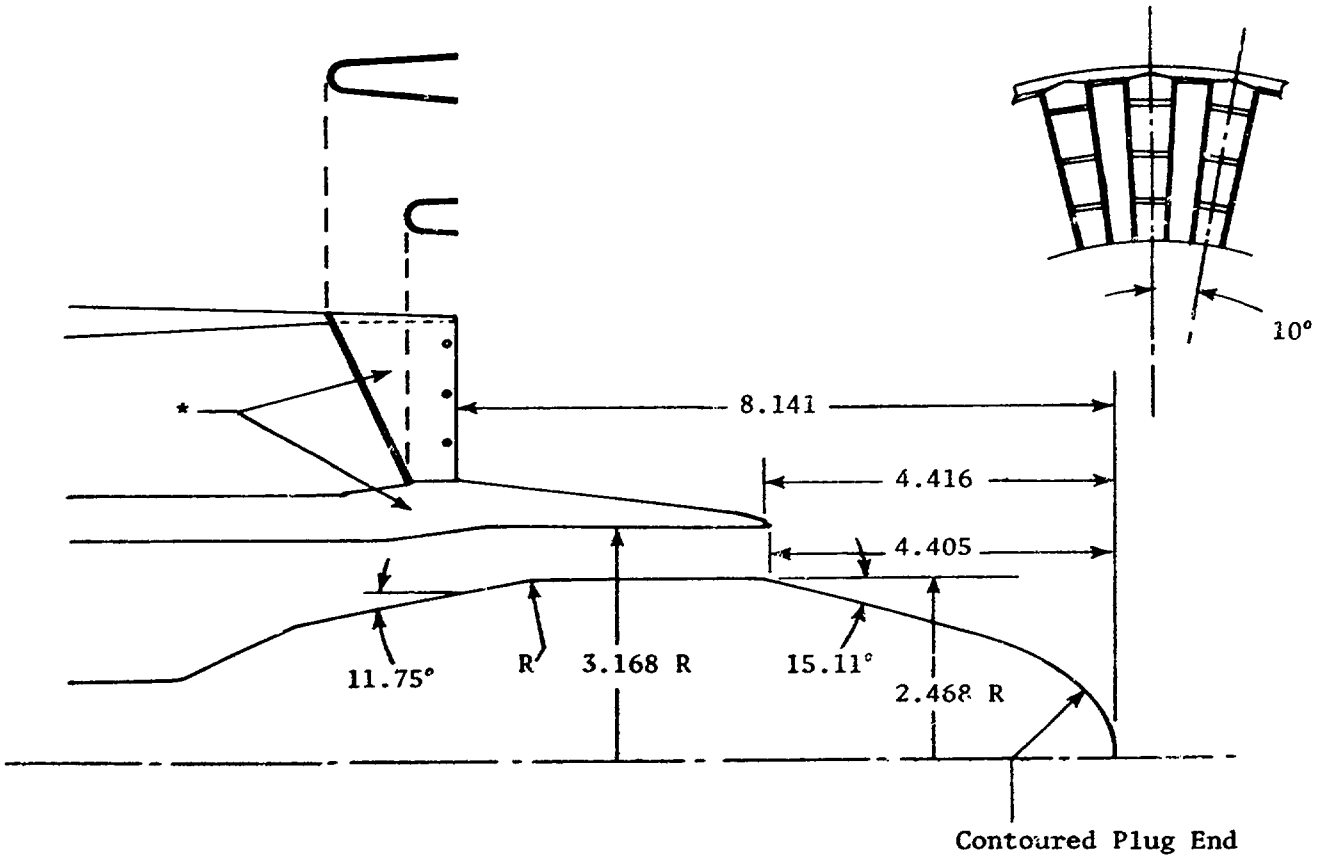

Figure A-16. Model 22 - 36-Chute, AR = 2.5, R_r^o = 0.653 Outer Suppressor; A_o/A_i = 1.92, R_r^i = 0.779 Inner Plug, Retracted.

* See Model 16, Figure A-10 for Dimensions of Chute Suppressor

● All Dimensions in Inches

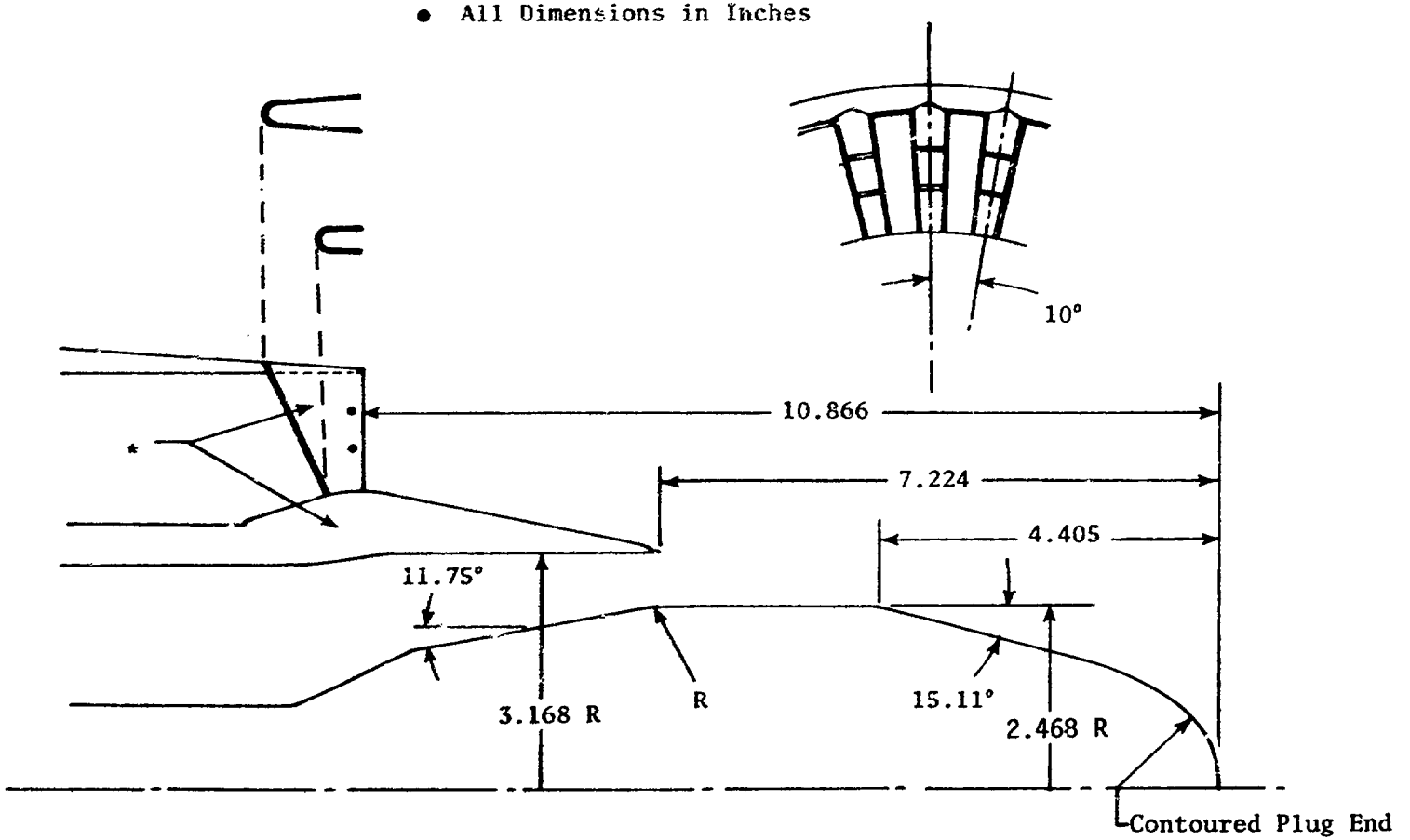

Figure A-17. Model 23 - 36-Chute, AR = 2.0, R_r^o = 0.716 Outer Suppressor; A_o/A_i = 1.92, R_r^i = 0.779 Inner Plug, In-Line.

• All Dimensions in Inches

* See Model 16, Figure A-10, for Dimensions of Chute Suppressor

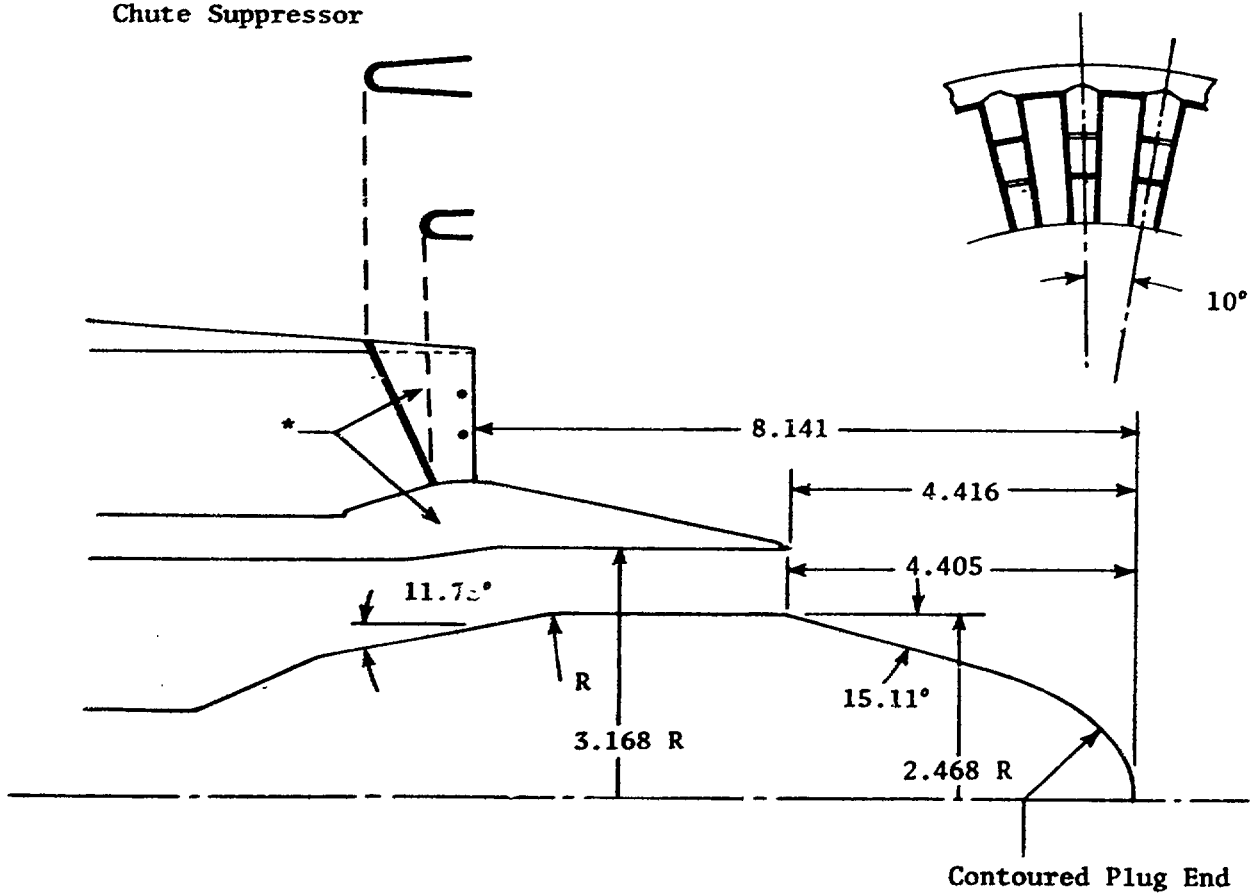

Figure A-18. Model 24 - 36-Chute, AR = 2.0, R_r^o = 0.716 Outer Suppressor; A_o/A_i = 1.92, R_r^i = 0.779 Inner Plug, Retracted.

• All Dimensions in Inches

* See Model 16, Figure A-10, for Dimensions of Chute Suppressor

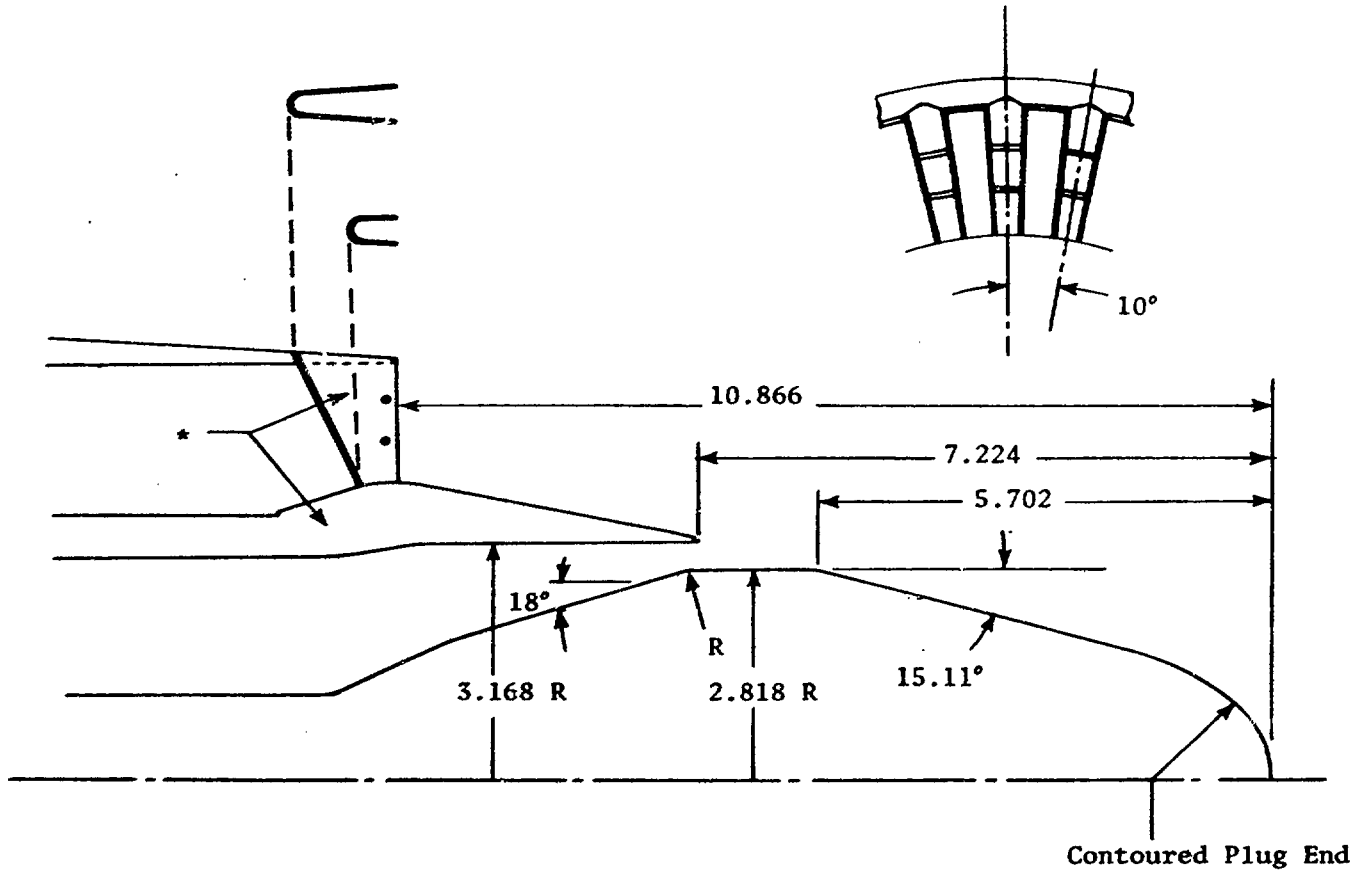

Figure A-19. Model 25 - 36-Chute, AR = 2.0, R_r^o = 0.716 Outer Suppressor; A_o/A_i = 3.61, R_r^i = 0.89 Inner Plug, In-Line.

• All Dimensions in Inches

* See Model 16, Figure A-10, for Dimensions of Chute Suppressor

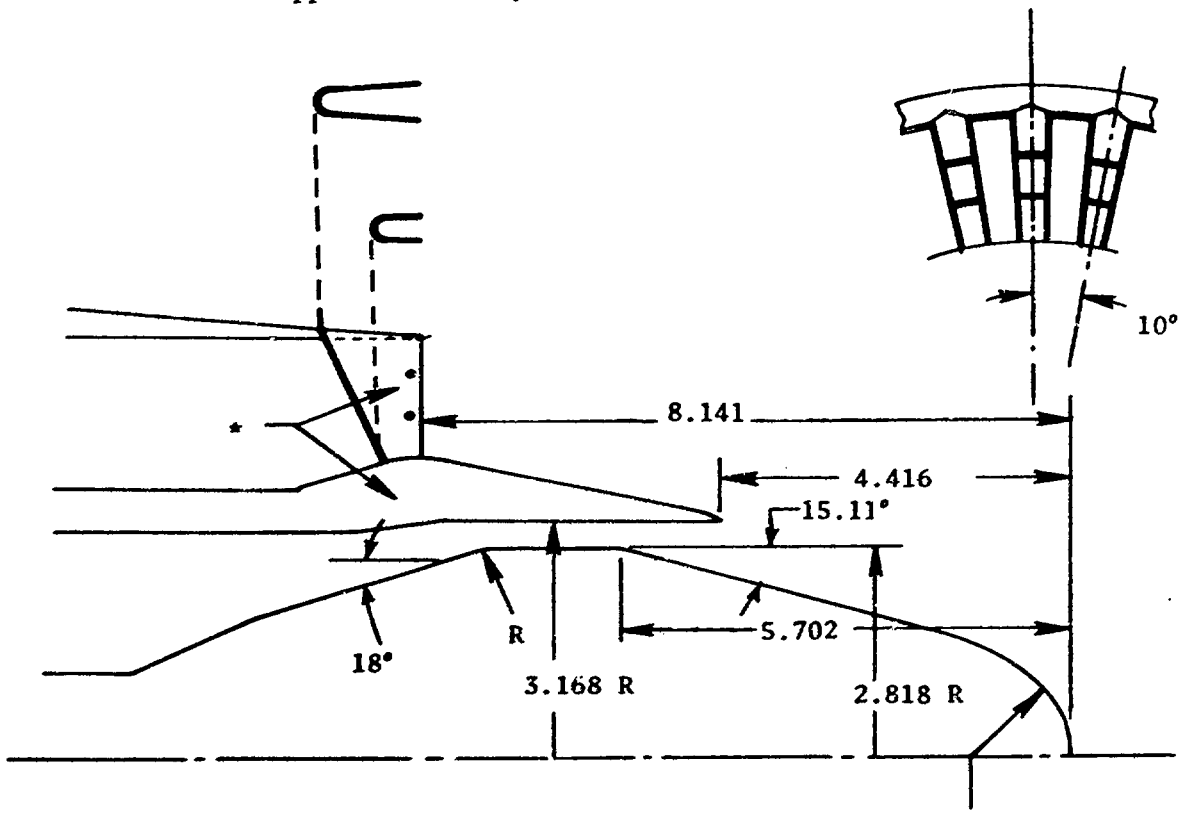

Figure A-20. Model 26 - 36-Chute, AR = 2.0, R_r^o = 0.716 Outer Suppressor; A_o/A_i = 3.61, R_r^i = 0.89 Inner Plug, Retracted.

● All Dimensions in Inches

* See Model 17, Figure A-11, for Dimensions of Chute Suppressor

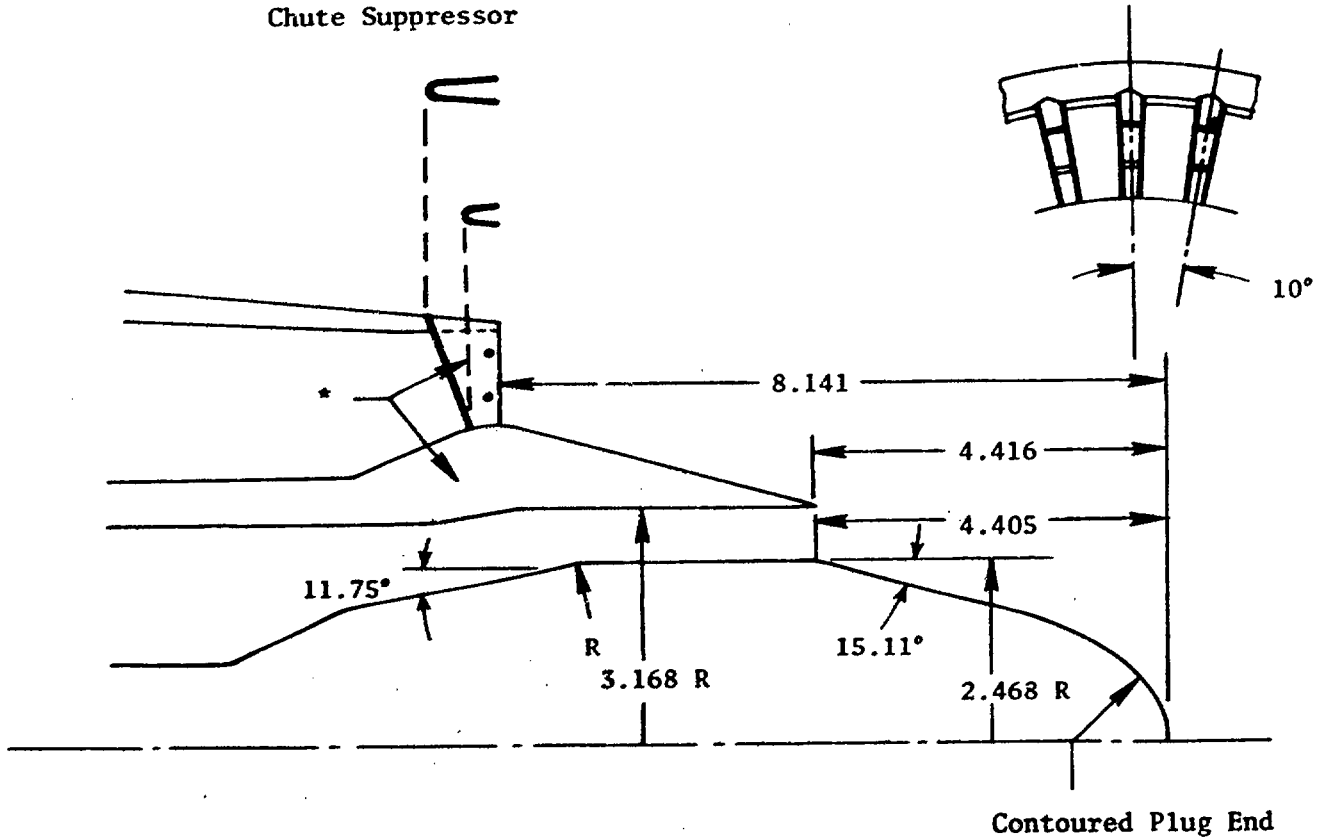

Figure A-21. Model 27 - 36-Chute, AR = 1.5, R_r^o = 0.782 Outer Suppressor; A_o/A_i = 1.92, R_r^i = 0.779 Inner Plug, Retracted.

- All Dimensions in Inches

* See Model 18, Figure A-12, for Dimensions of Spoke Suppressor

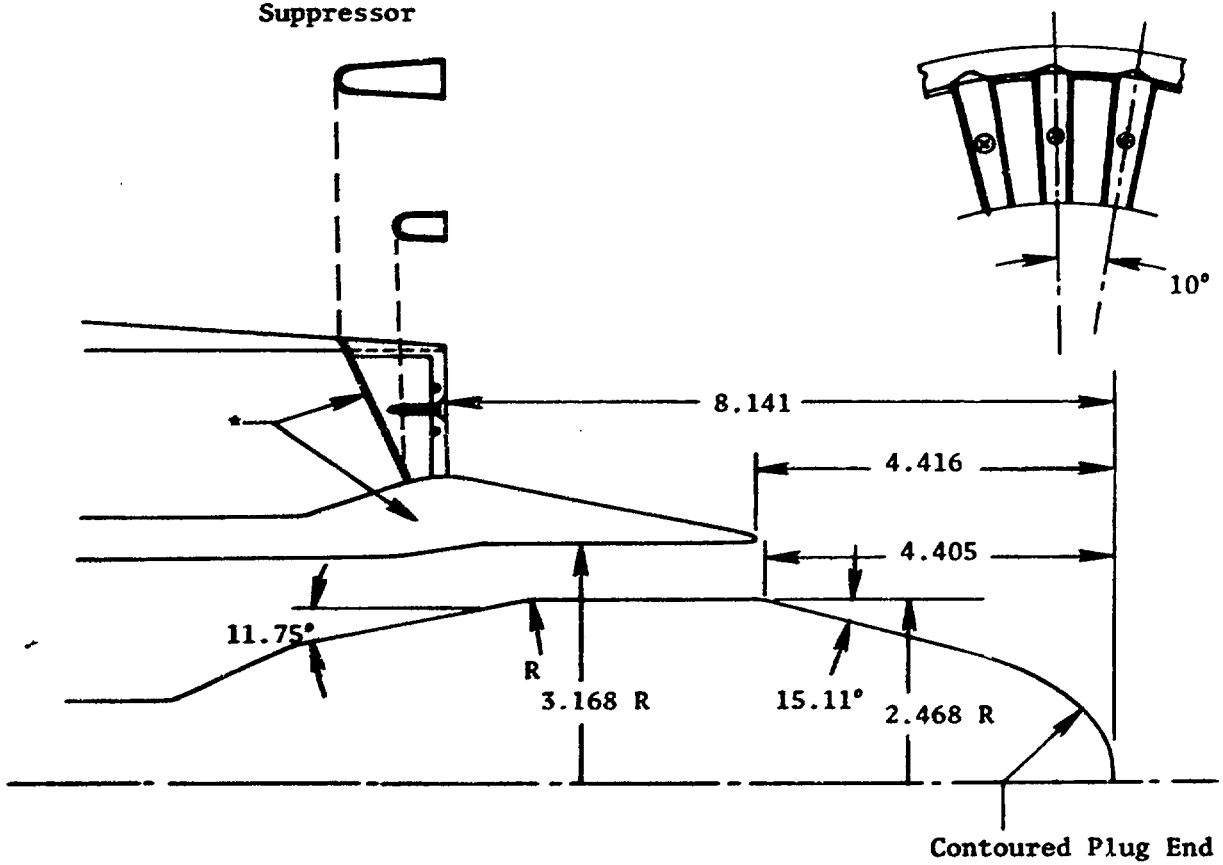

Figure A-22. Model 28 - 36-Spoke, AR = 2.0, R_r^o = 0.716 Outer Suppressor; A_o/A_i = 1.92, R_r^i = 0.779 Inner Plug, Retracted.

• All Dimensions in Inches

* See Model 18, Figure A-12, for Dimensions of Spoke Suppressor

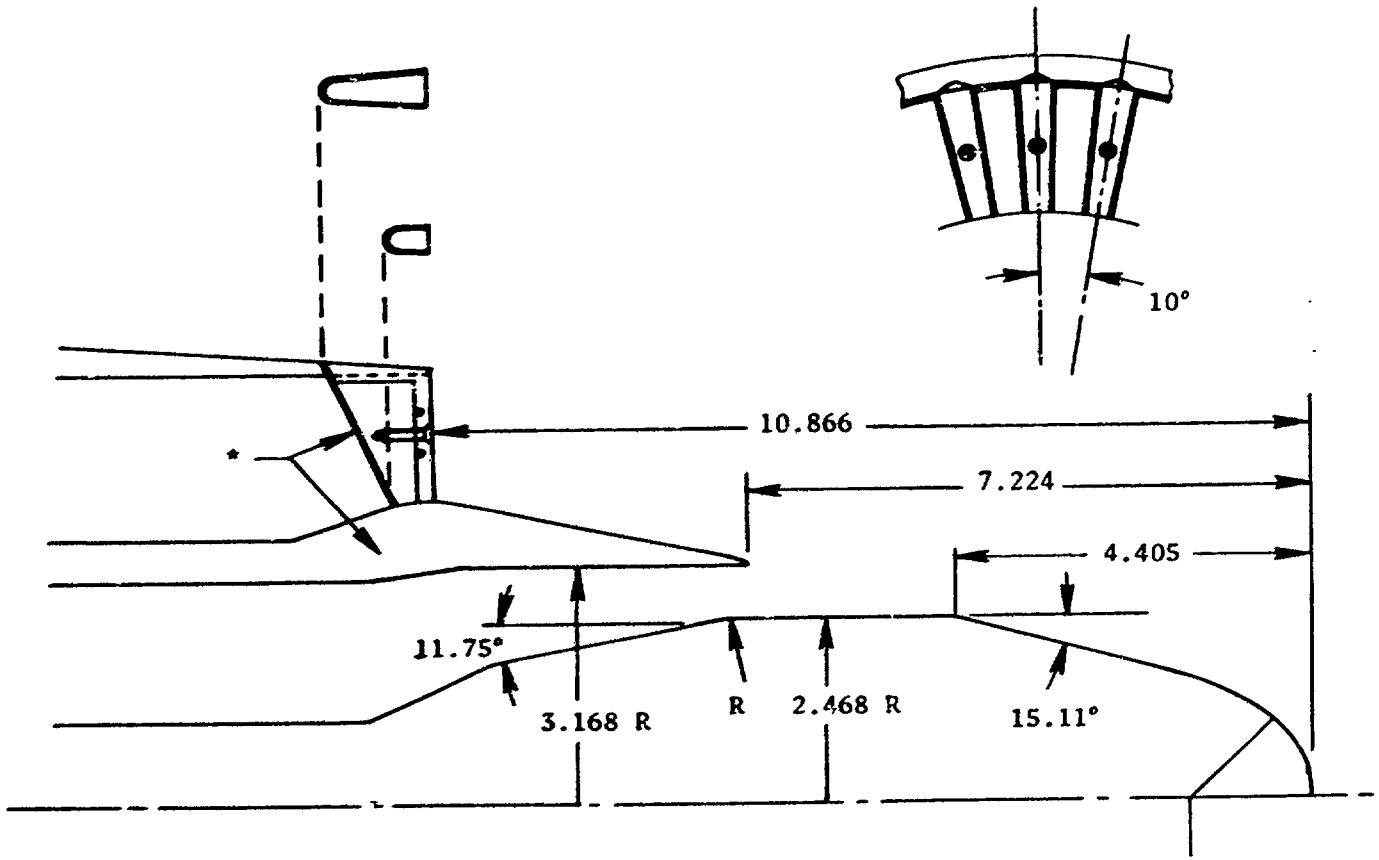

Figure A-23. Model 29 - 36-Spoke, AR = 2.0, R_r^o = 0.716 Outer Suppressor; A_o/A_i = 1.92, R_r^i = 0.779 Inner Plug, In-Line.

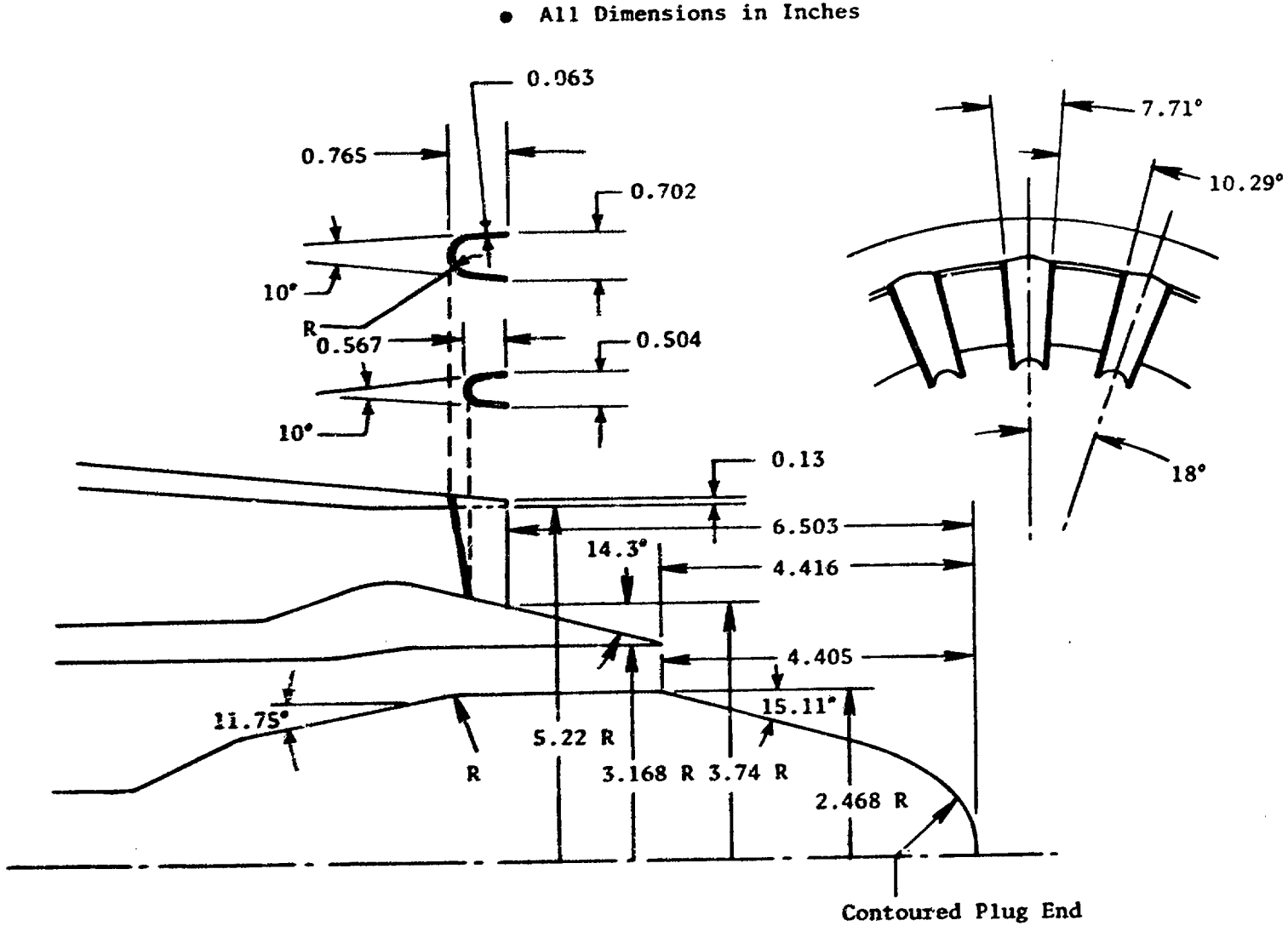

Figure A-24. Model 30 - 20-Shallow-Chute, AR = 1.75, R_r^o = 0.717 Outer Suppressor; A_o/A_i = 1.92, R_r^i = 0.779 Inner Plug, Retracted.

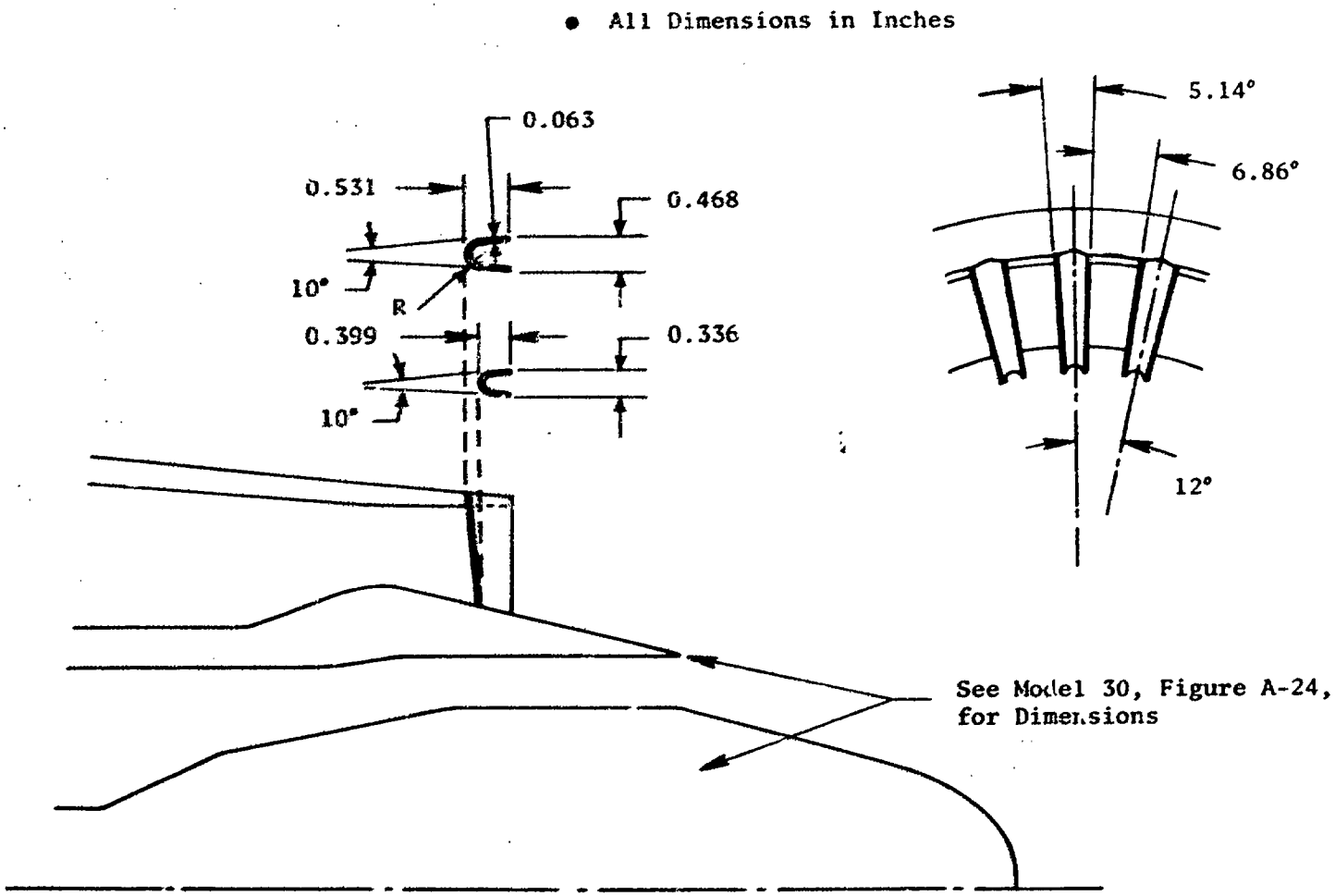

Figure A-25. Model 31 - 30-Shallow-Chute, AR = 1.75, R_r^o = 0.717 Outer Suppressor; A_o/A_i = 1.92, R_r^i = 0.779 Inner Plug, Retracted.

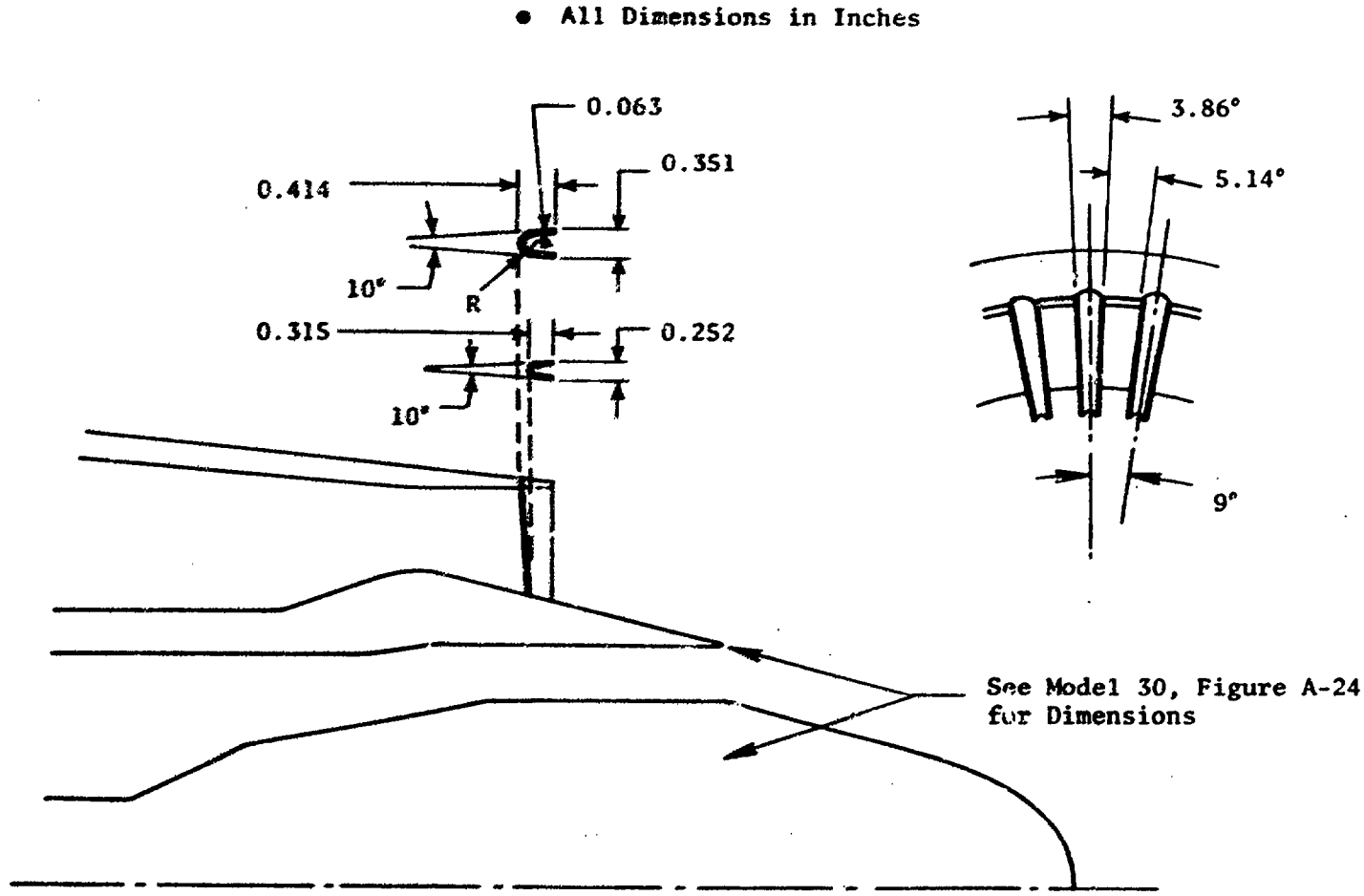

Figure A-26. Model 32 - 40-Shallow-Chute, AR = 1.75, R_r^o = 0.717 Outer Suppressor; A_o/A_i = 1.92, R_r^i = 0.779 Inner Plug, Retracted.

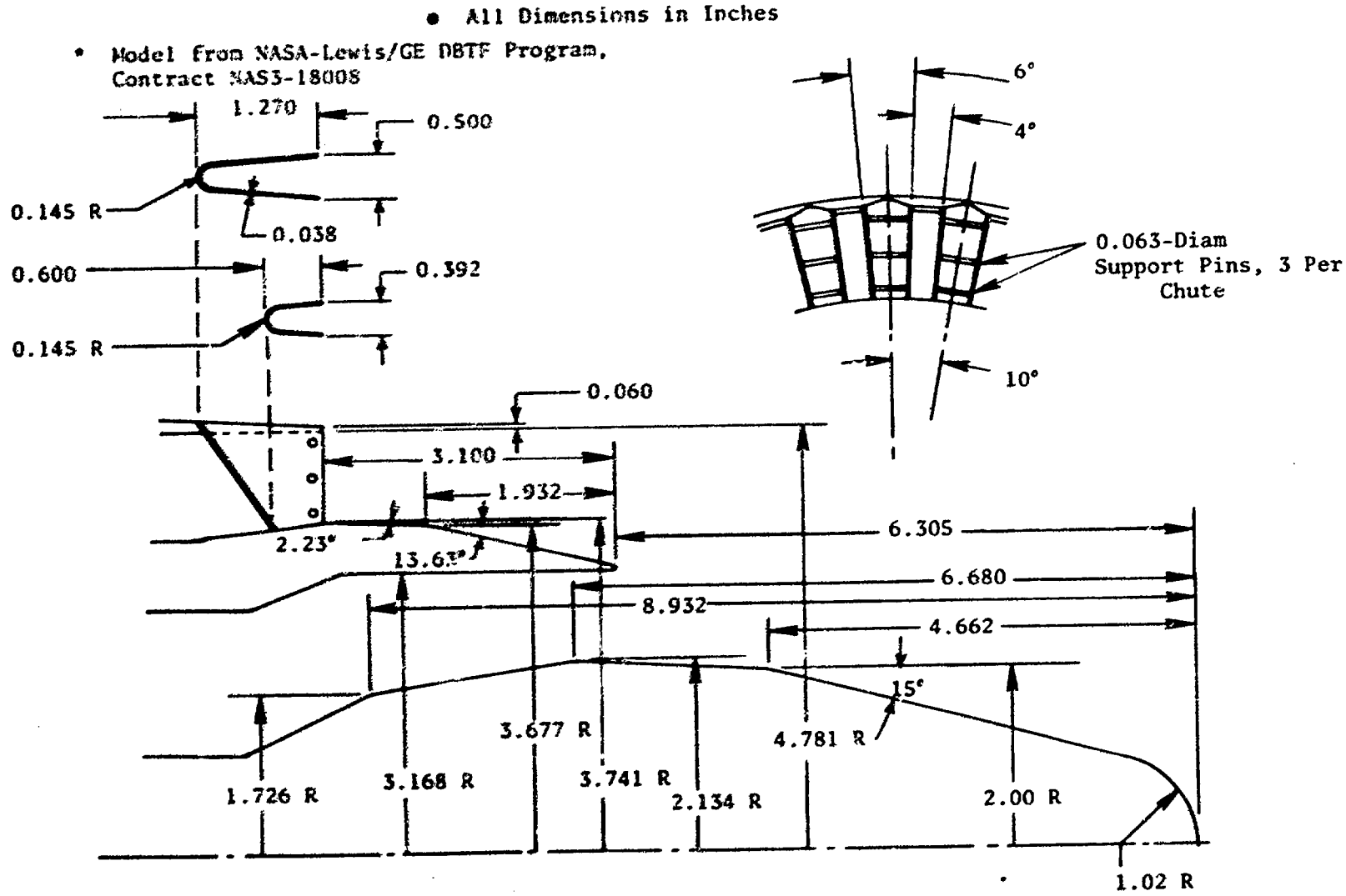

Figure A-27. • Model 33 - 36-Chute, AR = 2.5, R_T^o = 0.783 Outer Suppressor; A_o/A_i = 0.65, R_T^i = 0.674 Inner Plug, Retracted.

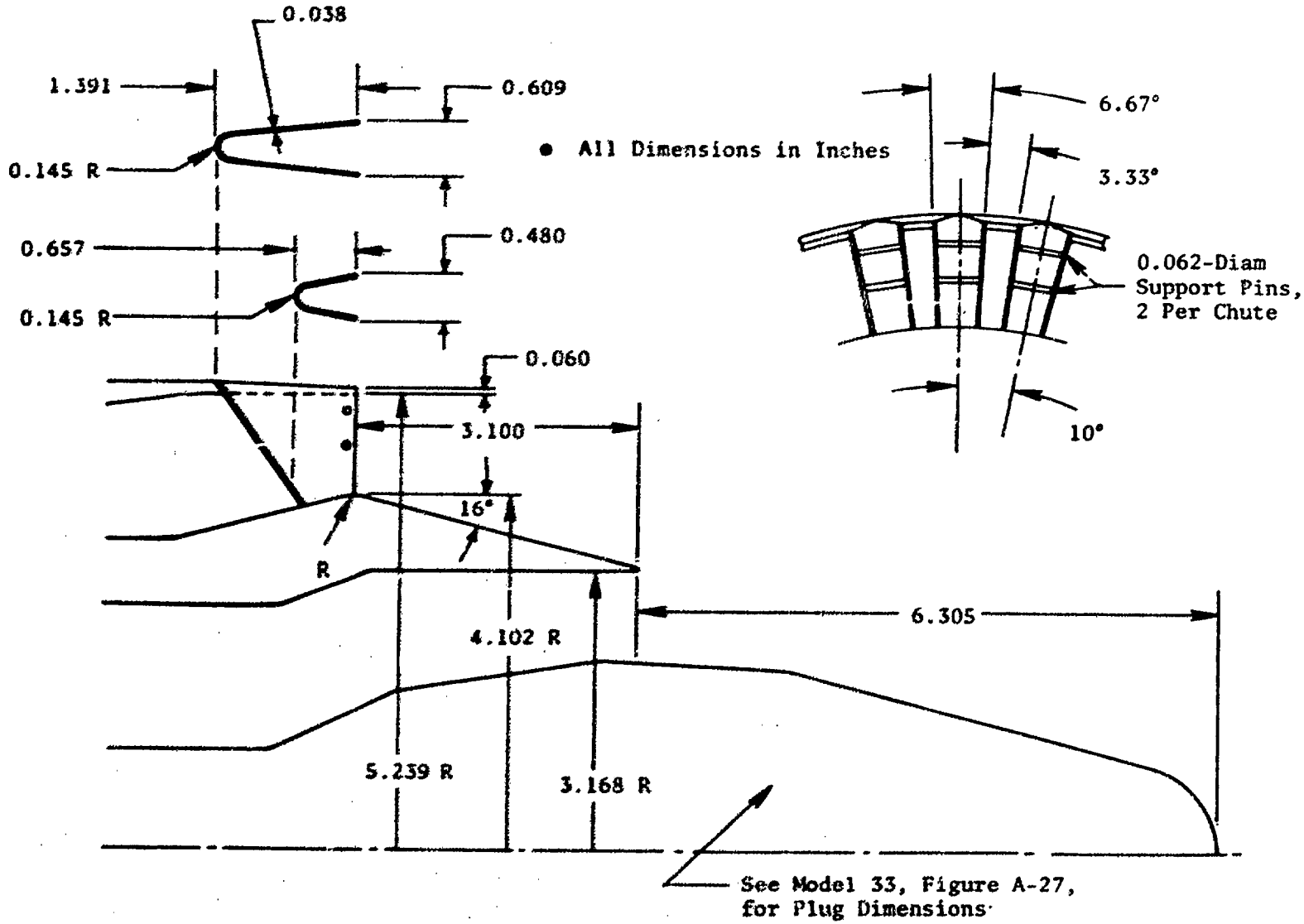

Figure A-28. Model 34 - 36-Chute, AR = 3.0, R_T^o = 0.783 Outer Suppressor; A_o/A_i = 0.65, R_T^i = 0.674 Inner Plug, Retracted.

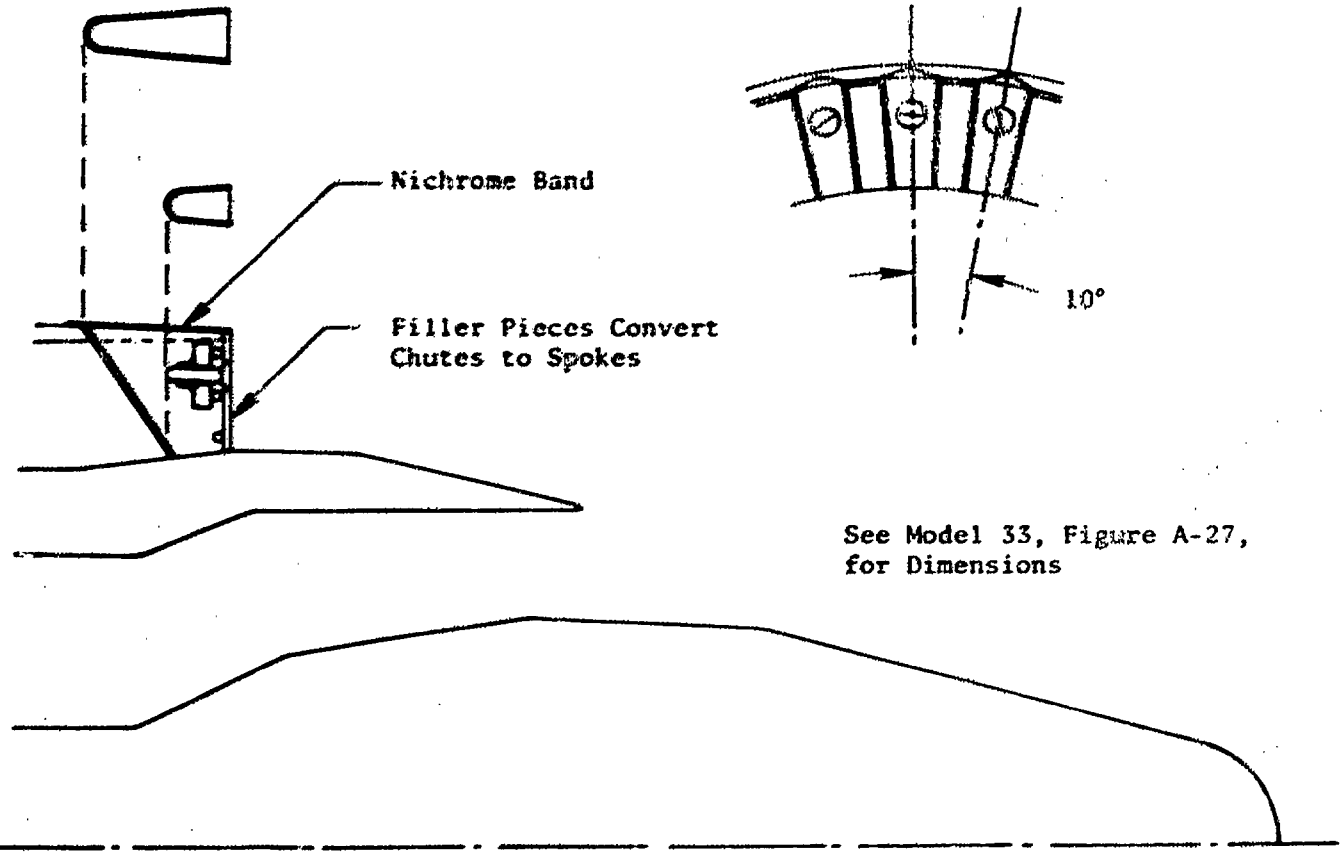

Figure A-29. Model 35 - 36-Spoke, AR = 2.5, R_r^o = 0.783 Outer Suppressor; A_o/A_i = 0.65, R_r^i = 0.674 Inner Plug, Retracted.

- All Dimensions in Inches

* See Model 16, Figure A-10, for Dimensions of Chute Suppressor

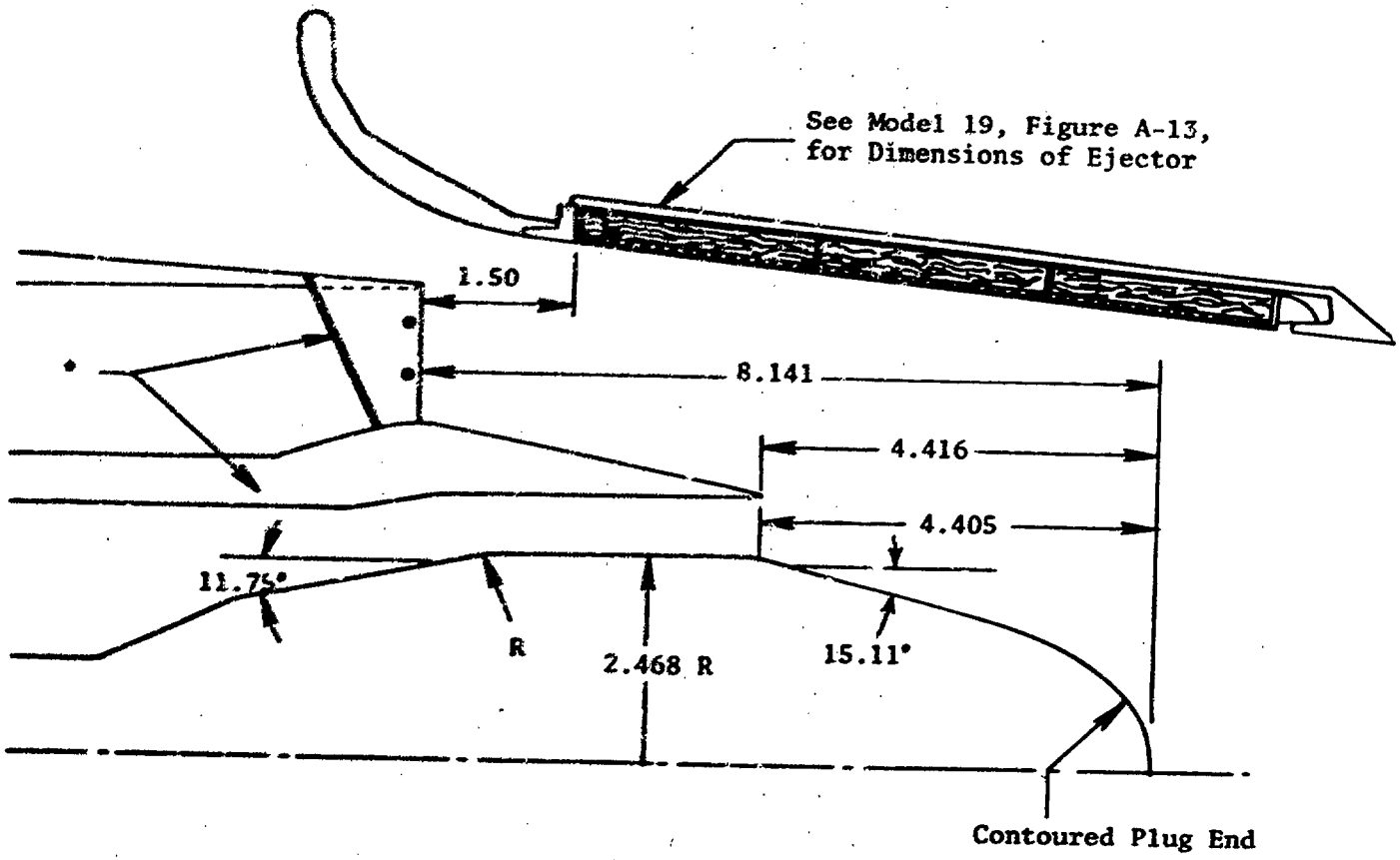

Figure A-30. Model 36 - 36-Chute, AR = 2.0, R_1^o = 0.716 Outer Suppressor; A_o/A_i = 1.92, R_1^I = 0.779 Inner Plug, Retracted with Acoustically Treated Ejector.

• All Dimensions in Inches

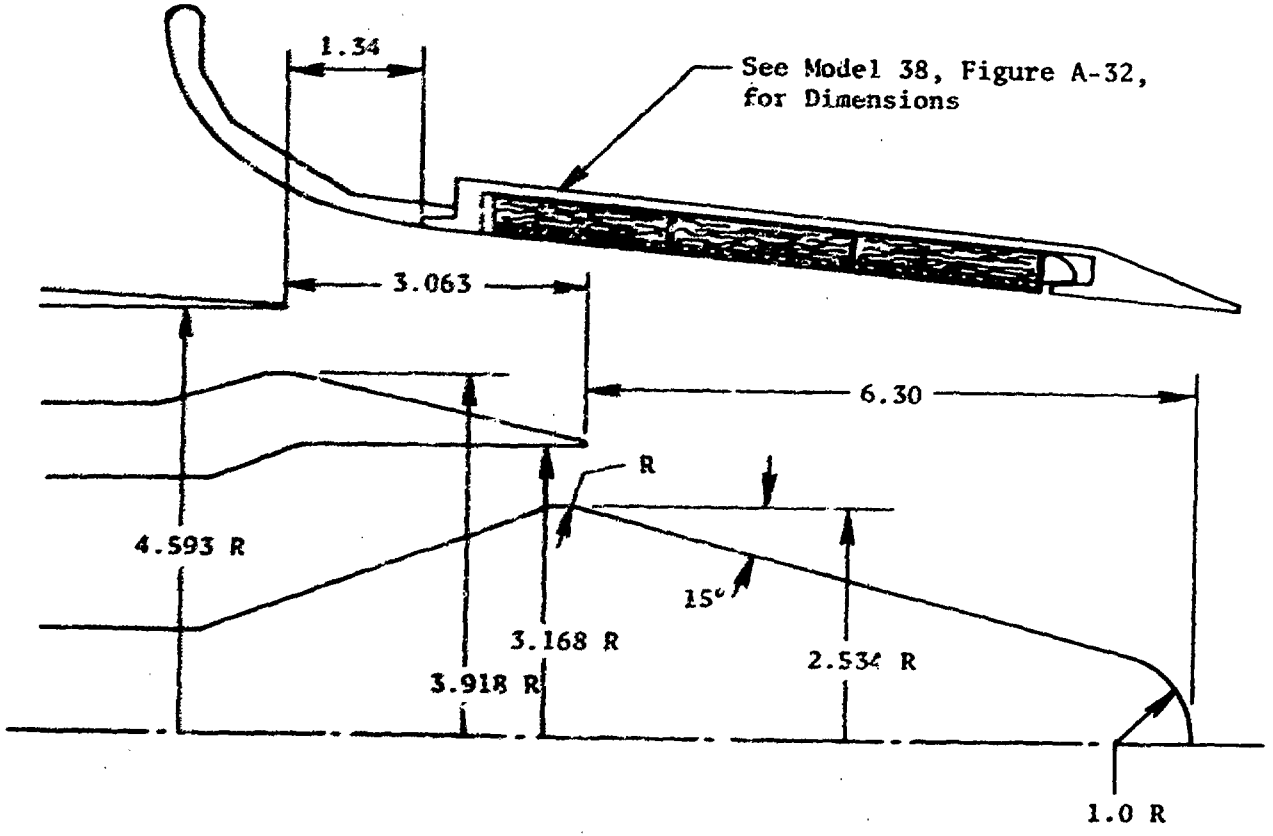

Figure A-31. Model 37 - Coannular-Noncoplanar Dual-Plug Nozzle, R_r^o = 0.853, A_o/A_j = 1.59, R_r^i = 0.800 with Acoustically Treated Secondary Ejector.

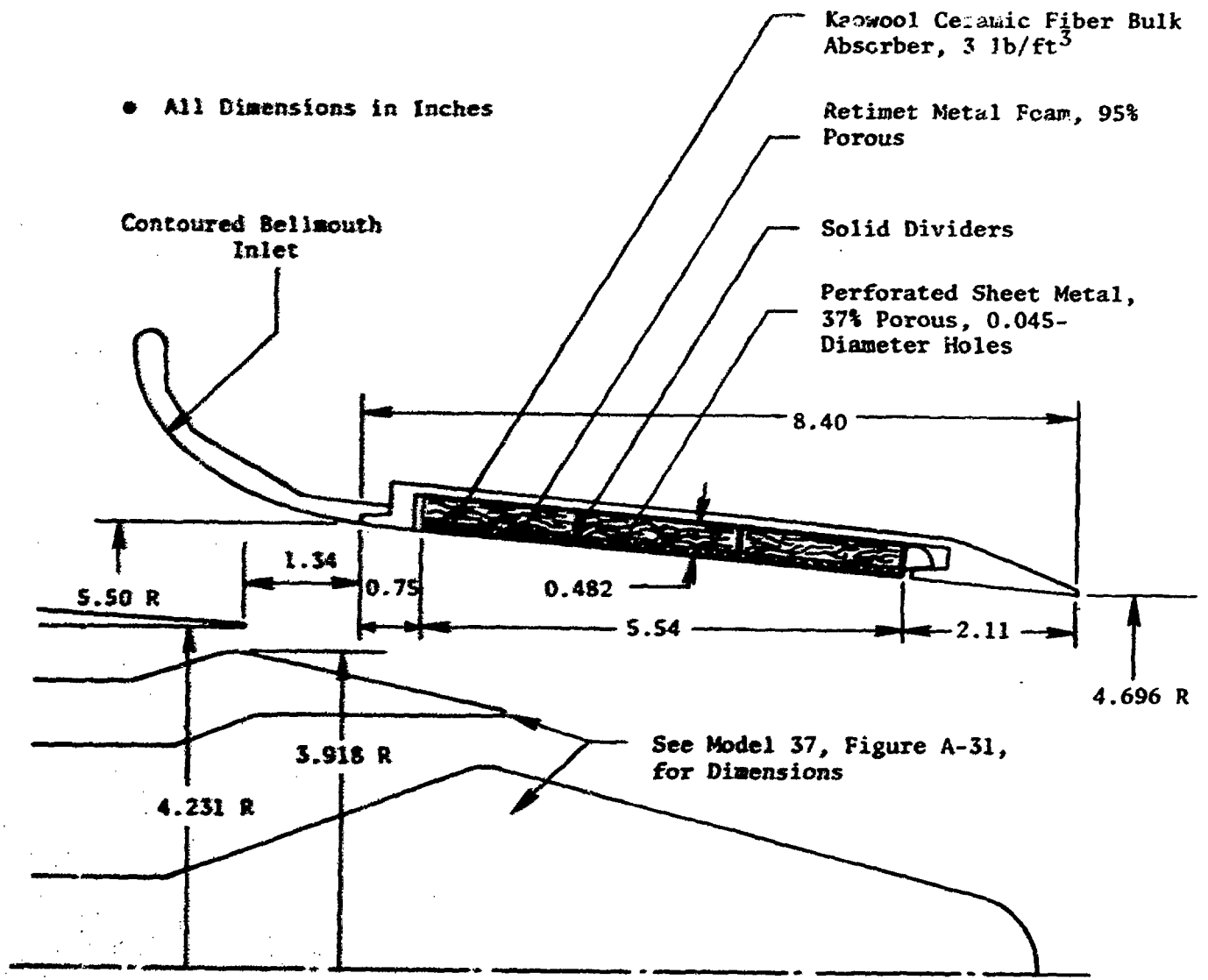

Figure A-32. Model 38 - Coannular-Noncoplanar Dual-Plug Nozzle, $R_r^o = 0.926$, $A_o/A_i = 0.71$, $R_r^i = 0.800$ with Acoustically Treated Secondary Ejector.

• All Dimensions in Inches

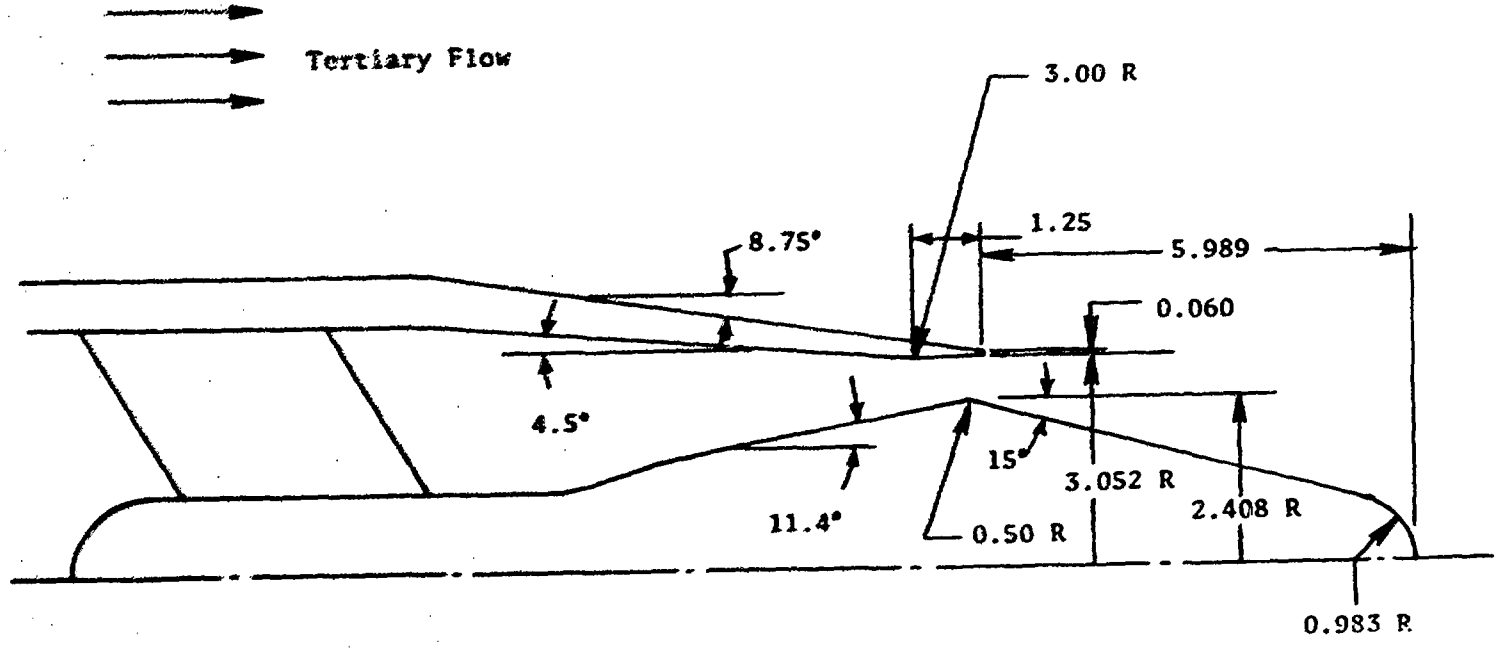

Figure A-33. Model 39 - Converging Plug, Single-Flow, R_r = 0.789.

• All Dimensions in Inches

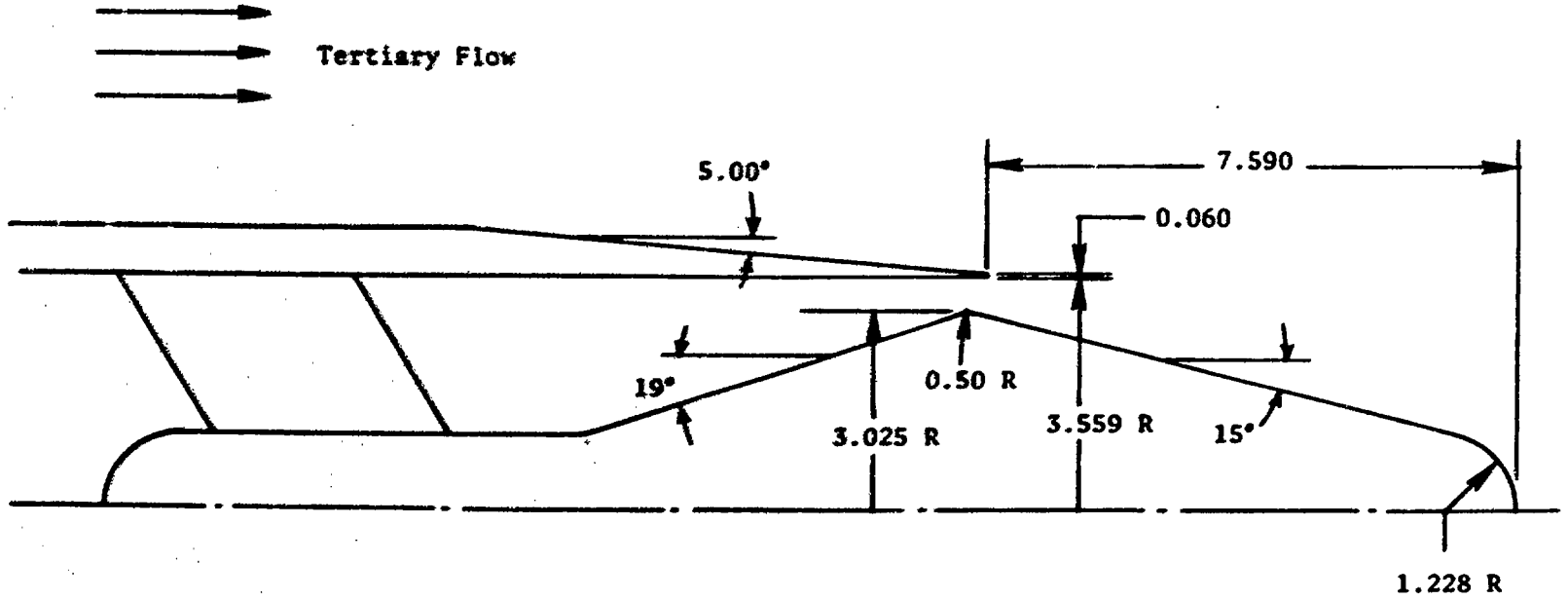

Figure A-34. Model 40 - Converging Plug, Single-Flow, R_r = 0.85.

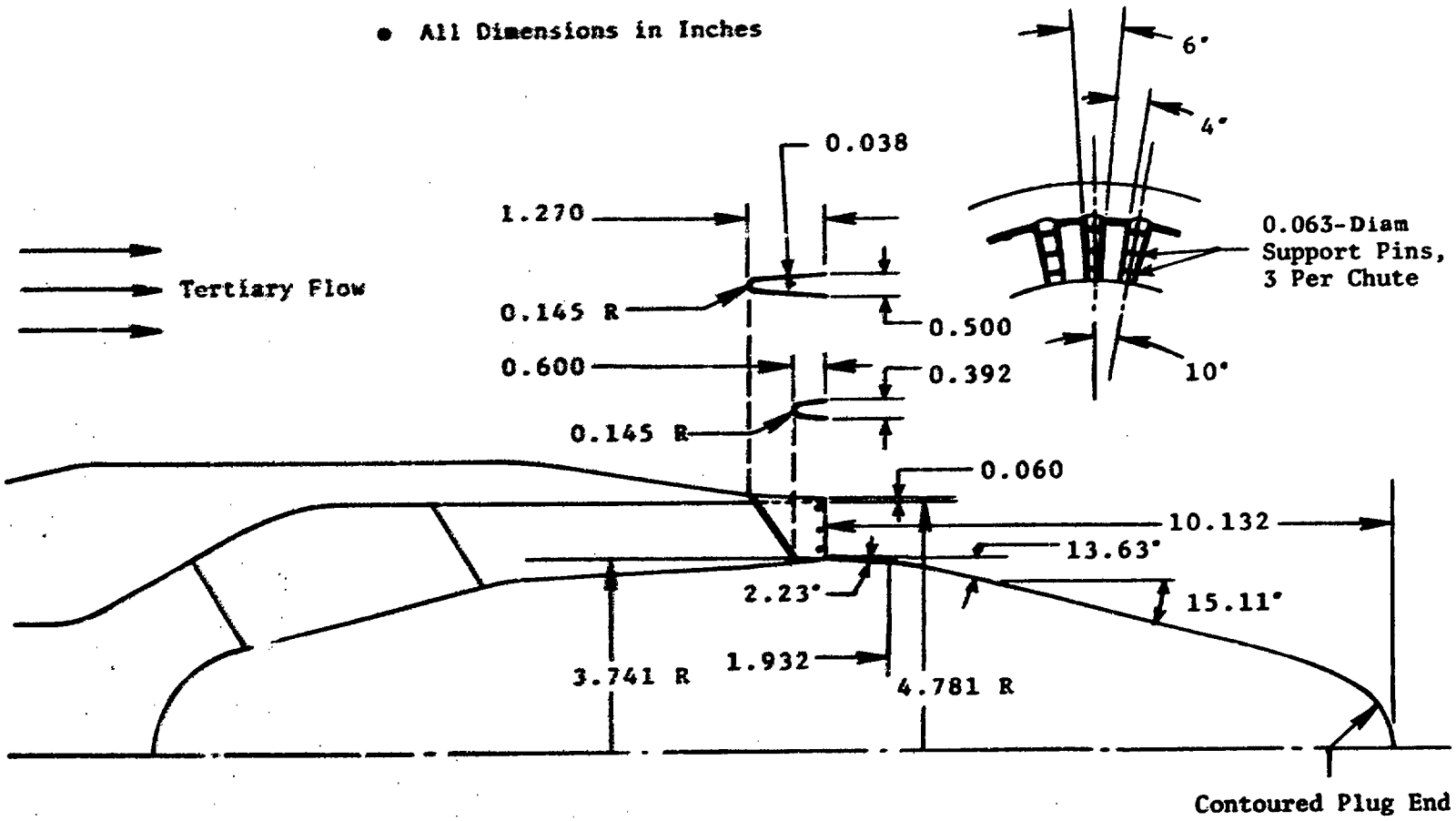

Figure A-35. Model 41 - 36-Chute, AR = 2.5, R_r = 0.78 Turbojet.

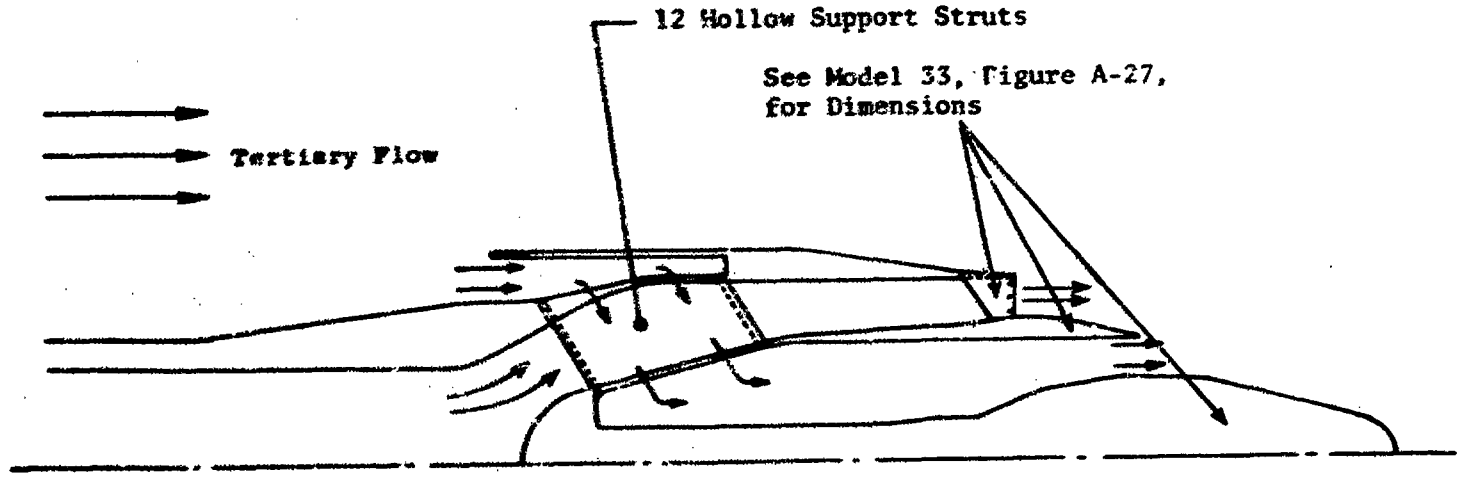

Figure A-36. Model 42 - 36-Chute, AR = 2.5, R_r^o = 0.78 Outer Suppressor with Induced Flow Through A_o/A_i = 0.65, R_r^i = 0.674 Inner Plug, Retracted.

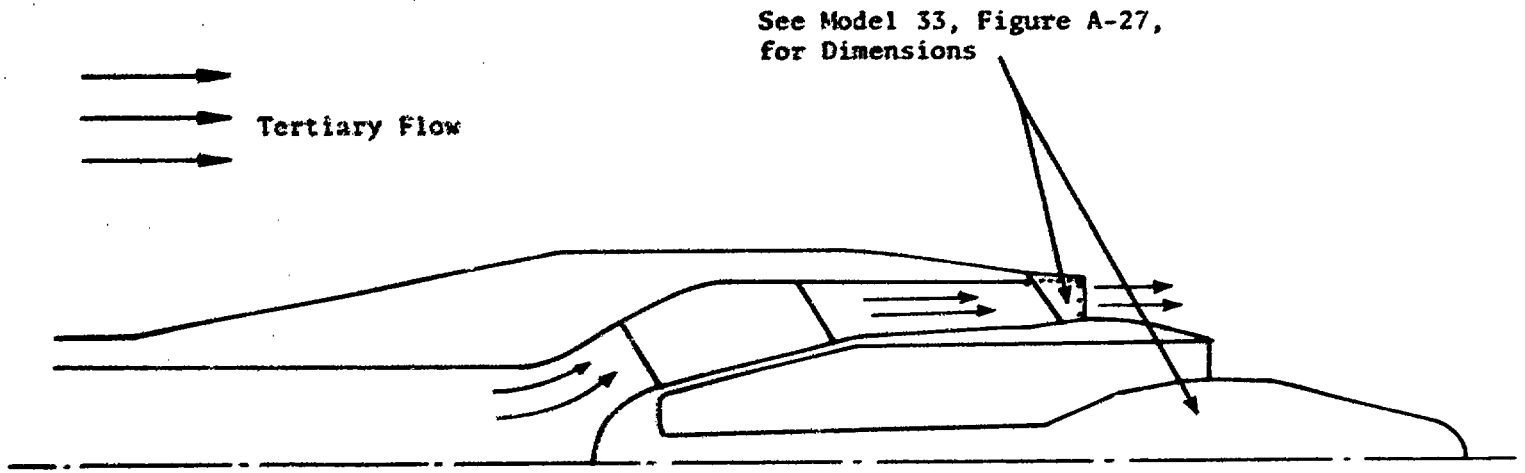

Figure A-37. Model 43 - 36-Chute, AR = 2.5, R_r^o = 0.78 Outer Suppressor with Abrupt Step Over A_o/A_i = 0.65, R_r^i = 0.674 Inner Plug, Retracted.

• All Dimensions in Inches

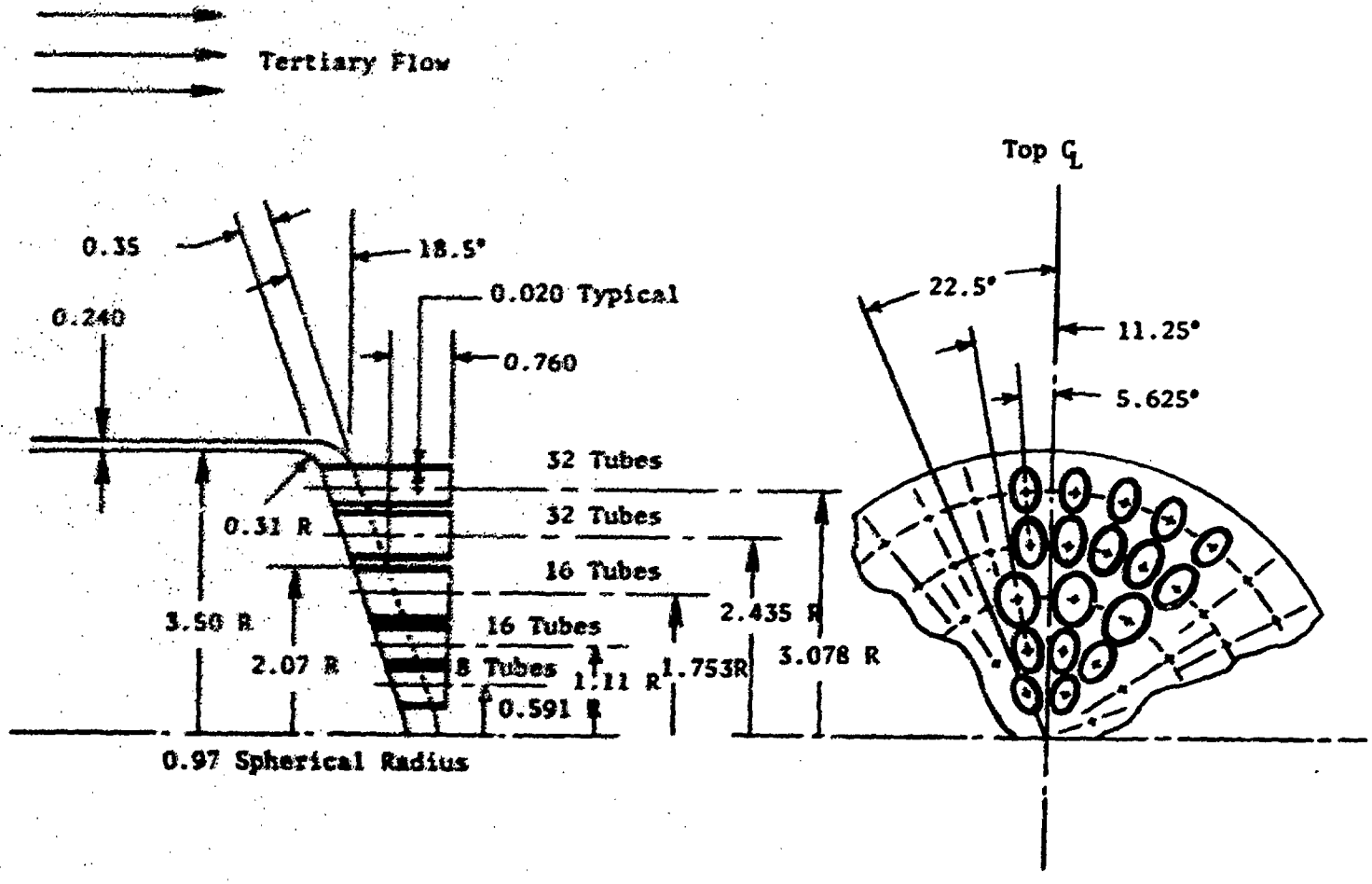

Figure A-38. Model 44 - 104 Elliptical Tubes, AR = 2.8.

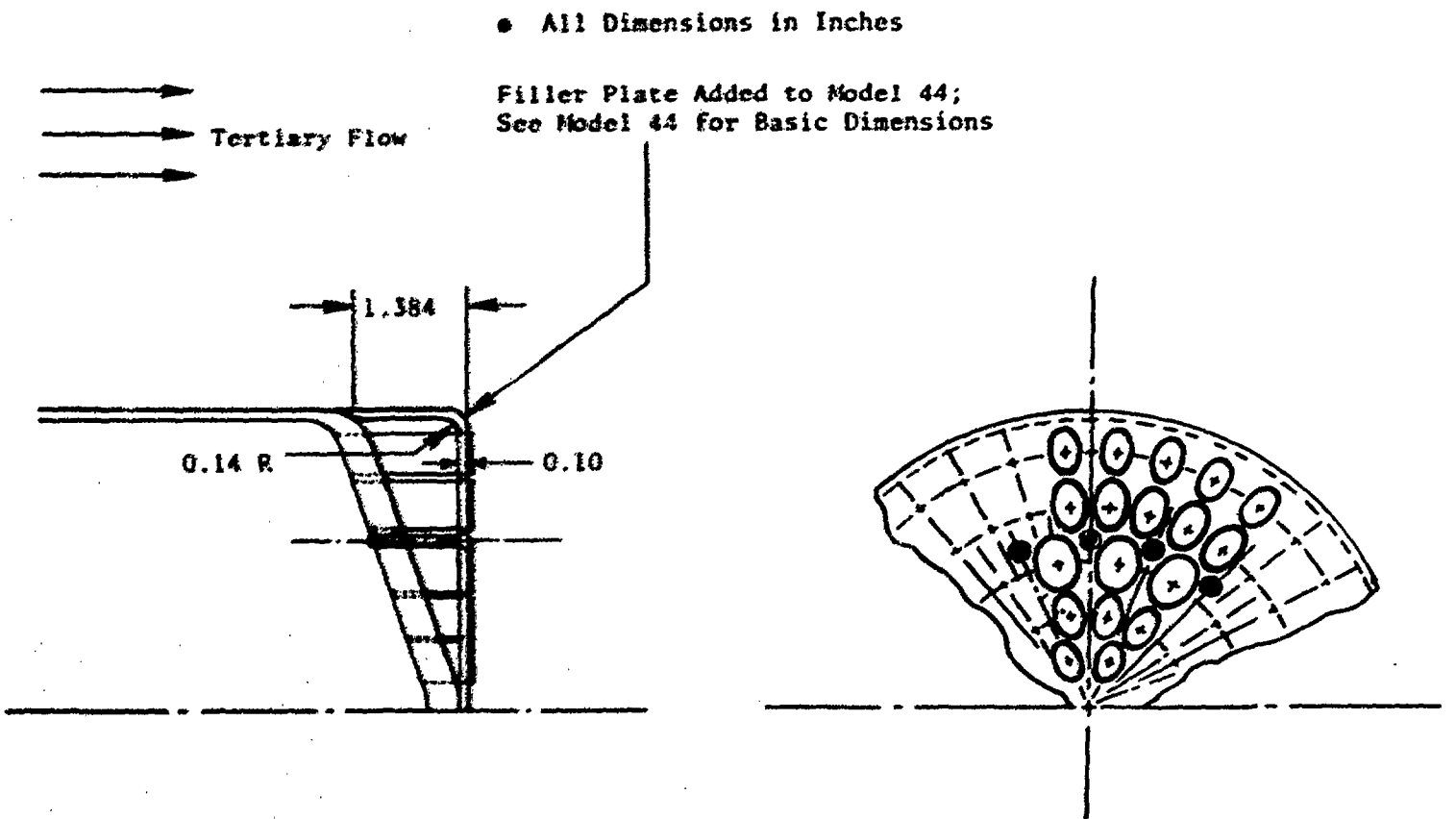

Figure A-39. Model 45 - 104 Elliptical Holes, AR = 2.8.

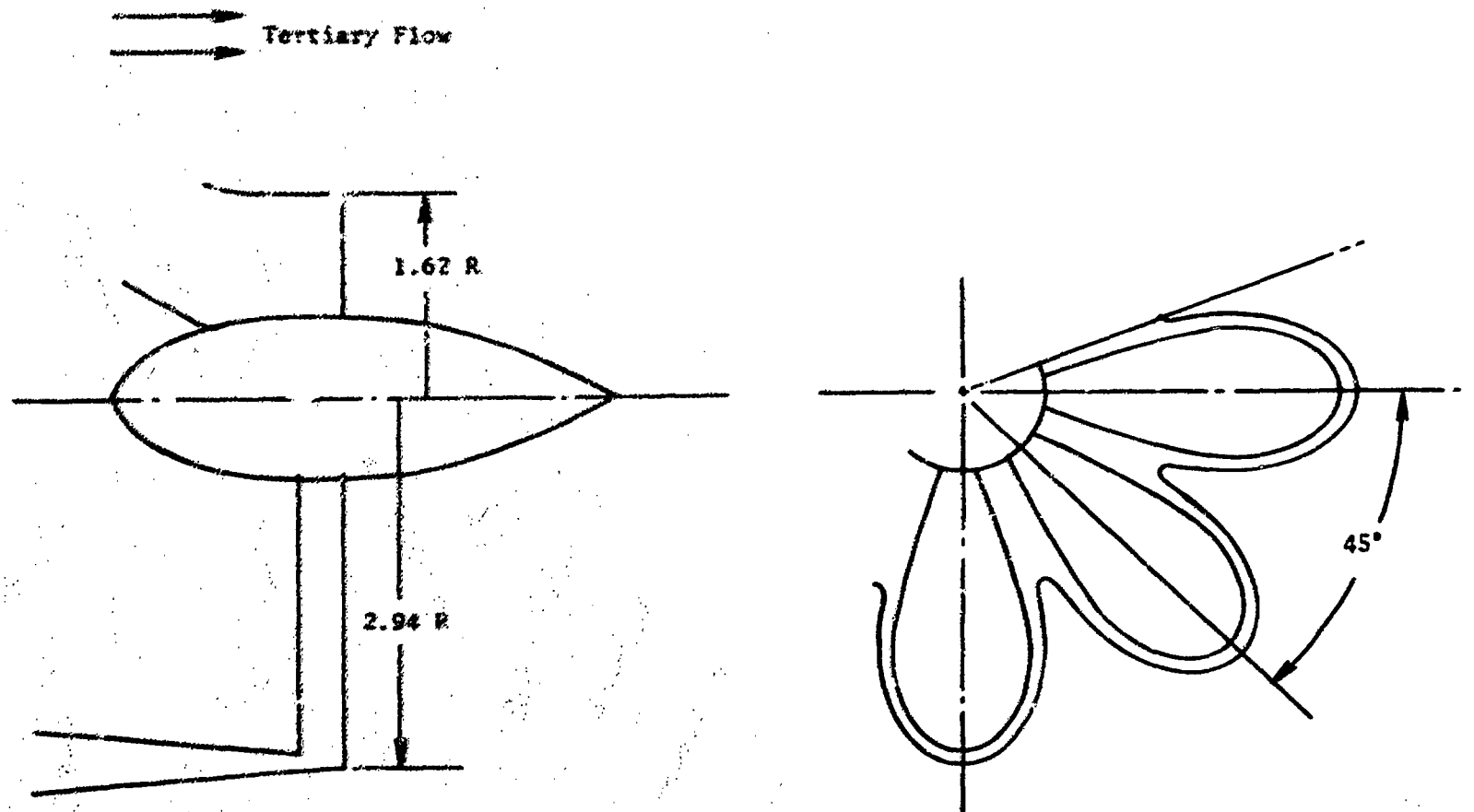

Figure A-40. Model 46 - 8-Lobe Daisy, AR = 2.1.

• All Dimensions in Inches

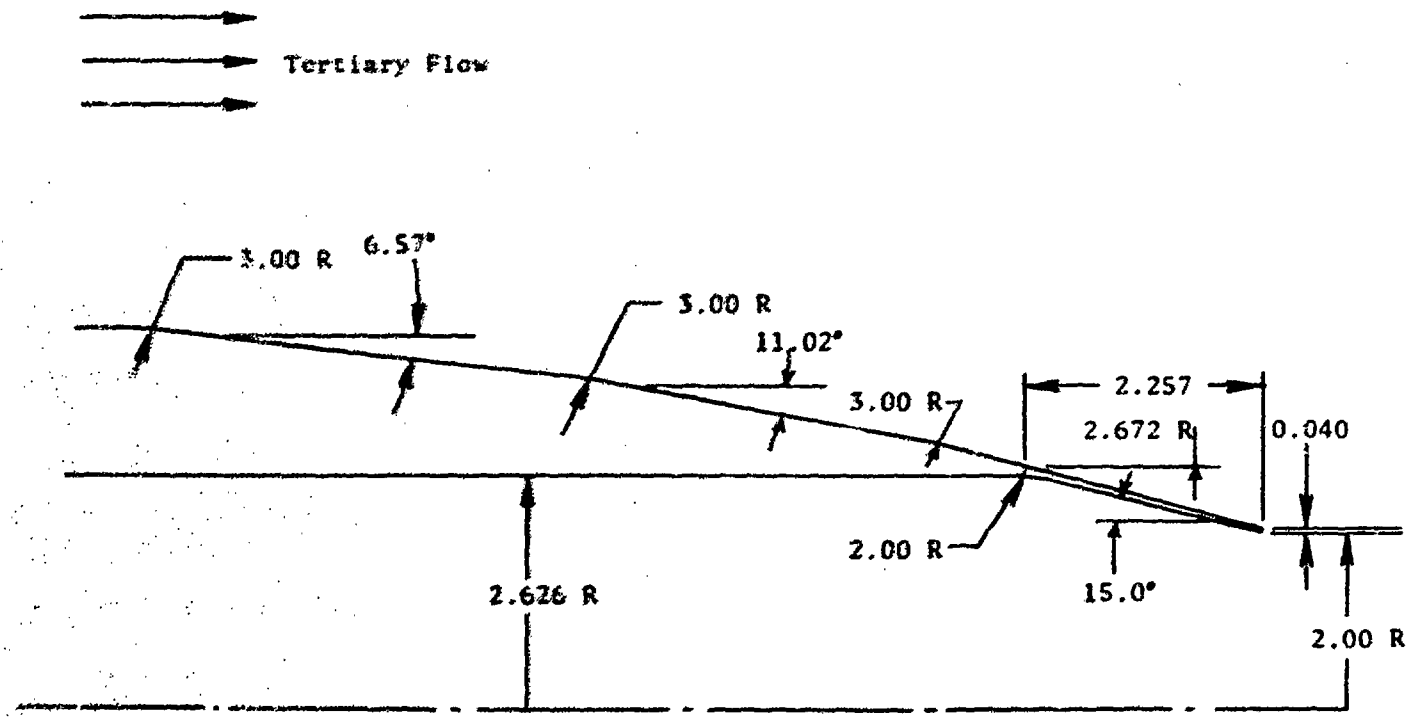

Figure A-41. Model 47 - 4.0-in.-Diameter Conical.

APPENDIX B

ACOUSTIC TEST MATRICES, AERODYNAMIC TEST CONDITIONS

The following tables summarize the aerodynamic cycle parameters, meteorological conditions, normalization parameters, and pertinent 2400-ft sideline acoustic data (scaled to a total flow area of 338 $in.^2$) associated with the far-field acoustic tests in support of Task 3, "Experimental Investigation of Suppression Principles." Table numbers B-1 through B-45 correspond to the model numbers defined in Section 4.3 and Appendix A (e.g., Model 1 through model 45); Table B-46 represents Model 47.

Table B-1. Model No. 1: 4.64-inch-Diameter Conical, Adapted to JENOTS.

A_i = 16.82 in.^{2} Linear Scale Factor to 338 in.^{2} = 4.48

Data Point No.	Inner			Meteorological Conditions		Normali Parameters		2400-ft S.L. Data							
								50°		90°					
	$(P_i/P_o)_i$	T_{T_i} (° R)	V_i (ft/sec)	T_{Dry} (° F)	T_{Wet} (° F)	10 $\log_{10}$ V/a_o	10 $F_s(T_o/T_{sm})^{\omega-1}$	OASPL	PNL	OASPL	PNL	PPNL	θ	POASPL	θ
8201	1.798	548	1085	79	65	-.438	37.8	66.3	71.4	71.7	77.5	79.2	130	74.8	140
8271	1.266	1298	1010	70	62	-.429	35.5	63.6	67.2	69.9	75.1	77.6	120	75.1	140
8289	3.936	541	1452	76	68	1.146	43.8	91.3	96.6	93.2	100.4	100.4	90	93.2	90
8290	1.842	1290	1580	79	70	1.510	35.8	76.0	80.8	81.4	87.9	94.8	130	90.0	130
8291	1.592	1297	1396	79	70	0.972	35.5	72.0	76.5	78.3	84.5	89.4	130	86.3	140
8292	1.407	1295	1205	79	70	0.333	35.5	68.1	72.2	74.2	80.0	83.6	130	80.6	140
8293	1.155	1287	791	79	70	-1.495	35.3	58.3	60.8	64.1	67.7	69.4	120	66.8	120
8294	1.060	1288	505	79	70	-3.435	34.4	49.9	47.8	53.1	51.5	54.6	110	55.8	110
8295	3.752	545	1436	76	60	1.098	43.4	90.9	96.2	93.2	100.3	100.3	90	93.2	90
8296	1.448	1467	1333	77	68	0.775	34.7	70.4	74.8	76.6	82.5	87.1	130	83.2	130
8287	1.626	765	1092	79	70	-.090	37.4	66.8	71.1	72.2	78.2	81.2	130	77.9	140
8298	1.523	1224	1293	77	68	0.649	35.8	70.0	74.4	76.4	82.4	86.8	130	83.6	140
8299	2.169	1496	1991	70	62	2.516	36.3	83.1	89.3	87.6	95.6	104.0	130	99.3	140
82100	2.651	1453	2099	89	77	2.746	37.2	86.8	93.6	90.3	98.6	105.8	130	100.6	140
82101	2.952	1497	2199	89	77	2.948	38.0	89.8	96.7	92.8	100.9	108.2	130	102.6	130
82102	3.322	1500	2299	89	77	3.139	38.8	92.0	98.5	94.9	103.0	109.8	130	104.1	130
82103	3.757	1500	2393	89	77	3.315	39.7	93.9	100.3	96.8	104.7	111.4	130	105.7	130
3	1.1	499	402			-4.43	29.2	40.0	42.9	44.9	50.0	50.9	100	45.6	100
4	1.15	501	485			-3.62	30.9	45.0	48.5	50.3	55.6	56.4	100	51.2	100
5	1.231	502	590			-2.77	32.6	50.4	54.2	56.2	61.0	62.0	100	57.2	120
6	1.348	503	703			-1.84	34.6	56.0	60.2	61.6	66.9	67.9	100	63.2	120
7	1.484	503	790			-1.50	35.4	59.8	64.2	65.8	71.6	72.5	110	67.1	130
8	1.632	504	890			-1.0	36.6	63.7	68.5	69.7	76.0	76.9	110	71.7	130
9	1.853	506	991			-0.5	37.7	69.6	72.8	73.1	79.6	81.0	130	76.3	140
10	2.516	507	1187			0.27	40.2	84.6	90.3	85.9	93.5	93.5	90	87.8	140
11	2.959	510	1278			0.59	4.5	90.9	96.3	93.3	100.9	100.9	90	93.8	80
12	1.046	993	390			-4.5	32.0	40.6	38.7	45.7	46.5	47.0	100	46.8	110
13	1.074	1001	494			-3.5	33.4	46.0	46.5	51.8	54.9	55.6	110	53.2	110
17	1.283	999	909			-0.9	85.8	61.3	65.5	68.2	73.7	75.9	120	72.7	140
18	1.355	1001	1001			-0.47	36.1	64.0	68.3	70.9	76.6	80.1	130	76.6	140
20	1.829	999	1386			0.94	37.3	73.3	78.1	79.8	86.7	92.6	140	89.4	140
22	1.031	1577	470			-3.76	34.9	46.1	43.5	50.7	48.8	50.7	100	53.7	120
23	1.044	1488	467			-3.78	34.6	47.0	46.6	51.5	53.7	54.4	100	52.9	110
24	1.068	1492	578			-2.86	35.0	51.6	52.8	56.8	60.1	61.2	110	58.5	120
25	1.101	1495	700			-2.03	35.2	56.0	58.7	61.8	66.0	67.3	110	64.1	120

Table B-1. Model No. 1: 4.64-inch-Diameter Conical, Adapted to JENOTS (Concluded).

A_1 = 16.82 in.^{2} Linear Scale Factor to 338 in.^{2} = 4.48

Data Point No.	Inner			Normalization Parameters		2400-ft S.L. Data							
						50°		90°					
	$(P_T/P_o)_i$	T_{T_i} (° R)	V_i (ft/sec)	10 $\log_{10}$ V/a_o	10 $\log_{10}$ $P_s(T_o/T_{ss})^{\omega-1}$	OASPL	PNL	OASPL	PNL	PPNL	θ	POASPL	θ
26	1.134	1493	796	-1.47	35.3	58.6	61.7	64.8	69.4	71.0	110	67.3	120
27	1.168	1500	887	-.997	35.3	61.2	64.9	67.4	72.5	74.3	120	70.7	140
28	1.219	1496	997	-.490	35.2	64.0	67.8	70.3	75.8	78.1	120	74.9	140
29	1.349	1494	1316	-.373	34.8	68.0	72.2	74.8	80.8	84.3	130	81.5	140
30	1.495	1496	1401	.988	34.5	73.1	77.5	79.4	85.8	91.0	130	88.0	140
31	2.362	1499	1990	2.51	36.3	84.8	91.1	88.3	97.6	105.9	140	100.8	140
62	1.577	997	1210	.351	36.8	68.8	73.4	76.0	82.3	87.0	130	83.8	140
63	1.518	1453	1485	1.000	34.7	72.5	77.5	79.0	85.7	90.8	130	87.3	140
64	1.806	1448	1652	1.701	34.9	76.7	82.0	82.8	89.8	97.1	130	92.4	140
65	2.047	1452	1804	2.086	35.4	80.4	86.0	86.2	93.3	101.9	140	97.0	140
66	2.48	1450	2004	2.542	36.8	85.6	92.3	89.9	98.5	106.5	130	100.7	140
67	1.519	714	983	-.551	36.8	64.3	69.7	70.9	77.4	80.2	130	75.9	140
117	1.058	896	414	-4.307	32.0	41.2	40.5	46.3	48.0	48.9	120	47.8	110
122	1.259	1255	982	-.556	85.6	63.4	67.5	70.0	75.4	78.3	110	74.6	140

Table B-2. Model No. 2: Convergent-Divergent Plug, Single Flow.

A_i = 37.40 $in.^2$, Linear Scale Factor to 338 $in.^2$ = 3.00

Data Point No.	Inner			Normalization Parameters		2128-ft S.L. Data							
						50°		90°					
	$(P_t/P_o)_1$	T_{T_1} (° R)	V_1 (ft/sec)	10 $\log_{10}$ V/a_o	10 $\log_{10}$ F_s $(T_o/T_{sm})^{\omega-1}$	OASPL	PNL	OASPL	PNL	PPNL	θ	POASPL	θ
1	1.116	1493	744	-1.756	35.3	65.7	66.6	71.4	74.9	78	120	75.7	120
2	1.226	1516	1016	-0.406	35.1	70.6	73.1	77.8	82.7	86.6	120	83.5	130
3	1.375	1497	1253	0.503	34.7	73.6	76.8	81.2	86.3	91	110	87.8	130
4	1.585	1485	1487	0.125	34.5	75.7	80.4	83.1	88.9	93.5	130	90.7	130
5	1.736	1485	1618	0.161	34.6	77.1	82.2	84.1	90.3	96.8	130	93.4	130
6	1.920	1501	1757	1.973	34.8	73.7	84.2	85.7	92.1	100.3	130	95.7	140
7	2.374	1501	1995	2.524	36.3	84	89.7	89.4	96.4	107.5	140	103	140
8	2.481	1515	2048	2.637	36.[illegible]	85.1	91	90.6	97.9	108.2	140	103.7	140
9	3.047	1556	2269	3.082	38.9	89.9	96.5	94.5	102.3	113.3	130	107.6	130
11	3.176	1541	2582	3.644	37.2	89.9	96	95.5	103.5	115.8	130	110.4	130
12	2.005	1939	2062	2.666	33.7	82.9	88.6	89.1	96.2	106.4	130	101.8	130
13	1.495	2006	1624	1.630	31.9	78.7	83.1	85.7	91.9	97.5	110	93.6	140
14	1.161	2018	1007	-0.442	34.4	71	73.2	77.2	81.5	86.3	110	82.5	110
15	1.192	1763	1019	-0.391	34.7	71	73.7	77.7	82.3	87.7	110	83.1	110
16	1.607	1757	1647	1.678	33.0	78.1	82.6	85.2	91.4	97.4	110	93.4	140
17	2.219	1734	2071	2.686	35.1	84.2	89.8	89.6	96.6	107.8	130	103.1	140
18	3.253	1285	2106	2.759	39.3	89.3	95.6	92.2	100.7	111	140	106.3	140
19	1.978	1249	1633	1.655	36.2	77.2	82.4	83.6	90.3	97.2	140	94.2	140
20	1.274	1266	1009	-0.435	32.0	70.5	73.3	76.3	81.2	86.5	110	82.7	130
21	1.369	1009	1020	-0.388	36.2	68.7	72.2	74.2	79.4	84.7	120	80	130
22	2.411	1019	1649	1.698	38.5	81.3	87.5	84.8	92.2	109	130	104.1	130
23	3.912	1107	2071	2.687	41.3	94.1	100.4	95.8	103.9	112.8	140	108.1	140
26	1.888	509	1007	-0.444	37.9	69	74.9	73.6	81.8	84.1	110	76.8	140
27	1.482	857	1046	-0.280	36.7	67.6	72.8	73.2	79.5	82.9	120	78.9	140
28	1.835	2259	2093	2.732	32.3	82.7	88	89.4	96.4	104.8	130	99.9	130
29	1.712	2511	2087	2.719	31.2	83.1	88.2	89.4	96.4	103.7	130	99.2	140
30	1.184	1507	924	-0.817	35.2	69.3	71.3	75.7	79.6	89.4	110	80.9	110
31	1.289	1511	1129	0.051	34.9	71.6	74.7	78.5	83.9	90.3	110	84.5	110
32	1.447	1506	1349	0.826	34.5	74.9	79	81.5	87.4	93.6	110	89.3	140
33	1.482	1560	1327	0.755	34.5	75.4	79.9	82	88	94	110	89.5	140
34	2.779	585	1239	0.456	41.0	86.1	92.6	86.4	94.3	94.5	100	90	150
36	1.632	1006	1257	0.517	34.8	71.1	75.9	77.6	83.7	87.4	120	83.6	140
37	1.469	1255	1254	0.509	35.6	72.7	77.2	89.6	85.5	90.5	110	85.9	140
38	1.321	1760	1274	0.578	33.8	73.9	77.6	81	87	94.5	110	87.3	110
39	1.274	2003	1271	0.568	33.1	79.3	77.3	80.8	86.3	92.8	110	87	110
40	1.[illegible]	2261	1667	1.744	30.8	78.9	83.2	85.5	91.7	97.2	120	99.3	140
41	1.399	2492	1667	1.731	29.9	78.7	82.6	85.2	91.1	96.5	120	94.2	140
42	1.234	2245	1257	0.518	32.6	74.6	77.4	80.9	85.8	90.7	110	87.3	120

Table B-3. Model No. 3. Convergent Plug, R_r = 0.59, Single Flow.

A_i = 33.63 in.^{2} Linear Scale Factor to 338 in.^{2} = 3.17

Data Point No.	Inner			Meteorological Conditions		Normalization Parameters		2400-ft S.L. Data							
								50°		90°					
	$(P_T/P_O)_i$	T_{T_i} (° R)	V_i (ft/sec)	T_{Dry} (° F)	T_{Wet} (° F)	10 $\log_{10}$ V/a_O	10 $\log_{10}$ $F_s(T_O/T_{sm})^{\omega-1}$	OASPL	PNL	OASPL	PNL	PPNL	θ	POASPL	θ
7245	1.535	701	986	86	73	-.538	37.0	64.0	68.9	68.5	74.3	75.8	130	71.8	140
7246	2.072	986	1493	88	73	1.264	38.0	75.0	81.3	80.8	88.2	91.9	140	88.5	150
7248	1.627	759	1088	86	73	-.110	37.4	66.3	71.2	71.0	76.8	79.4	130	75.8	140
7249	2.258	1085	1651	88	73	1.701	37.9	77.9	84.8	82.5	90.0	96.0	140	92.2	140
7251	1.737	812	1194	86	73	0.293	37.8	68.4	73.7	73.7	79.9	83.3	130	79.6	140
7252	2.452	1192	1804	88	73	2.086	37.7	79.9	85.9	84.7	92.2	99.5	140	95.6	140
7254	1.85	871	1299	86	73	0.659	37.9	70.8	76.2	75.9	82.3	86.1	130	82.7	140
7255	2.657	1288	1948	88	73	2.419	37.9	82.6	88.9	86.8	94.7	103.1	140	98.7	140
7257	1.963	927	1397	88	73	0.975	38.0	75.6	82.4	79.3	86.5	89.6	140	85.9	140

Table B-4. Model No. 4: Convergent Plug, R_r = 0.789, Single Flow.

A_i = 10.85 in.^{2} Linear Scale Factor to 338 in.^{2} = 5.58

Data Point No.	Inner			Meteorological Conditions		Normalization Parameters		2400-ft S.L. Data							
								50°		90°					
	$(P_T/P_o)_i$	T_{T_i} (° R)	V_i (ft/sec)	T_{Dry} (° F)	T_{Wet} (° F)	10 $\log_{10}$ V/a_o	10 $\log_{10}$ $F_s(T_o/T_{sm})^{\omega-1}$	OASPL	PNL	OASPL	PNL	PPNL	θ	POASPL	θ
7601	1.719	572	993	85	75	-.597	37.5	65.3	70.7	69.1	74.8	75.7	120	71.9	140
7602	1.513	684	958	85	75	-.663	36.8	63.2	67.8	66.6	72.3	73.4	130	69.6	140
7603	1.351	962	976	90	75	-.582	36.2	62.0	65.6	66.4	71.3	73.4	130	69.9	140
7604	1.263	1244	984	90	75	-.547	35.6	62.2	65.5	67.0	71.6	73.7	120	70.2	140
7605	1.213	1492	983	89	73	-.551	35.2	62.0	65.1	66.9	71.7	73.5	120	70.2	130
7606	1.184	1658	971	87	73	-.600	35.0	61.1	64.3	66.4	70.8	72.9	120	69.8	140
7607	1.177	1851	1008	87	73	-.442	34.7	62.8	66.3	67.3	71.8	73.7	120	70.3	130
7608	2.382	580	1238	85	75	.451	40.0	72.3	79.0	77.0	83.9	85.2	140	81.7	140
7609	1.628	982	1239	90	75	.454	37.0	70.2	76.2	74.6	80.8	85.5	120	80.2	140
7610	1.469	1236	1246	90	75	.479	35.8	67.0	71.4	72.5	78.0	81.7	130	78.9	140
7611	1.369	1486	1241	90	75	.461	34.8	66.5	70.6	72.0	77.2	80.7	130	77.7	140
7612	1.308	1743	1247	87	73	.482	34.0	66.7	70.7	72.1	77.3	80.7	130	77.9	140
7613	1.276	1895	1341	87	73	.461	33.6	65.7	69.2	72.2	77.3	80.3	120	77.6	140
7614	2.928	985	1628	90	75	1.640	38.8	78.8	86.8	82.3	90.1	95.6	140	92.2	140
7615	2.055	1227	1660	88	74	1.720	36.6	75.8	80.8	81.0	87.1	94.6	140	91.0	140
7616	1.749	1484	1628	90	75	1.640	34.6	73.3	77.9	79.2	85.1	91.5	140	88.6	140
7617	1.600	1734	1625	87	73	1.632	33.2	73.6	78.8	78.9	84.8	90.8	130	87.6	140
7618	1.541	1907	1639	87	73	1.669	32.4	72.6	77.1	78.6	84.3	90.5	130	87.4	140
7619	4.059	1061	2051	89	73	2.643	41.8	91.9	98.3	93.9	101.5	107.9	140	103.5	140
7620	3.301	1223	2065	89	73	2.673	39.7	87.5	94.0	90.4	98.3	108.0	140	102.5	140
7621	2.618	1487	2083	90	75	2.710	37.1	82.7	89.1	87.9	95.2	106.8	140	100.9	140
7622	2.236	1765	2101	89	73	2.748	35.1	80.8	86.8	86.3	93.2	103.7	140	98.6	140
7623	2.07	1901	2084	87	73	2.712	34.2	79.0	84.6	85.0	91.7	101.7	140	97.0	140
7645	1.534	715	995	88	73	-.498	37.0	64.6	69.0	68.5	74.4	76.0	130	72.2	140
7646	2.061	989	1491	99	74	1.258	37.9	73.6	78.9	78.7	84.9	90.6	140	87.6	140
7647	2.723	1333	2004	90	75	2.542	37.9	83.2	89.9	87.4	94.9	104.8	140	99.5	140
7648	1.622	762	1088	88	73	-.110	37.4	66.8	72.4	70.7	76.6	78.9	130	75.2	140
7649	2.262	1083	1647	88	74	1.690	37.9	77.1	84.5	81.7	88.1	95.2	140	91.7	140
7650	3.007	1468	2193	90	75	2.934	38.2	84.5	90.4	89.5	96.6	107.8	140	102.4	140
7651	1.734	821	1199	88	74	0.312	37.7	70.7	76.5	74.3	80.8	83.4	120	79.3	140
7652	2.45	1191	1802	88	74	2.081	37.7	81.0	88.4	85.5	93.0	101.4	140	96.7	140
7653	3.294	1557	2337	89	73	3.210	38.6	86.4	92.6	91.0	98.6	109.0	140	103.9	130
7654	1.841	880	1301	88	74	0.666	37.9	69.2	73.9	74.7	80.5	85.0	130	81.8	140
7655	2.635	1296	1947	90	75	2.417	35.0	82.7	89.1	87.4	94.8	109.7	140	99.3	140
7656	3.568	1764	2561	89	73	3.607	38.6	87.0	93.0	92.3	100.0	110.7	130	105.5	130
7657	1.95	934	1397	88	74	0.975	37.9	71.7	76.4	76.8	82.7	88.0	140	85.2	140
7658	2.861	1393	2093	90	75	2.731	38.1	83.8	90.2	88.2	96.0	105.5	140	100.5	140
7659	3.893	1950	2772	89	73	3.951	38.7	90.5	97.0	95.1	102.8	113.0	130	107.7	130

Table B-5. Model No. 5: Convergent Plug, R_r = 0.853, Single Flow.

A_i = 6.73 in.^{2} Linear Scale Factor to 338 in.^{2} = 7.09

Data Point No.	Inner			Meteorological Conditions		Normalization Parameters		2400-ft S.L. Data							
								50°		90°					
	$(P_t/P_o)_i$	T_{ti} (° R)	V_i (ft/sec)	T_{dry} (° F)	T_{wet} (° F)	1C $\log_{10} V/a_o$	10 $\log_{10} P_s(T_o/T_{amb})^{3.5}-1$	OASPL	PNL	OASPL	PNL	PPNL	θ	POASPL	θ
7445	1.543	718	1003	81	71	-0.464	37.1	64.1	68.9	68.5	73.8	75.3	130	71.4	140
7446	2.057	979	1481	82	72	0.123	38.1	72.8	77.7	78.2	84.0	89.2	140	86.5	140
7447	2.719	1310	1985	84	73	2.501	38.1	81.7	86.9	86.1	93.0	102.4	140	98.0	140
7448	1.632	764	1095	81	71	-0.008	37.6	65.7	70.5	70.5	75.9	77.8	130	74.4	140
7449	2.259	1096	1656	82	72	1.714	37.9	75.9	81.8	81.1	87.2	93.5	140	90.4	140
7450	2.99	1480	2197	84	73	2.942	38.3	84.2	91.2	88.5	95.7	105.8	140	100.9	140
7451	1.732	819	1197	81	71	0.301	37.9	67.5	72.1	72.5	78.0	80.6	140	77.9	140
7452	2.447	1200	1808	82	72	2.095	37.8	79.2	86.5	83.5	90.1	97.5	140	93.9	140
7453	3.26	1628	2382	84	73	3.293	38.4	86.8	93.1	91.5	98.4	108.1	130	103.1	130
7454	1.841	875	1298	81	71	0.656	38.0	69.2	74.0	74.5	80.2	83.4	140	80.7	140
7455	2.645	1297	1951	82	72	2.426	38.0	81.2	88.5	85.7	92.5	101.4	140	97.3	140
7456	3.545	1791	2572	85	73	3.631	38.6	88.5	95.3	93.7	101.0	113.9	130	107.2	130
7457	1.978	934	1396	81	71	0.972	38.0	70.9	75.6	76.0	81.7	86.2	140	83.4	140
7458	2.854	1398	2095	84	73	2.735	38.2	83.4	90.6	87.6	94.5	103.6	140	99.4	140
7459	3.861	1950	2765	85	73	3.940	38.8	88.5	94.5	94.3	101.6	111.7	130	106.7	130

Table B-6. Model No. 6: Dual-Flow Coannular-Coplanar, A_o/A_i = 2.0.

A_o = 33.63 in.^{2}, A_i = 16.82 in.^{2} Linear Scale Factor to 338 in.^{2} = 2.59

Data Point No.	Inner $(P_{t_i}/P_{s_o})_i$	Inner T_{t_i} (°R)	Inner V_i (ft/sec)	Outer $(P_{t_o}/P_{s_o})_o$	Outer T_{t_o} (°R)	Outer V_o (ft/sec)	Ratios T_{t_o}/T_{t_i}	Ratios V_o/V_i	Mass Averages $(P_{t_2}/P_{s_o})_{av}$	Mass Averages T_{t_2} (°R)	Mass Averages V_{av} (ft/sec)	Meteorological Conditions T_{Dry} (°F)	Meteorological Conditions T_{Wet} (°F)	Normalization Parameters 10 $\log_{10}(V/a_o)$	Normalization Parameters 10 $\log_{10} F_8(T_o/T_{amb})^{w-1}$	2400-ft S.L. Data 50° OASPL	50° PNL	90° OASPL	90° PNL	PPNL	θ	POASPL	θ
8202	1.851	552	1212	1.829	541	192	0.2	0.3	1.843	549	809	79	65	-1.396	33.3	59.4	64.8	65.3	71.1	73.1	130	69.2	150
8203	1.803	549	1212	1.804	544	427	0.4	0.7	1.803	547	762	79	65	-1.656	34.1	58.4	62.9	64.3	69.4	71.3	130	68.7	150
8204	1.802	548	1209	1.844	545	500	0.5	0.9	1.794	547	771	79	65	-1.606	34.6	57.7	61.8	63.6	68.4	70.6	130	67.8	150
8205	1.803	547	1209	1.920	543	652	0.6	1.1	1.830	546	799	80	62	-1.654	35.1	58.1	62.2	64.0	68.6	70.7	130	67.9	150
8206	1.797	546	1206	1.939	545	804	0.8	1.3	1.861	545	885	80	62	-1.009	36.2	60.8	65.2	66.5	71.3	73.1	130	70.0	150
8207	1.803	547	1209	1.948	545	1008	0.1	2.0	1.801	546	1007	80	62	-0.646	37.7	65.0	70.1	70.7	76.3	77.8	130	73.2	140
8208	1.791	545	1203	1.816	549	1184	0.3	1.0	1.803	549	1199	82	63	0.312	39.9	70.9	76.1	76.8	83.4	85.3	130	80.1	140
8210	1.972	549	1467	1.791	548	1825	0.7	0.9	1.572	549	1268	82	63	0.487	40.4	90.7	95.6	91.5	97.6	97.9	80	92.8	70
8211	2.611	551	1965	1.799	549	1819	0.8	1.4	2.083	550	1118	82	63	0.007	38.9	73.0	78.1	75.8	81.5	83.0	130	80.4	150
8212	1.448	551	854	1.797	551	1811	1.2	2.6	1.684	551	957	84	64	-0.668	37.1	63.7	69.0	69.1	74.8	76.2	120	70.9	130
8213	1.446	552	906	1.798	552	1511	2.0	4.6	1.612	552	920	84	64	-0.840	36.4	62.1	67.3	67.6	73.6	73.6	120	69.3	140
8214	1.084	553	388	1.800	552	1813	2.6	6.8	1.620	552	924	88	68	-0.819	36.2	62.0	67.2	67.6	73.6	74.8	120	69.7	130
8215	1.023	554	316	1.798	552	1211	4.7	11.0	1.659	552	945	83	63	-0.723	36.0	62.1	67.2	67.0	72.9	73.8	110	68.6	150
8216	1.593	554	1014	1.141	721	1803	1.0	1.4	1.623	654	1007	71	63	-0.444	37.2	63.2	67.9	69.0	74.6	77.2	130	73.4	150
8217	1.802	561	1222	2.078	996	1509	1.5	1.7	1.458	836	1325	71	61	-0.744	38.4	71.1	76.9	76.9	84.0	87.9	120	82.8	150
8218	1.781	561	1196	2.715	1211	1991	1.9	2.0	2.366	1069	1675	71	63	-1.763	38.3	78.2	85.3	83.6	92.7	97.4	140	91.1	140
8219	1.641	568	1185	1.637	771	1183	1.0	2.0	1.639	770	1104	83	69	-0.048	37.4	65.0	70.0	71.0	76.7	80.1	120	76.6	150
8220	1.834	582	1893	2.268	1675	1646	1.5	2.5	2.046	994	1486	63	69	1.245	37.8	73.6	81.6	79.4	87.1	91.4	130	86.1	140
8221	1.632	744	1895	2.642	1386	2835	1.9	2.5	2.321	1207	1766	89	77	1.989	37.3	79.1	86.9	84.3	93.4	97.9	150	91.7	160
8222	1.161	987	1195	1.733	823	1193	1.0	2.5	1.674	864	1194	83	63	0.292	37.4	67.0	72.2	72.9	78.5	82.9	130	79.8	150
8223	1.163	999	1209	2.645	1197	1899	1.5	3.0	2.166	1147	1655	83	63	1.710	37.2	76.2	84.2	81.6	89.8	94.6	130	89.6	150
8224	1.570	1511	1717	2.281	1679	2845	1.7	2.3	2.034	1452	1796	83	63	2.066	35.3	76.5	82.6	82.9	90.4	96.4	130	90.9	150
8225	1.542	1522	1318	1.842	682	1303	2.0	2.9	1.739	969	1305	83	69	0.679	37.2	69.3	74.5	75.5	81.5	86.7	140	83.6	160
8226	1.533	1522	1296	2.647	1297	1932	1.5	1.5	2.293	1278	1805	75	66	2.087	36.8	79.3	86.8	84.3	92.8	97.9	140	93.5	160
8227	1.525	1525	1296	2.695	1384	2835	1.6	1.2	2.325	1348	1869	89	77	2.239	36.6	79.7	87.1	85.2	94.0	98.6	120	93.5	160
8228	1.514	1452	1480	1.962	941	1408	1.0	1.6	1.806	1258	1406	83	69	1.004	36.9	71.4	70.6	77.5	83.7	89.7	150	86.6	160
8229	1.501	1453	1387	2.684	1364	2815	1.5	2.9	2.309	1382	1886	89	77	2.278	36.4	80.0	87.5	85.9	93.9	99.1	160	94.0	160
8230	1.501	1461	1391	1.875	1839	3052	1.4	6.6	3.157	1096	1920	84	76	2.356	39.8	86.6	93.6	89.6	98.4	104.1	160	98.9	160
8240	1.232	1481	1021	1.834	1521	617	0.5	0.8	1.115	1504	745	83	63	-1.757	34.4	55.5	57.7	61.4	64.8	67.9	120	66.3	150
8241	1.233	1463	1003	1.944	1512	482	0.5	0.9	1.118	1502	753	83	69	-1.707	34.6	55.9	57.5	63.0	65.3	69.2	120	69.1	120
8242	1.231	1499	1002	1.876	1527	656	0.6	1.3	1.130	1501	788	84	64	-1.512	35.0	56.6	58.6	61.9	65.2	68.6	120	66.9	150
8243	1.222	1481	1001	1.340	1494	813	0.8	1.6	1.169	1493	886	76	64	-1.005	35.2	60.7	63.2	66.6	70.2	73.2	120	71.1	120
8244	1.223	1494	1002	1.212	1497	985	1.0	2.0	1.217	1497	991	84	64	-0.514	35.2	61.3	65.2	67.4	72.2	75.1	120	71.2	150
8245	1.219	1487	996	1.387	1515	1273	1.3	2.8	1.332	1508	1195	76	64	0.298	34.7	66.1	70.7	72.7	78.5	81.6	120	76.9	140
8246	1.232	1504	1005	2.175	1506	2080	2.0	4.9	2.036	1506	1831	84	64	2.150	36.8	77.0	83.5	82.8	90.4	96.8	130	92.0	150

Table B-6. Model No. 6: Dual-Flow Coannular-Coplanar, A_o/A_1 = 2.0 (Concluded).

A_o = 73.63 in.^{2}, A_1 = 36.82 in.^{2} Linear Scale Factor to 35^2 in.^{2} = 2.59

Data Point No.	Inner			Outer			Ratios		Mass Averages			Meteorological Conditions		Normalization Parameters		2400-ft S.L. Data							
	$(P_T/P_a)_1$	T_{T_1} (°R)	V_1 (ft/sec)	$(P_T/P_a)_o$	T_{T_o} (°R)	V_o (ft/sec)	T_o/T_1	w_o/w_1	$(P_T/P_a)_{mx}$	$T_{T_{mx}}$ (°R)	V_{mx} (ft/sec)	T_{Dry} (°F)	T_{Wet} (°F)	10 $\log_{10}$ (W/σ_{sl})	10 $\log_{10}$ $F_o(T_o/T_{mx})^{m-1}$	50° OASPL	50° PNL	90° OASPL	90° PNL	PPNL	θ	POASPL	θ
8267	1.227	1499	1019	1.483	1478	2058	2.1	5.5	2.263	1478	1930	84	64	2.380	35.7	81.5	88.8	86.1	94.3	99.9	140	94.7	150
8268	1.152	1505	824	1.322	1506	1808	1.7	2.5	1.397	1506	956	83	69	-0.682	35.2	60.8	64.8	67.3	72.1	74.4	120	70.0	130
8269	1.059	1491	540	1.225	1502	1822	1.4	3.9	1.185	1500	924	83	69	-0.821	34.9	59.6	63.9	66.1	71.3	73.6	120	68.8	120
8270	1.047	1482	482	1.232	1505	1825	2.1	6.4	1.184	1501	924	83	69	-0.821	34.8	60.2	64.1	66.6	71.5	74.4	120	72.0	120
8272	1.214	1492	1008	1.825	582	573	0.2	0.7	1.128	996	650	70	62	-2.287	33.0	57.6	60.9	63.4	68.2	71.7	120	68.9	140
8273	1.236	1492	995	1.866	562	397	0.4	1.8	1.165	816	613	84	64	-2.602	33.8	63.2	67.0	70.0	74.5	78.4	120	74.5	120
8274	1.161	1492	999	1.149	563	513	0.5	2.1	1.180	784	660	84	64	-2.281	34.4	70.7	68.9	56.8	60.4	69.5	40	71.0	40
8275	1.265	1492	1003	1.321	559	597	0.6	2.7	1.219	754	706	84	64	-1.992	34.8	74.4	73.7	57.7	61.4	73.7	50	74.4	50
8276	1.265	1491	1006	1.437	553	818	0.8	3.9	1.266	705	850	84	64	-1.183	35.9	78.0	78.5	62.4	67.0	78.7	40	78.0	50
8277	1.283	1283	996	1.776	556	1006	1.0	5.2	1.593	676	1004	83	63	-0.658	37.1	75.6	76.2	67.0	72.8	73.8	110	68.5	120
8278	1.255	1282	984	2.628	552	1223	1.3	7.8	2.137	635	1233	84	64	-0.634	39.2	73.0	78.9	78.0	86.4	85.3	140	81.3	150
8279	1.862	1293	1578	1.793	555	1012	0.6	2.9	1.774	742	1161	84	64	0.170	38.1	68.7	73.4	74.4	80.0	88.8	140	95.5	140
8280	1.595	1292	1396	1.789	556	1816	0.7	3.5	1.696	719	1100	84	64	-0.063	37.8	66.5	71.1	72.5	77.9	84.3	140	81.8	150
8281	1.398	1296	1195	1.804	557	1819	0.9	4.1	1.665	696	1053	84	64	-0.252	37.5	65.1	70.1	71.0	76.4	80.0	130	77.8	150
8282	1.198	1293	869	1.791	556	1813	1.2	6.1	1.592	658	992	83	63	-0.511	37.0	63.0	68.1	69.2	74.9	77.0	120	72.2	140
8283	1.659	1304	505	1.788	556	1811	2.0	10.9	1.603	619	969	83	63	-0.615	36.4	63.5	68.6	64.8	72.0	75.4	40	74.4	40
8284	1.934	1270	383	1.804	555	1815	2.7	14.4	1.639	600	974	83	63	-0.592	36.3	61.2	66.1	66.0	72.1	73.5	120	67.9	120
8285	2.752	572	1471	2.373	2024	1457	1.0	0.4	2.083	947	1467	84	76	1.189	38.3	91.4	97.4	93.0	100.5	100.5	80	93.6	70
8286	2.518	567	1433	2.726	1534	1803	0.7	0.3	2.814	809	1332	84	76	0.768	38.2	88.9	95.0	90.5	97.8	98.5	80	91.4	80
8287	1.657	1444	1141	1.425	671	881	0.7	2.9	1.419	876	1000	79	66	-0.675	36.6	63.9	67.6	69.6	74.7	81.9	140	79.2	140
8288	1.885	1442	1458	1.796	590	1845	0.6	3.2	1.752	800	1192	79	66	0.287	38.0	69.8	74.5	75.2	81.0	90.7	140	87.2	140
9283	1.348	1490	1058	1.329	1504	786	0.8	1.5	1.169	1498	887	83	69	-0.996	35.2	59.1	62.8	65.3	68.8	71.5	120	70.1	140
9278	1.847	1498	459	1.232	1506	1827	2.7	4.7	1.185	1505	926	79	66	-0.808	34.8	59.9	63.9	65.7	71.1	73.9	120	68.9	120
9282	1.153	1283	783	1.799	559	1815	1.3	6.8	1.589	652	985	84	64	-0.502	36.8	62.7	68.0	68.7	74.5	76.9	120	71.9	140

Table B-7. Model No. 7: Dual-Flow Coannular-Coplanar, $A_o/A_i = 0.65$.

A_o = 28.41 in.^{2}, A_i = 18.82 in.^{2} Linear scale factor to 538 in.^{2} = 1.50

Data Point No.	Inner			Outer			Ratios		Mean Averages			Meteorological Conditions		Normalization Parameters		2400-ft S.L. Data							
	$(P_o/P_{a_o})_i$	T_{T_i} (°R)	V_i (ft/sec)	$(P_o/P_{a_o})_o$	T_{T_o} (°R)	V_o (ft/sec)	W_o/W_i	A_o/A_i	$(P_o/P_{a_o})_{av}$	$T_{T_{av}}$ (°R)	V_{mix} (ft/sec)	T_{Dry} (°F)	T_{Wet} (°F)	10 $\log_{10}$ (V/a_o)	10 $\log_{10}$ $F_n(T_o/T_{amb})^{n-1}$	50° OASPL	50° PNL	90° OASPL	90° PNL	PPNL	θ	POASPL	θ
601	1.705	1021	971	1.103	731	578	1.0	0.8	1.462	970	962	61	34	-0.665	37.2	84.1	89.5	89.5	95.6	98.2	120	93.9	140
602	1.760	1030	986	1.104	736	5841	1.0	0.8	1.487	987	1147	62	34	-0.119	38.4	89.3	95.4	95.0	82.6	86.2	120	96.5	140
603	1.760	1029	989	1.099	1037	3044	2.1	0.8	1.459	844	1381	61	34	0.925	38.9	96.2	83.6	80.1	89.1	93.8	120	86.2	130
604	1.14	963	1088	1.069	764	1068	1.0	0.7	1.190	764	1068	64	35	-0.193	37.3	85.0	70.2	71.2	77.1	81.5	140	78.6	140
605	1.421	963	1324	1.072	1090	1452	1.5	0.8	1.264	906	1332	64	35	-0.768	37.8	71.4	77.9	77.5	85.2	89.5	120	83.7	140
606	1.837	998	1595	1.087	1487	2005	2.0	0.8	1.335	1292	1601	65	35	1.966	37.6	76.9	86.7	82.5	91.7	96.6	130	89.3	130
607	1.76	994	1595	1.078	815	1190	1.0	0.8	1.434	914	1193	52	41	0.291	37.2	67.9	72.7	74.2	80.2	86.6	130	81.6	140
611	1.768	994	1595	1.074	1190	1787	1.5	0.9	1.409	1093	1490	52	41	1.256	36.9	72.9	80.4	79.6	87.4	92.3	130	86.9	140
615	1.76	994	1729	1.069	1503	2596	1.8	1.1	1.357	1327	1803	53	42	2.096	36.6	81.6	90.0	85.2	94.3	99.7	140	92.9	140
618	1.769	1729	1918	1.064	1797	2950	1.5	1.1	1.395	1253	1635	51	41	1.686	36.2	75.7	84.6	81.8	89.9	95.3	120	89.6	140
620	1.959	1989	1959	1.061	1781	2583	2.0	1.1	1.365	1543	2020	43	35	2.577	36.1	81.9	90.7	86.8	95.6	101.8	130	96.4	140
622	1.929	1475	1792	1.044	923	1389	1.0	1.1	1.440	1195	1391	51	41	0.958	36.3	71.6	76.8	78.1	84.3	91.0	130	87.7	140
627	1.918	1453	1815	1.039	1438	2102	1.5	1.9	1.403	1425	1801	44	36	2.079	35.4	79.2	87.8	86.9	93.7	100.8	140	93.0	140
625	1.897	1463	1888	1.006	1948	2788	2.0	1.5	1.309	1746	2225	44	36	2.996	35.8	83.6	90.6	88.3	95.6	104.1	140	99.6	140
626	1.913	959	972	1.033	959	990	1.0	0.9	1.423	955	982	52	41	-0.562	36.5	62.4	67.1	68.8	74.6	78.0	130	74.5	140
627	1.961	995	1002	1.066	994	1243	1.1	1.9	1.046	990	1257	52	41	0.515	36.8	68.5	79.6	75.1	82.4	86.4	130	80.5	140
628	1.983	993	1662	1.052	1480	2086	2.0	2.3	1.024	1178	1557	52	41	1.445	36.3	75.3	85.7	81.1	90.0	86.3	140	87.9	140
629	1.962	994	1795	1.050	1731	2395	1.8	2.7	1.037	969	1395	52	41	0.969	37.6	72.4	77.6	78.0	84.8	91.8	140	87.6	150
630	1.978	994	1685	1.035	1470	2096	1.5	2.8	1.036	1278	1717	53	42	1.870	37.3	72.2	84.0	83.5	91.3	92.8	140	92.6	140
631	1.915	1524	1612	1.004	1911	2775	2.0	1.9	1.436	1481	2080	44	35	2.704	37.2	82.8	89.2	88.5	97.1	103.8	140	96.8	140
632	1.992	990	975	1.146	722	1487	1.1	0.8	1.491	824	1196	61	34	1.292	39.2	72.9	82.6	77.7	87.2	89.3	120	81.7	130
634	1.972	979	974	1.153	1161	1489	2.0	0.8	1.251	991	1481	60	33	1.019	39.4	76.7	86.0	81.2	90.9	94.8	120	87.6	140
635	1.826	981	1089	1.126	926	1435	1.5	1.0	1.406	838	1348	44	35	0.820	38.4	73.5	82.8	75.3	87.1	90.8	120	84.4	140
636	1.838	966	1181	1.083	825	1437	1.5	1.2	1.296	796	1289	44	35	0.950	39.0	79.5	88.5	82.7	94.5	93.7	120	86.3	140
637	1.827	968	1295	1.091	1847	2185	2.0	0.7	1.983	1131	1545	53	42	1.416	37.0	74.4	83.3	86.4	90.1	95.2	120	87.7	130
638	1.576	986	1383	1.058	1213	1777	1.5	1.2	2.097	1201	1514	52	41	1.325	37.8	76.6	86.8	82.3	90.5	93.7	120	87.6	140
639	1.566	983	1539	1.086	1345	2371	2.0	1.0	2.069	1360	1736	43	35	1.968	35.9	77.6	86.0	83.7	92.2	97.9	130	91.3	140
640	1.568	1387	1708	1.038	1988	2812	2.0	0.8	1.906	1432	1746	43	35	1.939	35.4	77.2	86.0	83.8	92.2	92.5	120	90.7	150
641	1.574	1233	1795	1.098	1651	2597	2.0	1.1	2.190	1607	1973	44	35	2.484	35.3	80.2	88.6	81.3	94.8	100.9	130	94.9	140
642	1.770	537	976	1.168	555	537	0....	0.9	1.560	533	874	51	40	-1.061	36.0	62.5	69.1	68.1	73.8	75.9	130	72.4	140
643	1.783	535	963	1.337	638	781	0.8	0.4	1.603	550	912	42	34	-0.837	36.6	67.9	67.8	68.2	74.1	76.0	130	72.9	140
644	1.612	781	1888	1.323	565	606	2.6	0.3	1.468	692	929	51	40	-0.796	36.4	62.6	66.9	69.1	74.7	79.6	130	76.6	140
645	1.526	989	1372	1.134	542	541	7.5	0.5	1.369	840	961	51	40	-0.651	36.2	64.6	66.9	70.9	76.3	82.6	130	80.1	140
646	1.567	975	1385	1.252	655	780	0.6	0.5	1.446	876	1026	52	41	-0.365	36.5	65.3	69.5	71.8	77.2	83.2	140	81.0	140
647	1.558	990	2191	1.498	699	956	0.8	0.7	1.530	868	1092	52	41	-0.096	37.0	66.1	70.6	72.1	77.6	83.3	140	81.0	140
648	1.535	1312	1798	1.337	667	787	0.6	0.7	1.448	978	1086	51	41	-0.118	36.6	67.3	76.4	73.2	78.8	86.0	140	83.5	140
649	1.483	1453	1364	1.259	533	539	0.4	0.6	1.367	1096	1037	52	41	-0.317	36.0	68.2	72.6	78.5	80.3	87.5	140	88.7	140
650	1.586	1460	1592	1.453	842	849	0.6	0.9	1.455	1074	1146	51	41	-0.115	36.5	69.7	73.8	75.5	80.1	88.9	140	86.1	140
651	1.513	1445	1392	1.466	771	1189	0.8	1.0	1.551	1209	1255	51	41	-0.908	36.4	70.2	74.8	76.4	82.3	89.9	150	86.6	140
652	1.742	1453	1686	1.883	1992	2861	1.8	1.2	2.621	1750	2284	44	36	3.072	36.3	83.6	88.7	89.0	95.9	105.2	140	100.7	140
653	1.748	1462	1818	2.181	1869	1880	1.0	1.0	1.916	1569	1612	43	35	1.597	36.1	76.6	82.0	81.9	88.4	97.2	140	93.4	140
654	1.777	1452	1831	1.506	684	948	0.6	0.8	1.646	1122	1360	43	35	0.793	36.5	74.4	79.3	75.5	85.6	99.8	140	91.9	140
655	2.032	1436	1785	2.728	1981	2698	1.5	1.8	2.717	1577	2247	44	36	3.039	36.8	83.8	89.2	88.6	96.0	106.6	140	101.9	140
656	2.025	1460	1883	2.467	2281	1516	1.8	0.9	2.304	1340	1899	43	35	2.098	36.3	79.9	85.5	84.9	91.8	102.2	140	97.4	140
657	2.051	1453	1887	1.595	218	1987	0.6	0.7	1.867	1170	1506	43	35	1.301	36.6	72.4	62.7	82.2	88.6	102.4	140	85.6	140
658	2.458	1453	1988	3.918	1717	2489	1.3	0.9	2.843	1572	2219	44	36	2.986	37.4	86.2	92.4	96.3	98.1	101.9	140	107.6	140
659	2.446	1498	2088	2.723	1353	2823	1.8	0.8	2.525	1635	2010	43	35	2.556	37.0	85.8	92.2	89.2	98.1	106.7	140	101.2	140
660	2.448	1461	2085	1.725	832	1281	0.6	0.6	2.148	1215	1783	43	35	1.835	36.9	83.8	90.3	88.8	99.4	106.4	140	100.6	140

Table B-8. Model No. 8: Dual-Flow Coannular-Coplanar, $A_o/A_1 = 0.4$.

A_o = 0.57 in.^{2}, A_i = 10.82 in.^{2} Linear Scale Factor to 338 in.^{2} = 3.59

Data Point No.	Inner			Outer			Ratios		Mass Averages			Meteorological Conditions		Normalization Parameters		2400-ft S.L. Data							
	$(P_T/P_{a2})_i$	T_{T_i} (° R)	V_i (ft/sec)	$(P_T/P_{a2})_o$	T_{T_o} (° R)	V_o (ft/sec)	V_o/V_i	W_o/W_i	$(P_T/P_{a2})_{mx}$	$T_{T_{mx}}$ (° R)	V_{mx} (ft/sec)	T_{Dry} (° F)	T_{Wet} (° F)	10 $\log_{10}$ (V/a_o)	10 $\log_{10}$ $F_\theta(T_o/T_{ssm})^{w-1}$	50° OASPL	50° PNL	90° OASPL	90° PNL	PPNL	θ	POASPL	θ
8230	1.0492	534	1010	1.1279	525	884	1.0	0.7	1.214	588	1005	80	64	−0.455	37.5	65.1	69.4	70.4	75.7	77.4	120	74.0	140
8231	1.0486	535	10030	1.0841	10800	10499	1.0	0.4	1.044	669	1135	80	64	0.074	38.3	68.2	73.6	74.0	80.9	83.9	120	77.3	130
8248	1.0482	540	10079	1.0726	10867	10231	1.0	0.4	1.035	748	1202	80	64	0.670	38.7	72.0	80.5	78.3	86.6	90.5	120	83.5	130
8249	1.0523	548	10093	1.0829	545	10072	1.0	0.4	1.023	761	1087	78	64	−0.115	37.3	65.3	69.2	71.9	76.6	79.6	130	77.3	140
8250	1.0525	546	10092	1.0757	10995	10418	1.0	0.5	1.030	873	1273	78	64	0.572	37.7	69.3	74.8	75.8	82.9	86.3	120	80.9	140
8251	1.0531	559	10150	1.09	11474	11785	2.0	0.5	1.098	1017	1282	77	63	1.230	37.6	74.4	84.4	80.1	88.7	93.2	120	86.1	130
8252	1.0529	561	10194	1.0720	592	11174	1.0	0.5	1.007	926	1187	78	64	0.269	37.0	67.3	71.4	73.3	78.9	83.4	130	81.3	140
8253	1.0562	592	10295	1.0451	11538	10782	1.9	0.6	1.029	1060	1417	78	64	1.036	36.9	71.7	78.5	78.0	85.3	89.0	120	84.3	140
8254	1.0569	598	10283	1.0561	11697	11344	2.0	0.6	1.040	1244	1663	78	64	1.733	36.3	76.7	86.1	82.5	90.9	95.9	130	89.1	140
8255	1.0533	1574	10302	1.0837	864	11354	1.0	0.6	1.044	1087	1295	78	64	0.647	36.5	69.5	73.5	75.5	81.1	86.3	130	84.1	140
8256	1.0574	1594	10291	1.0437	1048	10924	1.1	0.7	1.054	1236	1553	77	63	1.434	36.0	73.8	81.5	80.0	87.4	91.5	120	87.0	140
8257	1.0576	1593	10295	1.0462	1087	11472	1.0	0.7	1.029	1471	1859	78	64	2.217	35.4	78.4	87.5	84.1	92.5	97.9	130	91.6	140
8258	1.0497	1548	10198	1.0715	936	11399	1.0	0.7	1.020	1240	1388	78	64	0.946	35.8	71.7	75.8	77.7	83.6	88.8	130	86.4	140
8259	1.0585	1592	10283	1.0544	11385	10983	1.1	0.8	1.004	1432	1700	77	63	1.828	35.0	76.0	84.7	81.9	89.5	93.9	120	90.0	140
8260	1.0595	1596	10284	1.0680	1098	11776	2.0	0.8	1.229	1694	2032	80	64	2.646	35.0	80.1	88.4	86.4	94.5	100.0	130	94.9	140

Table B-9. Model No. 9: Coannular-Coplanar, $A_o/A_1 = 2.0$, Low Inner Flow.

A_o = 33.61 in.^{2}, A_i = 16.82 in.^{2} Linear Scale Factor to 338 in.^{2} = 3.17 (Outer Only)

Data Point No.	Inner			Outer			Ratios		Meteorological Conditions		Normalization Parameters		2400-ft S.L. Data							
	$(P_T/P_{a2})_i$	T_{T_i} (° R)	V_i (ft/sec)	$(P_T/P_{a2})_o$	T_{T_o} (° R)	V_o (ft/sec)	V_o/V_i	W_o/W_i	T_{Dry} (° F)	T_{Wet} (° F)	10 $\log_{10}$ V/a_o	10 $\log_{10}$ $F_\theta(T_o/T_{ssm})^{w-1}$	50° OASPL	50° PNL	90° OASPL	90° PNL	PPNL	θ	POASPL	θ
8231	1.0432	553	1031	1.1160	547	523	2.8	5.4	78	69	−3.3	31.8	48.6	45.4	57.6	51.7	52.4	110	53.6	110
8232	1.0435	547	1016	1.1221	550	655	3.8	5.9	78	69	−2.7	33.0	48.0	49.7	53.7	56.4	57.4	110	54.7	110
8233	1.0422	553	1048	1.0446	551	814	3.3	7.3	78	69	−1.4	35.6	56.9	61.0	62.8	67.6	68.6	110	64.3	110
8234	1.0513	612	1095	1.0787	555	1013	6.2	16.6	73	63	−0.4	37.7	65.1	69.7	70.3	75.8	76.9	130	72.9	140
8235	1.0522	543	1049	1.0495	534	1246	8.4	22.4	71	63	0.4	40.7	76.2	82.6	79.6	86.4	89.2	120	82.9	140
8236	1.0555	543	1055	1.0830	543	1423	4.5	12.9	71	63	1.1	43.2	88.8	94.3	90.9	98.1	98.1	90	91.3	150
8237	1.0605	738	1052	1.0805	15056	161	1.4	1.4	70	62	−6.4	26.1	45.3	44.6	50.1	50.9	52.6	110	52.6	110
8238	1.0626	735	1033	1.0835	14997	399	4.9	4.9	70	62	−2.7	35.0	50.0	53.2	57.5	58.5	59.9	120	59.2	120
8239	1.0608	725	1041	1.1142	15024	822	5.8	5.8	70	62	−1.3	35.2	56.4	59.8	61.9	66.2	67.7	120	64.1	120
8240	1.0609	725	1049	1.1234	15024	1029	6.8	6.8	70	65	−0.4	35.1	64.0	64.7	67.2	72.1	74.2	110	70.1	130
8241	1.0611	692	1041	1.1385	15156	1276	7.9	7.8	70	62	0.6	34.6	66.7	70.8	73.0	78.7	82.3	120	78.2	140
8242	1.0612	742	1051	1.1385	14812	1938	10.7	14.1	81	74	0.2	36.6	80.5	86.2	85.6	93.2	100.3	140	96.1	150
8244	1.0614	742	1049	1.1377	15046	1443	7.7	6.5	76	65	1.1	32.4	69.3	73.8	75.5	81.4	85.1	120	81.1	130
8245	1.0607	726	1032	1.1533	710	490	7.5	17.3	70	62	−0.5	36.9	61.5	65.8	67.6	72.9	75.2	130	71.8	140
8246	1.0611	663	1058	1.0863	975	1581	5.4	15.7	76	65	1.2	38.0	72.9	79.1	78.6	85.3	90.6	130	86.8	140
8247	1.0618	756	1031	1.1732	1317	1984	9.8	14.7	75	66	2.5	37.9	84.0	90.7	87.5	95.7	103.1	140	98.7	140
8248	1.0612	681	1065	1.0825	775	1032	6.6	13.0	70	62	−0.1	37.2	64.4	68.8	70.7	76.0	78.9	120	75.2	140
8249	1.0611	707	1061	1.1182	1181	1642	10.3	15.4	81	74	1.7	37.7	77.9	84.9	82.6	90.8	95.2	130	91.3	150
8250	1.0633	761	1043	1.0499	1389	2039	8.4	11.9	89	77	2.6	37.6	83.9	90.9	87.8	96.0	103.0	140	98.4	140
8251	1.0615	677	1046	1.1728	857	1193	6.6	12.4	81	62	0.3	37.7	67.2	72.1	72.4	78.1	81.9	130	77.4	140
8252	1.0622	800	1073	1.1446	1189	1789	10.4	17.9	81	62	2.1	37.7	81.6	88.3	86.5	92.9	97.8	140	94.4	150
8253	1.0625	754	1042	1.1790	1041	2051	8.1	9.2	83	63	2.6	35.6	80.5	85.8	85.7	92.5	100.8	140	96.5	150
8254	1.0614	637	1054	1.1835	879	1308	7.5	13.0	71	63	0.7	37.9	65.0	69.7	70.3	75.7	87.3	120	82.9	140
8255	1.0656	782	1046	1.0635	1524	1953	13.4	20.8	81	74	2.4	37.7	83.0	89.6	87.1	95.2	101.9	140	97.3	150
8257	1.0610	680	1050	1.0952	932	1396	7.1	15.8	76	65	1.1	37.9	70.8	75.9	77.1	83.2	88.3	130	84.6	140
8258	1.0618	847	1030	1.1145	1645	1978	8.6	12.0	89	77	2.5	35.0	78.9	84.1	84.9	91.7	99.6	140	95.4	140
9251	1.0612	644	1051	1.1340	816	1199	7.0	13.7	71	63	0.3	37.7	66.8	71.4	72.9	78.8	82.4	130	78.7	140

Table B-10. Model No. 10: Dual-Flow Coannular-Coplanar, A_o/A_1 = 0.65 Low Inner Flow.

A_o = 18.67 in.^{2}, A_i = 28.67 in.^{2} Linear Scale Factor to 338 in.^{2} = 5.56 (Outer Only)

Data Point No.	Inner			Outer			Ratios		Meteorological Conditions		Normalization Parameters		2400-ft S.L. Data							
													50°		90°					
		T_{0i} (° R)	V_i (ft/sec)		T_{0o} (° R)	V_o (ft/sec)	V_o/V_i	W_o/W_i	T_{amb} (° F)	T_{det} (° F)	10 log10 V/V_{ao}	10 log10 $F_s(T_o/T_{ao})^{-1}$	OASPL	PNL	OASPL	PNL	PPNL	θ	POASPL	θ
65											-4.3	29.5	38.9	38.1	43.7	45.8	45.3	100	44.5	110
57											-3.5	31.2	42.4	43.9	47.1	51.1	51.8	110	47.8	110
56											-2.8	32.6	46.9	49.3	51.9	57.2	58.0	110	52.8	110
55											-2.0	34.2	52.0	56.1	57.6	63.8	64.7	110	58.7	110
54											-1.5	35.4	56.3	61.0	62.2	68.5	69.4	110	63.3	110
53											-0.9	36.9	61.0	65.8	66.0	73.0	74.5	110	68.5	130
52											-0.5	37.7	64.9	69.8	70.5	76.7	78.0	110	72.7	140
51											0.3	40.2	78.6	85.8	81.4	91.5	91.7	100	82.4	140
50											0.9	42.8	88.8	95.9	93.0	100.7	101.8	110	93.6	100
49											-0.4	36.4	60.8	60.7	65.2	67.6	68.0	100	65.8	110
48											-0.4	33.4	53.6	56.5	58.5	63.1	63.9	110	59.5	110
47											0.3	36.7	64.8	69.4	71.9	78.7	87.0	110	76.6	130
46											0.9	37.3	69.8	74.7	77.0	83.9	87.8	130	83.5	140
45											-2.8	35.0	47.8	50.3	53.1	57.5	58.7	110	54.6	110
44											2.3	35.2	50.2	53.3	55.7	60.6	61.8	110	57.5	120
43											-1.6	35.3	53.9	57.8	59.7	65.0	66.7	110	62.1	120
42											-1.0	35.3	56.9	61.2	63.1	68.8	70.6	110	65.6	120
41											0.5	35.1	59.6	64.0	65.9	72.0	74.0	110	68.9	120
40											0.3	36.7	64.2	68.8	71.2	77.9	80.5	110	75.1	130
39											1.0	36.3	68.8	73.3	75.9	82.6	85.9	130	81.2	130
38											2.5	36.2	81.9	89.3	87.2	95.1	100.7	130	96.2	140
37											1.1	36.0	55.7	60.9	62.5	68.8	69.7	110	64.6	120
36											-0.6	36.7	58.9	64.1	65.6	67.2	74.0	110	68.4	130
35											0.3	37.7	65.1	70.5	72.3	79.2	81.2	130	76.3	140
34											0.4	37.8	66.0	71.6	73.0	80.0	82.4	130	77.7	150
33											0.5	38.7	68.1	74.1	74.8	81.5	84.0	130	79.8	140
32											1.7	37.9	78.0	86.6	82.9	92.3	94.4	120	86.1	150
31											1.7	39.4	88.1	95.5	87.0	97.5	98.6	100	91.7	140
30											3.4	35.8	84.7	91.2	90.3	98.0	105.0	140	101.5	140
29											2.5	37.9	90.1	97.5	91.2	100.7	103.8	140	98.7	140
28											2.6	39.6	94.6	101.5	94.6	103.7	104.7	120	98.4	140
27											4.0	38.6	91.6	97.0	96.3	104.4	114.1	130	108.6	130
26											1.9	34.1	74.5	79.6	81.5	88.6	92.8	130	89.0	140
25											2.8	39.4	96.7	101.5	95.3	103.7	108.7	120	101.2	120

Table B-11. Model No. 11: Coannular-Coplanar, $A_o/A_1 = 0.65$, No Inner Flow.

$A_o = 10.85$ in.^{2}, $A_1 = 16.82$ in.^{2} Linear Scale Factor to 338 in.$^2 = 5.58$ (Outer Only)

Data Point No.	Outer $(P_t/P_a)_o$	Outer T_{T_o} (° R)	Outer V_o (ft/sec)	Meteorological Conditions T_{dry} (° F)	Meteorological Conditions T_{wet} (° F)	Normalization Parameters 20 log10 V/a_o	Normalization Parameters 10 log10 $F_o(T_o/T_{amb})^{m-1}$	2400-ft S.L. Data 50° OASPL	50° PNL	90° OASPL	90° PNL	PPNL	θ	POASPL	θ
8445	1.539	919	1090	83	75	-0.474	37.9	63	67	69.4	74.4	76	130	73.3	140
8446	2.053	995	1451	82	75	-0.126	37.8	74.8	79.7	81.1	86.8	91.9	140	89.5	140
8447	2.724	1334	2005	84	76	2.545	37.9	85.3	91.5	90.2	97.3	105.1	140	101.3	140
8448	1.62	786	1089	82	75	-0.104	37.4	65.6	69.7	71.9	77.2	79.5	130	77	140
8449	2.258	1095	1655	84	76	1.712	37.7	78.4	85.9	83.8	90	95.9	140	93.2	140
8450	2.977	1481	2200	84	76	2.949	38.1	88.5	94.2	93.2	100.1	108.6	130	104.5	140
8451	1.728	820	1195	82	75	-0.297	37.7	68	72.1	74.5	79.8	83.3	130	80.7	140
8452	2.45	1204	1812	84	76	2.106	37.6	81.6	89	85.6	93.3	99.6	140	96	140
8453	3.243	1631	2385	85	76	3.300	38.3	88.7	94.5	93.3	100.8	109.8	130	104.9	130
8454	1.837	880	1299	82	75	0.660	37.8	70.4	74.8	76.7	82.2	85.9	130	83.4	140
8455	2.433	1202	1950	84	76	2.425	37.7	83.4	90.6	87.8	95.3	102.7	140	99	140
8456	3.545	1793	2527	85	76	3.635	38.4	90.5	96.4	95.2	102.5	112.7	130	107.1	130
8457	1.955	928	1394	82	75	0.968	37.9	73	77.6	79.2	84.8	82.9	130	87	140
8458	2.853	1399	2095	84	76	2.735	38.0	86.9	92.6	91.6	98.6	106.9	140	103	140
8459	3.878	1970	2783	84	76	3.969	38.6	91.2	97	95.7	104.2	113.8	140	108.7	130

Table B-12. Model No. 12: Coannular-Coplanar, $A_o/A_1 = 0.4$, Low Inner Flow.

$A_o = 6.73$ in.^{2}, $A_1 = 16.82$ in.^{2} Linear Scale Factor to 338 in.$^2 = 7.09$ (Outer Only)

Data Point No.	Inner $(P_t/P_a)_i$	Inner T_{T_i} (° R)	Inner V_i (ft/sec)	Outer $(P_t/P_a)_o$	Outer T_{T_o} (° R)	Outer V_o (ft/sec)	Ratios V_o/V_i	Ratios W_o/W_i	Meteorological Conditions T_{dry} (° F)	Meteorological Conditions T_{wet} (° F)	Normalization Parameters 10 log10 V/a_o	Normalization Parameters 10 log10 $F_o(T_o/T_{amb})^{m-1}$	2400-ft S.L. Data 50° OASPL	50° PNL	90° OASPL	90° PNL	PPNL	θ	POASPL	θ
8443	1.013	588	101	1.526	735	989	9.8	2.3	75	69	8.5	36.9	60.5	64.3	65.8	71.4	74.4	120	72.8	120
8446	1.004	548	121	2.054	946	1472	12.2	5.5	80	64	1.2	37.9	69.7	74.4	76.0	81.8	85.8	130	82.2	140
8447	1.009	704	149	2.721	1342	1824	12.2	3.8	75	63	2.6	37.8	87.1	95.8	86.6	95.8	98.6	130	93.4	140
8448	1.017	601	186	1.623	749	1093	5.9	2.1	75	63	-0.1	37.3	62.6	67.1	68.2	74.1	76.6	120	71.7	130
8449	1.001	795	12	2.259	1345	1617	30.9	11.6	80	64	1.6	38.0	75.4	85.6	79.0	86.7	89.9	130	85.0	140
8450	1.002	720	10	2.994	1479	2198	33.3	8.3	77	63	2.9	38.1	89.1	96.8	89.9	98.7	102.3	130	97.5	140
8451	1.017	610	188	1.732	821	1198	6.4	2.2	80	64	0.1	37.7	64.3	68.5	70.8	76.0	76.4	130	74.8	140
8452	1.005	722	111	2.445	1336	1789	16.1	5.1	75	63	2.0	38.2	82.5	93.6	83.0	92.1	95.1	120	88.7	140
8453	1.009	905	127	3.274	1585	2362	18.6	6.0	80	64	3.3	38.4	89.3	96.6	91.3	99.5	104.9	140	100.8	140
8454	1.005	636	104	1.832	868	1295	12.4	4.3	80	64	0.6	37.8	66.6	70.8	72.7	78.3	81.6	130	78.2	140
8455				2.436	1194	1949			77	63	2.4	37.8	87.1	95.5	86.5	95.7	98.5	140	92.7	140
8456	1.009	966	172	3.538	1751	2549	14.8	4.4	80	64	3.6	38.5	89.8	96.7	92.2	100.0	107.3	130	102.9	140
8457	1.003	629	104	1.934	914	1384	13.3	4.5	80	64	0.9	38.0	68.7	72.8	76.8	80.9	83.8	130	80.0	140
8458	1.001	724	84	2.859	1409	2154	25.4	6.7	77	63	2.8	38.0	88.9	96.5	88.9	97.8	101.0	130	95.7	140
8459	1.017	982	238	3.873	1953	2775	11.6	3.3	80	64	3.9	38.4	90.5	97.3	94.2	101.6	110.5	130	105.8	130

Table B-13. Model No. 13: Coannular-Coplanar, A_0/A_1 = 0.4, No Inner Flow.

A_0 = 6.73 in.^{2}, A_1 = 16.82 in.^{2} Linear Scale Factor to 338 in.^{2} = 7.39 (Outer Only)

Data Point No.	Outer			Meteorological Conditions		Normalization Parameters		2400-ft S.L. Data							
								50°		90°					
	$(P_T/P_a)_0$	T_0 (°R)	V_0 (ft/sec)	T_{dry} (°F)	T_{wet} (°F)	10 $\log_{10} V/a_0$	10 $\log_{10} F_n(T_0/T_{std})^{m-1}$	OASPL	PNL	OASPL	PNL	PPNL	θ	POASPL	θ
8445	1.528	717	997	89	76	-0.510	36.9	64.9	68.5	70.9	75.3	76.7	120	74.5	120
8446	2.047	994	1438	90	77	1.249	37.6	76.7	81	83.1	88.2	92.8	130	90.1	140
8447	2.718	1334	2003	90	77	2.541	37.9	85.6	92.6	90.9	97.1	104.1	130	100.5	1
8448	1.62	770	1092	89	76	-0.094	37.4	67.9	71.9	74	78.6	80.3	130	78.3	140
8449	2.282	1106	1666	90	77	-1.740	37.7	80.2	86	86.1	91.5	97.1	130	94.3	140
8450	2.999	1474	2155	90	77	2.939	36.1	89	94.4	94.6	100.9	109.1	130	105	130
8451	1.716	823	1202	89	76	0.324	38.1	70.8	79.8	76.7	81.5	84.3	130	82.1	140
8452	2.416	1189	1748	90	77	2.048	37.6	82.6	90.6	88	93.7	100	130	96.6	140
8453	3.286	1634	2388	90	77	3.305	38.3	90.6	96.1	96	102.5	111.1	130	106.9	130
8454	1.834	875	1294	89	76	0.643	37.8	73	77.1	79	84	87.3	130	84.6	140
8455	2.64	1292	1945	90	77	2.414	37.8	88.9	91.8	90.5	96.5	103.4	130	99.8	140
8456	3.549	1784	2571	90	77	3.626	38.4	90.6	96	95.7	102.5	111.9	130	107.5	130
8457	1.942	940	1392	90	77	0.977	37.8	74.7	78.9	81.1	86	90	130	87.5	140
8458	2.855	1399	2095	90	77	2.737	38.0	86.8	93.5	92.1	98.8	105.9	130	100.8	130
8459	3.894	1899	2734	90	77	3.893	38.8	91.5	97.1	96.7	103.9	113.1	130	108.5	130

Table B-14. Model No. 14: 4.64-inch-Diameter Conical, Adapted to Cell 41, Anechoic.

A_I = 16.82 in.^{2} Linear Scale Factor to 333 in.^{2} = 4.48

Data Point No.	Inner			Meteorological Conditions		Normalization Parameters		2400-ft S.L. Data							
								50°		90°					
	$(P_T/P_o)_i$	T_{Ti} (° R)	V_i (ft/sec)	T_{dry} (° F)	T_{wet} (° F)	$10 \log_{10} V/a_o$	$10 \log_{10} F_s(T_o/T_{om})^{\omega-1}$	OASPL	PNL	OASPL	PNL	PPNL	θ	POASPL	θ
1	1.099	1017	570	52	54	-2.9	34.1	47.6	48.0	53.9	55.5	58.0	120	57.2	130
2	1.215	1309	824	52	44	-1.3	35.5	55.3	58.6	62.1	66.4	69.7	120	67.3	130
3	1.037	1084	981	51	44	-0.6	35.9	60.1	64.4	67.3	72.6	76.7	130	73.9	140
4	1.474	1109	1184	50	42	0.3	36.2	64.8	69.8	72.3	78.3	83.8	130	81.1	140
5	1.723	1173	1427	49	42	1.1	36.3	69.8	75.2	77.0	83.9	91.5	130	88.2	140
6	1.97[illegible]	1203	1602	49	42	1.6	36.5	72.8	78.3	80.1	87.5	96.6	130	92.7	140
7	2.25[illegible]	1266	1796	48	41	2.1	36.9	79.6	86.3	83.5	92.4	101.4	140	96.[illegible]	140
8	2.745	1320	2001	48	41	2.5	38.0	86.9	93.4	89.2	97.9	106.0	130	1[illegible].6	130
9	3.246	1380	2185	40	41	2.9	39.0	90.9	97.3	93.6	101.4	109.1	130	103.4	130
10	3.924	1466	2397	43	42	3.3	40.0	93.2	99.5	96.0	104.0	112.3	130	106.5	130
11	1.319	1625	1222	51	43	0.4	34.3	65.4	70.0	72.5	78.0	83.4	130	81.0	140
12	1.601	1697	1608	50	43	1.6	33.4	71.2	76.2	78.5	85.2	94.0	140	90.9	140
13	2.059	1739	1985	49	41	2.5	34.5	76.1	81.6	83.8	91.5	103.5	130	98.1	130
14	1.329	737	831	49	42	1.3	35.7	55.6	59.9	62.7	67.6	70.8	130	68.0	140
15	1.947	764	1211	49	42	0.4	38.6	67.8	74.1	73.8	80.8	86.1	130	82.7	140
16	2.493	707	1397	49	42	1.0	40.2	87.8	93.4	90.1	97.5	97.7	80	90.4	140
17	3.491	705	1595	48	41	1.6	42.5	91.1	97.1	92.6	100.4	100.8	120	95.5	140
18	1.559	990	1192	49	42	0.3	36.8	65.3	70.4	72.6	78.9	84.7	130	81.9	140
19	2.296	1009	1602	48	41	1.6	38.3	80.7	87.2	82.3	91.2	98.2	140	94.2	140
20	3.960	1004	1981	49	43	2.5	41.9	93.8	99.9	96.0	104.0	108.0	140	103.3	140
21	1.148	1501	836	52	45	1.3	35.3	[illegible].6	60.8	64.3	68.2	71.4	120	69.9	130
22	1.707	1500	1668	50	42	1.6	34.4	71.9	77.1	79.0	86.0	94.7	140	91.2	140
23	2.404	1526	2026	47	41	2.6	36.3	81.0	87.7	85.9	94.6	105.6	130	100.1	130
24	2.915	1512	2200	48	41	2.9	37.8	87.6	94.3	91.0	99.5	108.8	130	103.0	130
25	3.674	1504	2380	48	42	3.3	39.5	92.9	99.1	95.5	103.5	111.9	130	106.2	130
26	1.165	842	654	57	45	-2.3	34.3	49.8	52.2	56.6	60.2	62.9	120	61.0	130
27	1.251	2018	872	52	44	-1.1	35.7	56.1	59.7	62.9	67.5	70.9	120	66.9	120
28	2.998	1009	1808	48	42	2.1	39.9	89.8	96.2	91.2	99.0	104.4	140	99.7	140
29	1.381	1493	1260	50	43	0.5	34.7	66.0	70.9	73.2	79.0	85.2	130	82.3	140
30	2.013	1497	1813	49	42	2.1	35.1	74.7	80.3	82.3	89.7	100.1	130	95.5	140
64	2.650	1512	2279	48	41	3.1	36.4	84.6	91.1	89.0	97.8	108.9	130	103.1	130
65	1.979	1628	1871	49	42	2.2	34.4	75.1	80.7	82.9	90.4	101.5	130	96.5	130
66	1.197	1732	865	52	44	-1.1	35.5	57.6	61.2	64.3	68.7	72.3	120	70.1	140
67	1.787	862	1259	48	41	0.5	37.8	67.0	72.7	73.8	79.8	86.9	130	83.9	140
68	2.624	863	1368	48	41	0.9	38.3	69.7	75.9	76.3	83.4	90.2	130	87.1	140
69	2.196	849	1433	47	40	1.1	38.9	79.7	86.4	80.9	89.5	92.9	140	89.6	140
70	2.380	845	1502	47	41	1.3	39.3	82.6	89.3	84.2	92.0	97.3	150	92.8	140
71	2.646	850	1575	48	41	1.4	40.1	86.7	92.4	89.3	97.1	99.1	140	95.3	140
72	2.809	854	1620	49	42	1.6	40.3	88.1	94.0	91.8	99.7	100.8	140	96.6	147

Table B-15. Model No. 15: 36 Chute, AR = 2.5, R_r = 0.653, Turbojet.

A_j = 11.56 in.^{2} Linear Scale Factor to 138 in.^{2} = 3.62

Data Point No.	Jet (P_j/P_{a_j})	Jet T_j (°R)	Jet V_j (ft/sec)	Meteorological Conditions T_{dry} (°F)	Meteorological Conditions T_{wet} (°F)	Normalization Parameters 10 $\log_{10}$ V/a_o	Normalization Parameters 10 $\log_{10}$ $F_s(T_o/T_{sa})\omega-1$	2400-ft S.L. Data 50° OASPL	50° PNL	90° OASPL	90° PNL	PPNL	θ	POASPL	θ
1	2.718	1114	2013	80	73	2.162	37.9	77.9	82.6	82.7	93.0	95.2	120	86.2	140
2	2.096	1441	2229	81	74	1.934	38.3	76.2	85.7	84.3	94.1	97.3	110	89.7	140
3	2.456	1201	2112	80	73	2.105	37.7	71.7	80.3	80.6	90.9	93.1	120	83.1	120
4	2.283	1431	2192	80	73	2.039	38.3	78.3	88.2	85.9	96.0	98.5	110	92.4	140
5	1.988	1764	2346	76	72	1.819	38.6	79.9	89.0	87.6	97.5	100.0	140	95.6	140
6	1.952	933	1393	80	71	0.975	37.9	66.7	75.4	75.8	85.7	87.5	120	77.5	120
7	1.927	1115	1611	76	72	1.725	39.2	79.9	89.0	87.6	97.6	100.1	140	95.6	140
8	2.034	638	1194	80	72	0.293	39.0	65.5	73.9	73.4	83.5	83.7	100	74.1	110
9	2.614	625	1196	81	73	0.972	40.6	70.3	80.0	77.2	87.4	88.6	120	79.1	140
10	1.310	729	1597	81	73	1.556	42.1	76.0	86.5	80.9	91.9	92.4	80	84.3	140
11	1.994	1252	2400	76	72	1.325	37.3	75.3	83.5	84.7	95.2	97.3	110	88.0	120
12	2.693	1234	2296	76	72	1.133	36.5	73.3	81.5	83.2	93.8	96.2	120	86.3	120
13	2.375	1131	2148	78	72	2.844	35.6	71.8	80.2	81.8	92.5	94.5	110	84.1	120
14	2.018	1419	1890	80	73	2.258	34.6	70.4	78.8	80.7	91.4	93.7	120	83.4	120
15	2.140	1447	1998	80	73	2.332	35.0	71.8	80.2	81.8	92.5	94.5	110	84.1	120
16	1.716	825	1191	80	72	0.282	37.6	63.6	72.0	72.9	82.8	83.9	120	74.2	120
17	1.453	1112	1191	80	73	0.282	36.2	60.5	68.4	71.4	80.8	82.2	120	72.9	120
18	1.924	1204	1604	80	73	1.575	36.5	68.5	76.9	78.0	88.4	90.7	120	80.4	120
19	3.974	1449	2351	80	73	3.309	40.2	81.2	90.3	87.2	97.5	100.5	140	95.9	140
20	1.314	701	1295	80	72	4.471	35.4	53.7	60.5	63.6	71.7	72.2	100	64.0	110
21	1.952	697	1207	81	73	0.340	37.6	64.9	73.5	73.3	83.1	83.8	110	74.2	110
22	1.976	651	1345	80	73	0.811	38.3	65.9	74.3	75.1	35.1	86.7	120	76.7	120
23	2.201	844	1433	79	72	1.086	38.9	68.3	76.9	76.9	86.7	88.5	120	78.3	120
24	2.380	848	1496	80	73	1.273	39.3	69.4	78.0	77.8	87.8	89.8	120	79.9	120
25	2.623	848	1567	81	74	1.474	39.9	71.2	80.3	78.8	89.0	90.7	120	81.1	140
26	2.792	848	1610	80	73	1.542	40.3	78.2	82.3	79.6	89.7	91.7	120	81.9	120

Table B-16. Model No. 16: 36 Chute, AR = 2.0, R_r = 0.716, Turbojet.

A_i = 23.76 in.^{2} Linear Scale Factor to 338 in.^{2} = 3.77

Data Point No.	Inner			Meteorological Conditions		Normalization Parameters		2400-ft S.L. Data							
								50°		90°					
	$(P_T/P_o)_i$	T_{T_i} (° R)	V_i (ft/sec)	T_{Dry} (° F)	T_{Wet} (° F)	10 $\log_{10}$ V/a_o	10 $\log_{10}$ $F_g(T_o/T_{sm})^{\omega-1}$	OASPL	PNL	OASPL	PNL	PPNL	θ	POASPL	θ
1	2.745	1324	2004	75	66	2.542	38.0	73.9	83.9	82.4	92.5	95.2	120	88.2	140
2	3.002	1484	2204	71	64	2.955	38.1	76.4	86.6	84.4	94.6	97.2	120	91.4	140
3	2.436	1204	1807	71	64	2.093	37.6	71.4	79.9	80.5	90.7	93.1	120	84.5	140
4	3.264	1611	2371	76	67	3.273	38.3	78.2	87.7	86.0	96.1	99.5	140	94.6	140
5	3.566	1753	2552	78	68	3.592	38.6	79.1	87.2	87.2	96.7	101.5	140	97.4	140
6	1.928	947	1396	65	61	0.972	37.8	66.4	74.7	82.5	88.4	88.4	110	78.1	120
7	3.902	1756	2627	77	67	3.718	39.2	79.4	86.4	88.1	97.2	103.7	140	100.0	140
8	2.046	634	1188	70	62	0.272	38.9	65.6	73.7	73.7	83.6	84.5	120	74.6	120
9	2.565	685	1394	66	60	0.966	40.4	70.7	81.6	77.4	87.7	88.6	120	79.8	140
10	3.302	739	1603	66	62	1.573	41.9	77.9	88.1	82.1	93.7	94.5	80	85.5	140
11	2.953	1756	2387	76	67	3.325	37.3	75.7	84.8	85.3	95.3	98.6	140	93.0	140
12	2.665	1745	2279	76	67	3.101	36.5	73.9	81.7	84.0	94.2	96.8	120	90.1	140
13	2.368	1733	2146	78	69	2.840	35.6	72.4	79.7	82.9	93.6	95.9	110	87.3	140
14	2.009	1632	1892	77	68	2.293	34.6	70.2	78.0	80.8	91.6	93.9	110	84.1	120
15	2.134	1673	1990	77	68	2.252	35.0	70.9	78.5	81.4	92.2	94.4	110	84.9	140
16	1.734	820	1199	66	61	2.312	37.7	63.4	71.7	72.6	82.3	84.3	120	74.3	120

Table B-17. Model No. 17: 36 Chute, AR = 1.5, R_r = 0.782, Turbojet.

A_i = 23.76 in.^{2} Linear Scale Factor to 338 in.^{2} = 3.77

Data Point No.	Inner			Meteorological Conditions		Normalization Parameters		2400-ft S.L. Data							
								50°		90°					
	$(P_T/P_o)_i$	T_{T_i} (° R)	V_i (ft/sec)	T_{Dry} (° F)	T_{Wet} (° F)	10 $\log_{10}$ V/a_o	10 $\log_{10}$ $F_g(T_o/T_{sm})^{\omega-1}$	OASPL	PNL	OASPL	PNL	PPNL	θ	POASPL	θ
1	2.699	1347	2007	62	64	2.549	37.8	74.2	82.5	82.7	91.8	95.8	140	91.0	140
2	3.001	1493	2210	62	64	2.967	38.1	76.2	84.7	84.5	93.7	98.8	140	95.0	140
3	2.463	1194	1809	62	64	2.098	37.7	71.7	79.9	80.4	89.7	91.8	140	86.8	140
4	3.266	1620	2378	62	64	3.285	38.3	78.3	86.2	86.4	95.7	102.9	140	98.8	140
5	3.567	1758	2556	65	67	3.599	38.5	81.1	88.9	88.2	97.6	106.5	140	102.6	140
6	1.951	939	1401	63	65	0.988	37.9	66.0	73.4	75.4	84.8	86.6	120	78.1	140
7	3.924	1744	2623	64	66	3.711	39.2	83.0	90.0	89.5	99.0	108.4	140	104.4	140
8	2.077	634	1199	62	64	0.312	39.0	66.1	74.4	73.7	83.3	83.5	110	75.0	140
9	2.599	680	1397	62	64	0.975	40.6	70.6	80.9	77.3	87.0	87.0	90	80.7	140
10	3.316	734	1600	62	64	1.565	42.0	78.1	87.6	82.1	93.4	93.4	90	87.1	140
11	3.064	1766	2428	63	65	3.376	37.4	76.7	83.6	85.6	94.5	101.8	140	98.1	140
12	2.700	1768	2308	63	65	3.156	36.5	75.1	81.0	84.4	93.4	99.7	140	95.6	140
13	2.405	1735	2165	63	65	2.878	35.6	73.2	79.2	83.0	92.2	95.8	140	91.1	140
14	1.987	1618	1871	62	64	2.244	34.5	69.8	76.2	79.9	89.5	92.2	120	85.3	140
15	2.151	1665	1994	62	64	2.521	35.0	71.3	77.5	81.2	90.6	93.8	120	87.7	140
16	1.744	819	1204	63	65	0.330	37.7	63.0	70.7	72.9	82.1	82.9	120	74.2	140

Table B-18. Model No. 18: 36 Spoke, AR = 2.0, R_r = 0.716, Turbojet.

A_i = 23.76 in.^{2} Linear Scale Factor to 338 in.^{2} = 3.77

Data Point No.	Inner			Meteorological Conditions		Normalization Parameters		2400-ft S.L. Data							
								50°		90°					
	$(P_T/P_o)_1$	T_{T_1} (° R)	V_1 (ft/sec)	T_{Dry} (° F)	T_{Wet} (° F)	10 $\log_{10}$ V/a_o	10 $\log_{10}$ $F_s(T_o/T_{sm})^{\omega-1}$	OASPL	PNL	OASPL	PNL	PPNL	θ	POASPL	θ
1	2.723	1344	2012	79	67	2.560	37.9	72.2	79.7	81.3	90.7	93.0	120	88.4	140
2	3.000	1491	2209	80	68	2.965	38.1	74.3	80.7	82.9	91.7	95.7	140	92.1	140
3	2.440	1194	1801	79	67	2.078	37.7	70.8	79.0	79.6	89.4	91.5	110	84.4	140
4	3.288	1622	2355	80	68	3.298	39.3	76.2	82.0	84.9	93.4	98.7	140	95.3	140
5	3.560	1723	2528	80	68	3.551	38.6	78.9	85.4	87.0	95.5	103.8	140	100.0	140
6	1.926	939	1389	80	68	0.950	37.8	66.4	75.2	75.1	85.7	87.3	110	77.0	140
7	3.924	1738	2618	80	68	3.703	39.3	81.3	88.0	88.3	97.0	107.5	140	103.6	140
8	2.041	644	1194	79	67	0.293	38.9	66.0	74.4	73.7	84.1	84.9	110	74.5	110
9	2.611	673	1398	79	67	0.978	40.6	69.6	78.7	76.7	87.1	87.4	110	77.3	110
10	3.308	726	1590	79	68	1.537	42.0	73.9	83.2	79.7	89.8	89.8	90	85.1	140
11	2.948	1175	2384	80	68	3.330	37.2	75.6	81.7	84.0	92.6	97.4	140	93.9	140
12	2.664	1746	2280	80	68	3.103	36.5	74.2	81.0	83.2	92.3	95.7	140	91.2	140
13	2.398	1723	2154	80	68	2.856	35.7	72.8	80.2	81.9	91.6	94.1	120	88.1	140
14	2.030	1621	1899	80	68	2.309	34.7	69.3	77.1	79.4	89.6	92.2	110	82.9	140
15	2.132	1661	1982	80	68	2.494	35.0	70.8	78.4	80.5	90.5	93.3	110	84.9	140
16	1.718	823	1191	79	68	0.282	37.7	63.4	72.3	72.2	82.9	84.1	110	73.5	110

Table B-19. Model No. 19: 36 Chute, AR = 2.0, R_r = 0.716, Turbojet with Acoustically Treated Secondary Ejector.

A_i = 23.76 in.^{2} Linear Scale Factor to 338 in.^{2} = 3.77

Data Point No.	Inner			Meteorological Conditions		Normalization Parameters		2400-ft S.L. Data							
								50°		90°					
	(P_T/P_o)	T_{T_1} (° R)	V_1 (ft/sec)	T_{Dry} (° F)	T_{Wet} (° F)	10 $\log_{10}$ V/a_o	10 $\log_{10}$ $F_s(T_o/T_{sm})^{\omega-1}$	OASPL	PNL	OASPL	PNL	PPNL	θ	POASPL	θ
1	2.727	1336	2007	66	61	2.549	37.9	72.5	79.0	80.8	89.6	91.6	110	86.5	140
2	3.013	1465	2193	66	62	2.934	38.2	74.5	81.2	82.7	91.3	93.4	110	89.9	140
3	2.444	1202	1809	66	61	2.098	37.6	69.9	76.8	78.6	87.2	89.3	110	82.3	140
4	3.300	1620	2355	65	61	3.298	38.4	77.0	84.5	34.7	83.1	97.5	140	94.5	140
5	3.553	1748	2545	65	61	3.580	38.5	79.6	87.2	87.2	95.3	102.7	140	99.9	140
6	1.935	935	1390	68	62	0.954	37.9	64.3	71.0	72.7	80.9	82.8	120	74.6	120
7	3.897	1754	2624	65	62	3.713	39.2	81.8	88.0	88.9	96.7	107.8	140	104.5	140
8	2.042	658	1208	73	65	0.344	38.9	64.2	70.7	71.8	79.5	80.1	110	72.4	110
9	2.578	683	1395	67	62	0.969	40.5	69.2	76.2	76.5	84.8	85.2	110	78.3	140
10	3.303	742	1607	69	64	1.584	41.9	76.6	85.9	81.3	91.6	92.1	80	85.9	140
11	2.984	1745	2392	65	61	3.311	37.3	74.9	81.3	83.8	92.4	95.4	140	91.8	140
12	2.683	1756	2293	66	62	3.127	36.5	73.0	79.1	82.4	91.1	93.7	110	88.9	140
13	2.367	1722	2139	66	62	2.825	35.6	71.1	76.9	80.6	89.8	92.4	110	85.9	140
14	2.016	1621	1890	68	63	2.289	34.6	67.9	73.5	77.3	86.5	89.9	110	80.6	140
15	2.135	1659	1982	67	62	2.494	35.0	69.1	74.7	78.4	87.6	90.6	110	82.4	140
16	1.723	823	1194	71	65	0.293	37.7	61.2	87.8	69.3	77.2	78.5	120	70.5	120

Table B-20. Model No. 20: 72 Tube/Plug, AR = 2.95, Turbojet.

A_i = 30.87 in.^{2} Linear Scale Factor to 338 in.^{2} = 3.31

Data Point No.	Inner			Meteorological Conditions		Normalization Parameters		2400-ft S.L. Data							
								50°		90°					
	$(P_T/P_o)_i$	T_{T_i} (° R)	V_i (ft/sec)	T_{Dry} (° F)	T_{Wet} (° F)	10 $\log_{10}$ V/a_o	10 $\log_{10}$ $F_s(T_o/T_{sm})^{\omega-1}$	OASPL	PNL	OASPL	PNL	PPNL	θ	POASPL	θ
1	2.772	1309	2001	40	37	2.5	38.1	72.8	82.5	80.1	91.5	93.9	120	84.3	140
2	3.001	1240	2009	55	46	2.6	38.9	73.4	83.3	80.6	91.6	93.6	120	85.2	140
3	2.471	1180	1800	40	37	2.1	37.8	71.0	80.8	78.1	89.8	92.2	120	81.4	120
4	3.244	1171	2008	54	45	2.6	39.8	74.1	84.6	81.1	92.2	94.3	120	86.7	140
5	2.232	1081	1634	37	34	1.7	37.6	69.3	79.2	76.8	88.5	90.4	120	79.5	120
6	3.566	1116	2022	54	45	2.6	40.7	74.9	85.6	81.6	92.4	94.9	130	88.3	150
7	1.931	937	1390	37	34	1.0	37.8	66.1	76.0	73.7	85.3	86.8	120	75.6	120
8	3.880	1057	2020	54	45	2.6	41.5	75.8	86.7	82.0	92.7	95.2	130	90.0	150
9	2.986	1262	2024	55	46	2.6	38.8	73.5	83.4	80.6	91.6	93.9	120	85.5	140
10	2.378	1411	1936	55	46	2.4	36.6	71.4	81.2	78.8	90.3	92.4	110	81.7	120
11	1.780	1398	1603	41	37	1.6	35.1	67.4	77.4	74.6	86.4	88.8	120	77.8	120
12	1.490	1135	1214	39	36	0.4	36.1	62.1	71.7	69.2	80.2	82.5	120	71.7	120
13	2.061	646	1204	34	32	0.3	38.9	65.9	75.7	72.7	84.3	84.9	110	73.6	110
14	2.591	675	1390	35	33	1.0	40.5	69.6	79.8	75.8	87.4	88.3	110	77.4	130
15	3.305	764	1630	43	39	1.6	41.8	73.1	84.5	78.6	90.1	91.0	130	81.9	130
16	1.691	1163	1398	38	35	1.0	36.3	65.1	74.9	72.5	84.0	86.0	120	75.0	120

Table B-21. Model No. 21: 32 Chute, AR = 2.0, R_r = 0.498, Turbojet.

A_i = 30.83 in.^{2} Linear Scale Factor to 338 in.^{2} = 3.31

Data Point No.	Inner			Meteorological Conditions		Normalization Parameters		2400-ft S.L. Data							
								50°		90°					
	$(P_T/P_o)_i$	T_{T_i} (° R)	V_i (ft/sec)	T_{Dry} (° F)	T_{Wet} (° F)	10 $\log_{10}$ V/a_o	10 $\log_{10}$ $F_s(T_o/T_{sm})^{\omega-1}$	OASPL	PNL	OASPL	PNL	PPNL	θ	POASPL	θ
1	2.727	1326	2001	68	60	2.536	37.9	71.7	79.9	79.6	89.9	92.7	140	89.6	140
2	3.013	1257	2026	68	60	2.590	38.9	73.3	81.9	80.6	89.8	95.1	140	92.1	140
3	2.453	1183	1797	66	59	2.069	37.7	69.6	78.1	77.5	87.6	90.2	120	85.0	140
4	3.289	1206	2049	66	59	2.639	39.7	75.6	85.5	81.9	90.9	97.2	140	94.2	150
5	2.220	1072	1622	68	61	1.624	37.8	67.4	76.3	75.1	85.7	88.1	120	80.5	140
6	3.595	1124	2034	68	61	2.607	40.7	78.0	87.0	83.3	92.6	98.7	140	95.7	150
7	1.941	942	1398	68	61	0.978	37.8	64.0	73.4	71.8	83.1	85.1	120	75.4	140
8	3.925	1046	2016	68	60	2.568	41.6	81.9	89.1	85.4	94.9	100.6	140	97.4	150
9	3.017	1306	2067	66	59	2.677	38.7	73.4	81.8	80.8	89.8	95.4	140	92.2	140
10	2.388	1458	1973	66	59	2.475	36.5	70.7	79.0	78.9	89.0	91.6	120	87.3	140
11	1.811	1355	1599	66	59	1.562	35.4	65.6	74.6	73.8	84.9	87.1	120	78.3	140
12	1.497	1133	1219	64	58	0.383	36.1	59.4	68.5	67.6	79.0	80.6	120	70.2	120
13	2.077	636	1200	64	58	0.315	39.0	63.0	72.7	69.8	81.4	81.9	120	71.5	130
14	2.596	678	1395	64	58	0.909	40.5	67.2	76.8	73.7	84.6	85.5	120	77.9	140
15	3.368	741	1616	64	58	1.608	42.1	64.0	74.3	68.7	78.8	79.5	130	76.2	150
16	1.711	1107	1416	64	58	1.034	36.3	62.9	72.2	71.1	82.5	84.3	110	74.4	130

Table B-22. Model No. 22: 36 Chute, AR = 2.5, R_r^o = 0.653 Outer Suppressor; A_o/A_i = 1.92, R_r^i = 0.779 Inner Plug, Retracted.

A_o = 12.76 in.^{2}, A_i = 6.59 in.^{2} Linear Scale Factor to 338 in.^{2} = 3.06

Data Point No.	Inner			Outer			Ratios		Mass Averages			Meteorological Conditions		Normalization Parameters		2400-ft S.L. Data							
																50°		90°					
	$(P_T/P_o)_i$	T_{T_i} (°R)	V_i (ft/sec)	$(P_T/P_o)_o$	T_{T_o} (°R)	V_o (ft/sec)	V_o/V_i	W_o/W_i	$(P_T/P_o)_{ma}$	$T_{T_{ma}}$ (°R)	V_{ma} (ft/sec)	T_{DTY} (°F)	T_{WET} (°F)	$10\log_{10}(V/a_o)$	$10\log_{10}F_n(T_o/T_{ma})^{\omega-1}$	OASPL	PNL	OASPL	PNL	PPNL	θ	POASPL	θ
9	1.0955	898	520	1.0482	1046	2000	3.8	6.5	2.273	1286	1802	58	56	2.082	36.1	71.1	80.0	81.0	91.8	93.6	110	82.6	120
12	1.0867	914	698	1.0447	1182	1794	3.6	4.7	2.104	1148	1628	58	56	1.639	36.4	68.3	77.2	78.3	89.1	91.5	120	81.2	120
13	1.0865	912	503	1.0372	1046	2399	4.8	7.5	2.739	1560	2176	58	56	2.900	36.5	74.6	83.4	84.0	94.5	96.8	120	88.6	130
14	1.0948	941	546	1.0702	1761	2589	4.7	7.8	3.062	1667	2356	60	58	3.244	37.0	77.0	86.4	85.8	95.9	99.4	120	91.4	130
15	1.1314	698	798	1.096	913	1587	1.8	3.9	1.729	908	1257	59	56	0.516	37.1	64.1	72.7	73.4	83.8	85.9	120	75.3	120
16	1.1389	696	981	1.0697	1382	2017	2.1	3.2	2.258	1251	1771	59	56	2.004	36.7	71.4	80.0	80.6	91.3	93.9	120	84.1	120
17	1.2864	913	843	1.1449	1767	2296	2.7	3.6	2.206	1572	1964	58	56	2.454	35.3	73.0	81.3	82.4	93.4	95.5	110	86.0	120
18	1.35	896	941	1.141	1356	1799	1.9	3.1	2.059	1132	1595	58	56	1.551	36.9	69.2	78.0	78.9	89.7	91.7	120	81.6	120
19	1.44	936	1045	1.255	1651	2198	2.3	3.3	2.639	1481	2085	57	55	2.714	37.0	74.7	83.4	84.1	94.1	97.2	120	88.9	130
20	1.46	937	1058	1.328	1769	2601	2.5	3.6	2.984	1583	2265	58	56	3.073	37.6	77.1	86.2	86.0	96.1	99.0	120	91.5	130
23	1.3778	576	1024	1.665	1334	1992	1.9	1.8	2.309	1068	1653	60	57	1.706	38.1	71.1	79.5	80.5	91.2	93.3	110	83.6	120
24	1.533	1009	1182	1.728	860	1223	1.0	2.4	1.461	904	1211	59	56	0.354	37.2	60.9	68.4	71.1	80.9	82.4	120	72.9	120
25	1.536	992	1174	2.391	1224	1805	1.5	2.7	2.099	1161	1635	59	55	1.657	36.9	68.1	75.5	78.8	89.5	91.9	120	81.9	120
27	1.529	1249	1312	2.166	1690	1613	1.2	2.9	1.948	1130	1537	59	56	1.390	36.8	67.6	76.0	76.7	86.9	90.0	120	79.7	120
28	1.536	1227	1307	2.432	1837	1962	1.5	3.2	2.266	1296	1806	59	56	2.091	36.6	71.0	79.6	80.4	91.0	93.6	110	83.5	120
29	1.539	1217	1305	3.717	1754	2587	2.0	3.8	3.010	1643	2323	59	56	3.184	37.5	74.4	86.5	86.2	96.0	99.0	120	92.1	130
35	1.4687	1444	1363	1.931	966	1411	1.0	3.2	1.769	1081	1399	59	56	0.982	36.7	63.8	71.0	74.3	84.6	86.6	120	76.8	130
36	1.4673	1459	1359	2.801	1442	2112	1.6	3.7	2.366	1446	1954	59	55	2.433	36.3	72.7	81.2	82.0	92.3	95.3	120	86.3	130
37	1.4635	1470	1367	3.961	1745	2629	1.9	4.8	3.188	1696	2413	59	56	3.348	37.7	78.3	87.4	87.1	96.9	99.0	120	93.8	140

Table B-23. Model No. 23: 36 Chute, AR = 2.0, R_r^o = 0.716 Outer Suppressor: A_o/A_i = 1.92, R_r^i = 0.779 Inner Plug, In-Line.

A_o = 21.76 in.^{2}, A_i = 12.39 in.^{2}
No. 9-37 at 1.07 (Dual Flow)

Linear Scale Factor to 338 in.^{2}, No. 1-8 at 1.77 (Outer Only);

Data Point No.	Inner			Outer			Ratios		Mass Averages			Meteorological Conditions		Normalization Parameters		2400-ft S.L. Data							
																50°		90°					
	$(P_T/P_o)_i$	T_{T_i} (° R)	V_i (ft/sec)	$(P_T/P_o)_o$	T_{T_o} (° R)	V_o (ft/sec)	V_o/V_i	$\dot{w}_o/\dot{w}_i$	$(P_T/P_o)_{ms}$	$T_{T_{ms}}$ (° R)	V_{ms} (ft/sec)	T_{Dry} (° F)	T_{Wet} (° F)	10 $\log_{10}$ $(V/a_o)^2$	10 $\log_{10}$ $F_8(T_o/T_{ms})^{n-1}$	OASPL	PNL	OASPL	PNL	FPNL	θ	POASPL	θ
1	0	0	0	2.741	1332	2009			2.746	1332	2009	75	70	2.6	37.9	74.0	84.1	82.3	92.5	95.7	120	86.8	120
2	0	0	0	2.98	1787	2417			2.984	1787	2417	74	70	3.4	37.2	76.1	85.4	85.4	95.4	98.2	120	91.1	140
3	0	0	0	2.482	1192	1816			2.485	1192	1816	76	70	2.1	37.8	71.6	80.8	80.3	90.5	93.5	120	84.0	120
4	0	0	0	3.281	1619	2381			3.285	1619	2381	75	70	3.3	38.3	78.4	88.4	85.8	95.7	98.9	120	92.5	140
5	0	0	0	2.227	1069	1622			2.228	1069	1622	76	70	1.6	37.8	69.2	77.5	78.3	88.5	91.4	110	81.2	120
6	0	0	0	3.572	1783	2576			3.577	1783	2576	76	71	3.6	38.5	79.2	87.6	87.1	96.6	100.2	120	95.7	140
7	0	0	0	1.952	937	1400			1.953	937	1400	76	70	1.0	37.9	66.3	74.2	75.5	85.3	87.9	120	77.7	120
8	0	0	0	2.696	1780	2314			2.699	1780	2314	73	69	3.2	36.5	73.9	81.6	84.0	94.0	97.1	110	88.9	130
9	1.211	901	760	2.699	1329	1993	2.6	4.3	2.242	1249	1762	71	65	2.0	36.5	71.1	80.0	79.3	89.7	92.7	120	83.8	120
10	1.158	984	664	3.003	1788	2425	3.7	4.8	2.456	1633	2119	70	65	2.9	35.7	74.4	83.5	82.5	92.9	96.7	120	88.1	120
11	1.182	888	707	2.7	1784	2321	3.3	4.0	2.285	1607	1996	70	65	2.5	35.1	73.1	81.2	81.8	92.2	95.1	120	86.6	130
12	1.183	896	711	2.633	1185	1798	2.5	4.5	2.069	1132	1600	71	65	1.6	36.7	68.5	76.8	77.6	88.2	90.6	120	81.2	120
13	1.211	901	760	3.28	1622	2383	3.1	4.7	2.652	1497	2101	69	65	2.7	36.8	76.0	86.3	83.0	93.2	96.6	120	88.4	120
14	1.241	921	825	3.559	1766	2558	3.2	4.6	2.835	1612	2245	70	65	3.0	37.0	76.7	85.8	84.5	94.4	97.7	120	91.1	140
15	1.58	893	1167	1.94	928	1387	1.2	2.3	1.816	917	1314	70	64	0.7	37.5	65.3	73.7	72.9	83.1	85.6	120	75.4	120
16	2.253	840	1497	2.721	1329	2000	1.3	1.7	2.586	1145	1810	72	65	2.1	38.3	72.4	80.6	80.3	90.7	93.2	120	86.8	140
17	1.641	985	1158	2.69	1787	2317	1.9	2.2	2.291	1508	1963	66	64	2.5	36.0	73.4	81.2	82.1	92.2	95.3	120	86.6	120
18	2.842	898	1412	2.437	1189	1796	1.3	1.9	2.295	1089	1664	71	65	1.7	37.8	70.9	79.4	78.4	89.0	91.0	120	83.3	140
19	2.325	981	1523	3.255	1620	2375	1.6	1.9	2.883	1373	2082	72	61	2.7	38.2	76.9	86.5	83.6	93.8	97.0	120	91.2	140
20	2.407	903	1552	3.566	1762	2559	1.6	1.9	3.094	1469	2216	72	66	3.0	38.4	77.9	86.8	85.2	95.1	98.1	120	93.8	150
21	1.872	956	1845	1.766	836	1227	1.2	1.4	1.792	719	1152	76	66	0.1	38.0	61.9	69.8	70.3	80.7	82.3	110	72.3	120
22	1.683	937	1846	2.058	990	1490	1.4	1.5	1.965	820	1315	76	66	0.7	38.4	66.1	74.4	74.0	84.3	86.1	120	76.2	120
23	1.787	971	1814	2.783	1346	1992	1.9	1.7	2.256	1076	1639	78	67	1.7	38.0	70.9	79.2	79.5	89.8	92.6	120	83.8	120
24	1.54	976	1180	1.738	825	1204	1.0	2.4	1.669	876	1197	74	71	0.3	37.3	62.4	70.7	70.6	80.4	82.8	120	72.8	140
25	1.589	1887	1226	2.469	1381	1814	1.5	2.7	2.162	1148	1654	74	70	1.7	37.1	70.0	78.3	78.0	88.3	90.9	120	81.7	130
26	1.582	996	1221	3.256	1626	2379	1.9	3.0	2.678	1468	2089	76	69	2.7	37.2	76.0	85.8	83.1	93.0	96.5	120	89.1	140
27	1.579	1134	1293	2.236	1070	1627	1.3	2.8	2.010	1087	1529	74	66	1.4	37.1	67.6	75.5	76.2	86.6	89.3	120	79.9	140
28	1.521	1215	1277	2.648	1285	1943	1.5	3.3	2.268	1269	1788	77	67	2.0	36.7	70.9	79.1	79.1	89.1	92.4	120	83.6	130
29	1.575	1226	1342	3.572	1794	2584	1.9	3.5	2.908	1669	2310	76	68	3.2	37.2	77.0	85.7	84.7	94.4	98.3	120	91.2	140
30	2.981	841	1527	2.973	1763	2398	1.6	1.5	2.726	1394	2049	74	65	2.6	37.8	76.6	86.0	83.4	92.7	96.5	120	90..	140
31	2.981	845	1650	2.659	1734	2270	1.4	1.1	2.688	1318	1989	73	64	2.5	38.0	77.0	86.3	83.0	93.8	95.6	120	90.9	150
32	2.581	849	1534	2.343	1712	2221	1.4	1.2	2.339	1320	1835	72	64	2.2	36.9	74.0	83.0	80.9	91.9	93.5	110	87.1	140
33	2.887	850	1558	1.99	1687	1965	1.4	1.3	1.965	1280	1646	69	63	1.7	36.1	69.9	78.0	78.3	89.2	91.0	110	81.8	140
34	3.087	840	1631	2.112	1645	1961	1.2	0.9	2.376	1225	1799	70	63	2.1	37.4	75.6	85.2	81.0	92.2	93.2	110	88.3	140
35	1.486	1456	1369	1.934	932	1387	1.0	3.2	1.769	1057	1383	77	67	0.9	36.9	65.7	73.8	73.0	83.0	85.9	120	76.8	140
36	1.487	1455	1373	2.836	1683	2098	1.5	3.8	2.402	1424	1947	77	67	2.4	36.5	72.7	81.7	81.1	91.1	93.9	120	86.6	140
37	1.499	1459	1388	3.869	1744	2511	1.9	4.5	3.118	1693	2390	75	66	3.3	37.6	78.9	88.4	85.8	95.4	98.9	130	94.7	140

Table B-24. Model No. 24: 36 Chute, AR = 2.0, R_r^o = 0.716 Outer Suppressor; A_o/A_i = 1.92, R_r^i = 0.779 Inner Plug, Retracted.

A_o = 23.76 $in.^2$, A_i = 12.39 $in.^2$ Linear Scale Factor to 338 $in.^2$ No. 1-8 at 3.77 (Outer Only); No. 9-37 at 3.07 (Dual Flow)

Data Point No.	Inner			Outer			Ratios		Mass Averages			Meteorological Conditions		Normalization Parameters		2400-ft S.L. Data							
	$(P_T/P_a)_i$	T_{T_i} (° R)	V_i (ft/sec)	$(P_T/P_a)_o$	T_{T_o} (° R)	V_o (ft/sec)	T_o/T_i	V_o/V_i	$(P_T/P_a)_{ma}$	$T_{T_{ma}}$ (° R)	V_{ma} (ft/sec)	T_{Dry} (° F)	T_{Wet} (° F)	10 $\log_{10}$ (V/a_o)	10 $\log_{10}$ $F_a(T_o/T_{ma})^{n-1}$	50° OASPL	50° PNL	90° OASPL	90° PNL	PPNL	θ	POASPL	θ
1			0	2.679	1332	1989			2.683	1332	1989	61	59	2.5	37.8	75.4	85.9	83.4	93.8	96.9	120	89.0	140
2			0	2.958	1751	2385			2.962	1751	2385	63	61	3.3	37.2	77.4	87.0	86.8	96.8	99.5	120	93.7	140
3			0	2.43	1200	1802			2.433	1200	18[illegible]	60	59	2.1	37.6	72.4	81.1	81.7	92.1	94.9	110	85.6	140
4			0	3.261	1630	2384			3.265	1630	23[illegible]	62	60	3.3	38.3	79.0	88.7	87.0	97.0	100.5	140	95.4	140
5			0	2.185	1084	161[illegible]			2.188	1084	1617	62	60	1.6	37.6	70.0	78.1	79.0	89.4	92.7	120	82.5	120
6			0	3.738	1749	2588			3.745	1749	2588	62	60	3.7	38.9	80.3	88.2	89.0	98.3	103.8	140	99.9	140
7			0	1.943	946	1402			1.944	946	1402	62	60	1.0	37.8	67.8	75.8	76.4	86.3	89.3	120	79.2	120
8			0	2.681	1747	2287			2.686	1747	2287	63	61	3.1	36.5	75.8	84.3	85.4	95.6	98.9	120	91.3	140
9	1.168	912	691	2.732	1323	1999	2.9	4.9	2.273	1254	1799	79	73	2.0	36.5	71.0	80.4	79.2	89.6	92.7	140	86.3	140
10	1.25	936	663	2.962	1712	2359	3.4	0.5	2.437	1584	2078	73	71	2.7	35.8	74.0	83.5	82.6	93.0	96.9	140	90.3	140
11	1.147	911	648	2.681	1753	2291	3.4	4.5	2.664	1600	1992	74	72	2.5	35.0	72.6	81.1	81.4	91.9	95.4	140	88.5	140
12	1.184	924	681	2.398	1206	1784	2.6	4.7	2.031	1152	1595	80	73	1.6	36.4	68.6	77.2	77.2	87.7	90.8	120	82.5	140
13	1.182	922	675	3.371	1625	2383	3.5	5.5	2.664	1512	2116	79	74	2.8	36.7	75.2	85.9	82.8	92.9	97.1	140	91.5	140
14	1.182	918	717	3.739	1736	2578	3.6	5.6	3.004	1613	2299	73	71	3.1	37.3	77.2	86.2	84.9	94.5	97.6	140	92.5	140
15	1.604	907	1173	1.941	930	1389	1.2	2.3	1.824	923	1323	81	74	0.7	37.6	63.8	71.8	72.8	82.9	85.1	120	78.1	140
16	2.239	900	1652	2.715	1345	2011	1.3	1.8	2.533	1187	1827	80	74	2.1	37.9	72.0	80.2	80.3	90.2	94.8	140	89.9	140
17	1.698	902	1234	2.677	1737	2278	1.8	2.1	2.301	1667	1940	77	73	2.4	36.2	72.8	80.6	81.7	92.1	95.0	140	89.1	140
18	2.069	894	1520	2.436	1203	1804	1.3	1.9	2.301	1094	1670	80	74	1.8	37.8	69.2	77.0	78.1	88.3	92.2	140	86.7	140
19	2.431	900	1558	3.286	1634	2393	1.5	1.8	2.934	1375	2098	78	73	2.7	38.3	76.1	85.9	83.7	93.5	99.3	140	95.2	140
20	2.41	907	1556	3.748	1749	2590	1.7	2.0	2.217	1473	2251	72	70	3.0	38.7	78.6	87.6	85.8	95.2	101.9	140	97.7	140
21	1.79	552	1009	1.77	839	1232	1.2	1.5	1.767	723	1142	74	72	0.1	37.9	61.7	69.6	70.7	80.8	82.4	120	74.4	140
22	1.799	555	1015	2.056	990	1489	1.5	1.6	1.962	822	1306	74	72	0.6	38.3	65.8	74.5	74.2	84.4	86.6	120	78.3	140
23	1.783	582	1032	2.698	1526	1990	1.9	1.9	2.318	1065	1653	73	71	1.7	38.1	71.0	79.6	79.8	90.3	93.3	140	86.7	140
24	1.564	983	1175	1.721	825	1194	1.0	2.3	1.659	873	1188	81	75	0.2	37.3	61.2	68.7	70.1	80.0	81.8	120	75.1	140
25	1.558	997	1194	2.443	1208	1812	1.5	2.7	2.138	1151	1645	81	75	1.6	37.0	69.2	77.4	77.7	88.1	90.8	120	84.5	140
26	1.564	1000	1201	3.284	1629	2389	2.0	3.1	2.692	1476	2099	82	75	2.7	37.2	75.6	85.9	83.2	93.2	97.5	140	92.0	140
27	1.528	1213	1292	2.208	1076	1620	1.3	3.0	1.974	1111	1537	85	77	1.3	36.9	66.8	74.6	75.7	86.3	88.1	110	81.9	140
28	1.533	1218	1300	2.619	1297	1946	1.5	3.2	2.262	1278	1791	83	75	2.0	36.0	70.7	79.1	79.0	89.0	92.1	120	86.3	140
29	1.532	1223	1301	3.759	1742	2587	2.0	3.9	3.035	1636	2325	82	74	3.2	37.6	77.2	85.6	85.0	95.4	100.3	140	95.9	140
30	2.488	854	1534	3.177	1744	2446	1.6	1.6	2.856	1406	2099	82	75	2.7	38.1	76.3	86.0	83.8	93.4	98.9	140	94.6	140
31	3.819	846	1660	2.703	1730	2283	1.4	1.1	2.729	1317	1992	75	73	2.5	38.1	76.5	85.7	83.1	93.4	98.1	140	94.2	140
32	2.512	850	1537	2.321	1731	2122	1.4	1.2	2.326	1327	1856	82	74	2.2	36.8	72.2	80.6	80.0	90.1	93.8	140	89.6	140
33	2.081	848	1354	2.017	1630	1896	1.4	1.3	1.977	1294	1663	81	73	1.7	36.1	68.4	76.2	77.8	88.4	90.3	120	84.5	140
34	3.007	856	1646	2.123	1655	1973	1.2	0.9	2.383	1241	1814	75	73	2.1	37.3	75.7	85.1	81.2	92.1	95.7	140	91.8	140
35	1.5	1456	1388	1.95	929	1392	1.0	3.1	1.783	1055	1391	81	74	0.9	36.9	63.6	70.7	73.3	83.1	86.0	140	81.0	140
36	1.497	1461	1387	2.853	1418	2194	1.5	3.7	2.392	1427	1952	81	74	2.4	36.4	72.2	80.7	81.0	91.0	95.2	140	89.9	140
37	1.499	1463	1389	4.031	1750	2548	1.9	4.7	2.235	1700	2428	81	74	3.4	37.8	78.2	85.8	86.1	95.2	103.6	140	99.0	140

Table B-25. Model No. 25: 36 Chute, AR = 2.0, R_r^o = 0.716 Outer Suppressor; A_o/A_i = 3.61, R_r^i = 0.89 Inner Plug, In-Line.

A_o = 73.16 in.^{2}, A_i = 6.58 in.^{2} Linear Scale Factor to 338 in.^{2} = 3.38

Data Point No.	Inner			Outer			Ratios		Mass Averages			Meteorological Conditions		Normalization Parameters	2400-ft S.L. Data							
	$(P_T/P_o)_i$	T_{T_i} (° R)	V_i (ft/sec)	$(P_T/P_o)_o$	T_{T_o} (° R)	V_o (ft/sec)	V_o/V_i	W_o/W_i	$(P_T/P_o)_m$	T_{T_m} (° R)	V_m (ft/sec)	T_{DRY} (° F)	T_{WET} (° F)	$10 \log_{10}(V/a_o)$ $10 \log_{10} F_R(T_o/T_m)^{n-1}$	50° OASPL	50° PNL	90° OASPL	90° PNL	PPNL	θ	POASPL	θ
9	1.72	897	1244	2.498	1330	1994	1.1	4.5	2.479	1251	1857	68	63	2.2 37.5	72.2	80.8	80.7	91.0	93.3	110	85.1	140
10	1.569	899	1095	3.046	1709	2382	2.2	5.2	2.699	1579	2176	72	66	2.9 37.0	75.2	84.6	83.6	93.7	96.7	120	89.4	140
11	1.636	907	1196	2.742	1759	2318	1.9	4.2	2.477	1595	2102	72	66	2.8 36.4	73.7	81.6	82.4	92.8	95.9	120	87.6	130
12	1.678	903	1222	2.427	1187	1791	1.5	4.4	2.262	1135	1686	69	64	1.8 37.5	70.0	78.1	78.3	88.6	91.3	120	81.7	120
13	1.708	901	1240	3.284	1614	2378	1.9	4.9	2.925	1495	2188	68	64	2.9 37.9	76.2	85.7	84.7	94.4	97.0	120	90.2	140
14	1.752	915	1276	3.55	1756	2549	2.0	5.1	3.136	1615	2339	71	65	3.2 38.1	77.3	86.0	85.3	95.2	98.9	120	92.6	140
15	2.409	897	1576	1.94	934	1392	0.9	2.7	2.068	924	1442	68	63	1.1 38.2	67.8	76.5	74.9	85.5	87.1	110	78.9	140
16	3.331	900	1771	2.725	1335	2006	1.1	2.3	2.846	1204	1936	69	64	2.4 38.7	74.4	83.6	81.8	92.2	94.0	110	89.5	140
17	2.855	898	1658	2.679	1747	2286	1.4	2.4	2.653	1494	2099	70	65	2.7 37.3	75.7	84.0	82.7	93.1	96.2	120	88.9	140
18	3.121	898	1732	2.436	1187	1794	1.0	2.4	2.59	1101	1776	69	64	2.0 38.5	73.1	82.2	79.8	90.5	91.9	120	86.1	140
19	3.416	898	1922	3.262	1608	2368	1.3	2.3	3.282	1394	2204	69	64	2.9 39.1	79.3	89.1	85.4	95.6	97.9	120	94.4	140
20	3.89	889	1854	3.798	1742	2590	1.4	2.4	3.697	1490	2372	86	77	3.3 39.7	82.2	90.4	87.3	97.0	101.9	140	98.0	140
21	1.767	551	997	1.76	848	1234	1.2	2.8	1.755	770	1172	69	66	0.2 37.9	63.4	71.8	71.6	81.8	82.8	120	72.6	120
22	1.751	563	1000	2.048	964	1465	1.5	3.2	1.966	867	1352	75	69	0.8 38.3	66.0	74.0	74.5	84.9	86.3	120	76.3	120
23	1.674	598	997	2.675	1338	1992	2.0	3.8	2.614	1182	1781	74	68	2.0 37.7	70.9	78.8	80.4	90.9	93.1	120	84.1	120
24	1.542	1055	1186	1.732	815	1193	1.0	4.5	1.689	850	1192	83	75	0.3 37.5	61.6	69.7	70.2	80.3	82.0	120	71.8	120
25	1.556	997	1193	2.452	1184	1798	1.5	5.3	2.261	1154	1700	83	75	1.8 37.4	69.0	76.7	78.0	88.4	91.0	120	81.5	130
26	1.562	1003	1185	3.245	1631	2380	2.0	5.8	2.876	1540	2206	81	73	3.0 37.6	75.5	84.9	83.9	93.9	96.7	120	90.0	140
27	1.526	1222	1295	2.238	1063	1622	1.3	5.8	2.083	1087	1573	79	70	1.5 37.3	67.1	75.1	76.6	86.8	88.9	120	78.9	120
28	1.529	1227	1301	2.66	1289	1943	1.5	6.1	2.607	1286	1852	79	72	2.2 37.1	71.3	79.8	79.9	90.2	92.7	120	84.2	140
29	1.538	1230	1302	3.743	1747	2587	2.0	7.4	3.295	1685	2433	77	70	3.4 38.1	78.1	86.8	86.1	95.7	99.0	120	94.7	140
30	2.505	843	1530	3.034	1699	2371	1.5	2.9	2.857	1681	2157	69	65	2.9 37.9	76.1	85.4	84.0	94.1	96.9	120	90.6	140
31	2.997	843	1652	2.875	1699	2321	1.4	2.3	2.833	1441	2120	73	67	2.9 38.0	78.5	84.2	83.3	93.5	95.7	120	90.5	140
32	2.5	847	1534	2.371	1723	2161	1.4	2.3	2.354	1456	1956	75	69	2.4 36.5	73.0	81.2	81.5	92.1	93.9	110	85.9	140
33	2.056	857	1363	2.033	1602	1889	1.4	2.5	2.003	1392	1761	80	72	1.9 35.6	69.3	77.3	78.6	89.6	91 7	110	81.5	120
34	2.988	853	1659	2.122	1619	1950	1.2	1.8	2.279	1363	1845	81	73	2.2 36.6	72.7	81.6	86.3	91.2	92.6	110	85.6	140
35	1.526	1427	1601	1.937	932	1389	1.0	5.6	1.841	1006	1391	84	76	1.0 37.3	65.0	73.5	73.6	83.9	86.4	120	75.8	120
36	1.486	1456	1372	2.856	1405	2095	1.5	7.0	2.56	1411	2006	84	76	2.5 37.1	73.6	83.0	81.4	91.5	95.1	120	86.4	140
37	1.484	1460	1383	4.037	1781	2658	1.9	8.8	3.547	1731	2530	85	76	3.6 38.5	80.8	90.0	86.3	96.4	100.5	130	96.2	140

Table B-26. Model No. 26: 36 Chute, AR = 2.0, R_r^o = 0.716 Outer Suppressor; A_o/A_i = 3.61, R_r^i = 0.89 Inner Plug, Retracted.

A_o = 23.76, in.^{2} A_i = 6.58 in.^{2} Linear Scale Factor to 138 in.^{2} = 3.38

Data Point No.	Inner			Outer			Ratios		Mean Averages			Meteorological Conditions		Normalization Parameters		2400-ft S.L. Data							
																50°		90°					
	$(P_T/P_a)_i$	T_{T_i} (° R)	V_i (ft/sec)	$(P_T/P_a)_o$	T_{T_o} (° R)	V_o (ft/sec)	V_o/V_i	W_o/W_i	$(P_T/P_a)_{mx}$	$T_{T_{mx}}$ (° R)	V_{mx} (ft/sec)	T_{Dry} (° F)	T_{Wet} (° F)	10 $\log_{10}$ $(V/a_o)^2$	10 $\log_{10}$ $F_s(T_o/T_{mx})^{w-1}$	OASPL	PNL	OASPL	PNL	PPNL	θ	POASPL	θ
9	1.676	904	1221	2.72	1343	2010	1.6	4.6	2.485	1265	1870	68	66	2.2	37.4	71.4	79.4	80.4	90.7	93.3	120	84.5	120
10	1.542	902	1121	3.005	1751	2399	2.1	5.0	2.667	1608	2185	68	67	2.9	36.9	76.9	83.6	83.8	94.0	97.2	120	89.1	130
11	1.613	904	1178	2.689	1745	2288	1.9	4.1	2.469	1583	2075	67	65	2.7	36.3	73.4	81.1	82.4	92.6	95.7	120	87.4	130
12	1.63	920	1187	2.603	1255	1863	1.5	4.5	2.231	1157	1690	67	65	1.8	37.3	69.7	77.9	78.5	89.1	91.3	120	81.9	120
13	1.698	922	1241	3.243	1636	2384	1.9	5.0	2.89	1514	2192	67	65	2.9	37.8	75.8	85.4	83.9	94.0	97.6	120	89.5	130
14	1.798	909	1299	3.732	1751	2588	2.0	5.2	3.29	1615	2378	70	68	3.3	38.4	77.2	85.5	85.7	95.3	99.3	120	93.1	140
15	2.496	895	1573	1.948	930	1393	0.9	2.7	2.078	921	1442	67	65	1.1	38.2	67.8	77.1	74.7	85.1	87.4	120	78.1	140
16	2.352	897	1776	2.701	1314	1982	1.1	2.3	2.835	1188	1920	67	65	2.4	38.7	74.5	83.4	81.5	91.7	93.4	120	87.9	140
17	2.294	899	1658	2.705	1749	2297	1.4	2.4	2.671	1498	2108	68	66	2.8	37.3	74.6	82.8	83.1	93.3	96.0	120	89.4	140
18	3.14	896	1732	2.435	1191	1796	1.0	2.3	2.591	1102	1777	68	66	2.0	38.5	72.8	81.9	79.5	90.0	92.0	120	85.6	140
19	4.042	894	1836	3.283	1632	2391	1.3	2.3	3.316	1404	2220	75	72	3.0	39.2	79.2	88.8	85.0	95.0	97.8	120	93.6	140
20	3.925	901	1872	3.73	1750	2587	1.4	2.4	3.675	1496	2373	79	74	3.3	39.7	81.1	89.5	87.0	96.4	101.3	140	97.2	140
21	1.792	561	1552	1.778	840	1237	-1.2	2.8	1.771	767	1179	75	72	0.2	37.9	63.2	71.3	71.5	81.7	83.0	120	72.7	120
22	1.792	583	1037	2.045	985	1480	1.4	3.0	1.974	886	1371	75	73	0.9	38.2	65.8	73.6	74.8	85.3	87.0	110	77.0	120
23	1.799	603	1058	2.727	1335	2007	1.9	3.5	2.479	1174	1798	74	72	2.1	38.0	71.5	80.1	80.2	90.6	93.1	120	84.3	140
24	1.551	988	1186	1.77	824	1222	-1.0	4.5	1.723	854	1215	67	65	0.3	37.6	62.9	70.8	71.3	81.3	83.0	120	72.8	120
25	1.548	994	1185	2.429	1200	1801	1.5	5.1	2.239	1166	1700	67	66	1.8	37.3	69.4	77.4	78.6	88.9	91.6	120	82.0	120
26	1.557	1013	1206	3.237	1629	2377	2.0	5.9	2.875	1539	2205	67	65	3.0	37.6	75.9	85.7	83.9	94.1	97.1	120	89.7	120
27	1.52	1216	1297	2.212	1073	1619	1.3	5.7	2.062	1095	1569	67	66	1.5	37.3	68.5	76.5	77.1	87.4	89.6	120	79.7	120
28	1.523	1219	1291	2.666	1300	1961	1.5	6.2	2.43	1289	1867	67	66	2.2	37.1	72.1	80.5	80.3	90.6	81.3	120	84.2	120
29	1.518	1217	1285	3.703	1747	2579	2.0	7.3	3.259	1683	2422	71	69	3.4	38.0	77.6	85.8	86.0	95.6	99.1	120	94.2	140
30	2.518	821	1540	3.145	1743	2435	1.6	3.0	2.94	1520	2211	67	65	3.0	38.0	76.2	85.4	84.3	94.1	97.6	120	91.1	140
31	3.018	850	1663	2.708	1756	2383	1.4	2.1	2.709	1468	2100	66	65	2.7	37.5	75.3	81.5	83.0	93.4	95.8	120	89.5	140
32	2.493	851	1535	2.373	1727	2148	1.4	2.3	1.785	1902	1878	66	65	2.3	33.2	72.3	80.1	81.4	92.0	94.0	120	85.7	140
33	2.098	846	1366	2.816	1628	1994	1.4	2.6	1.987	1412	1745	67	66	1.9	35.5	69.8	78.0	78.9	89.9	92.0	120	82.4	120
34	3.001	845	1655	2.154	1675	2002	1.2	1.8	2.301	1373	1876	66	65	2.3	36.6	72.8	81.5	80.5	91.5	90.8	130	85.3	140
35	1.498	1431	1374	1.926	930	1382	1.0	5.9	1.826	1003	1381	68	67	0.9	37.3	67.7	75.0	75.2	85.1	87.1	120	76.8	120
36	1.494	1456	1381	2.902	1410	2118	1.5	7.2	2.614	1416	2028	68	66	2.6	37.2	73.5	82.3	81.8	92.0	94.9	120	87.0	140
37	1.493	1461	1383	3.997	1741	2634	1.9	8.8	3.511	1713	2508	71	69	3.5	38.4	78.7	86.4	87.1	96.3	100.6	140	96.3	140

Table B-27. Model No. 27: 36 Chute, AR = 1.5, R_r^o = 0.782 Outer Suppressor; A_o/A_i = 1.92, R_r^i = 0.779 Inner Plug, Retracted.

A_o = 13.34 in.^{2}, A_i = 12.39 in.^{2} Linear Scale Factor to 338 in.^{2} No. 9-37 at 3.07 (Dual Flow); No. 38-41 at 3.77 (Outer Only)

Data Point No.	Inner			Outer			Ratios		Mass Averages			Meteorological Conditions		Normalization Parameters		2400-ft S.L. Data							
	$(P_T/P_o)_i$	T_{T_i} (° R)	V_i (ft/sec)	$(P_T/P_o)_o$	T_{T_o} (° R)	V_o (ft/sec)	V_o/V_i	W_o/W_i	$(P_T/P_o)_{mx}$	$T_{T_{mx}}$ (° R)	V_{mx} (ft/sec)	T_{Dry} (° F)	T_{Wet} (° F)	$10\log_{10}(V/a_o)$	$10\log_{10}F_s(T_o/T_{mx})^{n-1}$	50° OASPL	50° PNL	90° OASPL	90° PNL	PPNL	θ	POASPL	θ
9	1.134	898	618	2.657	1344	1991	3.2	5.4	2.233	1274	1777	72	60	2.0	36.2	70	77.2	79.4	88.6	91.8	120	84.7	130
10	1.111	895	611	2.91	1767	2380	3.9	5.1	2.407	1626	2093	66	56	2.7	35.6	73.1	79.6	82.8	92.2	96.4	120	89.8	130
11	1.118	899	605	2.665	1361	2290	3.8	4.9	2.227	1613	2000	67	57	2.5	35.0	71.6	77.9	81.8	91.3	94.2	120	87.2	130
12	1.122	878	585	2.431	1375	1783	3.0	5.6	2.071	1129	1599	71	59	1.6	36.6	68.1	75.6	77.6	87	89.8	120	82	130
13	1.182	919	683	3.254	1627	2380	3.5	5.5	2.661	1519	2120	73	60	2.9	36.7	74.9	84.2	83.3	92.8	95.7	120	90.9	140
14	1.178	889	700	3.69	1751	2574	3.7	5.6	2.958	1621	2291	64	55	3.1	37.2	77.9	86.7	86.1	95.9	99.5	140	95.7	140
15	1.290	926	684	1.974	927	1403	1.6	3.3	1.754	927	1285	69	58	0.6	37.3	62.7	69.2	73.2	82.7	83.4	120	74.8	120
16	1.384	887	972	2.644	1339	1982	2.0	3.1	2.22	1231	1741	74	61	1.9	36.8	70.5	76	80.1	89.2	91.3	120	85	140
17	1.263	884	829	2.706	1747	2296	2.8	3.4	2.232	1552	1964	66	57	2.5	35.5	72.4	79	81.7	91.3	94.6	120	87.3	130
18	1.377	895	970	2.423	1187	1789	1.8	3.2	2.077	1117	1592	70	59	1.5	37.1	69	76.5	78.3	87.6	89.9	120	82.4	140
19	1.485	894	1072	3.185	1637	2395	2.2	3.2	2.669	1460	2080	74	61	2.7	37.3	75	83.8	83.7	92.9	96.6	120	90.7	140
20	1.507	890	1088	3.68	1755	2579	2.4	3.4	2.938	1557	2232	64	55	3.0	37.7	77.8	86.2	86.2	96	99.2	120	94.8	140
21	1.752	554	993	1.747	650	1227	1.2	1.5	1.739	733	1134	72	61	0.1	37.9	62.7	70.2	71.2	80.3	81.1	120	72.5	120
22	1.773	561	1009	2.04	1001	1490	1.5	1.6	1.924	834	1307	72	61	0.6	38.3	65.4	72.7	74.5	83.7	85.3	120	77.3	130
23	1.772	577	1023	2.701	1340	2002	2.0	1.9	2.318	1075	1662	55	50	1.7	38.2	71.5	79.4	80.8	90.3	93.3	120	85.8	130
24	1.362	1001	1221	1.763	818	1214	1.0	2.4	1.695	871	1210	73	61	0.4	37.4	61.7	67.7	71.5	80.2	81.3	120	75.4	140
25	1.345	980	1174	2.42	1186	1789	1.5	2.7	2.124	1133	1626	74	63	1.6	37.2	69.1	75.7	78.4	87.4	90	120	83.5	140
26	1.359	1005	1209	3.307	2611	2381	2.0	3.2	2.716	1468	2101	74	63	2.7	37.4	74.9	83.3	83.7	93.0	96.2	120	90.7	140
27	1.324	1230	1301	2.297	1085	1627	1.3	3.0	1.976	1122	1546	75	63	1.4	36.9	67.6	74	77	85.8	88	120	82.6	140
28	1.314	1234	1293	2.633	1302	1953	1.5	3.4	2.264	1287	1799	72	60	2.1	36.7	70.7	77.5	80.2	89.1	92.2	120	86.5	140
29	1.935	1218	1292	3.731	1756	2581	2.0	3.9	3.02	1647	2329	74	61	3.2	37.6	78.2	86.6	86.1	95.6	99.8	140	96	140
30	2.488	844	1526	3.136	1787	2450	1.6	1.6	2.826	1415	2097	56	50	2.7	38.1	76.7	83.9	85	94.1	98.4	140	95	150
31	2.996	861	1649	2.662	1745	2278	1.4	1.7	2.696	1336	1996	62	53	2.5	38.0	78.3	85.2	84.3	93.4	96.9	150	94.6	150
32	2.677	838	1517	2.396	1745	2166	1.4	1.2	2.357	1341	1877	57	51	2.3	36.9	72.9	79.9	81.9	91	94.4	120	89.9	150
33	2.883	840	1364	2.822	1618	1887	1.4	1.4	1.984	1294	1667	75	62	1.7	36.1	68.6	74	78.3	87.2	90.3	120	83.6	150
34	3.021	852	1445	2.181	1640	1995	1.2	1.0	2.42	1240	1828	74	61	2.1	37.5	80.3	87	83.5	93.2	95	140	91.7	150
35	1.486	1659	1376	1.987	966	1397	1.0	2.2	1.755	1083	1392	62	54	1.0	36.8	64.2	69.1	74.4	83.1	85.3	120	80.7	140
36	1.681	1467	1372	2.833	1399	2082	1.5	3.9	2.39	1406	1936	62	54	2.4	36.5	72.2	78	81.7	90.6	94.2	130	89.1	140
37	1.469	1481	1392	3.959	1764	2645	1.9	4.8	3.196	1715	2428	64	55	3.4	37.7	79.7	87.4	87.6	97.3	102.8	140	99.1	140
38				3.723	1723	2565			3.731	1723	2565	52	48	3.6	38.9	81.2	89	89.1	98.6	104.3	140	100.9	140
39				2.631	1739	2270			2.66	1739	2270	53	49	3.1	36.5	74.5	80.3	84.7	93.8	97.8	120	91.6	140
40				2.718	1327	1998			2.723	1327	1958	55	50	2.5	37.9	73.4	81.7	82.9	92.3	95.4	120	89.5	140
41				2.438	1267	1841			2.443	1347	1841	53	48	2.2	37.4	70.6	77.4	81	90.4	92.9	120	85.6	140

Table B-28. Model No. 28: 36 Spoke, AR = 2.0, R_r^o = 0.716 Outer Suppressor; A_o/A_i = 1.92, R_r^i = 0.779 Inner Plug, Retracted.

A_o = 31.14, (in.)^2, A_i = 12.99 (in.)^2 Linear Scale Factor to 358 (in.)^2 No. 1-8 at 3.77 (Outer Only); No 9-37 at 3.09 (Dual Flow)

Data Point No.	Inner			Outer			Ratios		Mass Averages			Meteorological Conditions		Normalization Parameters		2400-ft S.L. Data							
	$(P_T/P_a)_i$	T_{T_i} (° R)	V_i (ft/sec)	$(P_T/P_a)_o$	T_{T_o} (° R)	V_o (ft/sec)	V_o/V_i	W_o/W_i	$(P_T/P_a)_{ma}$	$T_{T_{ma}}$ (° R)	V_{ma} (ft/sec)	T_{Dry} (° F)	T_{Wet} (° F)	10 log10 (V/a_o)	10 log10 $F_n(T_o/T_{ao})^{n-1}$	50° OASPL	50° PNL	90° OASPL	90° PNL	PPNL	θ	POASPL	θ
1				2.726	1335	2007			2.726	1334	2007	65	63	2.549	37.9	75.2	83.4	82.9	92.5	95.1	130	89.4	140
5				2.983	1748	2390			2.983	1749	2390	67	65	3.302	37.3	77.4	84.8	85.6	94.6	98.8	140	94.6	140
2				2.647	1197	1806			2.647	1197	1806	66	64	2.091	37.7	73.7	82.2	81.4	91.4	93.9	110	85.4	140
4				3.398	1626	2391			3.398	1626	2391	66	64	3.309	38.4	77.9	84.9	86.4	95.2	100	140	96.2	140
5				2.223	1076	1626			2.223	1076	1626	67	65	1.635	37.6	72.1	80.7	79.6	90	92.3	110	82	120
6				3.754	1752	2594			3.754	1752	2594	66	64	3.663	38.9	82.1	89.9	89.1	98.1	105.5	140	101.9	140
7				1.963	938	1407			1.963	938	1407	68	66	1.006	37.9	69.3	77.5	77.1	87.5	89.5	120	79	120
8				2.701	1751	2297			2.701	1751	2297	67	65	3.135	38.6	76.2	83.7	84.7	96	97.7	120	89.8	120
9	1.123	858	1444	2.744	1534	2027	1.4	1.2	2.351	1289	1820	78	70	2.125	36.3	70.7	79.1	79.3	89.4	90.9	120	82.8	130
10	1.893	962	1.89	3.043	1748	2398	1.4	1.6	2.513	1443	2150	76	68	2.847	35.7	73.1	80.4	82.2	91.4	94.7	120	88	130
11	1.882	865	1404	2.702	1543	2358	1.6	1.9	2.281	1637	2042	75	68	2.624	35.0	72.4	80.3	81.3	91.2	94.4	120	86.5	130
12	1.878	902	1480	2.434	1397	1805	1.6	1.9	2.094	1159	1631	76	68	1.647	36.3	68.8	76.6	77.8	88.1	90.1	120	80.8	120
13	1.827	914	1438	3.328	1836	2401	1.8	2.2	2.721	1536	2153	76	68	2.854	36.7	74.1	81.1	83.1	92.2	95.9	120	89.2	130
14	1.145	980	1446	3.715	1748	2400	4.0	4.2	3.015	1647	2327	75	68	3.191	37.2	77.6	86.4	85.7	94.7	99.2	130	93.8	140
15	1.231	903	1.26	1.953	941	1463	1.7	1.4	1.728	932	1273	67	65	.570	37.1	64.2	73	73.5	84.4	86	120	75.2	120
16	1.42	891	1819	3.075	1331	1987	2.0	3.1	2.249	1223	1766	69	66	1.946	36.9	71	79	80	89.8	91.6	120	83.7	130
17	1.274	952	1646	3.716	1773	2317	2.7	3.3	2.283	1571	1977	74	67	2.483	35.4	72.5	79.9	81.6	91.4	94.4	120	86.2	120
18	1.286	925	984	3.415	1556	1853	1.8	3.1	2.069	1132	1599	68	65	1.562	37.0	69.3	77.7	78.4	88.9	90.4	110	81.3	130
19	1.249	926	1584	3.563	1626	2381	2.2	3.2	2.645	1454	2067	69	64	2.037	37.2	74.6	81.9	83.7	92.6	96.8	120	89.1	120
20	1.91	889	1290	3.715	1375	2402	2.4	3.3	2.951	1569	2251	75	68	3.047	37.7	77.9	86.6	85.9	95	99	120	93.1	140
21	1.381	536	990	1.978	653	1349	1.3	1.5	1.767	724	1143	54	50	.103	38.9	63.7	72.8	72.3	83.4	84.4	100	73.4	120
22	1.389	542	999	2.072	1265	1522	1.5	1.4	1.944	825	1310	55	51	.695	38.4	66.6	75.3	75.7	86.3	87.7	110	77.4	120
23	1.399	562	1218	2.73	1352	1905	2.0	1.8	2.334	1058	1655	55	51	1.712	38.3	71.5	79.4	80.2	90	92.6	120	84.3	120
24	1.325	995	1278	1.693	875	1178	1.0	1.3	1.66	877	1178	53	50	.235	37.3	61.6	70.1	70.9	81.7	82.5	100	72.5	120
25	1.55	1014	1250	2.472	1181	1802	1.5	2.0	2.158	1138	1644	54	51	1.683	37.2	69.6	77.8	78.7	88.8	90.4	120	81.9	140
26	1.515	1015	1187	3.236	1634	2391	2.0	3.2	2.682	1486	2104	54	51	2.753	37.2	75.1	82	84.1	92.9	96.8	120	90.2	140
27	1.534	1253	1299	2.192	1105	1672	1.3	2.9	1.963	1134	1547	53	50	1.419	36.8	67.9	76.1	77.2	87.4	89.9	120	80.7	140
28	1.579	1236	1355	2.565	1324	1927	1.5	3.1	2.216	1295	1784	53	50	2.036	37.5	71	78.9	80.3	90.1	92.2	120	85	140
29	1.515	1226	1282	2.722	1370	2000	2.0	3.9	3.003	1659	2332	53	50	3.201	37.5	78.4	87	86.6	95.4	100	120	95.1	140
30	2.45	843	1535	3.157	1751	2445	1.6	1.4	2.838	1402	2092	56	52	2.729	38.1	76.5	82.6	84.7	93.4	96.3	140	93.4	150
31	2.476	853	1457	2.712	1734	2404	1.4	1.2	2.717	1338	2006	56	52	2.543	38.0	77.6	86.3	83.8	93.7	96.1	140	92.7	140
32	2.498	852	1515	2.342	1525	2129	1.4	1.2	2.336	1329	1859	57	52	2.217	36.9	72.8	81	81.3	91	93.4	120	88.4	150
33	2.801	852	1383	2.049	1638	1988	1.4	1.4	1.985	1304	1676	58	53	1.761	36.1	69.8	77.9	78.9	89.2	91.2	120	82.6	140
34	2.992	846	1452	2.214	1415	1948	1.2	.9	2.367	1235	1803	59	54	2.084	37.4	75.8	85	81.5	92.2	93.1	110	89.6	150
35	1.483	1484	1385	1.898	941	1375	.9	1.1	1.745	1072	1377	61	56	0.914	36.8	65.4	73.9	74.7	85.2	87.3	120	78.3	140
36	1.484	1441	1372	2.782	1398	2079	1.5	2.7	2.353	1608	1923	63	57	2.362	36.4	72.2	79.6	81.1	90.1	92.9	120	87.2	140
37	1.486	1480	1385	2.992	1749	2832	1.9	4.8	3.207	1695	2417	67	60	3.356	37.8	79.6	87.5	87.5	96.8	102.4	140	97.8	140

Table B-29. Model No. 29: 36 Spoke, AR = 2.0, R_r^o = 0.716 Outer Suppressor; A_o/A_i = 1.92, R_r^i = 0.779 Inner Plug, In-Line.

A_o = [illegible] sq. ft. A_c = [illegible] sq. ft. Thrust Scale Factor to FAE sq. ft. No. 9-12 at 3.09 (Dual Flow); No. 13-41 at 1.77 (Outer Only)

Data Point No.	Thrust			Nozzle			Ratios		Mass Averages			Meteorological Conditions		Normalization Parameters		2400-ft S.L. Data							
																50°		90°					
																OASPL	PNL	OASPL	PNL	PPNL	θ	POASPL	θ
9	[illegible]	[illegible]	[illegible]	[illegible]	[illegible]	[illegible]	3.7	3.4	2.372	1285	1801	62	61	2.1	36.3	70.7	78.4	79.8	89.8	92	120	83.6	120
10	[illegible]	[illegible]	[illegible]	[illegible]	[illegible]	[illegible]	3.9	3.2	2.31	1438	2138	63	62	2.3	35.8	73.9	80.5	82.6	92.1	95.2	120	88.4	130
11	[illegible]	[illegible]	[illegible]	[illegible]	[illegible]	[illegible]	4.2	3.4	2.376	1632	2212	64	63	2.6	36.8	72	79.2	81.5	91.6	94.5	120	86.6	130
12	[illegible]	[illegible]	[illegible]	[illegible]	[illegible]	[illegible]	3.5	3.9	2.491	1159	1829	62	61	1.6	36.4	68.2	76	77.9	88.4	90.5	120	81.2	120
13	[illegible]	[illegible]	[illegible]	[illegible]	[illegible]	[illegible]	3.3	3.3	2.47	1583	2111	62	61	2.8	36.8	74	80.9	83.3	92.4	96.7	120	90.2	130
14	[illegible]	[illegible]	[illegible]	[illegible]	[illegible]	[illegible]	3.3	3.2	2.999	1831	2310	63	62	3.2	37.3	77.3	86.1	86	95.6	99.2	120	94.1	140
15	[illegible]	[illegible]	[illegible]	[illegible]	[illegible]	[illegible]	3.4	3.2	2.712	914	1251	63	61	0.5	37.2	62.7	70	73.4	84.2	85.5	120	75.2	140
16	[illegible]	[illegible]	[illegible]	[illegible]	[illegible]	[illegible]	3.0	3.0	2.549	1235	1735	62	61	2.0	36.9	71.6	79.3	79.9	89.8	92.1	120	84.4	130
17	[illegible]	[illegible]	[illegible]	[illegible]	[illegible]	[illegible]	3.4	3.2	2.19	1544	1938	65	64	2.4	35.4	72.6	80.2	82	92.1	94.8	120	86.3	120
18	[illegible]	[illegible]	[illegible]	[illegible]	[illegible]	[illegible]	3.5	3.0	2.086	1144	1814	62	60	1.6	37	68.5	76	78	88.3	90.4	120	81.4	120
19	[illegible]	[illegible]	[illegible]	[illegible]	[illegible]	[illegible]	3.5	3.5	2.66	1486	2096	63	62	2.7	37.1	74.3	81.3	83.6	92.7	96.4	120	89.6	130
20	[illegible]	[illegible]	[illegible]	[illegible]	[illegible]	[illegible]	3.7	3.7	3.036	1547	2200	65	64	3.1	38	77.7	87.4	85.9	95.6	98.9	120	92.8	140
21	[illegible]	[illegible]	[illegible]	[illegible]	[illegible]	[illegible]	3.3	3.6	1.884	732	1169	80	70	2.0	38.1	64.3	73.1	72.1	83.2	84.3	100	73.3	120
22	[illegible]	[illegible]	[illegible]	[illegible]	[illegible]	[illegible]	3.1	3.4	1.922	825	1278	79	69	0.6	38.3	66.3	74.9	74.6	85	86.3	110	76.1	120
23	[illegible]	[illegible]	[illegible]	[illegible]	[illegible]	[illegible]	3.9	3.8	2.325	1073	1656	79	69	1.7	38.1	71.1	78.8	79.7	89.9	91.7	120	83.6	130
24	[illegible]	[illegible]	[illegible]	[illegible]	[illegible]	[illegible]	3.0	3.3	1.673	693	1211	71	67	0.4	37.3	63	71.3	71.4	82.3	83.5	120	73.2	120
25	[illegible]	[illegible]	[illegible]	[illegible]	[illegible]	[illegible]	3.5	3.5	2.125	1155	1644	69	66	1.7	37.1	69.8	77.6	78.4	88.6	90.9	120	81.9	120
26	[illegible]	[illegible]	[illegible]	[illegible]	[illegible]	[illegible]	3.8	3.7	2.71	1448	2100	68	65	2.7	37.4	75	82.6	83.4	92.4	96.6	120	89	140
27	[illegible]	[illegible]	[illegible]	[illegible]	[illegible]	[illegible]	3.5	3.6	1.957	1121	1539	67	65	1.4	36.8	67.3	75.1	76.6	86.8	88.9	120	79.6	140
28	[illegible]	[illegible]	[illegible]	[illegible]	[illegible]	[illegible]	3.5	3.3	2.183	1288	1798	66	64	2.1	36.6	71.3	78.8	80.2	89.9	92.1	120	84.5	130
29	[illegible]	[illegible]	[illegible]	[illegible]	[illegible]	[illegible]	3.8	3.9	2.611	1543	2223	66	66	3.2	37.5	78.7	88.5	86.1	95.6	99.4	120	94.4	140
30	[illegible]	[illegible]	[illegible]	[illegible]	[illegible]	[illegible]	3.6	3.6	2.915	1399	2112	63	61	2.8	38.3	76.7	84.5	84.5	93.9	96.9	120	92.6	150
31	[illegible]	[illegible]	[illegible]	[illegible]	[illegible]	[illegible]	3.4	3.1	2.252	1322	1987	63	61	2.5	38.1	77.6	86	83.7	94.1	95.6	120	92	150
32	[illegible]	[illegible]	[illegible]	[illegible]	[illegible]	[illegible]	3.4	3.7	2.332	1329	1858	62	60	2.2	36.9	76.1	83	81.8	92.5	93.9	120	88.4	150
33	[illegible]	[illegible]	[illegible]	[illegible]	[illegible]	[illegible]	3.4	3.3	1.973	1284	1834	63	61	1.7	36.2	69.9	77.7	78.8	89.4	91	110	81.5	120
34	[illegible]	[illegible]	[illegible]	[illegible]	[illegible]	[illegible]	3.3	.9	2.389	1237	1806	63	61	2.1	37.5	75	84.3	81.1	92.3	92.9	100	88.9	150
35	[illegible]	[illegible]	[illegible]	[illegible]	[illegible]	[illegible]	3.8	3.3	1.754	1271	1785	66	64	0.9	36.8	64.5	71.9	74.7	85.2	87.6	120	78.5	140
36	[illegible]	[illegible]	[illegible]	[illegible]	[illegible]	[illegible]	3.5	3.7	2.418	1434	1967	65	64	2.5	36.5	72.4	79.4	81.3	90.6	93.7	120	87.6	140
37	[illegible]	[illegible]	[illegible]	[illegible]	[illegible]	[illegible]	3.9	4.8	2.323	1588	2213	67	65	3.4	37.8	80.5	89.7	87.1	96.9	101.6	140	97	140
38				[illegible]	[illegible]	[illegible]																	

Table B-30. Model No. 30: 20 Shallow Chute, AR = 1.75, R_r^o = 0.717 Outer Suppressor; A_o/A_i = 1.92, R_r^i = 0.779 Inner Plug, Retracted.

A_o = 69.75 sq. ft A_i = 36.39 sq. ft Internal Nozzle Fraction = 0.34 Ref. No. 9-52 at 1.68 (Dual Flow); No. 58-41 at 3.77 (Outer Only)

Data Point No.	Outer			Inner			Ratios		Mass Averages			Meteorological Conditions		Normalization Parameters		2400-ft S.L. Data							
																50°		90°					
																OASPL	PNL	OASPL	PNL	PPNL	θ	POASPL	θ
9	0.4855	857	1046	0.4577	1.2157	1111.5	0.94	0.7	0.2902	1.3835	1180.6	73	40	2.094	38.0	71.7	82	80.4	90.9	93.7	120	84.5	120
10	0.4856	858.2	1046	0.4576	1.2160	1111.8	0.94	0.7	0.2902	1.3840		72	40	2.861	35.5	74.8	84.9	84	94.8	96.7	120	88.3	140
11	0.4859	858.6	1047	0.4566	1.2171	1112.5	0.94	0.7	0.2896	1.3840	2245	73	40	1.622	36.3	72.7	81.4	82.9	93.7	95.9	120	86.8	130
12	0.4859	858.5	1046	0.4566	1.2169	1112.4	0.94	0.7	0.2901	1.3838	2245	72	40	1.622	36.3	69.4	78.5	98.3	88.9	91.7	120	82.2	120
13	0.4856	858.2	1046	0.4576	1.2160	1111.8	0.94	0.7	0.2902	1.3840	2247	71	39	2.921	36.4	75.5	86.7	84.3	95.1	98	120	89.7	130
14	0.4852	858.6	1047	0.4566	1.2171	1112.5	0.94	0.7	0.2900	1.3840	2246	66	36	3.249	37.1	79.1	89.8	86.2	96.6	100	120	92.9	140
15	0.4856	858.2	1046	0.4576	1.2160	1111.8	0.94	0.7	0.2902	1.3840	2246	64	35	2.500	37.1	63.2	70.7	73.2	83.3	84.3	120	75	120
16	0.4853	858.0	1046	0.4574	1.2158	1111.7	0.94	0.7	0.2901	1.3843	2246	64	35	1.936	36.8	71.6	81.3	80.4	90.6	93.5	120	84.7	130
17	0.4849	857.8	1046	0.4566	1.2154	1111.4	0.94	0.7	0.2900	1.3844	2246	64	35	2.454	35.3	73.3	82.1	82.7	93.3	95.8	120	86.5	120
18	0.4847	857.9	1046	0.4566	1.2156	1111.5	0.94	0.7	0.2900	1.3845	2246	64	35	1.539	36.0	69.3	78	78.6	89	91	120	81.9	120
19	0.4850	858.1	1046	0.4576	1.2160	1111.8	0.94	0.7	0.2902	1.3840	2246	64	35	2.672	37.1	76.6	88.2	84.3	94.6	97.4	120	89.3	120
20	0.4853	858.3	1046	0.4576	1.2162	1111.9	0.94	0.7	0.2902	1.3840	2246	64	35	3.053	37.5	78.7	89.4	85.9	96.2	99.8	120	92.1	140
21	0.4852	858.4	1046	0.4576	1.2163	1112.0	0.94	0.7	0.2902	1.3840	2246	65	39	0.815	38.0	62.9	71	71.3	80.8	82.2	120	73.4	120
22	0.4849	858.2	1046	0.4566	1.2159	1111.8	0.94	0.7	0.2902	1.3840	2246	65	39	0.677	38.1	66.2	74.2	75	85	87.1	120	77.8	120
23	0.4846	858.0	1046	0.4566	1.2156	1111.6	0.94	0.7	0.2901	1.3840	2246	65	39	1.779	38.2	72.4	82.7	80.9	91.7	93.7	120	84.6	120
24	0.4852	858.4	1046	0.4576	1.2163	1112.0	0.94	0.7	0.4462	1.3841	2243	72	40	0.853	37.3	61.1	67.3	70.7	80	81.4	100	74.3	140
25	0.4849	858.2	1046	0.4566	1.2159	1111.8	0.94	0.7	0.4455	1.3838	2243	71	40	1.653	37.2	69.4	77.7	78.9	89.3	91.7	120	83.1	130
26	0.4847	858.1	1046	0.4566	1.2158	1111.7	0.94	0.7	0.4454	1.3840	2243	70	39	2.736	37.2	75.9	86.7	84.6	95	98	120	89.9	130
27	0.4847	858.1	1046	0.4566	1.2158	1111.7	0.94	0.7	0.4454	1.3840	2243	71	40	3.380	36.9	68	75.5	77.4	87.7	89.6	120	82.2	140
28	0.4849	858.2	1046	0.4566	1.2159	1111.8	0.94	0.7	0.44	1.3840	2243	72	40	2.036	36.6	73.3	80	80.3	90.5	93.1	120	85.1	140
29	0.4852	858.4	1046	0.4576	1.2163	1112.0	0.94	0.7	0.4459	1.3839	2243	73	41	3.180	37.4	78.5	88.9	86.2	96.1	99.5	120	93	140
30	0.4853	858.5	1046	0.4576	1.2164	1112.1	0.94	0.7	0.4454	1.3838	2243	72	41	2.746	38.1	77.4	87.8	85	95	98	120	92.2	140
31	0.4856	858.6	1046	0.4576	1.2165	1112.2	0.94	0.7	0.4452	1.3842	2242	72	41	2.505	38.0	78.5	86.4	84	93.6	96.3	140	92.9	150
32	0.4852	858.4	1046	0.4576	1.2163	1112.0	0.94	0.7	0.44	1.3840	2243	71	40	2.206	36.9	73.2	81.4	82	92.1	94.7	120	88.8	150
33	0.4852	858.4	1046	0.4576	1.2163	1112.0	0.94	0.7	0.4459	1.3840	2243	70	40	1.780	36.1	69.5	76.9	79.5	89.8	91.5	120	83.7	140
34	0.4853	858.5	1046	0.4576	1.2164	1112.1	0.94	0.7	0.975	1.3838	2246	69	39	3.096	37.4	76.2	85.7	81.7	92	93.9	140	90.1	140
35	0.4851	858.3	1046	0.4576	1.2161	1111.9	0.94	0.7	0.9748	1.3840	2246	72	40	0.938	36.9	64.7	71.5	74.6	84.4	86.1	120	80.4	140
36	0.4849	858.2	1046	0.4576	1.2159	1111.8	0.94	0.7	0.9745	1.3839	2246	74	41	1.471	36.6	71.7	81.9	82	92	95.3	120	84	140
37	0.4848	858.2	1046	0.4576	1.2159	1111.8	0.94	0.7	0.9744	1.3840	2246	73	41	3.557	37.7	79.5	89.5	86.8	96.7	100.4	120	95.4	140
38	"	"	"	"	"	"	"	"	0.9743	1.3840	2246	68	36	3.641	37.0	82.5	92.1	89.3	99.6	102.1	120	96.9	140
39	"	"	"	"	"	"	"	"	0.9742	1.3840	2247	66	36	3.154	36.7	76.1	84.1	86.2	96.8	98.8	120	90.1	120
40	"	"	"	"	"	"	"	"	0.9741	1.3840	2250	65	36	2.524	35.6	74.9	83.9	83.7	94.3	96.5	120	87.5	120
41	"	"	"	"	"	"	"	"	0.9741	1.3840	2250	65	36	2.161	35.7	72.3	82.1	81.8	92.2	94.6	120	85.4	120

Table B-31. Model No. 31: 30 Shallow Chute, AR = 1.75, R_r^o = 0.717 Outer Suppressor; A_o/A_i = 1.92, R_r^i = 0.779 Inner Plug, Retracted.

A_o = 21.76, in.^{2} A_i = 11.39 in.^{2} Linear Scale Factor to 338 in.^{2} No. 1-8 at 3.77 (Outer Only); No.9-37 at 3.08 (Dual Flow)

Data Point No.	Inner			Outer			Ratios		Mass Averages			Meteorological Conditions		Normalization Parameters		2400-ft S.L. Data							
																50°		90°					
	$(P_T/P_o)_i$	T_{T_i} (° R)	V_i (ft/sec)	$(P_T/P_o)_o$	T_{T_o} (° R)	V_o (ft/sec)	V_o/V_i	W_o/W_i	$(P_i/P_o)_{ma}$	$T_{T_{ma}}$ (° R)	V_{ma} (ft/sec)	T_{Dry} (° F)	T_{Wet} (° F)	10 $\log_{10}$ (V/a_o)	10 $\log_{10}$ $F_a(T_o/T_{sm})^{\omega-1}$	CASPL	PNL	OASPL	PNL	PPNL	θ	POASPL	ϕ
1	-	-	-	2.711	1339	2005	-	-	2.711	1339	2005	64	63	2.545	37.8	75.8	85.1	83.2	92.8	95.9	140	91.1	140
2	-	-	-	3.005	1756	2402	-	-	3.005	1756	2402	65	64	3.329	37.3	77.9	85.4	86.2	95.5	101.1	140	97.5	140
3	-	-	-	3.450	1198	1808	-	-	3.450	1198	1808	65	64	2.095	37.7	73.4	81.9	81.2	91	93.6	110	87.2	140
4	-	-	-	3.278	1626	2385	-	-	3.278	1626	2385	65	64	3.298	38.3	79.9	88.4	86.9	96	102.6	140	98.4	140
5	-	-	-	2.232	1070	1626	-	-	2.232	1070	1626	65	64	1.635	37.8	71.1	79.2	79.2	89.2	91.7	120	83.5	140
6	-	-	-	3.785	1752	2600	-	-	3.785	1752	2600	65	64	3.673	39.0	81.3	87.6	89	98.4	107.3	140	103	140
7	-	-	-	1.942	938	1396	-	-	1.942	938	1396	65	64	0.972	37.9	68.1	76.6	75.9	86.2	87.9	110	78.3	120
8	-	-	-	2.702	1752	2298	-	-	2.702	1752	1355	64	63	3.137	36.5	76.1	83.4	85	94.4	97.8	140	94.2	140
9	1.954	914	1695	2.711	1341	2007	5.0	8.7	2.348	1297	1841	79	74	2.175	36.1	71.4	79.9	79.7	89.7	93	120	87.5	140
10	1.913	2066	1413	2.994	1751	2396	7.7	12.6	2.656	1705	2246	70	68	3.037	35.5	75	83.2	83.1	92.5	98.2	140	93.8	140
11	1.912	1645	1328	2.715	1744	2298	6.6	10.5	2.498	1683	2126	69	67	2.860	34.8	73.2	80.6	81.9	91.8	95.7	120	90	140
12	1.848	971	1483	2.44	1215	1817	4.7	8.9	2.139	1185	1670	74	70	1.751	36.1	68.8	76.6	77.8	88.1	90.5	110	83.5	140
13	1.864	934	1456	3.306	1628	2593	5.2	8.5	2.797	1554	2191	70	68	2.931	36.6	75.4	83.9	83.6	93	97.1	120	93.9	140
14	1.8078	1019	1512	3.757	1745	2593	5.1	9.4	3.16	1672	2388	70	68	3.303	37.2	78.6	86.6	85.9	95.6	102.9	140	98.7	140
15	1.2256	665	781	1.976	955	1410	1.9	3.7	1.738	925	1274	69	67	0.575	37.1	64.4	72.3	73.2	83.4	85.1	120	76.3	140
16	1.823	909	903	2.726	1345	2014	2.2	3.6	2.269	1247	1773	68	66	2.009	36.8	72.6	81.4	80.2	90.2	93.4	120	86.8	140
17	1.220	688	798	3.73	1750	2307	3.1	6.0	2.249	1574	1987	68	65	2.505	35.4	73.1	80.3	81.7	91.5	95.6	120	89.2	140
18	1.832	906	936	2.698	1201	1826	2.0	3.5	2.315	1134	1623	68	66	1.626	37.0	70.3	78.5	78.4	88.5	90.7	110	84.1	140
19	1.4658	932	10500	3.284	1431	2530	2.4	3.4	2.651	1465	2077	68	66	2.698	37.1	76.2	85.5	83.5	93	98.5	140	93.1	140
20	1.445	889	10353	3.77	1717	2586	2.5	3.7	2.993	1555	2253	67	65	3.051	37.8	78.8	86.8	86	95.9	101.9	140	96.9	140
21	1.767	914	15008	1.938	851	1265	1.2	1.5	1.77	732	1151	74	71	0.132	38.0	64.3	73.1	71.3	81.2	82.2	120	74.3	140
22	1.783	917	15010	2.051	986	1483	1.2	1.6	1.934	922	1302	74	71	0.670	38.4	67.4	76.1	74.8	84.8	86.7	120	79	140
23	1.802	948	10942	2.739	1348	2015	1.9	1.9	2.353	1076	1675	74	71	1.764	38.2	73.1	82.3	80.2	90.1	93.2	120	87.1	140
24	1.36	914	1163	1.73	858	1201	1.0	2.1	1.672	878	1200	67	65	0.314	37.4	62.2	68.7	71	80.2	81.8	110	77.3	140
25	1.859	987	10980	2.448	1168	1799	1.5	2.7	2.145	1134	1636	69	66	1.662	37.2	69.9	76.5	78.7	88.2	90.8	120	85.3	140
26	1.540	986	11850	3.268	1427	2581	2.0	3.2	2.488	1473	2096	67	65	2.737	37.3	76.5	85	84.1	93.4	99.1	140	93.7	140
27	1.531	1235	1278	3.321	1563	1836	1.2	3.0	1.985	1102	1537	70	68	1.390	37.0	68.4	75.1	77	86.8	89.2	120	83.6	140
28	1.527	1211	1787	2.813	1303	1943	1.5	3.2	2.248	1280	1787	69	67	2.045	36.6	72.3	79.7	80.7	89.7	92.8	140	88.2	140
29	1.533	1722	1801	3.767	1715	2598	2.0	4.0	3.042	1647	2335	69	67	3.205	37.6	79.1	86.5	86.4	96	103.1	140	98	140
30	1.909	845	1552	1.895	1741	2451	1.6	1.6	2.071	1403	2102	68	66	2.749	38.2	77.7	85.9	84.7	93.9	99.8	140	95.4	140
31	1.905	844	1855	2.875	1746	2791	1.4	1.2	2.716	1326	1995	67	65	2.522	38.1	79.6	86.8	84.3	93.6	99.1	140	95.4	140
32	1.92	851	1944	2.958	1721	2752	1.4	1.2	2.38	1330	1878	66	64	2.261	37.0	74.9	83.1	82.2	92	95.4	140	91.4	140
33	1.9078	841	1983	2.85	1678	2684	1.4	1.3	1.984	1283	1660	69	67	1.724	36.2	70.3	77.1	78.8	88.9	91.1	120	85.6	140
34	1.864	852	1672	2.153	1671	1999	1.2	0.9	2.411	1247	1829	68	66	2.146	37.5	77.4	85.3	82.2	92.2	96.7	140	93	140
35	1.1078	1434	1107	1.952	928	1393	1.0	1.2	1.79	1054	1394	70	68	0.966	37.0	65.8	72	74.6	84.1	86.4	120	82.7	140
36	1.934	2439	1484	2.895	1797	2706	1.5	3.8	2.441	1410	1960	71	69	2.445	36.7	74.2	83.2	81.8	91.1	94.7	140	91	140
37	1.905	2434	1886	3.995	1759	2645	1.9	4.7	3.215	1702	2624	72	69	3.369	37.8	80.2	87.4	87.1	96.6	104.3	140	99.8	140

Table B-32. Model No. 32: 40 Shallow Chute, AR = 1.75, R_r^o = 0.717 Outer Suppressor; A_o/A_i = 1.92, R_r^i = 0.779 Inner Plug, Retracted.

a_o = 51.46 sq. in. a_i = 26.80 sq. in. Diameter Scale Factor to 250 sq. ft. = 0.06

Data Point No.	Nozzle			Model			Ratios		Mass Averages			Meteorological Conditions		Normalization Parameters		2400-ft S.L. Data							
																50°		90°					
																OASPL	PNL	OASPL	PNL	PPNL	θ	PCASPL	θ
1	0.1845	4866	4778	0.050	5376	5006	3.0	4.9	2.265	1273	1790	69	66	2.051	30.4	71	78.4	79	88.1	91.4	120	86.4	140
2	0.1838	4823	4737	0.0474	5071	5004	4.2	5.5	2.468	1856	1826	67	65	2.800	35.7	74	80.9	81.9	91	96.1	140	91.2	140
3	0.1820	4817	4685	0.0466	5040	4924	3.9	5.0	2.256	1835	2019	68	65	2.576	35.1	72.7	79.6	80.8	90	93.8	140	88.9	140
4	0.1848	4845	4756	0.0478	5203	4851	3.8	5.1	2.086	1159	1627	69	66	1.637	30.5	69.2	77	77	86.5	88.7	120	83	140
5	0.1840	4823	4736	0.0474	5161	5004	3.8	5.2	2.038	1533	2143	69	66	2.833	36.8	75.3	82.2	83.1	92	97.2	140	92.7	140
6	0.1835	4810	4722	0.0466	5076	4805	3.7	5.2	2.02	1832	2517	68	65	3.173	37.3	78.5	87.3	85.7	95.3	101.5	140	97.2	140
7	0.1	4800	4800	0.0462	4966	4620	3.8	5.3	1.795	932	1512	70	67	0.704	37.5	64.9	72.9	72.6	82.2	83.2	110	77.5	140
8	0.1	4798	4798	0.0458	4966	4966	3.8	5.4	2.4	1213	1797	69	66	2.070	37.5	72.3	79.2	79.8	88.4	91.9	120	87.7	140
9	0.1832	4815	4727	0.0458	5076	4805	3.8	5.3	2.269	1527	1965	68	65	2.458	35.9	73.2	79.7	81.3	90.3	94.4	120	88.9	140
10	0.1826	4806	4720	0.046	5029	4850	3.4	5.3	2.198	1135	1653	70	68	1.705	37.4	70	77	78	87	89.6	120	85.3	140
11	0.1836	4834	4746	0.050	5047	5004	3.6	5.5	2.755	1430	2086	67	65	2.717	37.7	75.7	82.2	83.6	92.1	97.8	140	93.6	140
12	0.1856	4887	4797	0.0466	5042	5003	3.6	5.6	3.072	1524	2253	67	65	3.050	38.2	79.1	86.5	86	95.1	101.3	140	96.2	140
13	0.1849	4868	4780	0.0474	5130	4948	3.5	5.5	1.774	730	1151	78	70	0.135	36.0	62.8	70.8	70.1	79.5	80.4	110	73.2	140
14	0.1846	4857	4771	0.0466	5042	4948	3.6	5.7	1.946	822	1308	78	70	0.690	38.4	66	73.4	73.4	82.7	84.4	170	78	140
15	0.1797	4734	4650	0.046	5046	4850	3.6	5.9	2.319	1078	1664	77	70	1.736	38.1	71.2	78.2	78.9	87.8	90.9	120	85.7	140
16	0.1	4800	4800	0.050	4966	4805	3.6	5.4	1.674	478	1201	73	69	0.319	37.4	62.3	69.7	70.2	79.6	80.7	110	76.6	140
17	0.1849	4874	4787	0.046	5089	4787	3.5	5.8	2.134	1133	1626	74	71	1.635	37.2	69.5	76.4	77.5	86.3	89.1	120	84.1	140
18	0.1847	4867	4779	0.050	5036	4966	3.6	5.8	2.732	1484	2119	72	69	2.764	37.4	75.4	82.2	83.1	91.7	97.6	140	92.9	140
19	0.1832	4827	4739	0.0458	5089	4819	3.4	5.8	1.979	1131	1554	72	68	1.438	36.9	68.3	75.6	76	85.2	87.3	120	83.7	140
20	0.1836	4836	4746	0.0454	5083	4966	3.9	5.9	2.284	1292	1912	72	69	2.105	36.7	71.7	78.5	79.6	88.0	91.8	120	87.9	140
21	0.1827	4810	4720	0.050	5089	4805	3.8	6.0	2.03	1659	2138	71	68	2.213	37.6	79.7	86.8	86	95.4	102.7	140	97.8	140
22	0.1819	4792	4702	0.0466	5046	4966	3.5	6.0	2.871	1413	2109	71	68	2.765	38.2	76.9	83.5	84	92.6	99	140	95	140
23	0.1845	4859	4768	0.0470	5095	4966	3.4	6.2	2.706	1345	2006	70	67	2.547	38.0	78.7	85.6	83.7	92.6	98.7	140	95.1	140
24	0.1828	4814	4724	0.0474	5083	4819	3.4	6.2	2.384	1317	1863	71	70	2.225	37.0	73.7	80.6	80.5	89.4	93.7	140	90.3	140
25	0.1828	4813	4723	0.0458	5046	4805	3.4	6.4	1.984	1096	1666	71	70	1.743	36.2	70.2	77.4	77.7	86.8	89.2	120	84.8	140
26	0.1853	4878	4786	0.0482	5130	4966	3.2	6.9	2.379	1245	1815	76	68	2.213	37.4	77.1	84.6	81.3	90.8	95.4	140	92.1	140
27	0.1	4800	4800	0.0482	4966	4805	3.0	6.3	1.776	1066	1393	71	68	0.986	36.9	65.4	73.7	73.6	82.4	85.9	140	82.9	140
28	0.15	14400	14400	0.0474	5036	4966	3.5	6.8	2.429	1439	1976	72	69	2.480	36.6	73.1	79.4	81.1	89.6	94.1	140	91	140
29	0.1836	4836	4746	0.0458	5046	4966	4.9	6.9	3.213	1715	2433	71	68	3.385	37.8	81.5	88.7	87.1	96.7	104.3	140	99.7	140

Table B-33. Model No. 33: 36 Chute, AR = 2.5, R_r^o = 0.783 Outer Suppressor; A_o/A_i = 0.65, R_r^i = 0.674 Inner Plug, Retracted.

A_o = [illegible] $in.^2$ A_p = [illegible] $in.^2$
A_m = [illegible] at 3.45 (Wet/Dry Ratio)

Linear Scale Factor to 128 $in.^2$, No. 1-35 and No. 44-59 at 3.45 (Dual Flow):

Data Point No.	Corr $(\dot{m}_p/\dot{m}_p)_c$	Corr T_{T_p} (°F)	Corr V_p (ft/sec)	Outer $(\dot{m}_p/\dot{m}_p)_o$	Outer T_{T_o} (°F)	Outer V_{mo} (ft/sec)	Ratios V_p/V_s	Ratios V_o/V_s	Mass Averages $(\dot{m}_p/\dot{m}_p)_{av}$	Mass Averages $T_{T_{av}}$ (°F)	Mass Averages V_{ma} (ft/sec)	Meteorological Conditions T_{DRY} (°F)	Meteorological Conditions T_{WET} (°F)	Normalization Parameters 10 log10 (V/a_o)	Normalization Parameters 10 log10 $F_s(T_o/T_{ma})^{-1}$	2400-ft S.L. Data 50° OASPL	50° PNL	90° OASPL	90° PNL	PWL	θ	POASPL	θ
1	[illegible]	[illegible]	[illegible]	[illegible]	[illegible]	[illegible]	1.0	0.5	1.642	585	985	44	42	0.564	37.3	59.7	66.3	65.5	74.4	75.1	130	69.6	140
2	[illegible]	[illegible]	[illegible]	[illegible]	[illegible]	[illegible]	1.0	0.5	1.781	638	1083	44	42	0.140	38.0	60.7	68.1	67.8	77.7	80	120	71.2	130
3	[illegible]	[illegible]	[illegible]	[illegible]	[illegible]	[illegible]	1.5	0.6	2.878	713	1188	44	42	0.272	38.4	63	72.1	70.1	80.6	83.5	120	73.7	130
4	[illegible]	[illegible]	[illegible]	[illegible]	[illegible]	[illegible]	1.9	0.6	2.118	912	1454	45	42	0.115	38.6	67.9	77.4	75.6	86.6	90.6	120	80	120
5	[illegible]	[illegible]	[illegible]	[illegible]	[illegible]	[illegible]	1.0	0.6	1.642	769	1100	60	51	-0.063	37.4	59	66	66	74.6	77.4	130	72.5	150
6	[illegible]	[illegible]	[illegible]	[illegible]	[illegible]	[illegible]	1.4	0.8	1.685	914	1349	57	49	0.823	37.8	64.5	73.8	71.9	82.8	85.6	120	76.9	140
7	[illegible]	[illegible]	[illegible]	[illegible]	[illegible]	[illegible]	1.9	0.9	2.184	1142	1659	56	48	1.721	37.3	69.5	78.7	77.4	88	92.4	120	82.2	120
8	[illegible]	[illegible]	[illegible]	[illegible]	[illegible]	[illegible]	1.0	0.6	1.669	926	1231	55	48	1.424	37.2	61.4	68.5	68.7	77.6	80.9	130	77.1	140
9	[illegible]	[illegible]	[illegible]	[illegible]	[illegible]	[illegible]	1.2	0.8	1.795	1004	1364	52	48	0.870	37.2	63.7	72.1	71.2	81.3	85	120	78.9	140
10	[illegible]	[illegible]	[illegible]	[illegible]	[illegible]	[illegible]	1.6	1.0	1.935	1195	1512	50	46	1.319	36.9	66.8	76	74.5	85.1	89.3	120	80.0	140
11	[illegible]	[illegible]	[illegible]	[illegible]	[illegible]	[illegible]	1.9	1.1	2.274	1237	1839	49	46	2.168	36.5	71.3	80.3	79.2	89.5	94.1	120	85.2	140
12	[illegible]	[illegible]	[illegible]	[illegible]	[illegible]	[illegible]	1.0	0.9	1.673	1075	1330	48	45	0.763	36.7	63.3	70.3	70.7	79.6	83.3	130	79.9	140
13	[illegible]	[illegible]	[illegible]	[illegible]	[illegible]	[illegible]	1.4	1.1	1.894	1190	1527	47	44	1.361	36.5	66.3	75	73.9	84.4	88.5	120	82.1	140
14	[illegible]	[illegible]	[illegible]	[illegible]	[illegible]	[illegible]	1.5	1.1	2.008	1273	1666	47	44	1.760	36.1	68.5	77.5	76	86.3	90.7	120	83.6	140
15	[illegible]	[illegible]	[illegible]	[illegible]	[illegible]	[illegible]	2.0	1.5	2.407	1554	2045	47	43	2.631	36.1	73	81.9	80.9	91.2	94.7	120	87.7	140
16	[illegible]	[illegible]	[illegible]	[illegible]	[illegible]	[illegible]	1.0	1.1	1.713	1160	1411	45	43	1.020	36.3	64.3	70.8	71.9	80.9	84.9	120	80.2	150
17	[illegible]	[illegible]	[illegible]	[illegible]	[illegible]	[illegible]	1.2	1.3	1.859	1303	1598	45	43	1.560	35.7	67	75.4	74.8	85.3	89.5	120	82.7	150
18	[illegible]	[illegible]	[illegible]	[illegible]	[illegible]	[illegible]	1.5	1.3	2.084	1436	1816	49	43	2.114	35.4	69.4	78.0	77.5	87.7	92.2	120	86.3	140
19	[illegible]	[illegible]	[illegible]	[illegible]	[illegible]	[illegible]	1.7	1.6	2.206	1566	2008	47	41	2.551	35.7	71.6	79.9	79.7	89.9	93.8	120	87.8	140
20	[illegible]	[illegible]	[illegible]	[illegible]	[illegible]	[illegible]	0.8	0.4	1.632	565	962	44	42	-0.739	36.9	59.5	64.8	64.8	72.5	74.1	130	70.1	140
21	[illegible]	[illegible]	[illegible]	[illegible]	[illegible]	[illegible]	0.6	0.6	1.416	898	1010	59	48	-0.432	36.4	59.2	63.4	66.6	71.9	78.8	130	77.1	140
22	[illegible]	[illegible]	[illegible]	[illegible]	[illegible]	[illegible]	0.8	0.7	1.529	896	1109	59	48	-0.028	36.9	59.2	64.1	66.7	73.4	78.8	130	76.7	140
23	[illegible]	[illegible]	[illegible]	[illegible]	[illegible]	[illegible]	0.6	0.7	1.45	988	1094	44	42	-0.087	36.3	62.1	66.4	69.1	75	82.4	130	80.3	140
24	[illegible]	[illegible]	[illegible]	[illegible]	[illegible]	[illegible]	0.6	0.9	1.434	1094	1136	44	42	0.075	36.3	63	67.4	70	76.3	83.7	130	81.6	140
25	[illegible]	[illegible]	[illegible]	[illegible]	[illegible]	[illegible]	0.8	1.0	1.552	1118	1261	44	42	0.529	36.4	63.6	68.9	70.9	78.2	84.7	130	82.5	140
26	[illegible]	[illegible]	[illegible]	[illegible]	[illegible]	[illegible]	1.0	1.0	1.928	1268	1617	44	41	1.611	36.1	67.7	75.4	75.1	84.5	90.4	140	87.6	140
27	[illegible]	[illegible]	[illegible]	[illegible]	[illegible]	[illegible]	0.6	0.8	1.667	1111	1349	50	43	0.822	36.6	65.6	70.9	73	79.6	88.3	140	85.9	140
28	[illegible]	[illegible]	[illegible]	[illegible]	[illegible]	[illegible]	1.0	0.8	2.24	1351	1833	59	48	2.156	36.4	70.9	78.1	78.1	87	95.8	140	92.4	140
29	[illegible]	[illegible]	[illegible]	[illegible]	[illegible]	[illegible]	0.6	0.7	1.876	1177	1528	55	46	1.365	36.5	68.7	74.5	75.8	82.8	93.9	140	90.7	140
30	[illegible]	[illegible]	[illegible]	[illegible]	[illegible]	[illegible]	1.2	0.8	2.927	1589	3258	59	49	3.061	37.6	76.8	84.7	83.8	92.9	102.2	130	98.1	140
31	[illegible]	[illegible]	[illegible]	[illegible]	[illegible]	[illegible]	1.0	0.7	2.609	1648	2050	45	42	2.641	37.2	75.3	82.8	82.1	91	101.2	130	97	140
32	[illegible]	[illegible]	[illegible]	[illegible]	[illegible]	[illegible]	0.6	0.6	2.158	1193	1685	45	42	1.789	37	73.4	80.9	79.8	88.4	100.0	140	95.5	140
33	----	----	----	[illegible]	[illegible]	[illegible]	----	----	2.759	1325	2009	81	71	2.553	38	70.4	80	78.3	89.4	93.6	120	82.4	120
34	----	----	----	[illegible]	[illegible]	[illegible]	----	----	3.044	1487	2217	82	72	2.981	38.2	72.6	82.3	80.5	91.6	95.3	120	84.7	120
35	----	----	----	[illegible]	[illegible]	[illegible]	----	----	2.465	1199	1813	81	71	2.107	37.7	68.1	77.4	76.1	87.4	90.6	120	79.3	120
36	----	----	----	[illegible]	[illegible]	[illegible]	----	----	3.356	1610	2388	84	74	3.304	38.5	73.9	83.1	82.2	93	97.4	120	87	120
60	----	----	----	[illegible]	[illegible]	[illegible]	----	----	2.253	1065	1630	80	67	1.645	37.9	66.1	76	74.2	95.6	88.1	120	76.7	120
41	----	----	----	[illegible]	[illegible]	[illegible]	----	----	3.622	1753	2565	85	75	3.614	38.7	75.4	84.6	83.7	94.6	98.7	120	88.5	120
42	----	----	----	[illegible]	[illegible]	[illegible]	----	----	1.953	945	1406	79	66	1.003	37.8	62.4	81.7	70.3	81.7	83.8	120	72.7	120
43	----	----	----	[illegible]	[illegible]	[illegible]	----	----	3.989	1749	2637	85	75	3.734	39.3	66.5	85.8	74.4	85.8	87.9	120	76.8	120
44	[illegible]	[illegible]	[illegible]	[illegible]	[illegible]	[illegible]	12.0	6.5	2.266	1243	1769	70	60	3.000	34.2	66.4	75.8	74.7	85.8	90.1	120	79	120
45	[illegible]	[illegible]	[illegible]	[illegible]	[illegible]	[illegible]	11.9	6.6	2 437	1393	1946	70	61	?.415	34.1	67.6	76.7	76.2	87.5	91.3	120	80.5	120
46	[illegible]	[illegible]	[illegible]	[illegible]	[illegible]	[illegible]	12.0	5.1	2.0	1106	1546	72	62	1.414	34.5	64	73.8	71.8	83.2	87.3	120	75.9	120
47	[illegible]	[illegible]	[illegible]	[illegible]	[illegible]	[illegible]	13.0	7.0	2.533	1523	2113	62	56	2.771	34.4	69.5	78.7	78.4	89.5	93.4	120	82.8	120
48	[illegible]	[illegible]	[illegible]	[illegible]	[illegible]	[illegible]	6.2	2.8	1.708	948	1271	74	63	0.564	35.5	62.1	72	69.9	81.5	84.8	120	73.1	120
49	[illegible]	[illegible]	[illegible]	[illegible]	[illegible]	[illegible]	9.9	6.1	2.736	1640	2232	62	56	3.010	34.6	71.1	80.2	79.5	90.4	94.4	120	84.5	120
50	[illegible]	[illegible]	[illegible]	[illegible]	[illegible]	[illegible]	5.7	2.9	1.559	845	1106	74	63	-0.063	35.2	58.9	68.3	66.1	77.4	79.9	120	68.9	130
51	[illegible]	[illegible]	[illegible]	[illegible]	[illegible]	[illegible]	11.9	6.8	3.026	1632	2319	60	56	?.338	35.3	73	82.4	81.1	92	95.4	120	87.2	140
52	[illegible]	[illegible]	[illegible]	[illegible]	[illegible]	[illegible]	7.2	3.0	2.005	1755	1584	70	60	1.521	35.1	65.5	74.9	74.2	85.4	89.8	120	78.7	120
53	[illegible]	[illegible]	[illegible]	[illegible]	[illegible]	[illegible]	6.7	3.2	2.136	1297	1747	70	60	1.947	34.7	67.7	77	76.1	87.3	91.3	120	80.7	120
54	[illegible]	[illegible]	[illegible]	[illegible]	[illegible]	[illegible]	6.6	2.9	1.841	1050	1422	71	61	1.053	35.3	63.8	73.5	71.8	83.2	86.7	120	75.4	120
55	[illegible]	[illegible]	[illegible]	[illegible]	[illegible]	[illegible]	7.0	3.2	2.294	1405	1495	64	58	2.299	34.7	69.6	79.1	78.2	89.2	93.4	120	82.9	120
56	[illegible]	[illegible]	[illegible]	[illegible]	[illegible]	[illegible]	10.8	5.4	1.855	996	1392	72	62	0.960	34.8	62.2	72	69.7	81.2	83.7	120	72.3	120
57	[illegible]	[illegible]	[illegible]	[illegible]	[illegible]	[illegible]	5.8	3.0	2.41	1532	2041	62	56	2.621	35.0	70.9	79.8	79.5	90.5	94.8	120	84.9	120
58	[illegible]	[illegible]	[illegible]	[illegible]	[illegible]	[illegible]	11.3	5.5	1.587	890	1218	74	63	0.380	34.6	58.9	68.2	66.5	77.7	79.9	120	68.8	120
59	[illegible]	[illegible]	[illegible]	[illegible]	[illegible]	[illegible]	5.9	3.1	2.593	1534	2105	60	56	0.2757	35.6	72	81	80.4	91.1	96	120	87	120

Table B-34. Model No. 34: 36 Chute, AR = 2.0, R_r^o = 0.783 Outer Suppressor; A_o/A_i = 0.65, R_r^i = 0.674 Inner Plug, Retracted.

A_o = 33.52 sq. ft A_i = 17.31 sq. ft
Wt. 24043 lbs (Outer Only)

Linear Scale Factor to 338 in.² No. 1-35 and No. 49-59 at 3.45 (Dual Flow):

Data Point No.	Inner			Outer			Ratios		Mass Averages			Meteorological Conditions		Normalization Parameters	2400-ft S.L. Data							
															50°		90°					
	$(P_T/P_o)_j$	T_{T_j} (° R)	V_j (ft/sec)	$(P_T/P_o)_o$	T_{T_o} (° R)	V_o (ft/sec)	V_o/V_j	A_o/A_j	$(P_T/P_o)_{ma}$	$T_{T_{ma}}$ (° R)	V_{ma} (ft/sec)	T_{Dry} (° F)	T_{Wet} (° F)	10 log10 $(V/a_o)^2$	10 log10 $F_s(T_o/T_{SM})^{\omega-1}$	OASPL	PNL	OASPL	PNL	PPNL	θ	POASPL	θ
1	1.781	707	983	1.569	709	1001	1.0	0.5	1.689	585	989	55	53	-0.526	37.4	57	64.1	64.8	74.2	75.3	130	71	150
2	1.774	685	984	1.559	691	1238	1.3	0.5	1.772	636	1073	54	52	-0.170	38	60	68.6	67.7	78.6	80.5	120	70.5	130
3	1.774	1465	998	1.956	992	1492	1.5	0.5	1.868	700	1173	54	53	0.219	38.4	62.7	72.4	70.7	82.3	84.8	120	73	120
4	1.793	1378	997	2.233	1388	2011	2.0	0.6	2.083	845	1386	54	53	0.941	38.8	67.2	77.2	75.9	87.5	91.2	120	79.5	120
5	1.863	744	1096	1.963	758	2085	1.9	0.6	1.631	760	1091	74	65	-0.098	37.4	57.6	64.8	65.4	74.9	76.9	130	71.4	140
6	1.863	771	1096	2.279	1084	1666	1.5	0.8	1.884	913	1348	73	65	0.819	37.8	63.9	73.9	72.3	84.3	86.4	120	74.6	140
7	1.863	778	1096	3.035	1473	2200	2.0	0.9	2.153	1102	1616	74	65	1.607	37.5	68.3	78	76.7	88.1	91.7	120	80.5	120
8	1.862	986	1340	1.75	858	1221	1.0	0.8	1.637	919	1204	77	66	0.331	37.2	59.3	67	67.2	77	79.4	130	74.1	140
9	1.862	980	1340	2.052	1000	1494	1.3	0.9	1.757	995	1334	76	66	0.775	37.1	61.7	70.5	70.1	81.1	84.1	120	75.5	140
10	1.862	984	1340	2.446	1169	1805	1.5	1.0	1.923	1090	1496	75	66	1.272	37	65	74.4	74.1	86	88.4	120	77.6	140
11	1.879	1001	1787	3.353	1436	2407	2.0	1.1	2.273	1333	1836	74	65	2.162	36.5	70.1	79.6	78.7	90.2	93.1	120	82.3	120
12	1.911	1781	1956	1.682	982	1336	1.0	0.9	1.658	1075	1320	73	63	0.728	36.6	61.2	68.8	69.7	79.5	82.6	120	77	140
13	1.936	1788	1929	2.295	1074	1630	1.2	1.0	1.814	1151	1473	73	64	1.206	36.4	64.4	73.6	73	84.7	87.7	120	78.9	140
14	1.936	1779	1927	3.013	1319	1930	1.5	1.1	1.987	1272	1654	72	63	1.707	36.0	66.7	75.9	75.6	87.2	90.3	120	80.3	140
15	1.945	1747	1927	3.697	1750	2566	1.9	1.3	2.403	1533	2030	71	62	2.597	36.2	71.2	79.9	79.9	90.8	94.1	110	85.3	140
17	1.568	1495	2452	2.331	1231	1787	1.1	1.2	1.834	1354	1613	68	61	1.600	35.3	65.7	74.7	74.8	86.5	88.7	120	80.7	140
18	1.602	1499	2450	2.92	1412	2125	1.5	1.3	2.082	1469	1821	68	61	2.126	35.4	68.4	77.7	76.9	88	91.6	120	83.1	140
19	1.611	1575	2432	3.428	1628	2424	1.7	1.5	2.308	1586	2023	68	61	2.583	35.7	70.7	79.7	79.4	90.4	93.4	120	86.2	140
20	1.601	1697	2430	4.653	1790	2766	2.0	1.8	2.807	1687	2289	71	62	3.120	36.8	73.9	83.1	82.4	92.5	95.7	120	89.3	140
21	1.785	521	983	1.366	636	825	0.8	0.4	1.632	559	936	56	54	-0.762	36.9	56.3	61.8	63.7	71.3	73.5	150	71	150
22	1.562	1004	1206	1.063	754	745	0.6	0.5	1.447	910	1047	56	54	-0.278	36.5	58.5	62.7	66.9	72.8	77.4	130	76	150
23	1.563	1599	1826	1.495	892	950	0.8	0.7	1.52	863	1081	57	55	-0.138	36.9	58.1	63.8	66.7	74.5	77	120	74.6	140
24	1.518	1780	1740	1.279	698	755	0.6	0.6	1.42	1023	1083	55	53	-0.131	36.3	60	64.3	68.5	74.6	80.2	140	78.4	140
25	1.581	1542	1740	1.427	675	886	0.6	0.9	1.453	1092	1154	55	53	0.146	36.4	61.9	66.6	70.5	77.3	82.6	140	80.6	140
26	1.649	1478	1898	1.656	773	1418	0.8	1.0	1.544	1120	1255	55	53	0.510	36.4	62.5	68.8	70.7	78.8	83.1	130	79.7	140
27	1.798	1547	1855	4.53	1786	2764	1.7	1.8	2.924	1693	2332	73	64	0.320	37.1	74.7	83.5	82.8	92.7	95.1	130	93.1	140
28	1.747	1436	1600	2.179	1130	1634	1.0	0.9	1.913	1279	1616	64	60	1.609	36	66.4	74.6	74.8	85.3	88.6	120	84.5	140
29	1.695	1429	1742	4.581	1700	2692	1.5	1.3	3.08	1583	2298	73	64	3.138	37.9	74.8	83.5	82.8	92.7	97.6	140	94.6	140
31	1.658	1456	1802	2.471	1194	1819	1.0	0.9	2.215	1324	1810	69	61	2.100	36.4	69.6	77.8	78.2	88.9	94.1	140	90.5	140
32	1.626	1418	1721	1.621	779	1087	0.6	0.7	1.839	1159	1494	64	60	1.265	36.6	68.1	74.1	75.8	84	93.4	140	89.9	140
33	2.422	1917	2028	3.457	1760	2516	1.2	0.9	2.841	1620	2253	66	60	3.052	37.3	74.1	82.3	82.6	92.6	99.6	140	96.2	140
34	2.424	1514	2028	2.763	1326	2017	1.0	0.8	2.569	1431	2023	64	60	2.584	37.1	72.9	81.7	80.7	90.6	98	140	94.4	140
35	2.44	1554	2034	1.74	843	1218	0.6	0.6	2.139	1257	1721	64	60	1.882	36.6	72.4	79.9	79.9	88.9	99.3	140	95.1	140
36	---	---	---	2.736	1327	2009	---	---	2.756	1327	2009	63	61	2.553	38	69.8	80.1	79.3	91.2	94.9	120	83.2	120
37	---	---	---	3.044	1469	2203	---	---	3.044	1469	2203	64	60	2.954	38.2	70.9	80.8	80.9	92.9	96.3	120	84.9	120
38	---	---	---	2.457	1192	1806	---	---	2.457	1192	1806	60	58	2.091	37.7	68.5	78.9	78.4	90.7	92.7	120	82.7	120
39	---	---	---	3.328	1619	2392	---	---	3.328	1619	2392	75	67	3.311	38.4	72.9	82.9	83	93.7	97.4	120	86.6	120
40	---	---	---	2.22	1072	1622	---	---	2.22	1012	1622	59	57	1.624	37.8	66.2	76.6	75.4	97.5	90.1	120	77.9	120
41	---	---	---	1.603	1754	2561	---	---	1.603	1754	2561	76	68	3.607	38.6	94.7	84.6	83.4	94.7	98.2	120	87.9	120
42	---	---	---	1.854	935	1399	---	---	1.954	935	1399	57	55	0.982	37.9	62.7	72.6	72.1	84	86.4	120	21.8	120
43	---	---	---	1.949	1749	2632	---	---	1.949	1749	2632	77	68	3.726	39.3	75.4	85.5	84.1	95.4	99.1	120	88.9	120
44	1.612	649	184	2.759	1330	2013	12.1	5.3	2.201	1229	1730	71	66	1.904	34.3	66.2	76.5	74.8	86.7	90.6	120	79.0	120
45	1.614	736	190	3.084	1472	2205	11.6	5.6	2.375	1360	1897	74	69	2.305	34.3	67.3	77.2	76.5	88.3	91.9	120	80.6	120
46	1.622	679	158	2.465	1198	1805	11.4	5.0	1.979	1105	1535	66	64	1.386	34.5	64.6	75.2	73.5	86	88.1	120	75.9	120
47	1.619	847	236	3.308	1620	2388	10.1	5.4	2.505	1497	2047	80	72	2.634	34.4	69.5	79.7	78.1	89.8	92.9	120	82.1	120
48	1.604	602	96	2.708	1070	1615	16.8	8.9	1.92	1017	1442	65	63	1.114	34.4	61.7	72	71.1	83.5	85.8	120	73.8	120
49	1.636	941	891	3.623	1725	2546	8.5	4.9	2.639	1592	2163	80	71	2.674	34.8	71.5	81.8	79.4	90.9	94.1	110	83.4	120
50	1.613	579	162	1.954	932	1397	8.6	4.2	1.625	864	1160	67	64	-1.66	34.8	59.5	69.4	67.6	79.3	82.1	120	70.5	120
51	1.637	945	241	4.024	1723	2625	7.7	4.8	2.843	1589	2232	79	70	3.009	35.5	72.6	83	80	91.4	94.8	120	84.6	120
52	1.639	619	203	2.742	1331	2009	7.1	2.6	1.988	1148	1570	69	66	1.483	35.1	66.2	76.5	74.9	86.8	90.3	120	78.8	120
53	1.644	648	156	3.021	1476	2202	7.0	2.9	2.121	1263	1717	72	67	1.871	34.9	67.3	77.2	76.4	88.3	91.9	120	80.7	120
54	1.634	658	274	2.451	1195	1806	6.6	3.1	1.84	1063	1430	65	63	1.078	35.2	64.2	74.7	73.8	86.4	88	120	76.1	120
55	1.657	705	364	3.306	1618	2386	6.6	2.8	2.252	1380	1859	78	71	2.215	34.8	69.5	79.7	77.9	89.6	93.1	120	82.2	120
56	1.628	566	232	2.234	1073	1620	7.0	3.1	1.712	946	1272	71	69	0.569	35.3	61.9	72.1	71	83.5	85.9	120	73.6	120
57	1.671	755	439	3.613	1716	2536	6.0	2.8	2.389	1462	1975	78	70	2.479	35.1	70.7	80.9	79.3	90.8	94.3	120	83.8	120
58	1.632	565	268	1.959	939	1605	5.7	2.6	1.55	837	1088	63	58	-0.111	35.3	58.9	68.8	67.4	79.2	82.1	120	70.5	120
59	1.884	768	459	3.96	1728	2617	5.7	2.8	2.556	1476	2051	80	70	2.644	35.7	72.5	82.8	80.1	91.4	94	120	83.8	120

Table B-35. Model No. 35: 36 Spoke, AR = 2.5, R_r^o = 0.783 Outer Suppressor; A_o/A_i = 0.65, R_r^i = 0.674 Inner Plug, Retracted.

A_o = 11.11, in.^{2}, A_i = 17.11 in.^{2}
Ea. No-41 at 5.43^2 (Outer Only)

Linear Scale Factor to 338 in.^{2} No. 1-35 and No. 44-59 at 3.45 (Dual Flow);

Data Point No.	Inner			Outer			Ratios		Mass Averages			Meteorological Conditions		Normalization Parameters		2400-ft S.L. Data							
	$(P_T/P_0)_i$	T_{T_i} (° R)	V_i (ft/sec)	$(P_T/P_0)_o$	T_{T_o} (° R)	V_o (ft/sec)	V_o/V_i	W_o/W_i	$(P_T/P_0)_{ms}$	$T_{T_{ms}}$ (° R)	V_{ms} (ft/sec)	T_{Dry} (° F)	T_{Wet} (° F)	$10\log_{10}(V/a_o)^2$	$10\log_{10}F_s(T_o/T_{ms})^{\omega-1}$	50° OASPL	50° PNL	90° OASPL	90° PNL	PPNL	θ	POASPL	θ
1	1.884	573	1021	1.553	704	1000	1.0	0.5	1.74	579	1009	54	47	-0.438	37.6	59.0	66.0	64.9	73.4	76.0	120	69.3	140
2	1.832	575	993	1.799	865	1268	1.3	0.5	1.791	638	1085	54	47	-0.124	38.0	61.0	69.4	67.4	77.0	80.3	120	71.1	130
3	1.787	582	987	2.079	991	1500	1.5	0.6	1.872	694	1169	54	47	-0.202	38.4	62.9	71.9	69.7	80.2	83.6	120	73.4	130
4	1.788	544	993	2.756	1331	2013	2.0	0.6	2.082	853	1392	54	47	0.960	38.8	67.2	76.2	74.4	85.0	89.3	120	79.4	120
5	1.832	585	1101	1.617	810	1118	1.0	0.6	1.618	795	1108	63	50	-0.033	37.3	59.4	66.6	6.57	74.3	78.0	130	72.7	140
6	1.844	777	1112	2.263	1120	1678	1.5	0.8	1.882	924	1355	63	50	0.841	37.8	65.0	73.6	71.5	81.6	85.6	120	76.9	130
7	1.682	854	1190	3.001	1485	2205	1.9	0.9	2.184	1149	1664	62	50	1.734	37.3	59.6	67.2	76.3	85.8	90.4	120	82.9	130
8	1.581	1000	1215	1.729	828	1202	1.0	0.8	1.639	924	1209	59	49	0.349	37.2	61.4	68.8	67.9	76.5	80.7	130	76.3	140
9	1.556	985	1188	2.078	1016	1519	1.3	0.9	1.765	999	1342	57	48	0.800	37.1	63.9	72.0	70.6	80.2	84.4	120	78.1	140
10	1.567	1087	1202	2.438	1206	1809	1.5	0.9	1.911	1101	1496	57	49	1.274	36.9	66.2	74.5	73.1	83.0	87.6	120	80.2	140
11	1.604	1103	1235	3.237	1625	2384	1.9	1.0	2.262	1321	1822	55	47	2.130	36.5	71.0	78.7	78.1	87.5	92.4	120	85.3	140
12	1.341	1197	1324	1.658	876	1307	1.0	0.9	1.676	1043	1312	54	47	0.702	36.8	62.7	69.4	69.9	78.5	83.3	130	79.9	140
13	1.582	1205	1319	2.26	1048	1619	1.2	1.0	1.839	1125	1572	54	47	1.201	36.6	64.9	71.8	72.3	81.5	86.5	120	81.4	140
14	1.598	1233	1366	2.692	1291	1962	1.4	1.1	2.04	1263	1676	54	47	1.767	36.2	67.8	74.9	75.3	84.8	90.0	120	84.5	140
15	1.554	1199	1329	3.576	1776	2572	2.0	1.2	2.379	1519	2010	55	47	2.555	36.2	72.6	79.9	79.8	89.1	94.2	130	86.4	150
16	1.545	1486	1430	1.952	972	1426	1.0	1.1	1.697	1214	1433	55	49	1.085	36.0	64.7	71.8	71.8	80.0	86.1	130	83.0	140
17	1.542	1492	1430	2.581	1187	1774	1.2	1.1	1.876	1311	1616	55	49	1.604	35.6	67.3	75.4	74.4	83.7	89.1	120	84.3	140
18	1.51	1419	1381	2.909	1415	2124	1.5	1.3	2.088	1417	1800	55	49	2.077	35.5	69.3	77.3	76.9	86.3	91.2	120	86.2	140
19	1.537	1436	1417	3.587	1664	2442	1.7	1.3	2.303	1567	2008	57	51	2.550	35.7	71.7	79.0	79.3	88.4	93.9	120	88.8	140
22	1.823	522	989	1.358	685	831	0.8	0.4	1.638	566	946	54	47	-0.720	36.9	58.0	63.5	63.8	70.5	73.3	120	68.7	140
23	1.571	1011	1214	1.302	700	783	0.6	0.6	1.466	898	1057	54	48	-0.239	36.6	59.4	63.8	66.2	71.7	78.6	130	76.1	140
24	1.55	1041	1214	1.482	685	936	0.8	0.7	1.517	888	1095	54	48	-0.83	36.9	59.6	65.3	66.4	73.3	79.0	130	75.9	140
25	1.552	1352	1341	1.355	654	809	0.6	0.7	1.467	1001	1118	54	49	0.007	36.6	61.4	66.0	68.3	74.1	81.4	130	79.1	140
26	1.498	1448	1381	1.392	660	847	0.6	0.9	1.438	1084	1134	55	49	0.007	36.4	61.9	66.5	69.0	74.9	82.4	130	79.9	140
27	1.504	1455	1394	1.648	768	1109	0.8	1.0	1.546	1110	1251	54	49	0.495	36.4	62.9	69.0	70.0	77.2	83.7	130	80.7	140
28	1.386	1490	1430	2.209	1140	1669	1.0	1.0	1.924	1320	1649	50	44	1.695	35.8	67.7	74.6	74.9	83.4	90.1	140	87.3	140
29	1.372	1438	1422	1.54	721	1003	0.6	0.8	1.66	1125	1352	65	55	0.832	36.5	66.1	71.4	73.2	79.6	89.0	140	86.2	140
30	2.071	1468	1788	3.824	1833	2670	1.5	1.0	2.786	1624	2237	52	47	3.021	37.1	75.9	82.7	82.6	91.1	100.3	140	96.7	140
31	2.082	1449	1814	2.507	1276	1843	1.0	0.9	2.24	1342	1827	56	50	2.142	36.4	70.8	77.5	78.1	86.3	95.6	140	92.5	140
32	2.083	1446	1832	1.573	758	1052	0.6	0.7	1.856	1182	1519	60	52	1.340	36.5	69.3	75.2	76.4	83.4	95.2	140	91.4	140
33	2.538	1470	2042	3.488	1700	2494	1.2	0.8	2.924	1574	2246	54	48	3.039	37.6	76.9	84.1	83.0	91.2	102.2	140	98.6	140
34	2.503	1484	2037	2.659	1336	1986	1.0	0.7	2.566	1422	2016	54	48	2.567	37.1	74.9	82.1	80.8	89.1	100.1	130	96.3	140
35	2.521	1480	2042	1.752	811	1205	0.6	0.5	2.139	1260	1724	54	48	1.882	36.9	73.7	80.8	79.9	88.1	99.9	140	95.8	140
36	—	—	—	2.73	1337	2009	—	—	2.73	1337	2009	78	67	2.553	37.9	70.1	79.4	77.6	88.4	91.9	120	81.8	140
37	—	—	—	3.022	1482	2207	—	—	3.022	1482	2207	78	67	2.961	38.2	71.8	80.4	79.4	89.9	93.2	120	85.1	140
38	—	—	—	2.462	1197	1812	—	—	2.462	1197	1812	78	67	2.105	37.7	68.3	77.8	75.6	86.4	90.0	120	79.2	120
39	—	—	—	3.281	1630	2389	—	—	3.281	1630	2389	78	67	3.306	38.3	74.1	82.7	81.5	91.7	95.2	120	88.3	140
40	—	—	—	2.235	1071	1627	—	—	2.235	1071	1627	78	67	1.637	37.8	65.9	75.3	73.1	84.4	87.9	120	76.7	120
41	—	—	—	3.624	1766	2556	—	—	3.624	1740	2556	78	67	3.599	38.7	76.1	84.4	83.1	92.6	94.7	120	92.5	140
42	—	—	—	1.986	934	1416	—	—	1.986	934	1414	78	67	1.028	38.0	63.1	72.6	70.0	81.3	83.6	120	72.5	120
43	—	—	—	3.918	1756	2631	—	—	3.918	1756	2631	78	67	3.725	39.2	78.1	86.5	84.5	94.0	99.1	140	95.2	140
44	1.81	716	160	2.753	1341	2020	12.6	6.4	2.226	1253	1758	62	54	1.974	34.2	65.8	75.2	73.9	85.1	88.5	120	77.9	120
45	1.814	724	164	2.014	1470	2198	11.9	5.6	2.369	1357	1893	62	54	2.295	34.3	68.0	77.5	75.9	86.8	91.0	120	80.8	120
46	1.814	712	183	2.448	1194	1811	9.9	5.1	1.979	1114	1542	65	57	1.404	34.5	64.0	74.0	71.5	83.0	85.9	120	75.0	120
47	1.812	825	186	3.3	1625	2390	12.8	6.3	2.603	1518	2098	62	54	2.742	34.4	69.3	77.9	77.6	88.3	91.9	120	82.3	120
48	1.81	418	145	2.217	1070	1619	11.2	5.3	1.836	996	1381	67	58	0.926	34.7	61.9	71.7	69.4	80.9	84.1	120	72.7	120
49	1.822	971	267	3.581	1695	2511	9.4	5.7	2.682	1587	2175	67	58	2.898	34.7	70.8	79.1	78.9	89.0	93.1	120	85.7	140
50	1.812	624	156	1.952	921	1387	8.9	4.6	1.637	869	1171	67	58	0.209	34.8	59.3	69.2	66.2	77.8	80.6	120	69.2	120
51	1.824	968	282	3.931	1740	2621	9.3	5.7	2.901	1627	2277	69	60	3.098	35.2	72.5	80.7	80.3	90.0	94.2	120	88.8	140
52	1.649	668	310	2.737	1332	2007	6.1	2.8	1.955	1154	1557	63	55	1.445	35.2	66.0	75.7	73.7	84.9	88.3	120	77.6	120
53	1.648	690	334	3.01	1478	2202	6.6	2.9	2.115	1276	1723	62	54	1.886	34.8	67.2	76.4	75.7	86.8	89.9	120	79.8	120
54	1.638	693	276	2.378	1197	1780	6.4	2.7	1.777	1037	1375	62	54	0.905	35.3	63.3	72.7	71.2	82.7	86.2	120	75.1	130
55	1.641	771	395	3.308	1612	2382	6.0	2.9	2.249	1394	1867	62	54	2.235	34.8	69.4	78.5	77.5	88.5	92.0	120	82.3	120
56	1.823	592	257	2.232	1080	1633	6.4	2.8	1.707	953	1274	67	58	0.575	35.4	62.4	72.2	69.3	80.8	83.7	120	72.6	120
57	1.674	824	448	3.588	1691	2510	5.6	2.8	2.38	1465	1973	67	58	2.476	35.1	72.2	81.1	78.6	89.0	92.8	120	84.3	130
58	1.836	622	274	1.956	931	1398	5.1	2.6	1.544	846	1090	67	58	-0.105	35.3	59.4	69.0	66.1	77.6	80.1	120	68.7	120
59	1.886	819	479	3.913	1756	2630	5.5	2.8	2.533	1511	2067	70	61	2.676	35.6	71.6	79.8	79.7	89.8	93.7	120	86.8	140

Table B-36. Model No. 36: 36 Chute, AR = 2.0, R_r^o = 0.716 Outer Suppressor; A_o/A_i = 1.92, R_r^i = 0.779 Inner Plug, Retracted with Acoustically Treated Secondary Ejector.

A_o = 21.7π, in.^{2} A_i = 17.39 in.^{2} Linear Scale Factor to 338 in.^{2} No. 9-37 at 3.09 (Dual Flow); No. 38-41 at 3.77 (Outer Only)

Data Point No.	Inner			Outer			Ratios		Mass Averages			Meteorological Conditions		Normalization Parameters		2400-ft S.L. Data							
																50°		90°					
	$(P_T/P_o)_i$	T_{T_i} (° R)	V_i (ft/sec)	$(P_T/P_o)_o$	T_{T_o} (° R)	V_o (ft/sec)	V_o/V_i	w_o/w_i	$(P_T/P_o)_{ma}$	$T_{T_{ma}}$ (° R)	V_{ma} (ft/sec)	T_{Dry} (° F)	T_{Wet} (° F)	$10\log_{10}(V/a_o)$	$10\log_{10}F_s(T_o/T_{SM})^{\omega-1}$	OASPL	PNL	OASPL	PNL	PPNL	θ	POASPL	θ
9	1.104	940	940	2.713	1336	2004	3.6	6.2	2.291	1282	1807	77	65	2.092	36.2	69	75	77.5	86.1	89.1	110	82.7	130
10	1.150	1002	970	2.934	1752	2378	4.2	6.1	2.452	1648	2127	78	66	2.802	35.5	72	77.6	80.9	89.5	92.1	130	87	130
11	1.104	974	571	2.733	1737	2300	4.0	5.8	2.285	1622	2040	76	64	2.619	35.1	70.6	76.5	79.3	88	91.2	110	85.1	130
12	1.050	895	341	2.456	1168	1802	3.3	6.0	2.095	1147	1622	76	65	1.625	36.5	66.3	72.6	74.8	83.4	86.5	120	78.7	130
13	1.127	887	564	3.27	1436	2391	4.3	6.1	2.69	1532	2139	75	64	2.825	36.6	72.8	78.6	81.7	90	93.6	130	88.6	140
14	1.182	986	760	3.727	1747	2584	3.7	6.2	3.013	1638	2320	76	65	3.178	37.2	74.5	80.3	83.4	91.7	96.2	130	91.4	150
15	1.224	898	794	1.905	952	1380	1.7	3.4	1.69	932	1249	68	61	0.489	37.0	62.1	68.5	70	78.7	80.3	120	72.5	120
16	1.408	928	999	2.673	1353	2003	2.0	3.1	2.243	1245	1760	71	63	1.977	36.8	69.1	75.5	77.6	86.6	89	110	81.9	130
17	1.286	934	849	2.659	1747	2278	2.6	3.2	2.195	1546	1942	73	64	2.406	35.4	70.8	76.9	79.6	88.5	91.6	110	84.8	130
18	1.327	895	970	2.434	1206	1800	2.0	3.2	2.055	1133	1593	74	64	1.546	36.9	66.6	73	75.2	84	85.9	110	78.6	120
19	1.460	890	1079	3.205	1641	2603	2.3	3.3	2.665	1466	2083	74	63	2.711	37.2	72.8	78.9	81.6	90.2	93.7	130	88.1	130
20	1.438	891	1026	3.759	1760	2592	2.5	3.6	2.948	1571	2251	75	64	3.048	37.6	74.7	80.6	83.5	91.8	96.3	130	90.8	130
21	1.271	938	937	1.745	871	1241	1.3	1.4	1.741	734	1137	56	51	0.079	37.9	61.5	68.7	68.9	77.2	78	120	70.7	120
22	1.259	942	984	2.025	984	1468	1.5	1.6	1.903	813	1281	51	48	0.598	38.3	64.1	71.4	72.3	81	82.2	110	74.6	120
23	1.264	940	1004	2.679	1344	1998	2.0	1.8	2.292	1065	1644	51	48	1.682	38.2	69.6	77	78.1	87.3	89.2	110	82.3	130
24	1.536	1008	1365	1.729	843	1211	1.0	2.3	1.661	893	1203	51	48	0.327	37.3	60.4	66.3	68.2	75.9	77.5	120	71	140
25	1.545	1000	1367	2.432	1215	1814	1.5	2.7	2.128	1157	1645	51	48	1.686	37.0	67.8	74.6	76.5	85.3	87.4	110	80.3	130
26	1.523	1001	1285	3.231	1656	2392	2.0	3.1	2.636	1496	2095	51	48	2.735	37.1	73.1	79.1	82.8	90.8	94.1	120	88.3	130
27	1.520	1002	1280	2.231	1073	1618	1.3	3.1	1.967	1110	1533	51	49	1.379	37.0	65.6	71.6	74.2	82.6	84.2	110	77.8	130
28	1.513	1012	1237	2.615	1300	1943	1.5	3.2	2.244	1279	1785	50	47	2.039	36.6	69.1	75.2	78	86.6	89.1	110	82.6	130
29	1.529	1237	1298	3.678	1747	2573	2.0	3.9	2.975	1643	2312	51	48	3.163	37.5	75.8	81.5	84.6	93	97.3	120	92.8	140
30	1.484	846	1528	3.159	1747	2442	1.5	1.6	2.839	1403	2092	57	53	2.730	38.1	74.5	81.1	83	91.6	94.6	130	90.9	150
31	2.975	847	1651	2.656	1750	2279	1.4	1.1	2.682	1327	1985	56	53	2.500	38.0	75	83.1	81.9	91.5	92.6	110	91	150
32	2.484	856	1535	2.165	1700	2135	1.4	1.2	2.362	1326	1867	53	50	2.234	37.0	70.9	77.6	79.3	88.0	89.5	110	86.4	150
33	1.978	858	1352	1.976	1623	1864	1.4	1.3	1.946	1294	1645	52	50	1.685	36.1	68.1	74.7	75.9	84.7	87.2	110	80.5	150
34	2.979	851	1656	2.168	1673	2009	1.2	0.9	2.399	1251	1828	53	50	2.142	37.4	75.2	83.5	80.1	90.4	90.4	100	88.4	150
35	1.484	1450	1367	1.905	945	1405	1.0	3.2	1.780	1066	1396	65	58	0.972	36.9	62.4	67.4	71.3	79.7	81.2	120	75.7	140
36	1.485	1453	1370	2.860	1411	2106	1.5	3.8	3.406	1420	1953	65	59	2.429	36.6	70.7	76.8	79.8	88.5	91.4	120	85.1	130
37	1.483	1470	1376	3.945	1758	2638	1.9	4.7	3.173	1708	2417	62	57	3.356	37.7	76.9	82.7	85.5	93.4	99.1	130	96.1	150
38	—	—	—	3.689	1756	2582	—	—	3.689	1756	2582	79	66	3.643	38.8	78.4	85.4	86.9	94.4	99	140	96.5	140
39	—	—	—	2.651	1782	2298	—	—	2.651	1782	2298	79	66	3.137	36.3	73.4	79.1	82.4	90.7	93.3	110	88.2	130
40	—	—	—	2.734	1322	1999	—	—	2.734	1322	1999	78	66	2.531	38.0	71.5	78	80.3	88.7	91.2	110	84.9	130
41	—	—	—	2.427	1207	1806	—	—	2.427	1207	1806	79	66	2.091	37.6	69.7	75.9	78	86.5	89.1	110	82	120

Table B-37. Model No. 37: Coannular-Nonconplanar Dual Plug Nozzle, $R_r^o = 0.853$, $A_o/A_i = 1.59$, $R_r^i = 0.800$ with Acoustically Treated Secondary Ejector.

A_o = 18.03 in.^{2}, A_i = 11.35 in.^{2} Linear Scale Factor to 338 in.^{2} = 3.38

Data Point No.	Inner $(P_T/P_a)_i$	Inner T_{T_i} (° R)	Inner V_i (ft/sec)	Outer $(P_T/P_a)_o$	Outer T_{T_o} (° R)	Outer V_o (ft/sec)	Ratios V_o/V_i	Ratios W_o/W_i	Mass Averages $(P_T/P_o)_{ma}$	Mass Averages $T_{T_{ma}}$ (° R)	Mass Averages V_{ma} (ft/sec)	Meteorological Conditions T_{Dry} (° F)	Meteorological Conditions T_{Wet} (° F)	Normalization Parameters 10 log10 (V/a_o)	Normalization Parameters 10 log10 $F_s(T_o/T_{sm})^{\omega-1}$	2400-ft S.L. Data 50° OASPL	50° PNL	90° OASPL	90° PNL	PPNL	θ	POASPL	θ
17	2.980	841	1438	3.950	1738	2624	1.6	1.5	3.453	1375	2226	64	59	2.999	39.6	85	91.7	89.2	98.2	105.8	140	100.9	140
18	1.350	850	65	2.680	1753	2291	3.5	3.8	2.171	1573	1947	60	57	2.417	34.9	75.1	82.7	82.5	91	97.2	120	92	140
20	1.780	890	865	3.740	1754	2590	3.0	3.8	2.873	1574	2230	60	57	3.007	37.3	85.7	93	89.3	99.4	104	140	99.2	140
21	1.368	545	992	1.762	849	1234	1.2	1.3	1.751	715	1127	69	61	0.044	37.9	69.4	74.1	72.8	79.1	80.3	120	74.5	120
22	1.349	555	1002	2.051	997	1492	1.5	1.4	1.917	811	1286	70	64	0.616	38.3	69.2	74.1	75.6	82.1	85.2	130	80.8	140
24	1.370	569	1015	2.710	1533	2000	2.0	1.6	2.283	1037	1619	68	60	1.615	38.3	74.8	63.6	80.9	90.2	93.7	130	88.5	140
25	1.518	1220	1278	2.300	1[illegible]	1619	1.3	2.6	1.942	1116	1524	66	60	1.353	36.8	72.6	78.9	79.2	85.9	90.6	130	87.6	140
28	1.569	1222	1271	2.590	1295	[illegible]	1.5	2.8	2.188	1276	1757	65	60	1.972	36.5	75.5	84.8	81.7	90.1	95.8	140	90.9	140
29	1.518	1221	1277	3.730	1750	2587	2.0	3.4	2.931	1630	2289	64	59	3.120	37.4	83	90.3	87.9	97.7	104.2	140	99.7	140
30	1.440	841	1525	[illegible]	1748	2440	1.6	1.4	2.806	1366	2054	62	57	2.649	38.2	81.8	88.5	86.5	95.4	102.6	140	97.8	140
31	1.[illegible]	829	1458	2.700	1739	2288	[illegible]	1.0	2.726	1291	1971	63	58	2.470	38.2	81.4	87.8	85.9	94.7	102	140	97.3	140
32	1.440	845	1597	2.390	[illegible]	2145	1.4	1.1	2.366	1291	1845	62	57	2.182	37.1	76.6	83.1	82.9	91	98.2	140	93.7	140
42	1.419	846	1167	2.779	1737	[illegible]	2.0	1.9	2.255	1426	1892	62	57	2.291	36.2	76	84	82.8	91.5	97.6	130	92.2	140

Table B-38. Model No. 38: Coannular-Nonconplanar Dual Plug Nozzle, $R_r^o = 0.926$, $A_o/A_i = 0.71$, $R_r^i = 0.800$ with Acoustically Treated Ejector.

A_o = 8.01 in.^{2}, A_i = 11.35 in.^{2} Linear Scale Factor to 338 in.^{2} = 4.17

Data Point No.	Inner $(P_T/P_a)_i$	Inner T_{T_i} (° R)	Inner V_i (ft/sec)	Outer $(P_T/P_a)_o$	Outer T_{T_o} (° R)	Outer V_o (ft/sec)	Ratios V_o/V_i	Ratios W_o/W_i	Mass Averages $(P_T/P_o)_{ma}$	Mass Averages $T_{T_{ma}}$ (° R)	Mass Averages V_{ma} (ft/sec)	Meteorological Conditions T_{Dry} (° F)	Meteorological Conditions T_{Wet} (° F)	Normalization Parameters 10 log10 (V/a_o)	Normalization Parameters 10 log10 $F_s(T_o/T_{sm})^{\omega-1}$	2400-ft S.L. Data 50° OASPL	50° PNL	90° OASPL	90° PNL	PPNL	θ	POASPL	θ
12	2.982	837	1643	3.969	1756	2641	1.6	0.6	3.266	1195	2032	55	53	2.603	39.9	85	91.4	88.3	96.7	103.5	140	98.8	140
22	1.765	541	987	2.034	1038	1514	1.5	0.6	1.844	725	1182	55	53	0.250	38.3	66.8	71.4	72.9	79	81.8	120	76.9	140
23	1.386	551	997	2.709	1329	1997	2.0	0.7	2.085	870	1407	55	53	1.006	38.7	71.2	77.2	77.7	85.7	89.3	120	83.1	130
27	1.565	1217	1272	2.224	1071	1623	1.3	1.2	1.807	1139	1461	56	54	1.169	36.5	69.5	74.3	76.4	82.3	86.9	130	84.7	140
28	1.535	1213	1271	2.662	1282	1945	1.5	1.3	2.0	1252	1648	55	53	1.691	36.2	72.3	80.7	79.2	86.8	91	130	87.3	140
29	1.504	1220	1274	3.780	1747	2591	2.0	1.5	2.691	1538	2069	56	54	2.681	36.4	77.5	84.5	84.7	93	99.5	130	94.3	140
30	2.741	840	1517	3.167	1753	2449	1.6	0.6	2.672	1188	1872	55	53	2.247	38.5	77.6	84.1	84	92.4	97.9	140	93.8	140
31	2.986	849	1647	2.713	1759	2307	1.4	0.4	2.782	1119	1848	56	54	2.189	39.1	87	93	88	96.4	99.7	140	95.7	140
32	2.478	843	1521	2.359	1721	2134	1.4	0.5	2.364	1121	1715	56	54	1.866	38	76.4	83	81.9	89.6	95	140	91.5	140
42	1.608	856	1143	2.765	1731	2300	1.5	0.9	2.044	1259	1676	55	53	1.765	36.4	72.8	78.6	80 3	88.2	92	130	87.1	140

Table B-39. Model No. 39: Converging Plug, Single-Flow, R_r = 0.789.

A_1 = 11.05 in.^{2} Linear Scale Factor to 338 in.^{2} = 5.51

Data Point No.	Inner			Free Stream	Meteorological Conditions		Normalization Parameters		2400-ft S.L. Data							
									50°		90°					
	$(P_T/P_o)_i$	T_{Ti} (° R)	V_i (ft/sec)	V_{FS} (ft/sec)	T_{Dry} (° F)	T_{Wet} (° F)	10 $\log_{10}$ V/a_o	10 $\log_{10}$ $F_s(T_o/T_{sm})^{\omega-1}$	OASPL	PNL	OASPL	PNL	PPNL	θ	POASPL	θ
A22030	1.710	821	1185	0	42	37	0.026	37.6	67.6	72.0	73.7	79.6	83.3	130	78.8	130
A22040	1.934	934	1388	0	42	37	0.095	37.9	71.9	76.6	77.6	83.6	89.5	140	86.7	140
A22060	2.429	1197	1799	0	42	37	0.208	37.6	79.7	85.3	84.5	91.2	100.5	140	96.7	140
A22070	2.699	1335	1998	0	42	37	0.253	37.8	83.8	89.9	87.5	94.9	104.5	140	100.2	140
A22080	3.000	1487	2206	0	42	36	0.296	38.1	86.1	92.0	89.8	96.6	108.0	140	103.5	140
A22090	3.268	1628	2384	0	33	37	0.330	38.3	89.0	95.0	91.7	99.0	110.2	130	105.0	140
A22100	3.543	1794	2577	0	42	36	0.364	38.4	88.7	94.6	92.6	99.6	111.7	130	106.2	130
A22110	1.947	1542	1800	0	33	37	0.208	34.7	77.5	82.0	82.2	88.2	96.6	140	93.3	140
A22120	2.536	1693	2194	0	33	37	0.294	36.2	83.3	88.2	87.8	94.2	105.9	140	101.4	140
B22030	1.726	821	1194	152	49	39	0.030	37.7	68.2	73.0	71.6	77.4	80.5	120	75.8	140
B22040	1.933	929	1384	153	49	39	0.094	37.9	70.8	76.2	75.1	81.2	85.8	130	81.8	140
B22060	2.445	1194	1803	154	53	41	0.208	37.7	79.1	85.5	82.4	89.7	96.2	140	91.7	140
B22070	2.707	1337	2002	155	53	41	0.254	37.8	83.4	89.9	85.8	93.6	101.1	140	95.8	140
B22080	2.980	1481	2195	157	53	41	0.294	38.1	85.7	92.4	88.3	96.0	104.4	130	98.6	140
B22090	3.259	1634	2386	152	53	41	0.330	38.2	89.2	95.8	91.0	98.8	106.7	130	100.5	140
B22100	3.556	1792	2579	143	53	41	0.364	38.4	88.6	94.8	92.0	99.8	109.2	130	103.2	130
B22110	1.930	1524	1779	153	53	41	0.203	34.7	76.4	81.4	80.5	86.9	93.4	130	88.8	140
B22120	2.528	1682	2183	147	53	41	0.292	36.3	82.7	88.2	86.6	93.8	102.4	140	97.1	140
C22030	1.743	823	1206	288	47	38	0.034	37.7	73.7	78.5	71.5	76.5	78.0	110	71.7	110
C22040	1.944	934	1393	275	47	38	0.097	37.9	72.7	77.4	74.4	81.2	84.1	120	78.6	140
C22060	2.436	1202	1806	282	47	38	0.209	37.6	78.8	86.1	81.3	89.4	93.6	130	88.6	140
C22070	2.708	1338	2003	284	47	38	0.254	37.8	83.3	90.7	85.0	93.8	98.0	130	92.4	140
C22080	2.986	1485	2200	287	47	38	0.294	38.1	85.8	92.9	87.7	96.5	102.6	130	96.2	130
C22090	3.256	1627	2380	286	47	38	0.329	38.3	89.4	96.7	90.7	99.6	105.9	130	99.1	130
C22100	3.534	1790	2572	269	47	38	0.363	38.4	88.5	95.4	91.5	100.2	108.2	130	101.7	130
C22110	1.925	1534	1781	281	42	37	0.203	34.7	79.0	84.1	79.4	86.7	90.5	130	85.3	130
C22120	2.541	1683	2189	288	47	38	0.293	36.3	82.1	88.6	85.7	93.9	100.1	130	94.3	130

Table B-40. Model No. 40: Converging Plug, Single-Flow, R_r = 0.85.

A_1 = 11.05 in.^{2} Linear Scale Factor to 338 in.^{2} = 5.51

Data Point No.	Inner			Free Stream	Meteorological Conditions		Normalization Parameters		2400-ft S.L. Data							
									50°		90°					
	$(P_t/P_o)_i$	T_{t_i} (° R)	V_i (ft/sec)	V_{FS} (ft/sec)	T_{Dry} (° F)	T_{Wet} (° F)	10 $\log_{10}$ V/a_o	10 $\log_{10}$ $F_s(T_o/T_{sm})^{\omega-1}$	OASPL	PNL	OASPL	PNL	PPNL	θ	POASPL	θ
A21030	1.742	814	1198	0	70	56	0.031	37.7	66.7	71.5	71.8	77.3	81.0	130	77.9	140
A21040	1.952	927	1392	0	70	56	0.096	37.9	70.5	75.1	75.9	81.4	86.9	140	83.9	140
A21050	2.273	1084	1652	0	70	56	0.171	37.8	76.3	82.1	81.1	87.7	95.0	140	91.6	140
A21060	2.462	1196	1810	0	70	56	0.210	37.7	81.5	87.9	85.4	92.3	99.8	140	96.0	140
A21070	2.762	1335	2018	0	70	56	0.257	38.0	81.2	87.2	85.9	92.4	103.3	140	99.0	140
A21080	3.037	1473	2204	0	70	56	0.296	38.2	83.7	89.5	88.3	94.9	106.6	140	102.1	140
A21090	3.305	1618	2386	0	70	56	0.330	38.4	86.7	93.0	90.5	97.8	108.6	130	103.8	140
A21100	3.595	1789	2585	0	70	56	0.365	38.5	89.0	95.6	92.8	100.4	111.6	130	105.8	130
A21110	1.973	1538	1814	0	70	56	0.211	34.8	75.6	80.4	81.2	87.1	94.7	140	91.5	140
A21120	2.585	1678	2203	0	70	56	0.296	36.4	82.0	87.9	87.0	93.3	105.0	140	100.2	140
A21150	2.436	991	1636	0	70	56	0.166	38.7	80.9	87.6	83.6	90.8	96.6	140	92.9	140
A21160	2.076	1245	1683	0	70	56	0.178	36.5	74.6	79.2	80.3	86.1	93.6	140	90.4	140
A21170	1.772	1492	1650	0	70	56	0.170	34.6	72.9	77.8	79.3	85.2	90.9	130	87.4	140
A21190	1.624	1789	1646	0	70	56	0.169	33.2	72.6	77.2	78.8	84.5	89.8	130	86.3	140
A21210	4.077	1090	2081	0	70	56	0.271	41.7	90.8	97.1	92.3	99.4	108.9	140	104.4	140
A21220	3.337	1236	2084	0	70	56	0.271	39.7	87.5	94.0	89.5	96.7	106.4	140	102.0	140
A21230	2.638	1490	2093	0	70	56	0.273	37.1	82.0	87.8	86.3	92.7	104.0	140	99.8	140
A21240	2.253	1741	2095	0	70	56	0.274	35.2	80.1	85.8	85.8	92.7	101.9	140	97.4	140
B21030	1.744	813	1199	147	70	56	0.031	37.8	67.4	72.6	70.7	76.8	77.9	120	72.3	120
B21040	1.972	902	1382	147	70	56	0.093	38.1	70.8	75.9	74.6	80.3	84.8	130	80.5	140
B21050	2.271	986	1574	146	70	56	0.149	38.4	76.3	82.9	79.9	87.2	91.5	130	87.1	140
B21060	2.466	1084	1723	150	70	56	0.189	38.3	82.0	88.9	84.3	91.7	95.7	130	91.2	140
B21070	2.758	1330	2013	150	70	56	0.256	38.0	82.0	88.5	85.2	92.1	100.4	140	95.2	140
B21080	3.024	1466	2196	149	70	56	0.294	38.2	84.5	90.6	87.5	94.6	103.4	140	98.1	140
B21090	3.300	1614	2382	145	70	56	0.327	38.4	87.9	94.4	89.8	97.4	106.2	130	100.4	140
B21100	3.596	1781	2580	143	70	56	0.364	38.5	90.1	96.8	92.0	99.7	108.8	130	102.6	130
B21110	1.964	1524	1800	149	70	56	0.208	34.8	75.9	80.8	79.9	86.1	92.6	130	88.0	140
B21120	2.573	1672	2194	149	70	56	0.294	36.4	82.2	87.8	85.8	92.3	101.6	140	96.5	140
C21030	1.723	829	1199	283	45	38	0.031	37.7	72.4	77.2	69.7	74.0	77.4	70	72.4	50
C21040	1.943	939	1397	279	45	38	0.098	37.9	75.6	81.2	74.9	81.5	83.2	120	77.2	140
C21050	2.235	1093	1644	286	45	38	0.169	37.7	80.0	86.6	79.7	87.7	90.3	130	84.3	140
C21060	2.429	1202	1803	289	45	38	0.209	37.6	80.7	88.2	83.7	92.1	94.5	130	88.3	130
C21070	2.730	1325	2000	284	45	38	0.253	37.9	81.7	90.0	84.6	93.6	97.5	130	92.3	140
C21080	3.001	1479	2200	278	45	38	0.295	38.1	83.9	91.4	87.1	95.8	101.2	130	95.1	130
C21090	3.246	1639	2387	280	45	38	0.330	38.2	88.5	95.8	89.9	98.7	104.8	130	98.4	130
C21100	3.589	1776	2575	286	45	38	0.363	38.5	90.1	97.2	92.0	100.7	107.4	130	101.1	130
C21110	1.945	1548	1802	273	38	31	0.208	34.7	78.4	83.6	78.7	86.3	90.7	120	84.7	130
C21120	2.541	1687	2192	267	38	31	0.293	36.3	81.4	88.1	85.2	93.3	99.2	130	93.4	130
C21150	2.413	994	1630	266	45	38	0.165	38.7	83.4	92.1	84.7	93.0	94.0	130	87.3	130

Table B-40. Model No. 40: Converging Plug, Single-Flow, R_r = 0.85 (Concluded).

A_i = 11.12 in.^{2} Linear Scale Factor to 338 in.^{2} = 5.50

Data Point No.	Inner			Free Stream	Meteorological Conditions		Normalization Parameters		2400-ft S.L. Data							
	$(P_T/P_o)_i$	T_{T_i} (°R)	V_i (ft/sec)	V_{FS} (ft/sec)	T_{Dry} (° F)	T_{Wet} (° F)	10 $\log_{10}$ V/a_o	10 $\log_{10}$ $F_s(T_o/T_{sm})^{\omega-1}$	50° OASPL	50° PNL	90° OASPL	90° PNL	PPNL	θ	POASPL	θ
C21160	1.966	1254	1631	272	45	38	0.165	36.1	77.7	81.7	77.1	84.4	87.8	120	82.3	130
C21170	1.755	1504	1645	277	38	31	0.169	34.5	77.1	81.5	77.3	84.4	87.4	120	80.8	120
C21190	1.607	1782	1655	275	38	31	0.171	32.9	76.7	81.2	77.1	83.8	86.9	120	80.5	120
C21210	4.057	1110	2098	271	38	31	0.274	41.6	92.8	99.5	93.6	101.9	105.6	140	100.3	140
C21220	3.304	1250	2089	271	38	31	0.272	39.6	89.2	96.7	89.2	98.1	101.6	130	95.8	140
C21230	2.608	1512	2097	271	38	31	0.274	37.0	81.4	88.9	85.0	93.4	98.7	130	93.4	140
C21240	2.231	1759	2075	278	38	31	0.274	35.1	80.4	87.5	84.2	92.1	97.5	130	91.1	130

Table B-41. Model No. 41: 36 Chute, AR = 2.5, R_r = 0.78 Turbojet.

A_i = 11.12 in.^{2} Linear Scale Factor to 338 in.^{2} = 5.50

Data Point No.	Inner			Free Stream	Meteorological Conditions		Normalization Parameters		2400-ft S.L. Data							
	$(P_T/P_o)_i$	T_{T_i} (°R)	V_i (ft/sec)	V_{FS} (ft/sec)	T_{Dry} (° F)	T_{Wet} (° F)	10 $\log_{10}$ V/a_o	10 $\log_{10}$ $F_s(T_o/T_{sm})^{\omega-1}$	50° OASPL	50° PNL	90° OASPL	90° PNL	PPNL	θ	POASPL	θ
A23030	1.735	816	1196	0	74	58	0.030	37.7	62.4	69.9	70.5	79.3	82.2	110	73.1	110
A23040	1.957	939	1404	0	74	58	0.100	37.9	65.6	73.6	73.5	82.8	86.0	120	76.8	120
A23060	2.452	1188	1800	0	74	58	0.208	37.7	70.9	79.3	78.4	87.9	92.5	120	82.7	120
A23070	2.731	1333	2007	0	74	58	0.255	37.9	73.4	82.0	80.9	90.5	94.9	120	85.3	120
A23090	3.264	1614	2372	0	73	58	0.328	38.3	76.8	85.9	84.5	93.7	98.4	120	89.4	120
A23100	3.573	1791	2582	0	73	58	0.364	38.5	78.2	85.9	86.1	95.1	99.5	120	91.7	140
A23110	1.951	1534	1798	0	74	58	0.207	34.7	69.1	77.2	77.5	87.0	91.7	120	82.0	120
A23120	2.547	1689	2195	0	74	58	0.294	36.3	73.9	82.1	81.3	90.8	96.0	120	86.3	120
B23030	1.727	816	1191	148	67	59	0.029	37.7	63.3	70.2	68.4	77.7	80.4	120	70.9	120
B23040	1.945	936	1396	157	67	59	0.097	37.9	68.1	75.9	71.9	81.3	84.8	120	74.9	120
B23060	2.454	1196	1807	155	67	59	0.209	37.7	72.6	81.6	77.4	87.4	92.1	120	81.6	120
B23070	2.716	1333	2001	153	67	59	0.254	37.9	74.4	83.8	79.3	89.2	94.2	120	84.0	120
B23090	3.268	1632	2387	156	74	59	0.330	38.3	78.0	87.7	83.2	93.0	98.0	120	86.0	120
B23100	3.566	1783	2574	159	74	59	0.363	38.5	79.7	89.4	84.4	94.0	99.1	120	89.4	120
B23110	1.955	1583	1802	159	67	59	0.208	34.7	71.2	79.5	76.3	86.0	90.7	120	80.5	120
B23120	2.549	1686	2194	156	74	59	0.294	36.3	75.1	83.8	80.1	90.1	95.2	120	84.9	120
C23030	1.708	823	1185	267	46	38	0.026	37.6	68.5	75.5	72.3	82.0	82.1	100	72.5	130
C23040	1.936	942	1396	270	46	38	0.097	37.8	77.6	81.2	79.5	86.2	87.2	110	80.4	110
C23060	2.432	1204	1806	271	46	38	0.209	37.6	75.5	83.4	78.6	90.3	92.5	120	81.8	130
C23070	2.699	1344	2004	272	46	38	0.254	37.8	75.1	84.0	80.6	92.4	95.2	130	84.6	130
C23090	3.246	1631	2380	274	40	38	0.329	38.2	77.5	87.8	84.0	95.4	98.6	130	87.8	130
C23100	3.535	1798	2578	276	40	38	0.363	38.4	79.9	90.0	85.8	97.3	100.8	120	90.3	120
C23110	1.937	1540	1793	274	38	31	0.206	34.7	76.1	82.7	77.5	88.8	91.4	120	80.5	120
C23120	2.531	1701	2197	274	40	38	0.294	36.2	75.6	84.0	81.5	93.1	95.8	120	84.6	120

Table B-42. Model No. 42: 36 Chute, AR = 2.5, R_r^o = 0.78 Outer Suppressor with Induced Flow Through A_o/A_i = 0.65, R_r^i = 0.674 Inner Plug, Retracted.

A_o = 11.12, in.^{2} A_i = 17.21 in.^{2} Linear Scale Factor to 338 in.^{2} = 5.50 (Outer Only)

Data Point No.	Outer			Free Stream	Meteorological Conditions		Normalization Parameters		2400-ft S.L. Data							
									50°		90°					
	$(P_T/P_o)_o$	T_{T_o} (° R)	V_o (ft/sec)	V_{FS} (ft/sec)	T_{Dry} (° F)	T_{Wet} (° F)	10 $\log_{10}$ V/a_o	10 $\log_{10}$ $F_s(T_o/T_{sm})^{\omega-1}$	OASPL	PNL	OASPL	PNL	PPNL	θ	POASPL	θ
A24030	1.723	817	1190	0	77	61	0.028	37.7	61.7	69.3	70.3	79.0	81.8	120	72.9	120
A24040	1.948	928	1391	0	77	61	0.096	37.9	63.1	73.0	73.5	82.7	86.1	120	76.7	120
A24060	2.447	1180	1793	0	77	61	0.206	37.7	70.4	79.1	78.7	88.2	92.7	120	82.8	120
A24070	2.715	1300	1976	0	77	61	0.248	38.0	72.4	81.3	80.4	90.0	95.1	120	85.2	120
A24090	3.253	1614	2370	0	75	61	0.327	38.3	76.0	85.7	83.9	93.3	98.7	120	89.2	120
A24100	3.549	1774	2564	0	75	61	0.361	38.5	77.8	87.4	85.7	95.1	99.8	120	90.8	120
A24110	1.940	1527	1787	0	75	61	0.205	34.7	68.8	77.3	77.2	86.7	91.5	120	81.6	120
A24120	2.533	1673	2179	0	75	61	0.291	36.3	73.3	81.8	81.3	91.0	95.9	120	86.1	120
B24030	1.714	818	1186	154	69	60	0.026	37.6	63.6	70.8	68.7	78.3	80.6	120	71.0	120
B24040	1.943	928	1389	153	69	60	0.095	37.9	66.0	76.2	72.1	81.9	85.2	120	75.2	120
B24060	2.453	1185	1799	151	68	60	0.207	37.7	72.2	81.7	77.7	88.0	92.3	120	81.8	120
B24070	2.714	1330	1999	151	68	60	0.253	37.9	73.7	83.4	79.5	89.7	94.8	120	84.4	120
B24090	3.265	1616	2374	154	68	60	0.328	38.3	77.5	87.4	83.2	93.2	98.6	120	88.5	120
B24100	3.561	1793	2580	151	66	59	0.364	38.4	79.1	89.1	84.9	94.6	99.7	120	89.8	120
B24110	1.940	1523	1784	151	68	60	0.204	34.8	70.7	79.3	76.3	86.2	91.2	120	80.9	120
B24120	2.544	1679	2187	153	68	60	0.292	36.3	74.8	83.8	80.5	90.7	95.9	120	85.4	120
C24030	1.714	827	1192	269	36	30	0.029	37.6	68.7	75.9	72.9	82.8	82.9	100	73.4	120
C24040	1.930	944	1394	270	36	30	0.097	37.8	72.0	79.3	76.1	86.5	86.8	120	76.4	130
C24060	2.427	1203	1803	272	36	30	0.208	37.6	76.2	84.2	79.8	91.6	93.3	120	82.2	120
C24070	2.697	1342	2002	270	36	30	0.254	37.8	82.3	88.4	81.9	93.8	96.0	120	84.8	120
C24090	3.248	1639	2387	270	36	30	0.330	38.2	79.4	89.0	85.4	97.0	99.7	120	88.5	120
C24100	3.539	1797	2578	269	37	30	0.364	38.4	79.8	90.0	87.2	98.7	101.0	120	90.0	120
C24110	1.948	1546	1803	270	37	30	0.209	34.7	76.0	83.2	78.6	89.8	92.4	120	81.3	120
C24120	2.529	1698	2194	270	36	30	0.294	36.2	77.1	85.6	82.9	94.8	97.1	120	85.8	120

Table B-43. Model No. 43: 36 Chute, AR = 2.5, R_r^o = 0.78 Outer Suppressor with Abrupt Step Over A_o/A_1 = 0.65, R_r^i = 0.674 Inner Plug, Retracted.

A_o = 11.12 in.^{2} Linear Scale Factor to 338 in.^{2} = 5.50 (Outer Only)

Data Point No.	Outer			Free Stream	Meteorological Conditions		Normalization Parameters		2400-ft S.L. Data							
	$(P_T/P_o)_o$	T_T (°R)	V_o (ft/sec)	V_{FS} (ft/sec)	$T_{D_{FS}}$ (° F)	T_{Wet} (° F)	10 $\log_{10}$ V/a_o	10 $\log_{10}$ $P_c(T_o/T_{sm})^{\omega-1}$	OASPL	50° PNL	OASPL	90° PNL	PPNL	θ	POASPL	θ
A25030	1.716	816	1185	0	76	61	0.026	37.7	62.0	69.6	70.0	79.0	81.7	120	72.8	120
A25040	1.930	930	1384	0	76	61	0.094	37.9	65.0	72.9	73.0	82.3	85.9	120	76.4	120
A25060	2.442	1192	1800	0	76	61	0.208	37.7	70.3	78.8	78.1	87.4	92.4	120	82.6	120
A25070	2.702	1328	1993	0	76	61	0.252	37.8	72.5	81.4	80.0	89.5	94.8	120	85.0	120
A25090	3.258	1620	2376	0	76	61	0.325	38.3	76.3	85.7	83.6	92.9	98.5	120	88.9	120
A25100	3.542	1769	2559	0	77	61	0.360	38.5	78.0	87.2	85.4	94.4	99.8	120	91.0	120
A25110	1.933	1533	1786	0	76	61	0.204	34.7	68.5	76.7	77.0	86.6	91.4	120	81.5	120
A25120	2.537	1678	2184	0	77	61	0.292	36.3	72.9	81.3	81.2	90.7	96.2	120	86.2	120
B25030	1.699	834	1187	152	38	33	0.027	37.6	64.4	71.9	70.4	80.1	80.9	120	71.1	130
B25040	1.931	945	1396	153	38	33	0.097	37.8	68.3	76.7	73.6	83.6	85.4	120	75.2	130
B25060	2.416	1195	1793	152	38	33	0.206	37.6	72.6	82.6	78.8	89.3	92.2	120	81.4	120
B25070	2.700	1348	2008	151	38	33	0.255	37.8	74.6	84.7	81.0	91.4	94.8	120	84.0	120
B25090	3.240	1641	2387	150	38	33	0.330	38.2	78.3	88.5	84.3	94.4	97.0	120	87.1	120
B25100	3.518	1801	2576	150	38	33	0.363	38.3	80.0	90.6	86.0	96.0	99.5	120	89.4	120
B25110	1.932	1537	1788	148	48	34	0.205	34.7	71.1	79.8	77.2	87.0	90.3	120	80.0	120
B25120	2.529	1701	2196	150	38	33	0.294	36.2	75.1	84.6	81.7	92.4	95.9	120	85.3	120
C25030	1.723	832	1200	277	40	33	0.032	37.6	69.9	76.5	72.3	82.1	82.3	120	72.9	120
C25040	1.928	945	1394	276	48	36	0.097	37.8	71.0	78.9	75.2	85.6	86.5	120	76.3	120
C25060	2.426	1204	1803	274	48	36	0.208	37.6	75.0	83.5	79.5	90.8	92.6	120	81.9	130
C25070	2.692	1344	2003	280	42	36	0.254	37.8	81.8	87.9	80.8	92.4	95.8	120	84.9	120
C25090	3.242	1645	2390	279	42	34	0.331	38.2	80.4	89.6	84.8	96.5	99.4	120	88.7	120
C25100	3.529	1811	2586	277	47	34	0.365	38.3	79.7	89.8	85.7	96.8	99.9	120	89.7	120
C25110	1.925	1555	1794	278	48	34	0.206	34.6	74.1	82.3	77.7	89.0	91.7	120	81.4	120
C25120	2.529	1704	2198	277	47	34	0.294	36.2	76.7	85.2	81.8	93.2	96.2	120	85.9	120

Table B-44. Model No. 44: 104 Elliptical Tube, AR = 2.8.

A_1 = 13.03 in.^{2} Linear Scale Factor to 338 in.^{2} = 5.08

Data Point No.	Inner			Free Stream	Meteorological Conditions		Normalization Parameters		2400-ft S.L. Data							
	$(P_T/P_O)_i$	T_{T_i} (°R)	V_i (ft/sec)	V_{FS} (ft/sec)	T_{Dry} (° F)	T_{Wet} (° F)	10 $\log_{10}$ V/a_o	10 $\log_{10}$ $F_s(T_O/T_{SS})^{\omega-1}$	50° OASPL	50° PNL	90° OASPL	90° PNL	PPNL	θ	POASPL	θ
A26090	3.261	1608	2167	0	75	58	0.327	38.3	77.7	82.2	83.6	90.6	96.4	140	94.3	140
A26110	1.934	1505	1771	0	75	58	0.201	34.8	66.5	71.3	74.3	83.4	87.3	110	78.7	140
A26120	2.546	1681	2189	0	75	63	0.293	36.3	73.6	77.4	80.1	87.9	91.8	110	88.9	140
A26130	4.053	694	1658	0	75	58	0.172	43.6	75.7	83.5	80.0	88.1	90.0	110	86.2	140
A26140	3.444	755	1641	0	75	58	0.168	42.2	72.4	79.6	77.9	86.1	88.7	120	84.0	140
A26150	2.421	1041	1672	0	76	59	0.176	38.4	67.9	72.0	75.4	83.6	86.8	120	81.4	140
A26160	1.995	1256	1649	0	76	59	0.170	36.2	66.1	70.4	73.7	82.3	86.1	120	78.5	140
A26170	1.793	1379	1628	0	76	59	0.164	34.6	64.8	68.7	72.6	81.4	85.1	120	76.5	120
A26180	1.666	1450	1647	0	76	59	0.169	33.6	64.3	68.7	72.5	81.8	85.1	110	76.0	120
A26200	1.793	1442	1717	0	76	59	0.187	33.8	65.5	69.7	73.3	82.4	86.2	110	77.3	120
B26090	3.328	1640	2409	147	64	48	0.334	38.4	78.4	84.3	81.6	89.8	94.6	140	91.3	140
B26110	1.976	1542	1818	152	65	49	0.212	34.8	68.9	76.9	72.8	83.3	87.4	120	77.1	120
B26120	2.592	1707	2226	153	65	49	0.300	36.4	74.3	81.5	78.1	87.4	91.5	120	84.8	140
B26130	4.107	672	1638	154	65	49	0.167	43.7	75.7	85.5	77.4	86.6	88.9	120	82.1	140
B26140	3.454	747	1637	152	65	49	0.166	42.2	72.8	82.5	75.4	85.0	87.8	120	79.6	140
B26150	2.469	993	1651	150	65	49	0.170	38.8	68.7	77.1	72.5	82.5	86.6	120	76.4	120
B26160	2.008	1250	1650	155	65	49	0.170	36.3	67.6	75.6	71.2	81.7	85.7	120	75.3	120
B26170	1.779	1395	1657	151	65	49	0.172	34.6	66.8	74.5	70.7	81.3	85.0	120	74.7	120
B26180	1.701	1492	1644	150	65	49	0.163	33.5	67.0	74.6	70.7	81.1	84.9	120	74.8	120
B26200	1.787	1491	1771	149	65	49	0.201	33.6	68.2	75.9	71.8	82.2	86.1	120	75.7	120
C26090	3.329	1638	2407	287	61	47	0.334	38.4	78.1	85.4	81.4	91.0	95.0	120	87.4	140
C26110	1.983	1547	1824	276	61	47	0.214	34.8	72.3	80.2	73.6	85.1	88.2	120	77.2	120
C26120	2.590	1700	2225	271	61	47	0.299	36.4	76.1	83.7	77.8	88.5	91.3	120	81.4	130
C26200	1.783	1685	1764	276	62	47	0.199	33.7	71.2	79.0	72.2	83.5	84.7	100	74.0	120

Table B-45. Model No. 45: 104 Elliptical Hole, AR = 2.8.

A_t = 13.03 in.^{2} Linear Scale Factor to 338 in.^{2} = 5.06

Data Point No.	Inner			Free Stream	Meteorological Conditions		Normalization Parameters		2400-ft S.L. Data							
									50°		90°					
	$(P_T/P_0)_t$	T_{T_2} (° R)	V_2 (ft/sec)	V_∞ (ft/sec)	T_{Dew} (° F)	T_{Max} (° F)	$10 \log_{10} V/a_0$	$10 \log_{10} F_s(T_0/T_{ss})^{w-1}$	OASPL	PNL	OASPL	PNL	PPNL	θ	POASPL	θ
A27090	1.359	1417	2389	0	70.0	98.0	0.331	38.2	78.6	82.6	84.3	90.6	97.9	140	95.5	140
A27110	1.944	1535	1794	0			0.206	34.7	68.1	72.3	75.4	84.6	88.1	110	80.6	140
A27120	2.562	1669	2202	0	70.0	98.0	0.295	36.3	74.9	78.7	81.1	88.9	92.7	130	89.8	140
A27130	4.071	641	1645	0	71.0	98.0	0.169	43.6	75.3	82.2	79.2	87.2	89.3	110	85.5	140
A27140	1.433	750	1411	0	71.0	98.0	0.167	42.2	72.1	78.3	77.6	85.9	88.3	120	83.7	140
A27150	2.411	983	1621	0	71.0	98.0	0.182	38.7	67.8	73.0	75.0	84.2	86.9	120	80.5	140
A27160	1.939	1224	1624	0	71.0	98.0	0.161	36.4	66.2	71.1	73.7	83.1	86.3	120	78.5	140
A27170	1.739	1462	1609	0	71.0	98.0	0.159	34.7	65.4	69.8	72.7	82.0	85.2	120	76.5	120
A27180	1.670	1661	1657	0	71.0	98.0	0.172	33.6	65.7	69.6	73.0	82.3	85.7	110	77.1	140
A27200	1.759	1664	1734	0	71.0	98.0	0.192	33.7	66.9	71.2	74.0	83.5	86.8	110	78.7	140
A27210	1.171	1205	799	0	70.0	98.0	-0.145	35.3	50.7	53.0	58.6	67.9	70.1	110	61.1	110
A27240	1.359	1354	1148	0	70.0	98.0	0.004	35.6	57.1	60.3	65.5	74.9	77.7	110	68.3	110
A27270	1.491	1273	1287	0	70.0	98.0	0.062	35.6	59.9	62.9	67.7	76.8	80.1	110	71.1	120
A27280	1.584	1309	1396	0	70.0	98.0	0.098	35.4	61.8	64.8	69.0	77.8	81.1	110	72.8	120
A27290	1.819	1415	1640	0	70.0	95.0	0.167	35.1	65.9	69.2	72.8	81.4	84.7	110	77.5	140
A27300	2.220	1683	2048	0	70.0	98.0	0.288	35.4	72.7	76.3	79.0	86.9	90.6	110	87.0	140
B27090	1.392	1427	2390	150.2	43.0	47.0	0.331	38.3	78.8	84.9	81.9	90.1	95.1	140	91.4	140
B27110	1.930	1543	1802	151.0	43.0	47.0	0.208	34.7	69.7	78.2	73.7	84.6	87.6	120	77.4	120
B27120	2.558	1687	2198	149.3	43.0	47.0	0.295	36.3	74.9	82.2	78.6	88.1	92.0	120	86.2	140
B27130	4.167	672	1643	142.9	60.0	45.5	0.169	43.8	75.3	84.1	77.1	86.2	88.6	120	82.2	140
B27143	3.445	739	1626	145.8	60.0	45.5	0.184	42.2	72.5	81.6	75.0	84.7	87.5	120	79.4	140
B27150	2.386	1001	1627	148.2	60.0	45.5	0.164	38.6	69.3	77.6	72.9	83.7	86.3	120	76.4	120
B27160	1.991	1353	1644	148.3	62.0	48.0	0.168	36.3	62.4	75.5	71.4	82.0	85.2	120	75.3	120
B27170	1.758	1496	1642	155.0	64.5	48.5	0.168	34.5	66.8	74.9	71.0	81.9	85.5	120	75.0	120
B27180	1.660	1684	1660	150.5	64.5	48.5	0.173	33.4	67.1	74.5	71.1	81.8	85.2	120	74.7	120
B27200	1.770	1693	1756	148.2	62.0	48.0	0.198	33.6	69.2	74.7	72.0	82.4	85.7	120	75.9	120
B27250	1.168	1199	791	194.1	64.5	48.5	0.149	35.3	56.0	60.8	58.6	67.6	69.7	110	60.4	110
B27260	1.357	1249	1121	150.9	64.5	48.5	0.002	35.7	55.7	62.4	63.4	74.0	76.6	100	65.4	120
B27270	1.475	1263	1263	151.8	64.0	48.5	0.055	35.6	60.3	67.0	66.2	77.2	79.9	110	69.3	120
B27280	1.594	1294	1398	152.8	64.0	48.5	0.098	35.5	62.3	69.5	68.0	78.9	82.0	120	71.4	120
B27190	1.825	1404	1633	154.4	64.0	46.5	0.167	35.1	67.3	75.5	71.4	82.5	85.8	120	75.1	120
B27300	2.292	1690	2062	150.5	63.0	47.0	0.271	35.5	72.8	80.3	76.9	86.6	90.1	120	82.8	140

Table B-46. Model No. 47: 4.0-inch-Diameter Conical.

A_1 = 12.57 in.^{2} Linear Scale Factor to 338 in.^{2} = 5.17

Data Point No.	Inner			Free Stream	Meteorological Conditions		Normalization Parameters		2400-ft S.L. Data							
									50°		90°					
	$(P_T/P_o)_i$	T_{T_i} (° R)	V_i (ft/sec)	V_{FS} (ft/sec)	T_{Dry} (° F)	T_{Wet} (° F)	10 $\log_{10}$ V/a_o	10 $\log_{10}$ $F_s(T_o/T_{sm})^{\omega-1}$	OASPL	PNL	OASPL	PNL	PPNL	θ	POASPL	θ
A29120	2.545	1693	2197	0	30.0	27.5	0.294	36.3	86.7	93.3	91.7	99.8	108.7	130	103.0	130
A29300	2.281	1692	2079	0	30.0	27.5	0.270	35.4	83.6	89.3	89.6	97.1	106.5	130	100.9	130
A29310	2.472	1002	1657	0	30.0	27.5	0.172	38.8	87.0	93.7	88.3	96.4	101.7	140	97.3	140
A29320	3.004	999	1800	0	30.0	27.5	0.208	40.0	91.5	98.2	93.1	101.1	105.7	140	101.0	140
A29330	3.506	1001	1904	0	30.0	27.5	0.232	41.0	94.5	100.9	96.3	103.9	108.4	140	103.7	140
A29340	2.497	1407	1980	0	30.0	27.5	0.249	37.0	86.1	92.9	90.1	98.3	105.7	130	100.9	140
A29350	2.994	1411	2145	0	30.0	27.5	0.284	38.3	91.3	98.2	94.0	101.8	109.4	130	103.7	130
A29360	3.489	1386	2244	0	30.0	27.5	0.304	39.5	93.9	100.5	96.7	104.5	111.4	130	105.7	130
A29370	2.389	1799	2197	0	30.0	27.5	0.294	35.5	84.8	90.9	90.8	98.4	108.0	130	102.4	130
A29380	3.135	1692	2395	0	30.0	27.5	0.332	37.8	91.8	98.7	95.5	103.6	111.5	130	105.9	130
A29390	3.432	1707	2486	0	30.0	27.5	0.348	38.4	93.4	100.3	96.8	104.9	112.6	130	107.0	130
B29120	2.548	1689	2195	145	30.0	27.5	0.294	36.3	87.5	94.4	90.5	98.9	105.9	130	99.6	130
B29300	2.274	1690	2074	149	30.0	27.5	0.269	35.4	83.4	89.2	88.0	95.7	103.8	130	97.7	130
B29310	2.482	1002	1660	150	31.0	26.5	0.172	38.8	87.8	94.4	88.6	96.2	98.8	130	93.6	140
B29320	3.009	994	1797	145	27.5	25.0	0.207	40.0	93.7	99.6	94.4	101.4	104.2	140	98.4	140
B29330	3.496	1005	1906	145	27.5	25.0	0.233	41.0	95.9	101.7	96.3	103.9	105.6	140	100.4	140
B29340	2.484	1400	1971	150	31.0	26.5	0.247	37.0	87.2	94.2	89.1	97.4	102.6	130	97.0	140
B29350	2.985	1400	2134	147	27.5	25.0	0.282	38.3	93.7	100.2	94.0	101.9	107.2	130	101.2	130
B29360	3.478	1400	2253	143	27.5	25.0	0.305	39.4	96.6	102.4	97.8	105.3	109.9	130	103.8	130
B29370	2.395	1803	2203	148	30.0	27.5	0.295	35.5	85.4	91.8	89.7	97.7	105.6	130	99.3	130
B29380	3.141	1690	2396	145	30.0	27.5	0.332	37.8	95.3	101.8	95.7	103.4	110.4	130	103.9	130
B29390	3.444	1712	2492	145	27.5	25.0	0.349	38.4	96.1	102.4	97.3	104.8	112.3	130	105.6	130
C29120	2.544	1696	2199	272	32.0	28.5	0.295	36.3	87.2	94.5	89.9	99.0	104.4	130	97.8	130
C29300	2.279	1683	2071	271	32.0	28.5	0.269	35.4	82.9	89.5	87.1	95.6	101.4	130	95.2	130
C29310	2.500	1000	1664	271	32.0	26.5	0.174	38.8	88.7	95.7	88.3	96.4	97.1	120	90.3	130
C29320	3.002	999	1799	272	30.0	27.0	0.207	40.0	94.6	101.4	93.5	101.9	102.7	70	95.4	70
C29330	3.459	998	1892	269	30.0	27.0	0.229	40.9	97.4	103.4	96.8	104.6	105.8	80	99.0	140
C29340	2.492	1402	1975	271	32.0	26.5	0.248	37.0	87.3	94.8	88.7	97.8	100.6	130	94.4	130
C29350	2.986	1397	2132	276	31.0	26.5	0.281	38.4	93.6	100.6	94.0	102.7	105.5	130	99.1	130
C29360	3.448	1403	2250	271	30.0	27.0	0.305	39.4	96.8	103.0	96.6	105.1	108.1	130	101.5	130
C29370	2.390	1802	2200	273	32.0	28.5	0.295	35.5	84.9	92.0	88.9	97.7	103.9	130	97.3	130
C29380	3.127	1684	2387	270	32.0	28.5	0.330	37.8	94.1	100.9	95.6	104.1	108.3	130	101.7	130
C29390	3.438	1704	2484	269	30.0	27.0	0.348	38.4	97.0	103.4	97.1	105.8	109.7	130	103.1	130

APPENDIX C

GENERAL ELECTRIC AIR-ATTENUATION MODEL

The air-attenuation model used for JENOTS data was developed in 1973 by R.G. Fogg of General Electric (Reference 17). Mr. Fogg noticed that a linear extrapolation of the SAE/ARP 866 curves (Reference 13) or the prediction of Harris (Reference 15) tended to distort the spectral shape for frequencies above 20 kHz when the data was scaled or PWL was calculated as seen in Figures C-1 and C-2. He hypothesized that this distortion was the result of applying excessive air attenuation at the high frequencies. From Harris' data, it was clear that the molecular absorption diminished in percent of the total absorption as the frequency increased, leaving the classical absorption as the dominant attenuator. By curve-fitting the trends of the classical and molecular absorption with frequency at various humidities and a temperature such as in Figure C-3, a family of prediction curves as shown in Figure C-4 was developed. For comparison, a similar presentation from Harris (Reference 15) and Evans (Reference 20), is given in Figures C-5 and C-6, respectively.

Table C-1 is a listing of the computer program used to generate the correction factors. With the wet and dry bulb temperatures given in Appendix B, one can calculate the values of the air-attenuation corrections applied to the data presented in this report.

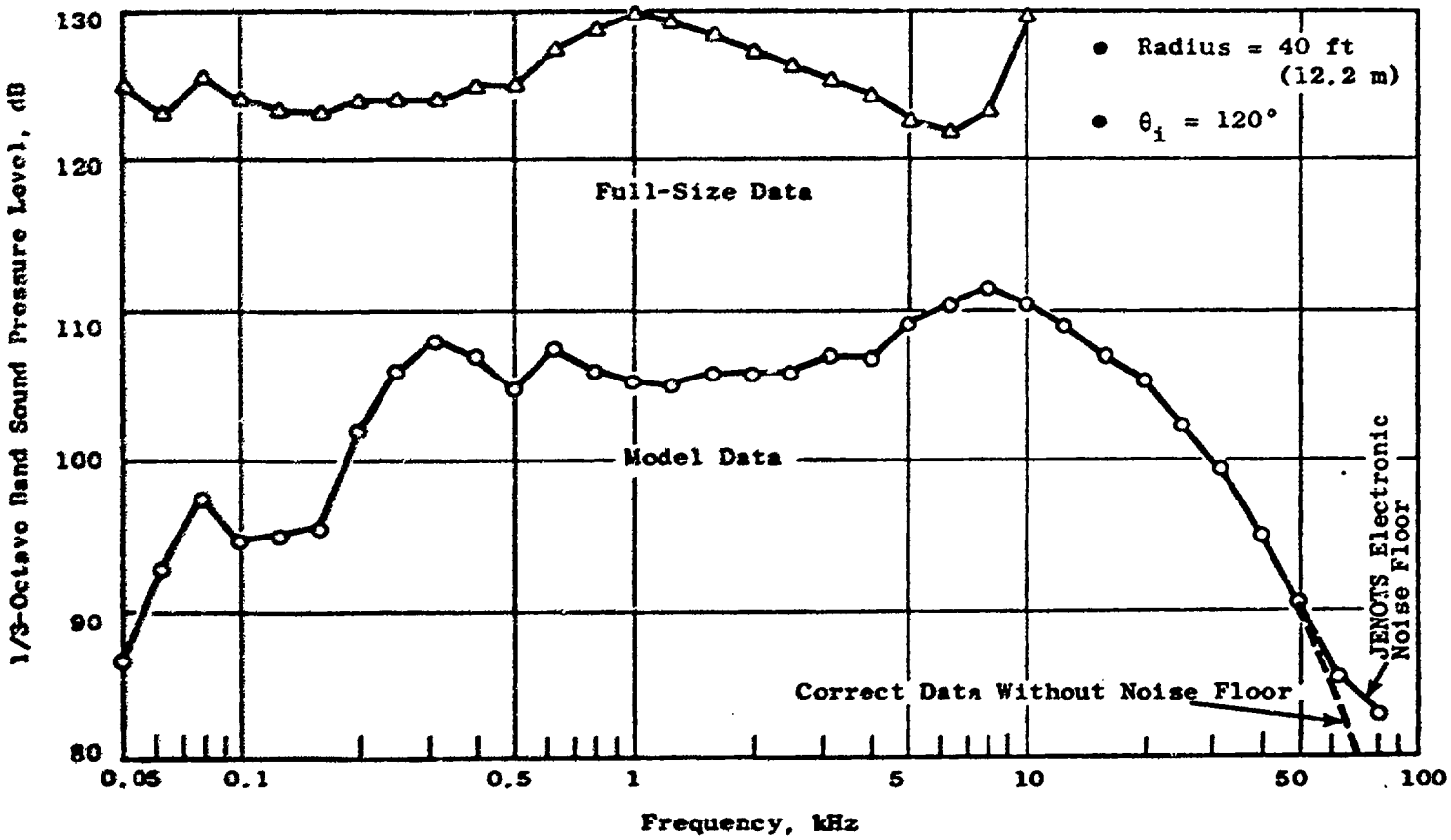

Figure C-1. JENOTS Data: SPL Spectra, FSDR Program Calculation.

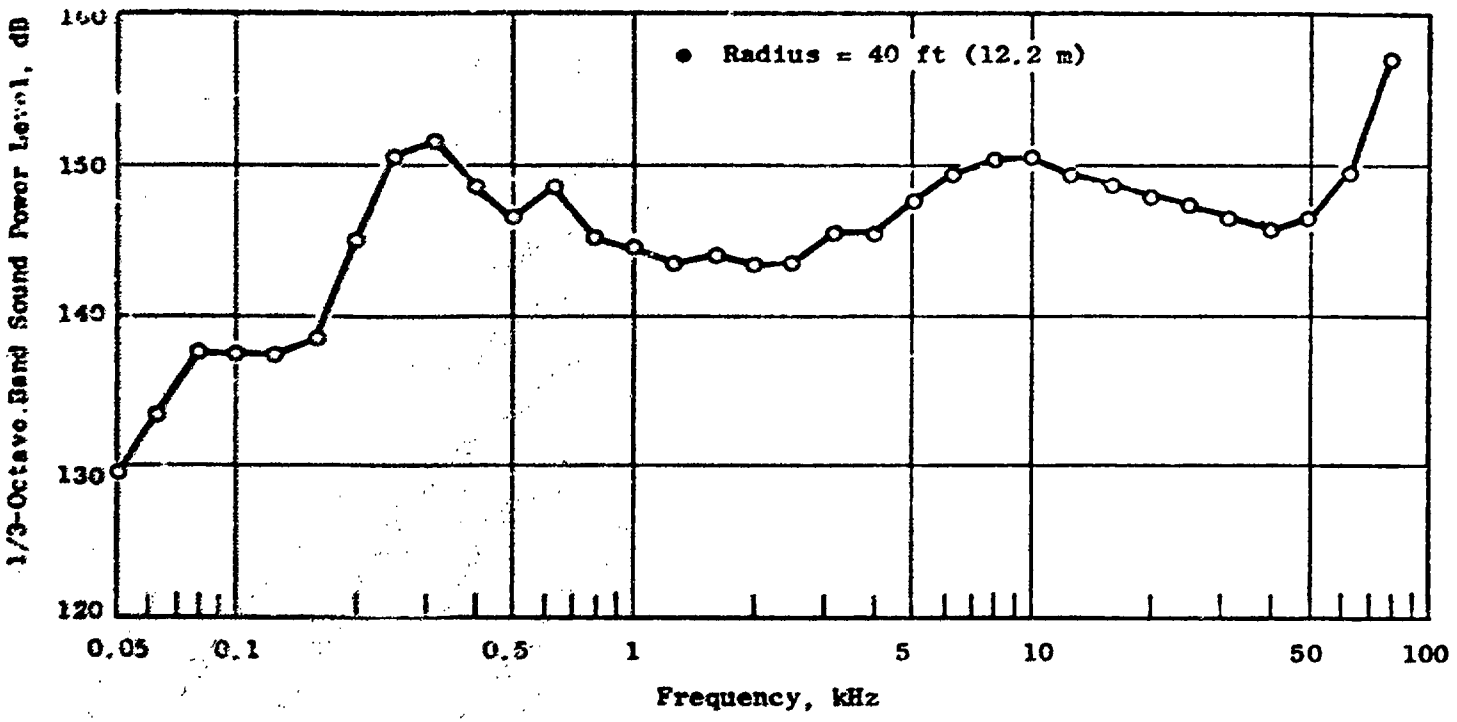

Figure C-2. JENOTS Data: SPL Spectra, FSDR Program Calculation.

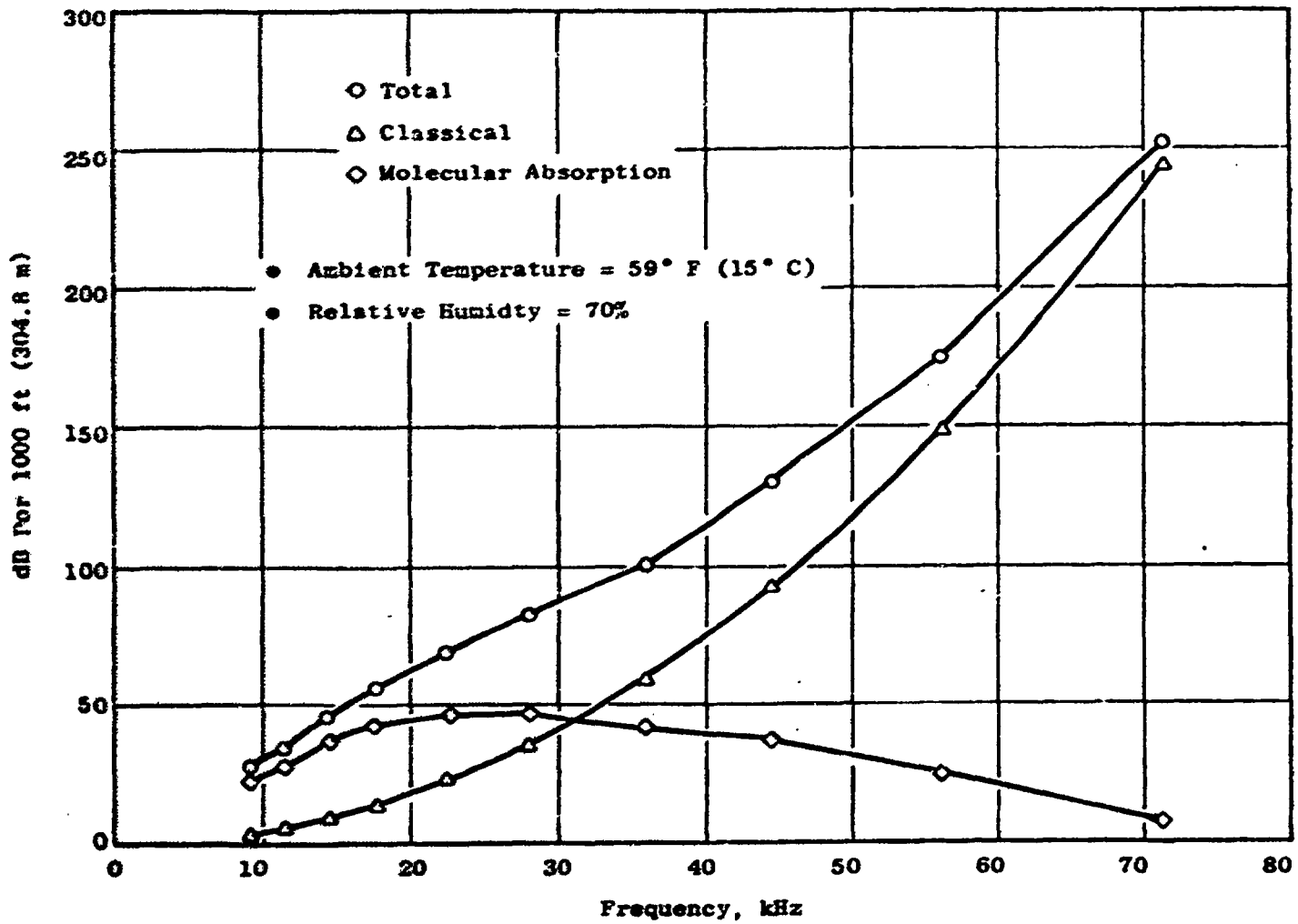

Figure C-3. Revised Atmospheric Correction Factors.

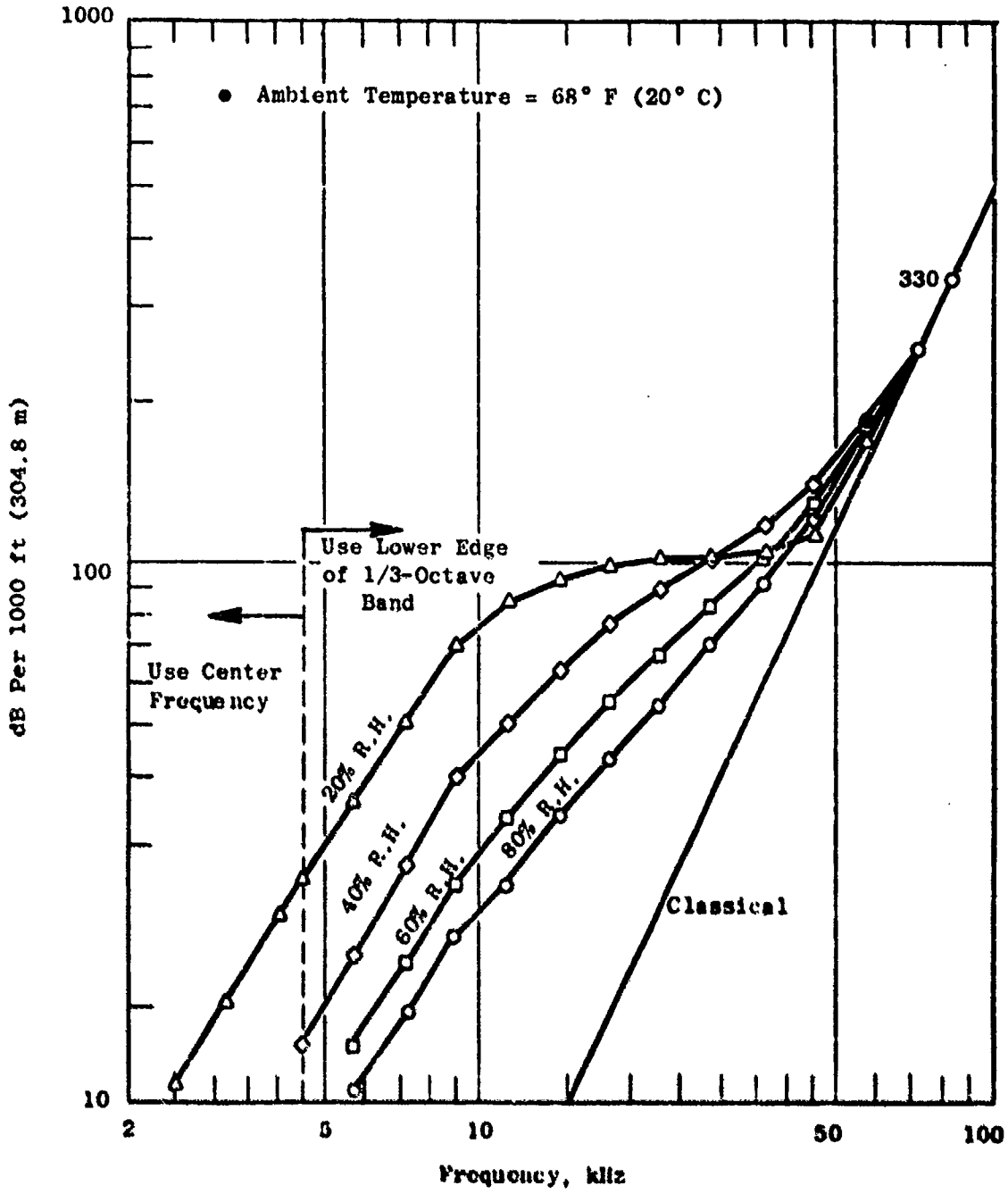

Figure C-4. Revised Atmospheric Absorption.

(Reference Figure 3.2, Page 3-3, "Harris Handbook of Noise"

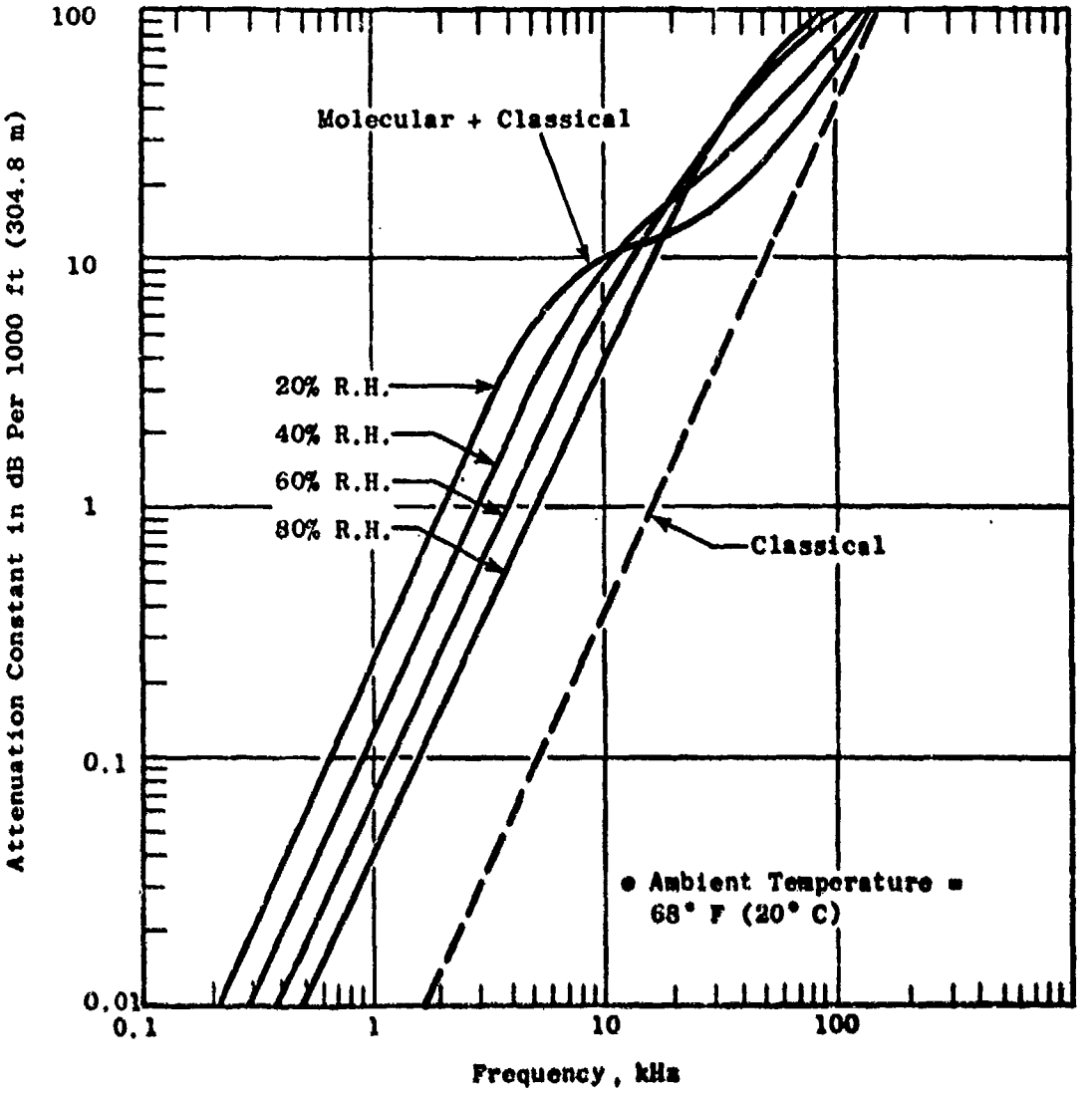

Figure C-5. Atmospheric Attenuation Factors.

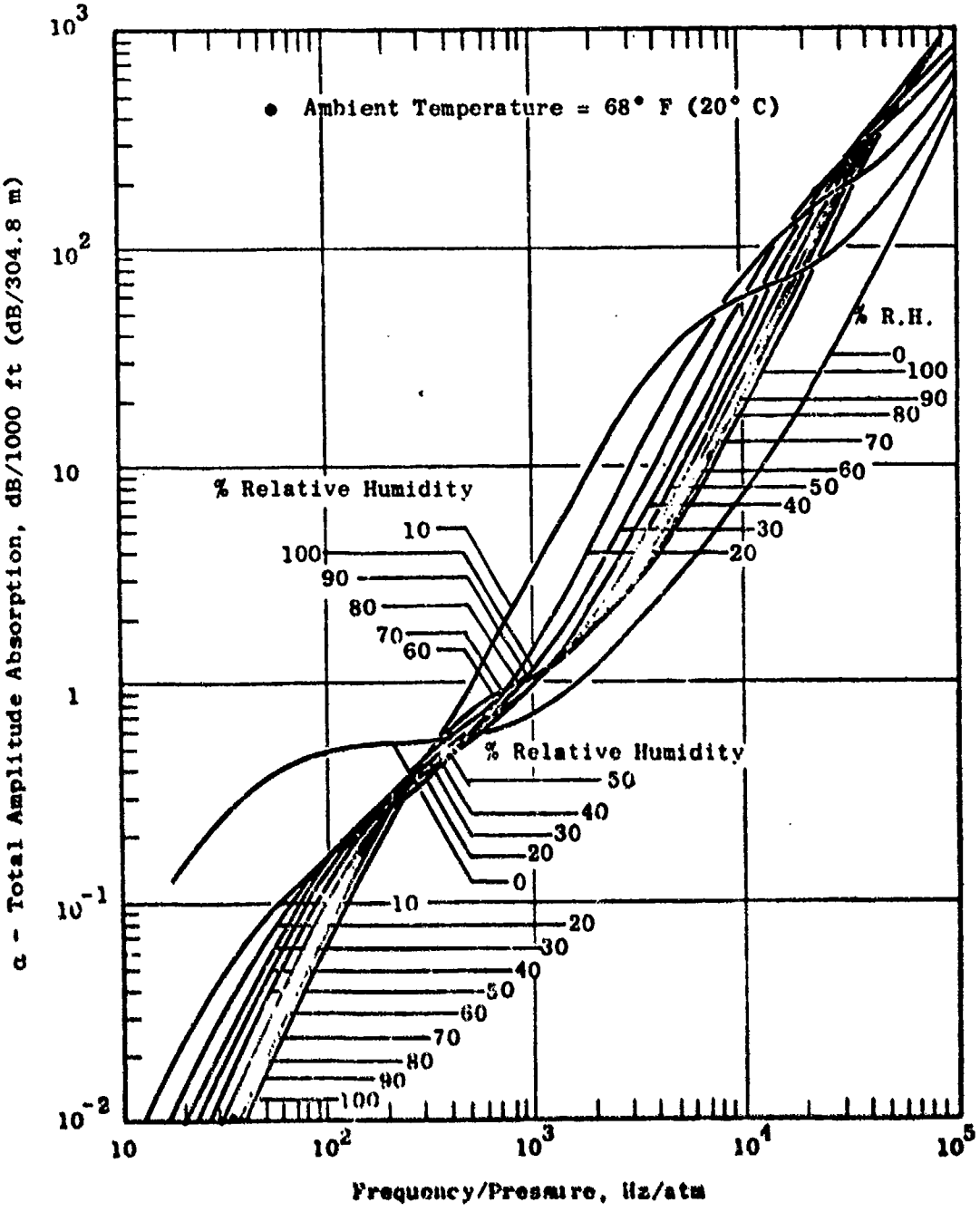

Figure C-6. Total Absorption of Sound in Air as a Function of Frequency.

Table C-1. Listing of the GE Air-Attenuation Correction Computer Program.

```
10 REM THIS PROGRAM PROVIDES CORRECTION FACTORS AND INCREMENTAL
11 REM SPHERICAL AREAS FOR THE FAR FIELD CALCULATIONS. SEE TIME
12 REM SHARE PROGRAM "FARFLD". INPUT AMBIENT ATMOSPHERIC
13 REM CONDITIONS AND ARC RADIUS AT LINE 90. INPUT MICROPHONE
14 REM ANGLE LOCATIONS AT LINE 840.
30 DIM C(24),E(24),F(24),G(24),H(24),K(24),M(20),N(20)
31 DIM P(20),S(20),Z(20)
40 FOR I = 1 TO 24
50 READ F(I)
60 DATA 500,630,800,1000,1250,1600,2000,2500,3150,4000,
70 DATA 5000,6300,8000,10000,12500,16000,20000,25000,
71 DATA 31500,40000,50000,63000,80000,100000
72 NEXT I
75 REM "T1" IS WET BULB TEMPERATURE IN DEGREES F, "T3" IS
76 REM ATMOSPHERIC TEMPERATURE IN DEGREES F. "P1" IS ATMOSPHERIC
77 REM PRESSURE IN INCHES OF HG. "R2" IS SPHERICAL RADIUS IN FT.
80 READ T1,T3,P1,R2
90 DATA 33,40,29.921,1000
95 REM THE FOLLOWING CALCULATIONS ARE FOR ABSOLUTE HUMIDITY.
100 LET T2 = ((5/9)*(T1 - 32)) + 273.16
110 LET X1 = 647.27 - T2
111 READ B6,B7,B8,B9
112 DATA 3.2437814,5.86826E-3,1.1702379E-8
113 DATA 0.89
120 LET A5 = B6 + B7*X1 + B8*X1↑3
130 LET A1 = 1 + 2.1878461E-3*X1
140 LET A2 = (X1/T2)*(A5/A1)
141 READ C6,C7
142 DATA 218.167,14.6959
150 LET P = (C6/10↑A2)*C7
160 LET A3 = ((P1*0.49115)-P)*(T3 - T1)
170 LET P2 = P - ((A3)/(2755 - 1.28*T1))
171 READ C8,C9,D5,D6
172 DATA 144,460,85.7,16.02E3
180 LET A4 = ((P2*C8)/((T3 + C9)*D5))*D6
181 PRINT "AMBIENT TEMPERATURE =";T3;"DEGREES F"
182 PRINT "WET BULB TEMPERATURE =";T1;"DEGREES F"
183 PRINT "BAROMETRIC PRESSURE =";P1;"INCHES OF HG"
184 PRINT
185 PRINT "ABSOLUTE HUMIDITY (HA) =";A4;"GRAMS PER CUBIC METER"
187 LET D1 = P1/29.921
188 LET D2 = (T3 + 460)/519
```

Table C-1. Listing of the GE Air-Attenuation Correction Computer Program (Continued).

```
189 LET D3 = (SQR(D2))/D1
190 PRINT " IMPEDENCE CORRECTED TO STD. DAY =";D3*2.227525E-6
191 PRINT
192 PRINT
193 REM THE FOLLOWING CALCULATIONS ARE FOR ALPHA MOL MAX
200 REM H MOL MAX
205 READ F1,F2,F3,F4,F5,F6
210 FOR I = 1 TO 24
220 IF F(I) > 4000 THEN 227
225 LET A6 = F(I)
226 GO TO 230
227 LET A6 = B9*F(I)
230 LET LET H(I) = 0.028961*A6↑0.51093
235 IF F(I) > 4000 THEN 250
240 LET A6 = F(I)
245 GO TO 260
250 LET A6 = B9*F(I)
260 LET C(I) = A6*0.00357451*EXP(0.0117537*T3)
261 IF A6 < 8900 THEN 266
263 DATA .15023777E02,.83707731E-02,.36541712E-06,.56857640E-11
264 DATA -0.31243498E-16,.0117537
265 LET C(I) = (F1+F2*A6+F3*A6↑2+F4*A6↑3+F5*A6↑4)*EXP(F6*(T3-59))
266 IF F(I) > 4000 THEN 269
267 LET A6 = F(I)
268 GO TO 270
269 LET A6 = B9*F(I)
270 LET Y4 = 0.279129E-7*A6↑2.05403
280 LET Y5 = 0.261933E-7*A6↑2.05081
290 LET K(I) = Y5 + (Y4 - Y5)*(T3 -32)/68
300 REM THE FOLLOWING CALCULATIONS ARE FOR ALPHA MOL OVER
301 REM ALPHA MOL MAX
305 LET A7 = A4/H(I)
310 IF A7 > 6.5 THEN 440
320 IF A7 < 1.0 THEN 380
330 LET Y1 = (0.16955546E-2*A7) - 0.35055924E-1
340 LET Y2 = (Y1*A7) + 0.28070773
350 LET Y3 = (Y2*A7) - 0.10581673E1
360 LET Z(I) = (Y3*A7) + 0.18209020E1
370 GO TO 450
380 LET Y1 = (0.74335316E1*A7) - 0.17186DE2
390 LET Y2 = (Y1*A7) + 0.11814166E2
400 LET Y3 = (Y2*A7) - 0.23792759E1
```

Table C-1. Listing of the GE Air-Attenuation Correction Computer Program (Continued).

```
410 LET Y4 = (Y3*A7) + 0.13220157E1
420 LET Z(I) = (Y4*A7) + 0.5230581E-3
430 GP TO 450
440 LET Z(I) = 0.2
450 LET Z(I) = 0.001*INT(1000*Z(I) + 0.5)
460 LET E(I) = Z(I)*C(I)
470 REM THE FOLLOWING CALCULATIONS ARE FOR THE EGA CORRECTION
480 LET R1 = R2
510 LET C1 = (0.20411435E-20*R1) - 0.66703093E-16
520 LET C2 = (C1*R1) + 0.72854603E-12
530 LET C3 = (C2*R1) - 0.32650913E-8
540 LET C4 = (C3*R1) + 0.49614255E-5
550 LET C5 = (C4*R1) + 0.44663072E-2
560 LET G1 = (C5*R1) + 0.59387702
570 LET E1 = (0.16573369E-24*R1) - 0.46152934E-20
580 LET E2 = (E1*R1) + 0.32361609E-16
590 LET E3 = (E2*R1) + 0.39118972E-13
600 LET E4 = (E3*R1) - 0.10464995E-8
610 LET E5 = (E4*R1) + 0.29126338E-5
620 LET E6 = (E5*R1) - 0.54370996E-3
630 LET G2 = (E6*R1) + 0.59506112
650 IF R1 <= 4000 THEN 680
660 LET G1 = 5.010264
670 LET G2 = 15.44041 + 0.0001*(R1 - 4000)
680 IF F(I) = 63 THEN 720
690 IF F(I) >= 2000 THEN 740
700 LET Z1 = 0.2*((LOG(F(I)/62.5))/LOG(2))
710 GO TO 750
720 LET Z1 = 0
730 GO TO 750
740 LET Z1 = 1.0
750 LET G(I) = (Z1*(G1 - G2)) + G2
760 NEXT I
765 PRINT "CORRECTION FACTORS IN DB AT ARC RADIUS ="; B2;
766 PRINT "FEET"
770 PRINT "FREQUENCY"; TAB(11); "CLASSICAL"; TAB(22);
771 PRINT "MOL.ABSORB."; TAB(36); "TOTAL ABSORB"; TAB(51);
772 PRINT "EGA"; TAB(63); "TOTAL CORR"
790 FOR I = 1 TO 24
802 PRINT F(I); TAB(8); K(I)*R2/1000; TAB(22); E(I)*R2/1000;
801 PRINT TAB (36); (K(I)+E(I))*R2/1000; TAB(51); G(I); TAB(63);
802 PRINT ((K(I)+E(I))*R2/1000)+G(I)
```

Table C-1. Listing of the GE Air-Attenuation Correction Computer Program (Concluded).

```
810 NEXT I
820 REM THE FOLLOWING CALCULATIONS APE FOR STRIP AREA
821 PRINT
822 PRINT
825 PRINT "ANGLE LOCATION","STRIP AREA FOR";R2;
826 PRINT "FOOT SPHERICAL RADIUS"
827 PRINT "(DEGREES)","SQ. FT.)"
830 REM "M(I)" AND "N(I)" ARE ANGLES WHICH DEFINE THE ARC
831 REM ASSIGNED TO EACH MICROPHONE. "P(I)" IS THE
840 REM MICROPHONE LOCATION ANGLE.
845 READ F1,F2,F3,F4
846 DATA 1.5,3.1416,2,0.0174533
850 READ N
855 DATA 17
860 FOR I = 1 TO N
870 READ P(I)
875 NEXT I
880 DATA 0,10,20,30,40,50,60,70,80,90,100,110
881 DATA 120,130,140,150,160
895 FOR I = 1 TO N
900 LET M(I) = P(I) - (P(I) - P(I-1))/F3
910 LET N(I) = (P(I+1) - P(I))/F3 +P(I)
915 IF I = 1 THEN 917
916 GO TO 920
917 LET M(I) = P(I) - (P(I+1)-P(I))/F3
920 IF M(I) < 0 THEN 940
930 GO TO 950
940 LET M(I) = 0
950 IF N(I) > 180 THEN 970
954 IF I = N THEN 962
958 GO TO 980
960 GO TO 980
962 LET N(I) = P(I) + (P(I) - P(I-1))/F3
966 GO TO 980
970 LET N(I) = 180
980 LET S(I) = F1*F2*R2*F3*(COS(M(I)*F4) - COS(N(I)*F4))
990 PRINT P(I),S(I)
995 NEXT I
1000 END
```

APPENDIX D

1.0 SUMMARY OF THE ELLIPSOIDAL MIRROR DEVELOPMENT

Ellipsodial mirror (EM) measurements of axial source intensity distributions were made for selected data points during the Task 3 test program.

This appendix describes the ellipsodial mirror technique as developed for Task 3. Section 1.1 describes the mirror configurations and test set-up. Section 1.2 discusses the mirror calibration. Section 1.3 discusses the data processing procedures and associated numerical techniques. Section 1.4 describes data analysis procedures. Section 2.0 is an evaluation of the ellipsoidal mirror technique and discusses theoretical limitations, data acquisition and data processing errors.

1.1 MIRROR CONFIGURATION AND TEST SETUP

The ellipsoidal mirror is a directional microphone system in which an ellipsoidal dish (mirror) is used to focus acoustic radiation from a specific source region in a jet onto a microphone placed outside the flow. Figure D-1 shows a schematic representation of the system. The EM is mounted on a remotely driven cart on tracks parallel to the jet axis. Surveys of the jet are then accomplished by making continuous traverses along the length of the jet. A microphone is placed at the primary focus of the ellipse, and the secondary focus is placed on the jet centerline (and the mirror axis is fixed normal to the jet axis).

All of the EM source location data reported in References 8 and 12 were obtained with an 18-inch-diameter shallow-dish mirror (Figure D-2). In the Task 3 program, this mirror was used for testing at the JENOTS freejet facility, while a new 34.654-inch-diameter deep-dish mirror (Figure D-3) was used in the jet noise anechoic facility. A summary of physical and operating characteristics of the two systems was shown in Figure 3-17. The new deep-dish mirror was designed to have a larger diameter and increased working distance for improved low frequency performance. In addition, a different microphone orientation is used. With the 18-inch mirror, the microphone is inserted through the rear of the mirror and directed toward the source region. A "reverse mounting" fixture is used on the deep-dish mirror (Figure D-4), so that the microphone can be turned and directed back toward the mirror surface. This change was made to allow better resolution of high frequency data.

The setup of the 18-inch mirror at JENOTS is shown in Figure D-5, and the setup of the deep-dish mirror in the anechoic facility is shown in Figure D-6. Note that the picture in Figure D-6 was taken prior to installation of the reverse mounting fixture in the mirror.

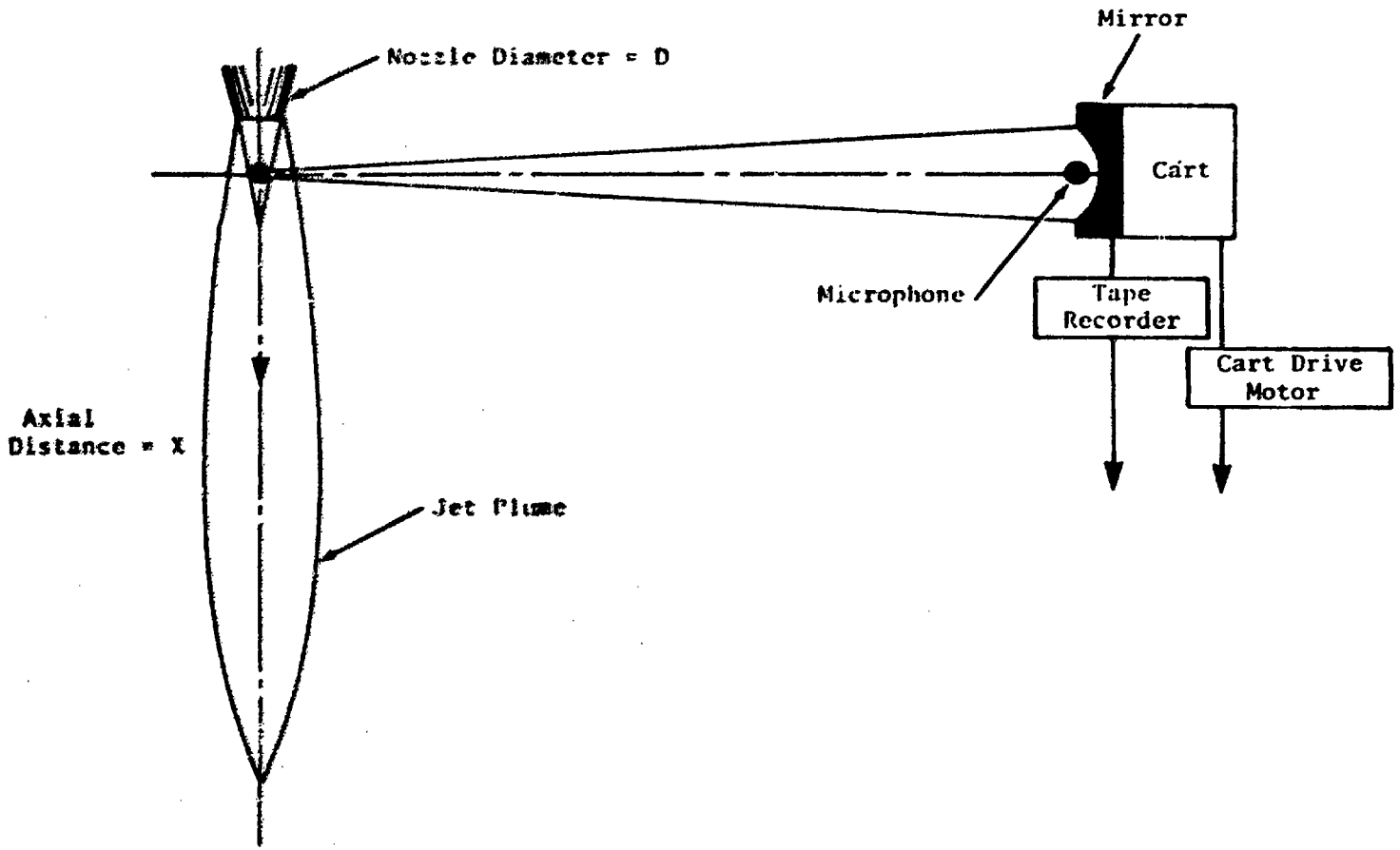

Figure D-1. Test Setup for Ellipsoidal Mirror Surveys.

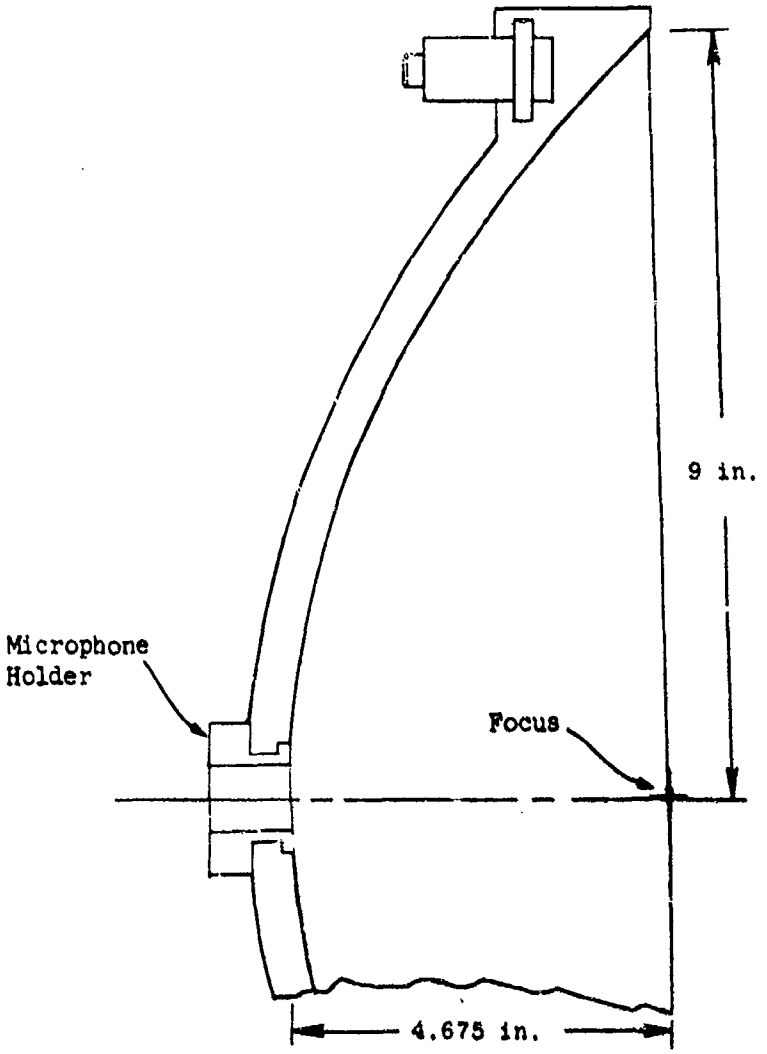

Figure D-2. 18-inch-Diameter Shallow-Dish EM with 9-foot Working Distance.

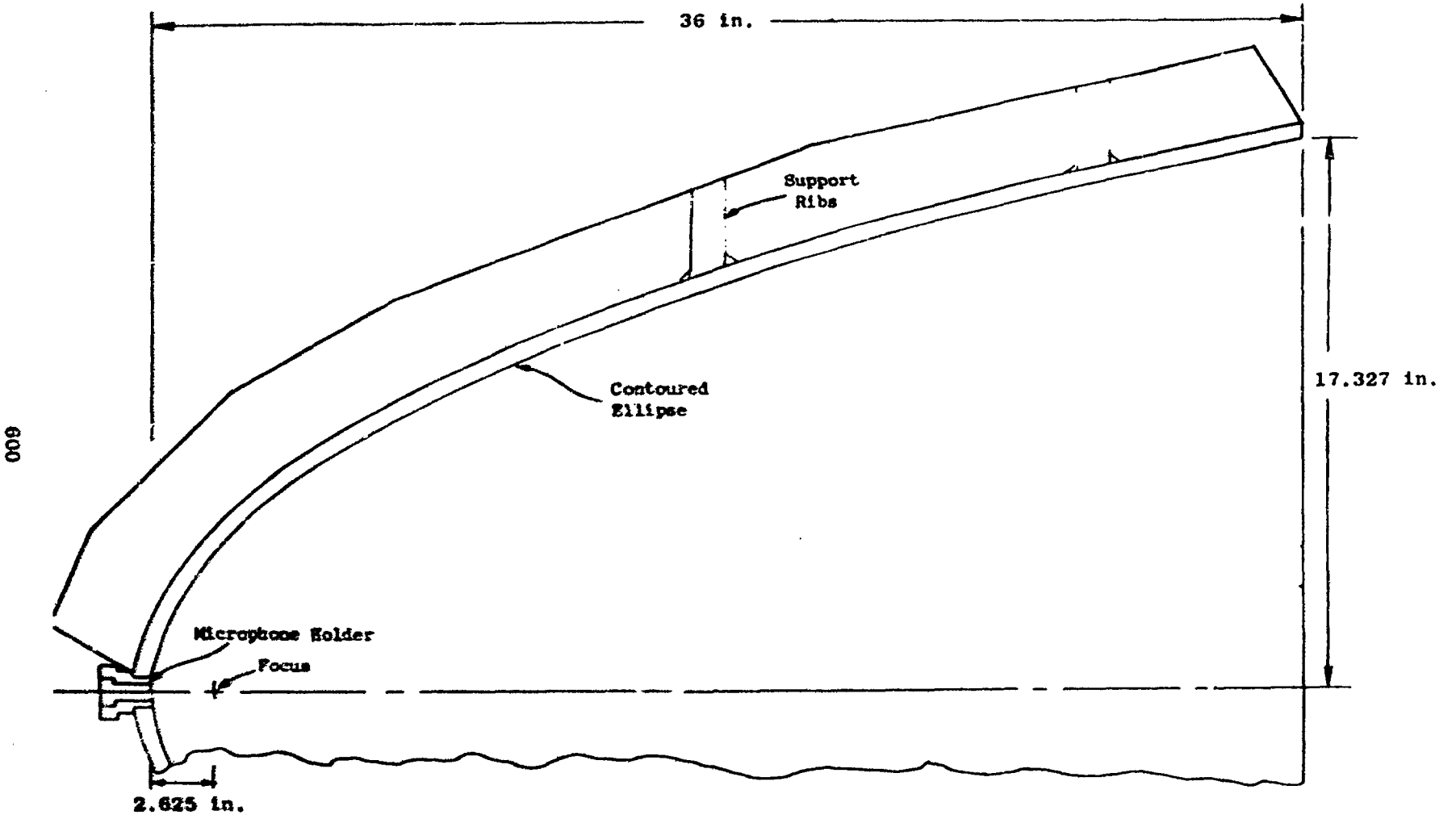

Figure D-3. 34.654-inch-Diameter Deep-Dish EM with 15-foot Working Distance.

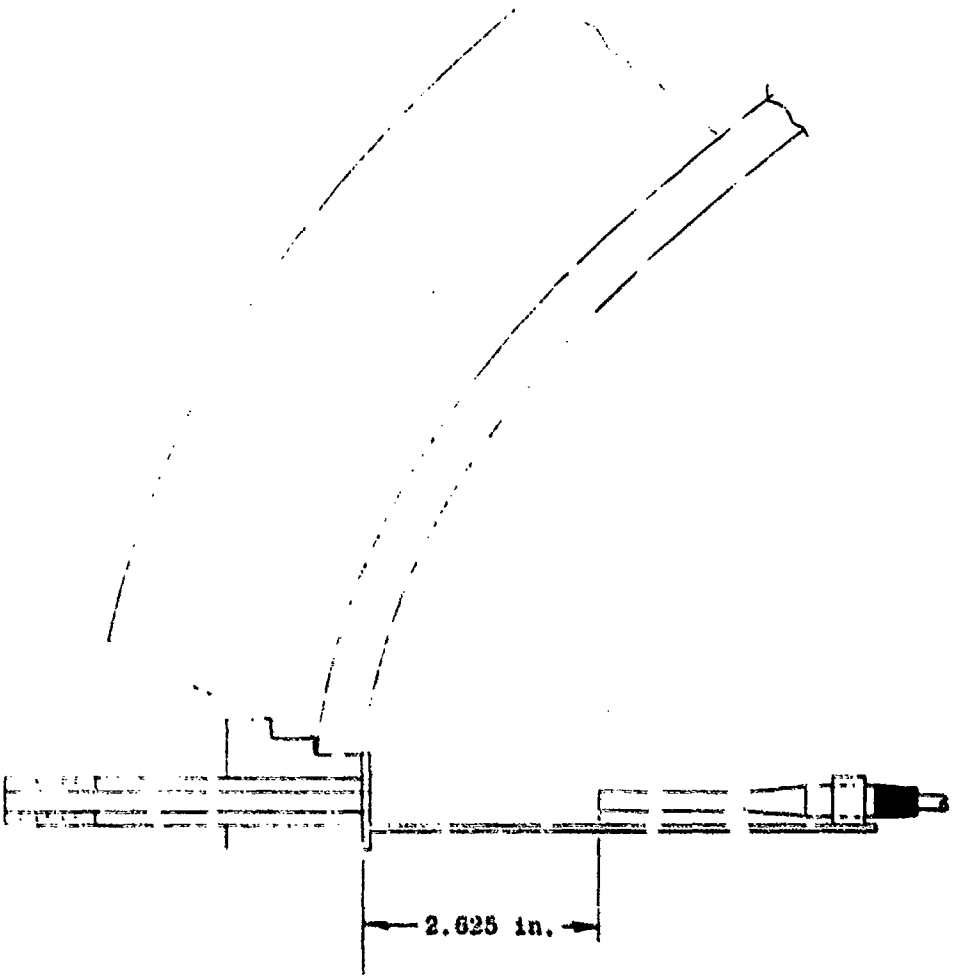

Figure D-4. "Reverse Mounting" Microphone Fixture for Deep-Dish Ellipsoidal Mirror.

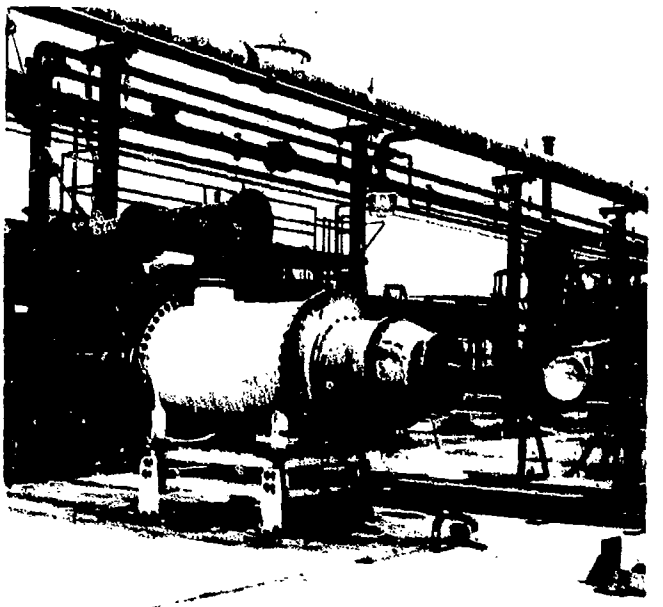

Figure D-5. Ellipsoidal Mirror Set-Up at JENOTS.

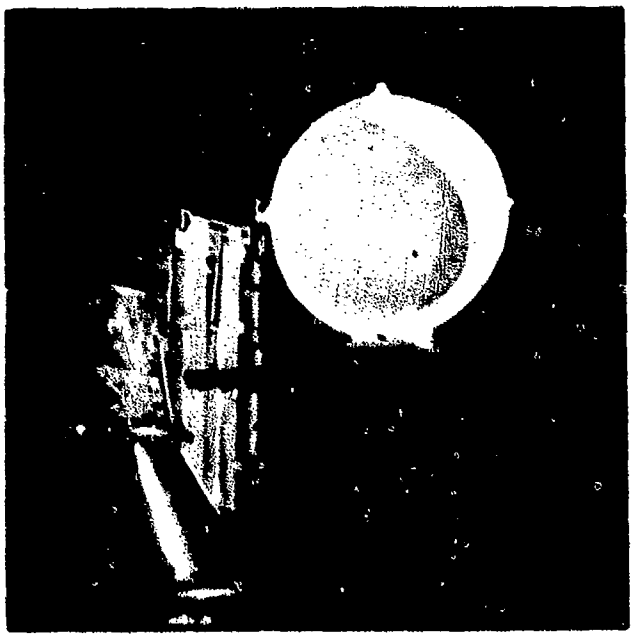

Figure D-6. Ellipsoidal Mirror Set-Up in the Anechoic Facility.

For each EM test point, data is recorded on magnetic tape over the full length of an "outbound" traverse. The microphone signal, a DC cart position signal and IRIG B-time code signal are all recorded using the standard acoustic data acquisition system for the particular facility (JENOTS or Anechoic).

1.2 MIRROR CALIBRATION

An ellipsoidal shape is used for the mirror surface because of its theoretical ability to resolve a point source of sound onto a microphone. The ellipse has the property that the tangent at any point makes equal angles with the two focal radii to that point. In the limit of high frequencies, with wavelengths very small relative to the mirror dimensions, acoustic radiation can be approximated as straight line rays and sound emanating from a source at one focal point would be reflected to the other focal point by any point on the surface. This focusing effect is characterized by the mirror gain, which theoretically increases with the square of frequency (6 dB/octave).

At lower frequencies, the wave character of sound becomes dominant, and resolution of source distributions by the mirror is limited by diffraction. The "point", which is resolved onto the microphone, spreads into a three-dimensional volume described by the frequency dependent diffraction pattern of the dish. A slice through the three-dimensional diffraction pattern along a plane parallel to the jet axis and normal to the mirror axis yields the window function. This function represents the sensitivity of the system to adjacent sources along the jet axis when the mirror is focused on a given point. The effect of diffraction is thus to smooth details and raise the overall level of measured distributions. The "width" of the window function is theoretically proportional to wavelength (inversely proportional to frequency).

The EM measurement of power spectral density at an arbitrary axial position in a jet can be expressed analytically in terms of a convolution integral:

$$p_m^2(x,f) = G(f) \int_{-\infty}^{\infty} p_a^2(\xi,f)\, H(x-\xi,f)\, d\xi \qquad (D\text{-}1)$$

where p_m^2 and p_a^2 are, respectively, the measured and actual values of mean square sound pressure, G is the mirror gain, and H is the diffraction window function. In order to obtain the true acoustic power distribution for a particular frequency, it is then necessary to solve (deconvolve) the integral equation for the excitation signal at each axial position, given knowledge of the system (mirror) characteristics and the response (measured) signal. Thus, each mirror must be calibrated to determine its gain and window function characteristics.

While the mirror gain is described by a single value for each frequency, the window function is actually a continuous function of distance from the focal point in the focal plane. The window function for a given frequency is mapped by placing a point source at the secondary focus of the mirror and translating it in the focal plane (normal to the mirror axis), or, conversely, by fixing the source and translating the mirror system. The gain is determined by fixing the point source at the secondary focus, and comparing measured levels of the primary focus with and without the mirror present. The algebraic difference (in dB) is the mirror gain.

Equation D-1 is strictly valid for discrete frequencies (1-Hz narrowband). However, to maintain consistency with farfield acoustic data, it is desirable to analyze source location data in 1/3 octave bands, with the necessary approximations made in the formulation of equation D-1. Thus, a broadband source is required for mirror calibration, so that the window function and gain can be determined on a 1/3 octave band basis.

Both of the ellipsoidal mirrors were calibrated in the anechoic facility. The test setup for calibration of the 18-inch mirror is shown in Figures D-7 and D-8. The mirror was mounted on a remotely driven cart so that it could be traversed past the stationary noise source, a 1/2 inch diameter nozzle operating at sonic pressure ratio. The nozzle was positioned with its axis in the secondary focal plane of the mirror, normal to both the mirror axis and the vertical tracks on which the cart moved (Figure D-7). A reference microphone (for gain calibration) was placed in the same horizontal plane as the source, at the same displacement from the source as the mirror microphone and at 180° to the mirror axis (Figure D-8). The same basic setup was used for calibration of the deep-dish mirror.

Calibration data was obtained for both mirrors over the range 0.4 to 40 kHz. In each case, the mirror and reference microphone signals, the cart position and time code, were recorded over the full length of an "outbound" vertical traverse. The data from this traverse was then played back through the appropriate filters and analyzed to obtain 1/3-octave band gains and window functions. The results are summarized in Figures D-9 through D-12. The gain of the 18-inch mirror (Figure D-9) is seen to follow the theoretical 6 dB/octave increase over a wide range of frequencies. Figure D-10 shows the width of the window functions, defined as the distance between points at 50% of the peak value (3 dB down) on either side, as normalized by the wavelengths corresponding to 1/3 octave band center frequencies. Again, it is seen that the theoretical trend (constant normalized width) is followed over a wide range of frequencies. Calibration results for the deep-dish mirror (Figures D-11 and D-12), while not showing as good agreement with theoretical trends, do indicate higher gain and slightly narrower window functions relative to the 18-inch mirror.

1.3 DATA REDUCTION

Ellipsoida mirror data reduction is accomplished as a two-stage procedure. The first step is a relatively straightforward conversion of raw

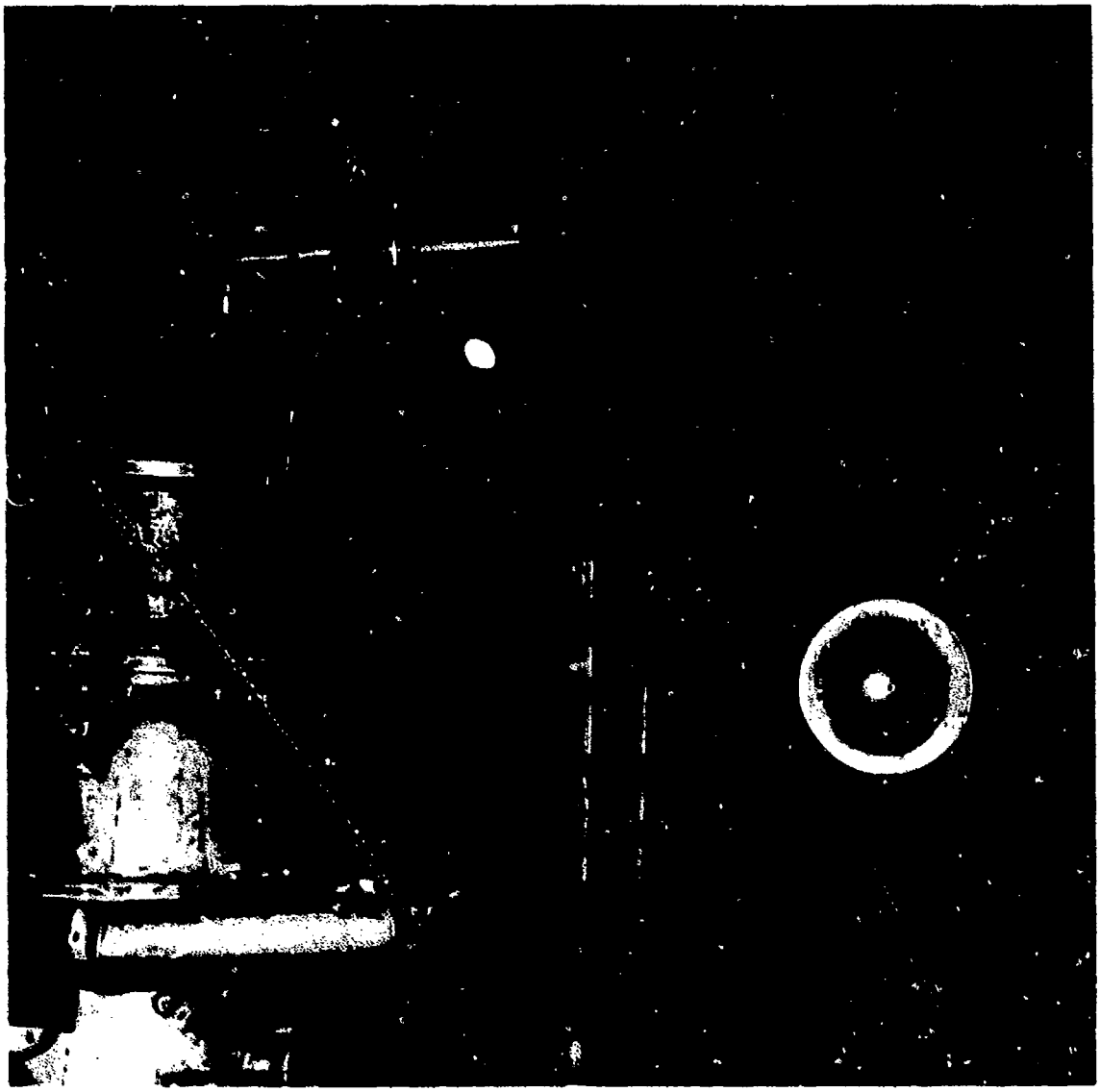

Figure D-7. Set-Up of Mirror and Noise Source for Calibration of 18-inch EM.

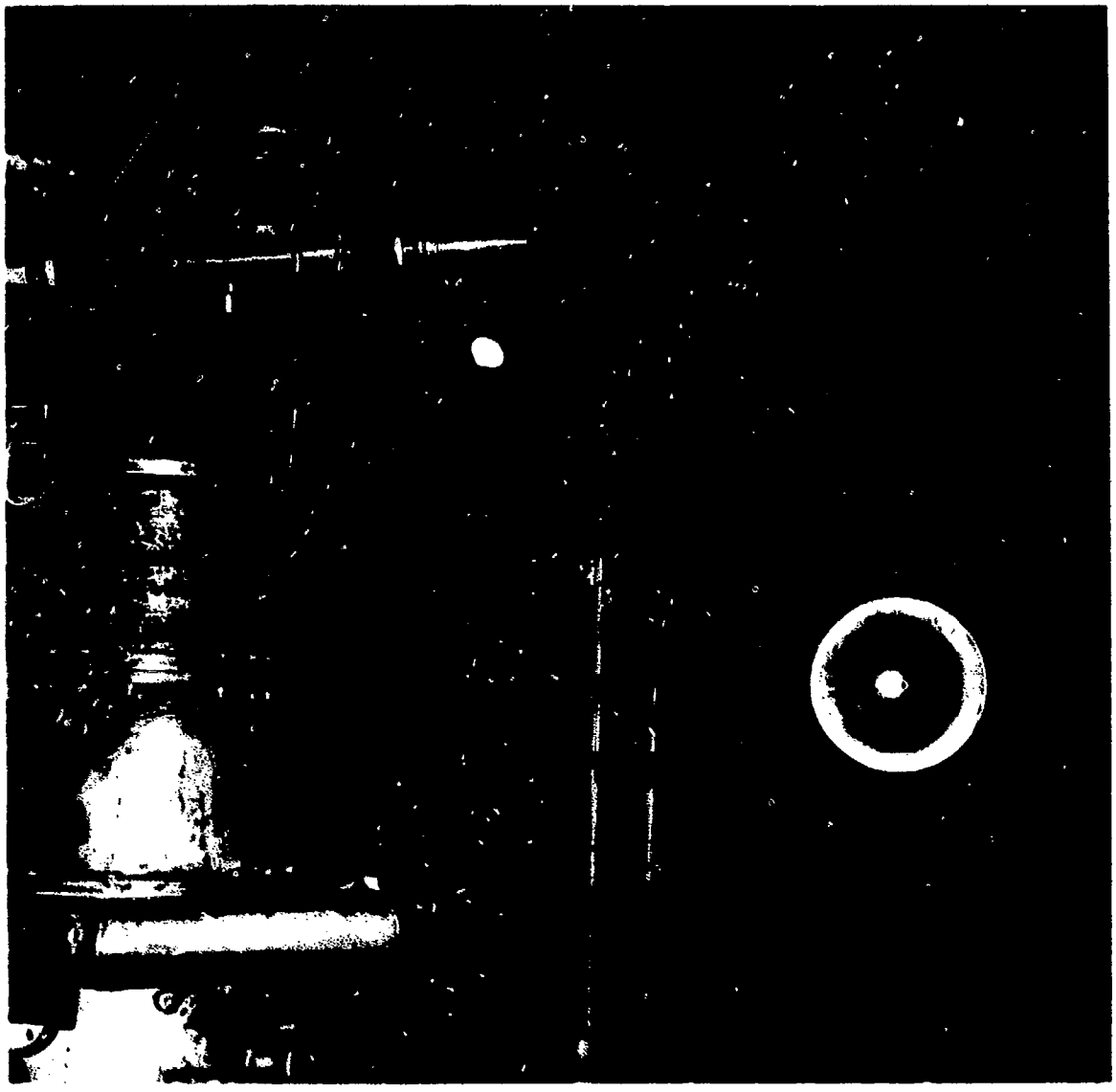

Figure D-7. Set-Up of Mirror and Noise Source for Calibration of 18-inch EM.

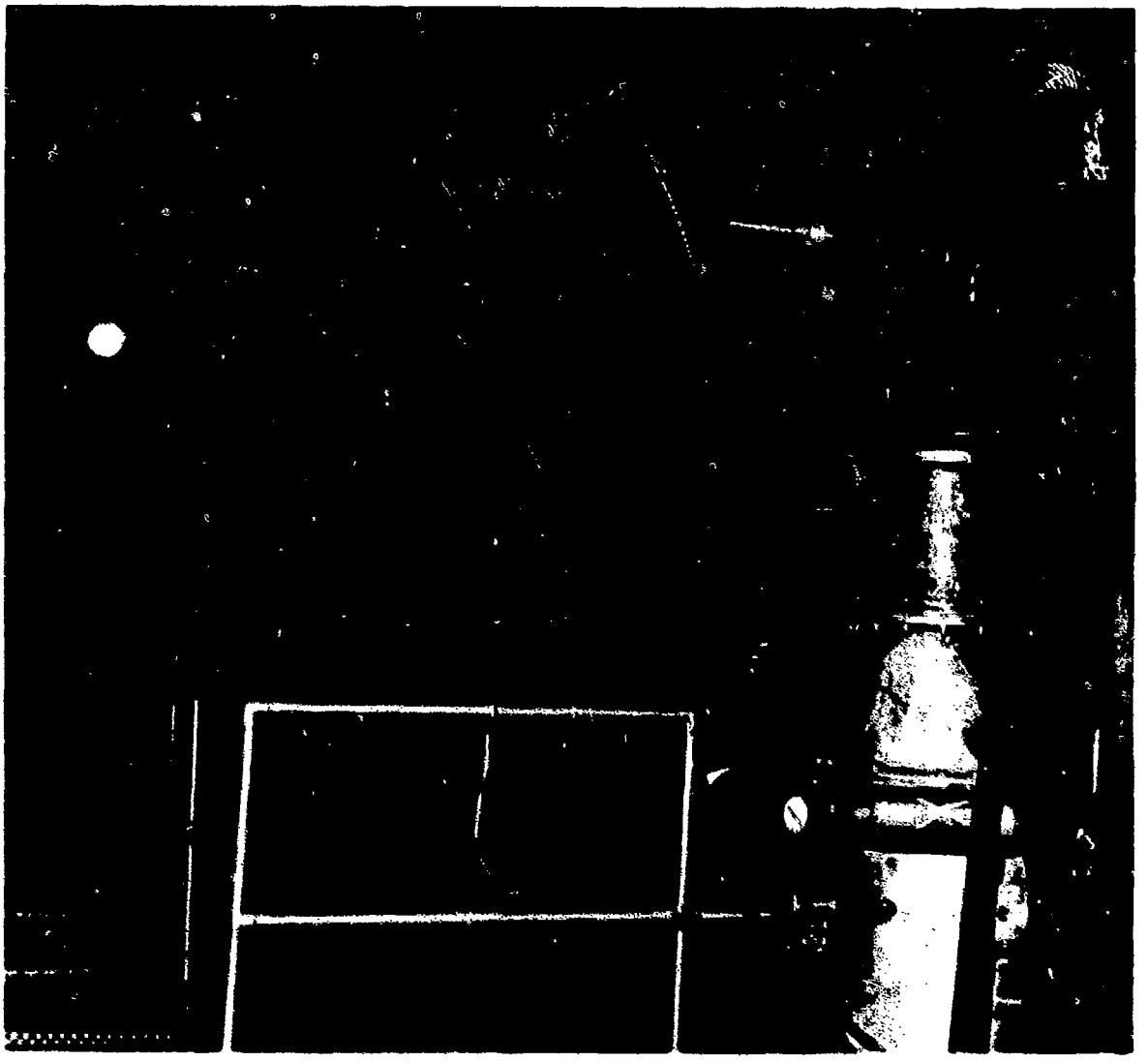

Figure D-8. Set-Up of Reference Microphone and Noise Source for Calibration of 18-inch EM.

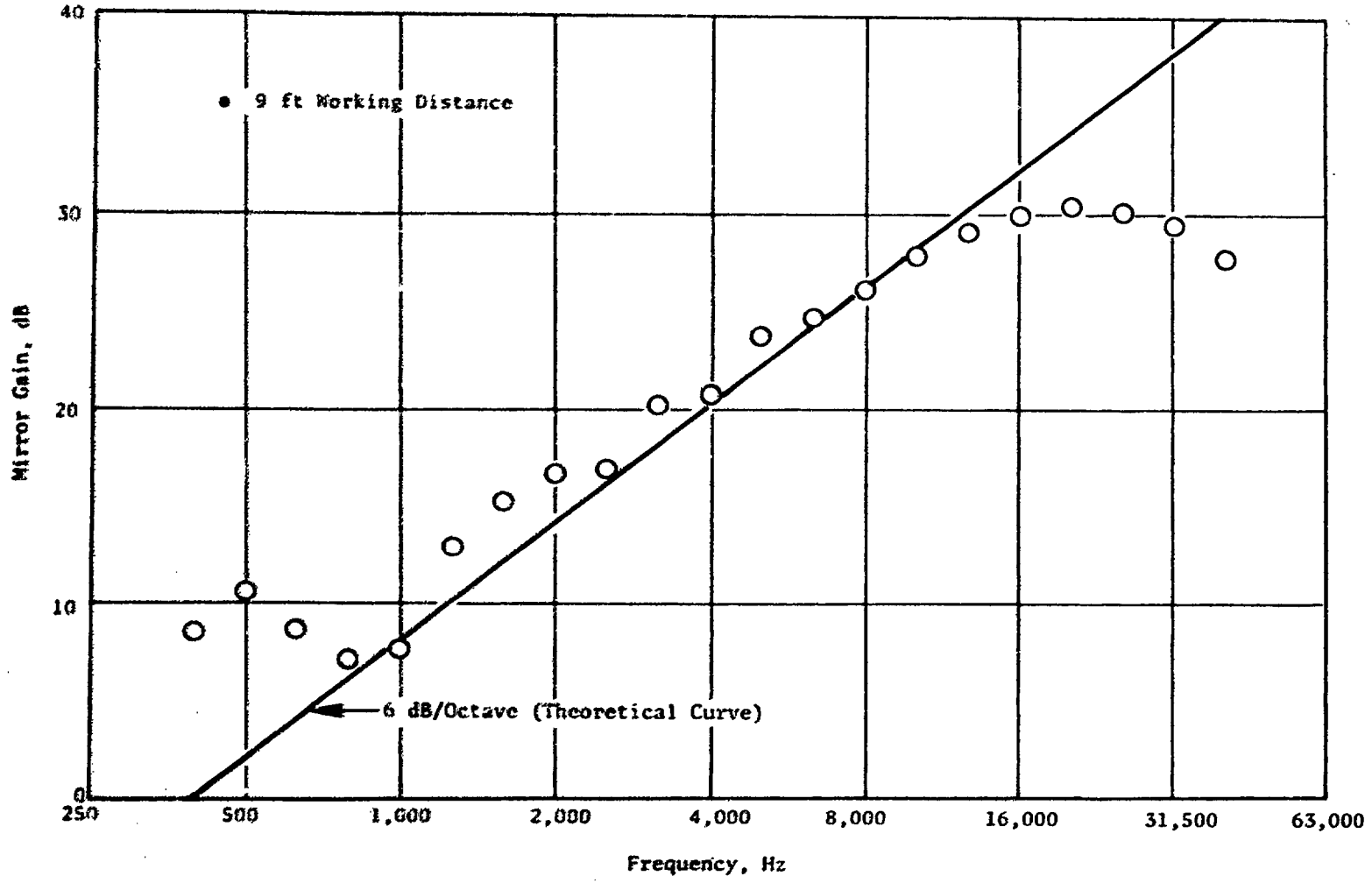

Figure D-9. Gain of the 18-inch-Diameter Ellipsoidal Mirror.

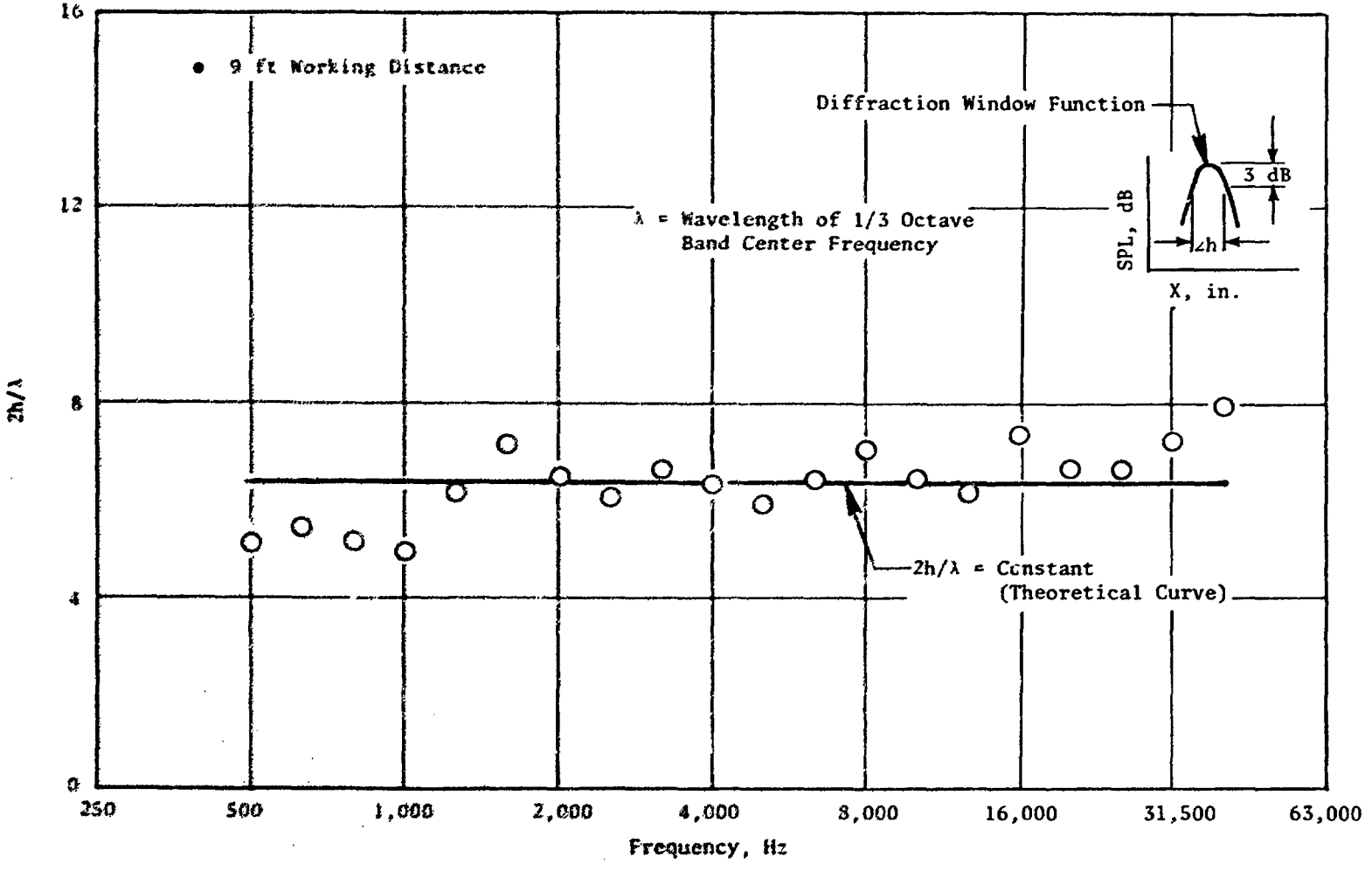

Figure D-10. Normalized Window Function Width for the 18-inch-Diameter Ellipsoidal Mirror.

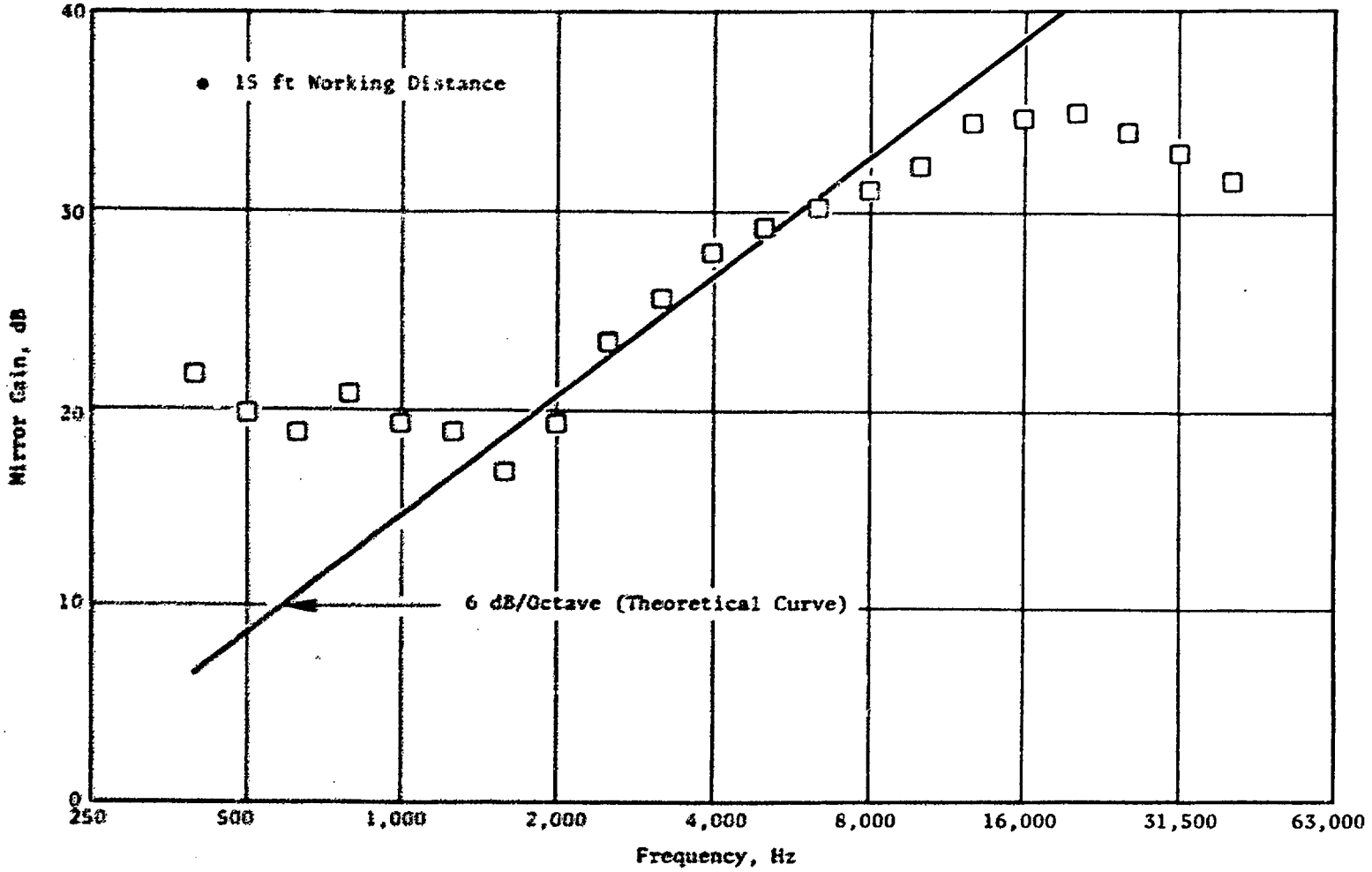

Figure D-11. Gain of the Deep-Dish Ellipsoidal Mirror.

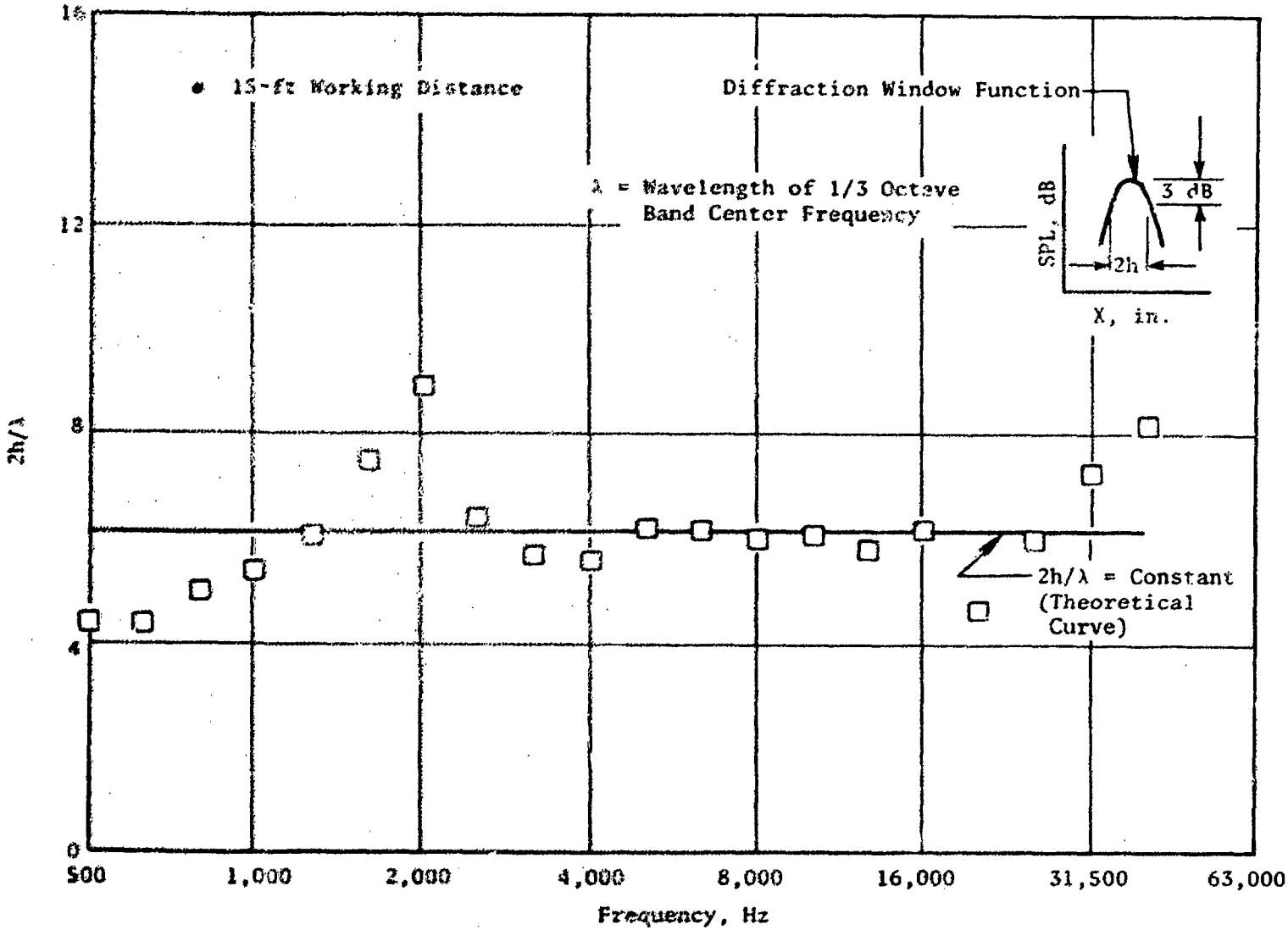

Figure D-12. Normalized Window Function Width for the Deep-Dish Ellipsoidal Mirror.

analog data to digitized spectral distributions. The second step involves numerical processing of these results to correct for the effects of mirror gain and diffraction window function.

1.3.1 One-third Octave Band Analysis

The initial stage of EM data reduction utilizes systems and procedures developed for handling of aircraft flyover noise data in the General Electric Acoustic Van (Figure D-13). The previously recorded EM microphone signal is played back through a Honeywell 7600 28-track recorder, set up for IRIG Wideband Group I operation. The playback signal is processed through a General Radio Model 1921 Real Time Analyzer coupled with a GE/PAC 30 minicomputer and a Terminent 300 printer/tape punch. Accurate event location is possible through the use of a CGS Datametrics SP-425 Time Code Reader and a CGS Datametrics Time Code Comparator.

The data is resolved into twenty-four 1/3-octave bands and averaged over each of eighty consecutive discrete time steps, then digitized and corrected for nonlinear frequency response and gain or attenuation of the data acquisition system. The length of the time steps (integration time) and the frequency range to be covered can be specified, within certain limits, to suit the requirements of a particular test. Integration time, while remaining constant during processing of an individual data point, can be set for 1/8, 1/4, 1/2, 1, 2, 4, 8, 16 or 32 seconds. A relatively short integration time is required for accurate definition of the details of high frequency source regions near the nozzle exit, especially for suppresser nozzles. However, for lower frequencies, a longer time step is generally necessary in order to allow coverage of the entire source region within eighty steps and to assure reasonable accuracy in resolution of the data (Figure D-14). An additional consideration is that the uncertainty in locating true axial source position increases with increasing integration time since data is averaged over this interval. In order to accommodate both high and low frequency requirements, each data point is processed twice, using two different integration times. The exact values are determined from the desired spacing/coverage and the cart speed. Based on the system characteristics shown in Figure 3-17, integration times of 1 and 4 seconds are used for EM data from JENOTS (18-inch mirror), while 2 and 8-second times are used for data from the anechoic facility (deep-dish mirror). The frequency range for data reduction, while not as flexible as integration time, can be regulated. Data can be resolved with twenty-four 1/3-octave bands over a range of 50Hz-10K Hz, 100Hz-20K Hz or 200Hz - 40K Hz. The range of 200Hz - 40K Hz is used for EM data reduction.

During this stage of data reduction, a three-channel brush chart is also prepared for each data point, showing traces of mirror cart position, overall sound level and time code (Figure D-15). Through use of the time code, an average cart position can thus be determined for each of the digitized spectra.

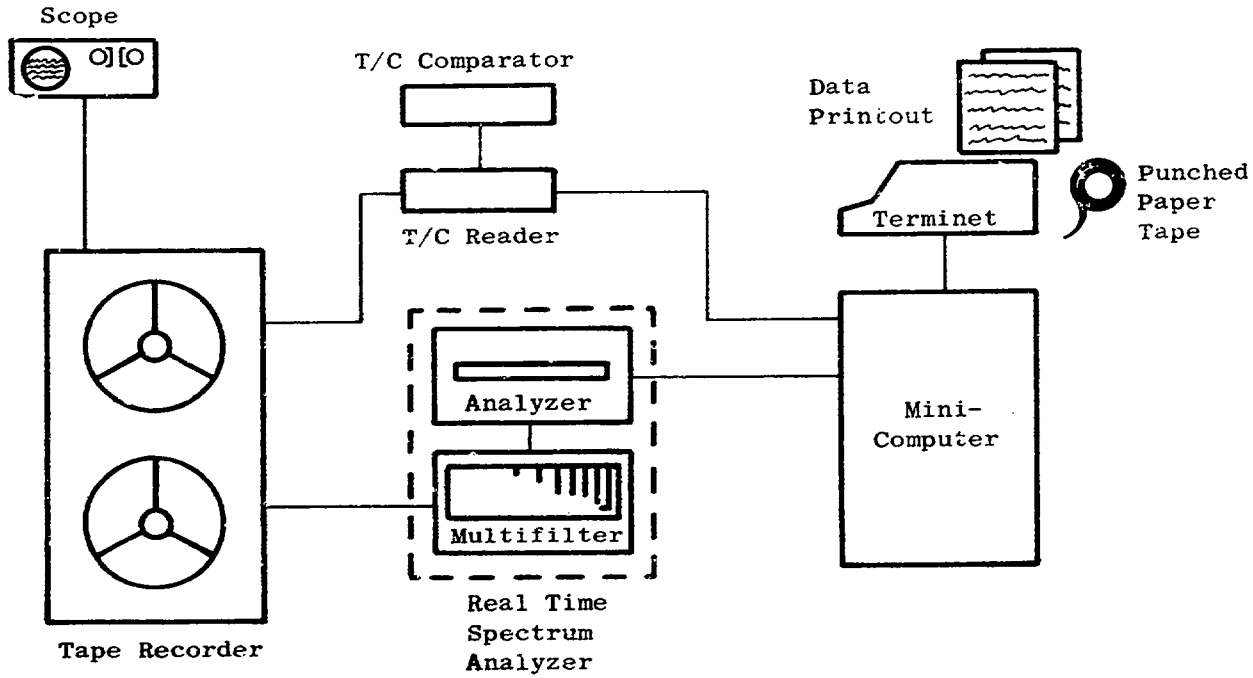

Figure D-13. Equipment Schematic for EM Data Processing - General Electric Acoustic Van.

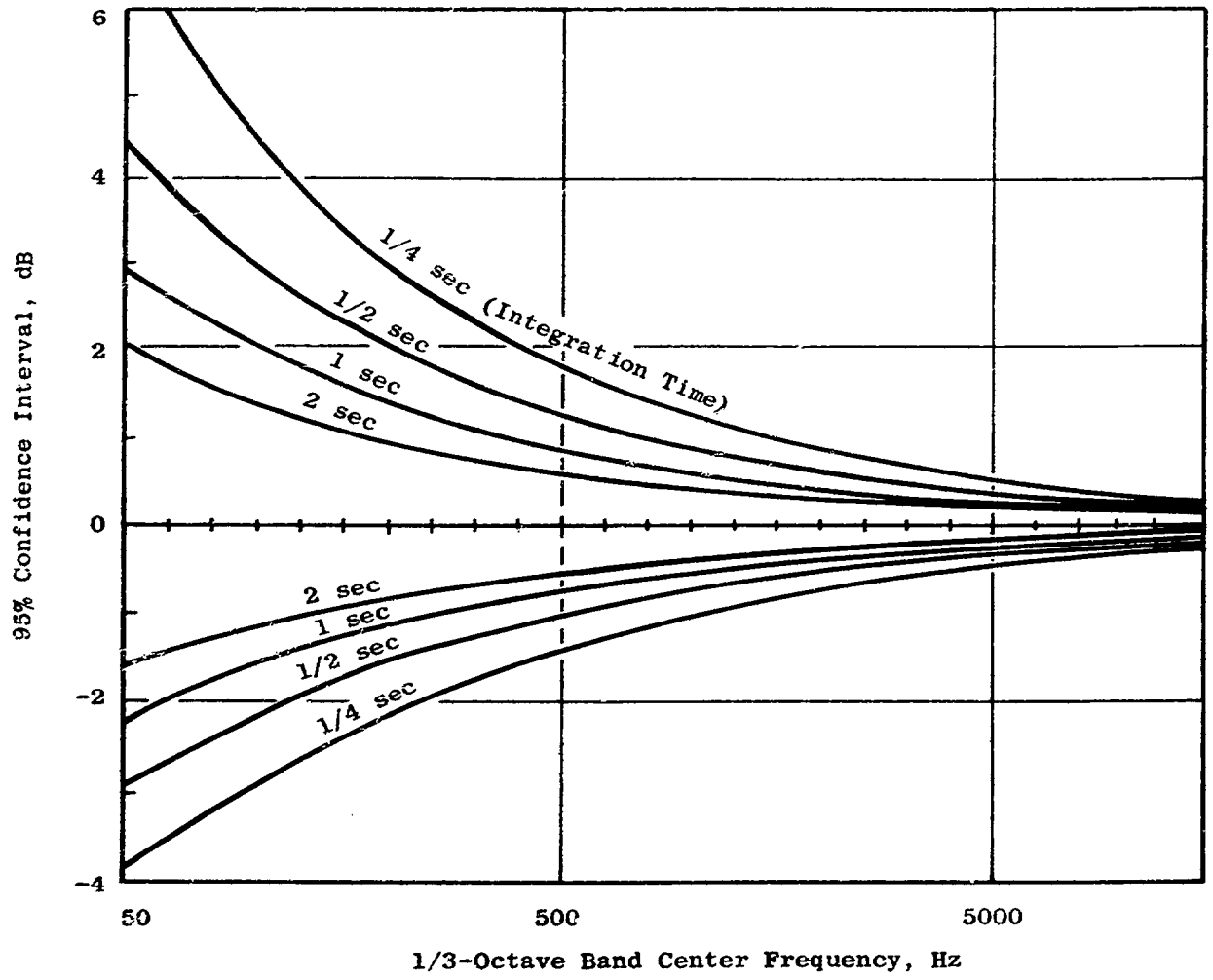

Figure D-14. 95% Confidence Interval Curves as a Function of Frequency and Integration Time.

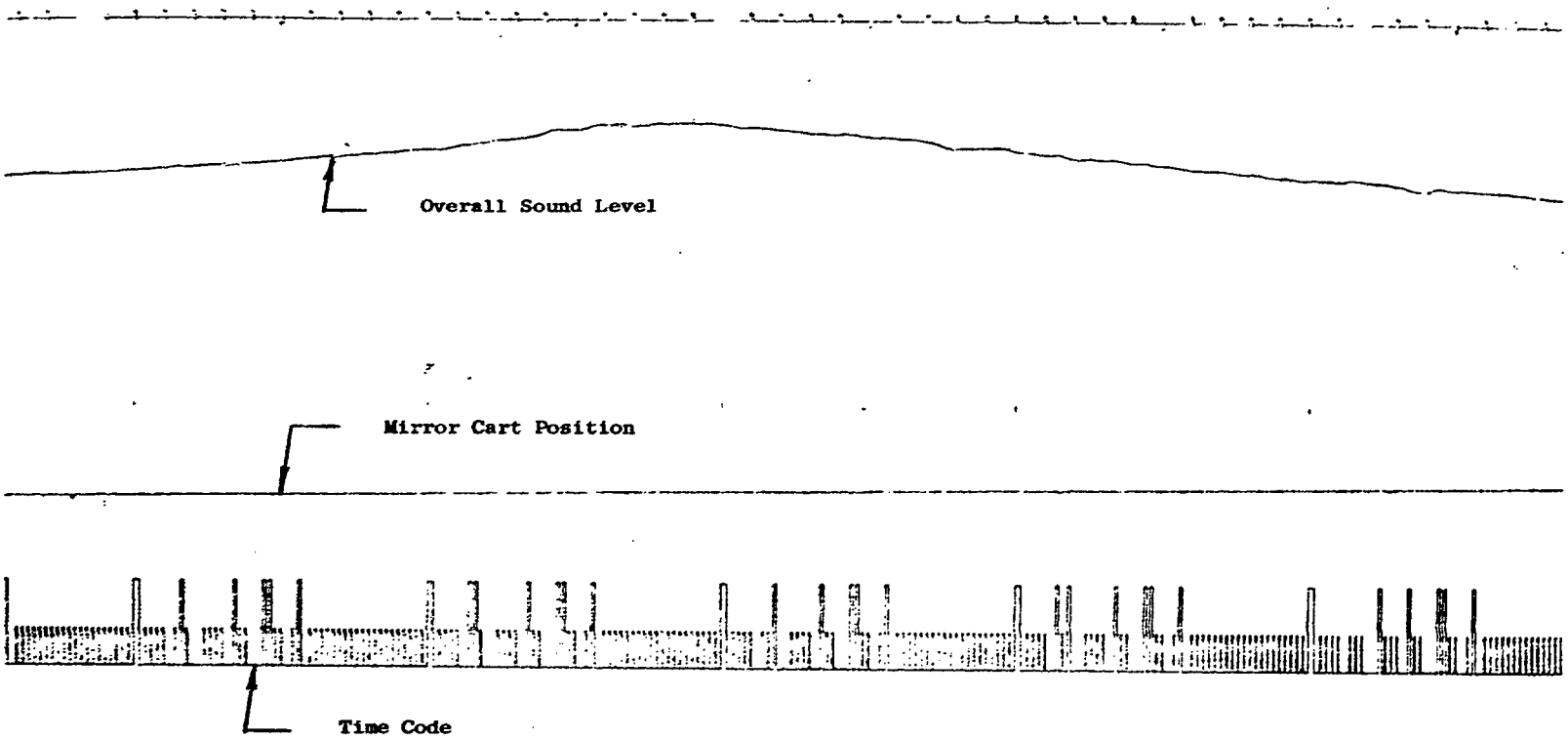

Figure D-15. Typical Brush Chart from EM Data Reduction.

1.3.2 Numerical Processing

The second stage of ellipsoidal mirror data reduction is the "correction" of the digitized source intensity distributions for the effects of mirror gain and diffraction window function.

Noise source intensity distributions obtained with a physical focusing device, such as the EM, are inevitably contaminated at lower frequencies by the effects of wave diffraction. However, if the window functions are known, the true source distribution can theoretically be determined from measurements with the use of a numerical deconvolution procedure. Since diffraction is a three-dimensional phenomenon, sources across the jet cross section, as well as along the axis, can be "heard" when the mirror is focused at a given point on the centerline. Thus, after deconvolution, the distributions represent total source contributions at each axial position (i.e., slice of jet measurements).

Recall that the actual and measured source intensity distributions, in terms of mean square sound pressures, are related by a convolution integral, equation D-1, which is formulated approximately for a 1/3-octave band. Due to the complexity of the problem, a numerical solution is mandatory. This reduces the continuous (in x) physical problem to a system with a finite number of degrees of freedom. In a numerical solution of equation D-1. The definite integral is expressed as the summation of integrals between discrete points within the continuous domain. The integrand is then approximated by a polynomial over each individual sub-range (e.q., trapezoidal rule). This leads to a series of simultaneous linear algebraic equations for each frequency band:

$$m_1 (f) = g (f) \sum_{j=1}^{n} h_{ij} (f) a_j (f) \qquad \text{(D-2)}$$

In tensor notation, this is expressed as:

$$\underline{M} (f) = g (f) \underline{\underline{H}} (f) \underline{A} (f) \qquad \text{(D-3)}$$

where the vectors $\underline{A}$ and $\underline{M}$ represent the actual and measured signals, respectively, at discrete values of x while $\underline{\underline{H}}$ is the matrix of window function coefficients and the scalar g is the mirror gain.

A non-homogeneous set of simultaneous linear algebraic equations has a unique solution only when the equations are linearly independent (i.e., when none of the equations in the set can be expressed as linear combinations of the others). The solution can be expressed as:

$$\underline{A} (f) = \frac{1}{g (f)} \underline{\underline{H}}^{-1} (f) \underline{M} (f) \qquad \text{(D-4)}$$

although solutions are rarely obtained by direct matrix inversion due to the monumental number of calculations required. For a linearly dependent set, the determinant of the coefficient matrix is identically zero and the inverse, expressed as the adjoint matrix divided by the determinant, does not exist. In this case, there is no unique solution, and the matrix is termed singular.

Deconvolution problems which occur in practice are often quite difficult to solve because the systems of equations are ill-conditioned. In this case, the coefficient matrix is "almost singular," with the value of the determinant very close to zero. While solutions exist for these systems, they are extremely sensitive to small changes or errors in the data. Thus, measurement accuracy and choice of a deconvolution technique become critical. An indirect, iterative solution may fail to converge if small successive corrections result in large changes. Direct solutions can fail if accumulated roundoff errors become significant.

The mode of operation of the EM is to make continuous constant-speed traverses parallel to the jet axis. The data is then averaged over each of eighty consecutive, constant time interval, discrete steps. In analyzing results, the integrated spectrum for each interval is assumed to represent the mid-point. Since the cart moves at (approximately) constant speed, the equally spaced time intervals translate to constant axial spacing. Symmetry of the window function and equal spacing of the assumed measurement locations allow the matrix of window function coefficients to be reduced to a form:

$$\underline{\underline{H}} = \begin{bmatrix} h_{11} & h_{12} & h_{13} & \cdots & h_{1\,n} \\ h_{12} & h_{11} & h_{12} & \cdots & h_{1(n-1)} \\ h_{13} & h_{12} & h_{11} & \cdots & h_{1(n-2)} \\ \vdots & \vdots & \vdots & & \vdots \\ h_{1\,n} & h_{1(n-1)} & h_{1(n-2)} & \cdots & h_{(11)} \end{bmatrix}$$

which is symmetric and has equal elements along any diagonal (Toplitz matrix). In this case, the matrix is completely defined by its first row, resulting in considerable simplification of the numerical deconvolution procedure. It is apparent from examination of the simplified matrix that the set of equations will become ill-conditioned as the window function "width" increases relative to point spacing, and the magnitudes of the individual elements approach a common value. This point is illustrated by the following example.

Consider the set:

$$a_1 + 0.9\, a_2 = 1.9$$
$$0.9\, a_1 + a_2 = 1.9$$

The determinant of the coefficient matrix is $|\underline{\underline{H}}| = 0.19$, and the inverse is:

$$\underline{\underline{H}}^{-1} = \begin{bmatrix} 5.26316 & -4.73684 \\ -4.73684 & 5.26316 \end{bmatrix}$$

The solution is $a_1 = 1.0$, $a_2 = 1.0$.

If the equations are altered slightly, to:

$$a_1 + 0.9\, a_2 = 1.9$$

$$0.9\, a_1 + a_2 = 1.899$$

The solution is now $a_1 = 1.00474$, $a_2 = 0.99474$. This is a relatively small change. Now, consider the set of equations:

$$a_1 + 0.999\, a_2 = 1.999$$

$$0.999\, a_1 + a_2 = 1.999$$

In this case, the determinant is $|\underline{\underline{H}}| = 0.001999$ and the inverse is:

$$\underline{\underline{H}}^{-1} = \begin{bmatrix} 500.25 & -499.75 \\ -499.75 & 500.25 \end{bmatrix}$$

The solution is again $a_1 = 1.0$, $a_2 = 1.0$.

It is apparent from the magnitude of the elements of $\underline{\underline{H}}^{-1}$ that any small changes in the right-hand-side terms (response signal) will be greatly magnifie in the solution. Thus, when the equations are altered slightly to:

$$a_1 + 0.999\, a_2 = 1.999$$

$$0.999\, a_1 + a_2 = 1.998$$

the solution is now $a_1 = 1.49975$, $a_2 = 0.49975$.

The major conclusion to be drawn from this discussion is that there is a practical limit to the width of window function which can be analytically "removed" from data. The critical dimension is the ratio of window function width (however defined) to point spacing. Thus, all other things being equal, it is as difficult to correct high frequency data at very close spacing as it is to correct low frequency data at wider spacings. There is no single magic number for the width-to-spacing ratio. Rather, it depends on the

degree of accuracy that is required in the calculation, the magnitude of errors and/or noise in the input data and the solution technique being used. The reported analytical error analysis provides further insight into this question.

A comparative study of numerical techniques for accomplishing the deconvolution of directional microphone data was made by Schlinker, et al. (Reference 30). Three different methods were considered:

1. Integral transform
2. Matrix inversion
3. Relaxation

Based on an evaluation in terms of resolution, sensitivity to noise and amount of computation, the relaxation procedure was found to be superior to the other techniques. Following a review of the results and recommendations of this study, the relaxation technique, which is actually an adaptation of the classical point Jacobi iterative method for solution of simultaneous linear algebraic equations, was chosen for use in processing source location data obtained with the ellipsoidal mirror.

The initial applications of relaxation to EM test data resulted in rather severe problems with non-converging solutions, for most frequency bands, due to ill-conditioning of the equations. In response to these problems, the solution algorithm was modified to limit the magnitude of corrections from one iteration to the next and to stop the iteration if and when the solution began to diverge. The incorporation of these modifications resulted in somewhat better convergence, although solutions still contained a relatively high degree of scatter. Another change was made by including a generalized relaxation factor in the iterative correction term. This allowed a solution to be obtained by over- (or under-) relaxation, if desired.

Since deconvolved data still exhibited a high degree of scatter, despite improvements made to the relaxation algorithm, alternative procedures were considered. A direct solution technique was discovered during the course of the error analysis, Appendix E. This method, due to Levinson (Reference 31), is applicable to symmetric, positive definite Toplitz matrices. Although the window function matrix is symmetric and Toplitz, it is not necessarily positive definite, even though all of the elements are positive. However, the potential savings in computation and the advantages of an "exact" solution suggested that this approach should be considered. A somewhat more efficient formulation of Levinson's recursion algorithm, presented as a FORTRAN subroutine in Reference 31, was evaluated after a coding error (in Reference 32) was found and corrected. The evaluation revealed that the technique did indeed require less computation than relaxation, while apparently producing much more accurate solutions. The latter fact was determined by "reconstructing" input data using equation D-3 from the known mirror gain and window function in combination with the deconvolved solution from each method. The actual input data was then compared with the two sets of "reconstructed"

data. However, it was found that solution obtained with the Levinson technique contained significantly more scatter than was found in solutions obtained by relaxation. Thus it became apparent that scatter was at least partially due to small fluctuations in the input data, which were magnified by the deconvolution, rather than just being the result at a non-converging solution. This meant that it should be possible to obtain more meaningful results by increasing point spacing to reduce the degree of ill-conditioning, or by applying a pre-smoothing procedure to lessen the impact of errors and/or noise in the input data.

Data which has been properly smoothed will be less influenced by random errors and should more nearly represent the underlying trends then will raw data. Thus, pre-smoothing of measured data can be expected to significantly reduce the scatter in deconvolved source distributions. It should be noted, however, that this is not a magic cure for "bad" data and that care must be exercised to avoid the loss of important details due to indiscriminate smoothing. Rather than being a standard procedure, smoothing should be used only when needed and when the point specifically required to desensitize the deconvolution with respect to small changes in data is too large for satisfactory definition of the measured distribution.

When the point spacing of sample EM data was doubled by averaging (combining) adjacent points, the slight improvement in scatter did not warrant the resultant loss of definition. Therefore, a study of smoothing procedures was undertaken. Source location measurements are resolved into 1/3 octave band spectra for several successive time steps, each step representing a discrete axial position in the jet. This spectral information is then recast as axial power distributions for given frequency bands. At this point the data is converted from dB to mean square sound pressure. It is these distributions of P^2 versus x which must be smoothed.

There are several techniques available which could be used for pre-smoothing. In Reference 30, for example, data is numerically convolved with a smoothing operator prior to processing. Although such an approach would appear to merely result in the substitution of an analytical window function for the physical one, this type of procedure was nevertheless considered. However, an evaluation of the technique failed to show any significant lessening of scatter in the data. A great many smoothing techniques use some form of least squares estimation. A common approach is to fit a polynomial of relatively low degree (say a parabola) to a set of $2N + 1$ data points (= five or seven). The ordinate of the approximating polynomial curve at the central point of the set is then taken as the new "corrected" value of that data point. Successive applications of this procedure, accomplished by indexing the set through the data one point at a time will result in a smoothed distribution. Further smoothing can be achieved by repeating the entire process. This technique was evaluated with over a dozen combinations of the three parameters:

1. Degree of the least squares polynomial
2. Number of points in the set
3. Number of passes through the data.

The results of this evaluation showed very significant improvements in scatter. The addition of increased point spacing, in combination with smoothing, did not have an appreciable effect. From the viewpoint of mathematical rigor, presmoothing is not a desirable step. However, as a practical matter, smoothing can be a useful technique for removing the effects of random errors from a set of data, and, in this way, can enhance the fidelity of deconvolved solutions. Also, the small changes in dB levels resulting from limited smoothing of the P^2 distribution seem almost insignificant when compared to the potential magnitude of measurement and sampling errors.

The studies of smoothing and deconvolution techniques have led to the adoption of improved data reduction procedures. The best results have been obtained using 2-7-3 least-squares smoothing (second degree polynomial, seven points, three passes) in combination with the modified relaxation method. It has been found that, for the smoothing techniques under study, application of the Levinson technique still results in an acceptable level of scatter. It is considered preferable to use relaxation with least-squares smoothing, rather than attempting more extensive smoothing for use with the Levinson procedure.

1.4 DATA ANALYSIS

Ellipsoidal mirror data can be interpreted as axial source intensity distributions for individual 1/3 octave bands, or as source spectra at discrete axial positions. The results are most readily summarized in terms of the axial location of the peak intensity for each frequency band. This is generally expressed by relating Strouhal Number (center frequency normalized by jet diameter and velocity, fD/V) to normalized axial position (x/D). Trends in the data can then be established by comparison of the summary plots between different nozzle configurations or operating conditions.

A typical data point for a conical converging nozzle was chosen for detailed examination as an illustration of EM data analysis. The sample case is a 3.56" conic nozzle operating statically at a velocity at 2253 ft/sec. This data was obtained on the JENOTS freejet facility with the 18-inch mirror, at a traverse speed approximately four times the value shown in Table 3-17. The data was processed at both 1/8 and 1-second integration times and deconvolved using 2-7-3 smoothing and modified relaxation. The data obtained with 1/8-second integration time is used to determine high frequency source distributions, while the 1-second data is used for low frequencies. The "dividing line" between the two is defined, case by case, from the results of the integral closure test. Far-field noise signatures are calculated from the two measured source distributions, and these predictions are then checked against actual farfield data to determine which gives the best results. The integral closure results (Figure D-16) indicate that the 1-second data should be used over the range 1 to 20 kHz.

Figures D-17 through D-20 show axial power distributions, obtained from 1-second integrations, for 1/3 octave bands centered at 16, 6.3, 2.5, and 1 kHz, respectively. In all four figures, the raw data and processed data,

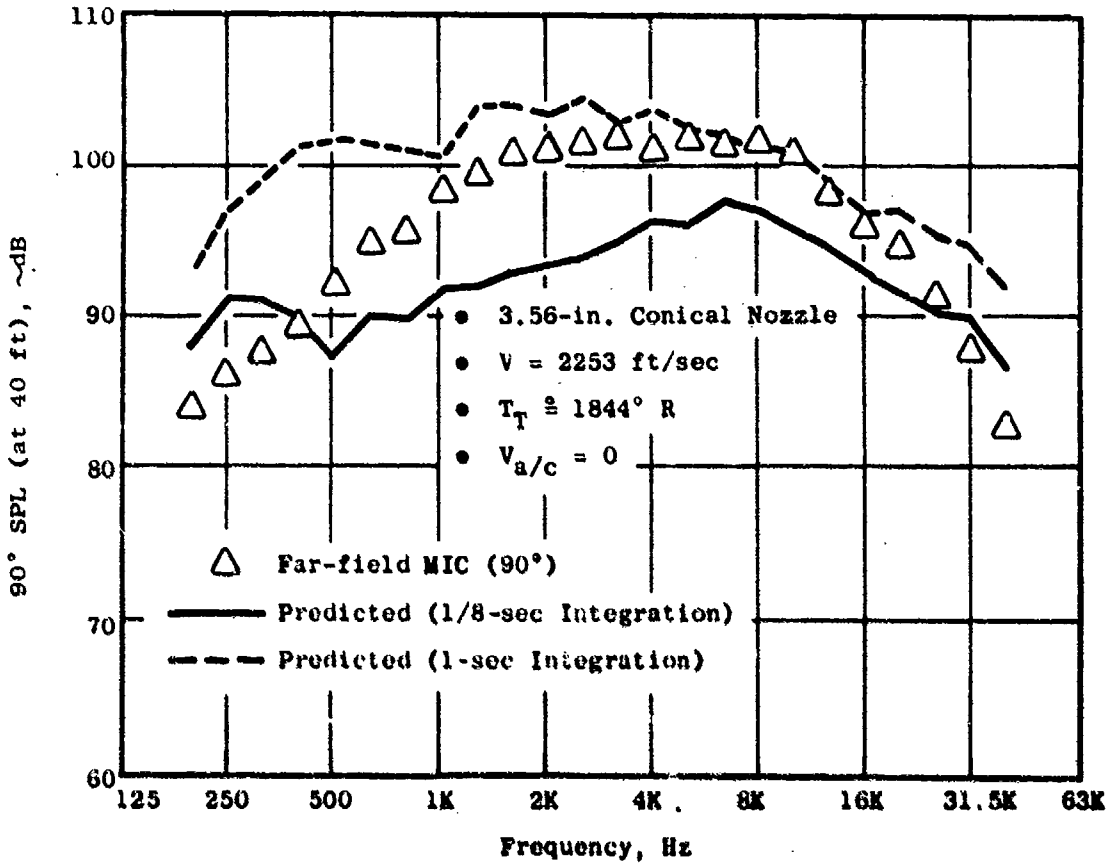

Figure D-16. Integral Closure Check for 3.56-Inch Conical Nozzle, V = 2253 ft/sec, $V_{a/c} = 0$.

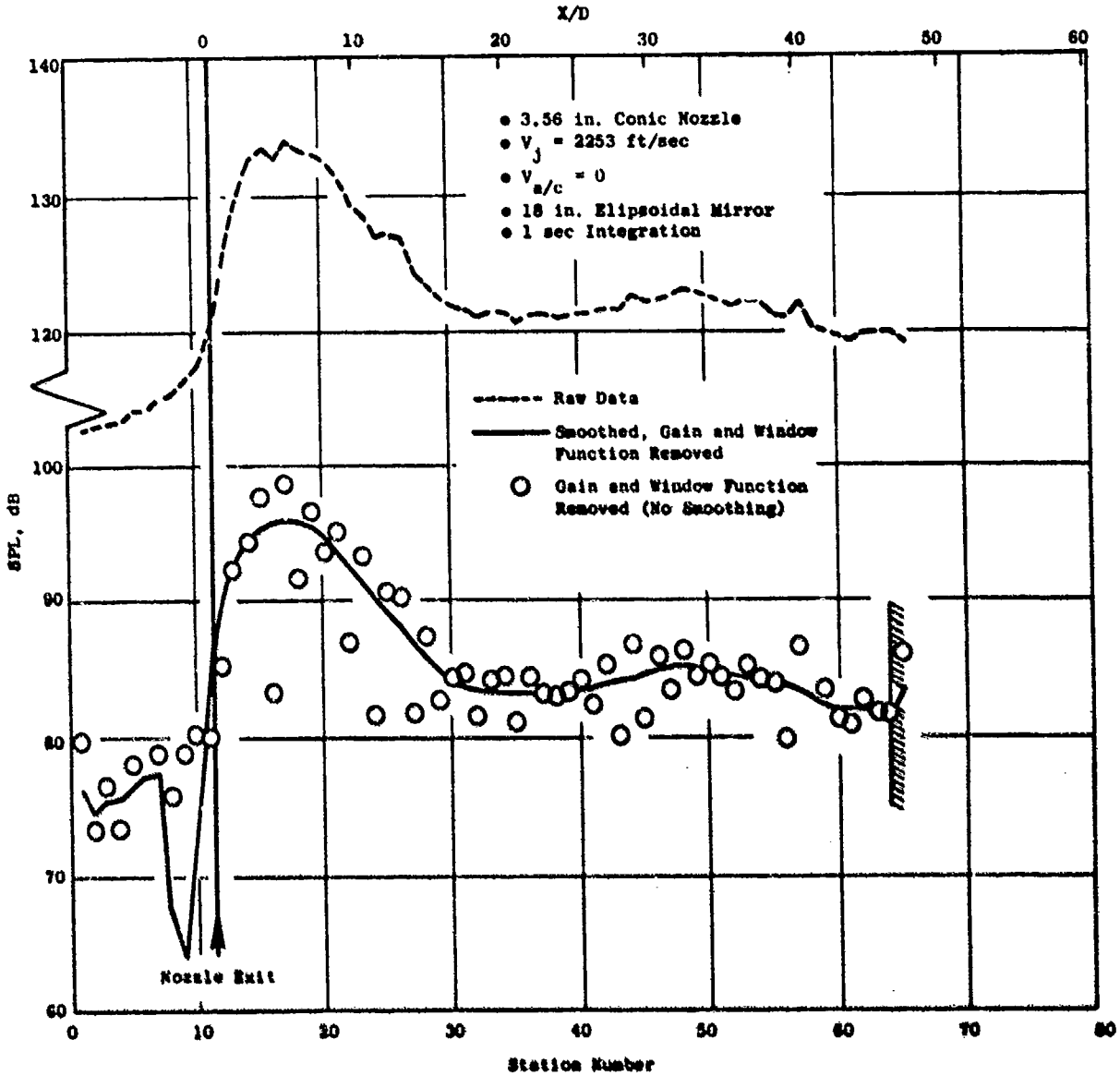

Figure D-17. Axial Distribution of Sound Source Intensity (16,000 Hz, 1/3 Octave Band).

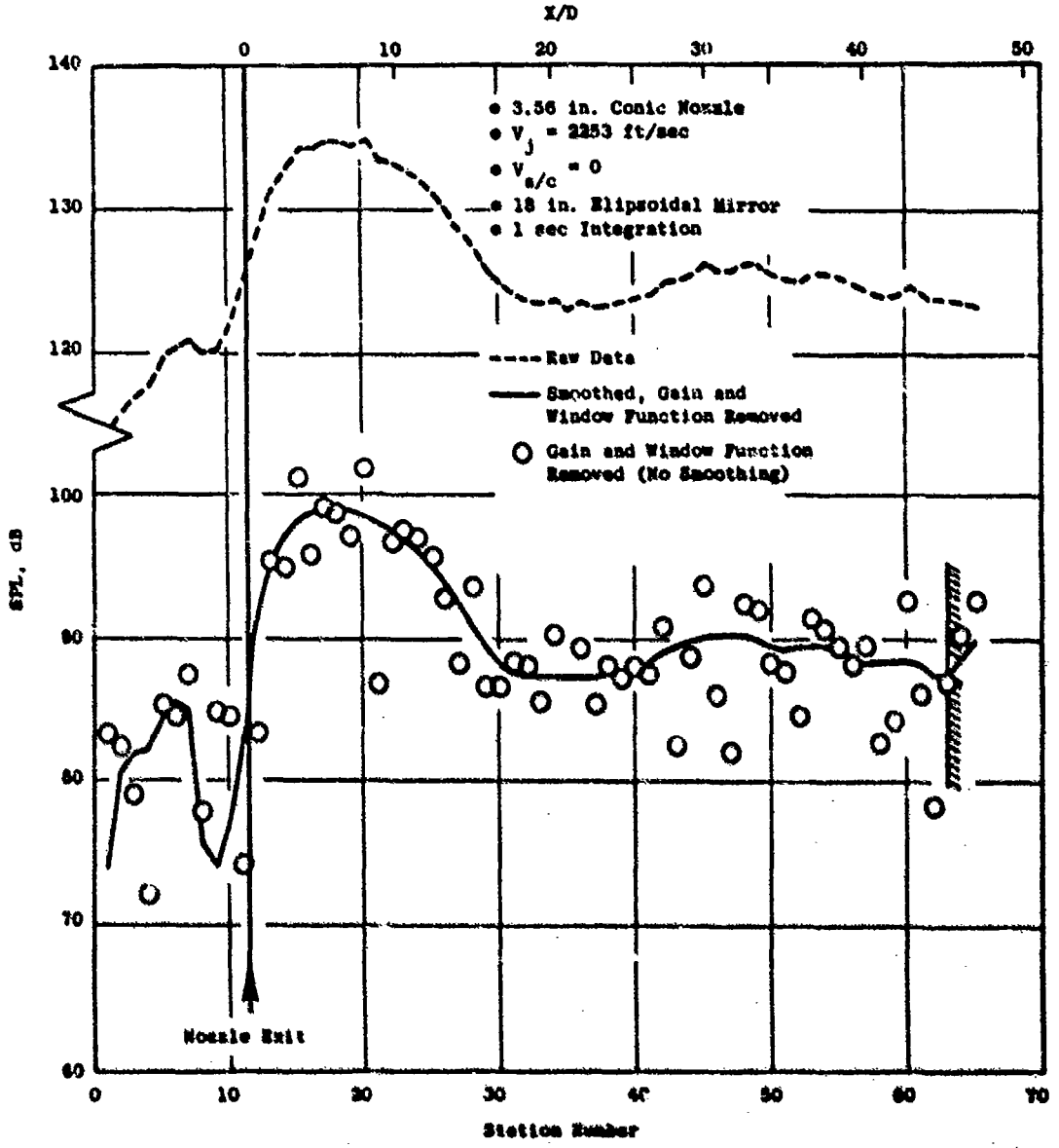

Figure D-18. Axial Distribution of Sound Source Intensity (6300 Hz, 1/3 Octave Band).

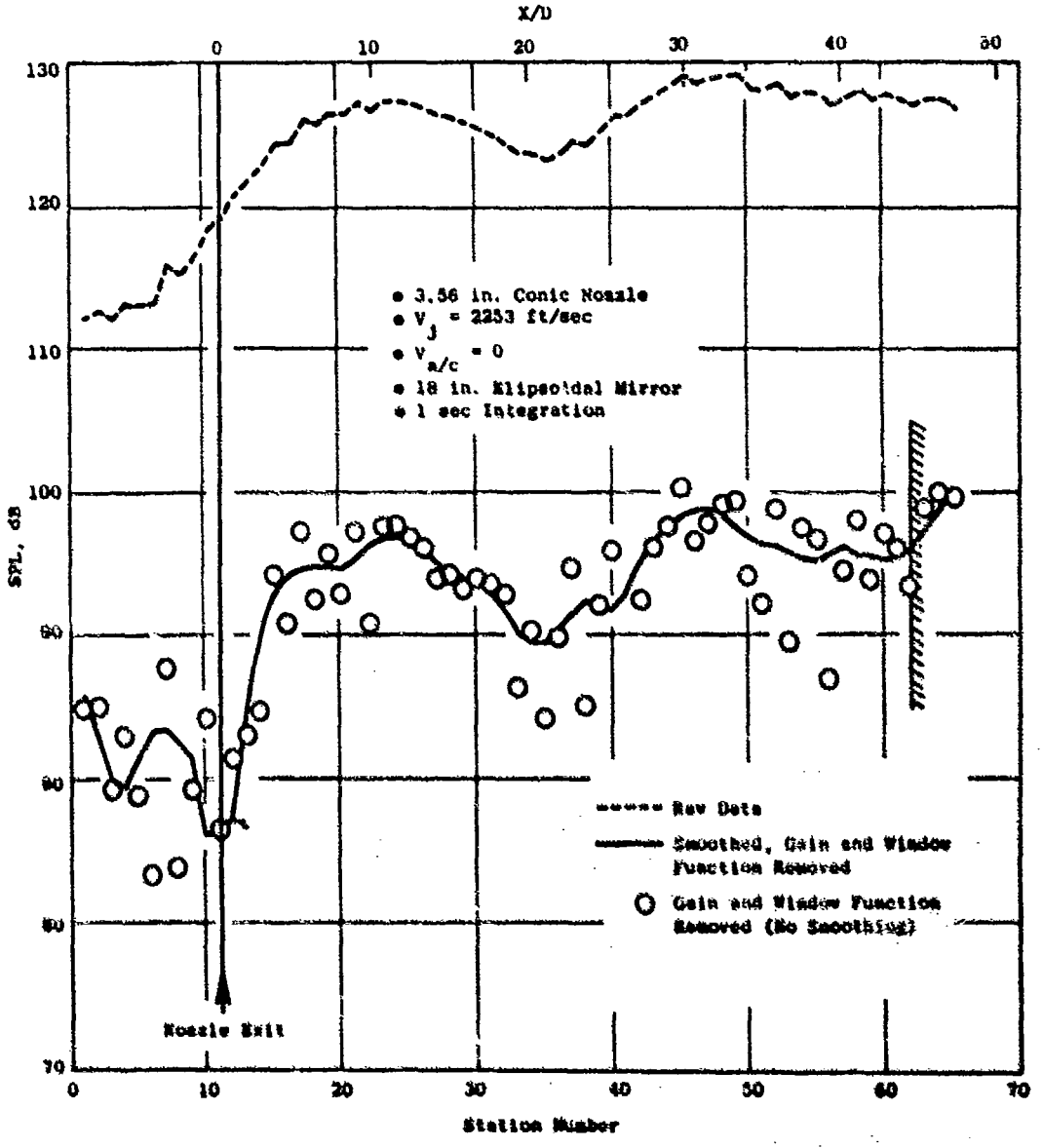

Figure D-19. Axial Distribution of Sound Source Intensity (2500 Hz, 1/3 Octave Band.

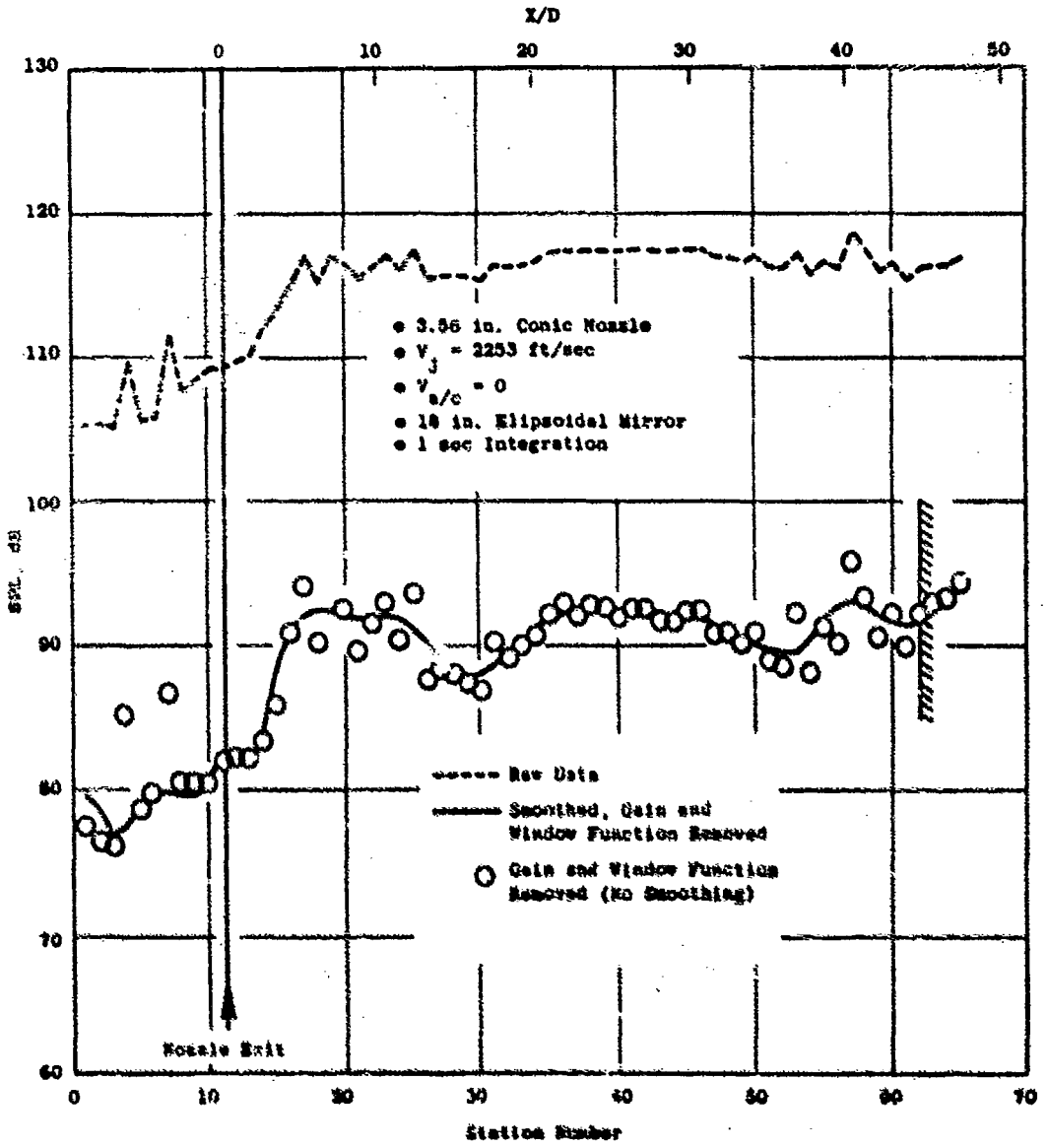

Figure D-20. Axial Distribution of Sound Source Intensity (1000 Hz, 1/3 Octave Band).

with and without presmoothing, are shown. The presmoothed data are seen to contain very little scatter, while retaining the basic trends of the unsmoothed data. As expected, the deconvolved distributions differ from the "as measured" distributions only in level, at higher frequencies, while the shapes of the curves are noticeably different at the two lowest frequencies. There are two distinct source regions apparent in the axial power distributions. At higher frequencies, the upstream region is dominant. With decreasing frequency, the peak source location (in the upstream region) moves downstream and the region broadens somewhat. At the same time, the downstream region is increasing in intensity to the point where the two sections are of approximately equal importance, with the downstream region barely dominant (Figure D-19). This phenomenon explains the seemingly discontinuous shift of the peak location to a high X/D at low frequencies (Strouhal numbers) in Figure D-21, which shows the peak and "3 dB down" curves for this case. It is interesting, and perhaps important, to note from Figure D-21 that the source intensity is still within 3 dB of the peak at X/D greater than 40 for Strouhal numbers below 0.4. The fictitious upturn at the "tail end" of the deconvolved source distributions (Figures D-17 through D-20) also results from the presence of additional sources downstream of the last measurement location. These indications of the sizable extent of the noise-producing region could have significant impact on practical, as well as theoretical, considerations of jet noise.

Typical spectra in the upstream and downstream source regions are shown in Figures D-22 and D-23, respectively. Each figure shows the "as measured" spectrum, as well as the deconvolved spectrum, with and without presmoothing. Also shown is the spectrum after smoothing and removal of mirror gain, but before deconvolution. Reductions in scatter in the deconvolved spectra, due to presmoothing, are obvious. These figures also illustrate the relative effects of mirror gain and window function on measured source spectra. Mirror gain increases with frequency (approximately as f^2) while an apparent gain due to the window function has a reciprocal trend. Thus, it is necessary to make both corrections in order to obtain unbiased spectra.

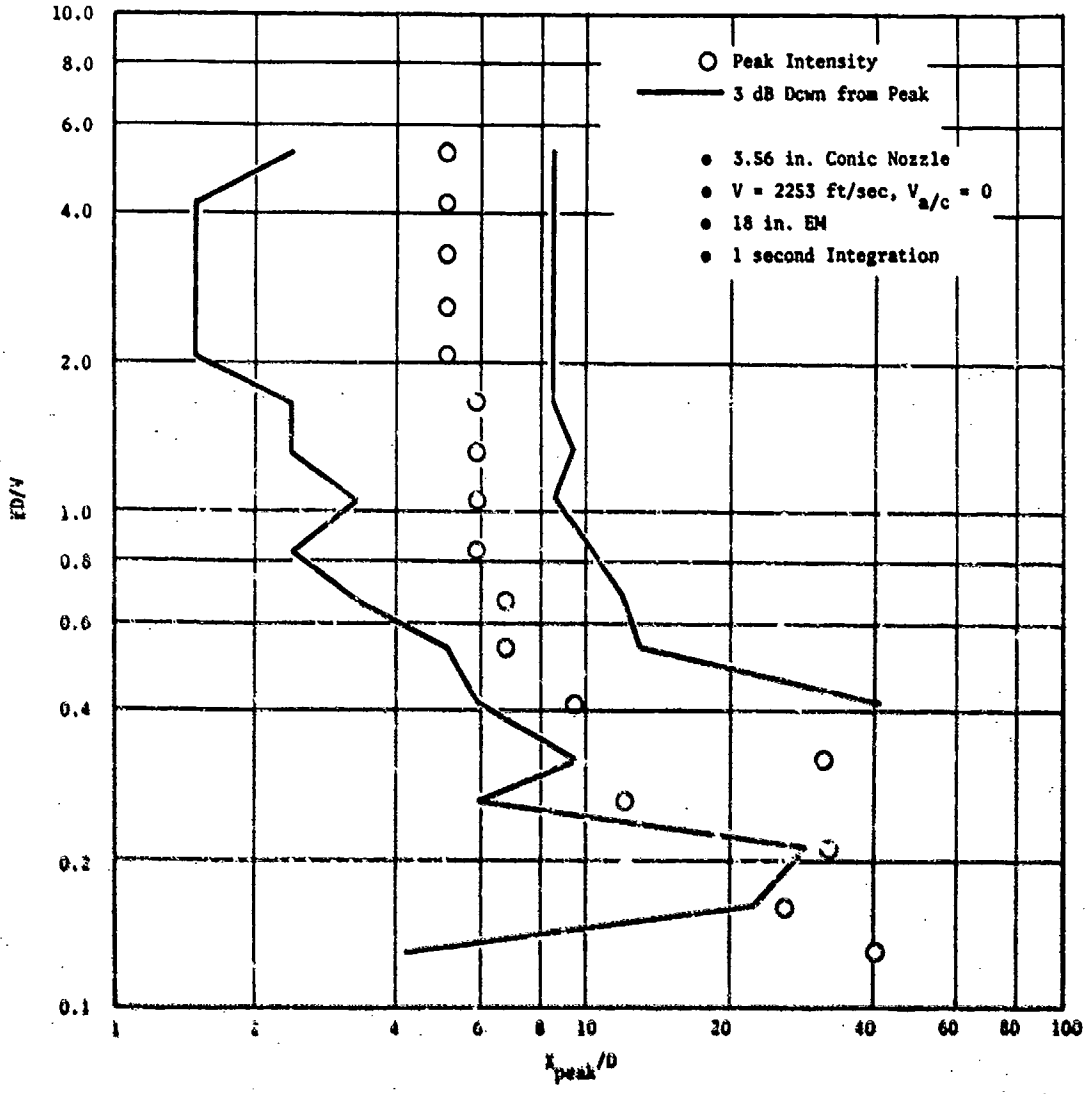

Figure D-21. Axial Location of Peak Sound Source Intensity.

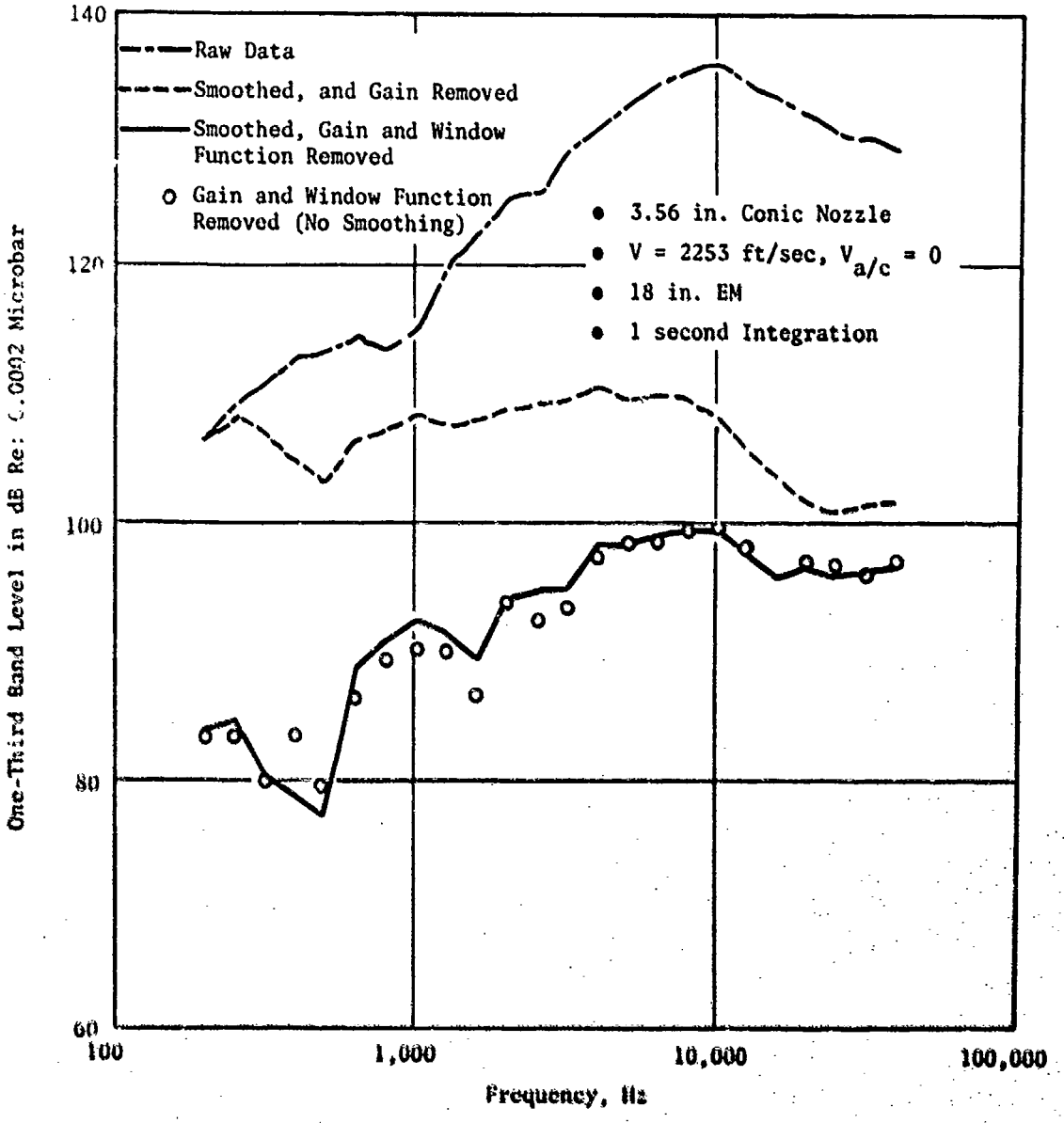

Figure D-22. Source Spectrum at Station 18 (x/D = 5.9).

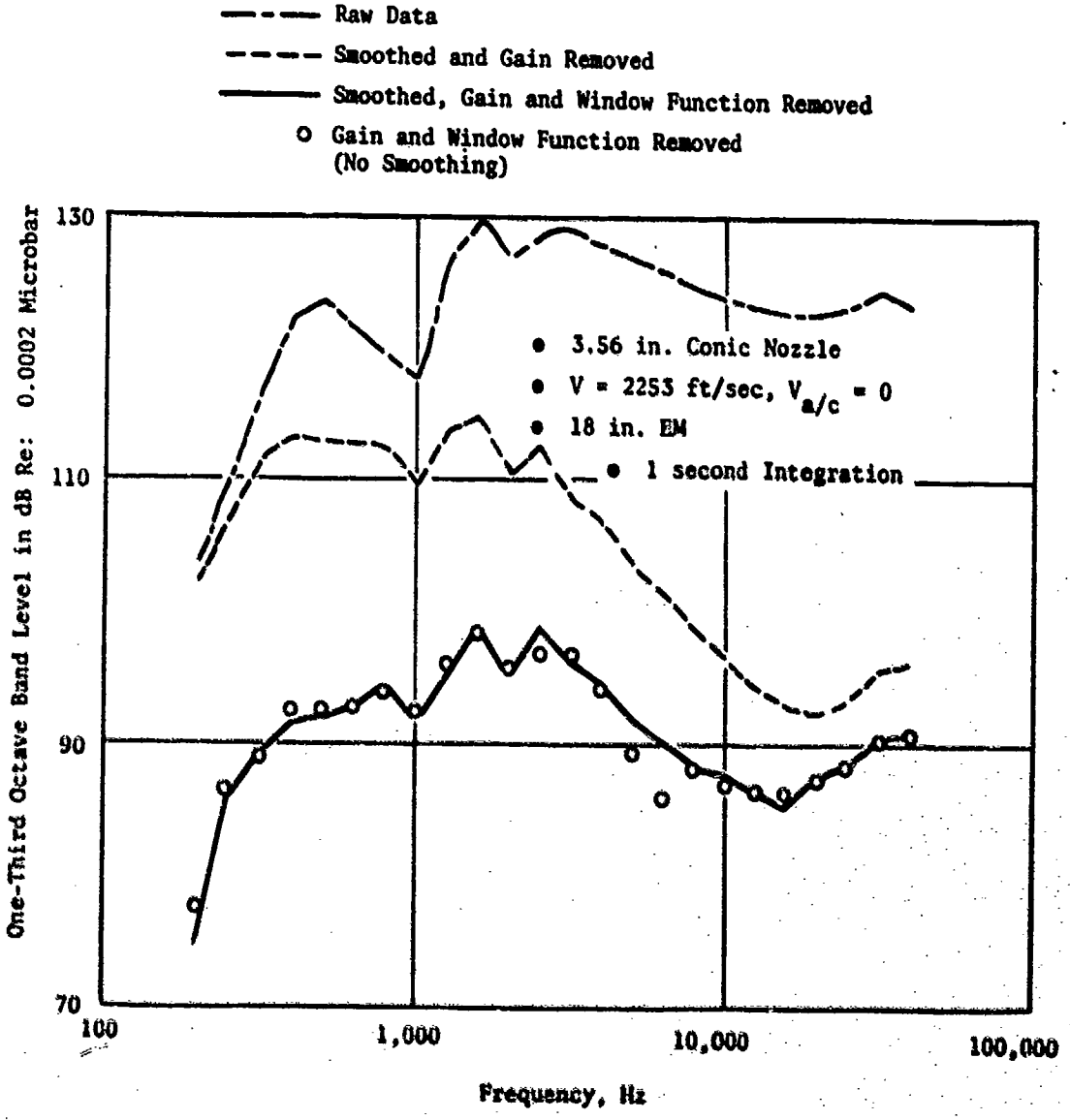

Figure D-23. Source Spectrum at Station 46 (x/D = 30.6).

2.0 EVALUATION OF THE EM TECHNIQUE

As in the case of any measurement system, it is necessary to assess the potential limitations and sources of error in the application of the ellipsoidal mirror technique. These can be separated into three distinct areas:

1. Theoretical limitations
2. Data acquisition errors
3. Data processing errors and limitations

In the realm of theoretical limitations, there are several items to be considered. Since the EM senses farfield acoustic radiation, measurements are affected by propagation phenomena such as convection, refraction, and turbulence scattering. Thus, even though these effects are minimized by alignment of the mirror axis normal to the jet (source) axis, it is still only possible to define "apparent" source distributions. In addition, there are limitations to the range of frequencies over which the EM provides meaningful data. These are dependent on the exact physical characteristics of the system in use. There are two potential limits at low frequencies. One occurs when the ratio of working distance to wavelength falls too low and the mirror is operating in the acoustic nearfield. The other occurs when the ratio of aperture diameters to wavelength falls too low and the mirror is unable to focus incoming waves. At high frequencies, the system is limited by microphone frequency response/directivity and by the dimensional tolerances at the mirror. The latter limit is reached when deviation from either the theoretical mirror surface contour or the focal point location become appreciable fractions of wavelength. It should also be noted that, since the width of a 1/3 octave band is proportional to the contour frequency, the formulation of equation D-1 in terms of 1/3-octave bands may not be a valid approximation at higher frequencies due to the large bandwidths.

In addition to the real or potential problems generally associated with acoustic data acquisition, there are particular sources of error associated with the mode of operation of the EM. As described in Section 1.1, measurements are made while the mirror is slowly traversed parallel to the jet axis. In data reduction, the signal is resolved into 1/3 octave bands, averaged over discrete time steps and digitized. Since the EM is moving during these time steps, the digitized spectra represent averages over some distance. This limits the resolution capability of the mirror to the width of an individual time step. Since the averaging time must be long enough to allow for extraction of a statistically valid sample (Figure D-14), this distance can be decreased only by a reduction in the traverse speed. Mirror misalignment and improper location of the microphone (relative to the primary focal point) are also potential sources of error during data acquisition. If the mirror axis is not normal to the jet axis, the window function is affected, becoming increasingly skewed as the mirror is tilted. Similarly, the measured data is distorted if the microphone is not properly located at the focal point.

The major sources of error encountered in processing EM data are:

1. Statistical errors due to insufficient averaging time.
2. Enhancement of ambient or electronic noise, or of statistical measurement errors, due to an ill-conditioned window function matrix.
3. Limits on achievable resolution due to numerical instabilities in the solution of an ill-conditioned set of equations.
4. Errors induced by uncertainty in window function measurements.

A discussion of these errors is included in Appendix E, along with some simplified numerical examples.

2.1 INTEGRAL CLOSURE TEST

An important test of a source location technique is to see if a measured farfield noise signature can be calculated from the measured source distribution. This test, referred to as integral closure, does not guarantee that the source measurements are correct since a given farfield signature could be generated by any of a number of different source distributions. However, it does provide some confidence in the results and can be used to identify ranges of variables for which a given technique is definitely not valid. For example, the results of integral closure checks on EM measurements reported in Reference 12 showed that it is an extremely valuable tool for determining the proper choice of integration time and for evaluating the range of frequencies over which the EM appears to yield valid source location data.

The farfield signal is predicted by logarithmically summing (integrating) the deconvolved source intensities (dB per unit length) over the length of the jet for each 1/3-octave band, after inverse square law and air attenuation adjustments have been made to correct the data to standard day conditions at the desired farfield position. The formulation of Reference 33, with an extrapolation to frequencies above 10 kHz, is used to calculate air attenuation corrections. The 90° farfield microphone is always chosen for closure checks since measurements at this location are known to most accurately reflect source generation mechanisms.

An integral closure check of 18-inch mirror measurements on a conical converging nozzle was illustrated in Figure D 16. Although results vary from case to case, the overall conclusion drawn from integral closure checks is that, as a minimum, the deconvolved source distributions generally appear to be valid over the following range of frequencies:

Mirror	Frequency Range
18" shallow-dish	1 kHz $\leq$ f $\leq$ 20 kHz
34.654" deep-dish	500 Hz $\leq$ f $\leq$ 10 kHz

2.2 POINT SOURCE EXPERIMENT

The measurement of a point source is a critical test for any noise source location technique, since the results can be used to infer the accuracy of the method in defining discrete sources and in discriminating among adjacent distributed sources. Although the window function width indicates the inherent resolution of a particular device, it is possible to enhance this capability with the use of numerical deconvolution procedures. Thus, the performance of a given source location technique is strongly dependent on the adequacy of the data processing routines. In the idealized case where a closed form solution of equation D-1 is possible, the function representing the measured point source distribution is resolved identically to a Dirac delta function, which is the analytical representation of a point source. However, a numerical solution will only yield an approximation to this result. The width of this deconvolved distribution is an accurate measure of the resolution of the technique.

An evaluation of the ellipsoidal mirror technique was made, using data obtained during calibration testing of the deep dish mirror (Section 1.2). The measured 1/3-octave band source distributions were first fitted with least-squares polynomial curves to reduce the influence of random measurement errors. The modeled data were then deconvolved using a modified relaxation. Typical results, for the 4KHz 1/3 octave band, are shown in Figure D-24. Note the relatively minor adjustment of measured data points due to the introduction of the polynomial model. The deconvolved distribution, while not a delta function, shows a marked improvement in resolution relative to the "raw" data. The overall results, illustrated in Figure D-25, indicate that the achievable resolution is an approximately constant fraction of wavelength. The point source can be located (within 3 dB) with a tolerance of ± 0.6 λ. While this is a five factor of improvement over the unprocessed results, it is not indicative of a precise measurement. For example, at 1 kHz, the error band is approximately ± 8 inches. The numerical study of the 18" mirror, which was conducted as part of the error analysis (Appendix E), indicates that it should be possible to achieve significantly better resolution than this with the proper numerical procedures. This indicates a need for further study to identify and implement a better numerical technique for deconvolution of ellipsoidal mirror data. It should also be noted here that it is still important to optimize a mirror design for a narrow window function, since, as a practical matter, precise numerical deconvolution is difficult to accomplish.

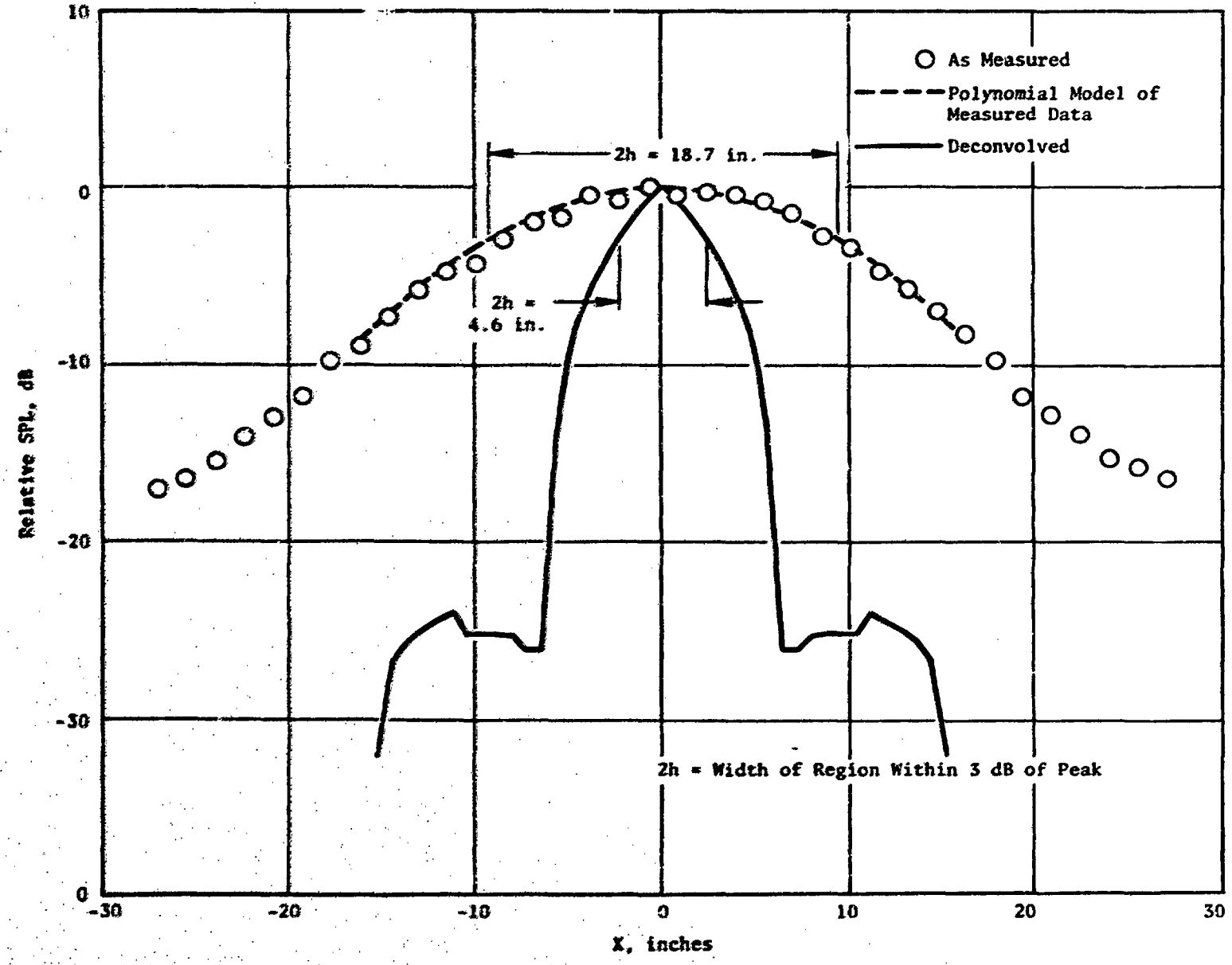

Figure D-24. Resolution of the Deep-Dish Ellipsoidal Mirror (Point Source Measurement), 4000 Hz.

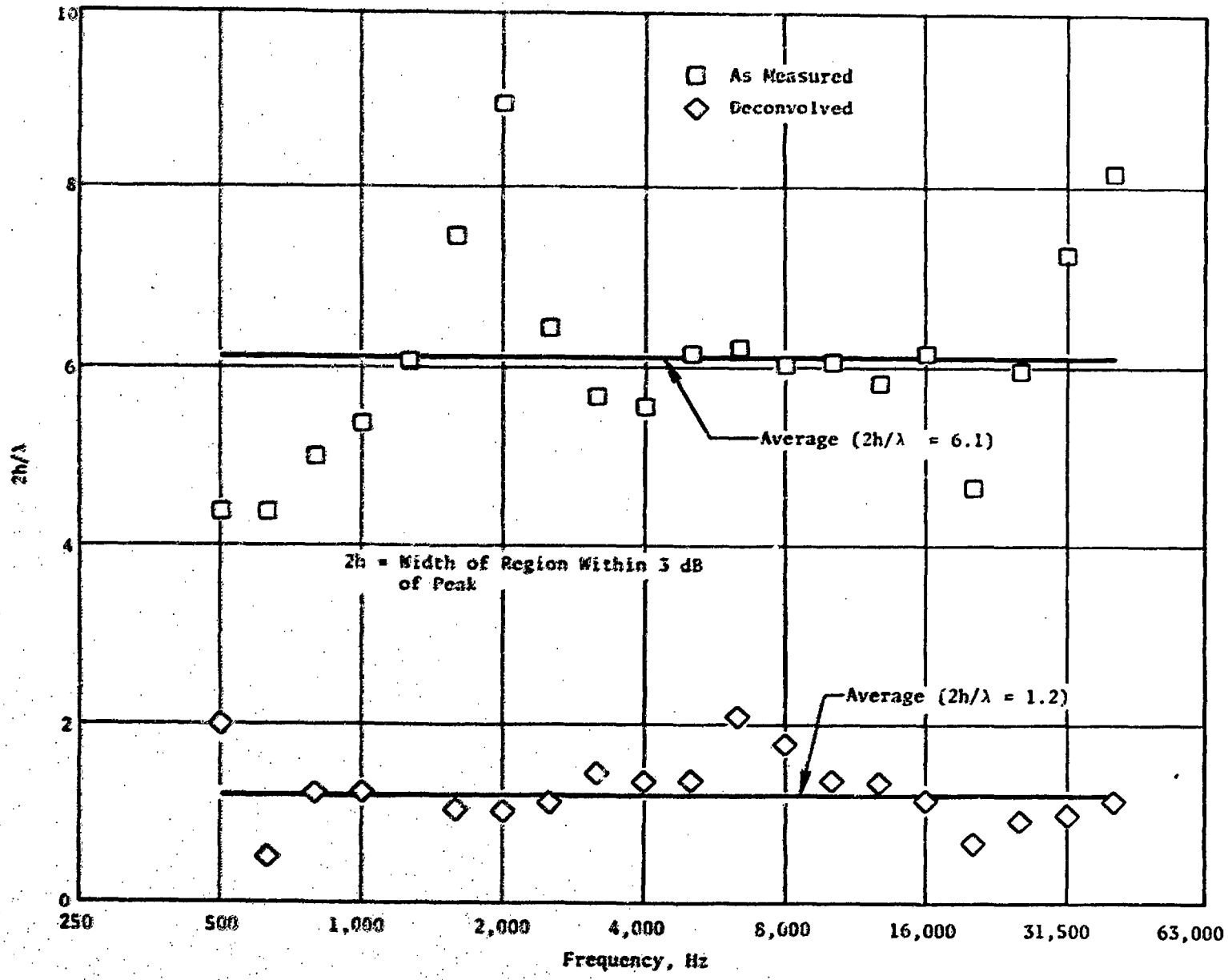

Figure D-25. Resolution of the Deep-Dish Ellipsoidal Mirror (Point Source Measurement).

APPENDIX E

ERROR ANALYSIS OF THE ELLIPSOIDAL MIRROR TECHNIQUE

1. MODEL FOR ELLIPSOIDAL MIRROR ERROR ANALYSIS

An analysis is developed herein of the window function removal technique for the ellipsoidal mirror. This analysis is based on a model for the device that describes the way in which acoustic sources are combined by the mirror to yield the measurement values. The following assumptions are made in the construction of this model (see Figure E-1):

1. The jet is composed of N statistically independent acoustic pressure sources equispaced along a line, x.

2. The M-measurements are made along a line, y, parallel to x, with the same spacing as the sources.

3. The measurements are the mean square outputs from a filter of sufficiently narrow bandwidth that the acoustic response of the mirror may be assumed constant for any frequency in the filter band.

4. The quantities of interest are the mean square values of the pressure sources.

Using the geometry illustrated in Figure E-1, each measured pressure signal is equal to a linear combination of the pressure sources which may be seen by application of the superposition principle of acoustics. The weights are determined by the pressure response of the ellipsoidal mirror (EM). Thus:

$$s_m(t) = \sum_{n=1}^{N} b(m,n)\, P_n(t) \qquad \text{(E-1)}$$

where $s_m(t)$ is the m^{th} measured pressure signal

$P_n(t)$ is the n^{th} source pressure signal and

$b(m,n)$ is the pressure response of the EM between the m^{th} measurement position and the n^{th} source position.

The mean square pressure measurements, corresponding to the outputs of a single filter, a GR third octave analyzer for example, are given by:

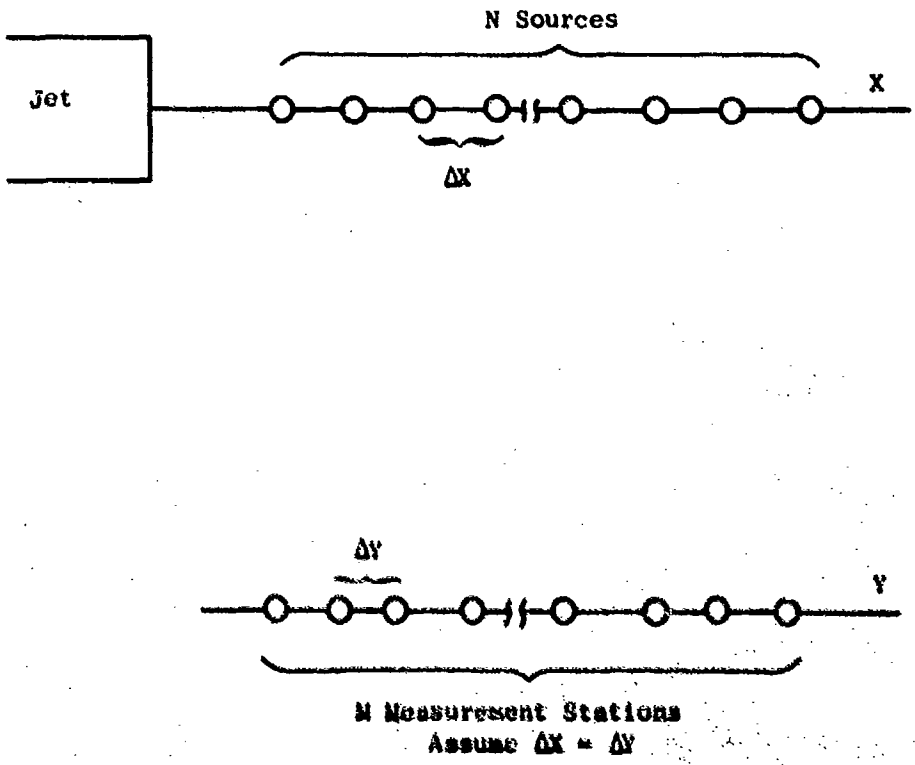

Figure E-1. Assumed Measurement Geometry.

$$S_m = \overline{|s_m(+)|^2} = \sum_{n=1}^{N} \sum_{k=1}^{N} b(m,n)\, b^*(m,k)\, \overline{P_n\, P_K^*} \qquad \text{(E-2)}$$

where * indicates the complex conjugate.

Since the sources are assumed to be statistically independent,

$$\overline{P_n\, P_m^*} = P_n\, \delta(n-m)$$

where $\delta(n)$ is the Kronecker delta function.

Then:

$$S_m = \sum_{n=1}^{N} \sum_{k=1}^{N} b(m,n)\, b^*(m,k)\, P_n\, \delta(n-k) = \sum_{n=1}^{N} |b(m,n)|^2\, P_n \qquad \text{(E-3)}$$

Finally, defining a (m,n) as the power response of the EM between measurement point m and source position n,

$$a(m,n) = |b(m,n)|^2 \qquad \text{(E-4)}$$

so that

$$S_m = \sum_{n=1}^{N} a(m,n)\, P_n \qquad \text{(E-5)}$$

where S_m are the filter mean square pressure measurements

P_n are the mean source strengths

and a(m,n) is the power response of the EM between m and n.

This may be written in matrix notation as

$$\underline{S} = A\, \underline{P} \qquad \text{(E-6)}$$

where $\underline{S}$ is the vector of N-measured powers, $\underline{P}$ is the vector of N source powers and A is the matrix of power response values that performs the operations indicated in Equation E-5.

Since the pressure fluctuations in the jet are random, the measurements will also be random. To include random data effects in the model, a slight modification to the definition of $\underline{S}$ and $\underline{P}$ is necessary. With $\underline{S}$ as the

vector of actual random measurements, $\underline{P}$ as the vector of true source values, and $\underline{\varepsilon}$ as the vector of zero mean random variables representing the uncertainty in $\underline{S}$, the random data model becomes:

$$\underline{S} = A\,\underline{P} + \underline{\varepsilon} \qquad \text{(E-7)}$$

To obtain an estimate of the source distribution, which will be denoted as $\hat{\underline{P}}$, from the measurement vector $\underline{S}$, the Fisher theory of estimation will be employed. This method is detailed in Schweppe, Reference 32, and provides the unbiased estimate of $\underline{P}$ with the minimum variance (statistical error) under the assumption that before the measurements are taken, $\underline{P}$ is completely unknown. Under this assumption, $\hat{\underline{P}}$ may be shown to be

$$\hat{P} = (A^T R^{-1} A)^{-1} A^T R^{-1} \underline{S} \qquad \text{(E-8)}$$

The covariance matrix of $\underline{P}$, defined as

$$K_{\hat{p}} = E\left\{(\hat{\underline{P}}-\underline{P})\ (\hat{\underline{P}}-\underline{P})^T\right\}$$

is then

$$K_{\hat{p}} = (A^T R^{-1} A)^{-1} \qquad \text{(E-9)}$$

where

$$R \triangleq E\left\{\underline{\varepsilon}\ \underline{\varepsilon}^T\right\}$$

is the covariance matrix of the statistical error, $\underline{\varepsilon}$.

In general, to evaluate Equation E-8, one must know R. However, if it is assumed that there are as many measurements as sources, N = M, A is a square matrix. Manipulating Equation E-8,

$$\hat{\underline{P}} = (A^T R^{-1} A)^{-1} A^T R^{-1} \underline{S} = A^{-1} R A^{-T} A^T R^{-1} S = A^{-1} \underline{S} \qquad \text{(E-10)}$$

Thus for this case, knowledge of the error covariance matrix is not required and the estimate is formed by inverting the A matrix. Under the above assumptions, $\underline{P}$ is unbiased and has minimum variance. In the following uncertainty analysis it will be assumed that A is a square matrix.

2. TECHNIQUES FOR COMPUTING THE ESTIMATE AND INVERTIBILITY OF THE A MATRIX

To compute the estimate of the source distribution given in Equation (E-10) it is necessary to solve the equation

$$\underline{S} = A\,\underline{\hat{P}} \qquad \text{(E-11)}$$

where $\underline{S}$ and A are given.

This may be done by:

(1) Iterative approaches such as the Jacobi or Gauss-Seidel procedures.

(2) Direct inversion of the A matrix.

(3) Direct, closed form solution of Equation E-11, taking advantage of a special property of A yet to be discussed.

Care must be taken in the solution of Equation E-11 because of its typical size (80 x 80) and the fact that A will generally be ill-conditioned particularly for low frequency conditions.

The invertibility of a matrix can be parameterized by its condition number. The condition number is an indication of how much the perturbation of an element of A will affect the values of the elements of A^{-1}. If the condition number is large, small changes in A, such as those that occur because of numerical truncation and roundoff errors, will drastically affect the value of A^{-1}. Conversely, if the condition number is small, small perturbation of the elements of A will have only small effects on the elements of A^{-1}. Zwicky (Reference 34) suggests that if the condition number is less than 1000, a matrix is easily inverted, and if it is more than 1000 special techniques should be employed. Zwicky defines this condition number as

$$u = \frac{\lambda_{max.}}{\lambda_{min.}} \qquad \text{(E-12)}$$

where $\lambda_{max.}$ is the maximum eigenvalue of A and $\lambda_{min.}$, is the minimum eigenvalue of A.

To examine the effect of this on the window function removal technique, consider the following approximate window function matrix:

$$A = (1-p)\,U + pI \qquad \text{(E-13)}$$

where I is the identity matrix and U is a matrix of all 1's. Thus the approximate window function has the form:

$$A = \begin{bmatrix} 1 & (1-p) & (1-p) & \cdots & (1-p) \\ (1-p) & 1 & (1-p) & \cdots & (1-p) \\ \vdots & & & & \vdots \\ (1-p) & (1-p) & \cdots & (1-p) & 1 \end{bmatrix} \qquad \text{(E-14)}$$

It may be shown that the eigenvalues for this choice of A are:

$$\lambda = \begin{cases} p \text{ (there are n-1 of these)} \\ n - p\ (n-1) \end{cases} \qquad \text{(E-15)}$$

Thus,

$$u = \frac{n - p\ (n-1)}{p} = \frac{n}{p} - (n-1) \qquad \text{(E-16)}$$

The table below gives the value of u for various values of p with n = 80.

Condition Number for N = 80

u	p
721	0.1
987	0.075
1521	0.05
3121	0.025
7921	0.01
15921	0.005

If the on and off diagonal elements of this matrix differ by less than 0.075, problems may be expected in computing A^{-1}.

Other observations can be made from the result in Equation E-16. For large n and small p (the case most relevant to ellipsoidal mirror window function removal),

$$u \approx \frac{N}{p} \qquad \text{(E-17)}$$

Therefore, the condition number is nearly proportional to the order of A. The condition number can be improved by reducing the number of measurement locations. Also, p should be nearly proportional to the reciprocal of the beamwidth for spatially broad window functions. Thus, the condition number should be proportional to the beamwidth of the mirror.

The Jacobi method is used to solve Equation (E-11) in the numerical processing of EM data. This method is in general use for solving equations of this type and is often recommended by numerical analysts. Direct inversion of the A matrix was examined in this study. Because of a general notion in numerical analysis that if one can directly compute A^{-1}, then the Jacobi and Gauss-Seidel methods will almost certainly work as well if they converge. Also, A^{-1} is required to evaluate some of the expressions to be developed later herein.

Two methods were evaluated for inverting the A-matrix. The first was a "Maximum Pivotal Gaussian Elimination" routine taken from Carnahan, Luther, and Wilkes (Reference 35) and the second was a program for inverting symmetric matrices based on the matrix inversion theorem in Appendix A of Schweppe (Reference 33). Both routines were able to obtain at least three place accuracy in the inverse, but only when the computations were performed using double precision arithmetic. Further precision was obtained by taking advantage of the superior word length of the CDC-7600 computer. The test case used in the evaluation was the inversion of the 1.25 KHz window function from the 18-inch ellipsoidal mirror at 0.375-inch spacing. The worst case conditions of the 1.25-KHz window function at 0.375-inch spacing and the 1.6 KHz window function at 0.125-inch spacing were also examined. The program based on the "Schweppe Theorem" ran in considerably less computer time (because the assumed symmetry of the window function was exploited) than the Maximum Pivotal program and for this reason was chosen as the preferred inversion procedure.

A method was also discovered for the direct solution of Equation E-11. This method uses the fact that if the A matrix is symmetric, then it is completely defined by its first row. This procedure was reported by Levinson, Reference 31. An evaluation of this approach was not made, but examination of the algorithm indicated that there may be a computational savings over the Jacobi iterative method. This, coupled with the advantage of obtaining an "exact" solution (over the "converged" approximation of the iterative method), suggests that the approach should be evaluated. A Fortran subroutine for performing the required calculations appears in Robinson, Reference 32.

The major conclusion of this section is that it should be possible to accurately solve Equation E-11 for measurement spacings as small as 0.125 inches if sufficient care is taken (such as use of double precision arithmetic) in writing the computation subroutines. While the Jacobi procedure should yield adequate results, a closed-form solution procedure is available and this should be evaluated.

3. ESTIMATOR VARIANCE AND BIAS

Under the assumptions that led to the model of Equation E-7 and estimator of Equation E-10, the estimate was unbiased and had covariance matrix:

$$K_p = A^{-1}RA^{-T} \qquad \text{(E-18)}$$

where R was the covariance matrix of the measurements. An ideal source distribution measurement is defined as $\underline{P}$, based on a direct observation of the sources. Then

$$\tilde{\underline{P}} = \underline{P} + \underline{\gamma} \tag{E-19}$$

is defined, where $\underline{\gamma}$ represents the uncertainty in $\tilde{\underline{P}}$ caused by finite observation time and bandwidth. One can do no better than a direct observation and therefore:

$$K_{\hat{\underline{p}}\ \text{min.}} = K_{\tilde{p}} = E\left\{\underline{\gamma}\underline{\gamma}^T\right\} \tag{E-20}$$

represents the minimum possible variance achievable. In the simple model of Equation E-7, the measurement uncertainty, $\underline{\varepsilon}$, is caused by the uncertainty in $\underline{P}$, and in going from Equation E-6 to Equation E-7 it is implied that

$$\underline{\varepsilon} = A\,\underline{\gamma} \tag{E-21}$$

Therefore, it follows that

$$R = A\,K_{\tilde{\underline{p}}}\,A^T \tag{E-22}$$

and from Equation 18,

$$K_{\tilde{\underline{p}}} = A^{-1}RA^{-T} = A^{-1}\,(AK_{\tilde{\underline{p}}}A^T)\,A^{-T} = K_{\tilde{\underline{p}}} \tag{E-23}$$

Thus, independent of the window function, the estimate achieves the same variance as a perfect observation of the source distribution. If $\underline{p}(t)$ is assumed to be a normally distributed random vector, then $\underline{P}$ is a Chi-Square random vector. The variance of a measurement P_n is

$$\text{VAR}\left\{\hat{P}_n\right\} = \frac{P_n^2}{BT} \tag{E-24}$$

and a 95% confidence statement on P_n is:

> "The true value of $\hat{P}_n$ which is P_n must lie between $\hat{P}_n\ (2\ BT)/\chi^2_{0.025,n}$ and $\hat{P}_n\ (2\ BT)/\chi^2_{0.975,n}$ with 95% confidence where B is the bandwidth of the one-third-octave filter and T is the integration time."

The curves in Figure E-2 may be used to determine the plus and minus 95% confidence limits in dB for P_n.

Another effect must be considered to complete the analysis of the variance and bias of the estimate. Generally ambient noise will be present

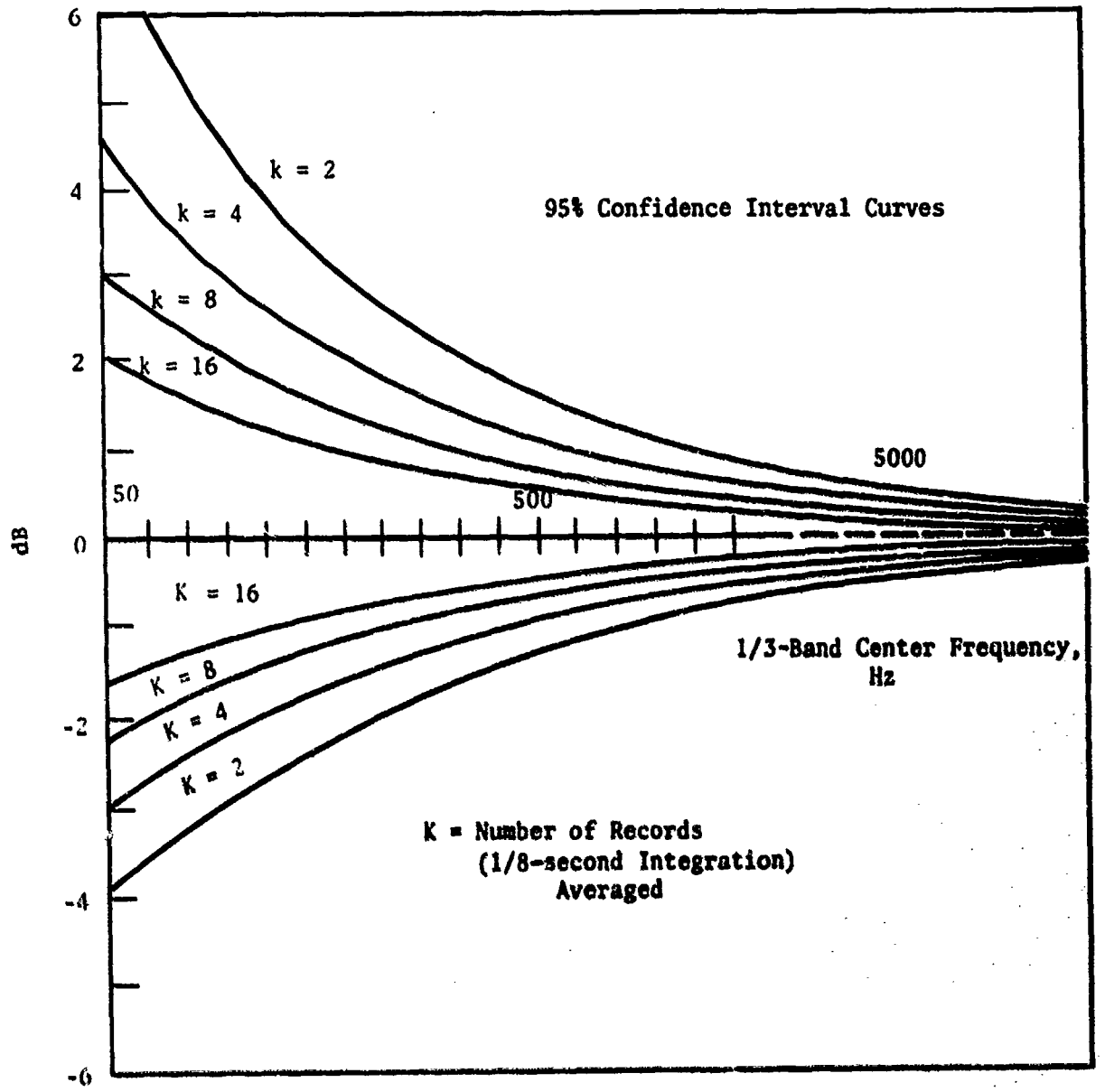

Figure E-2. 95% Confidence Interval Curves as a Function of Data Record Number.

in the enclosure in which measurements are made. In addition, instrument noise originating from the tape recorder, etc., will pollute the measurements. The effect of these noises is to add a bias error to the estimate as well as increase the variance. To evaluate these effects, the model is modified to include a vector of measurement noises $\underline{W}$ which are assumed to be independent of the jet sources so that

$$E\left\{\underline{\varepsilon}\ \underline{W}^T\right\} = 0 \tag{E-25}$$

The new model is

$$\underline{S} = A\underline{P} + \underline{\varepsilon} + \underline{W} \tag{E-26}$$

Using

$$\hat{P} = A^{-1}\ \underline{S} \tag{E-27}$$

as the estimator for $\underline{P}$. Note that the expected value of $\underline{P}$ is now

$$E\left\{\hat{\underline{P}}\right\} = \underline{P} + \underline{A}^{-1}\ \underline{W} \tag{E-28}$$

Thus the estimate has the bias $A^{-1}\underline{W}$. For the bias to be negligible,

$$\underline{P} >> A^{-1}\ W \tag{E-29}$$

This says that the "estimated" source distribution with the ambient noise as an input to the estimator must be significantly less than the true source distribution. Equation E-29 suggests that the following procedure would be useful in evaluating the bias error in EM data:

1. Measure the ambient noise using the standard data recording procedure.

2. Use the data reduction program to obtain

$$\tilde{\underline{P}} = A^{-1}\ W$$

3. Compare $\tilde{\underline{P}}$ to $\hat{\underline{P}}$'s obtained from the analysis of the jet data. $\tilde{\underline{P}} << \hat{\underline{P}}$ means the bias error is negligible. (Here << means about 3 to 6 dB).

Bias in the estimate due to acoustic sources is difficult to bound because of the gross variations in the magnitude and sign of the elements of A^{-1}. Such bounds have so far been too gross to be meaningful. A special and important case can be treated however. This is when the added noise

comes predominantly from the instrumentation (such as the tape recorder) and this dominates over the acoustic background noise. For this case it is reasonable to assume that

$$\underline{W} = \underline{U}\, W \tag{E-30}$$

or that the noise in each measurement has constant mean square value where $\underline{u}$ is a vector of all "one's". For this case one must have

$$P_n >> [A^{-1}\, \underline{U}]_n\, W \tag{E-31}$$

where $[A^{-1}\underline{u}]_n$ can be seen to be the sum of the elements of the n^{th} row of A^{-1}. Another way to write Equation E-31 is in terms of a Signal to Noise Ratio (SNR). This gives

$$SNR = 10 \log_{10} \left(\frac{P_n}{W}\right) >> 10 \log_{10} [A^{-1}\, \underline{U}]_n \tag{E-32}$$

Some typical values of $10 \log_{10} (A^{-1}\underline{u})_n$ are given in Table E-1. The bias error is more of a problem at the higher frequencies where the A matrix is well conditioned. As the A matrix becomes more singular, the sum of the elements of each row approaches zero and the sensitivity to bias error is reduced. The SNR given in Equation E-32 is not the recording SNR, but relates to the strength of the source distribution. The presence of bias error is best determined by the test given previously.

While the bias error might be small, the effect of ambient noise on the variance of the estimate may not be small. This effect may be determined by evaluating the variance of the estimator assuming the new model for the EM. With $K_{\underline{W}}$ as the covariance matrix of $\underline{W}$,

$$K_{\hat{\underline{P}}} = A^{-1}\, (AK_{\tilde{\underline{P}}}\, A^T + K_{\underline{W}})\, A^{-T} + K_{\tilde{\underline{P}}} + A^{-1}\, K_{\underline{W}}\, A^{-T} \tag{E-33}$$

If as before, it is assumed that the measurement noises are uncorrelated and equal in magnitude,

$$K_{\underline{W}} = I\, \sigma_W^2 = I\, W^2/BT \tag{E-34}$$

where W is the mean square noise power in each measurement, and $\underline{w}(t)$ is the assumed Gaussian noise vector. Thus

$$K_{\hat{\underline{P}}} = K_{\tilde{\underline{P}}} + A^{-1}\, A^{-T}\, W^2/BT$$

Table E-1. Sum and Sum of Squares of Row Elements of Typical A^{-1} EM Matrices.

Frequency (Hz)	Distance Between Measurement	Sum of 40th Row*		Sum of Squares of 40th Row*	
		Actual	$10^{*}\log_{10}$	Actual	$5^{*}\log_{10}$
1,250	0.375	0.00292	-25.35	15269.8	20.9
1,600	0.125	0.00127	-28.96	83684.7	24.6
1,600	0.375	0.00446	-23.51	9298.4	19.8
1,600	0.5	0.00635	-21.97	5230.4	18.6
63,000	0.375	8.976	9.53	7633.0	19.4

*The A-matrix was of dimension 80 x 80

and the individual estimate variances are

$$\mathrm{VAR}\left\{\hat{P}_n\right\} = \mathrm{VAR}\left\{\tilde{P}_n\right\} + [A^{-1}A^{-T}]_{n,n}\, W^2/BT \tag{E-35}$$

where $[A^{-1}A^{-T}]_{n,n}$ is the n^{th}, n^{th} diagonal element of $A^{-1}A^{-T}$. With the substitution used previously,

$$\mathrm{VAR}\left\{\tilde{P}_n\right\} = P_n^2/BT \tag{E-36}$$

and,

$$P_n >> [A^{-1}A^{-T}]^{1/2}_{n,n}\, W \tag{E-37}$$

or in DB, the "Signal to Noise Ratio" defined as $10 \log_{10} (P_n/W)$ must be

$$\mathrm{SNR} >> 5 \log_{10}\left\{ [A^{-1}A^{-T}]_{n,n} \right\} \tag{E-38}$$

if the noise variance is not to dominate the source distribution variance. Note that $[A^{-1}A^{-T}]_{n,n}$ is just the sum of the squares of the elements in the n^{th} row of A^{-1} if A is symmetric. Thus while the sum of the elements of a row may be near zero, implying a low bias error, the sum of squares might be very high, implying a drastic increase in the variance of the estimator. Values of the right-hand side of Equation E-38 are tabulated in Table E-1 for some typical cases.

The best way to evaluate this error is to approximate P_n by $\hat{P}_n$ and compare the value obtained from the estimation procedure with the ambient data before applying the analysis procedure. If the condition in Equation E-38 is satisfied, it is safe to use Figure E-2 to specify the confidence limits. If this condition is violated, the error in the estimate is probably much worse.

4. ERRORS INDUCED BY WINDOW FUNCTION MEASUREMENT UNCERTAINTY

In the previous sections perfect knowledge of the A matrix (the matrix of window function values) has been assumed. However, in the case of the EM, the elements of A are determined by a series of measurements, containing uncertainty, followed by some sort of modeling procedure which hopefully reduces this uncertainty. The errors in the elements of A cause an error in the estimated value of $\underline{P}$, $\hat{\underline{P}}$. The purpose of this section is to evaluate the variance of $\underline{P}$ due to this source of error. The simplifying assumption is made that there is no measurement uncertainty present, or that $\underline{\epsilon} = \underline{0}$ in Equation E-7. A total variance including all of the effects may be determined by summing the variances of the individual effects.

Employing the above assumptions,

$$\underline{S} = A\ (\underline{w_o})\ \underline{P} \tag{E-39}$$

where $\underline{w_o}$ is the vector of unique elements in the actual A matrix. The actual matrix used to estimate $\underline{P}$ will have values of $\underline{W}$ different from $\underline{w_o}$. Defining

$$\underline{W} = \underline{w_o} + \underline{\delta W} \tag{E-40}$$

and having as the estimate:

$$\underline{\hat{P}} = A^{-1}\ (\underline{W})\ \underline{S} = A^{-1}\ (\underline{W})\ A\ (\underline{w_o})\ \underline{P} \tag{E-41}$$

If $\underline{\delta w}$ is assumed to be "small", the above may be linearized to find the perturbation in $\underline{P}$, which will be called $\underline{\delta P}$, caused by the error in W, δw. Then

$$\underline{\hat{P}} = \underline{\hat{P}_o} + \underline{\delta \hat{P}} \approx A^{-1}\ (\underline{w_o})\ A\ (\underline{w_o})\ \underline{P} + \underline{\nabla_w}^T\ [A^{-1}(\underline{W})A(\underline{w_o})\ \underline{P}]\ \underline{\delta W}\Big|_{\underline{W}=\underline{w_o}} \tag{E-42}$$

Observing that

$$\underline{\hat{P}_o} = A^{-1}\ (\underline{w_o})\ A\ (\underline{w_o})\ \underline{P} = \underline{P} \tag{E-43}$$

yields

$$\underline{\delta \hat{P}} = \underline{\nabla_w}^T\ [A^{-1}(\underline{W})\ A\ (\underline{w_o})\ \underline{P}]\underline{\delta W}\Big|_{\underline{W}=\underline{w_o}} \tag{E-44}$$

as the error in $\underline{\hat{P}}$ due to a small error in $\underline{W}$. Since $A^{-1}(\underline{W})A(\underline{w_o})\underline{P_o}$ is a vector,

$$\underline{\nabla_w}^T\ [A^{-1}(\underline{W})\ A\ (\underline{w_o})]\ \underline{P_o} = \tag{E-45}$$

$$\begin{bmatrix} \frac{\partial}{\partial W_1}\ (A^{-1}(\underline{W})A(\underline{w_o})\underline{P_o})_1 & \cdots & \frac{\partial}{\partial W_n}\ (A^{-1}(\underline{W})\ A\ (\underline{w_o})\underline{P_o})_1 \\ \vdots & & \vdots \\ \frac{\partial}{\partial W_1}(A^{-1}(\underline{W})A(W_o)P_o)_n & \cdots & \frac{\partial}{\partial W_n}\ (A^{-1}\ (\underline{W})\ A\ (\underline{w_o})\underline{P_o})_n \end{bmatrix}$$

Where $(\ )_k$ is the k^{th} row of the enclosed vector. Since $\partial/\partial W_k\ (\ )_i = (\partial/\partial W_k\ )_i$, and since

$$\frac{\partial}{\partial W_k} A^{-1}(\underline{W})\Big|_{\underline{W}=\underline{W}_o} = -A^{-1}(\underline{w}_o)\left[\frac{\partial}{\partial W_k} A(\underline{W})\right] A^{-1}(\underline{w}_o)\Big|_{\underline{W}=\underline{W}_o} \tag{E-46}$$

Then:

$$\nabla_{\underline{W}}^{T}\left[A^{-1}(\underline{W})\, A(\underline{w}_o)\, \underline{P}_o\right]_{\underline{W}=\underline{w}_o} = \tag{E-47}$$

$$\left[-A^{-1}(\underline{w}_o)\frac{\partial}{\partial W_1}[A(\underline{W})]\,\underline{P}_{o_j} \cdots \quad -A^{-1}(\underline{w}_o)\frac{\partial}{\partial W_n}[A(\underline{W})]\,P_o\right]$$

$$= -A^{-1}(\underline{w}_o)\left[\frac{\partial}{\partial W_1}[A(\underline{W})]\underline{P}_{o_j} \cdots \quad \frac{\partial}{\partial W_n}[A(\underline{W})]\,\underline{P}_o\right]$$

If it is assumed that A is a Toplitz and symmetric matrix, then $A(\underline{W})$ may be written

$$A(\underline{W}) = \begin{bmatrix} W(1) & \cdots & W(n) \\ W(2), & W(1), & W(2). & W(n-1) \\ \vdots & & & \vdots \\ W(n) & \cdots & W(2) & W(1) \end{bmatrix} \tag{E-48}$$

where $\underline{W}$ is the defining row of the Toplitz matrix. Thus

$$[A(\underline{W})]_{ij} = W(|i-j| + 1) \quad \begin{matrix} i = 1 \ldots N \\ j = 1 \ldots N \end{matrix} \tag{E-49}$$

and

$$\left\{\frac{\partial}{\partial W_k} A(\underline{W})\right\}_{ij} = \delta(|i-j| + 1 - k)$$

If it is assumed that $\delta\underline{w}$ represents a random error, and the model used for $\underline{w}_o$ is such that

$$E(\underline{W}) = \underline{W}_o \tag{E-50}$$

Then the covariance matrix of the estimate due to the uncertainty in $\underline{w}$ may be written

$$K_{\underline{\hat{P}}} = A^{-1}(\underline{w_o})\ \phi\ K_{\underline{W}}\ \phi^T\ A^{-T}(\underline{w_o}) \tag{E-51}$$

where $K_{\underline{W}}$ is the covariance matrix of $\underline{w}$ and

$$[\phi]_{ij} = \sum_{k=1}^{N} \delta(|i-k| + 1 - j)P_k \tag{E-52}$$

The basic dependencies may be observed by examining the above.

The covariance of the estimation error is determined by the actual window function as embodied by $A^{-1}(w_o)$, the measured source distribution as embodied by ϕ, and the error in $\underline{w}$ as embodied by $K_{\underline{W}}$. Equations E-51 and E-52 may be evaluated for any assumed set of conditions.

5. NUMERICAL EVALUATION STUDY

The equations developed in the previous four sections of this Appendix were evaluated for four cases closely related to the experimental conditions encountered with the 18-inch elliptical mirror. Measured window function data was used in the analysis and the variance of this was estimated by fitting a cubic polynomial through the data and using the variance of the resulting regression. Details of the test cases are given in Figure E-3.

The source distribution assumed in all cases was a point source of unit magnitude at the center of the source distribution line. Other source distributions can be derived from this case by application of the superposition theorem of acoustics.

The output of this numerical study was an estimate of the error in the measurement values after window function removal due to:

- Error in the determination of the true window function of the mirror.
- Statistical error due to the fact the source is random.

Thus this result indicates an upper limit on the mirror's performance since such error sources as:

- Alignment and positioning errors in mirror placement
- Background and measurement noise

Number of Source and Measurement Points: 80

Band Width = 1/3-Octave Centered about Frequency Shown in Table E-2

Integration Time Used in Data Reduction Process: 0.125 sec

Measurement Spacing - As Shown in Table E-2

Source Distribution - Point Source of Unit Magnitude at Source Location Number 40:

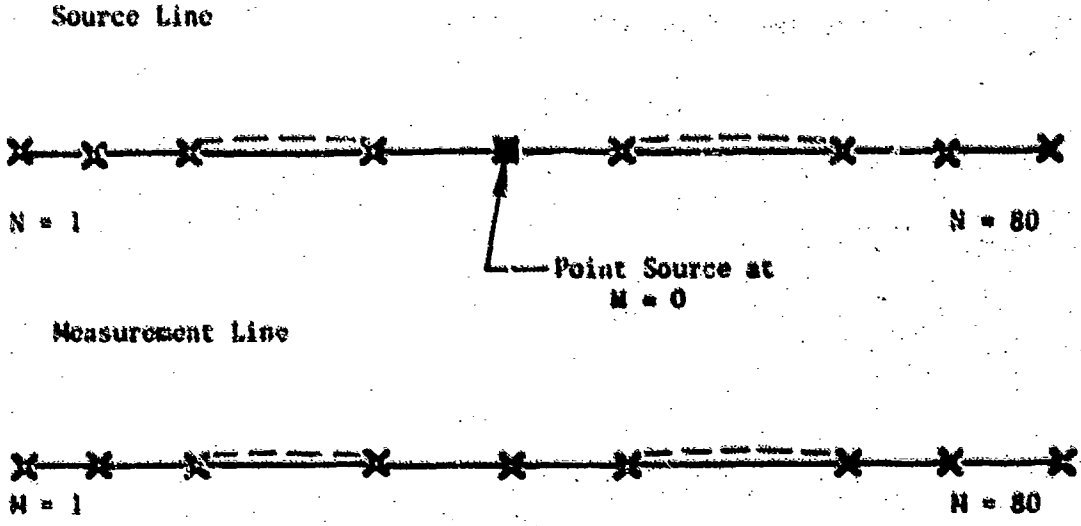

Figure E-3. Details of Test Cases Used in Numerical Analysis.

- Variation of mirror response with frequency within the bandwidth of the analysis filters
- Numerical "noise" errors in the data reduction process due to ill conditioning, etc.

are not included in this numerical evaluation.

In reducing this data, it was noted that the errors for the 80 source estimate points could be divided into two groups: the error at the source point and the errors at the other points where there was no source. The error at the source point represents the accuracy of determining the value of a strong source. The non-source point errors (which were all nearly the same magnitude) indicate the value of the "noise floor" of the measurement, and are thus a measure of the dynamic range of the procedure. Attempting to determine the strength of two sources whose magnitudes in dB differ by more than this noise floor value will result in the smaller of the two not being detected. The values obtained for the test cases are shown in Table E-2.

6. CONCLUSIONS

The following conclusions may be drawn from this study:

1. A small ellipsoidal mirror such as the 18" mirror developed for this program is capable of obtaining useful data when:
   a. The source frequency is greater than 1000 Hz.
   b. The source dynamic range is less than 25 dB
   c. The source spacing is greater than 0.5 inch
   d. The measurement accuracy required is less tight than ±2.5 dB.
2. The window function removal procedure is very sensitive to any error. Especially those in:
   a. The assumed shape of the window function. This includes measurement uncertainty in its determination, the mechanical repeatability of the mirror manipulation mechanism, and mathematical modeling errors.
   b. The numerical procedure used to solve the estimation equation and the word length specified in the analysis.
   c. Background and instrument noise.
3. The presence of errors in analyzed data may be difficult to detect due to high correlation between adjacent errors. Check procedures, like those suggested in this report, should be included in the data procedure to guarantee the quality of the data.

Table E-2. Theoretical Statistical Errors for a Single Point Source at Center of Measurement Set - 18-Inch Elliptical Mirror.

Frequency	Source Measurement Separation (inches)	Variance of Source Point	2 × Standard Deviation of Source Point	2 Standard Deviation Measurement Error (DB)
1600	0.125	0.014796	0.2433	(+0.95) (-1.2)
1600	0.375	0.01472	0.2427	(+0.95) (-1.2)
1600	0.5	0.014682	0.2423	(+0.95) (-1.2)
1250	0.375	0.044819	0.4234	(1.53) (-2.39)

Frequency	Source Measurement Separation (inches)	Typical Variance of Nonsource Point	2 × Standard Deviation of Nonsource Point	dB Below Source at 2 Standard Deviations
1600	0.125	2.6577×10^{-8}	3.26×10^{-4}	-34.9
1600	0.375	2.7×10^{-7}	1.64×10^{-3}	-29.8
1600	0.5	4.99×10^{-7}	1.41×10^{-3}	-28.5
1250	0.375	1.406×10^{-6}	2.037×10^{-3}	-26.2

APPENDIX F

1.0 DATA REDUCTION PROCEDURES

DETAILED DATA REDUCTION PROCEDURES

A detailed description of the data reduction procedure is given in the following sections. All the constants and equations in this appendix are given in English units as actually used in the data reduction programs.

FLOW RATES

The mass flow through the outer nozzle was measured with a 1.248-in. throat diameter choked venturi meter, located as shown in Figure 4-2, Section 4.2. The flow rate was calculated using the equation

$$W_o = C_{DV_o} \frac{K_{V_o} P_{TV_o} A_{V_o}}{\sqrt{T_{TV_o}}} \qquad \text{(F-1)}$$

The critical flow factor, K_{V_o}, was calculated as a function of total pressure and temperature:

$$K_{V_o} = 0.5282 + a\, T_{TV_o} + b\, T_{TV_o}^{\,2} + c\, T_{TV_o}^{\,3} + (1.86 \times 10^{-5})\, P_{TV_o} e^{-0.0067(T_{TV_o} - 500.00)} \qquad \text{(F-2)}$$

where

$$a = 1.654 \times 10^{-5}$$
$$b = -2.119 \times 10^{-8}$$
$$c = 6.008 \times 10^{-12}$$

where T_{TV_o} and P_{TV_o} are in ° R and psia, respectively.

This equation was obtained by curve-fitting tabulated values in Reference 36.

The meter flow coefficient was calculated as a function of the throat Reynolds number using the following semiempirical relation:

$$C_{DV_o} = 0.9983 \left(-.0691\, RN^{-0.183} \right) \qquad \text{(F-3)}$$

The 0.9983 factor in the equation is to account for the effects of sonic line distortion.

The meter total pressure, P_{TV_o}, was determined by measuring the static pressure, P_{V_o}, upstream of the venturi throat and calculating the total pressure as:

$$P_{TV_o} = P_{V_o}/0.995 \qquad \text{(F-4)}$$

The 0.9995 factor is the static-to-total pressure ratio for that Mach number based on the ratio of the area at the measurement plane to the meter throat area. The static pressure was measured by six taps, and each was sampled four times with dummy scanning valves during the taking of each data point. These 24 readings were averaged to determine the static pressure.

The meter total temperature, T_{TV_o}, was determined using five platinum resistance thermometers located upstream of the venturi. Each thermometer was read twice and the readings averaged.

The mass flow through the inner nozzle was measured with either of two choked venturi meters located as shown on Figure 4-2, Section 4.2. The flow for high inner flow rates was measured using the 1.1398-in.-throat-diameter venturi. The flow for the low inner flow rate testing was measured with the 0.3985-in.-throat-diameter venturi. For both meters, the flow rate was calculated using the equation

$$W_i = \frac{K_{V_i} P_{V_i}}{60.00 \sqrt{T_{T_{V_i}}}} \qquad \text{(F-5)}$$

This equation is based on calibration of the meters made by the manufacturer. The K_{Vi} factors based from the calibration were

$$K_{Vi} = (-1.9153 \times 10^{-7}) P_{V_i}^2 + (1.10896 \times 10^{-3}) P_{V_i} + 32.29807 \qquad \text{(F-6)}$$

for the 1.1398-in.-diameter meter, and

$$K_{V_i} = (-3.02076 \times 10^{-8}) P_{V_i}^2 + (9.49693 \times 10^{-5}) P_{V_i} + 3.93951 \qquad \text{F-7)}$$

for the 0.3985-in.-diameter meter.

The meter static pressure (P_{Vi}) was measured upstream of the venturi throat with four static taps, each was read twice, and the eight numbers averaged. The venturi total temperatures were measured with three thermocouples (each read twice) located upstream of the meter.

FLOW COEFFICIENTS

The flow coefficient of a nozzle is defined as the ratio of actual mass flow rate through the nozzle to the ideal isentropic flow rate at the temperature and pressure of the flow.

$$C_D = \frac{\text{measured } W}{\text{ideal } W} \qquad \text{(F-8)}$$

The ideal weight flow for the outer nozzle flow was calculated from the relation

$$W_{I_o} = \frac{K_o \, A_o \, P_{T_o}}{\sqrt{T_{T_o}}} \left(\frac{A^*}{A_o}\right). \qquad \text{(F-9)}$$

A_o is the outer nozzle physical throat area and

$$K_o = 0.5282 + a\, T_{T_o} + b\, T_{T_o}^{\,2} + c\, T_{T_o}^{\,3} + (1.86 \times 10^{-5}) P_{T_o} e^{-0.0067(T_{T_o} - 500.00)}$$

where a, b, and c are as given in the previous section, and T_{T_o} and P_{T_o} are in ° R and psia, respectively.

The nozzle temperature, T_{T_o}, and pressure, P_{T_o}, were measured upstream of the nozzle throat with multielement rakes. These rakes were placed downstream of choke plates and screens which provided a flow with no pressure profile distortion at the rakes to assure an accurate pressure measurement. The outer nozzle rakes contained eight total pressure probes, the readings of which were averaged to arrive at P_{T_o}, and two thermocouples, the readings of which were averaged. The inner nozzle rakes contained five Pitot tubes and one thermocouple.

For values of nozzle pressure ratio greater than 1.8929, A^*/A_o in the ideal weight flow equation is equal to one. For lower pressure ratios, A^*/A_o was calculated from the isentropic relationships

$$A^*/A_o = \frac{216}{125} M_o \left(1 + \frac{M_o^2}{5}\right)^{-3} \qquad \text{(F-10)}$$

where

$$M_o = \left\{ 5 \left[\left(\frac{P_{T_o}}{P_a} \right)^{0.28571} - 1 \right] \right\}^{1/2}$$

The inner nozzle ideal weight flow was calculated in identical fashion as the outer nozzle, but using the inner nozzle throat area, flow pressure, and temperature. For the low inner flow testing, the inner nozzle total pressures required to supply the low flow rates were generally lower than ambient pressure due to the pumping effect of the outer flow. In these cases, the ideal flow rate and flow coefficients are meaningless and were not calculated.

THRUST MEASUREMENTS

The thrust of the exhaust nozzles is defined as the axial exit momentum of the exhaust flow, plus the excess of exit pressure over ambient pressure times the exit area normal to the axis, minus the axial drag on the nozzle external surface; i.e.,

$$F = \int_{A_{exit}} d\,(WV)_{axial} + \int_{A_{exit}} (P-P_a)dA - D_{external}. \qquad \text{(F-11)}$$

The external drag consists of both the pressure drag on the boattail surface and the axial component of skin friction. Figure F-11 shows a control volume applied to the test nozzles. Writing the momentum equation in the axial direction for this control volume demonstrates how the thrust was measured for the tests:

$$F = F_{LC}+F_{AS}+A_1(P_1-P_a)+A_2(P_2-P_a)+A_3(P_3-P_a)+A_4(P_4-P_a) \qquad \text{(F-12)}$$

where F_{LC} is the axial force applied to the load cell and F_{AS} is the axial force applied at the boundary of the control volume by the air supply tubes. The static pressures P_1, P_2, P_3, and P_4 were measured with two static taps 180° apart at each of the four areas (see Figure 4-11, Section 4.4.3). The force measuring system was calibrated by applying known forces and correlating this force against the load cell output, as previously described in Section 3.0. This calibration provided a linear relationship between the applied load and the load cell output in millivolts which was used to determine the load cell plus air supply tube force as follows:

$$\text{Applied Load} = a(mv)+b = F_{LC} + F_{AS} \qquad \text{(F-13)}$$

where a and b are constants determined by the calibrations and mv is the load cell reading in millivolts. The load cell was sampled 48 times during the

taking of each point, the above calculation made for each sample, and the results averaged to yield the measured force.

An adjustment was made to the measured thrust to account for external friction drag on the cylindrical section upstream of the nozzle shroud. The axial force on this 8.0-in.-diameter section, which extended from the metric-break to the attach-point of the nozzle shrouds, was not included in the nozzle net thrust. The friction drag was calculated by the equation:

$$D_f = \frac{\gamma}{2} P_a M_a^2 A_c C_f \qquad \text{(F-14)}$$

where A_c is the wetted surface area of the cylindrical piece 8.0 in. in diameter and 7.0 in. in length. The drag coefficient was calculated from

$$C_f = 0.288 \ (1 + 0.2 \ M_a^2)^{-0.5} \ (\log_{10} RN_x)^{-2.45} \qquad \text{(F-15)}$$

where $RN_x = 9.37 \ RN_a$; RN_a being the Reynolds number per foot based on the ambient stream Mach number, temperature, and pressure.

The thrust of the nozzles for this test was therefore given by:

$$F = F_{LC}+F_{AS}+A_1(P_1-P_a)+A_2(P_2-P_a)+A_3(P_3-P_a)+A_4(P_4-P_a)+D_f \qquad \text{(F-16)}$$

or, substituting the equations by which $F_{LC} + F_{AS}$ and D_f were calculated:

$$F = a(mv)+b+A_1(P_1-P_a)+A_2(P_2-P_a)+A_3(P_3-P_a)+A_4(P_4-P_a)+ \frac{\gamma}{2} P_a M_a^2 A_c C_f$$

THRUST COEFFICIENT

The thrust coefficient is the ratio of the measured nozzle thrust to the ideal thrust of the inner duct flow plus the ideal thrust of the outer duct flow. The ideal thrust for each stream equals the actual mass flow rate times the ideal velocity; i.e., the velocity of the stream expanded isentropically from the total pressure to the ambient pressure. The equation for the thrust coefficient is thus:

$$C_T = \frac{F}{W_o \ V_{I_o} + W_i \ V_{I_i}} \qquad \text{(F-17)}$$

The ideal thrust for the nozzles was calculated using the dimensionless ideal-thrust function which is a function of only the nozzle pressure ratio.

$$\frac{W_I\ V_I}{P_T\ A^*} = \gamma \left(\frac{2}{\gamma+1}\right)^{\frac{\gamma}{\gamma-1}} \left(\frac{\gamma+1}{\gamma-1}\right)^{1/2} \left[1 - (P_a/P_T)^{\frac{\gamma-1}{\gamma}}\right]^{1/2}$$

$$= 1.81163 \sqrt{1 - (P_a/P_T)^{0.28571}} \text{ for } \gamma = 1.4 \qquad \text{(F-18)}$$

The ideal thrust for the inner and outer streams was then:

$$W_i\ V_{I_i} = C_{D_i}\ P_{T_i}\ A_i \left(\frac{A_i^*}{A_i}\right) \left(\frac{W_{I_i}\ V_{I_i}}{P_{T_i}\ A_i^*}\right)$$

$$W_o\ V_{I_o} = C_{D_o}\ P_{T_o}\ A_o \left(\frac{A_o^*}{A_i}\right) \left(\frac{W_{I_o}\ V_{I_o}}{P_{T_o}\ A_o^*}\right) \qquad \text{(F-19)}$$

For pressure ratios greater than 1.8929, $A^*/A = 1.0$. For pressure ratios less than this, A^*/A was calculated as described in the previous section on flow coefficients.

During much of the low inner flow rate testing, the total pressure of the inner nozzle flow was lower than ambient. In these cases, the ideal thrust of the inner nozzle was set equal to zero.

For the static thrust tests of the STA model, a dimensionless stream-thrust parameter was also calculated as:

$$f_9 = \frac{F + P_a A_9}{P_T\ A_9} \qquad \text{(F-20)}$$

where A_9 is the STA nozzle exit area.

PRESSURE DATA

Total pressures in the models and static pressures on the model surfaces were measured with scanning value/transducer arrangements. The individual static pressure readings were also nondimensionalized by the ambient pressure. Pressure forces on the aft-facing portions of the shroud, outer plug, inner plug, and suppressor bases were calculated by multiplying the difference between the static pressure at each tap and ambient pressure by an incremental projected area represented by the particular tap and summing the products, i.e.,

$$F_P + \Sigma\ (P-P_a)\Delta A \qquad \text{(F-21)}$$

These pressure forces were also nondimensionalized by the total ideal thrust of the nozzle:

$$\frac{F_P}{W_i V_{I_i} + W_o V_{I_o}}$$

DETAILED MODEL DESCRIPTION

Geometric details of the annular, suppressed models are presented in Figures F-1 through F-15.

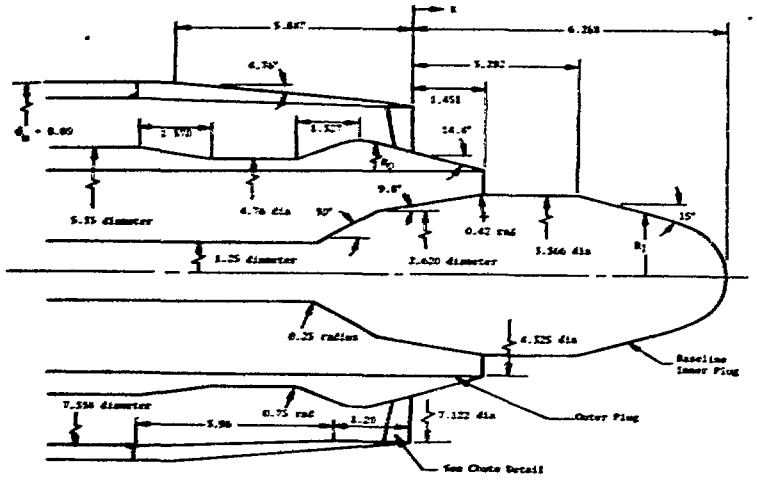

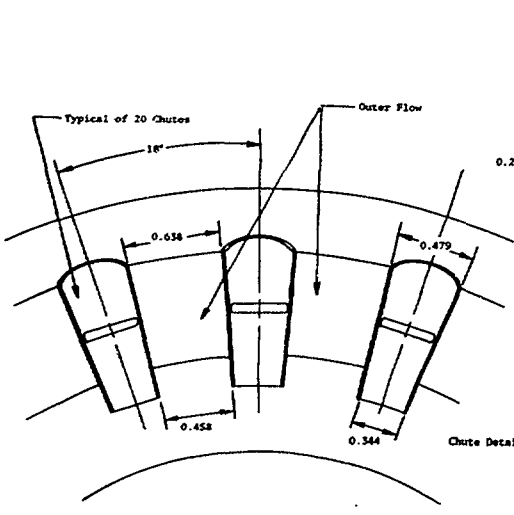

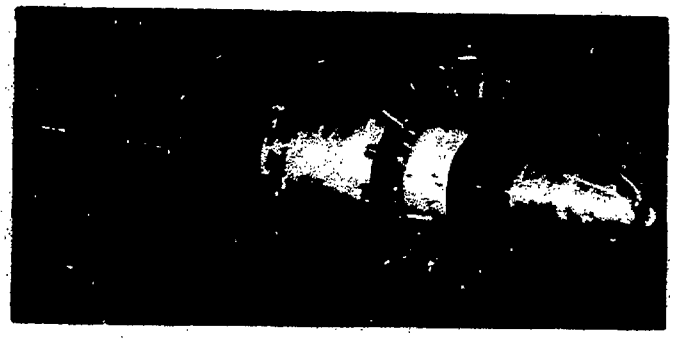

	Outer-Plug Geometry			Inner-Plug Geometry	
	Axial Coordinate, X/d_m	Radial Coordinate, R_o/d_m		Axial Coordinate, X/d_m	Radial Coordinate, R_i/d_m
Straight Line	- 0.306	0.298	Straight Line	0.411	0.210
	- 0.189	0.342		0.579	0.165
	- 0.179	0.345		0.584	0.164
	- 0.170	0.348		0.623	0.151
	- 0.160	0.350		0.662	0.138
	- 0.150	0.351		0.682	0.130
	- 0.140	0.352		0.701	0.121
	- 0.130	0.351		0.721	0.110
	- 0.120	0.350		0.740	0.095
Straight Line	- 0.111	0.348		0.759	0.075
	- 0.146	0.282		0.779	0.040
	- 0.181	0.275		0.786	0

Figure F-1. Geometric Details of Configuration SC-1, N = 20, Baseline Plug.

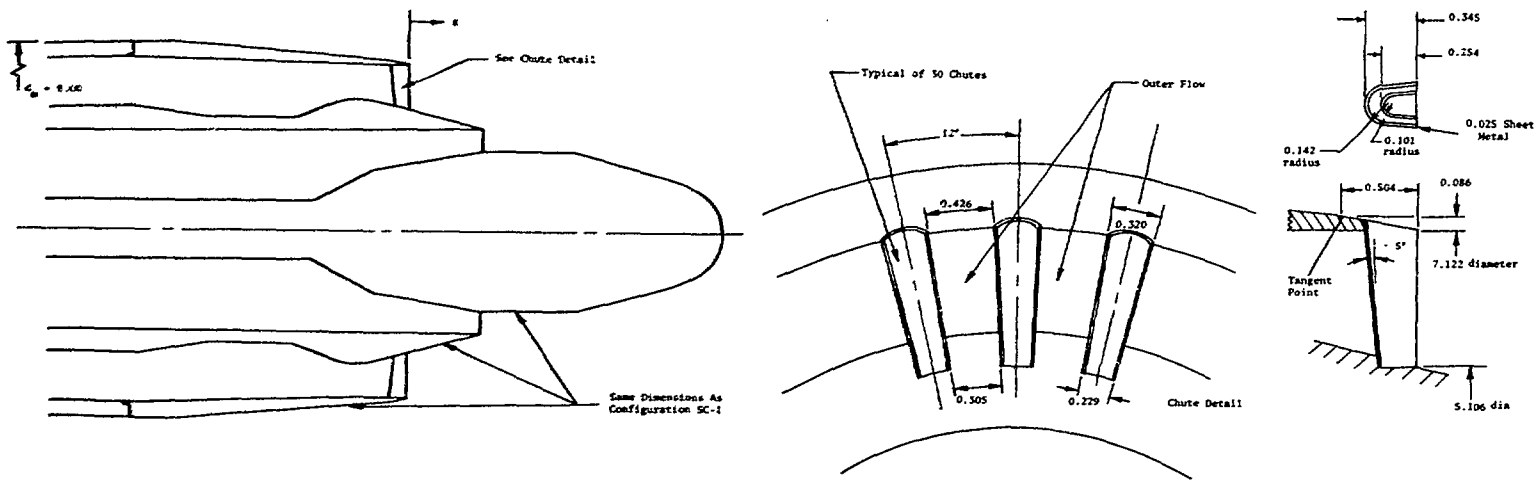

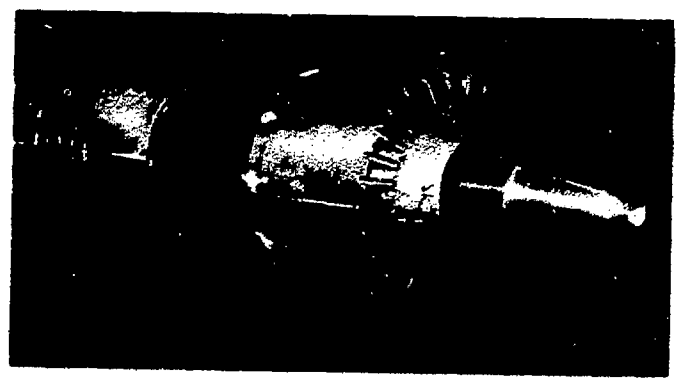

Figure F-2. Geometric Details of Configuration SC-2, N = 30, Baseline Plug.

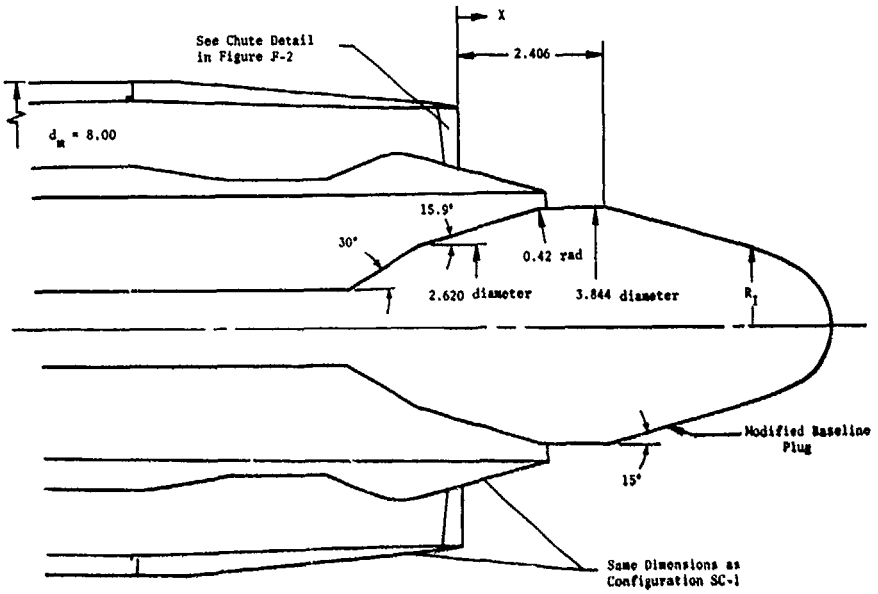

	Inner-Plug Geometry	
	Axial Coordinate, X/d_m	Radial Coordinate, R_I/d_m
Straight Line	0.300	0.240
	0.579	0.165
	0.584	0.164
	0.623	0.151
	0.662	0.138
	0.682	0.130
	0.701	0.121
	0.721	0.110
	0.740	0.095
	0.759	0.075
	0.779	0.040
	0.786	0

Figure F-3. Geometric Details of Configuration SC-3, Modified Baseline Plug.

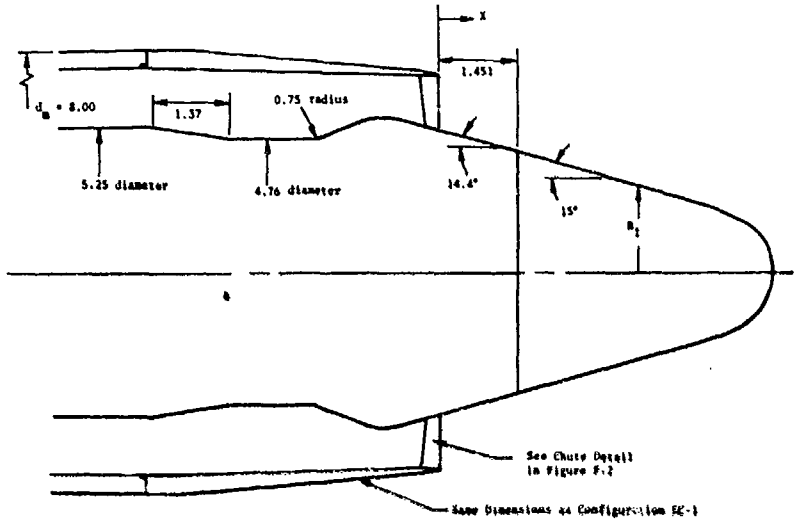

	Inner-Plug Geometry	
	Axial Coordinate, X/d_m	Radial Coordinate, R_i/d_m
Straight Line	- 0.306	0.298
	- 0.189	0.342
	- 0.179	0.345
	- 0.170	0.348
	- 0.160	0.350
	- 0.150	0.351
	- 0.140	0.352
	- 0.130	0.351
	- 0.120	0.350
	- 0.111	0.348
Straight Line	0.146	0.282
	0.579	0.165
	0.585	0.164
	0.623	0.151
	0.662	0.138
	0.682	0.130
	0.701	0.121
	0.721	0.110
	0.740	0.096
	0.759	0.075
	0.779	0.048
	0.786	0

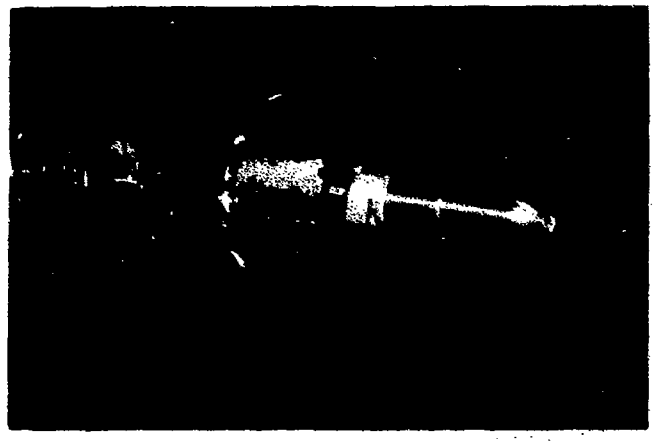

Figure F-4. Geometric Details of Configuration SC-4, N = 30, Full Plug.

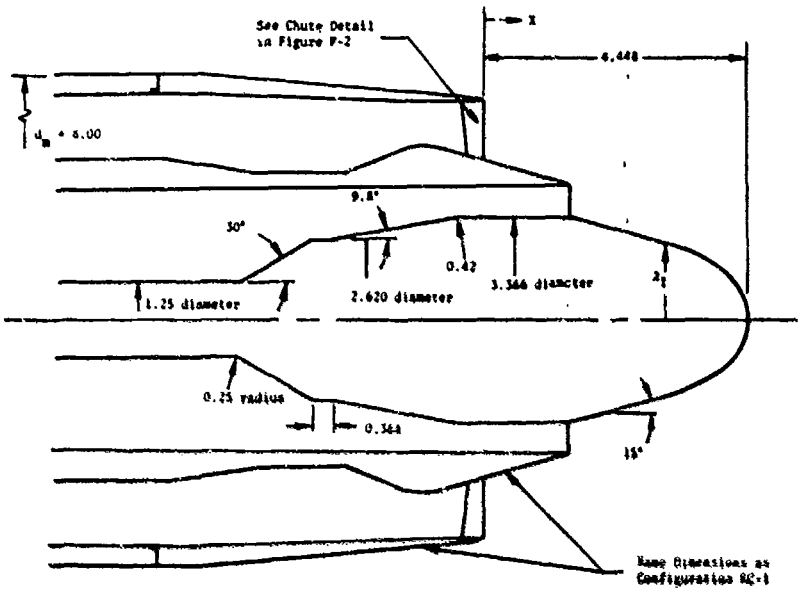

Inner-Plug Geometry		
	Axial Coordinate, X/d_m	Radial Coordinate, R_i/d_m
Straight Line	0.181	0.210
	0.349	0.165
	0.354	0.164
	0.383	0.151
	0.432	0.138
	0.452	0.130
	0.471	0.121
	0.491	0.110
	0.510	0.095
	0.529	0.075
	0.549	0.040
	0.556	0

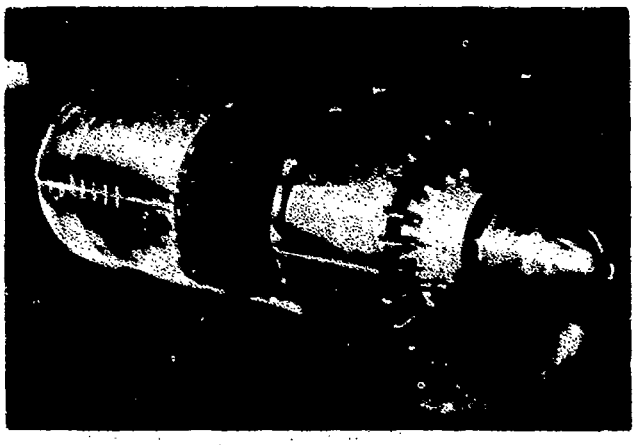

Figure F-5. Geometric Details of Configuration SC-5, N = 30, Forward Baseline Plug.

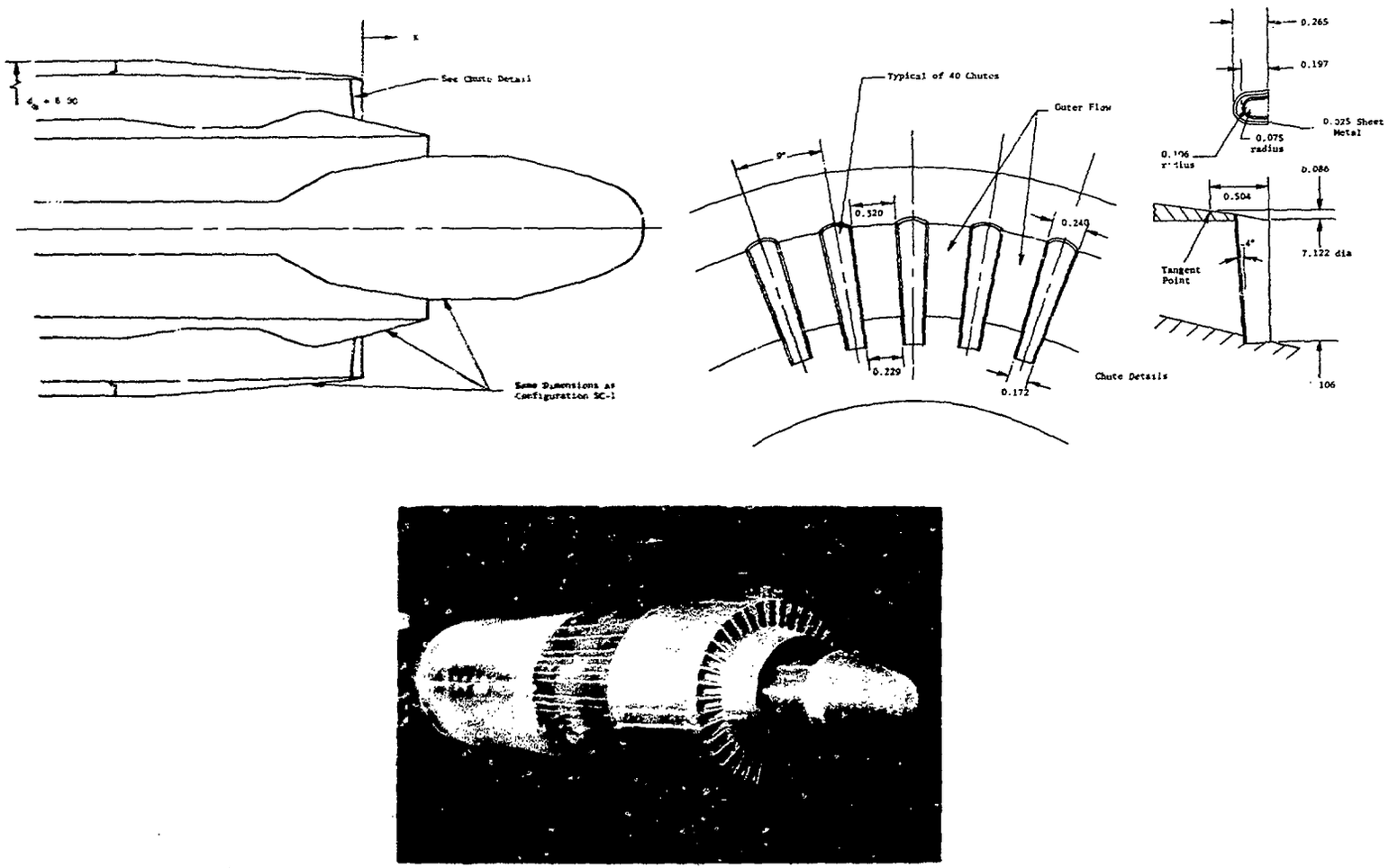

Figure F-6. Geometric Details of Configuration SC-6, N = 40, Baseline Plug.

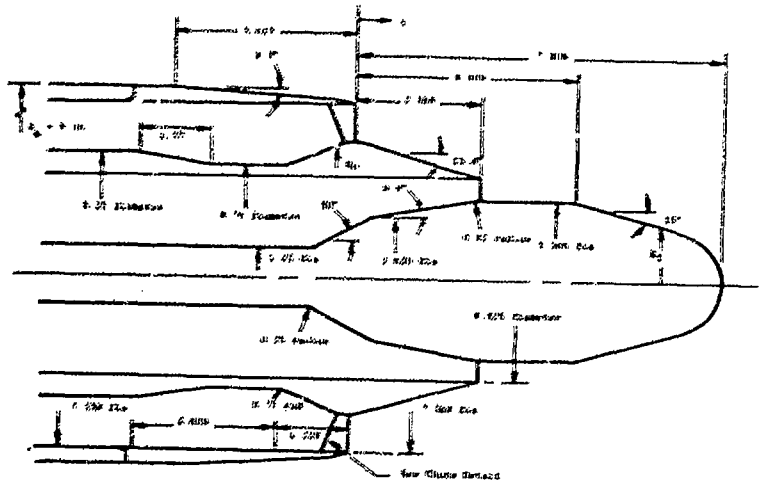

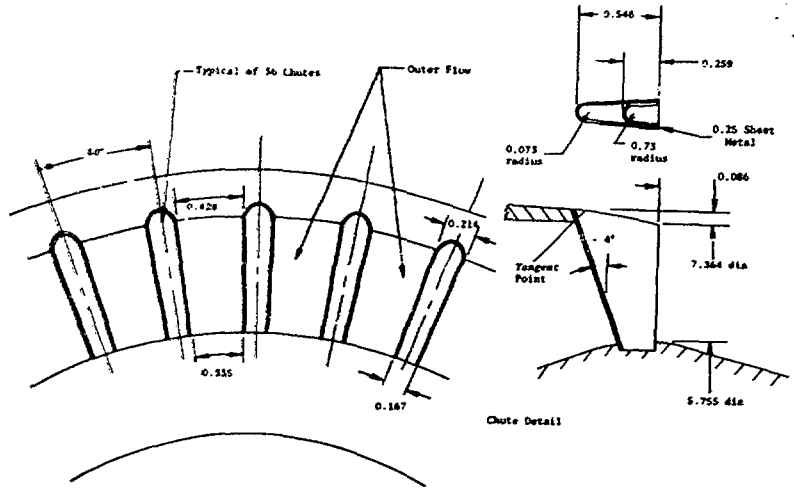

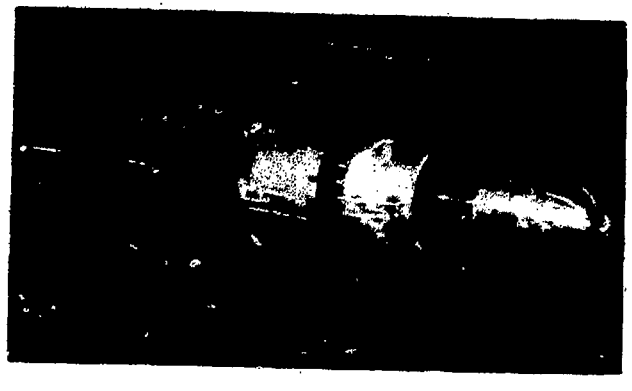

	Outer-Plug Geometry			Inner-Plug Geometry	
	Axial Coordinate, X/d_m	Radial Coordinate, R_o/d_m		Axial Coordinate, X/d_m	Radial Coordinate, R_o/d_m
Straight Line	- 0.170	0.298	Straight Line	0.551	0.210
	- 0.044	0.352		0.719	0.165
	- 0.039	0.354		0.724	0.164
	- 0.029	0.357		0.763	0.151
	- 0.020	0.358		0.802	0.138
	- 0.010	0.359		0.822	0.130
	0	0.360		0.841	0.121
	0.010	0.359		0.861	0.110
	0.020	0.357		0.880	0.095
	0.029	0.355		0.899	0.075
Straight Line	0.031	0.354		0.919	0.040
	0.266	0.282		0.926	0
	0.521	0.275			

Figure F-7. Geometric Details of Configuration DC-1, AR = 1.5, Full Plug.

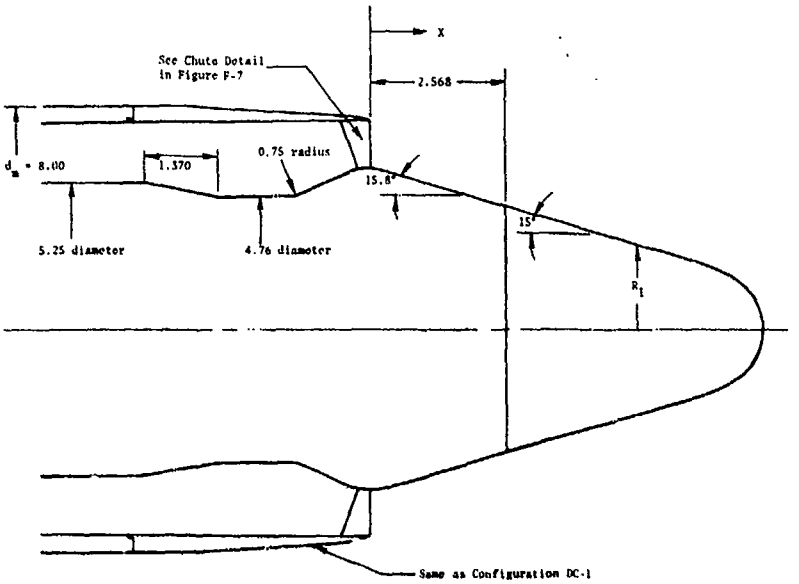

	Inner-Plug Geometry	
	Axial Coordinate, X/d_m	Radial Coordinate, R_I/d_m
Straight Line	- 0.170	0.298
	- 0.044	0.352
	- 0.039	0.354
	- 0.029	0.357
	- 0.020	0.358
	- 0.010	0.359
	0	0.360
	0.010	0.359
	0.020	0.357
	0.029	0.355
Straight Line	0.031	0.354
	0.286	0.282
	0.719	0.165
	0.724	0.164
	0.763	0.151
	0.802	0.138
	0.822	0.130
	0.841	0.121
	0.861	0.110
	0.880	0.095
	0.899	0.075
	0.919	0.040
	0.926	0

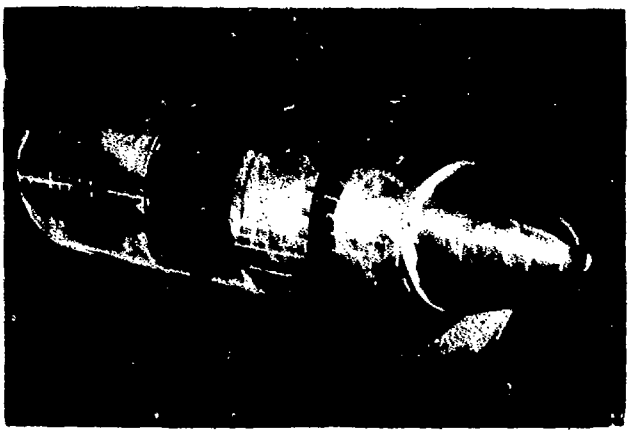

Figure F-8. Geometric Details of Configuration DC-2, AR = 1.5, Full Plug.

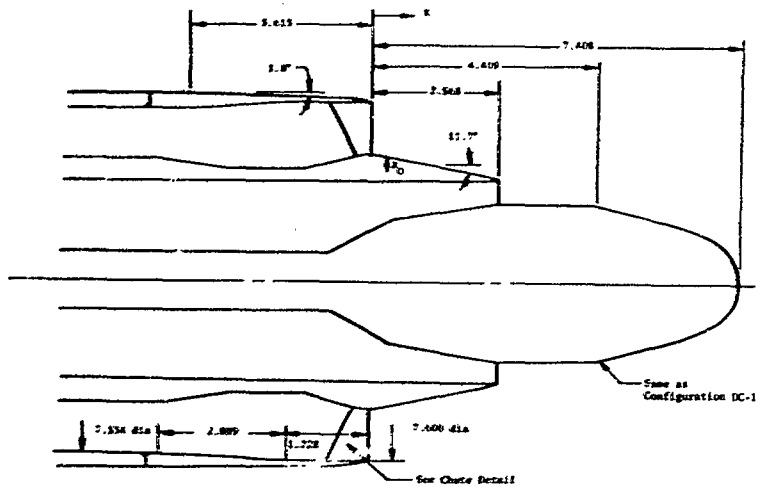

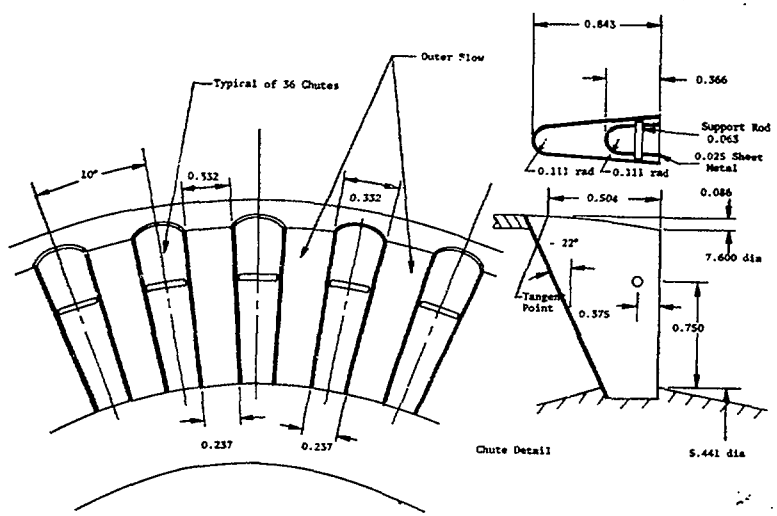

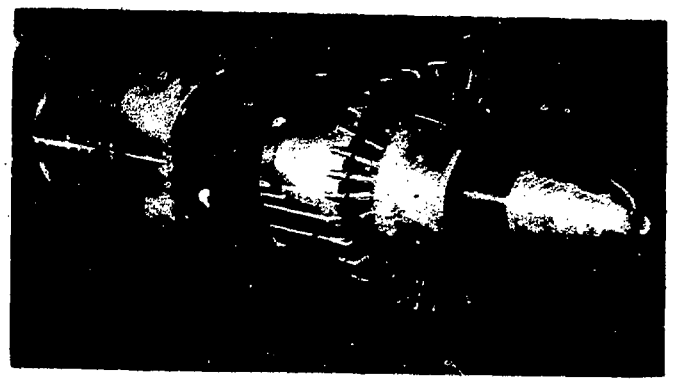

Outer-Plug Geometry		
	Axial Coordinate, X/d_m	Radial Coordinate, R_o/d_m
Straight Line	- 0.159	0.398
	- 0.056	0.329
	- 0.049	0.332
	- 0.039	0.335
	- 0.029	0.337
	- 0.020	0.338
	- 0.010	0.339
	0	0.340
	0.010	0.339
	0.020	0.337
	0.025	0.336
Straight Line	0.286	0.262
	0.321	0.275

Figure F-9. Geometric Details of Configuration DC-3, AR^c = 2.0, Baseline Plug.

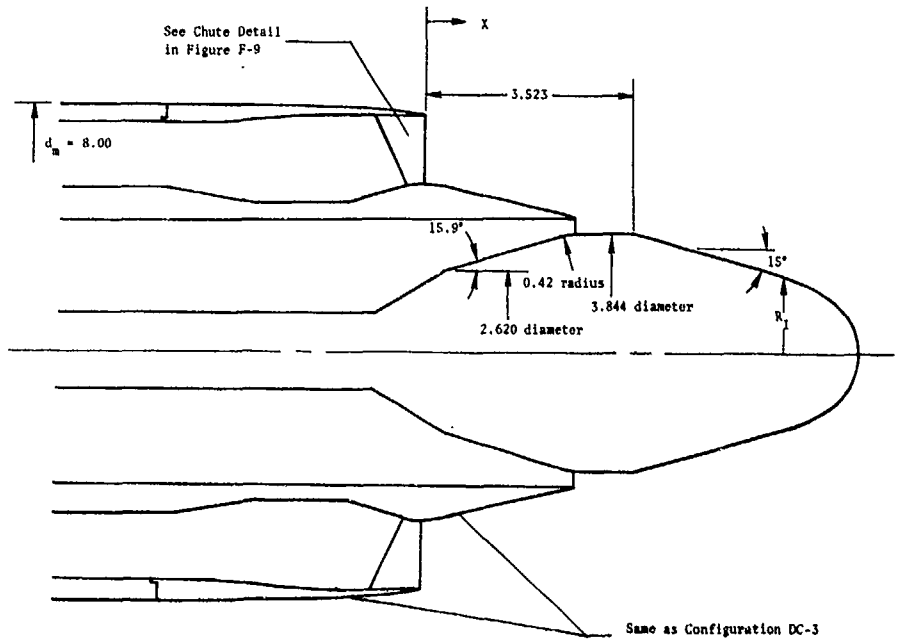

Inner-Plug Geometry	
Coordinate, X/d_m	Coordinate, R_I/d_m
0.440	0.240
0.719	0.165
0.724	0.164
0.763	0.151
0.802	0.138
0.822	0.130
0.841	0.121
0.861	0.110
0.880	0.095
0.899	0.075
0.919	0.040
0.926	0

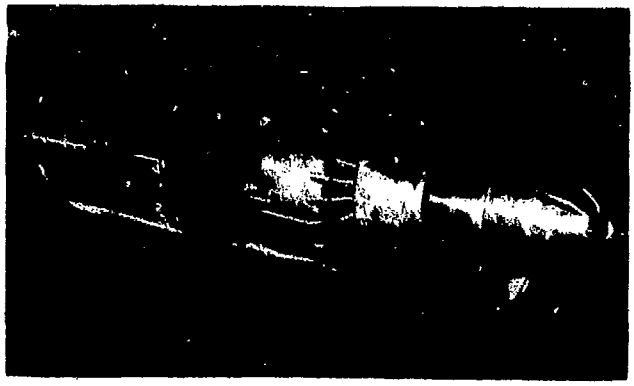

Figure F-10. Geometric Details of Configuration DC-4, AR = 2.0, Modified Baseline Plug.

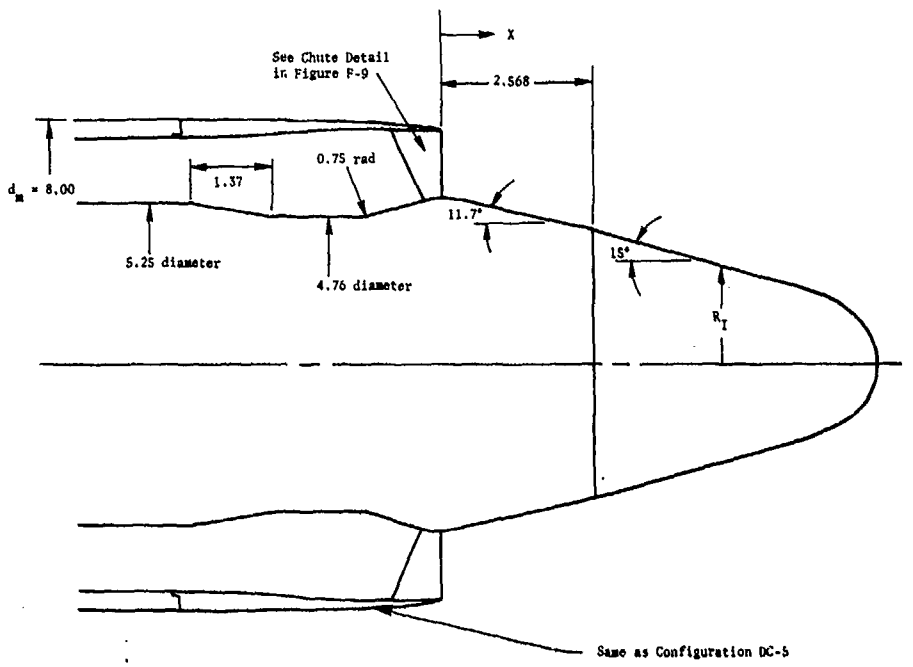

Inner-Plug Geometry	
Axial Coordinates, X/d_m	Radial Coordinates, R_I/d_m
- 0.159	0.298
- 0.056	0.329
- 0.049	0.332
- 0.039	0.335
- 0.029	0.337
- 0.020	0.338
- 0.010	0.339
0	0.340
0.010	0.339
0.020	0.337
0.025	0.336
0.286	0.282
0.719	0.165
0.724	0.164
0.763	0.151
0.802	0.138
0.822	0.130
0.841	0.121
0.861	0.110
0.880	0.095
0.899	0.075
0.919	0.040
0.926	0

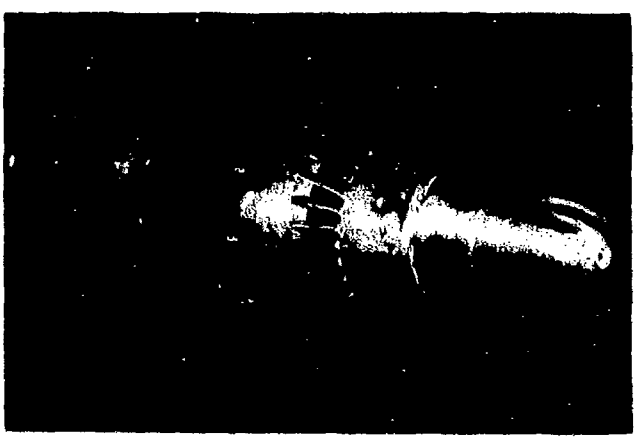

Figure F-11. Geometric Details of Configuration DC-5, AR = 2.0, Full Plug.

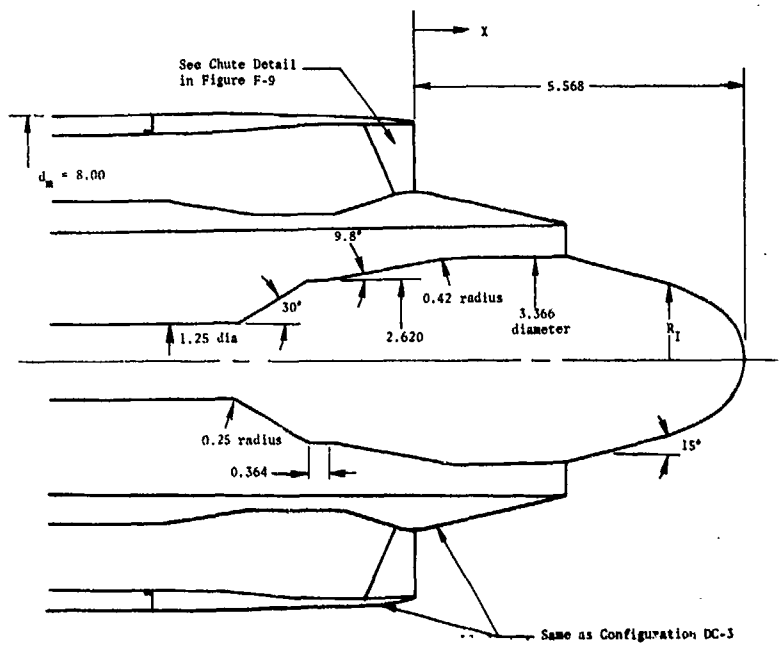

Inner-Plug Geometry	
Axial Coordinate, X/d_m	Radial Coordinate, R_I/d_m
0.321	0.210
0.489	0.165
0.494	0.164
0.533	0.151
0.572	0.138
0.592	0.130
0.611	0.121
0.631	0.110
0.650	0.095
0.669	0.075
0.689	0.040
0.706	0

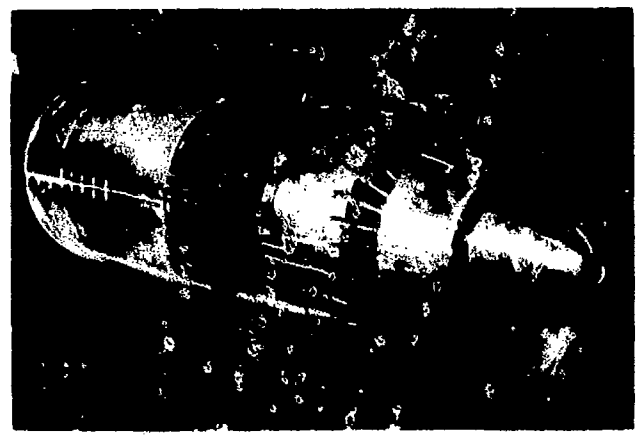

Figure F-12. Geometric Details of Configuration DC-6, AR = 2.0, Forward Plug.

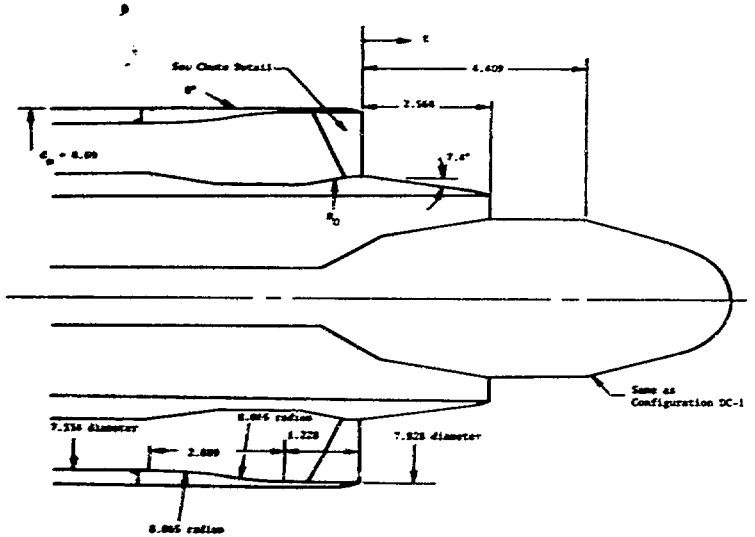

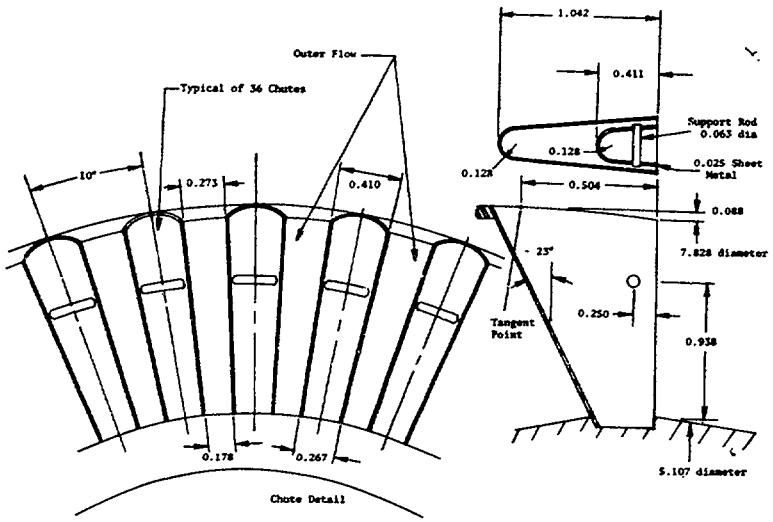

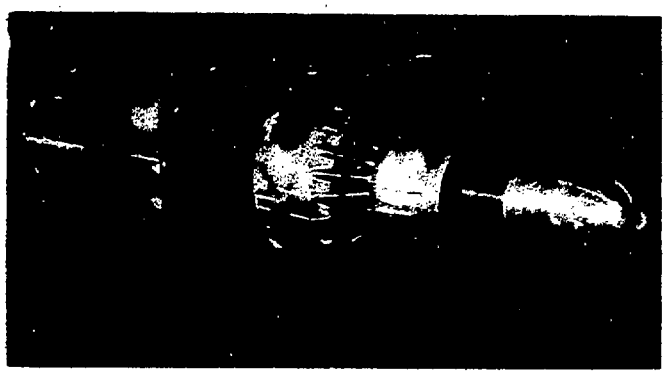

	Outer-Plug Geometry	
	Axial Coordinate, X/d_m	Radial Coordinate, R_i/d_m
Straight Line	- 0.157	0.298
	- 0.030	0.318
	- 0.020	0.319
	- 0.010	0.320
Straight Line	0	0 519
	0.286	0.282
	0.321	0.273

Figure F-13. Geometric Details of Configuration DC-7, AR = 2.5, Baseline Plug.

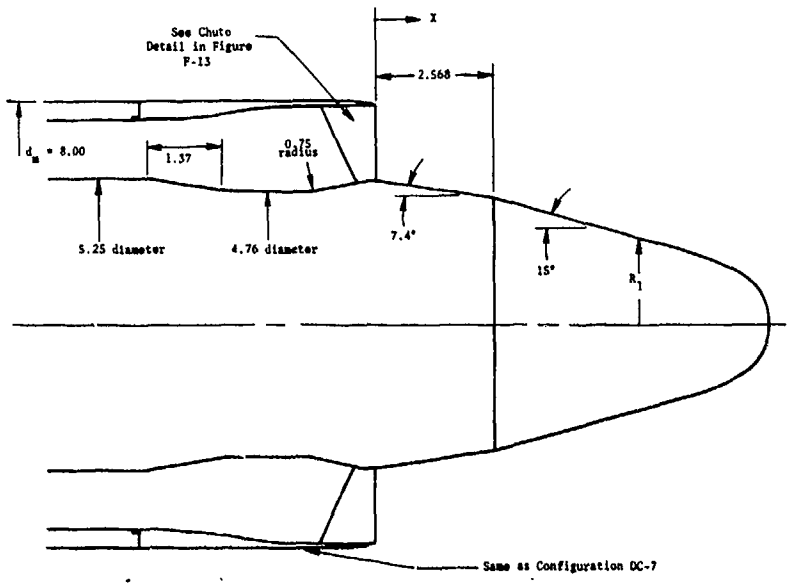

	Inner-Plug Geometry	
	Axial Coordinate, X/d_m	Radial Coordinate, R_1/d_m
Straight Line	- 0.137	0.298
	- 0.030	0.318
	- 0.020	0.319
	- 0.010	0.320
Straight Line	0	0.319
	0.286	0.282
	0.719	0.165
	0.724	0.164
	0.763	0.151
	0.802	0.138
	0.822	0.130
	0.841	0.121
	0.861	0.110
	0.880	0.095
	0.899	0.075
	0.919	0.040
	0.926	0

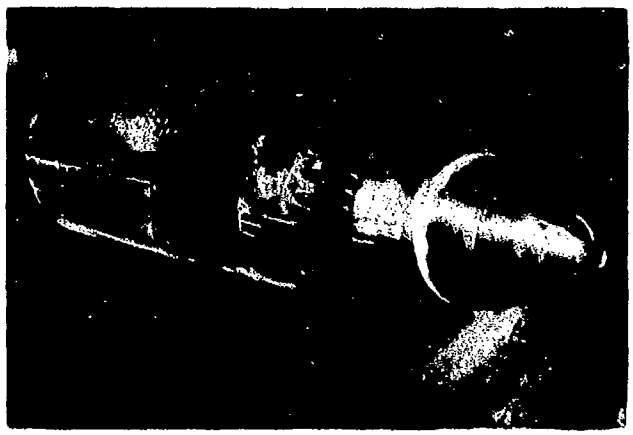

Figure F-14. Geometric Details of Configuration DC-8, AR = 2.5, Full Plug.

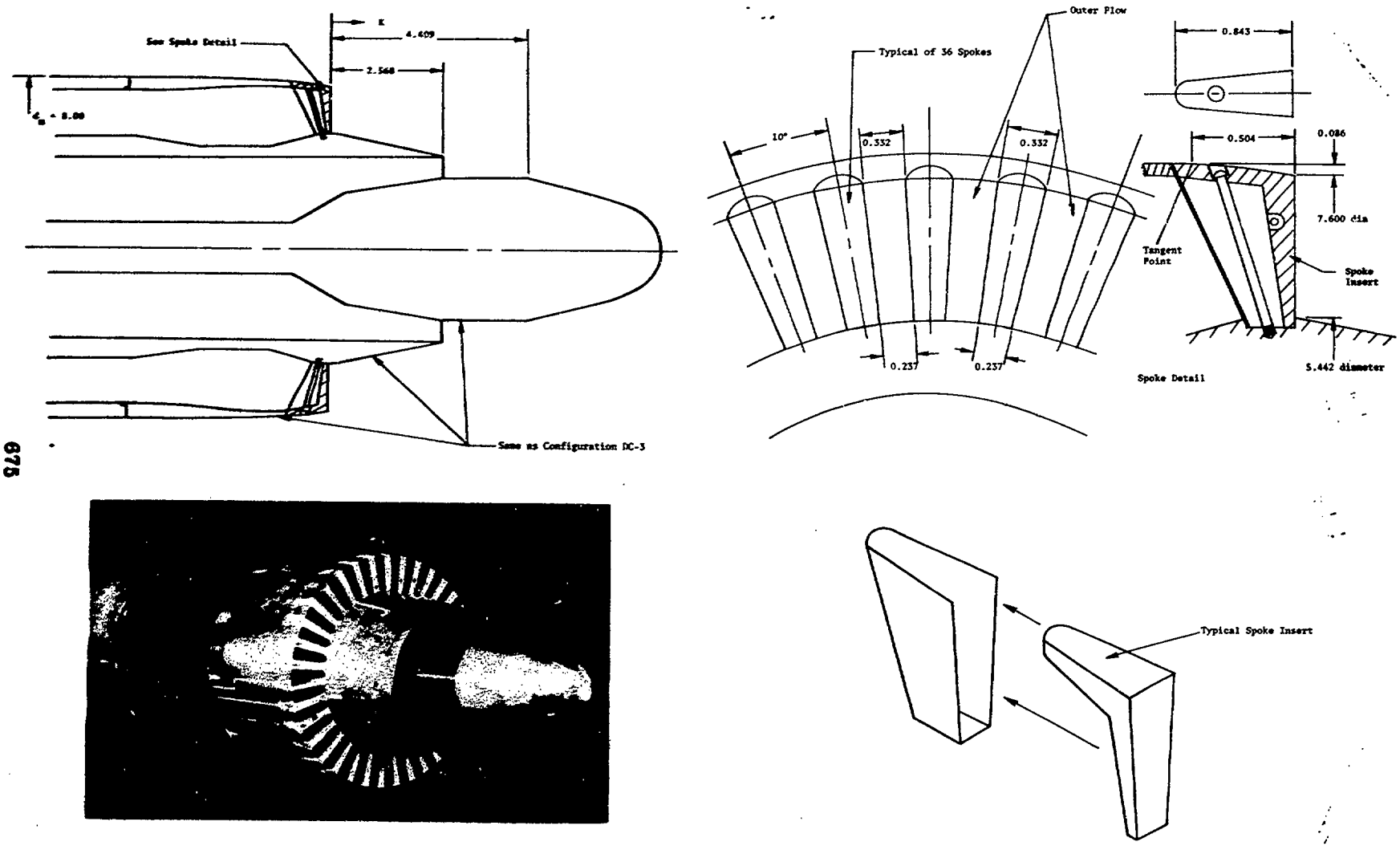

Figure F-15. Geometric Details of Configuration DC-3 (Spoke), N = 36, AR = 2.0, Baseline Plug.

INSTRUMENTATION LOCATION

Details of static pressure tap locations for all models tested are included in Figures F-16 through F-21.

Static-Pressure Locations

Orifice	Axial Location, X_β/d_m	Circumferential Location, θ deg
1	-0.167	90, 180, 270
2	0	↓
3	0.193	
4	0.373	
5	0.566	
6	0.746	
7	0.927	
8	1.107	
9	1.197	
10	1.274	

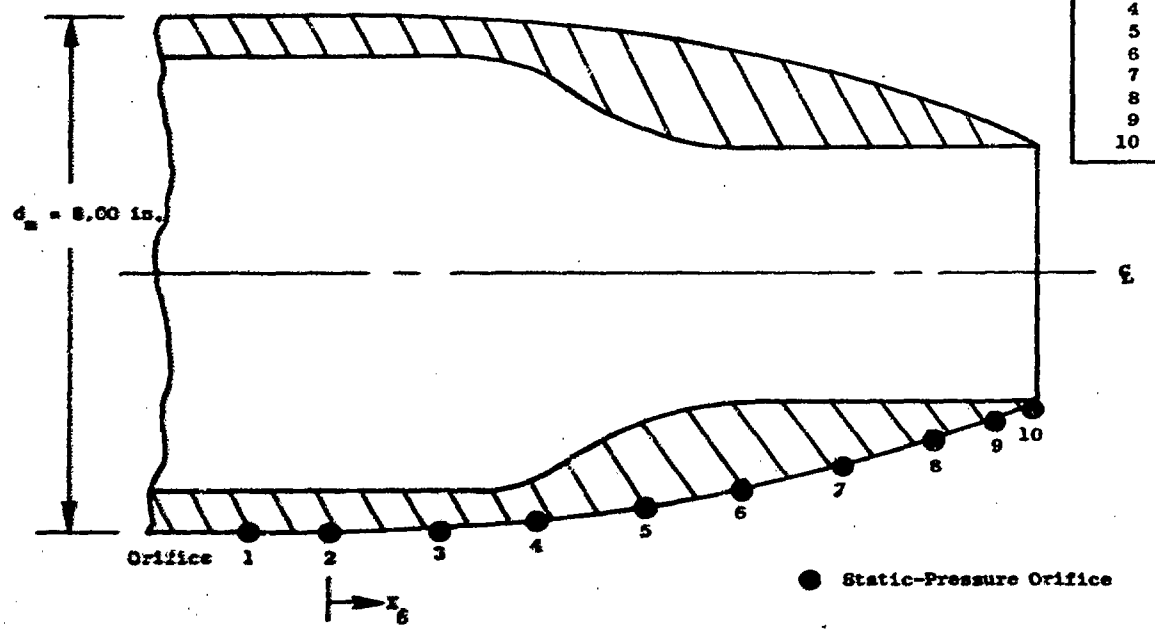

677

Figure F-16. Supersonic Tunnel Association (STA) Boattail Static-Pressure Instrumentation.

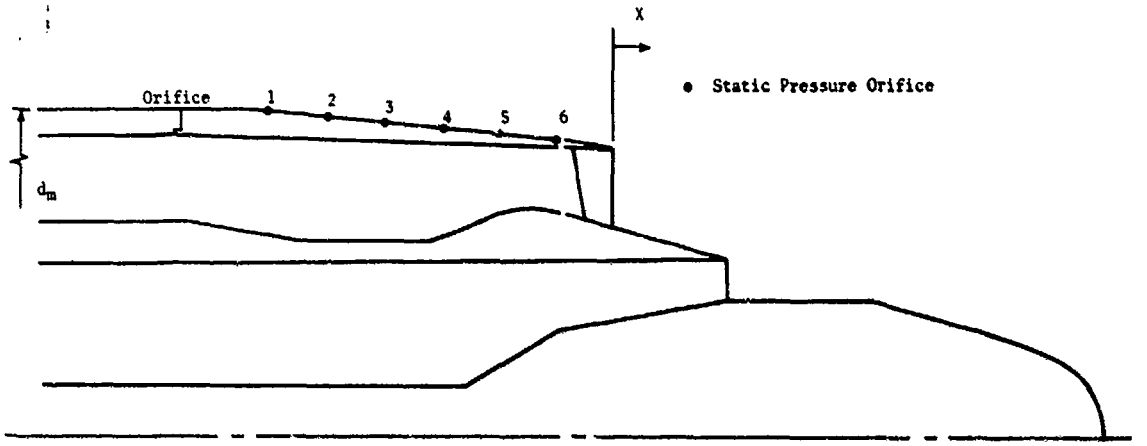

Shallow-Chute Nozzles

Orifice	SC-1		SC-2, SC-3, SC-4, SC-5		SC-6	
	Axial Location, X/d_m	Circumferential Location, θ degrees	Axial Location, X/d_m	Circumferential Location, θ degrees	Axial Location X/d_m	Circumferential Location, θ degrees
1	- 0.554	108	- 0.554	108	- 0.554	108
2	- 0.461	0	- 0.461	348	- 0.461	351
3	- 0.369	18	- 0.369	12	- 0.369	9
4	- 0.276	36	- 0.276	24	- 0.276	18
5	- 0.184	252	- 0.184	252	- 0.184	252
6	- 0.091	126	- 0.071	132	- 0.061	135

Deep-Chute and Spoke Nozzles

Orifice	DC-1, DC-2		DC-3, DC-4, DC-5, DC-6, DC-3 (Spoke)		DC-7, DC-8	
	Axial Location, X/d_m	Circumferential Location, θ degrees	Axial Location, X/d_m	Circumferential Location, θ degrees	Axial Location X/d_m	Circumferential Location, θ degrees
1	- 0.410	110	- 0.410	110	- 0.410	110
2	- 0.313	350	- 0.325	350	- 0.329	350
3	- 0.210	10	- 0.240	10	- 0.250	10
4	- 0.106	20	- 0.138	30	- 0.166	20
5	"	"	"	"	"	"
6	"	"	"	"	"	"

Figure F-17. Annular Nozzle Outer Shroud Static Pressures.

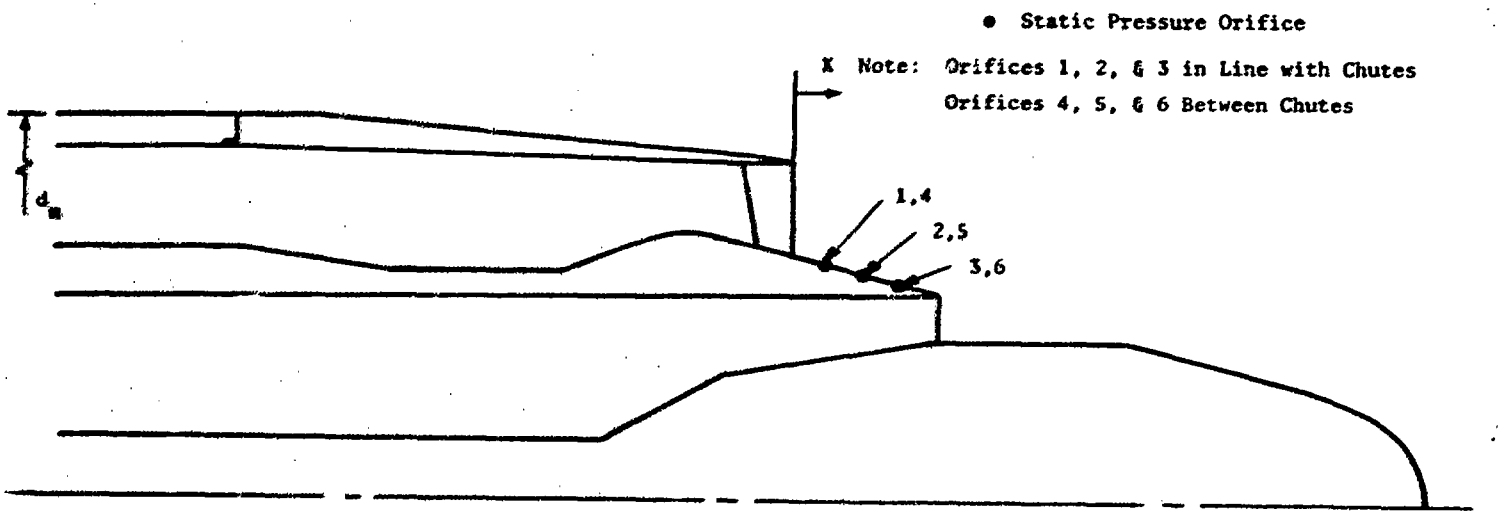

Orifice	Shallow-Chute Nozzles						Deep-Chute and Spoke Nozzles	
	SC-1		SC-2, SC-3, SC-4, SC-5		SC-6			
	Axial Location, X/d_m	Circumferential Location, θ degrees	Axial Location, X/d_m	Circumferential Location, θ degrees	Axial Location, X/d_m	Circumferential Location, θ degrees	Axial Location, X/d_m	Circumferential Location, θ degrees
1	0.042	126	0.042	132	0.042	135	0.081	120
2	0.088	252	0.088	252	0.088	261	0.163	260
3	0.133	270	0.133	264	0.133	261	0.244	270
4	0.042	54	0.042	48	0.042	63	0.081	60
5	0.088	342	0.088	336	0.088	342	0.163	330
6	0.133	162	0.133	156	0.133	162	0.244	160

Figure F-18. Outer Plug Static Pressures.

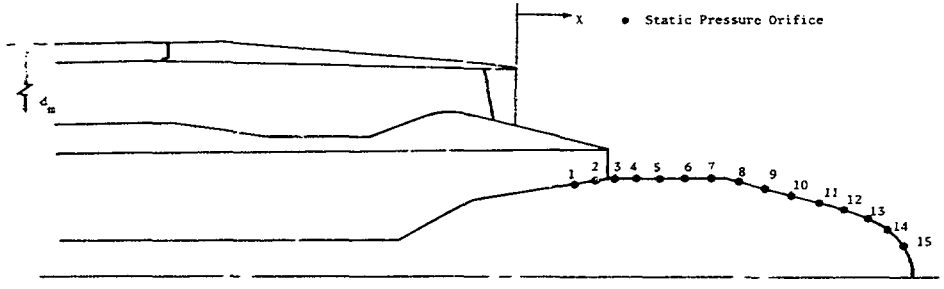

Shallow-Chute Nozzles

Orifice	SC-1, SC-2, SC-3, SC-4		SC-4		SC-5	
	Axial Location, X/d_m	Circumferential Location, θ degrees	Axial Location, X/d_m	Circumferential Location, θ degrees	Axial Location, X/d_m	Circumferential Location, θ degrees
1	0.331	300	0.208	180	- 0.107	300
2	0.360	240	0.242	120	- 0.055	240
3	0.360	180	0.286	60	- 0.023	180
4	0.392	120	0.358	0	0.018	120
5	0.396	60	0.398	0	0.064	60
6	0.358	0	0.444	0	0.114	0
7	0.394	0	--	--	0.171	0
8	0.444	0	--	--	0.224	0
9	0.530	45	0.500	45	0.277	45
10	0.553	90	0.555	90	0.329	90
11	0.637	135	0.637	135	0.385	135
12	0.659	180	0.659	180	0.436	180
13	0.797	225	0.797	225	0.483	225
14	0.748	270	0.766	270	0.524	270
15	0.777	315	0.777	315	0.555	315

Deep-Chute and Spoke Nozzles

Orifice	DC-1, DC-3, DC-4, DC-7 DC-3 (Spoke)		DC-2, DC-5, DC-8		DC-6	
	Axial Location, X/d_m	Circumferential Location, θ degrees	Axial Location, X/d_m	Circumferential Location, θ degrees	Axial Location, X/d_m	Circumferential Location, θ degrees
1	0.256	300	0.340	180	0.033	300
2	0.500	240	0.381	120	0.077	240
3	0.340	180	0.428	60	0.117	180
4	0.381	120	0.478	0	0.158	120
5	0.428	60	0.534	0	0.204	60
6	0.478	0	0.588	0	0.254	0
7	0.534	0	--	--	0.310	0
8	0.588	0	--	--	0.364	0
9	0.640	45	0.640	45	0.417	45
10	0.693	90	0.693	90	0.469	90
11	0.746	135	0.746	135	0.523	135
12	0.799	180	0.799	180	0.575	180
13	0.846	225	0.840	225	0.621	225
14	0.888	270	0.888	270	0.664	270
15	0.916	315	0.916	315	0.693	315

Figure F-19. Inner Plug Static Pressures.

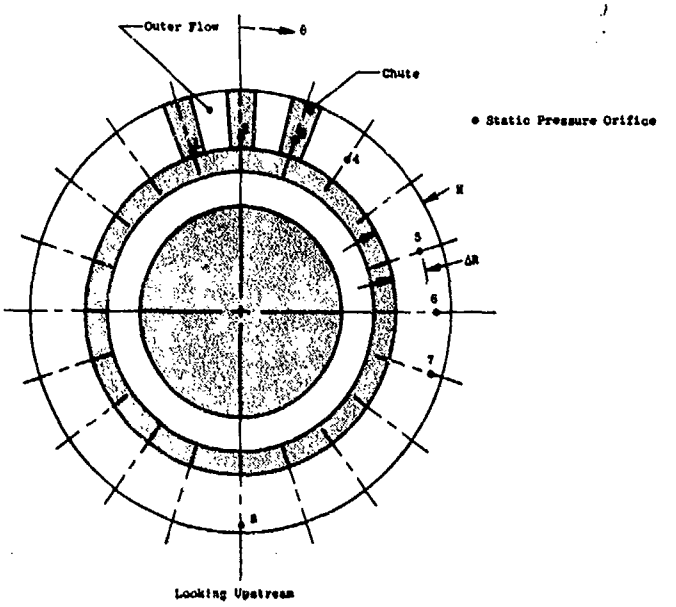

Shallow-Chute Nozzle

Orifice	SC-1		SC-2, SC-3, SC-4, SC-5		SC-6	
	Radial Location, Δ R/H	Circumferential Location, θ degrees	Radial Location, Δ R/H	Circumferential Location, θ degrees	Radial Location, Δ R/H	Circumferential Location, θ degrees
1	0.070	342	0.020	336	0	342
2	0.160	0	0.171	348	0.151	351
3	0.290	18	0.381	12	0.302	9
4	0.450	36	0.411	24	0.433	18
5	0.586	72	0.522	72	0.605	72
6	0.696	90	0.602	84	0.690	81
7	0.791	108	0.782	103	0.806	108
8	0.876	180	0.903	168	0.958	171
9	..	..	..	..	..	..
10	..	..	..	..	..	..

Deep-Chute and Spoke Nozzles

Orifice	DC-1, DC-2		DC-3, DC-4, DC-5, DC-6		DC-7, DC-8		DC-9 (Spoke)	
	Radial Location, Δ R/H	Circumferential Location, θ degrees	Radial Location, Δ R/H	Circumferential Location, θ degrees	Radial Location, Δ R/H	Circumferential Location, θ degrees	Radial Location, Δ R/H	Circumferential Location, θ degrees
1	0.035	340	0	340	0	340	..	..
2	0.110	350	0.120	350	0.154	354	0.126	350
3	0.247	10	0.255	10	0.311	10	0.255	10
4	0.381	20	0.424	20	0.475	20	0.424	20
5	0.609	70	0.556	70	0.593	70	0.556	70
6	0.753	90	0.756	90	0.766	90	0.756	90
7	0.858	110	0.8[illegible]	110	0.859	110	0.850	110
8	0.981	170	0.912	170	1.046	170	..	..
9	0.537	250	0.581	250	0.263	250	..	..
10	0.574	190	0.510	190	0.505	190	..	..

Figure F-20. Suppressor Element Base Static Pressures.

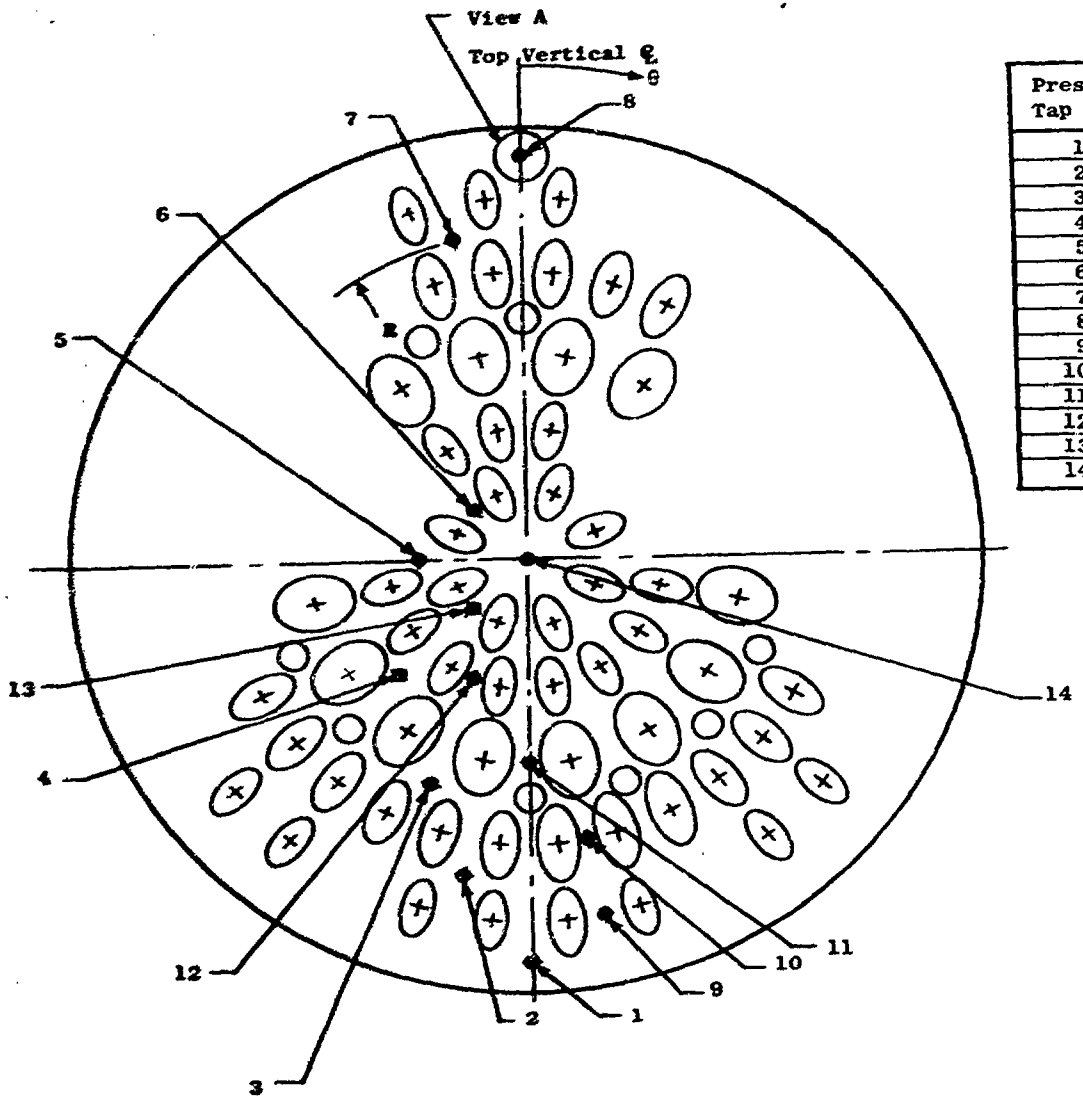

Pressure Tap No.	R Radial Location	θ Angular Location
1	3.432	180°
2	2.760	191° 15'
3	2.097	202° 30'
4	1.435	225°
5	0.857	270°
6	0.458	315°
7	2.760	348° 45'
8	3.432	0°
9	3.078	168° 45'
10	2.435	168° 45'
11	1.760	180°
12	1.110	202° 30'
13	0.591	225°
14	0.000	180°

Figure F-21. 104-Tube Nozzle Instrumentation.

ANNULAR SUPPRESSED-NOZZLE THRUST COEFFICIENTS

Annular suppressed-nozzle thrust coefficients are presented as a function of pressure ratio in Figures F-22 through F-36.

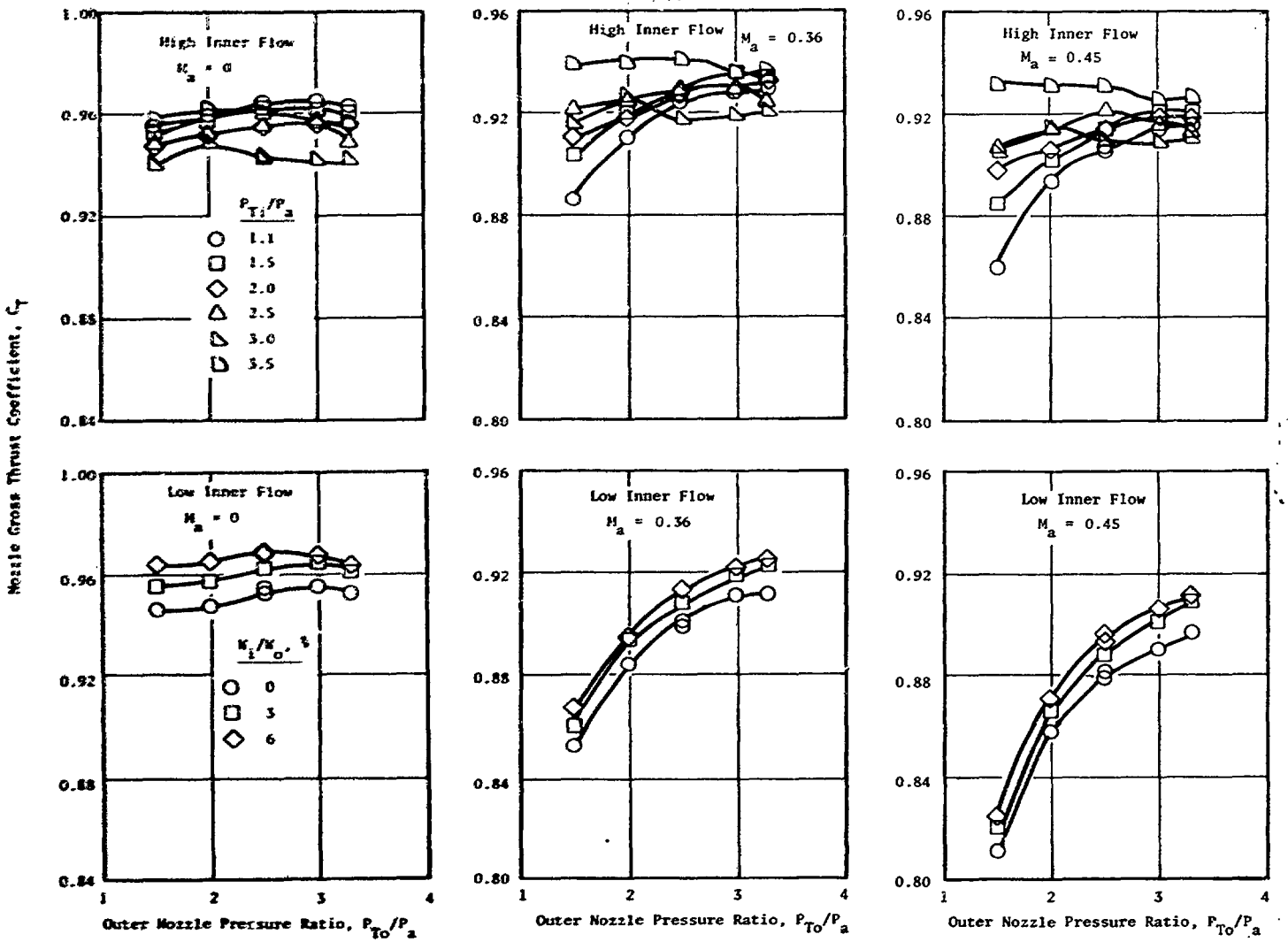

Figure F-22. Configuration SC-1 Performance.

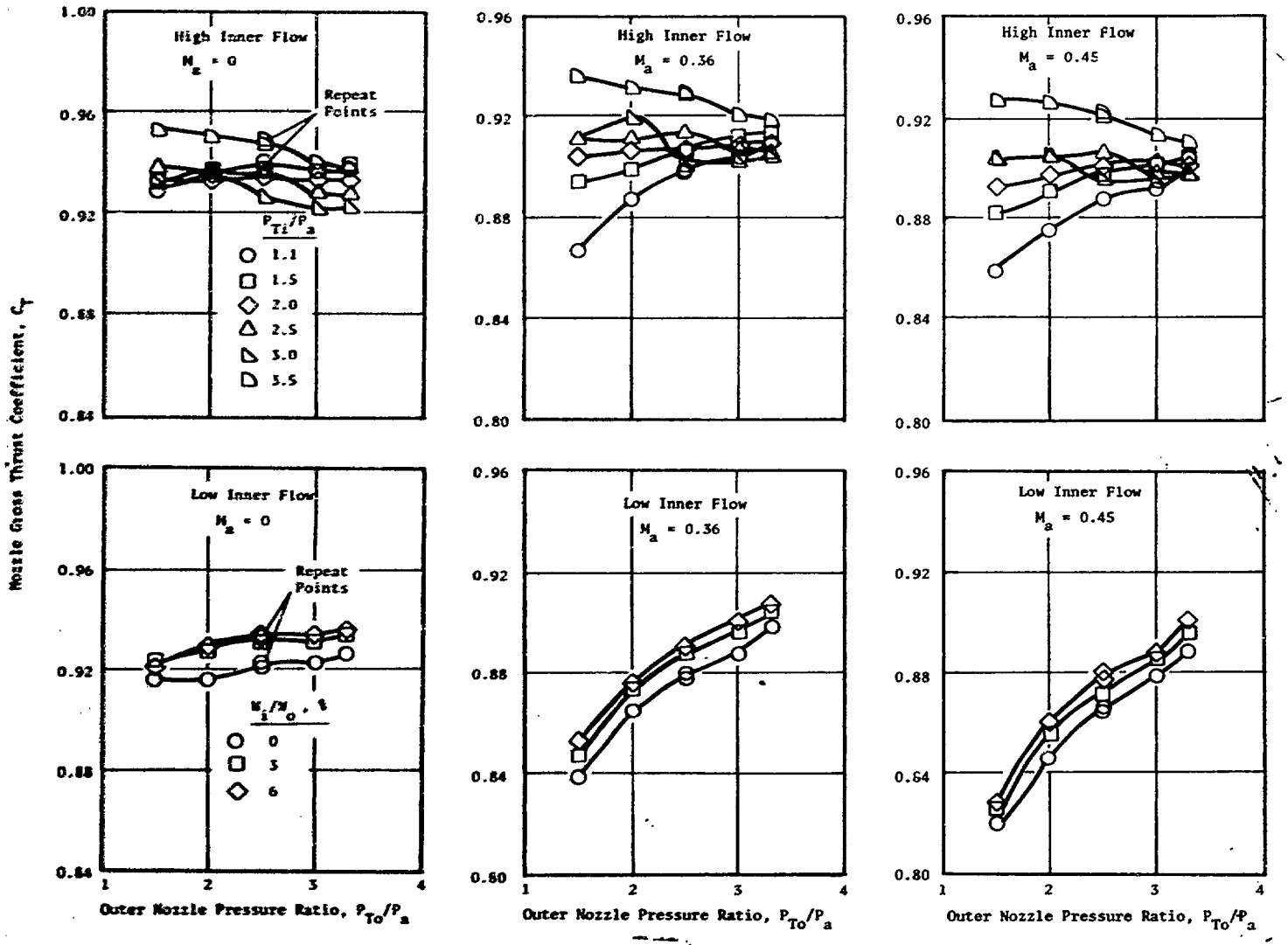

Figure F-23. Configuration SC-2 Performance.

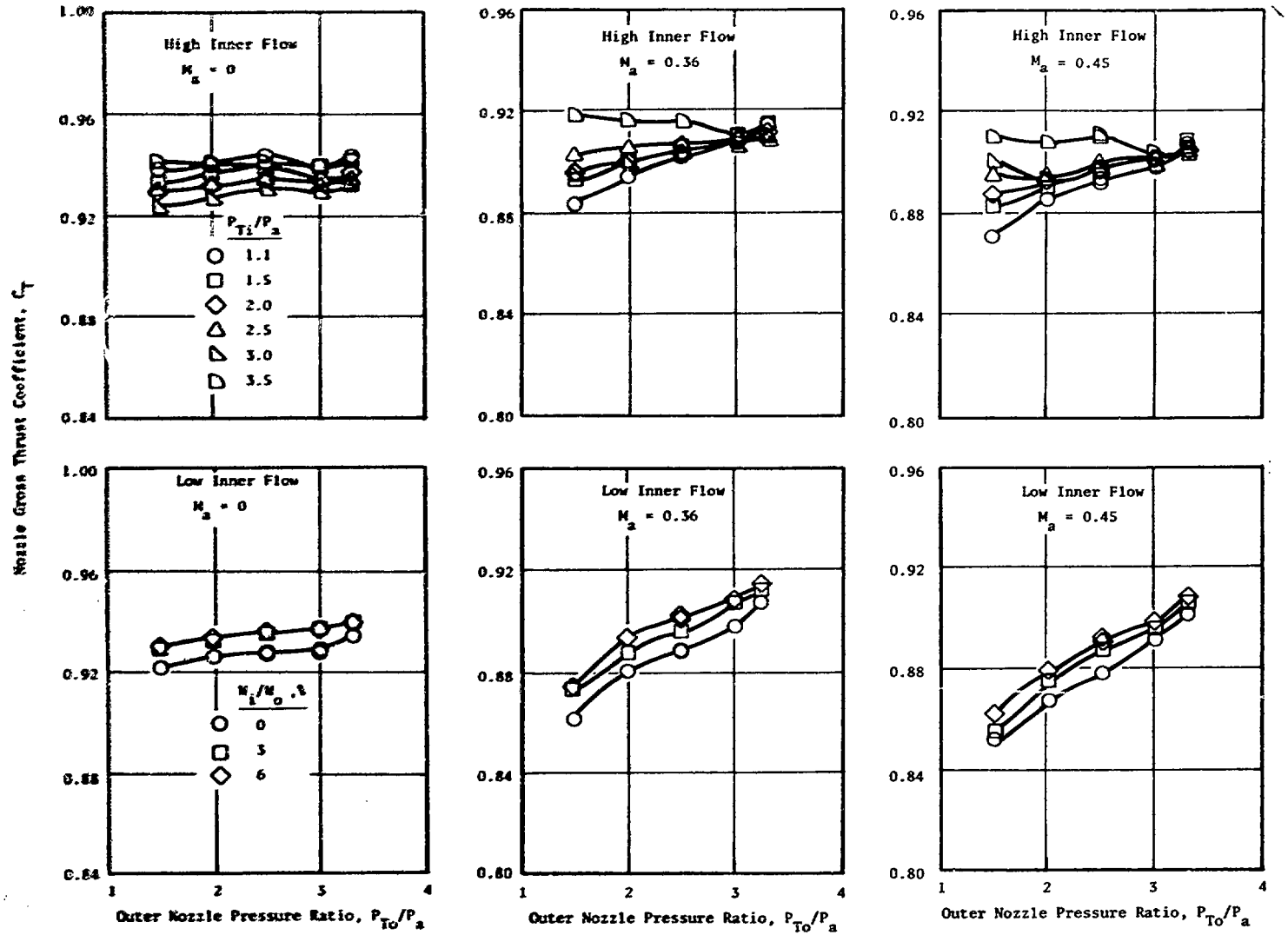

Figure F-24. Configuration SC-3 Performance.

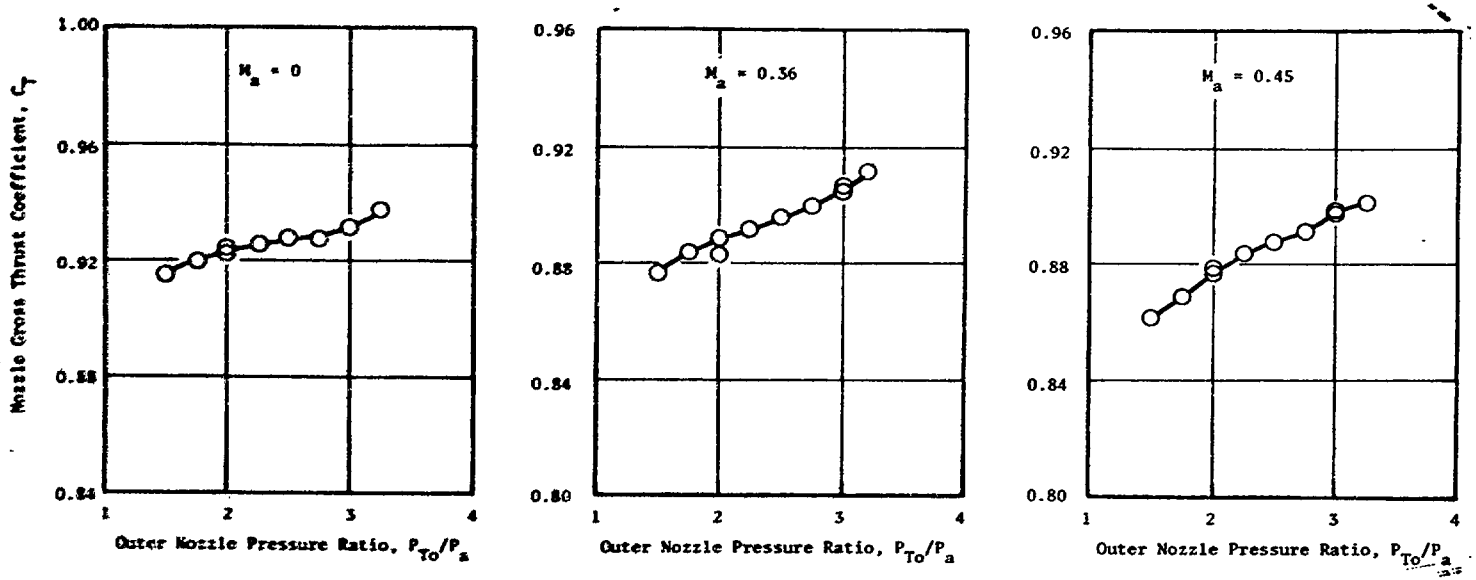

Figure F-25. Configuration SC-4 Performance.

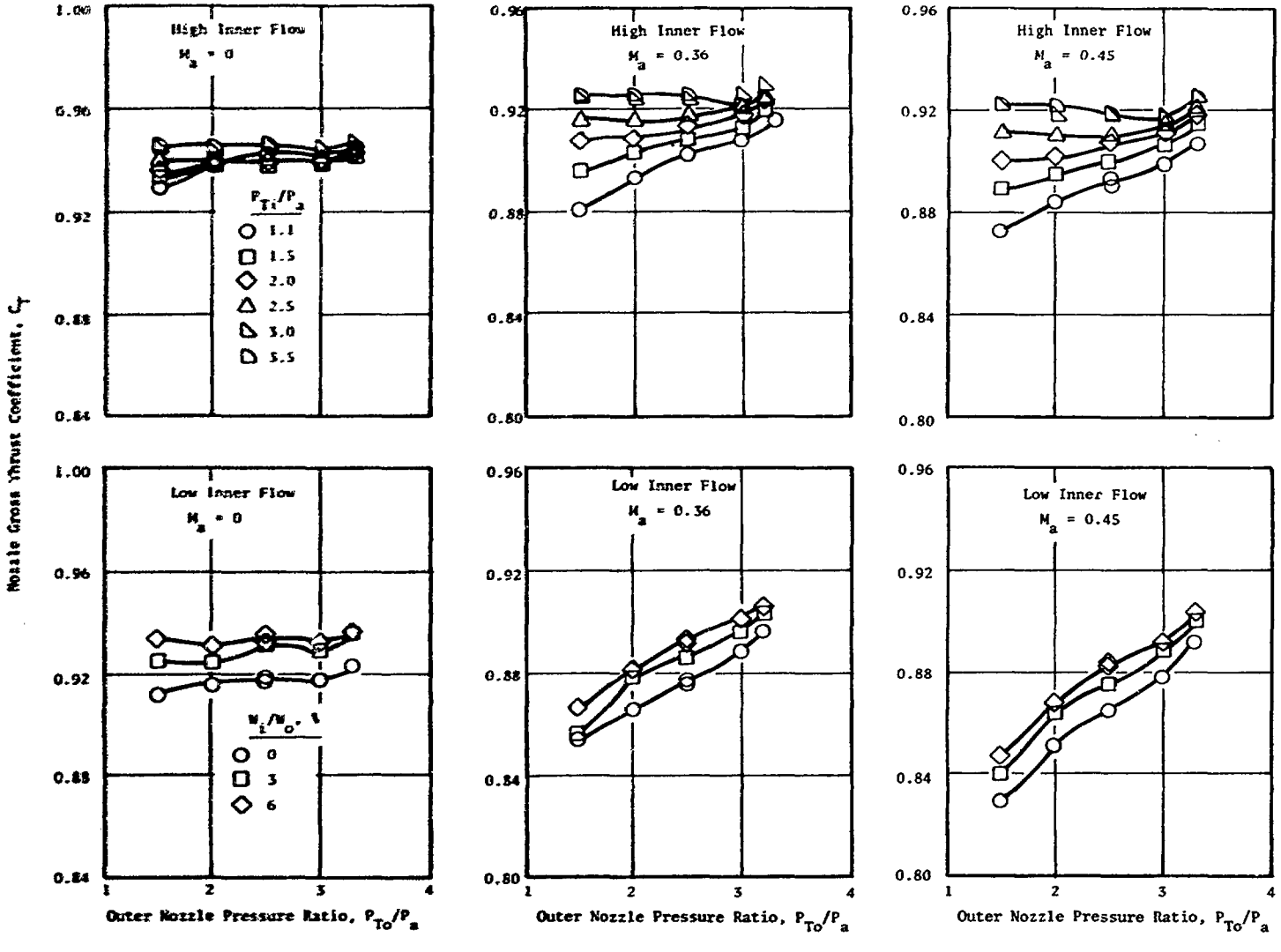

Figure F-26. Configuration SC-5 Performance.

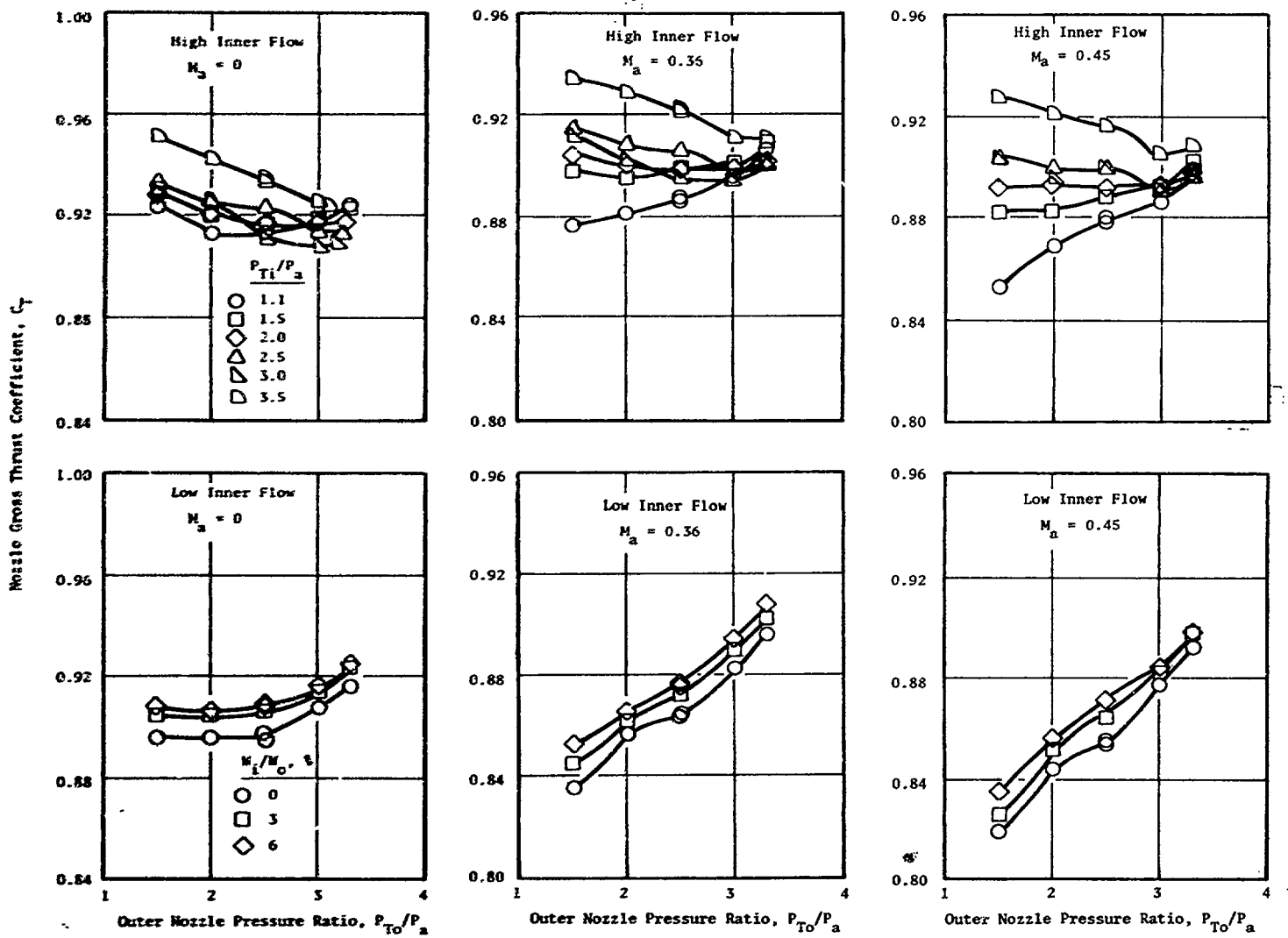

Figure F-27. Configuration SC-6 Performance.

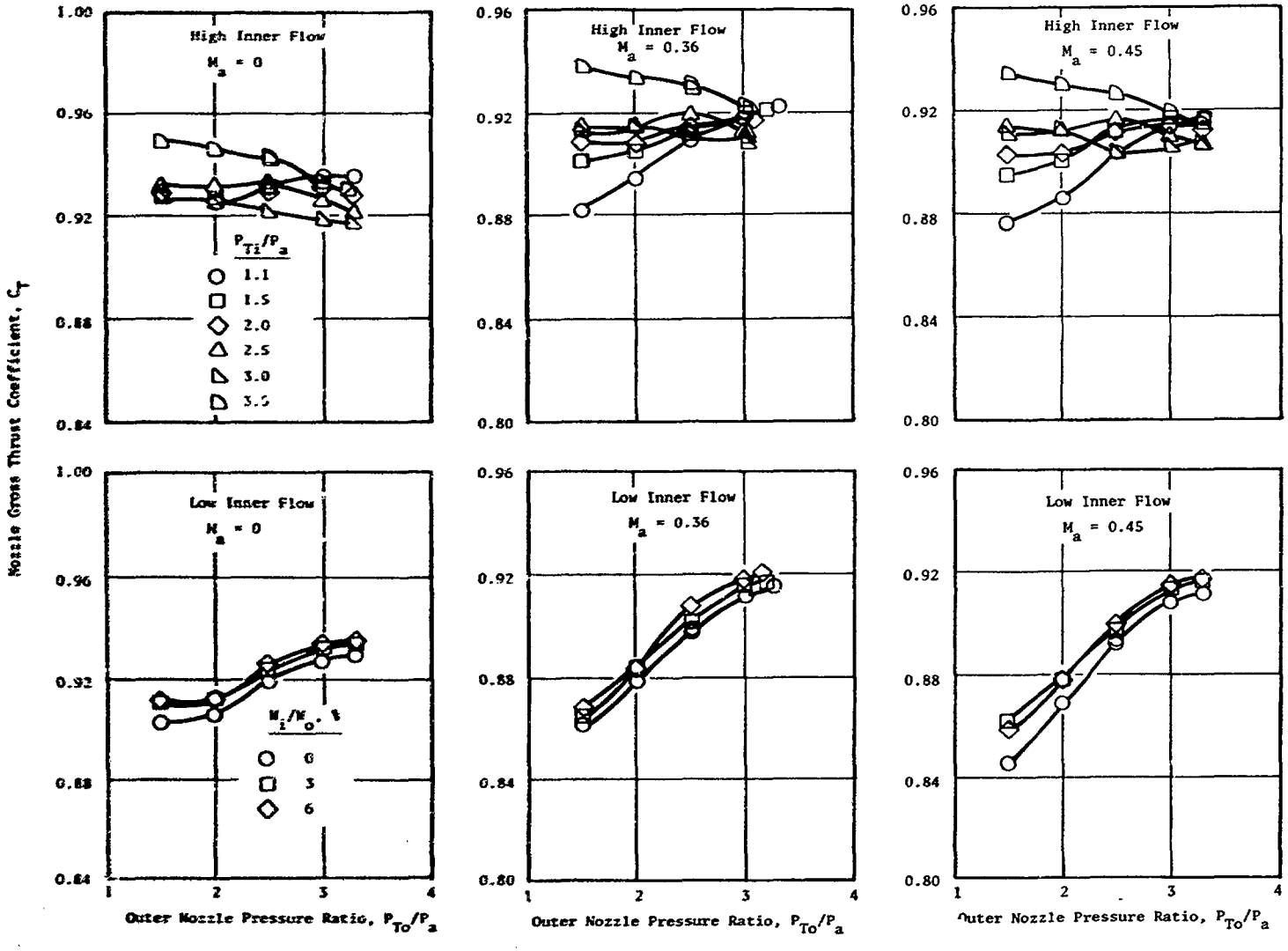

Figure F-28. Configuration DC-1 Performance.

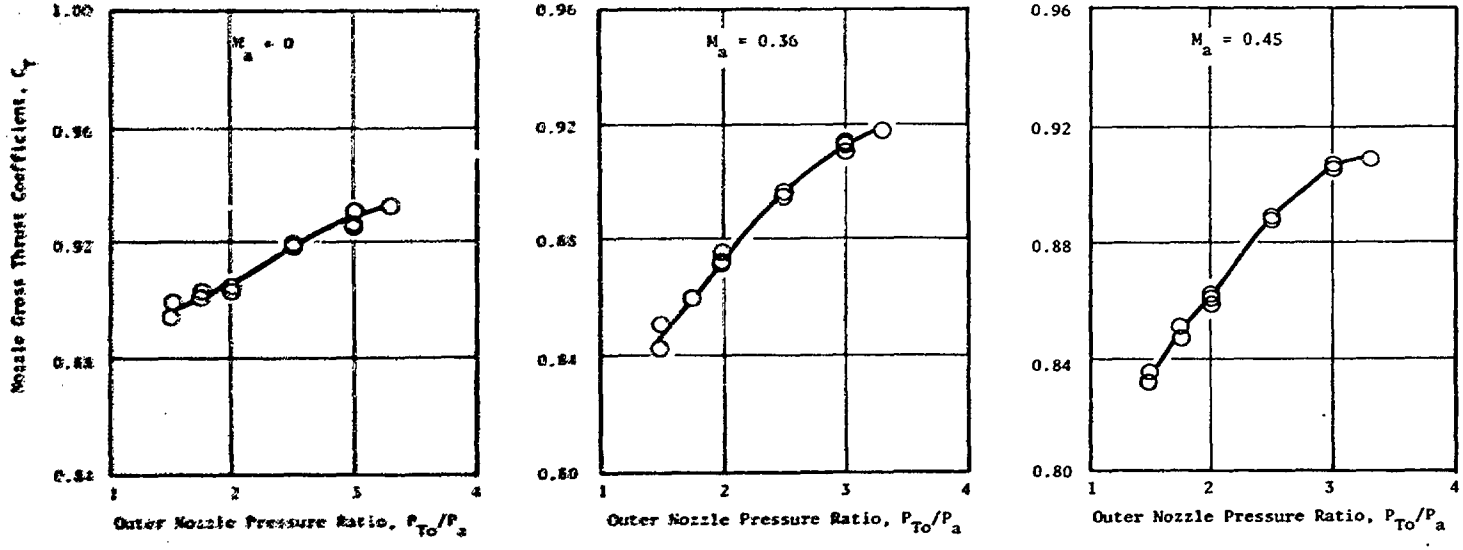

Figure F-29. Configuration DC-2 Performance.

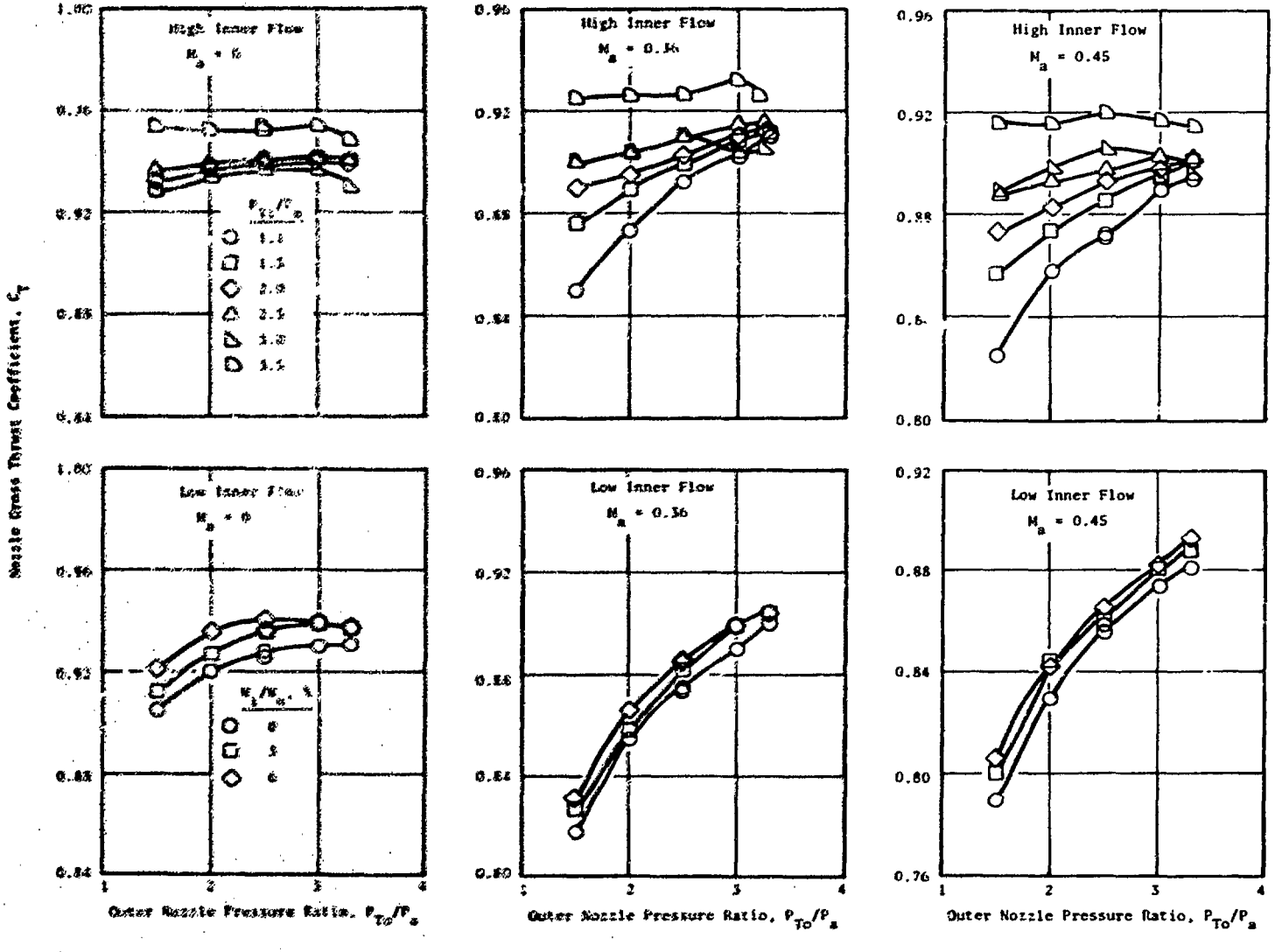

Figure F-30. Configuration DC-3 Performance.

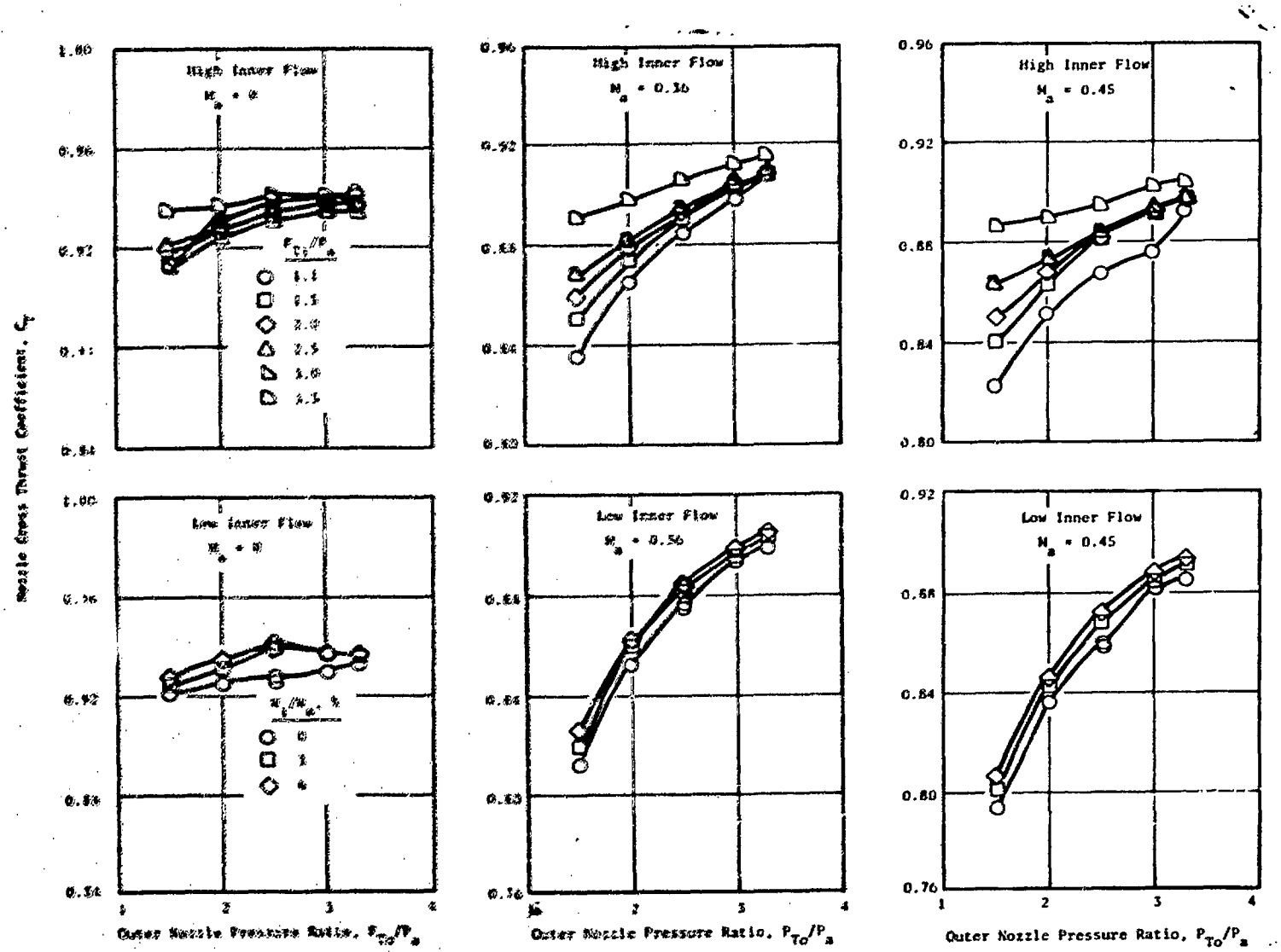

Figure F-31. Configuration DC-4 Performance.

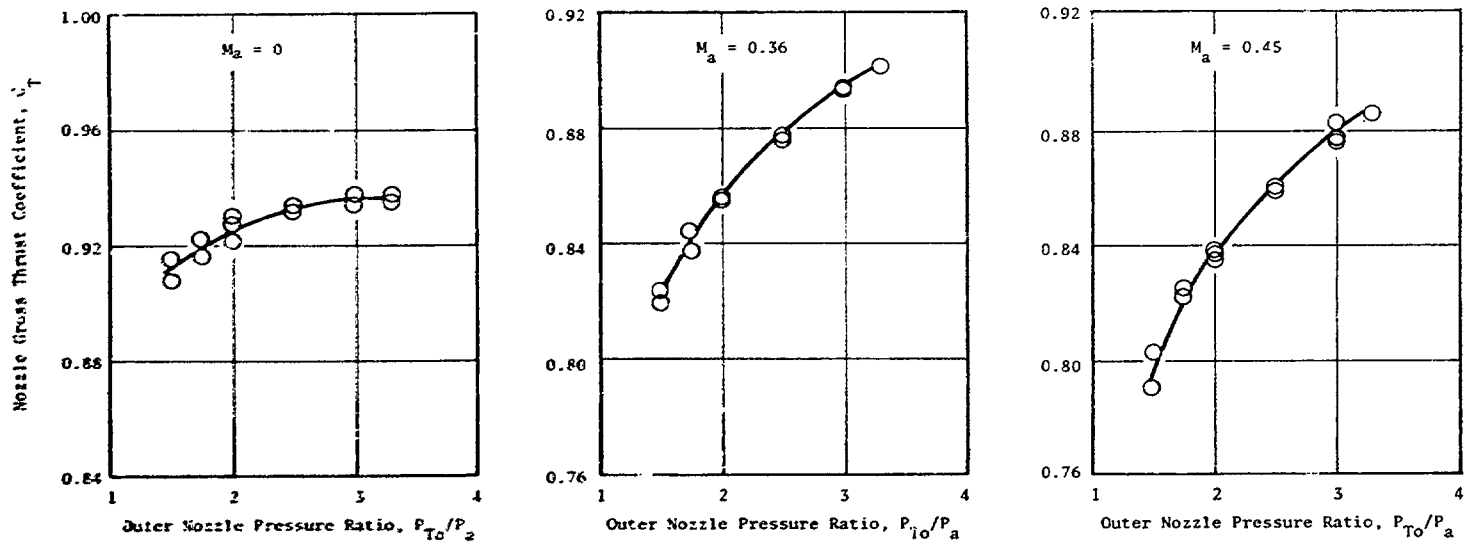

Figure F-32. Configuration DC-5 Performance.

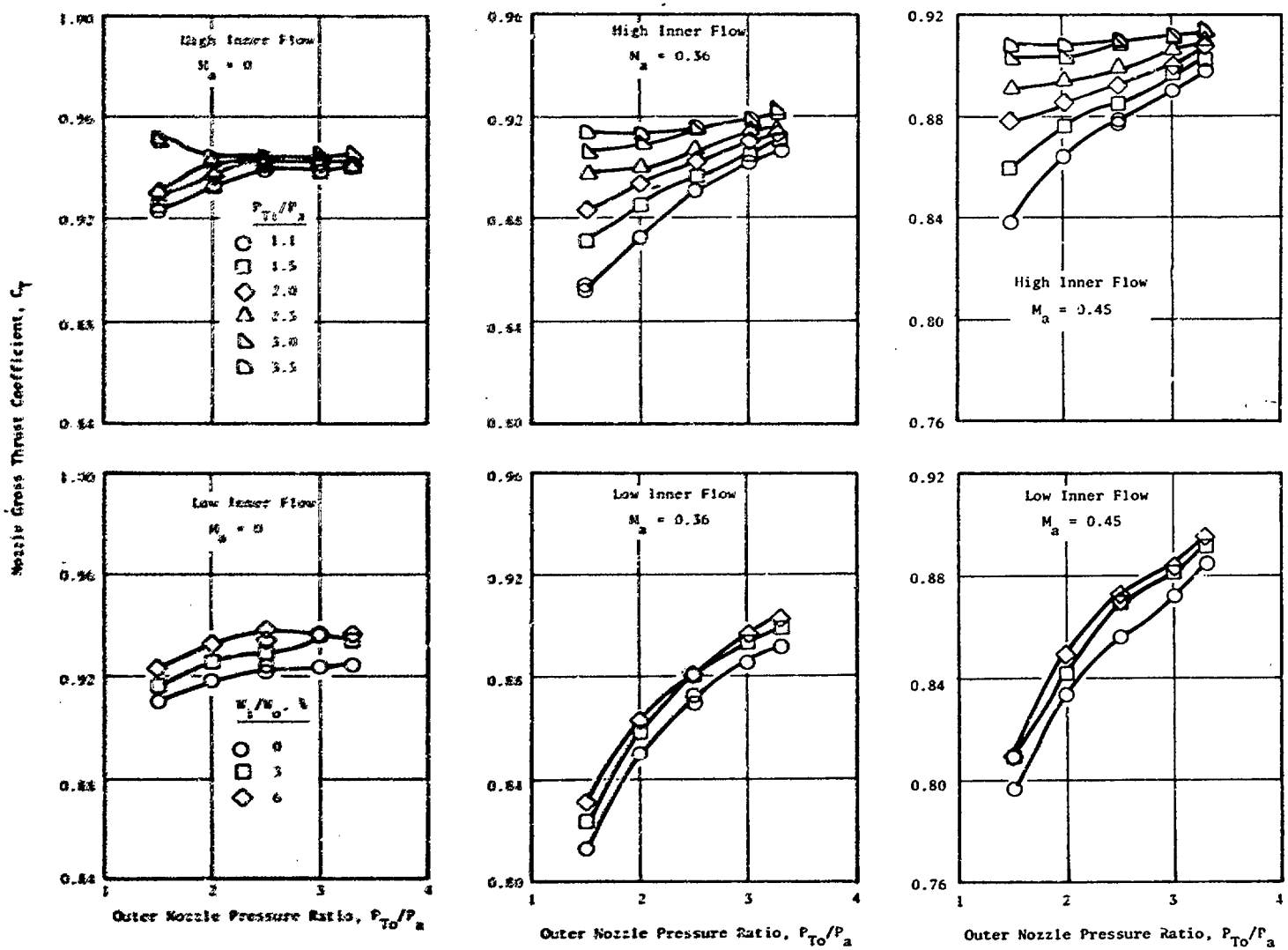

Figure F-33. Configuration DC-6 Performance.

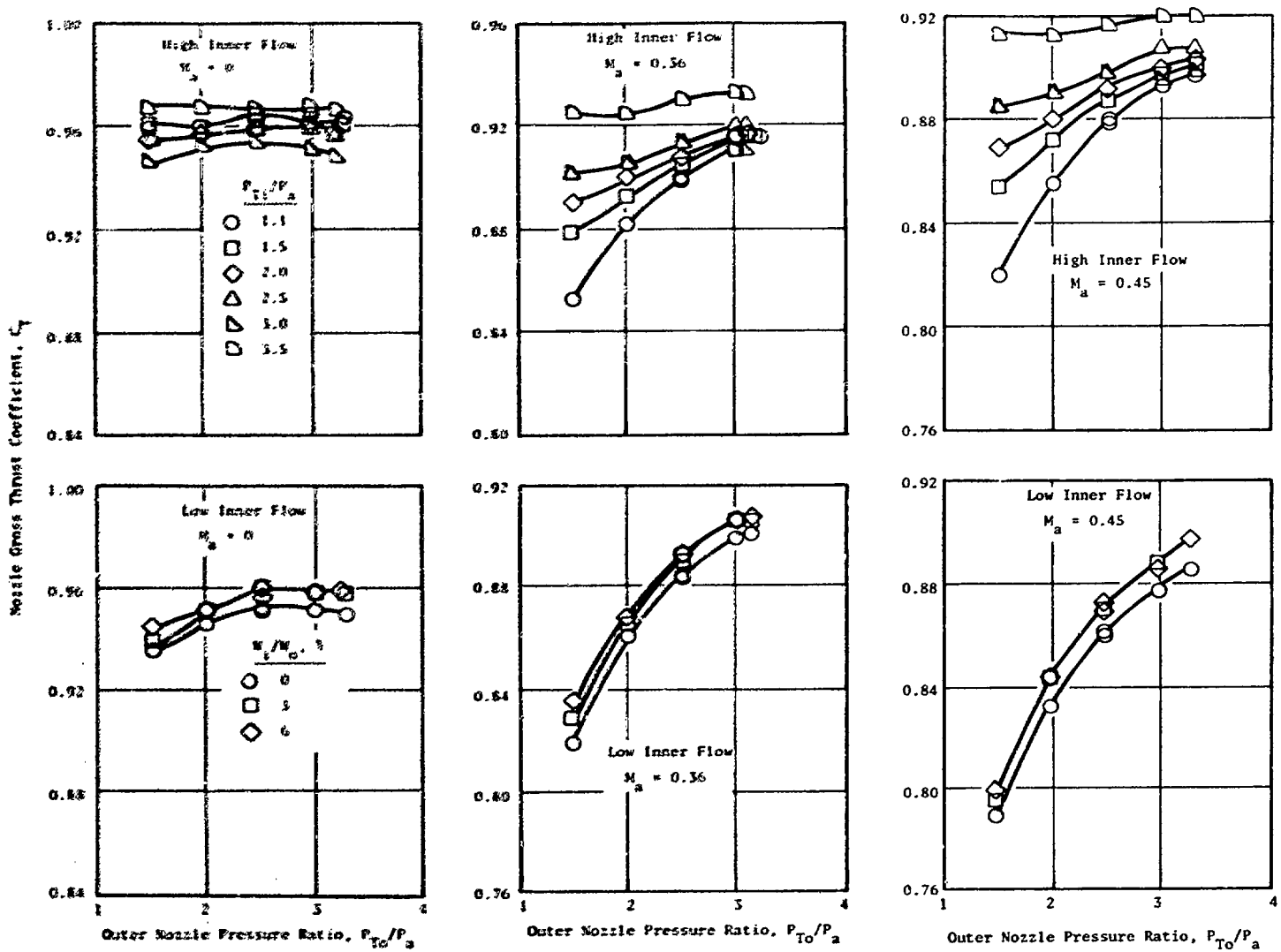

Figure F-34. Configuration DC-7 Performance.

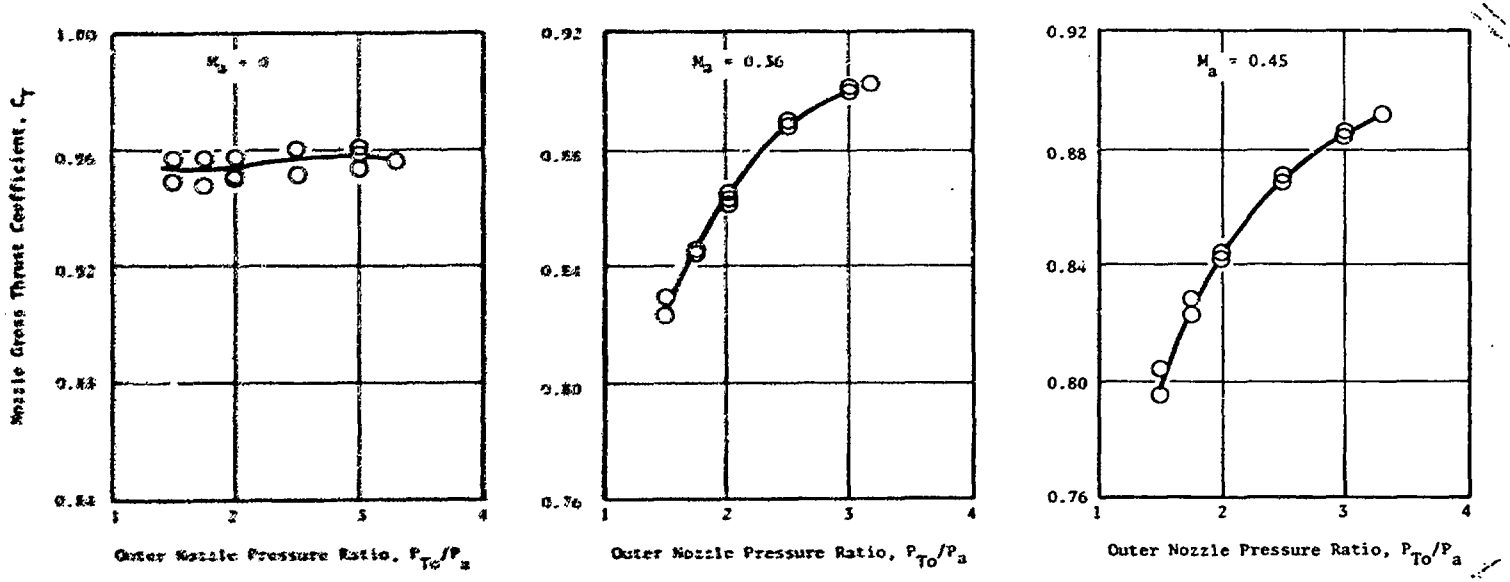

Figure F-35. Configuration DC-8 Performance.

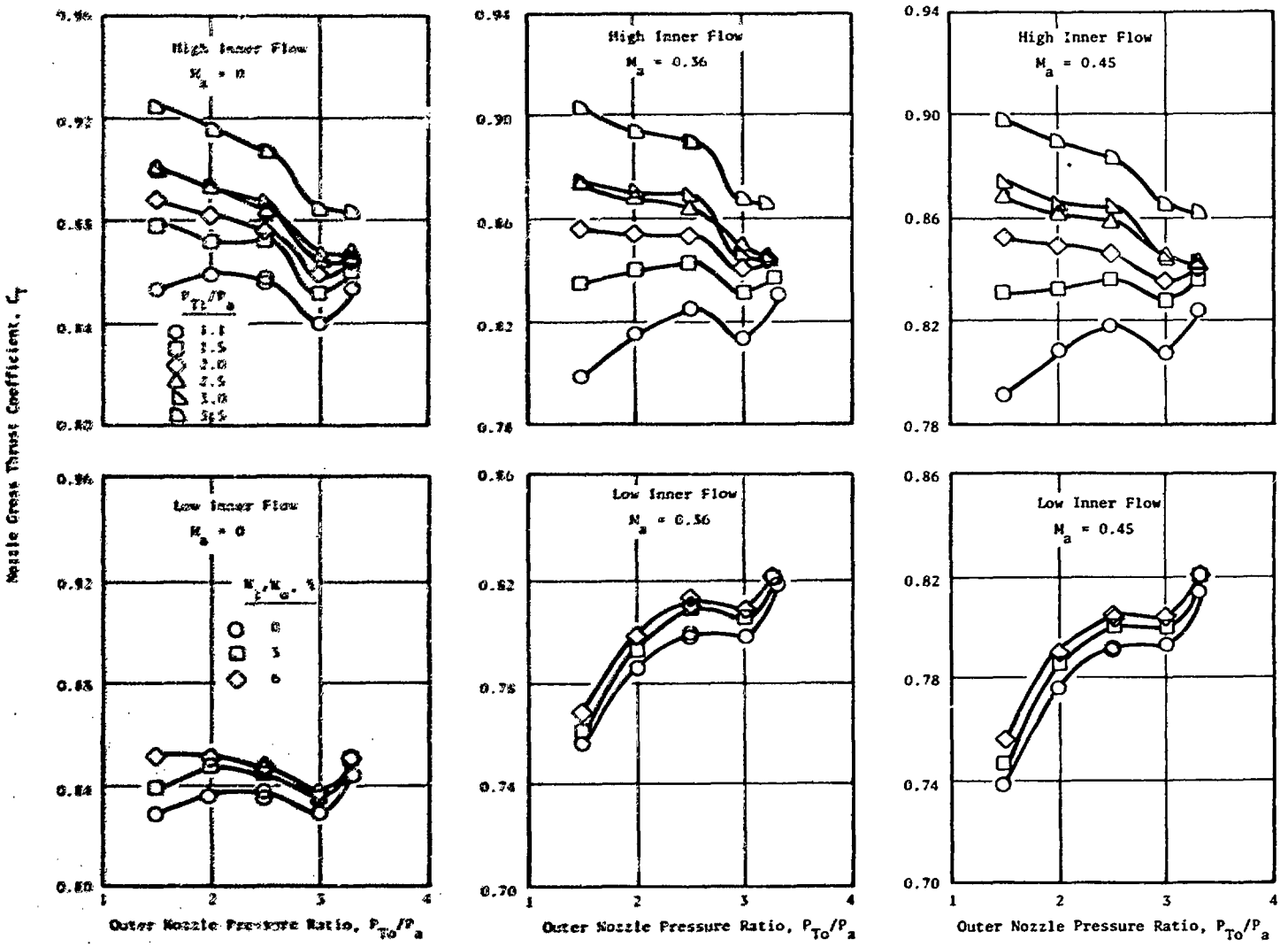

Figure F-36. Configuration DC-3 (Spoke) Performance.

OFF-LINE DATA SUMMARY

This section includes a data summary for each point taken in the test program. Listed below are the parameters presented in the summary.

Page 1 of data summary

D2	Inner nozzle venturi diameter, in.
MA	Tunnel Mach number
PTO/PA	Outer nozzle throat total-to-ambient pressure ratio
PTI/PA	Inner nozzle throat total-to-ambient pressure ratio
OMEGAT	Inner to outer nozzle flow ratio, W_i/W_o
CDO	Outer nozzle flow coefficient
CDI	Inner nozzle flow coefficient
CFNET1	Nozzle thrust coefficient based on sum of ideal thrusts of inner and outer streams, $(F-D)/(F_{I_o} + F_{I_i})$
CFNET2	Nozzle thrust coefficient based on outer stream ideal thrust, $(F-D)/F_{I_o}$
F9	Nozzle exit stream thrust parameter

Page 2 of data summary

DCS	Integrated suppressor base pressure drag divided by the sum of the ideal thrusts of the inner and outer streams, $D_{ch}/(F_{I_o} + F_{I_i})$
CDS	Suppressor base pressure drag coefficient referenced to free stream dynamic pressure and the model cross section area, $D_{ch}/q_a A_{max}$
DCSH	Integrated shroud axial boattail pressure drag referenced to the sum of the ideal thrusts of the inner and outer streams, $D_{sh}/(F_{I_o} + F_{I_i})$
CDSH	Integrated shroud axial boattail pressure drag coefficient referenced to free stream dynamic pressure and the model cross section area, $D_{sh}/q_a A_{max}$
DCPL,O	Integrated outer plug axial pressure force referenced to the sum of the inner and outer nozzle ideal thrust, $D_{PLo}/(F_{I_o} + F_{I_i})$
DCPL,I	Integrated inner plug axial pressure force referenced to the sum of inner and outer nozzle ideal thrust, $D_{PLi}/(F_{I_o} + F_{I_i})$
DCTOT	Summation of nozzle integrated axial pressure forces referenced to the sum of inner and outer nozzle ideal thrust, DSC + DCSH + DCPL,O + DCPL.I
PSUP/PA	Area averag d suppressor base pressure referenced to tunnel ambient pressure, P/P_a

STA CALIBRATION MODEL

FACILITY: [illegible] PROGRAM [illegible]

NOZZLE TYPE: High Inner Flow (4 INCH STRAIGHT STREAM ONLY)

AFTERBODY-STREAM PLUG CONFIGURATIONS

SUPPRESSOR CONFIGURATION

THRUST	DESIGNATED	CONFIGURATION NUMBER OF THIS SET	OUTER RADIUS RATIO	INNER RADIUS RATIO	D2	DVO
		05051	0.0000	0.0000	1.1398	1.9980

SEQ	WT	PITCH	RT/CA	AMBIENT	CDN	CDI	CPNET1	CPNET2	F9
31	0.0016	1.4007	0.0000	0.0000	0.0000	0.9798	1.0005	1.0005	1.2295
64	-0.0020	2.0150	0.0000	0.0000	0.0000	0.9839	0.9950	0.9950	1.2517
98	-0.0000	2.3198	0.0000	0.0000	0.0000	0.9830	0.9996	0.9996	1.2540
100	0.0016	1.5024	0.0000	0.0000	0.0000	0.9791	0.9985	0.9985	1.2294
101	0.0053	2.0198	0.0000	0.0000	0.0000	0.9823	0.9938	0.9938	1.2496
103	-0.0020	2.1109	0.0000	0.0000	0.0000	0.9841	0.9944	0.9944	1.2507
103	0.0033	2.0015	0.0000	0.0000	0.0000	0.9805	0.9985	0.9985	1.2564
104	-0.0030	1.5044	0.0000	0.0000	0.0000	0.9841	1.0050	1.0050	1.2366
135	-0.0000	1.4749	0.0000	0.0000	0.0000	0.9830	0.9924	0.9924	1.2768
136	-0.0000	2.0030	0.0000	0.0000	0.0000	0.9852	0.9931	0.9931	1.2513
137	-0.0000	2.3764	0.0000	0.0000	0.0000	0.9870	0.9930	0.9930	1.2519
138	-0.0003	2.0041	0.0000	0.0000	0.0000	0.9852	0.9952	0.9952	1.2536
139	0.0033	1.5048	0.0000	0.0000	0.0000	0.9833	0.9999	0.9999	1.2313
140	-0.0000	1.5047	0.0000	0.0000	0.0000	0.9841	0.9992	0.9992	1.2311
141	-0.0000	2.0044	0.0000	0.0000	0.0000	0.9863	0.9950	0.9950	1.2535
142	-0.0010	2.1440	0.0000	0.0000	0.0000	0.9877	0.9946	0.9946	1.2538
143	0.0013	2.0046	0.0000	0.0000	0.0000	0.9869	0.9944	0.9944	1.2536
144	-0.0003	1.5044	0.0000	0.0000	0.0000	0.9813	1.0016	1.0016	1.2326
145	0.0033	1.5077	0.0000	0.0000	0.0000	0.9829	1.0025	1.0025	1.2326
146	-0.0000	2.0049	0.0000	0.0000	0.0000	0.9856	0.9946	0.9946	1.2542
147	-0.0000	2.0431	0.0000	0.0000	0.0000	0.9867	0.9961	0.9961	1.2542
148	-0.0000	2.0049	0.0000	0.0000	0.0000	0.9861	0.9972	0.9972	1.2551
149	0.0016	1.5049	0.0000	0.0000	0.0000	0.9825	1.0043	1.0043	1.2335
150	0.0000	2.3343	0.0000	0.0000	0.0000	0.8757	1.0387	1.0387	1.1940
151	0.0000	2.3343	0.0000	0.0000	0.0000	0.9231	1.0618	1.0618	1.2520
120	0.0079	1.5046	0.0000	0.0000	0.0000	0.9858	1.0016	1.0016	1.1794
121	0.0046	1.4944	0.0000	0.0000	0.0000	0.9871	0.9951	0.9951	1.2543
122	0.0033	2.2145	0.0000	0.0000	0.0000	0.9885	0.9950	0.9950	1.2547
123	0.0020	1.5046	0.0000	0.0000	0.0000	0.9876	0.9960	0.9960	1.2553
124	0.0007	1.4987	0.0000	0.0000	0.0000	0.9833	1.0005	1.0005	1.2289
125	0.0026	1.4922	0.0000	0.0000	0.0000	0.9847	1.0045	1.0045	1.2318
126	0.0040	1.9529	0.0000	0.0000	0.0000	0.9863	0.9989	0.9989	1.2565
127	0.0013	2.2744	0.0000	0.0000	0.0000	0.9872	0.9991	0.9991	1.2570
128	0.0046	1.4854	0.0000	0.0000	0.0000	0.9853	1.0021	1.0021	1.2582
129	0.0007	1.4809	0.0000	0.0000	0.0000	0.9836	1.0076	1.0076	1.2329
130	0.0033	1.4844	0.0000	0.0000	0.0000	0.9762	0.9741	0.9741	1.2048
131	0.0020	1.4971	0.0000	0.0000	0.0000	0.9873	0.9802	0.9802	1.2421
132	0.0079	2.1774	0.0000	0.0000	0.0000	0.9870	0.9831	0.9831	1.2431
133	0.0026	1.4948	0.0000	0.0000	0.0000	0.9862	0.9826	0.9826	1.2432
134	0.0020	1.4911	0.0000	0.0000	0.0000	0.9737	0.9805	0.9805	1.2113
171	0.0092	1.4842	0.0000	0.0000	0.0000	0.9737	0.9758	0.9758	1.2081
172	0.0051	1.4876	0.0000	0.0000	0.0000	0.9867	0.9808	0.9808	1.2421
173	0.0092	2.2744	0.0000	0.0000	0.0000	0.9862	0.9847	0.9847	1.2434
174	0.0047	1.4849	0.0000	0.0000	0.0000	0.9874	0.9817	0.9817	1.2432
175	0.0092	1.4904	0.0000	0.0000	0.0000	0.9730	0.9791	0.9791	1.2097

FACILI [illegible] NOZZLE TYPE PER-STREAM PLUG CONFIGURATIONS SUPPRESSOR CONFIGURATION

High Inner Flow (4 INCH SPLITTER STREAM ONLY)

DATA REFERENCE CONFIGURATION NUMBER OF 0005 NASA 00051 OUTER RADIUS RATIO 0.0000 INNER RADIUS RATIO 0.0000 D2 1.1398 DV0 1.9980

ROW	VJ	PT/PA	PT/PA	OMEGAT	DCS	CDS	DCSH	CDSH	DCPL.0	DCPL.1	DCVAV
97	0.0000	1.5067	0.0000	0.0000	0.0000	0.0000	-0.0035	69.9187	0.0000	0.0000	-0.0035
98	-0.0000	1.7150	0.0000	0.0000	0.0000	0.0000	-0.0022	9.9999	0.0000	0.0000	-0.0022
99	-0.0000	2.0174	0.0000	0.0000	0.0000	0.0000	-0.0015	9.9999	0.0000	0.0000	-0.0015
100	0.0000	1.4944	0.0000	0.0000	0.0000	0.0000	-0.0033	65.8485	0.0000	0.0000	-0.0033
101	0.0000	2.0104	0.0000	0.0000	0.0000	0.0000	-0.0021	42.7067	0.0000	0.0000	-0.0021
102	-0.0000	2.1104	0.0000	0.0000	0.0000	0.0000	-0.0024	9.9999	0.0000	0.0000	-0.0024
103	0.0000	2.1104	0.0000	0.0000	0.0000	0.0000	-0.0020	101.5221	0.0000	0.0000	-0.0020
104	-0.0000	1.5244	0.0000	0.0000	0.0000	0.0000	-0.0024	9.9999	0.0000	0.0000	-0.0024
105	-0.0000	1.6244	0.0000	0.0000	0.0000	0.0000	-0.0042	9.9999	0.0000	0.0000	-0.0042
106	-0.0000	2.0744	0.0000	0.0000	0.0000	0.0000	-0.0018	9.9999	0.0000	0.0000	-0.0018
107	-0.0000	2.2744	0.0000	0.0000	0.0000	0.0000	-0.0020	9.9999	0.0000	0.0000	-0.0020
108	-0.0000	2.0744	0.0000	0.0000	0.0000	0.0000	-0.0018	9.9999	0.0000	0.0000	-0.0018
109	0.0000	1.5244	0.0000	0.0000	0.0000	0.0000	-0.0028	2168.7170	0.0000	0.0000	-0.0028
110	-0.0000	1.6244	0.0000	0.0000	0.0000	0.0000	-0.0039	3030.7646	0.0000	0.0000	-0.0039
111	-0.0000	2.0744	0.0000	0.0000	0.0000	0.0000	-0.0016	9.9999	0.0000	0.0000	-0.0016
112	-0.0000	2.2744	0.0000	0.0000	0.0000	0.0000	-0.0013	9.9999	0.0000	0.0000	-0.0013
113	0.0000	2.0744	0.0000	0.0000	0.0000	0.0000	-0.0012	392.0825	0.0000	0.0000	-0.0012
114	-0.0000	1.5244	0.0000	0.0000	0.0000	0.0000	-0.0018	9.9999	0.0000	0.0000	-0.0018
115	0.0000	1.6244	0.0000	0.0000	0.0000	0.0000	-0.0010	28.4233	0.0000	0.0000	-0.0010
116	-0.0000	2.0744	0.0000	0.0000	0.0000	0.0000	-0.0013	9.9999	0.0000	0.0000	-0.0013
117	-0.0000	2.2744	0.0000	0.0000	0.0000	0.0000	-0.0010	9.9999	0.0000	0.0000	-0.0010
118	-0.0000	2.0744	0.0000	0.0000	0.0000	0.0000	-0.0015	9.9999	0.0000	0.0000	-0.0015
119	0.0000	1.5244	0.0000	0.0000	0.0000	0.0003	-224.9377	0.0000	0.0000	0.0000	0.0003
120	0.0000	2.2744	0.0000	0.0000	0.0000	0.0000	-0.0029	0.7790	0.0000	0.0000	-0.0029
121	0.0000	2.0744	0.0000	0.0000	0.0000	0.0000	-0.0021	0.4978	0.0000	0.0000	-0.0021
122	0.0000	1.5244	0.0000	0.0000	0.0000	0.0000	-0.0113	2.8416	0.0000	0.0000	-0.0113
123	0.0000	1.6244	0.0000	0.0000	0.0000	0.0000	-0.0026	0.5937	0.0000	0.0000	-0.0026
124	0.0000	2.2744	0.0000	0.0000	0.0000	0.0000	-0.0023	0.5502	0.0000	0.0000	-0.0023
125	0.0000	1.6244	0.0000	0.0000	0.0000	0.0000	-0.0038	1.2289	0.0000	0.0000	-0.0038
126	0.0000	1.6244	0.0000	0.0000	0.0000	0.0000	-0.0078	5.3914	0.0000	0.0000	-0.0078
127	0.0000	1.6244	0.0000	0.0000	0.0000	0.0000	-0.0055	1.8547	0.0000	0.0000	-0.0055
128	0.0000	1.6244	0.0000	0.0000	0.0000	0.0000	-0.0039	0.9983	0.0000	0.0000	-0.0039
129	0.0000	2.2744	0.0000	0.0000	0.0000	0.0000	-0.0029	0.7361	0.0000	0.0000	-0.0029
130	0.0000	1.6244	0.0000	0.0000	0.0000	0.0000	-0.0026	0.6662	0.0000	0.0000	-0.0026
131	0.0000	1.6244	0.0000	0.0000	0.0000	0.0000	-0.0067	2.7061	0.0000	0.0000	-0.0067
132	0.0000	1.6244	0.0000	0.0000	0.0000	0.0000	-0.0155	0.0357	0.0000	0.0000	-0.0155
133	0.0000	1.6244	0.0000	0.0000	0.0000	0.0000	-0.0093	0.0392	0.0000	0.0000	-0.0093
134	0.0000	2.2744	0.0000	0.0000	0.0000	0.0000	-0.0086	0.0418	0.0000	0.0000	-0.0086
135	0.0000	1.6244	0.0000	0.0000	0.0000	0.0000	-0.0092	0.0390	0.0000	0.0000	-0.0092
136	0.0000	1.6244	0.0000	0.0000	0.0000	0.0000	-0.0162	0.0375	0.0000	0.0000	-0.0162
137	0.0000	1.6244	0.0000	0.0000	0.0000	0.0000	-0.0236	0.0443	0.0000	0.0000	-0.0236
138	0.0000	1.6244	0.0000	0.0000	0.0000	0.0000	-0.0118	0.0405	0.0000	0.0000	-0.0118
139	0.0000	2.2744	0.0000	0.0000	0.0000	0.0000	-0.0098	0.0415	0.0000	0.0000	-0.0098
140	0.0000	1.6244	0.0000	0.0000	0.0000	0.0000	-0.0143	0.0409	0.0000	0.0000	-0.0143
141	0.0000	1.6244	0.0000	0.0000	0.0000	0.0000	-0.0187	0.0352	0.0000	0.0000	-0.0187

FACILITY (E) PROGRAM CODE

NOZZLE TYPE — IN-STREAM PLUG CONFIGURATIONS — SUPPRESSOR CONFIGURATION

4 (NOZ STAG OUTER STREAM ONLY)

CONFIGURATION NUMBER — OUTER RADIUS RATIO — INNER RADIUS RATIO — D2 — DVO

GE 1000 NASA 10000 — 0.0000 — 0.0000 — 0.0000 — 1.2480

INPUT PARAMETERS

NOZ	MA	PTJ/PA	PTI/PA	CNEGAT	CDO	CDI	CFNET1	CFNET2	F9
297	0.0041	1.2480	0.9904	0.0000	0.9884	9.9999	0.9974	0.9974	1.1626
298	0.0285	1.5088	0.9927	0.0000	0.9818	9.9999	0.9879	0.9879	1.2227
299	0.0337	1.7406	0.9910	0.0000	0.9825	9.9999	0.9872	0.9872	1.2438
300	0.0472	1.9949	0.9917	0.0000	0.9848	9.9999	0.9898	0.9898	1.2485
301	0.0510	2.4995	0.9921	0.0000	0.9852	9.9999	0.9902	0.9902	1.2482
302	0.0565	2.9851	0.9926	0.0000	0.9875	9.9999	0.9888	0.9888	1.2507
303	0.0570	2.4988	0.9920	0.0000	0.9856	9.9999	0.9907	0.9907	1.2489
304	0.0421	1.9970	0.9913	0.0000	0.9854	9.9999	0.9896	0.9896	1.2488
305	0.0394	1.7385	0.9918	0.0000	0.9827	9.9999	0.9862	0.9862	1.2431
306	0.0307	1.5015	0.9909	0.0000	0.9829	9.9999	0.9858	0.9858	1.2223
307	0.0144	1.2533	0.9909	0.0000	0.9881	9.9999	0.9885	0.9885	1.1614
308	0.0765	1.7425	0.9912	0.0000	0.9869	9.9999	0.9966	0.9966	1.1676
309	0.0272	1.4991	0.9916	0.0000	0.9816	9.9999	0.9942	0.9942	1.2259
310	0.0356	1.7536	0.9916	0.0000	0.9818	9.9999	0.9942	0.9942	1.2485
311	0.0440	1.9966	0.9928	0.0000	0.9841	9.9999	0.9945	0.9945	1.2515
312	0.0520	2.4989	0.9921	0.0000	0.9840	9.9999	0.9943	0.9943	1.2506
313	0.0648	2.8719	0.9919	0.0000	0.9857	9.9999	0.9927	0.9927	1.2525
314	0.0515	2.4979	0.9916	0.0000	0.9854	9.9999	0.9939	0.9939	1.2515
315	0.0497	1.9963	0.9923	0.0000	0.9836	9.9999	0.9948	0.9948	1.2513
316	0.0341	1.7416	0.9920	0.0000	0.9823	9.9999	0.9905	0.9905	1.2459
317	0.0272	1.5019	0.9915	0.0000	0.9821	9.9999	0.9923	0.9923	1.2255
318	0.0110	1.2469	0.9911	0.0000	0.9886	9.9999	0.9980	0.9980	1.1624
319	0.0010	0.9909	0.9915	9999.0000	9.9999	9.9999	9.9999	9.9999	1.0160
320	-0.0000	0.9916	0.9911	9999.0000	9.9999	9.9999	9.9999	9.9999	1.0764
321	-0.0000	0.9915	0.9916	9999.0000	9.9999	9.9999	9.9999	9.9999	1.0130
322	0.0103	1.2527	0.9907	0.0000	0.9889	9.9999	0.9995	0.9995	1.1695
323	0.0214	1.5016	0.9913	0.0000	0.9826	9.9999	0.9948	0.9948	1.2271
324	0.0358	1.7478	0.9907	0.0000	0.9827	9.9999	0.9931	0.9931	1.2482
325	0.0498	1.9945	0.9910	0.0000	0.9856	9.9999	0.9941	0.9941	1.2524
326	0.0518	2.4987	0.9918	0.0000	0.9852	9.9999	0.9928	0.9928	1.2504
327	0.0537	2.8728	0.9922	0.0000	0.9856	9.9999	0.9908	0.9908	1.2504
328	0.0529	2.4977	0.9925	0.0000	0.9855	9.9999	0.9927	0.9927	1.2505
329	0.0440	1.9956	0.9916	0.0000	0.9849	9.9999	0.9913	0.9913	1.2497
330	0.0414	1.7459	0.9913	0.0000	0.9832	9.9999	0.9904	0.9904	1.2466
331	0.0278	1.4998	0.9905	0.0000	0.9873	9.9999	0.9901	0.9901	1.2241
332	0.0116	1.2503	0.9913	0.0000	0.9884	9.9999	0.9950	0.9950	1.1627
333	0.0078	0.9909	0.9912	9999.0000	9.9999	9.9999	9.9999	9.9999	1.0140
334	0.3589	1.2495	0.9962	0.0000	0.9821	9.9999	0.9747	0.9747	1.1437
335	0.3584	1.4957	0.9968	0.0000	0.9765	9.9999	0.9734	0.9734	1.2089
336	0.3599	1.7416	0.9953	0.0000	0.9799	9.9999	0.9771	0.9771	1.2344
337	0.3587	2.0061	0.9941	0.0000	0.9849	9.9999	0.9823	0.9823	1.2418
338	0.3599	2.5122	0.9934	0.0000	0.9854	9.9999	0.9848	0.9848	1.2429
339	0.3602	2.7337	0.9957	0.0000	0.9845	9.9999	0.9858	0.9858	1.2437
340	0.3592	2.4132	0.9956	0.0000	0.9847	9.9999	0.9843	0.9843	1.2419
341	0.3574	2.0085	0.9943	0.0000	0.9842	9.9999	0.9818	0.9818	1.2409

FACILITY: ARI PROGRAM CC31 — NOZZLE TYPE: 4 INCH STA(OUTER STREAM ONLY) — INNER-STREAM PLUG CONFIGURATIONS — SUPPRESSOR CONFIGURATION

DUCT PARAMETERS — CONFIGURATION NUMBER GE 1000 ASK 10000 — OUTER RADIUS RATIO 0.0000 — INNER RADIUS RATIO 0.0000 — D2 0.0000 — DVO 1.2480

ARC	MA	PTO/PA	PT1/PA	OMEGAT	DCS	CDS	DCSH	CDSH	DCPL.O	DCPL.I	DCTOT
297	0.0091	1.2480	0.9904	2.3000	0.0000	0.0000	-0.0169	33.1655	0.0000	0.0000	-0.0169
298	0.0295	1.5038	0.9877	0.0000	0.0000	0.0000	-0.0070	2.6064	0.0000	0.0000	-0.0070
299	0.0317	1.7404	0.9910	0.0000	0.0000	0.0000	-0.0047	1.7469	0.0000	0.0000	-0.0047
300	0.0423	1.8949	0.9917	0.0000	0.0000	0.0000	-0.0028	0.6786	0.0000	0.0000	-0.0028
301	0.0510	2.4085	0.9921	0.0000	0.0000	0.0000	-0.0034	0.9970	0.0000	0.0000	-0.0034
302	0.0545	2.8451	0.9926	0.0000	0.0000	0.0000	-0.0024	0.6989	0.0000	0.0000	-0.0024
303	0.0420	2.4488	0.9920	0.0000	0.0000	0.0000	-0.0026	0.7302	0.0000	0.0000	-0.0026
304	0.0421	1.9870	0.9913	0.0000	0.0000	0.0000	-0.0025	0.7656	0.0000	0.0000	-0.0025
305	0.0308	1.7145	0.9916	0.0000	0.0000	0.0000	-0.0041	1.9494	0.0000	0.0000	-0.0041
306	0.0207	1.5015	0.9909	0.0000	0.0000	0.0000	-0.0055	3.9085	0.0000	0.0000	-0.0055
307	0.0148	1.2513	0.9888	0.0000	0.0000	0.0000	-0.0123	9.1496	0.0000	0.0000	-0.0123
308	0.0284	1.2675	0.9917	0.0000	0.0000	0.0000	-0.0120	2.5082	0.0000	0.0000	-0.0120
309	0.0232	1.6991	0.9916	0.0000	0.0000	0.0000	-0.0074	3.0231	0.0000	0.0000	-0.0074
310	0.0356	1.7510	0.9918	0.0000	0.0000	0.0000	-0.0036	1.2074	0.0000	0.0000	-0.0036
311	0.0447	1.9966	0.9928	0.0000	0.0000	0.0000	-0.0029	0.7936	0.0000	0.0000	-0.0029
312	0.0430	2.4489	0.9921	0.0000	0.0000	0.0000	-0.0025	0.7092	0.0000	0.0000	-0.0025
313	0.0448	2.8719	0.9919	0.0000	0.0000	0.0000	-0.0025	0.7634	0.0000	0.0000	-0.0025
314	0.0415	2.4979	0.9916	0.0000	0.0000	0.0000	-0.0021	0.6092	0.0000	0.0000	-0.0021
315	0.0472	1.9961	0.9923	0.0000	0.0000	0.0000	-0.0022	0.4918	0.0000	0.0000	-0.0022
316	0.0347	1.7614	0.9920	0.0000	0.0000	0.0000	-0.0029	1.0361	0.0000	0.0000	-0.0029
317	0.0372	1.5019	0.9935	0.0000	0.0000	0.0000	-0.0052	2.1103	0.0000	0.0000	-0.0052
318	0.0110	1.2449	0.9911	0.0000	0.0000	0.0000	-0.0100	13.3538	0.0000	0.0000	-0.0100
319	0.0019	0.9909	0.9915	9999.0000	0.0000	0.0000	9.9999	331.1060	0.0000	0.0000	9.9999
320	0.0003	0.9916	0.9913	9999.0000	0.0000	0.0000	9.9999	9.9999	0.0000	0.0000	9.9999
321	0.0000	0.9915	0.9916	9999.0000	0.0000	0.0000	9.9999	9.9999	0.0000	0.0000	9.9999
322	0.0103	1.7671	0.9902	0.0000	0.0000	0.0000	-0.0126	20.0699	0.0000	0.0000	-0.0126
323	0.0214	1.9014	0.9913	0.0000	0.0000	0.0000	-0.0070	4.6583	0.0000	0.0000	-0.0070
324	0.0356	1.7475	0.9907	0.0000	0.0000	0.0000	-0.0044	1.4824	0.0000	0.0000	-0.0044
325	0.0469	1.9969	0.9910	0.0000	0.0000	0.0000	-0.0020	0.4368	0.0000	0.0000	-0.0020
326	0.0418	2.4447	0.9918	0.0000	0.0000	0.0000	-0.0023	0.6587	0.0000	0.0000	-0.0023
327	0.0433	2.8728	0.9927	0.0000	0.0000	0.0000	-0.0025	0.8136	0.0000	0.0000	-0.0025
328	0.0425	2.4977	0.9925	0.0000	0.0000	0.0000	-0.0025	0.6869	0.0000	0.0000	-0.0025
329	0.0440	1.9955	0.9918	0.0000	0.0000	0.0000	-0.0029	0.8099	0.0000	0.0000	-0.0029
330	0.0414	1.7490	0.9913	0.0000	0.0000	0.0000	-0.0033	0.8191	0.0000	0.0000	-0.0033
331	0.0378	1.4994	0.9908	0.0000	0.0000	0.0000	-0.0053	2.0514	0.0000	0.0000	-0.0053
332	0.0196	1.2523	0.9913	0.0000	0.0000	0.0000	-0.0111	9.7846	0.0000	0.0000	-0.0111
333	0.0028	0.9908	0.9912	9999.0000	0.0000	0.0000	9.9999	27.1657	0.0000	0.0000	9.9999
334	0.1594	1.2493	0.9942	0.0000	0.0000	0.0000	-0.0371	0.0452	0.0000	0.0000	-0.0371
335	0.1484	1.4982	0.9948	0.0000	0.0000	0.0000	-0.0165	0.0383	0.0000	0.0000	-0.0165
336	0.1528	1.7516	0.9951	0.0000	0.0000	0.0000	-0.0114	0.0377	0.0000	0.0000	-0.0114
337	0.1542	2.0081	0.9941	0.0000	0.0000	0.0000	-0.0102	0.0432	0.0000	0.0000	-0.0102
338	0.1550	2.5122	0.9934	0.0000	0.0000	0.0000	-0.0073	0.0439	0.0000	0.0000	-0.0073
339	0.1602	2.7737	0.9957	0.0000	0.0000	0.0000	-0.0051	0.0339	0.0000	0.0000	-0.0051
340	0.1592	2.5132	0.9956	0.0000	0.0000	0.0000	-0.0059	0.0355	0.0000	0.0000	-0.0059
341	0.1574	2.2484	0.9947	0.0000	0.0000	0.0000	-0.0084	0.0358	0.0000	0.0000	-0.0084

FACILIT (REKI PROGRAM C03)

NOZZLE TYPE — ER-STREAM
4 (NEW DISTRIBUTED STREAM ONLY) — PLUG CONFIGURATIONS — SUPPRESSOR CONFIGURATION

THRUST PARAMETERS					CONFIGURATION NUMBER GE 1000 MASA 10000	OUTER RADIUS RATIO 0.0000	INNER RADIUS RATIO 0.0000	D2 0.0000	DVD 1.2480
ENG	WA	BTOJPS	BTJPS	OMEGAT	CDO	CDI	CFNET1	CFNET2	F9
163	0.3588	1.7471	0.9967	0.0000	0.9800	9.9999	0.9773	0.9773	1.2346
164	0.3577	1.7004	0.9960	0.0000	0.9730	9.9999	0.9738	0.9738	1.2085
165	0.3574	1.7519	0.9954	0.0000	0.9579	9.9999	0.9632	0.9632	1.1392
166	0.3587	1.7665	0.9976	0.0000	0.9574	9.9999	0.9661	0.9661	1.1389
241	0.3958	1.5019	0.9976	0.0000	0.9722	9.9999	0.9761	0.9761	1.2092
242	0.3954	1.7607	0.9943	0.0000	0.9784	9.9999	0.9789	0.9789	1.2346
243	0.3961	1.7871	0.9929	0.0000	0.9853	9.9999	0.9817	0.9817	1.2414
244	0.3948	1.8004	0.9934	0.0000	0.9852	9.9999	0.9851	0.9851	1.2429
245	0.3944	1.8037	0.9948	0.0000	0.9855	9.9999	0.9847	0.9847	1.2443
246	0.3948	1.8022	0.9935	0.0000	0.9849	9.9999	0.9850	0.9850	1.2425
247	0.3940	1.8027	0.9944	0.0000	0.9846	9.9999	0.9810	0.9810	1.2405
248	0.3950	1.7977	0.9940	0.0000	0.9748	9.9999	0.9787	0.9787	1.2353
249	0.3948	1.8001	0.9935	0.0000	0.9731	9.9999	0.9735	0.9735	1.2081
170	0.3948	1.7407	0.9939	0.0000	0.9567	9.9999	0.9681	0.9681	1.1394
276	0.4444	1.7444	0.9934	0.0000	0.9441	9.9999	0.9637	0.9637	1.1329
277	0.4442	1.7809	0.9939	0.0000	0.9758	9.9999	0.9758	0.9758	1.2078
278	0.4437	1.7689	0.9945	0.0000	0.9774	9.9999	0.9770	0.9770	1.2319
279	0.4443	1.7966	0.9933	0.0000	0.9847	9.9999	0.9819	0.9819	1.2410
280	0.4448	1.8091	0.9936	0.0000	0.9857	9.9999	0.9848	0.9848	1.2428
281	0.4443	1.8040	0.9943	0.0000	0.9860	9.9999	0.9842	0.9842	1.2448
282	0.4432	1.8048	0.9942	0.0000	0.9859	9.9999	0.9830	0.9830	1.2440
283	0.4446	1.8150	0.9945	0.0000	0.9851	9.9999	0.9837	0.9837	1.2438
284	0.4435	1.8004	0.9948	0.0000	0.9855	9.9999	0.9835	0.9835	1.2414
285	0.4432	1.7942	0.9937	0.0000	0.9844	9.9999	0.9794	0.9794	1.2388
286	0.4440	1.7682	0.9933	0.0000	0.9791	9.9999	0.9754	0.9754	1.2319
287	0.4432	1.7806	0.9936	0.0000	0.9769	9.9999	0.9704	0.9704	1.2048
288	0.4428	1.7623	0.9934	0.0000	0.9697	9.9999	0.9630	0.9630	1.1321
[illegible]									

705

FACILITY ...XI PROGRAM CODE ... NOZZLE TYPE ... IN-STREAM PLUG CONFIGURATIONS ... SUPPRESSOR CONFIGURATION

(4 INCH STRAIGHT STREAM ONLY)

CASE PARAMETERS ... CONFIGURATION NUMBER CC 1000 NASA 10000 ... OUTER RADIUS RATIO 0.0000 ... INNER RADIUS RATIO 0.0000 ... D2 0.0000 ... DVO 1.2480

CASE	WA	P1/P2	P1/P2	GAMMA	PCS	COS	DCSH	COSH	DCPL,O	DCPL,I	DCTOT
1	0.3540	1.7421	0.5647	0.2000	0.0000	0.0000	-0.0101	0.0337	0.0000	0.0000	-0.0101
2	0.3477	1.7006	0.5660	0.2000	0.0000	0.0000	-0.0136	0.0317	0.0000	0.0000	-0.0136
3	0.3574	1.7619	0.5644	0.2000	0.0000	0.0000	-0.0197	0.0245	0.0000	0.0000	-0.0197
4	0.3487	1.7065	0.5658	0.2000	0.0000	0.0000	-0.0354	0.0354	0.0000	0.0000	-0.0354
5	0.3574	1.7619	0.5644	0.2000	0.0100	0.0000	-0.0194	0.0271	0.0000	0.0000	-0.0194
6	0.3574	1.7619	0.5644	0.2000	0.0000	0.0000	-0.0145	0.0398	0.0000	0.0000	-0.0145
7	0.3601	1.7801	0.5598	0.2000	0.0000	0.0000	-0.0128	0.0440	0.0000	0.0000	-0.0128
8	0.3574	1.7626	0.5674	0.2000	0.0000	0.0000	-0.0094	0.0457	0.0000	0.0000	-0.0094
9	0.3574	1.7626	0.5674	0.2000	0.0000	0.0000	-0.0071	0.0427	0.0000	0.0000	-0.0071
10	0.3574	1.7626	0.5674	0.2000	0.0000	0.0000	-0.0094	0.0459	0.0000	0.0000	-0.0094
11	0.3601	1.7801	0.5618	0.2000	0.0000	0.0000	-0.0117	0.0402	0.0000	0.0000	-0.0117
12	0.3643	1.7971	0.5565	0.2000	0.0000	0.0000	-0.0152	0.0418	0.0000	0.0000	-0.0152
13	0.3574	1.7626	0.5674	0.2000	0.0000	0.0000	-0.0193	0.0369	0.0000	0.0000	-0.0193
14	0.3574	1.7626	0.5674	0.2000	0.0000	0.0000	-0.0358	0.0362	0.0000	0.0000	-0.0358
15	0.4444	1.7442	0.5733	0.2000	0.0000	0.0000	-0.0425	0.0330	0.0000	0.0000	-0.0425
16	0.4447	1.7453	0.5729	0.2000	0.0000	0.0000	-0.0229	0.0347	0.0000	0.0000	-0.0229
17	0.4447	1.7440	0.5733	0.2000	0.0000	0.0000	-0.0179	0.0385	0.0000	0.0000	-0.0179
18	0.4447	1.7440	0.5733	0.2000	0.0000	0.0000	-0.0140	0.0382	0.0000	0.0000	-0.0140
19	0.4447	1.7440	0.5733	0.2000	0.0000	0.0000	-0.0103	0.0399	0.0000	0.0000	-0.0103
20	0.4447	1.7440	0.5733	0.2000	0.0000	0.0000	-0.0070	0.0353	0.0000	0.0000	-0.0070
21	0.4447	1.7440	0.5733	0.2000	0.0000	0.0000	-0.0079	0.0409	0.0000	0.0000	-0.0079
22	0.4444	1.7429	0.5736	0.2000	0.0000	0.0000	-0.0071	0.0360	0.0000	0.0000	-0.0071
23	0.4447	1.7440	0.5733	0.2000	0.0000	0.0000	-0.0098	0.0380	0.0000	0.0000	-0.0098
24	0.4447	1.7440	0.5733	0.2000	0.0200	0.0000	-0.0141	0.0387	0.0000	0.0000	-0.0141
25	0.4444	1.7429	0.5736	0.2000	0.0000	0.0000	-0.0168	0.0360	0.0000	0.0000	-0.0168
26	0.4447	1.7440	0.5733	0.2000	0.0000	0.0000	-0.0231	0.0350	0.0000	0.0000	-0.0231
27	0.4428	1.7371	0.5754	0.1999	0.0000	0.0000	-0.0432	0.0335	0.0000	0.0000	-0.0432
[illegible]											
[illegible]											
[illegible]											
[illegible]											

FACILITY EL PASO/SAN JUAN MODEL TYPE 2 INCH STAINLESS STEEL DUCT 12-STREAM PLANE CONFIGURATIONS SUPPRESSOR CONFIGURATION

CORE RADIUS RATIO 0.0000 INNER RADIUS RATIO 0.0000 DVD 1.2480

FREQUENCY	PARAMETERS							CDD	CDI	CENET1	CENET2	F9
3234	60000	60000	0.0000	0.0000	1.0000	0.0000	0.0000	0.0000	0.0000	0.9999	0.9999	1.2503
3236	60000	60000	1.1398	-0.0000	3.0033	0.0000	0.0000	0.0000	0.9966	0.9746	0.9746	1.2458
3238	60000	60000	1.1398	0.0000	3.0033	0.0000	0.0000	0.0000	0.9900	0.9805	0.9805	1.2565
3240	60000	60000	1.1398	1.2744	4.0148	0.0000	0.0000	0.0000	1.0064	0.9732	0.9732	1.2649
3242	60000	60000	1.1398	0.0132	3.0033	0.0000	0.0000	0.0000	1.0083	0.9713	0.9713	1.2649
3244	60000	60000	1.1398	0.0132	3.0033	0.0000	0.0000	0.0000	0.9959	0.9902	0.9902	1.2608
3246	60000	60000	1.1398	0.0132	3.0033	0.0000	0.0000	0.0000	0.9964	0.9923	0.9923	1.2591
3248	60000	60000	1.1398	0.0132	3.0033	0.0000	0.0000	0.0000	0.9949	0.9869	0.9869	1.2539
3250	60000	60000	1.1398	0.0132	3.0033	0.0000	0.0000	0.0000	0.9974	0.9826	0.9826	1.2551
3252	60000	60000	1.1398	0.0132	3.0033	0.0000	0.0000	0.0000	1.0061	0.9748	0.9748	1.2666
3254	60000	60000	1.1398	0.0132	3.0033	0.0000	0.0000	0.0000	1.0153	0.9652	0.9652	1.2785
3256	60000	60000	1.1398	0.0132	3.0033	0.0000	0.0000	0.0000	1.0103	0.9670	0.9670	1.2846
3258	60000	60000	1.1398	0.0132	3.0033	0.0000	0.0000	0.0000	1.0105	0.9816	0.9816	1.2780
3260	60000	60000	1.1398	0.0132	3.0033	0.0000	0.0000	0.0000	1.0076	0.9910	0.9910	1.2678
3262	60000	60000	1.1398	0.0132	3.0033	0.0000	0.0000	0.0000	0.9956	1.0011	1.0011	1.2552
3264	60000	60000	1.1398	0.0132	3.0033	0.0000	0.0000	0.0000	0.9897	0.9790	0.9790	1.2443
3266	60000	60000	1.1398	0.0132	3.0033	0.0000	0.0000	0.0000	0.9856	0.9801	0.9801	1.2507
3268	60000	60000	1.1398	0.0132	3.0033	0.0000	0.0000	0.0000	1.0070	0.9735	0.9735	1.2654
3270	60000	60000	1.1398	0.0132	3.0033	0.0000	0.0000	0.0000	1.0175	0.9647	0.9647	1.2795
3272	60000	60000	1.1398	0.0132	3.0033	0.0000	0.0000	0.0000	1.0187	0.9672	0.9672	1.2834
3274	60000	60000	1.1398	0.0132	3.0033	0.0000	0.0000	0.0000	1.0122	0.9784	0.9784	1.2757
3276	60000	60000	1.1398	0.0132	3.0033	0.0000	0.0000	0.0000	1.0000	0.9871	0.9871	1.2614
3278	60000	60000	1.1398	0.0132	3.0033	0.0000	0.0000	0.0000	0.9898	0.9893	0.9893	1.2521

FACILITY F 1 PROGRAM C031 INN STREAM

NOZZLE TYPE PLUG, CONFIGURATIONS SUPPRESSOR CONFIGURATION

2 INCH STA(OUTER STREAM ONLY)

THRUST PARAMETERS			OUTER RADIUS RATIO 0.0000			INNER RADIUS RATIO 0.0000		DVO 1.2480				
REG	GF	[illegible]SE	D2	MA	PTO/PA	PTI/PA	OMEGAT	COO	COI	CFNET1	CFNET2	F9
3230	7000	70000	0.0000	-0.0000	1.9780	1.1490	0.0000	0.9915	9.9999	0.9746	0.9746	1.2437
3231	7000	70000	0.0000	0.0100	2.9879	1.3169	0.0000	0.9905	9.9999	0.9799	0.9799	1.2456
3232	7000	70000	0.0000	0.0215	3.9683	1.4804	0.0000	0.9991	9.9999	0.9785	0.9785	1.2625
3233	7000	70000	0.0000	0.0308	3.9859	1.4797	0.0000	1.0060	9.9999	0.9747	0.9747	1.2656
3234	7000	70000	0.0000	0.0033	2.9882	1.3168	0.0000	0.9940	9.9999	0.9932	0.9932	1.2615
3235	7000	70000	0.0000	0.0117	1.9806	1.1494	0.0000	0.9884	9.9999	0.9978	0.9978	1.2574
3242	7000	70000	0.0000	0.0170	1.9843	1.1502	0.0000	0.9839	9.9999	1.0111	1.0111	1.2630
3243	7000	70000	0.0000	0.0072	2.9879	1.3159	0.0000	0.9952	9.9999	0.9890	0.9890	1.2587
3244	7000	70000	0.0000	0.0294	3.9742	1.4800	0.0000	1.0032	9.9999	0.9806	0.9806	1.2688
3245	7000	70000	0.0000	0.0483	3.9862	1.4801	0.0000	1.0043	9.9999	0.9809	0.9809	1.2709
3246	7000	70000	0.0000	0.0300	2.9918	1.3171	0.0000	0.9979	9.9999	0.9878	0.9878	1.2600
3247	7000	70000	0.0000	0.0248	1.9813	1.1497	0.0000	0.9914	9.9999	0.9959	0.9959	1.2582
3248	7000	70000	0.0000	0.0058	1.9827	1.1501	0.0000	0.9909	9.9999	0.9904	0.9904	1.2537
3249	7000	70000	0.0000	0.0144	2.9871	1.3157	0.0000	0.9854	9.9999	0.9922	0.9922	1.2526
3250	7000	70000	0.0000	0.0307	3.9801	1.4819	0.0000	1.0034	9.9999	0.9757	0.9757	1.2641
3251	7000	70000	0.0000	0.0287	5.0065	1.6444	0.0000	1.0101	9.9999	0.9665	0.9665	1.2738
3252	7000	70000	0.0000	-0.0000	4.9716	1.6397	0.0000	1.0116	9.9999	0.9732	0.9732	1.2824
3253	7000	70000	0.0000	-0.0000	3.9723	1.4763	0.0000	1.0053	9.9999	0.9840	0.9840	1.2745
3254	7000	70000	0.0000	0.0176	2.9779	1.3131	0.0000	1.0011	9.9999	0.9883	0.9883	1.2634
3255	7000	70000	0.0000	0.0058	1.9760	1.1473	0.0000	0.9931	9.9999	0.9994	0.9994	1.2622
3264	7000	70000	0.0000	0.0052	1.9863	1.1495	0.0000	0.9896	9.9999	0.9986	0.9986	1.2589
3265	7000	70000	0.0000	0.0227	2.9868	1.3184	0.0000	0.9930	9.9999	0.9868	0.9868	1.2546
3266	7000	70000	0.0000	0.0320	3.9816	1.4838	0.0000	0.9998	9.9999	0.9812	0.9812	1.2661
3267	7000	70000	0.0000	0.0513	4.9963	1.6446	0.0000	1.0103	9.9999	0.9684	0.9684	1.2765
3268	7000	70000	0.0000	0.0386	4.9848	1.6456	0.0000	1.0165	9.9999	0.9666	0.9666	1.2805
3269	7000	70000	0.0000	0.0407	3.9837	1.4799	0.0000	1.0092	9.9999	0.9740	0.9740	1.2681
3270	7000	70000	0.0000	0.0150	2.9838	1.3163	0.0000	1.0015	9.9999	0.9758	0.9758	1.2522
3271	7000	70000	0.0000	0.0026	1.9820	1.1500	0.0000	0.9934	9.9999	0.9765	0.9765	1.2450
3280	7000	70000	0.0000	0.0062	1.9825	1.1540	0.0000	0.9842	9.9999	0.9644	0.9644	1.2306
3281	7000	70000	0.0000	0.0190	2.9884	1.3165	0.0000	0.9929	9.9999	0.9748	0.9748	1.2432
3282	7000	70000	0.0000	0.0282	3.9505	1.4810	0.0000	1.0040	9.9999	0.9725	0.9725	1.2611
3283	7000	70000	0.0000	0.0432	4.9413	1.6454	0.0000	1.0149	9.9999	0.9667	0.9667	1.2783
3284	7000	70000	0.0000	0.0465	4.9413	1.6458	0.0000	1.0168	9.9999	0.9688	0.9688	1.2828
3285	7000	70000	0.0000	0.0328	3.9428	1.4807	0.0000	1.0108	9.9999	0.9775	0.9775	1.2729
3286	7000	70000	0.0000	0.0184	2.9614	1.3175	0.0000	0.9999	9.9999	0.9869	0.9869	1.2609
3287	7000	70000	0.0000	0.0236	1.9793	1.1545	0.0000	0.9874	9.9999	0.9805	0.9805	1.2435

MODEL SC-1, 20 SHALLOW CHUTES, AR = 1.75 BASELINE PLUG

FACILITY 8X6X1 PROGRAM C031

NOZZLE TYPE — DUAL FLOW (FAA)

INNER-STREAM PLUG CONFIGURATIONS — BASELINE PLUG WITH BLEED

SUPPRESSOR CONFIGURATION — 20-SPOKE, AREA RATIO = 1.75

THRUST PARAMETERS — OUTER RADIUS RATIO 0.0000 — INNER RADIUS RATIO 0.7700 — OVD 1.2480

ENG	GE	NASA	M2	MA	PTO/PA	PTI/PA	OMEGAT	CDT	CDI	CFNET1	CFNET2	FG
1209	0001	44530	0.398	0.021	1.499	0.579	0.000	0.971	9.999	0.946	0.946	1.149
1210	0001	44530	0.398	0.022	1.496	0.586	0.000	0.971	9.999	0.955	0.955	1.150
1211	0001	44530	0.398	0.020	1.495	0.598	0.000	0.970	9.999	0.964	0.964	1.150
1212	0001	44530	0.398	0.026	1.989	0.566	0.000	0.966	9.999	0.947	0.947	1.149
1213	0001	44530	0.398	0.028	1.991	0.581	0.000	0.965	9.999	0.957	0.957	1.170
1214	0001	44530	0.398	0.032	1.991	1.000	0.000	0.965	9.999	0.965	0.965	1.170
1215	0001	44530	0.398	0.054	2.492	0.556	0.000	0.967	9.999	0.954	0.954	1.176
1216	0001	44530	0.398	0.046	2.490	0.577	0.000	0.967	9.999	0.962	0.962	1.177
1217	0001	44530	0.398	0.053	2.494	1.003	0.000	0.966	2.410	0.968	0.972	1.178
1218	0001	44530	0.398	0.050	2.997	0.546	0.000	0.966	9.999	0.955	0.955	1.181
1219	0001	44530	0.398	0.053	3.005	0.976	0.000	0.964	9.999	0.964	0.964	1.181
1220	0001	44530	0.398	0.055	3.005	1.012	0.000	0.966	1.459	0.967	0.977	1.183
1221	0001	44530	0.398	0.057	3.317	0.497	0.000	0.966	9.999	0.952	0.957	1.192
1222	0001	44530	0.398	0.056	3.320	0.978	0.000	0.965	9.999	0.961	0.961	1.182
1223	0001	44530	0.398	0.055	3.315	1.021	0.000	0.966	1.134	0.963	0.971	1.184
1224	0001	44550	1.140	0.027	1.494	1.114	0.249	0.969	0.940	0.955	1.091	1.142
1225	0001	44550	1.140	0.027	1.493	1.509	0.545	0.968	0.986	0.952	1.477	1.198
1226	0001	44550	1.140	0.046	1.495	2.002	0.756	0.970	0.993	0.968	1.870	1.205
1227	0001	44550	1.140	0.050	1.497	2.504	0.846	0.969	0.995	0.968	2.262	1.206
1228	0001	44550	1.140	0.052	1.498	3.009	1.126	0.969	0.995	0.960	2.620	1.201
1229	0001	44550	1.140	0.053	1.497	3.488	1.326	0.968	0.997	0.959	3.071	1.219
1230	0001	44550	1.140	0.042	1.989	1.116	0.177	0.965	0.917	0.959	1.030	1.179
1231	0001	44550	1.140	0.048	1.985	1.509	0.388	0.965	0.977	0.957	1.250	1.208
1232	0001	44550	1.140	0.056	1.989	2.000	0.565	0.965	0.994	0.952	1.672	1.213
1233	0001	44550	1.140	0.055	1.992	2.501	0.691	0.966	0.995	0.952	1.688	1.213
1234	0001	44550	1.140	0.057	1.994	3.001	0.817	0.965	0.995	0.949	1.901	1.211
1235	0001	44550	1.140	0.059	1.992	3.505	0.966	0.966	0.996	0.962	2.155	1.225
1236	0001	44550	1.140	0.051	2.496	1.117	0.144	0.955	0.938	0.964	1.015	1.184
1237	0001	44550	1.140	0.052	2.487	1.507	0.369	0.967	0.978	0.961	1.167	1.207
1238	0001	44550	1.140	0.054	2.491	1.999	0.434	0.966	0.994	0.955	1.322	1.210
1239	0001	44550	1.140	0.057	2.496	2.503	0.544	0.956	0.995	0.955	1.474	1.210
1240	0001	44550	1.140	0.056	2.495	3.003	0.653	0.966	0.996	0.943	1.610	1.202
1241	0001	44550	1.140	0.062	2.494	3.500	0.763	0.966	0.996	0.961	1.800	1.220
1242	0001	44550	1.140	0.056	2.986	1.113	0.119	0.967	0.947	0.965	1.003	1.188
1243	0001	44550	1.140	0.056	2.984	1.510	0.259	0.967	0.979	0.961	1.121	1.207
1244	0001	44550	1.140	0.058	2.994	2.000	0.361	0.967	0.994	0.956	1.238	1.209
1245	0001	44550	1.140	0.060	3.006	2.507	0.463	0.964	0.994	0.957	1.358	1.209
1246	0001	44550	1.140	0.062	3.007	3.008	0.563	0.965	0.996	0.942	1.453	1.197
1247	0001	44550	1.140	0.065	3.005	3.504	0.634	0.965	0.996	0.957	1.597	1.213
1248	0001	44550	1.140	0.057	3.293	1.117	0.109	0.967	0.940	0.963	0.997	1.189
1249	0001	44550	1.140	0.060	3.293	1.509	0.233	0.966	0.974	0.960	1.099	1.206
1250	0001	44550	1.140	0.060	3.297	2.000	0.329	0.966	0.994	0.956	1.203	1.209
1251	0001	44550	1.140	0.062	3.299	2.501	0.411	0.966	0.995	0.949	1.297	1.203
1252	0001	44550	1.140	0.064	3.298	3.008	0.496	0.966	0.995	0.942	1.392	1.198
1253	0001	44550	1.140	0.067	3.295	3.507	0.577	0.967	0.997	0.958	1.520	1.214

FACILITY 1 PROGRAM CODE

NOZZLE TYPE — DUAL FLOW (FAA) — INT. STREAM PLUG CONFIGURATIONS — BASELINE PLUG WITH BLEED — SUPPRESSOR CONFIGURATION — 20-SPOKE, AREA RATIO = 1.75

OUTER RADIUS RATIO 0.9090 — INNER RADIUS RATIO 0.7790 — DVO 1.2980

PROG	PARAMETERS	NASA	M2	VA	PTC/PA	PTJ/PA	DNFGAT	DCS	CDS	DCSH	CDSH	DCPL,O	DCPL,I	DCTOT	PSUP/PA
1208	0001	44530	0.398	0.021	1.490	0.979	0.000	-0.014	9.199	-0.001	0.637	-0.007	0.006	-0.017	0.984
1210	0001	44530	0.398	0.022	1.484	0.986	0.029	-0.015	8.942	-0.001	0.533	-0.006	0.005	-0.016	0.986
1211	0001	44530	0.398	0.020	1.485	0.998	0.059	-0.014	8.799	-0.001	0.710	-0.006	0.003	-0.018	0.986
1212	0001	44530	0.398	0.028	1.486	0.964	0.000	-0.014	8.255	-0.001	0.540	-0.005	0.009	-0.012	0.975
1213	0001	44530	0.398	0.048	1.491	0.981	0.029	-0.013	2.602	-0.000	0.081	-0.004	0.008	-0.009	0.976
1214	0001	44530	0.398	0.037	1.491	1.000	0.059	-0.013	5.912	-0.001	0.369	-0.003	0.006	-0.011	0.977
1215	0001	44530	0.398	0.054	2.492	0.956	0.000	-0.012	2.666	-0.000	0.104	-0.004	0.010	-0.007	0.970
1216	0001	44530	0.398	0.044	2.490	0.977	0.029	-0.011	3.777	-0.001	0.200	-0.003	0.008	-0.007	0.971
1217	0001	44530	0.398	0.053	2.494	1.003	0.059	-0.011	2.545	-0.000	0.098	-0.001	0.006	-0.006	0.972
1218	0001	44530	0.398	0.053	2.997	0.946	0.000	-0.010	3.036	-0.001	0.170	-0.014	0.009	-0.016	0.967
1219	0001	44530	0.398	0.053	3.005	0.974	0.029	-0.009	2.904	-0.001	0.173	-0.012	0.007	-0.015	0.969
1220	0001	44530	0.398	0.055	3.005	1.012	0.059	-0.009	2.704	-0.000	0.141	-0.011	0.005	-0.016	0.969
1221	0001	44530	0.398	0.057	3.317	0.937	0.000	-0.010	2.853	-0.001	0.164	-0.013	0.009	-0.015	0.964
1222	0001	44530	0.398	0.058	3.320	0.979	0.029	-0.009	2.666	-0.000	0.137	-0.012	0.007	-0.015	0.965
1223	0001	44530	0.398	0.059	3.315	1.021	0.059	-0.009	2.891	-0.001	0.172	-0.011	0.006	-0.016	0.967
1224	0001	44550	1.140	0.022	1.494	1.114	0.269	-0.011	7.013	-0.001	0.596	-0.003	0.001	-0.014	0.987
1225	0001	44550	1.140	0.027	1.493	1.509	0.545	-0.008	4.208	-0.001	0.404	-0.002	-0.001	-0.012	0.987
1226	0001	44550	1.140	0.046	1.495	2.002	0.750	-0.006	1.435	-0.000	0.072	-0.001	-0.017	-0.025	0.988
1227	0001	44550	1.140	0.050	1.497	2.504	0.544	-0.005	1.241	-0.000	0.057	-0.001	-0.021	-0.027	0.988
1228	0001	44550	1.140	0.052	1.496	3.007	1.136	-0.004	1.086	-0.000	0.076	-0.001	-0.028	-0.033	0.988
1229	0001	44550	1.140	0.053	1.497	3.498	1.726	-0.004	1.070	-0.000	0.087	-0.000	-0.006	-0.011	0.988
1230	0001	44550	1.140	0.042	1.995	1.116	0.177	-0.010	2.883	-0.001	0.161	-0.001	0.002	-0.010	0.990
1231	0001	44550	1.140	0.048	1.995	1.509	0.388	-0.008	2.054	-0.000	0.106	-0.001	-0.000	-0.010	0.981
1232	0001	44550	1.140	0.054	1.989	2.000	0.545	-0.007	1.648	-0.000	0.087	-0.001	-0.019	-0.027	0.982
1233	0001	44550	1.140	0.055	1.992	2.501	0.681	-0.006	1.626	-0.000	0.116	-0.000	-0.017	-0.023	0.981
1234	0001	44550	1.140	0.057	1.994	3.001	0.818	-0.005	1.503	-0.000	0.095	0.000	-0.025	-0.031	0.981
1235	0001	44550	1.140	0.056	1.992	3.505	3.956	-0.005	1.402	-0.000	0.117	0.000	-0.010	-0.014	0.992
1236	0001	44550	1.140	0.051	2.494	1.117	0.144	-0.010	2.617	-0.000	0.123	0.001	0.002	-0.007	0.974
1237	0001	44550	1.140	0.052	2.487	1.507	0.309	-0.008	2.348	-0.000	0.131	0.001	-0.000	-0.007	0.975
1238	0001	44550	1.140	0.054	2.491	1.999	0.434	-0.007	2.206	-0.000	0.142	0.001	-0.014	-0.021	0.975
1239	0001	44550	1.140	0.057	2.496	2.503	0.544	-0.006	1.672	-0.000	0.150	0.001	-0.019	-0.025	0.975
1240	0001	44550	1.140	0.056	2.495	3.003	0.653	-0.006	1.996	-0.000	0.162	0.001	-0.030	-0.035	0.976
1241	0001	44550	1.140	0.062	2.494	3.504	0.763	-0.006	1.580	-0.000	0.129	0.001	-0.013	-0.017	0.977
1242	0001	44550	1.140	0.056	2.986	1.113	0.119	-0.003	2.413	-0.001	0.143	-0.009	0.002	-0.017	0.971
1243	0001	44550	1.140	0.056	2.984	1.510	0.259	-0.007	2.224	-0.001	0.158	-0.008	-0.000	-0.014	0.973
1244	0001	44550	1.140	0.058	2.994	2.000	0.361	-0.007	2.120	-0.000	0.159	-0.007	-0.012	-0.026	0.972
1245	0001	44550	1.140	0.060	3.006	2.507	0.453	-0.006	1.867	-0.000	0.155	-0.006	-0.016	-0.029	0.974
1246	0001	44550	1.140	0.063	3.007	3.008	0.543	-0.005	1.709	-0.000	0.143	-0.006	-0.028	-0.039	0.974
1247	0001	44550	1.140	0.065	3.005	3.504	0.634	-0.005	1.536	-0.000	0.142	-0.005	-0.015	-0.025	0.975
1248	0001	44550	1.140	0.057	3.293	1.117	0.109	-0.003	2.506	-0.000	0.154	-0.009	0.002	-0.016	0.969
1249	0001	44550	1.140	0.060	3.293	1.509	0.233	-0.007	2.147	-0.000	0.147	-0.008	-0.001	-0.017	0.971
1250	0001	44550	1.140	0.060	3.297	2.000	0.328	-0.006	2.102	-0.000	0.157	-0.007	-0.013	-0.027	0.970
1251	0001	44550	1.140	0.062	3.299	2.501	0.411	-0.006	2.024	-0.000	0.149	-0.007	-0.021	-0.034	0.970
1252	0001	44550	1.140	0.066	3.298	3.009	0.494	-0.005	1.791	-0.000	0.156	-0.006	-0.025	-0.036	0.972
1253	0001	44550	1.140	0.067	3.296	3.502	0.577	-0.005	1.564	-0.000	0.151	-0.005	-0.014	-0.024	0.973

FACILITY AI PROGRAM C031

NOZZLE TYPE — DUAL FLOW (FAA)

INT. STREAM PLUG CONFIGURATIONS — BASELINE PLUG WITH BLEED

SUPPRESSOR CONFIGURATION — 20-SPOKE, AREA RATIO = 1.75

THRUST PARAMETERS — OUTER RADIUS RATIO 0.0000 — INNER RADIUS RATIO 0.7790 — DVD 1.2480

PDC	GF	WASB	PZ	MA	PTO/PA	PTI/PA	OMEGAT	CDD	CDI	CFNET1	CFNET2	EG
1254	0001	44550	1.140	0.050	2.491	1.114	0.143	0.956	0.941	0.944	1.014	1.184
1255	0001	44550	1.140	0.059	2.494	3.007	0.455	0.965	0.996	0.944	1.613	1.202
1256	0001	44530	0.398	0.448	2.449	0.954	0.000	0.965	9.999	0.952	0.952	1.173
1257	0001	44530	0.398	0.443	2.488	1.003	0.000	0.967	2.448	0.947	0.970	1.177
[illegible]	[illegible]	[illegible]	[illegible]	[illegible]	[illegible]	[illegible]	[illegible]	[illegible]	[illegible]	[illegible]	[illegible]	[illegible]
1259	0001	44530	0.398	0.446	1.495	1.000	0.000	0.995	9.999	0.811	0.811	1.093
1260	0001	44530	0.398	0.446	1.491	1.010	0.029	0.995	0.372	0.820	0.824	1.095
1261	0001	44530	0.398	0.446	1.494	1.024	0.059	0.995	0.404	0.825	0.838	1.097
1262	0001	44530	0.398	0.448	1.999	0.997	0.000	0.996	9.999	0.858	0.858	1.107
1263	0001	44530	0.398	0.448	1.999	1.017	0.029	0.967	0.394	0.866	0.870	1.110
1264	0001	44530	0.398	0.448	1.997	1.042	0.059	0.967	0.514	0.871	0.885	1.113
1265	0001	44530	0.398	0.448	2.502	0.981	0.000	0.997	9.999	0.879	0.879	1.117
1266	0001	44530	0.398	0.448	2.504	1.015	0.029	0.967	0.527	0.888	0.892	1.119
1267	0001	44530	0.398	0.449	2.501	1.051	0.059	0.958	0.582	0.893	0.906	1.123
1268	0001	44530	0.398	0.450	3.005	0.964	0.000	0.968	9.999	0.890	0.890	1.126
1269	0001	44530	0.398	0.450	3.003	1.012	0.029	0.968	0.700	0.901	0.904	1.130
1270	0001	44530	0.398	0.450	3.004	1.067	0.059	0.968	0.635	0.906	0.919	1.133
1271	0001	44530	0.398	0.450	3.306	0.954	0.000	0.967	9.999	0.897	0.897	1.133
1272	0001	44530	0.398	0.450	3.307	1.014	0.029	0.966	0.686	0.909	0.912	1.136
1273	0001	44530	0.398	0.449	3.300	1.074	0.059	0.967	0.436	0.912	0.924	1.139
1274	0001	44530	0.398	0.448	2.503	0.980	0.000	0.967	9.999	0.882	0.882	1.119
1275	0001	44530	0.398	0.449	2.502	1.052	0.059	0.967	0.576	0.897	0.911	1.125
1276	0001	44550	1.140	0.447	1.494	1.112	0.208	0.993	0.814	0.840	0.954	1.119
1277	0001	44550	1.140	0.446	1.495	1.507	0.522	0.991	0.971	0.885	1.351	1.164
1278	0001	44550	1.140	0.449	1.496	2.006	0.737	0.991	0.988	0.898	1.749	1.176
1279	0001	44550	1.140	0.448	1.495	2.500	0.925	0.991	0.995	0.907	2.130	1.191
1280	0001	44550	1.140	0.447	1.495	3.012	1.117	0.991	0.994	0.905	2.500	1.178
1281	0001	44550	1.140	0.447	1.496	3.506	1.302	0.986	0.994	0.932	2.959	1.199
1282	0001	44550	1.140	0.447	1.996	1.118	0.141	0.964	0.731	0.894	0.947	1.129
1283	0001	44550	1.140	0.447	1.999	1.511	0.276	0.967	0.953	0.902	1.169	1.165
1284	0001	44550	1.140	0.447	1.998	2.001	0.541	0.967	0.992	0.906	1.396	1.177
1285	0001	44550	1.140	0.447	1.999	2.505	0.676	0.967	0.999	0.914	1.613	1.190
1286	0001	44550	1.140	0.448	1.999	3.011	0.816	0.967	0.995	0.914	1.827	1.181
1287	0001	44550	1.140	0.448	1.999	3.511	0.952	0.966	0.995	0.931	2.079	1.197
1288	0001	44550	1.140	0.448	2.500	1.116	0.107	0.967	0.705	0.906	0.941	1.133
1289	0001	44550	1.140	0.448	2.503	1.511	0.297	0.958	0.944	0.914	1.103	1.167
1290	0001	44550	1.140	0.448	2.513	2.003	0.431	0.964	0.991	0.914	1.262	1.171
1291	0001	44550	1.140	0.449	2.504	2.509	0.542	0.964	0.991	0.921	1.421	1.179
1292	0001	44550	1.140	0.449	2.501	3.010	0.651	0.966	0.993	0.909	1.550	1.170
1294	0001	44550	1.140	0.449	3.005	1.115	0.090	0.968	0.710	0.914	0.947	1.141
1295	0001	44550	1.140	0.448	3.003	1.511	0.246	0.958	0.936	0.921	1.066	1.168
1296	0001	44550	1.140	0.448	3.009	2.004	0.359	0.968	0.992	0.919	1.188	1.176
1297	0001	44550	1.140	0.447	3.004	2.504	0.450	0.968	0.994	0.917	1.298	1.174
1298	0001	44550	1.140	0.448	3.005	3.012	0.542	0.968	0.995	0.909	1.402	1.168
1299	0001	44550	1.140	0.448	3.002	3.509	0.633	0.969	0.996	0.926	1.546	1.186

FACILITY A , PROGRAM C031

NOZZLE TYPE — INNER TREAM PLUG CONFIGURATIONS — SUPPRESSOR CONFIGURATION
DUAL FLOW (FAAA) — BASELINE PLUG WITH BLEED — 20-SPOKE, AREA RATIO = 1.75

DRAG PARAMETERS — OUTER RADIUS RATIO 0.0000 — INNER RADIUS RATIO 0.7790 — DVD 1.3680

PDC	GE	MASA	D2	MA	PTO/PS	PT1/PA	THRUST	DCC	CDS	DCSH	CD_0	DCPL,0	DCPL,I	DCTOT	PSUP/PA
1254	0001	44550	1.140	0.050	2.491	1.114	0.143	-0.010	2.675	-0.000	0.114	0.001	0.003	-0.007	0.974
1255	0001	44550	1.140	0.059	2.496	3.007	0.455	-0.006	1.782	-0.000	0.132	0.001	-0.029	-0.034	0.976
1256	0001	44550	0.398	0.048	2.485	0.956	0.000	-0.012	3.309	-0.001	0.148	-0.004	0.011	-0.006	0.970
1257	0001	44550	0.398	0.043	2.488	1.003	0.059	-0.011	3.946	-0.001	0.208	-0.001	0.007	-0.006	0.972
~~1258~~	~~0001~~	~~44550~~	~~0.398~~	~~0.048~~	~~2.488~~	~~1.001~~	~~0.000~~	~~-0.012~~	~~3.003~~	~~-0.025~~	~~0.038~~	~~-0.001~~	~~0.016~~	~~-0.070~~	~~0.930~~
1259	0001	44550	0.398	0.446	1.466	1.000	0.000	-0.087	0.115	-0.029	0.038	-0.005	0.028	-0.093	0.912
1260	0001	44550	0.398	0.446	1.461	1.010	0.029	-0.085	0.110	-0.028	0.037	-0.005	0.025	-0.091	0.915
1261	0001	44550	0.398	0.446	1.464	1.024	0.059	-0.081	0.108	-0.026	0.035	-0.003	0.021	-0.089	0.917
1262	0001	44550	0.398	0.448	1.466	0.997	0.000	-0.072	0.165	-0.019	0.043	-0.002	0.021	-0.073	0.877
1263	0001	44550	0.398	0.448	1.469	1.017	0.029	-0.066	0.160	-0.019	0.043	-0.001	0.018	-0.070	0.876
1264	0001	44550	0.398	0.448	1.467	1.042	0.059	-0.064	0.155	-0.018	0.042	0.000	0.015	-0.069	0.890
1265	0001	44550	0.398	0.448	2.502	0.981	0.000	-0.042	0.233	-0.014	0.046	-0.003	0.017	-0.062	0.843
1266	0001	44550	0.398	0.448	2.504	1.015	0.029	-0.060	0.195	-0.014	0.045	-0.002	0.015	-0.060	0.848
1267	0001	44550	0.398	0.449	2.501	1.051	0.059	-0.057	0.190	-0.013	0.044	-0.000	0.012	-0.059	0.852
1268	0001	44550	0.398	0.450	3.005	0.964	0.000	-0.057	0.271	-0.011	0.046	-0.012	0.016	-0.059	0.827
1269	0001	44550	0.398	0.450	3.004	1.017	0.029	-0.051	0.215	-0.011	0.045	-0.010	0.013	-0.058	0.832
1270	0001	44550	0.398	0.450	3.004	1.067	0.059	-0.049	0.210	-0.010	0.043	-0.009	0.010	-0.059	0.836
1271	0001	44550	0.398	0.450	3.006	0.956	0.000	-0.047	0.274	-0.010	0.046	-0.012	0.016	-0.053	0.825
1272	0001	44550	0.398	0.450	3.007	1.014	0.029	-0.045	0.219	-0.009	0.045	-0.011	0.013	-0.053	0.829
1273	0001	44550	0.398	0.449	3.000	1.074	0.059	-0.044	0.216	-0.009	0.044	-0.010	0.010	-0.053	0.832
1274	0001	44550	0.398	0.448	2.500	0.933	0.000	-0.041	0.284	-0.014	0.044	-0.003	0.018	-0.041	0.841
1275	0001	44550	0.398	0.449	2.502	1.052	0.059	-0.057	0.189	-0.013	0.043	-0.000	0.012	-0.058	0.853
1276	0001	44550	1.140	0.447	1.464	1.112	0.208	-0.066	0.047	-0.023	0.034	-0.000	0.017	-0.073	0.925
1277	0001	44550	1.140	0.449	1.466	1.507	0.322	-0.047	0.093	-0.016	0.032	0.001	0.011	-0.051	0.927
1278	0001	44550	1.140	0.449	1.466	2.306	0.737	-0.037	0.093	-0.013	0.033	0.000	-0.006	-0.055	0.927
1279	0001	44550	1.140	0.448	1.465	2.503	0.525	-0.030	0.073	-0.011	0.032	0.001	-0.011	-0.051	0.928
1280	0001	44550	1.140	0.447	1.463	3.012	1.117	-0.025	0.090	-0.009	0.032	0.001	-0.025	-0.058	0.930
1281	0001	44550	1.140	0.447	1.464	3.504	1.302	-0.021	0.089	-0.008	0.032	0.001	-0.006	-0.035	0.931
1282	0001	44550	1.140	0.447	1.466	1.119	0.141	-0.059	0.144	-0.014	0.040	0.002	0.012	-0.062	0.889
1283	0001	44550	1.140	0.447	1.466	1.511	0.376	-0.045	0.136	-0.013	0.038	0.002	0.007	-0.049	0.895
1284	0001	44550	1.140	0.447	1.466	2.001	0.561	-0.038	0.135	-0.011	0.036	0.002	-0.014	-0.060	0.896
1285	0001	44550	1.140	0.447	1.466	2.505	0.674	-0.033	0.133	-0.009	0.038	0.002	-0.012	-0.052	0.897
1286	0001	44550	1.140	0.448	1.466	3.011	0.816	-0.028	0.128	-0.009	0.037	0.002	-0.025	-0.058	0.901
1287	0001	44550	1.140	0.448	1.466	3.511	0.952	-0.024	0.124	-0.007	0.036	0.002	-0.008	-0.037	0.904
1288	0001	44550	1.140	0.448	2.500	1.116	0.107	-0.053	0.181	-0.012	0.042	0.001	0.009	-0.055	0.860
1289	0001	44550	1.140	0.448	2.503	1.511	0.297	-0.043	0.169	-0.010	0.041	0.002	0.005	-0.046	0.869
1290	0001	44550	1.140	0.448	2.513	2.003	0.431	-0.037	0.166	-0.009	0.041	0.002	-0.011	-0.055	0.871
1291	0001	44550	1.140	0.449	2.504	2.509	0.542	-0.033	0.163	-0.008	0.039	0.002	-0.016	-0.055	0.873
1292	0001	44550	1.140	0.449	2.501	3.019	0.651	-0.028	0.157	-0.007	0.038	0.002	-0.030	-0.064	0.877
1294	0001	44550	1.140	0.449	3.006	1.115	0.260	-0.047	0.224	-0.010	0.043	-0.008	0.007	-0.057	0.841
1295	0001	44550	1.140	0.448	3.003	1.511	0.246	-0.039	0.192	-0.008	0.040	-0.005	0.004	-0.048	0.851
1296	0001	44550	1.140	0.448	3.000	2.004	0.359	-0.034	0.189	-0.007	0.041	-0.004	-0.010	-0.056	0.854
1297	0001	44550	1.140	0.447	3.003	2.504	0.450	-0.031	0.188	-0.007	0.040	-0.004	-0.020	-0.052	0.855
1298	0001	44550	1.140	0.448	3.005	3.012	0.542	-0.028	0.182	-0.006	0.039	-0.003	-0.031	-0.068	0.859
1299	0001	44550	1.140	0.448	3.002	3.509	0.633	-0.025	0.176	-0.005	0.039	-0.003	-0.014	-0.049	0.864

FACILITY R -1 PROGRAM C021

NOZZLE TYPE — DUAL FLOW (FAE)

FAN STREAM PLUG CONFIGURATIONS — BASELINE PLUG WITH BLEED

SUPPRESSOR CONFIGURATION — 20-SOCKE, AREA RATIO = 1.75

THRUST PARAMETERS — OUTER RADIUS RATIO 0.0000 — INNER RADIUS RATIO 0.7790 — DVD 1.2480

PNC	CF	MASS	P2	M2	PT2/P2	PT1/P2	OMEGAT	CDT	CDI	CFNET1	CFNET2	FG
1300	0001	44550	1.140	0.448	3.294	1.114	0.078	0.969	0.680	0.916	0.939	1.143
1301	0001	44550	1.140	0.448	3.298	1.510	0.270	0.969	0.924	0.921	1.047	1.168
1302	0001	44550	1.140	0.448	3.302	2.003	0.377	0.969	0.992	0.918	1.154	1.175
1303	0001	44550	1.140	0.448	3.303	2.506	0.410	0.968	0.994	0.913	1.248	1.170
1304	0001	44550	1.140	0.449	3.305	3.017	0.494	0.968	0.994	0.911	1.347	1.169
1305	0001	44550	1.140	0.448	3.259	3.506	0.576	0.968	0.996	0.927	1.472	1.186
1306	0001	44550	1.140	0.448	2.503	1.115	0.110	0.967	0.772	0.908	0.944	1.136
1307	0001	44550	1.140	0.447	2.501	1.506	0.760	0.968	0.997	0.931	1.740	1.193
1308	0001	44530	0.398	0.358	1.503	0.998	0.000	0.991	0.999	0.852	0.852	1.111
1309	0001	44570	0.398	0.358	1.496	1.000	0.079	0.991	0.403	0.860	0.864	1.112
1310	0001	44530	0.398	0.358	1.497	1.002	0.059	0.988	0.520	0.867	0.879	1.114
1311	0001	44530	0.398	0.359	2.004	0.999	0.000	0.967	0.999	0.884	0.884	1.125
1312	0001	44530	0.398	0.359	2.005	1.012	0.029	0.967	0.465	0.892	0.896	1.127
1313	0001	44530	0.398	0.360	2.005	1.008	0.059	0.967	0.536	0.895	0.909	1.127
1314	0001	44530	0.398	0.360	2.507	0.997	0.000	0.967	0.999	0.899	0.899	1.132
1315	0001	44530	0.398	0.359	2.503	1.011	0.029	0.967	0.429	0.909	0.911	1.134
1316	0001	44530	0.398	0.360	2.510	1.008	0.059	0.964	0.601	0.913	0.926	1.136
1317	0001	44530	0.398	0.360	3.011	0.992	0.000	0.965	0.999	0.911	0.911	1.142
1318	0001	44550	0.398	0.358	3.000	1.009	0.029	0.959	0.808	0.919	0.922	1.145
1319	0001	44530	0.398	0.359	3.007	1.007	0.059	0.958	0.662	0.922	0.935	1.147
1320	0001	44530	0.398	0.359	3.273	0.999	0.000	0.969	0.999	0.911	0.911	1.147
1321	0001	44530	0.398	0.359	3.272	1.009	0.029	0.959	0.886	0.923	0.925	1.149
1322	0001	44530	0.398	0.359	3.272	1.007	0.059	0.958	0.667	0.926	0.940	1.152
1323	0001	44530	0.398	0.360	2.503	0.995	0.000	0.967	0.999	0.901	0.901	1.134
1324	0001	44530	0.398	0.359	2.505	1.005	0.059	0.958	0.673	0.913	0.926	1.138
1325	0001	44550	1.140	0.359	1.499	1.112	0.213	0.989	0.831	0.886	0.905	1.132
1326	0001	44550	1.140	0.359	1.499	1.503	0.526	0.990	0.975	0.903	1.383	1.175
1327	0001	44550	1.140	0.359	1.498	2.014	0.764	0.983	0.993	0.910	1.782	1.186
1328	0001	44550	1.140	0.360	1.497	2.520	0.833	0.985	0.991	0.921	2.173	1.190
1329	0001	44550	1.140	0.360	1.495	3.009	1.117	0.987	0.994	0.916	2.530	1.186
1330	0001	44550	1.140	0.360	1.495	3.508	1.204	0.988	0.994	0.930	2.978	1.207
1331	0001	44550	1.140	0.359	2.005	1.115	0.145	0.965	0.765	0.910	0.964	1.141
1332	0001	44550	1.140	0.360	1.996	1.517	0.378	0.956	0.954	0.919	1.193	1.177
1333	0001	44550	1.140	0.359	1.997	2.013	0.544	0.968	0.993	0.917	1.619	1.197
1334	0001	44550	1.140	0.360	2.009	2.512	0.677	0.967	0.996	0.924	1.632	1.190
1335	0001	44550	1.140	0.360	2.007	3.005	0.813	0.964	0.992	0.926	1.847	1.199
1336	0001	44550	1.140	0.360	2.003	3.502	0.940	0.967	0.996	0.930	2.091	1.205
1337	0001	44550	1.140	0.361	2.504	1.117	0.115	0.955	0.756	0.924	0.963	1.147
1338	0001	44550	1.140	0.361	2.508	1.514	0.309	0.966	0.949	0.927	1.121	1.176
1339	0001	44550	1.140	0.361	2.513	2.018	0.433	0.966	0.989	0.927	1.283	1.185
1340	0001	44550	1.140	0.361	2.511	2.515	0.542	0.956	0.994	0.929	1.433	1.197
1341	0001	44550	1.140	0.360	2.506	3.010	0.651	0.967	0.995	0.917	1.562	1.178
1342	0001	44550	1.140	0.359	2.505	3.500	0.757	0.968	0.996	0.940	1.752	1.200
1343	0001	44550	1.140	0.359	2.997	1.116	0.093	0.958	0.735	0.927	0.957	1.153
1344	0001	44550	1.140	0.359	2.985	1.510	0.249	0.966	0.943	0.935	1.085	1.180

FACILITY : 1 PROGRAM CODE

NOZZLE TYPE — INV. STREAM PLUG CONFIGURATIONS — SUPPRESSOR CONFIGURATION

DUAL FLOW (FAST) — RADIAL PLUG WITH BLEED — 20-SPOKE, AREA RATIO = 1.75

PROG PARAMETERS — OUTER RADIUS RATIO 0.8000 — INNER RADIUS RATIO 0.7790 — OVD 1.2400

PROG	GE	MASP	MP	VA	PTP/PA	PTT/PA	OMEGAT	DCS	FDS	DCSH	FDSH	DCPL,O	DCPL,I	DCTOT	PSUP/PA
1300	0001	44550	1.140	0.448	3.296	1.114	0.273	-0.041	0.212	-0.009	0.044	-0.009	0.007	-0.054	0.836
1301	0001	44550	1.140	0.448	3.294	1.519	0.220	-0.037	0.201	-0.008	0.041	-0.006	0.000	-0.050	0.844
1302	0001	44550	1.140	0.448	3.302	2.003	0.327	-0.032	0.197	-0.007	0.040	-0.005	-0.013	-0.058	0.847
1303	0001	44550	1.140	0.448	3.303	2.501	0.410	-0.029	0.194	-0.006	0.041	-0.005	-0.023	-0.064	0.850
1304	0001	44550	1.140	0.449	3.303	3.017	0.494	-0.027	0.190	-0.005	0.039	-0.004	-0.030	-0.066	0.852
1305	0001	44550	1.140	0.448	3.299	3.504	0.576	-0.025	0.186	-0.005	0.040	-0.003	-0.032	-0.065	0.855
1306	0001	44550	1.140	0.446	2.503	1.115	0.110	-0.051	0.191	-0.013	0.043	0.001	0.009	-0.054	0.841
1307	0001	44550	1.140	0.447	2.501	1.506	0.760	-0.025	0.154	-0.006	0.039	0.002	-0.009	-0.038	0.881
1308	0001	44530	0.398	0.353	1.502	0.998	0.000	-0.071	0.152	-0.019	0.038	-0.002	0.014	-0.080	0.925
1309	0001	44530	0.398	0.353	1.496	1.002	0.029	-0.073	0.145	-0.019	0.038	-0.001	0.011	-0.079	0.928
1310	0001	44530	0.398	0.358	1.497	1.927	0.050	-0.067	0.140	-0.018	0.037	-0.000	0.008	-0.077	0.931
1311	0001	44530	0.398	0.359	2.006	0.992	0.000	-0.060	0.217	-0.013	0.046	-0.000	0.012	-0.061	0.892
1312	0001	44530	0.398	0.359	2.005	1.912	0.029	-0.051	0.209	-0.013	0.044	0.000	0.010	-0.061	0.896
1313	0001	44530	0.398	0.360	2.005	1.934	0.050	-0.050	0.202	-0.012	0.043	0.001	0.007	-0.059	0.899
1314	0001	44530	0.398	0.360	2.507	0.977	0.000	-0.062	0.261	-0.010	0.049	-0.002	0.011	-0.053	0.859
1315	0001	44530	0.398	0.359	2.500	1.351	0.023	-0.050	0.256	-0.010	0.050	-0.001	0.008	-0.052	0.873
1316	0001	44530	0.398	0.360	2.510	1.942	0.050	-0.047	0.245	-0.009	0.046	0.001	0.005	-0.050	0.878
1317	0001	44530	0.398	0.360	3.011	0.962	0.000	-0.064	0.287	-0.008	0.250	-0.012	0.010	-0.053	0.856
1318	0001	44530	0.398	0.358	3.009	1.388	0.028	-0.042	0.281	-0.007	0.050	-0.011	0.008	-0.053	0.861
1319	0001	44530	0.398	0.359	3.007	1.957	0.050	-0.041	0.273	-0.007	0.048	-0.009	0.005	-0.052	0.864
1320	0001	44530	0.398	0.359	3.280	0.951	0.000	-0.059	0.293	-0.007	0.060	-0.013	0.010	-0.068	0.855
1321	0001	44530	0.398	0.359	3.277	1.009	0.028	-0.037	0.287	-0.006	0.048	-0.012	0.009	-0.069	0.857
1322	0001	44530	0.398	0.359	3.275	1.867	0.050	-0.037	0.281	-0.006	0.048	-0.010	0.006	-0.069	0.860
1323	0001	44530	0.398	0.359	2.500	0.975	0.000	-0.052	0.264	-0.010	0.050	-0.002	0.011	-0.052	0.869
1324	0001	44530	0.398	0.359	2.505	1.365	0.050	-0.047	0.245	-0.009	0.047	0.001	0.005	-0.051	0.878
1325	0001	44550	1.140	0.359	1.503	1.112	0.213	-0.056	0.127	-0.015	0.034	0.002	0.005	-0.064	0.937
1326	0001	44550	1.140	0.359	1.504	1.509	0.526	-0.040	0.125	-0.011	0.035	0.002	0.002	-0.047	0.938
1327	0001	44550	1.140	0.359	1.499	2.016	0.744	-0.031	0.124	-0.009	0.035	0.001	-0.013	-0.051	0.938
1328	0001	44550	1.140	0.360	1.494	2.523	0.939	-0.024	0.123	-0.007	0.033	0.002	-0.017	-0.048	0.938
1329	0001	44550	1.140	0.360	1.495	3.002	1.117	-0.022	0.121	-0.006	0.033	0.001	-0.019	-0.045	0.940
1330	0001	44550	1.140	0.360	1.492	3.507	1.304	-0.018	0.117	-0.005	0.032	0.001	-0.020	-0.042	0.942
1331	0001	44550	1.140	0.359	2.005	1.115	0.145	-0.050	0.189	-0.011	0.043	0.002	0.004	-0.054	0.906
1332	0001	44550	1.140	0.360	1.498	1.512	0.378	-0.039	0.179	-0.009	0.040	0.003	0.000	-0.044	0.911
1333	0001	44550	1.140	0.359	1.997	2.017	0.566	-0.032	0.178	-0.007	0.041	0.002	-0.019	-0.056	0.911
1334	0001	44550	1.140	0.360	2.002	2.512	0.677	-0.028	0.176	-0.006	0.040	0.002	-0.016	-0.048	0.912
1335	0001	44550	1.140	0.360	2.002	3.005	0.811	-0.026	0.171	-0.006	0.041	0.002	-0.028	-0.056	0.915
1336	0001	44550	1.140	0.360	2.003	3.502	0.945	-0.021	0.165	-0.005	0.038	0.002	-0.029	-0.031	0.917
1337	0001	44550	1.140	0.361	2.509	1.117	0.115	-0.045	0.231	-0.009	0.045	0.002	0.003	-0.048	0.884
1338	0001	44550	1.140	0.361	2.508	1.514	0.300	-0.036	0.220	-0.007	0.043	0.003	0.000	-0.040	0.899
1339	0001	44550	1.140	0.361	2.510	2.018	0.493	-0.031	0.218	-0.006	0.043	0.002	-0.015	-0.050	0.891
1340	0001	44550	1.140	0.361	2.511	2.515	0.542	-0.027	0.215	-0.005	0.041	0.002	-0.019	-0.049	0.892
1341	0001	44550	1.140	0.360	2.508	3.010	0.651	-0.026	0.208	-0.005	0.042	0.002	-0.034	-0.060	0.896
1342	0001	44550	1.140	0.359	2.505	3.508	0.757	-0.021	0.202	-0.004	0.043	0.002	-0.011	-0.035	0.899
1343	0001	44550	1.140	0.359	2.997	1.116	0.063	-0.039	0.252	-0.007	0.046	-0.008	0.002	-0.051	0.869
1344	0001	44550	1.140	0.359	2.986	1.510	0.249	-0.032	0.246	-0.006	0.045	-0.006	0.001	-0.044	0.877

FACILITY AXI PROGRAM COST

NOZZLE TYPE — PLUG CONFIGURATIONS — SUPPRESSOR CONFIGURATION

DUAL FLOW (FAST) — RADIATIVE PLUG WITH BLEED — 20-SPOKE, AREA RATIO = 1.75

INPUT PARAMETERS — OUTER RADIUS RATIO 0.0000 — INNER RADIUS RATIO 0.7790 — DVD 1.2680

REC	CF	CASE	B2	W2	PTO/P2	PTI/P2	OMEGAT	CDO	CDI	CFNET1	CFNET2	F9
1345	0001	44550	1.140	0.359	2.982	2.978	0.365	0.969	0.992	0.929	1.208	1.186
1346	0001	44550	1.140	0.359	2.987	2.514	0.455	0.967	0.993	0.929	1.322	1.195
1347	0001	44550	1.140	0.358	2.968	3.004	0.542	0.968	0.995	0.918	1.417	1.177
1348	0001	44550	1.140	0.358	3.002	3.500	0.631	0.968	0.995	0.935	1.559	1.194
1349	0001	44550	1.140	0.358	3.244	1.115	0.083	0.967	0.712	0.929	0.954	1.155
1350	0001	44550	1.140	0.358	3.229	1.513	0.230	0.968	0.960	0.933	1.067	1.179
1351	0001	44550	1.140	0.359	3.214	2.014	0.338	0.968	0.993	0.931	1.183	1.197
1352	0001	44550	1.140	0.358	3.215	2.519	0.423	0.969	0.994	0.934	1.277	1.181
1353	0001	44550	1.140	0.359	3.215	3.004	0.506	0.968	0.995	0.919	1.373	1.177
1354	0001	44550	1.140	0.358	3.212	3.508	0.592	0.968	0.996	0.936	1.507	1.194
1355	0001	44550	1.140	0.357	2.510	1.114	0.114	0.956	0.759	0.923	0.962	1.148
1356	0001	44550	1.140	0.358	2.503	1.501	0.757	0.969	0.995	0.940	1.753	1.202

716

FACILITY AXI PROGRAM COST

NOZZLE TYPE — PLUG CONFIGURATIONS — SUPPRESSOR CONFIGURATION

DUAL FLOW (FAST) — RADIATIVE PLUG WITH BLEED — 20-SPOKE, AREA RATIO = 1.75

DRAG PARAMETERS — OUTER RADIUS RATIO 0.0000 — INNER RADIUS RATIO 0.7790 — DVD 1.2680

REC	CF	CASE	B2	W2	PTO/P2	PTI/P2	OMEGAT	DCS	CDS	DCSH	CDSH	DCPL,0	DCPL,1	DCTOT	PSUP/PA
1345	0001	44550	1.140	0.359	2.982	2.978	0.365	-0.024	0.242	-0.005	0.043	-0.005	-0.013	-0.051	0.880
1346	0001	44550	1.140	0.359	2.987	2.514	0.455	-0.024	0.242	-0.005	0.044	-0.004	-0.021	-0.055	0.880
1347	0001	44550	1.140	0.358	2.968	3.004	0.542	-0.023	0.237	-0.004	0.045	-0.004	-0.033	-0.064	0.883
1348	0001	44550	1.140	0.358	3.002	3.500	0.631	-0.021	0.231	-0.004	0.043	-0.003	-0.017	-0.045	0.885
1349	0001	44550	1.140	0.358	3.244	1.115	0.083	-0.036	0.375	-0.006	0.047	-0.010	0.003	-0.049	0.864
1350	0001	44550	1.140	0.358	3.229	1.513	0.230	-0.031	0.359	-0.006	0.046	-0.007	-0.001	-0.044	0.872
1351	0001	44550	1.140	0.359	3.214	2.014	0.338	-0.028	0.295	-0.005	0.045	-0.006	-0.014	-0.052	0.874
1352	0001	44550	1.140	0.358	3.215	2.519	0.423	-0.025	0.261	-0.004	0.043	-0.005	-0.026	-0.061	0.875
1353	0001	44550	1.140	0.359	3.215	3.004	0.506	-0.023	0.244	-0.004	0.042	-0.004	-0.032	-0.063	0.879
1354	0001	44550	1.140	0.358	3.212	3.508	0.592	-0.020	0.238	-0.004	0.042	-0.004	-0.015	-0.042	0.882
1355	0001	44550	1.140	0.357	2.510	1.114	0.114	-0.044	0.236	-0.009	0.046	0.002	0.004	-0.047	0.884
1356	0001	44550	1.140	0.358	2.503	1.501	0.757	-0.021	0.203	-0.004	0.042	0.007	-0.010	-0.034	0.899

MODEL SC-2, 30 SHALLOW CHUTES, AR = 1.75, BASELINE PLUG

FACILITY R. [illegible] PROGRAM COST

NOZZLE TYPE — FULL FLOW TESTS

TURBINE CONFIGURATIONS — BASELINE PLUS MID SLEEVE

SUPPRESSOR CONFIGURATION — 30-SPOKE, AREA RATIO = 1.75

THROAT PARAMETERS — THROAT RADIUS RATIO 0.9000 — EXIT RADIUS RATIO 0.7790 — OVR 1.2480

PPR	RF	RPSA	R2	FR	PTT/PA	PTT/PA	THRUST	CQT	CDI	CFTETL	CFTETL2	FG
1357	0002	45550	0.398	0.448	1.405	1.001	0.000	0.946	0.000	0.819	0.819	1.097
1358	0002	45550	0.398	0.448	1.404	1.012	0.979	0.987	0.342	0.825	0.829	1.099
1359	0002	45550	0.398	0.448	1.405	1.024	0.959	0.986	0.687	0.828	0.840	1.099
1360	0002	45550	0.398	0.448	1.407	1.035	0.000	0.955	0.000	0.846	0.846	1.100
1361	0002	45550	0.398	0.448	1.404	1.024	0.939	0.970	0.338	0.850	0.861	1.105
1362	0002	45550	0.398	0.448	1.407	1.047	0.960	0.970	0.689	0.860	0.874	1.107
1363	0002	45550	0.398	0.448	1.406	0.991	0.000	0.970	0.000	0.865	0.865	1.107
1364	0002	45550	0.398	0.448	1.533	1.024	0.939	0.971	0.408	0.872	0.877	1.109
1365	0002	45550	0.398	0.448	1.401	1.001	0.959	0.971	0.543	0.877	0.891	1.112
1366	0002	45550	0.398	0.448	1.399	1.024	0.000	0.969	0.000	0.879	0.879	1.112
1367	0002	45550	0.398	0.447	1.394	1.046	0.939	0.970	0.360	0.885	0.891	1.115
1368	0002	45550	0.398	0.447	1.397	1.024	0.959	0.971	0.523	0.888	0.904	1.119
1369	0002	45550	0.398	0.448	1.396	1.024	0.000	0.971	0.000	0.889	0.889	1.119
1370	0002	45550	0.398	0.448	1.393	1.024	0.939	0.971	0.310	0.896	0.903	1.122
1371	0002	45550	0.398	0.448	1.392	1.133	0.959	0.973	0.482	0.901	0.920	1.124
1372	0002	45550	0.398	0.447	2.488	1.001	0.000	0.969	0.000	0.881	0.895	1.113
1374	0002	45550	0.398	0.447	2.483	0.934	0.394	0.969	0.999X	0.866	0.866	1.107
1375	0002	45550	1.140	0.446	1.406	1.104	0.000	0.991	0.000	0.859	0.947	1.118
1376	0002	45550	1.140	0.446	1.401	1.068	0.514	0.993	0.000	0.882	1.343	1.152
1377	0002	45550	1.140	0.446	1.403	2.004	0.732	0.991	0.003	0.893	1.738	1.176
1378	0002	45550	1.140	0.447	1.402	2.406	0.814	0.991	0.005	0.904	2.108	1.180
1379	0002	45550	1.140	0.447	1.398	2.802	1.193	0.992	0.996	0.903	2.474	1.178
1380	0002	45550	1.140	0.447	1.403	3.206	1.286	0.992	0.996	0.927	2.920	1.197
1381	0002	45550	1.140	0.447	1.397	1.117	0.131	0.969	0.707	0.875	0.922	1.120
1382	0002	45550	1.140	0.446	1.402	1.420	3.160	0.979	0.996	0.891	1.150	1.159
1383	0002	45550	1.140	0.447	1.398	2.003	0.534	0.970	0.997	0.907	1.377	1.172
1384	0002	45550	1.140	0.447	1.398	2.406	0.670	0.970	0.996	0.905	1.691	1.176
1385	0002	45550	1.140	0.447	1.402	2.811	0.806	0.969	0.995	0.905	1.801	1.175
1386	0002	45550	1.140	0.447	1.401	3.207	0.940	0.968	0.996	0.926	2.055	1.193
1387	0002	45550	1.140	0.447	2.483	1.113	0.101	0.973	0.677	0.888	0.920	1.124
1388	0002	45550	1.140	0.447	2.474	1.420	0.732	0.972	0.937	0.858	1.089	1.154
1389	0002	45550	1.140	0.447	2.483	2.005	0.627	0.971	0.992	0.901	1.262	1.167
1390	0002	45550	1.140	0.447	2.487	2.593	0.135	0.971	0.996	0.906	1.391	1.170
1391	0002	45550	1.140	0.447	2.501	3.208	0.743	0.970	0.995	0.895	1.517	1.160
1392	0002	45550	1.140	0.447	2.531	3.804	0.751	0.970	0.996	0.920	1.710	1.184
1393	0002	45550	1.140	0.447	1.395	1.111	0.160	0.971	0.570	0.892	0.913	1.123
1394	0002	45550	1.140	0.447	2.483	1.420	0.737	0.970	0.914	0.901	1.037	1.151
1395	0002	45550	1.140	0.447	2.471	2.004	0.156	0.970	0.991	0.902	1.164	1.162
1396	0002	45550	1.140	0.448	2.482	2.593	0.445	0.971	0.994	0.898	1.269	1.159
1397	0002	45550	1.140	0.448	2.484	3.209	0.534	0.972	0.995	0.896	1.374	1.157
1398	0002	45550	1.140	0.448	2.501	3.811	0.274	0.973	0.995	0.915	1.515	1.175
1400	0002	45550	1.140	0.447	2.481	1.513	0.139	0.971	0.876	0.905	1.022	1.150
1401	0002	45550	1.140	0.448	2.270	2.034	0.173	0.972	0.985	0.903	1.130	1.160
1402	0002	45550	1.140	0.447	2.277	2.537	0.307	0.973	0.994	0.898	1.226	1.160
1403	0002	45550	1.140	0.447	2.301	3.084	0.486	0.971	0.997	0.898	1.319	1.160

FACILITY [illegible] NUCLEAR COST — NOZZLE TEST — DUAL FLOW STAGE — 1ST STAGE — BLADE CONFIGURATIONS — ASSEMBLE BLADE WITH SLEEVE — SUPPRESSOR CONFIGURATION — 30-SPOKE, AREA RATIO = 1.75

DRAG PARAMETERS — PIPE RADIUS RATIO = 0.0930 — TIP RADIUS RATIO = 0.7290 — MW = 1.2460

SEC	CE	MACH	M2	M3	P2/P0	P3/P0	CMFGE	MCS	FCS	DCSM	FCSN	DCPL/0	DCPL/1	DCTOT	PSUP/PA
1357	0002	45510	1.140	0.447	1.407	1.301	0.000	-0.117	0.154	-0.013	0.040	-0.016	0.029	-0.134	0.877
1358	0002	45510	1.140	0.446	1.404	1.312	0.029	-0.119	0.151	-0.009	0.039	-0.013	0.025	-0.131	0.881
1359	0002	45510	1.140	0.447	1.401	1.321	0.059	-0.120	0.149	-0.009	0.039	-0.011	0.022	-0.126	0.885
1360	0002	45510	1.140	0.447	1.399	1.331	0.088	-0.120	0.147	-0.021	0.047	-0.012	0.021	-0.119	0.892
1361	0002	45510	1.140	0.448	1.396	1.336	0.117	-0.120	0.145	-0.020	0.046	-0.009	0.018	-0.115	0.897
1362	0002	45510	1.140	0.448	1.393	1.347	0.147	-0.120	0.143	-0.019	0.045	-0.007	0.015	-0.112	0.902
1363	0002	45510	1.140	0.448	1.390	1.358	0.176	-0.119	0.141	-0.015	0.050	-0.009	0.017	-0.104	0.746
1364	0002	45510	1.140	0.448	1.387	1.370	0.205	-0.118	0.139	-0.014	0.048	-0.006	0.015	-0.100	0.753
1365	0002	45510	1.140	0.447	1.384	1.381	0.234	-0.118	0.137	-0.013	0.048	-0.004	0.012	-0.096	0.759
1366	0002	45510	1.140	0.447	1.381	1.393	0.263	-0.117	0.135	-0.012	0.050	-0.029	0.016	-0.108	0.718
1367	0002	45510	1.140	0.447	1.378	1.404	0.293	-0.117	0.134	-0.012	0.050	-0.025	0.013	-0.105	0.721
1368	0002	45510	1.140	0.447	1.375	1.416	0.322	-0.116	0.132	-0.011	0.050	-0.023	0.011	-0.103	0.724
1369	0002	45510	1.140	0.446	1.372	1.428	0.351	-0.116	0.130	-0.010	0.050	-0.020	0.014	-0.093	0.737
1370	0002	45510	1.140	0.446	1.369	1.441	0.380	-0.115	0.128	-0.010	0.049	-0.018	0.012	-0.091	0.739
1371	0002	45510	1.140	0.446	1.366	1.453	0.409	-0.114	0.127	-0.010	0.048	-0.016	0.009	-0.090	0.742
1372	0002	45510	1.140	0.446	1.363	1.466	0.438	-0.113	0.125	-0.010	0.047	-0.013	0.012	-0.084	0.760
1373	0002	45510	1.140	0.446	1.360	1.479	0.467	-0.112	0.123	-0.009	0.050	-0.009	0.010	-0.102	0.747
1374	0002	45510	1.140	0.446	1.357	1.492	0.496	-0.111	0.121	-0.009	0.049	-0.007	0.007	-0.100	0.753
1375	0002	45510	1.140	0.446	1.354	1.505	0.525	-0.110	0.119	-0.008	0.048	-0.005	0.005	-0.098	0.759
1376	0002	45510	1.140	0.446	1.351	1.518	0.554	-0.109	0.117	-0.007	0.047	-0.003	0.002	-0.096	0.765
1377	0002	45510	1.140	0.446	1.348	1.531	0.583	-0.108	0.115	-0.007	0.046	-0.001	0.000	-0.094	0.771
1378	0002	45510	1.140	0.446	1.345	1.545	0.612	-0.107	0.113	-0.006	0.045	0.000	-0.002	-0.092	0.777
1379	0002	45510	1.140	0.446	1.342	1.558	0.641	-0.106	0.111	-0.006	0.044	0.002	-0.004	-0.090	0.783
1380	0002	45510	1.140	0.446	1.339	1.572	0.670	-0.105	0.109	-0.005	0.043	0.003	-0.006	-0.088	0.789
1381	0002	45510	1.140	0.446	1.336	1.586	0.699	-0.104	0.107	-0.004	0.042	0.005	-0.008	-0.086	0.795
1382	0002	45510	1.140	0.446	1.333	1.600	0.728	-0.103	0.105	-0.004	0.041	0.006	-0.010	-0.084	0.801
1383	0002	45510	1.140	0.446	1.330	1.614	0.757	-0.102	0.103	-0.003	0.040	0.008	-0.012	-0.082	0.807
1384	0002	45510	1.140	0.446	1.327	1.628	0.786	-0.101	0.101	-0.002	0.039	0.009	-0.014	-0.080	0.813
1385	0002	45510	1.140	0.446	1.324	1.642	0.815	-0.100	0.099	-0.002	0.038	0.011	-0.016	-0.078	0.819
1386	0002	45510	1.140	0.446	1.321	1.656	0.844	-0.099	0.097	-0.001	0.037	0.012	-0.018	-0.076	0.825
1387	0002	45510	1.140	0.446	1.318	1.671	0.873	-0.098	0.095	0.000	0.036	0.014	-0.020	-0.074	0.831
1388	0002	45510	1.140	0.446	1.315	1.685	0.902	-0.097	0.093	0.000	0.035	0.015	-0.022	-0.072	0.837
1389	0002	45510	1.140	0.446	1.312	1.700	0.931	-0.096	0.091	0.001	0.034	0.017	-0.024	-0.070	0.843
1390	0002	45510	1.140	0.446	1.309	1.715	0.960	-0.095	0.089	0.002	0.033	0.018	-0.026	-0.068	0.849
1391	0002	45510	1.140	0.446	1.306	1.730	0.989	-0.094	0.087	0.003	0.032	0.020	-0.028	-0.066	0.855
1392	0002	45510	1.140	0.446	1.303	1.745	1.018	-0.093	0.085	0.004	0.031	0.021	-0.030	-0.064	0.861
1393	0002	45510	1.140	0.446	1.300	1.760	1.047	-0.092	0.083	0.005	0.030	0.023	-0.032	-0.062	0.867
1394	0002	45510	1.140	0.446	1.297	1.775	1.076	-0.091	0.081	0.006	0.029	0.024	-0.034	-0.060	0.873
1395	0002	45510	1.140	0.446	1.294	1.790	1.105	-0.090	0.079	0.007	0.028	0.026	-0.036	-0.058	0.879
1396	0002	45510	1.140	0.446	1.291	1.805	1.134	-0.089	0.077	0.008	0.027	0.027	-0.038	-0.056	0.885
1397	0002	45510	1.140	0.446	1.288	1.820	1.163	-0.088	0.075	0.009	0.026	0.029	-0.040	-0.054	0.891
1398	0002	45510	1.140	0.446	1.285	1.835	1.192	-0.087	0.073	0.010	0.025	0.030	-0.042	-0.052	0.897
1399	0002	45510	1.140	0.446	1.282	1.850	1.221	-0.086	0.071	0.011	0.024	0.032	-0.044	-0.050	0.903
1400	0002	45510	1.140	0.446	1.279	1.865	1.250	-0.085	0.069	0.012	0.023	0.033	-0.046	-0.048	0.909
1401	0002	45510	1.140	0.446	1.276	1.880	1.279	-0.084	0.067	0.013	0.022	0.035	-0.048	-0.046	0.915
1402	0002	45510	1.140	0.446	1.273	1.895	1.308	-0.083	0.065	0.014	0.021	0.036	-0.050	-0.044	0.921
1403	0002	45510	1.140	0.446	1.270	1.910	1.337	-0.082	0.063	0.015	0.020	0.038	-0.052	-0.042	0.927
1404	0002	45510	1.140	0.446	1.267	1.925	1.366	-0.081	0.061	0.016	0.019	0.039	-0.054	-0.040	0.933
1405	0002	45510	1.140	0.446	1.264	1.940	1.395	-0.080	0.059	0.017	0.018	0.041	-0.056	-0.038	0.939
1406	0002	45510	1.140	0.446	1.261	1.955	1.424	-0.079	0.057	0.018	0.017	0.042	-0.058	-0.036	0.945
1407	0002	45510	1.140	0.446	1.258	1.970	1.453	-0.078	0.055	0.019	0.016	0.044	-0.060	-0.034	0.951
1408	0002	45510	1.140	0.446	1.255	1.985	1.482	-0.077	0.053	0.020	0.015	0.045	-0.062	-0.032	0.957
1409	0002	45510	1.140	0.446	1.252	2.000	1.511	-0.076	0.051	0.021	0.014	0.047	-0.064	-0.030	0.963
1410	0002	45510	1.140	0.446	1.249	2.015	1.540	-0.075	0.049	0.022	0.013	0.048	-0.066	-0.028	0.969
1411	0002	45510	1.140	0.446	1.246	2.030	1.569	-0.074	0.047	0.023	0.012	0.050	-0.068	-0.026	0.975
1412	0002	45510	1.140	0.446	1.243	2.045	1.598	-0.073	0.045	0.024	0.011	0.051	-0.070	-0.024	0.981
1413	0002	45510	1.140	0.446	1.240	2.060	1.627	-0.072	0.043	0.025	0.010	0.053	-0.072	-0.022	0.987
1414	0002	45510	1.140	0.446	1.237	2.075	1.656	-0.071	0.041	0.026	0.009	0.054	-0.074	-0.020	0.993
1415	0002	45510	1.140	0.446	1.234	2.090	1.685	-0.070	0.039	0.027	0.008	0.056	-0.076	-0.018	0.999

719

PROPELLANT & ..AIL BURNING RATE

STAGE 1 AFT
SOLID MOTOR ROCKET

FINAL STAGE
MISSION CONFIGURATIONS
RESTART MOTOR WITH BLEED

SUPPRESSOR CONFIGURATION
30-SPOKE, AREA RATIO = 1.75

PROPELLANT PARAMETERS

PLATEAU BURNING RATE (INCHES/SEC) 0.4000
PRESSURE EXPONENT 0.7700
GMD 1.2480

BMC	CC	AREA	PD	PA	PROPPB	PTI/PB	PMAX/PI	FD1	FD2	CFNET1	CFNET2	FD
1424	0002	45550	1.140	0.449	2.509	1.369	0.464	0.972	0.995	0.910	1.436	1.171
1425	0002	45550	1.140	0.445	2.503	1.318	0.491	0.970	0.991	0.898	0.921	1.123
1426	0002	45550	1.140	0.444	2.494	1.305	0.491	0.979	0.992	0.922	1.715	1.194
1427	0002	45550	1.140	0.446	2.495	1.311	0.491	0.977	0.9977	0.904	0.910	1.130
1428	0002	45550	1.140	0.447	2.499	1.301	0.489	0.980	0.998	0.839	0.839	1.104
1429	0002	45550	0.994	0.197	1.499	1.018	0.495	0.997	0.964	0.847	0.851	1.106
1430	0002	45550	0.994	0.197	1.499	1.019	0.495	0.997	0.964	0.847	0.851	1.106
1431	0002	45550	0.994	0.197	1.499	1.019	0.495	0.997	0.964	0.847	0.851	1.106
1432	0002	45550	0.994	0.197	1.499	1.019	0.495	0.997	0.964	0.847	0.851	1.106
1433	0002	45550	0.994	0.197	1.499	1.019	0.495	0.997	0.964	0.847	0.851	1.106
1434	0002	45550	0.994	0.197	1.499	1.019	0.495	0.997	0.964	0.847	0.851	1.106
1435	0002	45550	0.994	0.197	1.499	1.019	0.495	0.997	0.964	0.847	0.851	1.106
1436	0002	45550	0.994	0.197	1.499	1.019	0.495	0.997	0.964	0.847	0.851	1.106
1437	0002	45550	0.994	0.197	1.499	1.019	0.495	0.997	0.964	0.847	0.851	1.106
1438	0002	45550	0.994	0.197	1.499	1.019	0.495	0.997	0.964	0.847	0.851	1.106
1439	0002	45550	0.994	0.197	1.499	1.019	0.495	0.997	0.964	0.847	0.851	1.106
1440	0002	45550	0.994	0.197	1.499	1.019	0.495	0.997	0.964	0.847	0.851	1.106
1441	0002	45550	1.140	0.340	2.495	1.301	0.491	0.979	0.998	0.839	0.839	1.104
1442	0002	45550	1.140	0.340	2.495	1.301	0.491	0.979	0.998	0.839	0.839	1.104
1443	0002	45550	1.140	0.340	2.495	1.301	0.491	0.979	0.998	0.839	0.839	1.104
1444	0002	45550	1.140	0.340	2.495	1.301	0.491	0.979	0.998	0.839	0.839	1.104
1445	0002	45550	1.140	0.340	2.495	1.301	0.491	0.979	0.998	0.839	0.839	1.104
1446	0002	45550	1.140	0.340	2.495	1.301	0.491	0.979	0.998	0.839	0.839	1.104
1447	0002	45550	1.140	0.340	2.495	1.301	0.491	0.979	0.998	0.839	0.839	1.104
1448	0002	45550	1.140	0.340	2.495	1.301	0.491	0.979	0.998	0.839	0.839	1.104

SUPPRESSOR CONFIGURATION
30-SERIES, AREA RATIO = 1.75

FACILITY [illegible] COMPRESSOR CODE

STAGE TYPE: QUAD FLOW (QUAD)

IMPELLER: SLOTS CONFIGURATIONS: BASELINE PLUG WITH BLEED

SUPPRESSOR CONFIGURATION: 30-SPOKE, AREA RATIO = 1.75

INLET PARAMETERS: OUTER RADIUS RATIO = 0.9000; INNER RADIUS RATIO = 0.3790; DAO = 1.2480

RPM	GG	WAVE	MN	WR	DP/DP0	PT/PT0	CP/CP0	EFF	SOI	EFFET1	EFFET2	FQ
1440	0002	45450	1.140	0.348	1.235	1.116	0.956	0.971	0.486	0.908	0.925	1.134
1440	0002	45450	1.140	0.348	1.231	1.112	0.952	0.971	0.481X	0.910	0.925	1.137
1441	0002	45450	1.140	0.348	1.284	1.511	0.708	0.972	0.678	0.914	1.032	1.159
1443	0002	45450	1.140	0.348	1.277	2.017	0.325	0.973	0.987	0.910	1.145	1.170
1437	0002	45450	1.140	0.348	1.281	2.516	0.098	0.973	0.996	0.905	1.237	1.167
1434	0002	45450	1.140	0.348	1.273	3.020	0.040	0.973	0.998	0.904	1.332	1.165
1435	0002	45450	1.140	0.348	1.274	3.522	0.022	0.973	0.996	0.918	1.455	1.179
1436	0002	45450	1.140	0.351	1.422	1.114	0.196	0.979	0.705	0.900	0.994	1.133
1437	0002	45450	1.140	0.350	1.409	1.507	0.768	0.972	0.946	0.929	1.723	1.193
1438	0002	45450	0.198	2.017	1.406	1.505	0.000	0.976	0.999	0.916	0.915	1.137
1439	0002	45450	0.198	0.011	1.405	0.996	0.329	0.976	0.999	0.923	0.923	1.137
1440	0002	45450	0.198	0.041	1.404	1.007	0.859	0.977	0.966	0.921	0.928	1.136
1441	0002	45450	0.198	0.024	1.388	0.990	0.000	0.978	0.999	0.916	0.915	1.149
1442	0002	45450	0.198	0.019	1.388	0.995	0.026	0.978	0.999	0.927	0.927	1.153
1443	0002	45450	0.198	0.019	1.387	1.010	0.059	0.978	0.834	0.929	0.927	1.154
1444	0002	45450	0.198	0.044	1.404	0.990	0.000	0.971	0.999	0.921	0.921	1.153
1445	0002	45450	0.198	0.024	1.404	0.995	0.029	0.969	0.999	0.931	0.931	1.154
1446	0002	45450	0.198	0.041	1.403	1.010	0.059	0.971	0.966	0.932	0.942	1.156
1447	0002	45450	0.198	0.043	1.404	0.992	0.000	0.972	0.999	0.923	0.923	1.155
1448	0002	45450	0.198	0.031	1.403	1.010	0.029	0.971	0.784	0.931	0.934	1.157
1449	0002	45450	0.198	0.042	1.404	1.002	0.059	0.973	0.700	0.934	0.945	1.161
1450	0002	45450	0.198	0.027	1.404	0.994	0.000	0.971	0.999	0.927	0.927	1.157
1451	0002	45450	0.198	0.054	1.417	1.016	0.029	0.972	0.603	0.934	0.939	1.160
1452	0002	45450	0.198	0.044	1.417	1.009	0.059	0.973	0.592	0.936	0.952	1.163
1453	0002	45450	0.198	0.043	1.404	0.989	0.000	0.971	0.999	0.923	0.923	1.155
1454	0002	45450	0.198	0.044	1.403	1.006	0.059	0.969	0.840	0.934	0.944	1.157
1455	0002	45450	1.140	0.022	1.405	1.106	0.723	0.975	0.896	0.929	1.035	1.150
1456	0002	45450	1.140	0.027	1.404	1.506	0.529	0.977	0.980	0.933	1.432	1.189
1457	0002	45450	1.140	0.031	1.441	1.507	0.744	0.977	0.994	0.933	1.828	1.198
1458	0002	45450	1.140	0.044	1.444	2.007	0.528	0.976	0.995	0.938	2.205	1.201
1459	0002	45450	1.140	0.059	1.447	2.502	0.114	0.976	0.996	0.932	2.569	1.197
1460	0002	45450	1.140	0.063	1.446	3.008	0.104	0.975	0.997	0.953	3.020	1.216
1461	0002	45450	1.140	0.034	1.445	1.117	0.159	0.957	0.925	0.925	0.996	1.153
1462	0002	45450	1.140	0.040	1.446	1.506	0.177	0.966	0.965	0.938	1.215	1.193
1463	0002	45450	1.140	0.044	1.444	2.004	0.438	0.970	0.994	0.933	1.438	1.201
1464	0002	45450	1.140	0.052	1.443	2.499	0.170	0.973	0.996	0.937	1.649	1.203
1465	0002	45450	1.140	0.052	1.442	3.001	0.105	0.969	0.993	0.936	1.851	1.201
1466	0002	45450	1.140	0.054	1.444	3.499	0.241	0.970	0.996	0.950	2.111	1.217
1467	0002	45450	1.140	0.051	1.444	1.113	0.129	0.971	0.868	0.938	0.981	1.166
1468	0002	45450	1.140	0.044	1.443	1.508	0.301	0.970	0.966	0.937	1.133	1.199
1469	0002	45450	1.140	0.052	1.442	2.003	0.479	0.971	0.993	0.934	1.289	1.196
1470	0002	45450	1.140	0.056	1.441	2.505	0.536	0.972	0.995	0.937	1.440	1.198
1471	0002	45450	1.140	0.049	1.442	3.000	0.443	0.970	0.995	0.926	1.571	1.189
1472	0002	45450	1.140	0.061	1.441	3.496	0.751	0.971	0.997	0.947	1.760	1.209
1473	0002	45450	1.140	0.053	1.441	1.106	0.094	0.973	0.702	0.937	0.955	1.166

FACILITY .1 PROGRAM CODE

MODEL TYPE — FINAL STAGE
DUAL FLOW (TAN)

PLUG CONFIGURATIONS
BASELINE PLUG WITH BLEED

SUPPRESSOR CONFIGURATION
30-SPOKE, AREA RATIO = 1.75

DRAG PARAMETERS — PIECE RADIUS RATIO 0.0030 — THICK RADIUS RATIO 0.7790 — OVR 1.2480

RPC	GS	NPSS	M2	V2	PTT/PS	PT1/P4	OVERAT	CDS	CDS	DCDSM	CDSM	DCPL,0	DCPL,1	DCTOT	PSUP/PA
1448	0002	45550	1.140	0.358	3.295	1.118	0.054	-0.041	0.466	-0.007	0.057	-0.024	0.005	-0.096	0.756
1450	0002	45550	1.140	0.358	3.292	1.112	0.052	-0.039	0.459	-0.007	0.053	-0.024	0.005	-0.094	0.769
1451	0002	45550	1.140	0.358	3.264	1.511	0.208	-0.042	0.448	-0.004	0.050	-0.016	-0.009	-0.092	0.775
1452	0002	45550	1.140	0.358	3.232	3.212	0.326	-0.046	0.443	-0.005	0.048	-0.013	-0.017	-0.081	0.776
1453	0002	45550	1.140	0.358	3.281	2.514	0.408	-0.043	0.443	-0.005	0.047	-0.012	-0.027	-0.086	0.777
1454	0002	45550	1.140	0.358	3.293	3.293	0.480	-0.044	0.439	-0.004	0.049	-0.010	-0.028	-0.092	0.779
1455	0002	45550	1.140	0.358	3.264	3.507	0.572	-0.037	0.438	-0.004	0.046	-0.008	-0.020	-0.069	0.778
1456	0002	45550	1.140	0.357	2.487	1.114	0.105	-0.038	0.472	-0.000	0.049	-0.001	0.004	-0.093	0.788
1457	0002	45550	1.140	0.358	2.520	3.501	0.348	-0.039	0.371	-0.005	0.046	0.004	-0.011	-0.051	0.813
1458	0002	45550	0.338	0.012	1.454	3.385	0.000	-0.054	121.079	-0.001	2.445	-0.016	0.010	-0.071	0.934
1459	0002	45550	0.334	0.013	1.443	0.295	0.029	-0.041	93.511	-0.001	1.931	-0.014	0.008	-0.068	0.937
1460	0002	45550	0.331	2.042	1.479	1.387	0.056	-0.060	459.634	-0.001	11.311	-0.012	0.005	-0.068	0.938
1461	0002	45550	0.334	0.025	1.484	0.979	0.000	-0.050	45.174	-0.001	0.722	-0.016	0.010	-0.067	0.890
1462	0002	45550	2.334	2.234	1.924	0.395	0.029	-0.047	20.658	-0.001	0.293	-0.013	0.007	-0.064	0.895
1463	0002	45550	0.343	0.039	1.994	1.014	0.059	-0.045	14.717	-0.001	0.253	-0.011	0.005	-0.062	0.899
1464	0002	45550	2.334	2.053	2.542	0.877	0.029	-0.047	20.147	-0.001	0.223	-0.011	0.009	-0.059	0.853
1465	0002	45550	2.343	2.044	2.498	2.454	0.079	-0.045	14.914	-0.001	0.246	-0.009	0.007	-0.057	0.857
1466	0002	45550	0.334	2.041	2.490	1.224	0.059	-0.051	21.554	-0.001	0.299	-0.006	0.004	-0.056	0.861
1467	0002	45550	2.334	0.051	2.494	0.972	0.000	-0.041	14.594	-0.001	0.168	-0.028	0.009	-0.071	0.828
1468	0002	45550	2.343	2.051	1.802	1.210	0.029	-0.053	14.486	-0.001	0.203	-0.025	0.007	-0.069	0.830
1469	0002	45550	0.334	0.052	2.496	1.059	0.059	-0.049	15.691	-0.001	0.193	-0.022	0.004	-0.067	0.833
1470	0002	45550	2.334	0.047	3.284	2.934	0.000	-0.045	12.174	-0.001	0.169	-0.029	0.008	-0.061	0.847
1471	0002	45550	0.334	0.055	3.277	1.335	0.029	-0.038	12.762	-0.001	0.185	-0.026	0.006	-0.060	0.848
1472	0002	45550	0.338	0.054	1.220	1.284	0.149	-0.044	12.151	-0.001	0.177	-0.024	0.004	-0.059	0.849
1473	0002	45550	0.343	0.041	2.491	3.965	0.000	-0.047	22.222	-0.001	0.204	-0.011	0.010	-0.058	0.853
1474	0002	45550	0.338	0.044	2.507	1.335	0.059	-0.044	15.093	-0.001	0.162	-0.006	0.005	-0.054	0.861
147	0002	45550	1.140	0.022	1.469	1.107	0.721	-0.043	29.156	-0.001	0.443	-0.008	0.003	-0.055	0.943
1476	0002	45550	1.140	0.027	1.493	1.504	0.529	-0.035	18.630	-0.001	0.455	-0.005	0.001	-0.040	0.945
1477	0002	45550	1.140	0.031	1.491	1.497	0.734	-0.037	15.041	-0.001	0.374	-0.004	-0.019	-0.051	0.944
1478	0002	45550	1.140	0.026	1.494	2.497	0.528	-0.035	6.496	-0.000	0.111	-0.003	-0.017	-0.043	0.945
1479	0002	45550	1.140	0.050	1.497	1.202	1.116	-0.045	5.333	-0.000	0.078	-0.002	-0.030	-0.051	0.947
1480	0002	45550	1.140	0.035	1.494	1.500	1.305	-0.039	6.552	-0.000	0.094	-0.001	-0.005	-0.022	0.948
1481	0002	45550	1.140	0.034	1.500	1.111	0.149	-0.049	21.129	-0.001	0.339	-0.008	0.002	-0.056	0.934
1482	0002	45550	1.140	0.060	1.494	1.504	0.377	-0.034	14.487	-0.001	0.258	-0.006	-0.001	-0.046	0.909
1483	0002	45550	1.140	0.064	1.488	2.305	0.558	-0.037	11.398	-0.001	0.197	-0.005	-0.020	-0.058	0.909
1484	0002	45550	1.140	0.052	1.493	2.438	0.470	-0.037	8.304	-0.000	0.128	-0.004	-0.017	-0.049	0.911
1485	0002	45550	1.140	0.042	1.492	3.491	0.605	-0.024	8.120	-0.000	0.167	-0.003	-0.029	-0.057	0.913
1486	0002	45550	1.140	0.056	1.488	3.493	0.941	-0.029	7.135	-0.000	0.172	-0.002	-0.008	-0.032	0.917
1487	0002	45550	1.140	0.041	2.494	1.113	0.128	-0.040	12.996	-0.000	0.124	-0.003	0.002	-0.050	0.867
1488	0002	45550	1.140	0.044	2.490	1.504	0.301	-0.046	14.973	-0.001	0.217	-0.002	-0.001	-0.044	0.873
1489	0002	45550	1.140	0.057	2.487	2.503	0.429	-0.034	12.053	-0.001	0.169	-0.001	-0.016	-0.053	0.874
1490	0002	45550	1.140	0.054	2.491	2.505	0.536	-0.035	10.468	-0.000	0.155	-0.001	-0.019	-0.052	0.873
1491	0002	45550	1.140	0.054	2.497	3.000	0.643	-0.035	9.289	-0.001	0.171	-0.001	-0.030	-0.058	0.878
1492	0002	45550	1.140	0.041	2.491	3.496	0.751	-0.024	7.819	-0.000	0.159	0.000	-0.015	-0.039	0.885
1493	0002	45550	1.140	0.043	2.491	1.106	0.096	-0.047	14.632	-0.001	0.184	-0.019	0.002	-0.065	0.836

FACILITY ...ASI WINDOW COST

NOZZLE TYPE — DUAL FLOW (SEAS)

FAN-STREAM PLUG CONFIGURATIONS — BASELINE PLUG WITH BLEED

SUPPRESSOR CONFIGURATION — 20-SPOKE, AREA RATIO = 1.75

INPUT PARAMETERS — INNER RADIUS RATIO 0.0032 — OUTER RADIUS RATIO 0.7790 — OVD 1.2680

PRES	FR	MASS	M2	MA	PT2/P0	PT1/PA	OMEGAT	CPO	CPI	CFNET1	CFNET2	F9
1494	0002	45550	1.140	0.054	2.959	1.504	0.747	0.972	0.992	0.937	1.086	1.188
1495	0002	45550	1.140	0.047	2.985	1.507	0.356	0.972	0.993	0.934	1.206	1.194
1496	0002	45550	1.140	0.042	2.992	2.503	0.446	0.972	0.995	0.928	1.312	1.188
1497	0002	45550	1.140	0.061	2.996	3.006	0.535	0.972	0.995	0.922	1.415	1.183
1498	0002	45550	1.140	0.067	3.003	3.507	0.624	0.972	0.996	0.940	1.559	1.201
1499	0002	45550	1.140	0.056	3.250	1.111	0.073	0.971	0.646	0.939	0.940	1.164
1500	0002	45550	1.140	0.047	3.305	1.504	0.216	0.973	0.925	0.940	1.065	1.189
1501	0002	45550	1.140	0.044	3.310	1.507	0.310	0.972	0.991	0.933	1.169	1.193
1502	0002	45550	1.140	0.038	3.309	2.503	0.402	0.972	0.995	0.928	1.261	1.187
1503	0002	45550	1.140	0.042	3.295	3.006	0.486	0.972	0.995	0.923	1.357	1.184
1504	0002	45550	1.140	0.045	3.298	3.507	0.564	0.973	0.996	0.938	1.480	1.200
1505	0002	45550	1.140	0.050	3.497	1.114	0.128	0.972	0.857	0.941	0.985	1.169
1506	0002	45550	1.140	0.059	3.497	1.498	0.751	0.973	0.997	0.949	1.766	1.213

FACILITY D... WINDOW COST

NOZZLE TYPE — DUAL FLOW (SEAS)

FAN-STREAM PLUG CONFIGURATIONS — BASELINE PLUG WITH BLEED

SUPPRESSOR CONFIGURATION — 20-SPOKE, AREA RATIO = 1.75

INPUT PARAMETERS — INNER RADIUS RATIO 0.0032 — OUTER RADIUS RATIO 0.7790 — OVD 1.2680

PRES	FR	MASS	M2	MA	PT2/P0	PT1/PA	OMEGAT	DCS	CDS	DCSH	CDSH	DCPL,O	DCPL,I	DCTOT	PSUP/PA
1494	0002	45550	1.140	0.055	2.949	1.504	0.747	-0.034	12.956	-0.001	0.179	-0.015	-0.001	-0.055	0.844
1495	0002	45550	1.140	0.047	2.985	1.507	0.356	-0.015	12.114	-0.001	0.191	-0.013	-0.015	-0.063	0.847
1496	0002	45550	1.140	0.042	2.992	2.503	0.446	-0.022	11.845	-0.001	0.194	-0.012	-0.020	-0.064	0.847
1497	0002	45550	1.140	0.061	2.996	3.006	0.535	-0.026	9.651	-0.000	0.160	-0.010	-0.027	-0.065	0.851
1498	0002	45550	1.140	0.067	3.003	3.507	0.624	-0.025	9.490	-0.000	0.183	-0.008	-0.018	-0.052	0.858
1499	0002	45550	1.140	0.056	3.250	1.111	0.073	-0.030	12.613	-0.001	0.192	-0.023	0.003	-0.059	0.848
1500	0002	45550	1.140	0.047	3.305	1.504	0.216	-0.014	11.595	-0.001	0.195	-0.018	-0.006	-0.058	0.852
1501	0002	45550	1.140	0.044	3.310	1.507	0.310	-0.020	10.748	-0.001	0.183	-0.016	-0.014	-0.062	0.854
1502	0002	45550	1.140	0.038	3.309	2.503	0.402	-0.026	10.296	-0.001	0.194	-0.015	-0.021	-0.064	0.852
1503	0002	45550	1.140	0.042	3.295	3.006	0.486	-0.026	9.597	-0.000	0.180	-0.013	-0.024	-0.063	0.853
1504	0002	45550	1.140	0.045	3.298	3.507	0.564	-0.023	8.791	-0.000	0.174	-0.011	-0.019	-0.055	0.857
1505	0002	45550	1.140	0.050	3.497	1.114	0.128	-0.049	13.630	-0.001	0.158	-0.003	0.003	-0.049	0.866
1506	0002	45550	1.140	0.059	3.497	1.498	0.751	-0.024	8.509	-0.000	0.156	-0.000	-0.011	-0.035	0.885

MODEL SC-3, 30 SHALLOW CHUTES, AR = 1.75, REDUCED AREA

FACILITY # PROGRAM CODE NOZZLE TYPE INLET FLOW CONFIGURATIONS SUPPRESSOR CONFIGURATION

DUAL FLOW (FAA) 1/2 BLEED AREA WITH BLEED 30-SPOKE, AREA RATIO = 1.75

THRUST PARAMETERS OUTER RADIUS RATIO 0.9000 INNER RADIUS RATIO 0.7490 OVD 1.2680

ARC	CF	MACH	P2	M2	P2/P0	P2/P0	DPOPAT	CDP	CDI	CFNET1	CFNET2	FG
1957	0003	45T30	0.398	0.447	1.592	1.001	0.000	0.999	0.000	0.851	0.851	1.127
1958	0003	45T30	0.398	0.448	1.586	1.022	0.029	0.995	0.406	0.856	0.860	1.127
1959	0003	45T30	0.398	0.448	1.585	1.047	0.059	0.995	0.688	0.862	0.879	1.132
1960	0003	45T30	0.398	0.448	2.006	1.002	0.000	0.970	0.000	0.867	0.867	1.125
1961	0003	45T30	0.398	0.448	2.010	1.027	0.029	0.970	0.520	0.875	0.881	1.130
1962	0003	45T30	0.398	0.448	2.007	1.056	0.059	0.971	0.699	0.879	0.898	1.135
1963	0003	45T30	0.398	0.448	2.011	0.990	0.000	0.971	0.999	0.878	0.878	1.127
1964	0003	45T30	0.398	0.448	2.017	1.046	0.029	0.970	0.585	0.887	0.893	1.131
1965	0003	45T30	0.398	0.447	2.027	1.114	0.059	0.970	0.751	0.850	0.909	1.135
1966	0003	45T30	0.398	0.448	2.014	1.005	0.000	0.973	0.000	0.891	0.891	1.134
1967	0003	45T30	0.398	0.447	2.021	1.082	0.029	0.971	0.524	0.896	0.904	1.136
1968	0003	45T30	0.398	0.447	2.027	1.177	0.059	0.971	0.725	0.898	0.920	1.140
1969	0003	45T30	0.398	0.448	2.019	1.003	0.000	0.971	0.000	0.901	0.901	1.139
1970	0003	45T30	0.398	0.448	2.024	1.123	0.029	0.971	0.472	0.906	0.915	1.144
1971	0003	45T30	0.398	0.448	2.027	1.254	0.059	0.972	0.695	0.909	0.932	1.149
1972	0003	45T30	0.398	0.447	2.424	0.999	0.000	0.969	0.999	0.878	0.878	1.125
1973	0003	45T30	0.398	0.448	2.431	1.115	0.029	0.972	0.752	0.893	0.912	1.139
1974	0003	45T50	1.140	0.446	1.594	1.003	0.000	0.957	0.000	0.850	0.850	1.123
1975	0003	45T50	1.140	0.447	1.597	1.003	0.000	0.995	0.000	0.853	0.853	1.127
1976	0003	45T50	1.140	0.446	1.594	1.119	0.125	0.995	0.916X	0.871	0.930	1.143
1977	0003	45T50	1.140	0.446	1.591	1.227	0.281	0.995	0.993	0.893	1.134	1.168
1978	0003	45T50	1.140	0.446	1.591	2.016	0.000	0.996	1.002	0.897	1.332	1.173
1979	0003	45T50	1.140	0.446	1.595	2.522	0.488	0.994	1.002	0.895	1.529	1.176
1980	0003	45T50	1.140	0.446	1.595	3.034	0.588	0.994	1.002	0.890	1.712	1.172
1981	0003	45T50	1.140	0.447	1.594	3.536	0.688	0.994	1.004	0.910	1.945	1.187
1982	0003	45T50	1.140	0.446	2.002	1.126	0.093	0.970	0.801X	0.885	0.917	1.141
1983	0003	45T50	1.140	0.446	2.007	1.324	0.306	0.970	0.977	0.890	1.034	1.161
1984	0003	45T50	1.140	0.447	2.004	2.024	0.388	0.970	1.000	0.892	1.149	1.166
1985	0003	45T50	1.140	0.446	2.011	2.538	0.488	0.969	1.002	0.895	1.260	1.167
1986	0003	45T50	1.140	0.447	2.009	3.033	0.632	0.970	1.003	0.892	1.365	1.166
1987	0003	45T50	1.140	0.447	2.004	3.535	0.736	0.970	1.003	0.908	1.500	1.179
1988	0003	45T50	1.140	0.448	2.514	1.128	0.366	0.970	0.796X	0.892	0.915	1.138
1989	0003	45T50	1.140	0.448	2.515	1.525	0.161	0.970	0.969	0.897	0.999	1.157
1990	0003	45T50	1.140	0.449	2.521	2.019	0.328	0.954	0.999	0.896	1.077	1.158
1991	0003	45T50	1.140	0.447	2.514	2.523	0.387	0.970	1.002	0.900	1.148	1.162
1992	0003	45T50	1.140	0.448	2.518	3.026	0.545	0.964	1.003	0.897	1.232	1.159
1993	0003	45T50	1.140	0.448	2.525	3.527	0.692	0.965	1.003	0.908	1.324	1.168
1994	0003	45T50	1.141	0.447	1.029	1.124	0.244	0.970	0.648X	0.898	0.912	1.138
1995	0003	45T50	1.140	0.447	1.014	1.523	0.130	0.971	0.942	0.901	0.978	1.155
1996	0003	45T50	1.140	0.448	2.521	2.534	0.400	0.972	1.003	0.910	1.325	1.174
1997	0003	45T50	1.140	0.447	2.027	2.025	0.190	0.970	0.998	0.901	1.042	1.159
1998	0003	45T50	1.140	0.448	2.014	2.525	0.239	0.972	1.002	0.901	1.101	1.161
1999	0003	45T50	1.140	0.448	2.022	3.032	0.287	0.970	1.003	0.899	1.158	1.158
2000	0003	45T50	1.141	0.448	2.015	3.530	0.335	0.974	1.003	0.904	1.225	1.167
2001	0003	45T50	1.140	0.450	2.335	1.125	0.300	0.969	0.000	0.916	0.916	1.143

FACILITY [illegible] PROGRAM CODE

NOZZLE TYPE — DUAL FLOW (FAA)

JET STREAM INTERFERENCE CONFIGURATIONS — 1/2 WING AREA WITH BLEED

SUPPRESSOR CONFIGURATION — 30-SPOKE, AREA RATIO = 1.75

OPER PARAMETERS — OUTER RADIUS RATIO 0.8030 — INNER RADIUS RATIO 0.9890 — DVD 1.2480

ACC	OF	MASS	PI2	W%	PI2/P0	PI1/P2	DWFOAT	DCS	DCAS	DCSH	DCSH	DCPL,O	DCPL,I	DCTOT	PSUP/PA
1557	0003	45750	1.140	0.448	1.507	1.001	0.000	-0.114	0.157	-0.030	0.040	-0.014	0.030	-0.130	0.876
1558	0003	45750	1.140	0.444	1.505	1.377	0.024	-0.110	0.151	-0.029	0.039	-0.011	0.026	-0.123	0.881
1559	0003	45750	1.140	0.444	1.504	1.347	0.054	-0.106	0.146	-0.027	0.038	-0.008	0.024	-0.118	0.885
1560	0003	45750	1.140	0.444	2.005	1.102	0.000	-0.105	0.247	-0.020	0.047	-0.011	0.023	-0.113	0.895
1561	0003	45750	1.140	0.444	2.010	1.317	0.029	-0.101	0.240	-0.019	0.046	-0.008	0.019	-0.109	0.811
1562	0003	45750	1.140	0.448	2.007	1.094	0.059	-0.096	0.232	-0.019	0.045	-0.006	0.017	-0.103	0.817
1563	0003	45750	1.140	0.448	2.011	0.000	0.000	-0.046	0.317	-0.014	0.048	-0.009	0.019	-0.099	0.750
1564	0003	45750	1.140	0.448	2.517	1.064	0.025	-0.041	0.307	-0.014	0.048	-0.005	0.016	-0.094	0.758
1565	0003	45750	1.140	0.447	2.520	1.116	0.050	-0.038	0.300	-0.014	0.047	-0.002	0.014	-0.090	0.764
1566	0003	45750	1.140	0.449	3.018	1.105	0.000	-0.041	0.350	-0.011	0.049	-0.029	0.029	-0.101	0.723
1567	0003	45750	1.140	0.447	3.024	1.089	0.029	-0.040	0.340	-0.011	0.049	-0.026	0.026	-0.099	0.725
1568	0003	45750	1.140	0.447	3.027	1.177	0.059	-0.037	0.344	-0.011	0.047	-0.021	0.013	-0.096	0.728
1569	0003	45750	1.140	0.449	3.515	1.093	0.000	-0.044	0.375	-0.010	0.049	-0.028	0.020	-0.084	0.742
1570	0003	45750	1.140	0.448	3.524	1.173	0.029	-0.035	0.363	-0.010	0.048	-0.024	0.016	-0.083	0.745
1571	0003	45750	1.140	0.448	3.527	1.256	0.059	-0.031	0.371	-0.009	0.047	-0.021	0.012	-0.082	0.747
1572	0003	45750	1.140	0.447	3.524	0.000	0.000	-0.045	0.422	-0.014	0.048	-0.009	0.021	-0.098	0.748
1573	0003	45750	1.140	0.448	3.511	1.119	0.059	-0.037	0.400	-0.013	0.046	-0.007	0.014	-0.089	0.765
1574	0003	45750	1.140	0.445	3.498	1.201	0.088	-0.027	0.371	-0.028	0.041	-0.014	0.030	-0.129	0.866
1575	0003	45750	1.140	0.447	3.507	1.004	0.000	-0.114	0.158	-0.029	0.040	-0.014	0.030	-0.129	0.876
1576	0003	45750	1.140	0.444	1.504	1.119	0.125	-0.097	0.142	-0.026	0.038	-0.006	0.026	-0.105	0.899
1577	0003	45750	1.140	0.444	1.501	1.572	0.281	-0.081	0.141	-0.021	0.037	-0.005	0.032	-0.074	0.889
1578	0003	45750	1.140	0.444	1.501	2.316	0.700	-0.029	0.161	-0.038	0.038	-0.004	0.039	-0.052	0.889
1579	0003	45750	1.140	0.444	1.504	2.532	0.488	-0.041	0.147	-0.014	0.037	-0.003	0.027	-0.053	0.889
1580	0003	45750	1.140	0.444	1.505	1.716	0.584	-0.045	0.139	-0.014	0.037	-0.002	0.044	-0.026	0.891
1581	0003	45750	1.140	0.447	1.504	3.536	0.686	-0.017	0.138	-0.013	0.037	-0.002	0.121	0.059	0.892
1582	0003	45750	1.140	0.444	2.002	1.124	0.093	-0.083	0.227	-0.018	0.044	-0.004	0.017	-0.098	0.822
1583	0003	45750	1.140	0.446	2.007	1.572	0.704	-0.071	0.226	-0.016	0.043	-0.002	0.023	-0.076	0.825
1584	0003	45750	1.140	0.447	2.008	2.324	0.288	-0.077	0.221	-0.014	0.042	-0.002	0.027	-0.061	0.826
1585	0003	45750	1.140	0.444	2.011	2.928	0.360	-0.070	0.221	-0.013	0.044	-0.001	0.022	-0.059	0.827
1586	0003	45750	1.140	0.447	2.008	3.011	0.432	-0.060	0.216	-0.012	0.043	-0.000	0.027	-0.044	0.831
1587	0003	45750	1.140	0.447	2.008	3.515	0.504	-0.055	0.216	-0.011	0.043	-0.000	0.040	0.013	0.831
1588	0003	45750	1.140	0.448	2.514	1.124	0.066	-0.097	0.297	-0.014	0.046	-0.002	0.013	-0.089	0.766
1589	0003	45750	1.140	0.448	2.516	1.525	0.181	-0.077	0.287	-0.012	0.045	0.001	0.018	-0.070	0.774
1590	0003	45750	1.140	0.447	2.526	2.019	0.228	-0.070	0.281	-0.011	0.044	0.001	0.015	-0.065	0.778
1591	0003	45750	1.140	0.447	2.514	2.525	0.287	-0.065	0.276	-0.010	0.045	0.002	0.027	-0.052	0.779
1592	0003	45750	1.140	0.448	2.518	3.014	0.345	-0.059	0.274	-0.010	0.044	0.003	0.026	-0.043	0.784
1593	0003	45750	1.140	0.448	2.525	3.517	0.402	-0.056	0.272	-0.009	0.044	0.003	0.049	-0.013	0.785
1594	0003	45750	1.140	0.447	3.029	1.125	0.046	-0.098	0.347	-0.011	0.048	-0.022	0.013	-0.098	0.727
1595	0003	45750	1.140	0.447	3.016	1.523	0.110	-0.077	0.339	-0.010	0.046	-0.015	0.015	-0.092	0.733
1596	0003	45750	1.140	0.448	3.524	1.594	0.400	-0.057	0.278	-0.009	0.045	0.003	0.009	-0.054	0.780
1597	0003	45750	1.140	0.447	3.027	2.325	0.190	-0.067	0.336	-0.009	0.046	-0.013	0.006	-0.083	0.735
1598	0003	45750	1.140	0.448	3.014	2.525	0.239	-0.063	0.334	-0.009	0.045	-0.011	0.000	-0.082	0.737
1599	0003	45750	1.140	0.448	3.022	3.332	0.287	-0.059	0.331	-0.008	0.045	-0.009	-0.001	-0.078	0.739
1600	0003	45750	1.140	0.449	3.010	3.534	0.335	-0.056	0.328	-0.008	0.044	-0.007	0.007	-0.064	0.740
1601	0003	45750	1.140	0.450	3.336	1.125	0.000	-0.015	0.321	-0.010	0.047	-0.025	0.016	-0.083	0.744

FACILITY SL PROGRAM CODE IN -STREAM

NOZZLE TYPE: DUAL FLOW ISOLATOR PLUG CONFIGURATIONS: 1/2 BLEED AREA WITH BLEED SUPPRESSOR CONFIGURATION: 30-SPOKE, AREA RATIO = 1.75

THRUST PARAMETERS OUTER RADIUS RATIO: 0.0000 INNER RADIUS RATIO: 0.8490 DVD: 1.2680

ERC	CF	MACH	M2	M8	PT2/P2	PT8/P8	CVFACT	CDD	CDI	CFNET1	CFNET2	FD
1402	0003	45730	1.140	0.445	3.319	1.923	0.113	0.978	0.901	0.909	0.973	1.158
1403	0003	45730	1.140	0.446	3.327	2.019	0.177	0.972	0.905	0.905	1.029	1.163
1404	0003	45730	1.142	0.445	3.324	2.523	0.216	0.971	1.001	0.904	1.079	1.167
1405	0003	45730	1.140	0.446	3.323	3.009	0.241	0.971	1.003	0.905	1.133	1.163
1406	0003	45730	1.140	0.446	3.322	3.581	0.304	0.971	1.004	0.903	1.183	1.163
1407	0003	45730	1.140	0.446	3.321	1.121	0.000	0.971	0.000	0.917	0.917	1.145
1408	0003	45730	1.140	0.446	3.319	1.122	0.043	0.970	0.780X	0.894	0.915	1.140
1409	0003	45730	1.140	0.447	3.322	2.403	0.403	0.974	1.002	0.911	1.337	1.176
1410	0003	45730	0.398	0.356	1.503	1.120	0.000	0.971	0.000	0.940	0.940	1.147
1411	0003	45730	0.398	0.357	1.503	1.119	0.029	0.971	0.211	0.926	0.940	1.147
1412	0003	45730	0.398	0.357	1.504	1.122	0.059	0.971	0.425	0.914	0.940	1.148
1413	0003	45730	0.398	0.357	1.503	1.121	0.000	0.972	0.000	0.923	0.923	1.148
1414	0003	45730	0.398	0.357	1.503	1.120	0.029	0.971	0.209	0.912	0.923	1.148
1415	0003	45730	0.398	0.356	1.503	1.119	0.059	0.969	0.426	0.901	0.924	1.146
1416	0003	45730	0.398	0.356	1.503	1.120	0.000	0.971	0.000	0.921	0.921	1.145
1417	0003	45730	0.398	0.356	1.503	1.120	0.029	0.971	0.209	0.911	0.921	1.142
1418	0003	45730	0.398	0.356	1.503	1.119	0.059	0.969	0.427	0.904	0.925	1.144
1419	0003	45730	0.398	0.356	1.503	1.120	0.000	0.971	0.000	0.920	0.920	1.146
1420	0003	45730	0.398	0.356	1.503	1.121	0.029	0.971	0.428	0.912	0.922	1.147
1421	0003	45730	0.398	0.356	1.503	1.120	0.059	0.969	0.741	0.908	0.929	1.147
1422	0003	45730	0.398	0.356	1.503	1.120	0.000	0.972	0.000	0.922	0.922	1.150
1423	0003	45730	0.398	0.356	1.504	1.122	0.029	0.971	0.449	0.916	0.925	1.151
1424	0003	45730	0.398	0.356	1.503	1.124	0.059	0.970	0.700	0.914	0.938	1.153
1425	0003	45730	0.398	0.356	1.503	1.121	0.000	0.970	0.000	0.923	0.923	1.146
1426	0003	45730	0.398	0.356	1.503	1.120	0.029	0.971	0.700	0.913	0.933	1.151
1427	0003	45730	1.140	0.356	1.503	1.121	0.122	0.971	0.880	0.893	0.941	1.147
1428	0003	45730	1.142	0.356	1.503	1.123	0.243	0.969	0.996	0.891	1.147	1.172
1429	0003	45730	0.398	0.356	1.503	1.120	0.029	0.971	0.175	0.909	0.909	1.145
1430	0003	45730	0.398	0.356	1.503	1.120	0.029	0.969	0.210	0.898	0.906	1.139
1431	0003	45730	0.398	0.356	1.504	1.121	0.029	0.969	0.209	0.897	0.887	1.133
1432	0003	45730	0.398	0.356	1.503	1.119	0.059	0.969	0.763	0.900	0.910	1.144
1433	0003	45730	0.398	0.356	1.504	1.000	0.000	0.971	0.000	0.861	0.861	1.130
1434	0003	45730	0.398	0.356	1.503	1.001	0.029	0.969	0.503	0.872	0.878	1.135
1435	0003	45730	0.398	0.356	1.503	1.000	0.059	0.967	0.497	0.873	0.890	1.136
1436	0003	45730	0.398	0.356	1.503	1.000	0.000	0.970	0.000	0.880	0.880	1.136
1437	0003	45730	0.398	0.356	1.503	1.001	0.029	0.970	0.501	0.887	0.903	1.138
1438	0003	45730	0.398	0.356	1.503	1.001	0.059	0.969	0.707	0.893	0.911	1.143
1439	0003	45730	0.398	0.356	1.503	0.998	0.000	0.969	0.000	0.888	0.888	1.133
1440	0003	45730	0.398	0.356	1.503	1.002	0.029	0.966	0.606	0.895	0.901	1.135
1441	0003	45730	0.398	0.356	1.503	1.109	0.059	0.969	0.765	0.902	0.921	1.145
1442	0003	45730	0.398	0.356	1.503	0.998	0.000	0.972	0.000	0.898	0.898	1.141
1443	0003	45730	0.398	0.356	1.503	1.002	0.029	0.971	0.555	0.907	0.914	1.146
1444	0003	45730	0.398	0.356	1.503	1.109	0.059	0.971	0.742	0.908	0.930	1.150
1445	0003	45730	0.398	0.356	1.503	1.000	0.000	0.971	0.000	0.907	0.907	1.146
1446	0003	45730	0.398	0.356	1.503	1.112	0.029	0.971	0.484	0.912	0.921	1.149

FACILITY P 1 PROGRAM CODE

NOZZLE TYPE — PLUG — CONFIGURATIONS — SUPPRESSOR CONFIGURATION
CONE FROM START — 1/2 BLEED AREA WITH BLEED — 30-SPOKE, AREA RATIO = 1.75

OUTER RADIUS RATIO 0.0000 — INNER RADIUS RATIO 0.8890 — DVO 1.2480

RUN	CONF	MACH	PT	PS	PT/PA	PT/PA	SPECAT	DCS	CDS	DCSH	CDSH	DCPL,O	DCPL,I	DCTOT	PSUP/PA
1402	0001	45750	1.140	0.449	3.319	1.421	0.113	-0.063	0.316	-0.002	0.046	-0.018	0.009	-0.077	0.749
1403	0001	45750	1.140	0.449	3.322	2.019	0.172	-0.058	0.315	-0.008	0.045	-0.016	-0.002	-0.082	0.751
1404	0001	45750	1.140	0.448	3.328	2.427	0.214	-0.053	0.314	-0.008	0.045	-0.015	-0.002	-0.077	0.752
1405	0001	45750	1.140	0.448	3.320	1.075	0.781	-0.051	0.314	-0.337	0.046	-0.014	-0.004	-0.075	0.752
1406	0001	45750	1.140	0.448	3.322	1.433	0.304	-0.048	0.313	-0.007	0.044	-0.012	-0.009	-0.077	0.753
1407	0001	45750	1.140	0.448	3.331	1.121	0.080	-0.055	0.325	-0.010	0.048	-0.025	0.016	-0.084	0.745
1408	0001	45750	1.140	0.448	3.319	1.173	0.099	-0.087	0.330	-3.014	0.047	-0.002	0.016	-0.087	0.765
1409	0001	45750	1.140	0.447	3.459	1.592	0.603	-0.047	0.276	-0.009	0.044	0.003	0.003	-0.060	0.783
[illegible]															
1411	0001	45750	0.198	0.351	1.501	1.119	0.039	-0.024	0.271	-0.018	0.039	-0.005	0.022	-0.095	0.899
1412	0001	45750	0.198	0.349	1.504	1.122	0.059	-0.027	0.281	-0.017	0.038	-0.004	0.021	-0.092	0.899
1413	0001	45750	0.198	0.352	1.518	1.121	0.080	-0.087	0.322	-0.013	0.048	-0.006	0.015	-0.088	0.838
1414	0001	45750	0.198	0.352	1.509	1.120	0.099	-0.085	0.325	-0.013	0.047	-0.004	0.014	-0.089	0.837
1419	0001	45750	0.198	0.348	1.506	1.124	0.059	-0.085	0.322	-0.013	0.047	-0.004	0.015	-0.087	0.838
1416	0001	45750	0.198	0.350	1.520	1.120	0.080	-0.080	0.417	-0.009	0.049	-0.001	0.011	-0.079	0.789
1417	0001	45750	0.198	0.348	1.523	1.120	0.099	-0.086	0.424	-0.009	0.050	-0.001	0.012	-0.079	0.786
1418	0001	45750	0.198	0.350	1.524	1.121	0.059	-0.073	0.419	-0.009	0.050	-0.001	0.012	-0.077	0.788
1419	0001	45750	0.198	0.350	1.505	1.123	0.080	-0.077	0.486	-0.008	0.052	-0.020	0.011	-0.090	0.754
1420	0001	45750	0.198	0.349	1.521	1.122	0.099	-0.071	0.485	-0.008	0.052	-0.020	0.011	-0.087	0.756
1421	0001	45750	0.198	0.348	1.527	1.149	0.059	-0.070	0.492	-0.007	0.051	-0.019	0.011	-0.086	0.755
1422	0001	45750	0.198	0.349	1.247	1.120	0.080	-0.061	0.460	-0.007	0.050	-0.024	0.013	-0.079	0.767
1423	0001	45750	0.198	0.348	1.528	1.152	0.099	-0.060	0.457	-0.007	0.052	-0.023	0.012	-0.078	0.768
1424	0001	45750	0.198	0.350	1.525	1.124	0.059	-0.059	0.455	-0.007	0.052	-0.021	0.010	-0.076	0.769
1425	0001	45750	0.198	0.350	1.520	1.121	0.080	-0.081	0.493	-0.009	0.049	-0.001	0.014	-0.078	0.786
[illegible]															
1427	0001	45750	1.140	0.358	1.505	1.121	0.122	-0.090	0.202	-0.017	0.039	-0.005	0.023	-0.089	0.898
1428	0001	45750	1.140	0.352	1.502	1.523	0.283	-0.076	0.198	-0.015	0.040	-0.003	0.023	-0.089	0.900
[illegible]															
1430	0001	45750	0.198	0.348	2.528	1.047	0.029	-0.087	0.414	-0.010	0.051	-0.006	0.015	-0.081	0.779
1431	0001	45750	0.198	0.350	2.524	0.984	0.080	-0.084	0.491	-0.010	0.052	-0.009	0.018	-0.086	0.771
1432	0001	45750	0.198	0.350	2.522	1.110	0.059	-0.079	0.426	-0.009	0.049	-0.001	0.012	-0.078	0.785
1433	0001	45750	0.198	0.350	1.509	1.007	0.080	-0.104	0.223	-0.020	0.041	-0.012	0.028	-0.108	0.887
1434	0001	45750	0.198	0.350	1.507	1.021	0.099	-0.101	0.212	-0.019	0.041	-0.009	0.024	-0.105	0.893
1435	0001	45750	0.198	0.350	1.502	1.045	0.059	-0.092	0.235	-0.019	0.040	-0.007	0.021	-0.100	0.896
1436	0001	45750	0.198	0.348	2.507	0.998	0.080	-0.093	0.365	-0.014	0.051	-0.011	0.019	-0.099	0.827
1437	0001	45750	0.198	0.350	2.514	1.035	0.099	-0.090	0.374	-0.013	0.048	-0.007	0.018	-0.094	0.831
1438	0001	45750	0.198	0.350	2.513	1.081	0.059	-0.097	0.376	-0.013	0.048	-0.005	0.016	-0.090	0.835
1439	0001	45750	0.198	0.350	2.515	0.984	0.080	-0.086	0.449	-0.010	0.053	-0.008	0.014	-0.089	0.773
1440	0001	45750	0.198	0.350	2.527	1.042	0.099	-0.087	0.433	-0.010	0.051	-0.006	0.016	-0.082	0.781
1441	0001	45750	0.198	0.349	2.517	1.109	0.059	-0.079	0.471	-0.009	0.050	-0.001	0.012	-0.079	0.787
1442	0001	45750	0.198	0.352	1.000	0.994	0.000	-0.074	0.497	-0.008	0.054	-0.026	0.017	-0.091	0.748
1443	0001	45750	0.198	0.350	1.010	1.072	0.099	-0.077	0.489	-0.008	0.054	-0.022	0.013	-0.090	0.753
1444	0001	45750	0.198	0.348	1.025	1.149	0.059	-0.070	0.493	-0.007	0.051	-0.019	0.010	-0.086	0.754
1445	0001	45750	0.198	0.350	1.257	1.020	0.000	-0.062	0.485	-0.007	0.053	-0.028	0.018	-0.079	0.764
1446	0001	45750	0.198	0.350	1.260	1.112	0.029	-0.081	0.450	-0.007	0.052	-0.024	0.013	-0.078	0.766

FACILITY XI PROGRAM CODE IN-STREAM

NOZZLE TYPE PLUG CONFIGURATIONS SUPPRESSOR CONFIGURATION

TEST FLOW LEVEL 1/3 BLEED AREA WITH BLEED 30-SPOKE, AREA RATIO = 1.75

INPUT PARAMETERS OUTER RADIUS RATIO 0.8000 INNER RADIUS RATIO 0.7900 OVR 1.2980

RPC	CF	NASA	M0	M8	PT0/P0	PT1/P0	THRUST	CDO	CDI	CFNETI	CFNET2	FD
1447	0001	45710	0.198	0.828	3.731	1.219	0.959	0.971	0.703	0.915	0.938	1.154
1448	0001	45710	0.198	0.836	3.731	1.219	0.959	0.971	0.703	0.915	0.938	1.154
1449	0001	45710	0.198	0.836	3.731	1.219	0.959	0.971	0.703	0.915	0.938	1.154
1450	0001	45710	0.198	0.836	3.731	1.219	0.959	0.971	0.703	0.915	0.938	1.154
1451	0001	45710	0.198	0.836	3.731	1.219	0.959	0.971	0.703	0.915	0.938	1.154
1452	0001	45710	0.198	0.836	3.731	1.219	0.959	0.971	0.703	0.915	0.938	1.154
1453	0001	45710	0.198	0.836	3.731	1.219	0.959	0.971	0.703	0.915	0.938	1.154
1454	0001	45710	0.198	0.836	3.731	1.219	0.959	0.971	0.703	0.915	0.938	1.154
1455	0001	45710	0.198	0.836	3.731	1.219	0.959	0.971	0.703	0.915	0.938	1.154
1456	0001	45710	0.198	0.836	3.731	1.219	0.959	0.971	0.703	0.915	0.938	1.154
1457	0001	45710	0.198	0.836	3.731	1.219	0.959	0.971	0.703	0.915	0.938	1.154
1458	0001	45710	0.198	0.836	3.731	1.219	0.959	0.971	0.703	0.915	0.938	1.154
1459	0001	45710	0.198	0.836	3.731	1.219	0.959	0.971	0.703	0.915	0.938	1.154
1460	0001	45710	0.198	0.836	3.731	1.219	0.959	0.971	0.703	0.915	0.938	1.154
1461	0001	45710	0.198	0.836	3.731	1.219	0.959	0.971	0.703	0.915	0.938	1.154
1462	0001	45710	0.198	0.836	3.731	1.219	0.959	0.971	0.703	0.915	0.938	1.154
1463	0001	45710	0.198	0.836	3.731	1.219	0.959	0.971	0.703	0.915	0.938	1.154
1464	0001	45710	0.198	0.836	3.731	1.219	0.959	0.971	0.703	0.915	0.938	1.154
1465	0001	45710	0.198	0.836	3.731	1.219	0.959	0.971	0.703	0.915	0.938	1.154
1466	0001	45710	0.198	0.836	3.731	1.219	0.959	0.971	0.703	0.915	0.938	1.154
1467	0001	45710	0.198	0.836	3.731	1.219	0.959	0.971	0.703	0.915	0.938	1.154
1468	0001	45710	0.198	0.836	3.731	1.219	0.959	0.971	0.703	0.915	0.938	1.154
1469	0001	45710	0.198	0.836	3.731	1.219	0.959	0.971	0.703	0.915	0.938	1.154
1470	0001	45710	0.198	0.836	3.731	1.219	0.959	0.971	0.703	0.915	0.938	1.154
1471	0001	45710	0.198	0.836	3.731	1.219	0.959	0.971	0.703	0.915	0.938	1.154
1472	0001	45710	0.198	0.836	3.731	1.219	0.959	0.971	0.703	0.915	0.938	1.154
1473	0001	45710	0.198	0.836	3.731	1.219	0.959	0.971	0.703	0.915	0.938	1.154
1474	0001	45710	0.198	0.836	3.731	1.219	0.959	0.971	0.703	0.915	0.938	1.154
1475	0001	45710	0.198	0.836	3.731	1.219	0.959	0.971	0.703	0.915	0.938	1.154
1476	0001	45710	0.198	0.836	3.731	1.219	0.959	0.971	0.703	0.915	0.938	1.154
1477	0001	45710	0.198	0.836	3.731	1.219	0.959	0.971	0.703	0.915	0.938	1.154
1478	0001	45710	0.198	0.836	3.731	1.219	0.959	0.971	0.703	0.915	0.938	1.154
1479	0001	45710	0.198	0.836	3.731	1.219	0.959	0.971	0.703	0.915	0.938	1.154
1480	0001	45710	0.198	0.836	3.731	1.219	0.959	0.971	0.703	0.915	0.938	1.154
1481	0001	45710	0.198	0.836	3.731	1.219	0.959	0.971	0.703	0.915	0.938	1.154
1482	0001	45710	0.198	0.836	3.731	1.219	0.959	0.971	0.703	0.915	0.938	1.154
1483	0001	45710	0.198	0.836	3.731	1.219	0.959	0.971	0.703	0.915	0.938	1.154
1484	0001	45710	0.198	0.836	3.731	1.219	0.959	0.971	0.703	0.915	0.938	1.154
1485	0001	45710	0.198	0.836	3.731	1.219	0.959	0.971	0.703	0.915	0.938	1.154
1486	0001	45710	0.198	0.836	3.731	1.219	0.959	0.971	0.703	0.915	0.938	1.154
1487	0001	45710	0.198	0.836	3.731	1.219	0.959	0.971	0.703	0.915	0.938	1.154
1488	0001	45710	0.198	0.836	3.731	1.219	0.959	0.971	0.703	0.915	0.938	1.154
1489	0001	45710	0.198	0.836	3.731	1.219	0.959	0.971	0.703	0.915	0.938	1.154
1490	0001	45710	0.198	0.836	3.731	1.219	0.959	0.971	0.703	0.915	0.938	1.154
1491	0001	45710	0.198	0.836	3.731	1.219	0.959	0.971	0.703	0.915	0.938	1.154

FACILITY A BOILER CODE

NOZZLE TYPE: DUAL FLOW THROAT

INLET THROAT BLOCK CONFIGURATIONS: 1/2 BLEED AREA WITH BLEED

SUPPRESSOR CONFIGURATION: 20-SPOKE, AREA RATIO = 1.75

NOZZLE FAMILY RATIO: 0.0000 INNER RADIUS RATIO: 0.3490 OVD: 1.2480

RUN	CONFIG	MACH	ALT	WF	PT/P2	PT/P2	SPECIAL	NPR	FG5	DCSH	CDSH	DCPL.0	DCPL.1	DCTOT	PSUP/PA
1467	0001	45730	0.198	0.169	3.751	1.217	0.056	-0.000	0.454	-1.337	3.052	-0.071	0.010	-0.077	0.767
1468	0001	45730	1.198	0.199	2.474	0.987	0.000	-0.046	0.452	-0.010	0.053	-0.008	0.020	-0.085	0.771
1469	0001	45730	0.398	0.348	2.518	1.110	0.000	-0.079	0.471	-0.010	0.051	-0.002	0.014	-0.077	0.787
1470	0001	45750	1.140	0.198	1.508	1.127	0.171	-0.044	0.703	-0.017	0.039	-0.006	0.024	-0.098	0.898
1471	0001	45750	1.140	0.199	1.485	1.122	0.142	-0.072	0.194	-0.014	0.038	-0.003	0.023	-0.048	0.899
1472	0001	45750	1.140	0.198	1.494	2.011	0.304	-0.041	0.193	-0.013	0.040	-0.003	0.016	-0.062	0.900
1473	0001	45750	1.140	0.359	1.501	2.514	0.491	-0.046	0.198	-0.011	0.039	-0.007	-0.008	-0.076	0.900
1474	0001	45750	1.140	0.348	1.502	1.315	0.962	-0.041	0.194	-0.010	0.040	-0.001	-0.014	-0.073	0.902
1475	0001	45750	1.140	0.359	1.501	1.520	0.684	-0.041	0.191	-0.009	0.040	-0.001	0.041	-0.013	0.902
1476	0001	45750	1.140	0.348	2.017	1.124	0.081	-0.084	0.318	-0.012	0.044	-0.004	0.017	-0.081	0.838
1477	0001	45750	1.140	0.349	2.008	1.499	0.255	-0.071	0.310	-0.011	0.047	-0.002	0.017	-0.069	0.843
1478	0001	45750	1.140	0.358	2.011	2.011	0.248	-0.044	0.312	-0.010	0.044	-0.002	0.011	-0.047	0.843
1479	0001	45750	1.140	0.359	2.014	2.514	0.760	-0.049	0.308	-0.009	0.047	-0.001	-0.007	-0.077	0.844
1480	0001	45750	1.140	0.348	2.017	1.024	0.450	-0.054	0.304	-0.008	0.047	-0.000	-0.013	-0.075	0.846
1481	0001	45750	1.140	0.359	2.015	1.499	0.502	-0.049	0.302	-0.008	0.047	0.000	0.010	-0.038	0.847
1482	0001	45750	1.140	0.348	2.524	1.126	0.044	-0.078	0.420	-0.009	0.050	-0.001	0.015	-0.074	0.797
1483	0001	45750	1.140	0.348	2.526	1.524	0.141	-0.070	0.417	-0.008	0.049	0.001	0.014	-0.064	0.793
1484	0001	45750	1.140	0.347	2.527	2.319	0.210	-0.064	0.400	-0.008	0.048	0.002	0.002	-0.058	0.796
1485	0001	45750	1.140	0.348	2.527	2.530	0.244	-0.063	0.396	-0.007	0.049	0.002	-0.002	-0.066	0.799
1486	0001	45750	1.140	0.348	2.522	1.731	0.444	-0.054	0.390	-0.007	0.048	0.003	-0.010	-0.059	0.892
1487	0001	45750	1.140	0.348	2.523	1.524	0.400	-0.051	0.395	-0.006	0.049	0.003	0.006	-0.052	0.892
1488	0001	45750	1.140	0.348	2.006	1.127	0.046	-0.071	0.442	-0.008	0.051	-0.020	0.014	-0.085	0.754
1489	0001	45750	1.140	0.348	2.008	1.524	0.137	-0.065	0.440	-0.007	0.050	-0.014	0.012	-0.073	0.761
1470	0001	45750	1.140	0.348	2.004	2.334	0.193	-0.060	0.446	-0.006	0.048	-0.011	-0.001	-0.079	0.761
1471	0001	45750	1.140	0.348	2.004	2.537	0.240	-0.059	0.444	-0.006	0.049	-0.010	-0.005	-0.078	0.763
1472	0001	45750	1.140	0.348	2.022	1.731	0.284	-0.051	0.460	-0.005	0.048	-0.008	-0.008	-0.074	0.764
1473	0001	45750	1.140	0.348	2.020	1.513	0.334	-0.045	0.440	-0.005	0.049	-0.007	-0.002	-0.065	0.765
1474	0001	45750	1.140	0.348	2.344	1.125	0.048	-0.057	0.435	-0.237	0.052	-0.024	0.015	-0.073	0.773
1475	0001	45750	1.140	0.348	2.344	1.523	0.115	-0.051	0.440	-0.206	0.051	-0.017	0.007	-0.071	0.772
1476	0001	45750	1.140	0.359	2.345	2.314	0.176	-0.045	0.446	-0.006	0.050	-0.015	-0.006	-0.079	0.773
1477	0001	45750	1.140	0.359	2.347	2.535	0.220	-0.040	0.448	-0.005	0.049	-0.014	-0.005	-0.073	0.774
1478	0001	45750	1.140	0.359	2.348	1.327	0.261	-0.047	0.445	-0.004	0.049	-0.013	-0.010	-0.075	0.774
1479	0001	45750	1.140	0.348	2.345	1.532	0.307	-0.043	0.442	-0.005	0.047	-0.011	-0.014	-0.075	0.774
1480	0001	45750	1.140	0.358	2.523	1.125	0.066	-0.079	0.425	-0.004	0.048	-0.001	0.013	-0.076	0.784
1481	0001	45750	1.140	0.358	2.521	1.525	0.480	-0.041	0.391	-0.006	0.049	0.003	0.001	-0.054	0.802
1482	0001	45730	0.198	0.025	1.501	0.989	0.000	-0.052	27.174	-0.001	0.452	-0.015	0.012	-0.066	0.935
1483	0001	45730	0.198	0.022	1.502	1.001	0.029	-0.041	31.615	-0.001	0.459	-0.012	0.010	-0.064	0.936
1484	0001	45730	0.198	0.016	1.501	1.022	0.054	-0.038	64.810	-0.001	1.175	-0.010	0.008	-0.061	0.938
1485	0001	45730	0.198	0.015	1.498	0.995	0.000	-0.040	31.325	-0.001	0.440	-0.015	0.012	-0.064	0.890
1486	0001	45730	0.198	0.031	2.003	1.007	0.029	-0.041	27.089	-0.001	0.426	-0.012	0.008	-0.062	0.893
1487	0001	45730	0.198	0.021	1.998	1.042	0.054	-0.054	24.634	-0.001	0.425	-0.010	0.006	-0.059	0.899
1488	0001	45730	0.198	0.049	2.509	0.965	0.038	-0.057	15.644	-0.001	0.150	-0.011	0.011	-0.058	0.850
1489	0001	45730	0.198	0.041	2.504	1.335	0.029	-0.055	29.425	-0.001	0.225	-0.007	0.007	-0.056	0.856
1490	0001	45730	0.198	0.041	2.516	1.076	0.054	-0.053	14.729	-0.001	0.205	-0.005	0.006	-0.053	0.858
1491	0001	45730	0.198	0.051	2.998	0.987	0.000	-0.052	17.503	-0.001	0.185	-0.027	0.011	-0.069	0.824

SUPPRESSOR CONFIGURATION
30-SPOKE, AREA RATIO = 1.75

FACILITY KI RECORD COIL

NOZZLE TYPE — 4° CONE
DATA FLOW LEVEL — 1/2 BLEED AREA WITH BLEED — CONFIGURATIONS — SUPPRESSOR CONFIGURATION — 30-SPOKE, AREA RATIO = 1.75

TEST PARAMETERS — DESIGN NOZZLE AREA RATIO 0.4001 — DESIGN NOZZLE PRESSURE RATIO 0.8490 — PVO 1.2480

RUN	CONFIG	MACH	ALT	NPR	FNCORR	FNTRUE	FNRATIO	EFF	FNS	DCSH	CDSH	DCPL,P	DCPL,T	DCTOT	PSUP/PA
1692	0001	45750	2.196	6.057	5.013	4.937	0.978	-0.050	16.163	-0.000	0.158	-0.023	0.007	-0.046	0.829
1693	0001	45750	0.398	2.042	2.018	1.126	0.549	-0.049	16.011	-0.001	0.173	-0.021	0.005	-0.053	0.832
1694	0001	45750	0.398	3.054	3.013	0.990	0.000	-0.019	12.684	-0.001	0.184	-0.029	0.011	-0.056	0.946
1695	0001	45750	0.198	2.044	2.019	1.139	2.679	-0.019	13.289	-0.001	0.193	-0.026	0.008	-0.056	0.946
1696	0001	45750	0.398	3.045	3.008	1.142	0.849	-0.018	12.852	-0.001	0.203	-0.021	0.006	-0.056	0.946
1697	0001	45750	0.398	2.043	2.017	0.781	0.000	-0.017	24.348	-0.001	0.224	-0.011	0.013	-0.056	0.850
1698	0001	45750	2.196	2.044	2.002	1.774	0.000	-0.041	16.314	-0.001	0.233	-0.005	0.004	-0.050	0.840
1699	0001	45750	0.398	0.051	1.006	0.330	0.000	-0.051	17.088	-0.001	0.190	-0.027	0.012	-0.047	0.875
1700	0001	45750	1.140	0.071	1.494	1.170	0.131	-0.054	33.197	-0.001	0.407	-0.000	0.014	-0.049	0.940
1701	0001	45750	1.140	0.071	1.498	1.170	0.290	-0.043	27.102	-0.001	0.580	-0.006	0.013	-0.037	0.942
1702	0001	45750	1.140	0.053	1.500	2.027	0.600	-0.018	12.436	-0.001	0.280	-0.005	0.006	-0.037	0.961
1703	0001	45750	1.140	0.074	1.501	2.515	0.488	-0.032	19.049	-0.001	0.426	-0.004	-0.026	-0.043	0.942
1704	0001	45750	1.140	0.053	1.501	3.010	0.368	-0.028	8.845	-0.000	0.153	-0.003	-0.020	-0.060	0.9
1705	0001	45750	1.140	0.042	1.502	3.427	0.298	-0.025	8.385	-0.001	0.179	-0.003	0.025	-0.006	0.944
1706	0001	45750	1.140	2.029	1.441	1.180	0.098	-0.057	31.352	-0.001	0.538	-0.000	0.011	-0.051	0.900
1707	0001	45750	1.140	0.035	2.000	1.522	0.707	-0.045	14.355	-0.001	0.237	-0.007	0.011	-0.042	0.903
1708	0001	45750	1.140	0.052	2.004	2.030	0.488	-0.040	14.124	-0.001	0.303	-0.006	0.005	-0.042	0.904
1709	0001	45750	1.140	0.041	2.003	2.493	0.361	-0.033	9.561	-0.000	0.108	-0.005	-0.015	-0.057	0.904
1710	0001	45750	1.140	0.041	2.006	3.022	0.293	-0.030	17.281	-0.000	0.177	-0.006	-0.019	-0.056	0.908
1711	0001	45750	1.140	0.040	2.004	3.421	0.304	-0.030	9.196	-0.000	0.131	-0.006	0.013	-0.022	0.909
1712	0001	45750	1.140	0.042	2.007	1.121	0.074	-0.051	13.112	-0.000	0.126	-0.006	0.010	-0.046	0.861
1713	0001	45750	1.140	0.041	2.004	1.521	0.145	-0.046	13.410	-0.001	0.156	-0.009	0.010	-0.040	0.865
1714	0001	45750	1.140	0.041	2.011	2.025	0.210	-0.042	17.913	-0.000	0.128	-0.006	-0.002	-0.048	0.866
1715	0001	45750	1.140	0.042	2.006	2.521	0.287	-0.039	12.531	-0.001	0.169	-0.002	-0.009	-0.050	0.868
1716	0001	45750	1.140	0.052	2.005	3.021	0.364	-0.036	12.023	-0.001	0.170	-0.001	-0.013	-0.050	0.871
1717	0001	45750	1.140	0.055	2.004	3.521	0.407	-0.035	10.687	-0.000	0.140	-0.001	-0.004	-0.039	0.872
1718	0001	45750	1.140	0.041	3.006	1.115	0.040	-0.049	15.151	-0.001	0.184	-0.021	0.009	-0.060	0.833
1719	0001	45750	1.140	0.041	3.004	1.519	0.135	-0.044	14.641	-0.001	0.171	-0.017	0.007	-0.054	0.837
1720	0001	45750	1.140	0.055	3.008	2.015	0.191	-0.041	13.461	-0.001	0.160	-0.015	-0.007	-0.063	0.860
1721	0001	45750	1.140	0.055	3.019	2.520	0.258	-0.038	13.546	-0.000	0.167	-0.014	-0.005	-0.057	0.862
1722	0001	45750	1.140	0.055	3.020	3.032	0.297	-0.035	13.561	-0.001	0.201	-0.012	-0.011	-0.059	0.864
1723	0001	45750	1.140	0.054	3.018	3.524	0.334	-0.034	11.746	-0.001	0.178	-0.012	-0.001	-0.047	0.864
1724	0001	45750	1.140	0.054	3.020	1.119	0.042	-0.038	12.514	-0.001	0.184	-0.023	0.009	-0.052	0.868
1725	0001	45750	1.140	0.042	3.018	1.520	0.110	-0.036	11.968	-0.001	0.169	-0.019	0.008	-0.048	0.868
1726	0001	45750	1.140	0.052	3.019	2.021	0.174	-0.035	12.009	-0.001	0.181	-0.017	-0.007	-0.060	0.846
1727	0001	45750	1.140	0.054	3.291	2.527	0.219	-0.033	11.200	-0.001	0.180	-0.016	-0.006	-0.056	0.847
1728	0001	45750	1.140	0.054	3.254	3.023	0.252	-0.031	11.455	-0.001	0.204	-0.015	-0.015	-0.062	0.848
1729	0001	45750	1.140	0.052	3.307	3.528	0.305	-0.030	10.035	-0.000	0.159	-0.014	-0.007	-0.051	0.849
1730	0001	45750	1.140	0.046	3.513	1.124	0.027	-0.051	14.737	-0.001	0.177	-0.004	0.012	-0.065	0.860
1731	0001	45750	1.140	0.054	3.504	1.524	0.403	-0.034	11.138	-0.001	0.171	-0.001	-0.004	-0.039	0.871

MODEL SC-4, 30 SHALLOW CHUTES, AR = 1.5, FULL PLUG

FACILITY A PROGRAM CODE

NOZZLE TYPE — DUAL FLOW (FSS)

TYPE TREAT PLUG CONFIGURATIONS — FULL PLUG W/O BLEED

SUPPRESSOR CONFIGURATION — 30-SPOKE, AREA RATIO = 1.75

TARGET PARAMETERS — OUTER RADIUS RATIO 0.8000 — INNER RADIUS RATIO 0.3000 — OVD 1.2680

RPM	CF	MASA	MJ	MP	PTO/P1	PT1/P1	ST	CDO	CD1	CFNET1	CFNET2	FG
1507	0005	45830	0.358	0.025	1.572	1.112	0.305	0.978	9.999	0.915	0.915	1.181
1508	0005	45830	0.358	0.031	1.756	1.121	.300	0.956	9.999	0.919	0.919	1.189
1509	0005	45830	0.358	0.038	2.003	1.137	.300	0.968	9.999	0.922	0.922	1.186
1510	0005	45830	0.358	0.037	2.257	1.162	0.000	0.970	9.999	0.925	0.925	1.184
1511	0005	45830	0.358	0.053	2.512	1.196	0.000	0.971	9.999	0.927	0.927	1.182
1512	0005	45830	0.358	0.041	2.769	1.237	0.000	0.970	9.999	0.927	0.927	1.180
1513	0005	45830	0.358	0.054	3.013	1.291	0.000	0.971	9.999	0.931	0.931	1.182
1514	0005	45830	0.358	0.047	3.274	1.408	0.000	0.970	9.999	0.937	0.937	1.188
1515	0005	45830	0.358	0.038	2.009	1.490	0.000	0.969	9.999	0.924	0.924	1.187
1516	0005	45830	0.358	0.052	3.005	1.493	0.000	0.971	9.999	0.930	0.930	1.182
[illegible]												
1518	0005	45830	0.358	0.447	1.758	1.142	0.000	0.972	9.999	0.865	0.865	1.152
1519	0005	45830	0.358	0.447	2.002	1.150	0.000	0.972	9.999	0.873	0.873	1.149
1520	0005	45830	0.358	0.447	2.261	1.167	0.000	0.970	9.999	0.878	0.878	1.143
1521	0005	45830	0.358	0.446	2.515	1.190	0.000	0.970	9.999	0.881	0.881	1.140
1522	0005	45830	0.358	0.446	2.763	1.220	0.000	0.971	9.999	0.884	0.884	1.141
1523	0005	45830	0.358	0.447	3.021	1.259	0.000	0.972	9.999	0.894	0.894	1.149
1524	0005	45830	0.358	0.446	3.280	1.330	0.000	0.971	9.999	0.905	0.905	1.157
1525	0005	45830	0.358	0.447	2.018	1.233	0.000	0.970	9.999	0.868	0.868	1.143
1526	0005	45830	0.358	0.446	2.263	1.[illegible]	0.000	0.970	9.999	0.894	0.894	1.147
1527	0005	45830	0.358	0.357	1.505	1.[illegible]	0.000	0.973	9.999	0.864	0.864	1.157
1528	0005	45830	0.358	0.356	1.753	1.150	0.000	0.973	9.999	0.872	0.872	1.158
1529	0005	45830	0.358	0.356	2.015	1.158	0.000	0.970	9.999	0.880	0.880	1.154
1530	0005	45830	0.358	0.357	2.264	1.172	0.000	0.970	9.999	0.885	0.885	1.150
1531	0005	45830	0.358	0.358	2.523	1.197	0.000	0.970	9.999	0.890	0.890	1.149
1532	0005	45830	0.358	0.358	2.783	1.233	0.000	0.972	9.999	0.894	0.894	1.152
1533	0005	45830	0.358	0.358	3.002	1.287	0.000	0.971	9.999	0.900	0.900	1.154
1534	0005	45830	0.358	0.361	3.143	1.454	0.000	0.971	9.999	0.905	0.905	1.158
1535	0005	45830	0.358	0.359	2.[illegible]	1.414	0.000	0.969	9.999	0.880	0.880	1.152
[illegible]												
1537	0005	45830	0.358	0.446	1.513	1.719	0.000	0.995	9.999	0.862	0.862	1.156
1538	0005	45830	0.358	0.446	1.776	1.701	0.000	0.976	9.999	0.869	0.869	1.157
1539	0005	45830	0.358	0.447	1.[illegible]	1.198	0.000	0.973	9.999	0.879	0.879	1.155
1540	0005	45830	0.358	0.446	2.254	1.205	0.000	0.971	9.999	0.884	0.884	1.150
1541	0005	45830	0.358	0.447	2.502	1.215	0.000	0.972	9.999	0.888	0.888	1.148
1542	0005	45830	0.358	0.446	2.771	1.241	0.000	0.971	9.999	0.892	0.892	1.147
1543	0005	45830	0.358	0.447	3.017	1.275	0.000	0.972	9.999	0.899	0.899	1.154
1544	0005	45830	0.358	0.447	3.269	1.313	0.000	0.971	9.999	0.911	0.911	1.163
1545	0005	45830	0.358	0.446	2.022	1.326	0.000	0.957	9.999	0.877	0.877	1.147
1546	0005	45830	0.358	0.447	2.005	1.341	0.000	0.970	9.999	0.898	0.898	1.151
1547	0005	45830	0.358	0.356	1.514	1.101	0.000	0.992	9.999	0.876	0.876	1.164
1548	0005	45830	0.358	0.357	1.757	1.105	0.000	0.973	9.999	0.883	0.883	1.165
1549	0005	45830	0.358	0.357	2.007	1.120	0.000	0.972	9.999	0.888	0.888	1.161
1550	0005	45830	0.358	0.358	2.271	1.144	0.000	0.970	9.999	0.891	0.891	1.155
1551	0005	45830	0.358	0.358	2.511	1.170	0.000	0.970	9.999	0.895	0.895	1.153

FACILITY XI PROGRAM FOR

INPUT STREAM

ROTOR TYPE — FLOW CONFIGURATIONS — SUPPRESSOR CONFIGURATION

DISK FLOW (FREE) — FULL PLAN W/O BLEED — 30-SPOKE, AREA RATIO = 1.75

ROTOR PARAMETERS — OUTER RADIUS RATIO 0.1000 — INNER RADIUS RATIO 0.0000 — OVD 1.2460

ROTOR	CF	MACH	QF	WR	PTOT/PI	PTOT/P1	EFFICIENCY	SOS	COS	DCSH	DOSH	DCPL,0	DCPL,1	DCTOT	PSUP/PA
1507	0005	45K10	0.398	0.320	1.406	1.117	0.000	-0.056	42.510	-0.001	0.545	-0.014	0.018	-0.061	0.932
1508	0005	45K10	0.398	0.041	1.396	1.121	0.000	-0.054	23.472	-0.001	0.321	-0.014	0.018	-0.058	0.910
1509	0005	45K10	0.398	0.018	2.000	1.132	0.000	-0.048	19.171	-0.001	0.254	-0.014	0.017	-0.058	0.899
1510	0005	45K10	0.398	0.017	2.757	1.182	0.000	-0.054	24.514	-0.001	0.314	-0.012	0.015	-0.056	0.847
1511	0005	45K10	0.398	0.051	2.651	1.196	0.000	-0.058	13.954	-0.000	0.006	-0.010	0.015	-0.053	0.848
1512	0005	45K10	0.398	0.051	2.756	1.237	0.000	-0.047	16.727	-0.001	0.156	-0.021	0.014	-0.063	0.830
1513	0005	45K10	0.398	0.056	2.816	1.241	0.000	-0.051	15.437	-0.000	0.147	-0.027	0.017	-0.062	0.826
1514	0005	45K10	0.398	0.057	2.503	1.408	0.000	-0.042	11.842	-0.001	0.156	-0.028	0.020	-0.048	0.846
1515	0005	45K10	0.398	0.036	2.908	1.400	0.000	-0.051	21.548	-0.001	0.263	-0.017	0.018	-0.060	0.887
1516	0005	45K10	0.398	0.052	3.004	1.421	0.000	-0.041	16.431	-0.001	0.169	-0.027	0.017	-0.051	0.824
[illegible]															
1518	0005	45K10	0.398	0.447	1.758	1.142	0.000	-0.114	0.298	-0.024	0.044	-0.013	0.035	-0.113	0.836
1519	0005	45K10	0.398	0.447	2.002	1.150	0.000	-0.106	0.260	-0.020	0.047	-0.012	0.031	-0.107	0.803
1520	0005	45K10	0.398	0.447	2.261	1.167	0.000	-0.101	0.293	-0.017	0.048	-0.009	0.028	-0.099	0.774
1521	0005	45K10	0.398	0.447	2.516	1.170	0.000	-0.096	0.320	-0.015	0.050	-0.008	0.027	-0.092	0.748
1522	0005	45K10	0.398	0.447	2.761	1.220	0.000	-0.092	0.353	-0.013	0.050	-0.017	0.027	-0.095	0.721
1523	0005	45K10	0.398	0.449	3.031	1.244	0.000	-0.087	0.393	-0.011	0.050	-0.028	0.030	-0.091	0.720
1524	0005	45K10	0.398	0.449	3.334	1.335	0.000	-0.067	0.329	-0.010	0.049	-0.029	0.031	-0.075	0.739
1525	0005	45K10	0.398	0.447	2.814	1.335	0.000	-0.107	0.255	-0.020	0.047	-0.012	0.032	-0.107	0.800
1526	0005	45K10	0.398	0.449	3.018	1.343	0.000	-0.[illegible]	0.353	-0.011	0.050	-0.028	0.029	-0.092	0.721
1527	0005	45K10	0.398	0.447	1.506	1.164	0.000	-0.[illegible]	0.273	-0.012	0.041	-0.016	0.033	-0.106	0.888
1528	0005	45K10	0.398	0.355	1.757	1.150	0.000	-0.099	0.[illegible]	-0.014	0.047	-0.014	0.029	-0.099	0.855
1529	0005	45K10	0.398	0.356	2.015	1.167	0.000	-0.094	0.352	-0.013	0.050	-0.012	0.026	-0.093	0.824
1530	0005	45K10	0.398	0.357	2.264	1.172	0.000	-0.090	0.404	-0.011	0.051	-0.009	0.024	-0.087	0.797
1531	0005	45K10	0.398	0.358	2.520	1.157	0.000	-0.087	0.456	-0.010	0.051	-0.008	0.023	-0.082	0.770
1532	0005	45K10	0.398	0.358	2.767	1.239	0.000	-0.082	0.494	-0.009	0.053	-0.007	0.024	-0.084	0.750
1533	0005	45K10	0.398	0.359	3.002	1.287	0.000	-0.074	0.499	-0.008	0.054	-0.027	0.026	-0.084	0.747
1534	0005	45K10	0.398	0.361	3.165	1.43-	0.000	-0.047	0.477	-0.007	0.053	-0.028	0.028	-0.074	0.756
1535	0005	45K10	0.398	0.359	2.834	1.414	0.000	-0.086	0.356	-0.014	0.051	-0.011	0.026	-0.093	0.820
[illegible]															
1537	0005	45K10	0.398	0.448	1.510	1.219	0.000	-0.117	0.151	-0.030	0.041	-0.015	0.037	-0.125	0.874
1538	0005	45K10	0.398	0.446	1.756	1.201	0.000	-0.111	0.205	-0.024	0.043	-0.012	0.033	-0.114	0.839
1539	0005	45K10	0.398	0.447	1.998	1.199	0.000	-0.106	0.248	-0.020	0.048	-0.012	0.031	-0.107	0.805
1540	0005	45K10	0.398	0.446	2.238	1.201	0.000	-0.101	0.284	-0.017	0.049	-0.010	0.028	-0.100	0.777
1541	0005	45K10	0.398	0.447	2.502	1.215	0.000	-0.096	0.321	-0.015	0.049	-0.009	0.026	-0.093	0.749
1542	0005	45K10	0.398	0.446	2.771	1.241	0.000	-0.092	0.357	-0.013	0.050	-0.019	0.027	-0.097	0.721
1543	0005	45K10	0.398	0.447	3.017	1.275	0.000	-0.087	0.356	-0.011	0.050	-0.029	0.029	-0.092	0.720
1544	0005	45K10	0.398	0.447	2.780	1.317	0.000	-0.048	0.333	-0.010	0.049	-0.029	0.031	-0.076	0.738
1545	0005	45K10	0.398	0.445	2.032	1.324	0.000	-0.107	0.258	-0.020	0.047	-0.011	0.031	-0.106	0.799
1546	0005	45K10	0.398	0.447	3.006	1.341	0.000	-0.092	0.356	-0.012	0.050	-0.028	0.029	-0.093	0.721
1547	0005	45K10	0.398	0.355	1.514	1.101	0.000	-0.104	0.226	-0.019	0.042	-0.015	0.033	-0.106	0.887
1548	0005	45K10	0.398	0.357	1.757	1.105	0.000	-0.099	0.291	-0.016	0.047	-0.013	0.029	-0.099	0.855
1549	0005	45K10	0.398	0.357	2.004	1.120	0.000	-0.094	0.350	-0.013	0.050	-0.011	0.027	-0.093	0.824
1550	0005	45K10	0.398	0.355	2.271	1.144	0.000	-0.090	0.403	-0.011	0.051	-0.009	0.024	-0.086	0.797
1551	0005	45K10	0.398	0.358	2.511	1.170	0.000	-0.087	0.454	-0.010	0.054	-0.008	0.023	-0.083	0.772

FACILITY XL PROGRAM COST

NOZZLE TYPE: DUAL FLOW (FAA)

TEST STREAM

PLUG CONFIGURATIONS: FULL PLUG W/O BLEED

SUPPRESSOR CONFIGURATION: 30-SPOKE, AREA RATIO = 1.75

THRUST PARAMETERS — OUTER RADIUS RATIO: 0.0000 — INNER RADIUS RATIO: 0.0000 — DVD: 1.2480

PNC	GF	MASA	M2	MA	PTM/PA	PT7/PA	OMEGAT	CDD	CDI	CFNET1	CFNET2	F9
1552	0005	45830	0.398	0.358	2.772	1.221	0.000	0.971	9.999	0.899	0.899	1.156
1553	0005	45830	0.399	0.359	3.007	1.273	0.000	0.969	9.999	0.906	0.905	1.158
1554	0005	45830	0.398	0.358	3.205	1.342	0.000	0.970	9.999	0.911	0.911	1.163
1555	0005	45830	0.398	0.357	2.000	1.377	0.000	0.967	9.999	0.882	0.882	1.153
1556	0005	45830	0.398	0.358	3.014	1.420	0.000	0.973	9.999	0.904	0.904	1.159

737

FACILITY XL PROGRAM COST

NOZZLE TYPE: DUAL FLOW (FAA)

TEST STREAM

PLUG CONFIGURATIONS: FULL PLUG W/O BLEED

SUPPRESSOR CONFIGURATION: 30-SPOKE, AREA RATIO = 1.75

THRUST PARAMETERS — OUTER RADIUS RATIO: 0.0000 — INNER RADIUS RATIO: 0.0000 — DVD: 1.2480

PNC	GF	MASA	M2	MA	PTM/PA	PT7/PA	OMEGAT	DCS	CDS	DCSH	CDSH	DCPL,O	DCPL,I	DCTOT	PSUP/PA
1552	0005	45830	0.398	0.358	2.772	1.221	0.000	-0.081	0.497	-0.009	0.052	-0.017	0.024	-0.085	0.749
1553	0005	45830	0.398	0.359	3.007	1.273	0.000	-0.074	0.497	-0.008	0.053	-0.027	0.026	-0.083	0.748
1554	0005	45830	0.398	0.358	3.206	1.342	0.000	-0.065	0.476	-0.007	0.055	-0.029	0.028	-0.073	0.760
1555	0005	45830	0.398	0.357	2.000	1.377	0.000	-0.095	0.351	-0.014	0.051	-0.012	0.027	-0.093	0.824
1556	0005	45830	0.398	0.358	3.014	1.420	0.000	-0.074	0.499	-0.008	0.054	-0.027	0.025	-0.083	0.748

MODEL SC-5, 30 SHALLOW CHUTES, AR = 1.75, FORWARD PLUG

FACILITY --ASI PROGRAM C031

NOZZLE TYPE — DUAL FLOW (FAA)

(4) X-STREAM PLUG CONFIGURATIONS — FORWARD PLUG WITH BLEED

SUPPRESSOR CONFIGURATION — 30-SPOKE, AREA RATIO = 1.75

THRUST PARAMETERS — OUTER RADIUS RATIO 0.8000 — INNER RADIUS RATIO 0.7790 — DVD 1.2480

ADC	CF	NASA	DJ	MA	RIC/RA	RII/RA	CNFCAT	CDD	CDI	CFNET1	CFNET2	F9
2505	0004	45630	0.398	0.446	1.506	0.995	0.000	0.995	9.999	0.830	0.830	1.104
2506	0004	45630	0.398	0.447	1.504	1.007	0.029	0.995	0.454	0.840	0.843	1.105
2507	0004	45630	0.398	0.445	1.503	1.017	0.059	0.994	0.604	0.847	0.857	1.108
2508	0004	45630	0.398	0.446	2.002	0.988	0.000	0.969	9.999	0.851	0.851	1.107
2509	0004	45630	0.398	0.445	2.001	1.013	0.029	0.970	0.469	0.864	0.867	1.111
2510	0004	45630	0.398	0.446	2.004	1.031	0.059	0.970	0.608	0.868	0.879	1.114
2511	0004	45630	0.398	0.447	2.515	0.973	0.000	0.968	9.999	0.865	0.865	1.109
2512	0004	45630	0.398	0.448	2.510	1.010	0.029	0.968	0.662	0.875	0.878	1.111
2513	0004	45630	0.399	0.448	2.508	1.038	0.059	0.965	0.685	0.884	0.895	1.116
2514	0004	45630	0.398	0.447	3.027	0.952	0.000	0.930	9.999	0.879	0.879	1.122
2515	0004	45630	0.398	0.448	3.019	1.013	0.029	0.970	0.703	0.888	0.891	1.121
2516	0004	45630	0.398	0.448	3.020	1.058	0.059	0.970	0.666	0.892	0.905	1.124
2517	0004	45630	0.398	0.450	3.322	0.947	0.000	0.970	9.999	0.892	0.892	1.133
2518	0004	45630	0.398	0.450	3.323	1.026	0.029	0.969	0.545	0.900	0.904	1.130
2519	0004	45630	0.398	0.449	3.324	1.080	0.059	0.970	0.625	0.906	0.918	1.133
2520	0004	45630	0.398	0.449	3.505	0.973	0.000	0.971	9.999	0.865	0.865	1.112
2521	0004	45630	0.398	0.449	2.512	1.038	0.059	0.968	0.683	0.882	0.893	1.116
2522	0004	45650	1.140	0.448	1.503	1.110	0.240	0.994	0.930	0.873	0.986	1.132
2523	0004	45650	1.140	0.447	1.503	1.526	0.523	0.993	0.975	0.889	1.362	1.169
2524	0004	45650	1.140	0.447	1.500	2.014	0.710	0.996	0.965	0.900	1.722	1.173
2525	0004	45650	1.140	0.448	1.502	2.517	0.884	0.995	0.966	0.911	2.083	1.175
2526	0004	45650	1.140	0.448	1.503	3.025	1.064	0.991	0.963	0.922	2.462	1.178
2527	0004	45650	1.140	0.448	1.504	3.527	1.247	0.990	0.969	0.922	2.826	1.179
2528	0004	45650	1.140	0.448	2.005	1.124	0.173	0.969	0.890	0.886	0.950	1.133
2529	0004	45650	1.140	0.447	2.003	1.525	0.384	0.969	0.973	0.895	1.168	1.165
2530	0004	45650	1.140	0.448	2.004	2.021	0.522	0.969	0.966	0.902	1.376	1.168
2531	0004	45650	1.140	0.448	2.004	2.518	0.652	0.970	0.966	0.910	1.583	1.171
2532	0004	45650	1.140	0.448	2.007	3.036	0.786	0.968	0.966	0.918	1.804	1.174
2533	0004	45650	1.140	0.448	2.001	3.524	0.916	0.970	0.968	0.922	2.016	1.179
2534	0004	45650	1.140	0.448	2.500	1.121	0.135	0.974	0.882	0.894	0.939	1.136
2535	0004	45650	1.140	0.448	2.511	1.525	0.306	0.968	0.973	0.900	1.093	1.159
2536	0004	45650	1.140	0.448	2.510	2.017	0.417	0.968	0.965	0.907	1.242	1.164
2537	0004	45650	1.140	0.448	2.510	2.519	0.521	0.969	0.967	0.911	1.386	1.166
2538	0004	45650	1.140	0.448	2.511	3.021	0.626	0.968	0.967	0.918	1.540	1.170
2539	0004	45650	1.140	0.449	2.508	3.525	0.731	0.970	0.968	0.919	1.687	1.172
2540	0004	45650	1.140	0.448	3.021	1.120	0.103	0.969	0.822	0.899	0.933	1.134
2541	0004	45650	1.140	0.450	3.015	1.525	0.252	0.971	0.963	0.907	1.055	1.161
2542	0004	45650	1.140	0.450	3.013	2.016	0.347	0.970	0.965	0.911	1.170	1.166
2543	0004	45650	1.140	0.450	3.021	2.522	0.433	0.970	0.966	0.915	1.282	1.167
2544	0004	45650	1.140	0.451	3.028	3.031	0.520	0.969	0.967	0.918	1.396	1.168
2545	0004	45650	1.140	0.450	3.018	3.528	0.607	0.970	0.968	0.917	1.505	1.168
2546	0004	45650	1.140	0.449	3.320	1.122	0.083	0.971	0.717	0.907	0.932	1.139
2547	0004	45650	1.140	0.450	3.310	1.525	0.226	0.971	0.948	0.915	1.044	1.166
2548	0004	45650	1.140	0.450	3.313	2.018	0.315	0.970	0.964	0.919	1.168	1.172
2549	0004	45650	1.140	0.450	3.321	2.520	0.393	0.971	0.966	0.921	1.245	1.173

FACILITY 6X8 PROGRAM CO3I

NOZZLE TYPE — DUAL FLOW (FAB)

II A-STREAM PLUG CONFIGURATIONS — FORWARD PLUG WITH PLEFD

SUPPRESSOR CONFIGURATION — 30-SPOKE, AREA RATIO = 1.75

CRAC PARAMETERS — OUTER RADIUS RATIO 0.0000 — INNER RADIUS RATIO 0.7790 — DVO 1.2480

RDC	CC	AMSA	G2	M6	RTC/CA	RTC/PA	ONECAT	DCS	COS	DCSM	CDSM	DCPL,0	DCPL,1	DCTOT	PSUR/PA
2505	0004	45630	0.398	0.446	1.504	0.995	0.000	-0.120	0.163	-0.024	0.033	-0.010	0.032	-0.122	0.873
2506	0004	45630	0.398	0.447	1.504	1.007	0.029	-0.114	0.156	-0.023	0.032	-0.008	0.029	-0.117	0.878
2507	0004	45630	0.398	0.445	1.503	1.017	0.059	-0.111	0.154	-0.023	0.032	-0.007	0.029	-0.112	0.880
2508	0004	45630	0.398	0.446	2.002	0.988	0.000	-0.110	0.259	-0.015	0.037	-0.008	0.023	-0.111	0.798
2509	0004	45630	0.398	0.446	2.001	1.013	0.029	-0.106	0.250	-0.015	0.035	-0.006	0.019	-0.108	0.804
2510	0004	45630	0.398	0.446	2.006	1.031	0.059	-0.102	0.245	-0.015	0.035	-0.005	0.020	-0.102	0.808
2511	0004	45630	0.398	0.447	2.515	0.973	0.000	-0.097	0.326	-0.011	0.038	-0.007	0.019	-0.097	0.744
2512	0004	45630	0.398	0.448	2.510	1.012	0.029	-0.094	0.312	-0.011	0.036	-0.004	0.014	-0.095	0.753
2513	0004	45630	0.398	0.448	2.509	1.038	0.059	-0.092	0.309	-0.011	0.036	-0.003	0.015	-0.091	0.756
2514	0004	45630	0.398	0.447	3.022	0.952	0.000	-0.083	0.360	-0.009	0.038	-0.024	0.023	-0.092	0.717
2515	0004	45630	0.398	0.448	3.019	1.013	0.029	-0.082	0.355	-0.008	0.036	-0.021	0.016	-0.096	0.719
2516	0004	45630	0.398	0.448	3.020	1.058	0.059	-0.080	0.353	-0.008	0.036	-0.020	0.015	-0.093	0.722
2517	0004	45630	0.398	0.450	3.322	0.967	0.000	-0.067	0.329	-0.008	0.037	-0.023	0.025	-0.073	0.738
2518	0004	45630	0.398	0.450	3.327	1.026	0.029	-0.066	0.325	-0.007	0.036	-0.021	0.019	-0.075	0.741
2519	0004	45630	0.398	0.449	3.324	1.080	0.059	-0.065	0.325	-0.007	0.036	-0.019	0.017	-0.074	0.742
2520	0004	45630	0.398	0.449	2.505	0.973	0.000	-0.098	0.325	-0.011	0.037	-0.007	0.019	-0.097	0.743
2521	0004	45630	0.398	0.449	2.512	1.038	0.059	-0.091	0.306	-0.010	0.035	-0.003	0.015	-0.089	0.757
2522	0004	45650	1.140	0.448	1.502	1.119	0.240	-0.096	0.166	-0.020	0.030	-0.005	0.010	-0.090	0.885
2523	0004	45650	1.140	0.447	1.503	1.526	0.523	-0.071	0.148	-0.015	0.030	-0.004	0.024	-0.065	0.894
2524	0004	45650	1.140	0.447	1.503	2.016	0.719	-0.058	0.150	-0.012	0.032	-0.004	0.015	-0.060	0.882
2525	0004	45650	1.140	0.448	1.502	2.517	0.886	-0.048	0.147	-0.010	0.031	-0.002	0.007	-0.053	0.884
2526	0004	45650	1.140	0.448	1.503	3.025	1.064	-0.040	0.146	-0.008	0.030	-0.002	0.015	-0.035	0.886
2527	0004	45650	1.140	0.448	1.504	3.527	1.247	-0.034	0.140	-0.007	0.031	-0.001	0.008	-0.034	0.890
2528	0004	45650	1.140	0.448	2.005	1.134	0.133	-0.094	0.237	-0.013	0.034	-0.004	0.021	-0.090	0.813
2529	0004	45650	1.140	0.447	2.003	1.525	0.384	-0.078	0.238	-0.012	0.035	-0.003	0.019	-0.073	0.813
2530	0004	45650	1.140	0.448	2.004	2.021	0.522	-0.067	0.238	-0.010	0.034	-0.003	0.013	-0.066	0.812
2531	0004	45650	1.140	0.448	2.004	2.518	0.652	-0.058	0.235	-0.009	0.035	-0.002	0.007	-0.061	0.815
2532	0004	45650	1.140	0.448	2.007	3.034	0.786	-0.050	0.228	-0.007	0.033	-0.001	0.006	-0.051	0.820
2533	0004	45650	1.140	0.448	2.001	3.524	0.916	-0.044	0.222	-0.007	0.035	0.000	0.007	-0.043	0.824
2534	0004	45650	1.140	0.449	2.500	1.121	0.135	-0.087	0.301	-0.010	0.034	-0.001	0.017	-0.081	0.761
2535	0004	45650	1.140	0.448	2.511	1.525	0.306	-0.075	0.304	-0.009	0.036	-0.001	0.016	-0.069	0.760
2536	0004	45650	1.140	0.448	2.510	2.017	0.417	-0.067	0.304	-0.008	0.035	-0.001	0.011	-0.065	0.759
2537	0004	45650	1.140	0.448	2.510	2.519	0.521	-0.059	0.300	-0.007	0.035	-0.000	0.008	-0.059	0.763
2538	0004	45650	1.140	0.449	2.511	3.021	0.626	-0.052	0.291	-0.006	0.035	0.001	0.007	-0.050	0.769
2539	0004	45650	1.140	0.449	2.508	3.525	0.731	-0.046	0.281	-0.006	0.035	0.002	0.004	-0.046	0.777
2540	0004	45650	1.140	0.448	3.031	1.120	0.108	-0.078	0.349	-0.008	0.036	-0.010	0.017	-0.088	0.723
2541	0004	45650	1.140	0.450	3.015	1.525	0.252	-0.069	0.344	-0.007	0.034	-0.010	0.017	-0.075	0.725
2542	0004	45650	1.140	0.450	3.013	2.014	0.347	-0.063	0.342	-0.006	0.035	-0.014	0.012	-0.072	0.724
2543	0004	45650	1.140	0.450	3.021	2.522	0.433	-0.057	0.345	-0.006	0.034	-0.012	0.007	-0.068	0.726
2544	0004	45650	1.140	0.451	3.028	3.031	0.520	-0.052	0.338	-0.005	0.034	-0.009	0.010	-0.056	0.729
2545	0004	45650	1.140	0.450	3.018	3.529	0.607	-0.047	0.333	-0.005	0.033	-0.006	0.002	-0.057	0.734
2546	0004	45650	1.140	0.445	3.320	1.122	0.083	-0.066	0.326	-0.007	0.036	-0.018	0.018	-0.072	0.743
2547	0004	45650	1.140	0.450	3.310	1.525	0.226	-0.058	0.321	-0.006	0.034	-0.015	0.017	-0.062	0.744
2548	0004	45650	1.140	0.450	3.313	2.019	0.315	-0.053	0.321	-0.005	0.033	-0.013	0.014	-0.058	0.744
2549	0004	45650	1.140	0.450	3.321	2.520	0.393	-0.048	0.320	-0.005	0.034	-0.011	0.008	-0.056	0.745

FACILITY TEST PROGRAM CO3I — NOZZLE TYPE: DUAL FLOW (FAA) — IN-...-STREAM PLUG CONFIGURATIONS: FORWARD PLUG WITH BLEED — SUPPRESSOR CONFIGURATION: 30-SPOKE, AREA RATIO = 1.75

THRUST PARAMETERS — OUTER RADIUS RATIO = 0.0000 — INNER RADIUS RATIO = 0.7790 — OVD = 1.2480

RDC	CC	MACH	NPR	WA	PTC/P4	PTI/P4	CWSCAT	CDC	CDI	CFNET1	CFNET2	E9
2550	CCC4	45650	1.140	0.450	3.322	3.024	0.477	0.970	0.967	0.926	1.349	1.176
2551	CCC4	45650	1.140	0.452	3.320	3.525	C.551	0.971	0.968	0.926	1.446	1.177
2552	0004	45650	1.140	0.450	2.516	1.117	0.133	0.967	C.882	0.890	0.934	1.129
2553	CCC4	45650	1.140	0.450	2.504	3.521	0.731	0.970	C.968	0.919	1.688	1.172
2554	0004	45630	0.398	0.361	1.504	0.991	0.000	0.989	9.999	0.854	0.854	1.113
2555	CCC4	45630	0.398	0.360	1.504	1.005	0.029	0.992	0.538	0.856	0.859	1.112
2556	CCC4	45630	0.399	0.340	1.503	1.015	C.059	0.990	0.634	0.867	0.877	1.117
2557	CCC4	45630	0.399	0.362	2.012	0.985	0.000	0.968	9.999	0.865	0.865	1.116
2558	CCC4	45630	0.398	0.362	2.005	1.010	C.029	0.972	0.517	0.878	0.881	1.121
2559	CCC4	45630	0.398	0.360	2.010	1.028	C.059	0.968	0.637	0.881	0.892	1.121
2560	0004	45630	0.399	0.363	2.572	0.972	0.000	0.968	9.999	0.875	0.875	1.117
2561	CCC4	45630	0.398	0.362	2.517	1.010	C.029	0.969	0.666	0.886	0.888	1.120
2562	0004	45630	0.398	0.362	2.513	1.035	C.059	0.970	0.715	0.891	0.902	1.126
2563	0004	45630	0.398	0.363	3.016	0.946	0.000	0.969	9.999	0.888	0.888	1.130
2564	CCC4	45630	0.399	0.364	3.020	1.008	C.029	0.970	0.875	0.896	0.898	1.128
2565	0004	45630	0.398	0.362	3.016	1.052	0.059	0.970	0.706	0.900	0.912	1.131
2566	0004	45630	0.399	0.363	3.198	0.942	0.000	0.968	9.999	0.896	0.896	1.135
2567	0004	45630	0.398	0.362	3.191	1.013	C.029	0.970	0.724	0.903	0.906	1.134
2568	0004	45630	0.398	0.360	3.167	1.064	0.059	0.970	0.668	0.906	0.919	1.136
2569	CCC4	45630	0.398	0.359	2.517	C.970	C.004	0.969	9.999X	0.877	0.877	1.119
2570	CCC4	45630	0.399	0.360	2.515	1.035	C.059	0.969	0.716	0.893	0.903	1.126
2571	0004	45650	1.140	C.360	1.504	1.121	0.246	0.990	0.945	0.981	0.999	1.137
2572	CCC4	45650	1.140	0.359	1.505	1.526	0.526	0.989	0.979	0.896	1.373	1.172
2573	0004	45650	1.140	0.360	1.502	2.031	C.717	0.992	0.966	0.908	1.748	1.177
2574	0004	45650	1.140	0.360	1.504	2.532	0.893	0.989	C.965	0.916	2.106	1.177
2575	CCC4	45650	1.140	0.362	1.503	3.033	1.071	0.990	0.967	0.924	2.480	1.181
2576	0004	45650	1.140	0.361	1.504	3.520	1.248	0.989	0.969	0.926	2.839	1.183
2577	CCC4	45650	1.140	0.361	2.015	1.124	C.174	0.969	0.903	0.893	0.959	1.139
2578	CCC4	45650	1.140	0.358	2.009	1.523	C.383	0.969	0.977	0.903	1.178	1.172
2579	0004	45650	1.140	C.359	2.013	2.032	0.525	0.968	0.966	0.909	1.389	1.174
2580	CCC4	45650	1.140	0.360	2.014	2.533	C.654	0.969	0.967	0.915	1.594	1.175
2581	0004	45650	1.140	C.359	2.011	3.021	C.702	0.968	0.968	0.924	1.808	1.180
2582	0004	45650	1.140	C.359	2.011	3.517	0.911	0.969	0.969	0.926	2.015	1.182
2583	CCC4	45650	1.140	0.360	2.522	1.121	0.138	0.969	C.908	0.902	0.948	1.140
2584	0004	45650	1.140	0.361	2.515	1.528	C.308	0.970	0.975	0.908	1.103	1.167
2585	CCC4	45650	1.140	0.360	2.515	2.031	C.419	0.969	0.966	0.913	1.254	1.170
2586	0004	45650	1.140	0.361	2.517	2.530	C.523	0.969	0.968	0.918	1.399	1.172
2587	CCC4	45650	1.140	0.361	2.525	3.023	0.624	0.967	0.968	0.924	1.547	1.175
2588	0004	45650	1.140	0.360	2.517	3.520	0.729	0.968	0.969	0.924	1.693	1.176
2589	CCC4	45650	1.140	0.360	3.014	1.120	0.107	0.970	0.843	0.908	0.941	1.142
2590	0004	45650	1.140	0.359	3.001	1.525	C.254	0.970	0.968	0.913	1.064	1.168
2591	0004	45650	1.140	0.360	3.005	2.034	C.350	C.971	0.965	0.917	1.182	1.172
2592	0004	45650	1.140	0.359	3.009	2.528	0.436	0.970	0.967	0.921	1.294	1.173
2593	0004	45650	1.140	0.360	3.012	3.021	C.521	0.970	0.968	0.926	1.409	1.177
2594	0004	45650	1.140	0.361	3.015	3.520	C.608	0.968	0.968	0.922	1.514	1.172

FACILITY 40X1 PROGRAM CODE

NOZZLE TYPE — DUAL FLOW (FAA) — INNER-STREAM PLUG CONFIGURATIONS — FORWARD PLUG WITH BLEED — SUPPRESSOR CONFIGURATION — 30-SPOKE, AREA RATIO = 1.75

CRUISE PARAMETERS — OUTER RADIUS RATIO = 0.0000 — INNER RADIUS RATIO = 0.7790 — DVO = 1.2480

RDC	CS	NOZZ	FD	PA	PI/PA	BI/PA	CHEGHT	DCS	CDS	CCSH	CDSH	DCPL,0	DCPL,I	DCTOT	PSUP/PA
2550	0004	45650	1.140	0.450	3.322	3.024	0.472	-0.045	0.318	-0.005	0.034	-0.009	0.010	-0.048	0.747
2551	0004	45650	1.140	0.452	3.320	3.523	0.551	-0.041	0.312	-0.004	0.032	-0.007	0.005	-0.047	0.749
2552	0004	45650	1.140	0.450	2.516	1.117	0.133	-0.087	0.301	-0.010	0.034	-0.002	0.017	-0.082	0.761
2553	0004	45650	1.140	0.450	2.504	3.521	0.731	-0.046	0.279	-0.006	0.034	0.002	0.004	-0.046	0.778
2554	0004	45650	0.398	0.341	1.504	0.991	0.000	-0.105	0.226	-0.017	0.035	-0.016	0.006	-0.136	0.884
2555	0004	45650	0.398	0.340	1.504	1.005	0.020	-0.105	0.221	-0.016	0.033	-0.016	0.002	-0.133	0.888
2556	0004	45650	0.398	0.360	1.503	1.015	0.059	-0.102	0.215	-0.015	0.032	-0.013	0.003	-0.127	0.891
2557	0004	45650	0.398	0.362	2.012	0.985	0.000	-0.097	0.352	-0.010	0.036	-0.012	0.007	-0.112	0.819
2558	0004	45650	0.398	0.362	2.005	1.010	0.029	-0.093	0.337	-0.010	0.037	-0.010	0.003	-0.110	0.826
2559	0004	45650	0.398	0.360	2.010	1.028	0.059	-0.091	0.341	-0.010	0.038	-0.008	0.005	-0.107	0.826
2560	0004	45650	0.398	0.363	2.522	0.972	0.000	-0.089	0.451	-0.007	0.038	-0.009	0.008	-0.097	0.766
2561	0004	45650	0.398	0.362	2.517	1.010	0.029	-0.086	0.439	-0.007	0.036	-0.006	0.003	-0.096	0.774
2562	0004	45650	0.398	0.362	2.513	1.025	0.059	-0.084	0.432	-0.007	0.037	-0.005	0.004	-0.092	0.777
2563	0004	45650	0.398	0.363	3.016	0.965	0.000	-0.075	0.494	-0.006	0.037	-0.026	0.014	-0.093	0.744
2564	0004	45650	0.398	0.364	3.020	1.003	0.029	-0.074	0.486	-0.006	0.037	-0.024	0.007	-0.096	0.747
2565	0004	45650	0.398	0.362	3.016	1.052	0.059	-0.073	0.489	-0.006	0.038	-0.022	0.007	-0.094	0.748
2566	0004	45650	0.398	0.363	3.198	0.962	0.000	-0.066	0.473	-0.006	0.040	-0.025	0.016	-0.081	0.755
2567	0004	45650	0.398	0.362	3.161	1.013	0.029	-0.066	0.472	-0.005	0.038	-0.023	0.009	-0.085	0.757
2568	0004	45650	0.398	0.360	3.167	1.064	0.059	-0.065	0.476	-0.005	0.037	-0.021	0.008	-0.084	0.758
2569	0004	45650	0.398	0.359	2.517	0.970	0.000	-0.088	0.459	-0.007	0.038	-0.009	0.008	-0.096	0.767
2570	0004	45650	0.398	0.360	2.515	1.035	0.059	-0.083	0.436	-0.007	0.036	-0.005	0.005	-0.090	0.778
2571	0004	45650	1.140	0.360	1.504	1.121	0.246	-0.088	0.207	-0.014	0.033	-0.008	0.009	-0.101	0.895
2572	0004	45650	1.140	0.359	1.506	1.526	0.576	-0.065	0.210	-0.010	0.033	-0.006	0.009	-0.073	0.894
2573	0004	45650	1.140	0.360	1.502	2.031	0.717	-0.053	0.210	-0.008	0.031	-0.005	0.004	-0.062	0.893
2574	0004	45650	1.140	0.360	1.504	2.532	0.893	-0.044	0.208	-0.007	0.032	-0.004	-0.004	-0.058	0.894
2575	0004	45650	1.140	0.362	1.503	3.033	1.071	-0.036	0.202	-0.006	0.031	-0.003	0.003	-0.042	0.896
2576	0004	45650	1.140	0.361	1.504	3.529	1.248	-0.031	0.197	-0.005	0.031	-0.002	0.000	-0.037	0.899
2577	0004	45650	1.140	0.361	2.015	1.124	0.174	-0.084	0.330	-0.009	0.037	-0.006	0.008	-0.091	0.831
2578	0004	45650	1.140	0.358	2.009	1.523	0.383	-0.070	0.335	-0.008	0.036	-0.005	0.009	-0.075	0.831
2579	0004	45650	1.140	0.359	2.013	2.032	0.525	-0.059	0.332	-0.006	0.036	-0.004	0.006	-0.066	0.832
2580	0004	45650	1.140	0.360	2.014	2.533	0.654	-0.051	0.328	-0.006	0.037	-0.003	-0.000	-0.060	0.833
2581	0004	45650	1.140	0.359	2.011	3.021	0.782	-0.045	0.323	-0.005	0.037	-0.002	-0.001	-0.053	0.837
2582	0004	45650	1.140	0.359	2.011	3.517	0.911	-0.039	0.313	-0.005	0.036	-0.001	0.000	-0.044	0.841
2583	0004	45650	1.140	0.360	2.522	1.121	0.138	-0.075	0.431	-0.006	0.035	-0.003	0.007	-0.082	0.780
2584	0004	45650	1.140	0.361	2.515	1.528	0.306	-0.068	0.428	-0.006	0.035	-0.003	0.008	-0.069	0.781
2585	0004	45650	1.140	0.360	2.515	2.031	0.419	-0.061	0.432	-0.005	0.037	-0.003	0.004	-0.065	0.780
2586	0004	45650	1.140	0.361	2.517	2.539	0.523	-0.054	0.421	-0.005	0.035	-0.001	0.001	-0.058	0.784
2587	0004	45650	1.140	0.361	2.525	3.021	0.624	-0.047	0.410	-0.004	0.036	0.000	0.002	-0.049	0.790
2588	0004	45650	1.140	0.360	2.517	3.520	0.729	-0.042	0.400	-0.004	0.036	0.001	-0.002	-0.047	0.796
2589	0004	45650	1.140	0.360	3.014	1.123	0.107	-0.070	0.488	-0.005	0.035	-0.020	0.009	-0.087	0.751
2590	0004	45650	1.140	0.359	3.001	1.525	0.254	-0.063	0.487	-0.004	0.037	-0.017	0.009	-0.075	0.752
2591	0004	45650	1.140	0.360	3.005	2.026	0.350	-0.057	0.485	-0.004	0.036	-0.015	0.005	-0.071	0.751
2592	0004	45650	1.140	0.359	3.009	2.528	0.436	-0.052	0.486	-0.004	0.037	-0.013	0.002	-0.066	0.754
2593	0004	45650	1.140	0.360	3.012	3.021	0.521	-0.047	0.476	-0.003	0.035	-0.010	0.005	-0.055	0.757
2594	0004	45650	1.140	0.361	3.015	3.520	0.608	-0.043	0.467	-0.003	0.033	-0.007	-0.003	-0.056	0.760

FACILITY XI PROGRAM COST

NOZZLE TYPE: DUAL FLOW (FAB)

IN-STREAM PLUG CONFIGURATIONS: FORWARD PLUG WITH BLEED

SUPPRESSOR CONFIGURATION: 30-SPOKE, AREA RATIO = 1.75

THRUST PARAMETERS

OUTER RADIUS RATIO 0.0000 | INNER RADIUS RATIO 0.7790 | DVD 1.2480

ROC	CC	MACH	P2	M6	PTO/P6	PTI/P6	CW/CAT	CDO	CDI	CFNET1	CFNET2	FG
2605	0004	45650	1.140	0.360	3.274	1.122	0.092	0.969	0.769	0.913	0.942	1.145
2606	0004	45650	1.140	0.360	3.137	1.627	0.239	0.968	0.958	0.918	1.057	1.168
2607	0004	45650	1.140	0.359	3.290	1.123	0.089	0.969	0.753	0.916	0.943	1.146
2608	0004	45650	1.140	0.359	3.718	1.526	0.234	0.969	0.956	0.920	1.057	1.171
2599	0004	45650	1.140	0.359	3.204	2.034	0.328	0.970	0.964	0.924	1.168	1.177
2600	0004	45650	1.140	0.360	3.205	2.511	0.409	0.970	0.965	0.926	1.269	1.177
2601	0004	45650	1.140	0.360	3.209	3.028	0.490	0.970	0.968	0.930	1.376	1.180
2602	0004	45650	1.140	0.360	3.209	3.517	0.572	0.970	0.970	0.924	1.471	1.176
2603	0004	45650	1.140	0.358	2.505	1.121	0.139	0.970	0.906	0.905	0.952	1.143
2604	0004	45650	1.140	0.361	2.504	1.510	0.230	0.970	0.969	0.926	1.696	1.178
2605	0004	45630	0.398	0.021	1.501	0.979	0.000	0.976	9.999	0.912	0.912	1.137
2606	0004	45630	0.398	0.020	1.501	0.980	0.020	0.976	9.999	0.925	0.925	1.139
2607	0004	45630	0.398	0.003	1.500	1.000	0.059	0.976	9.922	0.934	0.935	1.141
2608	0004	45630	0.398	0.016	1.499	0.971	0.000	0.977	9.999	0.916	0.916	1.150
2609	0004	45630	0.398	0.004	1.497	0.991	0.029	0.969	9.999	0.925	0.925	1.151
2610	0004	45630	0.398	0.015	1.497	1.008	0.059	0.969	1.186	0.931	0.937	1.154
2611	0004	45630	0.398	0.042	2.503	0.967	0.000	0.969	9.999	0.918	0.918	1.150
2612	0004	45630	0.398	0.056	2.498	0.988	0.029	0.972	9.999	0.931	0.931	1.155
2613	0004	45630	0.398	0.053	2.493	1.016	0.059	0.970	1.047	0.936	0.944	1.159
2614	0004	45630	0.398	0.046	3.008	0.960	0.000	0.971	9.999	0.918	0.918	1.157
2615	0004	45630	0.399	0.025	3.009	0.995	0.029	0.970	9.999	0.929	0.929	1.155
2616	0004	45630	0.398	0.055	3.011	1.031	0.059	0.970	0.908	0.933	0.943	1.160
2617	0004	45630	0.398	0.055	3.311	0.924	0.000	0.970	9.999	0.923	0.923	1.163
2618	0004	45630	0.398	0.036	3.260	0.996	0.029	0.970	9.999	0.936	0.936	1.162
2619	0004	45630	0.398	0.058	3.286	1.048	0.059	0.971	0.800	0.937	0.969	1.165
2620	0004	45630	0.398	0.055	3.502	0.967	0.000	0.967	9.999	0.919	0.919	1.149
2621	0004	45630	0.399	0.057	2.501	1.016	0.059	0.971	1.051	0.932	0.940	1.157
2622	0004	45650	1.140	0.005	1.501	1.120	0.267	0.975	1.011	0.929	1.063	1.158
2623	0004	45650	1.140	0.010	1.498	1.519	0.535	0.978	0.986	0.934	1.442	1.192
2624	0004	45650	1.140	0.015	1.498	2.013	0.723	0.978	0.967	0.936	1.808	1.193
2625	0004	45650	1.140	0.045	1.503	2.516	0.903	0.977	0.968	0.940	2.171	1.192
2626	0004	45650	1.140	0.055	1.505	3.015	1.083	0.975	0.968	0.945	2.547	1.194
2627	0004	45650	1.140	0.053	1.501	2.516	1.266	0.976	0.969	0.946	2.932	1.196
2628	0004	45650	1.140	0.036	1.499	1.117	0.101	0.969	1.011	0.938	1.012	1.172
2629	0004	45650	1.140	0.053	2.001	1.523	0.388	0.969	0.986	0.938	1.227	1.198
2630	0004	45650	1.140	0.040	1.856	2.017	0.526	0.969	0.966	0.940	1.437	1.199
2631	0004	45650	1.140	0.051	1.999	2.516	0.655	0.969	0.964	0.941	1.642	1.197
2632	0004	45650	1.140	0.053	1.998	3.017	0.787	0.969	0.969	0.947	1.862	1.201
2633	0004	45650	1.140	0.056	1.999	3.516	0.917	0.968	0.969	0.945	2.068	1.199
2634	0004	45650	1.140	0.035	2.501	1.118	0.155	0.969	1.016	0.939	0.992	1.171
2635	0004	45650	1.140	0.040	2.499	1.520	0.310	0.970	0.987	0.938	1.142	1.193
2636	0004	45650	1.140	0.055	2.500	2.017	0.419	0.970	0.966	0.940	1.290	1.194
2637	0004	45650	1.140	0.050	2.514	2.517	0.521	0.967	0.967	0.941	1.433	1.191
2638	0004	45650	1.140	0.057	2.504	3.018	0.627	0.969	0.966	0.947	1.589	1.195
2639	0004	45650	1.140	0.057	2.495	3.515	0.732	0.972	0.969	0.945	1.737	1.197

FACILITY ...ZI PROGRAM CD31 — MAIN-STREAM

NOZZLE TYPE — PLUG CONFIGURATIONS — SUPPRESSOR CONFIGURATION

DIAL FLOW (FAA) — FORWARD PLUG WITH BLEED — 30-SPOKE, AREA RATIO = 1.75

OUTER RADIUS RATIO 0.0000 — INNER RADIUS RATIO 0.7780 — DVD 1.2480

PRG	PARAMETERS														
PRG	CF	MACH	O2	M8	STG/FS	PT1/PA	OMEGAT	DCS	CDS	DCSH	CDSH	DCPL,O	DCPL,I	DCTOT	PSUR/PA
2595	0004	45650	1.140	0.360	3.224	1.172	0.092	-0.061	0.466	-0.005	0.036	-0.070	0.010	-0.076	0.763
2596	0004	45650	1.140	0.360	3.177	1.527	0.236	-0.057	0.473	-0.004	0.036	-0.017	0.011	-0.067	0.760
2597	0004	45650	1.140	0.359	3.290	1.123	0.089	-0.059	0.458	-0.005	0.036	-0.020	0.011	-0.072	0.768
2598	0004	45650	1.140	0.359	3.239	1.526	0.234	-0.055	0.467	-0.004	0.035	-0.016	0.011	-0.065	0.763
2599	0004	45650	1.140	0.359	3.204	2.034	0.328	-0.051	0.469	-0.004	0.037	-0.015	0.007	-0.063	0.763
2600	0004	45650	1.140	0.360	3.205	2.531	0.408	-0.046	0.463	-0.004	0.035	-0.012	0.003	-0.059	0.764
2601	0004	45650	1.140	0.360	3.205	3.028	0.490	-0.043	0.460	-0.003	0.036	-0.010	0.006	-0.050	0.765
2602	0004	45650	1.140	0.360	3.200	3.517	0.572	-0.040	0.455	-0.003	0.034	-0.008	-0.001	-0.052	0.766
2603	0004	45650	1.140	0.358	2.505	1.121	0.139	-0.079	0.430	-0.007	0.036	-0.003	0.008	-0.081	0.783
2604	0004	45650	1.140	0.361	2.508	3.510	0.779	-0.012	0.396	-0.004	0.034	0.002	-0.001	-0.045	0.798
2605	0004	45650	0.398	0.071	1.501	0.979	0.000	-0.045	37.181	-0.001	0.431	-0.015	0.008	-0.073	0.933
2606	0004	45650	0.398	0.072	1.501	0.993	0.026	-0.041	0.000	-0.001	0.009	-0.013	0.005	-0.070	0.936
2607	0004	45650	0.398	0.073	1.500	1.000	0.056	-0.036	12402.873	-0.001	38.144	-0.012	0.006	-0.069	0.936
2608	0004	45650	0.398	0.074	1.498	0.993	0.000	-0.041	417.279	-0.001	1.077	-0.014	0.006	-0.070	0.888
2609	0004	45650	0.398	0.074	1.497	0.991	0.025	-0.039	808.149	-0.001	31.635	-0.012	0.002	-0.070	0.892
2610	0004	45650	0.398	0.075	1.497	1.008	0.056	-0.037	419.615	-0.001	1.947	-0.011	0.004	-0.065	0.895
2611	0004	45650	0.398	0.042	2.505	0.987	0.000	-0.057	21.362	-0.000	0.182	-0.009	0.003	-0.064	0.850
2612	0004	45650	0.398	0.054	2.499	0.998	0.029	-0.055	12.413	-0.000	0.053	-0.006	0.001	-0.060	0.856
2613	0004	45650	0.398	0.053	2.493	1.016	0.059	-0.055	12.780	-0.000	0.100	-0.006	0.004	-0.057	0.857
2614	0004	45650	0.398	0.046	3.008	0.940	0.000	-0.051	20.800	-0.000	0.078	-0.026	0.009	-0.068	0.825
2615	0004	45650	0.398	0.025	3.009	0.995	0.029	-0.051	72.488	-0.001	0.876	-0.023	0.004	-0.070	0.826
2616	0004	45650	0.398	0.055	3.011	1.031	0.059	-0.050	14.241	-0.000	0.035	-0.021	0.005	-0.066	0.829
2617	0004	45650	0.398	0.055	3.311	0.924	0.000	-0.019	12.609	-0.000	0.049	-0.024	0.013	-0.050	0.848
2618	0004	45650	0.398	0.054	3.309	0.996	0.029	-0.048	25.530	-0.000	0.227	-0.022	0.007	-0.055	0.846
2619	0004	45650	0.398	0.058	3.298	1.048	0.059	-0.040	11.741	-0.000	0.037	-0.020	0.007	-0.053	0.846
2620	0004	45650	0.398	0.055	3.502	0.962	0.000	-0.037	12.624	0.000	-0.006	-0.010	0.003	-0.064	0.851
2621	0004	45650	0.398	0.052	2.503	1.016	0.059	-0.054	13.560	0.000	-0.000	-0.006	0.004	-0.056	0.858
2622	0004	45650	1.140	0.025	1.501	1.123	0.267	-0.054	606.353	-0.001	8.365	-0.011	0.009	-0.057	0.936
2623	0004	45650	1.140	0.010	1.498	1.519	0.535	-0.040	170.072	-0.001	3.626	-0.009	0.009	-0.042	0.936
2624	0004	45650	1.140	0.015	1.499	2.011	0.723	-0.032	71.782	-0.001	2.153	-0.007	0.002	-0.039	0.935
2625	0004	45650	1.140	0.045	1.503	2.516	0.903	-0.027	8.087	-0.000	0.089	-0.005	-0.003	-0.035	0.936
2626	0004	45650	1.140	0.055	1.505	3.015	1.083	-0.022	5.092	-0.000	0.023	-0.003	0.002	-0.024	0.939
2627	0004	45650	1.140	0.053	1.501	2.516	1.266	-0.018	5.298	-0.000	0.062	-0.003	0.002	-0.020	0.941
2628	0004	45650	1.140	0.054	1.498	2.517	0.451	-0.053	20.140	-0.001	0.201	-0.011	0.009	-0.056	0.895
2629	0004	45650	1.140	0.053	2.001	1.523	0.388	-0.044	9.398	-0.000	0.105	-0.009	0.009	-0.044	0.895
2630	0004	45650	1.140	0.040	1.996	2.017	0.525	-0.038	11.006	-0.000	0.070	-0.008	0.003	-0.043	0.894
2631	0004	45650	1.140	0.051	1.999	2.514	0.655	-0.033	10.324	-0.000	0.092	-0.007	0.000	-0.040	0.895
2632	0004	45650	1.140	0.053	1.998	3.012	0.782	-0.028	8.938	-0.000	0.068	-0.005	0.001	-0.032	0.900
2633	0004	45650	1.140	0.056	1.999	3.516	0.917	-0.024	7.640	-0.000	0.120	-0.004	0.001	-0.027	0.904
2634	0004	45650	1.140	0.025	2.502	1.119	0.154	-0.052	54.802	-0.000	0.489	-0.007	0.006	-0.053	0.856
2635	0004	45650	1.140	0.040	2.499	1.520	0.310	-0.044	23.646	-0.000	0.245	-0.006	0.007	-0.046	0.853
2636	0004	45650	1.140	0.055	2.500	2.017	0.466	-0.041	12.346	-0.000	0.023	-0.006	0.004	-0.043	0.853
2637	0004	45650	1.140	0.049	2.514	2.517	0.521	-0.036	10.630	-0.000	0.068	-0.004	0.002	-0.039	0.856
2638	0004	45650	1.140	0.057	2.506	3.018	0.627	-0.032	10.891	-0.000	0.119	-0.003	0.002	-0.033	0.860
2639	0004	45650	1.140	0.057	2.495	3.515	0.732	-0.028	10.275	-0.000	0.102	-0.001	-0.001	-0.030	0.868

FACILITY NAME PROGRAM CODE

NOZZLE TYPE: DUAL FLOW (FAA)

IN-STREAM PLUG CONFIGURATIONS: FORWARD PLUG WITH BLEED

SUPPRESSOR CONFIGURATION: 30-SPOKE, AREA RATIO = 1.75

THRUST PARAMETERS — OUTER RADIUS RATIO: 0.0000 — INNER RADIUS RATIO: 0.7790 — OVD: 1.2480

ADC	CF	AREA	M2	M8	RTO/P8	RTI/P8	CNECAT	CDO	CDI	CFNET1	CFNET2	F9
7840	CC04	45650	1.140	0.055	3.011	1.119	0.120	0.971	0.954	0.939	0.978	1.172
7841	CC04	45650	1.140	0.056	3.013	1.521	0.256	0.969	0.983	0.939	1.095	1.191
7842	CC04	45650	1.140	0.055	3.004	2.016	0.349	0.970	0.968	0.940	1.209	1.193
7843	CC04	45650	1.140	0.058	3.008	2.516	0.434	0.971	0.968	0.942	1.322	1.194
7844	CC04	45650	1.140	0.063	3.009	3.019	0.521	0.971	0.969	0.945	1.438	1.195
7845	CC04	45650	1.140	0.063	3.009	3.516	0.607	0.971	0.969	0.941	1.545	1.192
7846	CC04	45650	1.140	0.055	3.317	1.120	0.101	0.970	0.875	0.943	0.974	1.174
7847	CC04	45650	1.140	0.056	3.296	1.520	0.231	0.970	0.972	0.945	1.081	1.196
7848	CC04	45650	1.140	0.050	3.282	2.013	0.318	0.971	0.966	0.945	1.184	1.198
7849	CC04	45650	1.140	0.063	3.276	2.515	0.398	0.971	0.967	0.946	1.284	1.196
7850	CC04	45650	1.140	0.065	3.280	3.023	0.478	0.971	0.968	0.948	1.388	1.198
7851	CC04	45650	1.140	0.061	3.273	3.515	0.555	0.971	0.969	0.941	1.475	1.193
7852	CC04	45650	1.140	0.036	2.500	1.117	0.153	0.970	1.015	0.943	0.996	1.175
7853	CC04	45650	1.140	0.041	2.498	1.507	0.731	0.970	0.969	0.947	1.738	1.198

FACILITY NAME PROGRAM CODE

NOZZLE TYPE: DUAL FLOW (FAA)

IN-STREAM PLUG CONFIGURATIONS: FORWARD PLUG WITH BLEED

SUPPRESSOR CONFIGURATION: 30-SPOKE, AREA RATIO = 1.75

DRAG PARAMETERS — OUTER RADIUS RATIO: 0.0000 — INNER RADIUS RATIO: 0.7790 — OVD: 1.2480

ADC	CF	AREA	M2	M8	RTO/P8	RTI/P8	CNECAT	DCS	COS	DCSH	COSH	DCPL.O	DCPL.I	DCTOT	PSUP/PA
7840	CC04	45650	1.140	0.055	3.011	1.119	0.120	-0.048	14.548	-0.000	0.062	-0.020	0.007	-0.061	0.830
7841	CC04	45650	1.140	0.056	3.013	1.521	0.256	-0.043	13.762	-0.000	0.042	-0.015	0.008	-0.054	0.829
7842	CC04	45650	1.140	0.055	3.004	2.016	0.349	-0.039	14.455	-0.000	0.076	-0.017	0.004	-0.052	0.829
7843	CC04	45650	1.140	0.058	3.008	2.516	0.434	-0.036	12.627	-0.000	0.051	-0.015	0.003	-0.048	0.830
7844	CC04	45650	1.140	0.063	3.009	3.019	0.521	-0.032	10.568	-0.000	0.058	-0.012	0.004	-0.040	0.836
7845	CC04	45650	1.140	0.063	3.009	3.516	0.607	-0.028	10.110	-0.000	0.044	-0.010	-0.003	-0.041	0.842
7846	CC04	45650	1.140	0.055	3.317	1.120	0.101	-0.038	12.745	-0.000	0.013	-0.019	0.009	-0.048	0.848
7847	CC04	45650	1.140	0.056	3.296	1.520	0.231	-0.035	13.323	-0.000	0.076	-0.017	0.009	-0.043	0.846
7848	CC04	45650	1.140	0.050	3.282	2.013	0.318	-0.032	15.796	-0.000	0.129	-0.018	0.005	-0.043	0.844
7849	CC04	45650	1.140	0.063	3.276	2.515	0.398	-0.030	9.886	-0.000	0.035	-0.014	0.003	-0.040	0.845
7850	CC04	45650	1.140	0.065	3.280	3.023	0.478	-0.027	9.191	-0.000	0.046	-0.012	0.006	-0.033	0.847
7851	CC04	45650	1.140	0.061	3.273	3.515	0.555	-0.025	10.363	-0.000	0.078	-0.011	-0.002	-0.038	0.849
7852	CC04	45650	1.140	0.036	2.500	1.117	0.153	-0.052	28.650	-0.000	0.151	-0.006	0.007	-0.052	0.856
7853	CC04	45650	1.140	0.041	2.498	1.507	0.731	-0.028	9.038	-0.000	0.060	-0.001	-0.001	-0.030	0.868

MODEL SC-6, 40 SHALLOW CHUTES, AR = 1.75, BASELINE PLUG

FAC .IFT * PROGRAM CALL ...

NOZZLE TYPE — IN -STREAM
DUAL FLOW (CAL) — PLUG CONFIGURATIONS — SUPPRESSOR CONFIGURATION
PASELINE PLUG MIN BLEED — 60-SPACE, AREA RATIO = 1.75

INLET PARAMETERS — FIXED RADIUS RATIO 0.3870 — INNER RADIUS RATIO 0.7790 — DVD 1.2480

ERR	FI	VFSA	PI	MI	BETAPS	BETAPD	TURBAI	CFD	CDI	CFMFT1	CFMFT2	F9
1732	0004	44550	0.198	3.021	1.433	0.580	0.000	0.896	0.896	0.896	0.895	1.130
1733	0004	44550	0.198	0.014	1.461	1.000	0.079	0.905	0.909	0.904	0.904	1.131
1734	0004	44550	0.198	0.011	1.494	1.014	0.049	0.905	0.554	0.908	0.919	1.133
1735	0004	44550	0.198	3.020	2.005	0.998	0.000	0.565	0.909	0.896	0.896	1.134
1736	0004	44550	0.198	0.016	2.005	1.007	0.079	0.915	0.565	0.904	0.907	1.135
1737	0004	44550	0.198	0.020	2.004	1.028	0.049	0.914	0.535	0.906	0.918	1.136
1738	0004	44550	0.198	0.042	2.033	0.575	0.000	0.906	0.909	0.898	0.898	1.132
1739	0004	44550	0.198	0.021	2.004	1.005	0.079	0.905	0.910	0.906	0.909	1.133
1740	0004	44550	0.198	0.041	2.019	1.039	0.049	0.905	0.678	0.909	0.921	1.135
1741	0004	44550	0.198	0.052	2.011	0.991	0.000	0.906	0.909	0.908	0.908	1.136
1742	0004	44550	0.198	0.054	2.014	1.007	0.079	0.906	0.915	0.914	0.919	1.137
1743	0004	44550	0.198	0.062	2.011	1.004	0.059	0.906	0.568	0.916	0.931	1.140
1744	0004	44550	0.198	0.060	2.004	1.011	0.059	0.905	0.909	0.916	0.916	1.142
1745	0004	44550	0.198	0.064	2.009	1.000	0.029	0.904	0.554	0.923	0.933	1.145
1746	0004	44550	0.198	0.064	2.039	1.017	0.049	0.906	0.539	0.925	0.942	1.147
1747	0004	44550	0.198	0.053	2.022	0.975	0.000	0.914	0.909	0.894	0.894	1.128
1748	0004	44550	0.198	0.063	2.043	1.004	0.049	0.905	0.680	0.907	0.918	1.134
1749	0004	44550	1.140	0.017	1.402	1.123	0.231	0.982	0.883	0.923	1.040	1.151
1750	0004	44550	1.140	0.050	1.404	1.565	0.227	0.942	0.978	0.930	1.429	1.189
1751	0004	44550	1.140	0.040	1.431	2.019	0.295	0.982	0.993	0.928	1.035	1.197
1752	0004	44550	1.140	0.044	1.404	2.022	0.217	0.970	0.996	0.933	2.172	1.198
1753	0004	44550	1.140	0.048	1.405	1.021	0.000	0.958	0.996	0.928	2.521	1.194
1754	0004	44550	1.140	0.052	1.433	2.018	0.287	0.979	0.995	0.941	2.975	1.215
1755	0004	44550	1.140	0.031	1.404	1.122	0.158	0.957	0.821	0.913	0.974	1.148
1756	0004	44550	1.140	0.050	1.404	1.524	0.281	0.974	0.965	0.920	1.198	1.180
1757	0004	44550	1.140	0.049	1.431	2.015	0.337	0.965	0.993	0.921	1.418	1.189
1758	0004	44550	1.140	0.052	1.401	1.521	0.172	0.956	0.993	0.925	1.732	1.190
1759	0004	44550	1.140	0.044	1.404	1.020	0.057	0.965	0.994	0.926	1.843	1.192
1760	0004	44550	1.140	0.054	1.433	1.514	0.343	0.965	0.995	0.942	2.080	1.207
1761	0004	44550	1.140	0.040	1.401	1.122	0.174	0.967	0.820	0.914	0.958	1.146
1762	0004	44550	1.140	0.048	1.433	1.520	0.202	0.975	0.963	0.918	1.112	1.171
1763	0004	44550	1.140	0.053	1.401	1.016	0.120	0.956	0.991	0.917	1.266	1.178
1764	0004	44550	1.140	0.051	1.404	1.520	0.236	0.962	0.980	0.923	1.419	1.180
1765	0004	44550	1.140	0.047	1.431	1.014	0.046	0.965	0.965	0.911	1.566	1.172
1766	0004	44550	1.140	0.043	1.404	1.524	0.251	0.956	0.995	0.934	1.739	1.195
1767	0004	44550	1.140	0.051	1.433	1.013	0.084	0.967	0.674	0.917	0.966	1.143
1768	0004	44550	1.140	0.049	1.401	1.518	0.245	0.967	0.963	0.919	1.064	1.168
1769	0004	44550	1.140	0.038	1.401	1.016	0.157	0.967	0.992	0.917	1.185	1.175
1770	0004	44550	1.140	0.046	1.431	1.517	0.444	0.967	0.993	0.913	1.290	1.170
1771	0004	44550	1.140	0.044	1.403	1.023	0.537	0.965	0.995	0.908	1.396	1.164
1772	0004	44550	1.140	0.042	1.404	1.520	0.425	0.966	0.995	0.925	1.537	1.184
1773	0004	44550	1.140	0.044	1.433	1.121	0.086	0.967	0.561	0.924	0.944	1.147
1774	0004	44550	1.140	0.058	1.397	1.523	0.218	0.934	0.915	0.921	1.069	1.167
1775	0004	44550	1.140	0.042	1.396	2.022	0.330	0.965	0.993	0.917	1.159	1.173
1776	0004	44550	1.140	0.042	1.715	2.518	0.418	0.966	0.994	0.913	1.258	1.169

FACILITY C1 PROGRAM C031 NOZZLE TYPE IN STREAM
DUAL FLOW (FAA) PLUG CONFIGURATIONS SUPPRESSOR CONFIGURATION
BASELINE PLUG WITH BLEED 40-SPOKE, AREA RATIO = 1.75

OUTER RADIUS RATIO 0.0000 INNER RADIUS RATIO 0.7790 OVD 1.2480

DFAC PARAMETERS

RPG	CF	MASA	M2	MA	PT0/PA	PT1/P1	GMFGAT	FNF	FNS	DCSH	CDSH	DCPL,0	DCPL,T	DCTOT	PSUP/PA
1732	0006	46530	0.398	0.023	1.496	0.984	0.000	-0.006	49.070	-0.001	0.295	-0.015	0.006	-0.105	0.898
1733	0006	46530	0.398	0.014	1.495	1.000	0.029	-0.005	122.844	-0.001	1.433	-0.013	0.003	-0.105	0.899
1734	0006	46530	0.398	0.011	1.496	1.014	0.059	-0.332	202.104	-0.001	1.774	-0.011	0.001	-0.102	0.901
1735	0006	46530	0.398	0.029	2.005	0.986	0.000	-0.004	5[illegible]49	-0.001	0.324	-0.013	0.009	-0.099	0.823
1736	0006	46530	0.398	0.034	2.006	1.007	0.029	-0.002	37.863	-0.001	0.232	-0.010	0.006	-0.097	0.826
1737	0006	46530	0.398	0.027	2.004	1.028	0.059	-0.000	56.725	-0.001	0.337	-0.009	0.003	-0.096	0.830
1738	0006	46530	0.398	0.052	2.004	0.975	0.000	-0.007	33.849	-0.000	0.040	-0.014	0.010	-0.101	0.741
1739	0006	46530	0.398	0.035	2.005	1.005	0.029	-0.004	52.656	-0.001	0.286	-0.011	0.007	-0.098	0.749
1740	0006	46530	0.398	0.051	2.010	1.029	0.059	-0.000	23.832	-0.000	0.055	-0.009	0.004	-0.095	0.757
1741	0006	46530	0.398	0.053	3.011	0.993	0.000	-0.008	24.521	-0.000	0.072	-0.031	0.010	-0.100	0.729
1742	0006	46530	0.398	0.056	3.014	1.037	0.029	-0.008	23.166	-0.000	0.097	-0.029	0.008	-0.099	0.729
1743	0006	46530	0.398	0.052	3.011	1.080	0.059	-0.007	24.558	-0.000	0.089	-0.026	0.006	-0.097	0.729
1744	0006	46530	0.398	0.050	3.006	1.011	0.000	-0.001	23.896	-0.000	0.144	-0.036	0.010	-0.087	0.761
1745	0006	46530	0.398	0.038	3.009	1.060	0.029	-0.000	17.782	-0.000	0.083	-0.032	0.007	-0.085	0.767
1746	0006	46530	0.398	0.044	3.006	1.112	0.059	-0.000	20.451	-0.000	0.121	-0.028	0.005	-0.083	0.[illegible]
1747	0006	46530	0.398	0.052	2.527	0.975	0.000	-0.007	24.134	-0.000	0.104	-0.013	0.012	-0.099	0.[illegible]
1748	0006	46530	0.398	0.052	2.508	1.038	0.059	-0.000	22.695	-0.000	0.099	-0.008	0.005	-0.094	0.757
1749	0006	46550	1.140	0.037	1.502	1.123	0.233	-0.077	17.550	-0.001	0.114	-0.005	0.001	-0.082	0.907
1750	0006	46550	1.140	0.050	1.494	1.515	0.527	-0.[illegible]	9.000	-0.000	0.030	-0.003	-0.000	-0.059	0.909
1751	0006	46550	1.140	0.050	1.504	2.315	0.735	-0.[illegible]	9.211	-0.000	0.042	-0.002	-0.021	-0.068	0.908
1752	0006	46550	1.140	0.045	1.508	2.522	0.617	-0.007	11.429	-0.000	0.052	-0.002	-0.018	-0.057	0.908
1753	0006	46550	1.140	0.046	1.508	3.321	1.049	-0.[illegible]	10.641	-0.000	0.103	-0.001	-0.035	-0.067	0.909
1754	0006	46550	1.140	0.052	1.505	3.514	1.287	-0.[illegible]	7.966	-0.000	0.041	0.000	-0.032	-0.058	0.913
1755	0006	46550	1.140	0.031	1.998	1.122	0.158	-0.[illegible]92	74.520	-0.001	0.647	-0.005	0.003	-0.085	0.836
1756	0006	46550	1.140	0.050	2.001	1.526	0.381	-0.[illegible]	15.751	-0.000	0.071	-0.003	-0.000	-0.068	0.841
1757	0006	46550	1.140	0.052	1.998	2.315	0.537	-0.[illegible]	14.957	-0.000	0.058	-0.002	-0.018	-0.076	0.841
1758	0006	46550	1.140	0.052	2.003	2.521	0.672	-0.[illegible]	14.805	-0.000	0.124	-0.002	-0.019	-0.069	0.842
1759	0006	46550	1.140	0.054	1.999	3.320	0.807	-0.[illegible]	13.486	-0.000	0.130	-0.001	-0.020	-0.062	0.845
1760	0006	46550	1.140	0.046	2.000	3.518	0.940	-0.[illegible]	12.982	-0.000	0.127	0.000	-0.025	-0.061	0.850
1761	0006	46550	1.140	0.040	2.504	1.122	0.126	-0.[illegible]	37.251	-0.001	0.308	-0.006	0.003	-0.089	0.765
1762	0006	46550	1.140	0.053	2.505	1.529	0.302	-0.[illegible]	17.158	-0.000	0.066	-0.004	0.001	-0.073	0.773
1763	0006	46550	1.140	0.051	2.502	2.316	0.429	-0.[illegible]	20.225	-0.000	0.096	-0.004	-0.014	-0.080	0.772
1764	0006	46550	1.140	0.051	2.508	2.520	0.535	-0.[illegible]	21.972	-0.000	0.168	-0.003	-0.018	-0.077	0.773
1765	0006	46550	1.140	0.057	2.504	3.318	0.644	-0.[illegible]	17.421	-0.000	0.154	-0.002	-0.030	-0.083	0.776
1766	0006	46550	1.140	0.043	2.506	3.524	0.753	-0.[illegible]	13.474	-0.000	0.101	-0.001	-0.018	-0.063	0.784
1767	0006	46550	1.140	0.053	3.010	1.123	0.086	-0.[illegible]	24.017	-0.000	0.133	-0.023	0.004	-0.096	0.730
1768	0006	46550	1.140	0.058	3.009	1.518	0.245	-0.[illegible]	20.134	-0.000	0.130	-0.009	-0.001	-0.077	0.731
1769	0006	46550	1.140	0.058	3.001	2.316	0.357	-0.[illegible]	19.730	-0.000	0.110	-0.007	-0.016	-0.083	0.732
1770	0006	46550	1.140	0.056	3.008	2.517	0.446	-0.[illegible]	19.992	-0.000	0.175	-0.007	-0.021	-0.083	0.732
1771	0006	46550	1.140	0.065	3.006	3.323	0.537	-0.[illegible]	15.732	-0.000	0.125	-0.004	-0.025	-0.080	0.735
1772	0006	46550	1.140	0.064	3.005	3.520	0.625	-0.[illegible]	14.251	-0.000	0.100	-0.002	-0.017	-0.065	0.741
1773	0006	46550	1.140	0.055	3.330	1.123	0.066	-0.[illegible]	19.973	-0.001	0.173	-0.029	0.004	-0.085	0.741
1774	0006	46550	1.140	0.058	3.292	1.523	0.219	-0.[illegible]	17.841	-0.000	0.126	-0.015	-0.008	-0.077	0.759
1775	0006	46550	1.140	0.062	3.255	2.022	0.330	-0.[illegible]	16.749	-0.000	0.115	-0.012	-0.015	-0.078	0.755
1776	0006	46550	1.140	0.062	3.216	2.513	0.418	-0.[illegible]	16.448	-0.000	0.136	-0.010	-0.023	-0.081	0.750

FACILITY XI [illegible] CELL — IN-STREAM

NOZZLE TYPE — PLUG CONFIGURATIONS — SUPPRESSOR CONFIGURATION

FULL FLOW (FAA) — BASELINE PLUG WITH BLEED — 40-SPOKE, AREA RATIO = 1.75

THRUST PARAMETERS — OUTER RADIUS RATIO 0.0030 — INNER RADIUS RATIO 0.7790 — OVD 1.2480

PDC	FF	WAGE	PJ	PS	PTO/PJ	PTJ/PA	CVFGAT	CDD	CDI	CFNET1	CFNET2	FG
1177	0004	44440	1.140	0.440	3.143	3.020	0.512	0.965	0.994	0.909	1.368	1.167
1178	0004	44440	1.140	0.447	3.047	3.519	0.510	0.964	0.995	0.924	1.514	1.181
1179	0004	44440	1.141	0.449	2.512	1.172	0.176	0.966	0.823	0.913	0.955	1.144
1180	0004	44440	1.140	0.450	2.532	3.514	0.750	0.964	0.995	0.933	1.734	1.194
1181	0004	44440	0.198	0.446	1.502	1.001	0.000	0.936	0.000	0.819	0.819	1.096
1182	0004	44440	0.198	0.447	1.504	1.015	0.029	0.991	0.319	0.826	0.830	1.097
1183	0004	44440	0.198	0.447	1.501	1.024	0.059	0.991	0.484	0.835	0.848	1.100
1184	0004	44440	0.198	0.447	2.005	1.003	0.000	0.964	0.000	0.844	0.844	1.097
1185	0004	44440	0.198	0.447	2.004	1.025	0.029	0.965	0.331	0.851	0.856	1.099
1186	0004	44440	0.198	0.446	2.001	1.047	0.059	0.965	0.492	0.856	0.869	1.102
1187	0004	44440	0.198	0.447	2.513	0.996	0.000	0.966	0.000	0.855	0.855	1.097
1188	0004	44440	0.198	0.447	2.504	1.026	0.029	0.967	0.410	0.864	0.868	1.101
1189	0004	44440	0.198	0.447	2.495	1.060	0.059	0.973	0.566	0.871	0.885	1.110
1190	0004	44440	0.198	0.447	3.004	1.005	0.000	0.966	0.000	0.877	0.877	1.105
1191	0004	44440	0.198	0.448	3.001	1.031	0.029	0.965	0.298	0.882	0.889	1.106
1192	0004	44440	0.198	0.447	3.001	1.122	0.059	0.965	0.461	0.884	0.902	1.109
1193	0004	44440	0.198	0.448	3.193	1.042	0.000	0.966	0.000	0.891	0.891	1.115
1194	0004	44440	0.198	0.448	3.175	1.096	0.029	0.966	0.286	0.897	0.904	1.118
1195	0004	44440	0.198	0.447	3.181	1.140	0.059	0.965	0.461	0.898	0.918	1.120
1196	0004	44440	0.198	0.447	2.517	0.994	0.000	0.964	0.999	0.853	0.853	1.095
1197	0004	44440	0.198	0.447	2.513	1.059	0.059	0.955	0.551	0.866	0.880	1.101
1198	0004	44440	1.140	0.444	1.502	1.121	0.210	0.990	0.807	0.853	0.950	1.116
1199	0004	44440	1.140	0.444	1.503	1.519	0.215	0.991	0.966	0.882	1.342	1.162
1200	0004	44440	1.140	0.447	1.501	2.020	0.731	0.993	0.992	0.892	1.753	1.174
1201	0004	44440	1.141	0.444	1.504	2.522	0.910	0.990	0.993	0.904	2.098	1.179
1202	0004	44440	1.140	0.446	1.507	3.028	1.094	0.987	0.993	0.903	2.449	1.176
1203	0004	44440	1.140	0.446	1.504	3.531	1.279	0.989	0.994	0.920	2.897	1.197
1204	0004	44440	1.140	0.445	1.979	1.121	0.141	0.965	0.732	0.869	0.921	1.116
1205	0004	44440	1.140	0.447	2.001	1.523	0.373	0.954	0.947	0.883	1.145	1.150
1206	0004	44440	1.141	0.446	1.996	2.014	0.537	0.966	0.991	0.892	1.374	1.166
1207	0004	44440	1.140	0.447	2.003	2.524	0.672	0.965	0.992	0.899	1.586	1.169
1208	0004	44440	1.140	0.447	2.005	3.010	0.806	0.955	0.993	0.895	1.778	1.164
1209	0004	44440	1.141	0.447	2.008	3.527	0.939	0.964	0.995	0.921	2.041	1.187
1210	0004	44440	1.140	0.446	2.513	1.127	0.113	0.965	0.719	0.878	0.915	1.113
1211	0004	44440	1.140	0.447	2.501	1.521	0.296	0.954	0.941	0.888	1.072	1.144
1212	0004	44440	1.141	0.447	2.505	2.011	0.427	0.964	0.991	0.892	1.229	1.155
1213	0004	44440	1.140	0.448	2.507	2.520	0.535	0.966	0.993	0.899	1.381	1.161
1214	0004	44440	1.140	0.447	2.504	3.027	0.673	0.966	0.994	0.890	1.509	1.163
1215	0004	44440	1.140	0.448	2.507	3.526	0.751	0.965	0.995	0.916	1.703	1.177
1216	0004	44440	1.140	0.448	3.038	1.124	0.086	0.952	0.4978	0.886	0.905	1.109
1217	0004	44440	1.141	0.447	3.208	1.521	0.232	0.964	0.889	0.892	1.026	1.137
1218	0004	44440	1.140	0.447	3.009	2.016	0.354	0.966	0.986	0.893	1.153	1.152
1219	0004	44440	1.140	0.448	3.022	2.518	0.446	0.957	0.994	0.890	1.256	1.150
1220	0004	44440	1.141	0.444	3.014	3.023	0.534	0.962	0.994	0.868	1.351	1.145
1221	0004	44440	1.140	0.449	3.025	3.533	0.623	0.965	0.993	0.905	1.501	1.163

...ACILITY ... NAL PROGRAM COST

NOZZLE TYPE — IN... -STREAM
PI CONFIGURATIONS — SUPPRESSOR CONFIGURATION
NOZZLE FLOW (FAA) — BASELINE PLUG WITH BLEED — 40-SPOKE, AREA RATIO = 1.75

OUTER RADIUS RATIO 0.0000 — INNER RADIUS RATIO 0.7790 — DVO 1.2480

ROW	PARAMETERS														
ERC	EE	MASA	M2	M8	PTT/PA	PT1/PA	OMEGAT	DCS	CDS	DCSH	CDSH	DCPL,0	DCPL,T	DCTOT	PSUP/PA
1777	0004	46550	1.140	0.440	3.149	3.323	0.512	-0.046	17.879	-0.000	0.166	-0.007	-0.025	-0.078	0.745
1778	0004	46550	1.140	0.447	3.087	3.519	0.610	-0.044	14.584	-0.000	0.128	-0.003	-0.017	-0.064	0.742
1779	0004	46550	1.140	0.449	2.512	1.127	0.126	-0.094	24.631	-0.001	0.155	-0.006	0.004	-0.087	0.764
1780	0004	46550	1.140	0.449	2.502	3.514	0.750	-0.044	15.679	-0.001	0.183	-0.001	-0.018	-0.063	0.782
1781	0004	46550	0.398	0.445	1.502	1.301	0.000	-0.139	0.189	-0.015	0.020	-0.014	0.024	-0.143	0.850
1782	0004	46550	0.398	0.447	1.504	1.915	0.029	-0.134	0.193	-0.014	0.020	-0.010	0.022	-0.137	0.854
1783	0004	46550	0.398	0.447	1.503	1.924	0.059	-0.131	0.180	-0.015	0.020	-0.008	0.019	-0.135	0.856
1784	0004	46550	0.398	0.447	2.005	1.303	0.000	-0.127	0.299	-0.011	0.026	-0.009	0.019	-0.128	0.742
1785	0004	46550	0.398	0.447	2.006	1.325	0.029	-0.122	0.290	-0.011	0.026	-0.007	0.016	-0.124	0.749
1786	0004	46550	0.398	0.446	2.003	1.947	0.059	-0.118	0.283	-0.011	0.026	-0.005	0.013	-0.120	0.775
1787	0004	46550	0.398	0.447	2.510	0.995	0.000	-0.120	0.402	-0.009	0.028	-0.008	0.017	-0.120	0.679
1788	0004	46550	0.398	0.447	2.502	1.826	0.029	-0.117	0.393	-0.008	0.027	-0.005	0.013	-0.116	0.687
1789	0004	46550	0.398	0.447	2.495	1.348	0.059	-0.114	0.383	-0.008	0.027	-0.002	0.010	-0.114	0.694
1790	0004	46550	0.398	0.447	3.024	1.925	0.000	-0.091	0.339	-0.007	0.029	-0.030	0.015	-0.113	0.682
1791	0004	46550	0.398	0.446	3.023	1.871	0.029	-0.090	0.396	-0.007	0.029	-0.028	0.012	-0.113	0.683
1792	0004	46550	0.398	0.447	3.021	1.127	0.059	-0.089	0.337	-0.007	0.029	-0.026	0.009	-0.113	0.683
1793	0004	46550	0.398	0.448	3.320	1.042	0.000	-0.072	0.357	-0.006	0.030	-0.033	0.015	-0.096	0.714
1794	0004	46550	0.398	0.448	3.329	1.094	0.029	-0.071	0.356	-0.006	0.030	-0.030	0.011	-0.096	0.715
1795	0004	46550	0.398	0.447	3.331	1.150	0.059	-0.070	0.355	-0.006	0.030	-0.028	0.008	-0.095	0.717
1796	0004	46550	0.398	0.447	2.517	0.994	0.000	-0.120	0.404	-0.009	0.032	-0.008	0.017	-0.120	0.679
1797	0004	46550	0.398	0.447	2.510	1.359	0.059	-0.112	0.381	-0.009	0.030	-0.002	0.011	-0.112	0.696
1798	0004	46550	1.140	0.446	1.502	1.121	0.710	-0.111	0.169	-0.015	0.023	-0.001	0.014	-0.113	0.866
1799	0004	46550	1.140	0.446	1.499	1.519	0.515	-0.080	0.164	-0.011	0.022	0.002	0.010	-0.079	0.870
1800	0004	46550	1.140	0.446	1.501	2.320	0.731	-0.082	0.164	-0.009	0.023	0.001	-0.014	-0.085	0.870
1801	0004	46550	1.140	0.446	1.505	2.522	0.510	-0.082	0.164	-0.007	0.023	0.001	-0.012	-0.070	0.870
1802	0004	46550	1.140	0.446	1.507	3.028	1.094	-0.043	0.160	-0.006	0.023	0.002	-0.028	-0.075	0.873
1803	0004	46550	1.140	0.446	1.504	3.531	1.279	-0.037	0.157	-0.005	0.022	0.002	-0.026	-0.066	0.875
1804	0004	46550	1.140	0.445	1.998	1.121	0.141	-0.109	0.273	-0.012	0.030	-0.000	0.011	-0.110	0.784
1805	0004	46550	1.140	0.447	2.002	1.523	0.373	-0.085	0.259	-0.009	0.028	0.003	0.007	-0.084	0.794
1806	0004	46550	1.140	0.446	1.996	2.014	0.537	-0.071	0.259	-0.008	0.028	0.002	-0.014	-0.091	0.795
1807	0004	46550	1.140	0.447	2.003	2.524	0.472	-0.062	0.257	-0.007	0.028	0.002	-0.016	-0.083	0.795
1808	0004	46550	1.140	0.447	2.005	3.330	0.806	-0.064	0.251	-0.006	0.028	0.003	-0.027	-0.083	0.800
1809	0004	46550	1.140	0.448	2.009	3.527	0.939	-0.047	0.246	-0.005	0.027	0.004	-0.020	-0.069	0.803
1810	0004	46550	1.140	0.446	2.510	1.127	0.113	-0.106	0.371	-0.009	0.032	0.001	0.009	-0.105	0.705
1811	0004	46550	1.140	0.447	2.501	1.571	0.296	-0.038	0.351	-0.008	0.030	0.004	0.005	-0.086	0.720
1812	0004	46550	1.140	0.447	2.505	2.011	0.427	-0.076	0.349	-0.007	0.030	0.004	-0.011	-0.089	0.722
1813	0004	46550	1.140	0.448	2.507	2.520	0.535	-0.048	0.346	-0.006	0.030	0.004	-0.015	-0.085	0.722
1814	0004	46550	1.140	0.447	2.509	3.027	0.643	-0.050	0.341	-0.005	0.030	0.004	-0.030	-0.091	0.728
1815	0004	46550	1.140	0.448	2.507	3.526	0.751	-0.054	0.331	-0.005	0.029	0.005	-0.011	-0.065	0.735
1816	0004	46550	1.140	0.443	3.038	1.124	0.064	-0.038	0.393	-0.008	0.034	-0.026	0.009	-0.113	0.695
1817	0004	46550	1.140	0.447	3.009	1.521	0.232	-0.079	0.390	-0.006	0.032	-0.013	0.001	-0.097	0.688
1818	0004	46550	1.140	0.447	3.008	2.016	0.354	-0.078	0.389	-0.005	0.031	-0.007	-0.014	-0.096	0.689
1819	0004	46550	1.140	0.448	3.022	2.518	0.444	-0.063	0.385	-0.005	0.031	-0.007	-0.023	-0.098	0.692
1820	0004	46550	1.140	0.449	3.036	3.029	0.534	-0.058	0.383	-0.004	0.029	-0.005	-0.027	-0.094	0.692
1821	0004	46550	1.140	0.449	3.026	3.533	0.623	-0.053	0.380	-0.004	0.029	-0.001	-0.014	-0.074	0.694

FACILITY XE PROGRAM C231 — F- -STREAM

NOZZLE TYPE — PL. CONFIGURATIONS — SUPPRESSOR CONFIGURATION

DUAL FLOW (FAA) — BASELINE PLUG WITH BLEED — 40-SPOKE, AREA RATIO = 1.75

THRUST PARAMETERS — OUTER RADIUS RATIO 0.0000 — INNER RADIUS RATIO 0.7790 — OVD 1.2480

PPP	CF	WASA	WP	WR	PTO/PS	PTI/PA	WFGAT	EDD	EDI	CFNET1	CFNET2	FG
1822	0006	46550	1.140	0.447	3.327	1.122	0.045	0.965	0.388X	0.899	0.913	1.120
1823	0006	46550	1.140	0.448	3.305	1.522	0.208	0.934	0.873	0.902	1.020	1.143
1824	0006	46550	1.140	0.449	3.303	2.016	0.323	0.966	0.985	0.897	1.127	1.153
1825	0006	46550	1.140	0.447	3.303	2.522	0.406	0.967	0.991	0.895	1.220	1.152
1826	0006	46550	1.140	0.449	3.327	3.029	0.485	0.966	0.993	0.895	1.314	1.152
1827	0006	46550	1.140	0.449	3.333	3.535	0.565	0.963	0.991	0.908	1.432	1.163
1828	0006	46550	1.140	0.449	3.503	3.524	0.753	0.955	0.994	0.916	1.706	1.177
1829	0006	46530	0.398	0.357	1.506	0.999	0.000	0.481	0.999	0.836	0.836	1.104
1830	0006	46530	0.399	0.359	1.507	1.013	0.029	0.988	0.346	0.845	0.850	1.106
1831	0006	46530	0.398	0.359	1.507	1.026	0.059	0.998	0.487	0.853	0.867	1.109
1832	0006	46530	0.395	0.359	2.012	1.000	0.000	0.965	0.999	0.857	0.857	1.105
1833	0006	46530	0.398	0.361	2.012	1.022	0.029	0.965	0.360	0.862	0.867	1.107
1834	0006	46530	0.398	0.361	2.015	1.046	0.059	0.953	0.499	0.866	0.880	1.108
1835	0006	46530	0.393	0.361	2.525	0.991	0.000	0.963	0.999	0.863	0.863	1.102
1836	0006	46530	0.398	0.361	2.524	1.022	0.029	0.964	0.444	0.872	0.876	1.106
1837	0006	46530	0.398	0.361	2.523	1.056	0.059	0.964	0.565	0.875	0.889	1.108
1838	0006	46530	0.399	0.362	3.035	1.018	0.000	0.966	0.000	0.883	0.883	1.112
1839	0006	46530	0.398	0.360	3.007	1.054	0.029	0.955	0.314	0.890	0.897	1.114
1840	0006	46530	0.398	0.360	3.013	1.115	0.059	0.966	0.475	0.894	0.912	1.118
1841	0006	46530	0.398	0.361	3.295	1.036	0.000	0.966	0.000	0.896	0.896	1.120
1842	0006	46530	0.399	0.360	3.295	1.090	0.029	0.955	0.291	0.902	0.910	1.123
1843	0006	46530	0.398	0.361	3.287	1.143	0.059	0.962	0.463	0.908	0.927	1.125
1844	0006	46530	0.398	0.360	2.513	0.990	0.000	0.966	0.999	0.865	0.865	1.105
1845	0006	46530	0.398	0.360	2.511	1.055	0.059	0.968	0.573	0.877	0.890	1.112
1846	0006	46550	1.140	0.359	1.497	1.124	0.220	0.989	0.829	0.876	0.982	1.128
1847	0006	46550	1.140	0.359	1.499	1.519	0.518	0.989	0.970	0.897	1.368	1.171
1848	0006	46550	1.140	0.360	1.502	2.026	0.736	0.988	0.993	0.904	1.760	1.191
1849	0006	46550	1.140	0.359	1.503	2.533	0.910	0.987	0.994	0.914	2.137	1.186
1850	0006	46550	1.140	0.360	1.504	3.027	1.099	0.986	0.995	0.911	2.483	1.183
1851	0006	46550	1.140	0.361	1.503	3.526	1.283	0.985	0.995	0.934	2.919	1.201
1852	0006	46550	1.140	0.360	2.008	1.125	0.144	0.965	0.740	0.881	0.935	1.123
1853	0006	46550	1.140	0.360	2.016	1.531	0.375	0.965	0.953	0.895	1.161	1.160
1854	0006	46550	1.140	0.360	2.009	2.035	0.540	0.966	0.993	0.900	1.390	1.173
1855	0006	46550	1.140	0.360	2.015	2.537	0.672	0.965	0.993	0.908	1.599	1.175
1856	0006	46550	1.140	0.359	2.011	3.039	0.807	0.966	0.995	0.902	1.795	1.172
1857	0006	46550	1.140	0.361	2.012	3.526	0.937	0.965	0.995	0.928	2.050	1.194
1858	0006	46550	1.140	0.360	2.521	1.121	0.111	0.954	0.730	0.886	0.922	1.119
1859	0006	46550	1.140	0.360	2.508	1.528	0.298	0.967	0.948	0.899	1.087	1.155
1860	0006	46550	1.140	0.361	2.515	2.037	0.431	0.965	0.991	0.899	1.244	1.162
1861	0006	46550	1.140	0.361	2.519	2.539	0.536	0.956	0.992	0.906	1.394	1.167
1862	0006	46550	1.140	0.359	2.516	3.034	0.663	0.967	0.994	0.895	1.518	1.158
1863	0006	46550	1.140	0.361	2.513	3.525	0.749	0.965	0.996	0.922	1.709	1.183
1864	0006	46550	1.140	0.361	3.016	1.122	0.063	0.966	0.693	0.896	0.916	1.120
1865	0006	46550	1.140	0.360	2.993	1.528	0.238	0.965	0.902	0.901	1.041	1.147
1866	0006	46550	1.140	0.360	2.999	2.038	0.360	0.957	0.989	0.899	1.167	1.158

FACILITY 5X1 PROGRAM C031

NOZZLE TYPE — IF -STREAM
DUAL FLOW (EAA) — PL CONFIGURATIONS — SUPPRESSOR CONFIGURATION
BASELINE PLUG WITH BLEED — 40-SPOKE, AREA RATIO = 1.75

DRAG PARAMETERS — OUTER RADIUS RATIO 0.0000 — INNER RADIUS RATIO 0.7790 — OVD 1.2480

FDG	CE	MASS	D2	MA	PTO/PA	PTI/PA	OMEGAT	DCS	CDS	CDSH	CDSH	DCPL,O	DCPL,I	DCTOT	PSUP/PA
1822	0006	46550	1.140	0.447	3.327	1.122	0.045	-0.070	0.354	-0.007	0.035	-0.029	0.009	-0.097	0.718
1823	0006	46550	1.140	0.448	3.305	1.522	0.208	-0.063	0.349	-0.006	0.032	-0.018	-0.005	-0.092	0.720
1824	0006	46550	1.140	0.449	3.302	2.016	0.323	-0.056	0.347	-0.005	0.031	-0.015	-0.015	-0.091	0.722
1825	0006	46550	1.140	0.447	3.303	2.522	0.406	-0.052	0.347	-0.005	0.031	-0.014	-0.022	-0.092	0.723
1826	0006	46550	1.140	0.449	3.327	3.029	0.485	-0.047	0.342	-0.004	0.029	-0.012	-0.024	-0.087	0.726
1827	0006	46550	1.140	0.449	3.333	3.535	0.565	-0.044	0.339	-0.004	0.030	-0.011	-0.017	-0.075	0.727
1828	0006	46550	1.140	0.449	2.499	1.524	0.763	-0.054	0.330	-0.005	0.031	0.004	-0.012	-0.066	0.735
1829	0006	46550	0.398	0.357	1.506	0.000	0.000	-0.177	0.673	-0.029	0.009	-0.019	-0.010	-0.100	0.801
1830	0006	46530	0.398	0.358	1.507	1.013	0.029	-0.124	0.265	-0.028	0.060	-0.010	0.006	-0.156	0.865
1831	0006	46530	0.398	0.359	1.507	1.020	0.059	-0.120	0.758	-0.027	0.058	-0.006	0.005	-0.148	0.867
1832	0006	46530	0.398	0.359	2.012	1.006	0.000	-0.118	0.436	-0.018	0.065	-0.009	0.010	-0.135	0.776
1833	0006	46530	0.398	0.361	2.012	1.022	0.029	-0.115	0.421	-0.017	0.062	-0.006	0.008	-0.130	0.791
1834	0006	46530	0.398	0.361	2.015	1.026	0.059	-0.111	0.411	-0.017	0.061	-0.004	0.005	-0.126	0.786
1835	0006	46530	0.398	0.361	2.526	0.991	0.000	-0.113	0.582	-0.012	0.063	-0.007	0.011	-0.121	0.698
1836	0006	46530	0.398	0.361	2.524	1.022	0.029	-0.110	0.569	-0.012	0.062	-0.005	0.008	-0.118	0.704
1837	0006	46530	0.398	0.361	2.523	1.026	0.059	-0.106	0.557	-0.012	0.061	-0.002	0.006	-0.114	0.711
1838	0006	46530	0.398	0.362	3.006	1.018	0.000	-0.098	0.582	-0.010	0.063	-0.028	0.011	-0.115	0.697
1839	0006	46530	0.398	0.360	3.007	1.364	0.029	-0.087	0.585	-0.009	0.063	-0.026	0.008	-0.114	0.698
1840	0006	46530	0.398	0.360	3.013	1.415	0.059	-0.085	0.582	-0.009	0.062	-0.024	0.005	-0.113	0.699
1841	0006	46530	0.398	0.361	3.296	1.236	0.000	-0.070	0.526	-0.008	0.062	-0.031	0.011	-0.098	0.727
1842	0006	46530	0.398	0.360	3.295	1.090	0.029	-0.069	0.527	-0.008	0.061	-0.029	0.007	-0.099	0.727
1843	0006	46530	0.398	0.361	3.287	1.143	0.059	-0.069	0.525	-0.008	0.059	-0.027	0.004	-0.100	0.727
1844	0006	46530	0.398	0.360	2.518	0.993	0.000	-0.113	0.586	-0.012	0.060	-0.007	0.012	-0.120	0.698
1845	0006	46530	0.398	0.360	2.511	1.356	0.059	-0.106	0.560	-0.011	0.058	-0.002	0.006	-0.113	0.711
1846	0006	46550	1.140	0.359	1.497	1.126	0.220	-0.103	0.241	-0.021	0.049	-0.000	0.004	-0.121	0.876
1847	0006	46550	1.140	0.359	1.499	1.519	0.518	-0.074	0.237	-0.015	0.047	0.001	0.002	-0.086	0.878
1848	0006	46550	1.140	0.360	1.502	2.026	0.734	-0.058	0.235	-0.012	0.047	0.001	-0.021	-0.089	0.878
1849	0006	46550	1.140	0.359	1.503	2.533	0.919	-0.048	0.235	-0.010	0.048	0.001	-0.017	-0.073	0.879
1850	0006	46550	1.140	0.360	1.504	3.027	1.099	-0.041	0.231	-0.008	0.046	0.002	-0.022	-0.069	0.881
1851	0006	46550	1.140	0.361	1.503	3.526	1.283	-0.035	0.226	-0.007	0.045	0.002	-0.019	-0.059	0.882
1852	0006	46550	1.140	0.360	2.008	1.125	0.144	-0.103	0.396	-0.013	0.051	0.000	0.004	-0.112	0.795
1853	0006	46550	1.140	0.360	2.016	1.531	0.375	-0.081	0.384	-0.010	0.049	0.003	0.001	-0.088	0.801
1854	0006	46550	1.140	0.360	2.008	2.035	0.540	-0.068	0.381	-0.009	0.050	0.002	-0.018	-0.092	0.803
1855	0006	46550	1.140	0.360	2.015	2.537	0.672	-0.059	0.381	-0.007	0.048	0.002	-0.020	-0.084	0.803
1856	0006	46550	1.140	0.359	2.011	3.030	0.807	-0.051	0.378	-0.007	0.048	0.003	-0.024	-0.079	0.808
1857	0006	46550	1.140	0.361	2.012	3.526	0.937	-0.045	0.362	-0.006	0.047	0.003	-0.023	-0.070	0.812
1858	0006	46550	1.140	0.360	2.521	1.121	0.111	-0.101	0.545	-0.010	0.052	0.001	0.004	-0.104	0.718
1859	0006	46550	1.140	0.360	2.508	1.529	0.298	-0.084	0.523	-0.008	0.051	0.004	0.002	-0.087	0.730
1860	0006	46550	1.140	0.361	2.516	2.037	0.431	-0.072	0.515	-0.007	0.050	0.004	-0.014	-0.089	0.733
1861	0006	46550	1.140	0.361	2.519	2.539	0.536	-0.065	0.513	-0.006	0.049	0.003	-0.016	-0.084	0.733
1862	0006	46550	1.140	0.359	2.516	3.034	0.643	-0.058	0.508	-0.006	0.049	0.004	-0.031	-0.090	0.738
1863	0006	46550	1.140	0.361	2.516	3.525	0.749	-0.052	0.492	-0.005	0.048	0.005	-0.019	-0.071	0.744
1864	0006	46550	1.140	0.361	3.014	1.122	0.053	-0.085	0.578	-0.008	0.053	-0.024	0.005	-0.112	0.700
1865	0006	46550	1.140	0.360	2.990	1.528	0.238	-0.076	0.581	-0.007	0.050	-0.009	-0.003	-0.094	0.700
1866	0006	46550	1.140	0.360	2.998	2.038	0.360	-0.066	0.575	-0.006	0.049	-0.006	-0.016	-0.095	0.703

FACILITY X1 PROGRAM C031 IN -STREAM

NOZZLE TYPE DUAL FLOW (FAA) PLUG CONFIGURATIONS BASELINE PLUG WITH BLEED SUPPRESSOR CONFIGURATION 40-SPOKE, AREA RATIO = 1.75

THRUST PARAMETERS OUTER RADIUS RATIO 0.0000 INNER RADIUS RATIO 0.7790 OVD 1.2480

PNC	GE	NASA	D2	M4	PT0/P4	PT1/P4	OMEGAT	CDP	CDI	CFNET1	CFNET2	FG
1667	0006	46550	1.140	0.360	3.012	2.535	0.448	0.966	0.993	0.897	1.271	1.156
1668	0006	46550	1.140	0.361	3.018	3.023	0.534	0.966	0.994	0.894	1.372	1.153
1669	0006	46550	1.140	0.361	3.015	3.526	0.625	0.966	0.995	0.911	1.513	1.170
1670	0006	46550	1.140	0.360	3.304	1.120	0.046	0.964	0.993X	0.907	0.921	1.126
1671	0006	46550	1.140	0.361	3.252	1.531	0.214	0.964	0.879	0.909	1.032	1.150
1672	0006	46550	1.140	0.360	3.224	2.035	0.334	0.966	0.986	0.902	1.145	1.159
1673	0006	46550	1.140	0.361	3.220	2.536	0.419	0.967	0.993	0.900	1.242	1.157
1674	0006	46550	1.140	0.361	3.230	3.028	0.499	0.963	0.990	0.902	1.342	1.157
1675	0006	46550	1.140	0.362	3.237	3.527	0.582	0.966	0.996	0.911	1.457	1.169
1676	0006	46550	1.140	0.359	2.519	1.121	0.111	0.965	0.726	0.888	0.924	1.122
1677	0006	46550	1.140	0.360	2.515	3.520	0.748	0.966	0.995	0.921	1.708	1.183

753

FACILITY X1 PROGRAM C031 IN -STREAM

NOZZLE TYPE DUAL FLOW (FAA) PLUG CONFIGURATIONS BASELINE PLUG WITH BLEED SUPPRESSOR CONFIGURATION 40-SPOKE, AREA RATIO = 1.75

DRAG PARAMETERS OUTER RADIUS RATIO 0.0000 INNER RADIUS RATIO 0.7790 OVD 1.2480

PNC	GE	NASA	D2	M4	PT0/P4	PT1/P4	OMEGAT	DCS	CDS	DCSH	CDSH	DCPL,O	DCPL,I	DCTOT	PSUP/P4
1667	0006	46550	1.140	0.360	3.012	2.535	0.448	-0.060	0.572	-0.005	0.049	-0.006	-0.024	-0.096	0.705
1668	0006	46550	1.140	0.361	3.018	3.023	0.534	-0.055	0.566	-0.005	0.047	-0.004	-0.031	-0.094	0.706
1669	0006	46550	1.140	0.361	3.015	3.526	0.625	-0.051	0.554	-0.004	0.047	-0.000	-0.022	-0.077	0.707
1670	0006	46550	1.140	0.360	3.304	1.120	0.046	-0.068	0.525	-0.007	0.051	-0.028	0.005	-0.098	0.728
1671	0006	46550	1.140	0.361	3.252	1.531	0.214	-0.063	0.528	-0.006	0.048	-0.017	-0.008	-0.093	0.726
1672	0006	46550	1.140	0.360	3.224	2.035	0.334	-0.057	0.533	-0.005	0.048	-0.014	-0.017	-0.094	0.724
1673	0006	46550	1.140	0.361	3.220	2.536	0.419	-0.053	0.528	-0.005	0.047	-0.013	-0.024	-0.094	0.725
1674	0006	46550	1.140	0.361	3.230	3.028	0.499	-0.048	0.526	-0.004	0.047	-0.011	-0.027	-0.091	0.727
1675	0006	46550	1.140	0.362	3.237	3.527	0.582	-0.044	0.521	-0.004	0.047	-0.008	-0.021	-0.077	0.728
1676	0006	46550	1.140	0.359	2.519	1.121	0.111	-0.101	0.546	-0.009	0.050	0.001	0.005	-0.104	0.719
1677	0006	46550	1.140	0.360	2.515	3.520	0.748	-0.052	0.494	-0.005	0.046	0.005	-0.011	-0.062	0.744

MODEL DC-1, 36 DEEP CHUTES, AR = 1.5, BASELINE PLUG

FACILITY X1 PROGRAM F031 IN-STREAM

NOZZLE TYPE: DUAL FLOW (FAA) — P&I CONFIGURATIONS: BASELINE PLUG WITH BLEED — SUPPRESSOR CONFIGURATION: 36-CHUTE, AREA RATIO = 1.5

THRUST PARAMETERS — OUTER RADIUS RATIO 0.9000 — INNER RADIUS RATIO 0.7790 — DVO 1.2480

PCC	CF	MASA	M2	PA	PTO/PA	PTI/PA	OMEGAT	CDO	CDI	CFNET1	CFNET2	F9
1878	0007	47530	0.398	0.447	1.503	0.998	0.000	0.994	0.999	0.846	0.846	1.111
1879	0007	47530	0.398	0.447	1.503	1.009	0.029	0.985	0.414	0.862	0.866	1.112
1880	0007	47530	0.398	0.447	1.504	1.022	0.059	0.934	0.558	0.858	0.870	1.114
1881	0007	47530	0.398	0.447	2.013	1.002	0.000	0.964	0.000	0.869	0.869	1.112
1882	0007	47530	0.398	0.448	2.014	1.023	0.029	0.966	0.367	0.878	0.893	1.117
1883	0007	47530	0.398	0.447	2.015	1.047	0.059	0.965	0.513	0.879	0.893	1.117
1884	0007	47530	0.398	0.447	2.516	1.016	0.000	0.968	0.000	0.894	0.894	1.122
1885	0007	47530	0.398	0.448	2.513	1.056	0.029	0.968	0.291	0.898	0.905	1.123
1886	0007	47530	0.398	0.447	2.532	1.094	0.059	0.963	0.456	0.900	0.918	1.121
1887	0007	47530	0.398	0.448	3.022	1.044	0.000	0.969	0.000	0.908	0.908	1.130
1888	0007	47530	0.398	0.448	3.028	1.096	0.029	0.969	0.267	0.913	0.921	1.131
1889	0007	47530	0.398	0.448	3.031	1.149	0.059	0.969	0.435	0.915	0.935	1.134
1890	0007	47530	0.398	0.447	3.333	1.063	0.000	0.969	0.000	0.911	0.911	1.131
1891	0007	47530	0.398	0.449	3.331	1.123	0.029	0.969	0.261	0.915	0.924	1.133
1892	0007	47530	0.398	0.449	3.331	1.180	0.059	0.969	0.436	0.917	0.939	1.136
1893	0007	47530	0.398	0.449	2.512	1.017	0.000	0.970	0.000	0.892	0.892	1.122
1894	0007	47530	0.398	0.448	2.535	1.094	0.059	0.962	0.456	0.898	0.916	1.120
1895	0007	47550	1.140	0.445	1.507	1.117	0.212	0.995	0.865	0.876	0.975	1.133
1896	0007	47550	1.140	0.447	1.509	1.528	0.601	0.993	0.974	0.895	1.350	1.172
1897	0007	47550	1.140	0.446	1.508	2.026	0.699	0.994	0.991	0.902	1.712	1.181
1898	0007	47550	1.140	0.447	1.508	2.523	0.974	0.994	0.994	0.913	2.068	1.187
1899	0007	47550	1.140	0.447	1.508	3.028	1.051	0.993	0.995	0.910	2.407	1.184
1900	0007	47550	1.140	0.447	1.505	3.530	1.227	0.995	0.995	0.934	2.831	1.204
1901	0007	47550	1.140	0.445	2.013	1.125	0.143	0.965	0.742	0.886	0.940	1.127
1902	0007	47550	1.140	0.446	2.005	1.528	0.364	0.959	0.960	0.900	1.161	1.166
1903	0007	47550	1.140	0.447	2.010	2.022	0.517	0.967	0.992	0.903	1.372	1.174
1904	0007	47550	1.140	0.447	2.008	2.524	0.646	0.969	0.994	0.911	1.578	1.179
1905	0007	47550	1.140	0.448	2.011	3.044	0.779	0.968	0.994	0.912	1.784	1.180
1906	0007	47550	1.140	0.448	2.015	3.533	0.906	0.966	0.995	0.929	2.016	1.195
1907	0007	47550	1.140	0.447	2.517	1.119	0.076	0.967	0.520	0.903	0.929	1.127
1908	0007	47550	1.140	0.447	2.512	1.528	0.273	0.970	0.902	0.911	1.085	1.160
1909	0007	47550	1.140	0.447	2.515	2.023	0.411	0.968	0.988	0.910	1.242	1.171
1910	0007	47550	1.140	0.447	2.514	2.523	0.516	0.969	0.994	0.916	1.389	1.177
1911	0007	47550	1.140	0.448	2.516	3.035	0.620	0.968	0.993	0.904	1.512	1.166
1912	0007	47550	1.140	0.448	2.515	3.530	0.723	0.968	0.995	0.926	1.691	1.187
1913	0007	47550	1.140	0.447	3.023	1.119	0.043	0.969	0.352X	0.913	0.926	1.131
1914	0007	47550	1.140	0.448	3.315	1.528	0.219	0.970	0.865	0.916	1.046	1.158
1915	0007	47550	1.140	0.447	3.027	2.022	0.339	0.959	0.982	0.914	1.169	1.171
1916	0007	47550	1.140	0.448	3.023	2.525	0.428	0.971	0.994	0.909	1.270	1.169
1917	0007	47550	1.140	0.448	3.335	3.040	0.516	0.967	0.995	0.905	1.373	1.163
1918	0007	47550	1.140	0.448	3.027	3.534	0.601	0.959	0.995	0.919	1.501	1.178
1919	0007	47550	1.140	0.448	3.332	1.127	0.000	0.969	0.000	0.926	0.925	1.134
1920	0007	47550	1.140	0.448	3.303	1.529	0.197	0.970	0.854	0.916	1.030	1.157
1921	0007	47550	1.140	0.448	3.296	2.021	0.311	0.910	0.982	0.911	1.136	1.168
1922	0007	47550	1.140	0.449	3.309	2.525	0.391	0.970	0.993	0.906	1.224	1.165

FACILITY B-1 PROGRAM C031 NOZZLE TYPE DUAL FLOW (FAA) TABLE TYPE PLUG CONFIGURATIONS BASELINE PLUG WITH BLEED SUPPRESSOR CONFIGURATION 36-CHUTE, AREA RATIO = 1.5

DRAG PARAMETERS OUTER RADIUS RATIO 0.9000 INNER RADIUS RATIO 0.7790 DVO 1.2460

PTC	CF	NASA	D2	MA	PTD/PA	PTI/PA	OMEGAT	DCS	CDS	DCSH	CDSH	DCPL,O	DCPL,I	DCTOT	PSUP/PA
1878	0007	47530	0.398	0.447	1.509	0.998	0.000	-0.102	0.146	-0.021	0.030	-0.038	0.024	-0.137	0.823
1879	0007	47530	0.398	0.447	1.508	1.009	0.029	-0.102	0.144	-0.021	0.029	-0.032	0.021	-0.133	0.825
1880	0007	47530	0.398	0.447	1.508	1.022	0.059	-0.098	0.142	-0.020	0.029	-0.027	0.018	-0.128	0.828
1881	0007	47530	0.398	0.447	2.018	1.002	0.000	-0.086	0.210	-0.014	0.035	-0.031	0.020	-0.111	0.744
1882	0007	47530	0.398	0.448	2.014	1.023	0.029	-0.084	0.208	-0.013	0.033	-0.027	0.016	-0.109	0.746
1883	0007	47530	0.398	0.447	2.015	1.047	0.059	-0.082	0.205	-0.013	0.032	-0.023	0.012	-0.106	0.750
1884	0007	47530	0.398	0.447	2.514	1.016	0.000	-0.058	0.201	-0.010	0.036	-0.028	0.017	-0.078	0.755
1885	0007	47530	0.398	0.448	2.519	1.036	0.029	-0.057	0.199	-0.010	0.035	-0.024	0.015	-0.076	0.756
1886	0007	47530	0.398	0.447	2.532	1.296	0.059	-0.056	0.200	-0.010	0.034	-0.021	0.010	-0.077	0.756
1887	0007	47530	0.398	0.448	3.022	1.044	0.000	-0.036	0.163	-0.009	0.035	-0.061	0.015	-0.090	0.801
1888	0007	47530	0.398	0.448	3.028	1.096	0.029	-0.036	0.162	-0.007	0.034	-0.056	0.012	-0.087	0.801
1889	0007	47530	0.398	0.448	3.031	1.149	0.059	-0.035	0.162	-0.007	0.034	-0.052	0.009	-0.086	0.802
1890	0007	47530	0.398	0.447	3.239	1.065	0.000	-0.027	0.141	-0.007	0.036	-0.081	0.014	-0.101	0.828
1891	0007	47530	0.398	0.449	3.231	1.123	0.029	-0.027	0.139	-0.006	0.032	-0.076	0.010	-0.099	0.828
1892	0007	47530	0.398	0.449	3.321	1.180	0.059	-0.027	0.140	-0.006	0.033	-0.076	0.008	-0.101	0.829
1893	0007	47530	0.398	0.449	2.512	1.017	0.000	-0.058	0.201	-0.010	0.034	-0.028	0.018	-0.079	0.753
1894	0007	47530	0.398	0.448	2.535	1.094	0.059	-0.056	0.199	-0.010	0.034	-0.021	0.010	-0.077	0.756
1895	0007	47550	1.140	0.446	1.507	1.117	0.212	-0.086	0.137	-0.017	0.027	-0.019	0.014	-0.109	0.834
1896	0007	47550	1.140	0.447	1.508	1.528	0.501	-0.063	0.136	-0.013	0.027	-0.012	0.010	-0.078	0.835
1897	0007	47550	1.140	0.445	1.508	2.026	0.699	-0.050	0.136	-0.010	0.027	-0.010	-0.012	-0.092	0.834
1898	0007	47550	1.140	0.447	1.508	2.523	0.874	-0.042	0.136	-0.008	0.027	-0.008	-0.011	-0.070	0.834
1899	0007	47550	1.140	0.447	1.508	3.028	1.051	-0.036	0.135	-0.007	0.028	-0.007	-0.022	-0.073	0.836
1900	0007	47550	1.140	0.447	1.505	3.530	1.227	-0.031	0.134	-0.007	0.028	-0.005	-0.017	-0.059	0.837
1901	0007	47550	1.140	0.445	2.018	1.125	0.143	-0.077	0.206	-0.012	0.032	-0.017	0.011	-0.096	0.754
1902	0007	47550	1.140	0.446	2.006	1.528	0.364	-0.063	0.201	-0.010	0.032	-0.011	0.006	-0.078	0.756
1903	0007	47550	1.140	0.447	2.010	2.022	0.517	-0.053	0.199	-0.008	0.032	-0.009	-0.013	-0.094	0.758
1904	0007	47550	1.140	0.447	2.006	2.526	0.646	-0.047	0.199	-0.007	0.031	-0.008	-0.012	-0.074	0.758
1905	0007	47550	1.140	0.448	2.011	3.044	0.779	-0.041	0.197	-0.006	0.031	-0.006	-0.012	-0.066	0.759
1906	0007	47550	1.140	0.448	2.015	3.533	0.906	-0.037	0.196	-0.006	0.031	-0.004	-0.010	-0.057	0.761
1907	0007	47550	1.140	0.447	2.517	1.119	0.076	-0.056	0.200	-0.009	0.034	-0.019	0.008	-0.077	0.757
1908	0007	47550	1.140	0.447	2.512	1.528	0.273	-0.047	0.197	-0.008	0.032	-0.008	0.005	-0.057	0.760
1909	0007	47550	1.140	0.447	2.516	2.023	0.411	-0.041	0.196	-0.007	0.033	-0.006	-0.011	-0.065	0.761
1910	0007	47550	1.140	0.447	2.514	2.523	0.516	-0.037	0.196	-0.006	0.032	-0.004	-0.010	-0.051	0.762
1911	0007	47550	1.140	0.448	2.516	3.035	0.620	-0.034	0.194	-0.005	0.031	-0.002	-0.030	-0.071	0.763
1912	0007	47550	1.140	0.448	2.516	3.530	0.723	-0.031	0.195	-0.005	0.031	-0.001	-0.013	-0.050	0.762
1913	0007	47550	1.140	0.447	3.023	1.119	0.043	-0.035	0.162	-0.007	0.034	-0.055	0.010	-0.089	0.802
1914	0007	47550	1.140	0.448	3.016	1.528	0.218	-0.031	0.159	-0.006	0.031	-0.036	0.000	-0.073	0.805
1915	0007	47550	1.140	0.447	3.027	2.027	0.339	-0.027	0.158	-0.005	0.031	-0.014	-0.019	-0.079	0.808
1916	0007	47550	1.140	0.448	3.023	2.525	0.428	-0.025	0.157	-0.005	0.030	-0.027	-0.020	-0.077	0.808
1917	0007	47550	1.140	0.448	3.035	3.040	0.516	-0.023	0.157	-0.004	0.031	-0.024	-0.026	-0.077	0.809
1918	0007	47550	1.140	0.448	3.027	3.534	0.601	-0.021	0.156	-0.004	0.030	-0.020	-0.018	-0.053	0.809
1919	0007	47550	1.140	0.449	3.332	1.127	0.000	-0.027	0.141	-0.006	0.033	-0.077	0.010	-0.101	0.828
1920	0007	47550	1.140	0.449	3.303	1.529	0.197	-0.024	0.137	-0.005	0.030	-0.043	-0.003	-0.075	0.831
1921	0007	47550	1.140	0.448	3.296	2.021	0.311	-0.022	0.138	-0.005	0.030	-0.034	-0.019	-0.080	0.831
1922	0007	47550	1.140	0.449	3.309	2.525	0.391	-0.020	0.136	-0.004	0.029	-0.035	-0.025	-0.043	0.833

FACILITY X1 PROGRAM C031

NOZZLE TYPE: DUAL FLOW (FAA)

IN-STREAM PLUG CONFIGURATIONS: BASELINE PLUG WITH BLEED

SUPPRESSOR CONFIGURATION: 36-CHUTE, AREA RATIO = 1.5

THRUST PARAMETERS: OUTER RADIUS RATIO 0.9000; INNER RADIUS RATIO 0.7790; DVD 1.2480

RDC	CE	WASA	P2	WA	PTC/P1	PTI/PA	OMEGAT	CDC	CDI	CFNETI	CFNET2	F9
1923	0007	47550	1.140	0.448	3.327	3.032	0.468	0.969	0.994	0.906	1.316	1.164
1924	0007	47550	1.140	0.449	3.327	3.551	0.546	0.969	0.995	0.914	1.423	1.173
1925	0007	47550	1.140	0.448	2.519	1.127	0.080	0.967	0.531	0.902	0.930	1.127
1926	0007	47550	1.140	0.446	2.503	3.528	0.724	0.969	0.995	0.926	1.592	1.188
1927	0007	47530	0.398	0.358	1.503	1.008	0.029	0.993	0.452	0.865	0.868	1.118
1928	0007	47530	0.398	0.358	1.508	0.998	0.000	0.994	9.999	0.861	0.861	1.118
1929	0007	47530	0.398	0.357	1.507	1.022	0.059	0.993	0.552	0.868	0.880	1.119
1930	0007	47530	0.398	0.358	2.015	1.001	0.000	0.957	0.000	0.879	0.879	1.120
1931	0007	47530	0.398	0.359	2.023	1.022	0.029	0.966	0.369	0.884	0.889	1.121
1932	0007	47530	0.398	0.359	2.023	1.043	0.059	0.966	0.641	0.894	0.897	1.122
1933	0007	47530	0.398	0.359	2.521	1.017	0.000	0.959	0.000	0.899	0.899	1.127
1934	0007	47530	0.398	0.357	2.528	1.055	0.029	0.968	0.203	0.901	0.908	1.125
1935	0007	47530	0.398	0.358	2.528	1.095	0.059	0.966	0.454	0.908	0.926	1.130
1936	0007	47530	0.398	0.358	3.003	1.040	0.000	0.970	0.000	0.911	0.911	1.133
1937	0007	47530	0.398	0.359	3.022	1.004	0.029	0.969	0.270	0.916	0.924	1.135
1938	0007	47530	0.398	0.359	3.030	1.150	0.059	0.969	0.435	0.918	0.939	1.137
1939	0007	47530	0.398	0.359	3.264	1.055	0.000	0.966	0.000	0.915	0.915	1.133
1940	0007	47530	0.398	0.360	3.189	1.110	0.029	0.968	0.264	0.917	0.926	1.134
1941	0007	47530	0.398	0.359	3.159	1.163	0.059	0.968	0.434	0.921	0.942	1.139
1942	0007	47530	0.398	0.359	2.521	1.017	0.000	0.946	0.000	0.899	0.899	1.125
1943	0007	47530	0.398	0.359	2.519	1.093	0.059	0.969	0.455	0.908	0.925	1.131
1944	0007	47540	1.140	0.358	1.510	1.120	0.215	0.991	0.864	0.882	0.983	1.135
1945	0007	47550	1.140	0.359	1.507	1.526	0.503	0.992	0.977	0.901	1.361	1.176
1946	0007	47550	1.140	0.359	1.505	2.053	0.706	0.994	0.992	0.909	1.735	1.186
1947	0007	47550	1.140	0.359	1.508	2.534	0.680	0.991	0.993	0.914	2.081	1.187
1948	0007	47550	1.140	0.360	1.503	3.023	1.051	0.991	0.995	0.912	2.410	1.185
1949	0007	47550	1.140	0.359	1.509	3.524	1.226	0.992	0.995	0.937	2.833	1.206
1950	0007	47550	1.140	0.360	2.018	1.124	0.145	0.967	0.777	0.894	0.949	1.135
1951	0007	47550	1.140	0.359	2.020	1.528	0.344	0.966	0.963	0.904	1.164	1.168
1952	0007	47550	1.140	0.359	2.017	2.037	0.519	0.957	0.991	0.908	1.382	1.176
1953	0007	47550	1.140	0.360	2.019	2.534	0.647	0.967	0.994	0.915	1.585	1.183
1954	0007	47550	1.140	0.360	2.023	3.024	0.772	0.967	0.995	0.914	1.776	1.182
1955	0007	47550	1.140	0.360	2.019	3.524	0.902	0.966	0.996	0.933	2.018	1.200
1956	0007	47550	1.140	0.360	2.522	1.125	0.079	0.969	0.532	0.909	0.935	1.132
1957	0007	47550	1.140	0.359	2.521	1.529	0.274	0.957	0.905	0.913	1.089	1.161
1958	0007	47550	1.140	0.359	2.524	2.036	0.413	0.968	0.989	0.914	1.250	1.175
1959	0007	47550	1.140	0.359	2.527	2.537	0.517	0.967	0.994	0.919	1.395	1.179
1960	0007	47550	1.140	0.360	2.513	3.038	0.620	0.972	0.995	0.910	1.522	1.174
1961	0007	47550	1.140	0.361	2.537	3.528	0.719	0.965	0.995	0.929	1.689	1.189
1962	0007	47550	1.140	0.360	3.015	1.125	0.046	0.968	0.369X	0.917	0.932	1.135
1963	0007	47550	1.140	0.360	2.950	1.528	0.220	0.968	0.843	0.920	1.051	1.160
1964	0007	47550	1.140	0.359	2.989	2.034	0.346	0.970	0.983	0.919	1.192	1.176
1965	0007	47550	1.140	0.359	3.008	2.536	0.433	0.970	0.993	0.912	1.279	1.171
1966	0007	47550	1.140	0.359	3.015	3.036	0.517	0.969	0.993	0.908	1.379	1.167
1967	0007	47550	1.140	0.359	3.007	3.524	0.604	0.968	0.994	0.923	1.513	1.182

FACILITY (1 PROGRAM CODE)

NOZZLE TYPE: DUAL FLOW (FAA)

INF STREAM PLUG CONFIGURATIONS: BASELINE PLUG WITH BLEED

SUPPRESSOR CONFIGURATION: 36-CHUTE, AREA RATIO = 1.5

DRAG PARAMETERS: OUTER RADIUS RATIO = 0.0000; INNER RADIUS RATIO = 0.7790; DVR = 1.2493

ENG	CF	MASA	M2	M1	PT2/P2	PT1/P1	OMEGAT	DCS	CDS	DCSH	CDSH	DCPL,0	DCPL,I	DCTOT	PSUP/PA
1923	0007	47550	1.140	0.448	3.227	3.032	0.468	-0.019	0.135	-0.004	0.030	-0.026	-0.026	-0.074	0.834
1924	0007	47550	1.140	0.449	3.327	3.531	0.546	-0.017	0.134	-0.004	0.029	-0.025	-0.025	-0.071	0.835
1925	0007	47550	1.140	0.448	2.515	1.127	0.080	-0.055	0.190	-0.009	0.034	-0.019	0.008	-0.075	0.757
1926	0007	47550	1.140	0.449	2.508	3.528	0.724	-0.031	0.195	-0.005	0.031	-0.000	-0.011	-0.047	0.762
1927	0007	47530	0.398	0.358	1.509	1.009	0.029	-0.088	0.196	-0.015	0.032	-0.032	0.007	-0.128	0.847
1928	0007	47530	0.398	0.358	1.508	0.998	0.000	-0.089	0.198	-0.014	0.031	-0.037	0.010	-0.130	0.845
1929	0007	47530	0.398	0.357	1.507	1.022	0.059	-0.086	0.193	-0.013	0.030	-0.030	0.004	-0.126	0.849
1930	0007	47530	0.398	0.358	2.015	1.001	0.000	-0.075	0.289	-0.009	0.036	-0.036	0.012	-0.109	0.774
1931	0007	47530	0.398	0.359	2.023	1.022	0.029	-0.074	0.287	-0.009	0.034	-0.032	0.007	-0.108	0.775
1932	0007	47530	0.398	0.359	2.023	1.043	0.059	-0.073	0.285	-0.009	0.035	-0.028	0.003	-0.107	0.776
1933	0007	47530	0.398	0.359	2.521	1.017	0.000	-0.051	0.276	-0.007	0.037	-0.030	0.011	-0.076	0.782
1934	0007	47530	0.398	0.357	2.528	1.035	0.029	-0.050	0.279	-0.007	0.036	-0.026	0.009	-0.075	0.783
1935	0007	47530	0.398	0.358	2.528	1.055	0.059	-0.050	0.277	-0.007	0.037	-0.023	0.004	-0.075	0.784
1936	0007	47530	0.398	0.358	3.023	1.040	0.000	-0.032	0.226	-0.005	0.037	-0.058	0.010	-0.085	0.824
1937	0007	47530	0.398	0.359	3.022	1.056	0.029	-0.031	0.222	-0.005	0.036	-0.055	0.008	-0.084	0.826
1938	0007	47530	0.398	0.359	3.030	1.150	0.059	-0.031	0.220	-0.005	0.035	-0.052	0.004	-0.083	0.827
1939	0007	47530	0.398	0.359	3.244	1.066	0.000	-0.025	0.197	-0.004	0.034	-0.063	0.010	-0.083	0.844
1940	0007	47550	0.398	0.360	3.185	1.110	0.029	-0.027	0.204	-0.005	0.036	-0.062	0.007	-0.077	0.839
1941	0007	47530	0.398	0.359	3.150	1.163	0.059	-0.027	0.207	-0.005	0.035	-0.049	0.005	-0.076	0.837
1942	0007	47530	0.398	0.359	2.531	1.017	0.000	-0.051	0.277	-0.007	0.037	-0.031	0.012	-0.076	0.793
1943	0007	47530	0.398	0.359	2.519	1.093	0.059	-0.050	0.275	-0.006	0.036	-0.024	0.005	-0.075	0.784
1944	0007	47550	1.140	0.358	1.510	1.120	0.215	-0.074	0.188	-0.012	0.029	-0.021	0.003	-0.105	0.853
1945	0007	47550	1.140	0.359	1.507	1.524	0.503	-0.056	0.196	-0.009	0.029	-0.015	0.002	-0.078	0.854
1946	0007	47550	1.140	0.359	1.505	2.033	0.706	-0.045	0.186	-0.007	0.029	-0.011	-0.018	-0.080	0.854
1947	0007	47550	1.140	0.359	1.509	2.534	0.880	-0.037	0.185	-0.006	0.029	-0.010	-0.016	-0.069	0.855
1948	0007	47550	1.140	0.359	1.509	3.025	1.051	-0.032	0.182	-0.005	0.028	-0.007	-0.025	-0.069	0.856
1949	0007	47550	1.140	0.359	1.508	3.524	1.226	-0.028	0.184	-0.004	0.028	-0.006	-0.030	-0.068	0.855
1950	0007	47550	1.140	0.360	2.018	1.124	0.145	-0.069	0.281	-0.008	0.032	-0.023	0.004	-0.096	0.779
1951	0007	47550	1.140	0.359	2.020	1.528	0.364	-0.056	0.279	-0.007	0.033	-0.015	0.002	-0.076	0.781
1952	0007	47550	1.140	0.359	2.017	2.027	0.519	-0.044	0.277	-0.006	0.033	-0.013	-0.017	-0.083	0.782
1953	0007	47550	1.140	0.359	2.018	2.534	0.647	-0.042	0.276	-0.005	0.032	-0.011	-0.015	-0.072	0.782
1954	0007	47550	1.140	0.360	2.020	3.024	0.772	-0.037	0.274	-0.004	0.032	-0.008	-0.015	-0.065	0.784
1955	0007	47550	1.140	0.360	2.019	3.524	0.902	-0.033	0.274	-0.004	0.033	-0.007	-0.020	-0.064	0.784
1956	0007	47550	1.140	0.360	2.522	1.125	0.079	-0.041	0.274	-0.006	0.035	-0.022	0.003	-0.075	0.783
1957	0007	47550	1.140	0.359	2.521	1.529	0.274	-0.042	0.273	-0.005	0.035	-0.011	0.002	-0.057	0.786
1958	0007	47550	1.140	0.359	2.524	2.036	0.413	-0.037	0.271	-0.005	0.033	-0.008	-0.014	-0.063	0.786
1959	0007	47550	1.140	0.359	2.527	2.537	0.517	-0.033	0.271	-0.004	0.033	-0.006	-0.014	-0.057	0.787
1960	0007	47550	1.140	0.360	2.518	3.038	0.620	-0.030	0.269	-0.004	0.033	-0.005	-0.030	-0.059	0.787
1961	0007	47550	1.140	0.361	2.537	3.528	0.719	-0.027	0.268	-0.003	0.033	-0.003	-0.016	-0.050	0.787
1962	0007	47550	1.140	0.360	3.016	1.125	0.046	-0.031	0.222	-0.005	0.036	-0.053	0.006	-0.084	0.824
1963	0007	47550	1.140	0.360	2.990	1.528	0.220	-0.028	0.220	-0.004	0.033	-0.037	-0.003	-0.072	0.826
1964	0007	47550	1.140	0.359	2.988	2.034	0.346	-0.029	0.220	-0.004	0.034	-0.030	-0.019	-0.078	0.827
1965	0007	47550	1.140	0.359	3.008	2.536	0.433	-0.027	0.217	-0.003	0.032	-0.027	-0.025	-0.078	0.829
1966	0007	47550	1.140	0.359	3.015	3.036	0.517	-0.020	0.217	-0.003	0.033	-0.024	-0.031	-0.079	0.829
1967	0007	47550	1.140	0.359	3.007	3.524	0.604	-0.019	0.217	-0.003	0.033	-0.021	-0.027	-0.070	0.829

FACILITY SXI PROGRAM C031 — PROFILE TYPE — DUAL FLOW (FAN) — FLOW-STREAM PLUG CONFIGURATIONS — BASELINE PLUG WITH BLEED — SUPPRESSOR CONFIGURATION 26-CHUTE, AREA RATIO = 1.5

THRUST PARAMETERS — OUTER RADIUS RATIO 0.7310 — INNER RADIUS RATIO 0.7790 — DVD 1.2480

PFG	CF	WASA	Q2	MA	PTO/PA	PTI/PA	DVEFAT	CDC	CDI	CFNET1	CFNET2	F9
1964	0007	47550	1.140	0.360	3.304	1.122	0.000	0.968	0.000	0.931	0.931	1.138
1965	0007	47550	1.140	0.360	3.193	1.526	0.204	0.965	0.855	0.921	1.040	1.158
1970	0007	47550	1.140	0.360	3.095	2.034	0.334	0.967	0.981	0.916	1.166	1.171
1971	0007	47550	1.140	0.359	3.037	2.531	0.429	0.968	0.994	0.912	1.274	1.170
1972	0007	47550	1.140	0.359	3.042	3.037	0.511	0.970	0.994	0.910	1.374	1.169
1973	0007	47550	1.140	0.360	3.082	3.529	0.587	0.971	0.994	0.921	1.489	1.182
1974	0007	47550	1.140	0.359	2.523	1.123	0.078	0.969	0.527	0.911	0.938	1.134
1975	0007	47550	1.140	0.359	2.517	1.521	0.721	0.969	0.995	0.931	1.697	1.193
1976	0007	47530	0.398	0.017	1.507	0.993	0.000	0.488	0.999	0.902	0.902	1.136
1977	0007	47530	0.398	0.017	1.507	1.001	0.329	0.998	1.100	0.911	0.912	1.138
1978	0007	47530	0.398	0.014	1.506	1.011	0.059	0.998	0.768	0.911	0.920	1.138
1979	0007	47530	0.398	0.027	2.031	0.996	0.000	0.967	0.999	0.905	0.905	1.139
1980	0007	47530	0.398	0.030	2.003	1.015	0.029	0.964	0.448	0.911	0.915	1.140
1981	0007	47530	0.398	0.025	2.017	1.035	0.059	0.964	0.595	0.911	0.923	1.139
1982	0007	47530	0.398	0.044	2.505	1.000	0.000	0.969	0.000	0.918	0.918	1.143
1983	0007	47530	0.398	0.043	2.515	1.044	0.029	0.957	0.326	0.923	0.929	1.143
1984	0007	47530	0.398	0.040	2.515	1.084	0.059	0.947	0.479	0.923	0.940	1.142
1985	0007	47530	0.398	0.042	3.017	1.030	0.000	0.969	0.000	0.926	0.926	1.147
1986	0007	47530	0.398	0.051	3.022	1.093	0.029	0.959	0.297	0.931	0.939	1.148
1987	0007	47530	0.398	0.051	3.024	1.139	0.059	0.968	0.449	0.933	0.953	1.150
1988	0007	47530	0.398	0.057	3.502	1.067	0.000	0.969	0.000	0.928	0.928	1.148
1989	0007	47530	0.398	0.056	3.281	1.108	0.029	0.968	0.275	0.933	0.941	1.149
1990	0007	47530	0.398	0.049	3.271	1.158	0.059	0.949	0.445	0.934	0.956	1.152
1991	0007	47530	0.398	0.037	2.517	1.098	0.000	0.958	0.000	0.919	0.919	1.143
1992	0007	47530	0.398	0.041	2.511	1.083	0.059	0.958	0.480	0.926	0.944	1.146
1993	0007	47550	1.140	0.044	1.506	1.120	0.234	0.998	0.939	0.926	1.042	1.159
1994	0007	47550	1.140	0.025	1.505	1.519	0.507	0.983	0.987	0.929	1.404	1.194
1995	0007	47550	1.140	0.040	1.504	2.017	0.706	0.948	0.983	0.929	1.769	1.199
1996	0007	47550	1.140	0.044	1.507	2.516	0.879	0.987	0.994	0.932	2.119	1.200
1997	0007	47550	1.140	0.044	1.508	3.018	1.055	0.987	0.995	0.926	2.453	1.196
1998	0007	47550	1.140	0.051	1.537	3.520	1.232	0.987	0.995	0.949	2.877	1.215
1999	0007	47550	1.140	0.044	2.005	1.121	0.155	0.967	0.839	0.923	0.984	1.156
2000	0007	47550	1.140	0.051	2.005	1.571	0.368	0.966	0.972	0.927	1.197	1.187
2001	0007	47550	1.140	0.051	2.032	2.018	0.518	0.967	0.992	0.925	1.407	1.193
2002	0007	47550	1.140	0.055	2.005	2.520	0.667	0.957	0.993	0.931	1.614	1.196
2003	0007	47550	1.140	0.052	2.004	3.028	0.778	0.967	0.995	0.927	1.810	1.193
2004	0007	47550	1.140	0.057	2.005	3.515	0.905	0.967	0.995	0.946	2.053	1.211
2005	0007	47550	1.140	0.043	2.505	1.119	0.086	0.973	0.586	0.932	0.961	1.153
2006	0007	47550	1.140	0.055	2.503	1.577	0.279	0.971	0.971	0.934	1.115	1.187
2007	0007	47550	1.140	0.051	2.513	2.019	0.412	0.967	0.990	0.930	1.270	1.189
2008	0007	47550	1.140	0.053	2.512	2.518	0.516	0.968	0.994	0.933	1.415	1.193
2009	0007	47550	1.140	0.058	2.505	3.020	0.621	0.970	0.994	0.921	1.541	1.184
2010	0007	47550	1.140	0.060	2.520	3.524	0.723	0.965	0.995	0.942	1.719	1.202
2011	0007	47550	1.140	0.054	3.027	1.117	0.047	0.968	0.3894	0.936	0.951	1.151
2012	0007	47550	1.140	0.051	3.035	1.522	0.218	0.969	0.867	0.935	1.068	1.174

FACILITY EI PROTEAN CO31 NOZZLE TYPE PL- STEAM CONFIGURATIONS SUPPRESSOR CONFIGURATION

DISK FLOW LEAKI BASELINE PLUG WITH BLEED 36-CHUTE, AREA RATIO = 1.5

PLUG BASELINE OUTER RADIUS RATIO 0.0000 INNER RADIUS RATIO 0.7790 DYN 1.2480

PDC	CF	MACH	RD	PR	PT/P2	PT/P2A	TPCAT	DCS	DCSH	DCSH	DCPL,O	DCPL,I	DCTOT	PSUP/PA
1000	0001	47550	1.140	0.300	3.504	1.127	0.000	-0.024	0.193	-0.004	0.036	-0.067	0.007	-0.089	0.848
1001	0001	47550	1.140	0.300	3.198	1.029	0.204	-0.024	0.201	-0.004	0.033	-0.037	-0.005	-0.070	0.842
1002	0001	47550	1.140	0.300	3.050	2.934	0.334	-0.024	0.210	-0.004	0.033	-0.030	-0.017	-0.073	0.835
1003	0001	47550	1.140	0.300	3.027	2.931	0.409	-0.022	0.215	-0.003	0.033	-0.028	-0.021	-0.074	0.831
1004	0001	47550	1.140	0.300	3.042	2.927	0.511	-0.020	0.213	-0.003	0.032	-0.024	-0.027	-0.074	0.833
1005	0001	47550	1.140	0.300	3.042	2.928	0.487	-0.018	0.207	-0.003	0.032	-0.020	-0.025	-0.066	0.836
1006	0001	47550	1.140	0.300	2.520	1.171	0.078	-0.019	0.277	-0.004	0.036	-0.023	0.003	-0.075	0.793
1007	0001	47550	1.140	0.300	2.517	1.171	0.771	-0.024	0.271	-0.003	0.037	-0.003	-0.011	-0.044	0.797
1010	0001	47550	0.720	0.002	1.607	0.291	0.000	-0.048	68.702	-0.000	0.719	-0.050	0.009	-0.091	0.917
1011	0001	47550	0.720	0.001	1.507	1.301	0.026	-0.046	46.501	-0.000	0.326	-0.044	0.005	-0.089	0.918
1012	0001	47550	0.720	0.001	1.408	1.311	0.050	-0.047	64.754	-0.001	0.725	-0.042	0.003	-0.087	0.919
1013	0001	47550	0.720	0.001	2.008	0.796	0.000	-0.047	31.682	-0.000	0.298	-0.044	0.009	-0.082	0.867
1020	0001	47550	0.960	0.002	2.008	1.315	0.029	-0.044	24.916	-0.000	0.201	-0.041	0.005	-0.083	0.863
1021	0001	47550	0.960	0.001	2.010	1.316	0.059	-0.045	34.605	-0.000	0.373	-0.038	0.002	-0.082	0.863
1022	0001	47550	0.960	0.001	2.008	1.320	0.000	-0.042	11.556	-0.000	0.102	-0.033	0.008	-0.057	0.865
1023	0001	47550	0.960	0.001	2.014	1.316	0.026	-0.041	8.933	-0.000	0.056	-0.031	0.006	-0.057	0.866
1024	0001	47550	0.960	0.001	2.010	1.316	0.060	-0.041	13.460	-0.000	0.163	-0.028	0.002	-0.057	0.866
1025	0001	47550	0.960	0.001	2.017	1.310	0.000	-0.038	4.052	-0.000	0.091	-0.051	0.007	-0.063	0.900
1026	0001	47550	0.960	0.001	2.022	1.282	0.026	-0.039	6.303	-0.000	0.115	-0.048	0.005	-0.062	0.900
1027	0001	47550	0.960	0.001	2.026	1.159	0.060	-0.039	5.861	-0.000	0.091	-0.046	0.002	-0.062	0.900
1028	0001	47550	0.960	0.001	2.702	1.047	0.000	-0.031	4.069	-0.000	0.077	-0.056	0.009	-0.062	0.919
1029	0001	47550	0.960	0.001	2.703	1.134	0.026	-0.033	6.334	-0.000	0.098	-0.054	0.005	-0.063	0.917
1030	0001	47550	0.960	0.001	2.703	1.134	0.060	-0.031	5.841	-0.000	2.085	-0.051	0.002	-0.062	0.917
1031	0001	47550	0.960	0.001	2.712	1.308	0.000	-0.032	14.566	-0.000	0.172	-0.033	0.009	-0.057	0.865
1032	0001	47550	0.960	0.001	2.711	1.287	0.026	-0.031	13.061	-0.000	0.084	-0.028	0.002	-0.058	0.865
1033	0001	47550	1.140	0.044	1.508	0.820	0.235	-0.041	6.738	-0.000	0.016	-0.034	0.007	-0.072	0.922
1034	0001	47550	1.140	0.044	1.506	1.519	0.507	-0.041	19.086	-0.000	0.308	-0.025	0.002	-0.054	0.921
1035	0001	47550	1.140	0.044	1.504	1.317	0.304	-0.034	7.913	-0.000	0.101	-0.020	-0.016	-0.061	0.921
1036	0001	47550	1.140	0.044	1.507	1.518	0.539	-0.030	6.919	-0.000	0.100	-0.017	-0.017	-0.055	0.920
1037	0001	47550	1.140	0.044	1.508	1.514	1.055	-0.017	6.758	-0.000	0.065	-0.014	-0.030	-0.051	0.921
1040	0001	47550	1.140	0.044	1.509	1.520	1.252	-0.000	6.036	-0.000	0.044	-0.011	-0.024	-0.050	0.922
1041	0001	47550	1.140	0.044	2.008	1.121	0.166	-0.042	11.472	-0.000	0.070	-0.032	0.007	-0.072	0.866
1042	0001	47550	1.140	0.041	2.008	1.123	0.349	-0.035	8.370	-0.000	0.018	-0.024	0.001	-0.057	0.867
1043	0001	47550	1.140	0.041	2.007	2.718	0.518	-0.030	22.332	-0.000	0.250	-0.021	-0.017	-0.068	0.866
1044	0001	47550	1.140	0.044	2.008	2.520	0.647	-0.024	7.007	-0.000	0.057	-0.018	-0.016	-0.059	0.867
1045	0001	47550	1.140	0.043	2.008	2.524	0.778	-0.021	8.028	-0.000	0.070	-0.014	-0.015	-0.052	0.867
1046	0001	47550	1.140	0.042	2.008	2.519	0.905	-0.020	6.559	-0.000	0.046	-0.012	-0.020	-0.053	0.868
1047	0001	47550	1.140	0.041	2.006	1.119	0.084	-0.031	11.911	-0.000	0.087	-0.026	0.000	-0.057	0.865
1048	0001	47550	1.140	0.040	2.008	1.122	0.279	-0.027	7.146	-0.000	0.062	-0.016	0.001	-0.043	0.865
1049	0001	47550	1.140	0.041	2.007	2.019	0.412	-0.023	8.622	-0.000	0.040	-0.014	-0.014	-0.052	0.865
1050	0001	47550	1.140	0.041	2.012	2.518	0.516	-0.021	7.721	-0.000	0.065	-0.012	-0.016	-0.049	0.865
1060	0001	47550	1.140	0.042	2.008	1.020	0.021	-0.019	6.481	-0.000	0.065	-0.009	-0.029	-0.057	0.866
1010	0001	47550	1.140	0.042	2.009	1.524	0.723	-0.017	6.090	-0.000	0.076	-0.007	-0.019	-0.044	0.865
1011	0001	47550	1.140	0.044	1.007	1.117	0.067	-0.018	5.492	-0.000	0.063	-0.047	0.003	-0.062	0.900
1012	0001	47550	1.140	0.041	1.004	1.522	0.218	-0.016	9.253	-0.000	0.105	-0.034	-0.003	-0.054	0.899

760

FACILITY SL PROGRAM CODE

NOZZLE TYPE: CONV FLOW FRAME

IM STREAM
PLT CONFIGURATIONS: BASELINE PLUG WITH BLEED

SUPPRESSOR CONFIGURATION: 36-CHUTE, AREA RATIO = 1.5

TUNNEL PARAMETERS

OUTER RADIUS RATIO 0.0000 INNER RADIUS RATIO 0.7790 OVD 1.2680

RPM	CR	NPSA	M2	M1	PT/PA	PT/PA	OMEGA	CDN	CDJ	CFNET1	CFNET2	FG
2013	0007	47550	1.140	0.000	1.000	2.019	0.741	0.959	0.992	0.932	1.193	1.188
2014	0007	47550	1.140	0.041	1.018	2.020	0.478	0.970	0.993	0.926	1.293	1.186
2015	0007	47550	1.140	0.083	1.034	2.034	0.414	0.969	0.995	0.919	1.392	1.178
2016	0007	47550	1.140	0.089	1.038	2.071	0.399	0.969	0.994	0.933	1.524	1.193
2017	0007	47550	1.140	0.054	1.025	1.918	0.393	0.969	0.995	0.946	0.946	1.153
2018	0007	47550	1.140	0.044	1.027	1.924	0.178	0.958	0.996	0.934	1.051	1.173
2019	0007	47550	1.140	0.041	1.026	2.021	0.313	0.971	0.997	0.928	1.159	1.185
2020	0007	47550	1.140	0.061	1.034	2.020	0.193	0.973	0.998	0.922	1.267	1.180
2021	0007	47550	1.140	0.061	1.044	2.029	0.477	0.968	0.994	0.917	1.366	1.175
2022	0007	47550	1.140	0.085	1.033	2.015	0.544	0.967	0.995	0.930	1.471	1.189
2023	0007	47550	1.140	0.051	1.038	1.914	0.084	0.968	0.580	0.933	0.961	1.152
2024	0007	47550	1.140	0.041	1.031	2.018	0.723	0.969	0.995	0.943	1.723	1.204

FACILITY SL PROGRAM CODE

NOZZLE TYPE: CONV FLOW FRAME

IM STREAM
PLT CONFIGURATIONS: BASELINE PLUG WITH BLEED

SUPPRESSOR CONFIGURATION: 36-CHUTE, AREA RATIO = 1.5

DRAG PARAMETERS

OUTER RADIUS RATIO 0.0000 INNER RADIUS RATIO 0.7790 OVD 1.2680

RPM	CR	NPSA	M2	M1	PT/PA	PT/PA	OMEGA	CFS	CDS	DCSH	CDSH	DCPL.0	DCPL.1	DCTOT	PSUP/PA
2013	0007	47550	1.140	0.000	1.000	2.019	0.741	-0.014	4.707	-0.000	0.042	-0.029	-0.019	-0.062	0.899
2014	0007	47550	1.140	0.041	1.018	2.020	0.478	-0.013	4.662	-0.000	0.000	-0.026	-0.023	-0.053	0.899
2015	0007	47550	1.140	0.083	1.034	2.034	0.414	-0.012	4.179	-0.000	0.097	-0.023	-0.030	-0.065	0.900
2016	0007	47550	1.140	0.089	1.038	2.071	0.399	-0.011	4.175	-0.000	0.114	-0.020	-0.025	-0.056	0.899
2017	0007	47550	1.140	0.054	1.025	1.918	0.393	-0.013	4.411	-0.000	0.004	-0.055	0.006	-0.054	0.921
2018	0007	47550	1.140	0.044	1.027	1.924	0.178	-0.012	4.490	-0.000	0.119	-0.041	-0.007	-0.060	0.917
2019	0007	47550	1.140	0.041	1.026	2.021	0.313	-0.011	3.655	-0.000	0.078	-0.034	-0.021	-0.066	0.917
2020	0007	47550	1.140	0.061	1.034	2.020	0.193	-0.010	4.597	-0.000	0.117	-0.032	-0.028	-0.070	0.918
2021	0007	47550	1.140	0.061	1.044	2.029	0.477	-0.009	3.506	-0.000	0.093	-0.029	-0.031	-0.070	0.916
2022	0007	47550	1.140	0.085	1.033	2.015	0.544	-0.009	3.345	-0.000	0.099	-0.024	-0.029	-0.063	0.913
2023	0007	47550	1.140	0.051	1.038	1.914	0.084	-0.011	8.685	-0.000	0.047	-0.026	0.001	-0.056	0.866
2024	0007	47550	1.140	0.041	1.031	2.018	0.723	-0.010	5.001	-0.000	0.071	-0.007	-0.013	-0.038	0.864

MODEL DC-2, 36 DEEP CHUTES, AR = 1.5, FULL PLUG

FACILITY [illegible] PROGRAM CODE

NOZZLE TYPE: DUAL FLOW (FAA)

INNER-STREAM PLUG CONFIGURATIONS: FULL, C W/O BLEED

SUPPRESSOR CONFIGURATION: 36-CHUTE, AREA RATIO = 1.5

INPUT PARAMETERS: CUTOFF RADIUS RATIO 0.0000; INNER RADIUS RATIO 0.0000; OVD 1.2480

BOC	CF	AREA	M2	PR	PTC/PR	PTI/PA	CMFCAT	CDC	CDI	CFNET1	CFNET2	F9
2735	4783	47830	0.393	0.025	1.503	1.167	0.000	0.987	9.999	0.894	0.894	1.172
2736	4783	47830	0.395	0.030	1.746	1.169	0.000	0.966	9.999	0.901	0.901	1.175
2737	4783	47830	0.328	0.034	2.006	1.179	0.000	0.964	9.999	0.903	0.903	1.169
2738	4783	47830	0.393	0.039	2.299	1.205	0.000	0.967	9.999	0.920	0.920	1.174
[illegible]												
2740	4783	47830	0.398	0.035	3.316	1.338	0.000	0.965	9.999	0.933	0.933	1.180
2741	4783	47830	0.398	0.047	2.789	1.404	0.000	0.968	9.999	0.927	0.927	1.177
2742	4783	47830	0.399	0.041	2.515	1.422	0.000	0.965	9.999	0.919	0.919	1.171
2743	4783	47830	0.329	0.036	2.005	1.410	0.000	0.966	9.999	0.905	0.905	1.170
2744	4783	47830	0.398	0.032	1.758	1.371	0.000	0.969	9.999	0.904	0.904	1.179
2745	4783	47830	0.398	0.021	1.506	1.341	0.000	0.989	9.999	0.899	0.899	1.177
2746	4783	47830	0.344	0.050	2.383	1.330	0.000	0.966	9.999	0.905	0.905	1.171
2747	4783	47830	0.395	0.073	3.017	1.371	0.000	0.966	9.999	0.931	0.931	1.178
2748	4783	47830	0.394	0.447	1.505	1.114	0.000	0.994	9.999	0.832	0.832	1.138
2749	4783	47830	0.395	0.447	1.768	1.121	0.000	0.987	9.999	0.851	0.851	1.139
2750	4783	47830	0.394	0.446	2.026	1.135	0.000	0.985	9.999	0.861	0.861	1.136
2751	4783	47830	0.394	0.447	2.510	1.163	0.000	0.968	9.999	0.888	0.888	1.145
2752	4783	47830	0.394	0.447	3.023	1.206	0.000	0.966	9.999	0.907	0.907	1.156
2753	4783	47830	0.358	0.448	3.328	1.304	0.000	0.967	9.999	0.909	0.909	1.158
2754	4783	47830	0.358	0.447	3.020	1.344	0.000	0.983	9.999	0.905	0.905	1.151
2755	4783	47830	0.358	0.447	2.510	1.359	0.000	0.983	9.999	0.889	0.889	1.142
2756	4783	47830	0.398	0.447	2.006	1.358	0.000	0.986	9.999	0.860	0.860	1.136
2757	4783	47830	0.398	0.446	1.761	1.342	0.000	0.969	9.999	0.847	0.847	1.138
2758	4783	47830	0.398	0.445	1.507	1.317	0.000	0.994	9.999	0.836	0.836	1.140
2759	4783	47830	0.398	0.445	2.008	1.307	0.000	0.965	9.999	0.862	0.862	1.136
2760	4783	47830	0.394	0.447	3.016	1.330	0.000	0.967	9.999	0.907	0.907	1.157
2761	4783	47830	0.398	0.357	1.504	1.171	0.000	0.994	9.999	0.842	0.842	1.145
2762	4783	47830	0.398	0.356	1.766	1.171	0.000	0.988	9.999	0.859	0.859	1.146
2763	4783	47830	0.398	0.357	2.015	1.182	0.000	0.976	9.999	0.872	0.872	1.145
2764	4783	47830	0.399	0.358	2.523	1.205	0.000	0.966	9.999	0.895	0.895	1.150
2765	4783	47830	0.393	0.360	3.023	1.269	0.000	0.971	9.999	0.913	0.913	1.166
2766	4783	47830	0.398	0.360	3.288	1.356	0.000	0.966	9.999	0.916	0.916	1.164
2767	4783	47830	0.398	0.361	2.559	1.412	0.000	0.966	9.999	0.910	0.910	1.159
2768	4783	47830	0.399	0.360	2.524	1.428	0.000	0.967	9.999	0.896	0.896	1.152
2769	4783	47830	0.398	0.361	2.016	1.417	0.000	0.966	9.999	0.871	0.871	1.144
2770	4783	47830	0.393	0.361	1.768	1.397	0.000	0.967	9.999	0.859	0.859	1.146
2771	4783	47830	0.398	0.361	1.505	1.363	0.000	0.992	9.999	0.851	0.851	1.149
2772	4783	47830	0.398	0.361	2.013	1.349	0.000	0.966	9.999	0.875	0.875	1.147
2773	4783	47830	0.398	0.362	2.275	1.366	0.000	0.969	9.999	0.913	0.913	1.164

FACILITY AEL PROGRAM CODE

NOZZLE TYPE — DUAL FLOW (FAA)

PL -STREAM CONFIGURATIONS — FULL PLUG W/O BLEED

SUPPRESSOR CONFIGURATION — 36-CHUTE, AREA RATIO = 1.5

FREE PARAMETERS — OUTER RADIUS RATIO 0.0000 — INNER RADIUS RATIO 0.0000 — DVD 1.2480

POS	GE	MASA	P2	MA	PTO/PA	PT1/PA	DMFCAT	DCS	CDS	DCSH	CDSH	DCPL,C	DCPL,T	DCTOT	PSUP/PA
2735	4783	47830	0.398	0.075	1.503	1.167	0.000	-0.047	21.520	-0.000	0.165	-0.038	0.012	-0.074	0.919
2736	4783	47830	0.398	0.050	1.756	1.169	0.000	-0.046	7.296	0.000	-0.014	-0.036	0.015	-0.067	0.891
2737	4783	47830	0.398	0.054	2.006	1.179	0.000	-0.045	7.550	-0.000	0.028	-0.034	0.016	-0.063	0.866
2738	4783	47830	0.398	0.059	2.499	1.205	0.000	-0.031	6.179	-0.000	0.036	-0.025	0.018	-0.039	0.868
[illegible]															
2740	4783	47830	0.398	0.075	3.316	1.338	0.000	-0.013	2.291	-0.000	0.020	-0.041	0.019	-0.035	0.922
2741	4783	47830	0.398	0.067	2.580	1.404	0.000	-0.019	3.731	-0.000	0.037	-0.035	0.020	-0.033	0.899
2742	4783	47830	0.398	0.061	2.515	1.422	0.000	-0.031	5.777	-0.000	0.021	-0.026	0.022	-0.035	0.868
2743	4783	47830	0.398	0.056	2.005	1.419	0.000	-0.045	7.089	-0.000	0.019	-0.034	0.020	-0.059	0.865
2744	4783	47830	0.398	0.052	1.758	1.371	0.000	-0.046	6.583	0.000	-0.042	-0.036	0.018	-0.064	0.891
2745	4783	47830	0.398	0.073	1.504	1.341	0.000	-0.048	25.605	-0.000	0.083	-0.039	0.018	-0.068	0.919
2746	4783	47830	0.398	0.050	2.003	1.330	0.000	-0.045	8.691	-0.000	0.015	-0.034	0.019	-0.060	0.867
2747	4783	47830	0.398	0.077	3.017	1.374	0.000	-0.018	3.037	-0.000	0.029	-0.036	0.019	-0.035	0.901
2748	4783	47830	0.398	0.447	1.506	1.114	0.000	-0.103	0.145	-0.022	0.030	-0.032	0.044	-0.112	0.823
2749	4783	47830	0.398	0.447	1.768	1.121	0.000	-0.093	0.183	-0.017	0.033	-0.031	0.039	-0.102	0.778
2750	4783	47830	0.398	0.446	2.004	1.135	0.000	-0.086	0.210	-0.015	0.036	-0.029	0.034	-0.095	0.746
2751	4783	47830	0.398	0.447	2.510	1.163	0.000	-0.058	0.201	-0.010	0.035	-0.023	0.033	-0.057	0.755
2752	4783	47830	0.398	0.447	3.023	1.206	0.000	-0.036	0.164	-0.008	0.035	-0.045	0.032	-0.057	0.800
2753	4783	47830	0.398	0.448	3.528	1.304	0.000	-0.028	0.142	-0.007	0.034	-0.066	0.031	-0.070	0.826
2754	4783	47830	0.398	0.447	3.020	1.344	0.000	-0.037	0.166	-0.008	0.035	-0.044	0.033	-0.056	0.797
2755	4783	47830	0.398	0.447	2.510	1.359	0.000	-0.059	0.202	-0.010	0.036	-0.023	0.036	-0.055	0.754
2756	4783	47830	0.398	0.447	2.004	1.358	0.000	-0.085	0.208	-0.014	0.034	-0.028	0.039	-0.088	0.746
2757	4783	47830	0.398	0.446	1.761	1.347	0.000	-0.093	0.183	-0.017	0.033	-0.030	0.042	-0.099	0.778
2758	4783	47830	0.398	0.445	1.507	1.317	0.000	-0.103	0.147	-0.021	0.031	-0.031	0.047	-0.109	0.823
2759	4783	47830	0.398	0.445	2.009	1.307	0.000	-0.085	0.210	-0.014	0.034	-0.028	0.038	-0.090	0.746
2760	4783	47830	0.398	0.447	3.016	1.330	0.000	-0.037	0.164	-0.008	0.035	-0.045	0.033	-0.056	0.800
2761	4783	47830	0.398	0.397	1.504	1.171	0.000	-0.089	0.197	-0.014	0.031	-0.031	0.015	-0.119	0.847
2762	4783	47830	0.398	0.356	1.766	1.171	0.000	-0.081	0.252	-0.011	0.033	-0.031	0.017	-0.106	0.806
2763	4783	47830	0.398	0.356	2.015	1.182	0.000	-0.075	0.292	-0.009	0.036	-0.029	0.019	-0.095	0.775
2764	4783	47830	0.398	0.358	2.523	1.205	0.000	-0.051	0.280	-0.007	0.036	-0.023	0.021	-0.061	0.782
2765	4783	47830	0.398	0.360	3.023	1.269	0.000	-0.031	0.221	-0.005	0.036	-0.042	0.022	-0.056	0.826
2766	4783	47830	0.398	0.360	3.288	1.356	0.000	-0.025	0.196	-0.005	0.035	-0.044	0.022	-0.052	0.846
2767	4783	47830	0.398	0.361	2.759	1.412	0.000	-0.034	0.228	-0.005	0.037	-0.043	0.023	-0.059	0.819
2768	4783	47830	0.398	0.360	2.524	1.426	0.000	-0.051	0.276	-0.007	0.039	-0.023	0.025	-0.057	0.782
2769	4783	47830	0.398	0.361	2.014	1.417	0.000	-0.076	0.286	-0.010	0.036	-0.030	0.023	-0.092	0.773
2770	4783	47830	0.398	0.361	1.768	1.397	0.000	-0.082	0.247	-0.011	0.034	-0.030	0.023	-0.100	0.804
2771	4783	47830	0.398	0.361	1.505	1.363	0.000	-0.090	0.195	-0.014	0.031	-0.031	0.023	-0.113	0.845
2772	4783	47830	0.398	0.361	2.013	1.349	0.000	-0.076	0.285	-0.010	0.036	-0.030	0.022	-0.093	0.773
2773	4783	47830	0.398	0.362	2.525	1.366	0.000	-0.033	0.224	-0.006	0.038	-0.043	0.024	-0.058	0.821

MODEL DC-3, 36 DEEP CHUTES, AR = 2.0, BASELINE PLUG

FACILITY KI PROGRAM COM

NOZZLE TYPE — DUAL FLOW (FAA)

INT STREAM PLUG CONFIGURATIONS — BASELINE PLUG WITH BLEED

SUPPRESSOR CONFIGURATION — 36-CHUTE, AREA RATIO = 2.0

OUTER RADIUS RATIO 0.0000 — INNER RADIUS RATIO 0.7790 — DVO 1.2480

THRUST PARAMETERS

FDC	CF	WASA	M2	M8	PTO/P4	PTI/P8	OMEGAT	CDO	CDI	CFNET1	CFNET2	F9
2025	0008	48530	0.398	0.009	1.502	0.980	0.000	0.952	9.999	0.905	0.905	1.125
2026	0008	48530	0.398	0.009	1.506	0.986	0.029	0.951	9.999	0.912	0.912	1.126
2027	0008	48530	0.398	0.009	1.504	0.994	0.059	0.950	9.999	0.921	0.921	1.127
2028	0008	48530	0.398	0.019	2.004	0.974	0.000	0.944	9.999	0.920	0.920	1.138
2029	0008	48530	0.398	0.016	2.001	0.987	0.029	0.945	9.999	0.927	0.927	1.140
2030	0008	48530	0.398	0.009	1.999	1.000	0.059	0.946	10.119	0.935	0.935	1.143
2031	0008	48530	0.398	0.026	2.513	0.968	0.000	0.944	9.999	0.928	0.928	1.140
2032	0008	48530	0.398	0.041	2.505	0.987	0.029	0.946	9.999	0.936	0.936	1.144
2033	0008	48530	0.398	0.018	2.494	1.000	0.059	0.950	1.358	0.941	0.947	1.149
2034	0008	48530	0.398	0.016	3.011	0.965	0.000	0.948	9.999	0.930	0.930	1.145
2035	0008	48530	0.398	0.042	3.015	0.997	0.029	0.948	9.999	0.939	0.939	1.145
2036	0008	48530	0.398	0.042	3.016	1.029	0.059	0.948	0.924	0.939	0.948	1.148
2037	0008	48530	0.398	0.030	3.313	0.968	0.000	0.949	9.999	0.931	0.931	1.147
2038	0008	48530	0.398	0.035	3.313	1.008	0.029	0.949	0.961	0.937	0.939	1.147
2039	0008	48530	0.398	0.026	3.311	1.051	0.059	0.949	0.769	0.938	0.950	1.149
2040	0008	48530	0.398	0.028	2.507	0.967	0.000	0.945	9.999	0.926	0.926	1.140
2041	0008	48530	0.398	0.015	2.503	1.010	0.059	0.947	1.324	0.936	0.942	1.143
2042	0008	48550	1.140	0.007	1.502	1.111	0.266	0.951	1.027	0.928	1.056	1.148
2043	0008	48550	1.140	0.015	1.501	1.513	0.547	0.952	0.996	0.932	1.447	1.184
2044	0008	48550	1.140	0.008	1.503	2.008	0.753	0.952	0.993	0.932	1.831	1.190
2045	0008	48550	1.140	0.021	1.504	2.508	0.940	0.951	0.993	0.936	2.210	1.192
2046	0008	48550	1.140	0.047	1.505	3.023	1.133	0.951	0.993	0.929	2.580	1.188
2047	0008	48550	1.140	0.039	1.502	3.515	1.323	0.952	0.996	0.953	3.042	1.210
2048	0008	48550	1.140	0.020	2.003	1.111	0.191	0.945	1.017	0.938	1.010	1.159
2049	0008	48550	1.140	0.021	1.966	1.508	0.394	0.946	0.996	0.937	1.227	1.187
2050	0008	48550	1.140	0.020	1.969	2.006	0.545	0.945	0.993	0.936	1.446	1.191
2051	0008	48550	1.140	0.039	2.003	2.514	0.682	0.945	0.993	0.939	1.665	1.193
2052	0008	48550	1.140	0.039	2.000	3.013	0.819	0.946	0.995	0.934	1.872	1.191
2053	0008	48550	1.140	0.045	2.007	3.518	0.957	0.944	0.997	0.952	2.129	1.208
2054	0008	48550	1.140	0.032	2.498	1.113	0.150	0.949	0.995	0.942	0.992	1.159
2055	0008	48550	1.140	0.021	2.493	1.512	0.315	0.948	0.993	0.940	1.146	1.182
2056	0008	48550	1.140	0.037	2.503	2.004	0.434	0.947	0.993	0.939	1.299	1.185
2057	0008	48550	1.140	0.047	2.503	2.507	0.544	0.947	0.995	0.941	1.453	1.188
2058	0008	48550	1.140	0.045	2.506	3.021	0.655	0.947	0.994	0.937	1.602	1.196
2059	0008	48550	1.140	0.046	2.513	3.511	0.763	0.944	0.996	0.952	1.781	1.201
2060	0008	48550	1.140	0.047	1.008	1.114	0.117	0.951	0.930	0.942	0.978	1.158
2061	0008	48550	1.140	0.041	3.037	1.515	0.259	0.949	0.993	0.941	1.099	1.178
2062	0008	48550	1.140	0.053	3.012	2.008	0.361	0.949	0.994	0.939	1.216	1.183
2063	0008	48550	1.140	0.051	3.016	2.515	0.451	0.949	0.994	0.941	1.334	1.185
2064	0008	48550	1.140	0.045	3.015	3.014	0.542	0.949	0.995	0.937	1.444	1.183
2065	0008	48550	1.140	0.052	3.012	3.518	0.634	0.949	0.996	0.954	1.592	1.201
2066	0008	48550	1.140	0.037	3.314	1.119	0.099	0.950	0.848	0.941	0.972	1.156
2067	0008	48550	1.140	0.018	3.292	1.509	0.232	0.950	0.970	0.940	1.076	1.176
2068	0008	48550	1.140	0.044	3.299	2.008	0.328	0.951	0.993	0.939	1.183	1.183
2069	0008	48550	1.140	0.051	3.323	2.509	0.405	0.950	0.994	0.940	1.282	1.184

FACILITY C1 PROGRAM C031

NOZZLE TYPE: DUAL FLOW (FAA)

INJ. STREAM PLUG CONFIGURATIONS: BASELINE PLUG WITH BLEED

SUPPRESSOR CONFIGURATION: 36-CHUTE, AREA RATIO = 2.0

DRAG PARAMETERS — OUTER RADIUS RATIO 0.0030 — INNER RADIUS RATIO 0.7790 — PVO 1.2480

PDC	CF	NASA	M2	MA	PTO/PA	PTI/PA	DMFGAT	DCS	CDS	DCSH	CDSH	DCPL,O	DCPL,I	DCTOT	PSUP/PA
2025	0008	48530	0.398	0.009	1.502	0.980	0.000	-0.047	170.144	-0.001	2.276	-0.028	0.004	-0.073	0.964
2026	0008	48530	0.398	0.009	1.504	0.986	0.029	-0.046	165.018	-0.001	1.953	-0.025	-0.001	-0.073	0.965
2027	0008	48530	0.398	0.009	1.504	0.994	0.059	-0.045	139.283	-0.001	2.126	-0.022	-0.003	-0.071	0.966
2028	0008	48530	0.398	0.019	2.006	0.974	0.000	-0.041	52.318	-0.001	0.739	-0.026	0.006	-0.062	0.945
2029	0008	48530	0.398	0.015	2.001	0.987	0.029	-0.040	74.725	-0.001	1.158	-0.023	0.002	-0.061	0.947
2030	0008	48530	0.398	0.009	1.999	1.000	0.059	-0.040	251.187	-0.001	3.612	-0.020	-0.000	-0.061	0.947
2031	0008	48530	0.398	0.026	2.512	0.958	0.000	-0.035	35.496	-0.001	0.502	-0.026	0.007	-0.055	0.933
2032	0008	48530	0.398	0.041	2.506	0.987	0.029	-0.034	13.586	-0.000	0.178	-0.022	0.003	-0.054	0.935
2033	0008	48530	0.398	0.018	2.494	1.000	0.059	-0.034	70.998	-0.001	1.164	-0.019	0.001	-0.053	0.936
2034	0008	48530	0.398	0.015	3.011	0.965	0.000	-0.031	106.947	-0.001	1.735	-0.026	0.007	-0.051	0.923
2035	0008	48530	0.398	0.042	3.016	0.997	0.029	-0.030	14.704	-0.000	0.186	-0.023	0.003	-0.050	0.925
2036	0008	48530	0.398	0.042	3.016	1.029	0.059	-0.029	14.287	-0.000	0.203	-0.020	0.002	-0.048	0.927
2037	0008	48530	0.398	0.030	3.313	0.968	0.000	-0.027	30.067	-0.000	0.513	-0.023	0.007	-0.044	0.924
2038	0008	48530	0.398	0.035	3.313	1.000	0.029	-0.027	20.535	-0.000	0.319	-0.021	0.003	-0.044	0.925
2039	0008	48530	0.398	0.034	3.311	1.051	0.059	-0.026	19.872	-0.000	0.314	-0.019	0.002	-0.043	0.925
2040	0008	48530	0.398	0.023	2.507	0.967	0.000	-0.036	29.171	-0.001	0.440	-0.025	0.008	-0.054	0.933
2041	0008	48530	0.398	0.015	2.503	1.010	0.059	-0.034	99.156	-0.001	1.705	-0.019	0.001	-0.053	0.935
2042	0008	48550	1.140	0.007	1.502	1.111	0.266	-0.040	272.905	-0.001	4.330	-0.019	-0.000	-0.050	0.966
2043	0008	48550	1.140	0.015	1.501	1.515	0.547	-0.020	53.337	-0.001	0.899	-0.015	0.002	-0.044	0.965
2044	0008	48550	1.140	0.008	1.503	2.009	0.753	-0.024	198.765	-0.001	4.430	-0.013	-0.010	-0.047	0.964
2045	0008	48550	1.140	0.021	1.504	2.509	0.940	-0.020	28.040	-0.000	0.601	-0.010	-0.020	-0.051	0.964
2046	0008	48550	1.140	0.047	1.505	3.023	1.133	-0.017	5.553	-0.000	0.086	-0.008	-0.032	-0.057	0.965
2047	0008	48550	1.140	0.039	1.502	3.515	1.323	-0.015	8.196	-0.000	0.179	-0.007	-0.021	-0.043	0.964
2048	0008	48550	1.140	0.020	2.003	1.111	0.191	-0.037	47.014	-0.001	0.776	-0.018	0.001	-0.054	0.947
2049	0008	48550	1.140	0.021	1.996	1.508	0.394	-0.031	61.801	-0.000	0.654	-0.015	0.002	-0.044	0.947
2050	0008	48550	1.140	0.020	1.995	2.006	0.545	-0.026	47.165	-0.000	0.912	-0.013	-0.011	-0.050	0.947
2051	0008	48550	1.140	0.039	2.003	2.514	0.682	-0.023	17.332	-0.000	0.237	-0.011	-0.013	-0.048	0.947
2052	0008	48550	1.140	0.039	2.000	3.013	0.819	-0.020	12.354	-0.000	0.225	-0.009	-0.020	-0.050	0.946
2053	0008	48550	1.140	0.049	2.007	3.518	0.957	-0.018	7.523	-0.000	0.135	-0.008	-0.020	-0.046	0.947
2054	0008	48550	1.140	0.032	2.498	1.113	0.150	-0.032	27.456	-0.000	0.346	-0.017	0.001	-0.048	0.936
2055	0008	48550	1.140	0.021	2.493	1.512	0.315	-0.028	50.858	-0.000	0.837	-0.015	0.001	-0.042	0.935
2056	0008	48550	1.140	0.037	2.503	2.004	0.434	-0.025	16.719	-0.000	0.254	-0.013	-0.013	-0.052	0.935
2057	0008	48550	1.140	0.047	2.503	2.507	0.544	-0.022	10.372	-0.000	0.159	-0.012	-0.010	-0.045	0.935
2058	0008	48550	1.140	0.045	2.506	3.021	0.655	-0.020	11.210	-0.000	0.187	-0.010	-0.011	-0.041	0.935
2059	0008	48550	1.140	0.046	2.513	3.511	0.763	-0.018	10.508	-0.000	0.200	-0.009	-0.014	-0.041	0.936
2060	0008	48550	1.140	0.047	3.008	1.114	0.117	-0.028	11.511	-0.000	0.149	-0.018	0.001	-0.045	0.928
2061	0008	48550	1.140	0.041	3.007	1.515	0.259	-0.025	15.182	-0.000	0.229	-0.015	0.001	-0.040	0.927
2062	0008	48550	1.140	0.053	3.012	2.008	0.361	-0.023	8.891	-0.000	0.136	-0.013	-0.011	-0.048	0.927
2063	0008	48550	1.140	0.051	3.016	2.515	0.451	-0.021	9.622	-0.000	0.147	-0.012	-0.012	-0.046	0.927
2064	0008	48550	1.140	0.045	3.016	3.014	0.542	-0.019	12.612	-0.000	0.236	-0.010	-0.014	-0.044	0.927
2065	0008	48550	1.140	0.052	3.012	3.518	0.634	-0.017	9.378	-0.000	0.192	-0.009	-0.013	-0.040	0.928
2066	0008	48550	1.140	0.037	3.314	1.119	0.099	-0.025	18.946	-0.000	0.288	-0.017	0.001	-0.041	0.926
2067	0008	48550	1.140	0.018	3.292	1.509	0.232	-0.024	76.676	-0.000	1.574	-0.014	0.001	-0.037	0.925
2068	0008	48550	1.140	0.044	3.299	2.008	0.328	-0.021	13.255	-0.000	0.246	-0.012	-0.011	-0.044	0.926
2069	0008	48550	1.140	0.051	3.323	2.509	0.408	-0.019	9.721	-0.000	0.174	-0.011	-0.011	-0.041	0.927

FACILITY [illegible]X1 PROGRAM C031 — NOZZLE TYPE DUAL FLOW (FAA) — TWO-STREAM PLUG CONFIGURATIONS BASELINE PLUG WITH BLEED — SUPPRESSOR CONFIGURATION 36-CHUTE, AREA RATIO = 2.0

THRUST PARAMETERS — OUTER RADIUS RATIO 0.9030 — INNER RADIUS RATIO 0.7790 — DVD 1.2480

EPS	CF	PASA	D2	PA	PTO/PA	PTI/PA	OMEGAT	CDO	CDI	CFNET1	CFNET2	F9
2070	0008	48550	1.140	0.453	3.329	3.018	0.492	0.950	0.995	0.930	1.373	1.176
2071	0008	48550	1.140	0.451	3.307	3.517	0.576	0.950	0.996	0.948	1.506	1.196
2072	0008	48550	1.140	0.012	2.509	1.112	0.150	0.945	0.999	0.940	0.990	1.155
2073	0008	48550	1.140	0.450	2.499	3.507	0.764	0.950	0.996	0.954	1.789	1.206
2074	0008	48530	0.398	0.449	1.504	0.990	0.000	0.970	9.999	0.790	0.790	1.079
2075	0008	48530	0.398	0.449	1.501	1.000	0.029	0.970	9.999	0.800	0.800	1.081
2076	0008	48530	0.398	0.447	1.503	1.009	0.059	0.969	0.811	0.806	0.813	1.083
2077	0008	48530	0.398	0.448	2.007	0.990	0.000	0.947	9.999	0.830	0.830	1.082
2078	0008	48530	0.398	0.449	2.005	1.006	0.029	0.939	0.658	0.845	0.847	1.085
2079	0008	48530	0.398	0.447	2.007	1.026	0.059	0.946	0.650	0.842	0.852	1.087
2080	0008	48530	0.398	0.448	2.515	0.985	0.000	0.943	9.999	0.856	0.856	1.086
2081	0008	48530	0.398	0.449	2.517	1.012	0.029	0.945	0.596	0.861	0.864	1.087
~~2082~~	~~0008~~	~~48530~~	~~0.398~~	~~0.448~~	~~2.517~~	~~1.040~~	~~0.059~~	~~0.956~~	~~0.630~~	~~0.870~~	~~0.888~~	~~1.100~~
2083	0008	48530	0.398	0.448	3.019	0.984	0.000	0.948	9.999	0.874	0.874	1.098
2084	0008	48530	0.398	0.448	3.017	1.022	0.029	0.949	0.526	0.880	0.884	1.100
2085	0008	48530	0.398	0.449	3.008	1.064	0.059	0.952	0.626	0.882	0.895	1.103
2086	0008	48530	0.398	0.449	3.322	0.985	0.000	0.950	9.999	0.881	0.881	1.104
2087	0008	48530	0.398	0.448	3.322	1.032	0.029	0.949	0.483	0.888	0.892	1.105
2088	0008	48530	0.398	0.449	3.322	1.080	0.059	0.945	0.603	0.893	0.908	1.107
2089	0008	48530	0.398	0.448	2.513	0.984	0.000	0.943	9.999	0.859	0.859	1.087
2090	0008	48530	0.398	0.447	2.521	1.040	0.059	0.943	0.654	0.861	0.872	1.086
2091	0008	48550	1.140	0.447	1.501	1.113	0.441	0.966	0.934	0.825	0.929	1.101
2092	0008	48550	1.140	0.447	1.502	1.516	0.533	0.969	0.987	0.857	1.318	1.144
2093	0008	48550	1.140	0.448	1.507	2.015	0.743	0.968	0.993	0.873	1.705	1.155
2094	0008	48550	1.140	0.447	1.502	2.514	0.927	0.970	0.995	0.888	2.083	1.162
2095	0008	48550	1.140	0.449	1.503	3.022	1.115	0.969	0.995	0.889	2.444	1.161
2096	0008	48550	1.140	0.448	1.502	3.516	1.302	0.959	0.997	0.916	2.891	1.184
2097	0008	48550	1.140	0.448	2.010	1.112	0.160	0.945	0.854	0.858	0.914	1.103
2098	0008	48550	1.140	0.446	2.305	1.515	0.386	0.946	0.975	0.873	1.139	1.139
2099	0008	48550	1.140	0.448	2.006	2.016	0.545	0.946	0.993	0.885	1.366	1.151
2100	0008	48550	1.140	0.447	2.007	2.510	0.680	0.946	0.994	0.893	1.580	1.156
2101	0008	48550	1.140	0.448	2.007	3.020	0.814	0.944	0.997	0.898	1.793	1.157
2102	0008	48550	1.140	0.448	2.008	3.522	0.954	0.946	0.995	0.916	2.045	1.[illegible]
2103	0008	48550	1.140	0.447	2.520	1.113	0.121	0.945	0.805	0.872	0.910	1.100
2104	0008	48550	1.140	0.447	2.499	1.513	0.305	0.951	0.965	0.886	1.074	1.137
2105	0008	48550	1.140	0.447	2.495	2.014	0.435	0.953	0.993	0.893	1.238	1.151
2106	0008	48550	1.140	0.448	2.513	2.519	0.544	0.947	0.993	0.898	1.388	1.151
2107	0008	48550	1.140	0.448	2.510	3.018	0.652	0.942	0.988	0.906	1.546	1.154
2108	0008	48550	1.140	0.448	2.480	3.522	0.762	0.959	0.995	0.920	1.727	1.179
2109	0008	48550	1.140	0.448	3.322	1.116	0.093	0.945	0.735	0.890	0.918	1.107
2110	0008	48550	1.140	0.448	3.013	1.517	0.250	0.949	0.948	0.895	1.039	1.135
2111	0008	48550	1.140	0.448	3.011	2.015	0.361	0.950	0.991	0.898	1.163	1.146
2112	0008	48550	1.140	0.448	3.022	2.513	0.450	0.948	0.993	0.903	1.279	1.150
2113	0008	48550	1.140	0.449	3.022	3.028	0.543	0.948	0.994	0.893	1.379	1.142
2114	0008	48550	1.140	0.450	3.327	3.525	0.632	0.947	0.993	0.917	1.529	1.164

FACILITY X1 PROGRAM C031 — NOZZLE TYPE: DUAL FLOW (FAA) — PLUG CONFIGURATIONS: BASELINE PLUG WITH BLEED — SUPPRESSOR CONFIGURATION: 36-CHUTE, AREA RATIO = 2.0

DRAG PARAMETERS — OUTER RADIUS RATIO 0.0000 — INNER RADIUS RATIO 0.7790 — DVO 1.2480

PDG	CF	WASE	D2	M8	PTO/PA	PTT/PA	OMEGAT	DCS	CDS	DCSH	CDSH	DCPL,O	DCPL,T	DCTOT	PSUP/PA
2070	0008	48550	1.140	0.453	3.320	3.018	0.492	-0.018	8.959	-0.000	0.152	-0.009	-0.021	-0.048	0.927
2071	0008	48550	1.140	0.451	3.307	3.517	0.576	-0.017	9.916	-0.000	0.214	-0.008	-0.013	-0.038	0.926
2072	0008	48550	1.140	0.012	2.509	1.117	0.150	-0.032	159.386	-0.001	2.841	-0.017	0.001	-0.049	0.936
2073	0008	48550	1.140	0.050	2.489	3.507	0.764	-0.018	8.813	-0.000	0.156	-0.009	-0.015	-0.043	0.936
2074	0008	48530	0.398	0.449	1.504	0.990	0.000	-0.152	0.202	-0.015	0.019	-0.020	0.022	-0.165	0.883
2075	0008	48530	0.398	0.449	1.501	1.000	0.029	-0.151	0.198	-0.014	0.018	-0.017	0.018	-0.164	0.885
2076	0008	48530	0.398	0.447	1.500	1.005	0.059	-0.146	0.195	-0.014	0.019	-0.015	0.015	-0.160	0.888
2077	0008	48530	0.398	0.448	2.007	0.999	0.000	-0.128	0.295	-0.010	0.022	-0.012	0.018	-0.141	0.829
2078	0008	48530	0.398	0.448	2.005	1.006	0.029	-0.126	0.291	-0.010	0.022	-0.010	0.014	-0.132	0.832
2079	0008	48530	0.398	0.447	2.007	1.026	0.059	-0.122	0.285	-0.008	0.022	-0.008	0.011	-0.128	0.835
2080	0008	48530	0.398	0.448	2.515	0.985	0.000	-0.112	0.367	-0.007	0.024	-0.014	0.015	-0.119	0.798
2081	0008	48530	0.398	0.449	2.517	1.012	0.029	-0.109	0.358	-0.007	0.023	-0.011	0.011	-0.116	0.792
[illegible]															
2083	0008	48530	0.398	0.448	3.014	0.984	0.000	-0.094	0.399	-0.006	0.024	-0.015	0.014	-0.101	0.769
2084	0008	48530	0.398	0.448	3.017	1.022	0.029	-0.092	0.395	-0.006	0.024	-0.013	0.010	-0.101	0.771
2085	0008	48530	0.398	0.449	3.008	1.064	0.059	-0.090	0.390	-0.006	0.024	-0.011	0.008	-0.099	0.774
2086	0008	48530	0.398	0.449	3.322	0.985	0.000	-0.081	0.393	-0.005	0.024	-0.016	0.014	-0.088	0.772
2087	0008	48530	0.398	0.448	3.322	1.032	0.029	-0.080	0.390	-0.005	0.024	-0.013	0.010	-0.088	0.774
2088	0008	48530	0.399	0.449	3.322	1.083	0.059	-0.079	0.386	-0.005	0.023	-0.011	0.007	-0.087	0.776
2089	0008	48530	0.398	0.448	2.510	0.985	0.000	-0.117	0.366	-0.007	0.024	-0.014	0.016	-0.117	0.789
2090	0008	48530	0.398	0.447	2.521	1.040	0.059	-0.106	0.355	-0.007	0.024	-0.009	0.009	-0.113	0.796
2091	0008	48550	1.140	0.447	1.501	1.113	0.241	-0.125	0.187	-0.012	0.018	-0.009	0.013	-0.133	0.892
2092	0008	48550	1.140	0.447	1.502	1.516	0.838	-0.091	0.187	-0.008	0.017	-0.007	0.012	-0.095	0.892
2093	0008	48550	1.140	0.448	1.503	2.015	0.743	-0.073	0.188	-0.007	0.017	-0.006	-0.006	-0.091	0.891
2094	0008	48550	1.140	0.447	1.502	2.514	0.927	-0.060	0.187	-0.006	0.018	-0.005	-0.012	-0.082	0.892
2095	0008	48550	1.140	0.449	1.503	3.022	1.115	-0.050	0.183	-0.005	0.017	-0.004	-0.028	-0.087	0.894
2096	0008	48550	1.140	0.448	1.502	3.516	1.302	-0.044	0.183	-0.004	0.018	-0.003	-0.016	-0.067	0.894
2097	0008	48550	1.140	0.448	2.010	1.112	0.160	-0.112	0.276	-0.009	0.021	-0.009	0.009	-0.114	0.840
2098	0008	48550	1.140	0.446	2.006	1.515	0.386	-0.091	0.276	-0.007	0.022	-0.001	0.008	-0.091	0.841
2099	0008	48550	1.140	0.448	2.006	2.016	0.545	-0.077	0.274	-0.006	0.021	-0.001	-0.011	-0.095	0.841
2100	0008	48550	1.140	0.447	2.007	2.510	0.680	-0.067	0.274	-0.005	0.021	-0.001	-0.008	-0.081	0.842
2101	0008	48550	1.140	0.448	2.007	3.020	0.814	-0.059	0.270	-0.004	0.021	-0.000	-0.015	-0.079	0.843
2102	0008	48550	1.140	0.448	2.008	3.522	0.954	-0.052	0.271	-0.004	0.021	0.000	-0.016	-0.072	0.843
2103	0008	48550	1.140	0.447	2.520	1.113	0.121	-0.101	0.348	-0.007	0.023	-0.006	0.007	-0.106	0.799
2104	0008	48550	1.140	0.447	2.499	1.513	0.305	-0.086	0.343	-0.006	0.023	-0.003	0.005	-0.090	0.803
2105	0008	48550	1.140	0.447	2.495	2.014	0.435	-0.075	0.340	-0.005	0.023	-0.003	-0.010	-0.093	0.804
2106	0008	48550	1.140	0.448	2.516	2.519	0.544	-0.067	0.339	-0.004	0.022	-0.002	-0.009	-0.082	0.804
2107	0008	48550	1.140	0.448	2.510	3.018	0.652	-0.060	0.333	-0.004	0.022	-0.001	-0.011	-0.075	0.807
2108	0008	48550	1.140	0.448	2.480	3.522	0.762	-0.054	0.330	-0.004	0.022	-0.000	-0.009	-0.067	0.809
2109	0008	48550	1.140	0.448	3.022	1.116	0.093	-0.089	0.388	-0.005	0.024	-0.009	0.007	-0.096	0.775
2110	0008	48550	1.140	0.448	3.013	1.517	0.250	-0.077	0.380	-0.005	0.023	-0.005	0.004	-0.083	0.780
2111	0008	48550	1.140	0.448	3.011	2.015	0.361	-0.069	0.379	-0.004	0.023	-0.004	-0.009	-0.085	0.781
2112	0008	48550	1.140	0.448	3.022	2.513	0.450	-0.062	0.377	-0.004	0.023	-0.003	-0.011	-0.081	0.782
2113	0008	48550	1.140	0.449	3.022	3.028	0.543	-0.057	0.373	-0.003	0.023	-0.002	-0.025	-0.087	0.783
2114	0008	48550	1.140	0.450	3.027	3.525	0.632	-0.052	0.369	-0.003	0.022	-0.001	-0.011	-0.067	0.784

FACILITY B* * PROGRAM CODE

NOZZLE TYPE — INNER STREAM PLUG CONFIGURATIONS — SUPPRESSOR CONFIGURATION
DUAL FLOW (FAA) — BASELINE PLUG WITH BLEED — 36-CHUTE, AREA RATIO = 2.0

THRUST PARAMETERS — OUTER RADIUS RATIO 0.9930 — INNER RADIUS RATIO 0.7790 — DVD 1.2480

PCS	CF	PASA	D2	MA	PTO/PA	PTI/PA	DMFGAT	CDO	CDI	CFNET1	CFNET2	F9
2115	0008	48550	1.140	0.448	3.328	1.116	0.077	0.949	0.670	0.894	0.915	1.111
2116	0008	48550	1.140	0.449	3.317	1.517	0.223	0.949	0.930	0.901	1.025	1.136
2117	0008	48550	1.140	0.449	3.310	2.014	0.328	0.950	0.991	0.901	1.135	1.147
2118	0008	48550	1.140	0.449	3.322	2.516	0.409	0.950	0.994	0.903	1.233	1.149
2119	0008	48550	1.140	0.450	3.325	3.024	0.491	0.950	0.994	0.896	1.321	1.143
2120	0008	48550	1.140	0.450	3.320	3.525	0.575	0.950	0.995	0.915	1.442	1.163
2121	0008	48550	1.140	0.448	2.524	1.118	0.124	0.944	0.810	0.873	0.913	1.100
2122	0008	48550	1.140	0.449	2.501	3.517	0.760	0.950	0.993	0.920	1.720	1.173
2123	0008	48530	0.398	0.447	2.517	1.041	0.059	0.946	0.649	0.866	0.878	1.092
2124	0008	48530	0.399	0.358	1.505	0.992	0.000	0.964	9.999	0.817	0.817	1.089
2125	0008	48530	0.398	0.359	1.503	0.999	0.029	0.964	9.999	0.827	0.827	1.091
2126	0008	48530	0.398	0.362	1.504	1.009	0.059	0.963	0.800	0.831	0.838	1.092
2127	0008	48530	0.398	0.362	2.011	0.989	0.006	0.946	9.999X	0.854	0.854	1.097
2128	0008	48530	0.398	0.361	2.017	1.006	0.029	0.943	0.654	0.858	0.860	1.095
2129	0008	48530	0.398	0.362	2.005	1.024	0.059	0.948	0.678	0.866	0.876	1.103
[illegible]												
2131	0008	48530	0.398	0.362	2.520	1.017	0.029	0.948	0.589	0.882	0.885	1.104
2132	0008	48530	0.398	0.362	2.521	1.041	0.059	0.946	0.647	0.885	0.896	1.105
2133	0008	48530	0.398	0.361	3.007	0.980	0.000	0.950	9.999	0.890	0.890	1.112
2134	0008	48530	0.398	0.362	3.020	1.019	0.029	0.945	0.558	0.899	0.902	1.112
2135	0008	48530	0.398	0.362	3.021	1.059	0.059	0.949	0.654	0.899	0.912	1.115
2136	0008	48530	0.398	0.362	3.302	0.980	0.000	0.947	9.999	0.900	0.900	1.117
2137	0008	48530	0.398	0.361	3.295	1.027	0.029	0.948	0.514	0.904	0.908	1.117
2138	0008	48530	0.398	0.362	3.274	1.073	0.059	0.950	0.638	0.904	0.918	1.120
2139	0008	48530	0.398	0.362	2.517	0.984	0.000	0.948	9.999	0.874	0.874	1.102
2140	0008	48530	0.398	0.362	2.513	1.039	0.059	0.946	0.660	0.886	0.897	1.106
2141	0008	48530	0.398	0.361	2.510	0.993	0.030	0.950	9.999	0.875	0.875	1.104
2142	0008	48550	1.140	0.362	1.503	1.113	0.241	0.965	0.938	0.850	0.957	1.112
2143	0008	48550	1.140	0.361	1.501	1.516	0.532	0.965	0.986	0.876	1.345	1.154
2144	0008	48550	1.140	0.361	1.501	2.014	0.746	0.966	0.994	0.890	1.744	1.166
2145	0008	48550	1.140	0.362	1.502	2.520	0.933	0.966	0.995	0.900	2.122	1.171
2146	0008	48550	1.140	0.362	1.504	3.017	1.118	0.955	0.996	0.900	2.477	1.169
2147	0008	48550	1.140	0.362	1.504	3.519	1.305	0.965	0.996	0.925	2.923	1.190
2148	0008	48550	1.140	0.361	2.015	1.117	0.166	0.945	0.872	0.873	0.933	1.113
2149	0008	48550	1.140	0.362	2.009	1.512	0.385	0.946	0.978	0.889	1.158	1.150
2150	0008	48550	1.140	0.362	2.008	2.017	0.645	0.947	0.995	0.895	1.385	1.161
2151	0008	48550	1.140	0.363	2.010	2.524	0.683	0.947	0.995	0.904	1.603	1.166
2152	0008	48550	1.140	0.363	2.012	3.019	0.816	0.946	0.995	0.904	1.805	1.165
2153	0008	48550	1.140	0.363	2.009	3.515	0.951	0.947	0.995	0.926	2.063	1.186
2154	0008	48550	1.140	0.363	2.517	1.116	0.124	0.949	0.820	0.892	0.933	1.117
2155	0008	48550	1.140	0.363	2.519	1.515	0.306	0.946	0.958	0.899	1.090	1.144
2156	0008	48550	1.140	0.362	2.511	2.017	0.435	0.949	0.994	0.903	1.251	1.157
2157	0008	48550	1.140	0.362	2.511	2.519	0.565	0.948	0.995	0.910	1.406	1.161
2158	0008	48550	1.140	0.362	2.519	3.020	0.651	0.948	0.995	0.910	1.550	1.162
2159	0008	48550	1.140	0.363	2.527	3.520	0.760	0.944	0.996	0.926	1.728	1.177

FACILITY XI PROGRAM CO3I

NOZZLE TYPE: DUAL FLOW (FAAI)

IN-STREAM PLUG CONFIGURATIONS: BASELINE PLUG WITH BLEED

SUPPRESSOR CONFIGURATION: 36-CHUTE, AREA RATIO = 2.0

DRAG PARAMETERS

OUTER RADIUS RATIO: 0.0000

INNER RADIUS RATIO: 0.7790

DVD: 1.2480

PRG	GE	NASA	D2	MA	PT2/PA	PT1/PA	OMEGAT	DCS	CDS	DCSH	CDSH	DCPL,O	DCPL,I	DCTOT	PSUP/PA
2115	0008	48550	1.140	2.449	3.328	1.114	0.077	-0.077	0.394	-0.005	0.024	-0.010	0.006	-0.085	0.777
2116	0008	48550	1.140	0.449	3.317	1.517	0.223	-0.069	0.379	-0.004	0.023	-0.005	0.003	-0.075	0.780
2117	0008	48550	1.140	0.449	3.310	2.014	0.328	-0.062	0.377	-0.004	0.023	-0.004	-0.009	-0.079	0.781
2118	0008	48550	1.140	0.449	3.322	2.516	0.409	-0.057	0.376	-0.003	0.023	-0.003	-0.014	-0.077	0.782
2119	0008	48550	1.140	0.450	3.325	3.024	0.491	-0.052	0.372	-0.003	0.022	-0.002	-0.027	-0.084	0.783
2120	0008	48550	1.140	0.450	3.320	3.525	0.575	-0.048	0.370	-0.003	0.022	-0.001	-0.013	-0.065	0.784
2121	0008	48550	1.140	0.449	2.524	1.119	0.124	-0.101	0.348	-0.007	0.023	-0.006	0.008	-0.106	0.799
2122	0008	48550	1.140	0.449	2.501	1.517	0.760	-0.056	0.333	-0.004	0.022	-0.000	-0.015	-0.074	0.806
2123	0008	48530	0.398	0.447	2.517	1.041	0.059	-0.106	0.345	-0.007	0.023	-0.009	0.009	-0.113	0.795
2124	0008	48530	0.398	0.358	1.505	0.992	0.000	-0.133	0.276	-0.010	0.021	-0.018	0.010	-0.151	0.898
2125	0008	48530	0.398	0.359	1.503	0.992	0.029	-0.130	0.267	-0.010	0.021	-0.016	0.006	-0.150	0.901
2126	0008	48530	0.398	0.362	1.504	1.009	0.059	-0.128	0.267	-0.010	0.020	-0.013	0.002	-0.148	0.901
2127	0008	48530	0.398	0.362	2.011	0.989	0.006	-0.115	0.408	-0.007	0.024	-0.015	0.010	-0.126	0.846
2128	0008	48530	0.398	0.361	2.017	1.006	0.029	-0.112	0.403	-0.007	0.024	-0.011	0.006	-0.124	0.848
2129	0008	48530	0.398	0.362	2.006	1.024	0.059	-0.110	0.396	-0.007	0.024	-0.010	0.004	-0.123	0.851
2130	0008	48530	0.398	0.362	2.013	0.986	0.000	-0.107	0.403	-0.005	0.024	-0.010	0.004	-0.107	0.848
2131	0008	48530	0.398	0.362	2.520	1.012	0.029	-0.094	0.474	-0.005	0.026	-0.013	0.007	-0.105	0.820
2132	0008	48530	0.398	0.362	2.521	1.041	0.059	-0.092	0.468	-0.005	0.025	-0.011	0.004	-0.103	0.823
2133	0008	48530	0.398	0.361	3.007	0.980	0.000	-0.081	0.529	-0.004	0.027	-0.018	0.009	-0.094	0.801
2134	0008	48530	0.398	0.362	3.020	1.019	0.029	-0.079	0.519	-0.004	0.027	-0.015	0.006	-0.093	0.804
2135	0008	48530	0.398	0.362	3.021	1.059	0.059	-0.078	0.514	-0.004	0.027	-0.013	0.003	-0.091	0.805
2136	0008	48530	0.398	0.362	3.302	0.980	0.000	-0.070	0.516	-0.004	0.028	-0.018	0.009	-0.083	0.805
2137	0008	48530	0.398	0.361	3.296	1.027	0.029	-0.069	0.515	-0.004	0.026	-0.015	0.006	-0.082	0.806
2138	0008	48530	0.398	0.362	3.274	1.073	0.059	-0.069	0.511	-0.003	0.026	-0.013	0.003	-0.082	0.807
2139	0008	48530	0.398	0.362	2.517	0.984	0.000	-0.096	0.482	-0.005	0.026	-0.016	0.010	-0.107	0.818
2140	0008	48530	0.398	0.362	2.513	1.039	0.059	-0.092	0.470	-0.005	0.025	-0.011	0.004	-0.104	0.823
2141	0008	48530	0.398	0.361	2.510	0.983	0.000	-0.095	0.485	-0.005	0.027	-0.016	0.010	-0.107	0.817
2142	0008	48550	1.140	0.362	1.503	1.113	0.241	-0.110	0.250	-0.008	0.018	-0.007	0.004	-0.121	0.905
2143	0008	48550	1.140	0.361	1.501	1.510	0.532	-0.081	0.252	-0.006	0.019	-0.007	0.004	-0.090	0.905
2144	0008	48550	1.140	0.361	1.501	2.014	0.746	-0.063	0.250	-0.005	0.020	-0.005	-0.009	-0.082	0.906
2145	0008	48550	1.140	0.362	1.502	2.520	0.933	-0.052	0.249	-0.004	0.019	-0.004	-0.017	-0.078	0.906
2146	0008	48550	1.140	0.362	1.504	3.017	1.118	-0.045	0.248	-0.003	0.019	-0.003	-0.031	-0.082	0.906
2147	0008	48550	1.140	0.362	1.504	3.519	1.305	-0.039	0.247	-0.003	0.019	-0.003	-0.032	-0.076	0.907
2148	0008	48550	1.140	0.361	2.016	1.117	0.156	-0.101	0.386	-0.006	0.023	-0.006	0.003	-0.110	0.855
2149	0008	48550	1.140	0.362	2.008	1.512	0.386	-0.083	0.382	-0.005	0.023	-0.005	0.003	-0.090	0.856
2150	0008	48550	1.140	0.362	2.008	2.017	0.545	-0.069	0.381	-0.004	0.023	-0.003	-0.013	-0.090	0.856
2151	0008	48550	1.140	0.363	2.010	2.524	0.683	-0.060	0.378	-0.004	0.023	-0.003	-0.011	-0.078	0.857
2152	0008	48550	1.140	0.363	2.012	3.019	0.816	-0.053	0.376	-0.003	0.023	-0.002	-0.017	-0.075	0.857
2153	0008	48550	1.140	0.363	2.009	3.515	0.951	-0.047	0.375	-0.003	0.023	-0.001	-0.022	-0.074	0.858
2154	0008	48550	1.140	0.363	2.517	1.116	0.124	-0.088	0.461	-0.005	0.025	-0.008	0.003	-0.098	0.825
2155	0008	48550	1.140	0.363	2.519	1.515	0.306	-0.075	0.455	-0.004	0.025	-0.005	0.002	-0.082	0.828
2156	0008	48550	1.140	0.362	2.511	2.017	0.435	-0.065	0.452	-0.004	0.025	-0.004	-0.013	-0.086	0.829
2157	0008	48550	1.140	0.362	2.511	2.519	0.565	-0.058	0.453	-0.003	0.025	-0.003	-0.010	-0.075	0.829
2158	0008	48550	1.140	0.362	2.519	3.020	0.691	-0.052	0.449	-0.003	0.025	-0.002	-0.012	-0.070	0.830
2159	0008	48550	1.140	0.363	2.527	3.520	0.760	-0.047	0.444	-0.003	0.024	-0.001	-0.016	-0.068	0.831

FACILITY X1 PROGRAM C031 NOZZLE TYPE DUAL FLOW (FAA) IN-STREAM PLUG CONFIGURATIONS BASELINE PLUG WITH BLEED SUPPRESSOR CONFIGURATION 36-CHUTE, AREA RATIO = 2.0

THRUST PARAMETERS OUTER RADIUS RATIO 0.0000 INNER RADIUS RATIO 0.7790 OVD 1.2480

PTG	CF	NASA	D2	MA	PTO/PA	PTI/PA	OMEGAT	CDD	CDI	CFNET1	CFNET2	F9
2160	0008	48550	1.140	0.362	3.013	1.114	0.095	0.949	0.758	0.902	0.930	1.120
2161	0008	48550	1.140	0.362	3.009	1.511	0.250	0.949	0.953	0.908	1.054	1.147
2162	0008	48550	1.140	0.363	3.007	2.017	0.363	0.950	0.994	0.910	1.181	1.157
2163	0008	48550	1.140	0.363	3.013	2.523	0.453	0.950	0.994	0.915	1.299	1.162
2164	0008	48550	1.140	0.363	3.021	3.020	0.542	0.949	0.995	0.904	1.394	1.153
2165	0008	48550	1.140	0.363	3.017	3.522	0.633	0.945	0.991	0.932	1.555	1.177
2166	0008	48550	1.140	0.363	3.323	1.116	0.080	0.949	0.698	0.910	0.934	1.125
2167	0008	48550	1.140	0.363	3.275	1.511	0.227	0.949	0.943	0.912	1.041	1.148
2168	0008	48550	1.140	0.362	3.273	2.024	0.339	0.950	0.992	0.911	1.158	1.157
2169	0008	48550	1.140	0.362	3.232	2.530	0.423	0.950	0.994	0.916	1.267	1.162
2170	0008	48550	1.140	0.362	3.243	3.017	0.504	0.949	0.994	0.905	1.349	1.152
2171	0008	48550	1.140	0.363	3.223	3.517	0.591	0.951	0.996	0.926	1.490	1.175

FACILITY : 1 PROGRAM C031 NOZZLE TYPE DUAL FLOW (FAA) IN-STREAM PLUG CONFIGURATIONS BASELINE PLUG WITH BLEED SUPPRESSOR CONFIGURATION 36-CHUTE, AREA RATIO = 2.0

DRAG PARAMETERS OUTER RADIUS RATIO 0.0000 INNER RADIUS RATIO 0.7790 OVD 1.2480

PTG	CF	NASA	D2	MA	PTO/PA	PTI/PA	OMEGAT	DCS	CDS	DCSH	CDSH	DCPL,D	DCPL,T	DCTOT	PSUP/PA
2160	0008	48550	1.140	0.362	3.013	1.116	0.095	-0.075	0.512	-0.004	0.026	-0.011	0.003	-0.087	0.807
2161	0008	48550	1.140	0.362	3.009	1.511	0.250	-0.067	0.505	-0.003	0.026	-0.007	0.001	-0.076	0.809
2162	0008	48550	1.140	0.363	3.007	2.017	0.363	-0.059	0.500	-0.003	0.025	-0.006	-0.011	-0.079	0.810
2163	0008	48550	1.140	0.363	3.013	2.523	0.453	-0.054	0.500	-0.003	0.026	-0.005	-0.011	-0.073	0.810
2164	0008	48550	1.140	0.363	3.021	3.020	0.542	-0.049	0.495	-0.002	0.025	-0.003	-0.024	-0.079	0.812
2165	0008	48550	1.140	0.363	3.017	3.522	0.633	-0.046	0.493	-0.002	0.025	-0.002	-0.014	-0.055	0.812
2166	0008	48550	1.140	0.363	3.323	1.116	0.080	-0.064	0.501	-0.003	0.026	-0.012	0.003	-0.078	0.810
2167	0008	48550	1.140	0.363	3.275	1.511	0.227	-0.060	0.500	-0.003	0.025	-0.008	0.001	-0.070	0.810
2168	0008	48550	1.140	0.362	3.273	2.024	0.339	-0.055	0.503	-0.003	0.026	-0.006	-0.011	-0.075	0.810
2169	0008	48550	1.140	0.362	3.232	2.530	0.423	-0.050	0.499	-0.003	0.026	-0.005	-0.010	-0.068	0.811
2170	0008	48550	1.140	0.362	3.243	3.017	0.504	-0.046	0.496	-0.002	0.026	-0.004	-0.026	-0.079	0.813
2171	0008	48550	1.140	0.363	3.223	3.517	0.591	-0.043	0.493	-0.002	0.025	-0.003	-0.014	-0.062	0.812

MODEL DC-4, 36 DEEP CHUTES, AR = 2.0, REDUCED AREA

FACILITY P 1 PROGRAM CODE

NOZZLE TYPE: DUAL FLOW (FAN)

FAN STREAM PLUG CONFIGURATIONS: 1/2 BLEED AREA WITH BLEED

SUPPRESSOR CONFIGURATION: 36-CHUTE, AREA RATIO = 2.0

TARGET PARAMETERS: OUTER RADIUS RATIO 0.9370 INNER RADIUS RATIO 0.8890 OVD 1.2480

ECC	CS	PASS	M2	M1	PT2/P0	PT1/P0	AMFGAT	CDD	CDI	CFNET1	CFNET2	F9
2177	0005	68750	0.448	0.450	1.504	0.993	0.000	0.969	9.999	0.794	0.796	1.090
2178	0006	68750	0.448	0.450	1.501	1.003	0.029	0.970	0.992	0.801	0.804	1.093
2179	0006	68750	0.448	0.450	1.502	1.027	0.059	0.970	0.882	0.806	0.810	1.096
2179	0006	68750	0.448	0.449	2.005	0.986	0.000	0.965	9.999	0.836	0.836	1.093
2178	0006	68750	0.448	0.449	2.005	1.017	0.029	0.965	0.751	0.842	0.846	1.097
2177	0006	68750	0.448	0.449	2.007	1.058	0.059	0.965	0.822	0.846	0.851	1.100
2178	0006	68750	0.448	0.448	2.509	0.978	0.000	0.963	9.999	0.860	0.860	1.099
2179	0006	68750	0.448	0.448	2.512	1.027	0.029	0.963	0.742	0.868	0.873	1.100
2180	0006	68750	0.448	0.448	2.511	1.087	0.059	0.963	0.838	0.871	0.877	1.106
2181	0006	68750	0.448	0.448	3.016	0.974	0.000	0.967	9.999	0.881	0.881	1.108
2182	0006	68750	0.448	0.448	3.015	1.044	0.029	0.969	0.700	0.884	0.890	1.111
2183	0006	68750	0.448	0.448	3.017	1.131	0.059	0.969	0.823	0.888	0.907	1.117
2184	0006	68750	0.448	0.448	3.517	0.972	0.000	0.950	9.999	0.885	0.885	1.114
2185	0006	68750	0.448	0.448	3.523	1.061	0.029	0.969	0.654	0.891	0.897	1.115
2186	0006	68750	0.448	0.448	3.516	1.164	0.059	0.950	0.811	0.896	0.914	1.122
2187	0006	68750	0.446	0.447	2.508	0.978	0.000	0.963	9.999	0.858	0.858	1.097
2188	0006	68750	0.448	0.448	2.507	1.068	0.059	0.967	0.830	0.872	0.889	1.108
2189	0006	68750	1.140	0.447	1.501	1.114	0.135	0.964	0.979	0.822	0.881	1.109
2190	0006	68750	1.140	0.447	1.502	1.523	0.291	0.970	1.007	0.839	1.088	1.135
2191	0006	68750	1.140	0.448	1.501	2.019	0.397	0.971	0.999	0.850	1.285	1.141
2192	0006	68750	1.140	0.447	1.501	2.518	0.506	0.970	0.998	0.863	1.486	1.145
2193	0006	68750	1.140	0.448	1.502	3.024	0.596	0.970	1.000	0.863	1.671	1.144
2194	0006	68750	1.140	0.447	1.502	3.526	0.694	0.970	0.999	0.886	1.907	1.160
2195	0006	68750	1.140	0.448	2.007	1.120	0.056	0.967	0.917	0.851	0.885	1.108
2196	0006	68750	1.140	0.448	2.006	1.624	0.212	0.967	0.997	0.863	1.008	1.131
2197	0006	68750	1.140	0.448	2.006	2.020	0.292	0.967	0.999	0.867	1.121	1.135
2198	0006	68750	1.140	0.448	2.005	2.524	0.395	0.966	1.000	0.873	1.235	1.139
2199	0006	68750	1.140	0.448	2.006	3.030	0.499	0.966	1.001	0.873	1.342	1.138
2200	0006	68750	1.140	0.448	2.005	3.527	0.612	0.967	1.002	0.890	1.490	1.154
2201	0006	68750	1.140	0.448	2.503	1.127	0.034	0.939	0.873	0.872	0.896	1.103
2202	0006	68750	1.140	0.448	2.501	1.626	0.168	0.967	0.997	0.881	0.895	1.130
2203	0006	68750	1.140	0.448	2.507	2.021	0.253	0.969	0.999	0.881	1.063	1.134
2204	0006	68750	1.140	0.448	2.507	2.521	0.371	0.968	1.000	0.894	1.143	1.136
2205	0006	68750	1.140	0.448	2.511	3.030	0.490	0.966	1.001	0.886	1.219	1.136
2206	0006	68750	1.140	0.448	2.509	3.529	0.608	0.965	1.002	0.895	1.312	1.146
2207	0006	68750	1.140	0.448	3.014	1.118	0.028	0.969	1.376	0.875	0.902	1.114
2208	0006	68750	1.140	0.448	3.013	1.525	0.137	0.967	0.973	0.892	0.971	1.131
2209	0006	68750	1.140	0.449	3.019	2.020	0.199	0.966	0.994	0.892	1.033	1.134
2210	0006	68750	1.140	0.448	3.018	2.522	0.342	0.969	0.998	0.894	1.096	1.138
2211	0006	68750	1.140	0.448	3.015	3.030	0.490	0.950	1.000	0.891	1.151	1.137
2212	0006	68750	1.140	0.448	3.017	3.526	0.610	0.960	1.001	0.902	1.226	1.148
2213	0006	68750	1.140	0.448	3.313	1.119	0.046	0.969	0.762X	0.893	0.907	1.119
2214	0006	68750	1.140	0.448	3.307	1.525	0.123	0.951	0.959	0.897	0.966	1.135
2215	0006	68750	1.140	0.449	3.316	2.020	0.175	0.950	0.996	0.895	1.020	1.138
2216	0006	68750	1.140	0.450	3.314	2.523	0.719	0.951	0.998	0.898	1.075	1.141

FACILITY LF PROGRAM CODE NOZZLE TYPE PLUG CONFIGURATIONS SUPPRESSOR CONFIGURATION

1/2 BLEED AREA WITH BLEED 26-CHUTE, AREA RATIO = 2.0

DRAG PARAMETERS OUTER RADIUS RATIO 0.8000 INNER RADIUS RATIO 0.8000 NPR 1.2480

RPC	RS	RUN#	M2	M6	PT2/P0	PT6/P0	DNOZZLE	DCS	FDS	DCSH	CDSH	DCPL,O	DCPL,I	DCTOT	PSUP/PA
2172	0000	44750	0.335	0.450	1.534	0.903	0.000	-0.163	0.201	-0.014	0.018	-0.021	0.021	-0.167	0.893
2173	0000	44750	0.334	0.450	1.403	1.005	0.029	-0.160	0.197	-0.014	0.018	-0.018	0.014	-0.167	0.885
2174	0000	44750	0.335	0.450	1.402	1.007	0.056	-0.164	0.192	-0.014	0.019	-0.017	0.012	-0.163	0.888
2175	0000	44750	0.334	0.449	2.005	0.984	0.000	-0.130	0.298	-0.010	0.023	-0.013	0.020	-0.133	0.827
2176	0000	44750	0.334	0.449	2.003	1.317	0.029	-0.126	0.291	-0.010	0.022	-0.010	0.015	-0.131	0.830
2177	0000	44750	0.334	0.449	2.001	1.054	0.056	-0.123	0.284	-0.009	0.022	-0.007	0.013	-0.127	0.832
2178	0000	44750	0.334	0.448	2.004	0.926	0.000	-0.112	0.367	-0.007	0.024	-0.015	0.010	-0.117	0.787
2179	0000	44750	0.333	0.448	2.003	1.327	0.029	-0.110	0.360	-0.007	0.024	-0.012	0.013	-0.116	0.792
2180	0000	44750	0.334	0.448	2.002	1.057	0.056	-0.107	0.354	-0.007	0.023	-0.010	0.011	-0.112	0.794
2181	0000	44750	0.334	0.448	2.014	0.976	0.000	-0.095	0.401	-0.006	0.025	-0.017	0.016	-0.101	0.767
2182	0000	44750	0.334	0.448	2.014	1.264	0.029	-0.093	0.395	-0.006	0.025	-0.013	0.011	-0.100	0.770
2183	0000	44750	2.333	0.448	2.009	1.131	0.056	-0.091	0.390	-0.006	0.024	-0.011	0.010	-0.098	0.772
2184	0000	44750	0.333	0.448	2.013	0.979	0.000	-0.095	0.396	-0.006	0.025	-0.017	0.016	-0.097	0.771
2185	0000	44750	0.333	0.448	2.009	1.261	0.029	-0.090	0.391	-0.006	0.024	-0.013	0.011	-0.097	0.773
2186	0000	44750	0.333	0.448	2.010	1.144	0.056	-0.088	0.388	-0.006	0.024	-0.011	0.009	-0.095	0.774
2187	0000	44750	0.333	0.447	2.008	0.979	0.000	-0.112	0.368	-0.007	0.024	-0.015	0.019	-0.115	0.788
2188	0000	44750	0.333	0.448	2.007	1.088	0.029	-0.107	0.357	-0.007	0.024	-0.009	0.012	-0.111	0.794
2189	0000	44750	1.140	0.447	1.501	1.116	0.135	-0.136	0.193	-0.013	0.018	-0.014	0.012	-0.151	0.889
2190	0000	44750	1.140	0.446	1.502	1.523	0.291	-0.129	0.195	-0.011	0.018	-0.012	0.016	-0.121	0.888
2191	0000	44750	1.140	0.446	1.501	2.017	0.397	-0.098	0.195	-0.009	0.018	-0.011	0.009	-0.109	0.897
2192	0000	44750	1.140	0.447	1.501	2.419	0.486	-0.096	0.196	-0.008	0.019	-0.010	-0.006	-0.110	0.897
2193	0000	44750	1.140	0.446	1.502	3.024	0.596	-0.094	0.196	-0.007	0.019	-0.008	-0.019	-0.110	0.898
2194	0000	44750	1.140	0.447	1.501	1.524	0.604	-0.090	0.197	-0.007	0.018	-0.043	-0.025	-0.145	0.887
2195	0000	44750	1.140	0.446	2.007	1.120	0.004	-0.119	0.297	-0.009	0.022	-0.006	0.013	-0.122	0.834
2196	0000	44750	1.140	0.446	2.006	1.529	0.212	-0.104	0.296	-0.008	0.022	-0.005	0.014	-0.105	0.835
2197	0000	44750	1.140	0.446	2.004	2.120	0.392	-0.095	0.294	-0.007	0.022	-0.005	0.008	-0.100	0.835
2198	0000	44750	1.140	0.447	2.004	2.574	0.565	-0.091	0.293	-0.007	0.022	-0.004	-0.002	-0.100	0.835
2199	0000	44750	1.140	0.448	2.004	1.040	0.619	-0.079	0.202	-0.006	0.022	-0.004	-0.021	-0.110	0.837
2200	0000	44750	1.140	0.448	2.004	1.527	0.812	-0.074	0.282	-0.006	0.022	-0.003	0.016	-0.067	0.837
2201	0000	44750	1.140	0.448	2.932	1.192	0.071	-0.105	0.354	-0.007	0.023	-0.009	0.011	-0.111	0.795
2202	0000	44750	1.140	0.448	2.931	1.532	0.168	-0.097	0.351	-0.006	0.023	-0.007	0.011	-0.099	0.796
2203	0000	44750	1.140	0.448	2.927	2.321	0.273	-0.090	0.350	-0.006	0.023	-0.007	0.007	-0.095	0.797
2204	0000	44750	1.140	0.448	2.927	2.921	0.391	-0.083	0.351	-0.006	0.023	-0.006	-0.006	-0.101	0.797
2205	0000	44750	1.140	0.448	2.931	3.030	0.350	-0.077	0.349	-0.005	0.023	-0.004	-0.017	-0.104	0.798
2206	0000	44750	1.140	0.448	2.930	3.530	0.498	-0.073	0.349	-0.005	0.023	-0.004	0.000	-0.073	0.797
2207	0000	44750	1.140	0.448	3.018	1.118	0.000	-0.089	0.394	-0.005	0.024	-0.011	0.010	-0.096	0.772
2208	0000	44750	1.140	0.448	3.018	1.525	0.137	-0.084	0.391	-0.005	0.024	-0.008	0.010	-0.088	0.774
2209	0000	44750	1.140	0.447	3.019	2.020	0.263	-0.080	0.389	-0.005	0.024	-0.007	0.006	-0.086	0.774
2210	0000	44750	1.140	0.449	3.014	2.477	0.242	-0.076	0.387	-0.005	0.024	-0.007	-0.006	-0.091	0.775
2211	0000	44750	1.140	0.448	3.015	3.020	0.200	-0.070	0.385	-0.004	0.024	-0.005	-0.013	-0.092	0.776
2212	0000	44750	1.140	0.448	3.013	3.524	0.339	-0.067	0.384	-0.004	0.024	-0.005	0.008	-0.067	0.776
2213	0000	44750	1.140	0.448	3.019	1.114	0.046	-0.079	0.390	-0.005	0.025	-0.011	0.010	-0.086	0.774
2214	0000	44750	1.140	0.448	3.017	1.524	0.173	-0.074	0.387	-0.005	0.024	-0.008	0.008	-0.079	0.776
2215	0000	44750	1.140	0.448	3.016	2.020	0.175	-0.070	0.385	-0.004	0.024	-0.007	0.003	-0.078	0.776
2216	0000	44750	1.140	0.448	3.016	2.523	0.219	-0.066	0.382	-0.004	0.024	-0.006	-0.005	-0.082	0.776

FACILITY SL_PROGRAM C031 — INP STREAM

NOZZLE TYPE: DUAL FLOW (EAA) — PLUG CONFIGURATIONS: 1/2 BLEED AREA WITH BLEED — SUPPRESSOR CONFIGURATION: 36-CHUTE, AREA RATIO = 2.0

THRUST PARAMETERS — OUTER RADIUS RATIO 0.0000 — INNER RADIUS RATIO 0.9890 — DVO 1.2480

ENG	GE	MASA	M2	MA	PTO/PA	PTI/PA	OMEGAT	CDO	CDI	CFNET1	CFNET2	F9
2217	0009	48750	1.140	0.449	3.317	3.029	0.764	0.951	0.999	0.896	1.125	1.140
2218	0009	48750	1.140	0.450	3.373	3.531	0.307	0.949	1.000	0.904	1.187	1.148
2219	0009	48750	1.140	0.448	2.911	1.119	0.075	0.947	0.923X	0.867	0.891	1.105
2220	0009	48750	1.140	0.448	2.521	3.530	0.409	0.949	1.001	0.895	1.315	1.148
~~2221~~	~~0009~~	~~48750~~	~~1.140~~	~~0.360~~	~~1.561~~	~~1.561~~	~~0.000~~	~~0.967~~	~~0.000~~	~~1.107~~	~~1.107~~	~~1.107~~
2223	0009	48750	0.398	0.360	1.500	0.990	0.000	0.967	9.999	0.812	0.812	1.099
2224	0009	48750	0.398	0.360	1.503	1.005	0.029	0.965	1.017	0.819	0.822	1.100
2225	0009	48750	0.398	0.359	1.501	1.025	0.059	0.964	0.911	0.826	0.838	1.104
2226	0009	48750	0.399	0.360	2.013	0.984	0.000	0.946	9.999	0.852	0.852	1.105
2227	0009	48750	0.398	0.361	2.011	1.015	0.029	0.946	0.788	0.860	0.864	1.109
2229	0009	48750	0.398	0.361	2.013	1.054	0.059	0.945	0.851	0.862	0.877	1.111
2229	0009	48750	0.398	0.359	2.512	0.978	0.000	0.948	9.999	0.875	0.875	1.110
2230	0009	48750	0.398	0.359	2.513	1.025	0.029	0.948	0.775	0.882	0.887	1.114
2231	0009	48750	0.398	0.358	2.514	1.084	0.059	0.949	0.852	0.894	0.901	1.118
2232	0009	48750	0.398	0.359	3.014	0.972	0.000	0.946	9.999	0.894	0.894	1.119
2233	0009	48750	0.398	0.359	3.015	1.041	0.029	0.948	0.721	0.896	0.902	1.121
2234	0009	48750	0.398	0.359	3.013	1.125	0.059	0.948	0.842	0.899	0.918	1.126
2235	0009	48750	0.398	0.359	3.513	0.971	0.000	0.948	9.999	0.899	0.899	1.125
2236	0009	48750	0.398	0.358	3.512	1.054	0.029	0.950	0.694	0.903	0.909	1.127
2237	0009	48750	0.398	0.359	3.507	1.158	0.059	0.950	0.826	0.905	0.925	1.132
2238	0009	48750	0.398	0.358	2.515	0.977	0.000	0.946	9.999	0.877	0.877	1.110
2239	0009	48750	0.398	0.358	2.522	1.086	0.059	0.943	0.841	0.885	0.902	1.114
2240	0009	48750	1.140	0.358	1.503	1.112	0.134	0.953	0.980	0.835	0.893	1.114
2241	0009	48750	1.140	0.359	1.504	1.522	0.293	0.967	1.008	0.850	1.103	1.141
2242	0009	48750	1.140	0.359	1.499	2.031	0.403	0.967	1.001	0.859	1.307	1.146
2243	0009	48750	1.140	0.359	1.501	2.527	0.503	0.966	1.003	0.868	1.504	1.149
2244	0009	48750	1.140	0.359	1.503	3.018	0.599	0.967	1.003	0.878	1.685	1.148
2245	0009	48750	1.140	0.359	1.503	3.526	0.700	0.967	1.003	0.891	1.927	1.164
2246	0009	48750	1.140	0.359	2.013	1.117	0.094	0.947	0.930	0.845	0.898	1.118
2247	0009	48750	1.140	0.359	2.013	1.523	0.212	0.946	1.001	0.873	1.020	1.139
2248	0009	48750	1.140	0.359	2.006	2.028	0.293	0.946	1.002	0.878	1.137	1.144
2249	0009	48750	1.140	0.359	2.009	2.532	0.366	0.947	1.003	0.883	1.251	1.148
2250	0009	48750	1.140	0.361	2.011	3.030	0.439	0.947	1.003	0.892	1.356	1.147
2251	0009	48750	1.140	0.360	2.011	3.522	0.510	0.946	1.003	0.898	1.490	1.160
2252	0009	48750	1.140	0.361	2.517	1.112	0.073	0.949	0.920X	0.864	0.907	1.119
2253	0009	48750	1.140	0.359	2.512	1.522	0.168	0.948	0.994	0.890	0.995	1.139
2254	0009	48750	1.140	0.360	2.514	2.032	0.234	0.948	1.002	0.891	1.077	1.142
2255	0009	48750	1.140	0.360	2.517	2.534	0.292	0.948	1.003	0.894	1.156	1.145
2256	0009	48750	1.140	0.359	2.519	3.026	0.349	0.945	1.002	0.894	1.231	1.144
2257	0009	48750	1.140	0.359	3.013	1.113	0.057	0.950	0.857X	0.898	0.915	1.126
2258	0009	48750	1.140	0.360	3.012	1.524	0.138	0.950	0.982	0.903	0.984	1.143
2260	0009	48750	1.140	0.360	3.009	2.031	0.195	0.950	0.999	0.902	1.047	1.147
2261	0009	48750	1.140	0.360	3.014	2.532	0.243	0.950	1.001	0.906	1.111	1.150
2262	0009	48750	1.140	0.360	3.014	3.028	0.291	0.949	1.002	0.902	1.166	1.147

FACILITY [illegible]

PROFILE TYPE — STREAM
DUCT FLOW (F33) — PLUG CONFIGURATIONS — SUPPRESSOR CONFIGURATION
1/2 BLEED AREA WITH BLEED — 36-CHUTE, AREA RATIO = 2.0

OUTER RADIUS RATIO 0.5030 — INNER RADIUS RATIO 0.8890 — DVD 1.2480

PT#	PARAMETERS					PTI/PA	PTI/P4	OMEGAT	DCS	CDS	CDSH	CDSH	DCPL,O	DCPL,I	DCTOT	PSUP/PA
2212	0000	48750	1.140	0.348	2.442	3.319	3.022	0.264	-0.063	0.382	-0.004	0.023	-0.005	-0.011	-0.082	0.778
2218	0000	48750	1.140	0.350	2.373	3.531	0.307	-0.060	0.381	-0.004	0.024	-0.005	-0.005	-0.073	0.778
2219	0000	48750	1.140	0.445	2.511	1.112	0.075	-0.105	0.354	-0.007	0.024	-0.009	0.012	-0.110	0.795
2220	0000	48750	1.140	0.448	2.581	1.530	0.409	-0.073	0.348	-0.005	0.023	-0.004	0.007	-0.075	0.798
[illegible]																
[illegible]																
2223	0000	48730	0.348	0.343	1.500	0.300	0.000	-0.133	0.271	-0.010	0.021	-0.020	0.018	-0.145	0.899
2224	0000	48730	0.348	0.340	1.502	1.006	0.029	-0.129	0.265	-0.010	0.020	-0.016	0.013	-0.142	0.901
2225	0000	48730	0.348	0.339	1.501	1.025	0.059	-0.125	0.260	-0.010	0.020	-0.014	0.010	-0.141	0.903
2226	0000	48730	0.348	0.340	2.013	0.000	0.000	-0.114	0.410	-0.007	0.025	-0.015	0.018	-0.118	0.846
2227	0000	48730	0.348	0.341	2.011	1.015	0.029	-0.112	0.403	-0.007	0.025	-0.011	0.012	-0.118	0.849
2228	0000	48730	0.348	0.341	2.013	1.054	0.059	-0.109	0.397	-0.007	0.024	-0.009	0.011	-0.114	0.851
2229	0000	48730	0.348	0.339	2.512	0.000	0.000	-0.096	0.490	-0.005	0.026	-0.017	0.016	-0.102	0.818
2230	0000	48730	0.348	0.339	2.510	1.025	0.029	-0.094	0.484	-0.005	0.026	-0.013	0.011	-0.101	0.820
2231	0000	48730	0.348	0.338	2.514	1.084	0.059	-0.091	0.478	-0.005	0.026	-0.011	0.011	-0.097	0.823
2232	0000	48730	0.348	0.338	3.014	0.972	0.000	-0.080	0.533	-0.004	0.028	-0.019	0.014	-0.089	0.803
2233	0000	48730	0.348	0.340	3.014	1.041	0.029	-0.079	0.528	-0.004	0.026	-0.015	0.009	-0.089	0.804
2234	0000	48730	0.348	0.339	3.013	1.125	0.059	-0.076	0.518	-0.004	0.027	-0.013	0.009	-0.085	0.807
2235	0000	48730	0.348	0.339	3.318	0.971	0.000	-0.069	0.571	-0.004	0.027	-0.019	0.014	-0.077	0.806
2236	0000	48730	0.348	0.338	3.312	1.054	0.029	-0.068	0.517	-0.004	0.028	-0.015	0.009	-0.077	0.809
2237	0000	48730	0.348	0.339	3.307	1.158	0.059	-0.064	0.512	-0.003	0.026	-0.013	0.008	-0.074	0.810
2238	0000	48730	0.348	0.338	2.515	0.977	0.000	-0.098	0.493	-0.005	0.027	-0.017	0.017	-0.102	0.817
2239	0000	48730	0.348	0.338	2.477	1.084	0.059	-0.092	0.480	-0.005	0.026	-0.011	0.010	-0.098	0.822
2240	0000	48750	1.140	0.338	1.500	1.112	0.134	-0.119	0.760	-0.009	0.020	-0.013	0.013	-0.128	0.904
2241	0000	48750	1.140	0.338	1.498	1.522	0.293	-0.098	0.760	-0.007	0.020	-0.012	0.015	-0.102	0.904
2242	0000	48750	1.140	0.339	1.499	2.031	0.403	-0.084	0.761	-0.006	0.020	-0.010	0.007	-0.093	0.903
2243	0000	48750	1.140	0.339	1.501	2.533	0.503	-0.075	0.753	-0.006	0.020	-0.009	-0.005	-0.094	0.902
2244	0000	48750	1.140	0.339	1.500	3.018	0.599	-0.065	0.261	-0.005	0.020	-0.007	-0.020	-0.098	0.903
2245	0000	48750	1.140	0.339	1.503	3.526	0.700	-0.059	0.761	-0.005	0.020	-0.007	0.018	-0.052	0.903
2246	0000	48750	1.140	0.339	2.010	1.117	0.096	-0.106	0.397	-0.006	0.024	-0.010	0.011	-0.111	0.853
2247	0000	48750	1.140	0.339	2.010	1.573	0.212	-0.094	0.396	-0.006	0.025	-0.008	0.012	-0.095	0.854
2248	0000	48750	1.140	0.339	2.008	2.025	0.293	-0.085	0.396	-0.005	0.025	-0.007	0.006	-0.091	0.853
2249	0000	48750	1.140	0.339	2.009	2.532	0.396	-0.078	0.396	-0.005	0.024	-0.006	-0.002	-0.091	0.853
2250	0000	48750	1.140	0.341	2.011	3.030	0.439	-0.071	0.389	-0.004	0.024	-0.005	-0.024	-0.104	0.854
2251	0000	48750	1.140	0.340	2.011	3.527	0.510	-0.066	0.394	-0.004	0.024	-0.005	0.016	-0.059	0.853
2252	0000	48750	1.140	0.341	2.517	1.112	0.073	-0.091	0.477	-0.005	0.026	-0.011	0.009	-0.097	0.823
2253	0000	48750	1.140	0.339	2.512	1.527	0.168	-0.083	0.476	-0.005	0.026	-0.009	0.010	-0.096	0.824
2254	0000	48750	1.140	0.340	2.516	2.032	0.234	-0.077	0.473	-0.004	0.025	-0.008	0.006	-0.083	0.823
2255	0000	48750	1.140	0.340	2.517	2.536	0.292	-0.071	0.472	-0.004	0.026	-0.007	-0.006	-0.089	0.824
2256	0000	48750	1.140	0.339	2.519	3.026	0.349	-0.067	0.469	-0.004	0.026	-0.006	-0.021	-0.097	0.825
2257	0000	48750	1.140	0.339	3.013	1.113	0.057	-0.077	0.520	-0.004	0.027	-0.013	0.008	-0.086	0.807
2258	0000	48750	1.140	0.340	3.017	1.526	0.138	-0.072	0.515	-0.004	0.027	-0.010	0.009	-0.077	0.808
2260	0000	48750	1.140	0.340	3.009	2.031	0.195	-0.067	0.516	-0.003	0.027	-0.009	0.005	-0.075	0.807
2261	0000	48750	1.140	0.339	3.014	2.532	0.243	-0.063	0.515	-0.003	0.026	-0.008	-0.008	-0.083	0.808
2262	0000	48750	1.140	0.340	3.014	3.028	0.291	-0.060	0.510	-0.003	0.026	-0.007	-0.015	-0.084	0.809

FACILITY YI PROGRAM C-3L NOZZLE TYPE TAB-STREAM
DUAL FLOW (SEAL) PLUG CONFIGURATIONS SUPPRESSOR CONFIGURATION
1/2 BLEED AREA WITH BLEED 36-CHUTE, AREA RATIO = 2.0

THRUST PARAMETERS OUTER RADIUS RATIO 0.0000 INNER RADIUS RATIO 0.9890 OVD 1.2480

RPC	GE	WASA	M2	M8	PT8/P8	PT2/P8	OMEGAT	CDD	CDI	CFNETI	CFNET2	FG
2263	0009	48750	1.140	0.360	3.515	3.524	0.339	0.949	1.003	0.912	1.239	1.158
2264	0009	48750	1.140	0.360	3.511	1.115	0.049	0.949	0.781X	0.907	0.921	1.131
2265	0009	48750	1.140	0.360	3.502	1.524	0.125	0.949	0.970	0.909	0.980	1.146
2266	0009	48750	1.140	0.359	3.209	2.030	0.177	0.950	0.999	0.908	1.036	1.150
2267	0009	48750	1.140	0.360	3.309	2.523	0.221	0.949	0.997	0.911	1.091	1.152
2268	0009	48750	1.140	0.360	3.315	3.031	0.264	0.951	1.001	0.907	1.138	1.151
2269	0009	48750	1.140	0.360	3.311	3.523	0.308	0.950	1.002	0.915	1.203	1.160
2270	0009	48750	1.140	0.360	2.515	1.111	0.073	0.948	0.924X	0.884	0.907	1.119
2271	0009	48750	1.140	0.360	2.505	1.520	0.408	0.949	1.003	0.906	1.328	1.158
2272	0009	48730	0.398	0.037	1.494	0.971	0.000	0.954	9.999	0.921	0.921	1.147
2273	0009	48730	0.398	0.031	1.498	0.970	0.029	0.953	9.999	0.925	0.925	1.147
2274	0009	48730	0.398	0.026	1.501	1.007	0.058	0.951	1.683	0.927	0.934	1.147
2275	0009	48730	0.398	0.053	1.996	0.971	0.000	0.947	9.999	0.925	0.925	1.155
2276	0009	48730	0.398	0.056	1.995	0.964	0.029	0.946	9.999	0.931	0.931	1.156
2277	0009	48730	0.398	0.053	1.995	1.027	0.059	0.942	1.187	0.935	0.946	1.158
2278	0009	48730	0.398	0.040	2.496	0.963	0.000	0.947	9.999	0.928	0.928	1.153
2279	0009	48730	0.398	0.040	2.496	0.999	0.029	0.945	9.999	0.939	0.939	1.155
2280	0009	48730	0.398	0.040	2.497	1.049	0.059	0.943	1.104	0.939	0.953	1.158
2281	0009	48730	0.398	0.065	3.005	0.958	0.000	0.949	9.999	0.930	0.930	1.154
2282	0009	48730	0.398	0.064	2.997	1.013	0.029	0.951	1.274	0.938	0.941	1.159
2283	0009	48730	0.398	0.070	3.006	1.089	0.059	0.949	0.997	0.937	0.953	1.160
2284	0009	48730	0.398	0.074	3.511	0.958	0.000	0.949	9.999	0.932	0.932	1.156
2285	0009	48730	0.398	0.074	3.508	1.060	0.029	0.950	0.925	0.936	0.941	1.157
2286	0009	48730	0.398	0.074	3.507	1.126	0.059	0.950	0.921	0.937	0.956	1.162
2287	0009	48730	0.398	0.059	2.691	0.962	0.000	0.949	9.999	0.926	0.926	1.153
2288	0009	48730	0.398	0.058	2.495	1.049	0.059	0.948	1.106	0.932	0.946	1.156
2289	0009	48750	1.140	0.037	1.498	1.112	0.148	0.952	1.064	0.914	0.985	1.152
2290	0009	48750	1.140	0.041	1.697	1.521	0.299	0.950	1.014	0.914	1.192	1.172
2291	0009	48750	1.140	0.053	1.500	2.016	0.605	0.949	0.996	0.919	1.399	1.176
2292	0009	48750	1.140	0.053	1.499	2.514	0.906	0.951	0.997	0.922	1.600	1.178
2293	0009	48750	1.140	0.054	1.500	3.018	0.608	0.952	1.002	0.913	1.786	1.175
2294	0009	48750	1.140	0.053	1.995	1.111	0.105	0.945	1.052	0.931	0.971	1.164
2295	0009	48750	1.140	0.054	1.996	1.522	0.216	0.946	1.011	0.930	1.089	1.180
2296	0009	48750	1.140	0.056	1.995	2.017	0.293	0.946	1.000	0.926	1.200	1.181
2297	0009	48750	1.140	0.060	1.995	2.519	0.366	0.947	1.000	0.928	1.314	1.183
2298	0009	48750	1.140	0.064	1.995	3.020	0.440	0.946	1.001	0.924	1.423	1.180
2299	0009	48750	1.140	0.065	1.995	3.520	0.514	0.945	1.003	0.937	1.562	1.193
23C1	0009	48750	1.140	0.060	2.495	1.114	0.084	0.947	1.046	0.938	0.955	1.163
23C2	0009	48750	1.140	0.063	2.495	1.522	0.172	0.948	1.010	0.935	1.048	1.177
23C3	0009	48750	1.140	0.066	2.497	2.017	0.234	0.947	0.997	0.934	1.128	1.177
23C4	0009	48750	1.140	0.070	2.496	2.518	0.292	0.947	0.998	0.936	1.210	1.179
23C5	0009	48750	1.140	0.071	2.496	3.015	0.351	0.948	1.002	0.931	1.285	1.178
23C6	0009	48750	1.140	0.070	2.495	3.520	0.410	0.948	1.002	0.940	1.382	1.188
23C7	0009	48740	1.140	0.067	3.007	1.117	0.067	0.948	0.988	0.939	0.960	1.162
23C8	0009	48750	1.140	0.073	3.005	1.523	0.142	0.949	1.003	0.938	1.025	1.175

FACILITY TF PROGRAM CODE NOZZLE TYPE IN-STREAM

DUAL FLOW (FAAT) FLOW CONFIGURATIONS SUPPRESSOR CONFIGURATION

1/2 BLEED AREA WITH BLEED 36-CHUTE, AREA RATIO = 2.0

OPER PARAMETERS OUTER RADIUS RATIO 0.0000 INNER RADIUS RATIO 0.8890 DVO 1.2480

RPG	CF	PRSR	M2	PA	PT2/PE	PT1/PE	DREGAT	DCS	CDS	DCSH	CDSH	DCPL,O	DCPL,I	DCTOT	PSUP/PA
2283	0000	48750	1.140	0.360	3.015	3.524	0.330	-0.057	0.509	-0.003	0.026	-0.006	0.007	-0.059	0.810
2284	0000	48750	1.140	0.360	3.311	1.115	0.068	-0.067	0.513	-0.003	0.027	-0.014	0.008	-0.076	0.809
2285	0000	48750	1.140	0.359	3.300	1.524	0.125	-0.063	0.509	-0.003	0.026	-0.010	0.008	-0.069	0.810
2286	0000	48750	1.140	0.359	3.299	2.030	0.177	-0.059	0.509	-0.003	0.027	-0.009	0.003	-0.069	0.810
2287	0000	48750	1.140	0.360	3.309	2.533	0.221	-0.056	0.506	-0.003	0.026	-0.008	-0.007	-0.074	0.810
2288	0000	48750	1.140	0.360	3.316	3.031	0.264	-0.054	0.506	-0.003	0.026	-0.006	-0.011	-0.074	0.811
2289	0000	48750	1.140	0.360	3.313	3.523	0.308	-0.051	0.505	-0.003	0.027	-0.006	0.001	-0.060	0.811
2270	0000	48750	1.140	0.360	2.516	1.111	0.073	-0.031	0.475	-0.005	0.025	-0.011	0.010	-0.097	0.823
2271	0000	48750	1.140	0.359	2.496	1.520	0.108	-0.053	0.468	-0.004	0.026	-0.005	0.004	-0.057	0.826
2272	0000	48730	0.398	0.037	1.496	0.979	0.000	-0.046	8.780	-0.000	0.034	-0.030	0.006	-0.071	0.966
2273	0000	48730	0.398	0.031	1.498	0.980	0.029	-0.044	12.074	-0.000	0.065	-0.026	0.000	-0.071	0.967
2274	0000	48730	0.398	0.026	1.501	1.337	0.058	-0.043	16.417	-0.000	0.135	-0.025	-0.000	-0.069	0.967
2275	0000	48730	0.398	0.053	1.496	0.971	0.000	-0.039	6.465	-0.020	0.041	-0.027	0.008	-0.058	0.948
2276	0000	48730	0.398	2.056	1.496	0.994	0.029	-0.039	6.059	-0.000	0.020	-0.023	0.003	-0.059	0.949
2277	0000	48730	0.398	0.053	1.495	1.027	0.059	-0.038	6.253	-0.000	0.034	-0.022	0.004	-0.056	0.950
2278	0000	48730	0.398	0.060	2.495	0.963	0.000	-0.034	6.112	-0.000	0.035	-0.027	0.009	-0.052	0.936
2279	0000	48730	0.398	0.060	2.494	0.999	0.029	-0.033	5.907	-0.000	0.025	-0.022	0.004	-0.051	0.938
2280	0000	48730	0.398	0.060	2.497	1.369	0.059	-0.032	5.881	-0.000	0.027	-0.020	0.005	-0.048	0.939
2281	0000	48730	0.398	0.060	3.005	0.958	0.000	-0.029	5.206	-0.000	0.021	-0.027	0.010	-0.046	0.929
2282	0000	48730	0.398	0.065	2.992	1.313	0.029	-0.029	5.611	-0.000	0.030	-0.023	0.005	-0.046	0.930
2283	0000	48730	0.398	0.070	3.006	1.099	0.059	-0.028	6.990	-0.000	0.020	-0.021	0.005	-0.044	0.930
2284	0000	48730	0.398	0.074	3.311	0.958	0.000	-0.025	4.527	-0.000	0.034	-0.024	0.010	-0.040	0.929
2285	0000	48730	0.398	0.074	3.308	1.030	0.029	-0.025	4.516	-0.000	0.025	-0.020	0.005	-0.040	0.929
2286	0000	48730	0.398	0.074	3.307	1.126	0.059	-0.025	4.437	-0.000	0.027	-0.019	0.005	-0.039	0.930
2287	0000	48730	0.398	2.059	2.491	0.962	0.000	-0.024	6.298	-0.000	0.024	-0.026	0.011	-0.049	0.936
2288	0000	48730	0.398	0.058	2.494	1.046	0.059	-0.017	6.345	-0.000	0.035	-0.020	0.005	-0.048	0.939
2289	0000	48750	1.140	0.037	1.499	1.117	0.148	-0.041	8.154	-0.000	0.033	-0.024	0.005	-0.061	0.967
2290	0000	48750	1.140	0.041	1.498	1.521	0.209	-0.034	6.741	-0.000	0.031	-0.021	0.009	-0.046	0.967
2291	0000	48750	1.140	0.053	1.500	2.016	0.405	-0.029	3.989	0.000	-0.003	-0.018	0.003	-0.044	0.967
2292	0000	48750	1.140	0.053	1.499	2.516	0.504	-0.025	4.044	-0.000	0.016	-0.016	-0.011	-0.053	0.967
2293	0000	48750	1.140	0.055	1.500	3.215	0.608	-0.023	3.967	-0.000	0.014	-0.014	-0.029	-0.065	0.967
2294	0000	48750	1.140	0.053	1.496	1.111	0.106	-0.037	6.234	-0.000	0.030	-0.021	0.005	-0.054	0.949
2295	0000	48750	1.140	0.056	1.496	1.522	0.216	-0.033	6.061	-0.000	0.035	-0.020	0.008	-0.065	0.950
2296	0000	48750	1.140	0.056	1.495	2.017	0.293	-0.030	5.648	-0.000	0.028	-0.018	0.003	-0.045	0.949
2297	0000	48750	1.140	0.060	1.495	2.519	0.366	-0.027	4.859	-0.000	0.027	-0.016	-0.006	-0.050	0.949
2298	0000	48750	1.140	0.044	1.496	3.020	0.440	-0.025	4.277	-0.000	0.026	-0.014	-0.029	-0.068	0.950
2299	0000	48750	1.140	0.045	1.495	3.520	0.514	-0.023	4.080	-0.000	0.024	-0.014	0.016	-0.020	0.950
2300	0000	48750	1.140	0.060	2.496	1.114	0.094	-0.032	5.964	-0.000	0.027	-0.021	0.005	-0.048	0.938
2301	0000	48750	1.140	0.061	2.495	1.522	0.172	-0.029	5.382	-0.000	0.034	-0.019	0.007	-0.041	0.938
2302	0000	48750	1.140	0.066	2.497	2.017	0.234	-0.027	4.956	-0.000	0.026	-0.018	0.004	-0.041	0.938
2303	0000	48750	1.140	0.070	2.496	2.518	0.292	-0.025	4.435	-0.000	0.022	-0.016	-0.004	-0.046	0.938
2304	0000	48750	1.140	0.071	2.494	3.315	0.351	-0.024	4.201	-0.000	0.030	-0.015	-0.024	-0.062	0.939
2305	0000	48750	1.140	0.070	2.495	3.520	0.410	-0.022	4.411	-0.000	0.030	-0.014	0.013	-0.023	0.938
2307	0000	48750	1.140	0.067	3.009	1.117	0.067	-0.028	5.432	-0.000	0.031	-0.021	0.005	-0.043	0.930
2308	0000	48750	1.140	0.073	3.005	1.523	0.142	-0.026	4.534	-0.000	0.025	-0.019	0.007	-0.038	0.930

FACILITY CI PROGRAM COST

NOZZLE TYPE — DUAL FLOW (ERA)

IN STREAM PLUG CONFIGURATIONS — 1/2 BLEED AREA WITH BLEED

SUPPRESSOR CONFIGURATION — 36-CHUTE, AREA RATIO = 2.0

THRUST PARAMETERS

OUTER RADIUS RATIO 0.0000 — INNER RADIUS RATIO 0.8890 — DVO 1.2480

PPC	PE	WASA	M2	PA	PTO/PA	PTI/PA	OMEGAT	CDO	CDI	CFNET1	CFNET2	F9
2309	0009	48750	1.140	0.072	3.001	2.017	0.194	0.950	0.999	0.937	1.086	1.178
2310	0009	48750	1.140	0.075	3.001	2.517	0.243	0.950	1.001	0.937	1.148	1.178
[illegible]												
2312	0009	48750	1.140	0.081	3.005	3.523	0.340	0.949	1.002	0.941	1.280	1.186
2313	0009	48750	1.140	0.075	3.309	1.120	0.057	0.950	0.913	0.938	0.955	1.163
2314	0009	48750	1.140	0.077	3.302	1.522	0.127	0.950	0.992	0.940	1.014	1.176
2315	0009	48750	1.140	0.078	3.302	2.018	0.176	0.950	0.998	0.937	1.068	1.177
2316	0009	48750	1.140	0.081	3.302	2.518	0.220	0.951	1.000	0.937	1.122	1.178
2317	0009	48750	1.140	0.083	3.307	3.018	0.264	0.950	1.001	0.934	1.172	1.176
2318	0009	48750	1.140	0.085	3.308	3.523	0.308	0.950	1.002	0.942	1.238	1.186
2319	0009	48750	1.140	0.060	2.495	1.118	0.085	0.948	1.042	0.940	0.959	1.166
2320	0009	48750	1.140	0.072	2.493	3.521	0.410	0.948	1.003	0.942	1.384	1.190
2321	0009	48750	1.140	0.079	3.001	3.027	0.292	0.950	1.001	0.935	1.209	1.179
2322	0009	48750	1.140	0.058	1.499	3.519	0.711	0.952	1.003	0.935	2.039	1.193

780

FACILITY P I PROGRAM COST

NOZZLE TYPE — DUAL FLOW (ERA)

IN STREAM PLUG CONFIGURATIONS — 1/2 BLEED AREA WITH BLEED

SUPPRESSOR CONFIGURATION — 36-CHUTE, AREA RATIO = 2.0

DEAC PARAMETERS

OUTER RADIUS RATIO 0.0000 — INNER RADIUS RATIO 0.8890 — DVO 1.2480

PPC	PE	WASA	M2	M4	PTO/PA	PTI/PA	OMEGAT	DCS	DDS	DCSH	CDSH	DCPL,O	DCPL,I	DCTOT	PSUP/PA
2309	0009	48750	1.140	0.072	3.001	2.017	0.194	-0.026	4.697	-0.000	0.029	-0.018	0.004	-0.039	0.930
2310	0009	48750	1.140	0.075	3.001	2.517	0.243	-0.023	4.293	-0.000	0.019	-0.016	-0.007	-0.046	0.930
[illegible]															
2312	0009	48750	1.140	0.081	3.005	3.523	0.340	-0.021	3.685	-0.000	0.020	-0.014	0.009	-0.026	0.931
2313	0009	48750	1.140	0.075	3.309	1.120	0.057	-0.024	4.297	-0.000	0.024	-0.019	0.005	-0.038	0.930
2314	0009	48750	1.140	0.077	3.302	1.522	0.127	-0.023	4.115	-0.000	0.024	-0.017	0.006	-0.034	0.930
2315	0009	48750	1.140	0.078	3.302	2.018	0.176	-0.022	3.930	-0.000	0.022	-0.015	0.003	-0.034	0.930
2316	0009	48750	1.140	0.081	3.302	2.518	0.220	-0.021	3.682	-0.000	0.021	-0.014	-0.007	-0.043	0.930
2317	0009	48750	1.140	0.083	3.307	3.018	0.264	-0.020	3.462	-0.000	0.012	-0.013	-0.013	-0.046	0.931
2318	0009	48750	1.140	0.085	3.308	3.523	0.308	-0.019	3.312	-0.000	0.023	-0.012	0.004	-0.027	0.931
2319	0009	48750	1.140	0.060	2.495	1.118	0.085	-0.032	6.031	-0.000	0.044	-0.020	0.005	-0.047	0.938
2320	0009	48750	1.140	0.072	2.493	3.521	0.410	-0.022	4.132	-0.000	0.029	-0.014	0.013	-0.024	0.938
2321	0009	48750	1.140	0.079	3.001	3.027	0.292	-0.021	3.748	-0.000	0.013	-0.015	-0.019	-0.055	0.932
2322	0009	48750	1.140	0.058	1.499	3.519	0.711	-0.020	3.488	-0.000	0.018	-0.013	0.022	-0.011	0.967

MODEL DC-5, 36 DEEP CHUTES, AR = 2.0, FULL PLUG

FACILITY PL PROGRAM C031

NOZZLE TYPE
DUAL FLOW (EDAL

INNER-STREAM
PL CONFIGURATIONS
FULL ...UG W/O BLEED

SUPPRESSOR CONFIGURATION
36-CHUTE, AREA RATIO = 2.0

OUTER RADIUS RATIO 0.0000 INNER RADIUS RATIO 0.0000 DVO 1.2480

THRUST PARAMETERS

EDG	GE	PASS	D2	PA	PTO/PA	PTI/PA	ONEGAT	CDO	CDI	CFNET1	CFNET2	F9
2654	4883	48C30	0.399	0.019	1.504	1.179	0.000	0.951	9.999	0.907	0.907	1.162
2655	4883	48E30	0.399	0.027	1.760	1.173	0.000	0.945	9.999	0.916	0.916	1.172
2656	4883	48830	0.399	0.033	2.001	1.178	0.000	0.945	9.999	0.921	0.921	1.169
2657	4883	48830	0.399	0.038	2.504	1.192	0.000	0.946	9.999	0.932	0.932	1.166
2658	4883	48830	0.399	0.046	3.010	1.224	0.000	0.948	9.999	0.934	0.934	1.166
2659	4883	48830	0.398	0.055	3.312	1.269	0.000	0.949	9.999	0.935	0.935	1.168
2660	4883	48830	0.399	0.036	2.502	1.295	0.000	0.947	9.999	0.933	0.933	1.168
2661	4883	48830	0.398	0.044	2.004	1.295	0.000	0.944	9.999	0.930	0.930	1.174
2662	4883	48830	0.399	0.005	1.503	1.217	0.000	0.951	9.999	0.916	0.916	1.166
2663	4883	48830	0.399	0.022	1.754	1.205	0.000	0.945	9.999	0.922	0.922	1.176
2664	4883	48830	0.399	0.047	2.001	1.205	0.000	0.946	9.999	0.928	0.928	1.174
2665	4883	48830	0.399	0.057	3.002	1.210	0.000	0.948	9.999	0.938	0.938	1.170
2666	4883	48830	0.399	0.053	3.306	1.267	0.000	0.949	9.999	0.938	0.938	1.170
2667	4883	48830	0.398	0.447	1.510	1.497	0.000	0.968	9.999	0.790	0.790	1.102
2668	4883	48830	0.398	0.447	1.763	1.444	0.000	0.947	9.999	0.822	0.822	1.108
2669	4883	48830	0.399	0.447	2.005	1.417	0.000	0.946	9.999	0.835	0.835	1.104
2670	4883	48830	0.399	0.447	2.510	1.412	0.000	0.947	9.999	0.860	0.860	1.106
2671	4883	48830	0.398	0.448	3.022	1.421	0.000	0.942	9.999	0.883	0.883	1.113
2672	4883	48830	0.399	0.448	3.320	1.438	0.000	0.948	9.999	0.886	0.886	1.120
2673	4883	48830	0.398	0.449	3.027	1.453	0.000	0.947	9.999	0.877	0.877	1.113
2674	4883	48830	0.398	0.447	2.511	1.450	0.000	0.947	9.999	0.859	0.859	1.105
2675	4883	48830	0.399	0.447	2.005	1.426	0.000	0.946	9.999	0.836	0.836	1.105
2676	4883	48830	0.398	0.447	1.763	1.399	0.000	0.948	9.999	0.825	0.825	1.110
2677	4883	48830	0.398	0.446	1.506	1.367	0.000	0.968	9.999	0.803	0.903	1.109
2678	4883	48830	0.398	0.447	2.006	1.344	0.000	0.946	9.999	0.838	0.838	1.106
2679	4883	48830	0.398	0.448	3.017	1.357	0.000	0.948	9.999	0.878	0.878	1.114
2680	4883	48830	0.398	0.356	1.506	1.083	0.000	0.966	9.999	0.824	0.824	1.121
2681	4883	48830	0.398	0.358	1.768	1.092	0.000	0.945	9.999	0.845	0.845	1.123
2682	4883	48830	0.398	0.358	2.015	1.104	0.000	0.945	9.999	0.857	0.857	1.119
[illegible]	[illegible]	[illegible]	[illegible]	[illegible]	[illegible]	[illegible]	[illegible]	[illegible]	[illegible]	[illegible]	[illegible]	[illegible]
2684	4883	48830	0.398	0.359	3.014	1.161	0.000	0.949	9.999	0.895	0.895	1.131
2685	4883	48830	0.399	0.359	3.311	1.234	0.000	0.948	9.999	0.902	0.902	1.135
2686	4883	48830	0.398	0.361	3.021	1.782	0.000	0.948	9.999	0.893	0.893	1.128
2687	4883	48830	0.398	0.358	2.522	1.294	0.000	0.945	9.999	0.877	0.877	1.120
2688	4883	48830	0.399	0.358	2.017	1.294	0.000	0.944	9.999	0.854	0.854	1.116
2689	4883	48830	0.398	0.357	1.767	1.281	0.000	0.947	9.999	0.838	0.838	1.119
2690	4883	48830	0.398	0.359	1.508	1.262	0.000	0.962	9.999	0.820	0.820	1.117
2691	4883	48830	0.398	0.359	2.015	1.253	0.000	0.944	9.999	0.856	0.856	1.119
2692	4883	48830	0.398	0.359	3.009	1.274	0.000	0.947	9.999	0.894	0.894	1.129
2693	4883	48830	0.398	0.358	2.508	1.200	0.000	0.950	9.999	0.878	0.878	1.124

FACILITY TEST PROGRAM CODE — IN-STREAM

NOZZLE TYPE — CONFIGURATIONS — SUPPRESSOR CONFIGURATION

DUCT FLOW (FAA) — FULL PLUG W/C BLEED — 36-CHUTE, AREA RATIO = 2.0

OUTER RADIUS RATIO — INNER RADIUS RATIO — OVD

READ PARAMETERS — 0.0000 — 0.0000 — 1.2480

RDG	CE	WASA	M2	MA	PT0/PA	PT1/PA	OMEGAT	DCS	CDS	DCSH	CDSH	DCPL,O	DCPL,I	DCTOT	PSUP/PA
2654	4883	48830	0.398	0.019	1.504	1.179	0.000	-0.047	34.135	-0.000	0.328	-0.028	0.004	-0.071	0.965
2655	4883	48830	0.398	0.027	1.760	1.173	0.000	-0.043	22.209	-0.000	0.179	-0.027	0.006	-0.064	0.954
2656	4883	48830	0.398	0.031	2.001	1.178	0.000	-0.040	17.520	-0.000	0.119	-0.026	0.008	-0.059	0.946
2657	4883	48830	0.398	0.039	2.504	1.192	0.000	-0.035	15.407	-0.000	0.172	-0.025	0.008	-0.052	0.934
2658	4883	48830	0.398	0.046	3.010	1.274	0.000	-0.030	11.972	-0.000	0.128	-0.026	0.010	-0.047	0.926
2659	4883	48830	0.398	0.055	3.512	1.269	0.000	-0.026	8.484	-0.000	0.093	-0.025	0.010	-0.041	0.926
2660	4883	48830	0.398	0.036	2.502	1.295	0.000	-0.035	17.128	-0.000	0.161	-0.027	0.009	-0.054	0.934
2661	4883	48830	0.398	0.044	2.004	1.295	0.000	-0.040	9.411	-0.000	0.050	-0.028	0.008	-0.060	0.947
2662	4883	48830	0.398	0.055	1.503	1.237	0.000	-0.047	600.396	-0.001	7.921	-0.029	0.003	-0.074	0.964
2663	4883	48830	0.398	0.022	1.754	1.205	0.000	-0.044	32.528	-0.000	0.358	-0.028	0.005	-0.067	0.954
2664	4883	48830	0.398	0.047	2.001	1.295	0.000	-0.040	9.411	-0.000	0.034	-0.026	0.007	-0.059	0.947
2665	4883	48830	0.398	0.057	3.002	1.210	0.000	-0.030	7.823	-0.000	0.069	-0.026	0.009	-0.047	0.926
2666	4883	48830	0.398	0.053	1.306	1.267	0.000	-0.046	8.888	-0.000	0.053	-0.024	0.010	-0.040	0.927
2667	4883	48830	0.398	0.447	1.810	1.497	0.000	-0.153	0.206	-0.014	0.019	-0.021	0.034	-0.155	0.881
2668	4883	48830	0.398	0.447	1.763	1.444	0.000	-0.139	0.258	-0.017	0.021	-0.014	0.032	-0.133	0.851
2669	4883	48830	0.398	0.448	2.005	1.417	0.000	-0.129	0.297	-0.010	0.022	-0.012	0.029	-0.121	0.828
2670	4883	48830	0.398	0.447	2.510	1.412	0.000	-0.111	0.365	-0.007	0.024	-0.014	0.025	-0.108	0.790
2671	4883	48830	0.398	0.448	3.022	1.421	0.000	-0.095	0.401	-0.006	0.025	-0.016	0.023	-0.094	0.767
2672	4883	48830	0.398	0.448	3.320	1.438	0.000	-0.092	0.397	-0.005	0.025	-0.017	0.021	-0.082	0.770
2673	4883	48830	0.398	0.449	3.027	1.453	0.000	-0.094	0.401	-0.006	0.025	-0.016	0.023	-0.093	0.767
2674	4883	48830	0.398	0.447	2.511	1.450	0.000	-0.111	0.366	-0.007	0.025	-0.015	0.025	-0.108	0.789
2675	4883	48830	0.398	0.447	2.005	1.426	0.000	-0.128	0.298	-0.010	0.023	-0.012	0.031	-0.119	0.828
2676	4883	48830	0.398	0.447	1.763	1.299	0.000	-0.139	0.257	-0.011	0.021	-0.012	0.033	-0.129	0.852
2677	4883	48830	0.398	0.446	1.506	1.362	0.000	-0.153	0.205	-0.014	0.019	-0.019	0.038	-0.148	0.882
2678	4883	48830	0.398	0.447	2.006	1.344	0.000	-0.128	0.298	-0.010	0.022	-0.011	0.030	-0.119	0.828
2679	4883	48830	0.398	0.448	3.017	1.357	0.000	-0.094	0.401	-0.006	0.025	-0.016	0.022	-0.094	0.768
2680	4883	48830	0.398	0.356	1.506	1.093	0.000	-0.133	0.279	-0.010	0.020	-0.018	0.011	-0.150	0.898
2681	4883	48830	0.398	0.358	1.768	1.092	0.000	-0.123	0.355	-0.008	0.023	-0.015	0.015	-0.131	0.869
2682	4883	48830	0.398	0.358	2.015	1.104	0.000	-0.114	0.414	-0.007	0.025	-0.015	0.014	-0.121	0.847
[illegible]															
2684	4883	48830	0.398	0.359	3.016	1.161	0.000	-0.090	0.530	-0.004	0.028	-0.018	0.013	-0.089	0.803
2685	4883	48830	0.398	0.359	3.311	1.234	0.000	-0.069	0.519	-0.004	0.027	-0.019	0.013	-0.078	0.807
2686	4883	48830	0.398	0.361	3.021	1.282	0.000	-0.075	0.521	-0.004	0.027	-0.018	0.013	-0.088	0.804
2687	4883	48830	0.398	0.358	2.522	1.294	0.000	-0.096	0.497	-0.005	0.026	-0.016	0.015	-0.103	0.816
2688	4883	48830	0.398	0.358	2.017	1.294	0.000	-0.113	0.411	-0.007	0.024	-0.014	0.017	-0.117	0.848
2689	4883	48830	0.398	0.357	1.767	1.281	0.000	-0.123	0.357	-0.008	0.024	-0.016	0.015	-0.132	0.868
2690	4883	48830	0.398	0.359	1.508	1.262	0.000	-0.133	0.275	-0.010	0.020	-0.018	0.012	-0.149	0.898
2691	4883	48830	0.398	0.359	2.015	1.253	0.000	-0.114	0.412	-0.007	0.025	-0.014	0.016	-0.118	0.847
2692	4883	48830	0.398	0.359	3.009	1.274	0.000	-0.090	0.529	-0.004	0.028	-0.019	0.013	-0.090	0.804
2693	4883	48830	0.398	0.358	2.508	1.200	0.000	-0.097	0.497	-0.005	0.027	-0.016	0.014	-0.104	0.816

MODEL DC-6, 36 DEEP CHUTES, AR = 2.0, FORWARD PLUG

FACILITY 8X6X1 PROGRAM C031

NOZZLE TYPE: DUAL FLOW (FAA)

INNER-STREAM PLUG CONFIGURATIONS: FORWARD PLUG WITH BLEED

SUPPRESSOR CONFIGURATION: 36-CHUTE, AREA RATIO = 2.0

THRUST PARAMETERS

OUTER RADIUS RATIO 0.0000

INNER RADIUS RATIO 0.7790

DVO 1.2480

ADC	CF	MASS	02	P4	PTI/PA	PTI/PA	ONEGAT	CDO	CDI	CFNET1	CFNET2	F9
2321	0010	48630	0.398	0.023	1.500	0.984	0.000	0.952	9.999	0.910	0.910	1.126
2324	0010	48630	0.398	0.011	1.502	0.989	0.029	0.951	9.999	0.916	0.916	1.126
2325	0010	48630	0.398	0.019	1.504	0.995	0.059	0.950	9.999	0.923	0.923	1.128
2326	0010	48630	0.398	0.048	1.998	0.982	0.000	0.946	9.999	0.918	0.918	1.136
2327	0010	48630	0.398	0.026	1.997	0.990	0.029	0.946	9.999	0.925	0.925	1.139
2328	0010	48630	0.398	0.024	1.997	0.999	0.059	0.946	9.999	0.932	0.932	1.141
2329	0010	48630	0.398	0.041	2.496	0.977	0.000	0.949	9.999	0.922	0.922	1.137
2330	0010	48630	0.398	0.046	2.500	0.993	0.029	0.946	9.999	0.929	0.929	1.136
2331	0010	48630	0.398	0.050	2.507	1.008	0.059	0.945	1.435	0.933	0.939	1.140
2332	0010	48630	0.398	0.047	3.012	0.973	0.000	0.949	9.999	0.923	0.923	1.138
2333	0010	48630	0.398	0.052	3.012	0.998	0.029	0.946	9.999	0.935	0.935	1.141
2334	0010	48630	0.398	0.056	3.013	1.022	0.059	0.947	1.051	0.936	0.945	1.145
2335	0010	48630	0.398	0.066	3.309	0.988	0.000	0.949	9.999	0.924	0.924	1.141
2336	0010	48630	0.398	0.055	3.307	1.005	0.029	0.948	1.174	0.933	0.935	1.143
2337	0010	48630	0.398	0.057	3.309	1.033	0.059	0.949	0.959	0.936	0.946	1.148
2338	0010	48630	0.398	0.041	2.500	0.977	0.000	0.943	9.999	0.924	0.924	1.135
2339	0010	48630	0.398	0.052	2.499	1.008	0.059	0.947	1.497	0.938	0.943	1.145
2340	0010	48650	1.140	0.025	1.504	1.118	0.286	0.949	1.069	0.923	1.044	1.148
2341	0010	48650	1.140	0.054	1.502	1.518	0.545	0.951	0.989	0.925	1.436	1.179
2342	0010	48650	1.140	0.050	1.502	2.013	0.735	0.951	0.966	0.929	1.807	1.180
2343	0010	48650	1.140	0.024	1.501	2.514	0.919	0.952	0.967	0.930	2.171	1.178
2344	0010	48650	1.140	0.050	1.504	3.020	1.097	0.943	0.953	0.950	2.586	1.183
2345	0010	48650	1.140	0.056	1.502	3.514	1.277	0.944	0.954	0.952	2.965	1.186
2346	0010	48650	1.140	0.042	2.002	1.124	0.211	0.946	1.064	0.932	1.016	1.159
2347	0010	48650	1.140	0.023	1.994	1.517	0.396	0.946	0.990	0.931	1.223	1.182
2348	0010	48650	1.140	0.048	1.996	2.013	0.533	0.946	0.966	0.936	1.437	1.184
2349	0010	48650	1.140	0.051	1.998	2.518	0.663	0.944	0.963	0.942	1.655	1.185
2350	0010	48650	1.140	0.056	2.001	3.020	0.793	0.945	0.968	0.939	1.860	1.184
2351	0010	48650	1.140	0.062	2.000	3.518	0.931	0.943	0.965	0.944	2.083	1.187
2352	0010	48650	1.140	0.055	2.498	1.119	0.165	0.948	1.069	0.940	0.997	1.160
2353	0010	48650	1.140	0.051	2.503	1.519	0.315	0.943	0.985	0.940	1.147	1.178
2354	0010	48650	1.140	0.057	2.501	2.015	0.423	0.943	0.959	0.943	1.297	1.179
2355	0010	48650	1.140	0.053	2.507	2.514	0.529	0.938	0.959	0.949	1.491	1.179
2356	0010	48650	1.140	0.053	2.507	3.018	0.637	0.946	0.967	0.943	1.592	1.181
2357	0010	48650	1.140	0.048	2.515	3.518	0.739	0.935	0.955	0.953	1.764	1.180
2358	0010	48650	1.140	0.028	3.007	1.118	0.133	0.940	1.043	0.939	0.981	1.158
2359	0010	48650	1.140	0.058	3.004	1.517	0.262	0.948	0.989	0.938	1.097	1.176
2360	0010	48650	1.140	0.057	3.010	2.017	0.352	0.948	0.966	0.939	1.211	1.177
2361	0010	48650	1.140	0.066	3.011	2.516	0.440	0.949	0.967	0.941	1.324	1.176
2362	0010	48650	1.140	0.066	3.012	3.021	0.529	0.948	0.967	0.945	1.445	1.181
2363	0010	48650	1.140	0.061	3.002	3.521	0.617	0.952	0.968	0.943	1.558	1.183
2364	0010	48650	1.140	0.063	3.306	1.118	0.117	0.949	1.000	0.941	0.977	1.159
2365	0010	48650	1.140	0.058	3.289	1.522	0.239	0.949	0.985	0.940	1.080	1.177
2366	0010	48650	1.140	0.056	3.295	2.010	0.320	0.949	0.965	0.940	1.179	1.178
2367	0010	48650	1.140	0.062	3.307	2.512	0.399	0.950	0.967	0.941	1.278	1.179

FACILITY 8X6X1 PROGRAM CO3L

NOZZLE TYPE: DUAL FLOW (FAA) | INNER-STREAM PLUG CONFIGURATIONS: FORWARD PLUG WITH BLEED | SUPPRESSOR CONFIGURATION: 36-CHUTE, AREA RATIO = 2.0

CASE PARAMETERS: OUTER RADIUS RATIO 0.0000 | INNER RADIUS RATIO 0.7390 | DVO 1.2480

ROC	CE	MASA	M2	MA	PTO/PA	PT1/PA	OMEGAT	DCS	CDS	DCSH	CDSH	DCPL,O	DCPL,I	DCTOT	PSUP/PA
2323	0010	48630	0.398	0.023	1.500	0.984	0.000	-0.046	21.938	-0.001	0.282	-0.026	-0.002	-0.075	0.965
2324	0010	48630	0.398	0.011	1.502	0.999	0.029	-0.045	95.310	-0.001	1.337	-0.023	-0.001	-0.069	0.966
2325	0010	48630	0.398	0.019	1.504	0.995	0.059	-0.045	32.792	-0.000	0.308	-0.022	0.001	-0.066	0.966
2326	0010	48630	0.398	0.040	1.958	0.982	0.000	-0.040	7.975	-0.000	0.049	-0.023	0.000	-0.063	0.947
2327	0010	48630	0.398	0.026	1.997	0.990	0.029	-0.040	26.874	-0.000	0.314	-0.021	0.000	-0.061	0.948
2328	0010	48630	0.398	0.024	1.997	0.995	0.059	-0.040	31.398	-0.001	0.398	-0.021	0.002	-0.059	0.948
2329	0010	48630	0.398	0.041	2.496	0.977	0.000	-0.035	13.514	-0.000	0.125	-0.023	0.001	-0.058	0.935
2330	0010	48630	0.398	0.044	2.509	0.993	0.029	-0.034	11.322	-0.000	0.096	-0.020	0.001	-0.054	0.936
2331	0010	48630	0.398	0.050	2.507	1.008	0.059	-0.033	8.784	-0.000	0.066	-0.020	0.003	-0.051	0.937
2332	0010	48630	0.398	0.047	3.017	0.973	0.000	-0.030	11.823	-0.000	0.096	-0.025	0.002	-0.053	0.925
2333	0010	48630	0.398	0.052	3.012	0.998	0.029	-0.030	9.561	-0.000	0.076	-0.022	0.002	-0.050	0.927
2334	0010	48630	0.398	0.055	3.013	1.022	0.059	-0.030	8.494	-0.000	0.067	-0.021	0.004	-0.047	0.927
2335	0010	48630	0.398	0.056	3.309	0.968	0.000	-0.026	5.985	-0.000	0.055	-0.023	0.004	-0.046	0.926
2336	0010	48630	0.398	0.055	3.307	1.005	0.029	-0.026	8.558	-0.000	0.099	-0.021	0.002	-0.046	0.926
2337	0010	48630	0.398	0.057	3.309	1.033	0.059	-0.026	7.873	-0.000	0.059	-0.020	0.004	-0.042	0.926
2338	0010	48630	0.398	0.041	2.500	0.977	0.000	-0.035	13.638	-0.000	0.112	-0.023	0.001	-0.058	0.934
2339	0010	48630	0.398	0.057	2.499	1.008	0.059	-0.034	8.107	-0.000	0.063	-0.019	0.003	-0.050	0.936
2340	0010	48630	1.140	0.025	1.506	1.119	0.286	-0.040	19.892	-0.000	0.204	-0.023	0.006	-0.060	0.965
2341	0010	48650	1.140	0.054	1.502	1.519	0.545	-0.030	4.205	-0.000	0.024	-0.018	0.005	-0.044	0.965
2342	0010	48650	1.140	0.050	1.502	2.013	0.735	-0.024	4.866	-0.000	0.012	-0.015	0.000	-0.039	0.965
2343	0010	48650	1.140	0.026	1.501	2.514	0.919	-0.021	22.161	-0.000	0.419	-0.013	-0.003	-0.037	0.963
2344	0010	48650	1.140	0.050	1.504	3.020	1.097	-0.017	6.847	-0.000	0.049	-0.011	0.009	-0.019	0.965
2345	0010	48650	1.140	0.056	1.502	3.514	1.277	-0.015	3.963	-0.000	0.038	-0.009	0.000	-0.024	0.964
2346	0010	48650	1.140	0.062	2.002	1.124	0.210	-0.037	10.674	-0.000	0.091	-0.021	0.006	-0.052	0.947
2347	0010	48650	1.140	0.023	1.994	1.517	0.396	-0.032	37.095	-0.000	0.427	-0.020	0.005	-0.046	0.945
2348	0010	48650	1.140	0.048	1.996	2.013	0.533	-0.027	8.208	-0.000	0.079	-0.017	0.001	-0.043	0.945
2349	0010	48650	1.140	0.051	1.998	2.519	0.665	-0.023	7.323	-0.000	0.049	-0.014	0.001	-0.037	0.946
2350	0010	48650	1.140	0.056	2.001	3.020	0.799	-0.020	5.918	-0.000	0.047	-0.012	0.007	-0.026	0.946
2351	0010	48650	1.140	0.067	2.000	3.518	0.931	-0.018	4.919	-0.000	0.048	-0.011	0.001	-0.028	0.946
2352	0010	48650	1.140	0.055	2.498	1.119	0.165	-0.033	7.600	-0.000	0.062	-0.021	0.005	-0.049	0.934
2353	0010	48650	1.140	0.051	2.503	1.519	0.315	-0.029	8.758	-0.000	0.046	-0.019	0.007	-0.042	0.934
2354	0010	48650	1.140	0.057	2.501	2.015	0.423	-0.026	7.144	-0.000	0.059	-0.018	0.002	-0.042	0.933
2355	0010	48650	1.140	0.053	2.507	3.018	0.637	-0.021	8.221	-0.000	0.062	-0.014	0.003	-0.031	0.934
2358	0010	48650	1.140	0.028	3.007	1.118	0.133	-0.029	12.918	-0.000	0.610	-0.021	0.005	-0.046	0.926
2359	0010	48650	1.140	0.056	3.004	1.517	0.262	-0.026	8.314	-0.000	0.080	-0.020	0.006	-0.041	0.926
2360	0010	48650	1.140	0.057	3.010	2.017	0.352	-0.023	8.024	-0.000	0.070	-0.019	0.002	-0.040	0.926
2361	0010	48650	1.140	0.066	3.011	2.516	0.440	-0.021	5.968	-0.000	0.056	-0.016	0.002	-0.036	0.926
2362	0010	48650	1.140	0.064	3.012	3.021	0.529	-0.020	6.202	-0.000	0.042	-0.014	0.001	-0.033	0.927
2363	0010	48650	1.140	0.061	3.002	3.521	0.617	-0.018	6.781	-0.000	0.067	-0.012	0.001	-0.030	0.927
2364	0010	48650	1.140	0.063	3.306	1.118	0.117	-0.025	6.447	-0.000	0.068	-0.020	0.006	-0.040	0.926
2365	0010	48650	1.140	0.058	3.289	1.522	0.239	-0.023	7.643	-0.000	0.036	-0.019	0.006	-0.036	0.926
2366	0010	48650	1.140	0.056	3.295	2.010	0.320	-0.021	8.174	-0.000	0.052	-0.017	0.002	-0.037	0.926
2367	0010	48650	1.140	0.062	3.307	2.512	0.399	-0.019	6.535	-0.000	0.060	-0.015	0.002	-0.033	0.927

FACILITY AEDC PROGRAM COST

NOZZLE TYPE — DUAL FLOW (FAA)

IN-STREAM PLUG CONFIGURATIONS — FORWARD PLUG WITH BLEED

SUPPRESSOR CONFIGURATION — 36-CHUTE, AREA RATIO = 2.0

SUPPRESSOR PARAMETERS — OUTER RADIUS RATIO 0.0000 — INNER RADIUS RATIO 0.7740 — OVD 1.2480

ARC	CC	NOZZLE	PR	MA	AEC/A8	AII/A8	CNFCAT	CDD	CDI	CFNET1	CFNET2	FG
2369	0010	48A50	1.140	0.448	3.315	3.020	0.480	0.949	0.967	0.945	1.382	1.181
2370	0010	48A50	1.140	0.446	2.502	1.122	0.167	0.947	1.067	0.939	0.998	1.160
2372	0010	48A50	1.140	0.440	2.498	2.513	0.530	0.950	0.967	0.941	1.442	1.182
2376	0010	48A30	0.398	0.450	1.500	1.008	0.059	0.969	0.857	0.794	0.860	1.078
2378	0010	48A30	0.398	0.450	2.005	1.011	0.029	0.938	0.484	0.830	0.833	1.075
2380	0010	48A30	0.398	0.452	2.503	0.986	0.000	0.938	9.999	0.851	0.851	1.080
2382	0010	48A30	0.398	0.453	2.509	1.006	0.059	0.944	0.750	0.859	0.869	1.086
2384	0010	48A30	0.398	0.454	3.010	1.021	0.029	0.946	0.546	0.873	0.876	1.092
2386	0010	48A30	0.398	0.454	3.313	0.979	0.004	0.944	9.999X	0.877	0.877	1.097
2388	0010	48A30	0.398	0.452	3.318	1.055	0.059	0.942	0.731	0.894	0.903	1.104
2390	0010	48A30	0.398	0.449	2.505	1.028	0.059	0.942	0.772	0.861	0.871	1.087
2392	0010	48A30	0.398	0.448	1.501	0.991	0.000	0.972	9.999	0.797	0.797	1.082
2394	0010	48A30	0.398	0.445	1.503	1.009	0.059	0.969	0.794	0.809	0.817	1.085
2396	0010	48A30	0.398	0.445	2.001	1.006	0.029	0.947	0.642	0.841	0.844	1.087
2398	0010	48A30	0.398	0.446	2.509	0.987	0.000	0.947	9.999	0.856	0.856	1.088
2400	0010	48A30	0.398	0.445	2.504	1.028	0.059	0.944	0.782	0.873	0.883	1.097
2402	0010	48A30	0.398	0.446	3.014	1.017	0.029	0.950	0.596	0.881	0.885	1.101
2404	0010	48A30	0.398	0.446	3.317	0.978	0.000	0.946	9.999	0.885	0.885	1.104
2406	0010	48A30	0.398	0.446	3.315	1.054	0.059	0.947	0.744	0.895	0.907	1.111
2408	0010	48A30	0.398	0.443	2.503	1.027	0.059	0.947	0.793	0.869	0.878	1.095
2410	0010	48A50	1.140	0.443	1.501	1.519	0.534	0.970	0.984	0.860	1.325	1.145
2412	0010	48A50	1.140	0.444	1.502	2.512	0.900	0.970	0.986	0.691	2.055	1.154

FACILITY NO. 1 PROGRAM CO11

NOZZLE CASE — INNER-STREAM PLUG CONFIGURATIONS — SUPPRESSOR CONFIGURATION

CORE FLOW (SEA) — FORWARD PLUG WITH BLEED — 36-CHUTE, AREA RATIO = 2.0

OUTER RADIUS RATIO 0.6000 — INNER RADIUS RATIO 0.7300 — DVO 1.2480

CASE	PARAMETER													
2369	CO10	48410	1.140	0.444	1.315	3.029	0.480	-0.010	5.473	-0.000	0.066	-0.013	0.003	-0.029	0.926
2368	CO10	48450	1.140	0.444	1.316	3.030	0.560	-0.017	6.547	-0.000	0.062	-0.011	-0.001	-0.029	0.926
2373	CO10	48410	1.140	0.444	1.317	1.177	0.167	-0.033	18.989	-0.000	0.087	-0.021	0.005	-0.049	0.934
2371	CO10	48450	1.140	0.444	1.318	1.178	0.744	-0.019	8.146	-0.000	0.101	-0.017	0.002	-0.029	0.934
2372	CO10	48450	1.140	0.444	1.316	2.517	0.530	-0.023	14.902	-0.000	0.197	-0.016	0.002	-0.038	0.932
2371	CO10	48450	1.140	0.444	1.317	1.178	0.743	-0.019	8.147	-0.000	0.101	-0.017	0.002	-0.029	0.934
2370	CO10	48410	1.140	0.444	1.315	3.029	0.480	-0.010	5.473	-0.000	0.066	-0.013	0.003	-0.029	0.926
2374	CO10	48410	0.394	0.450	1.500	1.008	0.059	-0.146	0.192	-0.014	0.018	-0.015	0.029	-0.146	0.888
2373	CO10	48410	0.394	0.450	1.500	0.991	0.000	-0.125	0.294	-0.010	0.022	-0.013	0.020	-0.132	0.828
2379	CO10	48410	0.394	0.450	1.501	1.011	0.029	-0.126	0.287	-0.010	0.023	-0.008	0.020	-0.124	0.832
2380	CO10	48410	0.394	0.450	1.504	1.026	0.059	-0.123	0.283	-0.010	0.022	-0.009	0.020	-0.121	0.834
2380	CO10	48410	0.394	0.442	2.503	0.994	0.000	-0.112	0.357	-0.008	0.024	-0.015	0.016	-0.119	0.789
2381	CO10	48410	0.394	0.443	2.503	1.011	0.029	-0.116	0.352	-0.007	0.023	-0.012	0.014	-0.116	0.793
2382	CO10	48410	0.394	0.443	2.504	1.010	0.059	-0.120	0.348	-0.007	0.023	-0.011	0.017	-0.109	0.795
2383	CO10	48410	0.394	0.443	2.504	0.981	0.000	-0.091	0.396	-0.006	0.025	-0.016	0.013	-0.104	0.766
2384	CO10	48410	0.394	0.444	2.503	1.011	0.029	-0.093	0.385	-0.006	0.024	-0.013	0.012	-0.099	0.769
2385	CO10	48410	0.394	0.444	2.504	1.026	0.058	-0.093	0.386	-0.006	0.024	-0.012	0.014	-0.095	0.771
2386	CO10	48410	0.394	0.443	3.503	0.979	0.000	-0.082	0.388	-0.005	0.025	-0.016	0.013	-0.090	0.770
2387	CO10	48410	0.394	0.443	3.503	1.015	0.029	-0.081	0.388	-0.005	0.025	-0.014	0.012	-0.089	0.771
2388	CO10	48410	0.394	0.443	3.504	1.014	0.059	-0.090	0.385	-0.005	0.024	-0.012	0.013	-0.084	0.773
2389	CO10	48410	0.394	0.450	2.503	0.994	0.000	-0.112	0.362	-0.007	0.024	-0.015	0.015	-0.119	0.789
2390	CO10	48410	0.394	0.449	2.504	1.028	0.059	-0.108	0.355	-0.007	0.023	-0.011	0.015	-0.113	0.794
2391	CO10	48410	0.394	0.444	1.501	1.014	0.059	-0.108	0.355	-0.007	0.023	-0.011	0.015	-0.113	0.794
2392	CO10	48410	0.394	0.445	1.501	0.991	0.000	-0.153	0.205	-0.014	0.019	-0.021	0.025	-0.162	0.883
2393	CO10	48410	0.394	0.445	1.502	1.001	0.029	-0.149	0.198	-0.014	0.019	-0.018	0.023	-0.157	0.887
2394	CO10	48410	0.394	0.445	1.502	1.005	0.059	-0.146	0.197	-0.014	0.019	-0.014	0.026	-0.148	0.887
2395	CO10	48410	0.394	0.444	1.998	0.989	0.000	-0.129	0.300	-0.010	0.023	-0.013	0.017	-0.134	0.829
2396	CO10	48410	0.394	0.445	2.001	1.005	0.029	-0.125	0.294	-0.010	0.023	-0.011	0.015	-0.131	0.832
2397	CO10	48410	0.394	0.446	2.001	1.019	0.059	-0.124	0.290	-0.009	0.022	-0.009	0.017	-0.126	0.834
2398	CO10	48410	0.394	0.444	2.504	0.987	0.000	-0.111	0.366	-0.007	0.025	-0.015	0.014	-0.119	0.790
2399	CO10	48410	0.394	0.445	2.505	1.012	0.029	-0.109	0.361	-0.007	0.023	-0.012	0.012	-0.116	0.794
2400	CO10	48410	0.394	0.445	2.504	1.026	0.059	-0.107	0.358	-0.007	0.024	-0.011	0.014	-0.112	0.796
2401	CO10	48410	0.394	0.444	3.721	0.982	0.000	-0.095	0.401	-0.006	0.025	-0.016	0.012	-0.103	0.770
2402	CO10	48410	0.394	0.445	3.014	1.017	0.029	-0.092	0.398	-0.006	0.024	-0.013	0.010	-0.101	0.772
2403	CO10	48410	0.394	0.444	3.021	1.042	0.059	-0.091	0.393	-0.006	0.025	-0.012	0.013	-0.096	0.773
2404	CO10	48410	0.394	0.444	3.312	0.978	0.000	-0.081	0.396	-0.005	0.025	-0.016	0.012	-0.091	0.772
2405	CO10	48410	0.394	0.446	3.312	1.024	0.029	-0.080	0.393	-0.005	0.024	-0.014	0.010	-0.089	0.774
2406	CO10	48410	0.394	0.446	3.319	1.054	0.059	-0.079	0.391	-0.005	0.024	-0.013	0.012	-0.085	0.775
2407	CO10	48410	0.394	0.443	2.503	0.988	0.000	-0.111	0.364	-0.007	0.024	-0.015	0.014	-0.118	0.790
2408	CO10	48410	0.394	0.443	2.503	1.027	0.059	-0.107	0.361	-0.007	0.024	-0.011	0.014	-0.112	0.795
2409	CO10	48410	1.140	0.444	1.501	1.514	0.358	-0.123	0.182	-0.012	0.018	-0.013	0.026	-0.126	0.890
2410	CO10	48410	1.140	0.443	1.501	1.519	0.534	-0.095	0.198	-0.009	0.019	-0.011	0.021	-0.094	0.888
2411	CO10	48410	1.140	0.443	1.501	2.008	0.712	-0.078	0.200	-0.007	0.019	-0.009	0.012	-0.083	0.885
2412	CO10	48410	1.140	0.444	1.502	2.512	0.900	-0.065	0.201	-0.006	0.019	-0.008	0.007	-0.072	0.886

FACILITY 21 INCHER CO2L NOZZLE TYPE IN...-STREAM

DUEL FLOW (FAA) PLUG CONFIGURATIONS SUPPRESSOR CONFIGURATION

FORWARD PLUG WITH BLEED 36-CHUTE, AREA RATIO = 2.0

INPUT PARAMETERS OUTER RADIUS RATIO 0.0000 INNER RADIUS RATIO 0.7790 DVD 1.2480

ROC	CC	NASA	M3	M1	P1/P0A	A1/A8	CVEFF	CDO	CDI	CFNET1	CFNET2	F9
2413	CC10	48410	1.140	0.446	1.401	1.074	1.086	0.970	0.967	0.903	2.443	1.160
2414	CC10	48420	1.140	0.446	1.500	1.519	1.264	0.970	0.968	0.908	2.816	1.163
2415	CC10	48430	1.140	0.446	2.000	1.112	0.184	0.945	0.975	0.864	0.929	1.111
2416	CC10	48440	1.140	0.446	2.000	1.518	0.302	0.946	0.984	0.876	1.147	1.141
2417	CC10	48440	1.140	0.445	1.998	2.012	0.532	0.946	0.967	0.885	1.358	1.147
2418	CC10	48440	1.140	0.445	2.000	2.514	0.666	0.946	0.966	0.896	1.567	1.148
2419	CC10	48440	1.140	0.446	2.002	3.026	0.799	0.946	0.967	0.903	1.788	1.153
2420	CC10	48450	1.140	0.446	2.000	3.523	0.932	0.946	0.968	0.908	2.005	1.158
2421	CC10	48490	1.140	0.445	2.401	1.115	0.145	0.947	0.953	0.879	0.925	1.111
2422	CC10	48450	1.140	0.446	2.403	1.514	0.312	0.947	0.982	0.885	1.072	1.136
2423	CC10	48440	1.140	0.446	2.404	2.016	0.424	0.948	0.965	0.892	1.228	1.141
2424	CC10	48450	1.140	0.446	2.408	2.518	0.530	0.947	0.967	0.899	1.376	1.144
2425	CC10	48450	1.140	0.447	2.507	3.024	0.637	0.947	0.967	0.908	1.534	1.150
2426	CC10	48450	1.140	0.448	2.508	3.523	0.741	0.947	0.968	0.909	1.680	1.152
2427	CC10	48440	1.140	0.448	3.004	1.114	0.115	0.947	0.917	0.890	0.924	1.113
2428	CC10	48450	1.140	0.448	3.003	1.514	0.258	0.950	0.980	0.897	1.047	1.141
[illegible]												
2430	CC10	48440	1.140	0.445	3.014	2.517	0.428	0.946	0.966	0.906	1.275	1.146
2431	CC10	48450	1.140	0.446	3.027	3.019	0.528	0.947	0.967	0.911	1.392	1.150
2432	CC10	48450	1.140	0.445	3.008	3.523	0.616	0.951	0.968	0.912	1.507	1.153
2433	CC10	48440	1.140	0.445	3.315	1.120	0.104	0.949	0.884	0.897	0.928	1.119
2434	CC10	48450	1.140	0.445	3.310	1.518	0.236	0.949	0.975	0.902	1.034	1.143
2435	CC10	[illegible]	1.140	0.446	3.313	2.008	0.218	0.949	0.964	0.907	1.135	1.148
2436	CC10	48450	1.140	0.446	3.314	2.516	0.328	0.949	0.966	0.910	1.234	1.148
2437	CC10	48450	1.140	0.446	3.315	3.023	0.440	0.949	0.966	0.914	1.338	1.152
2438	CC10	48450	1.140	0.446	3.313	3.525	0.561	0.949	0.967	0.913	1.437	1.152
2439	CC10	48450	1.140	0.446	3.508	1.114	0.144	0.947	0.953	0.877	0.923	1.109
2440	CC10	48450	1.140	0.446	3.501	1.524	0.243	0.948	0.967	0.910	1.683	1.153
2441	CC10	48450	1.140	0.445	3.519	2.009	0.350	0.947	0.964	0.900	1.158	1.142
2442	CC10	48430	0.398	0.350	1.502	0.992	0.000	0.967	0.999	0.815	0.815	1.089
2443	CC10	48430	0.398	0.349	1.504	0.991	0.000	0.965	0.999	0.813	0.813	1.087
2444	CC10	48430	0.398	0.348	1.505	1.002	0.029	0.964	0.901	0.824	0.826	1.090
2445	CC10	48430	0.398	0.350	1.503	1.008	0.059	0.965	0.896	0.831	0.838	1.093
2446	CC10	48430	0.398	0.348	2.122	0.987	0.000	0.946	0.999	0.850	0.850	1.095
2447	CC10	48430	0.398	0.348	2.120	1.005	0.029	0.946	0.759	0.858	0.860	1.097
2448	CC10	48430	0.398	0.348	2.015	1.018	0.058	0.945	0.771	0.863	0.872	1.099
2449	CC10	48430	0.398	0.349	2.517	0.985	0.000	0.947	0.999	0.873	0.873	1.100
2450	CC10	48430	0.398	0.348	2.509	1.011	0.029	0.952	0.622	0.880	0.883	1.105
2451	CC10	48430	0.398	0.348	2.521	1.027	0.059	0.945	0.798	0.881	0.891	1.103
2452	CC10	48430	0.398	0.348	3.015	0.981	0.000	0.950	0.999	0.886	0.886	1.109
2453	CC10	48430	0.398	0.348	3.018	1.015	0.029	0.948	0.647	0.893	0.896	1.109
2454	CC10	48430	0.398	0.348	3.021	1.040	0.058	0.947	0.791	0.897	0.907	1.113
2455	CC10	48430	0.398	0.348	3.296	0.977	0.000	0.949	0.999	0.892	0.892	1.113
2456	CC10	48430	0.398	0.348	3.301	1.022	0.029	0.949	0.581	0.899	0.903	1.114
2457	CC10	48430	0.398	0.348	3.305	1.051	0.059	0.949	0.766	0.903	0.915	1.120

FACILITY X1 PROGRAM C031 NOZZLE TYPE DUAL FLOW (FAA) IN...-STREAM PLUG CONFIGURATIONS FOPPARD PLUG WITH PLEED SUPPRESSOR CONFIGURATION 36-CHUTE, AREA RATIO = 2.0

DRAG PARAMETERS OUTER RADIUS RATIO 0.0000 INNER RADIUS RATIO 0.7790 DVD 1.2480

EOS	CE	MASA	M2	M6	RTO/PA	RTI/PA	OMEGAT	DCS	CDS	DCSH	CDSH	DCPL,C	DCPL,I	DCTOT	PSUP/PA
2413	0010	48650	1.140	0.446	1.501	3.024	1.086	-0.055	0.197	-0.005	0.018	-0.006	0.016	-0.050	0.887
2414	0010	48650	1.140	0.446	1.500	3.519	1.266	-0.048	0.197	-0.005	0.019	-0.006	0.007	-0.051	0.887
2415	0010	48650	1.140	0.446	2.000	1.112	0.184	-0.115	0.285	-0.009	0.022	-0.009	0.017	-0.115	0.836
2416	0010	48650	1.140	0.446	2.000	1.518	0.392	-0.095	0.287	-0.007	0.022	-0.007	0.016	-0.092	0.835
2417	0010	48650	1.140	0.445	1.998	2.012	0.532	-0.081	0.290	-0.006	0.021	-0.007	0.009	-0.085	0.834
2418	0010	48650	1.140	0.445	2.000	2.514	0.664	-0.071	0.290	-0.005	0.022	-0.006	0.006	-0.076	0.834
2419	0010	48650	1.140	0.446	2.002	3.026	0.799	-0.062	0.286	-0.005	0.022	-0.005	0.011	-0.060	0.836
2420	0010	48650	1.140	0.446	2.000	3.523	0.932	-0.055	0.284	-0.004	0.022	-0.003	0.006	-0.057	0.837
2421	0010	48650	1.140	0.445	2.503	1.115	0.145	-0.102	0.355	-0.007	0.023	-0.011	0.014	-0.106	0.797
2422	0010	48650	1.140	0.446	2.499	1.514	0.312	-0.089	0.360	-0.006	0.024	-0.010	0.014	-0.092	0.795
2423	0010	48650	1.140	0.446	2.504	2.016	0.424	-0.079	0.357	-0.005	0.023	-0.009	0.009	-0.085	0.795
2424	0010	48650	1.140	0.446	2.508	2.518	0.530	-0.071	0.357	-0.005	0.023	-0.007	0.007	-0.076	0.795
2425	0010	48650	1.140	0.447	2.507	3.024	0.637	-0.063	0.351	-0.004	0.022	-0.006	0.003	-0.070	0.797
2426	0010	48650	1.140	0.446	2.508	3.523	0.743	-0.057	0.347	-0.004	0.023	-0.004	0.006	-0.059	0.799
2427	0010	48650	1.140	0.446	3.024	1.114	0.115	-0.088	0.393	-0.005	0.024	-0.011	0.012	-0.092	0.774
2428	0010	48650	1.140	0.446	3.008	1.516	0.258	-0.079	0.394	-0.005	0.024	-0.011	0.013	-0.082	0.774
2429	0010	48650	1.140	0.446	3.002	1.970	0.369	-0.071	0.392	-0.005	0.024	-0.013	0.004	-0.085	0.785
2430	0010	48650	1.140	0.445	3.016	2.517	0.439	-0.065	0.394	-0.004	0.024	-0.008	0.006	-0.071	0.775
2431	0010	48650	1.140	0.446	3.022	3.019	0.528	-0.059	0.391	-0.004	0.024	-0.006	0.006	-0.064	0.776
2432	0010	48650	1.140	0.445	3.008	3.523	0.616	-0.055	0.389	-0.003	0.024	-0.005	0.004	-0.059	0.776
2433	0010	48650	1.140	0.445	3.315	1.120	0.104	-0.077	0.391	-0.005	0.024	-0.012	0.012	-0.083	0.776
2434	0010	48650	1.140	0.445	3.310	1.518	0.234	-0.070	0.392	-0.004	0.024	-0.011	0.012	-0.073	0.776
2435	0010	48650	1.140	0.446	3.313	2.008	0.318	-0.064	0.391	-0.004	0.024	-0.011	0.007	-0.071	0.776
2436	0010	48650	1.140	0.446	3.314	2.514	0.395	-0.059	0.388	-0.004	0.024	-0.009	0.006	-0.065	0.777
2437	0010	48650	1.140	0.446	3.315	3.023	0.480	-0.054	0.388	-0.003	0.024	-0.007	0.008	-0.056	0.778
2438	0010	48650	1.140	0.446	3.313	3.525	0.561	-0.050	0.385	-0.003	0.024	-0.005	0.002	-0.056	0.779
2439	0010	48650	1.140	0.444	2.506	1.114	0.144	-0.102	0.356	-0.007	0.023	-0.010	0.013	-0.106	0.797
2440	0010	48650	1.140	0.446	2.501	3.524	0.743	-0.057	0.347	-0.004	0.023	-0.004	0.005	-0.060	0.801
2441	0010	48650	1.140	0.445	3.019	2.009	0.350	-0.071	0.395	-0.004	0.024	-0.010	0.007	-0.079	0.774
2442	0010	48630	0.398	0.359	1.502	0.292	0.000	-0.133	0.273	-0.010	0.020	-0.015	-0.003	-0.165	0.898
2443	0010	48630	0.398	0.360	1.505	0.993	0.000	-0.133	0.272	-0.010	0.021	-0.018	-0.003	-0.163	0.898
2444	0010	48630	0.398	0.361	1.505	1.002	0.029	-0.129	0.263	-0.010	0.020	-0.015	-0.005	-0.159	0.901
2445	0010	48630	0.398	0.359	1.503	1.008	0.059	-0.128	0.264	-0.009	0.019	-0.015	-0.003	-0.155	0.902
2446	0010	48630	0.398	0.360	2.009	0.997	0.000	-0.114	0.411	-0.007	0.024	-0.014	-0.000	-0.136	0.847
2447	0010	48630	0.398	0.358	2.010	1.005	0.029	-0.112	0.407	-0.007	0.025	-0.012	-0.002	-0.134	0.850
2448	0010	48630	0.398	0.359	2.015	1.019	0.059	-0.110	0.402	-0.007	0.025	-0.011	0.000	-0.127	0.851
2449	0010	48630	0.398	0.359	2.517	0.995	0.000	-0.095	0.484	-0.005	0.026	-0.016	0.001	-0.114	0.820
2450	0010	48630	0.398	0.360	2.505	1.011	0.029	-0.094	0.478	-0.005	0.025	-0.013	-0.000	-0.112	0.822
2451	0010	48630	0.398	0.359	2.521	1.027	0.059	-0.092	0.479	-0.005	0.026	-0.012	0.002	-0.107	0.822
2452	0010	48630	0.398	0.361	3.015	0.901	0.000	-0.079	0.520	-0.004	0.026	-0.018	0.003	-0.099	0.804
2453	0010	48630	0.398	0.360	3.016	1.015	0.029	-0.078	0.517	-0.004	0.027	-0.015	0.001	-0.097	0.807
2454	0010	48630	0.398	0.359	3.021	1.060	0.059	-0.077	0.516	-0.004	0.027	-0.015	0.003	-0.092	0.808
2455	0010	48630	0.398	0.362	3.294	0.977	0.000	-0.069	0.511	-0.004	0.027	-0.018	0.003	-0.088	0.807
2456	0010	48630	0.398	0.361	3.301	1.022	0.029	-0.068	0.507	-0.004	0.027	-0.016	0.002	-0.086	0.809
2457	0010	48630	0.398	0.361	3.305	1.051	0.059	-0.067	0.507	-0.004	0.027	-0.015	0.004	-0.081	0.810

FACILITY -GRC PROGRAM CODE

NOZZLE TYPE: DUAL FLOW (FAN)

1. 4-STREAM PLUG CONFIGURATIONS: FORWARD PLUG WITH BLEED

SUPPRESSOR CONFIGURATION: 36-CHUTE, AREA RATIO = 2.0

TUNNEL PARAMETER				OUTER RADIUS RATIO 0.0000			INNER RADIUS RATIO 0.7790		OVR 1.2480			
RUN	CE	MACH	DP	P1	P1C/P4	P11/P4	(UNCAL	CPD	CDI	CFNET1	CFNET2	F9
2458	0010	48650	0.360	0.360	2.517	0.984	0.000	0.947	9.999	0.870	0.870	1.099
2459	0010	48650	0.360	0.360	2.515	1.029	-0.059	0.947	0.775	0.881	0.891	1.104
2460	0010	48650	0.360	0.360	2.508	1.117	-0.264	0.946	1.000	0.910	0.924	1.008
2461	0010	48650	1.140	0.360	1.506	1.517	0.534	0.965	0.985	0.871	1.342	1.151
2462	0010	48650	1.140	0.359	1.505	2.026	0.727	0.965	0.966	0.883	1.709	1.153
2463	0010	48650	1.140	0.360	1.505	2.533	0.907	0.964	0.961	0.898	2.082	1.157
2464	0010	48650	1.140	0.360	1.503	3.018	1.086	0.966	0.967	0.906	2.451	1.161
2465	0010	48650	1.140	0.361	1.502	3.523	1.270	0.965	0.967	0.914	2.838	1.167
2466	0010	48650	1.140	0.361	2.016	1.124	0.191	0.948	0.977	0.872	0.943	1.118
2467	0010	48650	1.140	0.360	2.011	1.515	0.390	0.945	0.982	0.885	1.157	1.148
2468	0010	48650	1.140	0.360	2.012	2.028	0.531	0.947	0.965	0.893	1.370	1.152
2469	0010	48650	1.140	0.361	2.014	2.530	0.664	0.946	0.967	0.900	1.577	1.153
2470	0010	48650	1.140	0.361	2.014	3.025	0.794	0.945	0.967	0.909	1.791	1.159
2471	0010	48650	1.140	0.361	2.013	3.528	0.927	0.944	0.967	0.918	2.005	1.162
2472	0010	48650	1.140	0.359	2.514	1.119	0.148	0.947	0.965	0.890	0.938	1.119
2473	0010	48650	1.140	0.359	2.512	1.519	0.312	0.947	0.983	0.896	1.090	1.145
2474	0010	48650	1.140	0.360	2.512	2.020	0.424	0.948	0.966	0.902	1.241	1.150
2475	0010	48650	1.140	0.361	2.526	2.532	0.530	0.944	0.966	0.907	1.389	1.149
2476	0010	48650	1.140	0.360	2.516	3.021	0.634	0.947	0.967	0.915	1.542	1.157
2477	0010	48650	1.140	0.360	2.515	3.524	0.752	0.946	0.967	0.924	1.710	1.162
2478	0010	48650	1.140	0.361	3.015	1.123	0.122	0.949	0.934	0.901	0.939	1.125
2479	0010	48650	1.140	0.358	3.005	1.522	0.260	0.948	0.980	0.906	1.059	1.148
2480	0010	48650	1.140	0.361	3.017	2.527	0.441	0.947	0.966	0.914	1.289	1.153
2481	0010	48650	1.140	0.358	3.018	3.031	0.529	0.948	0.967	0.919	1.406	1.157
2482	0010	48650	1.140	0.361	3.016	3.527	0.617	0.949	0.968	0.919	1.518	1.159
2483	0010	48650	1.140	0.445	2.501	1.117	0.146	0.948	0.956	0.876	0.922	1.109
2484	0010	48650	1.140	0.445	2.501	1.522	0.744	0.948	0.968	0.908	1.682	1.152
2485	0010	48650	1.140	0.356	2.507	1.119	0.148	0.951	0.960	0.890	0.939	1.122
2486	0010	48650	1.140	0.357	2.511	1.527	0.313	0.949	0.981	0.897	1.094	1.147
2487	0010	48650	1.140	0.357	2.516	2.034	0.424	0.948	0.966	0.902	1.266	1.149
2488	0010	48650	1.140	0.358	2.514	2.530	0.531	0.947	0.967	0.908	1.391	1.152
2489	0010	48650	1.140	0.358	2.515	3.024	0.635	0.947	0.968	0.915	1.543	1.157
2490	0010	48650	1.140	0.360	2.513	3.520	0.740	0.948	0.969	0.916	1.691	1.160
2491	0010	48650	1.140	0.360	3.025	1.123	0.122	0.949	0.937	0.902	0.941	1.126
2492	0010	48650	1.140	0.359	3.006	1.528	0.262	0.949	0.981	0.906	1.060	1.148
2493	0010	48650	1.140	0.358	3.006	2.032	0.356	0.949	0.966	0.910	1.177	1.152
2494	0010	48650	1.140	0.359	3.008	2.532	0.443	0.949	0.967	0.915	1.291	1.155
2495	0010	48650	1.140	0.356	3.016	3.040	0.531	0.949	0.967	0.919	1.409	1.158
2496	0010	48650	1.140	0.359	3.017	3.522	0.616	0.949	0.969	0.919	1.517	1.159
2497	0010	48650	1.140	0.359	3.295	1.121	0.107	0.949	0.901	0.906	0.939	1.128
2498	0010	48650	1.140	0.359	3.265	1.525	0.240	0.949	0.979	0.911	1.048	1.151
2499	0010	48650	1.140	0.360	3.229	2.030	0.331	0.948	0.966	0.913	1.156	1.153
2500	0010	48650	1.140	0.358	3.216	2.533	0.414	0.951	0.967	0.916	1.260	1.156
2501	0010	48650	1.140	0.361	3.237	3.038	0.493	0.951	0.967	0.923	1.367	1.162
2502	0010	48650	1.140	0.360	3.258	3.520	0.569	0.949	0.968	0.920	1.458	1.159

FACILITY 6 1 PROGRAM COST [illegible] [illegible] [illegible]

FACILITY ,E1 PROGRAM COST

NOZZLE TYPE: DUAL FLOW (FAN)

IN...-STREAM PLUG CONFIGURATIONS: FORWARD PLUG WITH BLEED

SUPPRESSOR CONFIGURATION: 36-CHUTE, AREA RATIO = 2.0

INPUT PARAMETERS: OUTER RADIUS RATIO C.0000; INNER RADIUS RATIO 0.7790; DVO 1.2480

ROC	CE	AREA	C3	FN	FIC/FA	RTI/FA	CWEGAT	CDO	CDI	CENET1	CENET2	FG
2503	0010	48650	1.140	0.359	1.506	1.121	0.267	0.966	1.007	0.853	0.976	1.118
2504	0010	48650	1.140	0.358	1.504	1.121	0.267	0.966	1.003	0.850	0.973	1.117

FACILITY ,E1 PROGRAM COST

NOZZLE TYPE: DUAL FLOW (FAN)

IN... STREAM PLUG CONFIGURATIONS: FORWARD PLUG WITH BLEED

SUPPRESSOR CONFIGURATION: 36-CHUTE, AREA RATIO = 2.0

DRAG PARAMETERS: OUTER RADIUS RATIO C.0000; INNER RADIUS RATIO 0.7790; DVO 1.2480

ROC	CE	AREA	C3	FN	FIC/FA	RTI/FA	CWEGAT	DCS	CDS	DCSH	CDSH	DCPL,O	DCPL,I	DCTOT	PSUP/PA
2503	0010	48650	1.140	0.359	1.504	1.121	0.267	-0.111	0.263	-0.008	0.020	-0.012	0.005	-0.126	0.902
2504	0010	48650	1.140	0.358	1.504	1.121	0.267	-0.111	0.262	-0.008	0.019	-0.013	0.006	-0.128	0.903

MODEL DC-7, 36 DEEP CHUTES, AR = 2.5, BASELINE PLUG

FACILITY [illegible] [illegible] [illegible]

INLET-STREAM CONFIGURATIONS — SUPPRESSOR CONFIGURATION

CORE FLOW (FAN) — BASELINE PLUG WITH BLEED — 36-CHUTE, AREA RATIO = 2.5

INPUT PARAMETERS — OUTER FISCUS RATIO 0.8000 — LEAD RADIUS RATIO 0.7790 — OVC 1.2480

RPC	RF	RPCO	P2	W2	P16/P2	P13/P2	CMFRAT	CDC	CDI	CFNET1	CFNET2	FG
2774	0012	48530	0.998	0.063	1.505	0.991	0.000	0.977	0.999	0.936	0.936	1.149
2775	0012	48530	0.998	0.029	1.507	0.992	0.029	0.975	0.999	0.939	0.939	1.146
2776	0012	48530	0.998	0.019	1.508	1.001	0.059	0.976	2.219	0.945	0.949	1.148
2777	0012	48530	0.998	0.063	3.007	0.973	0.000	0.976	0.999	0.946	0.946	1.173
2778	0012	48530	0.998	0.062	3.008	0.992	0.029	0.976	0.999	0.951	0.951	1.172
2779	0012	48530	0.998	0.035	3.008	1.011	0.059	0.976	1.066	0.951	0.959	1.172
2780	0012	48530	0.998	0.063	3.013	0.963	0.000	0.975	0.999	0.952	0.952	1.180
2781	0012	48530	0.998	0.061	3.006	0.995	0.029	0.978	0.999	0.960	0.960	1.181
[illegible]												
2783	0012	48530	0.998	0.052	3.012	1.022	0.059	0.977	0.944	0.956	0.965	1.179
2784	0012	48530	0.998	0.052	3.008	0.993	0.000	0.979	0.999	0.952	0.952	1.187
2785	0012	48530	0.998	0.027	3.015	0.992	0.029	0.980	0.999	0.958	0.958	1.186
2786	0012	48530	0.998	0.054	3.022	1.010	0.059	0.978	0.947	0.958	0.968	1.187
2787	0012	48530	0.998	0.035	3.009	0.966	0.000	0.980	0.999	0.950	0.950	1.191
2788	0012	48530	0.998	0.027	3.011	0.992	0.029	0.979	0.999	0.958	0.958	1.188
2789	0012	48530	0.998	0.027	3.022	1.033	0.059	0.980	0.978	0.959	0.969	1.191
2790	0012	48530	0.998	0.054	3.012	0.965	0.000	0.978	0.999	0.953	0.953	1.187
2791	0012	48530	0.998	0.040	3.017	1.027	0.059	0.978	0.939	0.960	0.969	1.192
2792	0012	48530	1.149	0.032	1.508	1.117	0.263	0.976	0.986	0.959	1.085	1.172
2793	0012	48530	1.149	0.056	1.509	1.113	0.515	0.977	0.983	0.960	1.458	1.207
2794	0012	48530	1.149	0.034	1.509	2.017	0.715	0.977	0.990	0.954	1.927	1.211
2795	0012	48530	1.149	0.051	1.507	2.018	0.805	0.976	0.991	0.954	2.189	1.211
2796	0012	48530	1.149	0.044	1.508	1.018	1.076	0.976	0.991	0.945	2.529	1.205
2797	0012	48530	1.149	0.041	1.509	3.012	1.252	0.977	0.993	0.967	2.966	1.225
2798	0012	48530	1.149	0.027	1.509	1.018	0.271	0.976	0.983	0.959	1.240	1.216
2799	0012	48530	1.149	0.047	3.013	3.014	0.516	0.976	0.989	0.956	1.451	1.220
2800	0012	48530	1.149	0.031	3.006	3.012	0.643	0.976	0.990	0.955	1.651	1.218
2801	0012	48530	1.149	0.057	3.007	3.017	0.773	0.976	0.991	0.951	1.850	1.214
2802	0012	48530	1.149	0.038	3.004	3.019	0.902	0.976	0.992	0.967	2.095	1.231
2803	0012	48530	1.149	0.025	3.010	1.116	0.173	0.976	0.944	0.967	1.036	1.192
2804	0012	48530	1.149	0.046	3.013	1.118	0.134	0.977	0.934	0.964	1.012	1.193
2805	0012	48530	1.149	0.063	3.010	1.520	0.245	0.979	0.979	0.961	1.159	1.216
2806	0012	48530	1.149	0.046	3.013	3.018	0.411	0.979	0.988	0.958	1.307	1.218
2807	0012	48530	1.149	0.063	3.010	3.016	0.513	0.979	0.990	0.958	1.450	1.218
2808	0012	48530	1.149	0.047	3.015	3.022	0.617	0.977	0.991	0.953	1.590	1.214
2809	0012	48530	1.149	0.040	3.009	3.019	0.719	0.976	0.993	0.967	1.761	1.230
2810	0012	48530	1.149	0.064	3.021	1.119	0.119	0.980	0.946	0.964	1.002	1.199
2811	0012	48530	1.149	0.047	3.019	1.519	0.246	0.978	0.978	0.961	1.113	1.215
2812	0012	48530	1.149	0.064	3.008	2.013	0.341	0.980	0.988	0.959	1.227	1.219
2813	0012	48530	1.149	0.050	3.012	2.017	0.427	0.980	0.990	0.959	1.337	1.219
2814	0012	48530	1.149	0.033	3.022	3.020	0.512	0.980	0.991	0.951	1.437	1.213
2815	0012	48530	1.149	0.044	3.021	3.017	0.596	0.980	0.992	0.967	1.575	1.229
2816	0012	48530	1.149	0.060	3.106	1.121	0.106	0.980	0.946	0.963	0.997	1.202
2817	0012	48530	1.149	0.047	3.020	1.514	0.224	0.979	0.978	0.960	1.094	1.216
2818	0012	48530	1.149	0.063	3.109	2.019	0.322	0.980	0.989	0.958	1.205	1.219

SUPPRESSOR CONFIGURATION
36-CHUTE, AREA RATIO = 2.5

1 P-STREAM
5 CONFIGURATIONS
BASELINE PLUG WITH BLEED
SUPPRESSOR CONFIGURATIO
36-CHUTE, AREA RATIO = 2.5

CROSS RADIUS RATIO 0.6000
INNER RADIUS RATIO 0.7750
OVD 1.2480

2823	0012	40550	1.140	0.446	2.514	1.040	0.059	0.975	0.691	0.871	0.882	1.114
2824	0012	40551	1.140	0.447	2.515	1.120	0.222	1.001	0.918	0.819	0.920	1.110
2825	0012	40552	1.140	0.447	2.516	1.517	0.581	1.001	0.980	0.854	1.285	1.152
2826	0012	40553	1.140	0.447	2.517	2.010	0.696	1.000	0.989	0.869	1.643	1.161
2827	0012	40554	1.140	0.447	2.518	2.514	0.869	0.999	0.984	0.885	1.998	1.166
2828	0012	40555	1.140	0.447	2.519	3.026	1.053	0.999	0.992	0.885	2.344	1.165
2829	0012	40556	1.140	0.448	2.520	3.519	1.226	1.001	0.992	0.913	2.759	1.187
2830	0012	40557	1.140	0.447	2.520	1.121	0.140	0.976	0.966	0.855	0.913	1.118
2831	0012	40558	1.140	0.448	2.520	1.520	0.367	0.977	0.972	0.872	1.126	1.153
2832	0012	40559	1.140	0.448	2.520	2.017	0.514	0.977	0.991	0.880	1.333	1.161
2833	0012	40560	1.140	0.447	2.520	2.519	0.643	0.977	0.991	0.890	1.538	1.166
2834	0012	40561	1.140	0.448	2.520	3.024	0.774	0.977	0.992	0.891	1.737	1.166
2835	0012	40562	1.140	0.448	2.520	3.523	0.902	0.976	0.992	0.913	1.978	1.184
2836	0012	40563	1.140	0.447	2.519	1.122	0.124	0.975	0.960	0.880	0.921	1.126
2837	0012	40564	1.140	0.447	2.519	1.520	0.291	0.978	0.966	0.887	1.067	1.154
2838	0012	40565	1.140	0.447	2.518	2.011	0.410	0.977	0.991	0.892	1.215	1.162
2839	0012	40566	1.140	0.447	2.519	2.517	0.513	0.974	0.991	0.898	1.360	1.166
2840	0012	40567	1.140	0.448	2.518	3.027	0.617	0.973	0.992	0.899	1.500	1.166
2841	0012	40568	1.140	0.447	2.517	3.519	0.722	0.979	0.993	0.917	1.674	1.184
2842	0012	40569	1.140	0.447	2.521	1.523	0.241	0.979	0.961	0.958	1.038	1.159
2843	0012	40570	1.140	0.448	2.521	2.022	0.341	0.980	0.990	0.900	1.151	1.167
2845	0012	40550	1.140	0.448	3.025	2.518	0.429	0.976	0.992	0.908	1.268	1.170

SUPPRESSOR CONFIGURATION
36-CHUTE, AREA RATIO = 2.5

FACILITY [illegible] CO'L

NOZZLE TYPE — DUAL FLOW LEAKI

IN-STREAM CONFIGURATIONS — BASELINE PLUG WITH BLEED

SUPPRESSOR CONFIGURATION — 36-CHUTE, AREA RATIO = 2.5

IMPACT PARAMETERS — OUTER RADIUS RATIO 0.0000 — INNER RADIUS RATIO 0.7790 — DVC 1.2480

PRC	CF	MASS	PT	MA	PTP/PA	PTI/PA	CF/CAT	CDD	CDI	CFNET1	CFNET2	F9
2844	0012	40553	1.160	0.446	3.010	1.623	0.511	0.979	0.992	0.896	1.354	1.161
2847	0012	40553	1.160	0.446	3.022	1.525	0.554	0.980	0.993	0.920	1.501	1.184
2848	0012	40553	1.160	0.447	3.025	1.170	0.101	0.981	0.893	0.924	0.924	1.138
2849	0012	40553	1.160	0.448	3.015	1.119	0.000	0.981	0.820	0.897	0.924	1.142
2850	0012	40553	1.160	0.448	3.021	1.522	0.217	0.981	0.956	0.901	1.024	1.163
2851	0012	40553	1.160	0.448	3.024	2.018	0.310	0.981	0.990	0.903	1.125	1.170
2852	0012	40553	1.160	0.448	3.031	2.612	0.396	0.981	0.992	0.908	1.221	1.173
2871	0012	40553	1.160	0.448	3.034	3.024	0.463	0.981	0.992	0.899	1.301	1.164
2874	0012	40553	1.160	0.449	3.036	3.024	0.542	0.980	0.993	0.920	1.428	1.185
2875	0012	40553	1.160	0.447	2.417	1.121	0.124	0.978	0.847	0.878	0.919	1.126
2876	0012	40553	1.160	0.448	2.421	1.521	0.721	0.978	0.994	0.917	1.673	1.183
2877	0012	40553	0.358	0.358	1.586	0.991	0.000	0.998	9.999	0.819	0.819	1.102
2878	0012	40553	0.358	0.358	1.588	1.001	0.029	0.996	1.118	0.828	0.829	1.104
2879	0012	40553	0.358	0.358	1.587	1.012	0.059	0.997	0.733	0.835	0.844	1.107
2880	0012	40553	0.358	0.358	2.018	0.986	0.000	0.977	9.999	0.860	0.860	1.117
2881	0012	40553	0.358	0.358	2.019	1.004	0.029	0.976	0.819	0.865	0.867	1.117
2882	0012	40553	0.358	0.358	2.018	1.016	0.059	0.977	0.691	0.869	0.878	1.119
2883	0012	40553	0.358	0.358	2.023	0.975	0.000	0.978	9.999	0.884	0.884	1.129
2884	0012	40553	0.358	0.358	2.026	1.007	0.029	0.978	0.939	0.890	0.892	1.130
2885	0012	40553	0.358	0.358	2.022	1.017	0.059	0.978	0.729	0.892	0.903	1.132
2886	0012	40553	0.358	0.358	3.020	0.967	0.000	0.980	9.999	0.898	0.898	1.143
2887	0012	40553	0.358	0.358	3.044	1.007	0.029	0.981	1.027	0.905	0.907	1.144
2888	0012	40553	0.358	0.358	3.020	1.048	0.059	0.979	0.761	0.905	0.917	1.143
2889	0012	40553	0.358	0.358	3.156	0.958	0.000	0.980	9.999	0.900	0.900	1.145
2890	0012	40553	0.358	0.361	3.134	1.008	0.029	0.980	1.086	0.905	0.907	1.143
2891	0012	40553	0.358	0.361	3.129	1.051	0.059	0.981	0.768	0.907	0.919	1.146
2892	0012	40553	0.358	0.358	2.574	0.976	0.000	0.978	9.999	0.883	0.883	1.129
2893	0012	40553	0.358	0.358	2.574	1.038	0.059	0.979	0.712	0.891	0.902	1.131
2894	0012	40553	1.160	0.361	1.510	1.171	0.232	0.995	0.925	0.852	0.958	1.125
2895	0012	40553	1.160	0.360	1.595	1.527	0.509	0.997	0.984	0.879	1.333	1.166
2896	0012	40553	1.160	0.359	1.597	2.032	0.709	0.996	0.991	0.890	1.702	1.175
2897	0012	40553	1.160	0.359	1.597	2.530	0.883	0.996	0.993	0.900	2.054	1.178
2898	0012	40553	1.160	0.359	1.597	3.019	1.056	0.996	0.993	0.901	2.386	1.177
2899	0012	40553	1.160	0.360	1.585	3.518	1.232	0.997	0.994	0.925	2.809	1.197
2900	0012	40553	1.160	0.361	2.018	1.124	0.165	0.977	0.891	0.881	0.943	1.136
2901	0012	40553	1.160	0.359	2.018	1.528	0.369	0.977	0.977	0.892	1.153	1.147
2902	0012	40553	1.160	0.359	2.018	2.035	0.518	0.976	0.991	0.899	1.366	1.175
2903	0012	40553	1.160	0.360	2.018	2.533	0.645	0.977	0.992	0.906	1.568	1.179
2904	0012	40553	1.160	0.359	2.017	3.025	0.772	0.977	0.993	0.905	1.758	1.178
2905	0012	40553	1.160	0.361	2.017	3.520	0.899	0.976	0.994	0.925	1.996	1.195
2906	0012	40553	1.160	0.360	2.524	1.121	0.126	0.978	0.861	0.899	0.941	1.143
2907	0012	40553	1.160	0.359	2.521	1.530	0.293	0.978	0.960	0.905	1.091	1.169
2908	0012	40553	1.160	0.360	2.522	2.035	0.413	0.979	0.991	0.908	1.241	1.176
2909	0012	40553	1.160	0.361	2.523	2.534	0.515	0.979	0.992	0.914	1.385	1.180
2910	0012	40553	1.160	0.360	2.525	3.030	0.617	0.978	0.993	0.913	1.522	1.179

FACILITY NSWC SCCOSAM COIL — NOZZLE TYPE: C-D-STREAM — CONFIGURATIONS — SUPPRESSOR CONFIGURATIC

FUEL FLOW (GAS) — BASELINE PLUG WITH BLEED — 36-CHUTE, AREA RATIO = 2.5

BASE PRESSURES — OUTER RADIUS RATIO 0.9000 — INNER RADIUS RATIO 0.7720 — OVO 1.2480

RUN	PT	MACH	PJ	PA	PT/PJ	PT/PA	OMEGAT	DCS	CDS	DCSH	CDSH	DCPL,C	DCPL,I	DCTOT	PSUP/PA
2964	0013	40000	1.140	3.449	1.030	3.071	0.511	-0.065	0.439	-0.001	0.007	0.002	-0.024	-0.087	0.823
2965	0013	40000	1.140	3.449	1.022	3.025	0.598	-0.060	0.435	-0.001	0.007	0.003	-0.005	-0.063	0.824
2966	0013	40000	1.140	3.449	1.025	3.129	0.101	-0.097	0.457	-0.002	0.007	0.001	0.007	-0.091	0.817
2967	0013	40000	1.140	3.448	1.115	1.110	0.050	-0.030	0.477	-0.001	0.007	-0.001	0.006	-0.086	0.808
2968	0013	40000	1.140	3.448	1.131	1.527	0.717	-0.091	0.470	-0.001	0.007	0.001	0.002	-0.079	0.811
2969	0013	40000	1.140	3.448	1.124	2.018	0.319	-0.073	0.467	-0.001	0.007	0.001	-0.011	-0.084	0.812
2970	0013	40000	1.140	3.448	1.131	2.517	0.386	-0.068	0.466	-0.001	0.007	0.001	-0.013	-0.080	0.812
2971	0013	40000	1.140	3.448	1.130	1.024	0.661	-0.062	0.463	-0.001	0.007	0.002	-0.025	-0.087	0.813
2974	0013	40000	1.140	3.448	1.134	1.524	0.542	-0.068	0.460	-0.001	0.007	0.002	-0.006	-0.063	0.814
2975	0013	40000	1.140	3.447	1.117	1.121	0.174	-0.117	0.408	-0.002	0.007	0.001	0.008	-0.105	0.836
2976	0013	40000	1.140	3.448	1.111	1.521	0.721	-0.062	0.391	-0.001	0.007	0.002	-0.006	-0.067	0.842
2977	0013	40000	1.140	3.448	1.104	0.991	0.000	-0.149	0.327	-0.003	0.004	-0.008	0.012	-0.148	0.916
2978	0013	40000	1.140	3.448	1.105	1.001	0.079	-0.145	0.319	-0.003	0.004	-0.005	0.010	-0.143	0.918
2979	0013	40000	1.140	3.448	1.107	1.012	0.050	-0.141	0.313	-0.003	0.006	-0.004	0.007	-0.140	0.920
2980	0013	40000	1.140	3.448	1.111	1.511	0.000	-0.124	0.477	-0.002	0.008	-0.004	0.012	-0.119	0.877
2981	0013	40000	1.140	3.448	1.111	2.010	1.004	0.025	-0.172	0.472	-0.002	0.008	-0.002	0.008	-0.118	0.879
2982	0013	40000	1.140	3.448	1.110	1.024	0.050	-0.118	0.458	-0.002	0.007	-0.001	0.006	-0.115	0.882
2983	0013	40000	1.140	3.448	1.109	0.995	0.000	-0.134	0.563	-0.003	0.009	-0.004	0.011	-0.099	0.855
2984	0013	40000	1.140	3.448	1.109	1.001	0.025	-0.127	0.554	-0.002	0.009	-0.002	0.007	-0.099	0.856
2985	0013	40000	1.140	3.448	1.107	1.007	0.050	-0.120	0.548	-0.001	0.008	-0.001	0.005	-0.097	0.859
2986	0013	40000	1.140	3.448	1.107	0.987	0.000	-0.093	0.616	-0.001	0.009	-0.006	0.010	-0.085	0.841
2987	0013	40000	1.140	3.448	1.104	1.007	0.025	-0.085	0.601	-0.001	0.009	-0.003	0.006	-0.083	0.844
2988	0013	40000	1.140	3.448	1.103	1.041	0.050	-0.083	0.589	-0.001	0.009	-0.002	0.004	-0.083	0.847
2989	0013	40000	1.140	3.448	1.104	0.991	0.000	-0.084	0.620	-0.001	0.009	-0.007	0.010	-0.082	0.839
2990	0013	40000	1.140	3.448	1.104	1.004	0.029	-0.082	0.604	-0.001	0.009	-0.006	0.006	-0.082	0.842
2991	0013	40000	1.140	3.448	1.105	1.051	0.050	-0.081	0.598	-0.001	0.009	-0.002	0.004	-0.081	0.844
2992	0013	40000	1.140	3.448	1.104	0.974	0.000	-0.106	0.659	-0.002	0.008	-0.004	0.011	-0.098	0.855
2993	0013	40000	1.140	3.448	1.104	1.021	0.050	-0.099	0.642	-0.001	0.008	-0.000	0.006	-0.095	0.860
2994	0013	40000	1.140	3.448	1.110	1.121	0.232	-0.173	0.300	-0.002	0.006	-0.000	0.007	-0.119	0.922
2995	0013	40000	1.140	3.448	1.106	1.521	0.589	-0.091	0.297	-0.002	0.004	-0.001	-0.001	-0.094	0.923
2996	0013	40000	1.140	3.448	1.107	2.017	0.708	-0.073	0.304	-0.001	0.006	-0.001	-0.017	-0.093	0.922
2997	0013	40000	1.140	3.448	1.107	2.520	0.821	-0.061	0.304	-0.001	0.006	-0.001	-0.026	-0.089	0.921
2998	0013	40000	1.140	3.448	1.107	3.014	1.054	-0.053	0.303	-0.001	0.006	-0.000	-0.020	-0.083	0.922
2999	0013	40000	1.140	3.448	1.105	3.514	1.232	-0.045	0.297	-0.001	0.006	-0.001	-0.014	-0.061	0.923
3000	0013	40000	1.140	3.448	2.010	1.124	0.146	-0.105	0.443	-0.002	0.007	0.001	-0.005	-0.105	0.884
3001	0013	40000	1.140	3.448	2.010	1.524	0.365	-0.090	0.446	-0.001	0.007	0.002	-0.000	-0.090	0.885
3002	0013	40000	1.140	3.448	2.010	2.023	0.518	-0.077	0.444	-0.001	0.007	0.001	-0.020	-0.096	0.885
3003	0013	40000	1.140	3.448	2.010	2.521	0.648	-0.067	0.441	-0.001	0.007	0.001	-0.018	-0.085	0.886
3004	0013	40000	1.140	3.448	2.011	3.025	0.772	-0.059	0.442	-0.001	0.007	0.001	-0.029	-0.088	0.886
3005	0013	40000	1.140	3.448	2.013	3.528	0.890	-0.053	0.434	-0.001	0.007	0.001	-0.010	-0.063	0.887
3006	0013	40000	1.140	3.448	2.014	1.121	0.176	-0.096	0.533	-0.001	0.008	0.001	0.004	-0.090	0.862
3007	0013	40000	1.140	3.448	2.011	1.520	0.293	-0.081	0.527	-0.001	0.009	0.001	-0.000	-0.081	0.864
3008	0013	40000	1.140	3.448	2.012	2.025	0.413	-0.071	0.528	-0.001	0.009	0.001	-0.018	-0.089	0.863
3009	0013	40000	1.140	3.448	2.013	2.524	0.515	-0.064	0.521	-0.001	0.008	0.002	-0.015	-0.079	0.864
3010	0013	40000	1.140	3.448	2.015	3.030	0.617	-0.058	0.521	-0.001	0.008	0.002	-0.024	-0.081	0.864

FACILITY AEDC PROPULSION CELL NOZZLE TYPE CONTOUR PLUG WITH BLEED FLOW-STREAM CONFIGURATIONS SUPPRESSOR CONFIGURATION

CONTOUR PLUG WITH BLEED SUPPRESSOR CONFIGURATION 36-CHUTE, AREA RATIO = 2.5

FIXED FLOW (FAN) BASELINE

FIXED RADIUS RATIO 0.0000 INNER RADIUS RATIO 0.7790 OVD 1.2480

RUN	PT	TAT	M3	M9	PT3/P0	PT3/P9	EFFFAN	CFG	CDI	CFNET1	CFNET2	F9
2911	0011	49550	1.140	0.358	2.524	3.525	0.717	0.978	0.992	0.930	1.689	1.194
2912	0012	49550	1.140	0.358	2.521	3.519	0.717	0.978	0.992	0.930	1.690	1.196
2913	0013	49550	1.140	0.358	2.516	3.512	0.717	0.978	0.994	0.930	1.690	1.196
2914	0011	49550	1.140	0.358	2.524	3.525	0.717	0.978	0.992	0.930	1.689	1.194
2915	0012	49550	1.140	0.358	2.521	3.519	0.717	0.978	0.992	0.930	1.690	1.196
2916	0013	49550	1.140	0.358	2.516	3.512	0.717	0.978	0.994	0.930	1.690	1.196
2917	0011	49550	1.140	0.358	2.524	3.525	0.717	0.978	0.992	0.930	1.689	1.194
2918	0012	49550	1.140	0.358	2.521	3.519	0.717	0.978	0.992	0.930	1.690	1.196
2919	0013	49550	1.140	0.358	2.516	3.512	0.717	0.978	0.994	0.930	1.690	1.196
2920	0011	49550	1.140	0.358	2.524	3.525	0.717	0.978	0.992	0.930	1.689	1.194
2921	0012	49550	1.140	0.358	2.521	3.519	0.717	0.978	0.992	0.930	1.690	1.196
2922	0013	49550	1.140	0.358	2.516	3.512	0.717	0.978	0.994	0.930	1.690	1.196
2923	0011	49550	1.140	0.358	2.524	3.525	0.717	0.978	0.992	0.930	1.689	1.194
2924	0012	49550	1.140	0.358	2.521	3.519	0.717	0.978	0.992	0.930	1.690	1.196
2925	0013	49550	1.140	0.358	2.516	3.512	0.717	0.978	0.994	0.930	1.690	1.196

FACILITY AEDC PROPULSION CELL NOZZLE TYPE CONTOUR PLUG WITH BLEED FLOW-STREAM CONFIGURATIONS SUPPRESSOR CONFIGURATION

CONTOUR PLUG WITH BLEED SUPPRESSOR CONFIGURATION 36-CHUTE, AREA RATIO = 2.5

FIXED FLOW (FAN) BASELINE

FIXED RADIUS RATIO 0.0000 INNER RADIUS RATIO 0.7790 OVD 1.2480

RUN	PT	TAT	M3	M9	PT3/P0	PT3/P9	EFFFAN	MFS	CDS	DFSH	CDSH	DCPL,0	DCPL,1	DCTOT	PSUP/PA
2911	0011	49550	1.140	0.361	2.524	3.525	0.717	-0.043	0.515	-0.001	0.008	0.002	-0.008	-0.059	0.866
2912	0012	49550	1.140	0.358	2.521	3.519	0.717	-0.043	0.514	-0.001	0.008	-0.001	0.004	-0.079	0.848
2913	0013	49550	1.140	0.358	2.516	3.512	0.717	-0.043	0.514	-0.001	0.008	0.000	-0.000	-0.073	0.850
2914	0011	49550	1.140	0.358	2.524	3.525	0.717	-0.044	0.578	-0.001	0.008	0.001	-0.015	-0.079	0.851
2915	0012	49550	1.140	0.358	2.521	3.519	0.717	-0.044	0.578	-0.001	0.008	0.001	-0.017	-0.076	0.851
2916	0013	49550	1.140	0.358	2.516	3.512	0.717	-0.044	0.577	-0.001	0.008	0.001	-0.017	-0.076	0.851
2917	0011	49550	1.140	0.358	2.524	3.525	0.717	-0.044	0.572	-0.001	0.008	0.001	-0.029	-0.082	0.852
2918	0012	49550	1.140	0.358	2.521	3.519	0.717	-0.044	0.565	-0.001	0.008	0.002	-0.007	-0.056	0.853
2919	0013	49550	1.140	0.358	2.516	3.512	0.717	-0.044	0.604	-0.001	0.008	-0.002	0.004	-0.075	0.844
2920	0011	49550	1.140	0.358	2.524	3.525	0.717	-0.043	0.515	-0.001	0.008	-0.000	-0.000	-0.070	0.847
2921	0012	49550	1.140	0.358	2.521	3.519	0.717	-0.043	0.514	-0.001	0.008	0.000	-0.014	-0.078	0.849
2922	0013	49550	1.140	0.358	2.516	3.512	0.717	-0.043	0.514	-0.001	0.008	0.001	-0.017	-0.076	0.850
2923	0011	49550	1.140	0.358	2.524	3.525	0.717	-0.044	0.572	-0.001	0.008	0.001	-0.029	-0.081	0.851
2924	0012	49550	1.140	0.358	2.521	3.519	0.717	-0.044	0.571	-0.001	0.008	0.002	-0.007	-0.055	0.852
2925	0013	49550	1.140	0.358	2.516	3.512	0.717	-0.044	0.519	-0.001	0.008	0.002	-0.008	-0.059	0.866

MODEL DC-8, 36 DEEP CHUTES, AR = 2.5, FULL PLUG

FACILITY 6FT PROPAN CCTL — NOZZLE TYPE: DUAL FLOW THRU — 1-STREAM PL.. CONFIGURATIONS: ELLI PLUG W/C BLEED — SUPPRESSOR CONFIGURATION: 36-CHUTE, AREA RATIO = 2.5

THROAT DIAMETERS — OUTER RADIUS RATIO: 0.0000 — INNER RADIUS RATIO: 0.0000 — DVD: 1.2480

ENG	RE	MACH	PJ	PS	PTS/PA	PTI/PA	PMFGRT	KDD	KDI	CFNET1	CFNET2	F9
2695	4981	49810	0.398	0.445	1.504	1.334	0.000	1.001	9.999	0.796	0.796	1.121
2696	4981	49810	0.398	0.445	1.748	1.552	0.000	0.979	9.999	0.824	0.824	1.128
2697	4981	49810	0.398	0.445	2.004	1.784	0.000	0.977	9.999	0.843	0.843	1.130
2698	4981	49810	0.398	0.446	2.416	1.582	0.000	0.978	9.999	0.869	0.869	1.136
2700	4981	49810	0.398	0.446	3.026	1.373	0.000	0.980	9.999	0.885	0.885	1.148
2701	4981	49810	0.398	0.447	1.374	1.408	0.000	0.979	9.999	0.893	0.893	1.154
2702	4981	49810	0.398	0.447	1.631	1.652	0.000	0.981	9.999	0.887	0.887	1.150
2703	4981	49810	0.398	0.447	2.416	1.460	0.000	0.975	9.999	0.872	0.872	1.137
2704	4981	49810	0.398	0.446	2.007	1.446	0.000	0.976	9.999	0.845	0.845	1.130
2705	4981	49810	0.398	0.446	1.734	1.439	0.000	0.977	9.999	0.829	0.829	1.130
2706	4981	49810	0.398	0.446	1.503	1.387	0.000	1.001	9.999	0.805	0.805	1.126
2707	4981	49810	0.398	0.446	2.334	1.869	0.000	0.978	9.999	0.843	0.843	1.130
2708	4981	49810	0.398	0.446	2.012	1.500	0.000	0.982	9.999	0.885	0.885	1.149
2709	4981	49810	0.398	0.354	1.506	1.341	0.000	0.997	9.999	0.823	0.823	1.135
2710	4981	49810	0.398	0.355	1.748	1.528	0.000	0.980	9.999	0.845	0.845	1.143
2711	4981	49810	0.398	0.357	2.029	1.717	0.000	0.973	9.999	0.863	0.863	1.142
2712	4981	49810	0.398	0.357	2.424	1.526	0.000	0.975	9.999	0.890	0.890	1.153
2713	4981	49810	0.398	0.358	3.004	1.351	0.000	0.983	9.999	0.901	0.901	1.165
2714	4981	49810	0.398	0.358	3.454	1.260	0.000	0.981	9.999	0.903	0.903	1.165
2715	4981	49810	0.398	0.355	2.024	1.439	0.000	0.980	9.999	0.902	0.902	1.163
2716	4981	49810	0.398	0.358	2.427	1.460	0.000	0.975	9.999	0.888	0.888	1.153
2717	4981	49810	0.398	0.358	2.814	1.479	0.000	0.977	9.999	0.862	0.862	1.145
2718	4981	49810	0.398	0.358	1.748	1.410	0.000	0.979	9.999	0.846	0.846	1.144
2719	4981	49810	0.398	0.359	1.978	1.374	0.000	0.995	9.999	0.829	0.829	1.138
2720	4981	49810	0.398	0.358	2.012	1.358	0.000	0.977	9.999	0.865	0.865	1.147
2721	4981	49810	0.398	0.359	1.002	1.389	0.000	0.980	9.999	0.901	0.901	1.163
2722	4981	49810	0.398	0.039	1.503	1.025	0.000	0.977	9.999	0.957	0.957	1.203
2723	4981	49810	0.398	0.047	1.742	1.049	0.000	0.973	9.999	0.957	0.957	1.218
2724	4981	49810	0.398	0.056	1.994	1.089	0.000	0.978	9.999	0.957	0.957	1.219
2725	4981	49810	0.398	0.066	2.493	1.101	0.000	0.978	9.999	0.960	0.960	1.215
2726	4981	49810	0.398	0.076	2.988	1.169	0.000	0.978	9.999	0.960	0.960	1.216
2727	4981	49810	0.398	0.077	3.139	1.286	0.000	0.980	9.999	0.956	0.956	1.216
2728	4981	49810	0.398	0.041	1.028	1.365	0.000	0.974	9.999	0.954	0.954	1.210
2729	4981	49810	0.398	0.047	2.519	1.144	0.000	0.975	9.999	0.951	0.951	1.206
2730	4981	49810	0.398	0.056	2.007	1.341	0.000	0.975	9.999	0.950	0.950	1.211
2731	4981	49810	0.398	0.057	1.760	1.343	0.000	0.971	9.999	0.948	0.948	1.210
2732	4981	49810	0.398	0.046	1.504	1.314	0.000	0.974	9.999	0.949	0.949	1.197
2733	4981	49810	0.398	0.043	2.052	1.313	0.000	0.972	9.999	0.951	0.951	1.210
2734	4981	49810	0.398	0.043	2.005	1.335	0.000	0.980	9.999	0.958	0.958	1.216

FACILITY 6X1 PROGRAM CQ31 — INNER-STREAM

NOZZLE TYPE: DUAL FLOW (FAAJ) — PL CONFIGURATIONS: FULL ..UG W/O BLEED — SUPPRESSOR CONFIGURATION: 36-CHUTE, AREA RATIO = 2.5

DRAG PARAMETERS — OUTER RADIUS RATIO 0.0000 — INNER RADIUS RATIO 0.0000 — DVC 1.2480

RDG	GE	NASA	O2	MA	PTO/PA	PTI/PA	OMEGAT	DCS	CDS	DCSH	CDSH	DCPL,O	DCPL,I	DCTOT	PSUP/PA
2696	4983	49830	0.398	0.445	1.506	1.375	0.000	-0.178	0.253	-0.004	0.006	-0.009	0.033	-0.156	0.899
2697	4983	49830	0.398	0.445	1.758	1.352	0.000	-0.160	0.315	-0.003	0.006	-0.006	0.030	-0.140	0.875
2698	4983	49830	0.398	0.446	2.008	1.346	0.000	-0.148	0.366	-0.003	0.007	-0.005	0.027	-0.129	0.854
2699	4983	49830	0.398	0.446	2.514	1.352	0.000	-0.124	0.433	-0.002	0.007	-0.005	0.021	-0.111	0.827
2700	4983	49830	0.398	0.446	3.024	1.371	0.000	-0.106	0.480	-0.002	0.008	-0.005	0.017	-0.095	0.808
2701	4983	49830	0.398	0.447	3.334	1.408	0.000	-0.097	0.502	-0.002	0.008	-0.007	0.016	-0.090	0.799
2702	4983	49830	0.398	0.447	3.021	1.452	0.000	-0.106	0.479	-0.002	0.008	-0.006	0.017	-0.096	0.808
2703	4983	49830	0.398	0.447	2.516	1.460	0.000	-0.124	0.431	-0.002	0.007	-0.005	0.022	-0.110	0.827
2704	4983	49830	0.398	0.446	2.007	1.446	0.000	-0.149	0.364	-0.003	0.007	-0.005	0.027	-0.129	0.855
2705	4983	49830	0.398	0.445	1.764	1.423	0.000	-0.161	0.317	-0.003	0.006	-0.006	0.029	-0.141	0.874
2706	4983	49830	0.398	0.446	1.503	1.387	0.000	-0.176	0.249	-0.004	0.006	-0.009	0.034	-0.155	0.901
2707	4983	49830	0.398	0.444	2.005	1.369	0.000	-0.149	0.368	-0.003	0.007	-0.005	0.025	-0.131	0.855
2708	4983	49830	0.398	0.446	3.019	1.389	0.000	-0.105	0.481	-0.002	0.008	-0.006	0.017	-0.096	0.809
2709	4983	49830	0.398	0.355	1.506	1.341	0.000	-0.151	0.336	-0.003	0.007	-0.007	0.009	-0.152	0.915
2710	4983	49830	0.398	0.355	1.768	1.323	0.000	-0.135	0.421	-0.002	0.007	-0.005	0.011	-0.132	0.894
2711	4983	49830	0.398	0.357	2.022	1.317	0.000	-0.122	0.473	-0.002	0.008	-0.005	0.011	-0.118	0.879
2712	4983	49830	0.398	0.357	2.523	1.326	0.000	-0.104	0.568	-0.002	0.009	-0.005	0.010	-0.101	0.855
2713	4983	49830	0.398	0.358	3.005	1.351	0.000	-0.097	0.613	-0.001	0.009	-0.007	0.009	-0.086	0.842
2714	4983	49830	0.398	0.358	3.156	1.380	0.000	-0.093	0.625	-0.001	0.009	-0.007	0.008	-0.083	0.840
2715	4983	49830	0.398	0.358	3.024	1.430	0.000	-0.097	0.614	-0.001	0.009	-0.007	0.009	-0.086	0.842
2716	4983	49830	0.398	0.358	2.522	1.440	0.000	-0.104	0.565	-0.002	0.009	-0.005	0.011	-0.100	0.855
2717	4983	49830	0.398	0.358	2.014	1.429	0.000	-0.125	0.479	-0.002	0.008	-0.005	0.011	-0.121	0.877
2718	4983	49830	0.398	0.358	1.768	1.410	0.000	-0.135	0.412	-0.002	0.007	-0.005	0.012	-0.130	0.894
2719	4983	49830	0.398	0.359	1.508	1.374	0.000	-0.151	0.330	-0.003	0.006	-0.007	0.010	-0.151	0.915
2720	4983	49830	0.398	0.358	2.012	1.358	0.000	-0.124	0.473	-0.002	0.008	-0.005	0.011	-0.120	0.878
2721	4983	49830	0.398	0.359	3.002	1.389	0.000	-0.098	0.612	-0.001	0.008	-0.006	0.009	-0.086	0.842
2722	4983	49830	0.398	0.030	1.503	1.025	0.000	-0.045	13.726	-0.000	0.035	-0.015	0.003	-0.057	0.975
2723	4983	49830	0.398	0.057	1.762	1.045	0.000	-0.041	4.871	-0.000	0.005	-0.014	0.006	-0.049	0.968
2724	4983	49830	0.398	0.056	1.995	1.069	0.000	-0.039	6.077	-0.000	0.016	-0.014	0.006	-0.047	0.962
2725	4983	49830	0.398	0.066	2.503	1.101	0.000	-0.035	5.588	-0.000	0.012	-0.014	0.006	-0.043	0.952
2726	4983	49830	0.398	0.074	2.998	1.149	0.000	-0.029	4.796	-0.000	0.010	-0.014	0.005	-0.038	0.948
2727	4983	49830	0.398	0.072	3.325	1.284	0.000	-0.026	5.214	-0.000	0.011	-0.015	0.005	-0.036	0.945
2728	4983	49830	0.398	0.063	3.008	1.345	0.000	-0.030	6.841	-0.000	0.010	-0.014	0.005	-0.039	0.946
2729	4983	49830	0.398	0.062	2.517	1.364	0.000	-0.035	6.193	-0.000	0.013	-0.014	0.007	-0.041	0.952
2730	4983	49830	0.398	0.054	2.007	1.361	0.000	-0.039	6.484	-0.000	0.017	-0.013	0.007	-0.046	0.961
2731	4983	49830	0.398	0.032	1.759	1.343	0.000	-0.043	16.422	-0.000	0.032	-0.014	0.005	-0.053	0.966
2732	4983	49830	0.398	0.039	1.504	1.319	0.000	-0.043	7.768	-0.000	0.026	-0.015	0.003	-0.055	0.976
2733	4983	49830	0.398	0.053	2.002	1.313	0.000	-0.039	6.703	-0.000	0.012	-0.013	0.006	-0.047	0.962
2734	4983	49830	0.398	0.065	2.995	1.335	0.000	-0.030	6.368	-0.000	0.015	-0.014	0.005	-0.038	0.947

MODEL DC-3 (SPOKE), 36 SPOKES, AR = 2.0, BASELINE PLUG

FACILITY [illegible] PROGRAM C031

NOZZLE TYPE — [illegible]-STREAM PL CONFIGURATIONS — SUPPRESSOR CONFIGURATION

DUAL FLOW (SAA) — BASELINE PLUG WITH BLEED — 36-SPOKE(CHUTE INSERT),AREA RATIO=2.0

THRUST PARAMETERS — OUTER RADIUS RATIO 0.0000 — INNER RADIUS RATIO 0.7790 — DVD 1.2480

PDG	CF	MASA	F2	MA	PTC/PA	PTI/PA	OMEGAT	CDC	CDI	CFNET1	CFNET2	F9
2926	0011	410530	0.393	0.450	1.506	0.584	0.002	0.964	9.999	0.739	0.739	1.058
2927	0011	410530	0.393	0.450	1.507	0.989	0.028	0.963	9.999	0.747	0.747	1.059
2928	0011	410530	0.398	0.450	1.507	0.999	0.059	0.962	9.999	0.756	0.756	1.060
2929	0011	410530	0.398	0.450	2.004	0.986	0.000	0.946	9.999	0.776	0.776	1.052
2930	0011	410530	0.398	0.451	2.006	0.997	0.029	0.945	9.999	0.785	0.785	1.054
2931	0011	410530	0.393	0.451	2.008	1.013	0.059	0.945	0.926	0.790	0.796	1.057
2932	0011	410530	0.398	0.451	2.516	0.990	0.000	0.944	9.999	0.792	0.792	1.062
2933	0011	410530	0.398	0.450	2.511	1.010	0.029	0.946	0.651	0.800	0.802	1.046
2934	0011	410530	0.393	0.449	2.509	1.033	0.059	0.946	0.718	0.805	0.815	1.050
2935	0011	410530	0.393	0.450	3.030	1.005	0.000	0.947	0.000	0.793	0.793	1.030
2936	0011	410530	0.399	0.450	3.021	1.048	0.029	0.948	0.357	0.800	0.805	1.035
2937	0011	410530	0.393	0.450	3.026	1.091	0.059	0.947	0.526	0.804	0.818	1.037
2938	0011	410530	0.393	0.450	3.328	1.013	0.000	0.949	0.000	0.814	0.814	1.044
2939	0011	410530	0.393	0.449	3.317	1.065	0.029	0.948	0.337	0.820	0.825	1.046
2940	0011	410530	0.398	0.449	3.315	1.120	0.059	0.949	0.502	0.821	0.837	1.048
2941	0011	410530	0.398	0.448	2.511	0.989	0.000	0.947	9.999	0.791	0.791	1.042
2942	0011	410530	0.393	0.447	2.512	1.034	0.059	0.945	0.708	0.803	0.813	1.048
[illegible]												
[illegible]												
[illegible]												
2946	0011	410550	1.140	0.448	1.506	2.021	0.747	0.963	0.994	0.852	1.669	1.141
2947	0011	410550	1.140	0.448	1.508	1.118	0.263	0.962	1.000	0.791	0.902	1.088
2948	0011	410550	1.140	0.447	1.506	1.528	0.546	0.963	0.996	0.831	1.291	1.129
2949	0011	410550	1.140	0.448	1.506	2.521	0.933	0.963	0.994	0.868	2.043	1.147
2950	0011	410550	1.140	0.448	1.508	3.030	1.121	0.959	0.992	0.874	2.407	1.146
2951	0011	410550	1.140	0.449	1.508	3.536	1.309	0.963	0.996	0.898	2.843	1.168
2952	0011	410550	1.140	0.448	2.007	1.118	0.183	0.945	0.948	0.808	0.870	1.076
2953	0011	410550	1.140	0.448	2.008	1.632	0.398	0.945	0.988	0.832	1.096	1.112
2954	0011	410550	1.140	0.449	2.005	2.022	0.549	0.945	0.995	0.849	1.317	1.125
2955	0011	410550	1.140	0.451	2.008	2.528	0.685	0.945	0.995	0.861	1.531	1.131
2956	0011	410550	1.140	0.450	2.009	3.039	0.824	0.944	0.995	0.865	1.739	1.132
2957	0011	410550	1.140	0.450	2.006	3.535	0.960	0.946	0.996	0.890	1.997	1.155
2958	0011	410550	1.140	0.449	2.509	1.122	0.138	0.946	0.884	0.817	0.859	1.065
2959	0011	410550	1.140	0.449	2.506	1.527	0.314	0.948	0.980	0.836	1.021	1.099
2960	0011	410550	1.140	0.449	2.508	2.021	0.437	0.946	0.994	0.846	1.175	1.109
2961	0011	410550	1.140	0.449	2.511	2.524	0.546	0.947	0.995	0.858	1.327	1.117
2962	0011	410550	1.140	0.449	2.513	3.032	0.656	0.946	0.995	0.864	1.479	1.121
2963	0011	410550	1.140	0.450	2.514	3.534	0.765	0.945	0.995	0.884	1.658	1.140
2964	0011	410550	1.140	0.449	3.019	1.125	0.093	0.949	0.632	0.808	0.832	1.044
2965	0011	410550	1.140	0.449	3.020	1.528	0.249	0.947	0.937	0.828	0.962	1.078
2966	0011	410550	1.140	0.450	3.020	2.023	0.362	0.948	0.992	0.835	1.083	1.091
2967	0011	410550	1.140	0.450	3.027	2.526	0.451	0.945	0.990	0.846	1.199	1.097
2968	0011	410550	1.140	0.449	3.022	3.034	0.543	0.946	0.991	0.844	1.303	1.095
2969	0011	410550	1.140	0.451	3.021	3.535	0.634	0.949	0.994	0.865	1.445	1.118
2970	0011	410550	1.140	0.451	3.326	1.123	0.060	0.948	0.507	0.824	0.841	1.050

FACILITY (NEXT PROGRAM COPY)

NOZZLE TYPE — OUTER-STREAM CONFIGURATIONS — SUPPRESSOR CONFIGURATION

DUAL FLOW (EAS) — BASELINE PLUG WITH BLEED — 36-SPOKE(CHUTE INSERT),AREA RAT...=2.0

DATA	PARAMETERS		OUTER RADIUS RATIO 0.0000		INNER RADIUS RATIO 0.7790		DVD 1.2480							
POS	GE	MAS*	O2	PA	PTT/PA	PTT/PA	DMEGAT	DCS	CPS	DCSH	COSH	DCPL,O	DCPL,I	DCTOT	PSUP/PA
2926	0011	410530	0.398	0.450	1.506	0.894	0.000	-0.124	0.162	-0.010	0.013	-0.035	0.029	-0.140	0.905
2927	0011	410530	0.398	0.450	1.507	0.993	0.028	-0.120	0.158	-0.010	0.013	-0.031	0.025	-0.136	0.908
2928	0011	410530	0.398	0.450	1.507	0.992	0.059	-0.117	0.154	-0.009	0.012	-0.029	0.022	-0.134	0.910
2929	0011	410530	0.398	0.450	2.004	0.994	0.000	-0.114	0.260	-0.007	0.015	-0.028	0.023	-0.126	0.848
2930	0011	410530	0.398	0.451	2.006	0.997	0.029	-0.112	0.256	-0.007	0.015	-0.026	0.019	-0.126	0.850
2931	0011	410530	0.398	0.451	2.008	1.013	0.059	-0.109	0.252	-0.006	0.015	-0.023	0.016	-0.122	0.853
2932	0011	410530	0.398	0.451	2.514	0.990	0.000	-0.108	0.351	-0.005	0.015	-0.027	0.018	-0.122	0.794
2933	0011	410530	0.398	0.450	2.511	1.010	0.029	-0.106	0.343	-0.005	0.015	-0.024	0.015	-0.119	0.800
2934	0011	410530	0.398	0.449	2.509	1.033	0.059	-0.103	0.340	-0.004	0.015	-0.022	0.012	-0.117	0.802
2935	0011	410530	0.398	0.450	3.030	1.009	0.000	-0.111	0.470	-0.004	0.015	-0.021	0.014	-0.122	0.726
2936	0011	410530	0.398	0.450	3.021	1.048	0.029	-0.110	0.469	-0.004	0.015	-0.020	0.012	-0.121	0.727
2937	0011	410530	0.398	0.450	3.026	1.091	0.059	-0.108	0.465	-0.003	0.014	-0.018	0.010	-0.119	0.729
2938	0011	410530	0.398	0.450	3.320	1.013	0.000	-0.096	0.462	-0.003	0.016	-0.024	0.012	-0.111	0.731
2939	0011	410530	0.398	0.449	3.317	1.065	0.029	-0.096	0.466	-0.003	0.015	-0.022	0.010	-0.111	0.729
2940	0011	410530	0.398	0.449	3.315	1.120	0.059	-0.095	0.468	-0.003	0.015	-0.020	0.008	-0.110	0.728
2941	0011	410530	0.398	0.448	2.511	0.989	0.000	-0.113	0.369	-0.005	0.015	-0.028	0.019	-0.127	0.786
2942	0011	410530	0.398	0.447	2.512	1.034	0.029	-0.107	0.364	-0.004	0.015	-0.027	0.013	-0.120	0.796
~~2943~~	~~0011~~	~~410530~~	~~0.398~~	~~0.448~~	~~1.506~~	~~1.110~~	~~0.000~~	~~-0.133~~	~~0.176~~	~~-0.002~~	~~0.012~~	~~-0.030~~	~~0.021~~	~~-0.119~~	~~0.870~~
~~2944~~	~~0011~~	~~410530~~	~~0.398~~	~~0.448~~	~~1.506~~	~~1.136~~	~~0.029~~	~~-0.130~~	~~0.173~~	~~-0.002~~	~~0.012~~	~~-0.029~~	~~0.020~~	~~-0.119~~	~~0.870~~
~~2945~~	~~0011~~	~~410530~~	~~0.398~~	~~0.448~~	~~1.506~~	~~1.161~~	~~0.059~~	~~-0.127~~	~~0.169~~	~~-0.002~~	~~0.012~~	~~-0.027~~	~~0.018~~	~~-0.117~~	~~0.870~~
2946	0011	410550	1.140	0.448	1.506	2.021	0.747	-0.070	0.182	-0.005	0.012	-0.015	-0.007	-0.097	0.894
2947	0011	410550	1.140	0.448	1.508	1.118	0.269	-0.117	0.177	-0.008	0.012	-0.023	0.018	-0.130	0.897
2948	0011	410550	1.140	0.447	1.506	1.529	0.546	-0.099	0.183	-0.006	0.012	-0.019	0.010	-0.104	0.995
2949	0011	410550	1.140	0.448	1.506	2.521	0.933	-0.059	0.193	-0.004	0.012	-0.013	-0.021	-0.096	0.894
2950	0011	410550	1.140	0.449	1.508	3.030	1.121	-0.050	0.182	-0.004	0.013	-0.010	-0.025	-0.099	0.894
2951	0011	410550	1.140	0.449	1.508	3.526	1.309	-0.030	0.163	-0.003	0.013	-0.009	-0.001	-0.052	0.905
2952	0011	410550	1.140	0.448	2.007	1.118	0.183	-0.109	0.272	-0.006	0.014	-0.020	0.013	-0.122	0.843
2953	0011	410550	1.140	0.448	2.008	1.532	0.398	-0.020	0.275	-0.005	0.014	-0.016	0.007	-0.103	0.841
2954	0011	410550	1.140	0.449	2.005	2.022	0.549	-0.077	0.275	-0.004	0.014	-0.014	-0.010	-0.105	0.840
2955	0011	410550	1.140	0.451	2.009	2.528	0.685	-0.067	0.272	-0.003	0.013	-0.012	-0.013	-0.095	0.841
2956	0011	410550	1.140	0.450	2.009	3.039	0.824	-0.059	0.273	-0.003	0.014	-0.010	-0.026	-0.098	0.840
2957	0011	410550	1.140	0.450	2.004	3.535	0.960	-0.053	0.274	-0.003	0.014	-0.009	0.001	-0.064	0.840
2958	0011	410550	1.140	0.449	2.509	1.122	0.138	-0.104	0.356	-0.004	0.015	-0.020	0.010	-0.118	0.793
2959	0011	410550	1.140	0.449	2.504	1.527	0.314	-0.099	0.352	-0.004	0.014	-0.014	0.005	-0.103	0.795
2960	0011	410550	1.140	0.449	2.503	2.021	0.437	-0.078	0.353	-0.003	0.014	-0.014	-0.014	-0.109	0.795
2961	0011	410550	1.140	0.449	2.511	2.524	0.546	-0.070	0.354	-0.003	0.014	-0.012	-0.014	-0.099	0.794
2962	0011	410550	1.140	0.449	2.513	3.032	0.656	-0.063	0.350	-0.003	0.014	-0.011	-0.017	-0.093	0.796
2963	0011	410550	1.140	0.450	2.514	3.534	0.765	-0.057	0.349	-0.002	0.014	-0.009	-0.002	-0.071	0.796
2964	0011	410550	1.140	0.449	3.010	1.125	0.093	-0.113	0.492	-0.003	0.014	-0.019	0.008	-0.126	0.713
2965	0011	410550	1.140	0.449	3.020	1.529	0.249	-0.097	0.481	-0.003	0.014	-0.015	0.005	-0.110	0.721
2966	0011	410550	1.140	0.450	3.020	2.023	0.362	-0.087	0.477	-0.003	0.014	-0.013	-0.011	-0.114	0.722
2967	0011	410550	1.140	0.450	3.027	2.526	0.451	-0.080	0.478	-0.002	0.013	-0.012	-0.013	-0.107	0.721
2968	0011	410550	1.140	0.449	3.027	3.034	0.543	-0.073	0.477	-0.002	0.014	-0.011	-0.030	-0.116	0.722
2969	0011	410550	1.140	0.451	3.021	3.535	0.634	-0.066	0.467	-0.002	0.013	-0.009	-0.010	-0.088	0.726
2970	0011	410550	1.140	0.451	3.326	1.123	0.060	-0.101	0.496	-0.003	0.015	-0.020	0.006	-0.116	0.709

FACILITY "AX1 PROGRAM CC3L

NOZZLE TYPE — DUAL FLOW (FAA)

F 2-STREAM
9. CONFIGURATIONS — BASELINE PLUG WITH BLEED

SUPPRESSOR CONFIGURATION — 36-SPOKE(CHUTE INSERT),AREA RATIO=2.0

THRUST PARAMETERS — OUTER RADIUS RATIO 0.0000 — INNER RADIUS RATIO 0.7790 — DVD 1.7480

RUN	CF	MASS	D2	MA	PT2/PA	PT1/PA	DUCCAT	CDO	CDI	CFMET1	CFMET2	F9
2971	0011	410550	1.140	0.450	3.316	1.528	0.217	0.948	0.898	0.935	0.949	1.078
2972	0011	410550	1.140	0.450	3.318	2.022	0.329	0.948	0.988	0.941	1.059	1.092
2973	0011	410550	1.140	0.451	3.325	2.523	0.411	0.948	0.994	0.943	1.153	1.094
2974	0011	410550	1.140	0.450	3.327	3.024	0.493	0.948	0.995	0.942	1.244	1.093
2975	0011	410550	1.140	0.451	3.328	3.523	0.576	0.949	0.996	0.942	1.368	1.112
2976	0011	410550	1.140	0.450	2.516	1.120	0.136	0.944	0.880	0.818	0.859	1.064
2977	0011	410550	1.140	0.451	2.524	1.528	0.265	0.948	0.996	0.883	1.657	1.140
2978	0011	410530	0.398	0.360	1.507	0.998	0.000	0.984	0.999	0.756	0.756	1.064
2979	0011	410530	0.398	0.361	1.507	0.994	0.029	0.943	0.999	0.761	0.761	1.065
2980	0011	410530	0.398	0.361	1.509	1.003	0.059	0.941	1.467	0.768	0.772	1.066
2981	0011	410530	0.398	0.361	2.016	0.988	0.000	0.946	0.999	0.785	0.785	1.056
2982	0011	410530	0.398	0.360	2.021	1.021	0.029	0.944	1.390	0.792	0.794	1.058
2983	0011	410530	0.398	0.361	2.021	1.017	0.059	0.942	0.802	0.798	0.805	1.060
2984	0011	410530	0.398	0.362	2.524	0.990	0.000	0.946	0.999	0.799	0.799	1.048
2985	0011	410530	0.398	0.361	2.519	1.010	0.029	0.946	0.639	0.809	0.812	1.053
2986	0011	410530	0.398	0.361	2.520	1.033	0.059	0.944	0.719	0.813	0.823	1.055
2987	0011	410530	0.398	0.362	3.017	1.007	0.000	0.948	0.000	0.799	0.799	1.036
2988	0011	410530	0.398	0.362	3.023	1.045	0.029	0.948	0.352	0.805	0.810	1.039
2989	0011	410530	0.398	0.361	3.020	1.089	0.059	0.948	0.529	0.809	0.823	1.042
2990	0011	410530	0.398	0.361	3.309	1.010	0.000	0.948	0.000	0.818	0.818	1.048
2991	0011	410530	0.398	0.360	3.291	1.061	0.029	0.948	0.344	0.821	0.827	1.048
2992	0011	410530	0.398	0.361	3.296	1.113	0.059	0.945	0.508	0.821	0.837	1.047
2993	0011	410530	0.398	0.361	2.522	0.989	0.000	0.947	0.999	0.798	0.798	1.048
2994	0011	410530	0.398	0.360	2.524	1.035	0.059	0.946	0.710	0.810	0.820	1.054
2995	0011	410550	1.140	0.360	1.505	1.118	0.262	0.962	0.997	0.798	0.909	1.091
2996	0011	410550	1.140	0.360	1.505	1.527	0.545	0.963	0.995	0.835	1.298	1.132
2997	0011	410550	1.140	0.360	1.506	2.026	0.753	0.964	0.994	0.856	1.688	1.144
2998	0011	410550	1.140	0.361	1.508	2.537	0.938	0.962	0.995	0.873	2.062	1.150
2999	0011	410550	1.140	0.361	1.507	3.030	1.122	0.963	0.996	0.874	2.412	1.150
3000	0011	410550	1.140	0.362	1.509	3.526	1.306	0.961	0.994	0.903	2.950	1.172
3001	0011	410550	1.140	0.361	2.024	1.125	0.183	0.965	0.931	0.815	0.879	1.080
3002	0011	410550	1.140	0.361	2.028	1.530	0.395	0.964	0.987	0.840	1.103	1.117
3003	0011	410550	1.140	0.360	2.026	2.037	0.549	0.965	0.994	0.854	1.327	1.129
3004	0011	410550	1.140	0.360	2.028	2.536	0.684	0.965	0.994	0.867	1.539	1.136
3005	0011	410550	1.140	0.361	2.019	3.033	0.818	0.966	0.995	0.870	1.740	1.137
3006	0011	410550	1.140	0.361	2.022	3.530	0.952	0.965	0.996	0.894	1.990	1.158
3007	0011	410550	1.140	0.362	2.522	1.123	0.135	0.968	0.971	0.825	0.867	1.071
3008	0011	410550	1.140	0.362	2.521	1.529	0.312	0.967	0.979	0.843	1.028	1.104
3009	0011	410550	1.140	0.360	2.520	2.035	0.438	0.967	0.993	0.853	1.185	1.115
3010	0011	410550	1.140	0.361	2.522	2.534	0.546	0.967	0.995	0.863	1.335	1.121
3011	0011	410550	1.140	0.362	2.524	3.029	0.652	0.966	0.995	0.869	1.482	1.126
3012	0011	410550	1.140	0.361	2.523	3.522	0.760	0.967	0.996	0.890	1.660	1.145
3013	0011	410550	1.140	0.361	3.017	1.120	0.030	0.968	0.619	0.813	0.835	1.047
3014	0011	410550	1.140	0.360	3.006	1.529	0.250	0.968	0.937	0.831	0.966	1.081
3015	0011	410550	1.140	0.359	3.007	2.036	0.366	0.968	0.992	0.840	1.093	1.096

FACILITY 4X1 PROGRAM CODE

NOZZLE TYPE — DUAL FLOW (F44)

1 2-STREAM CONFIGURATIONS — PL. BASELINE PLUG WITH BLEED

SUPPRESSOR CONFIGURATION — 36-SPOKE(WHITE INSERT),AREA RATIO=2.0

DRAG PARAMETERS — OUTER RADIUS RATIO 0.9999 — INNER RADIUS RATIO 0.7790 — DVD 1.2480

PPG	CF	PTSA	M2	M8	PT0/P8	PT7/P8	CMSCAT	NCS	CDS	DCSH	CDSH	DCPL,0	DCPL,T	DCTOT	PSUP/P8
2971	0011	410550	1.140	0.450	3.316	1.527	0.717	-0.121	0.496	-0.003	0.014	-0.014	0.002	-0.105	0.710
2972	0011	410550	1.140	0.450	3.318	2.022	0.329	-0.382	0.497	-0.002	0.014	-0.011	-0.011	-0.106	0.710
2973	0011	410550	1.140	0.451	3.326	2.523	0.411	-0.275	0.495	-0.002	0.014	-0.010	-0.023	-0.111	0.710
2974	0011	410550	1.140	0.450	3.327	3.024	0.493	-0.170	0.495	-0.002	0.013	-0.006	-0.032	-0.113	0.710
2975	0011	410550	1.140	0.451	3.328	3.533	0.578	-0.065	0.494	-0.002	0.014	-0.008	-0.013	-0.088	0.710
2976	0011	410550	1.140	0.450	2.516	1.120	0.134	-0.106	0.373	-0.004	0.014	-0.019	0.011	-0.121	0.783
2977	0011	410550	1.140	0.451	2.506	1.528	0.745	-0.040	0.364	-0.002	0.014	-0.010	-0.003	-0.075	0.787
2978	0011	410550	0.398	0.360	1.507	0.984	0.000	-0.176	0.361	-0.006	0.013	-0.032	0.017	-0.197	0.865
2979	0011	410550	0.398	0.361	1.507	0.996	0.029	-0.173	0.353	-0.006	0.013	-0.029	0.013	-0.195	0.867
2980	0011	410550	0.398	0.361	1.509	1.005	0.059	-0.170	0.348	-0.006	0.013	-0.025	0.011	-0.190	0.869
2981	0011	410550	0.398	0.361	2.016	0.989	0.000	-0.143	0.512	-0.004	0.016	-0.029	0.014	-0.160	0.808
2982	0011	410550	0.398	0.360	2.021	1.001	0.029	-0.140	0.506	-0.004	0.015	-0.024	0.011	-0.158	0.810
2983	0011	410550	0.398	0.361	2.021	1.017	0.059	-0.137	0.495	-0.004	0.015	-0.022	0.008	-0.155	0.814
2984	0011	410550	0.398	0.362	2.524	0.990	0.000	-0.132	0.667	-0.003	0.016	-0.027	0.012	-0.150	0.748
2985	0011	410550	0.398	0.361	2.519	1.010	0.029	-0.130	0.655	-0.003	0.015	-0.024	0.010	-0.146	0.754
2986	0011	410550	0.398	0.361	2.520	1.033	0.059	-0.127	0.650	-0.003	0.015	-0.022	0.007	-0.145	0.756
2987	0011	410550	0.398	0.362	3.017	1.007	0.000	-0.130	0.845	-0.002	0.015	-0.021	0.009	-0.144	0.680
2988	0011	410550	0.398	0.362	3.023	1.049	0.029	-0.128	0.841	-0.002	0.015	-0.019	0.009	-0.141	0.682
2989	0011	410550	0.398	0.361	3.020	1.089	0.059	-0.126	0.843	-0.002	0.014	-0.018	0.006	-0.141	0.683
2990	0011	410550	0.398	0.361	3.509	1.010	0.000	-0.113	0.842	-0.002	0.016	-0.023	0.008	-0.130	0.684
2991	0011	410550	0.398	0.360	3.501	1.061	0.029	-0.114	0.847	-0.002	0.016	-0.021	0.006	-0.130	0.683
2992	0011	410550	0.398	0.361	3.506	1.113	0.059	-0.115	0.851	-0.002	0.016	-0.018	0.005	-0.130	0.681
2993	0011	410550	0.398	0.361	2.522	0.999	0.000	-0.134	0.679	-0.003	0.016	-0.027	0.012	-0.152	0.744
2994	0011	410550	0.398	0.360	2.524	1.035	0.059	-0.128	0.660	-0.003	0.014	-0.022	0.008	-0.144	0.753
2995	0011	410550	1.140	0.360	1.505	1.119	0.262	-0.156	0.362	-0.004	0.013	-0.023	0.008	-0.176	0.864
2996	0011	410550	1.140	0.360	1.505	1.527	0.545	-0.116	0.368	-0.004	0.013	-0.017	0.002	-0.136	0.862
2997	0011	410550	1.140	0.360	1.506	2.034	0.753	-0.092	0.371	-0.003	0.013	-0.014	-0.014	-0.123	0.861
2998	0011	410550	1.140	0.361	1.508	2.537	0.938	-0.076	0.367	-0.003	0.013	-0.013	-0.025	-0.115	0.862
2999	0011	410550	1.140	0.361	1.507	3.039	1.122	-0.065	0.364	-0.002	0.013	-0.010	-0.029	-0.105	0.863
3000	0011	410550	1.140	0.362	1.509	3.524	1.306	-0.057	0.362	-0.002	0.012	-0.008	-0.005	-0.071	0.863
3001	0011	410550	1.140	0.361	2.024	1.125	0.183	-0.130	0.505	-0.004	0.014	-0.018	0.006	-0.146	0.810
3002	0011	410550	1.140	0.361	2.020	1.530	0.365	-0.107	0.506	-0.003	0.015	-0.015	0.002	-0.124	0.810
3003	0011	410550	1.140	0.360	2.018	2.037	0.549	-0.091	0.509	-0.003	0.015	-0.013	-0.017	-0.124	0.810
3004	0011	410550	1.140	0.360	2.018	2.534	0.644	-0.080	0.508	-0.002	0.015	-0.011	-0.017	-0.110	0.810
3005	0011	410550	1.140	0.361	2.019	3.033	0.818	-0.070	0.502	-0.002	0.013	-0.010	-0.029	-0.110	0.811
3006	0011	410550	1.140	0.361	2.022	3.530	0.992	-0.062	0.501	-0.002	0.014	-0.008	-0.002	-0.074	0.811
3007	0011	410550	1.140	0.362	2.522	1.123	0.135	-0.121	0.644	-0.003	0.014	-0.019	0.006	-0.137	0.757
3008	0011	410550	1.140	0.362	2.521	1.529	0.312	-0.103	0.635	-0.002	0.014	-0.016	0.002	-0.119	0.760
3009	0011	410550	1.140	0.360	2.520	2.035	0.498	-0.091	0.646	-0.002	0.014	-0.014	-0.017	-0.124	0.758
3010	0011	410550	1.140	0.361	2.522	2.534	0.546	-0.082	0.644	-0.002	0.015	-0.012	-0.016	-0.112	0.758
3011	0011	410550	1.140	0.362	2.524	3.029	0.652	-0.074	0.636	-0.002	0.015	-0.011	-0.020	-0.106	0.760
3012	0011	410550	1.140	0.361	2.523	3.522	0.760	-0.067	0.634	-0.002	0.014	-0.010	-0.004	-0.082	0.762
3013	0011	410550	1.140	0.361	3.017	1.120	0.080	-0.128	0.862	-0.002	0.015	-0.017	0.005	-0.142	0.676
3014	0011	410550	1.140	0.360	3.008	1.539	0.256	-0.110	0.842	-0.002	0.015	-0.014	0.001	-0.125	0.686
3015	0011	410550	1.140	0.359	3.007	2.034	0.366	-0.098	0.840	-0.002	0.014	-0.012	-0.013	-0.125	0.687

FACILITY [6X] PROGRAM [C3] NOZZLE TYPE: 8-STREAM

FUEL FLOW (FAA) CONFIGURATIONS: PASSIVE PLUG WITH BLEED SUPPRESSOR CONFIGURATION: 36-SPOKE(CHUTE INSERT),AREA RATIO=2.0

THRUST	PARAMETERS			OUTER RADIUS RATIO 0.0000		INNER RADIUS RATIO 0.7790		DVO 1.2480				
PDC	CF	WFS2	P2	PA	P20/P2	PT1/PA	CNFGAT	CDD	CDI	CFNET1	CFNET2	F9
3016	0011	410550	1.140	0.360	3.018	2.535	0.455	0.948	0.993	0.849	1.209	1.103
3017	0011	410550	1.140	0.360	3.022	3.022	0.543	0.948	0.995	0.845	1.304	1.099
3018	0011	410550	1.140	0.361	3.025	3.527	0.633	0.948	0.995	0.968	1.448	1.120
3019	0011	410550	1.140	0.360	3.017	1.123	0.062	0.948	0.521	0.830	0.947	1.055
3020	0011	410550	1.140	0.359	3.016	1.520	0.223	0.946	0.905	0.837	0.955	1.078
3021	0011	410550	1.140	0.358	3.028	2.035	0.340	0.949	0.990	0.844	1.074	1.097
3022	0011	410550	1.140	0.358	3.026	2.537	0.425	0.948	0.994	0.846	1.171	1.097
3023	0011	410550	1.140	0.358	3.027	3.018	0.507	0.948	0.995	0.844	1.267	1.096
3024	0011	410550	1.140	0.358	3.026	3.523	0.594	0.949	0.996	0.846	1.396	1.117
3025	0011	410550	1.140	0.357	2.519	1.123	0.134	0.947	0.882	0.825	0.868	1.071
3026	0011	410550	1.140	0.358	2.518	1.516	0.209	0.947	0.999	0.890	1.661	1.147
3027	0011	410550	1.398	0.015	1.505	0.984	0.000	0.960	9.999	0.830	0.830	1.096
3028	0011	410550	1.398	0.026	1.504	0.993	0.022	0.959	9.999	0.835	0.835	1.097
3029	0011	410550	1.398	0.027	1.506	1.000	0.059	0.958	9.999	0.851	0.851	1.100
3030	0011	410550	1.398	0.023	2.006	0.583	0.000	0.965	9.999	0.836	0.836	1.088
3031	0011	410550	1.398	0.023	2.009	0.994	0.029	0.964	9.999	0.847	0.847	1.092
3032	0011	410550	1.398	0.026	2.007	1.011	0.059	0.964	1.006	0.851	0.858	1.094
3033	0011	410550	1.398	0.024	2.003	0.983	0.008	0.965	9.999	0.838	0.838	1.076
3034	0011	410550	1.398	0.026	2.007	1.002	0.029	0.966	1.316	0.844	0.845	1.079
3035	0011	410550	1.398	0.013	2.506	1.024	0.059	0.946	0.850	0.847	0.855	1.081
3036	0011	410550	1.398	0.047	3.015	0.996	0.000	0.948	9.999	0.829	0.829	1.062
3037	0011	410550	1.398	0.057	3.015	1.018	0.029	0.948	0.412	0.835	0.840	1.064
3038	0011	410550	1.398	0.047	3.015	1.026	0.059	0.947	0.573	0.836	0.849	1.064
3039	0011	410550	1.398	0.051	3.012	0.999	0.000	0.947	9.999	0.844	0.844	1.071
3040	0011	410550	1.398	0.054	3.006	1.049	0.079	0.947	0.394	0.851	0.856	1.073
3041	0011	410550	1.398	0.052	3.001	1.104	0.059	0.949	0.537	0.850	0.866	1.074
3042	0011	410550	1.398	0.027	2.506	0.982	0.000	0.965	9.999	0.835	0.935	1.075
3043	0011	410550	1.398	0.027	2.503	1.024	0.059	0.946	0.819	0.846	0.855	1.081
3044	0011	410550	1.140	0.031	1.504	1.116	0.241	0.959	0.995	0.853	0.970	1.116
3045	0011	410550	1.140	0.028	1.504	1.529	0.543	0.959	0.993	0.878	1.361	1.156
3046	0011	410550	1.140	0.030	1.503	2.024	0.747	0.957	0.993	0.889	1.736	1.163
3047	0011	410550	1.140	0.033	1.505	2.516	0.936	0.959	0.995	0.900	2.121	1.170
3048	0011	410550	1.140	0.037	1.502	3.009	1.119	0.961	0.993	0.899	2.475	1.167
3049	0011	410550	1.140	0.050	1.504	3.514	1.313	0.957	0.996	0.924	2.932	1.188
3050	0011	410550	1.140	0.015	2.001	1.119	0.187	0.945	0.967	0.859	0.927	1.110
3051	0011	410550	1.140	0.021	2.001	1.521	0.394	0.945	0.990	0.872	1.146	1.142
3052	0011	410550	1.140	0.045	2.003	2.021	0.548	0.945	0.993	0.892	1.368	1.151
3053	0011	410550	1.140	0.038	2.002	2.519	0.696	0.945	0.994	0.893	1.586	1.157
3054	0011	410550	1.140	0.053	2.003	3.014	0.871	0.944	0.995	0.893	1.701	1.157
3055	0011	410550	1.140	0.060	2.003	3.516	0.956	0.946	0.996	0.915	2.048	1.177
3056	0011	410550	1.140	0.030	2.506	1.118	0.142	0.947	0.924	0.856	0.901	1.095
3057	0011	410550	1.140	0.047	2.505	1.522	0.315	0.944	0.984	0.872	1.064	1.126
3058	0011	410550	1.140	0.050	2.504	2.021	1.437	0.947	0.993	0.876	1.216	1.134
3059	0011	410550	1.140	0.054	2.504	2.521	0.545	0.947	0.993	0.884	1.368	1.140
3060	0011	410550	1.140	0.054	2.507	3.017	0.654	0.947	0.995	0.887	1.514	1.143

FACILITY AYI PROGRAM C031 — NOZZLE TYPE — T (=STREAM — SUPPRESSOR CONFIGURATION

DUAL FLOW (SAA) — PL CONFIGURATIONS — BASELINE PLUG WITH PLUG — 34-SOOKE(CHUTE INSERT), AREA RATIO=2.0

DRAG PARAMETERS — OUTER RADIUS RATIO C.0000 — INNER RADIUS RATIO 0.7790 — DVM 1.2490

EOS	GE	PASS	M0	M1	PTO/P1	PT1/PA	PPEGAT	DCS	CDS	CDSH	CDSH	DCPL,0	DCPL,I	DCTOT	PSUP/PA
3016	0011	410550	1.140	0.360	3.013	2.539	0.455	-0.000	0.842	-0.001	0.014	-0.011	-0.015	-0.117	0.685
3017	0011	410550	1.140	0.360	3.022	3.027	0.543	-0.042	0.835	-0.001	0.014	-0.010	-0.032	-0.126	0.687
3018	0011	410550	1.140	0.361	3.025	3.527	0.631	-0.075	0.824	-0.001	0.014	-0.009	-0.013	-0.098	0.690
3019	0011	410550	1.140	0.360	3.017	1.123	0.052	-0.117	0.861	-0.002	0.015	-0.018	0.005	-0.128	0.678
3020	0011	410550	1.140	0.359	3.024	1.535	0.223	-0.104	0.873	-0.002	0.014	-0.012	0.001	-0.116	0.676
3021	0011	410550	1.140	0.358	3.029	2.035	0.340	-0.004	0.877	-0.002	0.014	-0.010	-0.012	-0.118	0.675
3022	0011	410550	1.140	0.358	3.026	2.537	0.425	-0.034	0.880	-0.001	0.014	-0.009	-0.022	-0.115	0.675
3023	0011	410550	1.140	0.358	3.027	3.013	0.507	-0.030	0.875	-0.001	0.014	-0.007	-0.035	-0.124	0.676
3024	0011	410550	1.140	0.358	3.026	3.521	0.594	-0.074	0.870	-0.001	0.014	-0.007	-0.015	-0.097	0.676
3025	0011	410550	1.140	0.357	2.519	1.123	0.138	-0.123	0.870	-0.003	0.015	-0.019	0.007	-0.138	0.754
3026	0011	410550	1.140	0.358	2.518	1.516	0.760	-0.068	0.851	-0.002	0.015	-0.009	-0.004	-0.092	0.759
3027	0011	410550	0.398	0.019	1.505	0.994	0.000	-0.144	199.270	-0.000	0.146	-0.033	0.017	-0.163	0.888
3028	0011	410550	0.398	0.020	1.504	0.993	0.028	-0.144	125.063	-0.000	2.329	-0.030	0.015	-0.159	0.890
3029	0011	410550	0.398	0.038	1.504	1.000	0.059	-0.142	527.058	-0.000	0.588	-0.028	0.014	-0.156	0.892
3030	0011	410550	0.398	0.023	2.009	0.991	0.000	-0.130	191.709	-0.000	0.134	-0.029	0.013	-0.136	0.840
3031	0011	410550	0.398	0.013	2.008	0.994	0.026	-0.119	323.873	-0.000	0.434	-0.026	0.011	-0.134	0.842
3032	0011	410550	0.398	0.034	2.001	1.011	0.058	-0.116	47.482	-0.000	0.078	-0.023	0.010	-0.130	0.844
3033	0011	410550	0.398	0.034	2.509	0.993	0.000	-0.111	53.904	-0.000	0.056	-0.028	0.011	-0.128	0.790
3034	0011	410550	0.398	0.034	2.507	1.002	0.035	-0.110	54.475	-0.000	0.030	-0.024	0.010	-0.124	0.793
3035	0011	410550	0.398	0.013	2.506	1.024	0.059	-0.107	421.294	-0.000	0.816	-0.023	0.007	-0.123	0.796
3036	0011	410550	0.398	0.047	3.015	0.994	0.000	-0.106	41.375	-0.000	0.007	-0.020	0.009	-0.121	0.732
3037	0011	410550	0.398	0.052	3.015	1.014	0.029	-0.108	34.811	0.000	-0.005	-0.019	0.007	-0.119	0.733
3038	0011	410550	0.398	0.047	3.018	1.014	0.059	-0.106	40.974	-0.000	0.004	-0.017	0.006	-0.117	0.735
3039	0011	410550	0.398	0.051	3.017	0.998	0.000	-0.096	35.027	-0.000	0.011	-0.022	0.007	-0.111	0.732
3040	0011	410550	0.398	0.056	3.356	1.049	0.029	-0.095	32.171	-0.000	0.008	-0.020	0.006	-0.110	0.732
3041	0011	410550	0.398	0.052	3.361	1.104	0.059	-0.094	34.458	-0.000	0.010	-0.018	0.006	-0.108	0.732
3042	0011	410550	0.398	0.027	2.504	0.992	0.000	-0.112	103.571	-0.000	0.147	-0.029	0.011	-0.128	0.790
3043	0011	410550	0.398	0.033	2.503	1.004	0.059	-0.107	64.607	-0.000	0.101	-0.023	0.007	-0.123	0.797
3044	0011	410550	1.140	2.031	1.504	1.116	0.261	-0.175	39.816	-0.000	0.062	-0.024	0.010	-0.140	0.892
3045	0011	410550	1.140	2.029	1.504	1.520	0.543	-0.202	48.428	-0.000	0.061	-0.019	0.002	-0.108	0.891
3046	0011	410550	1.140	0.029	1.513	2.024	2.767	-0.073	44.749	-0.000	0.109	-0.014	-0.014	-0.102	0.890
3047	0011	410550	1.140	0.033	1.505	2.515	0.936	-0.041	34.455	-0.000	0.077	-0.012	-0.025	-0.098	0.890
3048	0011	410550	1.140	0.037	1.507	3.005	1.119	-0.052	27.577	-0.000	0.035	-0.010	-0.028	-0.090	0.891
3049	0011	410550	1.140	0.250	1.504	3.515	1.311	-0.045	14.918	-0.000	0.017	-0.008	-0.005	-0.058	0.892
3050	0011	410550	1.140	0.019	2.001	1.119	0.187	-0.108	240.709	-0.000	0.510	-0.021	0.007	-0.123	0.845
3051	0011	410550	1.140	0.021	2.001	1.521	0.394	-0.099	117.330	-0.000	0.297	-0.018	0.002	-0.105	0.845
3052	0011	410550	1.140	0.245	2.003	2.021	0.548	-0.075	26.747	-0.000	0.036	-0.015	-0.016	-0.106	0.845
3053	0011	410550	1.140	0.018	2.007	2.519	0.684	-0.048	30.606	-0.000	0.053	-0.013	-0.017	-0.096	0.845
3054	0011	410550	1.140	0.253	2.002	3.014	0.821	-0.058	19.328	-0.000	0.025	-0.011	-0.028	-0.097	0.846
3055	0011	410550	1.140	0.250	2.003	3.516	0.956	-0.051	21.068	-0.000	0.035	-0.010	-0.003	-0.064	0.847
3056	0011	410550	1.140	0.030	2.506	1.119	0.142	-0.101	78.130	-0.000	0.070	-0.020	0.006	-0.115	0.799
3057	0011	410550	1.140	0.047	2.505	1.527	0.315	-0.087	30.082	-0.000	0.027	-0.017	0.002	-0.102	0.800
3058	0011	410550	1.140	0.050	2.506	2.021	0.437	-0.076	27.430	-0.000	0.002	-0.015	-0.017	-0.107	0.901
3059	0011	410550	1.140	0.054	2.504	2.521	0.565	-0.068	23.484	-0.000	0.030	-0.013	-0.015	-0.096	0.801
3060	0011	410550	1.140	0.054	2.507	3.017	0.694	-0.061	23.126	-0.000	0.025	-0.012	-0.021	-0.094	0.803

FACILITY [illegible] PROGRAM CODE

NOZZLE TYPE: DUAL FLOW (FAA) — F-STREAM CONFIGURATIONS: PASSIVE PLUG WITH BLEED — SUPPRESSOR CONFIGURATION: 36-SPOKE(CHUTE INSERT),AREA RATIO=2.0

INFLIGHT PARAMETERS — OUTER RADIUS RATIO 0.3090 — INNER RADIUS RATIO 0.7790 — DVC 1.7480

RUN	PT	MACH	M0	M8	PT8/P0	PT8/P8	THRUST	CDD	CDI	CFNET1	CFNET2	F9
3061	0011	410550	1.140	0.056	2.508	1.523	0.763	0.947	0.996	0.907	1.698	1.162
3062	0011	410550	1.140	0.038	2.[illegible]	1.120	0.[illegible]	0.946	0.689	0.840	0.846	1.070
3063	0011	410550	1.140	0.053	2.507	1.522	0.751	0.947	0.947	0.852	0.990	1.100
3064	0011	410550	1.140	0.051	2.[illegible]	2.020	0.363	0.948	0.992	0.869	1.115	1.113
3065	0011	410550	1.140	0.053	3.010	2.523	0.493	0.948	0.994	0.867	1.230	1.118
3066	0011	410550	1.140	0.066	3.[illegible]17	3.018	0.561	0.946	0.999	0.864	1.330	1.114
3067	0011	410550	1.140	0.057	3.016	3.520	0.694	0.948	0.996	0.886	1.476	1.136
3068	0011	410550	1.140	0.056	2.514	1.120	0.064	0.946	0.566	0.854	0.673	1.076
3069	0011	410550	1.140	0.052	2.[illegible]	1.522	0.220	0.949	0.998	0.860	0.978	1.101
3070	0011	410550	1.140	0.055	2.506	2.021	0.329	0.950	0.999	0.864	1.090	1.115
3071	0011	410550	1.140	0.050	2.516	2.521	0.411	0.949	0.992	0.868	1.187	1.117
3072	0011	410550	1.140	0.057	3.[illegible]	3.013	0.491	0.949	0.994	0.864	1.273	1.114
3073	0011	410550	1.140	0.056	3.[illegible]18	3.517	0.575	0.949	0.996	0.883	1.402	1.134
3074	0011	410550	1.140	0.022	2.[illegible]	1.117	0.142	0.947	0.925	0.858	0.902	1.096
3075	0011	410550	1.140	0.042	2.502	3.512	0.764	0.947	0.997	0.907	1.700	1.163

812

FACILITY [illegible] PROGRAM CODE

NOZZLE TYPE: DUAL FLOW (FAA) — F-STREAM CONFIGURATIONS: PASSIVE PLUG WITH BLEED — SUPPRESSOR CONFIGURATION: 36-SPOKE(CHUTE INSERT),AREA RATIO=2.0

INFLIGHT PARAMETERS — OUTER RADIUS RATIO 0.3090 — INNER RADIUS RATIO 0.7790 — DVC 1.7480

RUN	PT	MACH	M0	M8	PT8/P0	PT8/P8	THRUST	DCS	CDS	DCSH	CDSH	DCPL,0	DCPL,1	DCTOT	PSUP/PA
3061	0011	410550	1.140	0.056	2.503	1.521	0.763	-0.[illegible]	19.434	-0.000	0.007	-0.010	-0.003	-0.069	0.805
3062	0011	410550	1.140	0.038	2.[illegible]	1.121	0.[illegible]69	-0.104	44.827	-0.000	0.041	-0.017	0.004	-0.117	0.735
3063	0011	410550	1.140	0.053	2.509	1.522	0.751	-0.091	32.694	0.000	-0.004	-0.013	0.001	-0.103	0.739
3064	0011	410550	1.140	0.051	2.509	2.020	0.363	-0.092	34.086	-0.000	0.031	-0.011	-0.014	-0.108	0.737
3065	0011	410550	1.140	0.053	2.[illegible]	2.523	0.493	-0.075	27.032	-0.000	0.034	-0.010	-0.017	-0.101	0.738
3066	0011	410550	1.140	0.065	3.[illegible]19	3.014	0.561	-0.[illegible]	21.446	-0.000	0.026	-0.009	-0.030	-0.107	0.740
3067	0011	410550	1.140	0.057	3.016	3.520	0.694	-0.063	27.469	-0.000	0.025	-0.008	-0.009	-0.081	0.741
3068	0011	410550	1.140	0.056	2.514	1.120	0.066	-0.094	29.915	-0.000	0.014	-0.017	0.005	-0.106	0.732
3069	0011	410550	1.140	0.052	2.[illegible]	1.522	0.220	-0.096	34.743	-0.000	0.029	-0.012	-0.000	-0.097	0.732
3070	0011	410550	1.140	0.055	2.[illegible]	2.021	0.329	-0.[illegible]	30.267	-0.000	0.030	-0.010	-0.012	-0.099	0.732
3071	0011	410550	1.140	0.050	2.516	2.521	0.411	-0.070	27.134	-0.000	0.021	-0.010	-0.020	-0.099	0.732
3072	0011	410550	1.140	0.057	3.[illegible]	3.013	0.491	-0.065	29.095	-0.000	0.031	-0.009	-0.012	-0.106	0.732
3073	0011	410550	1.140	0.[illegible]	3.[illegible]18	3.517	0.575	-0.060	26.511	-0.000	0.029	-0.007	-0.013	-0.080	0.732
3074	0011	410550	1.140	0.022	2.[illegible]	1.117	0.142	-0.101	142.635	-0.000	0.237	-0.020	0.006	-0.115	0.800
3075	0011	410550	1.140	0.042	2.502	3.512	0.764	-0.055	17.635	-0.000	0.026	-0.010	-0.003	-0.069	0.804

104-TUBE NOZZLE

FACILITY [illegible] PROGRAM FOR [illegible] TYPE [illegible] P-STREAM CONFIGURATIONS SUPPRESSOR CONFIGURATION

[illegible]-TIME SUPPRESSOR (FAST)

THRUST	[illegible]	OUTER RADIUS RATIO	INNER RADIUS RATIO	OVP
		0.0000	0.0000	1.2480

[illegible]	[illegible]	[illegible]	F2	F6	F10/F6	F11/F6	CFCCAT	CFP	F01	CFNET1	CFNET2	F9
397	2000	20000	0.000	0.000	1.139	0.992	0.000	0.864	0.999	0.887	0.887	1.052
398	2000	20000	0.000	0.000	1.140	0.991	0.000	0.859	0.999	0.880	0.880	1.071
399	2000	20000	0.000	0.000	1.139	0.992	0.000	0.864	0.999	0.883	0.883	1.066
400	2000	20000	0.000	0.000	1.139	0.992	0.000	0.864	0.999	0.887	0.887	1.064
401	2000	20000	0.000	0.000	1.140	0.992	0.000	0.864	0.999	0.879	0.879	1.060
402	2000	20000	0.000	0.000	1.141	0.993	0.000	0.864	0.999	0.883	0.883	1.057
403	2000	20000	0.000	0.000	1.132	0.992	0.000	0.867	0.999	0.887	0.887	1.054
404	2000	20000	0.000	0.000	1.141	0.992	0.000	0.866	0.999	0.883	0.883	1.057
405	2000	20000	0.000	0.000	1.139	0.992	0.000	0.866	0.999	0.878	0.878	1.060
406	2000	20000	0.000	0.000	1.140	0.991	0.000	0.865	0.999	0.868	0.868	1.063
407	2000	20000	0.000	0.000	1.000	0.992	0.000	0.864	0.999	0.855	0.855	1.067
410	2000	20000	0.000	0.000	1.139	0.992	0.000	0.859	0.999	0.828	0.828	1.074
411	2000	20000	0.000	0.000	1.000	0.000	0.000	0.867	0.999	0.762	0.762	1.038
412	2000	20000	0.000	0.000	1.000	0.000	0.000	0.867	0.999	0.817	0.817	1.039
413	2000	20000	0.000	0.000	1.000	0.000	0.000	0.864	0.999	0.836	0.836	1.038
414	2000	20000	0.000	0.000	1.000	0.000	0.000	0.865	0.999	0.849	0.849	1.037
415	2000	20000	0.000	0.000	1.000	0.000	0.000	0.866	0.999	0.858	0.858	1.036
416	2000	20000	0.000	0.000	1.000	0.000	0.000	0.865	0.999	0.864	0.864	1.035
417	2000	20000	0.000	0.000	1.000	0.000	0.000	0.866	0.999	0.865	0.865	1.035
418	2000	20000	0.000	0.000	1.000	0.000	0.000	0.867	0.999	0.864	0.864	1.036
419	2000	20000	0.000	0.000	1.000	0.000	0.000	0.867	0.999	0.858	0.858	1.037
420	2000	20000	0.000	0.000	1.000	0.000	0.000	0.866	0.999	0.849	0.849	1.037
421	2000	20000	0.000	0.000	1.000	0.000	0.000	0.865	0.999	0.836	0.836	1.038
422	2000	20000	0.000	0.000	1.000	0.000	0.000	0.864	0.999	0.818	0.818	1.040
423	2000	20000	0.000	0.000	1.000	0.000	0.000	0.858	0.999	0.770	0.770	1.043
424	2000	20000	0.000	0.000	1.000	0.000	0.000	0.869	0.999	0.757	0.757	1.036
425	2000	20000	0.000	0.000	1.000	0.000	0.000	0.866	0.999	0.813	0.813	1.038
426	2000	20000	0.000	0.000	1.000	0.000	0.000	0.865	0.999	0.832	0.832	1.035
427	2000	20000	0.000	0.000	1.000	0.000	0.000	0.864	0.999	0.845	0.845	1.033
428	2000	20000	0.000	0.000	1.000	0.000	0.000	0.865	0.999	0.856	0.856	1.034
429	2000	20000	0.000	0.000	1.000	0.000	0.000	0.866	0.999	0.863	0.863	1.034
430	2000	20000	0.000	0.000	1.000	0.000	0.000	0.866	0.999	0.866	0.866	1.034
431	2000	20000	0.000	0.000	1.000	0.000	0.000	0.865	0.999	0.863	0.863	1.034
432	2000	20000	0.000	0.000	1.000	0.000	0.000	0.864	0.999	0.855	0.855	1.034
433	2000	20000	0.000	0.000	1.000	0.000	0.000	0.866	0.999	0.846	0.846	1.035
434	2000	20000	0.000	0.000	1.000	0.000	0.000	0.865	0.999	0.833	0.833	1.036
435	2000	20000	0.000	0.000	1.000	0.000	0.000	0.863	0.999	0.814	0.814	1.037
436	2000	20000	0.000	0.000	1.000	0.000	0.000	0.859	0.999	0.789	0.789	1.037
437	2000	20000	0.000	0.000	1.000	0.000	0.000	0.860	0.999	0.749	0.749	1.032
438	2000	20000	0.000	0.000	1.000	0.000	0.000	0.861	0.999	0.748	0.748	1.032
439	2000	20000	0.000	0.000	1.000	0.000	0.000	0.864	0.999	0.805	0.805	1.031
440	2000	20000	0.000	0.000	1.000	0.000	0.000	0.864	0.999	0.825	0.825	1.030
441	2000	20000	0.000	0.000	1.000	0.000	0.000	0.864	0.999	0.840	0.840	1.030
442	2000	20000	0.000	0.000	1.000	0.000	0.000	0.866	0.999	0.851	0.851	1.031
443	2000	20000	0.000	0.000	1.000	0.000	0.000	0.866	0.999	0.858	0.858	1.029

SUPPRESSOR CONFIGURATION

SUPPRESSOR CONFIGURATION

444	2000	200000	0.000	0.444	1.000	0.000	0.000	0.000	0.864	0.864	1.030
445	2000	200000	0.000	0.444	1.000	0.000	0.000	0.000	0.858	0.858	1.031
446	2000	200000	0.000	0.444	1.000	0.000	0.000	0.000	0.850	0.850	1.031
447	2000	200000	0.000	0.444	1.000	0.000	0.000	0.000	0.840	0.840	1.030
448	2000	200000	0.000	0.444	1.000	0.000	0.000	0.000	0.824	0.824	1.030
449	2000	200000	0.000	0.444	1.000	0.000	0.000	0.000	0.804	0.804	1.031
450	2000	200000	0.000	0.444	1.000	0.000	0.000	0.000	0.745	0.749	1.032
[illegible]											

SUPPRESSOR CONFIGURATION

444	2000	200000	1.000	1.444	1.000	0.000	0.000	-0.039	0.000	0.000	0.000	0.000	-0.078	0.000
445	2000	200000	1.000	1.444	1.000	0.000	0.000	-0.039	0.000	0.000	0.000	0.000	-0.079	0.000
446	2000	200000	1.000	1.444	1.000	0.000	0.000	-0.039	0.000	0.000	0.000	0.000	-0.081	0.000
447	2000	200000	1.000	1.444	1.000	0.000	0.000	-0.039	0.000	0.000	0.000	0.000	-0.084	0.000
448	2000	200000	1.000	1.444	1.000	0.000	0.000	-0.039	0.000	0.000	0.000	0.000	-0.087	0.000
449	2000	200000	1.000	1.444	1.000	0.000	0.000	-0.039	0.000	0.000	0.000	0.000	-0.094	0.000
450	2000	200000	1.000	1.444	1.000	0.000	0.000	-0.039	0.000	0.000	0.000	0.000	-0.122	0.000
[illegible]														

8-LOBE NOZZLE

FACILITY [illegible] PROGRAM CODE _____ NOZZLE TYPE _____ 1 STREAM

DAISY SUPPRESSOR (FAA) PLUG CONFIGURATIONS SUPPRESSOR CONFIGURATION

TARGET PARAMETERS — OUTER RADIUS RATIO 0.0000 — INNER RADIUS RATIO 0.0000 — OVD 1.2460

ANG	CE	LAMA	D2	PA	PTC/PA	PTI/PA	CMECAT	CDO	CDI	CFNET1	CFNET2	F9
3177	1000	10000	0.000	-0.000	1.407	1.075	0.000	1.006	9.999	0.906	0.906	1.189
3178	1000	10000	0.000	0.027	1.735	1.116	0.000	0.977	9.999	0.942	0.942	1.210
3179	1000	10000	0.000	0.042	2.009	1.162	0.000	0.976	9.999	0.947	0.947	1.209
3180	1000	10000	0.000	0.051	2.481	1.240	0.000	0.975	9.999	0.938	0.938	1.195
[illegible]												
3182	1000	10000	0.000	0.051	2.921	1.313	0.000	0.980	9.999	0.931	0.931	1.191
3183	1000	10000	0.000	0.051	2.434	1.241	0.000	0.976	9.999	0.937	0.937	1.194
3184	1000	10000	0.000	0.046	1.990	1.155	0.000	0.977	9.999	0.950	0.950	1.213
3185	1000	10000	0.000	0.035	1.743	1.118	0.000	0.978	9.999	0.945	0.945	1.212
3186	1000	10000	0.000	0.035	1.496	1.077	0.000	1.006	9.999	0.914	0.914	1.193
3187	1000	10000	0.000	0.047	1.978	1.158	0.000	0.972	9.999	0.950	0.950	1.209
3188	1000	10000	0.000	0.051	2.239	1.199	0.000	0.978	9.999	0.950	0.950	1.210
3189	1000	10000	0.000	0.443	1.495	1.081	0.000	1.003	9.999	0.898	0.898	1.177
3190	1000	10000	0.000	0.444	1.731	1.119	0.000	0.978	9.999	0.916	0.916	1.187
3191	1000	10000	0.000	0.445	1.979	1.163	0.000	0.974	9.999	0.922	0.922	1.185
3192	1000	10000	0.000	0.445	2.249	1.206	0.000	0.976	9.999	0.919	0.919	1.180
3193	1000	10000	0.000	0.445	2.492	1.248	0.000	0.979	9.999	0.909	0.909	1.170
3194	1000	10000	0.000	0.447	2.995	1.331	0.000	0.981	9.999	0.925	0.925	1.184
3195	1000	10000	0.000	0.446	3.049	1.335	0.000	0.981	9.999	0.926	0.926	1.184
3196	1000	10000	0.000	0.447	2.995	1.330	0.000	0.981	9.999	0.924	0.924	1.183
3197	1000	10000	0.000	0.445	2.513	1.250	0.000	0.980	9.999	0.908	0.908	1.170
3198	1000	10000	0.000	0.445	2.236	1.204	0.000	0.978	9.999	0.919	0.919	1.181
3199	1000	10000	0.000	0.445	1.989	1.162	0.000	0.975	9.999	0.920	0.920	1.185
3200	1000	10000	0.000	0.444	1.497	1.080	0.000	1.005	9.999	0.896	0.896	1.176
3201	1000	10000	0.000	0.445	2.742	1.288	0.000	0.980	9.999	0.913	0.913	1.173
3202	1000	10000	0.000	0.445	2.752	1.291	0.000	0.981	9.999	0.915	0.915	1.176
3203	1000	10000	0.000	0.395	1.492	1.080	0.000	1.004	9.999	0.901	0.901	1.179
3204	1000	10000	0.000	0.395	1.747	1.122	0.000	0.977	9.999	0.914	0.914	1.186
[illegible]												
3206	1000	10000	0.000	0.397	2.241	1.205	0.000	0.978	9.999	0.920	0.920	1.182
3207	1000	10000	0.000	0.397	2.496	1.247	0.000	0.981	9.999	0.911	0.911	1.174
3208	1000	10000	0.000	0.398	2.718	1.287	0.000	0.976	9.999	0.919	0.919	1.175
3209	1000	10000	0.000	0.398	2.876	1.314	0.000	0.982	9.999	0.920	0.920	1.181
3210	1000	10000	0.000	0.399	2.757	1.291	0.000	0.980	9.999	0.915	0.915	1.175
3211	1000	10000	0.000	0.398	2.498	1.248	0.000	0.976	9.999	0.914	0.914	1.172
3212	1000	10000	0.000	0.397	2.250	1.206	0.000	0.975	9.999	0.918	0.918	1.179
[illegible]												
3214	1000	10000	0.000	0.398	1.744	1.122	0.000	0.978	9.999	0.916	0.916	1.188
3215	1000	10000	0.000	0.398	1.499	1.082	0.000	1.003	9.999	0.900	0.900	1.179
3216	1000	10000	0.000	0.397	1.977	1.160	0.000	0.974	9.999	0.922	0.922	1.186
3217	1000	10000	0.000	0.398	1.991	1.163	0.000	0.976	9.999	0.922	0.922	1.187
3218	1000	10000	0.000	0.397	1.496	1.082	0.000	1.003	9.999	0.905	0.905	1.182
3219	1000	10000	0.000	0.357	1.743	1.124	7.671	0.977	9.999X	0.917	0.917	1.189
3220	1000	10000	0.000	0.358	1.986	1.164	0.000	0.972	9.999	0.927	0.927	1.189
3221	1000	10000	0.000	0.358	2.242	1.206	0.000	0.977	9.999	0.923	0.923	1.185

FACILITY SEI PROGRAM COST

NOZZLE TYPE — PLUG — CONFIGURATIONS — SUPPRESSOR CONFIGURATION

DEISY SUPPRESSOR (FAR)

DRAG PARAMETERS — OUTER RADIUS RATIO 0.0000 — INNER RADIUS RATIO 0.0000 — DVD 1.2480

RDG	GE	MASS	EP	MA	PTO/PA	PT/PA	OMEGAT	CDS	CDS	DCSH	CDSH	DCPL,C	DCPL,T	DCTOT	PSUP/PA
3177	3000	30000	0.000	-0.000	1.497	1.075	0.000	0.000	0.000	0.000	0.000	0.000	0.000	0.000	0.000
3178	3000	30000	0.000	0.022	1.735	1.116	0.000	0.000	0.000	0.000	0.000	0.000	0.000	0.000	0.000
3179	3000	30000	0.000	0.042	2.009	1.162	0.000	0.000	0.000	0.000	0.000	0.000	0.000	0.000	0.000
3180	3000	30000	0.000	0.063	2.481	1.240	0.000	0.000	0.000	0.000	0.000	0.000	0.000	0.000	0.000
[illegible]															
3182	3000	30000	0.000	0.061	2.921	1.313	0.000	0.000	0.000	0.000	0.000	0.000	0.000	0.000	0.000
3183	3000	30000	0.000	0.051	2.484	1.241	0.000	0.000	0.000	0.000	0.000	0.000	0.000	0.000	0.000
3184	3000	30000	0.000	0.046	1.990	1.159	0.000	0.000	0.000	0.000	0.000	0.000	0.000	0.000	0.000
3185	3000	30000	0.000	0.035	1.743	1.118	0.000	0.000	0.000	0.000	0.000	0.000	0.000	0.000	0.000
3186	3000	30000	0.000	0.005	1.496	1.077	0.000	0.000	0.000	0.000	0.000	0.000	0.000	0.000	0.000
3187	3000	30000	0.000	0.047	1.978	1.156	0.000	0.000	0.000	0.000	0.000	0.000	0.000	0.000	0.000
3188	3000	30000	0.000	0.054	2.239	1.199	0.000	0.000	0.000	0.000	0.000	0.000	0.000	0.000	0.000
3189	3000	30000	0.000	0.443	1.495	1.081	0.000	0.000	0.000	0.000	0.000	0.000	0.000	0.000	0.000
3190	3000	30000	0.000	0.444	1.731	1.119	0.000	0.000	0.000	0.000	0.000	0.000	0.000	0.000	0.000
3191	3000	30000	0.000	0.445	1.977	1.163	0.000	0.000	0.000	0.000	0.000	0.000	0.000	0.000	0.000
3192	3000	30000	0.000	0.445	2.245	1.206	0.000	0.000	0.000	0.000	0.000	0.000	0.000	0.000	0.000
3193	3000	30000	0.000	0.445	2.497	1.248	0.000	0.000	0.000	0.000	0.000	0.000	0.000	0.000	0.000
3194	3000	30000	0.000	0.447	2.665	1.331	0.000	0.000	0.000	0.000	0.000	0.000	0.000	0.000	0.000
3195	3000	30000	0.000	0.446	3.045	1.319	0.000	0.000	0.000	0.000	0.000	0.000	0.000	0.000	0.000
3196	3000	30000	0.000	0.447	2.495	1.310	0.000	0.000	0.000	0.000	0.000	0.000	0.000	0.000	0.000
3197	3000	30000	0.000	0.445	2.513	1.253	0.000	0.000	0.000	0.000	0.000	0.000	0.000	0.000	0.000
3198	3000	30000	0.000	0.445	2.238	1.204	0.000	0.000	0.000	0.000	0.000	0.000	0.000	0.000	0.000
3199	3000	30000	0.000	0.445	1.979	1.162	0.000	0.000	0.000	0.000	0.000	0.000	0.000	0.000	0.000
3200	3000	30000	0.000	0.444	1.492	1.080	0.000	0.000	0.000	0.000	0.000	0.000	0.000	0.000	0.000
3201	3000	30000	0.000	0.445	2.742	1.288	0.000	0.000	0.000	0.000	0.000	0.000	0.000	0.000	0.000
3202	3000	30000	0.000	0.445	2.252	1.291	0.000	0.000	0.000	0.000	0.000	0.000	0.000	0.000	0.000
3203	3000	30000	0.000	0.395	1.492	1.080	0.000	0.000	0.000	0.000	0.000	0.000	0.000	0.000	0.000
3204	3000	30000	0.000	0.395	1.747	1.122	0.000	0.000	0.000	0.000	0.000	0.000	0.000	0.000	0.000
[illegible]															
3206	3000	30000	0.000	0.397	2.246	1.205	0.000	0.000	0.000	0.000	0.000	0.000	0.000	0.000	0.000
3207	3000	30000	0.000	0.397	2.494	1.247	0.000	0.000	0.000	0.000	0.000	0.000	0.000	0.000	0.000
3208	3000	30000	0.000	0.398	2.750	1.287	0.000	0.000	0.000	0.000	0.000	0.000	0.000	0.000	0.000
3209	3000	30000	0.000	0.398	2.876	1.311	0.000	0.000	0.000	0.000	0.000	0.000	0.000	0.000	0.000
3210	3000	30000	0.000	0.399	2.752	1.291	0.000	0.000	0.000	0.000	0.000	0.000	0.000	0.000	0.000
3211	3000	30000	0.000	0.398	2.498	1.248	0.000	0.000	0.000	0.000	0.000	0.000	0.000	0.000	0.000
3212	3000	30000	0.000	0.397	2.250	1.206	0.000	0.000	0.000	0.000	0.000	0.000	0.000	0.000	0.000
[illegible]															
3214	3000	30000	0.000	0.398	1.744	1.122	0.000	0.000	0.000	0.000	0.000	0.000	0.000	0.000	0.000
3215	3000	30000	0.000	0.398	1.499	1.082	0.000	0.000	0.000	0.000	0.000	0.000	0.000	0.000	0.000
3216	3000	30000	0.000	0.397	1.977	1.164	0.000	0.000	0.000	0.000	0.000	0.000	0.000	0.000	0.000
3217	3000	30000	0.000	0.398	1.991	1.163	0.000	0.000	0.000	0.000	0.000	0.000	0.000	0.000	0.000
3218	3000	30000	0.000	0.357	1.499	1.082	0.000	0.000	0.000	0.000	0.000	0.000	0.000	0.000	0.000
3219	3000	30000	0.000	0.357	1.743	1.124	7.671	0.000	0.000	0.000	0.000	0.000	0.000	0.000	0.000
3220	3000	30000	0.000	0.358	1.996	1.164	0.000	0.000	0.000	0.000	0.000	0.000	0.000	0.000	0.000
3221	3000	30000	0.000	0.358	2.242	1.206	0.000	0.000	0.000	0.000	0.000	0.000	0.000	0.000	0.000

FACILITY 421 PROGRAM CODE

NOZZLE TYPE
DAISY SUPPRESSOR (FAA)

1 1-STREAM
PLUG CONFIGURATIONS

SUPPRESSOR CONFIGURATION

THRUST PARAMETERS

OUTER RADIUS RATIO 0.0000 INNER RADIUS RATIO 0.0000 OVD 1.2480

NOZ	GE	PASA	O2	MA	PTC/PA	PTI/PA	OMEGAT	CDO	CDI	CFNET1	CFNET2	F9
3222	30000	30000	0.000	0.357	2.500	1.247	0.000	0.981	9.999	0.912	0.912	1.176
3223	30000	30000	0.000	0.358	2.744	1.287	0.000	0.980	9.999	0.919	0.919	1.179
3224	30000	30000	0.000	0.358	2.507	1.249	0.000	0.978	9.999	0.914	0.914	1.174
3225	30000	30000	0.000	0.358	2.254	1.207	0.000	0.974	9.999	0.924	0.924	1.183
3226	30000	30000	0.000	0.359	2.003	1.165	0.000	0.976	9.999	0.926	0.926	1.191
3227	30000	30000	0.000	0.358	1.752	1.125	0.000	0.977	9.999	0.916	0.916	1.188
3228	30000	30000	0.000	0.358	1.496	1.082	0.000	0.994	9.999	0.912	0.912	1.181

FACILITY AFL PROGRAM CODE

NOZZLE TYPE
DAISY SUPPRESSOR (FAA)

1 1-STREAM
PLUG CONFIGURATIONS

SUPPRESSOR CONFIGURATION

DRAG PARAMETERS

OUTER RADIUS RATIO 0.0000 INNER RADIUS RATIO 0.0000 OVD 1.2480

NOZ	GE	PASA	O2	MA	PTC/PA	PTI/PA	OMEGAT	DCS	CDS	DCSH	CDSH	DCPL,O	DCPL,I	DCTOT	PSUP/PA
3222	30000	30000	0.000	0.357	2.500	1.247	0.000	0.000	0.000	0.000	0.000	0.000	0.000	0.000	0.000
3223	30000	30000	0.000	0.358	2.744	1.287	0.000	0.000	0.000	0.000	0.000	0.000	0.000	0.000	0.000
3224	30000	30000	0.000	0.358	2.507	1.249	0.000	0.000	0.000	0.000	0.000	0.000	0.000	0.000	0.000
3225	30000	30000	0.000	0.358	2.254	1.207	0.000	0.000	0.000	0.000	0.000	0.000	0.000	0.000	0.000
3226	30000	30000	0.000	0.359	2.003	1.165	0.000	0.000	0.000	0.000	0.000	0.000	0.000	0.000	0.000
3227	30000	30000	0.000	0.358	1.752	1.125	0.000	0.000	0.000	0.000	0.000	0.000	0.000	0.000	0.000
3228	30000	30000	0.000	0.358	1.496	1.082	0.000	0.000	0.000	0.000	0.000	0.000	0.000	0.000	0.000

REFERENCES

1. Lee, R., Kendall, R.M., et al., "Research Investigation of the Generation and Suppression of Jet Noise," General Electric Company, NOAS 59-6160-C, January 1961.

2. Simcox, C.S., et al., "SST Technology Follow-On Program - Phase I - A Summary of the SST Jet Noise Suppression Test Program," Boeing Company, FAA-SS-72-41, February 1972.

3. Brausch, J.F. and Doyle, V.L., "Summary of GE4/SST Acoustic Suppression Research, Supersonic Transport Noise Reduction Technology Program, Phase I," General Electric Company, FAA-SS-72-42, December 1972.

4. Stringas, E.J. and Kazin, S.B., "Supersonic Transport Noise Reduction Technology Program - Phase II," General Electric Company, FAA-SS-73-29-1, September 1975.

5. Atvars, J., et al., "SST Technology Follow-On Program - Phase II," Boeing Company, FAA-SS-73-11, March 1975.

6. Hawkins, R. and Hoch, R., "Studies into Concorde's Engine Noise Reduction," NATO, AGARD-CPP-131.

7. Mani, R. and Stringas, E.J., et. al., "High Velocity Jet Noise Source Location and Reduction - Task 2 - Theoretical Developments and Basic Experiments," General Electric Company, FAA-RD-76-79, II, May 1978.

8. Savell, C.T., Stringas, E.J., et al., "High Velocity Jet Noise Source Location and Reduction - Task 1, Activation of Facilities and Validation of Source Location Techniques," General Electric Company, FAA-RD-76-79, I, February 1977.

9. Savell, C.T. and Stringas, E.J., "High Velocity Jet Noise Source Location and Reduction - Task I Supplement - Certification of the General Electric Jet Noise Anechoic Test Facility," General Electric Company, FAA-RD-76-79, IA, February 1977.

10. Knott, P.R., Stringas E.J., et al., "Acoustic Tests of Duct-Burning Turbofan Jet Noise Simulation," General Electric Company, NASA Contract Report 2966, July 1978.

11. Knott, P.R., Blozy, J.T., and Staid, P.S., "Acoustic and Performance Investigation of Coannular Plug Nozzles," General Electric Company, NASA Contract NAS3-19777, May 1977 (to be published).

12. Clapper, W.S., Stringas, E.J., et al., "High Velocity Jet Noise Source Location and Reduction - Task 4 - Development/Evaluation of Techniques for In-Flight Investigations," General Electric Company, FAA-RD-76-79, IV, February 1977.

13. Anon., "Standard Values of Atmospheric Absorption as a Function of Temperature and Humidity for Use in Evaluating Aircraft Flyover Noise," SAE ARP 866, 1964.

14. Ibid., Proposed Revision to SAE ARP 866, October 1973.

15. Harris, C.M., "Absorption of Sound in Air in the Audio Frequency Range," JASA Vol. 35, 1963.

16. Knesner, H.O., "Interpretation of the Anomalous Sound Absorption in Air and Oxygen in Terms of Molecular Collisions," JASA Vol. 5, 1933.

17. Fogg, R.G., "Internal Memorandum," of the General Electric Aircraft Engine Group, Evendale, Ohio, December 1973.

18. Anon., "Acoustic Effects Produced by a Reflecting Plane," SAE AIR 876, October 1973.

19. Anon., "Jet Noise Predictions," SAE AIR 876, July 1965.

20. Evans., L.B., Bass, H.E., and Sutherland, L.C., "Atmospheric Absorption of Sound: Theoretical Predictions," Part 2, JASA, Vol. 51, 1972.

21. Knott, P.R., et al., "Supersonic Jet Exhaust Noise Investigation - Final Report," General Electric Company, AFAPL-TR-76-68, July 1976.

22. Knott, P.R., et al., "Supersonic Jet Exhaust Noise Investigation - Interim Report," General Electric Company, AFAPL-TR-74-25, June 1974.

23. Benzakein, M.J., and Knott, P.R., (editors), "Supersonic Jet Exhaust Noise - Final Report," General Electric Company, AFAPL-TR-72-52, August 1972.

24. "Prediction of Single Stream Shock Cell Noise," SAE ARP 876 (Proposed), April 1975.

25. Hoch, R.G., Duponchel, J.P., Cocking, B.J., and Bryce, W.D., "Studies of the Influence of Density on Jet Noise," Journal of Sound and Vibration, Vol. 28, No. 4, 1973, pp. 649-668.

26. Williams, T.J., Ali, M.R.M., and Anderson, J.S., "Noise and Flow Characteristics of Coaxial Jets," Journal of Mechanical Engineering Science, Vol. II, No. 2, April 1969, pp. 133-142.

27. Olsen, W. and Friedman, R., "Jet Noise from Coaxial Nozzles Over a Wide Range of Geometric and Flow Parameters," AIAA Paper No. 74-43, 1974.

REFERENCES (Concluded)

28. Kazin, S.B., et al., "Core Engine Noise Control Program - Final Report," General Electric Company, FAA-RD-75-125, 1974.

29. Von Glahn, U., Groesbeck, D., and Goodykoontz, J., "Velocity Decay and Acoustic Characteristics of Various Nozzle Geometries with Forward Velocity," NASA TMX-68259, July 1973.

30. Schlinker, R.H., Peterson, R.A., and Kaplan, R.E., "Enhancement of Directional Microphone Measurements," AIAA Paper 73-1040, October 1973.

31. Levinson, N., "The Wiener RMS Error Criterion in Filter Design and Prediction," Journal of Mathematics and Physics, Vol. 25, 1946, pp. 261-278.

32. Robinson, E.A., Multichannel Time Series Analysis with Digital Computer Programs, Holden-Day, 1967.

33. Anon., "Standard Values of Atmospheric Absorption as a Function of Temperature and Humidity," SAE ARP 866A, March 1975.

34. Zwicky, E.E., Jr., "Solution of Linear Algebraic Equations," from the General Electric ABC Course Notes, 1972.

35. Carnahan, Luther, and Wilkes, Applied Numerical Analysis, Wiley, 1969.

36. Johnson, R.D., "Real-Gas Effects in Critical Flow Through Nozzles and Tabulated Thermodynamic Properties," NASA TN-D-2565, 1965.

37. Siegfried, R.G., and Kuchar, A.P., "A Standard for Exhaust Nozzle Tests," General Electric Company, ESAD Technical Brief 71006, April 6, 1971.

38. Harrington, D.E., Schloemer, J.J., Skebe, S.A., "Thrust Performance of Isolated 36-Chute Suppressor Plug Nozzles With and Without Ejectors at Mach Numbers from 0 to 0.45," NASA TMX-3298, October 1975.

39. Staid, Paul S., "Wind Tunnel Performance Tests of Coannular Plug Nozzles," NASA Contract NAS3-19777, April 1977.